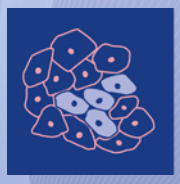

cancers

Volume 2

Cancer Nanomedicine

Edited by

Clare Hoskins

Printed Edition of the Special Issue Published in *Cancers*

www.mdpi.com/journal/cancers

MDPI

Cancer Nanomedicine

Cancer Nanomedicine

Editor

Clare Hoskins

MDPI • Basel • Beijing • Wuhan • Barcelona • Belgrade • Manchester • Tokyo • Cluj • Tianjin

Editor
Clare Hoskins
University of Strathclyde
UK

Editorial Office
MDPI
St. Alban-Anlage 66
4052 Basel, Switzerland

This is a reprint of articles from the Special Issue published online in the open access journal *Cancers* (ISSN 2072-6694) (available at: https://www.mdpi.com/journal/cancers/special_issues/Cancer_Nanomedicine).

For citation purposes, cite each article independently as indicated on the article page online and as indicated below:

LastName, A.A.; LastName, B.B.; LastName, C.C. Article Title. *Journal Name* **Year**, *Article Number*, Page Range.

Volume 2
ISBN 978-3-03943-104-5 (Hbk)
ISBN 978-3-03943-105-2 (PDF)

Volume 1-2
ISBN 978-3-03943-106-9 (Hbk)
ISBN 978-3-03943-107-6 (PDF)

Contents

About the Editor

Clare, Hoskins, Ph.D., Dr Clare Hoskins is a Reader in the School of Pure and Applied Chemistry. She has published >40 peer reviewed articles and filed 1 patent. Her research has been supported with over £2M by national (e.g., EPSRC, BBSRC/FAPESP, Wellcome Trust) and international (e.g., Newton-Bhabha & British Council, Iraqi Ministry of Higher Education and Scientific Research) research funding. Clare is the Elected Secretary to the Royal Society of Chemistry, Chemical Nanosciences and Nanotechnology Network, she is a committee member of the UK and Ireland Controlled Release Society and she sits on the British Council Grant Review Panel for Newton Grants. In 2019 Clare was awarded the Academy of Pharmaceutical Sciences 'Emerging Scientist' sponsored by Pfizer and also the North Staffordshire Medical Institute Researcher Award. Clare sits on the editorial board of numerous journals in her field, she leads a vibrant interdisciplinary research group within the them of Bionanotechnology and Analytical Chemistry within the Technology Innovation Centre. The focus of her research is the development of a range of multifunctional nanoparticles and their translation into medical therapies and agricultural products.

Preface to "Cancer Nanomedicine"

Welcome to the special issue on Cancer Nanomedicine within Cancers. It has been a real delight to edit this special edition bringing together cutting edge research within the field with insightful reviews and opinions reflecting our community.

Cancer nanomedicine is a large umbrella under which researchers spanning the physical, chemical and biological sciences. I think this is well reflected in this edition.

Cancer treatments are often hindered by the lack of drug specificity, poor physicochemical properties of active pharmaceutical ingredients, poor penetration ability and drug resistance. With the discovery and characterization of an increasing number of cancer types with little improvement of the ability to diagnose, treatment options or patient prognosis, more advanced technologies are urgently required. Nanotechnology defines particulates within the 1×10^{-9} m range. Particulates within the nano-sized domain often exhibit unique properties compared to their larger size scale. These can be exploited in biomedicine for applications such as imaging, cell sorting, drug delivery and targeting. Cancer nanomedicine is rapidly becoming one of the leading areas of promise for cancer therapy, with first-generation treatments already available to patients.

The exciting advances within this field have lead to cancer nanomedicines already been used clinically today. Sceptics would argue that the translation of nanotechnologies into the clinic have not matched the initial hype, however, I believe moving forward more and more commercial success will be achieved. It is estimated that the global nanomedicine market will be worth US$334 billion by 2025, with cancer nanomedicine dominating in this field. As the science develops and leads us down new avenues, the findings and their meaning are closely scrutinised and debated within the community. This all leads to a thriving and exciting field in which to work.

I hope you enjoy reading the manuscripts within this special edition, since it has been such a great success with 46 papers being accepted for publication. In order to continue to showcase work in our strong field, a Topical Collection has been permanently opened within Cancers, and I invite you all to consider submitting your next manuscripts into this.

Clare Hoskins
Editor

cancers

MDPI

Article

Hyaluronidase-Responsive Mesoporous Silica Nanoparticles with Dual-Imaging and Dual-Target Function

Zhi-Yuan Wu [1], Cheng-Chang Lee [1] and Hsiu-Mei Lin [1,2,3,*]

[1] Department of Bioscience and Biotechnology, National Taiwan Ocean University, Keelung City 20224, Taiwan; j18185202000@yahoo.com.tw (Z.-Y.W.); d91051238@gmail.com (C.-C.L.)
[2] Center of Excellence for the Oceans, National Taiwan Ocean University, Keelung City 20224, Taiwan
[3] Center of Excellence for Ocean Engineering, National Taiwan Ocean University, Keelung City 20224, Taiwan
* Correspondence: hmlin@mail.ntou.edu.tw; Tel./Fax: +886-2-2462-2192

Received: 24 April 2019; Accepted: 15 May 2019; Published: 20 May 2019

Abstract: Nanoparticle-based drug delivery systems are among the most popular research topics in recent years. Compared with traditional drug carriers, mesoporous silica nanoparticles (MSN) offer modifiable surfaces, adjustable pore sizes and good biocompatibility. Nanoparticle-based drug delivery systems have become a research direction for many scientists. With the active target factionalized, scientists could deliver drug carriers into cancer cells successfully. However, drugs in cancer cells could elicit drug resistance and induce cell exocytosis. Thus, the drug cannot be delivered to its pharmacological location, such as the nucleus. Therefore, binding the cell membrane and the nuclear target on the nanomaterial so that the anticancer drug can be delivered to its pharmacological action site is our goal. In this study, MSN-EuGd was synthesized by doping Eu^{3+} and Gd^{3+} during the synthesis of MSN. The surface of the material was then connected to the TAT peptide as the nucleus target for targeting the cancer nucleus and then loaded with the anticancer drug camptothecin (CPT). Then, the surface of MSN-EuGd was bonded to the hyaluronic acid as an active target and gatekeeper. With this system, it is possible and desirable to achieve dual imaging and dual targeting, as well as to deliver drugs to the cell nucleus under a hyaluronidase-controlled release. The experimental approach is divided into three parts. First, we conferred the material with fluorescent and magnetic dual-imaging property by doping Eu^{3+} and Gd^{3+} into the MSN. Second, modification of the cell membrane target molecule and the nucleus target molecule occurred on the surface of the nanoparticle, making the nanoparticle a target drug carrier. Third, the loading of drug molecules into the carrier gave the entire carrier a specific target profile and enabled the ability to treat cancer. In this study, we investigated the basic properties of the drug carrier, including physical properties, chemical properties, and in vitro tests. The result showed that we have successfully designed a drug delivery system that recognizes normal cells and cancer cells and has good anticancer effects.

Keywords: Mesoporous silica nanoparticle; drug delivery system; target treatment; lanthanide metal; TAT peptide; hyaluronic acid; hyaluronidase

1. Introduction

Drug release systems based on nanoparticles have been widely used for cancer treatment. An effective drug release system needs to have sufficient drug loading capability and the ability to target to bring nanoparticles into the cancer cells preferentially [1]. However, drugs in cancer cells could elicit drug resistance and induce cell exocytosis. Thus, the drug cannot be delivered to its pharmacological location [2], such as the nucleus. Therefore, we will bind the cell membrane

target and the nuclear target on the nanomaterial so that the anticancer drug can be delivered to its pharmacological action site and increase therapeutic efficiency.

A good drug carrier for a drug release system must have large drug loading efficiency, good biocompatibility, uniform size, and high stability. In recent years, many drug carriers have been developed [3]. Examples include liposomes [4], polymers [5], micelle [6], magnetic nanoparticles [7] and quantum dots [8]. Almost all nanoparticles are limited by instability and insufficient drug loading or toxicity and cannot be widely used. Mesoporous silica nanoparticles (MSN) as the carrier of the drug delivery system could overcome the previous disadvantage because: their high specific surface area allows MSN to modify more molecules on the surface [9]. Large and tunable pore volume can load more drug molecules [10], it has good biocompatibility, can be biodegraded and does not easily accumulate in the body [11]. The overall structure is composed of silica and Si-OH groups, which can provide a good environment to load and protect drugs and create many chemical surface modifications.

Most of the nanoparticle-based drug delivery systems enter the tumor tissue via the enhanced permeability and retention effect (EPR effect) [12], a postulate that nanoparticles, as well as molecules of certain size, are prone to accumulate in tumor tissue more than in normal tissue. To further enable nanoparticles to be effectively endocytosed by tumor cells, scientists will modify the active target on the surface of the nanoparticle [13,14]. Active targets are usually molecules that bind to receptors that are overexpressed on the surface of tumor cells compared to normal cells so that the nanoparticles can recognize the difference between normal cells and tumor cells.

However, successful entry of the nanoparticles through the cell membrane does not guarantee that the drug can be smoothly delivered to the desired pharmacological site. The drug carriers may be re-extracted out of a cancer cell via exocytosis, resulting in the insufficient concentration of the drug in the cell and reducing the cytotoxic effect. To solve this problem, scientists have simultaneously modified the cell membrane target and its drug-acting organelle target on the surface of the drug carrier. After the drug carrier enters the cell by endocytosis, the organelle target can lead the drug carrier to its targeting organelle [15].

Hyaluronic acid (HA) is the target selected for this experiment, and it is one of the main components of the extracellular matrix, which plays an important role in cell proliferation and migration [16]. Because cancer need to perform a large amount of proliferation and migration, hyaluronic acid receptors (CD44 receptor) are expressed to an excessive degree on the cancer cell surface [17], and the drug carrier can enter the cell by endocytosis through the binding of HA and CD44 receptor.

The nucleus is an important storage space for genetic material and plays an important role in the processes of cell metabolism, growth, and differentiation. Some anticancer drugs such as doxorubicin (DOX) or camptothecin (CPT) [18] induce cell apoptosis through drug entry into the nucleus, so it is very important to ensure that the drugs can enter the nucleus. For the drug carrier to pass through the nuclear membrane, it is necessary to interact with the nuclear pore complexes (NPC) on the nuclear membrane through a protein target which contains a nuclear localization signal (NLS) to allow the carrier to enter the nucleus [19]. TAT peptides [20], like other nuclear targets, such as dexamethasone (DEX) [21], are common nuclear targets. In this study, besides modifying HA, we will further modify the NLS contained TAT peptide, which can transport the drug carrier to the nucleus for drug release.

In addition to carrying the drug to the pharmacological site through the target on the surface of the drug carrier, we must have a gatekeeper to keep the drug in the drug carrier pore so that the drug does not release prematurely. Controlled release systems are mainly divided into external stimuli response and intrinsic stimuli response. External stimuli response is to make the gatekeeper decompose or structurally change by light or magnetic stimulation and then release the drug [22]. The intrinsic response is to use the difference between the internal and external environment of the cell, such as the change in pH or the difference in enzyme concentration, the gatekeeper can break down and release the drug after entering the cell due to environmental changes [23–25]. In this study, HA is not only used as an active target but also as a gatekeeper because of its polymer properties. Hyaluronidase (HAase) is an enzyme that catalyzes the hydrolysis of HA. There are six types of HAase

in the human body [26], of which type I and type II are the primary enzymes that hydrolyze HA in the majority of tissues. Type II is mainly linked to the CD44 receptor and is responsible for cleaving the HA of the polymer, then further hydrolyzing the HA into the cell via endocytosis by type II [27]. Studies have shown that cancer cells use hyaluronidase to hydrolysis hyaluronic acid into smaller molecular fragments and elicit significant angiogenic effect [28]. When the drug carrier enters the cancer tissue and penetrates into the cell through endocytosis, the gatekeeper collapses due to the action of HAase, thereby achieving the purpose of releasing the drug into the cell [18].

According to previous laboratory research [29], two kinds of lanthanide metals with fluorescence [30] and magnetic imaging [31] functions, Eu^{3+} and Gd^{3+}, are added to the synthetic process of MSN. The nuclear penetrating peptide (TAT peptide (sequence: YGRKKRRQRRR)) as a nuclear target was attached to the surface of MSN, then the anti-cancer drug (CPT) was loaded into the pore. Finally, the hyaluronic acid (HA) is used to attach to the surface of MSN as cell membrane target and gatekeeper. When the nanoparticles enter the cancer cells, the HA is decomposed by the HAase in the lysosome, and the nuclear target TAT is exposed, introduced nanoparticle into the nucleus for drug release. The study combines three functions of dual imaging with a controlled release switch and dual targeted treatment so that the material can simultaneously manifest the controlled release effect and increase the accumulation of drugs within cancer tissues. Finally, the imaging function is used to track the lesion location in clinical application (Scheme 1).

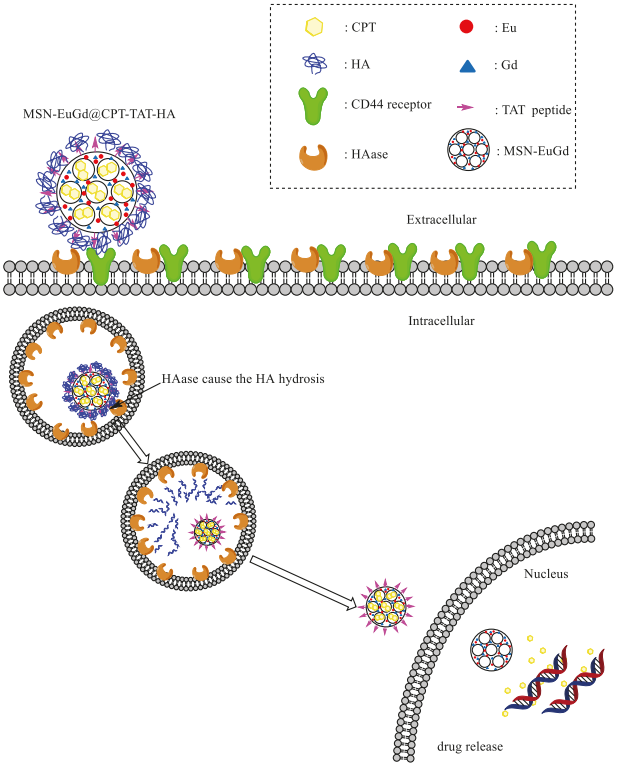

Scheme 1. MSN-EuGd@CPT-TAT-HA enters the cell membrane by binding to CD44 receptor on tumor cells. Then, after the HA (Hyaluronic acid) is hydrolyzed by the HAase (Hyaluronidase) between the cell membrane and the endosome and caused the proton sponge effect [32] to escape endosome, the exposed TAT peptide on MSN (mesoporous silica nanoparticles) is used to deliver the MSN to the nucleus for drug release.

2. Materials and Methods

2.1. Materials

Tetraethyl orthosilicate (TEOS), hexadecyltrimethylammonium bromide (CTAB), 1-ethyl-3-(3-dimethylaminopropyl) carbodiimide (EDC), N-hydroxysuccinimide (NHS), hyaluronic acid sodium salt from *Streptococcus equi* (HA, mol wt: ~1.5–1.8 × 10^6 Da), (3-aminopropyl) triethoxysilane (APTES), hyaluronidase from bovine test: Type I-S (HAase), camptothecin (CPT), and thiazolyl blue tetrazolium bromide (MTT) were purchased from Sigma-Aldrich (St. Louis, MI, USA). Sodium hydroxide (NaOH), toluene, and dimethyl sulfoxide (DMSO) were purchased from J.T.Baker and the N-acetyl TAT peptide (YGRKKRRQRRR) was synthesized by @GenMark company (Carlsbad, CA, USA). Minimum essential media (MEM), F-12K (Kaighn's) medium, fetal bovine serum (FBS), and antibiotic-antimycotic (AA) were purchased from Gibco (Waltham, MA, USA).

2.2. Synthesis of $Eu(NO_3)_3$ and $Gd(NO_3)_3$

Here, 4.40 g and 4.53 g of Eu_2O_3 and Gd_2O_3 were mixed with 4.89 mL and 5.03 mL of 16 M HNO_3, respectively, and then hydrothermally heated at 180 °C for 24 h, after which the mixed mixture was added to the D.I. water to obtain 50 mL of 0.5 M $Eu(NO_3)_3$ and $Gd(NO_3)_3$.

2.3. Synthesis of MSN-EuGd-NH_2

Ninety-seven milliliters of deionized water was added into 1.4 mL of 1 M NaOH and 0.2 g of surfactant CTAB. After stirring at 80 °C for one hour, 1 mL of TEOS and 3 mL of 0.5 M $Eu(NO_3)_3$, $Gd(NO_3)_3$ were added dropwise and stirred for two hours. The substances were washed with water, ethanol, and methanol and then calcinated at 650 °C for six hours to generate MSN-EuGd. Next, 0.1 g of MSN-EuGd was added to 15 mL of toluene and 0.2 mL of APTES, and it was stirred at 120 °C for four hours, centrifuged, and washed twice with alcohol to obtain MSN-EuGd-NH_2.

2.4. MSN-EuGd-NH_2 loaded into CPT (MSN-EGd-NH_2@CPT)

10 mg of CPT was dissolved in 5 mL of dimethyl sulfoxide (DMSO), and 50 mg of MSN-EuGd-NH_2 was added and mixed with ultrasonic waves for one hour. It was then stirred for 24 h, centrifuged three times and wash with deionized water to remove the most of solvent, then dried under vacuum for 48 h.

2.5. Synthesis of MSN-EuGd-TAT (or MSN-EuGd@CPT-TAT)

10 mg of N-acetylated TAT peptide was dissolved in 10 mL phosphate-buffered saline (PBS) (0.2 M, pH 7.4), and then, 9.6 mg EDC and 5.8 mg NHS were added at room temperature for half an hour. Next, 40 mL PBS (0.2 M, 80 mg of MSN-EuGd-NH_2 (or MSN-EuGd-NH_2@CPT) at pH 7.4) was dissolved, stirred for 12 h, centrifuged to remove the supernatant and lyophilized.

2.6. Synthesis of MSN-EuGd-TAT-HA (or MSN-EuGd@CPT-TAT-HA)

10 mg of MSN-EuGd-TAT (or MSN-EuGd@CPT-TAT) were dissolved in 4 mL MES solution (0.01 M, pH 5.5), 10 mg HA, 10 mg EDC and 10 mg NHS were added. After stirring at room temperature for 12 h, the supernatant liquid was removed by centrifugation and lyophilized.

2.7. Characterization

X-ray powder diffraction (XRD) was performed using a Bruker D2 Phase instrument. Particle size and zeta potential analyses were performed using dynamic light scattering (Malvern Zetasizer Nano ZS system, Malvern, Worcestershire, UK). Transmission electron microscopy images and energy dispersive X-ray (EDX) spectra were taken using a Tecnai F30 instrument. The analysis of nitrogen adsorption isotherms was performed using a Barrett–Joyner–Halenda (BJH) analysis (ASAP 2020,

Micromeritics, Norcross, GA, USA). The surface area and pore size distribution curves of the undoped or various-doped mesoporous silica nanoparticles were determined by the Brunauer–Emmett–Teller (BET) method. The Fourier transform infrared (FTIR) spectra of the functionalized MSNs were recorded by using a BRUKER TENSOR Series II Spectrometer (Billerica, MA, USA). The luminescence excitation spectra were recorded using a Jasco FP-6300 photoluminescence spectrophotometer (Easton, MD, USA) with an excitation wavelength of 394 nm. The thermal gravimetric analysis (TGA) curves were obtained using a Netzsch TG 209 F3 apparatus to determine the conjugation efficiency of the TAT and HA when the temperature was increased to 800 °C. The drug release curve of the camptothecin was analyzed using an Enzyme-Linked Immunosorbent Assay (ELISA) reader (BioTek Synergy Mx, Winooski, VT, USA) at 430 nm. The T1-weighted magnetic resonance (MR) imaging was performed using conventional spin-echo acquisition (TR/TE = 300 ms/10.6 ms, slice thickness = 2.00 mm) using a 7 T scanner (BRUKER S300 BIOSPEC/MEDSPEC MRI, Karlsruhe, Germany). The concentrations of Eu^{3+} and Gd^{3+} ions that were doped into the MSNs were measured by inductively coupled plasma AES spectrometry (ICP-MS, Santa Clara, CA, USA) and reported as mass percentages.

2.8. Drug Release

10 mg of MSN-EuGd@CPT-HA was first stirred with 150 U/mL of 3 mL of HAase/PBS aqueous solution for 12 h, then the supernatant was removed by centrifugation and dried under vacuum. Next, the HAase-treated MSN-EuGd@CPT-HA and the HAase-untreated MSN@CPT-HA were compressed into bracts, placed in 3 mL of DMSO and shaken evenly, and 100 μL of the supernatant was aspirated into the 96-well disk at 10, 20, 30, 40, 50, 60, 80, 100, 120, 150, 180, 210, 240, 270, 300, 360, 420, and 480 min. The ELISA reader then measured the optical density (OD) value at 430 nm, and the total drug release amount was calculated according to the concentration calibration curve of the OD value of 430 nm previously read by ELISA.

2.9. In Vitro Experiments

2.9.1. Cell Culture

L929 (Mus musculus fibroblast cell line) was cultured in minimum essential medium (MEM) supplemented with 10% fetal bovine serum (FBS) and 1% antibiotics (AA) at 37 °C in an environment containing 5% CO_2, A549 (adenocarcinomic human alveolar basal epithelial cells) was cultured in F-12K supplemented with 10% FBS and 1% antibiotics (AA) at 37 °C in an environment containing 5% CO_2.

2.9.2. Cell Viability Assay

Normal cell model L929 and cancer cell model A549 were selected as test cells in this experiment. The procedures were as follows:

First, we seed 10,000 cells/well of cells in a 96-well culture dish and incubate the cell for 24 h in a 37 °C cell culture incubator. Then we add 25/50/100/200 μg/mL of drug carrier/culture solution in each well respectively. Next, after co-culture with the drug carrier for 24 h, 20 μL of MTT was added into the wells for four hours' reaction. Finally, after the reaction, we add 100 μL of DMSO into each well and shake the dish for 15 min to induce its color. By reading the OD value at 540 nm with an enzyme immunoassay analyzer (ELISA reader, Winooski, VT, USA), the ability of cells reducing MTT can be known and can be used as an indicator of cell viability. The cell viability is calculated by the following formula:

$$\text{Cell viability} = \text{OD540 (test group)}/\text{OD540 (control group)} \times 100\%$$

2.9.3. Confocal Image Analysis

The sterilized 13 mm glass coverslip was placed in a 24-well plate. Then, 2×10^4 cells were seeded in each well, cultured for 24 h (5% CO_2, 37 °C), and then cultured with a 500 μL (100 μg/mL) mixture of

the drug carrier and the culture solution for six hours. After the completion of the culture, the culture medium was washed with PBS, and then 300 µL of a 3.7% formaldehyde/PBS solution was added for 10 min to fix the current state of the cells. After the end of the reaction time, the cells were washed with PBS, and then 4',6-diamidino-2-phenylindole (DAPI) was used to stain the nuclei for five minutes. After washing with PBS, the coverslips were mounted onto a glass slide, and the cells were visualized and observed under a confocal laser-scanning microscope (CLSM, SP5, Leica, Wetzlar, Germany).

3. Results and Discussion

3.1. Structure, Formation, Morphology, and Properties of MSNs and EuGd-MSNs

Figure 1a shows the results of the low-angle XRD pattern. Both MSN and MSN-EuGd have characteristic peaks at (100) (110) (200), indicating that they are in the form of MCM-41 with regular hexagonal pore structure [33]. It can be seen that the structure of MSN-EuGd is similar to that of MSN, and MSN-EuGd does not cause a large change in structure due to the doping of Eu and Gd, its structural arrangement is similar to MSN. The MSN d-spacing was calculated by XRD pattern to be 3.68 nm, and the MSN-EuGd d_{100}-spacing was 3.99 nm (Table 1). These results indicate that the MSN pore structure will change through the doping of metal ions, but this does not affect the main structure of MSN. The experiment uses BET analysis of MSN and MSN-EuGd. From Figure 1b nitrogen constant temperature adsorption and the pore size distribution pattern, it can be seen that the curve is of type IV and that all structures have a mesoporous structure as determined by hysteresis loop. MSN properties can be known by BET model calculation. The pore diameter of MSN-EuGd is 2.75 nm (Figure S1). After analysis, the specific surface area of MSN-EuGd is 608.19 m^2/g, it is much larger than non-porous silica nanoparticle compared with the previous research [34], and the pore volume is 0.93 cm^3/g (Table 1). The structure and size can be observed by TEM analysis. MSN has a regular hexagonal hole structure, and each particle has a uniform size. From Figure 1c–d, the hole size is approximately 2~3 nm as determined by XRD and BET. The measured data is consistent, and the particle size is approximately 120 nm. All of these geometric parameters are summarized in Table S1. The DLS can transmit the laser light through the solution containing the nanoparticles, and the receiver receives the light and is affected by the particles to generate a scattering signal to calculate the hydration radius of the particles. It can be seen from Table 1 that the size of MSN-EuGd is 271 nm, and the size of the organic molecule can be changed as it is grafted onto the material. The surface charge of the nanoparticles is also measured. Confirming that each molecule connected to MSN-EuGd: The surface charge of MSN-EuGd is −14.5 mV, and the potential rises to −10 mV due to its positive charge when connected to -NH_2 [35]. After the TAT peptide was attached, the potential was raised to 4.08 because the TAT peptide itself was positively charged [36]. Regarding HA attachment, the potential reached −17.3 because the HA itself was rich in negatively charged -COOH [37].

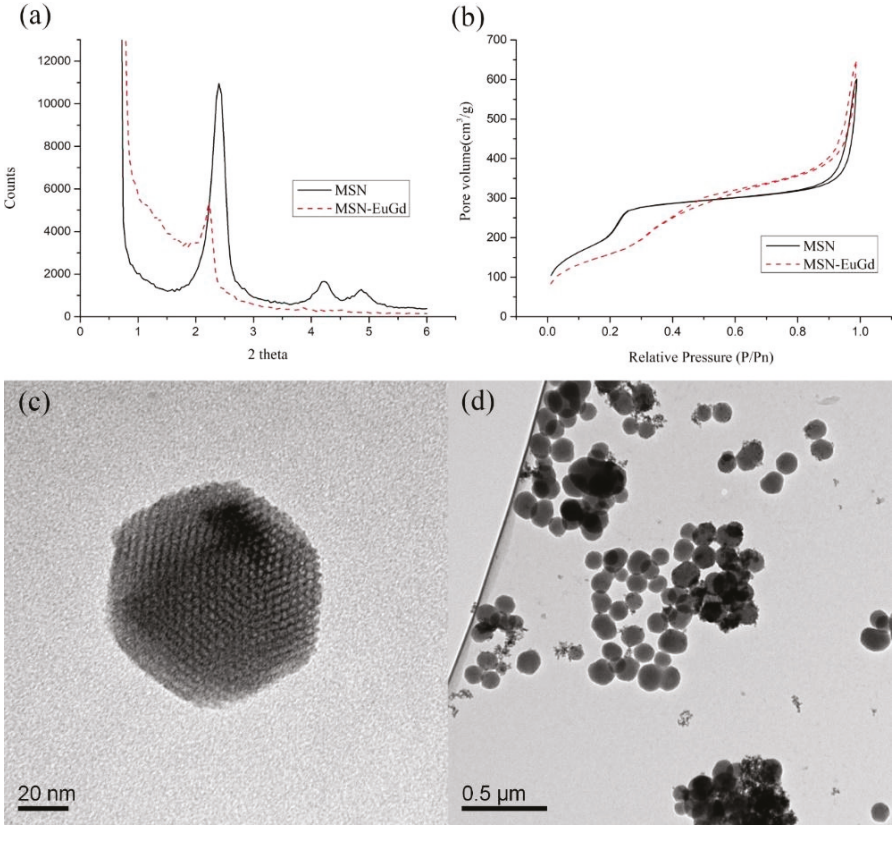

Figure 1. (**a**) Small-angle X-ray powder diffraction (XRD) analysis of mesoporous silica nanoparticles (MSN) and MSN-EuGd, (**b**) isothermal nitrogen adsorption of MSN and MSN-EuGd, (**c**,**d**) analysis of MSN structure and size using transmission electron microscopy (TEM). Scale bar: (**c**) 20 nm, (**d**) 0.5 μm.

Table 1. Properties analysis of mesoporous silica nanoparticles (MSNs) and MSN-EuGd.

Physical Data	**MSN**	**MSN-EuGd**
Brunauer–Emmett–Teller (BET) Surface Area (m^2/g)	947.57	608.19
Pore Volume (cm^3/g)	0.77	0.93
Barrett–Joyner–Halenda (BJH) Desorption Diameter (nm)	2.29	2.75
X-ray diffraction (XRD) 2θ (°)	2.40	2.21
d_{100}-spacing (nm)	3.68	3.99
Wall thickness (nm)	1.95	1.86
Mean particle diameters (nm)	197	271

The EDX can be used to determine the elements contained in the material. From Figure S2, it can be found that elements such as silicon, oxygen, europium, and gadolinium are detected in MSN-EuGd, while MSN is only silicon (Si), oxygen (O), and then further quantified by inductively coupled plasma mass spectrometry (ICP-MS) to obtain Eu and Gd contents of 4.91% and 4.82%, respectively, as shown in Table S2.

The MSN-EuGd measurement by PL found that: if 394 nm is used as the excitation wavelength, it will produce radiation absorption peaks at 590 nm and 615 nm, primarily from the red light emission peak of Eu^{3+} from $5D_0 \rightarrow 7F_1$ (590 nm) and $5D_0 \rightarrow 7F_2$ (614 nm) after receiving excitation light [38]. If a radiation wavelength of 615 nm is used, an absorption peak is observed at 394 nm as shown in Figure 2a, and Eu^{3+} is indeed dopeddop into MSN. In addition, if the material is irradiated with 254 nm UV light, MSN-EuGd will emit red excitation light, as shown in Figure S3. We used IVIS to illuminate MSN-EuGd at 430 nm excitation wavelength. From Figure 2b, MSN and blank were observed to have no obvious fluorescence characteristics, while MSN-EuGd showed very obvious fluorescence excitation, confirming that IVIS can effectively detect materials. The nature of the fluorescent light also confirms that the MSN-EuGd can use the IVIS system as an imaging tracking function.

For the magnetic properties of the material, we synthesized MSN-EuGd with different ratios of lanthanides and measured the results with a superconducting quantum interference device. It was found that the undoped Gd^{3+} material showed no magnetic properties, but MSN-EuGd doped with Gd^{3+} exhibits a paramagnetic phenomenon. As the concentration of Gd^{3+} escalates, the paramagnetic property is more pronounced, confirming that the material is paramagnetic (Figure 2c) [39]. MSN-EuGd can also be applied to MR imaging to perform in vitro MRI testing. The parameters are set in a magnetic field of 7 T, setting the parameter value TR/TE = 300 ms, FOV = 7 cm, NEX = 1, slice thickness = 2.00, matrix = 256 × 256, and material concentration from 4 to 0.25 mg/mL[3]. From Figure 2d, it can be seen that the T1-weighted image appears increasingly bright as the material concentration increases, confirming that MSN-EuGd can be used as the T1 positive development image [40].

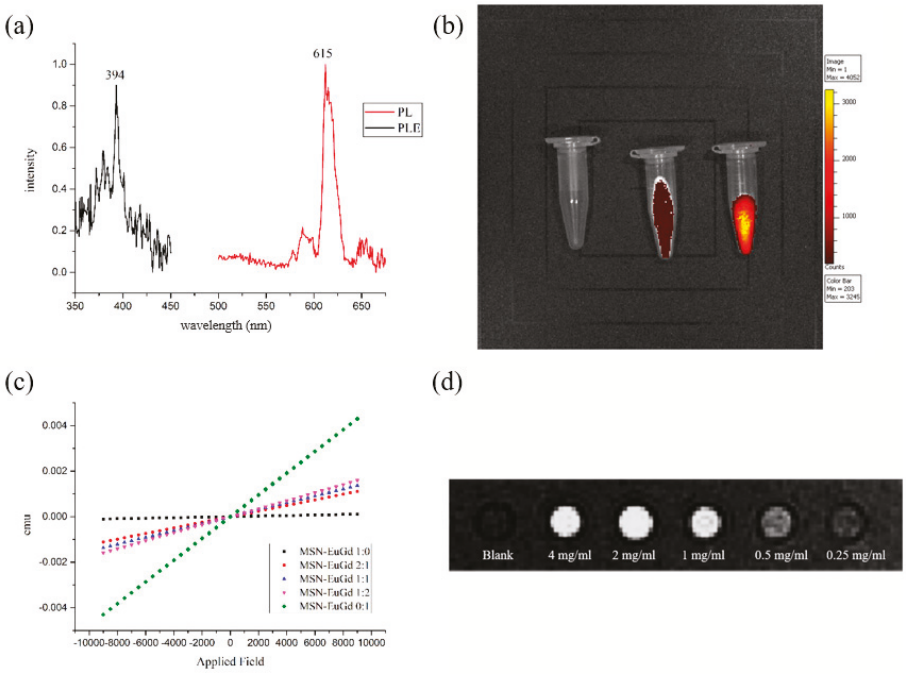

Figure 2. (**a**) PLE and PL results showing emission spectra of the MSN-EuGd. (**b**) IVIS optical imaging of Blank, MSN, and MSN-EuGd. (**c**) The magnetization curves of MSN-EuGd. (**d**) T_1-weighted MRI of MSN-EuGd.

To confirm whether the organic molecule was successfully attached to MSN-EuGd, we can use the FTIR to analyze the functional groups on the material (Figure S4). The -OH group was observed

at 3400 cm^{-1} and 2931 cm^{-1}, and the Si-O-Si signal [41] at 1068 cm^{-1} and 953 cm^{-1}. When the -NH_2 was modified, it was found that an additional N-H bond peak [42] on the amine group at 1552 cm^{-1} confirmed that the amino group was successfully attached to MSN-EuGd. Then, when TAT was modified, it was observed that 1415 cm^{-1} and 1715 cm^{-1}, respectively, represent the C-O-H stretching vibration of the amide bond and the stretching vibration of C = O, which proved that TAT was successfully connected to MSN-EuGd. MSN-EuGd-TAT-HA showed an additional peak at 1409 cm^{-1}, representing the asymmetric stretching vibration of the -COOH group of HA [43]. The amount of MSN-EuGd modified by organic molecules and its drug loading were determined by TGA analysis. In this experiment, the temperature of each material is increased to 800 degrees from 40 degrees Celsius in the environment of pure oxygen, and the mass loss percentage of each material is observed. Finally, the amount of each molecule connected to MSN-EuGd is converted into Table S3. The modification amount of -NH_2, -TAT and HA is approximately 129.17 mg/g, 26.27 mg/g, and 65.53 mg/g, respectively. The loading amount of CPT is 15.22 mg/g.

To confirm that MSN-EuGd@CPT-TAT-HA can be utilized for drug release, we first reacted MSN-EuGd@CPT-HA with 150 U/mL HAase for 12 h, then centrifuged to remove the supernatant liquid and added the residual material into DMSO for drug release test. As a result, it was found that the amount of MSN@CPT-HA that was not treated with HAase was approximately 44.86%, and the material treated with HAase was approximately 83.57% at eight hours. It can be seen that the design of this experiment can achieve the purpose of drug-controlled release, as shown in Figure 3.

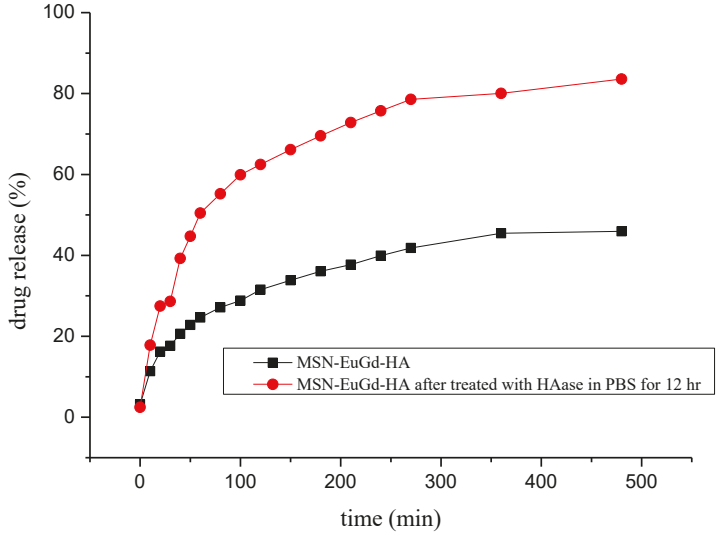

Figure 3. Drug release of MSN-EuGd@CPT-HA and HAase-treated MSN-EuGd@CPT-HA in Dimethyl sulfoxide (DMSO).

3.2. In Vitro Cytotoxicity and Cellular Uptake of Functionalized MSN-EuGd

To confirm the phagocytosis between cells for each material, mouse fibroblasts (L929) were compared with human lung adenocarcinoma cells (A549) as a CD44 receptor control group, and CLSM images were taken after six hours of coculture with each material. As shown in Figure 4, the bare MSN-EuGd is barely phagocytized by L929 cells and A549 cells, while the MSN-EuGd-TAT demonstrates a slight overlap of the material signal (red) and the nuclear signal (blue). It is speculated that MSN-EuGd-TAT can successfully enter the nucleus by TAT after being phagocytized. The MSN-EuGd-HA also exhibited that A549 cells contained more phagocytic material than did L929

cells. It is speculated that the overexpressed CD44 receptor on A549 cells enables MSN-EuGd-HA to be introduced into the cells by receptor-mediated endocytosis of A549 cells. The MSN-EuGd-TAT-HA can be found to be similar to MSN-EuGd-HA, but it can be observed that the signal of MSN-EuGd-TAT-HA overlaps with the nuclear signal of A549 cells. The material is successfully predicted by cell membrane target (HA), and nuclear target (TAT) enter the nucleus of cancer cells.

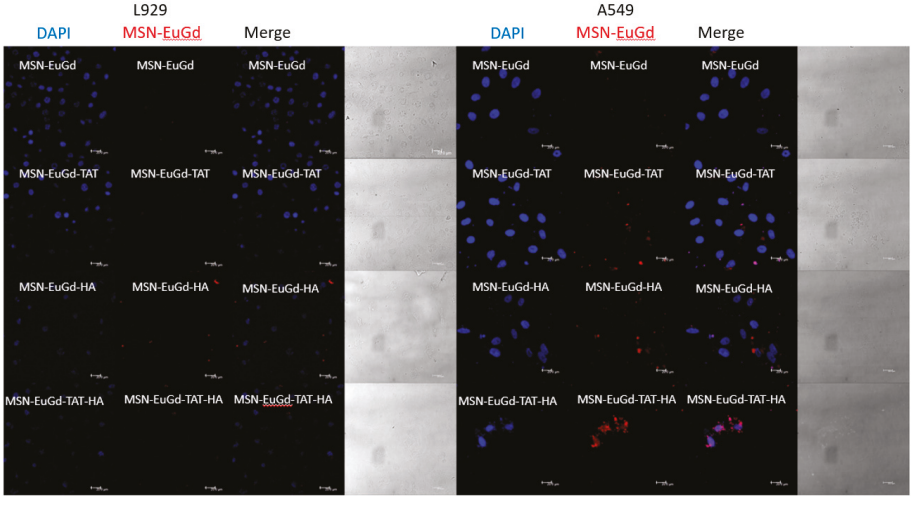

Figure 4. Confocal Laser Scanning Microscope (CLSM) image of MSN-EuGd, MSN-EuGd-TAT, MSN-EuGd-HA, and MSN-EuGd-TAT-HA incubated with L929 cell line and A549 cell line for six hours. Blue: 4′,6-diamidino-2-phenylindole (DAPI), red: MSN-EuGd, scale bar: 20 μm.

Cell viability tests confirm that the material is cytotoxic to cancer cells and less harmful to normal cells. As shown in Figures 5 and 6. In order to avoid possible cytotoxic interference caused by excessive uptake of MSNs by the cells, therefore, referred to the results of Chou et al. in 2017 and we choose the concentration of 200 μg/mL as the highest dose [44]. The results obtained were that L929 and A549 cells had a cell viability of more than 80% when using a drug carrier without a loading drug, indicating that the material itself is not cytotoxic to the cells. However, it was observed in the A549 group that MSN-EuGd@CPT-TAT was slightly more toxic to cells than MSN-EuGd, and the reason was that MSN-EuGd@CPT-TAT was introduced into the nucleus after entering the cells. Different concentrations of MSN-EuGd@CPT-HA showed that MSN-EuGd@CPT-HA had a better cytotoxic effect on A549 compared with A549 and L929. It is speculated that the binding of the CD44 receptor on the HA and A549 cells causes the cells to increase drug phagocytosis. Finally, MSN-EuGd@CPT-TAT-HA exhibits better cytotoxic effects against A549 than does MSN-EuGd@CPT-HA. This is primarily because MSN-EuGd@CPT-TAT-HA enters the cancer tissue and then carries the drug into the cell and onward to the nucleus via cell membrane and nucleus targeting, thus furthering cytotoxicity.

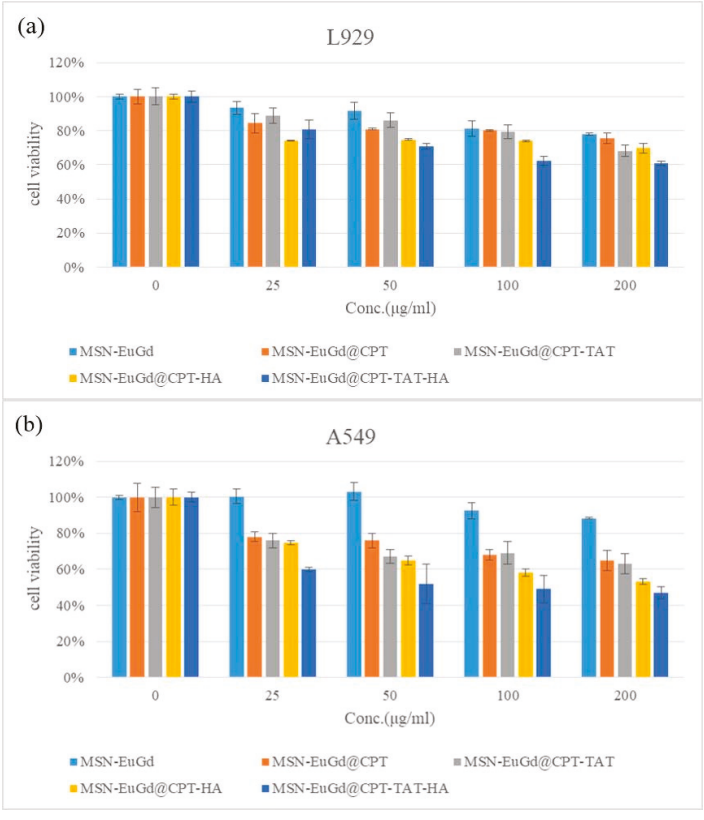

Figure 5. MTT assays for MSN-EuGd, MSN-EuGd@CPT, MSN-EuGd@CPT-TAT, MSN-EuGd@CPT-HA, and MSN-EuGd-TAT-HA using L929 and A549 cells.

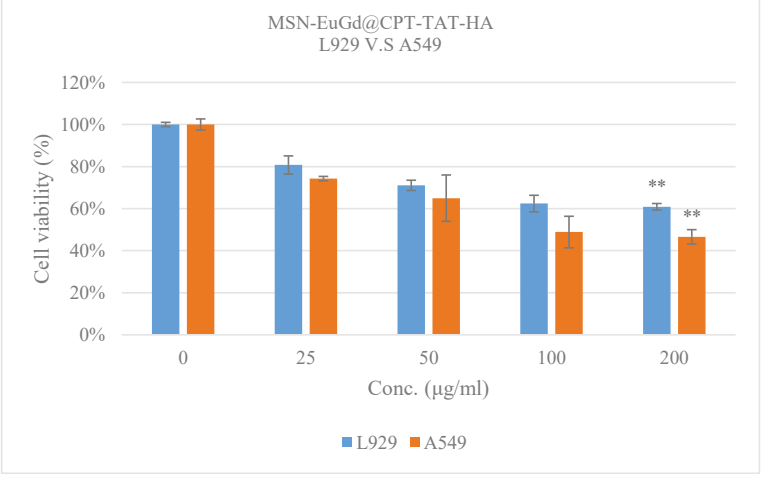

Figure 6. Comparison of cell viability between L929 cells and A549 cells at various concentrations of MSN-EuGd@CPT-TAT-HA, ** $p < 0.01$.

4. Conclusions

This study demonstrates the successful synthesis of a novel drug delivery system (MSN-EuGd@CPT-TAT-HA) that possesses dual development and dual targets and controls the release of drugs into the nucleus. The system is used to overcome the side effects of chemotherapy and multiple drug resistance problems.

The experiment used MSN with Eu and Gd as the carrier and loaded the anticancer drug CPT. After attaching the nuclear target TAT, it was connected with the HA which functions as both cell membrane target and gatekeeper. A nanoparticle, MSN-EuGd@CPT-TAT-HA, with dual target and dual development and HAase as a release switch was synthesized as a drug delivery system. After the material enters the tumor via the cell membrane target HA, HA is decomposed by HAase in the cytosol to expose the nuclear target TAT on the surface of MSN-EuGd, and the remaining particle enters the nucleus by TAT to release the drug.

The material confirms that doped lanthanides Eu and Gd through the PL and SQUID provided the material with a fluorescent imaging and magnetic imaging function. It is also confirmed from the IVIS and MRI images that the cancer tissue distribution can be tracked in vitro. The drug release test also confirmed the sealing ability of HA and the release of the drug by HAase decomposition of HA.

It was confirmed from the CLSM image that the MSN-EuGd was attached to the cell membrane target HA and the nuclear target TAT. The material can be introduced into the cell by endocytosis via the expression receptor and then onward into the nucleus. The cell viability test showed that MSN-EuGd alone demonstrated excellent cytocompatibility. When the material is loaded with the drug, it can also obtain better cancer cell cytotoxic effects with the cell membrane target HA and the nuclear target TAT attached to MSN-EuGd. Hopefully, this intelligent drug carrier can successfully become a potential therapeutic material for cancer.

Supplementary Materials: The following are available online at http://www.mdpi.com/2072-6694/11/5/697/s1, Table S1: Hydrodynamic size and zeta potential for MSN-EuGd and functionalized MSN-EuGd, Table S2: ICP-MS analyze of MSN and MSN-EuGd, Table S3: TGA for the MSN-EuGd@CPT-TAT-PEG-FA, Figure S1: BJH pore size distribution of MSN and MSN-EuGd, Figure S2: EDX spectral analyses of the (a) MSN and (b) MSN-EuGd, Figure S3: MSN and MSN-EuGd powder taken under illumination by a 254 nm UV lamp, Figure S4: FTIR spectrum of MSN-EuGd and functionized MSN-EuGd, Figure S5: TGA patterns for the MSN-EuGd and functionized MSN-EuGd.

Author Contributions: Data curation, Z.-Y.W.; formal analysis, Z.-Y.W.; methodology, Z.-Y.W.; supervision, H.-M.L.; writing—original draft, Z.-Y.W.; writing—review & editing, C.-C.L. and H.-M.L.

Funding: This research received no external funding.

Acknowledgments: We thank the National Science Council MOST 102-2113-M-019002; 103-2113-M-019-001-; 104-2113-M-019-002-; 105-2119-M-019-002-; 106-2113-M-019-003-; 107-2113-M-019-001-, National Taiwan Ocean University, the Center of Excellence for the Ocean and Center of Excellence for Ocean Engineering of National Taiwan Ocean University for financial support.

Conflicts of Interest: The authors declare no conflict of interest.

References

1. Robert, C.; Wilson, C.S.; Venuta, A.; Ferrari, M.; Arreto, C.D. Evolution of the scientific literature on drug delivery: A 1974-2015 bibliometric study. *J. Control. Release* **2017**, *260*, 226–233. [CrossRef]
2. Szakacs, G.; Paterson, J.K.; Ludwig, J.A.; Booth-Genthe, C.; Gottesman, M.M. Targeting multidrug resistance in cancer. *Nat. Rev. Drug Discov.* **2006**, *5*, 219–234. [CrossRef]
3. Florek, J.; Caillard, R.; Kleitz, F. Evaluation of mesoporous silica nanoparticles for oral drug delivery—Current status and perspective of MSNs drug carriers. *Nanoscale* **2017**, *9*, 15252–15277. [CrossRef]
4. Allen, T.M.; Cullis, P.R. Liposomal drug delivery systems: From concept to clinical applications. *Adv. Drug Deliv. Rev.* **2013**, *65*, 36–48. [CrossRef]
5. Soppimath, K.S.; Aminabhavi, T.M.; Kulkarni, A.R.; Rudzinski, W.E. Biodegradable polymeric nanoparticles as drug delivery devices. *J. Control. Release* **2001**, *70*, 1–20. [CrossRef]

6. Jiang, S.L.; Li, M.Y.; Hu, Y.; Zhang, Z.H.; Lv, H.X. Multifunctional self-assembled micelles of galactosamine-hyaluronic acid-vitamin E succinate for targeting delivery of norcantharidin to hepatic carcinoma. *Carbohydr. Polym.* **2018**, *197*, 194–203. [CrossRef] [PubMed]
7. Hegazy, M.; Zhou, P.; Wu, G.Y.; Wang, L.; Rahoui, N.; Taloub, N.; Huang, X.; Huang, Y.D. Construction of polymer coated core-shell magnetic mesoporous silica nanoparticles with triple responsive drug delivery. *Polym. Chem.* **2017**, *8*, 5852–5864. [CrossRef]
8. Zhao, M.X.; Zhu, B.J. The Research and Applications of Quantum Dots as Nano-Carriers for Targeted Drug Delivery and Cancer Therapy. *Nanoscale Res. Lett.* **2016**, *11*, 1–9. [CrossRef]
9. He, Y.J.; Liang, S.Q.; Long, M.Q.; Xu, H. Mesoporous silica nanoparticles as potential carriers for enhanced drug solubility of paclitaxel. *Mater. Sci. Eng. C Mater. Biol. Appl.* **2017**, *78*, 12–17. [CrossRef]
10. Rashidi, L.; Vasheghani-Farahani, E.; Rostami, K.; Ganji, F.; Fallahpour, M. Mesoporous silica nanoparticles with different pore sizes for delivery of pH-sensitive gallic acid. *Asia Pac. J. Chem. Eng.* **2014**, *9*, 845–853. [CrossRef]
11. He, Q.J.; Shi, J.L. Mesoporous silica nanoparticle based nano drug delivery systems: Synthesis, controlled drug release and delivery, pharmacokinetics and biocompatibility. *J. Mater. Chem.* **2011**, *21*, 5845–5855. [CrossRef]
12. Mikada, M.; Sukhbaatar, A.; Miura, Y.; Horie, S.; Sakamoto, M.; Mori, S.; Kodama, T. Evaluation of the enhanced permeability and retention effect in the early stages of lymph node metastasis. *Cancer Sci.* **2017**, *108*, 846–852. [CrossRef]
13. Cui, X.J.; Dong, L.L.; Zhong, S.L.; Shi, C.; Sun, Y.X.; Chen, P. Sonochemical fabrication of folic acid functionalized multistimuli-responsive magnetic graphene oxide-based nanocapsules for targeted drug delivery. *Chem. Eng. J.* **2017**, *326*, 839–848. [CrossRef]
14. Zhang, Q.; Colazo, J.; Berg, D.; Mugo, S.M.; Serpe, M.J. Multiresponsive Nanogels for Targeted Anticancer Drug Delivery. *Mol. Pharm.* **2017**, *14*, 2624–2628. [CrossRef]
15. Li, L.J.; Sun, W.; Li, L.; Liu, Y.Y.; Wu, L.; Wang, F.L.; Zhou, Z.; Zhang, Z.R.; Huang, Y. A pH-responsive sequential-disassembly nanohybrid for mitochondrial targeting. *Nanoscale* **2017**, *9*, 314–325. [CrossRef]
16. Gomes, J.A.P.; Amankwah, R.; Powell-Richards, A.; Dua, H.S. Sodium hyaluronate (hyaluronic acid) promotes migration of human corneal epithelial cells in vitro. *Br. J. Ophthalmol.* **2004**, *88*, 821–825. [CrossRef]
17. Yu, M.H.; Jambhrunkar, S.; Thorn, P.; Chen, J.Z.; Gu, W.Y.; Yu, C.Z. Hyaluronic acid modified mesoporous silica nanoparticles for targeted drug delivery to CD44-overexpressing cancer cells. *Nanoscale* **2013**, *5*, 178–183. [CrossRef]
18. Zhang, M.Z.; Xu, C.L.; Wen, L.Q.; Han, M.K.; Xiao, B.; Zhou, J.; Zhang, Y.C.; Zhang, Z.; Viennois, E.; Merlin, D. A Hyaluronidase-Responsive Nanoparticle-Based Drug Delivery System for Targeting Colon Cancer Cells. *Cancer Res.* **2016**, *76*, 7208–7218. [CrossRef]
19. Pan, L.M.; He, Q.J.; Liu, J.N.; Chen, Y.; Ma, M.; Zhang, L.L.; Shi, J.L. Nuclear-Targeted Drug Delivery of TAT Peptide-Conjugated Monodisperse Mesoporous Silica Nanoparticles. *J. Am. Chem. Soc.* **2012**, *134*, 5722–5725. [CrossRef]
20. Li, Z.H.; Dong, K.; Huang, S.; Ju, E.G.; Liu, Z.; Yin, M.L.; Ren, J.S.; Qu, X.G. A Smart Nanoassembly for Multistage Targeted Drug Delivery and Magnetic Resonance Imaging. *Adv. Funct. Mater.* **2014**, *24*, 3612–3620. [CrossRef]
21. Xiong, L.; Du, X.; Kleitz, F.; Qiao, S.Z. Cancer-Cell-Specific Nuclear-Targeted Drug Delivery by Dual-Ligand-Modified Mesoporous Silica Nanoparticles. *Small* **2015**, *11*, 5919–5926. [CrossRef]
22. Watermann, A.; Brieger, J. Mesoporous Silica Nanoparticles as Drug Delivery Vehicles in Cancer. *Nanomaterials* **2017**, *7*, 189. [CrossRef]
23. Webb, B.A.; Chimenti, M.; Jacobson, M.P.; Barber, D.L. Dysregulated pH: A perfect storm for cancer progression. *Nat. Rev. Cancer* **2011**, *11*, 671–677. [CrossRef]
24. Schafer, F.Q.; Buettner, G.R. Redox environment of the cell as viewed through the redox state of the glutathione disulfide/glutathione couple. *Free Radic. Biol. Med.* **2001**, *30*, 1191–1212. [CrossRef]
25. Liu, X.; Shao, W.; Zheng, Y.J.; Yao, C.H.; Peng, L.M.; Zhang, D.M.; Hu, X.Y.; Wang, L.Y. GSH-Responsive supramolecular nanoparticles constructed by beta-D-galactose-modified pillar 5 arene and camptothecin prodrug for targeted anticancer drug delivery. *Chem. Commun.* **2017**, *53*, 8596–8599. [CrossRef] [PubMed]
26. Csoka, A.B.; Scherer, S.W.; Stern, R. Expression analysis of six paralogous human hyaluronidase genes clustered on chromosomes 3p21 and 7q31. *Genomics* **1999**, *60*, 356–361. [CrossRef]

27. Chanmee, T.; Ontong, P.; Itano, N. Hyaluronan: A modulator of the tumor microenvironment. *Cancer Lett.* **2016**, *375*, 20–30. [CrossRef]
28. Khegai, I.I. Neurohormonal Regulation of Tumor Growth. *Russ. J. Genet.* **2018**, *54*, 36–44. [CrossRef]
29. Chan, M.H.; Lin, H.M. Preparation and identification of multifunctional mesoporous silica nanoparticles for in vitro and in vivo dual-mode imaging, theranostics, and targeted tracking. *Biomaterials* **2015**, *46*, 149–158. [CrossRef]
30. Yang, P.P.; Huang, S.S.; Kong, D.Y.; Lin, J.; Fu, H.G. Luminescence functionalization of SBA-15 by YVO4: Eu3+ as a novel drug delivery system. *Inorg. Chem.* **2007**, *46*, 3203–3211. [CrossRef] [PubMed]
31. Damasco, J.A.; Chen, G.Y.; Shao, W.; Agren, H.; Huang, H.Y.; Song, W.T.; Lovell, J.F.; Prasad, P.N. Size-Tunable and Monodisperse Tm3+/Gd3+-Doped Hexagonal NaYbF4 Nanoparticles with Engineered Efficient Near Infrared-to-Near Infrared Upconversion for In Vivo Imaging. *ACS Appl. Mater. Interfaces* **2014**, *6*, 13884–13893. [CrossRef] [PubMed]
32. Smith, S.A.; Selby, L.I.; Johnston, A.P.R.; Such, G.K. The Endosomal Escape of Nanoparticles: Toward More Efficient Cellular Delivery. *Bioconjug. Chem.* **2019**, *30*, 263–272. [CrossRef]
33. Zemtsova, E.G.; Arbenin, A.Y.; Plotnikov, A.F.; Smirnov, V.M. Pore radius fine tuning of a silica matrix (MCM-41) based on the synthesis of alumina nanolayers with different thicknesses by atomic layer deposition. *J. Vac. Sci. Technol. A* **2015**, *33*, 6. [CrossRef]
34. Da Silva, C.R.; Wallau, M.; Urquieta-Gonzalez, E.A. Mesoporous carbons prepared by nano-casting with meso- or non-porous silica nanoparticles. *J. Braz. Chem. Soc.* **2006**, *17*, 1170–1180. [CrossRef]
35. Tao, C.L.; Zhu, Y.F.; Xu, Y.; Zhu, M.; Morita, H.; Hanagata, N. Mesoporous silica nanoparticles for enhancing the delivery efficiency of immunostimulatory DNA drugs. *Dalton Trans.* **2014**, *43*, 5142–5150. [CrossRef]
36. Han, L.; Tang, C.; Yin, C.H. pH-Responsive Core-Shell Structured Nanoparticles for Triple-Stage Targeted Delivery of Doxorubicin to Tumors. *ACS Appl. Mater. Interfaces* **2016**, *8*, 23498–23508. [CrossRef] [PubMed]
37. Zhang, Y.; Xu, J. Mesoporous silica nanoparticle-based intelligent drug delivery system for bienzyme-responsive tumour targeting and controlled release. *R. Soc. Open Sci.* **2018**, *5*, 1–10. [CrossRef]
38. O'Donnell, K.P.; Roqan, I.S.; Wang, K.; Lorenz, K.; Alves, E.; Bockowski, M. The photoluminescence/excitation (PL/E) spectroscopy of Eu-implanted GaN. *Opt. Mater.* **2011**, *33*, 1063–1065. [CrossRef]
39. Chen, F.; Huang, P.; Zhu, Y.J.; Wu, J.; Zhang, C.L.; Cui, D.X. The photoluminescence, drug delivery and imaging properties of multifunctional Eu3+/Gd3+ dual-doped hydroxyapatite nanorods. *Biomaterials* **2011**, *32*, 9031–9039. [CrossRef]
40. Ashokan, A.; Menon, D.; Nair, S.; Koyakutty, M. A molecular receptor targeted, hydroxyapatite nanocrystal based multi-modal contrast agent. *Biomaterials* **2010**, *31*, 2606–2616. [CrossRef]
41. Fisichella, M.; Dabboue, H.; Bhattacharyya, S.; Lelong, G.; Saboungi, M.L.; Warmont, F.; Midoux, P.; Pichon, C.; Guerin, M.; Hevor, T.; et al. Uptake of Functionalized Mesoporous Silica Nanoparticles by Human Cancer Cells. *J. Nanosci. Nanotechnol.* **2010**, *10*, 2314–2324. [CrossRef]
42. Antsiferova, Y.; Sotnikova, N.; Parfenyuk, E. Different Effects of the Immunomodulatory Drug GMDP Immobilized onto Aminopropyl Modified and Unmodified Mesoporous Silica Nanoparticles upon Peritoneal Macrophages of Women with Endometriosis. *Biomed Res. Int.* **2013**, *2013*, 924362. [CrossRef] [PubMed]
43. Jiang, B.P.; Zhang, L.; Zhu, Y.; Shen, X.C.; Ji, S.C.; Tan, X.Y.; Cheng, L.; Liang, H. Water-soluble hyaluronic acid-hybridized polyaniline nanoparticles for effectively targeted photothermal therapy. *J. Mater. Chem. B* **2015**, *3*, 3767–3776. [CrossRef]
44. Chou, C.C.; Chen, W.; Hung, Y.; Mou, C.Y. Molecular Elucidation of Biological Response to Mesoporous Silica Nanoparticles in Vitro and in Vivo. *ACS Appl. Mater. Interfaces* **2017**, *9*, 22235–22251. [CrossRef]

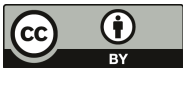

cancers

MDPI

Article

Antitumor Effects of Intra-Arterial Delivery of Albumin-Doxorubicin Nanoparticle Conjugated Microbubbles Combined with Ultrasound-Targeted Microbubble Activation on VX2 Rabbit Liver Tumors

Jae Hwan Lee [1,†], Hyungwon Moon [1,†], Hyounkoo Han [2], In Joon Lee [3], Doyeon Kim [2], Hak Jong Lee [1,4,5], Shin-Woo Ha [5], Hyuncheol Kim [2,*] and Jin Wook Chung [4,6,*]

1 Department of Radiology, Seoul National University Bundang Hospital, 82 Gumi-ro 173, Bundang-gu, Seongnam 13620, Korea; lzhwanmd@gmail.com (J.H.L.); moondaeng82@naver.com (H.M.); hakjlee@gmail.com (H.J.L.)
2 Department of Chemical & Biomolecular Engineering, Sogang University, 35 Baekbeom-ro, Mapo-gu, Seoul 04107, Korea; 507513@hanmail.net (H.H.); doyeon777@naver.com (D.K.)
3 Department of Radiology, National Cancer Center, 323 Ilsan-ro, Ilsandong-gu, Goyang 10408, Korea; cheolh@gmail.com
4 Department of Radiology, Seoul National University College of Medicine, Daehak-ro, Jongno-gu, Seoul 03080, Korea
5 IMGT Co., Ltd., 172 Dolma-ro, Bundang-gu, Seongnam 13605, Korea; shinwoo.ha@gmail.com
6 Institute of Radiation Medicine, Seoul National University Hospital, 101, Daehak-ro, Jongno-gu, Seoul 03080, Korea
* Correspondence: hyuncheol@sogang.ac.kr (H.K.); chungjw@snu.ac.kr (J.W.C.); Tel.: +82-2-705-8922 (H.K.); +82-2-2072-2057 (J.W.C.); Fax: +82-2-3273-0331 (H.K.); +82-2-743-6385 (J.W.C.)
† These authors contributed equally to this work.

Received: 4 March 2019; Accepted: 22 April 2019; Published: 24 April 2019

Abstract: Image-guided intra-arterial therapies play a key role in the management of hepatic malignancies. However, limited clinical outcomes suggest the need for new multifunctional drug delivery systems to enhance local drug concentration while reducing systemic adverse reactions. Therefore, we developed the albumin-doxorubicin nanoparticle conjugated microbubble (ADMB) to enhance therapeutic efficiency by sonoporation under exposure to ultrasound. ADMB demonstrated a size distribution of 2.33 ± 1.34 μm and a doxorubicin loading efficiency of 82.7%. The echogenicity of ADMBs was sufficiently generated in the 2–9 MHz frequency range and cavitation depended on the strength of the irradiating ultrasound. In the VX2 rabbit tumor model, ADMB enhanced the therapeutic efficiency under ultrasound exposure, compared to free doxorubicin. The intra-arterial administration of ADMBs sufficiently reduced tumor growth by five times, compared to the control group. Changes in the ADC values and viable tumor fraction supported the fact that the antitumor effect of ADMBs were enhanced by evidence of necrosis ratio (over 70%) and survival tumor cell fraction (20%). Liver toxicity was comparable to that of conventional therapies. In conclusion, this study shows that tumor suppression can be sufficiently maximized by combining ultrasound exposure with intra-arterial ADMB administration.

Keywords: albumin nanoparticles; microbubble; ultrasound; theranostics; hepatocellular carcinoma; VX2 tumor; intra-arterial chemotherapy

1. Introduction

Image-guided intra-arterial (IA) therapies, such as hepatic arterial infusion chemotherapy (HAIC) or trans-arterial chemoembolization (TACE) are frequently used for the treatment of primary or

secondary liver cancers [1–6]. HAIC involves the local and targeted delivery of high concentrations of chemotherapeutic drugs directly to the tumor, whereas TACE, with or without drug-eluting beads, combines local and targeted drug delivery with concurrent tumor-feeding artery embolization. The theory behind this treatment recommends delivering the maximal dose of the chemotherapeutic agent to the target tissue while minimizing systemic toxicity. However, clinical response is still unsatisfactory, as local tumor control rates achieved following TACE is only 15–60%, and increases median survival without treatment from 16 months to 20 months [7,8]. One possible reason for these poor results is perhaps the limited delivery of the drug to the target tumor [9–11]. Changes in tumor microenvironment including decreased pH, hypoxia, and abnormal vascularity impede drug delivery to the target. Moreover, local tumor recurrences at the periphery of the treated area are common and are often a cause for treatment failures [12]. Another limitation in clinical field is side effects. Concentrations of drugs in the bloodstream are increased even though drugs are administered via IA injection. Therefore, a decrease of the drug concentration in the bloodstream is also necessary to reduce the side effects caused by target delivery of drugs. The simultaneous monitoring of drug delivery is an unmet clinical need for enhancing tumor control. Thus, novel drug delivery carriers for IA chemotherapy are mandatory for better drug delivery and to allow multimodal imaging which enables the carriers to be simultaneously visualized with various imaging modalities.

In the last decade, studies have used ultrasound as an external trigger for enhancing local drug penetration through artificial pore formation in the cell membrane. This phenomenon is known as the sonoporation effect [13,14]. Theoretically, sonoporation is based on the cavitation between ultrasound and microbubbles. Microbubbles are made to repetitively expand and shrink under ultrasound irradiation. This behavior of microbubbles induces a microstream in the blood vessel and continually puts the cellular membrane under stress (stable cavitation). The microbubbles upon extreme oscillations finally explode at the critical elastic point under the strong ultrasound intensity. At the moment of microbubble explosion, microjets and shock waves are generated and temporally drill the cell membrane near the microbubble with pores of 100–300 nm in size (inertial cavitation) [15]. This cavitation approach is utilized for enhancing local drug delivery to the target site and for improving the intracellular uptake of large molecules and non-permeable drugs. Several groups have shown that sonoporation can enhance the therapeutic efficiency of chemotherapy and gene therapy [16,17]. These researches successfully demonstrated that microbubble-encapsulated drugs induce the well-penetration to target site and functionalization for therapeutic effect. However, the use of microbubbles as drug carriers has been limited since a small portion of drug encapsulation is possible structurally, and the undesirable release of drugs by degradation in the blood stream. To overcome these limitations, nanoparticles are studied for increasing drug loading and protection. In our previous study, human serum albumin nanoparticles (HSA-NPs) were effectively delivered to the tumor site by sonoporation [18,19]. Microbubble-conjugated anticancer drug-loaded HSA-NPs enhanced the selective delivery of drugs to the tumor and led to the improvement of therapeutic efficiency, compared to the administration of pure drugs and administration without ultrasound irradiation. Nanoparticle-based drug delivery has been advantageous for improving drug loading efficiency, protection of drugs from degradation, and intracellular penetration via characteristics of the nanoparticles which allow a sustained drug release. These advantages have progressed tumor-selective delivery and functional release of the drug to the target site. However, the systemic circulation of all agents including nanoparticles is biologically limited for clearance by accumulation in the liver or kidney rather than in the tumor region [20]. Therefore, the therapeutic efficiency is not maximized for tumor treatment owing to drug cleavage. Thus, some of microbubble during the circulation are ruptured by diffusion of gas in the core part. Sequentially, the sonoporation effect should be decreased at the tumor site, compared to direct administration such as IA injection. Therefore, a more effective administration route for maximizing therapeutic efficiency would be tumor vessels rather than the systemic circulation. Unfortunately, there are few or no studies that compare the therapeutic efficiency of systemic administration to that of specific administration routes, which is a surgical

procedure performed at present on humans in the clinic. In the case of hepatocellular carcinoma, the IA administration of drugs using microcatheters has been intensively applied in clinical practice, for the local administration of anticancer drugs and chemotherapeutic embolic agents [1,3,4]. The purpose of our study was to explore the antitumor effect of ADMBs combined with ultrasound-targeted microbubble activation (ADMB/US) in rabbit VX2 liver tumor model. (Figure 1A) and to compare antitumor effect via IA administration to IV administration. (Figure 1B).

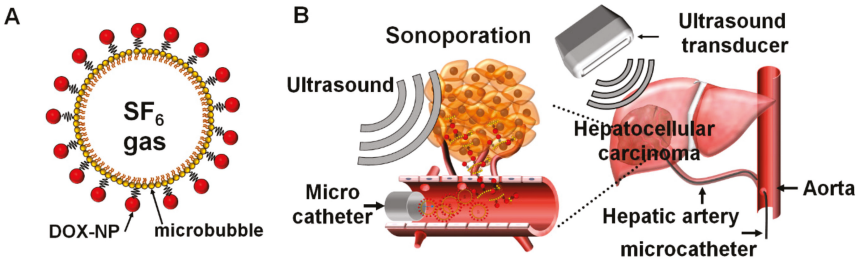

Figure 1. Schematic illustrations of (**A**) the ADMB complex and (**B**) treatment procedure for the intra-arterial administration of the ADMB complex using microcatheters under ultrasound exposure.

2. Results

2.1. Preparation of the ADMB Complex

For the enhancement of therapeutic effect by sonoporation phenomenon, ADMB complex was developed by self-assembled microbubble and albumin-doxorubicin nanoparticles. Albumin-doxorubicin nanoparticles were fabricated by the dropwise addition of ethanol to albumin. A size distribution of albumin-doxorubicin nanoparticles of 205.5 ± 45.3 nm. (PDI; 0.172) was demonstrated. Transmission electron microscope images of the albumin-doxorubicin nanoparticles demonstrated a uniform and spherical morphology (Figure 2A). The loading efficiency of doxorubicin into the albumin-doxorubicin nanoparticles was 82.7%. The doxorubicin was released in a sustained manner from the albumin-doxorubicin nanoparticles at an in vitro release rate of 24.2% for 50 h with the initial burst. Thus, albumin-doxorubicin nanoparticles demonstrated a similar release profile as doxorubicin in cell culture medium containing 10% fetal bovine serum and 1% antibiotics (25.2%). The size distribution of albumin-doxorubicin nanoparticles in cell culture medium (158.23 ± 42.9 nm; PDI: 0.155) demonstrated a similar size distribution to albumin-doxorubicin nanoparticles in PBS (Figure S2). According to these results, albumin-doxorubicin nanoparticles are sufficiently stable against serum proteins. However, compared to the in vitro release profile of doxorubicin in PBS and cell culture medium, doxorubicin was more rapidly released from the albumin-doxorubicin nanoparticles at pH 4.7. 41.5 % of doxorubicin was released at pH 4.7 for 50 h. Regarding to this result, doxorubicin was electrostatically bound to albumin and was pH-dependently released (Figure 2B).

The phospholipid-based microbubbles were filled with a SF_6 gas core and had size distributions of 1.73 ± 0.34 μm (PDI: 0.297). The albumin-doxorubicin nanoparticles were conjugated onto the surface of the microbubbles and the subsequent size distribution was 2.33 ± 1.34 μm (PDI: 0.395). Following albumin-doxorubicin nanoparticle conjugation, the size distribution of the ADMB complex was slightly larger in comparison to that of the free microbubbles. To increase doxorubicin loading efficiency by raising conjugation ratio of albumin-doxorubicin nanoparticles to microbubbles, albumin-doxorubicin nanoparticles (2 mg of doxorubicin loaded nanoparticle) were conjugated to microbubbles so that the number of microbubbles was 1×10^9. However, the ADMBs were aggregated heterogeneously (Figure S3) Aggressive aggregates of ADMBs were observed by optical microscopy images and the size distribution was incorrectly defined by DLS. This aggregation was induced by numerous reactions between both amine groups on the albumin-doxorubicin nanoparticles and N-hydroxysuccinimide

on the microbubble surface. Hence, ADMBs were optimized with a ratio of 1 mg of doxorubicin in albumin-doxorubicin nanoparticles to 1×10^9 microbubbles. In optimized ADMBs, the conjugation of the albumin-doxorubicin nanoparticles to the microbubbles was confirmed by fluorescence emission from the doxorubicin conjugated onto the surface of microbubble without ADMB aggregates (Figure 2C).

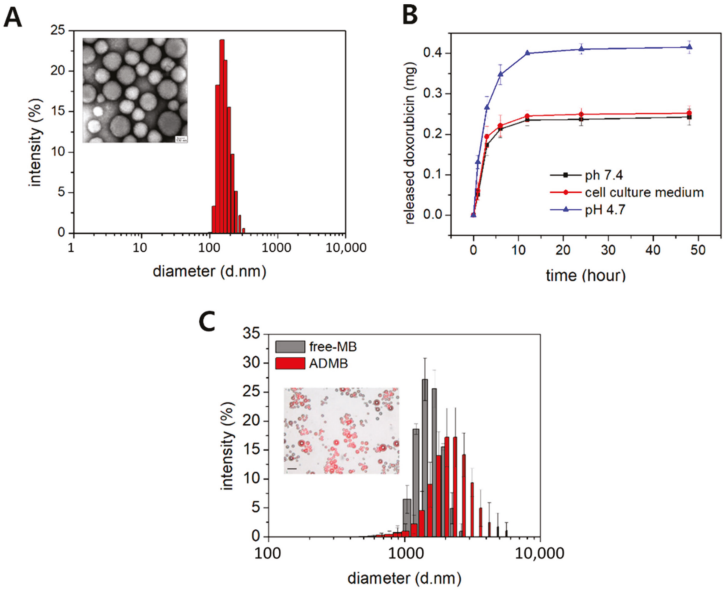

Figure 2. Characteristics of the albumin-doxorubicin nanoparticle and the ADMB complex (**A**) size distribution and TEM image (inset image, scale bar:100 nm) of the albumin-doxorubicin nanoparticle. (**B**) In vitro release of doxorubicin from albumin-doxorubicin nanoparticles at pH 7.4, pH 4.7 and DMEM containing 10% of fetal bovine serum and 1% of antibiotics. (**C**) size distribution of free MB (gray) and ADMB (red). Merged fluorescence and optical images (inset image, scale bar: 20 μm).

2.2. Phantom Study for Echogenicity of ADMB Complex

To investigate if the ADMB complex was capable of resonance to ultrasound irradiation for the cavitation effect, the echogenicity was evaluated by visualization with a clinical ultrasound scanner.

For the ultrasound imaging, 2% of home-made agarose phantom containing 2-holes was used. A contrast-enhanced ultrasound imaging mode demonstrated echogenicity only from the microbubbles. At a low MI of 0.06, the ADMB complexes were stably visualized by microbubble oscillations. However, the echogenicity decreased upon microbubble destruction, depending on the number of manual flashes (mechanical index: 0.68). Manual flashes strengthen the intensity of ultrasound exposure and lead to the destruction of the microbubbles. About 100 times of manual flashing decreased the echogenicity of the microbubbles by about half (55.45%). The echogenicity consistently decreased upon increasing the number of manual flashes (Figure 3A,B). The differences of echogenicity between the free microbubbles and the ADMB complexes were also investigated from the ultrasound images in the same frame, to analyze whether the cavitation effect was altered by conjugation with the doxorubicin-albumin nanoparticles. The echogenicity of the ADMB complexes did not differ from the free microbubbles. The percentages of echogenic area of the ADMB complexes and the free microbubbles were 79.6% and 76.5% respectively, in a relatively equal area (Figure 3C, Table S1).

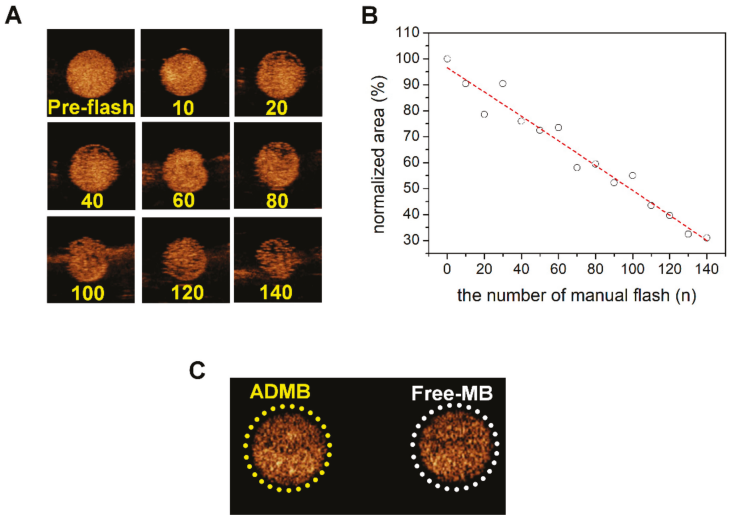

Figure 3. Contrast-enhanced ultrasound images and relative quantification of ultrasound images. (**A**) contrast-enhanced ultrasound images captured at varying numbers of manual flashes. (**B**) Relative quantification of ultrasound image. (**C**) Ultrasound image of the ADMB complex and the free microbubble.

2.3. Enhancement of Cell Uptake and Cell Viability of ADMBs by Sonoporation Effect

Intracellular uptake and cell viability of ADMB with or without ultrasound exposure were evaluated to investigate the enhancement of the anticancer effect by the sonoporation phenomenon. For tracking nanoparticle uptake into the cell, Alexa555 dye was conjugated to the nanoparticles and the nucleus was stained by DAPI. As shown in Figure 4, albumin nanoparticles were rarely permeable into the cytoplasm within 3 h without ultrasound exposure. A slight fluorescence intensity was detected from nanoparticles at 6 and 24 h post-incubation in the group without ultrasound exposure, because the large size of MBs disturbed the cellular uptake of nanoparticlesr. On the other hands, albumin nanoparticles rapidly penetrated into the cytoplasm within 3 h with the ultrasound exposure. Thus, cellular uptake of albumin nanoparticles was continuously increased time-dependently. At 6 and 24 h post-incubation, albumin nanoparticles were effectively located in the cytoplasm. Regarding these results, the cell viability of ADMBs was evaluated with or without ultrasound exposure. In vitro cell viability was confirmed using a hepatocellular carcinoma cell line (HepG2). To accurately verify that the sonoporation effect between microbubbles and ultrasound is non-toxic, we evaluated the cell viability under various ultrasound exposure conditions with or without microbubbles (Figure S4). Hence, we analyzed cell viability with 1 W/cm^2 of ultrasound strength and 5% duty cycle (Figure 5). At 24 h post-incubation, the cell viability in all groups was demonstrably similar. However, cell viability was decreased time-dependently after 48 h of incubation. Specifically, ADMBs only demonstrated enhancement of cell viability under the ultrasound exposure after 72 h ($p < 0.05$). As microbubbles resonate with the ultrasound and generated cavitation, albumin-doxorubicin nanoparticles were capable of penetration through the cell membrane more easily than other treatment groups. The treatment groups without microbubbles showed similar levels of cytotoxicity regardless of the ultrasound exposure. In conclusion, cellular uptake and cell viability results demonstrated that ADMBs were capable of not only generating sonoporation effects by cavitation with ultrasound, but also enhancing nanoparticle penetration through the pores in cellular membranes, hence the anticancer effect was enhanced by ADMBs under ultrasound exposure.

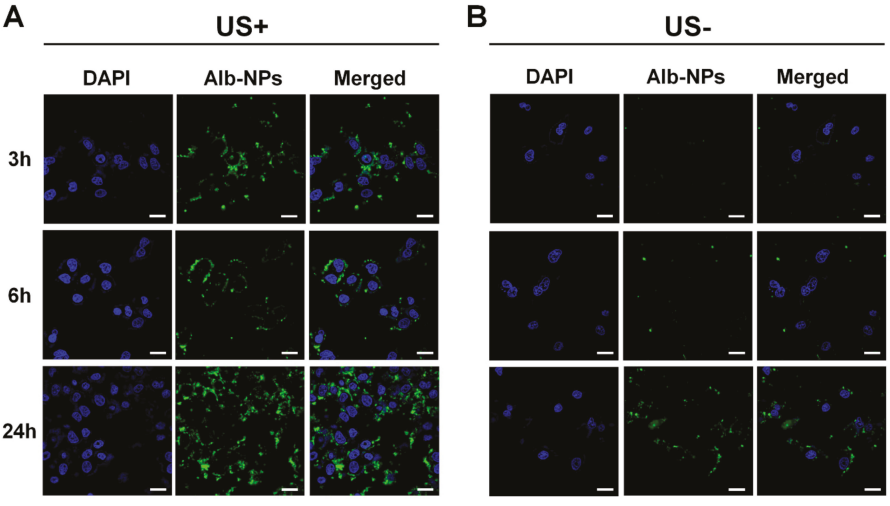

Figure 4. Cellular uptake of albumin nanoparticles after exposure of HepG2 cells to ADMBs. fluorescent image of albumin nanoparticles (**A**) under the ultrasound exposure and (**B**) without ultrasound exposure at 3, 6 and 24 h, respectively (blue; nucleus, green; albumin nanoparticle). Scale bar: 20 μm.

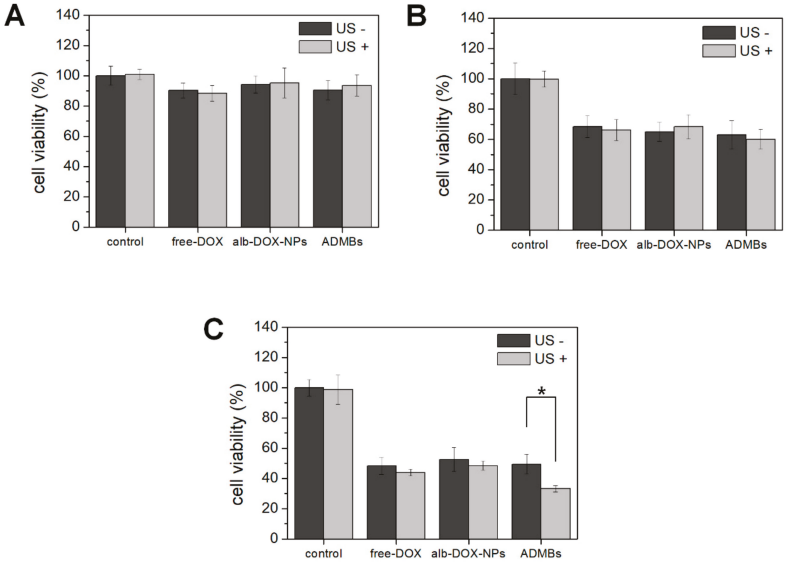

Figure 5. Cytotoxicity of doxorubicin (free-DOX) albumin-doxorubicin nanoparticle (alb-DOX-NPs) and ADMBs at (**a**) 24 h, (**b**) 48 h and (**c**) 72 h with (light gray) or without (dark gray) ultrasound exposure (* $p < 0.05$).

2.4. Animal Models and Ultrasound Imaging during Treatment Procedure

A total of 25 VX2 liver tumor rabbit models were created. All rabbits having tumors survived through the tenure of the experiment. The tumors were visualized using ultrasound during the experiments. A strong enhancement of intra-tumoral vessels was clearly demonstrated from the beginning of the injection in the IA-ADMBs and IA-free MB groups (Figure 6B,D). Individuals receiving

IV microbubbles (Figure 6C) showed a moderate tumor parenchymal enhancement accompanied by enhanced liver parenchyma and liver vessels. Ultrasound images without microbubbles demonstrated non-enhanced echogenicity (Figure 6A,E) The enhancement of ultrasound echogenicity demonstrated that the delivery efficiency of ADMB in the groups receiving IA microbubbles was higher than that of the groups receiving IV microbubbles. Interestingly, echogenicity of the both IA-ADMBs and IA-free MB demonstrated a similar degree of enhancement. However, the echogenicity enhancement patterns were slightly different. In the US image of ADMBs, increased echogenicity was noted separately at the tumor vessels and tumor parenchyma, whereas the echogenicity of the tumor and adjacent liver tissue in the US image of IA-free MB was enhanced simultaneously. This discrepancy was probably due to the fact that albumin was capable of binding glycoprotein 60 receptor around liver tumor epithelium and of enhancing the anti-cancer effect by targeted delivery [21].

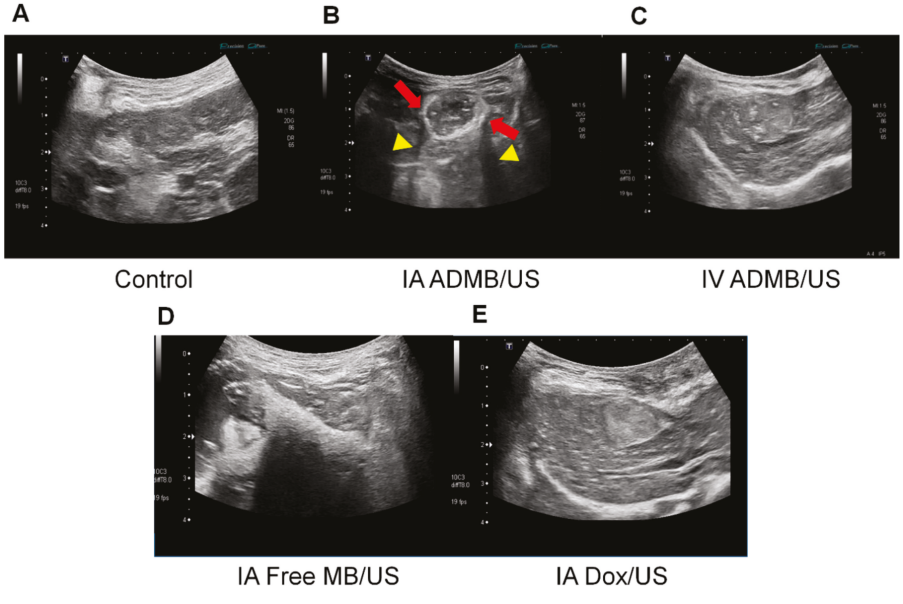

Figure 6. Representative ultrasound images of (**A**) control, (**B**) intraarterial injection of ADMB (IAMB/US), (**C**) intravenous injection of ADMB (IVMB/US), (**D**) intraarterial injection of microbubble (IA Free MB/US) and (**E**) intraarterial doxorubicin (IA Dox/US). Note that strong rim-like enhancement of intratumoral vessels (arrow) with posterior shadow (arrowhead) in IAMB/US group.

2.5. Antitumor Efficacy of Albumin-Doxorubicin Nanoparticle-MB Complex by Quantitative MR Imaging and Pathology

The anticancer efficacy of ADMB was evaluated using quantitative MR imaging (Figure 8A). The measured mean tumor volume at baseline and at 7 days after drug administration, volume inhibition rate (VIR), and change in ADC values are summarized in Figure 7. There was no significant difference in tumor size among groups at baseline ($p = 0.614$). The mean tumor volume of IA-ADMB.US (2156.57 ± 849.86 mm^3) was significantly small compared to that of IV-ADMB/US (3777.47 ± 1950.72 mm^3). The mean tumor volume of IV-ADMB/US was larger than that of IA-ADMB/US. And the tumor volume of IA-Dox/US, IA-free MB/US and control were 4811.02 ± 2132.69 mm^3, 5770.06 ± 1382.78 mm^3, and 6063.97 ± 3432.51 mm^3, respectively. Comparison of tumor volume IA-Dox/US, IA-free MB/US and control was not statistically significant. Among the five groups, IA-ADMB/US achieved a maximal reduction in tumor volume of 64.44 ± 15.35% on day 7 as indicated by the MRI (Table 1). Both the IA-ADMB/US and IV-ADMB/US showed an increase in the ADC values

after treatment by more than 50%, compared to pre-treatment values, which suggested the loss of diffusion-restrictive lesions such as tumor parenchyma. For group of IA-ADMB/US, the VIR and percent change in ADC value were significantly higher than others (Figure 7). In addition, the VIR and percent change in ADC value in IV-ADMB/US tended to be lower than the corresponding values of group IA-ADMB/US and higher than the corresponding values of IA-Dox/US, IA-free MB/US and control. However, the results were not statistically significant. The histologically viable tumor percentage was quantified using a slide-by-slide segmentation of the H&E staining images and TUNEL-stained images that were generated to investigate the entire section of the whole tumors. The pathological analysis performed on day 7 showed low viable tumors in IA-ADMB/US (19.60 ± 12.1%, 25.29 ± 14.00% and 33.65 ± 4.09%, 42.48 ± 8.85%, 37.42 ± 5.80% for IA-ADMB/US, IV-ADMB/US, IA- Dox/US, IA-free MB/US and control, respectively; Figure 8A,B, Figure S5 and Table 2). IA-ADMB/US demonstrated a significantly higher necrotic fraction and a lower estimated viable tumor volume, compared to IA- Dox/US, IA-free MB/US and control (Figure 8B,C). Similar to the MR-based analysis, the viable tumor percentage and the estimated viable tumor volume of IV-ADMB/US tended to be higher than the corresponding values of IA-ADMB/US and lower than the corresponding values of others; the difference, however, was not statistically significant.

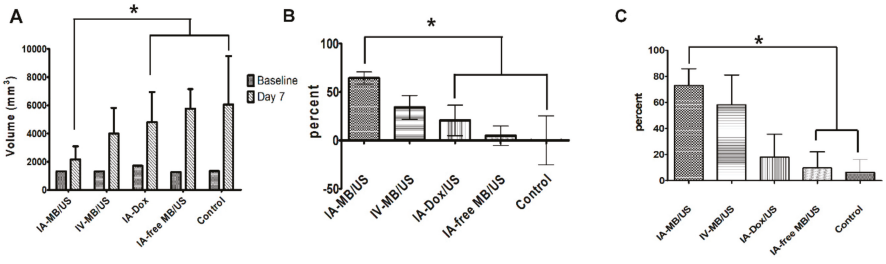

Figure 7. Quantitative volumetric image analysis at baseline and on day 7 after treatment, in IA ADMB/US, IV ADMB/US, IA Doxorubicin/US, IA free MB/US, and the untreated control groups. (**A**) Change in tumor volumes. (**B**) The Volume Inhibition Rate (VIR) of each group. (**C**) Percent change in ADC values across the experimental period among the groups. Each bar represents mean SD, * $p < 0.05$ versus IA Doxorubicin/US, IA free MB/US, and untreated control group.

Table 1. The tumor volume and volume inhibition rate (VIR) of each group.

Group	Tumor Volume (mm^3) at Baseline	Tumor Volume (mm^3) at 7 Days after Delivery	VIR (%)
Control	1331.21 ± 481.67	6063.97 ± 3432.51	-
IA-free MB/US	1266.54 ± 527.06	5770.06 ± 1382.78	4.85 ± 22.80
IA-Dox/US	1712.71 ± 431.79	4811.02 ± 2132.69	20.66 ± 35.16
IV-ADMB/US	1245.30 ± 811.94	3777.47 ± 1950.72	34.10 ± 30.09 *
IA-ADMB/US	1313.08 ± 740.77	2156.57 ± 849.86	64.44 ± 15.35 *,**

* $p < 0.05$ compared with the control group; ** $p < 0.05$ compared with IA-Dox/US and IA-free MB/US groups.

Table 2. The viable tumor percentage and estimated viable tumor volume of each group.

Group	Viable Tumor (%)	Estimated Viable Tumor Volume (mm^3)
Control	37.42 ± 5.80	2339.55 ± 1433.18
IA-free MB/US	42.48 ± 8.85	2503.82 ± 975.32
IA-Dox/US	33.65 ± 4.09	1526.89 ± 731.75
IV-ADMB/US	25.29 ± 14.00	1130.98 ± 1003.78
IA-ADMB/US	19.60 ± 10.55 *,**	429.0 ± 291.09 *,**

* $p < 0.05$ compared with the control group. ** $p < 0.05$ compared with IA Dox/US and IA free MB/US groups.

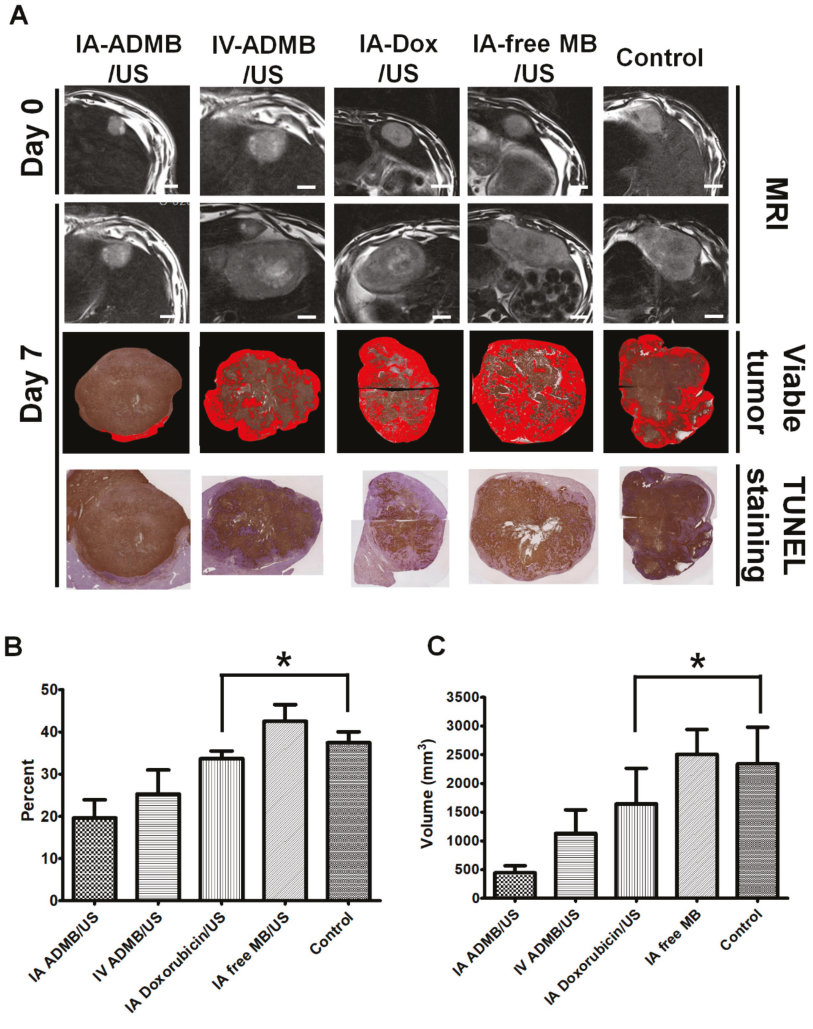

Figure 8. Representative MRI and histo-segmentation images of each group, Scale bar: 10 mm (**A**). Quantitative analysis of viable tumor fraction (**B**). Estimated viable tumor volume (**C**) at day 7 after treatment. Red area represents the viable portion of tumor; each bar represents mean SEM., * $p < 0.05$ versus IA doxorubicin/US, IA free MB/US, and untreated control group.

2.6. Biochemical Liver Toxicity Evaluation

All the animals showed a tendency to reach the highest values of AST and ALT enzymes at 24 h after treatment, which gradually decreased and returned to baseline values at 7 days after treatment. The AST and ALT values, noted at specific intervals of time starting from baseline to the end of the observation period, did not differ significantly among the five groups (Figure 9).

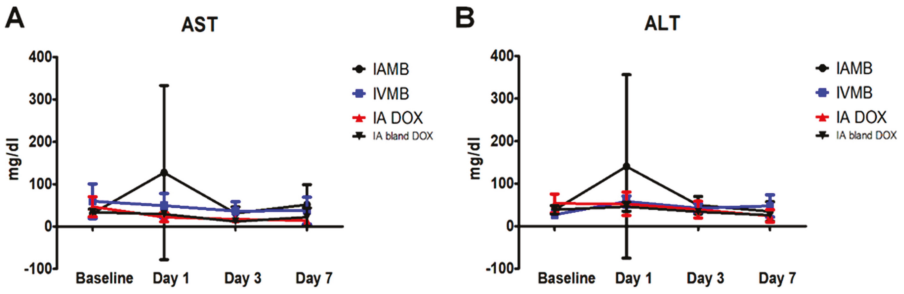

Figure 9. Graphs depicting liver enzyme values (AST and ALT) changes over the observation period for each treatment group. (**A**) Graph depicting the plasma concentration changes in aspartate transaminase (AST) over the 7-day observation period (expressed in mg/dl). (**B**) Graph depicting the plasma concentration changes in alanine transaminase (ALT) over the 7-day observation period. No significant changes in AST and ALT levels at each time interval throughout the observation period among the five groups.

3. Discussion

In this study, we prepared a novel drug delivery system with a dual function, acting as a drug carrier and an ultrasound contrast, by combining the advantages of microbubbles and bio-compatible nanoparticles. Albumin-doxorubicin nanoparticles were synthesized by a desolvation technique. The doxorubicin was strongly bound to the albumin and the correlation coefficient between doxorubicin and albumin was 0.98 [22]. The albumin-doxorubicin complexes were conjugated to the nanoparticles by cross-links between the amine group of albumins and aldehyde groups [23]. Being covalent in nature, these bonds were extremely strong. The doxorubicin molecules were stably loaded by both surface absorption and incorporation into the nanoparticles [22,24]. This structure is advantageous since the nanoparticles are not easily degraded and the doxorubicin incorporated within the nanoparticle is safely protected from different enzymes in the blood vessels. In addition, as shown in Figure 2B and Figure S2, doxorubicin was released in a sustained manner for a long period of time owing to the solid structure [25]. The conjugation of albumin-doxorubicin nanoparticles onto the surface of the microbubbles was also based on the amide bonding previously described. This amide bond forms between the numerous primary amines of albumin and N-hydroxysuccinimide of the microbubbles [18]. This rapid and strong bond is also easily induced within 1 h. The albumin-doxorubicin nanoparticles do not easily extravasate owing to the large size of the microbubbles, and are capable of safely delivering doxorubicin to the target site without mid-way losses, until the target site is exposed to ultrasound irradiation.

To confirm that the ADMBs resonate to ultrasound, we investigated the echogenicity of ADMBs using a commercial ultrasound scanner, which is equipped with a transducer having a frequency range of 2–9 MHz. In an in vitro phantom experiment, microbubbles were continuously visualized during ultrasound irradiation at a low MI of 0.06. The results showed that the microbubbles oscillated and generated acoustic wave pressure necessary for a stable cavitation. However, at a MI of 0.06, this behavior is not enough to generate sonoporation, because a MI of 0.06 is sufficiently low and this MI value is only for adaptation to diagnosis by ultrasound. However, collapse of microbubbles was demonstrated under the ultrasound radiation with MI 0.68 by manual flash. The destruction of microbubbles by the application of strong, intense ultrasound irradiation leads to an asymmetric gas infusion with high pressure from the core, which induces a temporary stress on the cellular membrane. This phenomenon is known as inertial cavitation and our ADMB complex was proven to induce inertial cavitation, as depicted in Figure 3. In addition, the driving frequency for inertial cavitation was 2–9 MHz, and this is the frequency which is generally applied to abdominal organs in the clinical field. Theoretically, the penetration depth and frequency of ultrasound are critically related. A lower

frequency permeates more to deeper regions, whereas the resolution of ultrasound imaging is clear in the diagnostic field. However, in clinical research, studies generally use low frequency ultrasounds for a deeper penetration and high intensity ultrasounds for an enhanced ultrasound trigger. In our previous study, we measured that the optimal resonance frequency of the albumin nanoparticle-conjugated microbubble is 3 MHz [18]. Therefore, a resonance frequency of 2–9 MHz was optimum for both our ADMBs and the hepatocellular carcinoma. We also analyzed the influence of albumin-doxorubicin nanoparticle conjugation on the echogenicity. As conjugation induces changes in the microbubble surface, corresponding changes in shell elasticity and stiffness are possible [26,27]. It is perhaps this change which is able to reduce the echogenicity. However, as shown in Figure 3C, the echogenicity was rarely influenced.

Regarding these characteristics of ADMBs, intracellular uptake and anticancer effect was evaluated, in order to study the generation of sonoporation effects by ADMBS and to enhance the anticancer effect. Cytotoxicity of ADMBs was enhanced under ultrasound, whereas the cytotoxicity of doxorubicin or albumin-doxorubicin was not related to ultrasound exposure. Theoretically, a high intensity of ultrasound such as HIFU can generate sonoporation and enhance intracellular delivery. However, high intensity of ultrasound to open cellular membranes usually stresses the surroundings and occasionally induces cytotoxicity to the normal cells or organs. Therefore, microbubbles were sufficiently beneficial for the generation of sonoporation effects with lower ultrasound pressure and enhancement of drug delivery into the cytoplasm. In our study we proved, as shown in Figures 4 and 5, that intracellular delivery and anticancer effects in the presence of microbubbles under ultrasound were enhanced within 3 h, whereas ADMBs without ultrasound exposure did not penetrate in 6 h, because sonoporation was not induced and large size of microbubbles interfered with penetration through the cell membrane. Therefore, the cytotoxicity of ADMBs under the ultrasound exposure was strongest, compared to doxorubicin and albumin-doxorubicin nanoparticles.

The second section of our study comprehensively evaluated the in vivo antitumor effect of ADMB following ultrasound activation. As we had expected, the combined therapy of IA ADMB/US administration led to the highest reduction in tumor volume. This was also supported by the fact that IA-ADMB/US group showed the maximal increase in ADC values post-treatment in MR, the highest necrotic fraction and the lowest viable tumor volume revealed by histosegmentation analyses. Moreover, pathological analysis revealed intense and homogeneous necrosis throughout the whole tumor section in the IA-ADMB/US group and viable tumors were nearly absent on the tumor periphery. In contrast, tumor necrosis in the untreated control group was focal and heterogeneous, and there were abundant finger-like viable tumor portions in the periphery. It is presumed that the IA route delivered a high concentration of ADMB which resulted in maximal cavitation and sonoporation in the target tumor site, causing enhanced drug penetration and cytotoxicity to tumor tissues. To our knowledge, this study a first of its kind to investigate and report the promise of IA delivery of ADMB following ultrasound activation in an orthotropic liver tumor animal model larger than rodents. Interestingly, tumor suppression in the IV ADMB/US group was modest but not statistically significant to other groups. Unlike previous studies which primarily used small animals [28–30], our study used rabbits, which are relatively large animals with more blood volumes, and have longer distances between tumors and ultrasound probes. It is perhaps these differences which resulted in the diverse treatment outcomes in the IV ADMB/US group. Previous studies [18,19,28,31–33] used high-intensity, low-intensity focused ultrasound or self-made ultrasound transducers to elucidate the feasibility of sonochemotherapy. However, these probes are not generally used in diagnostic imaging, and therefore cannot be applied for the same. In our study, we used an ultrasound scanner used for clinical purposes to simultaneously visualize the tissues of the target tumor and to deliver ultrasound irradiation for activating microbubble-assisted drug delivery. This allows the advantage of directly monitoring drug delivery while treating the target tumor, which means that it can be easily applied to clinical studies in the future. It is important to evaluate the safety profile while investigating new drug delivery systems. In our study, there were no significant differences in the liver enzyme levels analyzed at specific time

intervals, between the IA ADMB/US group and other groups. In addition, no animal deaths occurred due to complications arising from microbubble injection. This indicates that the IA ADMB/US therapy could be effective and safe for the treatment of liver cancers.

We acknowledge several limitations of our study. First, we did not study the treatment outcomes when only ADMB was administered without ultrasound irradiation. However, the efficacy of drug-loaded microbubbles in combination with microbubble destruction is a well-known drug delivery system, as many previous reports suggest [18,28,31–36]. Second, the concentration of doxorubicin in tumors was not directly measured. However, the IA ADMB/US group showed excellent tumor suppression as observed by both volumetric and quantitative analyses, indicated by changes in the ADC values, MR and necrotic fraction, and viable tumor volume. Moreover, the free MB/US group did not show significant tumor inhibition compared to the control group. These findings indirectly support that the enhanced anticancer effect in the IA ADMB/US group was caused by the application of an improved drug delivery system.

4. Materials and Methods

4.1. Materials

1,2-Distearoyl-sn-glycero-3-phosphocholine (DSPC) was purchased from NOF Corporation (Tokyo, Japan). 1,2-Distearoyl-sn-glycero-3-phosphoethanolamine-N-[succinyl(polyethylene glycol)-2000] (DSPE-PEG2k-NHS) was purchased from Nanocs Incorporated (Boston, MA, USA). Human serum albumin, 8%-glutaraldehyde, and 99%-ethanol were purchased from Sigma-Aldrich (St. Louis, MO, USA). Doxorubicin was purchased from the Il-Dong Pharmaceutical Company (Seoul, Korea). Microcatheters (Progreat 2.0F, Terumo, Japan) were obtained from the Terumo Korea Corporation (Seoul, Korea). The animals were purchased from Orient Bio Co. (Seongnam, Korea). All the other chemicals and solvents were of analytical grade.

4.2. Preparation of ADMB Complex

The ADMB complex consisted of two main parts: the albumin nanoparticle loaded with doxorubicin and the phospholipid-based microbubble; the complex was fabricated as per the sequence of procedures mentioned hereafter. First, the albumin nanoparticle was fabricated by a desolvation method; 150 mg of human serum albumin and 5 mg of doxorubicin were dissolved in water and the pH was adjusted to 8.5 by using 1 M NaOH. After stirring (at 600 rpm) for 2 h, 8 mL of ethanol (99.9%) was continuously added in a dropwise manner for transforming the mixture into doxorubicin-albumin nanoparticles, indicated by the development of turbidity in the mixture; 100 μL of 8%-glutaraldehyde was added cross-linking the nanoparticles. After stirring overnight, the albumin-doxorubicin nanoparticles were purified by centrifugation for 10 min at 4 °C at 15,000 rpm, and were resuspended in equal volume of 0.01 M phosphate buffer saline (pH 7.4). The loading efficiency of doxorubicin was calculated by analyzing the quantity of unloaded doxorubicin in the supernatant after centrifugation. The amount of doxorubicin in the supernatant was measured by a UV-Vis spectrometer.

DSPC and DSPE-PEG2k-NHS dissolved in chloroform in a 9:1 molar ratio. The chloroform was fully evaporated for fabrication of a thin phospholipid film. This thin phospholipid film was hydrated by 0.01 M PBS at a temperature above the phase transition temperature of DSPC (55 °C). A 2 mL vial was filled with the volume of phospholipid solution (at a concentration of 0.5 mg/mL) and sulfur hexafluoride gas (SF_6) at the headspace. Sequentially, the microbubbles were formulated by activation with Vialmix^{TM} for 45 s.

The albumin-doxorubicin nanoparticles were conjugated with the microbubbles by adding the albumin-doxorubicin nanoparticles to the microbubbles at a concentration of 1 mg/mL. The albumin-doxorubicin nanoparticles were conjugated to the microbubbles via amide bonds between the primary amine of the nanoparticles and the NHS from the microbubble surface. After 1 h for conjugation

of albumin-doxorubicin to surface of NHS functionalize microbubble, centrifugation at 3000 rpm for 5 min was performed at three times for purification of ADMBs. Unbound albumin-doxorubicin was removed and ADMBs were re-suspended by 0.01 M PBS.

4.3. In Vitro Release Test for the ADMB Complex

In order to investigate doxorubicin release from the ADMB complex, the complex was sealed with a 3000 Da (MW) cut-off dialysis membrane. The ADMBs loading 1 mg of doxorubicin in the dialysis membrane was placed into the tube filled with 10 mL of phosphate buffer saline, saline with adjustment to pH 4.7 or cell culture medium containing 10% of fetal bovine serum and 1% of antibiotics. This ADMBS was stored at 37 °C and 500 rpm of shakes (n = 3). The released doxorubicin was measured by a UV-Vis spectrometer.

4.4. Phantom Study for Echogenicity of the ADMB Complex

The echogenicity of the ADMB complex was evaluated using a commercial ultrasound scanner equipped with a transducer having a frequency range of 2–9 MHz. For the ultrasound imaging, home-made agarose phantoms containing two holes of 2 cm depth was used. The holes in the agarose phantoms were filled with the ADMB complex at the concentration of 5 μg/mL and degassed water, respectively. For studying microbubble stability, ultrasound imaging was performed at a Mechanical Index (MI) of 0.06 and manual flash mode (MI:0.68) was performed with 3 s time interval for microbubble destruction (iu-22 Philips Medical System, Philips, Bothell, WA, USA). The stability of the ADMB complex was analyzed by decreasing the ratio of echogenic area (pixel) with the ImageJ software (version 1.45 s; National Institutes of Health, Bethesda, MD, USA).

4.5. Cellular Uptake and Cell Viability of ADMB under the Ultrasound Exposure

To determine that ADMB enhances cell permeability under the ultrasound exposure, hepatic cellular carcinoma cell line, HepG2, was applied. HepG2 cells (5×10^4) were seed to the 8 well cell culture chamber and incubated for overnight. To fluorescently visualize, fluorescence dye, NHS-alexa488, was labeled to human serum albumin nanoparticle without doxorubicin loadings. Florescence dye was conjugated by amide bond between albumin nanoparticle and NHS. Fluorescently labeled ADMBs were treated and were exposed to the ultrasound wave (Sonidel SP100 sonoporator, Sonidel Ltd., Dublin, Ireland). Ultrasound was irradiated to each well with the 1 W/cm^2 of strength and 5% of duty cycle for the 1 min. At the post-incubation of 3, 6 and 24, HepG2 cells were washed three times and fixed by 4%-paraformaldehyde. And nucleus was stained by DAPI. Cellular uptake of ADMBs were observed by confocal laser microscopy.

Cell viability of ADMBs under the ultrasound exposure was measured by MTT assay. HepG2 cells (1×10^4) were seeded in each well of 96 well plate. After overnight for incubation, doxorubicin, free-microbubble, doxorubicin loaded albumin nanoparticles or ADMBs were treated to each well. The mass of doxorubicin in each well was equalized to 5 μg. Ultrasound was irradiated with the 1 W/cm^2 of strength and 5% of duty cycle for 30 s. And each well was washed 3 times at the post incubation of 3 h. And cell viability after 24, 48, 72 h was measured at the wavelength of 540 nm by ELIZA reader.

4.6. Animal Model Preparation

The animal research protocols followed in this study were approved by Seoul National University of medicine institutional Animal Care and Use Committee. Twenty-five male New Zealand white rabbits weighing between 3000 and 3500× g were used for our study. The animals were housed in cages with a 12-hour light/dark cycle and ad libitum access to standard rabbit chow diet and water. During all procedures, the animals were anesthetized with intramuscular injections of 5 mg/kg body weight of tiletamine-zolazepam (Zoletil 50; Virbac, Carros, France) and a 2 mg/kg body weight of 2% xylazine hydrochloride (Rompun; Bayer, Seoul, Korea). The VX2 carcinoma strain was maintained in the right hind limb of a carrier rabbit through deep intramuscular injection throughout the study. Briefly, the

left lobe of the animal's liver was exposed surgically and a small piece of tumor tissue (1 mm^3) freshly harvested from the maintained tumor was directly implanted at the subcapsular area of the liver for each rabbit, as described in previous studies [10,37,38]. The tumor was incubated for 17–18 days.

4.7. MR Imaging

All animals underwent MR imaging at day 0 (baseline before treatment) and at day 7 following IA or IV infusion in the groups A to D which received treatment, and the untreated group E. A 3.0-T clinical MR scanner (TimTrio; Siemens Healthcare, Erlangen, Germany) with a knee coil was used to improve SNR and spatial resolution. The animals were fixed on a board in a supine position, and an abdominal bandage was tightly applied to reduce any movement artifact. Axial T_2-weighted turbo spin-echo (repetition time/echo time: 4100 milliseconds/150 milliseconds; echo train length: 14; section thickness: 3 mm; field of view: 130 × 130 mm, matrix: 512 × 358; number of excitations: 2.0) and IVIM Diffusion-weighted image (free breathing single-shot echo-planar imaging pulse sequence with diffusion gradients applied in three orthogonal directions: 2700/63; section thickness: 3 mm; number of sections: 20; number of signals acquired: 8; field of view: 14 × 14 cm^2; matrix: 128 × 128; and four b values (0, 15, 200, and 800 s/mm^2)) were acquired [39]. The images were evaluated using a dedicated workstation for picture archiving and communication system (m-view; Marotech, Seoul, Korea).

4.8. Grouping and Drug Delivery

The study design is summarized in Figure S1. On the basis of the treatment procedure, the animals were divided into five groups having similar tumor volumes: animals receiving an intra-arterial (IA) infusion of ADMB/US (group IA-ADMB/US, n = 6), animals receiving an intravenous (IV) infusion of ADMB/US (group IV-ADMB/US, n = 6), animals receiving an IA infusion of free MB/US (group IA-free MB/US, n = 5), animals receiving an IA infusion of doxorubicin/US (group IA- Dox/US, n = 3), and the untreated control (n = 5). The dose of doxorubicin delivered was 1 mg for all groups except for groups of IA-free MB/US and control. In each group except the control, an infusion pump (Genie plus, Kent Scientific Corporation, Torrington, CT, USA) was used. IA-ADMB/US underwent an IA delivery of ADMB in 3 mL of Iopamidol (Pamiray®, Seoul, Korea) contrast media via the proper hepatic artery. ADMB was administered in group of IV-ADMB/US via the left marginal ear vein. In IA-free MB/US, the microbubble-contrast solution without doxorubicin was administered via the proper hepatic artery under the same conditions as group of IA-ADMB/US. The number of microbubbles in group IA-and IV-ADMB/US and IA-free MB/US were 9×10^8 in 3 mL of Iopamidol, respectively. Group of IA- Dox/US received a mixture of 1 mg of doxorubicin in 3 mL of contrast media via the proper hepatic artery. All the injections for groups were administered at a rate of 1 mL/min for 3 min, using the infusion pump for an accurate and homogenous infusion.

For the IA delivery, an 18-gauge catheter (BD Angiocath Plus with intravenous catheter, Becton-Dickinson, Korea) was inserted into the right central auricular artery for arterial access. To reach the proper hepatic artery, a 2.0-Fr microcatheter (Progreat; Terumo, Tokyo, Japan) was advanced via the catheter into the descending aorta [37,40]. After performing hepatic arteriography to confirm tumor staining and following visualization of the proper hepatic artery, the microcatheter was advanced selectively until the catheter tip was gently positioned at the proximal portion of the proper hepatic artery. The solution prepared for each group was then administered using an infusion pump (Genie plus, Kent Scientific Corporation) through the microcatheter at a rate of 1 mL/min for 3 min, to avoid reflux of the injected complex from the proper hepatic artery [31,37]. To access the systemic venous system, an 18-gauge catheter was inserted into the left marginal ear vein. The pressure line was then connected to catheter, and the solution was infused similarly. When the solution was completely injected, the microcatheter was removed, and the puncture site was compressed carefully to achieve hemostasis.

4.9. Ultrasound and Microbubble Activation

The abdominal hairs of the rabbits were carefully removed just prior to ultrasonography. The ultrasonography was performed by a radiologist both before and during drug administration in groups IA-ADMB/US, IV-ADMB/US, IA- Dox/US and IA-free MB/US using the Aplio 500 ultrasonographic system (Toshiba Medical Systems, Otawara, Japan), with 674 BT with an 8 MHz center frequency convex transducer. A fundamental B-mode ultrasound (a dynamic range of 65; a mechanical index of 1.5; a gain of 90; and a depth of 4 cm) was used to detect the VX2 tumors. After localization and a morphological examination of the tumor, the optimal plane was determined and the skin was marked. The vascular recognition imaging mode with a low MI of 0.06 was used to detect signals generated by the microbubbles. As soon as an IA or IV delivery of the mixture through the infusion pump began, the vascular recognition mode was used to confirm the presence of tumor enhancement. Simultaneously, using a continuous up-and-down sweeping of the probe at the skin marking site, the B-mode was used to irradiate ultrasound energy to the tumor for 3 min (J.H.L). After cessation of infusion, additional ultrasound irradiation was applied for 5 min for activating the microbubbles, resulting in a total of 8 min of bubble activation for each rabbit using the B-mode ultrasound.

4.10. Imaging Analysis

A radiologist who was blind to the information regarding the experimental group evaluated the MR images on a picture archiving and communications system workstation. The T_2-weighted images were used to confirm tumor formation and to measure the maximal longitudinal diameter (length) and maximal transverse diameter (width) of the tumors. Tumor volume was calculated from the measurements determined by MR imaging, using the modified ellipsoidal formula, tumor volume = 1/2(length × width^2) [34,38]. The volume inhibition rate (VIR) of tumor growth was calculated using the formula IR = $(T_c - T_t)/T_c \times 100\%$, where T_c represented the tumor volume of group E (control group) and Tt represents the tumor volume of each treatment group. The value of the Apparent Diffusion Coefficient (ADC) was measured quantitatively using the largest cross-section of the tumor visualized on the ADC map. The changes in the ADC values before and after TACE were evaluated.

4.11. Pathological Analysis

On day 7, all animals were pre-anesthetized and sacrificed with an intravenous injection of xylazine hydrochloride, and the whole tumor was harvested after follow-up imaging. Each tumor was fixed in 10% buffered formalin. The specimen was then embedded in paraffin, cut into 4 μm sections, and the largest cross-section of the tumor was stained with hematoxylin and eosin for basic histopathological examinations. The section was consecutively treated with terminal deoxynucleotidyl transferase dUTP nick end labeling (TUNEL) staining (ApopTag® Peroxidase in situ Apoptosis Detection Kit, Merck KGaA, Darmstadt, Germany) for evaluating tumor viability. After digital images of the histology slides were obtained (Leica Microsystems, Mannheim, Germany), the viable tumor percentage per tumor was calculated using image analysis software (ImageJ, version 1.45 s; National Institutes of Health, Bethesda, MD, USA). In brief, the viable portion of each TUNEL stained image of the whole tumor was measured by threshold intensity. Then, percentage of viable tumor region was calculated by ratio between whole tumor area and viable tumor region. This analysis was performed by an experienced radiologist who was blind to all experimental data, in order to ensure concordance. The estimated viable tumor volume after treatment was calculated as follows: Calculated tumor volume on day 7× viable percentage of the tumor.

4.12. Biochemical Liver Toxicity Assessment

Blood samples for assessing liver toxicity were gathered at baseline and at 1-, 3-, and 7-day intervals after treatment. Liver function tests included the assessment of liver enzymes (aspartate transaminase (AST) and alanine transaminase (ALT)).

4.13. Statistical Analysis

All the data in the study are reported as the mean ± SD. The nonparametric analysis was conducted using the Kruskal-Wallis test to compare the tumor volume, volume inhibition rate, changes in ADC value, tumor viability, and estimated viable tumor volume in the 5 experimental groups. When positive results were encountered, the Mann-Whitney post-hoc test was used for one-to-one group comparisons. Data processing and analysis were performed using the Statistical Package for the Social Sciences version 18.0 (SPSS Inc, IBM, Chicago, IL, USA). A two-sided *p*-value of less than 0.05 indicated that the groups differed significantly in terms of statistical results.

5. Conclusions

In the present study, the ADMB complex was developed for enhancing the therapeutic efficiency of drugs used in hepatocellular carcinoma. This complex can resonate to ultrasound irradiation and induce sonoporation. Using orthotopic experiments, we proved the anticancer effect of this treatment strategy using the VX2 rabbit tumor model. Our strategy is more effective than existing systems because it: (1) has an enhanced loading efficiency; (2) is optimized to resonate at ultrasound frequencies of 2–9 MHz, making it ideal for the treatment of hepatocellular carcinomas, and (3) induces a more effective anticancer effect when combined with an intra-arterial administration route in rabbits. In conclusion, the IA administration of ADMB followed by microbubble activation using a clinical ultrasound probe can take advantage of simultaneously monitoring drug delivery while treating the target, to achieve a better antitumor effect. This novel drug delivery system may help to effectively deliver chemotherapeutics to liver tumors and warrants further investigation for the treatment of advanced liver cancers.

Supplementary Materials: The following are available online at http://www.mdpi.com/2072-6694/11/4/581/s1, Figure S1: Study design of the VX2 rabbit liver tumor treatment protocol, Figure S2: Size distribution of albumin-doxorubicin nanoparticle in DMEM containing 10% fetal bovine serum and 1% antibiotics after 1 day, Figure S3: Heterogenous ADMBs, Figure S4: Cell viability under the various conditions of ultrasound exposure and microbubble, Figure S5:TUNEL assay images of tumor region in (A) IA-ADMBs, (B)IV-ADMBs (C) blend microbubble, Table S1: Percentage of echogenic area depending on the number of manual flashes.

Author Contributions: This study was designed by H.K. and J.W.C.; J.H.L. and H.M. performed in vitro and in vivo experiments with priority; H.H and D.K. analyzed characteristics of nanoparticles, and I.J.L. analyzed in vivo data; H.J.L. and S.-W.H academically supported in vitro and in vivo experiment. All authors were involved in writing manuscript and had final confirmation for submission of this article.

Funding: This research was funded by The Ministry of Health & Welfare, Korea, grant number HI15C2797.

Acknowledgments: This work was supported by the Korean Health Industry Development Institute (KHIDI), funded by the Ministry of Health & Welfare, Korea. (Grant Number: HI15C2797).

Conflicts of Interest: The authors declare no conflict of interest.

References

1. Karanicolas, P.J.; Metrakos, P.; Chan, K.; Asmis, T.; Chen, E.; Kingham, T.P.; Kemeny, N.; Porter, G.; Fields, R.C.; Pingpank, J.; et al. Hepatic arterial infusion pump chemotherapy in the management of colorectal liver metastases: Expert consensus statement. *Curr. Oncol. Toronto Ont.* **2014**, *21*, e129–e136. [CrossRef]
2. Chan, D.L.; Alzahrani, N.A.; Morris, D.L.; Chua, T.C. Systematic review and meta-analysis of hepatic arterial infusion chemotherapy as bridging therapy for colorectal liver metastases. *Surg. Oncol.* **2015**, *24*, 162–171. [CrossRef] [PubMed]
3. Obi, S.; Sato, S.; Kawai, T. Current status of hepatic arterial infusion chemotherapy. *Liver Cancer* **2015**, *4*, 188–199. [CrossRef] [PubMed]
4. Song, M.J. Hepatic artery infusion chemotherapy for advanced hepatocellular carcinoma. *World J. Gastroenterol.* **2015**, *21*, 3843–3849. [CrossRef]
5. Choi, J.W.; Chung, J.W.; Lee, D.H.; Kim, H.C.; Hur, S.; Lee, M.; Jae, H.J. Portal hypertension is associated with poor outcome of transarterial chemoembolization in patients with hepatocellular carcinoma. *Eur. Radiol.* **2018**, *28*, 2184–2193. [CrossRef] [PubMed]

6. Lewandowski, R.J.; Geschwind, J.F.; Liapi, E.; Salem, R. Transcatheter intraarterial therapies: Rationale and overview. *Radiology* **2011**, *259*, 641–657. [CrossRef] [PubMed]
7. Peter, R.G.; Alejandro, F.; Josep, M.L.; Vincenzo, M.; Fabio, P.; Jean-Luc, R.; Peter, S.; Valérie, V. EASL-EORTC clinical practice guidelines: Management of hepatocellular carcinoma. *J. Hepatol.* **2012**, *56*, 908–943.
8. Vogl, T.J.; Zangos, S.; Balzer, J.O.; Nabil, M.; Rao, P.; Eichler, K.; Bechstein, W.O.; Zeuzem, S.; Abdelkader, A. Transarterial chemoembolization (TACE) in hepatocellular carcinoma: Technique, indication and results. *Rofo* **2007**, *179*, 1113–1126. [CrossRef] [PubMed]
9. Liang, B.; Xiong, F.; Wu, H.; Wang, Y.; Dong, X.; Cheng, S.; Feng, G.; Zhou, G.; Xiong, B.; Liang, H.; et al. Effect of transcatheter intraarterial therapies on the distribution of Doxorubicin in liver cancer in a rabbit model. *PLoS ONE* **2013**, *8*, e76388. [CrossRef]
10. Gaba, R.C.; Emmadi, R.; Parvinian, A.; Casadaban, L.C. Correlation of doxorubicin delivery and tumor necrosis after drug-eluting bead transarterial chemoembolization of rabbit VX2 liver tumors. *Radiology* **2016**, *280*, 752–761. [CrossRef]
11. Sheth, R.A.; Hesketh, R.; Kong, D.S.; Wicky, S.; Oklu, R. Barriers to drug delivery in interventional oncology. *J. Vasc. Interv. Radiol.* **2013**, *24*, 1201–1207. [CrossRef] [PubMed]
12. Matsui, Y.; Horikawa, M.; Jahangiri, N.Y.; Kaufman, J.A.; Kolbeck, K.J.; Farsad, K. Baseline tumor lipiodol uptake after transarterial chemoembolization for hepatocellular carcinoma: Identification of a threshold value predicting tumor recurrence. *Radiol. Oncol.* **2017**, *51*, 393–400. [CrossRef]
13. Moghimi, S.M.; Hunter, A.C.; Murray, J.C. Long-circulating and target-specific nanoparticles: Theory to practice. *Pharmacol. Rev.* **2001**, *53*, 283–318.
14. Vancraeynest, D.; Havaux, X.; Pouleur, A.C.; Pasquet, A.; Gerber, B.; Beauloye, C.; Rafter, P.; Bertrand, L.J.L.; Vanoverschelde, J.L. Myocardial delivery of colloid nanoparticles using ultrasound-targeted microbubble destruction. *Eur. Heart J.* **2006**, *27*, 237–245. [CrossRef]
15. Zarnitsyn, V.; Rostad, C.A.; Prausnitz, M.R. Modeling transmembrane transport through cell membrane wounds created by acoustic cavitation. *Biophys. J.* **2008**, *95*, 4124–4138. [CrossRef] [PubMed]
16. Lentacker, I.; Geers, B.; Demeester, J.; De Smedt, S.C.; Sanders, N.N. Design and evaluation of doxorubicin-containing microbubbles for ultrasound-triggered doxorubicin delivery: Cytotoxicity and mechanisms involved. *Mol. Ther.* **2010**, *18*, 101–108. [CrossRef]
17. Yin, T.; Wang, P.; Li, J.; Zheng, R.; Zheng, B.; Cheng, D.; Li, R.; Lai, J.; Shuai, X. Ultrasound-sensitive siRNA-loaded nanobubbles formed by hetero-assembly of polymeric micelles and liposomes and their therapeutic effect in gliomas. *Biomaterials* **2013**, *34*, 4532–4543. [CrossRef] [PubMed]
18. Moon, H.; Yoon, C.; Lee, T.W.; Ha, K.-S.; Chang, J.H.; Song, T.-K.; Kim, K.; Kim, H. Therapeutic ultrasound contrast agents for the enhancement of tumor diagnosis and tumor therapy. *J. Biomed. Nanotechnol.* **2015**, *11*, 1183–1192. [CrossRef]
19. Han, H.; Lee, H.; Kim, K.; Kim, H. Effect of high intensity focused ultrasound (HIFU) in conjunction with a nanomedicines-microbubble complex for enhanced drug delivery. *J. Control. Release* **2017**, *266*, 75–86. [CrossRef] [PubMed]
20. Yan, F.; Li, L.; Deng, Z.; Jin, Q.; Chen, J.; Yang, W.; Yeh, C.-K.; Wu, J.; Shandas, R.; Liu, X. Paclitaxel-liposome–microbubble complexes as ultrasound-triggered therapeutic drug delivery carriers. *J. Control. Release* **2013**, *166*, 246–255. [CrossRef] [PubMed]
21. Mocan, L.; Matea, C.; Tabaran, F.A.; Mosteanu, O.; Pop, T.; Mocan, T.; Lancu, C. Photothermal treatment of liver cancer with albumin-conjugated gold nanoparticles initiates Golgi Apparatus-ER dysfunctionand caspase-3 apoptotic pathway activation by selective targeting of Gp60 receptor. *Int. J. Nanomed.* **2015**, *10*, 5435–5445.
22. Dreis, S.; Rothweiler, F.; Michaelis, M.; Cinatl, J.; Kreuter, J.; Langer, K. Preparation, characterisation and maintenance of drug efficacy of doxorubicin-loaded human serum albumin (HSA) nanoparticles. *Int. J. Pharm.* **2007**, *341*, 207–214. [CrossRef]
23. Weber, C.; Kreuter, J.; Langer, K. Desolvation process and surface characteristics of HSA-nanoparticles. *Int. J. Pharm.* **2000**, *196*, 197–200. [CrossRef]
24. Bae, S.; Ma, K.; Kim, T.H.; Lee, E.S.; Oh, K.T.; Park, E.-S.; Lee, K.C.; Youn, Y.S. Doxorubicin-loaded human serum albumin nanoparticles surface-modified with TNF-related apoptosis-inducing ligand and transferrin for targeting multiple tumor types. *Biomaterials* **2012**, *33*, 1536–1546. [CrossRef]

25. Byeon, H.J.; Lee, S.; Min, S.Y.; Lee, E.S.; Shin, B.S.; Choi, H.-G.; Youn, Y.S. Doxorubicin-loaded nanoparticles consisted of cationic-and mannose-modified-albumins for dual-targeting in brain tumors. *J. Control. Release* **2016**, *225*, 301–313. [CrossRef]
26. Hoff, L.; Sontum, P.C.; Hovem, J.M. Oscillations of polymeric microbubbles: Effect of the encapsulating shell. *J. Acoust. Soc. Am.* **2000**, *107*, 2272–2280. [CrossRef]
27. Khismatullin, D.B. Resonance frequency of microbubbles: Effect of viscosity. *J. Acoust. Soc. Am.* **2004**, *116*, 1463–1473. [CrossRef] [PubMed]
28. Moon, H.; Kang, J.; Sim, C.; Kim, J.; Lee, H.; Chang, J.H.; Kim, H. Multifunctional theranostic contrast agent for photoacoustics- and ultrasound-based tumor diagnosis and ultrasound-stimulated local tumor therapy. *J. Control. Release* **2015**, *218*, 63–71. [CrossRef] [PubMed]
29. Yousefian, B.; Firoozabadi, S.M.; Mokhtari-Dizaji, M. Sonochemotherapy of breast adenocarcinoma: An experimental in vivo model. *J. Ultrasound* **2015**, *18*, 165–171. [CrossRef] [PubMed]
30. Chang, S.; Si, T.; Zhang, S.; Merrick, M.A.; Cohn, D.E.; Xu, R.X. Ultrasound mediated destruction of multifunctional microbubbles for image guided delivery of oxygen and drugs. *Ultrason. Sonochem.* **2016**, *28*, 31–38. [CrossRef]
31. Yoon, Y.I.; Kwon, Y.-S.; Cho, H.-S.; Heo, S.-H.; Park, K.S.; Park, S.G.; Lee, S.-H.; Hwang, S.I.; Kim, Y.I.; Jae, H.J.; et al. Ultrasound-mediated gene and drug delivery using a microbubble-liposome particle system. *Theranostics* **2014**, *4*, 1133–1144. [CrossRef]
32. Gong, Y.; Wang, Z.; Dong, G.; Sun, Y.; Wang, X.; Rong, Y.; Li, M.; Wang, D.; Ran., H. Low-intensity focused ultrasound mediated localized drug delivery for liver tumors in rabbits. *Drug Deliv.* **2016**, *23*, 2280–2289. [CrossRef]
33. Alzaraa, A.; Gravante, G.; Chung, W.Y.; Al-Leswas, D.; Bruno, M.; Dennison, A.R.; Lloyd, D.M. Targeted microbubbles in the experimental and clinical setting. *Am. J. Surg.* **2012**, *204*, 355–366. [CrossRef]
34. Kang, J.; Wu, X.; Wang, Z.; Ran, H.; Xu, C.; Wu, J.; Wang, Z.; Zhang, Y. Antitumor effect of docetaxel-loaded lipid microbubbles combined with ultrasound-targeted microbubble activation on VX2 rabbit liver tumors. *J. Ultrasound Med.* **2010**, *29*, 61–70. [CrossRef]
35. Ma, J.; Du, L.F.; Chen, M.; Wang, H.H.; Xing, L.X.; Jing, L.F.; Li, Y.H. Drug-loaded nano-microcapsules delivery system mediated by ultrasound-targeted microbubble destruction: A promising therapy method. *Biomed. Rep.* **2013**, *1*, 506–510. [CrossRef]
36. Lammertink, B.H.; Bos, C.; Deckers, R.; Storm, G.; Moonen, C.T.; Escoffre, J.M. Sonochemotherapy: From bench to bedside. *Front. Pharmacol.* **2015**, *6*, 138. [CrossRef] [PubMed]
37. Lee, I.J.; Ahn, C.H.; Cha, E.J.; Chung, I.J.; Chung, J.W.; Kim, Y.I. Improved drug targeting to liver tumors after intra-arterial delivery using superparamagnetic iron oxide and iodized oil preclinical study in a rabbit model. *Investig. Radiol.* **2013**, *48*, 826–833. [CrossRef]
38. Bize, P.; Duran, R.; Fuchs, K.; Dormond, O.; Namur, J.; Decosterd, L.A.; Jordan, O.; Doelker, E.; Denys, A. Antitumoral effect of sunitinib-eluting beads in the rabbit VX2 tumor model. *Radiology* **2016**, *280*, 425–435. [CrossRef]
39. Joo, I.; Lee, J.M.; Han, J.K.; Choi, B.I. Intravoxel incoherent motion diffusion-weighted MR imaging for monitoring the therapeutic efficacy of the vascular disrupting agent CKD-516 in rabbit VX2 liver tumors. *Radiology* **2014**, *272*, 417–426. [CrossRef]
40. Jeon, M.J.; Gordon, A.C.; Larson, A.C.; Chung, J.W.; Kim, Y.I.; Kim., D.H. Transcatheter intra-arterial infusion of doxorubicin loaded porous magnetic nano-clusters with iodinated oil for the treatment of liver cancer. *Biomaterials* **2016**, *88*, 25–33. [CrossRef] [PubMed]

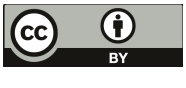

cancers

MDPI

Article

Plant Virus-Like Particle In Situ Vaccine for Intracranial Glioma Immunotherapy

Amber Kerstetter-Fogle [1,†], Sourabh Shukla [2,†], Chao Wang [2], Veronique Beiss [2], Peggy L. R. Harris [1], Andrew E. Sloan [1,3,4,*] and Nicole F. Steinmetz [2,5,6,7,*]

1 Department of Neurological Surgery, Case Western Reserve University, 10900 Euclid Avenue, Cleveland, OH 44106, USA; aek20@case.edu (A.K.-F.); plr2@case.edu (P.L.R.H.)
2 Department of NanoEngineering, University of California San Diego, La Jolla, CA 92093, USA; sshukla@ucsd.edu (S.S.); chw022@eng.ucsd.edu (C.W.); vbeiss@eng.ucsd.edu (V.B.)
3 University Hospitals-Cleveland Medical Center & the Seidman Cancer Center, Case Western Reserve University, 10900 Euclid Avenue, Cleveland, OH 44106, USA
4 Case Comprehensive Cancer Center, Case Western Reserve University, 10900 Euclid Avenue, Cleveland, OH 44106, USA
5 Department of Radiology, University of California San Diego, La Jolla, CA 92093, USA
6 Department of Bioengineering, University of California San Diego, La Jolla, CA 92093, USA
7 Moores Cancer Center, University of California San Diego, La Jolla, CA 92093, USA
* Correspondence: Andrew.Sloan@uhhospitals.org (A.E.S.); nsteinmetz@ucsd.edu (N.F.S.)
† These authors contributed equally to this work.

Received: 12 March 2019; Accepted: 8 April 2019; Published: 10 April 2019

Abstract: Despite aggressive multi-modality treatment with surgery, radiation and chemotherapies, malignant glioma inevitably recurs and has dismal survival rates. Recent progress in immunotherapy has led to a resurgence of interest, and immunotherapies are being investigated for treatment of glioma. However, the unique brain anatomy and a highly immunosuppressive glioma microenvironment pose significant challenges to achieving efficacy. Thus, there is a critical need for assessment of next-generation immunotherapies for glioma. In this study, we have investigated the efficacy of the nanoparticle platform technology based on plant-derived Cowpea mosaic virus like particles (empty CPMV or eCPMV) to instigate a potent immune response against intracranial glioma. CPMV immunotherapy has been shown to efficiently reverse the immunosuppressive tumor microenvironments in pre-clinical murine models of dermal melanoma and metastatic melanoma, metastatic breast cancer, intraperitoneal ovarian cancer and in canine patients with oral melanoma. In the present study, we demonstrate that in situ administration of CPMV immunotherapy in the setting of glioma can effectively recruit unique subset of effector innate and adaptive immune cells to the brain parenchyma while reducing immune suppressive cellular population, leading to regression of intracranial glioma. The in situ CPMV nanoparticle vaccine offers a potent yet safe and localized immunotherapy for intracranial glioma.

Keywords: intracranial glioma; immunotherapy; CPMV; viral nanoparticles; in situ vaccine

1. Introduction

Malignant glioma represents one of the most aggressive forms of cancer, with poor survival rates that have not changed in the past three decades despite advancements in detection and treatment modalities. Even with aggressive treatments including debulking, chemotherapy and radiation the median survival rates for malignant glioma is 12 months, with a five-year relative survival of about 5% [1,2]. Glioma is also associated with high rates of morbidity due to damage to functional regions of the brain. Surgery, radiation and chemotherapy are the mainstay of treatment regimens [3]. Malignant

glioma is incurable surgically due to the infiltrative nature of these tumors and the surgeon's inability to safely resect a "margin" as is typical in most other solid cancers. The blood brain barrier (BBB) also limits the penetration and clinical efficacy of most systemic chemotherapies [4]. Moreover, residual tumor subpopulations resistant to radio- and chemotherapy eventually lead to recurrence and treatment failure [5,6].

Success of immunotherapies for other solid tumors has led to renewed interest in immunotherapy for gliomas [7,8]. However, the unique anatomical and physiological features of the brain are critical barriers for such interventions [9]. The BBB, blood-cerebrospinal fluid (CSF) and blood-meningeal barriers limit the entry of most small molecules as well as immune cells into the brain [10]. Recent advances in the understanding of the central nervous system (CNS) have however, reversed the longstanding theory that the brain is "immunologically privileged" and demonstrated that the BBB in patients with malignant glioma is typically disrupted [11]. It has recently been noted that activated T cells can cross the blood-brain-barrier, however, many of the inflammatory cells recruited to malignant gliomas contribute to the highly immunosuppressive tumor microenvironment (TME). The glioma TME is characterized by the prevalence of M2 polarized resident macrophages and microglial cells, myeloid-derived suppressor cells (MDSCs), and a significantly smaller population of antigen presenting cells (APCs) including exhausted dendritic cells (DCs) and T cells. The expression of vascular endothelial growth factor (VEGF), tumor growth factor-β (TGF-β), prostaglandin E2 (PGE2) and interleukin-10 (IL-10) further impair T cell proliferation and activation in response to pro-inflammatory signals, and downregulate expression of major histocompatibility complexes (MHCs) and DC maturation [12]. Malignant glioma also has a considerable infiltration of regulatory T cells (Tregs), which can further suppress proliferation and activation of tumor infiltrating T lymphocytes [13]. Additionally, glioma stem cells (GSCs) and glioma initiating cells (GIC), which drive glioma growth and invasion, contribute to the immunosuppressive tumor microenvironment by recruiting tumor-supportive macrophages and microglia, expressing immunosuppressive cytokines, and down regulating Toll-like receptors (TLRs) thereby avoiding immune-mediated rejection [14].

Several immunotherapeutic approaches targeting gliomas are currently under pre-clinical development and clinical evaluation. These include vaccines, adoptive T cell therapies, monoclonal antibodies, checkpoint inhibitors and oncolytic virotherapies [8]. Immune escape with loss of targeted antigens and glioma heterogeneity pose significant challenges for vaccines based on single or multiple antigens, respectively [15]. Additionally, lack of a robust population of resident APCs in the brain contributes to the reduced efficacy of glioma vaccines [12]. DC vaccines can overcome this hurdle by reintroducing the patient's own antigen pulsed DCs, however besides the technological challenges, this approach suffers from low efficacy attributed to poor migration of DCs to secondary lymphoid tissues for T cell activation [16]. Adoptive cell therapies (ACT) [17] that can circumvent DC dependence have proven to be challenging in malignant gliomas due to their low densities within tumors, tumor mediated exhaustion, and inefficient delivery through intravenous administrations [8,9]. Similarly, restrictive delivery through the BBB and lack of effector cells or cytotoxic T cells (CTLs) renders antibody drug conjugates and checkpoint inhibitors less effective as brain tumor treatments [18,19].

Oncolytic virotherapy utilizing genetically engineered mammalian viruses to selectively invade glioma cells and express cytotoxic proteins has emerged as a potent therapeutic strategy for glioma. Several oncolytic viruses have been studied including adenoviral vector Ad-RTS-hIL-12 that expresses IL12 in the presence of an orally administered ligand, which can efficiently cross the BBB to reach the tumor bed [20]. Similarly, engineered poliovirus PVSRIPO [21], oncolytic herpes simplex virus type-1 (oHSV-1) [22], measles virus [23] and Zika virus [24] have been shown to selectively replicate in and lyse CNS tumor cells or tumor stem cells. While highly effective, applicability of virotherapy to the brain remains under investigation, as uncontrolled inflammatory responses posing a threat to healthy brain cells and delivery to the brain remain major hurdles [9].

Here, we present data from an in situ vaccine immunotherapy against malignant glioma utilizing the plant virus like particles (VLPs) derived from Cowpea mosaic virus (CPMV). The CPMV VLPs

lacks their nucleic acids and are referred to as empty CPMV (eCPMV). Recently, we have shown that eCPMV (as well as CPMV) can induce anti-tumor responses in several murine models of cancers when introduced into the tumor microenvironment (TME) as an in situ vaccine [25]. Results from canine trials have also demonstrated efficacy in large animals with spontaneous melanoma [26]. Mechanistic insights have indicated that CPMV stimulates an anti-tumor response through recruitment of innate cells including monocytes, tumor infiltrating neutrophils (TINs) and natural killer (NK) cells, which exert cancer cell toxicity resulting in the release of tumor antigens. Furthermore, through elevated influx of APCs into the treated tumors, the CPMV in situ vaccine also facilitates priming of an adaptive anti-tumor response with $CD4^+/CD8^+$ cells, therefore leading to systemic efficacy and immunological memory [25]. Thus, CPMV activates the innate immune response, recalibrating the cancer–immunity cycle to eliminate cancer cells via the adaptive immune system. Unlike the oncolytic viruses, plant viruses are non-infectious and non-replicative in mammalian cells and the immune modulation is driven by the unique proteinaceous architecture of the viral capsid. While previously validated in various mouse model of dermal and metastatic melanoma, lung metastasis from breast cancer, and intraperitoneal ovarian cancer, in the present study we set out to assess the efficacy of eCPMV in situ vaccine against intracranial glioma using the syngeneic GL261 glioma mouse model.

2. Results

CPMV VLPs were produced by co-expression of the precursor to the L and S coat proteins (VP60) and the viral proteinase (24K) using *N. benthamiana* plants and agroinfiltration as previously described (Figure 1A) [27]. Typical purification yields are around 0.5 mg of VLP from each gram of leaf tissue. The eCPMV VLP is a 30 nm-sized icosahedral particle devoid of nucleic acid and consists of 60 copies each of a small (S) and large (L) coat protein subunits (Figure 1B) [28]. Post-purification quality assurance of the self-assembled VLP was performed using TEM imaging and size exclusion chromatography (SEC) confirming the presence of intact 30 nm particles with the typical elution profiles from the Superose column; the absorbance ratio of A260:280 of 0.67 indicates that particles devoid of RNA were produced (in contrast RNA-containing wild-type CPMV has a A260:280 of 1.8 [29] (Figure 1C,D). For imaging and tracking studies, *N*-hydroxysuccinimide chemistry was used to conjugate the NHS esters of sulfo-Cy5 fluorophores to eCPMV capsid via the exposed lysine residues [30] (Figure 1E). SDS-gel electrophoresis was used to confirm fluorescent tagging of the viral coat proteins (Figure 1F). Unmodified eCPMV is represented by two distinct bands corresponding to the ~24 kDa small coat protein (S-CP) subunit and the ~42 kDa large coat protein subunit (L-CP). In eCPMV-Cy5 particles both these protein bands appear fluorescent when excited at 632 nm, indicating successful dye conjugation. The ratio of Cy5 dyes per eCPMV particle were quantified by UV/Vis spectroscopy and using the particles' specific extinction coefficient ε_{eCPMV} of 1.28 mL mg^{-1} cm^{-1} at 280 nm and the molar extinction coefficient ε_{Cy5} of 271,000 at 660 nm. The reaction yielded ~50 dyes per eCPMV.

To assess the potential for development of CPMV immunotherapy for treatment of glioma, we first determined the feasibility of delivering VLP immunotherapy through intracranial injections into the brain using fluorescently labeled eCPMV-Cy5 VLPs. All mouse studies were performed in compliance with the Institutional Animal Care and Use Committee of Case Western Reserve University.

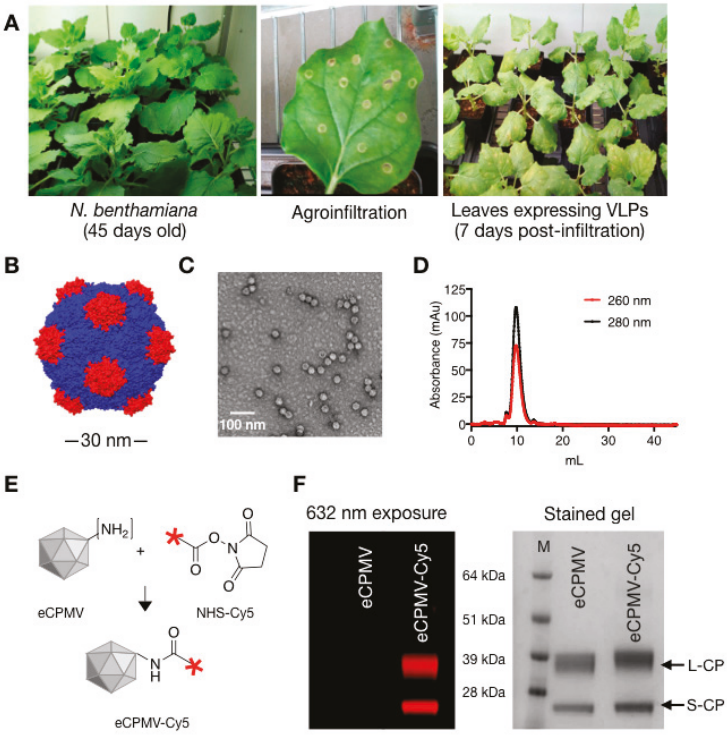

Figure 1. eCPMV propagation, purification and characterization. (**A**) eCPMV VLPs were propagated using *N. benthamiana* plants; leaves were infiltrated when plants were 45 days old. (**B**) Structure of eCPMV, chimera image created using PDB file 1NY7 (CPMV) (**C**,**D**) Purified eCPMV particles were characterized for structural integrity using TEM and size exclusion chromatography (FPLC). (**E**) One-step-NHS chemistry was used to bioconjugate Cy5 dyes to the lysine residues on eCPMV CPs. (**F**) SDS-gel electrophoresis was used to confirm conjugation of Cy5 dyes to eCPMV coat proteins: the fluorescence derived from conjugated Cy5 is detected by exposing the gel to 632 nm excitation; the small (S) and large (L) protein are detected after protein staining (GelCode™ Blue Safe protein stain) and visualization under white light.

Following the intracranial injection, presence and retention of VLPs in brain was detected using ex vivo Maestro fluorescence imaging (Figure 2A). At 24 h post injection eCPMV can be readily detected at and around the injection site as evident by a strong fluorescent signal, whereas at day 7 the weak signal intensity suggested degradation and loss of proteinaceous VLPs from the brain microenvironment (Figure 2A). This observation is consistent with clearance of viral nanoparticles from other tissues [31]. During this period, mice were monitored for any signs of stress and discomfort resulting from particle administration and no apparent adverse effects were observed. We also evaluated intravenous route for eCPMV VLP administration as a mean of delivery immunotherapy to the brain. However, the VLPs were sequestered in the liver and spleen by the mononuclear phagocyte system (MPS) system with minimal doses reaching other tissues, including the brain. Therefore, we selected the intracranial injection as the mode of delivery for our studies. Based on the weeklong retention of eCPMV in brain, we set weekly intratumoral administration schedules for glioma immunotherapy.

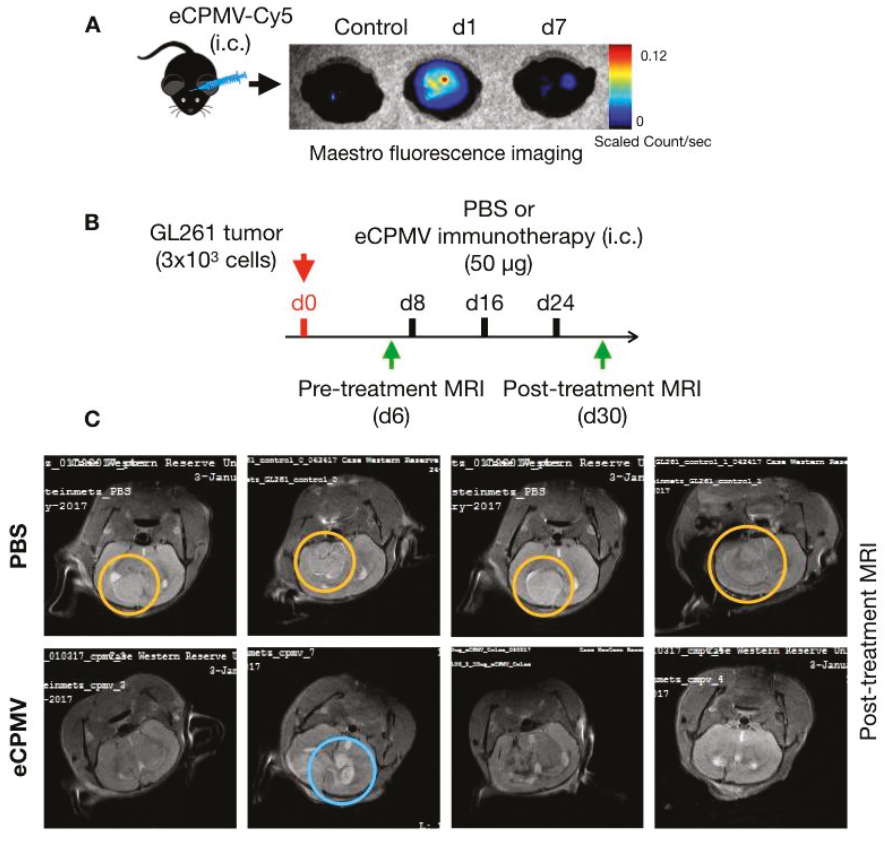

Figure 2. Intracranial eCPMV injection and immunotherapy. (**A**) eCPMV retention in brain following intracranial administration was determined using eCPMV-Cy5 and Maestro fluorescence imaging system. (**B**) For in situ immunotherapy, C57BL6 mice ($n = 4$) were inoculated with 3×10^3 GL261 cells intracranially and administered PBS or eCPMV via intracranial injections on days 8, 16 and 24. (**C**) On day 30, MRI imaging (7 Tesla) was used to visualize glioma post-treatment. Yellow circles highlight solid tumors in PBS administered mice, whereas blue circle highlights the residual tumor and/or edema in one of the mice in the eCPMV treatment group.

Next, we assessed the immunotherapeutic potential of the eCPMV in situ vaccine in a mouse model of GL261 glioma. This syngeneic model based on immunocompetent mice is one of the most widely used animal models for gliomas [32]. C57BL6 mice were challenged with syngeneic GL261 tumors via intracranial injections of 3×10^3 cells in 3 µL of PBS. Pre-treatment MRI was performed on day 6 post-tumor inoculations to establish onset of tumor growth; then mice were randomly assigned to treatment groups (Figure 2B). eCPMV immunotherapy at a dose of 50 µg VLP in 3 µL sterilized PBS was administered via weekly intracranial injections starting on day 8 post tumor inoculation. The control group received sterile PBS. Mice were observed for signs associated with glioma progression including weight loss, irregular breathing, hunched back and decreased activity; upon appearance of these signs, mice were euthanized. Following three intracranial injections, a second MRI was performed on day 30 post-tumor inoculations to assess treatment efficacy (Figure 2B).

Representative brain MRI images from PBS or eCPMV treated mice highlighted the therapeutic effects of the eCPMV in situ vaccination. Untreated mice developed large intracranial tumors by day thirty following the tumor inoculation (Figure 2C, upper panel; area marked with orange circle). In some mice, peritumoral edema was also observed as bright spots at the tumor edges. These mice also displayed the characteristic neurological and physiological symptoms associated with glioma including hunched posture, lack of activity and labored breathing. In stark contrast, eCPMV-treated mice showed absence of tumors or appeared to have regressed intracranial tumors (Figure 2C, lower panel) suggesting a therapeutic effect of the intratumoral eCPMV administrations. Presence of cerebral edema (blue circle) indicates stimulation of an inflammatory response to the in situ eCPMV.

To validate the underlying immunology of the eCPMV in situ vaccine, we used flow cytometry and IHC analysis. For flow cytometry, brains were harvested from immunized mice 24 hours post single or three weekly eCPMV administrations (Figure 3A). The single cell suspension from brains that received a single dose of CPMV VLPs were used for characterization of the innate immune response (Figure 3A) whereas tissues and cells derived from animals that received multiple eCPMV doses were used to characterize the adaptive immune response (Figure 3B). Flow cytometry analysis after a single intracranial injection indicates enhanced immune cells infiltration into the brain of mice receiving eCPMV in situ vaccine (black bars) over tumor bearing mice receiving PBS (white bars). Specifically, eCPMV treated mice showed significantly elevated levels of leukocytes ($CD45^+$ cells), $CD11b^+CD11c^+$ DCs, $CD11b^{int\text{-}low}NK1.1^+$ NK cells, $CD11b^+Ly6G^-$ monocytes, and $CD11b^+Ly6G^+MHCII^+CD86^+$ TINs compared with PBS-treated tumor bearing mice. Several other immune cells including macrophages, granulocytes, activated neutrophils and G-MDSCs showed an increasing trend, but were not statistically significantly different from PBS treated mice.

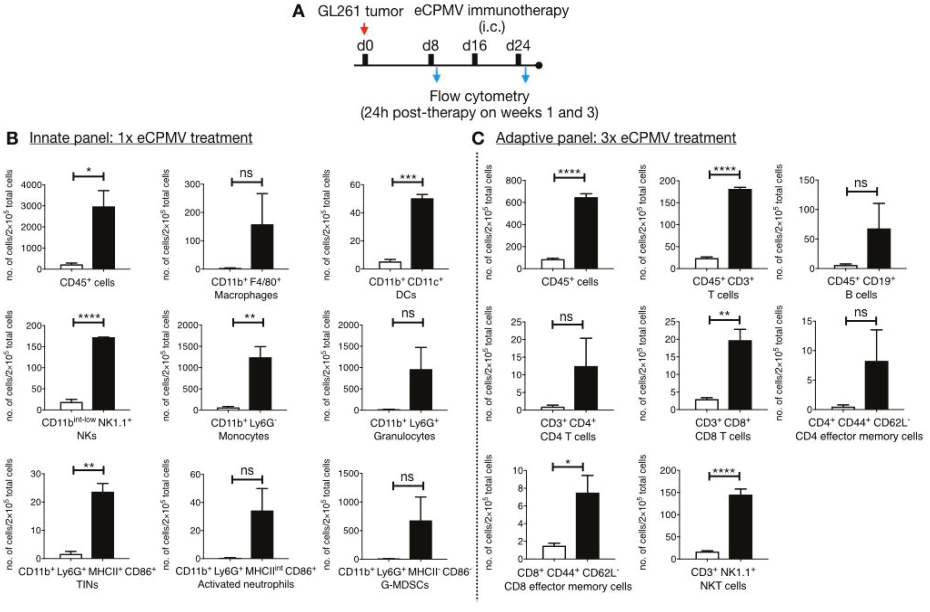

Figure 3. Flow cytometry analysis to characterize immune infiltration in the brain parenchyma. (**A**) GL261 glioma bearing C57BL6 mice ($n = 3$) were treated 1× or 3× with eCPMV immunotherapy and the brain tissues were harvested 24 h following the last treatments to determine innate (**B**) and adaptive (**C**) immune cell infiltrates in eCPMV treated (black bars) or untreated (white bars) GL261 bearing brain tissues. Error bars represent SEM. Statistical comparisons were performed using unpaired *t*-test (**** $p < 0.0001$, *** $p < 0.001$, ** $p < 0.01$ and * $p < 0.05$).

The innate response to the in situ vaccine is consistent with our earlier studies using mouse models of melanoma [33]. Here, we observed monocytes being recruited; in particular elevated levels of $CD11b^+Ly6G^-$ monocytes in eCPMV-treated brain could suggest local inflammation in response to the intracranial injection of the VLPs. Further, both monocytic $CD11b^+CD11c^+$ DCs and $CD11b^+F4/80^+$ macrophages were elevated in response to eCPMV immunotherapy. Additionally, eCPMV treatment also resulted in significant influx of the $CD11b^+Ly6G^+MHCII^+CD86^+$ tumor infiltrating neutrophils (TINs) that also displayed high expression levels of CD86 and MHCII molecules (Figure 3B).

Next, brain tissues harvested from mice following three treatments of eCPMV or PBS were analyzed by flow cytometry to evaluate the role of adaptive immunity (Figure 3C). Unlike the innate response, tumor-specific $CD8^+$ and $CD4^+$ T cells proliferate in an antigen-specific manner following stimulation by APCs. The potent innate response generated by the eCPMV in situ vaccine indeed led to significant recruitment of $CD3^+$ T cells. Specifically, $CD8^+$ T cell levels were significantly higher in eCPMV-treated mice over PBS-treated tumor-bearing mice. The increase in the $CD4^+$ T cell population was not significantly different comparing eCPMV-vs PBS-treated tumor-bearing mice. A similar trend was observed for the effector memory T cells (EMTs), where a significant increase in the levels of $CD8^+$ $CD44^+$ $CD62L^-$ EMTs and a non-significant increase in the levels of $CD4^+CD44^+CD62L^-$ EMTs was noted comparing eCPMV- vs. PBS-treated animals. Interestingly, eCPMV treated mice also demonstrated significantly enhanced levels of $CD3^+NK1.1^+$ NKT cells. Overall, these results demonstrate efficient recruitment of both innate and adaptive immune cells to the brain tissue as a result of the eCPMV in situ vaccination, indicating that the anti-tumor response is indeed immune-mediated.

Finally, we used immunohistochemistry (IHC) to characterize the changing cellular landscape of the innate immune system within the glioma itself. To gauge the effects of single or multiple doses of eCPMV, brains from tumor-bearing mice were harvested 24 h after either a single dose or three doses (Figure 4A). Fixed tissue sections were then stained for immune cell markers IBA-1, CD68, CD45 and FoxP3 and cellular densities were quantified using Zeiss image analysis program (Axiovision Rel 4.5, Zeiss, Thornwood, NY, USA) (Figure 4B). IHC staining revealed significantly elevated levels of $CD45^+$ leucocytes in the tumor tissue following the eCPMV treatment, which mirrors the flow cytometry data indicating an overall increase in the $CD45^+$ cells in the brain parenchyma. When compared to a single administration, the overall $CD45^+$ optical density doubled following three doses of eCPMV in situ vaccine; this may indicate engagement of adaptive cell response that results in an influx of effector cells including T lymphocytes and NKT cells. Further, we quantified the changes in IBA-1 and CD68 expression to evaluate microglia/macrophage (IBA-1/CD68) invasion into the tumors. As observed in IHC panel (Figure 4B), eCPMV administration resulted in increased intratumoral expression levels of both IBA-1 and CD68. We also compared the population of Tregs in glioma bearing mice with and without CPMV immunotherapy by staining for FoxP3 expression, which is a regulatory T cells specific transcription factor [34]. Our results indicate abundance of $FoxP3^+$ Tregs in non-treated glioma, whereas a significant reduction in intratumoral $FoxP3^+$ Tregs is observed with CPMV immunotherapy (Figure 4B).

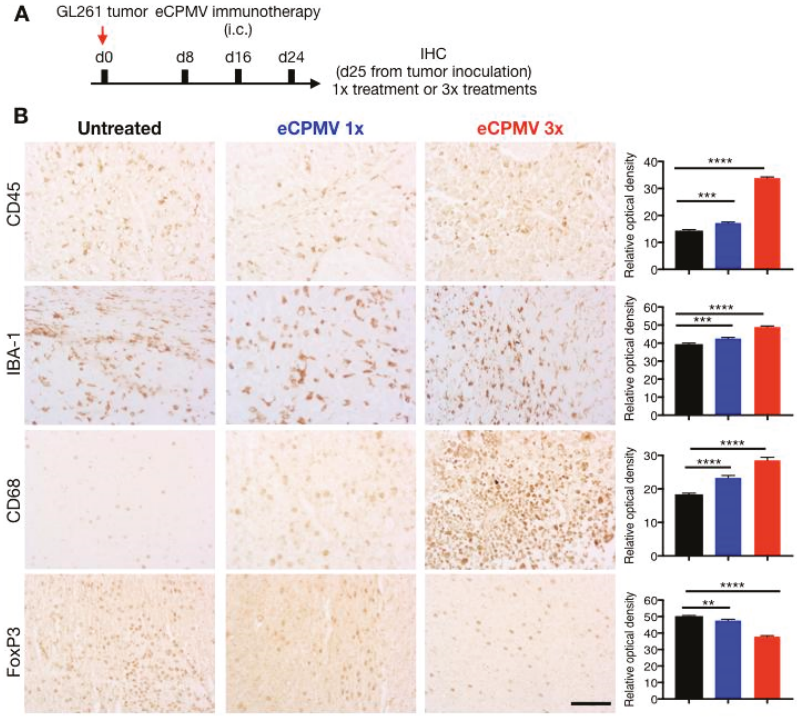

Figure 4. Immunohistochemical analysis. (**A**) Brain tissues from GL261 glioma bearing mice ($n = 3$) were harvested on day 25 from tumor inoculation after 24 h of receiving 1× eCPMV treatment or the last dose of 3× eCPMV treatment. (**B**) Tumor sections (6 μm thick) were stained with α-CD45 antibody, α-IBA-1 antibody, α-CD68 antibody and α-FoxP3 antibody. The scale bar is 50 μm in all images. Quantitative analysis was performed using Zeiss software to determine relative optical densities of the stained sections. Error bars represent SEM. Statistical analysis was performed using ordinary one-way ANOVA (Tukey's multiple comparison test (**** $p < 0.0001$, *** $p < 0.001$, ** $p < 0.01$).

3. Discussion

We and others have demonstrated that intratumorally administered VLPs can modulate the local tumor microenvironment via recruitment and activation of immune cells [25,35]. The immunomodulatory properties of VLPs arise from the repetitive architectures of the coat proteins that present potent pathogen-associated molecular patterns (PAMPs) [36]. VLPs are recognized by TLRs [37] and TLR signaling can stimulate innate as well as adaptive immune responses. Previously, GL261 cells have also been shown to express TLR2, TLR3 and TLR4, and TLR ligands have been used as treatments against established glioma [38,39]. Here we show that intratumoral administration of the eCPMV VLP generates an antitumor immune response leading to immunological regression of glioma. In some cases, inflammatory responses were also noted. The formation of such cerebral edema induced by inflammatory response has been previously observed following glioma radiotherapy [40] and oncolytic viral therapies [41]. The risk management of the immune responses in the brain as part of the immunotherapy will require future detailed investigation.

Profiling of the innate and adaptive immune cells following the in situ vaccination provides insight into the mechanism. Consistent with our previous studies in other tumor models, the innate immune cell cohort consists of monocytic DCs and macrophages and TINs. TINs have been identified as the primary modulators of the anti-tumor innate responses. Direct physical contact between neutrophils and cancer cells has been shown as a pre-requisite for cancer cell cytotoxicity. The cytotoxicity is attributed to

neutrophil-secreted H_2O_2 that induces influx of Ca^{2+} in cancer cells leading to apoptosis [42] or to neutrophil Fas ligand-cancer cell Fas receptor interactions, which stalls tumor cell cycle progression from G1 to S phase [43]. In addition to direct cytotoxicity, neutrophils also mediate anti-tumor immune response through recruitment of effector immune cells. Pro-inflammatory N1 neutrophils promote $CD8^+$ T recruitment and activation by secreting chemokines (e.g., CCL3, CXCL9, and CXCL10) and cytokines (e.g., IL-12, TNF-α, GM-CSF) that attract T cells [44]. Moreover, neutrophils can also coordinate adaptive immune responses through interactions with dendritic cells [44].

Another significant population of infiltrating innate immune cells was identified as NK cells. NK cells are among the most potent cytotoxic cells against tumor cells and high levels of tumor infiltrating NK cells are associated with a favorable tumor outcome in patients [45]. Transformed cells with reduced or absent MHC-I expression are therefore NK cells targets. Additionally, cellular stress and DNA damage results in upregulation of NK cell activation ligands on tumors. NK cells can kill tumor cells by releasing cytolytic granules containing perforin and granzymes, which leads to cancer cell apoptosis; NK cells also induce death receptor-mediated apoptosis [45,46]. Furthermore, activated NK cells secrete IFN-γ that can induce $CD8^+$ T cells to CTL transformation and promote $CD4^+$ T cells towards Th1 response, which promotes CTL differentiation. NK cells also promote recruitment of conventional DC-type 1 (cDCs) in the tumor microenvironment via secreted CCL5 and XCL1 cytokines [47]. cDCs are particularly efficient in carrying tumor antigens and cross presenting them to CD8 T cells to stimulate an adaptive immune response [48]. Therefore, tumor antigens released from cells lysed by activated NK cells can be taken up by APCs including the DCs and TINs described above, which subsequently can contribute towards development of an adaptive immune response mediated by tumor-specific CTLs [45].

Recent advances in the understanding of the structural and functional aspects of CNS lymphatic vessels have revealed the mechanism of CNS immune surveillance, including the entrance and exit of immune cells [11]. Functional studies of such meningeal lymphatic vessels have revealed their role in transporting $CD11c^+$ cells, $B220^+$ cells and T cells. Additionally, these meningeal lymphatic vessels have been shown connected to deep cervical lymph nodes, which are known to elicit immune responses to antigens from cerebrospinal fluids [49,50]. Thus, APCs carrying tumor antigens from lysed cells following eCPMV treatment are likely transported to the draining deep cervical lymph nodes and present the tumor antigens to naïve T cells resulting in expansion of tumor antigen specific adaptive immune response.

Indeed, our data indicate engagement of cells of the adaptive immune system. We note a significant increase in $CD8^+$ T cells levels, effector memory CD8 T cells and NKT cells. NKTs are a unique lineage of innate T cells that express markers for T lymphocytes as well as NK cells. These cells can kill tumor cells by direct cytolysis using perforin and granzyme B, but also by modulating the recruitment of other effector immune including T cells, B cells, NK cells and DCs [51]. Thus, NKT cells may also play a key role in linking the innate and adaptive immune response against tumors. NKT cells can also reverse the immunosuppression mediated by MDSCs and tumor associated macrophages [52]. In the case of glioma that display highly immunosuppressive tumor microenvironment, the role of NKT as boosters of adaptive immune response and suppressor of immune regulation is therefore considered critical.

Furthermore, IHC highlighted the changing immunological landscape following in situ vaccination with eCPMV. Our data indicate significantly elevated levels of $CD45^+$ cells in the brain paranchyma following CPMV administration, which corroborates earlier studies in melanoma models where intratumoral administrations of CPMV lead to massive influx of effector immune cells [33]. In particular, we observed enhanced influx of IBA-1/$CD68^+$ microglia/macrophage cells. Microglia are the resident innate immune cells of CNS that participate in immune surveillance and host defense against infectious agents. Together with infiltrating bone marrow-derived macrophages, microglia functions to restore homeostasis in brain parenchyma to counter inflammatory responses including malignancies. The dual role of microglia/macrophages in gliomas has been extensively studied. Under immunosuppressive TME, microglia/macrophages appear to promote glioma proliferation and invasiveness [53,54].

However, microglia-secreted factors and TLR agonists have been shown to simulate apoptosis in glioma cells [55,56]. Also, while genetic ablation of monocytoid cells has been shown to promote glioma, drug mediated activation of monocytoid cells in brain results in microglia-mediated reduction of brain tumor initiating cells [57]. This functional duality has been attributed to the polarization of microglia to tumor suppressive M1 and tumor supportive M2 cells [58,59]. M1 cells are activated by type I cytokines such as interferon-γ (IFN-γ) and tumor necrosis factor-α (TNF-α) and other immunostimulants such as lipopolysaccharide (LPS), and lipoproteins. The activated M1 polarized microglia have been shown to possess antigen-presenting capabilities to Th1 cells leading to anti-tumor CTL activity [58]. CPMV has been shown to stimulate IFN-γ and TNF-α in the TME in our previous studies, and therefore is likely to influence the glioma TME similarly. These results are consistent with elevated staining observed in glioma treated with LPS or myeloid cell activation agents that also lead to increased iNOS expression (M1 phenotype) and a significant reduction in tumor volumes [57].

Tumor-mediated immune suppression is a critical barrier to glioma immunotherapies. In addition to M2 polarized microglia/macrophages described above, regulatory T cells (Tregs) accumulated in the TME contribute to glioblastoma-mediated immune suppression [60]. In high grade brain tumors, Tregs suppress activation, proliferation and cytokine production of $CD4^+$/$CD8^+$ T cells via secreted cytokines such as TGF-B and IL-10 or via cell-to cell contact mediated by the constitutively expressed CTLA-4 and PD-L1 checkpoints [61]. Thus, expansion of Tregs is associated with decreased efficacy of immunotherapies and therapeutic targeting of Tregs has been used to improve survival in glioma studies [62,63]. The significant reduction in intratumoral $FoxP3^+$ Tregs following CPMV immunotherapy mirrors the effects of intratumoral IL-12^+ CTLA-4 combination therapy which enhanced infiltration of CD4/CD8 cells while significantly reducing the $FoxP3^+$ Tregs [64]. Pro-inflammatory cytokines including IL-12 are key component of eCPMV-mediated immune response and likely contribute to reduced Tregs population in the glioma TME [25,33]. Overall, eCPMV immunotherapy leads to an effective reversal of the immunosuppressive tumor microenvironment. In conjugation with the elevated $CD8^+$ T cells and NKT cells infiltration and enhanced activation of resident microglia, this immunomodulation renders the glioma TME conducive for progression of an anti-tumor immune response.

4. Materials and Methods

4.1. Production of eCPMV VLPs

eCPMV VLP was produced as described elsewhere [25,27]. Briefly, Agrobacterium LBA4404 cultures harboring the binary plasmid pEAQexpress-VP60-24K that encodes the coat protein precursor VP60 and viral proteinase 24K, were introduced into *N. benthamiana* leaves using syringe-infiltration. Infiltrated tissue was harvested 6 days post-infiltration, homogenized in 0.1 M sodium phosphate buffer (pH 7.0) and purified using established protocols [27]. VLP concentration was determined by UV/vis spectroscopy ($\varepsilon_{280\,nm}$ = 1.28 mg^{-1} mL cm^{-1}). Particle integrity was examined using transmission electron microscopy (TEM) on a FEI Technai20 and by size exclusion chromatography using a Superose 6 column on the AKTA Explorer chromatography system (GE Healthcare, Chicago, IL, USA).

4.2. Synthesis and Characterization of eCPMV-Cy5 Particles

eCPMV VLPs were covalently modified with Cy5 using N-hydroxysuccinimide-activated ester targeting surface exposed lysine residues on the capsid. Briefly, 3000 molar excess of Sulfo-Cyanine5 NHS ester (NHS-Sulfo Cy5) were reacted with eCPMV in 0.1M KP buffer at final protein concentration of 2 mg/mL in presence of 10% (*v*/*v*) DMSO. Following overnight reactions, eCPMV-Cy5 was purified from unconjugated reactants over a 40% (*w*/*v*) sucrose cushion at 160,000× *g* for 3 h and resuspended in sterile KP buffer. UV spectroscopy was used to determine the eCPMV-Cy5 concentrations and to determine Cy5/VLPs ratios using molar extinction coefficient ε_{eCPMV} of 1.28 mL mg^{-1} cm^{-1} at 280 nm and sulfo-Cy5-specific molar extinction coefficient ε_{Cy5} of 271,000 at 660 nm.

The conjugation of fluorophore on eCPMV was determined using SDS-gel electrophoresis. Briefly, 10 μg of unmodified eCPMV and eCPMV-Cy5 mixed with SDS running buffer and heated at 100 °C for 5 min were loaded on pre-cast NuPAGE™ 4–12% Bis-Tris proteins gels (ThermoFisher Scientific, Hampton, NH, USA) and electrophoresis was performed for 40 min at 200 V. Fluorescent bands representing Cy5 modified eCPMV coat proteins were visualized on an AlphaImage gel documentation system (Protein simple) using a 632 nm excitation. The gels were then stained using GelCode™ Blue Safe protein stain (ThermoFisher Scientific).

4.3. Cell Line

GL261 cell line was obtained from the Tumor Repository at National Cancer Institute (NCI) and maintained in suspension culture prior to engraftment intracranially. Briefly, cells were grown in a suspension flask (CytoOne, CC-672-4175, USA Scientific, Oscala, FL, USA) and kept in a 5% CO_2 37 °C humidified incubator in serum-free neuro medium (MACs neuro medium with Neurobrew-21 (130-093-570 and 130-097-263 respectively, Miltenyi Biotec Inc., Auburn, CA, USA), 20 ng/mL EGF (AF-100-15, Peprotech, Rocky Hill, NJ, USA) and 20 ng/mL FGF (100-18B, Peprotech) with 1% (*w*/*v*) pencillin-streptomycin (15140122, Gibco Invitrogen, Waltham, MA, USA) and 1% (*w*/*v*) L-glutamine (25030081, Gibco Invitrogen). Cultured cells were pelleted and re-suspended in media to 3×10^3 cells per 3 μL in growth medium and placed on ice prior to implantation.

4.4. Tumor Inoculation

All mouse studies were performed in compliance with the Institutional Animal Care and Use Committee of Case Western Reserve University (Assurance number is A-3145-01, valid until 20 April 2019). Immunocompetent animals (C57BL6, Jackson Labs, Bar Harbor, MA, USA), 4–6 weeks of age, males and females, were utilized for intracranial implantation of GL261 cells ($n = 4$). Briefly, animals were placed under anesthesia (inhaled isoflurane). Once fully anesthetized, lidocaine was applied and a small incision was made through the scalp and the bregma was identified. A small 25-gauge burr hole was made 2 mm caudal and 3 mm to the right of bregma. A 22-gauge Hamilton syringe (88011, ThermoFisher Scientific) was inserted and placed 3 mm below the skull and then retracted 0.5 mm to establish a pocket for implantation of cells. Cells, 3×10^3 cells per 3 μL PBS, were slowly injected into the right frontal lobe and the Hamilton syringe was held in place for 3 min post injection to prevent reflux. The burr hole was sealed with bone wax and the incision was closed with surgical glue and non-dissolvable sutures. Animals were given analgesia and maintained on a heating pad until recovery. Control and CPMV treated animals were placed under anesthesia weekly and given intratumoral injections of either vehicle or CPMV (50 μg) in 3 μL dosages. Injections were made within the same burr hole as done with inoculation of tumor. This was performed weekly for a total of 3 weeks.

Care and housing of the animals was provided by the University Animal Resource Center following IACUC oversight. The facility follows recommendations from the Guide for the Care and Use of Laboratory Animals of the National Institutes of Health. Mice were maintained in microisolator cages and exposed to 12 h light/12 h darkness cycles with standard food and water *ad libitum*. Mice were weighed weekly and checked daily for tumor growth symptoms according to the IACUC tumor burden policy.

4.5. Small Animal MRI

MRI imaging was performed prior to start of immunotherapy at day 6 from tumor inoculation and post-treatment on day 30. The in vivo MRI studies were performed on the same Biospec 7 T scanner equipped with a 3 cm birdcage ^{1}H coil (Bruker, Erlangen, Germany). During MR imaging, mice were anesthetized by isoflurane, respiration rate was maintained at 70–80/min. After reaching surgical plane of anesthesia, the mouse was placed on an animal holder with its nose inserted into a nose cone. A head restrainer was utilized to prevent potential motion. An animal monitoring system was in place to monitor body temperature and respiration/cardiac cycle. After securing the animal and monitoring the components, the animal was positioned at the center of the RF coil. The RF coil was placed into the

magnet. We conducted shimming process using a single pulse sequence and the RF pulse was maximized to keep the pulse length constant and a long enough recycle delay to conduct an image. A fast image acquisition was used to acquire sample images to determine animal placement and imaging setup.

4.6. Flow Cytometry

The following antibodies and reagents were used for flow cytometry, all obtained from BioLegend (San Diego, CA, USA): Pacific Blue anti-mouse CD45 (clone 30-F11), FITC anti-mouse CD11b (clone M1/70), APC anti-mouse CD11c (clone N418), PE anti-mouse F4/80 (clone BM8), Brilliant Violet 605 anti-mouse CD86 (clone GL-1), Alexa Fluro 700 anti-mouse I-A/I-E (clone M5/114.15.2), APC/Cy7 anti-mouse CD3 (clone 145-2C11), FITC anti-mouse CD4 (clone Gk1.5), APC anti-mouse CD8 (clone 53-6.7), Alexa Fluor 700 anti-mouse CD25 (clone PC61), PE anti-mouse FOXP3 (clone MF-14), Zombie yellow fixable viability kit, and anti-mouse CD16/32 (clone 93). GL261 Glioma bearing mice (n = 3) were treated once or thrice with CPMV immunotherapy or PBS and brain tissues were harvested 24 h following the intratumoral therapy. Single-cell suspensions were prepared as previously described [25] and incubated for 15 min at 4 °C with a CD16/CD32 antibody (diluted in PBS) to block Fc receptors before washing with PBS. Tumor cells harvested on following single CPMV dose were tested using the innate panel and were incubated at 4 °C in triplicate with the cocktail of zombie yellow viability, CD45, CD11b, CD11c, F4/80, CD86 and I-A/I-E antibodies diluted in PBS. Tumor cells harvested at 24 h following three doses of CPMV immunotherapy were tested using the adaptive panel and were incubated at 4 °C in triplicate with the cocktail of zombie yellow viability, CD45, CD3, CD25, CD4, CD8 and FOXP3 antibodies. Cells were washed twice with PBS and then fixed with 3% (*v*/*v*) paraformaldehyde for flow cytometry using an LSR II (BD Biosciences, San Jose, CA, USA). The data were analyzed using the FlowJo v8.6.3 software (Flow Jo, Ashland, OR, USA).

4.7. Immunohistochemistry and H&E-Staining

Brain tissues harvested from treated and untreated mice (n = 3) were fixed in 10% (*v*/*v*) buffered formalin, embedded in paraffin, sectioned at 6 µm, and mounted on Superfrost® Plus slides (12-550-15, ThermoFisher Scientific). Sections were then hydrated through descending ethanol to water. Endogenous peroxidase activity was eliminated by incubation in 3% (*v*/*v*) H_2O_2 for 30 min prior to heat induced epitope retrieval (HIER). HIER was performed using a citrate based retrieval buffer, pH 6.1 (S1699, Dako, Santa Clara, CA, USA) for 10 min in a 96 °C water bath. The mouse antigen blocking kit (PK-2200, Vector laboratories, Burlingame, CA, USA) was utilized to reduce background staining according to manufacturer protocols for mouse derived antibodies. To reduce non-specific binding sections were incubated in 10% (*v*/*v*) normal goat serum (PCN5000, ThermoFisher Scientific) in Tris-buffered saline, (TBS; 50 mM Tris-HCl 150 mM NaCl, pH 7.6, Bio-Rad, 170-6435, Hercules, CA, USA) for 30 min prior to application of the primary antibody. Antibodies used in this study were mouse monoclonal antibody specific CD68 (ab201340, Abcam, Cambridge, UK) and rabbit monoclonal antibodies to IBA1 (ab178846, Abcam); CD45 (ab10558, Abcam) and Foxp3 (700914, Invitrogen, Camarillo, CA, USA). Immunohistochemistry was visualized via the peroxidase-anti-peroxidase method using 3,3′-diaminobenzidine (DAB) as a chromogen (TA-125-QHDX, ThermoFisher Scientific, Waltham, MA, USA). Serial sections were stained with hematoxylin and eosin to note the areas of tumor cell growth. Images were acquired with an Azio Scope A.1 (Zeiss, Thronwood, NY, USA) from three adjacent fields containing tumor. The immunoreactive intensity of positive cells were measured utilizing the Zeiss image analysis program (Axiovision Red 4.5, Zeiss) with background levels substracted from the stroma of the tumor. Statistical analysis was completed by ordinary one-way ANOVA using the Tukey's multiple comparisons test on the GraphPad Prism software (GraphPad Software, San Diego, CA, USA).

5. Conclusions

In conclusion, our results illustrate that eCPMV-mediated modulation of the immunological landscape in the brain TME supports anti-tumor response in our murine model. With its non-pathogenic

and non-replicating nature, ability to reverse the tumor immunosuppression and recruit immune effector cells, eCPMV nanoparticles offer a promising immunotherapy for glioma. In this study, we performed multiple intracranial treatments; in the future one may consider the development of slow-release formulations, or continuous low flow infusion to better control the immune response and alleviate the edema and complications associated with immunotherapy. Delivery of therapeutics to the brain is an active area of research that has evolved from biodegradable polymer implants [65,66] to more recent miniaturized implantable system MiNDS [67]. We have already developed and tested slow-release formulations for VLP vaccines [68], including in situ vaccines [69]. By formulating slow-release devices or implants incorporating VLPs, it will likely be possible to circumvent the need for repeated invasive administrations; thereby improving the translational potential of plant virus based immunotherapy for glioma.

Author Contributions: N.F.S. and A.E.S. conceptualize the research; A.K.-F. and S.S. developed the methodology and conducted experiments. V.B. carried out VLP expression in plants; C.W. carried out flow cytometry experiments; P.L.R.H. contributed to the IHC analysis. S.S. and A.K.-F. wrote the first drafts of the manuscript; N.F.S. and A.E.S. and S.S. edited the manuscript.

Funding: This work was supported by the NCI-Nanotechnology Alliance Grant U01CA218292 to (N.F.S.). A.E.S. is supported by NIH CA217956; as well as the Peter D Cristal Chair, the Center of Excellence for Translational Neuro-Oncology, the Kimble Family Foundation, the Gerald Kaufman Fund for Glioma Research, and the Ferry Family Foundation at University Hospitals of Cleveland.

Conflicts of Interest: The authors declare no conflict of interest.

References

1. Siegel, R.L.; Miller, K.D.; Jemal, A. Cancer statistics, 2018. *CA Cancer J. Clin.* **2018**, *68*, 7–30. [CrossRef]
2. Ostrom, Q.T.; Gittleman, H.; Truitt, G.; Boscia, A.; Kruchko, C.; Barnholtz-Sloan, J.S. CBTRUS Statistical Report: Primary Brain and Other Central Nervous System Tumors Diagnosed in the United States in 2011–2015. *Neuro Oncol.* **2018**, *20* (Suppl. 4), iv1–iv86. [CrossRef]
3. Schima, W.; Ba-Ssalamah, A.; Kolblinger, C.; Kulinna-Cosentini, C.; Puespoek, A.; Gotzinger, P. Pancreatic adenocarcinoma. *Eur. Radiol.* **2007**, *17*, 638–649. [CrossRef] [PubMed]
4. Ningaraj, N.S. Drug delivery to brain tumours: Challenges and progress. *Expert Opin. Drug Deliv.* **2006**, *3*, 499–509. [CrossRef]
5. Chen, J.; Li, Y.; Yu, T.S.; McKay, R.M.; Burns, D.K.; Kernie, S.G.; Parada, L.F. A restricted cell population propagates glioblastoma growth after chemotherapy. *Nature* **2012**, *488*, 522–526. [CrossRef]
6. Rich, J.N. Cancer stem cells in radiation resistance. *Cancer Res.* **2007**, *67*, 8980–8984. [CrossRef]
7. Boussiotis, V.A.; Charest, A. Immunotherapies for malignant glioma. *Oncogene* **2018**, *37*, 1121–1141. [CrossRef] [PubMed]
8. Hoang-Minh, L.B.; Mitchell, D.A. Immunotherapy for Brain Tumors. *Curr. Treat. Options Oncol.* **2018**, *19*, 60. [CrossRef] [PubMed]
9. Lyon, J.G.; Mokarram, N.; Saxena, T.; Carroll, S.L.; Bellamkonda, R.V. Engineering challenges for brain tumor immunotherapy. *Adv. Drug Deliv. Rev.* **2017**, *114*, 19–32. [CrossRef]
10. Ratnam, N.M.; Gilbert, M.R.; Giles, A.J. Immunotherapy in CNS Cancers: The Role of Immune Cell Trafficking. *Neuro Oncol.* **2018**, *21*, 37–46. [CrossRef]
11. Louveau, A.; Smirnov, I.; Keyes, T.J.; Eccles, J.D.; Rouhani, S.J.; Peske, J.D.; Derecki, N.C.; Castle, D.; Mandell, J.W.; Lee, K.S.; et al. Structural and functional features of central nervous system lymphatic vessels. *Nature* **2015**, *523*, 337–341. [CrossRef] [PubMed]
12. Quail, D.F.; Joyce, J.A. The Microenvironmental Landscape of Brain Tumors. *Cancer Cell* **2017**, *31*, 326–341. [CrossRef] [PubMed]
13. Jacobs, J.F.; Idema, A.J.; Bol, K.F.; Grotenhuis, J.A.; de Vries, I.J.; Wesseling, P.; Adema, G.J. Prognostic significance and mechanism of Treg infiltration in human brain tumors. *J. Neuroimmunol.* **2010**, *225*, 195–199. [CrossRef] [PubMed]
14. Alvarado, A.G.; Thiagarajan, P.S.; Mulkearns-Hubert, E.E.; Silver, D.J.; Hale, J.S.; Alban, T.J.; Turaga, S.M.; Jarrar, A.; Reizes, O.; Longworth, M.S.; et al. Glioblastoma Cancer Stem Cells Evade Innate Immune Suppression of Self-Renewal through Reduced TLR4 Expression. *Cell Stem Cell* **2017**, *20*, 450–461.e4. [CrossRef] [PubMed]

15. Sampson, J.H.; Heimberger, A.B.; Archer, G.E.; Aldape, K.D.; Friedman, A.H.; Friedman, H.S.; Gilbert, M.R.; Herndon, J.E.; McLendon, R.E.; Mitchell, D.A.; et al. Immunologic escape after prolonged progression-free survival with epidermal growth factor receptor variant III peptide vaccination in patients with newly diagnosed glioblastoma. *J. Clin. Oncol.* **2010**, *28*, 4722–4729. [CrossRef] [PubMed]
16. Bregy, A.; Wong, T.M.; Shah, A.H.; Goldberg, J.M.; Komotar, R.J. Active immunotherapy using dendritic cells in the treatment of glioblastoma multiforme. *Cancer Treat. Rev.* **2013**, *39*, 891–907. [CrossRef] [PubMed]
17. Kuramitsu, S.; Yamamichi, A.; Ohka, F.; Motomura, K.; Hara, M.; Natsume, A. Adoptive immunotherapy for the treatment of glioblastoma: Progress and possibilities. *Immunotherapy* **2016**, *8*, 1393–1404. [CrossRef] [PubMed]
18. Reardon, D.A.; Lassman, A.B.; van den Bent, M.; Kumthekar, P.; Merrell, R.; Scott, A.M.; Fichtel, L.; Sulman, E.P.; Gomez, E.; Fischer, J.; et al. Efficacy and safety results of ABT-414 in combination with radiation and temozolomide in newly diagnosed glioblastoma. *Neuro Oncol.* **2017**, *19*, 965–975. [CrossRef] [PubMed]
19. Sirachainan, N.; Boongird, A.; Swangsilpa, T.; Klaisuban, W.; Lusawat, A.; Hongeng, S. Reported outcomes of children with newly diagnosed high-grade gliomas treated with nimotuzumab and irinotecan. *Childs Nerv. Syst.* **2017**, *33*, 893–897. [CrossRef]
20. Lang, F.F.; Conrad, C.; Gomez-Manzano, C.; Yung, W.K.A.; Sawaya, R.; Weinberg, J.S.; Prabhu, S.S.; Rao, G.; Fuller, G.N.; Aldape, K.D.; et al. Phase I Study of DNX-2401 (Delta-24-RGD) Oncolytic Adenovirus: Replication and Immunotherapeutic Effects in Recurrent Malignant Glioma. *J. Clin. Oncol.* **2018**, *36*, 1419–1427. [CrossRef]
21. Dobrikova, E.Y.; Broadt, T.; Poiley-Nelson, J.; Yang, X.; Soman, G.; Giardina, S.; Harris, R.; Gromeier, M. Recombinant oncolytic poliovirus eliminates glioma in vivo without genetic adaptation to a pathogenic phenotype. *Mol. Ther.* **2008**, *16*, 1865–1872. [CrossRef]
22. Delwar, Z.M.; Liu, G.; Kuo, Y.; Lee, C.; Bu, L.; Rennie, P.S.; Jia, W.W. Tumour-specific triple-regulated oncolytic herpes virus to target glioma. *Oncotarget* **2016**, *7*, 28658–28669. [CrossRef]
23. Hardcastle, J.; Mills, L.; Malo, C.S.; Jin, F.; Kurokawa, C.; Geekiyanage, H.; Schroeder, M.; Sarkaria, J.; Johnson, A.J.; Galanis, E. Immunovirotherapy with measles virus strains in combination with anti-PD-1 antibody blockade enhances antitumor activity in glioblastoma treatment. *Neuro Oncol.* **2017**, *19*, 493–502. [CrossRef]
24. Zhu, Z.; Gorman, M.J.; McKenzie, L.D.; Chai, J.N.; Hubert, C.G.; Prager, B.C.; Fernandez, E.; Richner, J.M.; Zhang, R.; Shan, C.; et al. Zika virus has oncolytic activity against glioblastoma stem cells. *J. Exp. Med.* **2017**, *214*, 2843–2857. [CrossRef]
25. Lizotte, P.H.; Wen, A.M.; Sheen, M.R.; Fields, J.; Rojanasopondist, P.; Steinmetz, N.F.; Fiering, S. In situ vaccination with cowpea mosaic virus nanoparticles suppresses metastatic cancer. *Nat. Nanotechnol.* **2016**, *11*, 295–303. [CrossRef]
26. Hoopes, P.J.; Wagner, R.J.; Duval, K.; Kang, K.; Gladstone, D.J.; Moodie, K.L.; Crary-Burney, M.; Ariaspulido, H.; Veliz, F.A.; Steinmetz, N.F.; et al. Treatment of Canine Oral Melanoma with Nanotechnology-Based Immunotherapy and Radiation. *Mol. Pharm.* **2018**, *15*, 3717–3722. [CrossRef]
27. Wen, A.M.; Shukla, S.; Saxena, P.; Aljabali, A.A.; Yildiz, I.; Dey, S.; Mealy, J.E.; Yang, A.C.; Evans, D.J.; Lomonossoff, G.P.; et al. Interior engineering of a viral nanoparticle and its tumor homing properties. *Biomacromolecules* **2012**, *13*, 3990–4001. [CrossRef]
28. Lin, T.; Chen, Z.; Usha, R.; Stauffacher, C.V.; Dai, J.B.; Schmidt, T.; Johnson, J.E. The refined crystal structure of cowpea mosaic virus at 2.8 A resolution. *Virology* **1999**, *265*, 20–34. [CrossRef]
29. Van Wezenbeek, P.; Verver, J.; Harmsen, J.; Vos, P.; van Kammen, A. Primary structure and gene organization of the middle-component RNA of cowpea mosaic virus. *EMBO J.* **1983**, *2*, 941–946. [CrossRef]
30. Chatterji, A.; Ochoa, W.F.; Paine, M.; Ratna, B.R.; Johnson, J.E.; Lin, T. New addresses on an addressable virus nanoblock; uniquely reactive Lys residues on cowpea mosaic virus. *Chem. Biol.* **2004**, *11*, 855–863. [CrossRef]
31. Singh, P.; Prasuhn, D.; Yeh, R.M.; Destito, G.; Rae, C.S.; Osborn, K.; Finn, M.G.; Manchester, M. Bio-distribution, toxicity and pathology of cowpea mosaic virus nanoparticles in vivo. *J. Control. Release* **2007**, *120*, 41–50. [CrossRef]
32. Szatmari, T.; Lumniczky, K.; Desaknai, S.; Trajcevski, S.; Hidvegi, E.J.; Hamada, H.; Safrany, G. Detailed characterization of the mouse glioma 261 tumor model for experimental glioblastoma therapy. *Cancer Sci.* **2006**, *97*, 546–553. [CrossRef]
33. Murray, A.A.; Wang, C.; Fiering, S.; Steinmetz, N.F. In Situ Vaccination with Cowpea vs. Tobacco Mosaic Virus against Melanoma. *Mol. Pharm.* **2018**, *15*, 3700–3716. [CrossRef]

34. Fontenot, J.D.; Gavin, M.A.; Rudensky, A.Y. Foxp3 programs the development and function of CD4+CD25+ regulatory T cells. *Nat. Immunol.* **2003**, *4*, 330–336. [CrossRef]
35. Lebel, M.E.; Chartrand, K.; Tarrab, E.; Savard, P.; Leclerc, D.; Lamarre, A. Potentiating Cancer Immunotherapy Using Papaya Mosaic Virus-Derived Nanoparticles. *Nano Lett.* **2016**, *16*, 1826–1832. [CrossRef]
36. Akira, S.; Uematsu, S.; Takeuchi, O. Pathogen recognition and innate immunity. *Cell* **2006**, *124*, 783–801. [CrossRef]
37. Kawai, T.; Akira, S. The role of pattern-recognition receptors in innate immunity: Update on Toll-like receptors. *Nat. Immunol.* **2010**, *11*, 373–384. [CrossRef]
38. Alizadeh, D.; Zhang, L.; Brown, C.E.; Farrukh, O.; Jensen, M.C.; Badie, B. Induction of anti-glioma natural killer cell response following multiple low-dose intracerebral CpG therapy. *Clin. Cancer Res.* **2010**, *16*, 3399–3408. [CrossRef]
39. Chicoine, M.R.; Zahner, M.; Won, E.K.; Kalra, R.R.; Kitamura, T.; Perry, A.; Higashikubo, R. The in vivo antitumoral effects of lipopolysaccharide against glioblastoma multiforme are mediated in part by Toll-like receptor 4. *Neurosurgery* **2007**, *60*, 372–380, Discussion 81. [CrossRef]
40. Brandsma, D.; Stalpers, L.; Taal, W.; Sminia, P.; van den Bent, M.J. Clinical features, mechanisms, and management of pseudoprogression in malignant gliomas. *Lancet Oncol.* **2008**, *9*, 453–461. [CrossRef]
41. Kleijn, A.; Chen, J.W.; Buhrman, J.S.; Wojtkiewicz, G.R.; Iwamoto, Y.; Lamfers, M.L.; Stemmer-Rachamimov, A.O.; Rabkin, S.D.; Weissleder, R.; Martuza, R.L.; et al. Distinguishing inflammation from tumor and peritumoral edema by myeloperoxidase magnetic resonance imaging. *Clin. Cancer Res.* **2011**, *17*, 4484–4493. [CrossRef]
42. Hara, Y.; Wakamori, M.; Ishii, M.; Maeno, E.; Nishida, M.; Yoshida, T.; Yamada, H.; Shimizu, S.; Mori, E.; Kudoh, J.; et al. LTRPC2 Ca2+-permeable channel activated by changes in redox status confers susceptibility to cell death. *Mol. Cell* **2002**, *9*, 163–173. [CrossRef]
43. Sun, B.; Qin, W.; Song, M.; Liu, L.; Yu, Y.; Qi, X.; Sun, H. Neutrophil Suppresses Tumor Cell Proliferation via Fas/Fas Ligand Pathway Mediated Cell Cycle Arrested. *Int. J. Biol. Sci.* **2018**, *14*, 2103–2113. [CrossRef]
44. Fridlender, Z.G.; Sun, J.; Kim, S.; Kapoor, V.; Cheng, G.; Ling, L.; Worthen, G.S.; Albelda, S.M. Polarization of tumor-associated neutrophil phenotype by TGF-beta: "N1" versus "N2" TAN. *Cancer Cell* **2009**, *16*, 183–194. [CrossRef]
45. Cheng, M.; Chen, Y.; Xiao, W.; Sun, R.; Tian, Z. NK cell-based immunotherapy for malignant diseases. *Cell. Mol. Immunol.* **2013**, *10*, 230–252. [CrossRef]
46. Screpanti, V.; Wallin, R.P.; Ljunggren, H.G.; Grandien, A. A central role for death receptor-mediated apoptosis in the rejection of tumors by NK cells. *J. Immunol.* **2001**, *167*, 2068–2073. [CrossRef]
47. Bottcher, J.P.; Bonavita, E.; Chakravarty, P.; Blees, H.; Cabeza-Cabrerizo, M.; Sammicheli, S.; Rogers, N.C.; Sahai, E.; Zelenay, S.; Reis e Sousa, C. NK Cells Stimulate Recruitment of cDC1 into the Tumor Microenvironment Promoting Cancer Immune Control. *Cell* **2018**, *172*, 1022–1037.e14. [CrossRef]
48. Roberts, E.W.; Broz, M.L.; Binnewies, M.; Headley, M.B.; Nelson, A.E.; Wolf, D.M.; Kaisho, T.; Bogunovic, D.; Bhardwaj, N.; Krummel, M.F. Critical Role for CD103(+)/CD141(+) Dendritic Cells Bearing CCR7 for Tumor Antigen Trafficking and Priming of T Cell Immunity in Melanoma. *Cancer Cell* **2016**, *30*, 324–336. [CrossRef]
49. Harris, M.G.; Hulseberg, P.; Ling, C.; Karman, J.; Clarkson, B.D.; Harding, J.S.; Zhang, M.; Sandor, A.; Christensen, K.; Nagy, A.; et al. Immune privilege of the CNS is not the consequence of limited antigen sampling. *Sci. Rep.* **2014**, *4*, 4422. [CrossRef]
50. Cserr, H.F.; Harling-Berg, C.J.; Knopf, P.M. Drainage of brain extracellular fluid into blood and deep cervical lymph and its immunological significance. *Brain Pathol.* **1992**, *2*, 269–276. [CrossRef]
51. Tian, G.; Courtney, A.N.; Jena, B.; Heczey, A.; Liu, D.; Marinova, E.; Guo, L.; Xu, X.; Torikai, H.; Mo, Q.; et al. CD62L+NKT cells have prolonged persistence and antitumor activity in vivo. *J. Clin. Investig.* **2016**, *126*, 2341–2355. [CrossRef]
52. Ko, H.J.; Lee, J.M.; Kim, Y.J.; Kim, Y.S.; Lee, K.A.; Kang, C.Y. Immunosuppressive myeloid-derived suppressor cells can be converted into immunogenic APCs with the help of activated NKT cells: An alternative cell-based antitumor vaccine. *J. Immunol.* **2009**, *182*, 1818–1828. [CrossRef]
53. Markovic, D.S.; Vinnakota, K.; Chirasani, S.; Synowitz, M.; Raguet, H.; Stock, K.; Sliwa, M.; Lehman, S.; Kalin, R.; van Rooijen, N.; et al. Gliomas induce and exploit microglial MT1-MMP expression for tumor expansion. *Proc. Natl. Acad. Sci. USA* **2009**, *106*, 12530–12535. [CrossRef]

54. Ye, X.Z.; Xu, S.L.; Xin, Y.H.; Yu, S.C.; Ping, Y.F.; Chen, L.; Xiao, H.L.; Wang, B.; Yi, L.; Wang, Q.L.; et al. Tumor-associated microglia/macrophages enhance the invasion of glioma stem-like cells via TGF-beta1 signaling pathway. *J. Immunol.* **2012**, *189*, 444–453. [CrossRef]
55. Hwang, S.Y.; Yoo, B.C.; Jung, J.W.; Oh, E.S.; Hwang, J.S.; Shin, J.A.; Kim, S.Y.; Cha, S.H.; Han, I.O. Induction of glioma apoptosis by microglia-secreted molecules: The role of nitric oxide and cathepsin B. *Biochim. Biophys. Acta* **2009**, *1793*, 1656–1668. [CrossRef]
56. Kees, T.; Lohr, J.; Noack, J.; Mora, R.; Gdynia, G.; Todt, G.; Ernst, A.; Radlwimmer, B.; Falk, C.S.; Herold-Mende, C.; et al. Microglia isolated from patients with glioma gain antitumor activities on poly (I:C) stimulation. *Neuro Oncol.* **2012**, *14*, 64–78. [CrossRef]
57. Sarkar, S.; Doring, A.; Zemp, F.J.; Silva, C.; Lun, X.; Wang, X.; Kelly, J.; Hader, W.; Hamilton, M.; Mercier, P.; et al. Therapeutic activation of macrophages and microglia to suppress brain tumor-initiating cells. *Nat. Neurosci.* **2014**, *17*, 46–55. [CrossRef]
58. Pyonteck, S.M.; Akkari, L.; Schuhmacher, A.J.; Bowman, R.L.; Sevenich, L.; Quail, D.F.; Olson, O.C.; Quick, M.L.; Huse, J.T.; Teijeiro, V.; et al. CSF-1R inhibition alters macrophage polarization and blocks glioma progression. *Nat. Med.* **2013**, *19*, 1264–1272. [CrossRef]
59. Lisi, L.; Stigliano, E.; Lauriola, L.; Navarra, P.; Dello Russo, C. Proinflammatory-activated glioma cells induce a switch in microglial polarization and activation status, from a predominant M2b phenotype to a mixture of M1 and M2a/B polarized cells. *ASN Neuro* **2014**, *6*, 171–183. [CrossRef]
60. Heimberger, A.B.; Abou-Ghazal, M.; Reina-Ortiz, C.; Yang, D.S.; Sun, W.; Qiao, W.; Hiraoka, N.; Fuller, G.N. Incidence and prognostic impact of FoxP3+ regulatory T cells in human gliomas. *Clin. Cancer Res.* **2008**, *14*, 5166–5172. [CrossRef]
61. DiDomenico, J.; Lamano, J.B.; Oyon, D.; Li, Y.; Veliceasa, D.; Kaur, G.; Ampie, L.; Choy, W.; Lamano, J.B.; Bloch, O. The immune checkpoint protein PD-L1 induces and maintains regulatory T cells in glioblastoma. *Oncoimmunology* **2018**, *7*, e1448329. [CrossRef]
62. Hanihara, M.; Kawataki, T.; Oh-Oka, K.; Mitsuka, K.; Nakao, A.; Kinouchi, H. Synergistic antitumor effect with indoleamine 2,3-dioxygenase inhibition and temozolomide in a murine glioma model. *J. Neurosurg.* **2016**, *124*, 1594–1601. [CrossRef]
63. Wainwright, D.A.; Chang, A.L.; Dey, M.; Balyasnikova, I.V.; Kim, C.K.; Tobias, A.; Cheng, Y.; Kim, J.W.; Qiao, J.; Zhang, L.; et al. Durable therapeutic efficacy utilizing combinatorial blockade against IDO, CTLA-4, and PD-L1 in mice with brain tumors. *Clin. Cancer Res.* **2014**, *20*, 5290–5301. [CrossRef]
64. Vom Berg, J.; Vrohlings, M.; Haller, S.; Haimovici, A.; Kulig, P.; Sledzinska, A.; Weller, M.; Bercher, B. Intratumoral IL-12 combined with CTLA-4 blockade elicits T cell-mediated glioma rejection. *J. Exp. Med.* **2013**, *210*, 2803–2811. [CrossRef]
65. Kaurav, H.; Kapoor, D.N. Implantable systems for drug delivery to the brain. *Ther. Deliv.* **2017**, *8*, 1097–1107. [CrossRef]
66. Pridgen, E.M.; Langer, R.; Farokhzad, O.C. Biodegradable, polymeric nanoparticle delivery systems for cancer therapy. *Nanomedicine* **2007**, *2*, 669–680. [CrossRef]
67. Dagdeviren, C.; Ramadi, K.B.; Joe, P.; Spencer, K.; Schwerdt, H.N.; Shimazu, H.; Delcasso, S.; Amemori, K.; Nunez-Lopez, C.; Graybiel, M.; et al. Miniaturized neural system for chronic, local intracerebral drug delivery. *Sci. Transl. Med.* **2018**, *10*, eaan2742. [CrossRef]
68. Lee, P.W.; Shukla, S.; Wallat, J.D.; Danda, C.; Steinmetz, N.F.; Maia, J.; Pokorski, J.K. Biodegradable Viral Nanoparticle/Polymer Implants Prepared via Melt-Processing. *ACS Nano* **2017**, *11*, 8777–8789. [CrossRef]
69. Czapar, A.E.; Tiu, B.D.B.; Veliz, F.A.; Pokorski, J.K.; Steinmetz, N.F. Slow-Release Formulation of Cowpea Mosaic Virus for In Situ Vaccine Delivery to Treat Ovarian Cancer. *Adv. Sci.* **2018**, *5*, 1700991. [CrossRef]

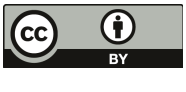

cancers

MDPI

Article

Improving Payload Capacity and Anti-Tumor Efficacy of Mesenchymal Stem Cells Using TAT Peptide Functionalized Polymeric Nanoparticles

Gopikrishna Moku [1,†], Buddhadev Layek [2,†], Lana Trautman [3], Samuel Putnam [3], Jayanth Panyam [1] and Swayam Prabha [1,2,*]

1 Department of Pharmaceutics, College of Pharmacy, University of Minnesota, Minneapolis, MN 55455, USA; gopikrishna.moku@gmail.com (G.M.); jpanyam@umn.edu (J.P.)
2 Department of Experimental and Clinical Pharmacology, College of Pharmacy, University of Minnesota, Minneapolis, MN 55455, USA; blayek@umn.edu
3 Breck School, 123 Ottawa Ave N, Golden Valley, MN 55422, USA; traula@student.breckschool.org (L.T.); putnsa@student.breckschool.org (S.P.)
* Correspondence: prabh025@umn.edu; Tel.: +1-612-626-3545
† These authors contributed equally to this work.

Received: 5 March 2019; Accepted: 2 April 2019; Published: 6 April 2019

Abstract: Mesenchymal stem cells (MSCs) accumulate specifically in both primary tumors and metastases following systemic administration. However, the poor payload capacity of MSCs limits their use in small molecule drug delivery. To improve drug payload in MSCs, we explored polymeric nanoparticles that were functionalized with transactivator of transcription (TAT) peptide. Paclitaxel loaded poly(DL-lactide-co-glycolide) (PLGA) nanoparticles (15–16% w/w paclitaxel; diameter of 225 ± 7 nm; and zeta potential of -15 ± 4 mV) were fabricated by emulsion-solvent evaporation method, followed by TAT-conjugation to the surface of nanoparticles via maleimide-thiol chemistry. Our studies demonstrated that TAT functionalization improved the intracellular accumulation and retention of nanoparticles in MSCs. Further, nano-engineering of MSCs did not alter the migration and differentiation potential of MSCs. Treatment with nano-engineered MSCs resulted in significant ($p < 0.05$) inhibition of tumor growth and improved survival ($p < 0.0001$) in a mouse orthotopic model of lung cancer compared to that with free or nanoparticle encapsulated drug. In summary, our results demonstrated that MSCs engineered using TAT functionalized nanoparticles serve as an efficient carrier for tumor specific delivery of anticancer drugs, resulting in greatly improved therapeutic efficacy.

Keywords: mesenchymal stem cells (MSCs); TAT peptide; PLGA; paclitaxel; nano-engineered MSCs; orthotopic lung tumor model

1. Introduction

Tumors are characterized by uneven vascular perfusion. The outer-most regions often have near normal blood flow while the inner regions can be avascular [1–3]. In addition, elevated interstitial fluid pressure and rigid extracellular matrix compromise intra-tumoral solute transport [4]. This leads to poor drug delivery to the under-perfused regions within the tumor and the eventual development of drug resistance [5–7]. Cell-based drug delivery can overcome these critical tissue barriers faced by synthetic nano drug delivery systems [8–10]. Because of their ability to respond to cytokine and chemokine gradients, various cell types including T cells [11], macrophages [12] and non-hematopoietic mesenchymal stem cells (MSCs) have been investigated for drug delivery [13]. Initial studies with these cell-based systems typically involved genetic modification of the cells to express anti-tumor

peptides and proteins [14]. More recently, techniques that allow the functionalization of cells with nano drug delivery systems without affecting their viability or migratory phenotype have enabled the utilization of MSCs for small molecule drug delivery [15–17].

A critical parameter that influences the effectiveness of cell-based drug delivery is payload capacity. Previous studies have loaded nanoparticle-encapsulated drugs into cells through either simple endocytosis mediated uptake of nanoparticles or by covalent conjugation of nanoparticles to cell surface [15,16,18]. Rapid recycling and exocytosis of internalized nanoparticles [19] results in low loading capacities when relying on non-specific endocytosis of drug-loaded nanoparticles. Similarly, cells continuously internalize and recycle their outer membranes, which can result in lysosomal degradation of membrane-conjugated nanoparticles.

In the current study, we evaluated nanoparticles functionalized with cell penetrating peptide (CPP) to enhance drug payload capacity of MSCs. CPPs are typically 5–30 amino acids long, and are characterized by their intrinsic ability to bypass lysosomes and enter cytoplasm through macropinocytosis [20]. Among the various CPPs identified so far, transactivator of transcription (TAT) peptide has been widely investigated to improve the intracellular delivery of various cargoes [21]. TAT peptide fragments are derived from the human immunodeficiency virus 1 protein containing 86–102 amino acid residues. The arginine-rich basic domain 48–60 (GRKKRRQRRRPPQ) is responsible for the transactivation [22]. TAT peptide (47 to 57 YGRKKRRQRRR, Figure 1A) has been successfully used to deliver biologically active antibodies [23], proteins [24], nucleic acids [25], small molecules [26], and nanocarriers [27,28] both in vitro and in vivo. TAT peptide and TAT conjugated systems are known to be internalized primarily through endocytic pathways [27,29,30]. Cellular internalization of TAT peptide is temperature-dependent, dynamin-1-independent, and is inhibited by drugs that block macropinocytosis [31]. However, some studies suggest that clathrin and caveolae-mediated endocytosis are likely also involved [32–34].

We hypothesized that surface functionalization of polymeric nanoparticles with TAT peptide will enable their improved internalization into and retention by MSCs, resulting in enhanced payload carrying capacity. We covalently conjugated TAT peptide to the surface of nanoparticles encapsulating paclitaxel (PTX) and used these nanoparticles to incorporate PTX in MSCs. Our studies show that these nano-engineered MSCs are effective in inhibiting tumor growth in a mouse orthotopic model of lung cancer.

2. Results

2.1. Synthesis of Thiolated TAT Peptide

To conjugate TAT peptide to nanoparticles having surface maleimide groups, the primary amine groups in the TAT peptide was converted into free thiol (-SH) using N-Succinimidyl 3-(2-pyridyldithio)propionate (SPDP) reagent and reducing agent tris(2-carboxyethyl)phosphine hydrochloride (TCEP). The detailed mechanism for the conversion is provided in the supporting information (Supplementary Figure S1). This reaction resulted in the conversion of one amine group (1.02 ± 0.12) per TAT peptide molecule into a free thiol as determined by thiol quantitation method.

2.2. Physicochemical Characterization of Nanoparticles

The hydrodynamic diameter (particle size) and zeta potential (surface charge) of nanoparticles were measured by dynamic light scattering (DLS) technique. Particle size of PTX loaded poly(DL-lactide-co-glycolide) (PLGA) nanoparticles (PTX NP), TAT functionalized PLGA nanoparticles (TAT NP), and PTX loaded TAT functionalized PLGA nanoparticles (TAT PTX NP) was 213 ± 6, 227 ± 18, and 225 ± 7 nm, respectively (Figure 1D). The surface charge of PTX NP, TAT NP, and TAT PTX NP was found to be -21 ± 1, -8.7 ± 2.5, and -15 ± 4 mV, respectively. PTX loading was in the range of 15–16% w/w. The efficiency of TAT peptide conjugation to NPs was $57 \pm 4\%$ (2.42 ± 0.14 μg/mg of NP).

The goal of the in vitro drug release study was to confirm that the incorporation of TAT peptide did not influence the drug release characteristics of nanoparticles. In order to maintain sink condition, PTX release study was conducted in cell culture medium supplemented with 10% (w/v) Captisol®. In vitro release of PTX from nanoparticles is shown in Figure 1E. An initial burst release of about 20% of the encapsulated PTX was observed in the first 1 h, followed by a steady release over the study period. The total PTX released over 8 days was ~76%. This was similar to that observed with non-functionalized PLGA nanoparticles in our previous studies [35], suggesting that TAT peptide functionalization did not affect the release profile of PTX from the nanoparticles. The initial burst release of PTX is primarily ascribed to the drug molecules present on or near the nanoparticle surface. However, it is noteworthy that the burst release took place within first 4 h, which is equivalent to optimal time for nano-engineering of MSCs. Thus, loosely bound PTX molecules are released during the nano-engineering process and nanoparticles loaded in the MSCs are in the sustained release phase.

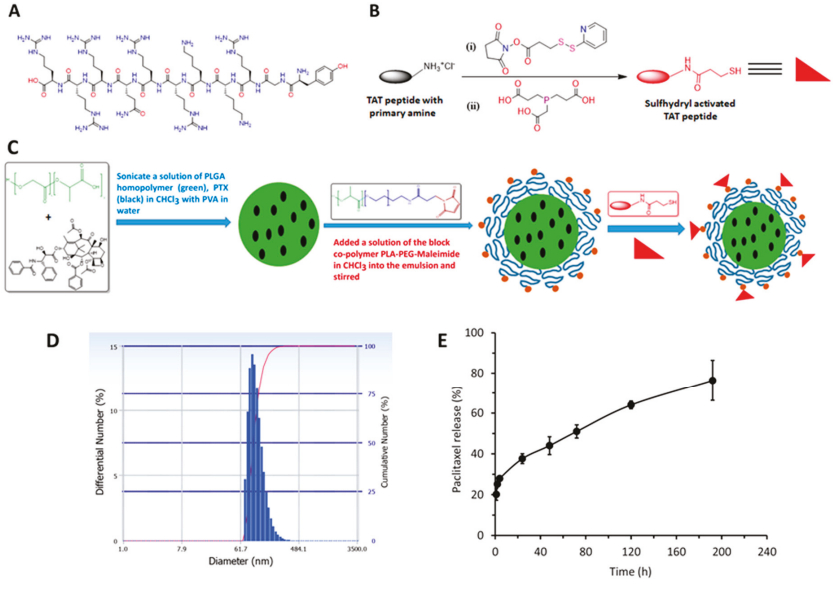

Figure 1. Preparation and characterization of PTX loaded TAT functionalized PLGA nanoparticles (TAT PTX NP). (**A**) Chemical structure of HIV-1 TAT peptide (47–57, YGRKKRRQRRR). (**B**) Synthetic scheme for the preparation of sulfhydryl activated TAT peptide using SPDP and TCEP. (**C**) Diagrammatic representation for the preparation of TAT PTX NP. (**D**) Particle size distribution of TAT PTX NP. (**E**) In vitro release profile of PTX from TAT PTX NP in cell culture medium supplemented with 10% (w/v) Captisol® at 37 °C. Data shown is mean ± SD (n = 4).

2.3. Nanoparticles Uptake and Retention in MSCs

In order to determine the optimal incubation time to achieve the maximum nanoparticle loading in MSCs, we performed quantitative uptake studies. The uptake of TAT NP was 3-fold higher when compared to that of non-TAT NP (Figure 2A). These findings demonstrated the effectiveness of TAT peptide-functionalized nanoparticles in increasing the drug payload in MSCs. However, there was no significant difference in amount of TAT NP taken up at 4 or 6 h and hence 4 h was used as the optimal incubation time for subsequent nano-engineering processes. The amount of PTX loading in nano-engineered MSCs was quantified using HPLC. The average PTX content was found to be 16.1 ± 0.9 pg/cell in MSCs incubated with TAT PTX NP. As shown in Figure 2B, TAT-NP demonstrated a 5-fold increase in the % retained in the cells when compared to non-TAT-NP, suggesting that the

TAT-functionalized nanoparticles not only enhanced payload capacity, but also improved the cellular retention of nanoparticles.

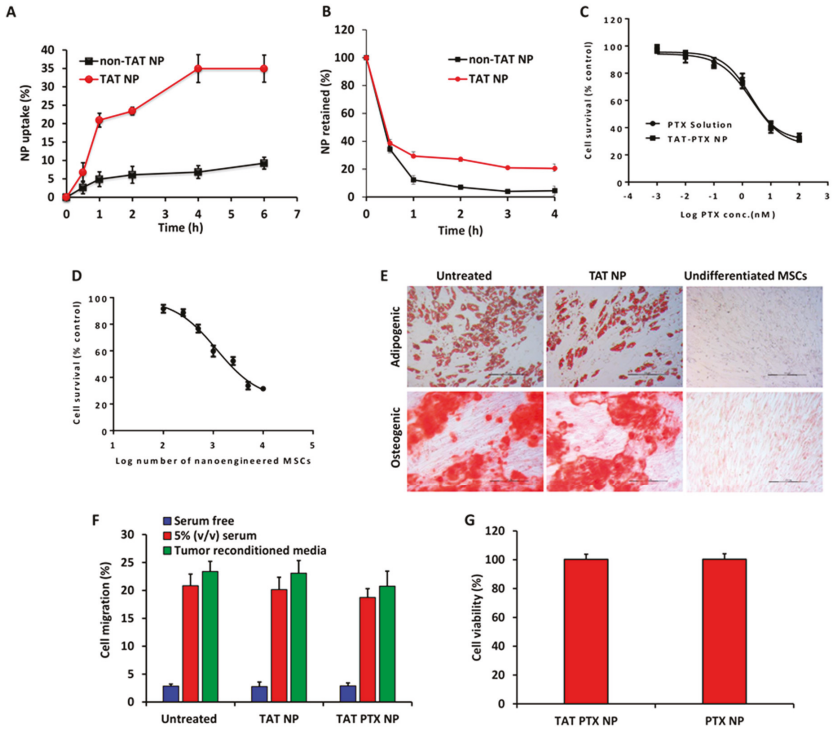

Figure 2. In vitro endocytosis (**A**) and exocytosis (**B**) of TAT-modified or non-TAT nanoparticles in MSCs. Cells were incubated with 100 μg/mL rhodamine-labeled PLGA nanoparticles. Data shown is mean ± SD, $n = 4$. (**C**,**D**) Cytotoxicity profiles of PTX solution, TAT PTX NP, and nano-engineered MSCs in A549 cells. Cells were treated with PTX solution or TAT PTX NP (**C**) or nano-engineered MSCs (**D**). MTS assay was performed after 72 h of treatment. Data shown is mean ± SD, $n = 6$. (**E**) Differentiation (adipogenic and osteogenic) potential of nano-engineered MSCs (MSCs engineered with TAT NP; TAT NP). Untreated MSCs and nano-engineered MSCs were grown in adipogenic and osteogenic differentiation media for 3 weeks. The cells were fixed and stained with oil red O or alizarin red to detect lipid vacuoles or calcium deposits, respectively. MSCs cultured in regular growth media were used as negative control. Scale bar: 200 μm. (**F**) The migratory potential of MSCs from a serum free media towards serum free, tumor reconditioned or 5% (*v*/*v*) serum containing media in a Transwell® plate. Data shown is mean ± SD, $n = 6$. (**G**) Cell viability of nano-engineered MSCs. Data shown is mean ± SD, $n = 5$.

2.4. In Vitro Cytotoxicity Studies

The in vitro cytotoxicity potential of nano-engineered MSCs was determined in A549 cells using a standard MTS assay. PTX solution and TAT PTX NP were used as controls. IC50 values for nano-engineered MSCs, PTX solution, and TAT PTX NP were 1171 MSCs (Figure 2D) (equivalent to 22 nM PTX), 1.96 nM, and 2.10 nM (Figure 2C), respectively.

2.5. Characterization of Nano-Engineered MSCs

Nano-engineered MSCs were characterized for adipogenic and osteogenic differentiation potential. There were no apparent differences in the formation of neutral lipid vacuoles and calcium deposits,

confirming that nano-engineered MSCs retain adipogenic and osteogenic differentiation potential, respectively (Figure 2E).

Next, we also confirmed the functional ability of the nano-engineered MSCs using an in vitro migration assay. As shown in Figure 2F, there was no significant change in the migration properties of nano-engineered MSCs when compared to untreated MSCs. In response to cytokines present in 5% serum media, 21% of untreated MSCs, 20% MSCs treated with TAT NP, and 19% MSCs treated with TAT PTX NP migrated to the lower chamber of the Transwell® plate (Figure 2F). Similarly, 23% of untreated MSCs, 23% of MSCs treated with TAT NP, and 20% MSCs treated with TAT PTX NP migrated towards tumor reconditioned media (Figure 2F). These findings clearly demonstrated that loading MSCs with TAT PTX NP did not significantly affect the migratory ability of the MSCs.

2.6. Cell Viability of Nano-Engineered MSCs

The effect of TAT PTX NP on MSCs survival was evaluated by incubating MSCs with 100 µg/mL nanoparticles. There was no significant effect of TAT PTX NP on viability of MSCs (Figure 2G). Further, there was no difference in cell viability of TAT PTX NP and PTX NP treated MSCs, suggesting TAT conjugation did not alter the cytotoxic potential of nanoparticles.

2.7. Therapeutic Efficacy of Nano-Engineered MSCs in Orthotopic Lung Tumor Model

The anticancer efficacy of nano-engineered MSCs was evaluated in an orthotopic lung tumor model. Mice treated with MSCs + TAT PTX NP showed significant inhibition of tumor progression ($p < 0.05$) compared to other treatment groups (Figure 3A). Furthermore, MSCs + TAT PTX NP treated mice had significantly longer survival than those in control groups (log-rank test, $p < 0.0001$) (Figure 3B). Notably, the median survival of MSCs + TAT PTX NP treated mice was 109 days after treatment initiation, while the median survival of mice in control groups was in the range of 76–86 days.

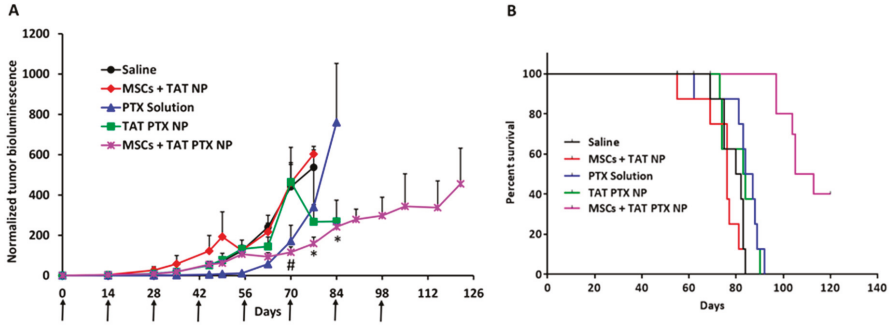

Figure 3. Nano-engineered MSCs were more effective in inhibiting orthotopic tumor growth and increased the overall survival of tumor bearing mice. (**A**) SCID beige mice bearing orthotopic A549 lung tumors were intravenously injected with Dulbecco's phosphate buffered saline (Saline); 4 Million MSCs engineered with TAT NP (MSCs + TAT NP); PTX solution; TAT PTX NP; 4 Million MSCs engineered with TAT PTX NP (MSCs + TAT PTX NP). Plot of normalized bioluminescence readings ($n = 10$ for MSCs + TAT PTX NP and $n = 8$ for all other groups). Arrowheads indicate injection days. (*) Indicates significantly different ($p < 0.05$) from PTX solution; # indicates significantly different ($p < 0.05$) from TAT PTX NP. (**B**) Kaplan–Meier survival curves for the different treatment groups. Log rank test of MSCs + TAT PTX NP and control groups yields $p < 0.0001$ (*).

2.8. Immunohistological Staining of Lung Tumors

In order to study the mechanism of improved anticancer efficacy with nano-engineered MSCs, lung tumor sections were stained for CD31, Ki-67, and cleaved caspase 3 (Figure 4A). Lung tumors from the mice treated with nano-engineered MSCs showed significantly fewer angiogenic blood vessels

compared to saline or MSCs + TAT NP treatment groups ($p < 0.05$). In addition, lung tumors from the mice treated with nano-engineered MSCs showed significantly fewer proliferating cells (Ki-67 positive cells) compared to other treatment groups ($p < 0.05$). Densities of the cleaved caspase 3 positive apoptotic cells in tumors from nano-engineered MSC treatment group was significantly higher (panel 3 of Figure 4A) than those in other groups ($p < 0.05$).

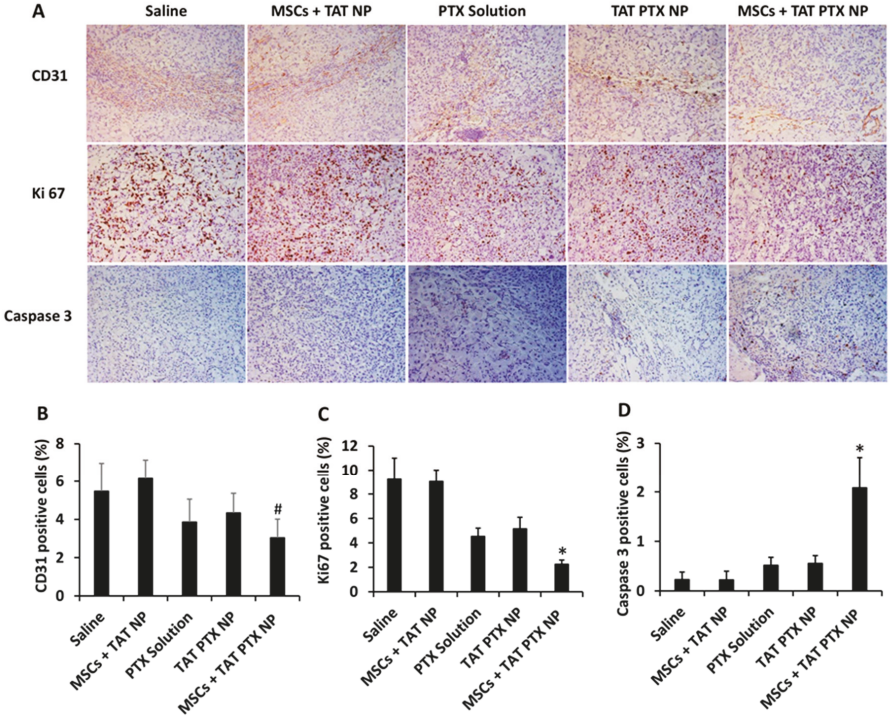

Figure 4. Immunohistological analysis of lung tumors collected from therapeutic efficacy study. (**A**) Lung tumors were stained for CD31 (angiogenesis marker), Ki-67 (proliferation marker), and caspase-3 (apoptosis marker). Images were taken at 20× magnification. Quantification of (**B**) CD31, (**C**) Ki67, and (**D**) cleaved caspase-3 staining. Data represented as mean ± SD, $n = 9$ images; * $p < 0.05$ compared with other treatment groups and # $p < 0.05$ compared with saline and MSCs + TAT NP.

2.9. Toxicology Assessment of Nano-Engineered MSCs

To examine the possible side effects of nano-engineered MSCs, we evaluated various biochemical and hematological parameters in healthy mice. We did not observe any signs of distress or significant differences in the body weights of the mice in different groups. Levels of aspartate aminotransferase (AST), alanine aminotransferase (ALT), gamma-glutamyl transferase (GGT), alkaline phosphatase (ALP), total protein (TP), albumin (ALB), globulin (GLOB), albumin/globulin (A/G) ratio, and total bilirubin (TBIL) in serum collected from treated mice were not different than those in the saline group (Table 1). Treatments with MSCs + TAT NP and MSCs + TAT PTX NP resulted in about 30% to 60% increase in platelet count (Table 2). Previous studies have shown that MSCs can increase platelet count through induction of interlukein-10 (IL-10) and TGF-β [36]. None of the other hematological parameters were affected by the treatments (Table 2, Table S1).

Table 1. Effect of different treatments on liver function test. Data represents mean ± SD (n = 4).

Parameters	Saline		MSCs + TAT NP		TAT PTX NP		MSCs + TAT PTX NP	
	Day 7	Day 18	Day 7	Day 18	Day 7	Day 18	Day 7	Day 18
ALT (U/L)	33.0 ± 7.0	37.0 ± 5.3	33.5 ± 4.7	36.0 ± 5.4	32.5 ± 4.5	33.5 ± 5.5	35.8 ± 6.4	40.0 ± 4.4
AST (U/L)	80.7 ± 9.7	87.3 ± 13.1	85.8 ± 11.5	90.0 ± 10.8	85.7 ± 7.7	90.3 ± 10.0	84.8 ± 11.7	91.5 ± 5.8
GGT(U/L)	1.0 ± 0.0	1.0 ± 0.0	1.0 ± 0.0	1.0 ± 0.0	1.0 ± 0.0	1.0 ± 0.0	1.0 ± 0.0	1.0 ± 0.0
ALP (U/L)	94.3 ± 5.9	100.7 ± 7.1	90.3 ± 4.9	96.8 ± 11.0	95.5 ± 4.2	98.0 ± 16.5	95.0 ± 6.5	100.8 ± 10.3
TP (g/dL)	5.8 ± 0.2	5.4 ± 0.3	5.8 ± 0.3	5.9 ± 0.3	5.7 ± 0.2	5.5 ± 0.1	5.8 ± 0.2	5.3 ± 0.1
ALB (g/dL)	3.5 ± 0.1	3.2 ± 0.1	3.5 ± 0.2	3.4 ± 0.2	3.5 ± 0.1	3.4 ± 0.1	3.5 ± 0.1	3.4 ± 0.1
GLOB (g/dL)	2.3 ± 0.1	1.9 ± 0.1	2.3 ± 0.2	2.5 ± 0.2	2.1 ± 0.2	2.0 ± 0.1	2.3 ± 0.1	2.4 ± 0.0
A/G	1.5 ± 0.1	1.7 ± 0.1	1.6 ± 0.1	1.4 ± 0.1	1.7 ± 0.1	1.7 ± 0.1	1.5 ± 0.1	1.4 ± 0.0
TBIL (mg/dL)	0.3 ± 0.1	0.4 ± 0.1	0.3 ± 0.0	0.2 ± 0.0	0.3 ± 0.1	0.3 ± 0.0	0.2 ± 0.0	0.3 ± 0.1

Abbreviations: ALT-alanine aminotransferase; AST-aspartate aminotransferase; GGT-gamma-glutamyl transferase; ALP-alkaline phosphatase; TP-total protein; ALB-albumin; GLOB-globulin; A/G-albumin/globulin ratio; TBIL-total bilirubin.

Table 2. Effect of different treatments on complete blood count. Data represents mean ± SD (n = 4).

Parameters	Saline		MSCs + TAT NP		TAT PTX NP		MSCs + TAT PTX NP	
	Day 7	Day 18	Day 7	Day 18	Day 7	Day 18	Day 7	Day 18
WBC ($\times 10^3$ cells/μL)	5.0 ± 1.4	6.3 ± 0.5	4.9 ± 0.8	5.0 ± 0.6	5.3 ± 0.6	4.4 ± 0.2	5.6 ± 1.2	4.7 ± 0.7
RBC ($\times 10^6$ cells/μL)	9.8 ± 0.3	9.7 ± 0.3	9.8 ± 0.2	9.5 ± 0.3	9.8 ± 0.1	9.1 ± 0.3	9.7 ± 0.2	9.1 ± 0.1
HGB (g/dL)	15.4 ± 0.4	15.5 ± 0.6	15.3 ± 0.3	15.0 ± 0.5	15.6 ± 0.2	14.8 ± 0.3	15.1 ± 0.3	14.3 ± 0.3
HCT (%)	50.9 ± 1.1	49.2 ± 1.7	50.2 ± 1.0	46.5 ± 1.6	51.4 ± 0.7	46.1 ± 1.5	49.5 ± 0.9	45.6 ± 0.9
PLT ($\times 10^3$ cells/μL)	840 ± 26	977 ± 50	1106 ± 224	1248 ± 131	914 ± 60	1060 ± 103	1349 ± 238	1234 ± 147

Abbreviations: WBC-white blood cell; RBC-red blood cell; HGB-hemoglobin concentration; HCT-hematocrit; PLT-platelets.

3. Discussion

Current approaches to tumor targeted drug delivery rely on passive accumulation of the drug carrier in the tumor through the 'enhanced permeation and retention' (EPR) effect, followed by internalization into tumor cells through either non-specific endocytosis or specific receptor-mediated endocytosis. However, the leaky tumor vasculature and dysfunctional lymphatics that allow for enhanced permeation of nano delivery systems also result in elevated interstitial fluid pressure that inhibits convective transport within the tumor microenvironment. In addition, tumors have a dense extracellular matrix that hinders diffusion. These physiologic and anatomic barriers constrain the extent of drug distribution within the tumor and limit the overall therapeutic effectiveness of synthetic delivery systems.

Recent studies have shown that cell-based drug carriers such as MSCs can infiltrate tumor tissue more uniformly, and thus improve the intra-tumoral distribution of the therapeutic payload. MSCs have been shown to actively traffic to both primary tumors and metastases, in response to inflammatory signals secreted by neutrophils and macrophages infiltrating the tumor, which enables the possibility of true active targeting of anticancer agents to the tumor tissue [13]. However, it is difficult to load small molecules in cells because of their diffusional clearance out of the cells. In addition, overexpression of drug efflux transporters such as P-glycoprotein in MSCs limits the loading of anticancer drugs, many of which are substrates for efflux transporters [37]. Several attempts have been made to load MSCs with anticancer therapeutics using polymeric nanoparticles [17,35,38], micelles [39], liposomes [40], carbon nanotubes [15], and dendrimers [41]. A key limitation with these methods is the limited drug loading efficiency [35,37]. For example, Zhang et al. investigated MSCs to deliver doxorubicin-polymer conjugates for glioma therapy [41]. However, the doxorubicin content in MSCs (5.81 ± 0.27 pg/cell) was found to be inadequate to meet the effective dose needed for systemic administration based on the maximum number of cells that could be injected. In our previous study, PTX loaded PLGA nanoparticles were used to load MSCs, but exocytosis of PLGA nanoparticles from MSCs reduced the amount of nanoparticle- and PTX payload that can could be loaded in MSCs (4.7 pg/cell) [35]. We hypothesized that this limitation can be overcome by increasing the cellular uptake and retention of nanoparticles. It has been previously shown that TAT peptide can be used to enhance the intracellular delivery of diverse bioactive molecules [23–28]. Attachment of TAT peptide to the surface of a drug carrier was shown to enhance the cellular uptake of the carrier [42]. Feiner-Gracia et al. also demonstrated that TAT functionalized PLGA nanoparticles were efficient in crossing plasma membrane and releasing their cargo inside the cells [43]. The increased uptake of TAT functionalized nanoparticles was attributed to the cationic nature of peptide, which was responsible for strong electrostatic interactions with anionic cell membrane, resulting in permeabilization and hence enhanced penetration inside the cells. Based on these findings, PLGA nanoparticles surface functionalized with TAT peptide were used to increase the drug loading capacity of MSCs. Our results further demonstrated that TAT functionalization improved drug loading in MSCs by ~3.4-fold compared to that with non-functionalized nanoparticles by increasing the uptake as well as retention of nanoparticles inside MSCs.

Although our aim was to generate nano-engineered MSCs with high drug loading, it was also critical to ensure that nano-engineering process did not alter MSCs phenotype or their viability. Our studies demonstrate that MSCs engineered with TAT NP retained their capacity to undergo osteogenic and adipogenic differentiation. Similarly, loading MSCs with TAT PTX NP did not affect their migration and tumor tropism, a property critical for their use in tumor-targeted drug delivery. Additionally, the viability of nano-engineered MSCs is essential for their tumor homing and sustained release of drugs at the tumor site. TAT conjugated nanoparticles did not result in toxicity when incubated with MSCs at the concentrations required for nano-engineering process. These results confirmed that TAT PTX NP loading had no negative impact on the phenotype or viability of MSCs.

Systemic injection of high number of MSCs can cause micro embolism, which could further lead to vascular obstruction, stroke and/or death. To evaluate the maximum number of MSCs that

can be administered intravenously without causing adverse effects, we dosed 2, 4, and 6 million MSCs/mouse. This preliminary study showed that a bolus dose of 2 or 4 million MSCs did not cause any gross toxicity or adverse effects over a one-week observation period. Based on the results of this study, we selected a dose of 4 million nano-engineered MSCs/mouse (equivalent to 3.2 mg per kg BW PTX). Despite significantly lower total dose of PTX (25.6 mg/kg total dose for MSCs + TAT PTX NP Vs 120 mg/kg total dose for free drug), nano-engineered MSCs resulted in significantly greater tumor inhibition compared to free drug. Importantly, the mean survival of mice treated with nano-engineered MSCs (109 days for MSCs + TAT PTX NP) was higher than that for the mice treated with PTX solution (86 days). Further, PTX has been shown to cause several dose-dependent toxicities such as leukopenia, neutropenia, and abnormalities in liver enzymes, including ALP, ALT and bilirubin [44,45]. Our previous studies also demonstrated that treatment with PTX solution (administered at 40 mg/kg on day 0, 4, and 8) led to decrease in both WBC and RBC count as well as abnormalities in liver enzyme induction [16]. However, in our current studies we did not observe any of these toxicities.

Finally, immunohistochemical studies confirmed that PTX delivered using nano-engineered MSCs resulted in greater inhibition of angiogenesis, decreased tumor cell proliferation and increased apoptosis, all of which point to improved tumor delivery of the drug with MSCs nano-engineered using TAT PTX NP.

4. Materials and Methods

4.1. Materials

TAT peptide, TCEP, polyvinyl alcohol (PVA), alizarin red and oil red O were obtained from Sigma (St. Louis, MO, USA). SPDP was purchased from Biovision (Milpitas, CA, USA). Amplite™ fluorimetric total thiol quantitation assay kit was purchased from AAT Bioquest, Inc. (Sunnyvale, CA, USA). PTX was purchased from TCI America, Portland, OR, USA. FITC labeled TAT peptide (FITC-LC-YGRKKRRQRRR-NH2) was purchased from AnaSpec (Fremont, CA, USA). Ester-terminated 50:50 poly (DL-lactide-co-glycolide) (inherent viscosity: 0.55–0.75 dL/g) was purchased from Lactel Absorbable Polymers (Birmingham, AL, USA). Poly (L-lactide)-b-polyethylene glycol-maleimide and poly (lactide-co-glycolide)-rhodamine B (lactide to glycolide ratio of 50:50, rhodamine B endcap, Mn 10,000–30,000 Da) were purchased from PolySciTech (West Lafayette, IN, USA). Fetal bovine serum (FBS) and penicillin/streptomycin were procured from Bioexpress (Kaysville, UT, USA). RPMI 1640, Dulbecco's phosphate buffered saline (DPBS), and trypsin-EDTA solutions were purchased from Invitrogen Corporation (Carlsbad, CA, USA). Mesenchymal stem cell media (MSCM) and human MSCs were obtained from ScienCell Research Laboratories (Carlsbad, CA, USA). A549-luc cell line was purchased from Caliper Life sciences (Waltham, MA, USA). D-Luciferin potassium salt was purchased from Gold Biotechnology (Saint Louis, MO, USA). Female Fox Chase SCID Beige mice (CB17.Cg-PrkdcscidLystbg-J/Crl) were purchased from Charles River Laboratories.

4.2. Synthesis of Sulfhydryl Activated TAT Peptide

Amine groups in the TAT peptide were converted into free thiols using the heterobifunctional cross-linker SPDP followed by treatment with TCEP (Figure 1B). TAT peptide (1 mg) was dissolved in PBS buffer. A 2-fold molar excess of SPDP was added to TAT peptide solution and incubated on a rotating platform for 2 h, followed by reduction with a 20-fold molar excess of TCEP for 2 h. The thiolated TAT peptide was purified using a polyacrylamide desalting column. The presence of thiol in TAT peptide was quantified using amplite™ fluorimetric total thiol quantitation assay kit (AAT Bioquest, Inc., Sunnyvale, CA, USA). The thiolated TAT peptide was subsequently used to functionalize nanoparticles containing surface maleimide groups.

4.3. Preparation of TAT-functionalized PLGA Nanoparticles

PTX loaded PLGA nanoparticles were prepared according to a previously described single emulsion-solvent evaporation technique (Figure 1C) [38]. In brief, PTX (7 mg) and PLGA (32 mg) were dissolved in 1 mL of chloroform and added to 8 mL of 2.5% *w*/*v* PVA solution. The mixture was sonicated using a probe sonicator set at an output of 18–21 W for 5 min (Sonicator XL, Misonix, NY, USA). The block co-polymer poly(L-lactide)-b-polyethylene glycol-maleimide (PLA-PEG-Mal; 8 mg) was dissolved in 0.2 mL chloroform and added to the emulsion with continuous stirring. The emulsion was further stirred overnight under ambient conditions, followed by 1 h stirring under vacuum to completely remove chloroform. The resulting nanoparticles were washed by ultracentrifugation at 35,000 rpm for 35 min at 4 °C (Optima XPN-80 Ultracentrifuge, Rotor type: 50.2 Ti, Beckman Coulter) followed by resuspension in deionized water three times. After the final wash, the nanoparticle pellet was dispersed in deionized water and centrifuged at 1000 rpm for 10 min. The supernatant was then reacted with thiolated TAT peptide. The resulting dispersion was stirred overnight at 4 °C. TAT peptide functionalized nanoparticles (TAT PTX NP) were then centrifuged to remove unreacted TAT peptide, and lyophilized (Labconco, FreeZone4.5). Blank nanoparticle formulation without the drug (TAT NP) was synthesized similarly. Drug-free, rhodamine-labeled nanoparticles were formulated by adding 5 mg PLGA-rhodamine B to 27 mg PLGA (total 32 mg polymer).

4.4. Characterization of Nanoparticles

Delsa Nano C particle analyzer (Beckman Coulter, California, USA) was used to determine the hydrodynamic diameter and zeta potential (surface charge). Nanoparticles were dispersed in deionized water (0.1 mg/mL) using probe sonication (18–21 W for one min). Analysis was performed at 25 °C and a scattering angle of 165°.

To determine PTX loading, nanoparticles were dispersed in methanol (1 mg/mL) and the drug was extracted overnight using a rotary extractor at room temperature. Nanoparticles were separated from free PTX by centrifugation at 13,000 rpm for 30 min, and PTX concentration of the methanolic extract was analyzed using HPLC [46].

To determine the extent of TAT peptide conjugation, nanoparticles were prepared with FITC-labeled TAT peptide and fluorescence spectroscopy was used to measure TAT associated fluorescence. Briefly, 1 mg of FITC-TAT nanoparticles was dispersed in deionized water and fluorescence intensity (λex: 493 and λem: 522 nm) was recorded using a SpectraMax i3x multi-mode microplate reader (Molecular Devices, LLC, CA, USA). Nanoparticles formulated without FITC-TAT were used as blank control. The amount of TAT peptide conjugated to nanoparticles was quantified using the standard curve of FITC-TAT solutions in deionized water (0.25–32 μg/mL).

The release of PTX from TAT PTX NPs was determined in MSC culture medium supplemented with 10% *w*/*v* Captisol® (Cydex Pharmaceuticals, Lawrence, KS). Aliquots of nanoparticle dispersion (0.5 mL, 0.1 mg/mL) were kept in an incubator shaker (37 °C; 100 rpm). At each time point (1 h, 2 h, 4 h, 1 day, 2 days, 3 days, 5 days, and 8 days), samples (n = 4) were centrifuged at 13,000 rpm for 15 min. The supernatant (0.45 mL) was collected and analyzed directly for PTX content by HPLC as described above.

4.5. Cell Culture

Human MSCs were cultured in human MSC complete medium (ScienCell Research Laboratories, Carlsbad, CA, USA). A549-luc cells were cultured in RPMI 1640 medium containing 10% FBS, penicillin (100 IU/mL) and streptomycin (100 μg/mL). All the cells were cultured at 37 °C in a humidified incubator containing 5% CO_2 and 95% air and monitored regularly for morphology and growth characteristics.

4.6. Nanoparticle Uptake and Retention in MSCs

For uptake studies, nanoparticles were fabricated using PLGA polymer that was covalently labeled with rhodamine. MSCs were plated onto a 24-well plate at a density of 1×10^4 cells/well in 0.5 mL of MSC growth medium. Next day, the growth medium was removed, and cells were incubated with nanoparticle dispersion in culture medium (100 μg/mL) for 0.5 h, 1 h, 2 h, 4 h, and 6 h at 37 °C. At each time point, a group of wells were washed 3 times with DPBS and the cells in those wells were lysed in 300 μL of DPBS by subjecting them to 3 freeze thaw cycles. The amount of nanoparticles in the cell lysates was determined by monitoring rhodamine fluorescence using an IVIS spectrum imaging system (Caliper Life Sciences, λex: 535 nm and λem: 580 nm). For the retention study, cells were incubated with nanoparticles for 4 h followed by two washes with DPBS (this was designated as the 0 h time point). Cells were further incubated with fresh culture medium at 37 °C. At various time points over 4 h, cells were washed with DPBS, lysed and the amount of nanoparticles in the cell lysate was determined. Data was represents % of nanoparticles retained insides cells relative to the 0 h time point.

4.7. Preparation of Nano-Engineered MSCs

MSCs in suspension (2×10^5 cells/mL) were incubated with nanoparticle dispersion in cell culture medium (100 μg/mL) in a rotating shaker at 37 °C. After 4 h of incubation, the cell suspension was washed thrice by centrifugation at 1000 rpm for 5 min (Allegra X-30R Centrifuge, Rotor type: SX4400, Beckman Coulter) followed by resuspension in DPBS to remove uninternalized nanoparticles. The final cell pellet was resuspended in DPBS for further studies.

4.8. In Vitro Migration Potential of Nano-Engineered MSCs

In vitro migration potential of nano-engineered MSCs was evaluated using a 96-Transwell® plate. MSCs were serum starved for 24 h prior to the migration study. To initiate the study, 5×10^3 untreated or nano-engineered MSCs in 50 μL serum-free medium were added to the top well of a 96-well Transwell® plate separated by an 8.0 μm pore size PET membrane (Corning Life Sciences, Lowell, MA, USA). Bottom wells were filled with 200 μL of 5% (v/v) serum containing, serum-free, or tumor-reconditioned media. Tumor reconditioned media was generated by incubating A549 cells with 5% (v/v) serum containing media for 24 h. After incubating at 37 °C for 24 h, both top and bottom wells were washed with DPBS and 150 μL of calcein AM solution (1.2 μg/mL) in cell dissociation media was added to the bottom well followed by 1 h incubation in the dark at 37 °C. The cell suspension was transferred to a black-walled 96-well plate and the fluorescence intensities were recorded at excitation and emission wavelengths of 485 nm and 520 nm, respectively. The number of migrated cells was quantified using standard curves constructed using untreated and nano-engineered MSCs stained with calcein AM.

4.9. Effect of Nano-Engineering on MSC Viability

MSCs were seeded in a 24 well plate at a density of 1×10^4 cells/well. Next day, cells were treated with 100 μg/mL nanoparticles at 37 °C. After 4 h incubation, nanoparticle dispersion was removed, cells were washed three times with DPBS, and the cell viability was determined by MTS assay. MSCs grown in cell culture medium was used as a control and percent cell survival was calculated using the following equation:

$$Cell\ survival\ (\%) = \frac{(Absorbance\ of\ treated\ cells - background)}{(Absorbance\ of\ untreated\ cells - background)} \times 100 \quad (1)$$

4.10. Differentiation Potential of Nano-Engineered MSCs

Nano-engineered MSCs were seeded at a density of ~4×10^4 cells/well in a 24-well plate, and then incubated with adipogenic or osteogenic differentiation media (StemPro Osteogenesis or Adipogenesis Differentiation Kits, Life Technologies, Carlsbad, CA, USA) for 3 weeks. The medium was replaced every 3–4 days. The untreated MSCs incubated with differentiation media and those incubated with regular culture media were used as positive and negative controls, respectively. After a 3-week incubation period, cells were fixed with 4% formalin and stained with alizarin red or oil red O to visualize osteogenic and adipogenic differentiation, respectively. Images were captured using a light microscope at 20× magnification.

4.11. In Vitro Cell Growth Inhibition Studies

The cytotoxicity of nano-engineered MSCs against A549 (human lung adenocarcinoma) cells was evaluated using MTS assay. A549 cells were seeded at a density of ~2×10^4 cells per well in 600 µL of RPMI 1640 medium in the bottom chamber of a 24 well Transwell® plate. Nano-engineered MSCs at different cell densities (in 100 µL medium) were added to the top well of the Transwell® plate separated by a 0.2 µm pore size PET membrane. PTX solution and TAT PTX NP were used as positive controls. After 3 days of incubation, A549 cell viability was determined by MTS assay. A549 cells grown in RPMI 1640 medium was used as a control, and the percentage of cell survival was calculated using Equation 1.

4.12. Therapeutic Efficacy of Nano-Engineered MSCs in Orthotopic Lung Tumor Model

All experiments involving animals were approved by the Institutional Animal Care and Use Committee (IACUC) of the University of Minnesota (Animal protocol No.: 1605-33821A, approval date: 25 July 2016). Female Fox Chase SCID Beige mice (CB17.Cg-PrkdcscidLystbg-J/Crl), 6–8 weeks old (each weighing 18–21 g), were injected intravenously with 1×10^6 A549-luc cells dispersed in 200 µL DPBS. Tumor growth in the lungs was monitored by bioluminescence imaging. Mice were injected intraperitoneally with 150 mg/kg of D-luciferin potassium salt solution prior to imaging on an IVIS spectrum in vivo imaging system (Caliper Life Sciences). When tumor bioluminescence reached ~5×10^5 photons/sec, mice were randomly assigned to five groups and were treated with intravenous injection of DPBS (200 µL at every 14 days, 'Saline'; $n = 8$), PTX solution (administered at 40 mg/kg on day 0, 4, and 8; 'PTX solution'; $n = 8$), TAT PTX NP (equivalent to 3.2 mg/kg PTX every 2 weeks; 'TAT PTX NP'; $n = 8$), MSCs loaded with TAT NP (4×10^6 every 2 weeks, 'MSCs + TAT NP', $n = 8$), or MSCs loaded with TAT PTX NP (4×10^6 MSCs equivalent to 3.2 mg/kg PTX every 2 weeks, 'MSCs + TAT PTX NP', $n = 10$). Dosing regimen for PTX solution was selected based on our previously published results [16]. Tumor growth was monitored by imaging tumor bioluminescence twice weekly initially and then once a week. Animals were euthanized using CO_2 when they showed signs of stress such as loss of appetite, weight loss, and/or ruffled hair. Tumor-bearing lungs were collected at the end of the study and processed for immunohistochemistry.

4.13. Toxicology Assessment of Intravenously Administered Nano-Engineered MSCs

Healthy SCID beige mice were administered with DPBS (control, $n = 8$), TAT PTX NP (administered at 3.2 mg per kg BW PTX on day 0 and 14, $n = 8$); MSCs + TAT NP (4×10^6 cells on day 0 and 14, $n = 8$); MSCs + TAT PTX NP (4×10^6 cells, equivalent to 3.2 mg per kg BW PTX on day 0 and 14, $n = 8$). For complete blood count (CBC), ~250 µL blood per mouse was collected from four mice in each group into EDTA tubes and gently mixed to prevent clotting. For liver function test, ~300 µL blood was collected from remaining four mice in each group into heparin-coated tubes. All the samples were analyzed by Charles River Clinical Pathology Services (Shrewsbury, MA, USA).

4.14. Immunohistological Staining of Lung Tumors

Lung tumors from the therapeutic study were fixed in 4% *w*/*v* formaldehyde solution for 24 h and subsequently transferred to 70% (*v*/*v*) ethanol. Tissue samples were embedded in paraffin and sectioned into 4 µm-thick slices. The sections were deparaffinized and stained for cleaved caspase-3, Ki67, and CD31. Both cleaved-caspase 3 (Cell Signaling Technology, Danvers, MA, USA) and Ki-67 clone SP-6 (Biocare Medical, Concord, CA, USA) staining used a 1:100 antibody concentration followed by Envision Rabbit Horseradish Peroxidase (HRP) detection system (Dako, Carpinteria, CA, USA). CD31 assay used a 1:1200 antibody concentration (Santa Cruz Biotechnology, Santa Cruz, CA, USA) followed by Goat-on-Rodent HRP polymer system (Biocare Medical). All the sections were developed using DAB chromogen (Dako) and counterstained with Mayer's Hematoxylin (Dako). The relative staining for each target was analyzed by Image J software (https://imagej.nih.gov/ij/download.html) to determine the fraction of positive stain per unit tissue area.

4.15. Statistical Analysis

The statistical significance of observed differences between groups was determined by one-way ANOVA, followed by Bonferroni-Holm post-hoc analysis for comparison between individual groups. Log-rank test was conducted to compare the survival distribution of different treatment groups. A probability level of $p < 0.05$ was considered significant.

5. Conclusions

In summary, we demonstrated significantly improved drug loading in MSCs by using TAT functionalized nanoparticles. These nano-engineered MSCs retained their osteogenic and adipogenic differentiation properties and tumor-tropism. Moreover, nano-engineered MSCs were effective in inhibiting tumor growth and increasing the overall survival in a mouse orthotopic lung tumor model.

Supplementary Materials: The following are available online at http://www.mdpi.com/2072-6694/11/4/491/s1, Figure S1: Preparation of TAT functionalized PLGA nanoparticles, Table S1: Effects of different treatments on complete blood count.

Author Contributions: G.M., B.L., S.P. (Swayam Prabha) and J.P. designed the experiments. G.M., B.L., L.T., and S.P. (Samuel Putnam) performed the experiments. S.P. (Swayam Prabha) and J.P. wrote the paper with the inputs from G.M. and B.L.

Funding: This work was supported by the NIH (EB022558 to S.P. (Swayam Prabha) and EB019893 to J.P.).

Acknowledgments: We acknowledge support provided by Tanmoy Sadhukha and Jairam Meena for preliminary studies. We sincerely thank Paula Overn (Comparative Pathology Shared Resource) for immunohistological staining of lung tumor tissues. Live animal imaging (bioluminescence imaging) was performed at the University Imaging Center (UIC) at the University of Minnesota.

Conflicts of Interest: The authors declare no conflict of interest.

References

1. Eberhard, A.; Kahlert, S.; Goede, V.; Hemmerlein, B.; Plate, K.H.; Augustin, H.G. Heterogeneity of angiogenesis and blood vessel maturation in human tumors: Implications for antiangiogenic tumor therapies. *Cancer Res.* **2000**, *60*, 1388–1393. [PubMed]
2. Forster, J.C.; Harriss-Phillips, W.M.; Douglass, M.J.; Bezak, E. A review of the development of tumor vasculature and its effects on the tumor microenvironment. *Hypoxia (Auckl)* **2017**, *5*, 21–32. [CrossRef] [PubMed]
3. Minchinton, A.I.; Tannock, I.F. Drug penetration in solid tumours. *Nat. Rev. Cancer* **2006**, *6*, 583–592. [CrossRef] [PubMed]
4. Stylianopoulos, T.; Martin, J.D.; Chauhan, V.P.; Jain, S.R.; Diop-Frimpong, B.; Bardeesy, N.; Smith, B.L.; Ferrone, C.R.; Hornicek, F.J.; Boucher, Y.; et al. Causes, consequences, and remedies for growth-induced solid stress in murine and human tumors. *Proc. Natl. Acad. Sci. USA* **2012**, *109*, 15101–15108. [PubMed]

5. Dewhirst, M.W.; Secomb, T.W. Transport of drugs from blood vessels to tumour tissue. *Nat. Rev. Cancer* **2017**, *17*, 738–750. [CrossRef]
6. Nichols, J.W.; Sakurai, Y.; Harashima, H.; Bae, Y.H. Nano-sized drug carriers: Extravasation, intratumoral distribution, and their modeling. *J. Control Release* **2017**, *267*, 31–46. [CrossRef] [PubMed]
7. Tan, Q.; Saggar, J.K.; Yu, M.; Wang, M.; Tannock, I.F. Mechanisms of Drug Resistance Related to the Microenvironment of Solid Tumors and Possible Strategies to Inhibit Them. *Cancer J.* **2015**, *21*, 254–262. [CrossRef] [PubMed]
8. Agrahari, V.; Mitra, A.K. Next generation drug delivery: Circulatory cells-mediated nanotherapeutic approaches. *Expert Opin. Drug Deliv.* **2017**, *14*, 285–289. [CrossRef] [PubMed]
9. Tan, S.; Wu, T.; Zhang, D.; Zhang, Z. Cell or cell membrane-based drug delivery systems. *Theranostics* **2015**, *5*, 863–881. [CrossRef] [PubMed]
10. Villa, C.H.; Anselmo, A.C.; Mitragotri, S.; Muzykantov, V. Red blood cells: Supercarriers for drugs, biologicals, and nanoparticles and inspiration for advanced delivery systems. *Adv. Drug Deliv. Rev.* **2016**, *106*, 88–103. [CrossRef] [PubMed]
11. Huang, B.; Abraham, W.D.; Zheng, Y.; Bustamante Lopez, S.C.; Luo, S.S.; Irvine, D.J. Active targeting of chemotherapy to disseminated tumors using nanoparticle-carrying T cells. *Sci. Transl. Med.* **2015**, *7*, 291ra294. [CrossRef] [PubMed]
12. Pang, L.; Qin, J.; Han, L.; Zhao, W.; Liang, J.; Xie, Z.; Yang, P.; Wang, J. Exploiting macrophages as targeted carrier to guide nanoparticles into glioma. *Oncotarget* **2016**, *7*, 37081–37091. [CrossRef] [PubMed]
13. Stuckey, D.W.; Shah, K. Stem cell-based therapies for cancer treatment: Separating hope from hype. *Nat. Rev. Cancer* **2014**, *14*, 683–691. [CrossRef] [PubMed]
14. Bago, J.R.; Alfonso-Pecchio, A.; Okolie, O.; Dumitru, R.; Rinkenbaugh, A.; Baldwin, A.S.; Miller, C.R.; Magness, S.T.; Hingtgen, S.D. Therapeutically engineered induced neural stem cells are tumour-homing and inhibit progression of glioblastoma. *Nat. Commun.* **2016**, *7*, 10593. [CrossRef]
15. Kim, S.W.; Lee, Y.K.; Hong, J.H.; Park, J.Y.; Choi, Y.A.; Lee, D.U.; Choi, J.; Sym, S.J.; Kim, S.H.; Khang, D. Mutual Destruction of Deep Lung Tumor Tissues by Nanodrug-Conjugated Stealth Mesenchymal Stem Cells. *Adv. Sci. (Weinh)* **2018**, *5*, 1700860. [CrossRef]
16. Layek, B.; Sadhukha, T.; Panyam, J.; Prabha, S. Nano-Engineered Mesenchymal Stem Cells Increase Therapeutic Efficacy of Anticancer Drug Through True Active Tumor Targeting. *Mol. Cancer* **2018**, *17*, 1196–1206. [CrossRef] [PubMed]
17. Zhao, Y.; Tang, S.; Guo, J.; Alahdal, M.; Cao, S.; Yang, Z.; Zhang, F.; Shen, Y.; Sun, M.; Mo, R.; et al. Targeted delivery of doxorubicin by nano-loaded mesenchymal stem cells for lung melanoma metastases therapy. *Sci. Rep.* **2017**, *7*, 44758. [CrossRef] [PubMed]
18. Wang, F.; Wang, Y.; Zhang, X.; Zhang, W.; Guo, S.; Jin, F. Recent progress of cell-penetrating peptides as new carriers for intracellular cargo delivery. *J. Control Release* **2014**, *174*, 126–136. [CrossRef] [PubMed]
19. Oh, N.; Park, J.-H. Endocytosis and exocytosis of nanoparticles in mammalian cells. *Int. J. Nanomed.* **2014**, *9* (Suppl. 1), 51–63. [CrossRef]
20. Guidotti, G.; Brambilla, L.; Rossi, D. Cell-Penetrating Peptides: From Basic Research to Clinics. *Trends Pharm. Sci.* **2017**, *38*, 406–424. [CrossRef] [PubMed]
21. Silhol, M.; Tyagi, M.; Giacca, M.; Lebleu, B.; Vives, E. Different mechanisms for cellular internalization of the HIV-1 Tat-derived cell penetrating peptide and recombinant proteins fused to Tat. *Eur. J. Biochem.* **2002**, *269*, 494–501. [CrossRef] [PubMed]
22. Brooks, H.; Lebleu, B.; Vives, E. Tat peptide-mediated cellular delivery: Back to basics. *Adv. Drug Deliv. Rev.* **2005**, *57*, 559–577. [CrossRef] [PubMed]
23. Kang, H.J.; Choe, W.; Kim, B.M.; Chung, S.J. IgG Fc-binding peptide (FcBP)-tat conjugate as a smart antibody carrier into live cells. *Macromol. Res.* **2015**, *23*, 876–881. [CrossRef]
24. Jo, J.; Hong, S.; Choi, W.Y.; Lee, D.R. Cell-penetrating peptide (CPP)-conjugated proteins is an efficient tool for manipulation of human mesenchymal stromal cells. *Sci. Rep.* **2014**, *4*, 4378. [CrossRef]
25. Zeng, Z.; Han, S.; Hong, W.; Lang, Y.; Li, F.; Liu, Y.; Li, Z.; Wu, Y.; Li, W.; Zhang, X.; et al. A Tat-conjugated Peptide Nucleic Acid Tat-PNA-DR Inhibits Hepatitis B Virus Replication In Vitro and In Vivo by Targeting LTR Direct Repeats of HBV RNA. *Mol. Nucleic Acids* **2016**, *5*, e295. [CrossRef] [PubMed]
26. Zhang, P.; Lock, L.L.; Cheetham, A.G.; Cui, H. Enhanced cellular entry and efficacy of tat conjugates by rational design of the auxiliary segment. *Mol. Pharm.* **2014**, *11*, 964–973. [CrossRef] [PubMed]

27. Layek, B.; Lipp, L.; Singh, J. Cell Penetrating Peptide Conjugated Chitosan for Enhanced Delivery of Nucleic Acid. *Int. J. Mol. Sci.* **2015**, *16*, 28912–28930. [CrossRef] [PubMed]
28. Majumder, P.; Bhunia, S.; Chaudhuri, A. A lipid-based cell penetrating nano-assembly for RNAi-mediated anti-angiogenic cancer therapy. *Chem. Commun. (Camb.)* **2018**, *54*, 1489–1492. [CrossRef] [PubMed]
29. Trabulo, S.; Cardoso, A.L.; Mano, M.; De Lima, M.C.P. Cell-Penetrating Peptides-Mechanisms of Cellular Uptake and Generation of Delivery Systems. *Pharmaceuticals (Basel)* **2010**, *3*, 961–993. [CrossRef] [PubMed]
30. Kauffman, W.B.; Fuselier, T.; He, J.; Wimley, W.C. Mechanism Matters: A Taxonomy of Cell Penetrating Peptides. *Trends Biochem. Sci.* **2015**, *40*, 749–764. [CrossRef] [PubMed]
31. Kaplan, I.M.; Wadia, J.S.; Dowdy, S.F. Cationic TAT peptide transduction domain enters cells by macropinocytosis. *J. Control. Release* **2005**, *102*, 247–253. [CrossRef] [PubMed]
32. Fittipaldi, A.; Ferrari, A.; Zoppé, M.; Arcangeli, C.; Pellegrini, V.; Beltram, F.; Giacca, M. Cell Membrane Lipid Rafts Mediate Caveolar Endocytosis of HIV-1 Tat Fusion Proteins. *J. Biol. Chem.* **2003**, *278*, 34141–34149. [CrossRef]
33. Duchardt, F.; Fotin-Mleczek, M.; Schwarz, H.; Fischer, R.; Brock, R. A Comprehensive Model for the Cellular Uptake of Cationic Cell-penetrating Peptides. *Traffic* **2007**, *8*, 848–866. [CrossRef]
34. Maiolo, J.R.; Ferrer, M.; Ottinger, E.A. Effects of cargo molecules on the cellular uptake of arginine-rich cell-penetrating peptides. *Biochim. Biophys. Acta (Bba) Biomembr.* **2005**, *1712*, 161–172. [CrossRef]
35. Sadhukha, T.; O'Brien, T.D.; Prabha, S. Nano-engineered mesenchymal stem cells as targeted therapeutic carriers. *J. Control. Release* **2014**, *196*, 243–251. [CrossRef] [PubMed]
36. Zhang, P.; Zhang, G.; Liu, X.; Liu, H.; Yang, P.; Ma, L. Mesenchymal stem cells improve platelet counts in mice with immune thrombocytopenia. *J. Cell. Biochem.* **2019**. [CrossRef] [PubMed]
37. Gao, Z.; Zhang, L.; Hu, J.; Sun, Y. Mesenchymal stem cells: A potential targeted-delivery vehicle for anti-cancer drug loaded nanoparticles. *Nanomed.: Nanotechnol. Biol. Med.* **2013**, *9*, 174–184. [CrossRef]
38. Layek, B.; Sadhukha, T.; Prabha, S. Glycoengineered mesenchymal stem cells as an enabling platform for two-step targeting of solid tumors. *Biomaterials* **2016**, *88*, 97–109. [CrossRef] [PubMed]
39. Tripodo, G.; Chlapanidas, T.; Perteghella, S.; Vigani, B.; Mandracchia, D.; Trapani, A.; Galuzzi, M.; Tosca, M.C.; Antonioli, B.; Gaetani, P.; et al. Mesenchymal stromal cells loading curcumin-INVITE-micelles: A drug delivery system for neurodegenerative diseases. *Colloids Surf. B Biointerfaces* **2015**, *125*, 300–308. [CrossRef] [PubMed]
40. Madeira, C.; Mendes, R.D.; Ribeiro, S.C.; Boura, J.S.; Aires-Barros, M.R.; da Silva, C.L.; Cabral, J.M.S. Nonviral gene delivery to mesenchymal stem cells using cationic liposomes for gene and cell therapy. *J. Biomed. Biotechnol.* **2010**, *2010*, 735349. [CrossRef] [PubMed]
41. Zhang, X.; Yao, S.; Liu, C.; Jiang, Y. Tumor tropic delivery of doxorubicin-polymer conjugates using mesenchymal stem cells for glioma therapy. *Biomaterials* **2015**, *39*, 269–281. [CrossRef] [PubMed]
42. Torchilin, V.P.; Rammohan, R.; Weissig, V.; Levchenko, T.S. TAT peptide on the surface of liposomes affords their efficient intracellular delivery even at low temperature and in the presence of metabolic inhibitors. *Proc. Natl. Acad. Sci. USA* **2001**, *98*, 8786–8791. [CrossRef]
43. Feiner-Gracia, N.; Dols-Perez, A.; Royo, M.; Solans, C.; Garcia-Celma, M.J.; Fornaguera, C. Cell penetrating peptide grafting of PLGA nanoparticles to enhance cell uptake. *Eur. Polym. J.* **2018**, *108*, 429–438. [CrossRef]
44. Alsharedi, M.; Gress, T.; Dotson, J.; Elmsherghi, N.; Tirona, M.T. Comparison of toxicity profile and tolerability between two standard of care paclitaxel-based adjuvant chemotherapy regimens in breast cancer. *Med. Oncol.* **2016**, *33*, 27. [CrossRef] [PubMed]
45. Mandaliya, H.; Baghi, P.; Prawira, A.; George, M.K. A Rare Case of Paclitaxel and/or Trastuzumab Induced Acute Hepatic Necrosis. *Case Rep. Oncol. Med.* **2015**, *2015*, 825603. [CrossRef] [PubMed]
46. Patil, Y.; Sadhukha, T.; Ma, L.; Panyam, J. Nanoparticle-mediated simultaneous and targeted delivery of paclitaxel and tariquidar overcomes tumor drug resistance. *J. Control Release* **2009**, *136*, 21–29. [CrossRef] [PubMed]

cancers

MDPI

Article

Targeted siRNA Nanoparticles for Mammary Carcinoma Therapy

Meital Ben-David-Naim [1], Arie Dagan [1], Etty Grad [1], Gil Aizik [1], Mirjam M. Nordling-David [1], Alisa Morss Clyne [2], Zvi Granot [3] and Gershon Golomb [1,*]

[1] Institute for Drug Research, Faculty of Medicine, The Hebrew University of Jerusalem, Jerusalem 9112001, Israel; meitalben@ekmd.huji.ac.il (M.B.-D.-N.); daganarie@gmail.com (A.D.); ettyg@ekmd.huji.ac.il (E.G.); gil.aizik@gmail.com (G.A.); mirjamd@ekmd.huji.ac.il (M.M.N.-D.)

[2] Department of Mechanical Engineering and Mechanics, Drexel University, Philadelphia, PA 19104, USA; alisam@coe.drexel.edu

[3] Institute for Medical Research Israel Canada, Faculty of Medicine, The Hebrew University of Jerusalem, Jerusalem 9112001, Israel; zvikag@ekmd.huji.ac.il

* Correspondence: gershong@ekmd.huji.ac.il; Tel.: +972-2-6758658; Fax: +972-2-6757126

Received: 17 February 2019; Accepted: 26 March 2019; Published: 29 March 2019

Abstract: Non-viral, polymeric-based, siRNA nanoparticles (NPs) have been proposed as promising gene delivery systems. Encapsulating siRNA in targeted NPs could confer improved biological stability, extended half-life, enhanced permeability, effective tumor accumulation, and therapy. In this work, a peptide derived from apolipoprotein B100 (ApoB-P), the protein moiety of low-density lipoprotein, was used to target siRNA-loaded PEGylated NPs to the extracellular matrix/proteoglycans (ECM/PGs) of a mammary carcinoma tumor. siRNA against osteopontin (siOPN), a protein involved in breast cancer development and progression, was encapsulated into PEGylated poly(D,L-lactic-co-glycolic acid) (PLGA) NPs using the double emulsion solvent diffusion technique. The NPs obtained possessed desired physicochemical properties including ~200 nm size, a neutral surface charge, and high siOPN loading of ~5 µg/mg. ApoB-P-targeted NPs exhibited both enhanced binding to isolated ECM and internalization by MDA-MB-231 human mammary carcinoma cells, in comparison to non-targeted NPs. Increased accumulation of the targeted NPs was achieved in the primary mammary tumor of mice xenografted with MDA-MB-231 mammary carcinoma cells as well as in the lungs, one of the main sites affected by metastases. siOPN NPs treatment resulted in significant inhibition of tumor growth (similar bioactivity of both formulations), accompanied with significant reduction of OPN mRNA levels (~40% knockdown of mRNA levels). We demonstrated that targeted NPs possessed enhanced tumor accumulation with increased therapeutic potential in mice models of mammary carcinoma.

Keywords: nanoparticles; targeted delivery system; siRNA; osteopontin; mammary carcinoma

1. Introduction

Polymeric nanoparticles (NPs), formulated with poly(D,L-lactic-co-glycolic acid) (PLGA) copolymer, have emerged as promising carriers for cancer therapy by delivering a wide variety of drugs, including small interfering RNAs (siRNAs) [1–5]. The unique characteristics that make PLGA-based NPs promising candidates for siRNA delivery include their ability to protect the siRNA molecules from degradation, overcoming the cell membrane absorption barrier thereby enabling siRNA internalization into the target cells, tunable sustained release properties, facile possibilities for surface functionalization, and their biocompatibility and biodegradability properties [6–9]. NPs accumulation in solid tumors is mediated mainly by a passive process (i.e., the enhanced permeability and retention effect (EPR)), based on the leaky vasculature and poor lymphatic drainage present in

the tumor [10–13]. Nanosized particles with neutral surface charges and/or a hydrophilic surfaces (PEGylation) have the propensity for increased circulation time because of decreased phagocytosis by the mononuclear phagocytic system (MPS), which consequently increases their EPR-based tumor accumulation [14]. Their ultimate fate is similar, however, to that of conventional NPs, and the liver/spleen will eventually take up the majority of circulating NPs [15,16]. Hence, for efficient NPs accumulation at the tumor site, a long circulation time and efficient particle targeting are critical. Incorporation of a targeting ligand in NPs' surfaces enables binding of the carrier with specific targets in the tumor tissue, which most often can be overexpressed, resulting in enhanced tumor accumulation and/or retention [17–19]. A broad range of ligands have been used for formulating targeted nanocarriers for enhanced tumor accumulation, including small molecules, carbohydrates, aptamers, peptides, proteins, or antibodies [20].

In our previous studies, PLGA-based NPs, containing antisense [7,21] and siRNAs [22,23] that were neither PEGylated nor targeted, have been examined in mammary carcinoma animal models. In the present study we sought to examine the feasibility of targeting siRNA-containing NPs to the cancer tissue by linking a specific navigator peptide to the NPs surface. In cancer, the tumor vasculature is highly permeable, and the sub-endothelial retention in the extracellular matrix (ECM) of low-density lipoproteins (LDLs) through their interaction with proteoglycans (PGs) is enhanced [24–26]. In vitro studies have identified sequences derived from the protein moiety of LDL, apolipoprotein B100 (apoB100), which binds the negatively charged PGs and LDL receptor (LDLr) with a high affinity [27–29]. We hypothesized that by linking an apoB100-derived peptide (25 AA; ApoB-P) to the NPs surface [30], the decorated NPs will be targeted to the tumor's ECM through their interaction with PGs in the tumor's microenvironment. As a model drug, we used an siRNA sequence specifically designed to knockdown the human osteopontin protein (OPN) [22,23]. OPN, a member of the small integrin-binding ligand N-linked glycoproteins (SIBLINGs) family [31], is considered as a multifunctional protein that plays a central role in malignancy [32–34]. Knockdown of OPN expression was shown by us and others to have antimetastatic and antitumorigenic effects [23,35–37]. We have shown that siRNA against OPN (siOPN) delivered by NPs inhibits tumor growth in an ectopic model of mammary carcinoma [22]. In this work, we examine whether the use of targeted NPs leads to both enhanced tumor accumulation and superior therapeutic efficacy. We evaluated the targeting efficiency of the ApoB-P NPs in vitro by examining their binding to both isolated basement membrane (BM) and ECM, and their uptake into breast cancer cells. In vivo, we further assessed their biodistribution and bioactivity in mammary carcinoma mice models.

2. Results

2.1. Poly(D,L-Lactic-Co-Glycolic Acid) Apolipoprotein B100 Peptide (PLGA-ApoB-P) Synthesis

The targeting peptide, ApoB-P, was linked to PLGA with a polyethylene glycol (PEG) spacer. PLGA-PEG-maleimide (PLGA-PEG-MAL) was synthesized by linking a heterobifunctional PEG containing a maleimide (MAL) group at one terminus to PLGA (Figure 1a). The successful linking between the PEG linker and PLGA was verified by ^{1}H NMR spectroscopy (Figure S1). ApoB-P linking in the final step of the synthesis (thiol-maleimide click reaction) was confirmed by amino acid analysis and by elemental analysis. The linking efficiency was >70%.

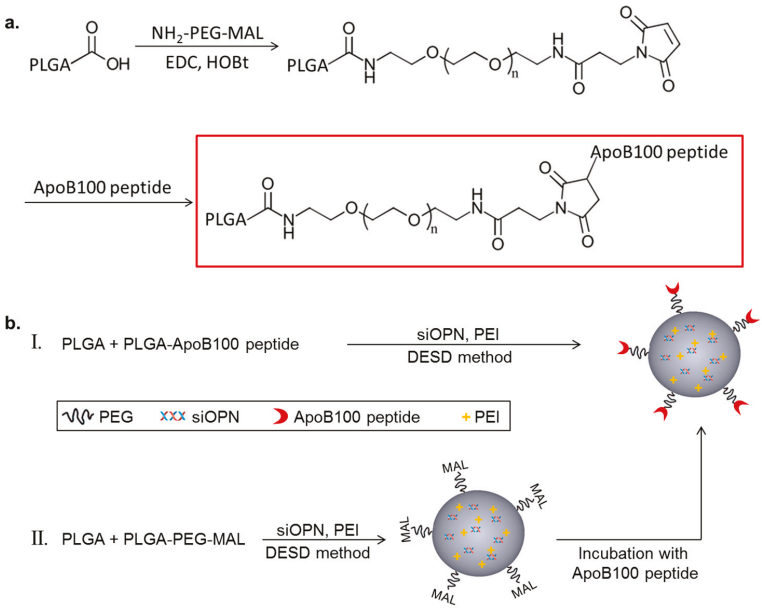

Figure 1. Schematic representation of PolyD,L-lactic-co-glycolic acid) apolipoprotein B100 peptide (PLGA-ApoB-P) synthesis (**a**), and targeted nanoparticle (NP) preparation (**b**), by two methods (I and II).

2.2. Nanoparticles (NPs) Physicochemical Properties

Targeted NPs (prepared by either method I or II, Figure 1b) and non-targeted NPs were successfully prepared using the double emulsion solvent diffusion (DESD) method. The NPs had a mean diameter of ~200 nm (empty and siOPN-loaded) with a narrow size distribution and a neutral surface charge (Table 1). siOPN was encapsulated in both targeted and non-targeted NPs, using polyethyleneimine (PEI) of 800 Da as the counter-ion for siOPN complexation, resulting in a relatively high siOPN loading of 4.9 and 5.1 μg/mg, and an encapsulation yield of 29.6% and 31.0%, respectively (Table 1).

Table 1. Physicochemical properties of targeted and non-targeted NPs (mean ± SD).

NP Type	Size (d., nm)	Polydispersity Index (PDI)	Surface Charge (ζ Potential, mV)	siOPN Loading (μg/mg NPs)	Encapsulation Yield (%)
Targeted empty	212.4 ± 3.6	0.21 ± 0.02	−0.9 ± 0.2	-	-
Non-targeted empty	207.3 ± 4.3	0.17 ± 0.02	−1.1 ± 0.1	-	-
Targeted siOPN	233.9 ± 3.7	0.29 ± 0.01	−0.6 ± 0.2	4.9 ± 0.2	29.6 ± 0.9
Non-targeted siOPN	228.5 ± 23.0	0.31 ± 0.04	−0.5 ± 0.1	5.1 ± 0.2	31.0 ± 1.4

2.3. In Vitro Binding and Uptake

2.3.1. Binding to Isolated Extracellular Matrix (ECM)

The binding affinity of targeted NPs to the ECM was evaluated by incubating the NPs with isolated ECM derived from porcine aortic endothelial cells. We validated the presence of ECM in the wells by fluorescent labeling for heparan sulfate proteoglycan (HSPG). No differences between targeted and non-targeted NPs were observed below NPs concentration of 5 mg/mL (Figure 2a). However, at a concentration of 10 mg/mL the targeted NPs showed enhanced binding to the ECM, compared to non-targeted NPs that remained almost undetected (Figure 2a).

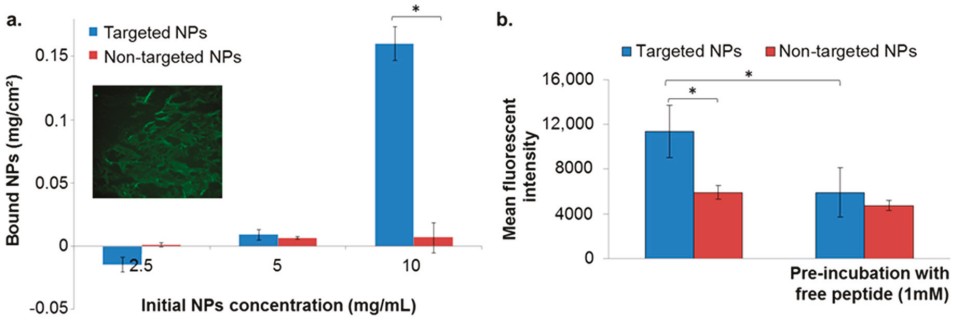

Figure 2. NPs binding to extracellular matrix (ECM) isolated from endothelial cells (**a**), and to basement membrane (**b**). Data is presented as mean ± SD, * $p < 0.05$. Validation of ECM matrix presence in the coated well is shown in the inset (**a**) conducted by fluorescent labeling for heparan sulfate proteoglycan (HSPG) (perlecan protein; basement membrane-specific heparan sulfate proteoglycan core protein).

2.3.2. Binding to the Basement Membrane (BM) Matrix

The binding affinity of targeted NPs to the BM was evaluated by incubating the NPs in wells pre-coated with Matrigel matrix, using 10 mg/mL of NPs. As in the isolated ECM model, targeted NPs exhibited higher binding affinities in comparison to non-targeted NPs (Figure 2b). Moreover, pre-incubation of the coated wells with free ApoB-P abolished the increased binding of the targeted NPs (Figure 2b). This further supported our hypothesis that the attachment of the NPs was to a specific target in the ECM, which was apparently saturated by the presence of the free ligand.

2.3.3. Uptake into the MDA-MB-231 Cell Line

To evaluate the enhanced uptake of the targeted NPs into MDA-MB-231 breast cancer cells, targeted and non-targeted fluorescent NPs were incubated with the cells for different durations, and internalized NPs were analyzed by flow cytometry (FACS). The number of cells with internalized targeted NPs was significantly higher at all time points (Figure 3(ai)), in comparison to cells with non-targeted NPs, by a factor of 4.4, 2.3, and 1.3 after 0.5, 1, and 2 h of incubation, respectively. At longer incubation time periods, the difference between the uptakes of targeted and non-targeted NPs declined.

In addition to the higher number of cells internalizing the targeted NPs, each cell engulfed a higher amount of the targeted formulation, demonstrated by the higher fluorescent intensity measured within the cells (Figure 3(aii)). The enhanced uptake of targeted NPs was further observed qualitatively by confocal laser scanning microscopy (Figure 3b), shown by the higher green staining of cells treated with the targeted formulation after 0.5 and 6 h (Figure 3b).

To further examine the mechanism of NPs internalization, targeted and non-targeted NPs were incubated with MDA-MB-231 cells at 4 °C and at 37 °C (Figure S2). Higher uptake of targeted compared to non-targeted NPs was observed at 37 °C (Figure S2). Lowering the temperature significantly reduced both targeted and non-targeted NPs uptakes, suggesting an active and energy-dependent endocytosis (Figure S2). Nevertheless, targeted NPs maintained their higher affinity and uptake at all time points examined, even at reduced temperatures (Figure S2). Of note, after 60 min of incubation, targeted NPs incubated at 4 °C demonstrated higher affinity compared with non-targeted NPs at 37 °C (Figure S2).

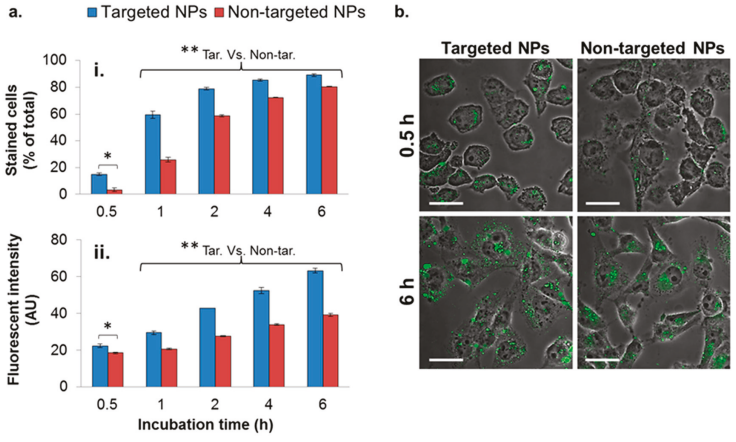

Figure 3. Cellular uptake of NPs by the MDA-MB-231 cell line. Cells internalizing NPs were analyzed quantitatively by means of flow cytometry (FACS) (**a**), and qualitatively by means of confocal laser scanning microscopy (**b**). A total of 10,000 cells were counted in each measurement ($n = 2$). Data is presented as the mean ± SD, * $p < 0.05$ for targeted (Tar) versus non-targeted (Non-tar) at 0.5 h. ** $p < 0.01$ at 1, 2, 4, and 6 h for targeted versus non-targeted comparisons. NPs are shown in green (PLGA-BODIPY); magnification 60×; size bar, 30 µm. The fluorescent intensity was normalized to untreated cells.

2.4. In Vivo Biodistribution—4T1 Intravenous (IV) Model

To evaluate the ability of NPs to accumulate at metastatic sites, the 4T1 IV model, a commonly employed model to study breast cancer lung metastasis, was used [38]. Metastatic lesions in the lungs were confirmed using bioluminescence (Figure S3), and the biodistribution of the NPs was studied as reported earlier [22]. Higher accumulation of the targeted NPs in the liver and spleen was noted after 8 h, but was similar after 24 h (Figure 4). There was no difference in the biodistribution of NPs in the kidneys. Significantly higher accumulation of the targeted NPs was observed in the metastatic lungs (1.8 times higher compared to non-targeted NPs) at 8 h after NPs injection (Figure 4). The same trend was observed after 24 h (borderline significance, $p = 0.07$).

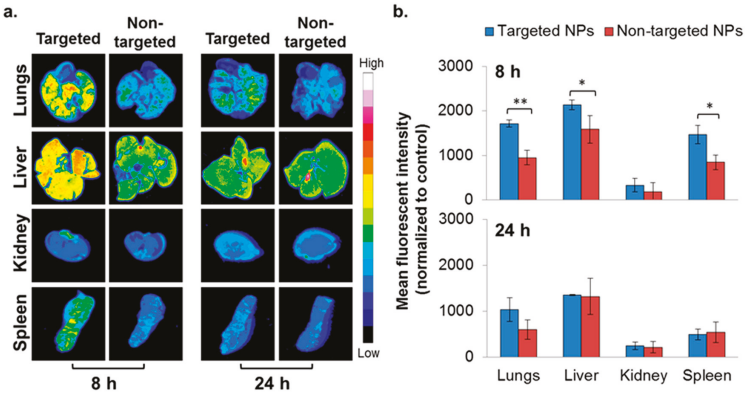

Figure 4. Biodistribution of NPs in the 4T1 intravenous (IV) model. Typhoon images (**a**) followed by ImageJ analysis (**b**) demonstrating targeted ($n = 3$) and non-targeted ($n = 3$) NPs accumulation in different organs. (Non-targeted NPs are described in [22].) The mean fluorescent intensity in each organ was normalized to untreated control. Data is presented as mean ± SD, * $p < 0.05$, and ** $p < 0.001$.

2.5. In Vivo Biodistribution—Orthotopic Xenograft Model

To evaluate the capability of the targeted formulation to accumulate in a primary tumor site, biodistribution was studied in the xenograft model of MDA-MB-231 human mammary carcinoma. Targeted NPs accumulated to a greater extent in the primary tumor site, at ~1.4 times higher than the non-targeted NPs (Figure 5c,d). A similar accumulation of targeted and non-targeted NPs was observed in the liver, spleen, and kidneys (Figure 5a,b). Of note, significantly increased uptake of the targeted NPs was observed in the lungs (Figure 5a,b).

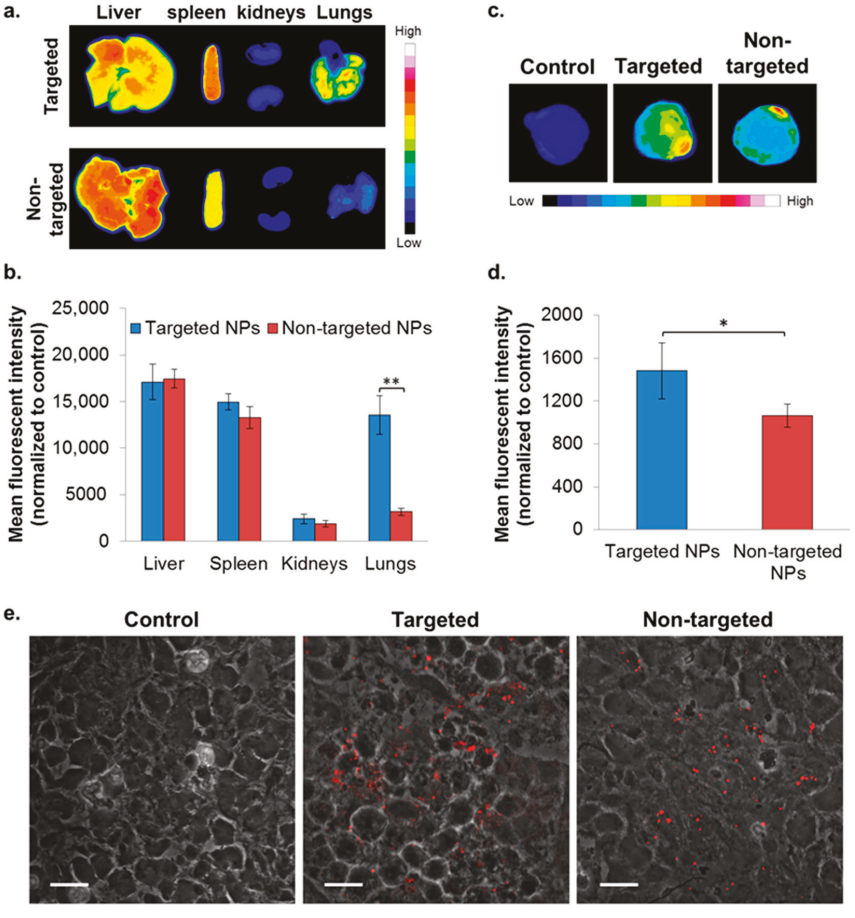

Figure 5. Biodistribution of NPs in the orthotopic xenografted mice model of MDA-MB-231 human mammary carcinoma cells. NPs biodistributions in selected organs (**a**,**b**) and in the primary tumor site (**c**,**d**) following treatment with targeted ($n = 2$) and non-targeted ($n = 3$) NPs was determined by Typhoon images followed by ImageJ analyses, 24 h after IV treatment. The mean fluorescent intensity in each organ was normalized to untreated control (mean ± SD, ** $p < 0.01$, and * $p < 0.05$). Representative confocal microscopy images for qualitative assessment of NPs accumulation in tumor cryosections is shown in (**e**); magnification 60×; size bar, 20 µm. NPs are shown in red (PLGA-Cy5). The fluorescent intensity was normalized to tumor cryosections of untreated control.

2.6. In Vivo Bioactivity—Orthotopic Xenograft Model

The bioactivity of the NPs was evaluated in the orthotopic MDA-MB-231 model, but not in the 4T1 model, because the siOPN sequence used was designed to knockdown human OPN, which is not expressed in the 4T1 cell line (mice origin). Treatment of mice xenografted with MDA-MB-231 human mammary carcinoma cells with targeted and non-targeted siOPN NPs resulted in a similar, significant suppression of tumor growth (Figure 6a). Congruent with significant tumor growth inhibition, a ~40% knockdown of OPN mRNA levels was also observed (Figure 6b).

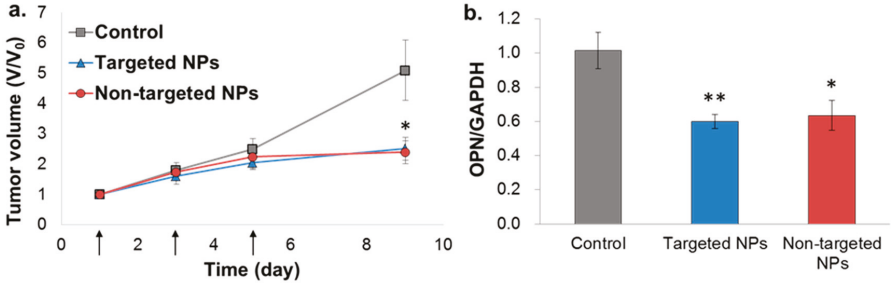

Figure 6. Tumor growth inhibition by siOPN NPs in the orthotopic xenograft MDA-MB-231 mammary carcinoma mice model. Targeted vs. non-targeted siOPN NPs were injected at a dose of 1 mg/kg by body weight of siOPN (arrows, (**a**)). Tumor size is presented as the tumor volume ratio, V/V_0. V and V_0, tumor volume measured at each time point and initial tumor volume (day 1), respectively, (mean ± SEM; n= 5–7 in each group, * $p < 0.05$, treatment vs. control). Knockdown of OPN mRNA levels evaluated by RT-PCR is shown in (**b**). OPN mRNA levels were normalized to GAPDH and to untreated control animals (mean ± SEM; n = 5–7 in each group, * $p < 0.05$, ** $p < 0.01$, treatment vs. control).

3. Discussion

Polymeric NPs based on the biocompatible and biodegradable PLGA have been explored for the delivery of siRNA [5,22,23,39]. PEGylated NPs, termed "stealth NPs", are characterized by increased residence times in the circulation and provide increased tumor accumulation via the EPR effect [1,40,41]. Nevertheless, a targeted delivery system (i.e., NPs decorated with a specific tissue/cell ligand) could further increase retention time at the diseased tissue [20,42,43]. In the present study, PLGA-PEG NPs containing siOPN were decorated with a navigator peptide (ApoB-P), which has affinity to PGs in the ECM of the tumor and to LDLr. We demonstrated that targeted NPs possessed significantly enhanced tumor accumulations and increased therapeutic potentials in mice models of mammary carcinoma.

The ligand, ApoB-P, is composed of two consecutive peptide dimers, derived from aa 3145 through 3157 and 3359 through 3367 (of apoB100), linked with a glycine–cysteine–glycine bridge (GCG; 3145–3157-GCG-3359–3367) [30]. The role of the individual dimers in the binding of LDL-apoB100 to PGs and to LDLr has been well established [44–47]. Olsson et al. [45] have shown that a heterodimer, linked by a glycine tripeptide (3145–3157-GGG-3359–3367), has higher affinity to PGs and LDLr than the two separated segments. We hypothesized that linking the two peptide dimers with the tripeptide, glycine–cysteine–glycine (GCG rather than GGG), could enable facile linking to PLGA-PEG, bestowing a U-shape orientation of the ligand—a conformation resembling that of the native apoB100 protein [27,44,48].

Targeted and non-targeted NPs containing siOPN, prepared by the DESD method, yielded NPs with a size of ~200 nm, a narrow size distribution (low PDI), and a neutral surface charge. The positively charged PEI of 800 Da, which was shown to be less toxic than the routinely used PEI of 25 kDa [22,49], was used as a counter-ion to the negatively charged siRNA in order to achieve efficient encapsulation. Depending on the N:P ratio (cation to anion molar ratio, e.g., the PEI nitrogen to siRNA

phosphate ratio), relatively high loading of siOPN was achieved (~5 μg of siOPN/mg of NPs). No difference in the loading of siOPN was found between targeted and non-targeted NPs, suggesting that the presence of PEG-linked ApoB-P to the surface of the NPs did not hamper the encapsulation of siOPN.

The competitive affinity studies, in the two models of BM and isolated ECM (Figure 2), validated the preferred binding of targeted NPs to BM/ECM, indicating their potential to bind and be retained in the tumor's extracellular space. In addition to the enhanced binding to BM/ECM, the targeted ApoB-P NPs demonstrated an increased uptake into MDA-MB-231 breast cancer cells up to 6 h of incubation (Figure 3). As expected, at longer incubation periods (4 and 6 h), differences between targeted and non-targeted NPs diminished since all the cells eventually engulfed the NPs. The increased uptake of targeted NPs by MDA-MB-231 cells, even at 4 °C (Figure S2), further supports the affinity of the targeted NPs to specific substrate(s) in the cells' membrane. Cell surface PGs [45] and LDLr, which are upregulated in tumor cells [50–52], are the most probable binding sites for the ApoB-P-decorated NPs. Taken together, we postulate that enhanced accumulation of the targeted NPs in the primary tumor could arise from their increased binding/retention at the tumor's ECM as well as their enhanced uptake into the tumor cells by receptor-mediated endocytosis.

Since Paget's "seed and soil" hypothesis [53], it is now well established that the lungs are among the primary organs affected in metastatic breast cancer [54,55]. We demonstrate preferred accumulation of the targeted NPs in the metastatic lungs of the 4T1-transplanted mice. A higher accumulation of the targeted NPs in the lungs was also observed in the orthotopic model of MDA-MB-231. Although lung macro-metastases were not observed at the time of sacrifice, micro-metastases are expected to form [56]. Another explanation for the higher accumulation in the lungs of the targeted NPs in the orthotopic model could be due to changes occurring in the pre-metastatic lungs. Evidence has emerged that early influx of neutrophils and other factors (including OPN) secreted by the primary tumor are key mechanisms in establishing the pre-metastatic niche for subsequent engraftment of tumor cells [57], and this leads to increased endothelial permeability and vascular leakiness [58,59]. In addition, PGs, being a major component of the ECM in the alveolar wall [60], are prevalent on the surface of lung capillary endothelium [61]. Nevertheless, the enhanced uptake in the lungs could be, at least in part, due to the abundant interstitial monocytes in this organ [62–64]. This is corroborated by the finding (Figure S4) that targeted NPs are engulfed to a higher extent than non-targeted NPs by white blood cells (WBCs), specifically by monocytes. This in turn is most likely because of the different PEGylation type of the NPs. PEG in non-targeted NPs (PLGA-PEG) is expected to be entirely functional in structure in comparison to that in targeted NPs since the PEG moiety is blocked at the end by the peptide (PLGA-PEG-ApoB-P). Taken together, the enhanced accumulation in the lungs of targeted NPs represents a significant potential for lung metastases therapy.

The major MPS organs responsible for particulate system sequestration and disposal are the liver and the spleen [21,65,66]. Indeed, in both mammary carcinoma models, substantial amounts of both targeted and non-targeted NPs were observed in these clearing organs, and similar levels were observed after 24 h (Figures 4 and 5a,b). Similarly, no difference in the disposition of targeted and non-targeted NPs was observed in kidneys, which exhibited the lowest level of biodistribution, probably because the size of the NPs was too large for renal filtration [65].

Finally, a significantly higher amount of the targeted vs. non-targeted NPs (1.4 times) was detected in the primary tumor site (Figure 5c,d). Of note, both targeted and non-targeted NPs were distributed throughout the tumor tissue, located in between the tumor cells (ECM) and inside the cells (Figure 5e). We anticipate that after reducing the uptake of targeted NPs by WBCs, higher levels in the tumor would be obtained. This can be achieved, for example, by adding PEG-PLGA chains in between the ApoB peptide-PEG-PLGA. Nonetheless, their accumulation in the tumor was significantly higher in comparison to non-targeted NPs, indicating their high affinity to the tumor tissue.

There are two possible explanations to the observation that both treatments of targeted and non-targeted siOPN NPs exhibited similar inhibition of tumor growth (Figure 6a). Perhaps the

higher levels of targeted NPs detected in the tumor were insufficient to exert a superior therapeutic effect. In addition, retention of the targeted NPs in the ECM of the tumor could have also limited their internalization into the cancer cells, resulting in similar bioactivity as the non-targeted NPs. Nevertheless, it is plausible to assume that the higher levels of targeted NPs found in the tumor could translate to superior efficacy at a later time period (tumor size was measured for a period of nine days since the first NPs injection). The therapeutic effect was in accord with that obtained in an ectopic xenograft model (MDA-MB-231 cells injected SC) treated with non-targeted siOPN NPs [22]. Although siOPN levels in the suppressed tumor were not determined, the therapeutic effect obtained by siOPN NPs was mediated by OPN mRNA knockdown (~40%; Figure 6b), validating our hypothesis. Overall, we developed a new platform for targeted siRNA delivery. This protean platform can be specifically tailored to deliver any siRNA of choice or, for that matter, any other drug intended to inhibit tumor growth. It should be noted that numerous reports describe tumor uptake of drugs following systemic administration by various types of NPs, mainly by the EPR principle [1,10,12,15,16,67–70]. The fate of nanomedicine has been criticized for lack of effective tumor accumulation [10,62,71–75]. In a recent review summarizing hundreds of studies performed in the field of tumor delivery systems [76], accumulation in the tumor tissue is on average 0.9% and 0.6% of the injected dose (ID), targeted and non-targeted NPs, respectively, and only 0.0014% ID of targeted NPs are detected in the tumor cells [77]. Our study provides a foundation for rationally developing new delivery strategies for cancer therapy.

4. Materials and Methods

4.1. Materials

PLGA (50:50, ester terminated, MW of 30–60 kDa), tris-EDTA buffer (TE buffer, RNase-free, 10 mM Tris-HCl, 1 mM EDTA), PEI (branched, 800 Da), poly(vinyl alcohol) (PVA, 30–70 kDa), *N*-(3-Dimethylaminopropyl)-N′-ethylcarbodiimide hydrochloride (EDC), 1-Hydroxybenzotriazole (HOBt), and Tris(2-carboxyethyl)phosphine hydrochloride (TCEP) were purchased from Sigma-Aldrich (Rehovot, Israel). PLGA 50:50, acid terminated, MW of 50–60 kDa was purchased from Lakeshore Biomaterials (Birmingham, AL, USA). PLGA-PEG copolymer (RGP d 50105, PLGA, 45 kDa, and PEG, 5 kDa) was purchased from Boehringer Ingelheim (Ingelheim, Germany). The heterobifunctional PEG, amine-PEG-maleimide (NH_2-PEG-MAL; PEG, 2 kDa) was purchased from Creative PEGWorks (Chapel Hill, NC, USA). siOPN (described in [22,23]) was custom synthesized by Thermo Fisher Scientific (Waltham, MA, USA). The navigator peptide, ApoB-P (a 25 AA sequence: SVKAQWKKNKHRHGCGRLTRKRGLK [30]; MW of ~3 kDa) was purchased from CASLO ApS (Lyngby, Denmark). Mannitol and organic solvents were obtained from J.T. Baker Chemicals (Radnor, PA, USA). Tissue culture reagents and phosphate buffered saline (PBS) were purchased from Biological Industries (Beit-Haemek, Israel).

4.2. PLGA-ApoB-P Synthesis

ApoB-P was linked to PLGA through a PEG spacer, as shown in Figure 1a. In the first step of the synthesis, a maleimide-functionalized di-block copolymer, PLGA-PEG-MAL, was synthesized by the conjugation of PLGA-COOH to the bi-functional NH_2-PEG-MAL. PLGA-COOH (0.017 mmol) dissolved in acetonitrile (ACN) was converted to an active ester using an excess of HOBt (0.7 mmol) and EDC (1 mmol), followed by a reaction with NH_2-PEG-MAL (0.034 mmol, NH_2-PEG-MAL/PLGA molar ratio of 2/1). The reaction mixture was left overnight, under constant stirring, at room temperature (RT; 23 °C). PLGA-PEG-MAL was precipitated by the addition of water, followed by centrifugation (4000 rpm, 10 min). PLGA-PEG-MAL was re-dissolved in ACN and precipitated again by the addition of water in order to eliminate residual HOBt, EDC, and unreacted PEG. These washing steps were repeated 3–4 times. After the final washing, the polymer was lyophilized and kept at −20 °C under nitrogen until further use. In order to confirm the linking of PEG-MAL to PLGA, a sample of the resultant polymer was dissolved in deuterated chloroform, and was analyzed by ^{1}H NMR (Bruker

Avance III 500 MHz NMR). The ^{1}H NMR analysis revealed four characteristic peaks, three of them originated from the PLGA at 1.6, 4.8, and 5.2 ppm, corresponding to CH_3, CH_2, and CH protons, respectively (Figure S1a,c), and the fourth originated from the PEG protons (CH_2–CH_2 protons) at 3.6 ppm (Figure S1a,b). A small peak was observed at 6.7 ppm corresponding to the MAL group protons (Figure S1a,b). These results confirmed the successful linking of the PEG linker as well as the presence of the MAL group, which was essential for further peptide-linking, utilizing a thiol-maleimide click-reaction [78]. In the final step of the synthesis, ApoB-P was reacted with the reducing agent TCEP (10× molar excess of TCEP) in order to break disulfide bonds in the peptide, forming free thiol groups for reacting with the MAL end group. Following 1 h of incubation, the reduced peptide was added (2× molar excess of peptide) to a solution of PLGA-PEG-MAL in ACN/dimethylformamide (DMF) under constant stirring. The reaction was left overnight at RT followed by three washing steps as described above. The final PLGA-ApoB-P was lyophilized and kept at −20 °C until further use. ApoB-P-linking in the final step of the synthesis was confirmed by amino acid analysis (Aminolab Ltd., Nes Ziona, Israel) and by elemental analysis, and the content of nitrogen was derived primarily from the peptide (Analytical Chemistry Lab, The Hebrew University of Jerusalem, Jerusalem, Israel).

4.3. Nanoparticles Preparation

The DESD method, previously described by us [22], was employed for preparing siOPN-loaded NPs. A solution of siOPN (1500 μg/mL) in RNase-free TE buffer was emulsified in 3 mL of ethyl acetate (EtAc), containing 90 mg of PLGA and PLGA-PEG-ApoB-P (8:1 weight ratio), and 325 μg PEI, by means of a microtip probe sonicator (Vibra-Cell tip sonicator, Sonic & Materials, Inc., CT, USA), at 20 W output for 90 s. The resulting primary emulsion was further emulsified into a 2% PVA solution (in 10 mL TE buffer), and was sonicated for 90 s at 50% amplitude to form a double emulsion (W/O/W). EtAc was evaporated under reduced pressure using a rotary evaporator (Buchi, Switzerland) resulting in the formation of NPs. NPs were washed twice (TE buffer and double-distilled water) using ultracentrifugation (25,000 rpm, 30 min, 4 °C), re-suspended in a sterile 2% mannitol solution, and lyophilized. Dry lyophilized NPs were stored at −20 °C until use. Fluorescent NPs were prepared by replacing 10% of the PLGA content in the NPs with PLGA-BODIPY (505/515) or PLGA-Cy5, both synthesized in our lab. For comparisons, non-targeted NPs were prepared containing PLGA and PLGA-PEG (8:1 weight ratio as above), and non-pegylated NPs as previously reported [22].

Additional method for preparing ApoB-P targeted NPs was examined by linking the navigator peptide, ApoB-P to pre-formed NPs of PLGA and PLGA-PEG-MAL (Figure 1b, II). The intermediate compound, PLGA-PEG-MAL, and PLGA were dissolved in EtAc, and the NPs were prepared as described above. NPs were washed once (ultracentrifuge) and were then incubated with the free ApoB-P (pre-incubated with TCEP) at a ×2 molar excess. The reaction was kept overnight at 4 °C, NPs were washed (ultracentrifuge) and lyophilized in 2% mannitol.

4.4. Determination of NP Size, Polydispersity, and Surface Charge

NPs size, size distribution, and surface charge (ζ potential) were determined by dynamic light scattering at 25 °C (Zetasizer Nano-ZSP, Malvern Instruments, UK) of 1 mg/mL NPs in TE buffer. The size distribution and mean diameter were analyzed by intensity. For each formulation, the mean value was recorded as the average of three measurements.

4.5. Determination of siOPN Content

For each batch, accurately weighted ~5 mg of NPs was dissolved in 1.5 mL of 0.5 N NaOH under constant stirring (100 rpm), at 37 °C, until a limpid solution was achieved. Following centrifugation (3000 rpm, 15 min), the supernatant was analyzed by UV spectrophotometry at 260 nm. siOPN concentration was calculated against a suitable calibration curve (degraded siRNA, dissolved in 0.5 N NaOH). Each batch was weighed and assayed in duplicates, and siOPN concentration and encapsulation yield (%) were calculated as previously described [22].

4.6. In Vitro Binding Studies

4.6.1. NPs Binding to the Isolated ECM

Porcine aortic endothelial cells were isolated from porcine aortae by the collagenase dispersion method [79], and passages four to nine were used. Cells were maintained in a low glucose Dulbecco's Modified Eagle's Medium (DMEM), supplemented with 5% fetal bovine serum (FBS), 1% L-glutamine and 1% penicillin–streptomycin. For ECM isolation, cells were seeded in 96-well plates and cultured for four days. ECM was isolated by 20 mM NH_4OH containing 0.5% Triton X-100. Solutions of fluorescently-labeled NPs (PLGA-BODIPY; 200 μL, 2.5, 5, and 10 mg/mL; targeted NPs prepared by method I, Figure 1b, I) were added to wells coated with ECM on a rocker, for 2 h at RT. The NPs suspension was aspirated, and the wells were washed three times with PBS. PBS (200 μL) was added to each well, and the fluorescence intensity was measured by means of a microplate reader (ex/em 484/515 nm). The number of NPs that remained bound to the ECM was extracted from a calibration curve.

4.6.2. NPs Binding to the BM Matrix

Plates (96 wells) were coated with a non-gelled protein layer of a Matrigel® matrix (from mouse sarcoma; Corning, Tewksbury, MA, USA), which contained heparan sulfate proteoglycans as a third major component after laminin and collagen IV. Coated wells (thin coating method according to the manufacturer's protocol) were incubated with either free ApoB-P (1 mM in PBS) or PBS only, for 1 h at 37 °C. The solution of unbound peptide was aspirated, and fluorescently labeled NPs (PLGA-Cy5; targeted NPs prepared by method II, Figure 1b, II) were then added at a concentration of 10 mg/mL and incubated at 37 °C for 4 h. The wells were washed three times with PBS, and 200 μL of PBS were added to each well. Fluorescent intensity was measured using the Typhoon scanner (FLA 9500 biomolecular imager, GE Healthcare, Hatfield, UK) followed by image analysis (ImageJ software, https://imagej.nih.gov).

4.7. Cellular Uptake Studies

The human breast adenocarcinoma cell line, MDA-MB-231, was obtained from ATCC (Manassas, VA, USA). Cells were routinely cultivated in RPMI 1640 medium supplemented with 10% FBS, 2 mM L-glutamine, 100 units/mL penicillin, and 100 μg/mL streptomycin at 37 °C and humidified 5% CO_2 atmosphere.

4.7.1. Quantification of NPs Cellular Uptake

MDA-MB-231 cells were seeded in 12-well plates (0.2×10^6 cells/well) and were left to attach overnight. The following day, the cells were treated with fluorescently labeled NPs (PLGA-BODIPY; targeted NPs prepared by method I, Figure 1b, I) at a concentration of 100 μg/mL and were incubated for 0.5, 1, 2, 4, and 6 h. The cells were washed with PBS three times, harvested, and analyzed for cell-associated NPs by FACS (BDTM LSR II, BD Biosciences, Franklin Lakes, NJ, USA). Non-treated cells were used as controls and were set as a background. The number of stained cells (expressed as the % of total cells) and the fluorescent intensities were calculated based on the obtained FACS histograms (Figure S5), using FCS Express 4 software (De Novo software, Glendale, CA, USA). The energy-dependent uptake was examined by incubating the cells at 37 °C and 4 °C.

4.7.2. Visualization of NPs Cellular Uptake

MDA-MB-231 cells were seeded on coverslips in 12-well plates (0.2×10^6 cells/well) and were left to attach overnight. Cells were incubated for 0.5 and 6 h with 100 μg/mL of fluorescently labeled NPs (PLGA-BODIPY; targeted NPs prepared by method I, Figure 1b, I). The cells were thereafter washed with PBS (×3), fixed using 4% formaldehyde solution for 10 min, washed again with PBS (×3),

and mounted onto a microscope slide. Slides were analyzed using an Olympus FV 10i confocal laser scanning microscope (magnification of 60×). Non-treated cells were used as controls and were set as a background.

4.8. In Vivo Mice Models

In all in vivo animal experiments, animals were used and treated according to the guidelines of the animal care and use committee of the Hebrew University of Jerusalem (MD-13-13685-5; 1 August 2013 and MD-17-15238-5; 20 October 2017), Israel, and the NIH. The biodistribution of the NPs was evaluated in the 4T1 model of tumor-bearing mice [22] and in the xenograft (human-derived, MDA-MB-231 cells) mammary carcinoma orthotopic mice model. The advantage of the 4T1 model is the formation of lung metastases (Figure S3) as in humans [54]. The bioactivity of siOPN was evaluated in the xenografted MDA-MB-231 mice model since the siOPN sequence, which was designed to human OPN, is inactive in the 4T1 model.

4.8.1. Mammary Carcinoma 4T1 IV Model

4T1 mouse breast cancer cells (ATCC) were cultured in DMEM containing 10% FBS. 4T1 cells, stably expressing firefly luciferase (4T1-Luc) suspended in PBS (1×10^5), were injected intravenously via the tail vein of 6–7 weeks old female BALB/c mice (Envigo Laboratories, Rehovot, Israel). Two weeks after tumor cell injection, metastatic lesions were observed only in the lungs (confirmed by bioluminescence [22], Figure S3). At this time, fluorescently labeled empty NPs (PLGA-BODIPY; targeted NPs prepared by method I, Figure 1b, I) were injected intravenously into the tail vein (10 mg/mice). The mice were sacrificed 8 and 24 h ($n = 3$ in each group) post-injection, perfused with PBS, and the lungs, liver, kidney, and spleen were harvested. Accumulation of the fluorescent NPs in the organs was evaluated by fluorescent imaging (Typhoon FLA 9500 biomolecular imager, GE Healthcare) followed by image analysis (ImageJ software). The mean fluorescent intensity in each organ was normalized to an untreated control (organ autofluorescence). To evaluate the fate of NPs in the circulation, 8 h after NPs injection, heparinized blood was drawn by cardiac puncture under anesthesia. The red blood cells were lysed (Erythrolyse, AbD, Serotec, Oxford, UK), and the pellet was washed twice with FACS buffer (1% BSA in PBS). Samples were analyzed for cell-associated NPs by FACS (BDTM LSR II), and FCS Express 4 software was used for quantitative analysis. The different populations of WBCs were gated according to their typical forward (size) and side (granularity) scattering, and the fluorescence of the gated cells was measured. The percentage of positive fluorescent WBCs and monocytes was extracted. Data were presented as mean ± SD.

4.8.2. Mammary Carcinoma Orthotopic Mice Model

The biodistribution and bioactivity of targeted and non-targeted NPs were evaluated in the orthotopic model of mice xenografted with MDA-MB-231 mammary carcinoma cells [80]. Mammary carcinoma cells (1×10^6 in 50 μL PBS) were injected into the inguinal mammary fat pad of 6–7 weeks old female athymic nude mice (Envigo). The tumor was visible 2–3 weeks after transplantation, measured externally by a caliper. Mice with similar tumor sizes were randomly assigned to treatments of targeted NPs vs. non-targeted NPs.

Empty NPs, fluorescently labeled with Cy5, were used for evaluating the accumulation of NPs in the tumor and selected organs (lungs, liver, kidneys, and spleen) and their uptake by WBC. Targeted ($n = 2$; NPs prepared by method II, Figure 1b, II) and non-targeted ($n = 3$) NPs (10 mg/mice) were intravenously injected via the tail vein. The mice were sacrificed 24 h post-injection, and the NPs fluorescent signal in the harvested organs was determined by means of fluorescent imaging (Typhoon FLA 9500 biomolecular imager) followed by image analysis (ImageJ software). The mean fluorescent intensity in each organ was normalized to an untreated control (organ autofluorescence). In addition, tumor cryo-sections were visualized by confocal laser scanning microscopy. Immediately after Typhoon scanning, the tumors were embedded in OCT (Bar-Naor, Ramat Gan, Israel) followed by snap-freezing

in liquid nitrogen, and stored at −80 °C for further cryo-sectioning (CM1950 cryostat, Leica Biosystems, Wetzlar, Germany). Tumor cryo-sections were performed at a 10 μm width, washed with PBS, fixed (4% formaldehyde), mounted, and visualized using an Olympus FV10I confocal laser scanning microscope. The fluorescent intensity was normalized to cryo-sections of untreated mice. For evaluating the NPs uptake by WBC, blood was collected (24 h post-injection) and analyzed for cell-associated NPs by FACS, as described above.

The bioactivity of siOPN NPs was evaluated in the mice orthotopic xenograft model since the siOPN sequence was designed for human OPN (expressed in the human-originated MDA-MB-231 cells, but not in the 4T1 cells, which are of mice origin). MDA-MB-231 cells were transplanted and examined as mentioned above. Mice having similar tumor sizes were randomly assigned to the different treatment groups and treated with either targeted siOPN NPs (n = 7; NPs prepared by method II, Figure 1b, II), non-targeted siOPN NPs (n = 5), or left untreated (n = 5). The NPs were intravenously injected (tail vein) at a siOPN dose of 1 mg/kg of body weight, every other day for a total of three injections. The tumor size was measured, blinded to the operator, externally by a caliper for a period of nine days after the first injection. Tumor volume was calculated by the formula $\frac{1}{2} \times L \times W^2$, where L is the length (in cm) and W is the width (cm).

For determining the mechanism of siOPN treatment, OPN mRNA levels in the excised tumors were analyzed using real-time PCR (RT-PCR). Tumor samples were embedded in 1 mL TRI reagent (Sigma-Aldrich), homogenized, and the total RNA was isolated according to the manufacturer's protocol. For each sample, RNA concentration was determined by means of a NanoDrop 1000 spectrophotometer (Thermo Fisher Scientific). cDNA was synthesized from 1 μg of extracted RNA using the Moloney murine leukemia virus reverse transcriptase (M-MLV RT, Promega, Madison, WI, USA), and oligo dT primer (Promega). mRNA levels of OPN and GAPDH (housekeeping gene) were quantified by SYBR green-based quantitative RT-PCR (qRT-PCR), performed using the CFX Connect™ Real-Time PCR Detection System (Bio-Rad, Hercules, CA, USA). The following primers were used: human OPN, forward: 5′-CGC AGA CCT GAC ATC CAG T-3′, reverse: 5′-GGC TGT CCC AAT CAG AAG G-3′; human GAPDH, forward: 5′-TCA AGC TCA TTT CCT GGT ATG-3′, reverse: 5′-GTG GTC CAG GGG TCT TAC TC-3′. Thermal cycling parameters for amplification were: 95 °C for 10 min, followed by 40 cycles of 95 °C for 5 s, and 60 °C for 15 s. OPN mRNA levels were normalized to GAPDH and to untreated control mice. Each cDNA sample was measured in triplicate, and mean cycle threshold (Ct) values were reported. ΔCt of each sample was calculated as follows: Ct of the target gene (OPN) minus Ct of the reference gene (GAPDH, housekeeping gene). Then, the mean ΔCt of the untreated control mice was chosen as the reference for the relative quantification calculation ($2^{-\Delta\Delta Ct}$). Data were expressed as OPN/GAPDH (mean ± SEM).

4.9. Statistical Analysis

Data was expressed as the mean ± standard deviation/error. For statistical analysis, the Student's t-test for independent means was used. Differences were termed significant at $p < 0.05$.

5. Conclusions

PLGA-PEG NPs containing siOPN, decorated with ApoB-P as a targeting ligand to the tumor, were successfully formulated. Because of the high affinity to ApoB substrates, both increased ECM binding and cellular uptake were obtained. Biodistribution studies revealed enhanced accumulation in the metastatic lungs of mice mammary carcinoma models (4T1 transplantable breast tumor, and orthotopic MDA-MB-231 mammary carcinoma). Despite the significantly higher retention of siOPN NPs in the tumor following intravenous treatment with targeted NPs, a similar therapeutic effect resulted following treatment with non-targeted siOPN NPs. It is suggested that further improvement of the targeting could be of value, and/or that a longer observation time is required. The obtained significant tumor growth suppression was accompanied by a significant reduction of OPN mRNA

levels. This validates our hypothesis that systemically administered ApoB-P-targeted siOPN NPs could inhibit tumor progression by inhibiting OPN.

Supplementary Materials: The following are available online at http://www.mdpi.com/2072-6694/11/4/442/s1, Figure S1: Confirmation of amine-PEG-maleimide (NH2-PEG-MAL) conjugation to PLGA by 1H-NMR analysis, Figure S2: Temperature-dependent uptake of targeted and non-targeted NPs by MDA-MB-231 cell line, Figure S3: A representative image of the metastatic lungs in the 4T1 IV model, Figure S4: NPs uptake by circulating WBC and monocytes, examined in the 4T1 IV model and in the orthotopic xenograft model, Figure S5: Cellular uptake of NPs by MDA-MB-231 cell line.

Author Contributions: Conceptualization, M.B.-D.-N. and G.G.; Data curation, M.B.-D.-N.; Formal analysis, M.B.-D.-N. and G.G.; Methodology, M.B.-D.-N., A.D., E.G., G.A., M.M.N.-D., A.M.C., Z.G., and G.G.; Supervision, G.G.; Visualization, M.B.-D.-N.; Writing—original draft, M.B.-D.-N. and G.G.; Writing—review & editing, G.G.

Funding: This study was supported in part by the DREXEL—HUJI Project (A.M.C. & G.G.), the Israel Science Foundation (ISF 2648/16; G.G.), and Yissum R&D of HUJI startup grants (G.G.).

Acknowledgments: G.G. is grateful to the Woll Sisters and Brothers Chair in Cardiovascular Diseases.

Conflicts of Interest: The authors declare no conflict of interest.

References

1. Shi, J.; Kantoff, P.W.; Wooster, R.; Farokhzad, O.C. Cancer nanomedicine: Progress, challenges and opportunities. *Nat. Rev. Cancer* **2017**, *17*, 20–37. [CrossRef]
2. Sarisozen, C.; Pan, J.; Dutta, I.; Torchilin, V.P. Polymers in the co-delivery of siRNA and anticancer drugs to treat multidrug-resistant tumors. *J. Pharm. Investig.* **2017**, *47*, 37–49. [CrossRef]
3. Mir, M.; Ahmed, N.; Rehman, A.U. Recent applications of PLGA based nanostructures in drug delivery. *Colloids Surf. B Biointerfaces* **2017**, *159*, 217–231. [CrossRef]
4. Danhier, F.; Ansorena, E.; Silva, J.M.; Coco, R.; Le Breton, A.; Preat, V. PLGA-based nanoparticles: An overview of biomedical applications. *J. Control. Release* **2012**, *161*, 505–522. [CrossRef] [PubMed]
5. Patil, Y.; Panyam, J. Polymeric nanoparticles for siRNA delivery and gene silencing. *Int. J. Pharm.* **2009**, *367*, 195–203. [CrossRef] [PubMed]
6. Cohen, H.; Levy, R.J.; Gao, J.; Fishbein, I.; Kousaev, V.; Sosnowski, S.; Slomkowski, S.; Golomb, G. Sustained delivery and expression of DNA encapsulated in polymeric nanoparticles. *Gene Ther.* **2000**, *7*, 1896–1905. [CrossRef] [PubMed]
7. Cohen-Sacks, H.; Najajreh, Y.; Tchaikovski, V.; Gao, G.; Elazer, V.; Dahan, R.; Gati, I.; Kanaan, M.; Waltenberger, J.; Golomb, G. Novel PDGFbetaR antisense encapsulated in polymeric nanospheres for the treatment of restenosis. *Gene Ther.* **2002**, *9*, 1607–1616. [CrossRef] [PubMed]
8. Panyam, J.; Labhasetwar, V. Biodegradable nanoparticles for drug and gene delivery to cells and tissue. *Adv. Drug Deliv. Rev.* **2003**, *55*, 329–347. [CrossRef]
9. Sah, H.; Thoma, L.A.; Desu, H.R.; Sah, E.; Wood, G.C. Concepts and practices used to develop functional PLGA-based nanoparticulate systems. *Int. J. Nanomed.* **2013**, *8*, 747–765. [CrossRef]
10. Prabhakar, U.; Maeda, H.; Jain, R.K.; Sevick-Muraca, E.M.; Zamboni, W.; Farokhzad, O.C.; Barry, S.T.; Gabizon, A.; Grodzinski, P.; Blakey, D.C. Challenges and key considerations of the enhanced permeability and retention effect for nanomedicine drug delivery in oncology. *Cancer Res.* **2013**, *73*, 2412–2417. [CrossRef]
11. Barua, S.; Mitragotri, S. Challenges associated with Penetration of Nanoparticles across Cell and Tissue Barriers: A Review of Current Status and Future Prospects. *Nano Today* **2014**, *9*, 223–243. [CrossRef]
12. Moghimi, S.M.; Simberg, D. Nanoparticle transport pathways into tumors. *J. Nanopart. Res.* **2018**, *20*, 169. [CrossRef]
13. Hare, J.I.; Lammers, T.; Ashford, M.B.; Puri, S.; Storm, G.; Barry, S.T. Challenges and strategies in anti-cancer nanomedicine development: An industry perspective. *Adv. Drug Deliv. Rev.* **2017**, *108*, 25–38. [CrossRef] [PubMed]
14. Peer, D.; Karp, J.M.; Hong, S.; Farokhzad, O.C.; Margalit, R.; Langer, R. Nanocarriers as an emerging platform for cancer therapy. *Nat. Nanotechnol.* **2007**, *2*, 751–760. [CrossRef]
15. Moghimi, S.M.; Hunter, A.C.; Andresen, T.L. Factors controlling nanoparticle pharmacokinetics: An integrated analysis and perspective. *Annu. Rev. Pharmacol. Toxicol.* **2012**, *52*, 481–503. [CrossRef] [PubMed]

16. Anchordoquy, T.J.; Barenholz, Y.; Boraschi, D.; Chorny, M.; Decuzzi, P.; Dobrovolskaia, M.A.; Farhangrazi, Z.S.; Farrell, D.; Gabizon, A.; Ghandehari, H.; et al. Mechanisms and barriers in cancer nanomedicine: Addressing challenges, looking for solutions. *ACS Nano* **2017**, *11*, 12–18. [CrossRef] [PubMed]
17. Farokhzad, O.C.; Cheng, J.; Teply, B.A.; Sherifi, I.; Jon, S.; Kantoff, P.W.; Richie, J.P.; Langer, R. Targeted nanoparticle-aptamer bioconjugates for cancer chemotherapy in vivo. *Proc. Natl. Acad. Sci. USA* **2006**, *103*, 6315–6320. [CrossRef] [PubMed]
18. Fasehee, H.; Dinarvand, R.; Ghavamzadeh, A.; Esfandyari-Manesh, M.; Moradian, H.; Faghihi, S.; Ghaffari, S.H. Delivery of disulfiram into breast cancer cells using folate-receptor-targeted PLGA-PEG nanoparticles: In vitro and in vivo investigations. *J. Nanobiotechnol.* **2016**, *14*, 32. [CrossRef]
19. Huang, J.; Zhang, H.; Yu, Y.; Chen, Y.; Wang, D.; Zhang, G.; Zhou, G.; Liu, J.; Sun, Z.; Sun, D.; et al. Biodegradable self-assembled nanoparticles of poly (D,L-lactide-co-glycolide)/hyaluronic acid block copolymers for target delivery of docetaxel to breast cancer. *Biomaterials* **2014**, *35*, 550–566. [CrossRef]
20. Nicolas, J.; Mura, S.; Brambilla, D.; Mackiewicz, N.; Couvreur, P. Design, functionalization strategies and biomedical applications of targeted biodegradable/biocompatible polymer-based nanocarriers for drug delivery. *Chem. Soc. Rev.* **2013**, *42*, 1147–1235. [CrossRef]
21. Elazar, V.; Adwan, H.; Rohekar, K.; Zepp, M.; Lifshitz-Shovali, R.; Berger, M.R.; Golomb, G. Biodistribution of antisense nanoparticles in mammary carcinoma rat model. *Drug Deliv.* **2010**, *17*, 408–418. [CrossRef]
22. Ben David-Naim, M.; Grad, E.; Aizik, G.; Nordling-David, M.M.; Moshel, O.; Granot, Z.; Golomb, G. Polymeric nanoparticles of siRNA prepared by a double-emulsion solvent-diffusion technique: Physicochemical properties, toxicity, biodistribution and efficacy in a mammary carcinoma mice model. *Biomaterials* **2017**, *145*, 154–167. [CrossRef]
23. Reufsteck, C.; Lifshitz-Shovali, R.; Zepp, M.; Bauerle, T.; Kubler, D.; Golomb, G.; Berger, M.R. Silencing of skeletal metastasis-associated genes impairs migration of breast cancer cells and reduces osteolytic bone lesions. *Clin. Exp. Metastasis* **2012**, *29*, 441–456. [CrossRef] [PubMed]
24. Theocharis, A.D.; Tsolakis, I.; Tzanakakis, G.N.; Karamanos, N.K. Chondroitin sulfate as a key molecule in the development of atherosclerosis and cancer progression. *Adv. Pharmacol.* **2006**, *53*, 281–295. [CrossRef] [PubMed]
25. Rensen, P.C.; de Vrueh, R.L.; Kuiper, J.; Bijsterbosch, M.K.; Biessen, E.A.; van Berkel, T.J. Recombinant lipoproteins: Lipoprotein-like lipid particles for drug targeting. *Adv. Drug Deliv. Rev.* **2001**, *47*, 251–276. [CrossRef]
26. Insua-Rodriguez, J.; Oskarsson, T. The extracellular matrix in breast cancer. *Adv. Drug Deliv. Rev.* **2016**, *97*, 41–55. [CrossRef] [PubMed]
27. Knott, T.J.; Pease, R.J.; Powell, L.M.; Wallis, S.C.; Rall, S.C., Jr.; Innerarity, T.L.; Blackhart, B.; Taylor, W.H.; Marcel, Y.; Milne, R.; et al. Complete protein sequence and identification of structural domains of human apolipoprotein B. *Nature* **1986**, *323*, 734–738. [CrossRef] [PubMed]
28. Weisgraber, K.H.; Rall, S.C., Jr. Human apolipoprotein B-100 heparin-binding sites. *J. Biol. Chem.* **1987**, *262*, 11097–11103. [PubMed]
29. Camejo, G.; Hurt-Camejo, E.; Wiklund, O.; Bondjers, G. Association of apo B lipoproteins with arterial proteoglycans: Pathological significance and molecular basis. *Atherosclerosis* **1998**, *139*, 205–222. [CrossRef]
30. Golomb, G.; Sacks, H.; Najajreh, Y.; Fishbein, I.; Chorny, M. Nanoparticles Containing Polymeric nucleic Acid Homologs. U.S. Patent US8178128B2, 15 May 2012.
31. Bellahcene, A.; Castronovo, V.; Ogbureke, K.U.; Fisher, L.W.; Fedarko, N.S. Small integrin-binding ligand N-linked glycoproteins (SIBLINGs): Multifunctional proteins in cancer. *Nat. Rev. Cancer* **2008**, *8*, 212–226. [CrossRef]
32. Wai, P.Y.; Kuo, P.C. Osteopontin: Regulation in tumor metastasis. *Cancer Metastasis Rev.* **2008**, *27*, 103–118. [CrossRef]
33. Shevde, L.A.; Samant, R.S. Role of osteopontin in the pathophysiology of cancer. *Matrix Biol.* **2014**, *37*, 131–141. [CrossRef]
34. Bramwell, V.H.; Doig, G.S.; Tuck, A.B.; Wilson, S.M.; Tonkin, K.S.; Tomiak, A.; Perera, F.; Vandenberg, T.A.; Chambers, A.F. Serial plasma osteopontin levels have prognostic value in metastatic breast cancer. *Clin. Cancer Res.* **2006**, *12*, 3337–3343. [CrossRef]

35. Adwan, H.; Bauerle, T.; Najajreh, Y.; Elazer, V.; Golomb, G.; Berger, M.R. Decreased levels of osteopontin and bone sialoprotein II are correlated with reduced proliferation, colony formation, and migration of GFP-MDA-MB-231 cells. *Int. J. Oncol.* **2004**, *24*, 1235–1244. [CrossRef]
36. Elazar, V.; Adwan, H.; Bauerle, T.; Rohekar, K.; Golomb, G.; Berger, M.R. Sustained delivery and efficacy of polymeric nanoparticles containing osteopontin and bone sialoprotein antisenses in rats with breast cancer bone metastasis. *Int. J. Cancer* **2010**, *126*, 1749–1760. [CrossRef]
37. Cho, W.Y.; Hong, S.H.; Singh, B.; Islam, M.A.; Lee, S.; Lee, A.Y.; Gankhuyag, N.; Kim, J.E.; Yu, K.N.; Kim, K.H.; et al. Suppression of tumor growth in lung cancer xenograft model mice by poly(sorbitol-co-PEI)-mediated delivery of osteopontin siRNA. *Eur. J. Pharm. Biopharm.* **2015**, *94*, 450–462. [CrossRef] [PubMed]
38. Rashid, O.M.; Nagahashi, M.; Ramachandran, S.; Dumur, C.I.; Schaum, J.C.; Yamada, A.; Aoyagi, T.; Milstien, S.; Spiegel, S.; Takabe, K. Is tail vein injection a relevant breast cancer lung metastasis model? *J. Thorac. Dis.* **2013**, *5*, 385–392. [CrossRef]
39. Woodrow, K.A.; Cu, Y.; Booth, C.J.; Saucier-Sawyer, J.K.; Wood, M.J.; Saltzman, W.M. Intravaginal gene silencing using biodegradable polymer nanoparticles densely loaded with small-interfering RNA. *Nat. Mater.* **2009**, *8*, 526–533. [CrossRef] [PubMed]
40. Torchilin, V. Tumor delivery of macromolecular drugs based on the EPR effect. *Adv. Drug Deliv. Rev.* **2011**, *63*, 131–135. [CrossRef] [PubMed]
41. Cuong, N.V.; Jiang, J.L.; Li, Y.L.; Chen, J.R.; Jwo, S.C.; Hsieh, M.F. Doxorubicin-loaded PEG-PCL-PEG micelle using xenograft model of nude mice: Effect of multiple administration of micelle on the suppression of human breast cancer. *Cancers* **2010**, *3*, 61–78. [CrossRef] [PubMed]
42. Tong, R.; Langer, R. Nanomedicines targeting the tumor microenvironment. *Cancer J.* **2015**, *21*, 314–321. [CrossRef]
43. Ahmadzada, T.; Reid, G.; McKenzie, D.R. Fundamentals of siRNA and miRNA therapeutics and a review of targeted nanoparticle delivery systems in breast cancer. *Biophys. Rev.* **2018**, *10*, 69–86. [CrossRef] [PubMed]
44. Innerarity, T.L.; Weisgraber, K.H.; Rall, S.C., Jr.; Mahley, R.W. Functional domains of apolipoprotein E and apolipoprotein B. *Acta Med. Scand. Suppl.* **1987**, *715*, 51–59. [CrossRef] [PubMed]
45. Olsson, U.; Camejo, G.; Hurt-Camejo, E.; Elfsber, K.; Wiklund, O.; Bondjers, G. Possible functional interactions of apolipoprotein B-100 segments that associate with cell proteoglycans and the ApoB/E receptor. *Arterioscler. Thromb. Vasc. Biol.* **1997**, *17*, 149–155. [CrossRef] [PubMed]
46. Boren, J.; Lee, I.; Zhu, W.; Arnold, K.; Taylor, S.; Innerarity, T.L. Identification of the low density lipoprotein receptor-binding site in apolipoprotein B100 and the modulation of its binding activity by the carboxyl terminus in familial defective apo-B100. *J. Clin. Investig.* **1998**, *101*, 1084–1093. [CrossRef]
47. Olsson, U.; Camejo, G.; Olofsson, S.O.; Bondjers, G. Molecular parameters that control the association of low density lipoprotein apo B-100 with chondroitin sulphate. *Biochim. Biophys. Acta* **1991**, *1097*, 37–44. [CrossRef]
48. Milne, R.; Theolis, R., Jr.; Maurice, R.; Pease, R.J.; Weech, P.K.; Rassart, E.; Fruchart, J.C.; Scott, J.; Marcel, Y.L. The use of monoclonal antibodies to localize the low density lipoprotein receptor-binding domain of apolipoprotein B. *J. Biol. Chem.* **1989**, *264*, 19754–19760. [PubMed]
49. Grayson, A.C.; Doody, A.M.; Putnam, D. Biophysical and structural characterization of polyethylenimine-mediated siRNA delivery in vitro. *Pharm. Res.* **2006**, *23*, 1868–1876. [CrossRef] [PubMed]
50. Antalis, C.J.; Uchida, A.; Buhman, K.K.; Siddiqui, R.A. Migration of MDA-MB-231 breast cancer cells depends on the availability of exogenous lipids and cholesterol esterification. *Clin. Exp. Metastasis* **2011**, *28*, 733–741. [CrossRef] [PubMed]
51. Koo, C.Y.; Sen, Y.P.; Bay, B.H.; Yip, G.W. Targeting heparan sulfate proteoglycans in breast cancer treatment. *Recent Pat. Anticancer Drug Discov.* **2008**, *3*, 151–158. [CrossRef]
52. Ibrahim, S.A.; Yip, G.W.; Stock, C.; Pan, J.W.; Neubauer, C.; Poeter, M.; Pupjalis, D.; Koo, C.Y.; Kelsch, R.; Schule, R.; et al. Targeting of syndecan-1 by microRNA miR-10b promotes breast cancer cell motility and invasiveness via a Rho-GTPase- and E-cadherin-dependent mechanism. *Int. J. Cancer* **2012**, *131*, E884–E896. [CrossRef]
53. Paget, S. The distribution of secondary growths in cancer of the breast. *Lancet* **1889**, *133*, 571–573. [CrossRef]
54. Minn, A.J.; Gupta, G.P.; Siegel, P.M.; Bos, P.D.; Shu, W.; Giri, D.D.; Viale, A.; Olshen, A.B.; Gerald, W.L.; Massague, J. Genes that mediate breast cancer metastasis to lung. *Nature* **2005**, *436*, 518–524. [CrossRef] [PubMed]

55. Weigelt, B.; Peterse, J.L.; van't Veer, L.J. Breast cancer metastasis: Markers and models. *Nat. Rev. Cancer* **2005**, *5*, 591–602. [CrossRef]
56. Zhang, H.; Wong, C.C.; Wei, H.; Gilkes, D.M.; Korangath, P.; Chaturvedi, P.; Schito, L.; Chen, J.; Krishnamachary, B.; Winnard, P.T., Jr.; et al. HIF-1-dependent expression of angiopoietin-like 4 and L1CAM mediates vascular metastasis of hypoxic breast cancer cells to the lungs. *Oncogene* **2012**, *31*, 1757–1770. [CrossRef]
57. Psaila, B.; Lyden, D. The metastatic niche: Adapting the foreign soil. *Nat. Rev. Cancer* **2009**, *9*, 285–293. [CrossRef]
58. Padua, D.; Zhang, X.H.; Wang, Q.; Nadal, C.; Gerald, W.L.; Gomis, R.R.; Massague, J. TGFbeta primes breast tumors for lung metastasis seeding through angiopoietin-like 4. *Cell* **2008**, *133*, 66–77. [CrossRef]
59. Hiratsuka, S.; Nakamura, K.; Iwai, S.; Murakami, M.; Itoh, T.; Kijima, H.; Shipley, J.M.; Senior, R.M.; Shibuya, M. MMP9 induction by vascular endothelial growth factor receptor-1 is involved in lung-specific metastasis. *Cancer Cell* **2002**, *2*, 289–300. [CrossRef]
60. Burns, A.R.; Smith, C.W.; Walker, D.C. Unique structural features that influence neutrophil emigration into the lung. *Physiol. Rev.* **2003**, *83*, 309–336. [CrossRef]
61. Uyechi, L.S.; Gagne, L.; Thurston, G.; Szoka, F.C., Jr. Mechanism of lipoplex gene delivery in mouse lung: Binding and internalization of fluorescent lipid and DNA components. *Gene Ther.* **2001**, *8*, 828–836. [CrossRef] [PubMed]
62. Bae, Y.H.; Park, K. Targeted drug delivery to tumors: Myths, reality and possibility. *J. Control. Release* **2011**, *153*, 198–205. [CrossRef] [PubMed]
63. Jiang, W.; von Roemeling, C.A.; Chen, Y.; Qie, Y.; Liu, X.; Chen, J.; Kim, B.Y.S. Designing nanomedicine for immuno-oncology. *Nat. Biomed. Eng.* **2017**, *1*, 0029. [CrossRef]
64. Rodero, M.P.; Poupel, L.; Loyher, P.L.; Hamon, P.; Licata, F.; Pessel, C.; Hume, D.A.; Combadiere, C.; Boissonnas, A. Immune surveillance of the lung by migrating tissue monocytes. *eLife* **2015**, *4*, e07847. [CrossRef]
65. Alexis, F.; Pridgen, E.; Molnar, L.K.; Farokhzad, O.C. Factors affecting the clearance and biodistribution of polymeric nanoparticles. *Mol. Pharm.* **2008**, *5*, 505–515. [CrossRef]
66. Owens, D.E., 3rd; Peppas, N.A. Opsonization, biodistribution, and pharmacokinetics of polymeric nanoparticles. *Int. J. Pharm.* **2006**, *307*, 93–102. [CrossRef] [PubMed]
67. Natfji, A.A.; Ravishankar, D.; Osborn, H.M.I.; Greco, F. Parameters Affecting the Enhanced Permeability and Retention Effect: The Need for Patient Selection. *J. Pharm. Sci.* **2017**, *106*, 3179–3187. [CrossRef]
68. Maeda, H. Polymer therapeutics and the EPR effect. *J. Drug Target.* **2017**, *25*, 781–785. [CrossRef] [PubMed]
69. Perry, J.L.; Reuter, K.G.; Luft, J.C.; Pecot, C.V.; Zamboni, W.; DeSimone, J.M. Mediating Passive Tumor Accumulation through Particle Size, Tumor Type, and Location. *Nano Lett.* **2017**, *17*, 2879–2886. [CrossRef] [PubMed]
70. Sykes, E.A.; Chen, J.; Zheng, G.; Chan, W.C. Investigating the impact of nanoparticle size on active and passive tumor targeting efficiency. *ACS Nano* **2014**, *8*, 5696–5706. [CrossRef]
71. Park, K. Facing the truth about nanotechnology in drug delivery. *ACS Nano* **2013**, *7*, 7442–7447. [CrossRef] [PubMed]
72. Chen, H.; Zhang, W.; Zhu, G.; Xie, J.; Chen, X. Rethinking cancer nanotheranostics. *Nat. Rev. Mater.* **2017**, *2*, 17024. [CrossRef]
73. Danhier, F. To exploit the tumor microenvironment: Since the EPR effect fails in the clinic, what is the future of nanomedicine? *J. Control. Release* **2016**, *244*, 108–121. [CrossRef] [PubMed]
74. Moghimi, S.M.; Farhangrazi, Z.S. Just so stories: The random acts of anti-cancer nanomedicine performance. *Nanomed. Nanotechnol. Biol. Med.* **2014**, *10*, 1661–1666. [CrossRef] [PubMed]
75. Nakamura, Y.; Mochida, A.; Choyke, P.L.; Kobayashi, H. Nanodrug Delivery: Is the Enhanced Permeability and Retention Effect Sufficient for Curing Cancer? *Bioconjug. Chem.* **2016**, *27*, 2225–2238. [CrossRef]
76. Wilhelm, S.; Tavares, A.J.; Dai, Q.; Ohta, S.; Audet, J.; Dvorak, H.F.; Chan, W.C.W. Analysis of nanoparticle delivery to tumours. *Nat. Rev. Mater.* **2016**, *1*, 16014. [CrossRef]
77. Dai, Q.; Wilhelm, S.; Ding, D.; Syed, A.M.; Sindhwani, S.; Zhang, Y.; Chen, Y.Y.; MacMillan, P.; Chan, W.C.W. Quantifying the ligand-coated nanoparticle delivery to cancer cells in solid tumors. *ACS Nano* **2018**, *12*, 8423–8435. [CrossRef]

78. Nair, D.P.; Podgórski, M.; Chatani, S.; Gong, T.; Xi, W.; Fenoli, C.R.; Bowman, C.N. The thiol-michael addition click reaction: A powerful and widely used tool in materials chemistry. *Chem. Mater.* **2014**, *26*, 724–744. [CrossRef]
79. Wong, M.K.; Gotlieb, A.I. In vitro reendothelialization of a single-cell wound. Role of microfilament bundles in rapid lamellipodia-mediated wound closure. *Lab. Investig.* **1984**, *51*, 75–81.
80. Muller, A.; Homey, B.; Soto, H.; Ge, N.; Catron, D.; Buchanan, M.E.; McClanahan, T.; Murphy, E.; Yuan, W.; Wagner, S.N.; et al. Involvement of chemokine receptors in breast cancer metastasis. *Nature* **2001**, *410*, 50–56. [CrossRef]

cancers

MDPI

Article

Graphene Oxide-Based Targeting of Extracellular Cathepsin D and Cathepsin L As A Novel Anti-Metastatic Enzyme Cancer Therapy

Tanveer A. Tabish [1,*], Md Zahidul I. Pranjol [2,3], David W. Horsell [1], Alma A. M. Rahat [1,4], Jacqueline L. Whatmore [2,*], Paul G. Winyard [2,*] and Shaowei Zhang [1,*]

1 College of Engineering, Mathematics and Physical Sciences, University of Exeter, Exeter EX4 4QF, UK; D.W.Horsell@exeter.ac.uk (D.W.H.); A.A.M.Rahat@exeter.ac.uk (A.A.M.R.)
2 Institute of Biomedical and Clinical Science, University of Exeter Medical School, St Luke's Campus, Exeter EX1 2LU, UK; z.pranjol@qmul.ac.uk
3 William Harvey Research Institute, Barts and the London School of Medicine and Dentistry, Queen Mary University of London, London EC1M 6BQ, UK
4 School of Computing, Electronics and Mathematics, University of Plymouth, Plymouth PL4 8AA, UK
* Correspondence: t.a.tabish2@exeter.ac.uk (T.A.T.); j.l.whatmore@exeter.ac.uk (J.L.W.); p.g.winyard@exeter.ac.uk (P.G.W.); s.zhang@exeter.ac.uk (S.Z.)

Received: 9 February 2019; Accepted: 27 February 2019; Published: 6 March 2019

Abstract: Overexpression and secretion of the enzymes cathepsin D (CathD) and cathepsin L (CathL) is associated with metastasis in several human cancers. As a superfamily, extracellularly, these proteins may act within the tumor microenvironment to drive cancer progression, proliferation, invasion and metastasis. Therefore, it is important to discover novel therapeutic treatment strategies to target CathD and CathL and potentially impede metastasis. Graphene oxide (GO) could form the basis of such a strategy by acting as an adsorbent for pro-metastatic enzymes. Here, we have conducted research into the potential of targeted anti-metastatic therapy using GO to adsorb these pro-tumorigenic enzymes. Binding of CathD/L to GO revealed that CathD/L were adsorbed onto the surface of GO through its cationic and hydrophilic residues. This work could provide a roadmap for the rational integration of CathD/L-targeting agents into clinical settings.

Keywords: graphene oxide; adsorption; cathepsin D; cathepsin L; anti-metastatic enzyme cancer therapy

1. Introduction

Every year more than 2.28 million new cases of breast and ovarian cancers are diagnosed worldwide, principally in developed countries and 807,440 women die of them [1–3], with these cancers representing the first and fifth most common cause of female malignancies, respectively [4,5]. Although these diseases have different pathologies they share a common set of molecular mechanisms such as the misfolding/aggregation, overexpression and hypersecretion of specific proteins typically involved in degrading cross-linked, abnormal, short-lived self- and foreign- proteins in lysosomes and phagocytosis. The intracellular and extracellular responses of the tumor microenvironment tend to be more prominent in response to conditions such as acidic pH [6], the enhanced permeability and retention effect [7], the enzyme abundance in the tumor extracellular matrix, [8] and overexpression of particular cell membrane receptors [9]. Typically, this emanates from the misfolding of proteins which potentially tend to form pathogenic aggregates, including harmful oligomeric and/or cytotoxic factors involved in the molecular etiology of these diseases and other pathologies (which are linked with the ability of the proteins to fully execute their physiological functions provided by certain regions of their protein sequence) [10]. When the intracellular protein degradation within the cells' acidic

endosomal/lysosome compartments increases, the proteolytic activity becomes particularly high in lysosomal proteases such as cathepsin D (CathD) and cathepsin L (CathL). However, in tumor invasion and development, these enzymes play a significant role by extracellularly influencing cell proliferation, differentiation, cell migration, programmed cell death, angiogenesis, immune defence, inflammation and extracellular tissue remodelling [11,12].

Higher CathL and CathD concentrations are closely related to an increased risk of metastasis [13]. For example, CathL is considered to be associated with tumor invasion and metastasis, by degrading subunits of extracellular matrix including proteoglycans, elastin, entactin (nidogen), laminin, fibronectin, perlecan and interstitial and basement-membrane collagens. Recently, we showed a significantly higher expression of CathL in the omentum hosting metastatic ovarian serous carcinoma compared with omentum from normal and benign controls with ovarian cystadenoma. We found that exogenous CathL induced pro-angiogenic effects on omental microvascular endothelial cells which may aid metastasis [14]. Recent studies have investigated the enhanced immunohistochemical CathD expression as an indicator of potential malignancy in serous ovarian cancer [13]. For example Losch et al. [15] demonstrated that CathD was detected in more than 70% of invasive ovarian cancers. Secreted CathD from breast cancer cells and its proteolytic role in degrading ECM proteins and subsequently releasing growth factors such as bFGF, have also been reported, which provide an ability for cancer cells to invade nearby tissue [16,17]. Misfolding, overexpression and hypersecretion of CathD and CathL have now been demonstrated in numerous cancer types such as ovarian, breast, lung and prostate, endometrial, as well as malignant glioma and melanoma and are recognized as critical players in cancer biology by regulating diverse proteolytic functions in triggering the breakdown of the tumor basement membrane and fueling tumor invasion [18–21]. Adsorption of these enzymes to two-dimensional materials opens a window of opportunity to develop a wide range of new approaches in the prevention of cancer.

Nanotechnology and its underpinning sciences have significantly contributed to the improvement of nanodrug bioavailability and therapeutic index in cancer therapy [22]. Recently, graphene oxide (GO) formulations have been developed into adaptable nanoscale platforms for medical interventions as one of the most sophisticated and minimally toxic tools [23] that permit direct contact with, and manipulation of, the intracellular environment. Graphene is a two-dimensional sheet composed of a single layer of sp^2-hybridized carbon atoms arranged in a honeycomb lattice [24]. Graphene and its analogues have attracted tremendous interest over the last decade for use in biomedicine owing to their unique physicochemical and mechanical properties, interesting optical and electronic properties, large surface area and good biofunctionality [25]. GO has many advantages over conventional nanosheets and other derivatives of graphene, such as a small size, chemical inertness, high specific surface area, photo-stability, good water solubility, high drug loading capacity, high purity, good fluorescence capability and biocompatibility. These properties make GO a promising candidate in novel delivery systems for target-specific therapeutic drugs and for the diagnosis of different medical conditions as well as for wound healing [26,27]. Furthermore, GO could offer a potential therapeutic tool by adsorbing the pro-metastatic enzymes, which are cancer-associated factors. GO has a large interfacial area and spatial constraints for biological interaction, ideally suited to constructing a robust and cost-effective extracellular tumor-specific enzyme binding method [28]. This capability of GO to bind and track an active enzyme could open the door to new clinical algorithms based on 'enzyme-targeted therapy'. GO nanoformulations which take up these enzymes could be key enablers of novel anti-metastatic enzyme therapy by breaking down the functional and structural integrity of extracellular enzymes. These GO nanoplatfoms offer a simple, safe and robust strategy in boosting the concept of 'anti-metastatic enzyme-targeted therapy', a neologism coined to indicate an innovative and revolutionary approach useful to adsorb and treat 'pro-tumorigenic' enzymes with a number of outcomes: notably the clearance of these enzymes, their structural breakdown, their digestion to active site-directed specific adsorbents and the deregulation of pro-tumorigenic enzymes. It is generally understood that the biocompatibility of graphene-based materials is limited by their sharp edges

and two-dimensional monolayered structures, which is evident from concentration-dependent toxic effects in numerous cell lines. Targeting and therapeutic adsorption of CathD and CathL in cancer treatment are currently unknown and undefined. The process of enzyme adsorption, and its therapeutic efficacy are affected by several factors such as: the properties of proteins and their concentrations in solution; pH and ionic strength; the temperature of the medium; pH-dependent adsorption performance; the structural stability of proteins; the selection and nature of adsorbent, porous sites/vacancies in adsorbents to take up the proteins; and strength/stability of adsorbate-adsorbent interface. The mechanistic aspects of protein adsorption and/or protein corona formation as a result of the interaction of proteins with graphene may involve electrostatic and hydrophobic interactions [29]. The intrinsic stability of the adsorbent matrix structure, which can be revealed by undergoing structural rearrangements, and conformational alterations, resulting in protein denaturation and/or loss of functional activities and a change in surface energy, allows a wide range of chemical changes in functional groups and wettabilities. The established method of fluorescence quenching and absorbance, together with vibrational spectrometry, wetting transparency, adsorption kinetics, and regression analysis can be used to reveal the fundamental aspects of the enzyme-graphene interaction and to address a variety of pre-clinical unknowns in the same theranostic session.

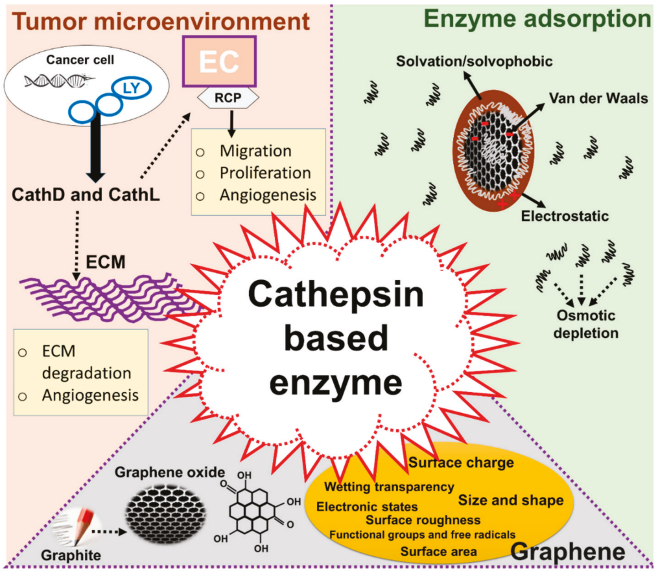

Figure 1. Proposed mechanism of cathepsin function in cancer metastasis and use of graphene oxide (GO) as an adsorbent to remove cathepsin from a living system. There are three panels in this diagram: (1) role of cathepsins in cancer progression: (2) structure of GO and its parameters relevant to the adsorption of cathepsins: and (3) the mechanism of adsorption. The left panel (1) illustrates possible tumorigenic and proangiogenic roles of cathepsin D (CathD) and cathepsin L (CathL) within the cancerous stroma or extracellular matrix (ECM) on endothelial cells (EC) acting via an unknown receptor(s) (RCP). The bottom panel (2) shows the structure of GO. This is prepared from graphite using the modified Hummer's method [26–28]. GO has suitable properties for the efficient adsorption of these enzymes such as surface charge, surface area, functional groups, electronic and chemical properties. The right panel (3) shows the potential mechanism involved in enzyme internalization, the interaction of GO with CathD/CathL and the further breakdown of cathepsins which may lead to cathepsin removal. Electrostatic and van der Waals forces, osmotic depletion and solvophobicity play a pivotal role in adsorption of such enzymes.

Secretion of CathD and CathL poses a unique therapeutic challenge in breast and ovarian cancers. Therefore, a fuller clearance of these proteins before their involvement in secondary tumour progression may help advancement of treatment modalities. We have previously reported on the expression and secretion of CathL and CathD in the omentum and ascites of ovarian malignant patients, as well as in the tumor-based conditioned media ovarian cancer cell lines [14]. In the present paper, we report the use of GO to investigate whether CathD and CathL might be cleared out through an adsorption process. To help visualize the role that GO plays, we used a cost-effective and scalable batch adsorption approach, where complementary information is channeled via multimodal kinetic and regression models as an analogy of a multiplexed toxicity-dependent clearance of pro-metastasis enzymes. Our study reveals that inhibition of CathD and CathL could indeed help overcome the therapeutic challenges faced in breast and ovarian cancers. The idea of enzyme-targeting therapy is explained in Figure 1.

2. Results

2.1. Synthesis and In Vitro Toxic Effects of GO on Lung Cancer Cells

Similar to our previously reported work, exfoliated GO was synthesized following the modified Hummer's method [30–32]. The basic characterization is given in Supplementary Note 1 and Figures S1–S9. TEM imaging showed the flake-like shapes of GO (Figure S1). We first characterized GO, referred to as GO sheets, indicating atomic compositions of C (1s) and O(1s) as 91%, and 9% (Figure S2A), respectively. The binding energy of 285.0 eV was related to the C−C, C=C, and C−H bonds (Figure S2B). The other C_{1s} peaks of GO contained three main components belonging to C−O (hydroxyl and epoxy, 286.7 eV), C=C/C−C (284.7 eV) and O=C−O (carboxyl, 288.8 eV) and a minor component of the C=O (carbonyl, 287.4 eV) and O=C−OH (289.1 eV) functional groups [33]. The Raman spectrum of GO (Figure S3) exhibited a D band at 1358 cm^{-1} (the presence of defects) and a G band at 1595 cm^{-1} (the in-plane stretching motion of pairs of sp^2 atoms) [34]. The surface area of the GO was measured by the N_2 absorption Brunauer−Emmett−Teller (BET) method and found to be 25 m^2/g with a pore volume of 0.07 cm^3/g (Figure S4). The surface charge of the GO sheets was determined by the zeta potential measurements (Figure S5). The GO sheets were highly negatively charged (−63.54 mV) due to the presence in their molecular structure of the carboxyl group in the free state. Furthermore, the FTIR spectrum of GO (Figure S6) showed the specific functional groups of C−O−C (~1000 cm^{-1}), C−O (1230 cm^{-1}), C=C (~1620 cm^{-1}) and C=O (1740–1720 cm^{-1}) bonds. The band in the region of 3600–3300 cm^{-1} corresponds to O−H stretching vibrations of hydroxyl and carboxyl groups of GO [35]. The Lambert–Beer law, which describes the linear relationship between the absorbance and the concentration of the compound in a given solution was used to examine the dispersibility of GO. A calibration curve was constructed by measuring the absorbance at 232 nm of nine different concentrations (0.039–10 mg/mL) of the GO solution, in which there was good water dispersibility of GO (Figure S7) [36]. The XRD pattern of GO, as prepared in the present study, gave a (001) reflection peak at $2\theta = 13.7^\circ$ (Figure S8), which corresponds to a d-spacing of 0.75 nm, and exhibits an increased interlayer distance compared to that (3.34 Å) (2 theta 1/4 26.7°) in the typical graphite oxide structure (sp^2 hybridization) [37]. This suggested the complete disintegration of the graphite structure to form GO under ultra-sonic vibration. Initially, GO exhibited weight loss of 8.7 wt% at temperature below 150 °C as a result of the loss of absorbed water, while in second stage GO lost more weight (23.6 wt%) in the temperature range of 180–250 °C due to thermal decomposition of oxygen-containing functional groups including hydroxyl and epoxy (Figure S9).

The in vitro toxic effects of GO were determined by measuring cell viability, early and late apoptosis, and necrosis in two well-characterized lung cancer cell lines at different concentrations of GO (5–500 μg/mL). We measured both early and late apoptosis, where the latter can be distinguished from the former by the presence of a disintegrated cell membrane (detected by PI internalization).

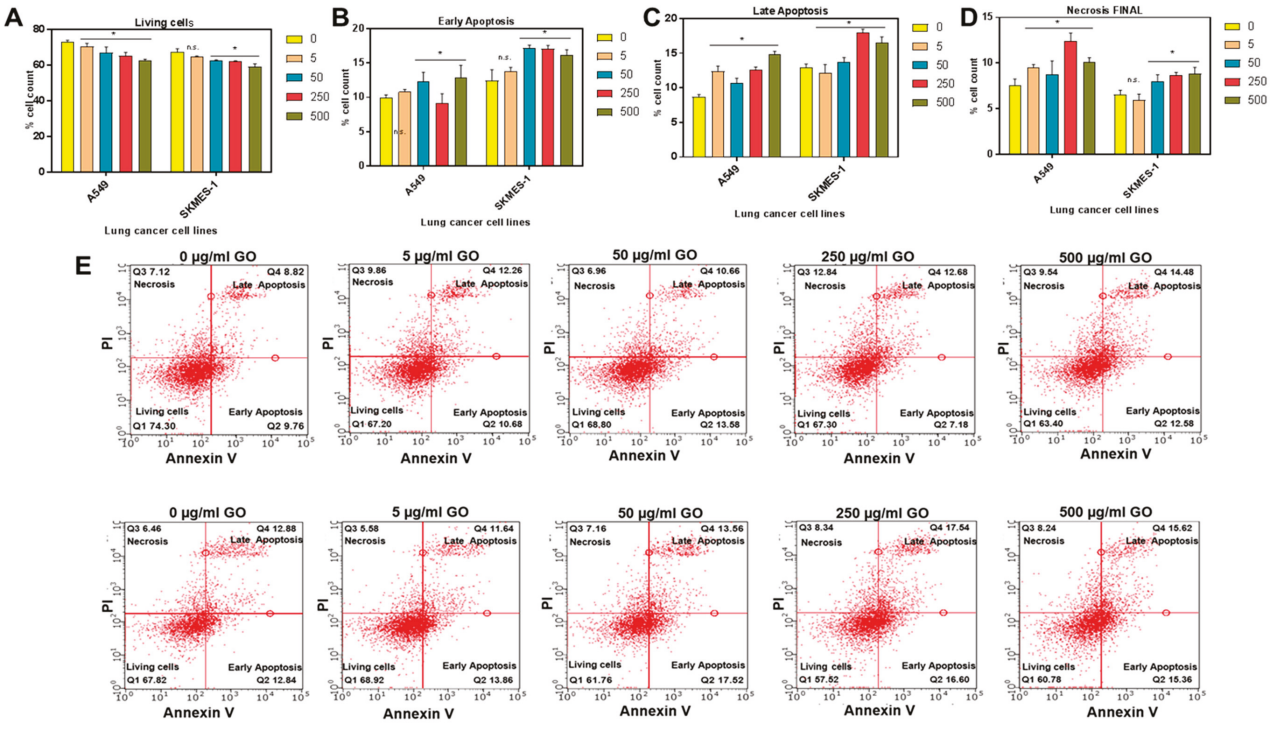

Figure 2. The percentages of living, apoptotic and necrotic lung cancer cells (A549 and SKMES-1) ± graphene oxide (GO) treatment. Cells were stained with annexin V (apoptosis) and propidium iodide (PI; late apoptosis and necrosis) following 24 h of treatment with varying concentrations of GO (0–500 μg/mL) and was assessed by flow cytometry and analysed using Guava 3.1.1 software. Percentage cell counts are shown for (**A**) living cells, (**B**) early apoptosis, (**C**) late apoptosis and (**D**) necrosis at increasing concentrations of GO. Data from three independent experiments are presented as mean ± SD. Groups are indicated as n.s and * $p < 0.05$, representing the outcomes of statistical tests vs control (0 μg/mL). (**E**) Shows scatterplots from one representative experiment in A549 (upper panel) and SKMES-1 (lower panel) cells.

Figure 2A demonstrates a slight but significant ($p < 0.05$) reduction in cell viability of both A549 and SKMES-1 cells after 24 h GO exposure statistically at concentrations of 250 and 500 μg/mL, compared to the control group (0 μg/mL). Significant early apoptosis was also detected (Figure 2B), in A549 cells at 500 μg/mL of GO ($p < 0.05$) compared to controls (0 μg/mL), and in SKMES-1 cells at 50 and 250 μg/mL of GO ($p < 0.05$) compared to controls. Late apoptosis (Figure 2C) and necrosis (Figure 2D) measurements were also carried out for A549 cells. Interestingly, in SKMES-1 cells, 250 and 500 μg/mL of GO significantly induced late apoptosis while necrotic cells were detected at GO concentrations of 50–500 μg/mL. Figure 2E illustrates the representative analysis of one flow cytometry experiment in SKMES-1 and A549. GO induced apoptosis and necrosis at concentrations higher than 50 μg/mL in both cell lines. However, the percentage count of apoptotic cells remained higher compared to necrosis, suggesting that GO may not cause significant damage to the cell membrane, allowing only the binding of annexin V to PS on the cell surface membrane. This indicates that the cell death observed at higher concentrations of GO is probably due to apoptosis rather than necrosis.

For the toxicity exposures undertaken, GO has been shown to be less toxic than other forms of graphene such as reduced GO, which we recently reported for similar cell lines [38]. However, GO has proven to be more toxic than graphene quantum dots as reported by Zhu et al. [39] where it was demonstrated that quantum dots have little toxicity to MG63 (80–90% of cell viability at low dose). This may be because dots are smaller than GO, and hence cause less damage to the cell membrane. GO has been proven to be less cytotoxic, with a reduced free radical production, and cell death compared to reduced GO because of the two-dimensional nature of thin sheets, functional groups and surface charges of GO that allows its efficient cellular uptake [40]. Oxidative stress is thought to be a key factor resulting in graphene toxicity, reducing the number of viable cells and hindering uptake of essential proteins and nutrients [41]. Furthermore, GO may induce various levels of toxicity in in vitro and in vivo models as a result of concentration and dosage patterns, administration routes, entry paths and accumulation of GO via barriers, distribution among different organs, cellular uptake, localisation and clearance [42]. These biological mechanisms depend on physio-chemical properties, sheet size, shape, lateral dimension, functional groups, surface charge and hydrodynamic diameter of the GO. It is evident that a sheet size of GO below 40 nm does not cause off-target toxicity [43–45]. We have explored the in vitro toxicity of GO in cancer cells at various concentrations, giving insights into the safe and biocompatible doses of GO to be used for the adsorption and clearance of enzymes. Our results demonstrate that GO at low concentrations did not exhibit obvious toxicity and did not interrupt the course of cell metabolism, gene transcription or cell death. Owing to the flake-like shape of the GO sheet, a readily available surface area is provided to adsorb enzymes while remaining non-toxic to healthy surrounding tissues. However, the neurotoxicity and neuroprotection of GO towards brain cells remain largely unknown and still need further research to explore the possible mechanism of interaction between GO and brain cells, and the capacity of GO not to cross the blood-brain barrier, in improving therapeutic responses to GO.

2.2. Basic Characterization of Enzymes

The proteolytic activity of CathD was investigated using a specific fluorogenic substrate at the two pHs, 3.6 and 7, while the proteolytic activity of CathL was investigated using the CathL-specific fluorogenic substrate ZVA (5 nM) at the two pHs 5 and 7. CathD was more active at pH (3.6). When the pH was increased to 7, the fluorescence signals were observed to be reduced (Figure 3A). The result suggests that CathD is not proteolytically active at neutral pHs. On the other hand, CathL was more active at pH 5.5 (Figure 3B). Fluorescence signals remained almost two times higher than the control at pH 7 (pH of the cell culture medium). The data suggested that CathL is proteolytically active at pH 7.

The representative FTIR spectra of CathD and CathL are given in Figure 3C for the spectral range (3200–500 cm^{-1}). In the case of CathD, most of the observed bands appearing at 1100, 1243, 1280, 1413, 1713, and 2050–2150 cm^{-1} are C−O stretch, CH wagging, C−O stretch, carboxylate ion (COO^{-}) symmetry, C=O stretch carboxylic acid and C−H alkyl stretch respectively [46,47]. The most

prominent band assignments of CathL at 1100, 1243, 1280, 1413, 1713, and 2050–2150 cm^{-1} are C−O stretch, CH wagging, C−O stretch, carboxylate ion (COO^-) symmetry, C=O stretch carboxylic acid and C−H alkyl stretch respectively [46–48]. These bands were not observed in control experiments without CathD/CathL and substrate agents (data not shown). The regions with the widest ranges and their corresponding spectral signatures have been given in Table S1. The representative Raman spectra of CathD and CathL are given in Figure 3D for the spectral range (500–2500 cm^{-1}). The most prominent band set of the CathD are 2243, 2024 and 1603 cm^{-1} while assignments of CathL are 2024 and 1603 cm^{-1}. The prominent peak at 1608 cm^{-1} relates to the known bands for the Fmoc group as reported earlier [49]. The Raman bands at 2024 and 2243 cm^{-1} could be assigned to the C≡C stretching vibration, which was present in the propargyl group [49]. The surface free energy and its polar and dispersive parts were calculated to investigate the binding capacity and weight of electrostatic and/or van der Waals interactions between GO and the enzymes. The binding capacity of GO, CathD and CathL were calculated using the contact angle method and their respective contact angles have been shown in Figure 3E. The surface free energies, polar and dispersive parts of GO, CathD and CathL are shown in Figure 3F. CathD has the highest total surface energy of 77.4 mN/m, although GO, CathD and CathL have similar trends of surface energies of total and their respective parts because of the similar amount and weight of functional groups. As a result, the use of GO as an adsorbent could allow enzymes to be adsorbed and substituted to improve the binding of CathD/CathL with GO. Therefore, it appeared that amino-acid replacement at the basal planes of GO can lead to protein-ligand binding. (See set of "snapshots" in Figure 3G).

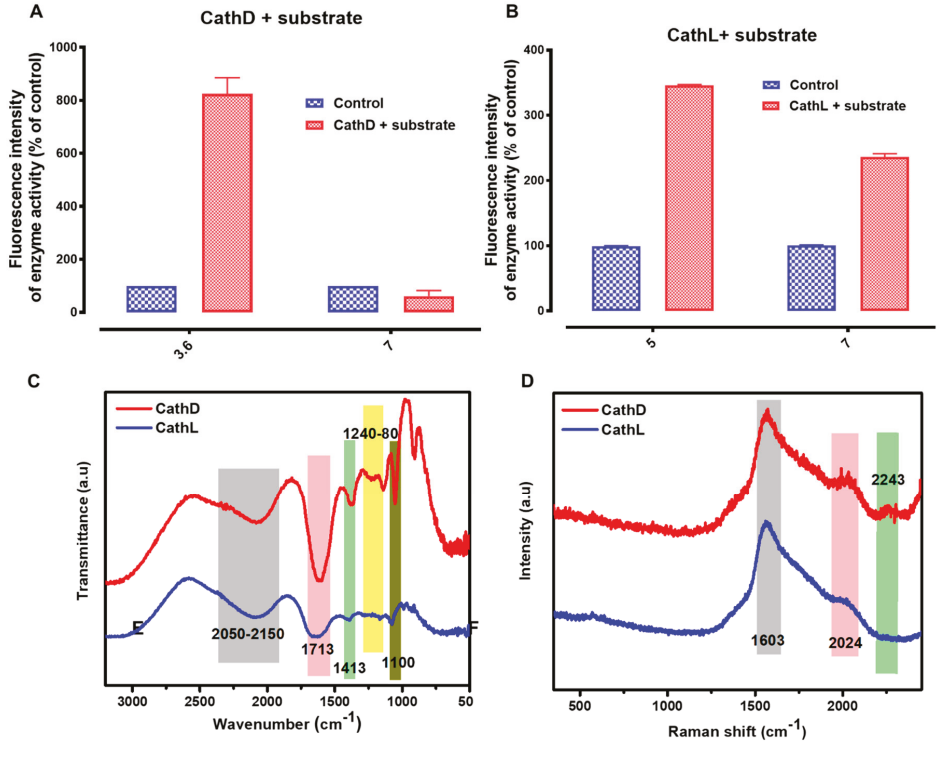

Figure 3. *Cont.*

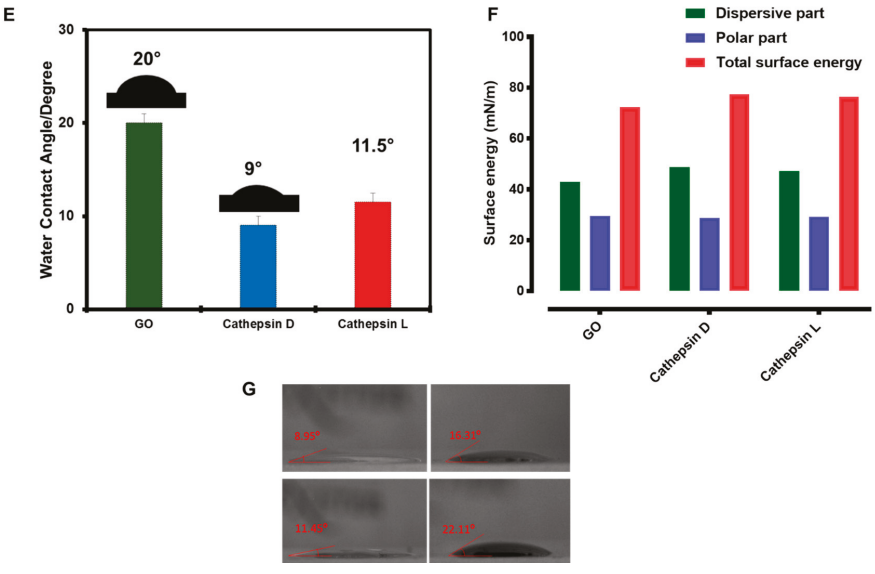

Figure 3. Characterization of cathepsin D (CathD) and cathepsin L (CathL). (**A**) CathD is highly active at pH 3.5–4 (optimum) and inactive at pH 7 and above. The CathD-specific fluorogenic substrate (10 μM) was incubated ± CathD (50 ng/mL) at the pH's 3.6 and 7, and fluorescence intensity was measured at Ex/Em: 320/393 nm. Each data point represents n = 4 experiments. The horizontal bars represent SDs. (**B**) CathL is highly active in ionic buffer. A specific fluorogenic substrate ZVA (5 nM) was incubated ± CathL (50 ng/mL) at pH's 5 and 7, and its fluorescence signals were measured at Ex/Em: 365/440 nm. Control wells contained substrate alone. The data are presented here as percentage of control (the relevant 100%). Each data point represents n = 4 experiments. The horizontal bars represent SDs. (**C**) FTIR spectra of CathD and CathL. (**D**) Raman spectra of CathD and CathL show bands at 1602 and 2024 cm^{-1}. (**E**) Water contact angle profile of GO, CathD and CathL gives the values of 20°, 9° and 11.5°. (**F**) Surface energy profile of GO, CathD and CathL. (**G**) Representative image of wettability quantification as measured by water and diiodomethane contact angles of GO, CathD and CathL. The images were taken using a digital camera and analysed for contact angle measurements using the ImageJ processing program.

2.3. Enzyme Interaction with GO

Batch adsorption studies were performed to measure the effect of pH on the adsorption process of CathD and CathL using GO as an adsorbent. Figure 4 shows absorbance variations at different concentrations of GO (0, 50, 500 and 1000 μg/mL) mixed with CathD and CathL at different time points (0–20 min). The decrease in absorbance signals of CathD and CathL at pH's of 3.6 and 5, respectively revealed the amount of CathD and CathL adsorbed to GO. At optimal incubation times and concentrations of GO, CathD and CathL were almost fully adsorbed onto the GO surface. The CathD and CathL adsorption process was found to be pH-dependent and concentration-dependent, demonstrating that the highest adsorbed amounts were at more acidic pHs (3.6 and 5). For pH 3.6, the amount of CathD adsorbed increased from 50 to 1000 μg/mL over a time scale of 0 to 20 min. The adsorption capacity of GO (1000 μg/mL) was above 90% after 20 min. CathL adsorption onto the GO surface followed a similar pattern at pH 5 and at 1000 μg/mL GO the highest value of efficiency was attained after 20 min. Figure 5 shows that an increase in adsorption capacity occurred for both enzymes over a 20 min time period, reaching a maximum capacity of above 90%. The capacity was found to be slightly greater for higher concentrations of GO. The results are in good agreement with experimental data (Figure 6A,B).

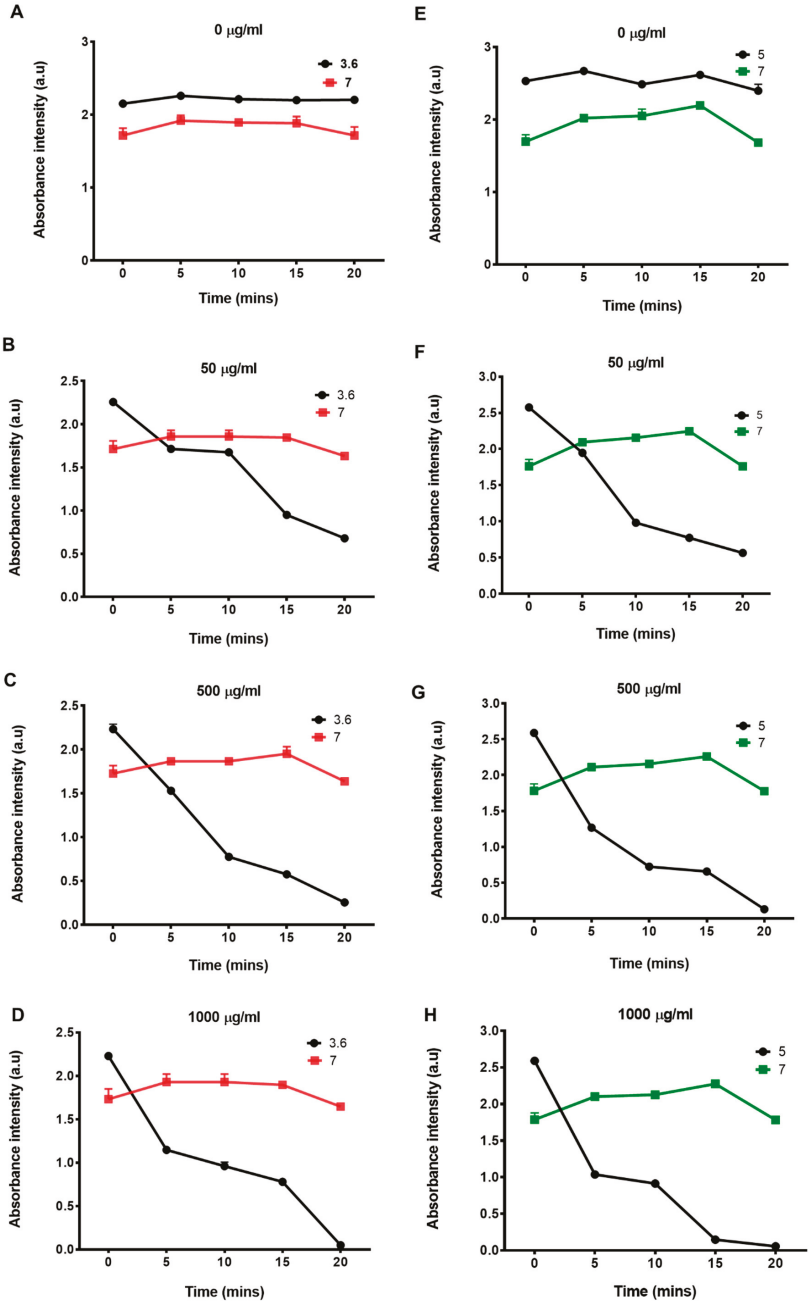

Figure 4. Effect of various concentrations of GO on CathD and CathL activities. Absorption of CathD (**A**–**D**) and CathL (**E**–**H**) by GO at different concentrations (50, 500, and 1000 μg/mL) incubated for 2, 5, 10, 15, and 20 min. Absorbance signals were measured using a PHERAstar BMG plate reader at λ = 280 nm. Each data point represents n = 4 experiments. The horizontal bars represent SDs. For some data points, the error bar is smaller than the diameter of the data point.

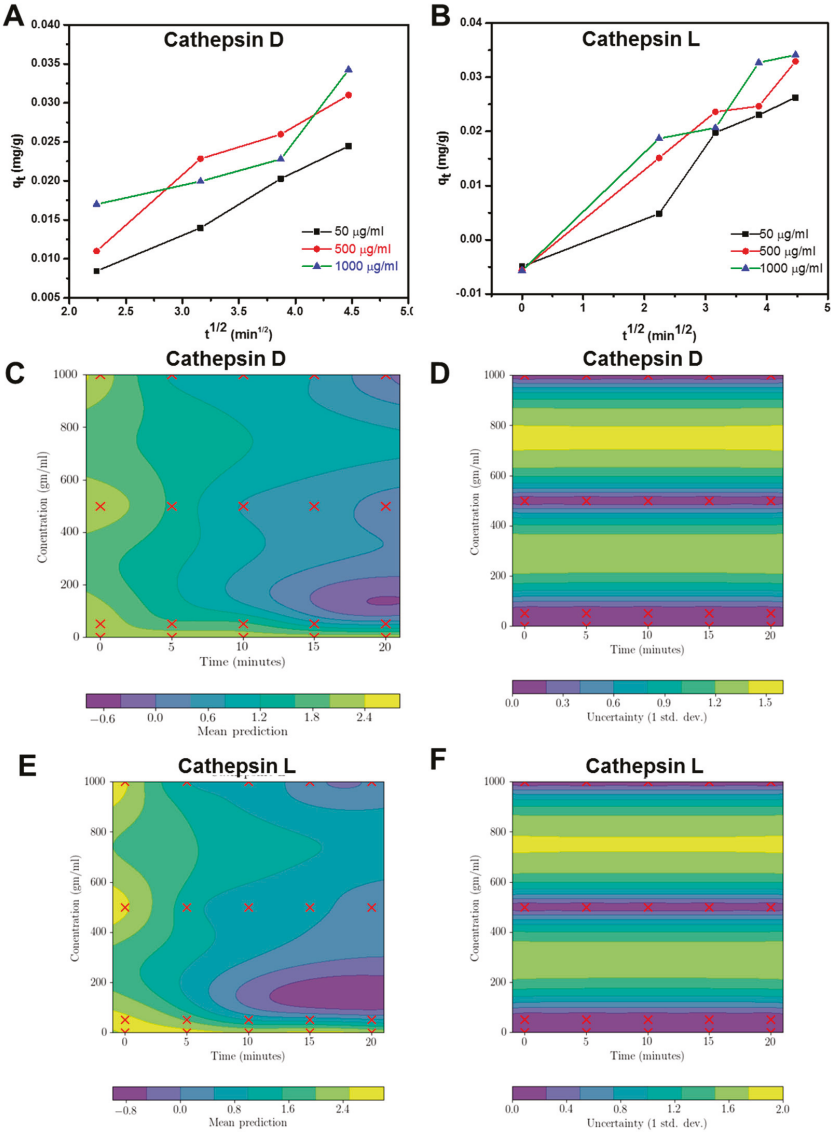

Figure 5. (**A**,**B**) Kinetic models fitting to the data for CathD and CathL using piecewise linear regression analysis of experiments in which (**A**) CathD and (**B**) CathL were adsorbed onto GO. (**C**–**F**) Gaussian process regression models to find the prediction and uncertainty in adsorption of CathD (**C**,**D**) and CathL (**E**,**F**) relating independent variables (time and concentration) to the dependent variable (absorption). In (**C**) and (**E**), the mean predictions are depicted, and the uncertainty in predictions is shown in (**D**) and (**F**).

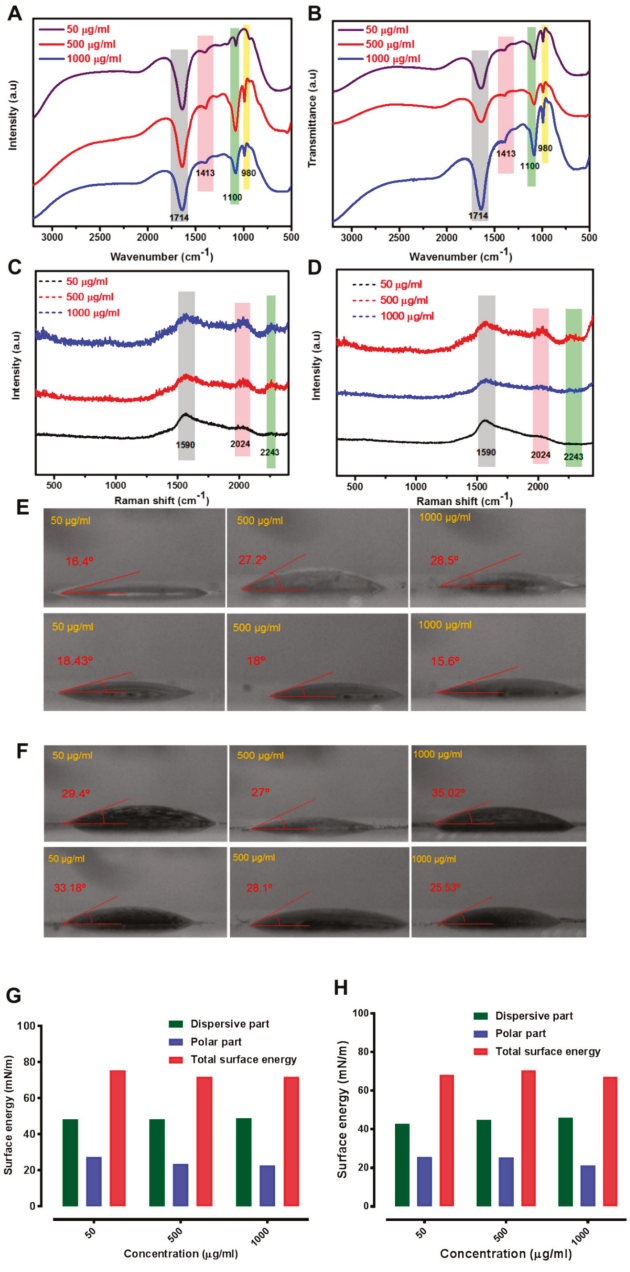

Figure 6. (**A**,**B**) FTIR spectra of CathD/CathL-linked graphene oxide (GO) at 50, 500 and 1000 µg/mL concentrations of GO. (**C**,**D**) Raman spectra of CathD/CathL-linked GO at 50, 500 and 1000 µg/mL GO concentrations. (**E**,**F**) Contact angle profiles of CathD/CathL-linked GO interfaces at 50, 500 and 1000 µg/mL concentrations of GO. The diiodomethane contact angle was determined to calculate the surface energy of the enzymes, GO and the interfaces of GO with enzymes. (**G**,**H**) The surface energy profile of GO-CathD/CathL interfaces which have three segments of total surface energy, dispersive surface energy and polar surface energy—the profiles correspond to 50, 500 and 1000 µg/mL concentrations of GO which had been treated with CathD and CathL.

Adsorption kinetics are useful to evaluate the adsorption process and adsorption rate. In this study, we have used an intraparticle diffusion model. This multi-linearity graph plot of intraparticle diffusion shows three segments: the first portion is the instantaneous adsorption segment which shows the adsorption of external surface of GO; the second step is the gradual adsorption stage assigned to intraparticle diffusion; and the third straight portion depicts the final equilibrium stage due to the low adsorbate concentration left in the solution. Figure 6A,B show that the intraparticle diffusion plot at each concentration did not pass through the origin, indicating that the intraparticle diffusion was not the only rate-controlling process. This is indicative of an additional role of boundary layer diffusion control. The intraparticle diffusion constant values are shown in Table S2. Gaussian process regression models for CathD and CathL relating independent variables (time and concentrations) to the dependent variable of adsorption are shown in Figure 5C–F. In Figure 5C,E, the mean predictions for CathD and CathL are depicted respectively, and the uncertainty in these predictions has been shown in Figure 5D,F. The mean predictions for CathD indicate that promising (lower) absorption can be achieved with a concentration of around 100 μg/mL when CathD is incubated with GO for 15 to 20 min. The models also revealed that concentrations of CathD greater than 900 μg/mL which are incubated for about 18 min could also be promising. Figure 5E,F show similar trends for CathL. The fluorescence of GO only has been shown in Figure S10. Figure S11 illustrates the measurement of normalised fluorescence intensities of various concentrations of GO (0, 50, 500 and 1000 μg/mL) exposed to CathD and CathL at different time points (0–20 min). CathD and CathL were enzymatically cleaving a GO substrate which gave rise to a fluorescent product, at increasing concentrations of GO (0, 50, 500 and 1000 μg/mL). GO was able to concentration-dependently increase the catalytic activity of CathD and CathL at all pHs tested. A slight difference in emission spectra also occurs, suggesting that lower pH values represent an improved exposure of non-polar sites of adsorbate in the enzymes. Fluorescence loss was observed in the case of CathL at pH 7, due to the reversible nature of CathL inhibition. The lack of any significant difference in fluorescence signals might be because of the adsorption of enzymes induced by GO. This uptake allows localization of internalized GO under different pH conditions [50,51]. This uptake could be attributable to the large size of GO which blocks fluorescence signals. The binding of CathD and CathL to GO shows that both the enzymes and GO sheets form a new tertiary structure. These tertiary structures may contribute significantly to the self-fluorescence characteristics of GO. Understanding the pre-clinical and clinical effects of such factors to allow the development and adsorption of pro-tumorigenic and pro-metastatic enzymes, released into the extracellular matrix from malignant tumors, will be the focus of further studies.

FTIR and Raman spectroscopic findings can be used to monitor the macromolecular movements and vibrational/rotational states of specific chemical groupings which bind target biomolecules with high specificity during the formation of the nano-bio-interface of CathD- and CathL-GO. Figure 6A,B illustrates FTIR spectra of GO-CathD/CathL at the concentrations of 50, 500 and 1000 μg/mL of GO after 20 min. The FTIR spectrum of CathD-linked GO revealed a range of CathD and CathL absorption bands including C=O ($\upsilon_{C=O}$ at 1714 cm^{-1}), and the peak of the C−N stretch mode ($\upsilon_{C=O}$ at 1100 cm^{-1}) at all the concentrations represents the CH stretching and NH bending. The specific band of GO-CathD (at two concentrations of 500 and 1000 μg/mL GO) (Figure 6A) showed the characteristic peak of an alkoxy group at 980 cm^{-1} which is associated with the C=O functional groups of GO and CathD. The peaks at 1413 cm^{-1}, ascribed to NH bending and CN stretching, also confirmed the presence of CathD and CathL. Figure 6C,D show Raman spectra of GO-CathD/CathL. The amide-1 vibration at 1590 cm^{-1} arose from the typical $\upsilon_{C=O}$ stretching vibration. The band in the range of 2020–2250 cm^{-1} was assigned to the specific C−H_3 and C−H_2 deformation vibrations which mainly arose from the side chains of different amino acids. The band in the range of 1200–1340 cm^{-1} was assigned to the amide-III vibration which typically arose from the combination of the N-H bending and C−C stretching vibration [52,53]. In the Raman spectra of GO and GO-CathD/CathL, the slight shifting of peaks towards lower wavenumber can be observed. GO has two typical peaks at ca. 1355 cm^{-1} and 1580 cm^{-1}. The spectra at 1600–1620 cm^{-1} can be assigned to the C=O stretching of carboxylate

and C−H_2 deformation vibrations. Based on these bands, it is concluded that the CathD and CathL interacted with GO through its amide groups. Both cathepsins have a deep bonding pocket with the binding groups identified by FTIR, which are held together with GO by electrostatic attractions.

The functional groups present at the outermost surface of GO readily facilitate its coverage with inert molecules, which increases surface hydrophilicity and subsequently enhances the bonding strength of these nanostructures [54]. Several site-specific variants of GO have been employed in attempts to alter the surface-inactivation of 'wild-type' enzymes. The extent of enzyme absorption (and the mechanistic insight this provides in relation to the proteins' interactions with surfaces) have been probed by water contact angle (WCA) measurements and surface energy determinations (Figure 6E,F). The CathD and CathL displayed higher binding activity towards GO, as demonstrated by the WCA values. Upon CathD and CathL interactions, the WCA profiles of GO shifted to higher values, suggesting that a good level of surface hydrophilicity was achieved (Figure 6F). The effect was more pronounced for the higher concentrations, whose average WCA value increased by 8.5 and 15.0 degrees for CathD and CathL, respectively. The changes in diiodomethane contact angle (Figure 6F) showed the surface energy profile (Figure 6G,H). The binding free energies of GO to CathD and CathL are shown in Figure 6G,H. The intermolecular vdW and electrostatic interactions are believed to improve the desolvation process because of the substitution of one oxygen-containing functional group with an amino group, which in turn increases the total free energy of the compound. However, the polar penalties upon binding of these two proteins to GO were decreased.

These findings have provided significant information about the surface interactions of GO sheets with CathD and CathL: (i) the number and amount of the functional groups and their reactivity; (ii) the critical role of surface hydrophobicity in the adsorption process. The WCA of CathD and CathL is shown in Figure 3. Moreover, the key differences in the amount and number of functional groups and bonding affinities are responsible for the rise in total and dispersive surface energy. The low polar and high dispersion parts (Figure 6G,H) of the surface energy profiles revealed that the polar and nonpolar side-chains of CathD/CathL facilitate conformational alterations in the CathD/CathL structure, which in turn lead to a high adsorption capacity of GO for CathD/CathL.

3. Discussion

Potential cancer therapies include the development of innovative treatment modalities that are capable of clearing the pro-tumorigenic enzyme by developing a novel platform based on biocompatible adsorbents. The currently available mainstream treatment options have resulted in improved survival and quality of life, although ovarian and breast cancers remain progressive diseases. Thus, there is an ever-growing need for the development of alternative approaches. Conventional biological drug therapies have limitations due to unwanted side effects on normal tissues/cells that adversely affect the efficacy and safety of the treatment. The emerging paradigm of personalised and precision medicine provokes the concept that adsorption of these enzymes in the local tumor environment could be achieved by using porous adsorbents. Enzyme-targeted therapy provides a great opportunity for this by addressing the mechanisms of pro-tumorigenic enzyme clearance and therapeutic action. In this study, we developed a GO that breaks down and takes up enzymes which promote increased invasiveness and metastasis. The surface charge, surface area, chemical reactivity and electronic characteristics of GO were used to target these enzymes with sustained release of functional groups, free radical and porous sites for entrapment of CathD and CathL. The inhibition of CathD and CathL was observed at specific pH values which support metastasis. Inhibition of CathD and CathL was verified by enzyme activity using specific substrates. The analysis of the released CathD and CathL libraries was carried out using a wide variety of analytical tools such as FTIR, Raman, WCA and surface energy profiles (see Figure 2; Figure 6), thus posing a significantly fast-tracked identification procedure and considerable output compared with conventional tools to analyse nanoparticle interactions with proteins. In this manner, the characterization of the studied

enzymes for their binding and bioactivity is carried out to better understand their structural and functional behaviours.

The current approach of enzyme targeting offers a number of important advantages over conventional approaches. First, it permits the simplistic tagging of cathepsins with very high transformation/removal efficiencies using GO, which considerably increases the likelihood of recognising biomolecular fractions. Secondly, the clinical relevance and biosafety of this modality would further benefit from utilising a GO system that is already used in clinical trials to introduce drug/gene carrier vehicles. Finally, the approach presented here is greatly adaptable and can be used largely for the innovation of theranostic saviours of disease-associated enzymes. The present work was mainly applied to targeting two ovarian and breast cancer-associated enzymes. The two-dimensional and adsorbing nature of GO could reduce the likelihood of abundance of these enzymes to induce tumor cell invasion and metastasis, and thereby maximize the broad applicability of GO. Furthermore, the GO not only allows for robust interactions with enzymes but also enables the compact packaging of the GO within dissolvable capsules, facilitating non-invasive oral administration to track these proteins, which could be used as a diagnostic tool. Given the clear benefits achievable by using enzyme-targeted therapy (compared with the currently available modalities such as chemotherapy, radiation therapy etc.), the cost-effectiveness involved in producing GO is another advantage for implementing this material as a standard-of-care in the treatment of cancer. Currently, clinical-scale manufacturing of GO entails a range of protocols to fabricate, modify, functionalise, deliver and selectively accumulate and administrate into the living systems. Future work will address cell-based and pre-clinical metastatic disease models and will possibly include further developments to integrate targeted and safe delivery of GO to the tumor sites with sufficient selectivity to facilitate the removal of disseminated enzymes.

4. Experimental Section

4.1. Synthesis and Characterization

Exfoliated graphene oxide (GO) flakes were synthesized from exfoliated graphite using the modified Hummer's method as previously reported by us [27,28,38]. $NaNO_3$ (1.5 g) and H_2SO_4 (150 mL, 98%) were added to a 800 mL round-bottom flask with graphite flakes (2 g). The reaction mixture was mixed under magnetic stirring following by the immersion of the flask in an oil bath. The mixture was then heated at the temperature of 35 °C, before adding $KMnO_4$ (9 g) into the flask. The mixture was subjected to constant continuous stirring for 24 h, followed by addition of more H_2SO_4 (280 mL, 5%) and the temperature was increased to 85–95 °C. The mixture was stirred for another 2 h before removing the bath. The flask was allowed to cool down to 60 °C. Finally, H_2O_2 (15 mL, 30 wt%) was added and the mixture was stirred for another 2 h. The resultant product was washed 7–8 times with HCl (3 wt%) and then washed 4–5 times with distilled water to eliminate any contaminants. As obtained GO was dispersed in water under stirring. As prepared GO was then used for further characterization. Transmission electron microscopy (TEM) (JEOL-2100 TEM, JEOL, Madrid, Spain), at an accelerating voltage of 200 kV) was used to obtain high resolution microstructural images. A drop of the as prepared GO was deposited on a holey carbon Cu grid to prepare the TEM samples. X-ray diffraction (XRD) analysis was conducted using Cu Kα radiation. X-ray measurements were performed at a voltage of 40 kV and a current of 40 mA and spectrum was collected a step size of 0.02° (2θ) and a step time of 1 s. Fourier-transform infrared (FTIR) spectroscopy was conducted by means of a Tensor-27 FTIR spectrometer (Bruker Optics, Champs-sur-Marne, France) in the wavenumber range of 4000–500 cm^{-1}. FTIR samples were prepared by mixing the sample with KBr. Raman spectroscopy was carried out with laser excitation at 532 nm (Renishaw, Stroud, UK). To calculate the surface charge of GO, zeta potential measurements were performed using a colloidal dynamics zeta probe. UV/Vis spectrophotometry was performed using a 6715 UV–Vis instrument (Jenway, Staffordshire, UK).

4.2. Cell Viability

Cell viability experiments using flow cytometry has been described elsewhere [34]. Briefly, cells were treated with or without 5, 50, 250, 500 and 1000 μg/mL of GO for 24 h. After trypsinisation, cells were stained with annexin V (BioLegend, London, UK) and propidium iodide (PI, Sigma-Aldrich, Gillingham, Dorset, UK)) and subjected to flow analysis using a Guava flow cytometer (Millipore UK Limited, Hertfordshire, UK). The data were analysed using the Guava 3.1.1 software. The experiment was carried out at least three times and the data obtained were analysed using GraphPad Prism 5.04 (GraphPad Software, San Diego, CA, USA), and expressed as % cell count ± SD, Mann Whitney.

4.3. Regression Model

We were particularly interested in determining a good estimate of the most effective level of concentration of CathD and CathL and the experiment time required for biological applications. As such we built a model that may indicate which pair of concentrations and times are promising and subsequently help in our decision making. However, we had limited data (due to the expense of conducting many experiments) and repeated measurements are always noisy (in that we obtained a slightly different measurement for the same concentration and time). Therefore, it is of paramount importance to consider these uncertainties in modelling the performance of these enzymes. Standard non-linear regression models usually predict the general trend without capturing such uncertainties. As an alternative, we used Gaussian processes (GPs) to model absorption (dependent variable) with respect to time and concentration (independent variables) for both CathD and CathL. A GP model allowed us to inspect the expected performance and the predictive uncertainty for the enzymes. Thus we were able to strike a balance between predicted performance and uncertainty to make an informed decision.

Formally, a GP may be considered as a collection of random variables, which is jointly Guassian distributed [38,52]. This essentially allows us to encapsulate the intuition that for a small change in concentration and time there should be a small change in performance. Let $D = \{x_i, y_i\}$ be a data set consisting of n data points, where the i-th vector x_i consists of a time and a concentration (independent variables), and y_i is the associated absorption (dependent variable). A trained GP model then produces the following posterior predictive Gaussian distribution: $P(y_{n+1} \mid x_{n+1}, D, \theta) \sim N(\mu(x_{n+1}), \sigma(x_{n+1}))$, where θ is a set of hyperparameters that are optimised using collected data D, $\mu(x_{n+1})$ is the expected performance for x_{n+1}, and $\sigma(x_{n+1})$ is the predictive uncertainty. The details of training a GP model can be found in [52].

4.4. Water Contact Angle Measurements and Surface Energy Calculations

A contact angle goniometer was used to calculate the wettability of GO, CathD and CathL. A digital camera was used to capture the images and the contact angle was measured using the ImageJ processing program. The contact angle surfaces were developed by dropping a 10 μL drop onto a glass slide. The surface free energies were estimated by quantifying the contact angle of diiodomethane (DIIO) on the surface of the sample. 10 μl drop of DIIO was used in each measurement. The surface free energy of a solid sample is expressed by Young's equation, where S is solid and L is liquid:

$$\sigma_S = \sigma_{SL} + \sigma_L \times \cos\theta \quad (1)$$

where σ_L, and σ_{SL} represent the surface tension of the liquid and the interfacial tension between the liquid and the solid, respectively and θ is the contact angle shaped by the liquid on the surface of the sample respectively. Here, we are measuring σ_S with the help of known value of σ_L and unknown value of σ_{SL}. According to the Fowkes method [53], the surface tension is given by:

$$\sigma_{SL} = \sigma_L + \sigma_S - 2((\sigma_L{}^D \times \sigma_S{}^D)^{1/2} + (\sigma_L{}^P \times \sigma_S{}^P)^{1/2}) \quad (2)$$

where the surface free energies are mixture of dispersive (D) and polar (P) parts together. This would be used to exclude the unknown value in Equation (1).

The polar part of liquid is zero for DIIO, so:

$$\sigma_S{}^D = \sigma_L \times (\cos\theta + 1)^2/4 \quad (3)$$

where $\sigma_L = \sigma_L{}^D = 50.8$ mN/m. The dispersive part of the surface free energy of the sample can directly be found from the contact angle.

The polar and dispersive parts of water are: $\sigma_L{}^D = 26.4$ mN/m and $\sigma_L{}^P = 46.4$ mN/m. Equations (1) and (2) can be reorganised to calculate the polar part of the surface energy of the sample:

$$\sigma_S{}^P = (\sigma_L \times (\cos\theta + 1)/2 - (\sigma_L{}^D \times \sigma_S{}^D)^{1/2})^2/\sigma_L{}^P \quad (4)$$

If the values of the dispersive and polar parts are known, the total surface energy of the sample will be:

$$\sigma_S = \sigma_S{}^D + \sigma_S{}^P \quad (5)$$

Contact angles of water and DIIO on surface of GO are 33.4° and 20° respectively. The dispersive component, polar component and total surface energies of GO are 42.8, 29.6 and 72.4 mN/m respectively [53]. The other surface energies were calculated in the same manner.

4.5. Proteolytic Activities

Citrate and phosphate buffer solutions were prepared at pHs 3.6, 5.0 and 7.0. Their composition is given in Supplementary notes 2 and 3. The measurement of proteolytic activities has been described elsewhere [18,20]. A brief description of each enzyme activity is presented below:

4.6. CathD Experiment

The buffers required to test CathD-proteolytic activities contained 0.005% of Tween20 (Sigma-Aldrich) and the pHs were adjusted to 3.6 and 7. CathD-fluorogenic substrate (100 nM; Enzo Life Sciences, Exeter, UK) was incubated ± CathD (50 ng/mL; recombinant from human liver, Sigma-Aldrich) and plates were read after 60 s of shaking at Ex/Em: 320/393 nm.

4.7. CathL Experiment

The buffers contained 1 mM DTT to disrupt the disulfide bonds, resulting in an active enzyme. CathL fluorogenic substrate Z-Val-Val-Arg-AMC (ZVA; 5 nM) was incubated ± CathL (50 ng/mL; recombinant from human liver, Sigma-Aldrich) at pHs 5 and 7. The plate was shaken for 60 s in a plate-reader prior to fluorescence reading at Ex/Em: 365/440 nm.

Both enzyme activities were measured using a SpectraMax plate reader (Molecular Devices UK Limited, Berkshire, UK). The data was normalised to control and represented as a percentage of the control.

4.8. Enzyme Interaction with GO

An interaction between CathD or CathL (50 ng/mL) and GO (50, 500 and 1000 μg/mL) was tested in pH buffers (pHs 3.6 and 7 for CathD, and pHs 5.5 and 7 for CathL). pH values of 3.6 and 5.5 are optimum for CathD and CathL activity, respectively. CathD and/or CathL was incubated with GO at different concentrations for 2, 5, 10, 15 and 20 min. The experiment was performed in ×4 96 well black opaque plates (Greiner Bio-One Ltd., Gloucestershire, UK). Plates were read at the same time scale as previously mentioned, of incubation at room temperature to measure absorbance at 280 nm for CathD and CathL using a SpectraMAX plate reader. The data normalised to the control and represented as a percentage of this control. The fluorescence intensity of the GO hydrolysis was identified kinetically using a SpectraMax plate reader. This was repeated ($n = 4$) with CathL at different

concentrations of GO (50, 500 and 1000 μg/mL). The control wells contained GO only. FTIR, Raman spectroscopy, wettabilities and surface energies were carried out in the same manner as explained in the previous section.

To verify the adsorption of CathD and CathL, an intra-particle diffusion model was used. Fick's second law was used to find out the intraparticle diffusion model as a rate-determining step during the adsorption experiment. It was carried out to verify whether it may control the kinetics of adsorption process [54,55]:

$$q_t = k_{id}\sqrt{t} + I \quad (6)$$

where I represents the boundary layer effect (a large value corresponds to a larger boundary layer thickness and k_{id} is the intraparticle rate constant and k_{int} (g/mg $min^{1/2}$) and C represent the adsorption constant and the intercept, respectively [56,57]. The intercept is measured from the plot of q_t versus $t^{1/2}$.

4.9. Statistical Analysis

Statistical analysis was carried out between two groups by the Mann-Whitney test, and between multiple groups were compared by one-way analysis of variance (ANOVA) with Tukey post-hoc testing or two-way ANOVA with a Bonferroni post-hoc test, using GraphPad Prism 5 software. The results are shown as mean ± s.d, (standard deviation) unless otherwise indicated. The value of $p < 0.05$ was considered statistically significant.

5. Conclusions

In summary, our findings represent a straightforward and highly reliable approach for the rapid and facile removal of pro-metastasis enzymes. GO with its variable zeta potential, variety of functional groups and very large (and in principle fully accessible) surface area, is an extremely promising candidate for the adsorption of such enzymes. Our results show that this material is compatible with cells. In addition, the adsorbent preparation is based on abundantly available and cost-effective graphite as the main precursor. Graphene oxide nanostructures are straightforward to prepare and are highly stable, which streamlines long-term storage at room temperature and correspondingly eases the manufacturing cost. Therefore, if employed in clinical settings as an innovative platform, this highly adaptable strategy could provide a real-world, cost-effective and broadly relevant procedure to treat chronic and complex diseases.

Supplementary Materials: The following are available online at http://www.mdpi.com/2072-6694/11/3/319/s1, Figure S1: Transmission electron microscopy image of graphene oxide, Figure S2: Basic characterization of exfoliated graphene oxide (GO). (A) XPS survey. (B) The C_{1s} spectrum of the GO shows three main components arising from C−O (hydroxyl and epoxy, 286.7 eV), C=C/C−C (284.7 eV) and O=C−O (carboxyl, 288.8 eV) and a minor component of the C=O (carbonyl, 287.4 eV) and O=C−OH (289.1 eV) species, Figure S3: Raman spectrum of the graphene oxide sample shows intense D (1358 cm^{-1}) and G peaks (1595 cm^{-1}) of defects and the in-plane stretching motion of pairs of sp^2 atoms, respectively, Figure S4: BET surface area of graphene oxide measured by nitrogen sorption isotherms measured at –196 °C. The BET surface area value obtained for this sample using the BET method was 25 m^2/g, Figure S5: Representative zeta potential of graphene oxide over a range of different pH values, Figure S6: The Fourier transformed infrared (FTIR) spectrum of graphene oxide shows vibrations of functional groups of C−O−C (~1000 cm^{-1}), C−O (1230 cm^{-1}), C=C (~1620 cm^{-1}), C=O (1740–1720 cm^{-1}) bonds and O−H (3600–3300 cm^{-1}), Figure S7: (A) UV/Vis absorption spectra of graphene oxide solutions with different concentrations (from 0.039–10 mg/mL) show the main peak around 232 nm. (B) The plot of the absorbance (λ = 232 nm) divided by the cell length, versus the concentration. The Lambert–Beer law ($A = \alpha \times C \times l$), allowed the determination of the absorption coefficient (α). This linear relationship fits well with the Lambert-Beer Law, indicating the good water solubility of the GO product, Figure S8: The XRD pattern recorded from graphene oxide shows a (001) peak at 2θ of 13.7°, Figure S9: TGA of exfoliated graphene oxide. TGA was performed in the nitrogen atmosphere, Figure S10: Photoluminescence emission spectrum of graphene oxide, Figure S11: Effect of different concentrations of GO on CathD and CathL fluorescence activities. GO at different concentrations (50, 500, and 1000 μg/mL) were incubated with CathD (A, B) and CathL (C, D) in 96 well plates at different time-points (2, 5, 10, 15, and 20 min) as shown where RFU is relative fluorescence units. Fluorescence signals were determined using a plate reader at Ex/Em: 355/450 nm. Each data point represents the mean of $n = 4$ experiments. Bars show SDs, Table S1: Characteristic IR bands of the protein linkages, Table S2: Kinetic parameters obtained for CathD and CathL for GO using an intraparticle diffusion model.

Author Contributions: Conceptualization, T.A.T., M.Z.I.P., J.L.W. and S.Z ; Data curation, J.L.W. and S.Z.; Formal analysis, T.A.T., M.Z.I.P., D.W.H. and J.L.W.; Funding acquisition, T.A.T., M.Z.I.P., J.L.W. and S.Z.; Investigation, T.A.T. M.Z.I.P.; Methodology, T.A.T., M.Z.I.P. and D.W.H.; Project administration, T.A.T., M.Z.I.P.; Resources, P.G.W., J.L.W. and S.Z; Software, A.A.M.R.; Supervision, J.L.W., P.G.W. and S.Z.; Validation, T.A.T., M.Z.I.P. and D.W.H.; Writing—original draft, T.A.T.; Writing—review & editing, J.L.W., S.Z. and P.G.W.

Funding: This work was supported by the EPSRC Centre for Doctoral Training in Metamaterials, XM2 (Grant no. EP/L015331/1) the University of Exeter, United Kingdom, and FORCE Cancer Charity (Grant No. 50703), United Kingdom.

Conflicts of Interest: The authors declare no conflicts of interest.

References

1. Michailidou, K.; Hall, P.; Gonzalez-Neira, A.; Ghoussaini, M.; Dennis, J.; Milne, R.L.; Wang, Q. Large-scale genotyping identifies 41 new loci associated with breast cancer risk. *Nat. Genet.* **2013**, *45*, 353–361. [CrossRef] [PubMed]
2. Eccles, S.A.; Aboagye, E.O.; Ali, S.; Anderson, A.S.; Armes, J.; Berditchevski, F.; Bundred, N.J. Critical research gaps and translational priorities for the successful prevention and treatment of breast cancer. *Breast Cancer Res.* **2013**, *15*, R92. [CrossRef] [PubMed]
3. Van Dam, G.M.; Themelis, G.; Crane, L.M.; Harlaar, N.J.; Pleijhuis, R.G.; Kelder, W.; Bart, J. Intraoperative tumor-specific fluorescence imaging in ovarian cancer by folate receptor-[alpha] targeting: First in-human results. *Nat. Med.* **2011**, *17*, 1315–1319. [CrossRef] [PubMed]
4. Aas, T.; Børresen, A.L.; Geisler, S.; Smith-Sørensen, B.; Johnsen, H.; Varhaug, J.E.; Lønning, P.E. Specific P53 mutations are associated with de novo resistance to doxorubicin in breast cancer patients. *Nat. Med.* **1996**, *2*, 811–814. [CrossRef] [PubMed]
5. Doufekas, K.; Olaitan, A. Clinical epidemiology of epithelial ovarian cancer in the UK. *Int. J. Women's Health* **2014**, *6*, 537.
6. Estrella, V.; Chen, T.; Lloyd, M.; Wojtkowiak, J.; Cornnell, H.H.; Ibrahim-Hashim, A.; Johnson, J. Acidity generated by the tumor microenvironment drives local invasion. *Cancer Res.* **2013**, *73*, 1524–1535. [CrossRef] [PubMed]
7. Trédan, O.; Galmarini, C.M.; Patel, K.; Tannock, I.F. Drug resistance and the solid tumor microenvironment. *J. Natl. Cancer Inst.* **2007**, *99*, 1441–1454. [CrossRef] [PubMed]
8. Liotta, L.A.; Kohn, E.C. The microenvironment of the tumour–host interface. *Nature* **2001**, *411*, 375–379. [CrossRef] [PubMed]
9. Coussens, L.M.; Fingleton, B.; Matrisian, L.M. Matrix metalloproteinase inhibitors and cancer—Trials and tribulations. *Science* **2002**, *295*, 2387–2392. [CrossRef] [PubMed]
10. Alberti, S.; Mateju, D.; Mediani, L.; Carra, S. Granulostasis: Protein quality control of RNP granules. *Front. Mol. Neurosci.* **2017**, *10*, 84. [CrossRef] [PubMed]
11. Berchem, G.; Glondu, M.; Gleizes, M.; Brouillet, J.P.; Vignon, F.; Garcia, M.; Liaudet-Coopman, E. Cathepsin-D affects multiple tumor progression steps in vivo: Proliferation, angiogenesis and apoptosis. *Oncogene* **2002**, *21*, 5951. [CrossRef] [PubMed]
12. Sudhan, D.R.; Rabaglino, M.B.; Wood, C.E.; Siemann, D.W. Cathepsin L in tumor angiogenesis and its therapeutic intervention by the small molecule inhibitor KGP94. *Clin. Exp. Metastasis* **2016**, *33*, 461–473. [CrossRef] [PubMed]
13. Pranjol, M.Z.I.; Gutowski, N.; Hannemann, M.; Whatmore, J. The potential role of the proteases cathepsin D and cathepsin L in the progression and metastasis of epithelial ovarian cancer. *Biomolecules* **2015**, *5*, 3260–3279. [CrossRef] [PubMed]
14. Winiarski, B.K.; Wolanska, K.I.; Rai, S.; Ahmed, T.; Acheson, N.; Gutowski, N.J.; Whatmore, J.L. Epithelial ovarian cancer-induced angiogenic phenotype of human omental microvascular endothelial cells may occur independently of VEGF signaling. *Transl. Oncol.* **2013**, *6*, 703–714. [CrossRef] [PubMed]
15. Losch, A.; Schindl, M.; Kohlberger, P.; Lahodny, J.; Breitenecker, G.; Horvat, R.; Birner, P. Cathepsin D in ovarian cancer: Prognostic value and correlation with p53 expression and microvessel density. *Gynecol. Oncol.* **2004**, *92*, 545–552. [CrossRef] [PubMed]
16. Xu, H.; Bao, K.; Tang, S.; Ai, J.; Hu, H.; Zhang, W. Cyanobacterial peptides as a prototype for the design of cathepsin D inhibitors. *J. Pept. Sci.* **2017**, *23*, 701–706. [CrossRef] [PubMed]

17. Westley, B.R.; May, F.E. Cathepsin D and breast cancer. *Eur. J. Cancer* **1996**, *32A*, 15–24. [CrossRef]
18. Pranjol, M.Z.I.; Gutowski, N.J.; Hannemann, M.; Whatmore, J.L. Cathepsin D non-proteolytically induces proliferation and migration in human omental microvascular endothelial cell via activation of the ERK1/2 and PI3K/AKT pathways. *Biochim. Biophys. Acta (BBA) Mol. Cell Res.* **2018**, *1865*, 25–33. [CrossRef] [PubMed]
19. Johansson, A.C.; Steen, H.; Öllinger, K.; Roberg, K. Cathepsin D mediates cytochrome c release and caspase activation in human fibroblast apoptosis induced by staurosporine. *Cell Death Differ.* **2003**, *10*, 1253–1259. [CrossRef] [PubMed]
20. Pranjol, M.Z.I.; Gutowski, N.J.; Hannemann, M.; Whatmore, J.L. Cathepsin L induces proangiogenic changes in human omental microvascular endothelial cells via activation of the ERK1/2 pathway. *Curr. Cancer Drug Targets* **2018**, in press. [CrossRef] [PubMed]
21. Sui, H.; Shi, C.; Yan, Z.; Wu, M. Overexpression of Cathepsin L is associated with chemoresistance and invasion of epithelial ovarian cancer. *Oncotarget* **2016**, *7*, 45995. [CrossRef] [PubMed]
22. Wason, M.; Lu, H.; Yu, L.; Lahiri, S.; Mukherjee, D.; Shen, C.; Zhao, J. Cerium Oxide Nanoparticles Sensitize Pancreatic Cancer to Radiation Therapy through Oxidative Activation of the JNK Apoptotic Pathway. *Cancers* **2018**, *10*, 303. [CrossRef] [PubMed]
23. Tabish, T.A. Graphene-based materials: The missing piece in nanomedicine? *Biochem. Biophys. Res. Commun.* **2018**, *504*, 686–689. [CrossRef] [PubMed]
24. Banerjee, A.N. Graphene and its derivatives as biomedical materials: Future prospects and challenges. *Interface Focus* **2018**, *8*, 20170056. [CrossRef] [PubMed]
25. Tabish, T.A.; Lin, L.; Ali, M.; Jabeen, F.; Ali, M.; Iqbal, R.; Zhang, S. Investigating the bioavailability of graphene quantum dots in lung tissues via Fourier transform infrared spectroscopy. *Interface Focus* **2018**, *8*, 20170054. [CrossRef] [PubMed]
26. Bugli, F.; Cacaci, M.; Palmieri, V.; Di Santo, R.; Torelli, R.; Ciasca, G.; De Spirito, M. Curcumin-loaded graphene oxide flakes as an effective antibacterial system against methicillin-resistant Staphylococcus aureus. *Interface Focus* **2018**, *8*, 20170059. [CrossRef] [PubMed]
27. Matharu, R.K.; Porwal, H.; Ciric, L.; Edirisinghe, M. The effect of graphene–poly (methyl methacrylate) fibres on microbial growth. *Interface Focus* **2018**, *8*, 20170058. [CrossRef] [PubMed]
28. Tabish, T.A.; Pranjol, M.Z.I.; Jabeen, F.; Abdullah, T.; Latif, A.; Khalid, A.; Zhang, S. Investigation into the toxic effects of graphene nanopores on lung cancer cells and biological tissues. *Appl. Mater. Today* **2018**, *12*, 389–401. [CrossRef]
29. Tabish, T.A.; Pranjol, M.Z.I.; Karadag, I.; Horsell, D.W.; Whatmore, J.L.; Zhang, S. Influence of luminescent graphene quantum dots on trypsin activity. *Int. J. Nanomed.* **2018**, *13*, 1525. [CrossRef] [PubMed]
30. Lin, L.; Wu, H.; Green, S.J.; Crompton, J.; Zhang, S.; Horsell, D.W. Formation of tunable graphene oxide coating with high adhesion. *Phys. Chem. Chem. Phys.* **2016**, *18*, 5086–5090. [CrossRef] [PubMed]
31. Lin, L.; Zhang, S. Effective solvothermal deoxidization of graphene oxide using solid sulphur as a reducing agent. *J. Mater. Chem.* **2012**, *22*, 14385–14393. [CrossRef]
32. Lin, L.; Zhang, S. Surface energy engineering in the solvothermal deoxidation of graphene oxide. *Adv. Mater. Interfaces* **2014**, *1*, 1300078. [CrossRef]
33. Wang, J.; Cheng, Y.; Chen, L.; Zhu, T.; Ye, K.; Jia, C.; Mo, X. In vitro and in vivo studies of electroactive reduced graphene oxide-modified nanofiber scaffolds for peripheral nerve regeneration. *Acta Biomater.* **2019**, *84*, 98–113. [CrossRef] [PubMed]
34. Tabish, T.A.; Memon, F.A.; Gomez, D.E.; Horsell, D.W.; Zhang, S. A facile synthesis of porous graphene for efficient water and wastewater treatment. *Sci. Rep.* **2018**, *8*, 1817. [CrossRef] [PubMed]
35. Wang, G.; Wang, B.; Park, J.; Yang, J.; Shen, X.; Yao, J. Synthesis of enhanced hydrophilic and hydrophobic graphene oxide nanosheets by a solvothermal method. *Carbon* **2009**, *47*, 68–72. [CrossRef]
36. Tabish, T.A.; Scotton, C.J.J.; Ferguson, D.C.; Lin, L.; der Veen, A.V.; Lowry, S.; Zhang, S. Biocompatibility and toxicity of graphene quantum dots for potential application in photodynamic therapy. *Nanomedicine* **2018**, *13*, 1923–1937. [CrossRef] [PubMed]
37. Tabish, T.A.; Chabi, S.; Ali, M.; Xia, Y.; Jabeen, F.; Zhang, S. Tracing the bioavailability of three-dimensional graphene foam in biological tissues. *Materials* **2017**, *10*, 336. [CrossRef] [PubMed]
38. Tabish, T.A.; Pranjol, M.Z.I.; Hayat, H.; Rahat, A.A.; Abdullah, T.M.; Whatmore, J.L.; Zhang, S. In vitro toxic effects of reduced graphene oxide nanosheets on lung cancer cells. *Nanotechnology* **2017**, *28*, 504001. [CrossRef] [PubMed]

39. Zhu, S.; Zhang, J.; Qiao, C.; Tang, S.; Li, Y.; Yuan, W.; Gao, H. Strongly green-photoluminescent graphene quantum dots for bioimaging applications. *Chem. Commun.* **2011**, *47*, 6858–6860. [CrossRef] [PubMed]
40. Tabish, T.A.; Zhang, S.; Winyard, P.G. Developing the next generation of graphene-based platforms for cancer therapeutics: The potential role of reactive oxygen species. *Redox Biol.* **2018**, *15*, 34–40. [CrossRef] [PubMed]
41. Lunova, M.; Smolková, B.; Lynnyk, A.; Uzhytchak, M.; Jirsa, M.; Kubinová, Š.; Lunov, O. Targeting the mTOR Signaling Pathway Utilizing Nanoparticles: A Critical Overview. *Cancers* **2019**, *11*, 82. [CrossRef] [PubMed]
42. Xu, M.; Zhu, J.; Wang, F.; Xiong, Y.; Wu, Y.; Wang, Q.; Liu, S. Improved in vitro and in vivo biocompatibility of graphene oxide through surface modification: Poly (acrylic acid)-functionalization is superior to PEGylation. *ACS Nano* **2016**, *10*, 3267–3281. [CrossRef] [PubMed]
43. Ou, L.; Song, B.; Liang, H.; Liu, J.; Feng, X.; Deng, B.; Shao, L. Toxicity of graphene-family nanoparticles: A general review of the origins and mechanisms. *Part. Fibre Toxicol.* **2016**, *13*, 57. [CrossRef] [PubMed]
44. Volkov, Y.; McIntyre, J.; Prina-Mello, A. Graphene toxicity as a double-edged sword of risks and exploitable opportunities: A critical analysis of the most recent trends and developments. *2d Mater.* **2017**, *4*, 022001. [CrossRef]
45. Seabra, A.B.; Paula, A.J.; de Lima, R.; Alves, O.L.; Durán, N. Nanotoxicity of graphene and graphene oxide. *Chem. Res. Toxicol.* **2014**, *27*, 159–168. [CrossRef] [PubMed]
46. Morhardt, C.; Ketterer, B.; Heißler, S.; Franzreb, M. Direct quantification of immobilized enzymes by means of FTIR ATR spectroscopy—A process analytics tool for biotransformations applying non-porous magnetic enzyme carriers. *J. Mol. Catal. B Enzym.* **2014**, *107*, 55–63. [CrossRef]
47. Rehman, S.; Movasaghi, Z.; Darr, J.A.; Rehman, I.U. Fourier transform infrared spectroscopic analysis of breast cancer tissues; identifying differences between normal breast, invasive ductal carcinoma, and ductal carcinoma in situ of the breast. *Appl. Spectrosc. Rev.* **2010**, *45*, 355–368. [CrossRef]
48. Movasaghi, Z.; Rehman, S.; Ur Rehman, D.I. Fourier transform infrared (FTIR) spectroscopy of biological tissues. *Appl. Spectrosc. Rev.* **2008**, *43*, 134–179. [CrossRef]
49. Sahoo, J.K.; Sirimuthu, N.M.; Canning, A.; Zelzer, M.; Graham, D.; Ulijn, R.V. Analysis of enzyme-responsive peptide surfaces by Raman spectroscopy. *Chem. Commun.* **2016**, *52*, 4698–4701. [CrossRef] [PubMed]
50. Sée, V.; Free, P.; Cesbron, Y.; Nativo, P.; Shaheen, U.; Rigden, D.J.; Brust, M. Cathepsin L digestion of nanobioconjugates upon endocytosis. *ACS Nano* **2009**, *3*, 2461–2468. [CrossRef] [PubMed]
51. Berciaud, S.; Cognet, L.; Blab, G.A.; Lounis, B. Photothermal Heterodyne Imaging of Individual Non-fluorescent Nanoclusters and Nanocrystals. *Phys. Rev. Lett.* **2004**, *93*, 257402. [CrossRef] [PubMed]
52. Rasmussen, C.E. Gaussian Processes in Machine Learning. In *Summer School on Machine Learning*; Springer: Berlin, Germany, 2003; pp. 63–71.
53. Fowkes, F.M. Attractive Forces at Interfaces. *Ind. Eng. Chem.* **1964**, *56*, 40. [CrossRef]
54. Malana, M.A.; Qureshi, R.B.; Ashiq, M.N. Adsorption studies of arsenic on nano aluminium doped manganese copper ferrite polymer (MA, VA, AA) composite: Kinetics and mechanism. *Chem. Eng. J.* **2011**, *172*, 721. [CrossRef]
55. Alkan, M.; Demirbaş, Ö.; Celikcapa, S.; Doğan, M. Sorption of acid red 57 from aqueous solution onto sepiolite. *J. Hazard. Mater.* **2004**, *116*, 135. [CrossRef] [PubMed]
56. Altenor, S.; Carene, B.; Emmanuel, E.; Lambert, J.; Ehrhardt, J.J.; Gaspard, S. Adsorption studies of methylene blue and phenol onto vetiver roots activated carbon prepared by chemical activation. *J. Hazard. Mater.* **2009**, *165*, 1029–1039. [CrossRef] [PubMed]
57. Qi, L.; Xu, Z. Lead sorption from aqueous solutions on chitosan nanoparticles. *Colloids Surf. A Physicochem. Eng. Aspects* **2004**, *251*, 183–190. [CrossRef]

cancers

MDPI

Article

PDL-1 Antibody Drug Conjugate for Selective Chemo-Guided Immune Modulation of Cancer

Samaresh Sau [1,*], Alex Petrovici [1], Hashem O. Alsaab [1,2], Ketki Bhise [1] and Arun K. Iyer [1,3,*]

[1] Department of Pharmaceutical Sciences, Wayne State University Eugene Applebaum College of Pharmacy and Health Sciences, 259 Mack Ave, Detroit, MI 48201, USA; alex.o.petrovici@gmail.com (A.P.); hashem.alsaab@wayne.edu (H.O.A.); ketki.bhise@wayne.edu (K.B.)

[2] Department of Pharmaceutics and Pharmaceutical Technology, College of Pharmacy, Taif University, Taif 26571, Saudi Arabia

[3] Molecular Imaging Program, Barbara Ann Karmanos Cancer Institute. Wayne State University School of Medicine, 4100 John R St, Detroit, MI 48201, USA

* Correspondence: samaresh.sau@wayne.edu (S.S.); arun.iyer@wayne.edu (A.K.I.); Tel.: +1-313-577-3220 (S.S.); +1-313-577-5875 (A.K.I.)

Received: 23 January 2019; Accepted: 14 February 2019; Published: 16 February 2019

Abstract: Targeting immune checkpoint molecules such as programmed death ligand-1 (PDL1) is an emerging strategy for anti-cancer therapy. However, transient expression of PDL1 and difficulty in tumor stroma penetration has limited the utility of anti-PDL1 therapy. To overcome these limitations, we report a new conjugate between the clinically approved PDL1 antibody (PDL1 AB) and drug Doxorubicin (Dox), named PDL1-Dox. We conjugated PDL1-Dox through a hydrazone linker containing a polyethylene glycol (PEG) spacer, which allows it to dissociate in a tumor environment and improves solubility. The purpose of using Dox is to disrupt the tumor extracellular environment so that PDL-1 antibody can penetrate the tumor core. PDL1-Dox demonstrates significant cell killing, disruption of tumor spheroid and induction of apoptosis in a breast cancer cell line. Significant release of IFN-γ suggests PDL1-Dox can upmodulate T cell activation. Optical imaging of dye conjugate supports the selective tumor targeting ability and core penetration of the construct.

Keywords: antibody drug conjugate (ADC); PD-L1; tumor spheroid disruption; immune modulation; doxorubicin

1. Introduction

Antibody-drug conjugates (ADCs) are a clinically effective treatment for targeted therapy of cancer. They typically consist of a monoclonal antibody, a cytotoxic drug, and a conditionally stable linker to conjugate the two. In cancer treatment, such combinations are especially useful because the antibody (Ab) serves as a specific targeting ligand to an overexpressed tumor cell surface protein in order to effectively deliver the cytotoxic drug [1]. So far, three ADCs (Adcetris, Kadcyla and Mylotarg) have been approved by the US FDA and more than 30 ADCs are currently being investigated in clinical trials for both solid tumors and hematological cancers [2]. Recently, groundbreaking results of immunotherapy have opened a new paradigm for several cancer treatments [3]. A promising target in anticancer therapy is immune checkpoint inhibition which resurrects the function of exhausted T-cells to kill tumor cells. Tumor cells evade immune surveillance by upmodulating immunosuppressive immune checkpoint molecules, resulting in downplay of antitumor immunity [3,4]. This involves the interaction between the surface receptor programmed death-1 (PD1) and its corresponding ligand (PDL1), which are expressed on the surface of immune cells (monocytes, T cells, B cells) and tumor cells, respectively [3]. The interaction between PD1 of T-cells with PDL1 of cancer cells inhibits T-cell mediated cancer cell killing. To alleviate the function of T-cells against cancer cells several

immune checkpoint antibody inhibitors have been developed that target either PD1 or PDL1 and stop this interaction.

Tecentriq®(Atezolizumab), an FDA approved antibody, has already been used for metastatic urothelial carcinoma, non-small cell lung cancer, and triple negative breast cancer (TNBC) [5]. Hypothetically, this antibody can be used against other types of tumors that have overexpression of PDL1. Several studies have shown that TNBC cells, including MDA-MB-231, have high expression of PDL1 [6], which suggests that an anti-PDL1 antibody is a promising platform for TNBC therapy [4]. Since TNBC cells lack receptors for estrogen, progesterone, and HER-2 [7], using the PDL1 biomarker is a rational option for its treatment. Alongside its clinical success, the treatment of anti-PDL1 antibody showed a patient specific response. However, its use is limited to the few types of tumors that are linked with several factors, such as the transient and heterogeneous expression of PDL1 in tumor microenvironment and poor penetration of the larger molecular weight PDL1 antibody (144.61 Kda) through dense tumor stroma [8,9]. Thus, an attempt to conjugate a cytotoxic drug with anti-PDL1 antibody would be a significant direction especially for solid tumors consisting of dense tumor stroma. In this regard, PDL1 antibody drug conjugate (ADC) can serve the purpose of chemo-guided immune therapy.

Chemotherapeutics such as Doxorubicin (Dox) have been utilized as potent anticancer agents for a long time. They work by slowing the growth of cancer cells through induction of apoptosis and arresting cell cycle that leads to cell death [10,11]. The poor selectivity and acute cardiotoxicity of Dox has limited its use in clinic, requiring a selective delivery system. Clinical use of Doxil is widespread and the predicted market size is expected to be $1.39 billion by 2024 [12]. Alongside this, a few antibody-Dox conjugates, including BR96-Dox (NCT00031187) and PL1-Dox (NCT01101594), have been studied in clinical trials for cancer [13]. These data support the idea that there is a significant scope in repurposing Dox for efficient therapy in cancer. Toward this end, we report for the first time a Dox conjugated PDL1 antibody (PDL1-Dox) for the broader application of chemo-guided immunotherapy.

As the tumor extracellular environment is acidic in nature, acidic pH responsive linkers have been utilized to conjugate ADCs so that they can selectively release drugs (Dox in this case) in the tumor environment [14]. Likewise, we have introduced a hydrazone linker to the PDL1-Dox ADC that will be selectively cleaved in the tumor cell environment. Additionally, we used a PEG-spacer for improving the aqueous solubility of the antibody and sustain the plasma circulation of PDL1-Dox. The hydrazone linker is extensively used for clinically approved ADCs such as Mylotarg. The monoclonal IgG1 antibody, PDL1 AB, has a high affinity for human PDL1 receptor with a dissociation constant (Kd) of 0.43 nM [15]. PDL1 AB binds to the PDL1 on the surface of the cancer cell and it does not internalize via endocytosis, resulting in inhibition of PDL1 with PD1 of T cells. Alongside the superior clinical outcome of PDL1 AB, several studies have revealed that its effect is limited to the small percent of patient population [16]. This is attributed to poor T cell infiltration through dense tumor stroma [17] and inadequate tumor core penetration of PDL1 AB, as depicted in Figure 1. To overcome these challenges, several combination therapies have emerged, including combination of PDL1 AB with chemotherapy and immunotherapies, namely anti-PD1 or CTLA-4 therapy [3–5]. Combination treatment, however, produced nonspecific toxicity and immune related adverse events (irAEs) [18,19]. To improve the selectivity and efficacy of PDL1 AB, we have developed the ADC, PDL1-Dox and evaluated its anticancer effect and mechanism of action in MDA-MB-231 cells. The chemical formation of PDL1-Dox was confirmed by MALDI-MS spectroscopy and UV-Vis spectrophotometry. We performed a tumor 3D- culture study to demonstrate the tumor spheroid disruption ability of PDL1-Dox and measured IFN-γ production in PDL1-Dox treated cell suspension, obtained from a co-culture of MDA-MB-231 and activated RAW 264.7 cells. We developed near-infrared (NIR) dye-conjugated PDL1-S0456 and tested its specificity as well as tumor retention ability in patient derived TNBC (BR1126) and NSCLC (LG703) model. The tumor specificity of PDL1-S0456 was confirmed by ex-vivo biodistribution on treated PDx mice. This proof-of-concept study demonstrates that PDL1-Dox can improve the current

therapeutic outcome beyond PDL1 AB and that PDL1 antibody can further be developed for tumor diagnosis and image-guided surgery [20].

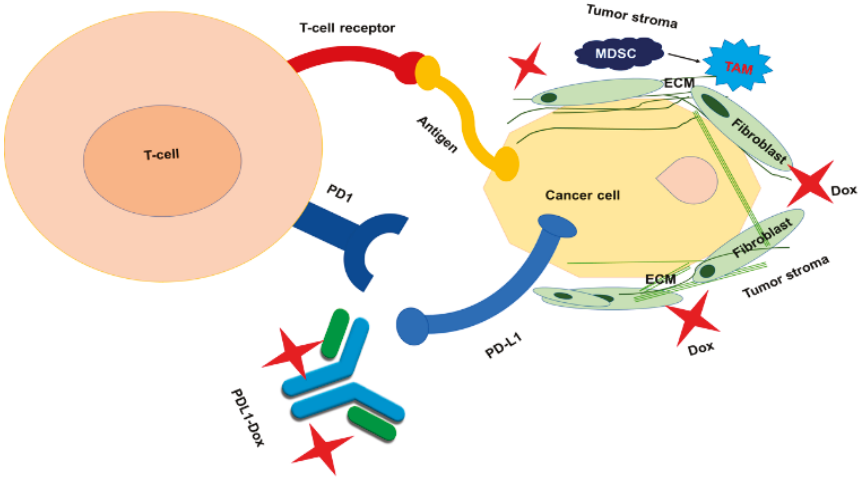

Figure 1. The interaction of the cancer cell with the T-cell through the binding of the major histocompatibility complex (MHC) and the T-cell receptor (TCR) leads to activation of the T-cell and releasing cancer cell death signal. The ligation of PD1 with PDL1 downmodulates the tumor cell killing function of T-cell. It is hypothesized that Dox of PDL1-Dox could disrupt the tumor stromal components and improve antitumor response of PDL1 antibody.

2. Materials and Methods

2.1. Materials

Atezolizumab (Tecentriq®, Genentech, South San Francisco, CA, USA) was obtained from Karmanos Cancer Institute pharmacy. SH-PEG-COOH was obtained from Biochempeg Scientific Inc., (Watertown, MA, USA). Other reagents and solvents were obtained from fisher scientific and Sigma Aldrich and used directly without further purification. RAW 264.7 cells were obtained as a kind gift of Shunbin Xu, Wayne State University School of Medicine (Detroit, MI, USA).

2.2. Synthesis of PDL1-Dox

The synthesis of the ADC began with the coupling of the monoclonal IgG antibody Atezolizumab (Tecentriq®, Genentech) to SH-PEG-COOH by EDC/sulfo-NHS, according to previously published method [21]. Clinically used PDL1 AB was dialyzed to separate the excipient and PDL1 AB was lyophilized to obtain the powered. For coupling between SH-PEG-COOH and PDL1 AB, SH-PEG-COOH (15 mg) was taken in a in mixture of water with catalytic amount DMSO in presence of EDC/sulfo-NHS and stirred for 1 h, followed by PDL1 AB powder (18 mg) was added to the mixture and stirred for 6 h. The resulting solution was transferred to a 12 Kd dialysis bag and dialyzed overnight at 4 °C to obtain PDL1-PEG-SH. Next PDL1-PEG-SH was then reacted with maleimide group of Aldoxorubicin in pH 7.4 using reagent free thiol-maleimide chemistry for 4 h. Followed by dialysis and lyophilization was performed with 12 Kd dialysis bag to obtain PDL1-Dox. The concentration of Dox was determined by the UV-Vis spectroscopy method.

2.3. Characterization of PDL1-Dox

PDL1-Dox was analyzed in UV/Vis spectroscopy (Agilent Technologies, Santa Clara, CA, USA) to evaluate the presence of Dox in the PDL1-Dox construct and compared with PDL1 AB.

2.4. Cell Culture

TNBC cell line (MDA-MB-231) was obtained from American Type Culture Collection (ATCC, Manassas, VA, USA) and grown in with Dulbecco's modified eagle medium, containing 1% antibiotic (penicillin and streptomycin) and 10% fetal bovine serum at 37 °C in a 5% CO_2 environment. MTT based cell viability assay was performed as per previously performed procedures [5,22,23]. Briefly, the cells were seeded in a 96 well plate at a density of 5000 cells per well and incubated overnight. Afterwards, the cells were treated with various concentrations of PDL1-DOX in a range of 2.5 μM to 0.156 μM with respect to Dox concentration and cells were incubated for 48 h or 72 h. The same amount of commercial Dox was used as a positive control. At the end of incubation, 3-(3,5-dimethyl-2-thiazolyl)-2,5-diphenyltetrazolium bromide (MTT) was added and cell viability was determined. Standard manufacturer procedure was followed for 3D-spheroid culture method. Briefly, 5000 MDA-MB-231 cells were slowly added to U-shaped well of 96-well plate and incubated for overnight. This was followed by PDL1-Dox, with Dox being treated for 48 h or kept untreated.

2.5. Apoptosis Assay

In preparation for the apoptosis assay, cells were seeded in 6-well plates for 24 hours. The cells were then treated with PDL1-DOX or kept untreated (UT) at concentrations of 2.5 μM and then incubated for 24 h, until a microscopically visible morphology change was occurred. The cells were then collected, centrifuged, counted, resuspended, and analyzed with a guava Guava®easyCyte™ flow cytometer (Austin, TX, USA).

2.6. Cellular Imaging with Confocal Microscopy

Confocal imaging was performed based on previously published literature [22]. Briefly, MDA-MB-231 cells were plated with a density of 200,000 cells per 60 mm petri dish and waited 48 h until confluency reached up to 70%, then cells were treated with 1 μM concentration of PDL1-Dox or Dox with respect to Dox concertation for 1 h in 10% FBS containing DMEM. The cells that followed were washed 3 times with PBS and fixed with 2% formalin in PBS for 15 min. 15 min prior to confocal imaging, cells were stained with Hoechst 33342. Dox was visualized in red channel (Ex. 488 nm and Em. 560 nm) and Hoechst was visualized in blue channel (Ex. 350 nm, Em. 461 nm) and images were merged to demonstrate the localization of PDL1-Dox and Dox in cells [11].

2.7. 3D-spheroid Culture Study

5,000 MDA-MB231 cells/well were plated in 3D-matrix containing 96-well plate and waited for 18 h to form 3D-spehroid. Following this, spheroids were treated with 5 μM and 2.5 μM of Dox and PDL1-Dox with respect to Dox concentration for 20 h and bight field images were taken in a phase contrast microscope under 4× objective.

2.8. IFN-γ ELISA

The enzyme linked immunosorbent assay (ELISA) of the IFN-γ cytokine was performed with bioligand ELISA kit as per manufacturer protocol. Briefly, 5000 RAW 264.7 cells/well were seeded to 96-well plate for 18 h. In day 2, media was changed with 1 μg/mL LPS containing DMEM for 24 h. On Day 3, 4000 MDA-MB-231 cells/well were co-cultured with RAW 264.7 cells containing wells in presence of 1 μg/mL LPS. Day 4, cells were treated with Dox (2.5 μM), PDL1-Dox (2.5 μM) or left UT for 24 h. Day 5, media was collected and run for Elisa assay. The quantity of IFN-γ was quantified with the IFN-γ standard.

2.9. Animal Studies

All animal procedures and imaging experiments was done according to protocols approved by the Institutional Laboratory Animal Care & Use Committee (IACUC) at the Wayne State University.

Near-infrared (NIR) dye, S0456 was conjugated with PDL1-PEG-SH to obtain PDL1-S0456 and free S0456 was separated by dialysis [7]. The 8-weeks old tumor bearing TNBC and NSCLC patient derived tumor xenograft (PDx) mice were intravenously injected with 10 nmole of PDL1-S0456 TNBC and the bio-distribution of NIR dye was monitored after 24 h of the single dose of 10 nmole NIR dye per mouse. Non-specific BSA-S0456 was used as a control. Fluorescence images were collected in Bruker Carestream Xtreme in vivo imaging system at excitation (750 nm) and emission (830 nm) wavelength as per previously published method [7]. The instrument has dual fluorescence and X-ray imaging modalities with light source and fluorescence and X-ray images of the mouse were merged to demonstrate the localization of NIR dye. PDx tumor mice were obtained from Jackson laboratory, and tumor fragments were passaged to Nod-Scid mice.

2.10. Statistical Analysis

The statistical analysis was done using GraphPad Prism 7 software (GraphPad Software Inc., La Jolla, CA, USA). The data were expressed as mean ± SD and analyzed using a two-tailed Student *t*-test, or one-way ANOVA followed by a post hoc test. A p-value of <0.05 was considered statistically significant.

3. Results

3.1. Synthesis and Characterization

The synthesis of the ADC was performed similar to previously published literature using the clinically used PDL1 antibody, COOH-PEG-SH and Aldoxorubicin [24]. The PDL1 AB itself does not have any significant absorbance at the same wavelength of max absorbance of Doxorubicin (481 nm) as can be found in Figure 2A. Therefore, the intensity of the absorbance at 481 nm was used to determine the concentration of Dox present in the PDL1-Dox formulation. This concentration of Dox in PDL1-Dox was considered as the basis for performing biological studies of PDL1-Dox, as it could be compared to free Dox. This is justified because the difference between in vitro activity of PDL1-Dox compared to free Dox could be attributed to the presence of PDL1 AB. The data from Figure 2A demonstrate the successful conjugation of Dox with PDL1 AB through PEG linker to produce PDL1-Dox ADC. As mentioned, the use of hydrazone linker in PDL1-Dox is needed to selectively deliver Dox to the extracellular acidic milieu of the tumor so that it can disrupt the tumor environment and enhance the penetration of PDL1-antibody into the core of the tumor [1]. To demonstrate the acidic pH responsive release of Dox from PDL1-Dox, we studied the release kinetics of PDL1-Dox in PBS of pH 5.5 and pH 7.4. Figure 2B indicates that 90% of Dox was released in pH 5.5 at 50 h, whereas the released amount of Dox was less than 30% in pH 7.5 at 50 h. The sustained and acidic pH stimuli-responsive release of Dox from PDL1-Dox supports the hypothesis of using PDL1-Dox ADC for chemo-guided immunotherapy in preclinical model.

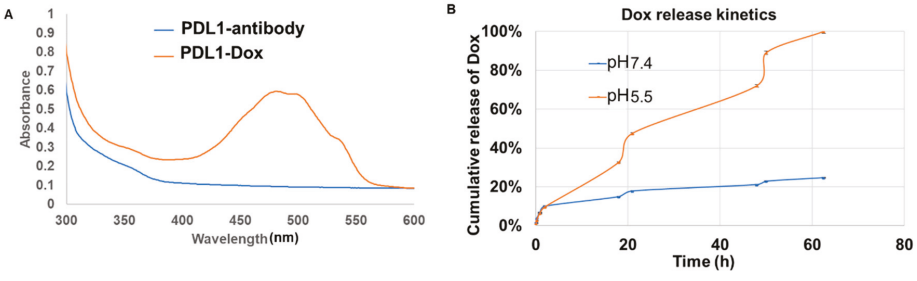

Figure 2. (**A**) The presence of the Dox absorbance peak in PDL1-Dox indicates successful conjugation of Dox. (**B**) The Dox is more completely released from the conjugate in more acidic conditions due to hydrazone linker degradation.

3.2. Cell Killing

Figure 3A shows the MTT-based cytotoxicity assay in MDA-MB-231 cells that displayed a dose dependent cell killing of PDL1-Dox treatment. The difference of cell killing of PDL1-Dox and Dox is more prominent at 72 h as compared to 48 h, indicating time dependent cell killing effect of PDL1-Dox in PDL1 overexpressing MDA-MB-231 cells [6]. The cell killing effect of PDL1-Dox is significantly higher in the range of 0.625 μM to 2.5 μM as compared to Dox treated cells for 72 h treatment. The reason for the superior cell killing effect of PDL1-Dox in the lower concentrations can be attributed to PDL-1 receptor mediated and acidic pH triggered Dox release. The IC50 of Dox and PDL1-Dox is 4 μM and 1.25 μM respectively. Thus, the cell viability data indicate conjugation of Dox with PDL-1 antibody significantly improved the cell killing effect of Dox at 72 h that corroborated with sustain drug release kinetics data obtained in acidic pH, as shown in Figure 2B. This observation supports the notion that PDL1-Dox will function as a potent tumor environment specific Dox delivery agent. To demonstrate the cell killing mechanism of PDL1-Dox, we performed Annexin-V/PE based apoptosis assay and the data is shown in Figure 3B. The results indicate a significant increase in early phase apoptosis in PDL1-Dox in comparison to untreated control (UT). The percent of early stage apoptosis in PDL1-Dox treated MDA-MB-231 is 2-fold higher compared to UT cells, suggesting that PDL1-Dox is highly efficient in inducing apoptosis-mediated cell death. With this efficient anticancer effect of PDL1-Dox, we sought to explore the cross-talk mechanism of PDL1-Dox with the MDA-MB-231 cells. The PDL1 AB binds with extracellularly overexpressed PDL1 receptor of cancer cells, resulting in the inhibition of interaction between PDL1 with PD-1 of T cell and the induction of T cell mediated tumor cell killing.

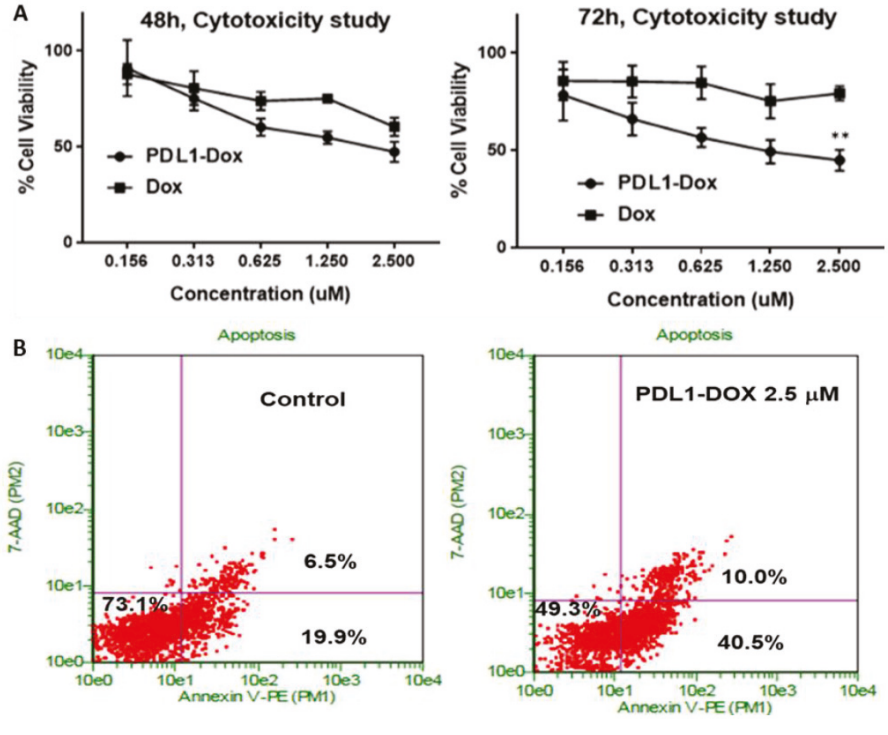

Figure 3. (**A**) The MTT based cell viability assay in MDA-MB-231 indicates the PDL1-Dox is more effective in killing PDL-1 overexpressing MDA-MB-231 cells as compared to Dox ($n = 6$). (**B**) The cell killing of PDL1-Dox is mediated by early apoptosis pathway. ** $p < 0.01$.

3.3. Cell Uptake

The data in Figure 4A,B clearly indicate that PDL1-Dox is unable to reach the nucleus of the MDA-MB-231 cells and thus localizes predominantly on the cell surface. This is in contrast to Dox treated cells in Figure 4C,D showing its non-specific accumulation in the nucleus. PDL1-Dox specifically binds to PDL1 receptor and the complex remains mainly on the surface of the cells 24. The presence of tumor stroma is a major barrier for any anti-tumor therapeutic as well as for PDL1 AB. In order to determine the efficacy of the tumor environment disruption of PDL1-Dox, we treated the MDA-MB-231 3D-spheroid culture with 2.5 μM PDL1-Dox, Dox or left it untreated (UT). The data from Figure 4E shows that PDL1-Dox is more effective in disrupting the tumor spheroid compared to Dox. This data resembles the observation in Figure 3A and indicates that the development of PDL1-Dox is a worthwhile approach for the disruption of tumor environment. Furthermore, to evaluate the activation of T-cells in PDL1-Dox treatment, we measured the production of IFN-γ, CD8+ T cell activation cytokine that is released during innate and adaptive immune responses, and its inhibition of the PD-1 stimulatory mechanism. From Figure 4F, it can be seen that the IFN-γ production in PDL1-Dox treatment is significantly higher compared to Dox in a co-cultured condition of MDA-MB-231 and activated RAW 264.7 cells. Literature reports indicate that activation of RAW 264.7 (macrophage) cells with lipopolysaccharide (LPS) can significantly upregulate the PD-1 expression [25,26]. Towards this end, we have utilized the LPS activated RAW 265.7 cells co-cultured with MDA-MB-231 and found the up-modulation of IFN-γ, suggesting the PDL1-Dox mediated inhibition of PD1 and PDL1 interaction. Thus, PDL1-Dox is compatible with the mechanism of ligand association, like the PDL1 AB antibody, and is effective in inducing the synergistic effect of destabilizing tumor spheroid formation and up-modulation of immune cell activation. The rationale of co-culturing the PD1 triggered macrophages with PDL-1 overexpressing MDA-MB-231 [6] would mimic the PD-1 and PDL-1 interaction model in cell culture condition. In this Raw-264.7 and MDA-MB231 co-cultured flask, treatment of PDL1-Dox can inhibit the PD-1 and PDL-1 interaction, resulting activation of macrophages and thus significant upregulation of tumor suppressing pro-inflammatory cytokine, such as IFN-γ.

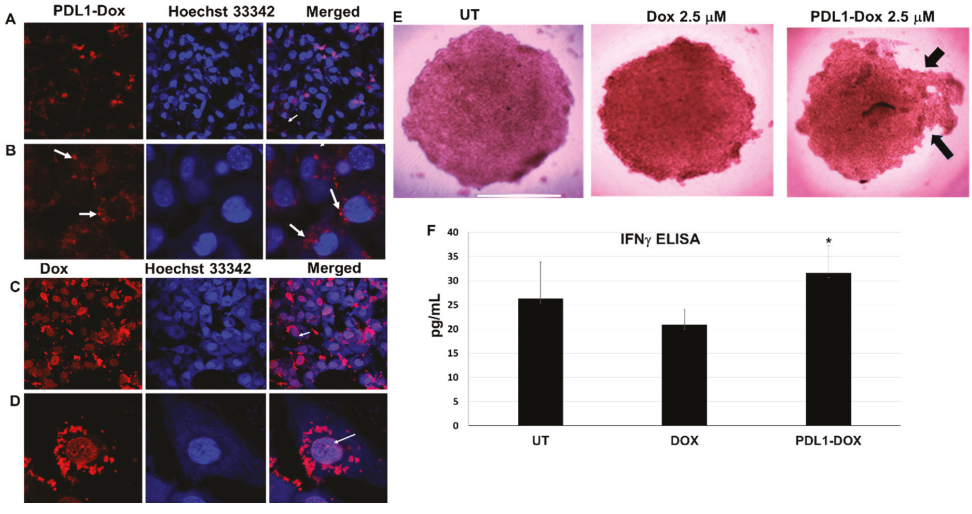

Figure 4. (**A**) Cell uptake study in MDA-MB-231 cells treated with PDL1-Dox indicates that PDL-Dox is predominately accumulated in cell surface and unable to reach the nucleus (40× magnified). (**B**) The magnified view of individual cells suggests presence of PDL1-Dox in cell surface (40× magnified). (**C**) Dox is non-specifically accumulated in the nucleus (40× magnified). (**D**) Magnified view suggests the colocalization of Dox with Hoechst dye (as indicated by arrow) (40× magnified). (**E**) The disruption of MDA-MB-231 tumor spheroid in PDL-1-Dox treatment supports the notion that PDL1-Dox can be a potential therapeutic for tumor environment disruption in preclinical tumor model. Arrows indicate the disruption of spheroid in PDL1-Dox treatment ($n = 3$). (**F**) Significant increase in IFN-γ production (pg/mL) in culture media treated with PDL1-Dox using coculture of MDA-MB-231 and activated RAW 264.5 cells as compared to Dox treatment is seen. * $p < 0.05$ ($n = 4$ independent experiment) and results are presented as STDEV in excel.

3.4. Imaging

With the selective anticancer effect and significant immune activation of PDL1-Dox at the cellular level, we performed near infrared (NIR) optical imaging in TNBC and NSCLC patient derived tumor xenograft (PDx) model with ATZ-conjugated NIR dye, PDL1-S0456. In this regard, we chose PDx models because it generates tumors with features that very closely mimic a human tumor microenvironment that is most ideal for future clinical translation. The rationale of performing NIR-imaging with PDL1-S0456 is due to its significant advantage as a (i) tumor image guided surgery tool in the clinic, and to (ii) understanding tumor selective delivery, tumor retention, and safety to predict therapeutic outcome in different tumor models. The results from Figure 5A,B clearly indicate the selective accumulation and tumor core penetration of PDL1-S0456. The sustained NIR intensity at 4 h and 24 h in NSCLC tumor as shown in Figure 5A indicates the retention of PDL1-S0456, suggesting tumor specificity. The biodistribution in Figure 5B confirms the tumor selectivity of PDL1-S0456 with low non-specific accumulation in liver and spleen. Similarly, PDL1-S0456 is selectively delivered to the TNBC PDx tumor and shows tumor specific delivery and favorable biodistribution as shown in Figure 5C,D. The bovine serum albumin (BSA) conjugated S0456, BSA-S0456 control showed poor specificity to tumor and majority of the dye is accumulated in the liver as compared to the tumor. This data indicates the longer retention and selectivity of PDL1-S0456 in tumors needed for achieving a tumor diagnosis.

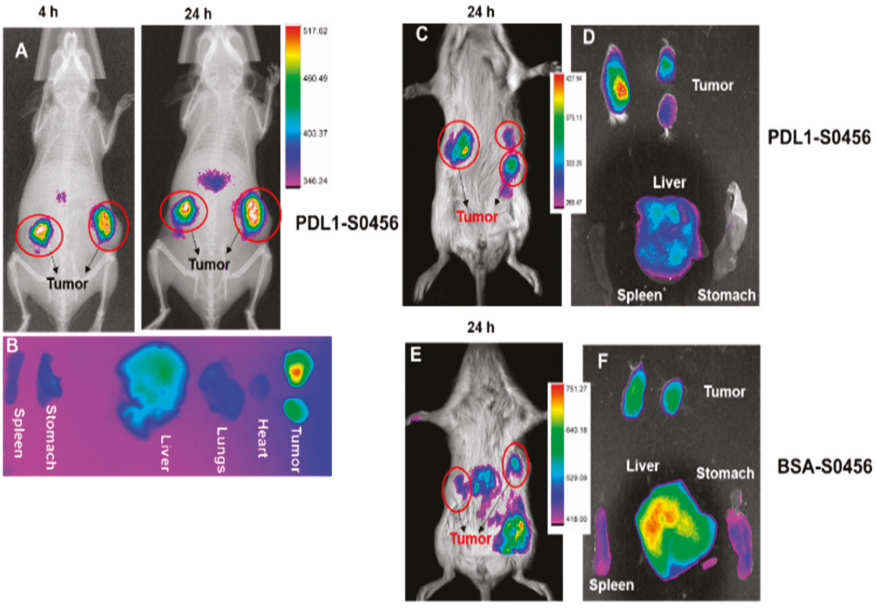

Figure 5. (**A**) NIR imaging of PDL1-S0456 in NSCLC PDx model indicates selective accumulation and retention of dye in tumor mass. (**B**) Higher accumulation of dye in tumor core as compared to other organs support tumor selectivity of the PDL1-S0456 formulation. (**C**,**D**) Higher tumor uptake compared to liver and spleen in TNBC PDX supports PDL1-S0456 as a smart diagnostic tracer for multiple tumor imaging and targeted therapy. (**E**,**F**) indicates high non-specific liver accumulation of non-targeted serum albumin-dye conjugate as compared to tumor (n = 2 independent experiment).

4. Discussion

Extensive research is ongoing to improve therapeutic outcome ADCs that can enhance their targetability and therapeutic efficacy against tumors. The majority of ADC are used to target the extracellular receptor of cancer cells, followed by receptor mediated-internalization of ADC in cytosol and delivery of payload in endosome [1,27]. Utilizing this mechanism, one can only achieve chemotherapeutic benefits against cancer. In contrast, our approach was to use PDL-1 antibody inhibitor in PDL1-Dox formulation that will bind to the surface of cancer cell and selectively delivery both PDL-1 inhibitor and Dox, resulting a synergistic outcome of chemotherapeutic and immunostimulatory effects. The extensive research majority (two out of three) of clinically approved ADCs are used blood cancer with limited benefits in solid tumor [28]. The phase I/II clinical study of anti-CD74 antibody-doxorubicin conjugate, (IMMU-110) was developed for multiple myeloma [29]. These limitations and challenges of current ADCs technology warranted us to develop PDL1-Dox conjugate for achieving the dual chemo and immunotherapeutic benefits against the solid tumor. In the clinical setting, several antibody-NIR imaging agents have shown an excellent ability to distinguish the tumor lesion from healthy tissue during image-guided surgery as noted in NCT01987375 and NCT01508572 [30] for targeting extracellularly overexpressed VEGF and EGFR receptor. With this note, PDL-1 is an excellent target for developing antibody-NIR or a radio imaging agent that can be utilized for multiple cancer diagnosis and for understanding the cross-talk between cancer cell and T-cell in immune evasion. The up modulation of tumor suppressing pro-inflammatory cytokines, such as IFN-γ in PDL1-Dox treatment supports PDL1-Dox mediated anti-tumor immune cell activation [31]. Furthermore, PDL1-S0456 can be engineered with potent drugs to obtain antibody-dye-drug conjugate for the multimodal image guided therapy and immune modulation. Towards this end, our first

approach in developing immune checkpoint antibody inhibitor-drug conjugate and imaging agent demonstrates a rational platform for chemo-guided immunotherapy that can be further developed for other types of cancer.

5. Conclusions

In this study we have demonstrated the development of PDL1 antibody drug conjugate to improve the antitumor efficacy of current treatment. The PDL1-Dox treatment has multimodal anticancer effects including tumor acidic pH responsive drug release, apoptosis mediated cancer cell death, targetability of PDL1 receptor and tumor 3D-spheroid disruption, and upmodulating of tumor suppressing IFN-γ mediated immune cell activation. The PDL1-S0456 tool has demonstrated the selective tumor targeting ability in a patient derived tumor model, which is a positive step towards further developing tumor NIR imaging tool for imaging guided surgery of PDL-1 positive tumor in a clinical set up.

Author Contributions: All the authors contributed substantially to this research project. Conceptualization, S.S., A.K.I., and A.P.; methodology, S.S.; validation, K.B. and H.O.A.; formal analysis, A.P. and S.S.; investigation, A.P, S.S., H.O.A., and K.B.; resources, A.K.I.; data curation, A.P. and S.S.; writing—original draft preparation, A.P. and S.S.; writing—review and editing, S.S. and A.K.I.; visualization, A.P. and S.S.; supervision, A.K.I.; project administration, S.S.; funding acquisition, A.K.I.

Funding: The funding for the imaging studies was supported, in part, by NIH Center grant P30 CA22453.

Acknowledgments: We appreciate Karmanos Cancer Institute pharmacy for kindly proving Atezolizumab. We also appreciate the kind gift of RAW 264.7 from Shunbin Xu, Wayne State University School of Medicine. S.S. acknowledges the support of Burroughs's welcome fund collaborative research travel grant (BWFCRTG). A.K.I. acknowledges the support of WSU start-up funds.

Conflicts of Interest: The authors declare no conflict of interest.

References

1. Sau, S.; Alsaab, H.O.; Kashaw, S.K.; Tatiparti, K.; Iyer, A.K. Advances in antibody–drug conjugates: A new era of targeted cancer therapy. *Drug Discov. Today* **2017**, *22*, 1547–1556. [CrossRef] [PubMed]
2. Diamantis, N.; Banerji, U. Antibody-drug conjugates—an emerging class of cancer treatment. *Br. J. Cancer* **2016**, *114*, 362–367. [CrossRef] [PubMed]
3. Alsaab, H.O.; Sau, S.; Alzhrani, R.; Tatiparti, K.; Bhise, K.; Kashaw, S.K.; Iyer, A.K. PD-1 and PD-L1 Checkpoint Signaling Inhibition for Cancer Immunotherapy: Mechanism, Combinations, and Clinical Outcome. *Front. Pharmacol.* **2017**, *8*, 1–15. [CrossRef] [PubMed]
4. Mittendorf, E.A.; Philips, A.V.; Meric-Bernstam, F.; Qiao, N.; Wu, Y.; Harrington, S.; Su, X.; Wang, Y.; Gonzalez-Angulo, A.M.; Akcakanat, A.; et al. PD-L1 Expression in Triple-Negative Breast Cancer. *Cancer Immunol. Res.* **2014**, *28*, 361–370. [CrossRef] [PubMed]
5. Sau, S.; Alsaab, H.O.; Bhise, K.; Alzhrani, R.; Nabil, G.; Iyer, A.K. Multifunctional nanoparticles for cancer immunotherapy: A groundbreaking approach for reprogramming malfunctioned tumor environment. *J. Control. Release* **2018**, *274*, 24–34. [CrossRef] [PubMed]
6. Chatterjee, S.; Lesniak, W.G.; Gabrielson, M.; Lisok, A.; Wharram, B.; Sysa-Shah, P.; Azad, B.B.; Pomper, M.G.; Nimmagadda, S. A humanized antibody for imaging immune checkpoint ligand PD-L1 expression in tumors. *Oncotarget* **2016**, *7*, 10215–10227. [CrossRef] [PubMed]
7. Wang, Z.; Sau, S.; Alsaab, H.O.; Iyer, A.K. CD44 Directed Nanomicellar Payload Delivery Platform for Selective Anticancer Effect and Tumor Specific Imaging of Triple Negative Breast Cancer. *Nanomedicine* **2018**, *14*, 1441–1454. [CrossRef]
8. Zou, W.; Wolchok, J.D.; Chen, L. PD-L1 (B7-H1) and PD-1 pathway blockade for cancer therapy: Mechanisms, response biomarkers, and combinations. *Sci. Transl. Med.* **2016**, *8*, 328rv4. [CrossRef]
9. Syn, N.L.; Teng, M.W.L.; Mok, T.S.K.; Soo, R.A. De-novo and acquired resistance to immune checkpoint targeting. *Lancet Oncol.* **2017**, *18*, e731–e741. [CrossRef]
10. Mukherjee, S.; Sau, S.; Madhuri, D.; Bollu, V.S.; Madhusudana, K.; Sreedhar, B.; Banerjee, R.; Patra, C.R. Green synthesis and characterization of monodispersed gold nanoparticles: Toxicity study, delivery of doxorubicin and its bio-distribution in mouse model. *J. Biomed. Nanotechnol.* **2016**, *12*, 165–181. [CrossRef]

11. Thorn, C.F.; Oshiro, C.; Marsh, S.; Hernandez-Boussard, T.; McLeod, H.; Klein, T.E.; Altman, R.B. Doxorubicin pathways: Pharmacodynamics and adverse effects. *Pharmacogenet. Genomics* **2011**, *21*, 440–446. [CrossRef] [PubMed]
12. Hare, J.I.; Lammers, T.; Ashford, M.B.; Puri, S.; Storm, G.; Barry, S.T. Challenges and strategies in anti-cancer nanomedicine development: An industry perspective. *Adv. Drug Deliv. Rev.* **2017**, *108*, 25–38. [CrossRef] [PubMed]
13. Tolcher, A.W. Antibody drug conjugates: Lessons from 20 years of clinical experience. *Ann. Oncol.* **2016**, *27*, 2168–2172. [CrossRef] [PubMed]
14. Tannock, I.F.; Rotin, D. Acid pH in Tumors and Its Potential for Therapeutic Exploitation. *Cancer Res.* **1989**, *49*, 4373–4384.
15. Powles, T.; Eder, J.P.; Fine, G.D.; Braiteh, F.S.; Loriot, Y.; Cruz, C.; Bellmunt, J.; Burris, H.A.; Petrylak, D.P.; Teng, S.L.; et al. MPDL3280A (anti-PD-L1) treatment leads to clinical activity in metastatic bladder cancer. *Nature* **2014**, *515*, 558–562. [CrossRef] [PubMed]
16. Jean, F.; Tomasini, P.; Barlesi, F. Atezolizumab: Feasible second-line therapy for patients with non-small cell lung cancer? A review of efficacy, safety and place in therapy. *Ther. Adv. Med. Oncol.* **2017**, *9*, 769–779. [CrossRef] [PubMed]
17. Pure, E.; Lo, A. Can Targeting Stroma Pave the Way to Enhanced Antitumor Immunity and Immunotherapy of Solid Tumors? *Cancer Immunol. Res.* **2016**, *4*, 269–278. [CrossRef]
18. Clinical, E.; Guidelines, P. Soft tissue and visceral sarcomas: ESMO clinical practice guidelines for diagnosis, treatment andfollow-up. *Ann. Oncol.* **2012**, *23*, vii92–vii99. [CrossRef]
19. Emens, L.A.; Middleton, G. The Interplay of Immunotherapy and Chemotherapy: Harnessing Potential Synergies. *Cancer Immunol. Res.* **2015**, *3*, 436–443. [CrossRef]
20. Mestel, R. Cancer: Imaging with antibodies. *Nature* **2017**, *543*, 743–746. [CrossRef]
21. Sau, S.; Banerjee, R. Cationic lipid-conjugated dexamethasone as a selective antitumor agent. *Eur. J. Med. Chem.* **2014**, *83*, 433–447. [CrossRef] [PubMed]
22. Luong, D.; Kesharwani, P.; Alsaab, H.O.; Sau, S.; Padhye, S.; Sarkar, F.H.; Iyer, A.K. Folic acid conjugated polymeric micelles loaded with a curcumin difluorinated analog for targeting cervical and ovarian cancers. *Surf. B Biointerfaces* **2017**, *157*, 490–502. [CrossRef] [PubMed]
23. Sau, S.; Mondal, S.K.; Kashaw, S.K.; Iyer, A.K.; Banerjee, R. Combination of cationic dexamethasone derivative and STAT3 inhibitor (WP1066) for aggressive melanoma: A strategy for repurposing a phase I clinical trial drug. *Mol. Cell. Biochem.* **2017**, *436*, 119–136. [CrossRef] [PubMed]
24. Knutson, S.; Raja, E.; Bomgarden, R.; Nlend, M.; Chen, A.; Kalyanasundaram, R.; Desai, S. Development and evaluation of a fluorescent antibody-drug conjugate for molecular imaging and targeted therapy of pancreatic cancer. *PLoS One* **2016**, *11*, e0157762. [CrossRef] [PubMed]
25. Bally, A.P.R.; Lu, P.; Tang, Y.; Austin, J.W.; Scharer, C.D.; Ahmed, R.; Boss, J.M. NF-κB Regulates PD-1 Expression in Macrophages. *J. Immunol.* **2015**, *194*, 4545–4554. [CrossRef] [PubMed]
26. Alsaab, H.O.; Sau, S.; Alzhrani, R.M.; Cheriyan, V.T.; Polin, L.A.; Vaishampayan, U.; Rishi, A.K.; Iyer, A.K. Tumor hypoxia directed multimodal nanotherapy for overcoming drug resistance in renal cell carcinoma and reprogramming macrophages. *Biomaterials* **2018**, *183*, 280–294. [CrossRef] [PubMed]
27. Beck, A.; Goetsch, L.; Dumontet, C.; Corvaïa, N. Strategies and challenges for the next generation of antibody-drug conjugates. *Nat. Rev. Drug Discov.* **2017**, *16*, 315–337. [CrossRef] [PubMed]
28. Lambert, J.M.; Morris, C.Q. Antibody–Drug Conjugates (ADCs) for Personalized Treatment of Solid Tumors: A Review. *Adv. Ther.* **2017**, *34*, 1015–1035. [CrossRef]
29. Sapra, P.; Stein, R.; Pickett, J.; Qu, Z.; Govindan, S.V.; Cardillo, T.M.; Hansen, H.J.; Horak, I.D.; Griffiths, G.L.; Goldenberg, D.M. Anti-CD74 antibody-doxorubicin conjugate, IMMU-110, in a human multiple myeloma xenograft and in monkeys. *Clin. Cancer Res.* **2005**, *11*, 5257–5264. [CrossRef]

30. Zhang, R.R.; Schroeder, A.B.; Grudzinski, J.J.; Rosenthal, E.L.; Warram, J.M.; Pinchuk, A.N.; Eliceiri, K.W.; Kuo, J.S.; Weichert, J.P. Beyond the margins: Real-time detection of cancer using targeted fluorophores. *Nat. Rev. Clin. Oncol.* **2017**, *14*, 347–364. [CrossRef]
31. Garcia-Diaz, A.; Shin, D.S.; Moreno, B.H.; Saco, J.; Escuin-Ordinas, H.; Rodriguez, G.A.; Zaretsky, J.M.; Sun, L.; Hugo, W.; Wang, X.; et al. Interferon Receptor Signaling Pathways Regulating PD-L1 and PD-L2 Expression. *Cell Rep.* **2017**, *19*, 1189–1201. [CrossRef] [PubMed]

cancers

MDPI

Case Report

Gold Nanorod-Assisted Photothermal Therapy Decreases Bleeding during Breast Cancer Surgery in Dogs and Cats

Moustafa R. K. Ali [1,*], Haithem A. M. Farghali [2], Yue Wu [1], Ivan El-Sayed [3], Ahmed H. Osman [2], Salah A. Selim [2] and Mostafa A. El-Sayed [1,*]

[1] Laser Dynamics Laboratory, School of Chemistry and Biochemistry, Georgia Institute of Technology, Atlanta, GA 30332-0400, USA; janewuyue@gmail.com

[2] Department of Veterinary Medicine, Cairo University, Giza 12211, Egypt; haithemfarghali@gmail.com (H.A.M.F.); AHOsman2007@hotmail.com (A.H.O.); dr.salahselim@hotmail.com (S.A.S.)

[3] Department of Otolaryngology, University of California, San Francisco, CA 94115, USA; Ivan.El-Sayed@ucsf.edu

* Correspondence: mali43@gatech.edu or Moustafa.r.k.ali@gmail.com (M.R.K.A); melsayed@gatech.edu (M.A.E); Tel.: +1-470-399-0571 (M.R.K.A); +1-404-894-0292 (M.A.E)

Received: 14 May 2019; Accepted: 18 June 2019; Published: 19 June 2019

Abstract: For localized tumors, gold nanorod (AuNR)-assisted plasmonic photothermal therapy (PPTT) is a potentially effective alternative to traditional surgery, in which AuNRs absorb near-infrared light and convert it to heat in order to kill cancer cells. However, for large tumors (volume ≥ 20 cm^3), an uneven distribution of AuNRs might cause inhomogeneity of the heat distribution inside the tumor. Surgery is frequently recommended for removing large tumors, but it is associated with a high risk of cancer recurrence and metastasis. Here, we applied PPTT before surgery, which showed improved treatment for large tumors. We divided the animals (eight cats/dogs) into two groups: Group I (control), where three cases were solely treated with surgery, laser, or AuNRs alone, resulting in recurrence and metastasis; and Group II, where animals were treated with PPTT before surgery. In Group II, four out of the five cases had tumor regression without any recurrence or metastasis. Interestingly, we observed that applying PPTT before surgery displayed reduced bleeding during tumor removal, supported by histopathology that showed altered blood vessels. In conclusion, our study showed that applying AuNR-assisted PPTT (AuNRs-PPTT) before surgery could significantly affect blood vessels inside the tumor, leading to a decreased amount of bleeding during surgery, which can potentially decrease the risk of metastasis and blood loss during surgery.

Keywords: plasmonic photothermal therapy; gold nanorods; surgery; bleeding; dogs; cats; breast cancer

1. Introduction

Gold nanorods (AuNRs)-based plasmonic photothermal therapy (PPTT) is a cancer therapy in which AuNRs are injected into the tumor before exposure to near-infrared (NIR) light [1,2]. The NIR light capable of deeply penetrating the tissue is transiently applied to the tumor, producing localized heat that could lead to tumor necrosis and apoptosis [3]. PPTT modulation to induce cell apoptosis might be a more favorable option than triggering necrosis, as during necrosis, the broken plasma membrane leads to the leaking of cytoplasmic components and inflammation, which could further induce cancer growth and metastasis [4–7]. The high efficiency of PPTT in getting rid of cancer cells by inducing apoptosis has been demonstrated both in vitro and in vivo [3,8]. The reason for using canines and felines is because of their molecular and biological similarity to human mammary tumors, which makes these animals a model system [9,10]. The surgery is usually the first line of treatment in

the animals. In many animal cases, the tumors often metastasize. We have shown the efficacy of this treatment in tumor-bearing mice [8,11] and have recently demonstrated the treatment of mammary carcinoma in dogs and cats, where the malignant mammary tumors of ≤20 cm^3 in volume could be treated by intratumoral inoculation of AuNRs, followed by PPTT [5]. During these studies, we observed that animals with induced or spontaneous tumors have noteworthy regression without any recurrence nor metastasis. Our recent studies have also shown the ability of gold nanorod-assisted plasmonic photothermal therapy (AuNRs-PPTT) in vitro to inhibit cancer cell migration [12,13]. In addition, the toxicity of this treatment has been examined in mice, dogs, and cats, which indicates that there are no toxic effects on the animals for long periods of time [5,8]. Therefore, PPTT is believed to be a favorable alternative for treating solid tumors with relatively small sizes and preventing metastasis [14].

For large tumors (volume ≥ 20 cm^3), PPTT could be hard to achieve because of an uneven distribution of injected AuNRs that causes an inhomogeneity of the heat in the tumor. In these cases, surgery is usually recommended to remove primary solid tumors. However, the surgical resection of primary breast cancer tumors commonly has a risk for metastatic recurrence [15]. It has been recognized that the tumors contain large amounts of blood vessels that provide nutrients that support tumor growth [16]. Blood vessels are also critical for metastasis, as extensive and highly permeable blood vessels provide ways for cancer cells to exit primary tumor sites and enter into the bloodstream. Surgery usually disrupts the blood and lymphatic vessels, thus releasing cancer cells into the vasculature and promoting metastasis [17]. Therefore, the development of novel therapies that aid in the surgical process to prevent blood loss, tumor recurrences, and metastasis are of great importance.

In this study, we are focusing on introducing a new treatment regimen featuring the combination of PPTT and surgery in dogs and cats with large tumors, as well as examining the efficacy of this new regimen. Interestingly, we observed that applying AuNRs-PPTT before surgery could significantly decrease bleeding, which could potentially avoid the risk of metastasis caused by surgery.

2. Results

2.1. Preparation and Characterization of the AuNRs

AuNRs with an average size of 27 (±5) × 6 (±1) nm (length × width) were used in this study, as they showed enhanced efficacy of PPTT [18]. AuNRs were synthesized according to our reported method [19], and these AuNRs are shown in the transmission electron microscope (TEM) image (Figure 1A). AuNRs have a surface plasmon resonance wavelength of around 800 nm (Figure 1B). After synthesis, AuNRs were successfully coated with Methoxy polyethylene glycol thiol (mPEG-SH) and Arg−Gly−Asp (RGD) peptides, as demonstrated by the red-shift of the surface plasmon peak (Figure 1B). The average number of ligands on each particle is quantified to be 1000 mPEG-SH and 10,000 RGD. RGD is known to bind to integrin, which is over-expressed on the surface of breast cancer cells and associated with breast cancer progression and metastasis [20]. RGD binding could enhance the receptor-mediated endocytosis of the nanoparticles [21].

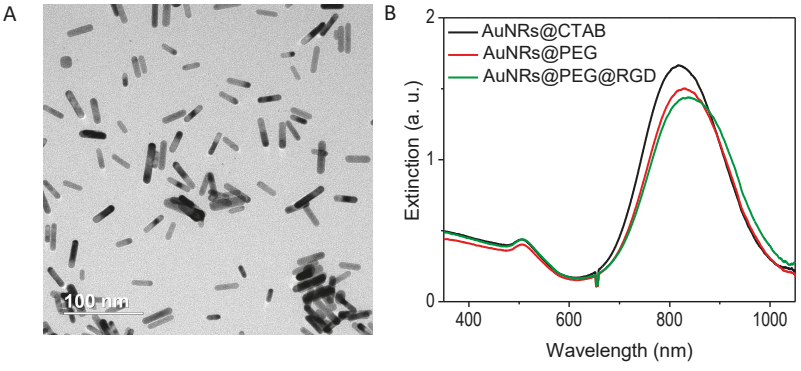

Figure 1. Characterization of gold nanorods (length 27 ± 5 nm, width 6 ± 1 nm). (**A**) Transmission electron microscope (TEM) image with 100 nm scale bar. (**B**) UV–VIS absorbance spectra showing the surface plasmon resonance peaks of gold nanorods (AuNRs) after synthesis (AuNRs@CTAB (cetyltrimethylammonium bromide)), then after conjugation with polyethylene glycol (PEG) (AuNRs@PEG), then after conjugation with (Arg−Gly−Asp) RGD (AuNRs@PEG@RGD).

2.2. PPTT Decreases Bleeding during Surgery

In our earlier studies, we optimized the PPTT conditions for treating dogs and cats, including the AuNR dosage and laser conditions (7.5 nM of AuNRs irradiated by NIR laser with 0.5 W/cm^2 intensity for 2 min). The optimized conditions were conducted multiple times (2 weeks apart) until complete regression via apoptosis was shown, and this apoptosis proved to be better than necrosis [5]. Herein, we devised a new treatment regimen for treating animals with tumor volumes ≥20 cm^3 by combining surgery with PPTT.

Before treatment, all animal tumors showed varied growth, as shown in Tables 1 and 2. In the control group (I), three cases with 10 tumors were solely treated by a mastectomy, laser, or AuNR treatment alone. As shown in Figure 2A,B, photographic images of case 1 (GI-1) revealed three large tumors located at the cranioabdominal and inguinal lymph nodes. All three tumors connected to form one chain. Figure 2C is a picture of a tumor during surgery with obvious bleeding (over 100 g). Figure 2D is a histopathology of the tumor tissue showing ductal carcinoma in situ, grade II.

In Group II, five cases with eleven tumors were treated with three sessions of PPTT (in 2 week intervals) and were followed by surgery after the last PPTT session. Figure 3A,B shows case 1 (GI-1), where the animal was treated with surgery only, and Figure 3C,D shows one case with surgery after PPTT. Interestingly, we observed that when applying PPTT before surgery, reduced bleeding during the surgery was observed for all of the treated tumors in Group II when compared to Group I (Figure 3A,C and Videos S1 [surgery only] and S2 [surgery after PPTT]).

The decrease of bleeding might be explained by the histopathology of the tumor bed vasculature (Figure 3B,D). With surgery only, the blood vessels were normal and intact (Figure 3B) while after PPTT, the tumor bed vasculature showed swelling and sloughing of the endothelial lining and destruction of the blood vessel walls Hematoxylin& Eosin (H&E ×400) (Figure 3D).

Table 1. Animal groups, tumor clinical features, and therapeutic approaches.

No. #	Species and Age	Site of Tumors	Size of Tumors (cm)	Grade	Therapy
GI-1	Dog—Mixed Boxer, 14 years	1-R caudoabdominal ulcerated	(8 × 5)	II	Only mastectomy
		2-R cranioabdominal	(18 × 4)		
		3-R inguinal Lymph node All the three connected to form one chain			
GI-2	Dog—Griffon, 7 years	1-R Cranioinquinal	(4.1 × 2.9)	II	Laser only, followed by mastectomy
GI-3	Cat—15 years	1-R caudo abdominal	(4 × 4.5).	II	1 + 2 + 3 tumors form chain; Laser only, followed by mastectomy
		2-R inguinal LN	(3 × 2.1).		
		3-L cranioabdominal	(5 × 2)		
		4-R inguinal	(1 × 2)	I	4 + 5 + 6 tumors treated by AuNRs only, followed by mastectomy
		5-L inguinal	(1 × 1)		
		6-L caudothoracic	(1 × 1)		
GII-1	Cat—9 years	L caudothoracic	(4.5 × 4)	III	Three sessions of plasmonic photothermal therapy (PPTT), followed by surgery
		R caudothoracic	(4 × 4)		
GII-2	Dog—Griffon, 10 years	R Caudoquinal	(3.1 × 3.6)	III	Three session of PPTT, followed by surgery
GII-3	Dog—Griffon, 11 years	1-L inguinal	(5 × 5)	II	Three session of PPTT, followed by surgery
		2-L inguinal	(2 × 1.5)		PPTT only
		3 small tumor	(1.5 × 1)		PPTT only
GII-4	Dog—Griffon, 5 years	1-R caudo thoracic	(3 × 2.5)	II	Three sessions of PPTT, followed by surgery
		2-R cranio abdominal both tumors form chain	(8 × 6.5)		
GII-5	Dog—Griffon, 8 years	1-L inguinal large calcified	(5 × 5)	III	Three session of PPTT, followed by surgery
		2-small caudal abdomenial	(2 × 1.5)		2 and 3 treated by PPTT only
		3-two attached small tumors	(1.5 × 1)		

The control group, GI, included three cases (two dogs and one cat with 10 tumors) treated with either surgery only, laser only, or AuNRs only. All cases developed metastasis and died after treatment. Group II (GII) included five cases (four dogs and one cat with 11 tumors) treated with PPTT (AuNRs and laser together) for three sessions, followed by surgery. At the time of death, there was no presence of disease; however, one case succumbed to metastatic disease.

Table 2. Survival, bleeding loss, and metastasis for both GI and GII.

No. #	EBL (g)	LR	DM (Time Mo)	OSS (mo)	Status
GI-1	>100	+1 month	+(CS, LN)	3	DOD
GI-2	66.5	-	+(CS, LN)	1	DOC
GI-3	47.5	-	+(LN)	1	DOC
GII-1	<1	-	-	24	ADF
GII-2	<1	-	-	48	ADF
GII-3	<1	-	-	3	DOC (pneumonia)
GII-4	<1	-	+(LN, CS)	1	DOD
GII-5	<1	-	-	6	DOC (pneumonia)

Group I (GI) were solely treated with surgery, laser, or AuNrs alone. Group II (GII) were treated with PPTT (AuNrs and laser together) before surgery. Estimate blood loss significant test p-value and statistical significance: the two-tailed p-value = 0.0010—by conventional criteria, this difference is considered to be statistically significant. ADF, alive disease free; DM, distant metastases; CS, clinical stage; DOC, dead other cause; DOD, dead of disease; EBL, estimated blood loss; LN, lymph node; LR, local recurrence.

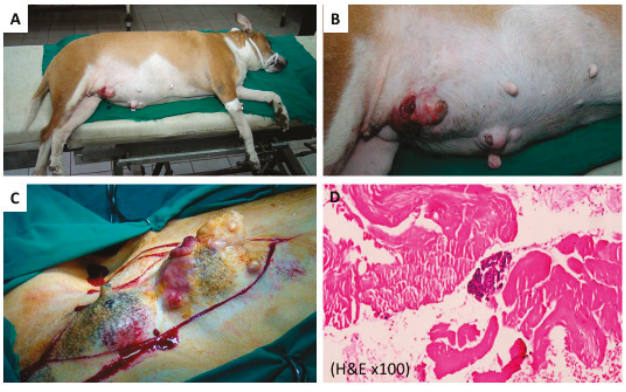

Figure 2. (**A**) Photographic image of control case 1 (Group 1, case 1) treated with surgery. (**B**) A magnified figure of (A) for the tumor area. (**C**) Photo of case during surgery with high amount of bleeding. (**D**) Photomicrograph of tumor tissue, showing ductal carcinoma in situ grade II (H&E ×100). Three images for each tumor were evaluated.

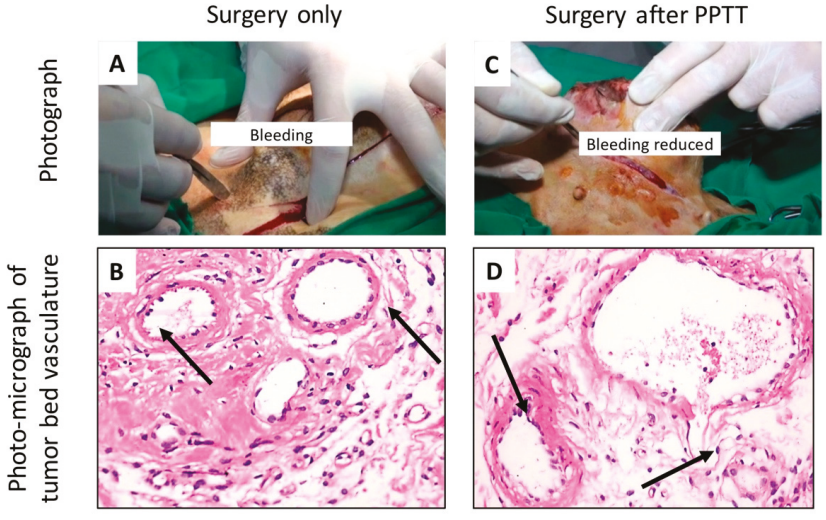

Figure 3. Left side (**A**,**B**) shows case 1 in Group I (surgery only). Right side (**C**,**D**) shows one case in Group II (treated with PPTT for three sessions (2 week intervals) before the surgery). (**A**,**C**) Photographic images indicating the decrease of bleeding after PPTT (**C**), compared with the control (**A**). (**B**,**D**) Photomicrograph of tumor bed vasculature showing (**B**) normal intact blood vessels with surgery only, and (**D**) swelling and sloughing of the endothelial lining and the destruction of the blood vessel wall (arrow) after PPTT (H&E ×400). Three images for each tumor were evaluated.

In addition, the regimen of PPTT before surgery has shown to be effective for achieving complete tumor regression, as shown in Table 2. For example, in one case from Group II, a nine-year-old mixed breed cat suffered from mammary neoplasms as shown in Figure 4A. The site of two tumors located at her left axillary lymph node (black arrow) and left cranial thoracic (blue arrow) is demonstrated in Figure 4B. After PPTT, followed by surgical excision of the tumors (Figure 4C), tumor regression was achieved. The histopathology showed that after PPTT, well-developed granulation tissues were

observed, indicating tumor recovery (Figure 4D). After 12 months, this case showed complete recovery from the surgery (Figure 4E) without evidence of recurrence or chest metastasis (Figure 4F).

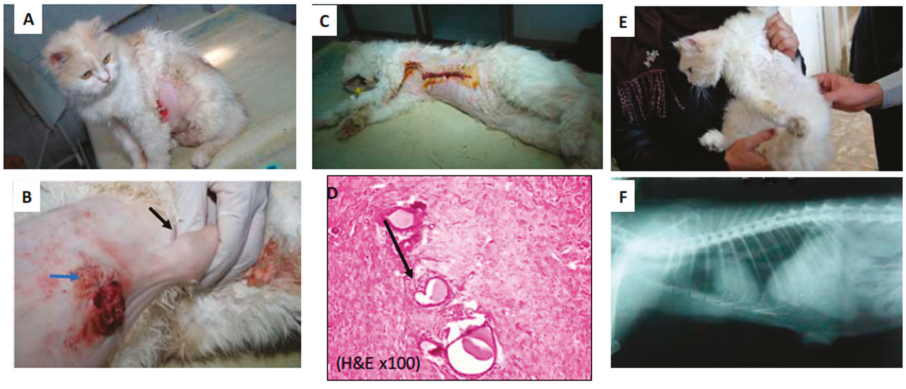

Figure 4. (**A**) A nine-year-old mixed breed cat suffered from mammary neoplasm (Group 2, case 1). (**B**) The sites of tumors at the left axillary lymph node (black arrow) and left cranial thoracic (blue arrow) (**C**) after surgical excision and (**D**) the subcutaneous layer showing well-developed granulation tissue at the site of suture (arrow) (H&E ×100). (**E**) The case after 12 months showed complete recovery from the surgery without any evidence of recurrence. (**F**) X-ray shows no metastasis in the chest. Three images for each tumor were evaluated.

3. Discussion

Three cases among the five in Group II died a few months after PPTT and surgery treatment because of viral pneumonia, but evidence of tumor recurrence or metastasis was not observed. Earlier, we have shown in our study on mice that there was no toxicity after 15 months of AuNRs injection, whose bio-distribution mainly locates at the liver and spleen [8]. However, we do find that other types of nanoparticles, such as TiO_2, iron, Cr^{3+}-doped zinc gallate, and silver, could accumulate in the lung, and might cause toxicity [22–25], while AuNPs have better biocompatibility than these nanoparticles. To the best of our knowledge, there are not many systematic studies discussing the blood circulating (not airborne) AuNRs and their relation with pneumonia thus far. This can be a separate study in future.

In this report, we observed that PPTT affected the tumor blood vessels that, in turn, decreased the blood flow inside the tumor. The reason is still not fully understood. Previous reports have shown that AuNPs could affect blood vessels and tumor angiogenesis [26–28]. In addition, the temperature increase would cause the destruction of blood vessels. For instance, it has been reported that photothermal ablation of breast cancer in mice models using doxorubicin-loaded DNA-wrapped AuNRs could disturb the blood vessels [29]. Furthermore, it is reported that AuNPs with sizes around 30 nm could induce tumor endothelial leakiness [30]. In addition, the abnormal vascular nature of the tumor tissues allows them to uptake more AuNRs [31], which might explain why the AuNRs-PPTT is more effective on the tumor blood vessels. The importance of applying AuNRs-PPTT before surgery could also be very important in decreasing blood loss, especially for the patients who have injury-healing problems, including chronic diseases such as diabetes, and need tumor surgery.

4. Materials and Methods

4.1. Synthesis and Surface Modification of AuNRs

AuNRs were prepared according to the seedless method [19]. Briefly, 5 mL of 1 mM $HAuCl_4$ (Sigma-Aldrich Co., St Louis, MO, USA) was mixed with 5 mL of 0.20 M cetyltrimethylammonium

bromide (CTAB; Sigma-Aldrich Co.), followed by adding 250 μL of 4 mM $AgNO_3$ (Sigma-Aldrich Co.) and adjusting the pH of the solution to be 1–1.15 by 37% HCl. Then, 70 μL of 78.8 mM ascorbic acid (Sigma-Aldrich Co.) was added to the solution until the solution became clear. A total of 15 μL of 0.01 M ice-cold $NaBH_4$ (Sigma-Aldrich Co.) was injected into the growth solution immediately, and the solution was left unstirred for 6 hours. To remove the extra CTAB and prepare for surface modification, the AuNRs were centrifuged at 19,000 rcf for 1 hour, and the pellet was redispersed in deionized water and centrifuged at 14,000 rcf for 15 min. The AuNRs were rinsed with water, then conjugated with different surface ligands (polyethylene glycol (PEG) thiol and Arg−Gly−Asp (RGD) peptides). For surface modification, methoxy PEG thiol (m-PEG-Th, PEG; Laysan Bio, Arab, AL, USA) was added to AuNRs and stirred overnight to achieve a concentration of around 1000 PEG molecules per AuNR. For preparation of the AuNRs@RGD, the PEGylated nanoparticles (1 nM) were treated with RGD (1 mM) to achieve 10,000 ligands on each AuNR. Afterward, the solution was kept overnight to be shaken at normal temperature, and the extra ligands were removed by centrifugation. A UV–VIS spectrometer was used to confirm the conjugation.

4.2. Characterization of AuNRs

A JEOL 100 CX transmission electron microscope (TEM) (JEOL Ltd., Tokyo, Japan) was used to measure the size and homogeneity of the samples. A Cary 500 UV–VIS spectrometer (Agilent Technologies, Santa Clara, CA, USA) was used for measuring the absorbance of the AuNRs. To characterize the surface conjugation with PEG, a ZetaSizer 3000 HAS (Malvern Instruments, Worcestershire, UK) was used for measuring the surface Zeta potentials. In addition, Ellman's reagents (Sigma-Aldrich Co.), which react with free-Thiol groups (calorimetrically measured at 412 nm), were used to quantify the number of PEG molecules boun to the surface of the AuNRs.

4.3. Animal Diagnosis and X-ray Examination

All animals were handled in accordance with Association for Assessment and Accreditation of Laboratory Animal Care and Office of Laboratory Animal Welfare guidelines under the direction of the Institutional Animal Care and Use Committee at Cairo University. The pet animals were admitted to the Department of Surgery Clinic of the Faculty of Veterinary Medicine at Cairo University. This research was approved by the Institutional Animal Care and Use Committee (CU-IACUC) Cairo University (code: CU II F 9 16).

All pets' owners claimed that their animals did not receive any treatment before their arrival at the university. Written informed consent was provided by the owners of the pets for the treatments. Eight female animals were treated in this study, including two canines and six felines, with a total of 21 tumors with varied grades (I to III). The tumor dimensions were measured using calipers. Histopathology tests were used to diagnose the tumor types/grades. At the tumor site, the animal's hair was shaved, and subsequently, radiographic recordings were taken with an X-ray machine (Fischer, Berlin, Germany). The radiographic setting factors were 58–70 kVp, 10 mAs, and a 90 cm focal spot film distance. The radiographic exposures were conducted dorsoventrally and right laterally. Blood loss was quantified by measuring the blood volume and weighing surgical sponges used for blood collection before and after the surgery.

General anesthesia was applied for animals during the surgical mastectomy and postsurgical application of PPTT. Under general injectable anesthesia, each animal was pre-medicated with atropine sulphate (1%, 0.05–0.1 mg/kg b. wt.; Adwia Co. S.A.E., Cairo, Egypt) and xylazine (Xyla-Ject 2%, 1 mg/kg b. wt.; Adwia Co. S.A.E.), and then anesthesia was induced using ketamine HCl (Ketalar, 10–15 mg/kg b. wt.; Sigma-Aldrich Co.) and maintained by ketamine HCl [32,33].

4.4. Performing PPTT in Animals

Each animal was subjected to three sessions of PPTT treatment in 2 week intervals using an 808 nm diode laser with a power of 0.5 W/cm^2 and a spot size of around 5.6 mm^2. An effective dose

of AuNR solution (7.5 nM AuNRs) for each 100 cm^3 was used for 2 min, and the amount used was scaled up based on the volume of the tumor, and then injected directly into the tumor. Five minutes after injection, the entirety of the tumor was irradiated with the laser. The AuNR concentration was decreased by 50% for each subsequent treatment. The temperature increase of a tumor during the laser irradiation was measured by placing a 33-gauge hypodermic thermocouple (OMEGA Engineering, Inc., Stamford, CT, USA) needle directly inside the tumor (42–44 °C).

4.5. Histopathology Evaluation of the Animal Tumors

The detailed pathologic evaluation of tumors was conducted by members of the pathology department of the Faculty of Veterinary Medicine at Cairo University. Histopathological analysis was performed on 5 µm sections from tumor tissue that were fixed in 10% buffered formalin. The samples were stained with H&E to assess pathology.

5. Conclusions

Surgery is often used for tumor removal; however, it might trigger metastasis [34]. PPTT could be a better alternative to replace traditional chemotherapy and radiotherapy for localized tumors, especially for tumors with a volume ≤20 cm^3 [5]. Therefore, for effective treatment of large tumors (volume ≥ 20 cm^3), we applied PPTT before surgical resection to naturally occurring tumors in the mammary glands of dogs and cats. Five cases were treated with this regimen and showed complete remission without any recurrence after therapy. Three cases died in the few months following treatment, but in two cases from three, there was no evidence of any tumors upon examination (the animals died because of other reasons, such as pneumonia). Histopathology results showed a decrease in cancer grades compared to before (variant grades from 1 to 4) and after 2 weeks of treatment via PPTT and surgery (grade 0). X-ray diffraction revealed an absence of metastasis 1–2 years after treatment. In conclusion, our study demonstrates the feasibility of applying PPTT before surgery to large tumors in dogs and cats. Applying AuNRs-PPTT before surgery in treating large tumors could significantly affect blood vessels inside the tumor and potentially avoid the risk of bleeding during surgery. PPTT could be incorporated before the surgery to decrease the bleeding and potentially avoid the risk of bleeding during surgery that could lead to excessive blood loss and metastasis.

6. Patents

This work has been filed in the US-Patent Publication of US20190008964A1.

Supplementary Materials: The following are available online at https://zenodo.org/record/3251162#.XR3I5_YRU2x, Video S1 [surgery only] and Video S2 [surgery after PPTT]).

Author Contributions: Conceptualization, M.R.K.A., S.A.S., and M.A.E.-S.; methodology, M.R.K.A., H.A.M.F., Y.W., A.H.O., S.A.S., and M.A.E.-S; software, M.R.K.A., Y.W., I.E.-S., A.H.O., and S.A.S.; validation, M.R.K.A., Y.W., I.E.-S., A.H.O., S.A.S., and M.A.E.-S; formal analysis, M.R.K.A., Y.W., I.E.-S., A.H.O., S.A.S., and M.A.E.-S.; investigation, M.R.K.A., H.A.M.F., Y.W., I.E.-S., A.H.O., S.A.S., and M.A.E.-S.; resources, M.R.K.A., H.A.M.F., I.E.-S., A.H.O., S.A.S., and M.A.E.-S.; data curation, M.R.K.A., H.A.M.F., Y.W., I.E.-S., A.H.O., S.A.S., and M.A.E.-S.; writing—original draft preparation, M.R.K.A., Y.W.; writing—review and editing, M.R.K.A., H.A.M.F., Y.W., I.E.-S., A.H.O., S.A.S., and M.A.E.-S.; visualization M.R.K.A., H.A.M.F., Y.W., I.E.-S., A.H.O., S.A.S., and M.A.E.-S.; supervision M.R.K.A., I.E.-S., S.A.S., and M.A.E.-S.; project administration, M.R.K.A., H.A.M.F., Y.W., I.E.-S., A.H.O., S.A.S., and M.A.E.-S.; funding acquisition, M.R.K.A., H.A.M.F., Y.W., I.E.-S., A.H.O., S.A.S., and M.A.E.-S.

Funding: This research was funded by the Joint Collaborative Efforts of the Egyptian Expatriates and Scientific Organizations toward Tackling National R&D Challenges (JESOR).

Acknowledgments: We thank the undergraduate research assistants, Paige Warner, Kamaria Dansby, Sarah Ghalayini, and Arusha Siddiqa and for their critical reading of the manuscript. We thank Tiegang Han for helping editing the videos and critically reading the manuscript. We thank Mahmoud Zawrah and Mahmoud Sakr for great support of this work. We thank Hala Ali for her help of assisting the work of Haithem A.M. Farghali.

Conflicts of Interest: The authors declare no conflict of interest.

References

1. Huang, X.; El-Sayed, I.H.; Qian, W.; El-Sayed, M.A. Cancer cell imaging and photothermal therapy in the near-infrared region by using gold nanorods. *J. Am. Chem. Soc.* **2006**, *128*, 2115–2120. [CrossRef] [PubMed]
2. El-Sayed, I.H.; Huang, X.; El-Sayed, M.A. Selective laser photo-thermal therapy of epithelial carcinoma using anti-EGFR antibody conjugated gold nanoparticles. *Cancer Lett.* **2006**, *239*, 129–135. [CrossRef] [PubMed]
3. Perez-Hernandez, M.; Del Pino, P.; Mitchell, S.G.; Moros, M.; Stepien, G.; Pelaz, B.; Parak, W.J.; Galvez, E.M.; Pardo, J.; de la Fuente, J.M. Dissecting the molecular mechanism of apoptosis during photothermal therapy using gold nanoprisms. *ACS Nano* **2015**, *9*, 52–61. [CrossRef] [PubMed]
4. Ali, M.R.; Ali, H.R.; Rankin, C.R.; El-Sayed, M.A. Targeting heat shock protein 70 using gold nanorods enhances cancer cell apoptosis in low dose plasmonic photothermal therapy. *Biomaterials* **2016**, *102*, 1–8. [CrossRef] [PubMed]
5. Ali, M.R.; Ibrahim, I.M.; Ali, H.R.; Selim, S.A.; El-Sayed, M.A. Treatment of natural mammary gland tumors in canines and felines using gold nanorods-assisted plasmonic photothermal therapy to induce tumor apoptosis. *Int. J. Nanomed.* **2016**, *11*, 4849–4863. [CrossRef]
6. Orosz, P.; Echtenacher, B.; Falk, W.; Ruschoff, J.; Weber, D.; Mannel, D.N. Enhancement of experimental metastasis by tumor necrosis factor. *J. Exp. Med.* **1993**, *177*, 1391–1398. [CrossRef] [PubMed]
7. Melamed, J.R.; Edelstein, R.S.; Day, E.S. Elucidating the fundamental mechanisms of cell death triggered by photothermal therapy. *ACS Nano* **2015**, *9*, 6–11. [CrossRef]
8. Ali, M.R.; Rahman, M.A.; Wu, Y.; Han, T.; Peng, X.; Mackey, M.A.; Wang, D.; Shin, H.J.; Chen, Z.G.; Xiao, H.; et al. Efficacy, long-term toxicity, and mechanistic studies of gold nanorods photothermal therapy of cancer in xenograft mice. *Proc. Natl. Acad. Sci. USA* **2017**, *114*, E3110–E3118. [CrossRef]
9. Antuofermo, E.; Miller, M.A.; Pirino, S.; Xie, J.; Badve, S.; Mohammed, S.I. Spontaneous mammary intraepithelial lesions in dogs—A model of breast cancer. *Cancer Epidemiol. Biomark. Prev.* **2007**, *16*, 2247–2256. [CrossRef]
10. Adega, F.; Borges, A.; Chaves, R. Cat mammary tumors: Genetic models for the human counterpart. *Vet. Sci.* **2016**, *3*, 17. [CrossRef]
11. Dickerson, E.B.; Dreaden, E.C.; Huang, X.; El-Sayed, I.H.; Chu, H.; Pushpanketh, S.; McDonald, J.F.; El-Sayed, M.A. Gold nanorod assisted near-infrared plasmonic photothermal therapy (PPTT) of squamous cell carcinoma in mice. *Cancer Lett.* **2008**, *269*, 57–66. [CrossRef] [PubMed]
12. Ali, M.R.K.; Wu, Y.; Tang, Y.; Xiao, H.; Chen, K.; Han, T.; Fang, N.; Wu, R.; El-Sayed, M.A. Targeting cancer cell integrins using gold nanorods in photothermal therapy inhibits migration through affecting cytoskeletal proteins. *Proc. Natl. Acad. Sci. USA* **2017**, *114*, E5655–E5663. [CrossRef] [PubMed]
13. Wu, Y.; Ali, M.R.K.; Dong, B.; Han, T.; Chen, K.; Chen, J.; Tang, Y.; Fang, N.; Wang, F.; El-Sayed, M.A. Gold nanorod photothermal therapy alters cell junctions and actin network in inhibiting cancer cell collective migration. *ACS Nano* **2018**, *12*, 9279–9290. [CrossRef]
14. Zou, L.; Wang, H.; He, B.; Zeng, L.; Tan, T.; Cao, H.; He, X.; Zhang, Z.; Guo, S.; Li, Y. Current approaches of photothermal therapy in treating cancer metastasis with nanotherapeutics. *Theranostics* **2016**, *6*, 762–772. [CrossRef] [PubMed]
15. Tohme, S.; Simmons, R.L.; Tsung, A. Surgery for cancer: A trigger for metastases. *Cancer Res.* **2017**, *77*, 1548–1552. [CrossRef] [PubMed]
16. Potente, M.; Gerhardt, H.; Carmeliet, P. Basic and therapeutic aspects of angiogenesis. *Cell* **2011**, *146*, 873–887. [CrossRef] [PubMed]
17. Park, Y.; Kitahara, T.; Takagi, R.; Kato, R. Does surgery for breast cancer induce angiogenesis and thus promote metastasis? *Oncology* **2011**, *81*, 199–205. [CrossRef] [PubMed]
18. Mackey, M.A.; Ali, M.R.; Austin, L.A.; Near, R.D.; El-Sayed, M.A. The most effective gold nanorod size for plasmonic photothermal therapy: Theory and in vitro experiments. *J. Phys. Chem. B* **2014**, *118*, 1319–1326. [CrossRef] [PubMed]
19. Ali, M.R.; Snyder, B.; El-Sayed, M.A. Synthesis and optical properties of small Au nanorods using a seedless growth technique. *Langmuir* **2012**, *28*, 9807–9815. [CrossRef]
20. Felding-Habermann, B.; O'Toole, T.E.; Smith, J.W.; Fransvea, E.; Ruggeri, Z.M.; Ginsberg, M.H.; Hughes, P.E.; Pampori, N.; Shattil, S.J.; Saven, A.; et al. Integrin activation controls metastasis in human breast cancer. *Proc. Natl. Acad. Sci. USA* **2001**, *98*, 1853–1858. [CrossRef]

21. Ali, M.; Wu, Y.; Ghosh, D.; Do, B.; Chen, K.; Dawson, M.; Fang, N.; Sulchek, T.; El-Sayed, M. Nuclear membrane-targeted gold nanoparticles inhibit cancer cell migration and invasion. *Acs Nano* **2017**, *11*, 3716–3726. [CrossRef] [PubMed]
22. Tate, J.A.; Petryk, A.A.; Giustini, A.J.; Hoopes, P.J. In vivo biodistribution of iron oxide nanoparticles: An overview. *Proc. SPIE Int. Soc. Opt. Eng.* **2011**, *7901*, 790117. [CrossRef] [PubMed]
23. Elgrabli, D.; Beaudouin, R.; Jbilou, N.; Floriani, M.; Pery, A.; Rogerieux, F.; Lacroix, G. Biodistribution and clearance of TiO_2 nanoparticles in rats after intravenous injection. *PLoS ONE* **2015**, *10*, e0124490. [CrossRef] [PubMed]
24. Sun, X.; Shi, J.; Fu, X.; Yang, Y.; Zhang, H. Long-term in vivo biodistribution and toxicity study of functionalized near-infrared persistent luminescence nanoparticles. *Sci. Rep.* **2018**, *8*, 10595. [CrossRef] [PubMed]
25. Yang, L.; Kuang, H.; Zhang, W.; Aguilar, Z.P.; Wei, H.; Xu, H. Comparisons of the biodistribution and toxicological examinations after repeated intravenous administration of silver and gold nanoparticles in mice. *Sci. Rep.* **2017**, *7*, 3303. [CrossRef] [PubMed]
26. Roma-Rodrigues, C.; Heuer-Jungemann, A.; Fernandes, A.R.; Kanaras, A.G.; Baptista, P.V. Peptide-coated gold nanoparticles for modulation of angiogenesis in vivo. *Int. J. Nanomed.* **2016**, *11*, 2633–2639. [CrossRef]
27. Arvizo, R.R.; Rana, S.; Miranda, O.R.; Bhattacharya, R.; Rotello, V.M.; Mukherjee, P. Mechanism of anti-angiogenic property of gold nanoparticles: Role of nanoparticle size and surface charge. *Nanomedicine* **2011**, *7*, 580–587. [CrossRef]
28. Wu, M.Z.Y.; Zhang, Y.; Wu, M.; Wu, H.; Cao, L.; Li, L.; Li, X.; Zhang, X. Tumor angiogenesis targeting and imaging using gold nanoparticle probe with directly conjugated cyclic NGR. *RSC Adv.* **2018**, *8*, 1706–1716. [CrossRef]
29. Wang, D.; Xu, Z.; Yu, H.; Chen, X.; Feng, B.; Cui, Z.; Lin, B.; Yin, Q.; Zhang, Z.; Chen, C.; et al. Treatment of metastatic breast cancer by combination of chemotherapy and photothermal ablation using doxorubicin-loaded DNA wrapped gold nanorods. *Biomaterials* **2014**, *35*, 8374–8384. [CrossRef]
30. Setyawati, M.I.; Tay, C.Y.; Bay, B.H.; Leong, D.T. Gold nanoparticles induced endothelial leakiness depends on particle size and endothelial cell origin. *ACS Nano* **2017**, *11*, 5020–5030. [CrossRef]
31. Greish, K. Enhanced permeability and retention (EPR) effect for anticancer nanomedicine drug targeting. *Methods Mol. Biol.* **2010**, *624*, 25–37. [CrossRef] [PubMed]
32. Farghali, H.A.; AbdElKader, N.A.; Khattab, M.S.; AbuBakr, H.O. Novel approach to gastric mucosal defect repair using fresh amniotic membrane allograft in dogs (experimental study). *Stem Cell Res. Ther.* **2017**, *8*, 235. [CrossRef]
33. Farghali, H.A.; AbdElKader, N.A.; Khattab, M.S.; AbuBakr, H.O. Evaluation of subcutaneous infiltration of autologous platelet-rich plasma on skin-wound healing in dogs. *Biosci. Rep.* **2017**, *37*. [CrossRef] [PubMed]
34. Krall, J.A.; Reinhardt, F.; Mercury, O.A.; Pattabiraman, D.R.; Brooks, M.W.; Dougan, M.; Lambert, A.W.; Bierie, B.; Ploegh, H.L.; Dougan, S.K.; et al. The systemic response to surgery triggers the outgrowth of distant immune-controlled tumors in mouse models of dormancy. *Sci. Transl. Med.* **2018**, *10*. [CrossRef] [PubMed]

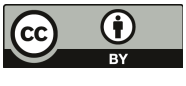

cancers

MDPI

Review

Effect of Flow-Induced Shear Stress in Nanomaterial Uptake by Cells: Focus on Targeted Anti-Cancer Therapy

Samar Shurbaji [1], Gulsen G. Anlar [2], Essraa A. Hussein [1], Ahmed Elzatahry [1,*] and Huseyin C. Yalcin [3,4,*]

[1] Materials Science and Technology Department, College of Arts and Sciences, Qatar University, Doha 2713, Qatar; samar.h.shurbaji1993@gmail.com (S.S.); essraa_88@yahoo.com (E.A.H.)
[2] College of Medicine, Department of Medical Sciences, Qatar University, Doha 2713, Qatar; guliz-y@hotmail.com
[3] Biomedical Research Center, Qatar University, Doha 2713, Qatar
[4] Department of Biomedical Sciences, College of Health Science-QU Health, Qatar University, Doha 2713, Qatar
* Correspondence: aelzatahry@qu.edu.qa (A.E.); hyalcin@qu.edu.qa (H.C.Y.); Tel.: +974-4403-6808 (A.E.); +974-4403-7719 (H.C.Y.)

Received: 30 October 2019; Accepted: 24 December 2019; Published: 16 July 2020

Abstract: Recently, nanomedicines have gained a great deal of attention in diverse biomedical applications, including anti-cancer therapy. Being different from normal tissue, the biophysical microenvironment of tumor cells and cancer cell mechanics should be considered for the development of nanostructures as anti-cancer agents. Throughout the last decades, many efforts devoted to investigating the distinct cancer environment and understanding the interactions between tumor cells and have been applied bio-nanomaterials. This review highlights the microenvironment of cancer cells and how it is different from that of healthy tissue. We gave special emphasis to the physiological shear stresses existing in the cancerous surroundings, since these stresses have a profound effect on cancer cell/nanoparticle interaction. Finally, this study reviews relevant examples of investigations aimed at clarifying the cellular nanoparticle uptake behavior under both static and dynamic conditions.

Keywords: nanomedicine; nanoparticle; targeted therapy; anti-cancer; shear stress; flow; in vitro

1. Introduction

In 1959, Richard Feynman delivered his pioneering lecture about nanotechnology in which he gave a foundation about materials miniaturization [1]. Since then, nano-scaled materials have been investigated and studied extensively for use in various fields, including the medical field [2]. When the power of nanotechnology is harnessed for biomedical applications, it is designated as nano-biotechnology or bio-nanotechnology to indicate the combination of nanotechnology with the biological system [3]. Nanomaterials are considered promising and favorable materials due to their unique properties as well as their extremely small size and high surface area to volume ratio, which means better surface interaction and effective cellular uptake. Nanobiotechnology has been applied in diverse medical applications, such as drug delivery platforms, contrast agents for magnetic resonance imaging, tissue engineering, and anti-cancer therapy.

Today, cancer is rated as the second leading cause of mortality worldwide [4]. In cancer cases, the signals that control normal cell division and normal cell death are disregarded due to genetic or environmental conditions. Consequently, uncontrolled cell division gives rise to rapid cell growth and the formation lumps, which is known as localized tumors. These tumor cells are characterized by fast proliferation, metastasis, and the ability to induce the formation of new blood vessels, which is also

known as "angiogenesis" [5]. Current cancer therapies are known for their lack of selectivity for tumor cells, as well as severe side effects such as damage to healthy organs, hair loss, and uncontrolled gastric problems. The integration of nano-scaled structures for anti-cancer therapy can be in the form of carriers for chemotherapeutic agents, cancer diagnostic agents, or targeting moieties. Nanomedicine holds the potential to minimize the undesired and severe adverse side effects of anti-cancer therapy, as well as to increase the efficacy and selectivity against tumor cells. In that regard, significant efforts have been devoted to developing nanoplatforms for specific cancer therapy or nanomedicine [6–9]. To design an effective nanomedicine, specific characteristics of cancer cells such as cancer cell mechanics or microenvironment of the tumor, which will influence the binding or internalization of the nanoparticles to cancer cells, should be taken into consideration.

Cancer cells are exposed to different forces and mechanical stresses than normal cells in the body, such as compressive forces due to tumor growth plus the interstitial pressure and shear stresses due to blood and interstitial fluid flow [10]. The biophysical microenvironment of tumor cells is different from normal cells. To illustrate this, blood flow in cancer microenvironment is irregular compared to normal circulation and subsequently, causes the tumor to be less oxygenated as the tumor grows [11]. Furthermore, the tumor site (extracellular fluid) is more acidic than normal tissues [12]. All these differences have substantial influences on the interactions of tumor cell with applied nanostructures. For example, shear forces in the extracellular environment can activate some cellular processes and affect the cellular uptake mechanism, which is important for targeted cancer therapy via nanoparticles [13].

Generally, fluid shear stress (FSS) in the biological systems can be categorized as resulting from blood flow, interstitial fluid flow or lymphatic fluid flow. Cancer cells mainly encounter interstitial fluid flow in localized tumor and also blood flow in case of metastasis [14]. Tumor cells can be exposed to additional fluid flows in the body, such as fluid flow in peritoneal cavity during ovarian cancer, which increases FSS [15]. Consequently, FSS is accepted as an important factor regulating the behavior of cancer cells and, more particularly, FSS acting on tumor cells will be discussed later in this article.

The major objectives of this review are to: (a) demonstrate the main types of physiological shear stresses that are affecting the tumor cells; (b) shed light on the interactions between cancer cells and applied nanomaterials in both static and dynamic conditions; (c) summarize findings on the influence of uptake of nanomaterials by cancer cells.

2. Physiological Shear Stresses Affecting the Tumor Cells

2.1. Shear Stress Due to Blood Flow

Circulating tumor cells (CTC) or metastatic cells are cancer cells that shed from the localized primary tumor and migrate to other body sites through the blood stream [16]. These cells experience shear stress due to blood flow [17,18]. Studies showed that, CTC can be influenced by FSS in two ways: either the cell cycle will be arrested due to mechanical force [19] or certain cellular process will be activated resulting in migration of CTC and invasion of other organs [20]. It has been reported that high levels of FSS (~60 dyn/cm^2) can induce apoptosis and eliminate 90% of cancer cells from the blood stream [21]. This elimination and cell death have been related to destruction of the cell's cytoskeleton due to high shear, thus preventing cell adhesion. Furthermore, at high shear rate, cells produce more reactive oxygen species, resulting in cell death due to oxidative stress [22]. On the other hand, low FSS (2 dyn/cm^2) can activate certain mechanosensitive cytokines such as IGF-2, VEGF, ROCK, and Cav-1. This activation prompts their downstream molecular pathways which induce metastasis [23].

2.2. Shear Stress Due to Interstitial Fluid Flow

Molecular diffusion and convection are the basic mechanism of biological mass transport. In molecular diffusion, random molecular movements lead to net transport of solutes or particles down the gradient in concentration. During convection, a solute or particle is carried by moving fluid.

In a region where a fluid (for example, blood or interstitial fluid) is flowing, diffusive and convective transport can occur simultaneously [24].

In normal tissue, the way that cells get their nutrition is by diffusion of the blood plasma to the stromal space between the cells, which is also known as the interstitial space. The cells excrete their wastes by diffusion of waste products to the nearby lymphatics that drain them to the venous blood stream [25] (Figure 1). In normal situations, the flow of interstitial fluid is only maintained by the diffusion of nutrients from the blood stream to the interstitial space, and waste products from the cells to the interstitial space, and then to the lymphatic vessels. This mechanism prevents excessive fluid accumulation in interstitial site. However, the situation is different in the cancer microenvironment. As cancer cells keep growing, it becomes difficult for them to support a good waste drainage. Furthermore, tumor endothelial cells proliferate fast due to production of vascular endothelial growth factor (VEGF) by tumor cells. However, they form less tight junctions than endothelial cells in normal tissue, causing leaky endothelial cell junctions and hyperpermeability [26]. Therefore, although the fluid will be absorbed from the blood vessels, it will not be drained back to the venous system. This fluid accumulation will cause pressure difference between cancer microenvironment and healthy tissue, resulting in fluid flow from tumor to its surroundings [25]. The flow of interstitial fluid was shown to induce shear stresses on the cancer cells within the localized tumor [27] with a shear stress level of 0.1 dyn/cm^2 [13]. Interstitial flow has much slower velocity than blood flow. The interstitial flow velocity ranges from 0.1–4 um/s compared to blood flow at 0.6–0.9 m/s in pulmonary artery [28]. Table 1 represents levels of FSS in the body and Figure 2 shows different types of FSS that cancer cells are exposed to.

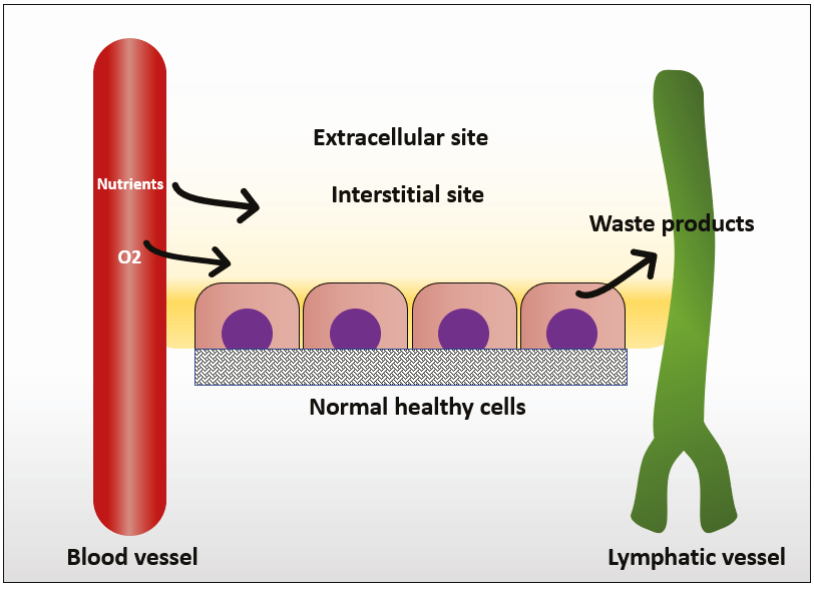

Figure 1. Mechanism in which normal cells get their nutrients and excrete their wastes.

Table 1. Different shear rate values in physiological and pathological conditions.

Fluid Flow	Shear Stress (Dyn/cm^2)	Reference
Interstitial flow	0.1	[13]
Normal vein	1–6	[29]
Normal artery	10–70	[29]
Lymphatic fluid flow	0.64	[14]
Liver	0.1–0.5	[30]
Peritoneal fluid flow	<5	[15]

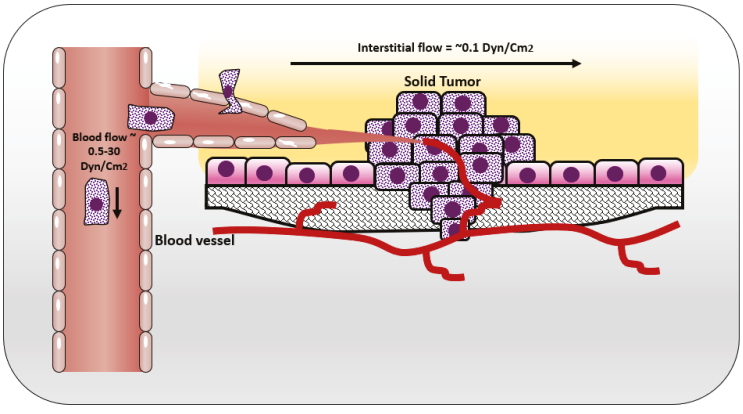

Figure 2. Shear stresses experienced by cells in solid tumor and circulating tumor cells.

2.3. Important Aspects for the Development of Nanomedicine for Targeted Cancer Therapy

One important aspect to consider is the mode of transport of drugs to cancer tumor, which is combination of convection and diffusion. Once infused, anti-cancer agent is transported in the systemic circulation via convection. Upon reaching to microcirculation, exchange occurs between blood and tissue. Here, drug passes through vessel walls toward cancer cells by combination of convection and diffusion in interstitial fluid. For low molecular mass drugs and small nanoparticles, diffusion is the dominant transport mechanism [31].

For efficient targeted anti-cancer therapy using nanoparticles, the tumor microenvironment should be considered during the design process. Ideally, nanomaterials, i.e., nanoparticles, or photothermal nano-agents should be tested on pre-clinical animal models of cancer therapy. However, using animal models is limited by ethical guidelines, also it is time and labor intensive [32]. To avoid the uncritical testing on animals, in-vitro and in-silico testing are used as preliminary evaluation due to their low cost, simplicity and better control on experimental conditions. In silico simulations are developed to analyze nanoparticle/cancer cell interactions by solving governing physical equations. These computational models provide quantitative analyses to describe biological mechanisms under certain conditions. However, in most situations, in-vitro experiments should be designed to verify in-silico test results [33]. For example, using a combination of in-vitro flow chamber set up and in-silico simulations, Boso et al. showed that artificial neural networks can determine the optimal nanoparticle size for maximal adherence to a targeted tissue. This optimal size depends on the wall shear rate in the target location [34]. The results suggested that the number of in-vitro experiments can be successfully reduced by using artificial neural networks, without compromising the accuracy of the study.

One of the major limitations for the in vitro approach is the discrepancies compared to in-vivo systems. The reason for these discrepancies is related to the fact that cells in the body are influenced

by many factors in their native environment. For example, FSS is one important factor affecting cell behavior. Therefore, static cell cultures are limited to mimicking the native cancer environment. To resemble the real conditions in organized system, FSS can be induced to static cell culture by using microfluidic devices [35]. FSS is the force experienced by cells as a result of flow of viscous fluids [17]. FSS can be applied on cells using parallel plate flow chambers (PPFCs), cone plate chambers or microfluidic chambers. Different chambers are used based on the site where FSS is intended to be mimicked. For example, cone-plate chambers are used to mimic FSS in abdominal aorta and brachial artery due to resemblance of their geometry [36], whereas parallel plate or microfluidic chambers are used to mimick FSS in smaller vessels.

PPFC were commonly used to mimick FSS in cancer microenvironment since cancer cells in the body are constantly exposed to FSS by interstitial flow or blood flow. It was previously suggested that FSS is an important factor for nanoparticle internalization by cancer cells. Therefore, association of FSS and cellular uptake of some nanomaterials has been studied [37,38]. We will explain this in detail in the following section. One of the first PPFCs was developed in 1995 by Ruel et al. [39]. A typical PPFC would have an inlet port and an outlet port for flow perfusion, silicon gaskets to form the flow chamber, and a coverslip where cells are grown on (Figure 4).

These flow chambers are mostly connected to syringe or peristaltic pumps that can pump a certain fluid (mostly cell media) at specific flow rates for extended flow perfusion. Shear stress can be calculated using Hagen–Poiseuille equation assuming Newtonian fluids under steady and laminar flows.

$$\tau = \frac{6.\mu.Q}{w.h^2}$$

where Q represents the fluid flow rate, τ is the shear stress acting on the cells, w and h are width and height of the flow chamber, and μ is the viscosity of the fluid, which is the cell medium [40]. Figure 4 illustrates a typical chamber setup representing the flow of the fluid in a closed circuit.

PPFCs offer a model that is not as simple as static cell culture, but not as complex as animal models; thus, cellular interactions and nanomaterials uptake can be studied in a practical and reliant manner as represented in Figure 3 [41].

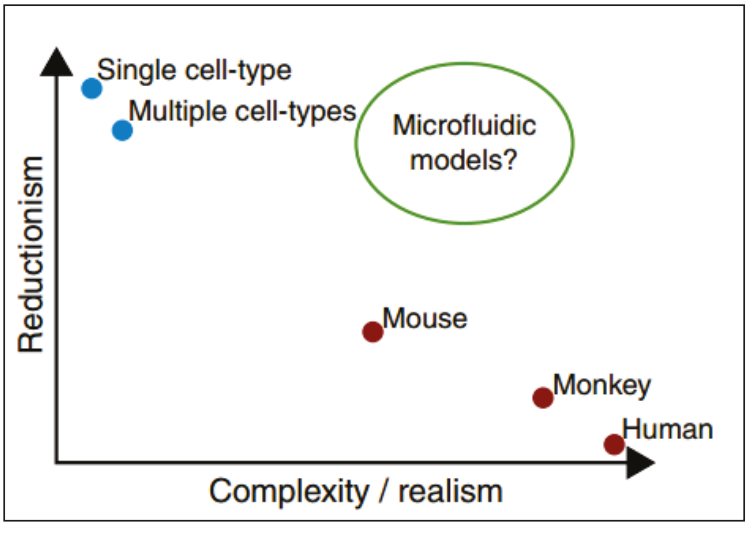

Figure 3. Microfluidic devices as models in which they provide conditions similar to in-vivo animal models and in-vivo models still retaining the simplicity of in-vitro testing. Adapted from Björnmalm et al. [41].

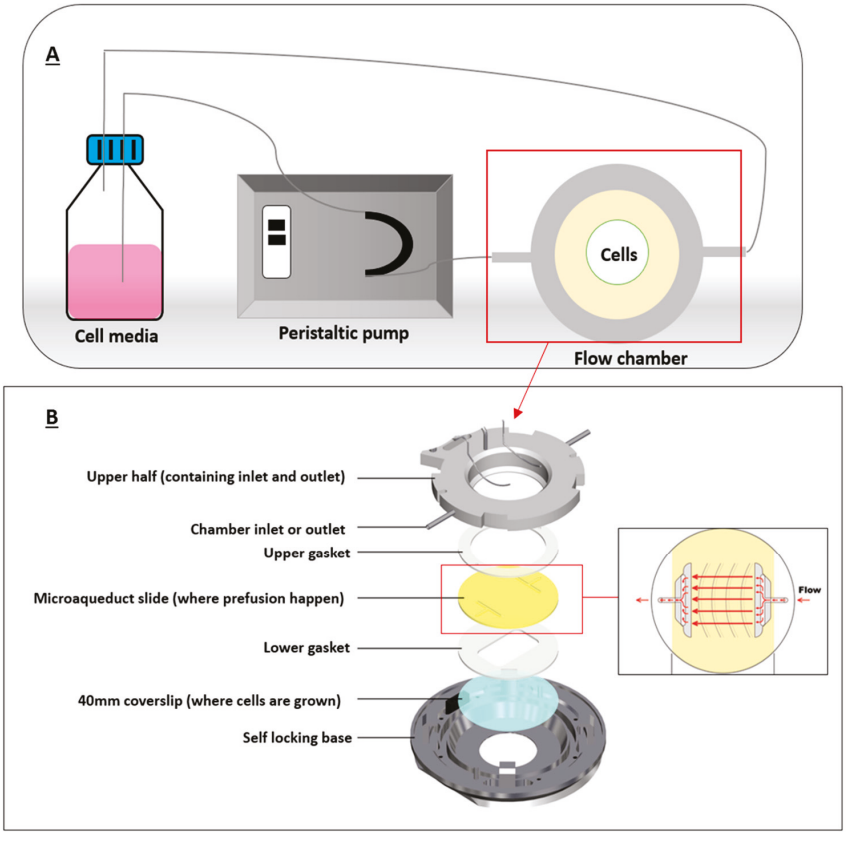

Figure 4. A typical flow chamber setup. (**A**) depicts a closed-circuit chamber, in which the chamber is connected to a peristaltic pump and a reservoir (cell media). (**B**) illustrates the flow chamber assembly where coverslip containing the cells is allowed for fluid flow. Adapted from bioptechs [42].

3. Interactions between Nanoparticles and Cancer Cells

Nanomaterials interact with cells differently in static and dynamic cultures. These differences include production of reactive oxygen species (ROS) [43] as well as the viability and uptake of the nanomaterials by cells [44]. Dynamic culture is more relevant to physiological conditions present in an animal or human body, as the biological systems are more complex and dynamic. Usually, it is easier to study the influence of nanomaterials using static cultures, but the results from such studies might be misleading and/or contradictory when compared to animal models or dynamic cultures. For example, nanomaterials tend to sediment and settle down in static cultures, inducing stresses on cells. Furthermore, nanomaterials form aggregates in static cultures, which might alter their uptake by the cells, and therefore, altering the viability of the results explained in Figure 5 [43].

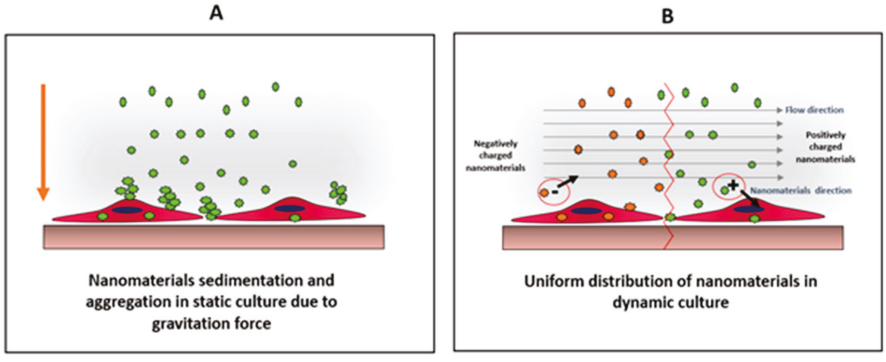

Figure 5. Comparison between distributions of nanomaterials under static (**A**) and dynamic (**B**) conditions. In static culture, nanoparticles tend to sediment and aggregate due to their high surface energy. This condition create physiochemical stress on cells, which might alter cells viability as well as particles uptake On the other hand, in dynamic culture, the particles will be uniformly distributed allowing better cellular interaction, which can be charge-dependent as the direction of the negatively-charged particles will be away from the cell surface, unlike positively-charged particles, where the particle direction will be towards the cell surface. Adapted from Mahto et al. [43].

When nanomaterials form aggregates, the aggregate size should be much smaller than the cell size for uptake. There are different mechanisms by which cells uptake nanomaterials. These include diffusion or passive penetration through the plasma membrane, and endocytosis that involves pinocytosis and phagocytosis. Pinocytosis involves the internalization of molecules or fluid by the formation of small vesicles, whereas phagocytosis involves the engulfment of large materials by the formation of intracellular phagosomes [45]. It was reported that the uptake of nanomaterials is size-dependent, and in some cases, it is easier for the cells to uptake larger nanomaterials by endocytosis, than smaller nanomaterials by diffusion [46]. Moreover, the formation of aggregates and sedimentation of nanomaterials will alter the effective concentration of nanomaterials delivered to the cells [47]. Therefore, nanoparticle aggregation should be prevented in most cases for nanoparticle studies. To uniformly distribute the nanomaterials over cells in culture without aggregate formation or sedimentation, it is suggested to use dynamic culture, and grow the cells under flow conditions using flow chambers [35].

It was reported that the uptake of nanomaterials is different under flow conditions compared to static cultures and that these changes are due to material's surface charge, surface ligands, stiffness, size and shape [48]. Cells can uptake nanomaterials in two steps: the first step is binding of the nanomaterial to cell surface and the second step is internalization of the nanoparticles. In the first step, electrostatic interactions, which are due to the physio-chemical properties of the nanomaterial, play an important role. As the cell membrane is negatively charged, it is more favorable for positively charged materials to interact with its surface than neutral or negatively charged particles. The second step is the internalization of the nanoparticle from the cell membrane. After nanomaterials interact and bind to the cell surface by electrostatic interactions, they can then be internalized by different uptake mechanisms [49]. Although surface charge is considered as an important contributor to higher uptake, other parameters influence the cellular uptake as well, such as elasticity [50] and the shape of the material especially under flow conditions [51]. Under flow conditions, the alignment of non-spherical nanomaterials can be different from that in static culture, thus altering the uptake. It has been reported that fibrous or 2D materials have a flow-aligning effect, which impacts their cellular adhesion and uptake [41], as demonstrated in Figure 6.

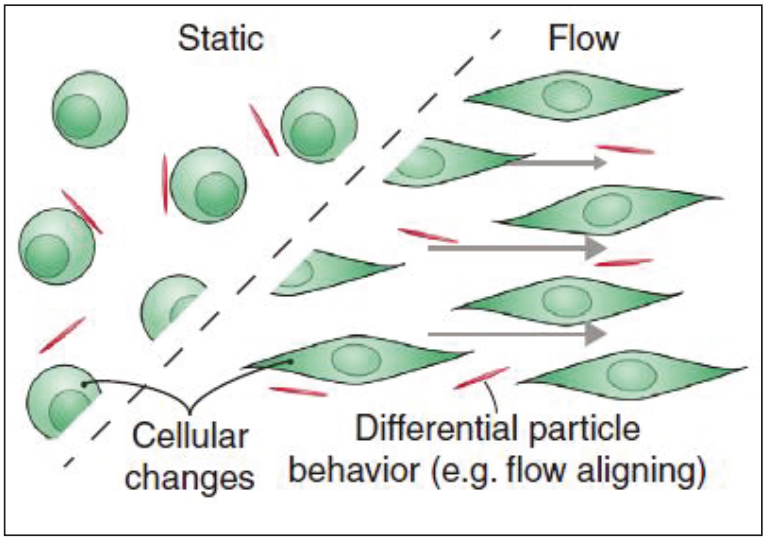

Figure 6. Filamentations or 2D nanomaterials align differently when there is fluid flow in cancer microenvironment. This flow-aligning effect can change the way that the cells interact with nanoparticles thus their cellular uptake would be influenced. Adapted from Björnmalm et al. [41].

4. Shear Stresses and Cellular Uptake of Nanomaterials for Cancer and Normal Cells

Owing to the effect of the dynamic environment in different biological processes, tissue engineering, and drug-delivery [52,53], many studies have investigated the role of FSS in the interactions between cells and nanoparticles [54–56]. One of these significant interactions is the cellular uptake of nanoparticles. To illustrate this, the uptake of the applied nanomaterials by cells is considered an important aspect, especially in drug-delivery and other therapeutic purposes, which require sufficient uptake by the targeted tissue. One important factor playing a role in cell-nanomaterial interaction under flow is the surface e charge of the nanoparticles. For instance, the interaction of endothelial cells with two negatively charged nanoparticles has been scrutinized by Samuel et al. by the application of varying levels of FSS on cells [57]. The authors revealed that, the cellular uptake increased under low shear stresses (0.05 Pa) compared to high shear stresses (0.5 Pa). In static conditions (0 Pa), cellular uptake was lower compared to low shear stress (0.05). The higher uptake of these particles under stress was mainly attributed to the formation of cytoskeletal stress fibers and membrane ruffles, which enhance endocytosis. Such changes in the cytoskeleton were not observed in the non-shear exposed cells. Additionally, Rigau and Städler correlated between the uptake of nano-sized drug delivery systems and the subsequent therapeutic effect using skeletal mouse myoblast cell model (C2C12) in the absence or presence of FSS [58]. They concluded that, the liposomes with positively charged lipids result in higher cellular interaction in the presence of shear, in contrast to those contained negatively charged lipids or zwitterionic ones. Furthermore, the authors investigated the therapeutic effect, in terms of cell viability, after treatment with the positively charged liposomes carrying a small cytotoxic molecule in static and dynamic conditions. Their findings stated that, there was a higher therapeutic response (i.e., higher cell mortality) in the case of dynamic conditions, which demonstrates the relationship between the higher cellular association of positive carriers and more effective therapy in the presence of shear. In another relevant study by Rinkenauer et al., authors investigated the effect of FSS on the uptake of co-polymers (negatively charged PMMA -co-PMAA with different ratios of MAA (3%, 5%, 8%, and 13%) and positively charged PMMA-co-PDMAEMA with 20% PDMAEMA) using different cell lines (HUVEC, HEK293, L929, and primary muscle cells). They found that, increasing the negative

charge (MMA) increases the uptake by different cells under static conditions. However, the uptake is not as efficient as that resulting from the use of positive particles (20 % PDMAEMA). A similar trend was observed in different cell lines, but not in co-culture which reduced the cellular uptake due to cellular interactions. When the uptake was assessed under flow conditions (0.7, 3, 6, and 10 Dyn/cm^2), it was observed that, increasing shear stress is positively correlated with cellular uptake. Nevertheless, compared to static culture, 13% PMMA showed more efficient uptake compared to positively charged 20% PDMAEMA. This is probably related to the differences in surface receptor patterns observed under flow conditions, which can alter the cellular uptake [38]. In our group, we are developing two-dimensional Mxene sheets as photothermal agents. Our initial findings show successful uptake on MXene sheets by MDA 231 breast cancer cells. When we compared static and dynamic cultures, we did not see any significant difference.

Another important aspect in cell-nanoparticle interaction is the surface modification. Toe et al. studied the cell response to modified liposomes with and without FSS using two cell lines. The former cell line was the immortalized skeletal mouse myoblast (C2C12), a tumor cell model, which is important to estimate the activity of the applied liposomes as drug carriers in drug delivery systems. The later cell model was hepatic cells (HepG2), which was chosen as a model for hepatic clearance due to their importance in eliminating drug-loaded nanocarriers from the body. To illustrate, the authors fabricated PEGylated poly (dopamine) coated liposomes and quantified their cellular uptake by myoblasts and hepatocytes using flow cytometry in both static and dynamic conditions. The results manifested that the hepatocytes response in the dynamic conditions was significantly higher after only 30 minutes, while the myoblasts demonstrated a significant increase after a relatively longer time (4 h). The authors explained these findings as the nature of the two cell lines were different. The hepatic cells were concerned with clearance, so their responses were instantaneous in the presence of physiological shear. On the other hand, the cancer cell model needed a longer time to show a response in low shear stress (0.146 dyn/cm^2) [59]. Additionally, the uptake of lipidic NPs by MCF-7 breast cancer cells and Hela human cervical cancer cells was reported by Palchetti et al., under flow conditions. Authors produced two types of lipidic NPs, one with surface modification (PEGylated) while the other without modification. They incubated the cells with particles at two different incubation durations (5 and 90 minutes). MCF-7 cells showed a significantly lower uptake of unmodified NPs in dynamic culture in comparison to static condition at both incubation durations, whereas Hela cells showed a higher NPs cellular uptake after 90 minutes incubation in dynamic culture [53]. On the other hand, an insignificant difference in uptake of modified NPs by MCF-7 was observed under flow and static conditions. However, NPs uptake by Hela cells in dynamic conditions was still higher than static culture. They clarified that shear stress can affect the protein corona (protein corona is formed when NPs absorb biomolecules as they interact with cells and the biological system) by changing its surface chemistry and properties, which in turn affect their uptake by cells [60].

Particle elasticity is suggested to affect cellular uptake [61,62]. In a very important investigation, Guo et al. revealed experimental evidence that indicates how elasticity alters in-vitro cellular uptake and in-vivo tumor uptake [50] They studied uptake of nanolipogels (NLGs) which consist of lipid bilayer capsule and hydrogel core with tunable elasticity. The elasticity of NLGs could be modulated independent from other physical properties such as size, shape and surface charge. Both normal cells and cancer cells showed higher uptake of soft NLGs (NLP-45KPa) compared to rigid NLGs (NLG-19MPa). Authors explained the higher uptake of soft particles by usage of different cell internalization pathways. While NLP-45KPa entered the cells through fusion and endocytosis, NLG-19MPa was internalized by only endocytosis (Figure 7). Fusion requires low energy compared to endocytosis. Therefore, cells take more time and energy to uptake the same amount of NLG-19MPa than NLP-45KPa. The in-vivo test results showed that particles with higher elasticity were more likely to accumulate into tumors. This is strong evidence that particle stiffness controls the tumor uptake of systematically applied nanoparticles.

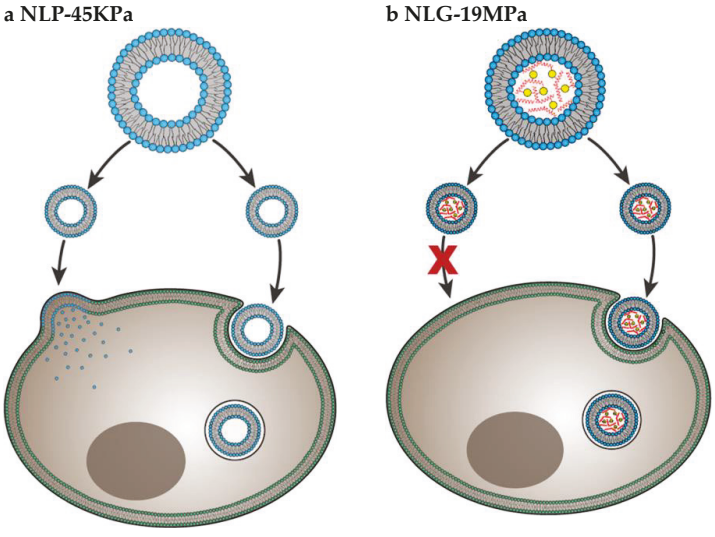

Figure 7. Cell internalization pathways of particles with different elasticity. Soft NLP-45KPa (**a**) enters the cell via two pathways: fusion and endocytosis. Hard NLG-19MPa (**b**) enters cell via only endocytosis. Adapted from Guo et al. [50].

Surface ligand is another aspect that affects cellular intake. Several studies were conducted on selective tumor targeting in order to eradicate tumor cells without harming normal body cells. The experiments were based on decorating nanoparticles with molecular recognition ligands that bind to selective proteins expressed on the surface of cancer cells. Engelberg et al. studied the internalization of quantum dots (QDs) decorated with S15-APT ligand into human non-small cell lung cancer A549 cells [63,64]. S15-APTs is a selective targeting moiety for uptake by A549 cells. These APT-decorated QDs bound themselves selectively to the target A549 cells and were internalized by them. However, they were neither bound to, nor were internalized by normal human bronchial epithelial BEAS2B, cervical carcinoma (HeLa), and colon adenocarcinoma CaCo-2 cells, thereby demonstrating high specificity. The shape and size of the particle is known to affect the uptake as well. Particle shape- and size-dependent uptake under physiological shear stress was reported by Jurney et al. They produced negatively charged rod-shaped PEG NPs with different aspect ratios and assessed their uptake by human umbilical vein endothelial cells (HUVEC) under flow conditions at different incubation durations (1, 12, and 24 hours). In all cases, the uptake of larger particles was found to be higher than smaller ones under flow in comparison to static culture. In contrast, smaller particles are internalized more in static conditions than in flow conditions. The trend of larger NPs being internalized more under flow conditions is contradictory with what was reported in literature with similar-sized spherical NPs. This indicates that particles with higher aspect ratios interact more with cells under flow conditions [65].

Moreover, Klingberg and Oddershede studied the effect of FSS on the uptake of spherical 80 nm gold nanoparticles (Au NPs) by HUVEC [66]. They categorized the cells into two groups, one group was cultured in static conditions for 24 hours (non-adapted group), while the other group was cultured for 24 hours under 10 dyn/cm^2 shear stress (shear adapted group). Then, each group was either kept in static culture for three hours in the presence of 5 μg/mL Au NPs or kept in dynamic culture for three hours in presence of 5 μg/mL Au NPs. The highest uptake was achieved by non-adapted group with three hours additional static culture and lowest uptake was realized by the shear adapted group with three hours additional dynamic culture. [66]. One more study was conducted by Fede et al. to reveal the effect of FSS and size of spherical citrate stabilized gold nanoparticles on HUVEC [32]. They tested two

batches of gold NPs (Batch 24 nm and Batch 13 nm). It was observed that, the viability is significantly more when testing gold NPs under flow conditions in comparison to static culture, regardless of NPs size or concentration. They measured the NPs concentration in two methods, one based on the surface area per unit volume, while the other based on the number of NPs per unit volume. They found that the cells were less viable when the surface area was increased per unit volume irrespective of the NPs size [32]. Yazdimamaghani et al. studied the effect of silica NPs density and flow conditions on cell cytotoxicity, uptake and sedimentation. They produced four types of silica NPs with different densities and surface charges and tested the cytotoxicity and uptake on RAW 264.7 macrophage cells after 24 hours of incubation with the cells, in static or under flow conditions. They found that the cell viability is enhanced under flow conditions, compared to static culture. Moreover, none of the four particles showed a toxic effect on macrophage cells up to 250 μg/mL in dynamic conditions. Also, particle sedimentation was reduced in dynamic conditions, and the distribution of particles was more homogeneous. Authors also found that, cellular uptake of silica NPs was more in static conditions compared to dynamic conditions. Furthermore, low density particles, showed lower uptake under flow conditions compared to high density particles [67].

Finally, application of different FSS levels is considered as an important parameter for detailed investigation of the effect of dynamic conditions on cellular responses, where the cellular uptake could be studied as a consequence of all applied FSS levels. Hence, more relevant correlation between the cell response and FSS levels can be stated. For instance, Kona and co-workers developed a novel drug delivery system that imitates the natural platelet adhesion to the injured vascular walls under different shear flow rates [68]. Their results implied that when the shear stress level was increased to 20dyn/cm^2, the cellular uptake fell dramatically by three folds when compared to the control static group. The authors explained their findings through computational model revealing that the high shear rates induce huge dislodging forces that are able to detach the adhered particles [69,70]. Table 2 summarizes important works on the effect of FSS nanoparticle internalization.

Table 2. Summary of findings on nanoparticle—cell interactions under shear stress.

Type & Properties of Nanomaterial Applied	Type of Cells	Flow Conditions	Shear Rate	Findings	Ref.
Different polymer-based NPs	HUVEC	One-hour incubation under optimum conditions (37 °C, 95% air & 5% CO_2)	0.7, 3, 6, and 10 Dyn/cm^2	Increasing the negative charge increases the uptake under static conditions. Positively charged particles showed more efficient uptake in static culture compared to negatively charged particles. Increasing shear stress is positively correlated with cellular uptake.	[38]
PEGylated lipidic NPs. Un-PEGylated lipidic NPs	MCF-7 Hela cells	Incubated under optimum conditions for 5 or 90 minutes under flow speed of 50 cm/s		MCF-7 cells showed significantly lower uptake of un-PEGylated NPs in dynamic culture at both incubation durations. PEGylated NPs showed similar uptake by MCF-7 in dynamic culture and static culture. Hela cells showed a higher NPs cellular uptake after 90 minutes incubation in dynamic culture.	[60]
Negatively charged PEG NPs with different aspect ratios	HUVEC	1,12, and 24 hours of exposure to dynamic conditions using 0.907 uL/min flow rate.	10 Dyn/cm^2	Larger particles have higher internalization than smaller ones, under flow in comparison to static culture.	[65]
Silica NPs with different densities	RAW 264.7 macrophage cells	24-hour incubation under flow (cell media agitation) at optimum conditions.		More Uptake in static conditions compared to dynamic conditions. Low density particles have lower uptake in dynamic conditions compared to high density particles.	[67]
Negatively charged NPs	Endothelial cells	24-hour incubation under optimum conditions.	0.05, 0.1, and 0.5 Pa	cellular uptake increased with low shear stresses when compared to high shear.	[57]
Negative, Positive & Zwitterionic lipidic NPS	Skeletal mouse myoblast cell model (C2C12)		0.0146 and 0.146 Dyn/cm^2	Higher cellular interaction in the presence of shear for positively-charged NPs compared to negatively-charged lipids or zwitterionic ones.	[58]

5. Conclusions

Cancer is a wide spreading disease with no definitive treatment. Researchers have been working on cancer therapy for decades with some improvements, yet many limitations remain. Lately, nanomaterials are being used for various biomedical applications including the targeted anti-cancer therapy due to their superior properties. Usually, when nanomaterials are tested for biomedical applications, cell culture techniques are used for preliminary testing. Cell culture is the most convenient method to test the toxicity and efficacy of nanomaterials, but it is limited due to particle aggregation, sedimentation and it does not mimic the native conditions in animal model and human body. FSS is one important parameter that affect nanomaterial-cell interaction, mainly cell viability and particle uptake. FSS can be due to blood flow, with variable flow rates based on the diameter size of the blood vessel where it affects endothelial cells lining the blood vessels or the circulating tumor cells. FSS can be due to interstitial fluid flow as well with very low flow rate, which occurs mainly around cancer cells in solid tumors. Here we summarized findings on the relation between shear stress and nanomaterials uptake mainly for cancer as well as for normal cells using in-vitro systems. There are variety of factors affecting nanomaterials uptake particularly under dynamic conditions. Some of these factors are related to the nanomaterials, while other factors are cell related. Nanomaterial size, shape surface charge, surface ligands, and particle elasticity are the main factors in cellular uptake under fluid flow. However, these factors are affecting nanomaterial-cell interaction differently depending on the cell type (i.e., origin of tissue and cancer vs healthy). There is no general rule on how nanomaterials will interact with cells. However, in most of the cases, negatively charged particles show less uptake by cells due to inefficient electrostatic interactions between nanomaterials and cells. Furthermore, soft particles show more uptake than rigid particles which can be attributed to the ability of the cell to uptake soft particles by different pathways compared to rigid particles. Additionally, the uptake of 2D materials will be different under flow conditions due to the effect of flow aligninment. Coating the cell surface with ligands is an efficient way to guarantee the uptake of particles, at the same time reducing the side effects by preventing internalization by non-cancerous cells. Other factors that might affect cellular uptake, are cell related. For example, the cytoskeletal structure and the formation of membrane ruffles after flow, as well as, cell rigidity under dynamic culture. However, these details are not the main focus of this paper. Further investigations will shed light on optimal nanoparticle parameters that can be used as smart nanoparticles for anti-cancer therapies.

Funding: This research received no external funding.

Acknowledgments: This work was supported by Qatar University under High Impact-Fund ProgramGrant (QUHI-CAS-19/20-1). Authors would like to acknowledge Qatar University Graduate Research Assistantship program offered to Samar Haroon (QUST-1-CAS-2019-37). The publication of this article was funded by the Qatar National Library.

Conflicts of Interest: The authors declare no conflict of interest.

References

1. Di Mauro, M.; Esposito, S.; Naddeo, A. When Physics Meets Biology: A Less Known Feynman. *Transversal Int. J. Hist. Sci.* **2018**, *4*, 163. [CrossRef]
2. Conde, J. The Golden Age in Cancer Nanobiotechnology: Quo Vadis? *Front. Bioeng. Biotechnol.* **2015**, *3*, 1–4. [CrossRef] [PubMed]
3. Athulya, K.; Anitha, T. Recent Advances in Nano Biotechnology: A Review. *Int. J. Adv. Sci. Res.* **2017**, *2*, 15–17.
4. Hussein, E.A.; Zagho, M.M.; Nasrallah, G.K.; Elzatahry, A.A. Recent Advances in Functional Nanostructures as Cancer Photothermal Therapy. *Int. J. Nanomed.* **2018**, *13*, 2897–2906. [CrossRef]
5. Hejmadi, M. *Introduction to Cancer Biology*; Garland: New York, NY, USA; Prentice Hall Publishing: Upper Saddle River, NJ, USA, 2010.

6. Nyoung, D.; Hyeok, D.; Moon, H.; Bok, J.; Soo, M.; Cheon, S.; Jun, W.; Sun, I.; Keun, I. Biomaterials Gold Nanoparticles Surface-Functionalized with Paclitaxel Drug and Biotin Receptor as Theranostic Agents for Cancer Therapy. *Biomaterials* **2012**, *33*, 856–866. [CrossRef]
7. Kumar, A.; Ma, H.; Zhang, X.; Huang, K.; Jin, S.; Liu, J.; Wei, T.; Cao, W.; Zou, G.; Liang, X. Biomaterials Gold Nanoparticles Functionalized with Therapeutic and Targeted Peptides for Cancer Treatment. *Biomaterials* **2012**, *33*, 1180–1189. [CrossRef] [PubMed]
8. Binh, L.; Yoshitomi, T.; Matsui, H.; Nagasaki, Y. Biomaterials Development of an Oral Nanotherapeutics Using Redox Nanoparticles for Treatment of Colitis-Associated Colon Cancer. *Biomaterials* **2015**, *55*, 54–63. [CrossRef]
9. Yang, Y.; Lin, Y.; Di, D.; Zhang, X.; Wang, D.; Zhao, Q.; Wang, S. Gold Nanoparticle-Gated Mesoporous Silica as Redox-Triggered Drug Delivery for Chemo-Photothermal Synergistic Therapy. *J. Colloid Interface Sci.* **2017**. [CrossRef]
10. Buchanan, C.F.; Voigt, E.; Vlachos, P.P.; Nichole, M. SBC2013-14592 Tissue Engineered Tumor Microvessels to Study the Role of Flow. In Proceedings of the ASME 2013 Summer Bioengineering Conference, Sunriver, OR, USA, 26–29 June 2013; pp. 6–7.
11. Huo, S.; Liu, J.; Wei, T. Superior Penetration and Retention Behavior of 50 Nm Gold Nanoparticles in Tumors. *Am. Assoc. cancer Res.* **2012**. [CrossRef]
12. Zhao, M.; Liu, Q.; Gong, Y.; Xu, X.; Zhang, C.; Liu, X.; Zhang, C.; Guo, H.; Zhang, X.; Gong, Y.; et al. GSH-Dependent Antioxidant Defense Contributes to the Acclimation of Colon Cancer Cells to Acidic Microenvironment. *Cell Cycle* **2016**, *15*, 1125–1133. [CrossRef]
13. Kang, T.; Park, C.; Choi, J.; Cui, J.; Lee, B. Journal of Drug Delivery Science and Technology Effects of Shear Stress on the Cellular Distribution of Polystyrene Nanoparticles in a Biomimetic Micro Fl Uidic System. *J. Drug Deliv. Sci. Technol.* **2016**, *31*, 130–136. [CrossRef]
14. Huang, Q.; Hu, X.; He, W.; Zhao, Y.; Hao, S.; Wu, Q.; Li, S.; Zhang, S. Fluid Shear Stress and Tumor Metastasis. *Am. J. Cancer Res.* **2018**, *8*, 763–777. [PubMed]
15. Hyler, A.R.; Baudoin, N.C.; Brown, M.S.; Stremler, M.A.; Cimini, D.; Davalos, R.V.; Schmelz, E.M. Fluid Shear Stress Impacts Ovarian Cancer Cell Viability, Subcellular Organization, and Promotes Genomic Instability. *PLoS ONE* **2018**, e0194170. [CrossRef] [PubMed]
16. Labelle, M.; Hynes, R.O. The Initial Hours of Metastasis: The Importance of Cooperative Host-Tumor Cell Interactions during Hematogenous Dissemination. *Cancer Discov.* **2013**, *2*, 1091–1099. [CrossRef]
17. Krog, B.L.; Henry, M.D. *Biomechanics of the Circulating Tumor Cell Microenvironment*; Springer: New York, NY, USA, 2018.
18. Franziska, M.; Jan, L.; Mauro, F.; Jonathan, W. What does physics have to do with cancer? *Nat. Rev. Cancer* **2013**, *11*, 657–670. [CrossRef]
19. Fan, R.; Emery, T.; Zhang, Y.; Xia, Y.; Sun, J.; Wan, J. Circulatory Shear Flow Alters the Viability and Proliferation of Circulating Colon Cancer Cells. *Nat. Publ. Gr.* **2016**, 1–8. [CrossRef]
20. Lee, H.J.; Diaz, M.F.; Price, K.M.; Ozuna, J.A.; Zhang, S.; Sevick-muraca, E.M.; Hagan, J.P.; Wenzel, P.L. Fluid Shear Stress Activates YAP1 to Promote Cancer Cell Motility. *Nat. Commun.* **2017**. [CrossRef]
21. Regmi, S.; Fu, A.; Luo, K.Q. High Shear Stresses under Exercise Condition Destroy Circulating Tumor Cells in a Microfluidic System. *Nat. Publ. Gr.* **2017**, 1–12. [CrossRef]
22. Fu, A.; Ma, S.; Wei, N.; Tan, B.X.X.; Tan, E.Y.; Luo, K.Q. High Expression of MnSOD Promotes Survival of Circulating Breast Cancer Cells and Increases Their Resistance to Doxorubicin. *Oncotarget* **2016**, *7*. [CrossRef]
23. Zhao, F.; Li, L.; Guan, L.; Yang, H.; Wu, C.; Liu, Y. Roles for GP IIb/IIIa and Avβ3 Integrins in MDA-MB-231 Cell Invasion and Shear Flow-Induced Cancer Cell Mechanotransduction. *Cancer Lett.* **2014**, *344*, 62–73. [CrossRef]
24. Dewhirst, M.W.; Secomb, T.W. Transport of Drugs from Blood Vessels to Tumour Tissue. *Nat. Publ. Gr.* **2017**, *17*, 738–750. [CrossRef]
25. Munson, J.M.; Shieh, A.C. Interstitial Fluid Flow in Cancer: Implications for Disease Progression and Treatment. *Cancer Manag. Res.* **2014**, 317–328. [CrossRef] [PubMed]
26. Ribatti, D.; Nico, B.; Crivellato, E.; Vacca, A. The Structure of the Vascular Network of Tumors. *Cancer Lett.* **2007**, *248*, 18–23. [CrossRef] [PubMed]
27. Yao, W.; Li, Y.; Ding, G. *Interstitial Fluid Flow: The Mechanical Environment of Cells and Foundation of Meridians*; Hindawi: London, UK, 2012. [CrossRef]

28. Bulwer, B.; Rivero, J. Echocardiography Pocket Guide: The Transthoracic Examination. In *Left Parasternal Views*; Jones and Bartlett Publishers: Burlington, MA, USA, 2011; pp. 95–194.
29. Malek, A.M.; Alper, S.L.; Izumo, S. Hemodynamic Shear Stress and Its Role. *J. Am. Med. Assoc.* **1999**, *282*, 2035–2042. [CrossRef] [PubMed]
30. Yu, D.; Li, N.; Yang, H.; Luo, C.; Gong, Y.; Tong, C.; Gao, Y.; lv, S.; Long, M. Mimicking Liver Sinusoidal Structures and Functions Using a 3D-Configured Microfluidic Chip. *R. Soc. Chem.* **2017**. [CrossRef]
31. Swabb, E.A.; Wei, J.; Cullino, P.M. Diffusion and Convection in Normal and Neoplastic Tissues1. *Am. Assoc. Cancer Res.* **1974**, *34*, 2814–2822.
32. Fede, C.; Albertin, G.; Petrelli, L.; De Caro, R.; Fortunati, I.; Weber, V.; Weber, V.; Ferrante, C. Influence of Shear Stress and Size on Viability of Endothelial Cells Exposed to Gold Nanoparticles. *J. Nanopaer. Res.* **2017**. [CrossRef]
33. Mascheroni, P.; Schrefler, B.A. In Silico Models for Nanomedicine: Recent Developments. *Curr. Med. Chem.* **2018**, 4192–4207. [CrossRef]
34. Lee, S.; Decuzzi, P. Optimizing Particle Size for Targeting Diseased Microvasculature: From Experiments to Artificial Neural Networks. *Int. J. Nanomed.* **2011**, 1517–1526. [CrossRef]
35. Mahto, S.K.; Charwat, V.; Ertl, P.; Rothen-rutishauser, B.; Rhee, S.W. Microfluidic Platforms for Advanced Risk Assessments of Nanomaterials. *Nanotoxicology* **2014**, *5390*, 1–15. [CrossRef]
36. Wang, Y.X.; Xiang, C.; Liu, B.; Zhu, Y.; Luan, Y.; Liu, S.T.; Qin, K.R. A Multi—Component Parallel—Plate Flow Chamber System for Studying the Effect of Exercise - Induced Wall Shear Stress on Endothelial Cells. *Biomed. Eng. Online* **2016**, *15*, 659–672. [CrossRef] [PubMed]
37. Han, J.; Shuvaev, V.V.; Davies, P.F.; Eckmann, D.M.; Muro, S.; Muzykantov, V.R. Flow Shear Stress Differentially Regulates Endothelial Uptake of Nanocarriers Targeted to Distinct Epitopes of PECAM-1. *J. Control. Release* **2015**, *210*, 39–47. [CrossRef] [PubMed]
38. Rinkenauer, A.C.; Press, A.T.; Raasch, M.; Pietsch, C.; Schweizer, S.; Schwörer, S.; Rudolph, K.L.; Mosig, A.; Bauer, M.; Traeger, A.; et al. Comparison of the Uptake of Methacrylate-Based Nanoparticles in Static and Dynamic in Vitro Systems as Well as in Vivo. *J. Control. Release* **2015**, *216*, 158–168. [CrossRef] [PubMed]
39. Ruel, J.; Lemay, J.; Dumas, G.; Doillon, C.; Charara, J. Development of Parallel Plate Flow Chamber for Studying Cell Behavior under Pulstile Flow. *ASAIO J.* **1995**, *41*, 876–883. [CrossRef]
40. Lane, W.O.; Jantzen, A.E.; Carlon, T.A.; Jamiolkowski, R.M.; Grenet, J.E.; Ley, M.M.; Haseltine, J.M.; Galinat, J.; Lin, F.; Allen, J.D.; et al. Parallel-Plate Flow Chamber and Continuous Flow Circuit to Evaluate Endothelial Progenitor Cells under Laminar Flow Shear Stress. *JoVE* **2012**, 1–11. [CrossRef] [PubMed]
41. Björnmalm, M.; Yan, Y.; Caruso, F. Engineering and Evaluating Drug Delivery Particles in Microfluidic Devices. *J. Control. Release* **2014**. [CrossRef]
42. Bioptechs. Available online: http://www.bioptechs.com/product/fcs2-system/ (accessed on 14 June 2019).
43. Mahto, S.K.; Yoon, T.H.; Rhee, S.W. A New Perspective on in Vitro Assessment Method for Evaluating Quantum Dot Toxicity by Using Microfluidics. *Biomicrofluidics* **2010**, 1–8. [CrossRef]
44. Huefner, A.; Septiadi, D.; Wilts, B.D.; Patel, I.I.; Kuan, W.; Fragniere, A.; Barker, R.A.; Mahajan, S. Gold Nanoparticles Explore Cells: Cellular Uptake and Their Use as Intracellular Probes. *Methods* **2014**, *68*, 354–363. [CrossRef]
45. Salatin, S.; Yari Khosroushahi, A. Overviews on the Cellular Uptake Mechanism of Polysaccharide Colloidal Nanoparticles. *J. Cell. Mol. Med.* **2017**, *21*, 1668–1686. [CrossRef]
46. Mustafa, T.; Watanabe, F.; Monroe, W.; Mahmood, M.; Xu, Y.; Saeed, L.M.; Karmakar, A. Impact of Gold Nanoparticle Concentration on Their Cellular Uptake by MC3T3-E1 Mouse Osteoblastic Cells as Analyzed by Transmission Electron Microscopy. *J. Nanomed. Nanotechnol.* **2011**, *2*. [CrossRef]
47. Ek, P.K.; Jansman, M.M.T.; Wohl, B.M. Interaction between Drug Delivery Vehicles and Cells under the Effect of Shear Stress. *J. Biomicrofludics* **2015**, *9*, 052605. [CrossRef]
48. Thurn, K.T.; Thurn, K.T.; Brown, Æ.E.M.B.; Wu, Æ.A.; Vogt, Æ.S.; Jo, B.L.Æ. Nanoparticles for Applications in Cellular Imaging Nanoparticles for Applications in Cellular Imaging. *J. Nanoscale Res. Lett.* **2007**. [CrossRef] [PubMed]
49. Forest, V.; Cottier, M.; Pourchez, J. Electrostatic Interactions Favor the Binding of Positive Nanoparticles on Cells: A Reductive Theory. *Nano Today* **2015**, *10*, 677–680. [CrossRef]
50. Guo, P.; Liu, D.; Subramanyam, K.; Wang, B.; Auguste, D.T.; Moses, M.A. Nanoparticle Elasticity Directs Tumor Uptake. *Nat. Commun.* **2018**, 1–9. [CrossRef]

51. Geng, Y.A.N.; Dalhaimer, P.; Cai, S.; Tsai, R.; Minko, T.; Discher, D.E. Shape effects of filaments versus spherical particles in flow and drug delivery. *Nat. Nanotechnol.* **2009**, *2*, 249–255. [CrossRef]
52. Chachisvilis, M.; Zhang, Y.-L.; Frangos, J.A. G Protein-Coupled Receptors Sense Fluid Shear Stress in Endothelial Cells. *Proc. Natl. Acad. Sci. USA* **2006**, *103*, 15463–15468. [CrossRef]
53. Holme, M.N.; Fedotenko, I.A.; Abegg, D.; Althaus, J.; Babel, L.; Favarger, F.; Reiter, R.; Tanasescu, R.; Zaffalon, P.-L.; Ziegler, A.; et al. Shear-Stress Sensitive Lenticular Vesicles for Targeted Drug Delivery. *Nat. Nanotechnol.* **2012**, *7*, 536. [CrossRef]
54. Korin, N.; Kanapathipillai, M.; Matthews, B.D.; Crescente, M.; Brill, A.; Mammoto, T.; Ghosh, K.; Jurek, S.; Bencherif, S.A.; Bhatta, D.; et al. Shear-Activated Nanotherapeutics for Drug Targeting to Obstructed Blood Vessels. *Science* **2012**, *337*, 738–742. [CrossRef]
55. Kim, D.; Lin, Y.; Haynes, C.L. On-Chip Evaluation of Shear Stress Effect on Cytotoxicity of Mesoporous Silica Nanoparticles. *Anal. Chem.* **2011**, 8377–8382. [CrossRef]
56. Han, J.; Zern, B.J.; Shuvaev, V.V.; Davies, P.F.; Muro, S.; Muzykantov, V. Acute and Chronic Shear Stress Differently Regulate Endothelial Internalization of Nanocarriers Targeted to Platelet-Endothelial Cell Adhesion Molecule-1. *ACS Nano* **2012**, *6*, 8824–8836. [CrossRef]
57. Samuel, S.P.; Jain, N.; Dowd, F.O.; Paul, T.; Gerard, V.A.; Gun, Y.K.; Prina-mello, A. Multifactorial Determinants That Govern Nanoparticle Uptake by Human Endothelial Cells under Flow. *Int. J. Nanomed.* **2012**, 2943–2956. [CrossRef]
58. Hosta-Rigau, L.; Städler, B. Shear Stress and Its Effect on the Interaction of Myoblast Cells with Nanosized Drug Delivery Vehicles. *Mol. Pharm.* **2013**, *10*, 2707–2712. [CrossRef] [PubMed]
59. Teo, B.M.; van der Westen, R.; Hosta-Rigau, L.; Städler, B. Cell Response to PEGylated Poly(Dopamine) Coated Liposomes Considering Shear Stress. *Biochim. Biophys. Acta Gen. Subj.* **2013**, *1830*, 4838–4847. [CrossRef] [PubMed]
60. Palchetti, S.; Pozzi, D.; Laura, A.; La, G.; Zenezini, R.; Digiacomo, L.; Peruzzi, G.; Caracciolo, G.; Laganà, A. Colloids and Surfaces B: Biointerfaces Influence of Dynamic Flow Environment on Nanoparticle-Protein Corona: From Protein Patterns to Uptake in Cancer Cells. *Colloids Surfaces B Biointerfaces* **2017**, *153*, 263–271. [CrossRef] [PubMed]
61. Liu, W.; Zhou, X.; Mao, Z.; Yu, D.; Wang, B.; Gao, C. Uptake of Hydrogel Particles with Different Stiffness and Its Influence On. *Soft Matter* **2012**, 9235–9245. [CrossRef]
62. Circulation, T.B.; Anselmo, A.C.; Zhang, M.; Kumar, S.; Vogus, D.R.; Menegatti, S.; Helgeson, M.E.; Mitragotri, S. Elasticity of Nanoparticles In Fl Uences. *ACS Nano* **2015**, 3169–3177. [CrossRef]
63. Engelberg, S.; Modrejewski, J.; Walter, J.G.; Livney, Y.D.; Assaraf, Y.G. Cancer Cell-Selective, Clathrin-Mediated Endocytosis of Aptamer- Decorated Nanoparticles. *Oncotarget* **2018**, *9*, 20993–21006. [CrossRef]
64. Engelberg, S.; Netzer, E.; Assaraf, Y.G. Selective Eradication of Human Non-Small Cell Lung Cancer Cells Using Aptamer-Decorated Nanoparticles Harboring a Cytotoxic Drug Cargo. *Cell Death Dis.* **2019**. [CrossRef]
65. Jurney, P.; Agarwal, R.; Singh, V.; Choi, D.; Roy, K.; Sreenivasan, S.V.; Shi, L. Unique Size and Shape-Dependent Uptake Behaviors of Non-Spherical Nanoparticles by Endothelial Cells Due to a Shearing Fl Ow. *J. Control. Release* **2017**, *245*, 170–176. [CrossRef]
66. Klingberg, H.; Oddershede, L.B. The influence of Flow, Shear Stress and Adhesion Molecule Targeting on Gold Nanoparticle Uptake in Human Endothelial Cells. *Nanosacle* **2015**. [CrossRef]
67. Yazdimamaghani, M.; Barber, Z.B.; Moghaddam, S.P.H.; Ghandehari, H. In Fluence of Silica Nanoparticle Density and Flow Conditions on Sedimentation, Cell Uptake, and Cytotoxicity. *J. Mol. Pharm.* **2018**. [CrossRef] [PubMed]
68. Kona, S.; Dong, J.-F.; Liu, Y.; Tan, J.; Nguyen, K.T. Biodegradable Nanoparticles Mimicking Platelet Binding as a Targeted and Controlled Drug Delivery System. *Int. J. Pharm.* **2012**, *423*, 516–524. [CrossRef] [PubMed]
69. Blackwell, J.E.; Dagia, N.M.; Dickerson, J.B.; Berg, E.L.; Goetz, D.J. Ligand Coated Nanosphere Adhesion to E- and P-Selectin under Static and Flow Conditions. *Ann. Biomed. Eng.* **2001**, *29*, 523–533. [CrossRef]
70. Lin, A.; Sabnis, A.; Kona, S.; Nattama, S.; Patel, H.; Dong, J.; Nguyen, K.T.; Al, L.I.N.E.T. Shear-Regulated Uptake of Nanoparticles by Endothelial Cells and Development of Endothelial-Targeting Nanoparticles. *J. Biomed. Mater. Res. A* **2009**, *93*, 833–842. [CrossRef] [PubMed]

cancers

MDPI

Review

Riboflavin-Targeted Drug Delivery

Milita Darguzyte [1], Natascha Drude [1], Twan Lammers [1] and Fabian Kiessling [1,2,*]

[1] Institute for Experimental Molecular Imaging, University Hospital Aachen, Forckenbeckstrasse 55, 52074 Aachen, Germany; mdarguzyte@ukaachen.de (M.D.); Ndrude@ukaachen.de (N.D.); tlammers@ukaachen.de (T.L.)

[2] Fraunhofer MEVIS, Institute for Medical Image Computing, Forckenbeckstrasse 55, 52074 Aachen, Germany

* Correspondence: fkiessling@ukaachen.de

Received: 13 November 2019; Accepted: 25 January 2020; Published: 27 January 2020

Abstract: Active targeting can improve the retention of drugs and drug delivery systems in tumors, thereby enhancing their therapeutic efficacy. In this context, vitamin receptors that are overexpressed in many cancers are promising targets. In the last decade, attention and research were mainly centered on vitamin B9 (folate) targeting; however, the focus is slowly shifting towards vitamin B2 (riboflavin). Interestingly, while the riboflavin carrier protein was discovered in the 1960s, the three riboflavin transporters (RFVT 1-3) were only identified recently. It has been shown that riboflavin transporters and the riboflavin carrier protein are overexpressed in many tumor types, tumor stem cells, and the tumor neovasculature. Furthermore, a clinical study has demonstrated that tumor cells exhibit increased riboflavin metabolism as compared to normal cells. Moreover, riboflavin and its derivatives have been conjugated to ultrasmall iron oxide nanoparticles, polyethylene glycol polymers, dendrimers, and liposomes. These conjugates have shown a high affinity towards tumors in preclinical studies. This review article summarizes knowledge on RFVT expression in healthy and pathological tissues, discusses riboflavin internalization pathways, and provides an overview of RF-targeted diagnostics and therapeutics.

Keywords: riboflavin; vitamin B2; targeted drug delivery; active targeting; theranostics; nanomedicines; molecular imaging; nanoparticle

1. Introduction

Nanomedicines are nano-sized systems conjugated to anti-cancer drugs. Owing to their size, the nanoparticles accumulate more at the tumor site based on the enhanced permeability and retention (EPR) effect and are expected to show less side effects compared to conventional chemotherapeutics [1]. The EPR effect occurs due to the leaky vasculature and the poor venous and lymphatic drainage of tumors. Nanomedicines can be further functionalized to actively target tumors or their microenvironment. Active targeting can increase the uptake and retention of nanomedicines and, thus, the therapeutic efficacy [2]. The most common targeting moieties are antibodies as well as peptides, aptamers, and small molecules. However, due to their considerably large size, antibodies can significantly alter drug pharmacokinetics and are relatively expensive to produce [3]. Moreover, the coupling of antibodies to drug delivery systems is difficult to control, and their receptor affinities tend to decrease upon conjugation [4–6]. Thus, researchers are shifting their focus to small (targeting) molecules, such as vitamins. Among the vitamins, folate-receptors were the most commonly selected cancer targets, particularly for ovarian cancers [7–10]. However, in recent years, the vitamin B2 (riboflavin (RF)) internalization pathway has also been gaining attention since its carrier protein and three transporters have been identified to be highly overexpressed in several cancers. Therefore, this review article will summarize the current knowledge of the mechanisms of RF internalization and report on studies using this pathway for targeted cancer diagnostics and nanomedicines.

2. Riboflavin and Its Transport

RF is a water-soluble molecule that is important for oxidation-reduction reactions [11], protein folding [12], and normal immune function [13,14]. It also has antioxidant and anti-inflammatory properties [15,16]. RF acts as a precursor for flavin mononucleotide (FMN) and flavin adenine dinucleotide (FAD), which are involved in various redox reactions that regulate the metabolism of carbohydrates, amino acids, and lipids (Figure 1) [17]. RF is considered to be relatively nontoxic as an excess of it is excreted via kidneys. Humans do not synthesize RF; thus, they need to get it from their diet. RF deficiency may result in oxidative damage, cell cycle arrest, and cell stress response. It also may impair iron absorption, cause hearing loss and cranial nerve deficits [18,19]. Besides an unbalanced diet, RF deficiency may also occur in inflammatory bowel diseases [20], chronic alcoholism [21], and diabetes mellitus [22].

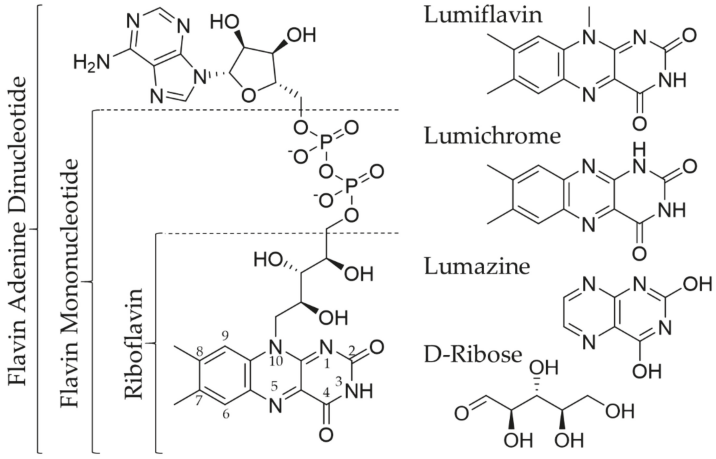

Figure 1. Chemical structures of riboflavin (RF) (with the numbering of isoalloxazine ring), Flavin Mononucleotide, Flavin Adenine Dinucleotide, Lumiflavin, Lumichrome, Lumazine, and D-Ribose.

2.1. Riboflavin Carrier Protein

The riboflavin carrier protein (RCP) is not a membrane-spanning carrier but a soluble protein that binds RF; however, the exact role in storing and transporting RF is still unknown. RCP was first identified in oviparous species in the 1960s [23,24]. Chicken RCP (cRCP) has been extensively investigated, as it is easy to isolate and purify in large quantities. cRCP has a high affinity to RF and its co-enzyme forms [23,25,26]. Further investigations using model compounds have indicated that the functionalization of either the isoalloxazine ring or the side-chain of RF results in decreased binding to cRCP [27,28]. During binding, the RF ring is stacked between parallel planes of cRCP [29], while the side chain is oriented inside the cRCP to form hydrogen bonds with it [27]. Furthermore, it was seen that the binding is pH-dependent, confirming the hydrophobic nature of the binding site. Based on these observations, only modification of the C-2 and N-3 positions of the isoalloxazine ring (see Figure 1) should not influence the binding affinity of RF to cRCP [27].

Human RCP (hRCP) shows many similarities to cRCP: molecular size, isoelectric point (pI), and preferential binding to RF over the flavin co-enzymes. hRCP is present during pregnancy and in umbilical cord serum [25]. Suppressing RCP during pregnancy induces abortion in mice and rats, while the well-being of the animals is not affected [30,31]. It is thus assumed that RCP is involved in RF transport to the fetus.

Moreover, overexpression of RCP in patients with malignant disease has been identified. RCP levels in serum were found to be higher in women with breast cancer (6.06 ng/mL) compared to

healthy women (0.70 ng/mL) [32]. Another study elucidated that RCP levels correlate with the stage of the disease. Women with early-stage breast cancer had 8.4 ng/mL RCP in serum, 3–4 folds higher than healthy controls (2.8 ng/mL), and patients with advanced tumor stages had even higher levels (20.4 ng/mL) [33]. Similar observations were made in hepatocellular carcinoma, where RCP serum levels were significantly increased (21.75 ng/mL) compared to healthy patients (0.73 ng/mL) [34]. Moreover, RCP overexpression was seen in prostate cancer cells (LnCaP, PC3, and DU-145) in vitro and in tumor tissues in vivo [35]. RCP overexpression in malignant cells makes it a potential biomarker for tumor detection, therapy monitoring, and a promising tool for targeted drug delivery systems.

2.2. Riboflavin Transporters

Solute carriers (SLC) transport diverse substrates through membranes such as inorganic ions, amino acids, lipids, and drugs [36,37]. Recently, the SLC52 transporter family has been identified, consisting of riboflavin transporters: RFVT1/SLC52A1, RFVT2/SLC52A2, and RFVT3/SLC52A3 [38–43]. RFVT1 and RFVT2 show the most similarity to each other (86.7% amino acid identity), while RFVT3 shows only 42.9% identity with RFVT1 and 44.1% with RFVT2 [43]. RFVT1 is expressed in the placenta, small intestine, plasma membrane, kidney, colon, lungs, uterus, and thymus [38,40]. RFVT2 can be mainly found in the brain, small intestine, and salivary gland [40]. Whereas, RFVT3 is found in the testis, small intestine, and prostate [39,44]. RFVT1, RFVT2, and RFVT3 have Michaelis-Menten constants of 1.38, 0.33, and 0.98 μM, respectively [45]. All three transporters exhibit sodium-independent and temperature-dependent behavior [40,46–49]; however, only RFVT3 has higher activity in acidic environments; the other transporters do not show pH-dependent behavior [39].

Substances can enter a cell via pinocytosis (Figure 2a), a form of fluid endocytosis, where the cell membrane forms a vesicle encapsulating the fluids and molecules. By this mechanism, small (RF) and large (RF-conjugates) molecules can be transported across the membrane. In addition to pinocytosis, RF is internalized with the help of RCP and RFVTs; however, the exact mechanism remains unclear. It is assumed to be a combination of clathrin-mediated endocytosis (Figure 2b) and carrier-mediated transport (Figure 2c). In the case of clathrin-mediated endocytosis, the substrate binds to receptors (RFVTs) located on the cell surface; and with the help of clathrin, a vesicle containing absorbed substrate is formed. In this way, small and large molecules can be internalized. Moreover, the uptake can be inhibited by receptor saturation. In carrier-mediated transportation, membrane proteins have substrate binding sites that allow specific molecules to pass through the membrane. The substrate size is very important, as it has been shown that upon conjugation to larger molecules, the substrate can lose the ability to pass through the membrane.

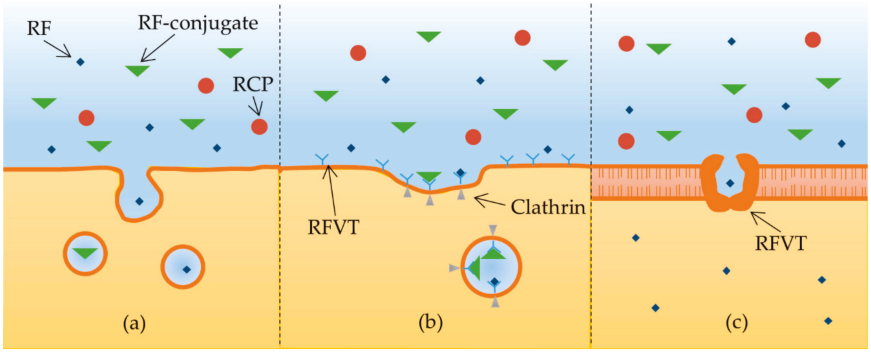

Figure 2. Internalization pathways: (**a**) pinocytosis; (**b**) clathrin-mediated endocytosis; (**c**) carrier-mediated transport. Abbreviations are defined as follows: riboflavin (RF); riboflavin transporter (RFVT); riboflavin carrier protein (RCP).

In vitro, high RFVT expression was observed in human epidermoid carcinoma (A431), human renal proximal tube epithelial cells (HK-2), and human umbilical vein endothelial cells (HUVEC) [50]. In vivo, low levels of all three RF transporters have been found in most healthy tissues, whilst tumors seem to overexpress RFVTs: all three transporters were significantly overexpressed in squamous cell carcinoma (SCC), melanoma, and luminal A breast cancer. RFVT3, in particular, was shown to be 187-fold more expressed in SCC compared to healthy tissue [50]. High amounts of RFVT3 were also found in esophageal squamous cell carcinoma, squamous cell carcinoma, and glioma [51–53]. Moreover, the SLC42A3 protein level was seen to increase with the stepwise development of esophageal squamous cell carcinoma [54]. RFVTs are thus promising cancer biomarkers and may act as targets for therapeutic drugs or diagnostics, due to their solute carrier function and high overexpression in cancerous tissue.

2.3. Riboflavin Internalization

Riboflavin transport processes have been investigated in various cell lines. In all tested cell lines, it was seen that RF uptake is a temperature-dependent and sodium-independent process. The rate of transport decreases with temperature from 37 to 4 °C, whereas the presence or absence of sodium ions in the incubation buffer does not change the uptake kinetics. Additionally, pH-dependent RF internalization was observed in some cases. In human pancreatic cells, RF uptake was increased with decreasing pH from 8 to 6. This cell line has a high expression of RFVT3, which shows better activity at acidic pH [39,55]. Interestingly, in human liver and human retinal pigment epithelial cells, the opposite trend was observed, most likely because these cells function better at a neutral rather than acidic pH. Thus, since tumors are usually characterized by an acidic pH, RFVT3 may be particularly active in tumors and, thus, the receptor to be preferentially targeted.

The kinetic parameters of RF transport vary depending on the cell line (Table 1). It is assumed that this is due to differences in the dominant transport mechanisms, which have not been investigated in detail yet. Among the tested cell lines, the Michaelis-Menten constants (K_m) of rat brain capillary endothelial cells were almost 50 times higher compared to other cell lines. This means that RF internalization into rat brain capillary cells is an extremely slow process compared to other cell lines. As for the transport rate (V_{max}), human intestinal epithelial cells stand out with a relatively high V_{max} value. This is not surprising since humans receive RF mainly from their diet. Taken into account that most other cell lines display K_m values below 1 μM, and V_{max} values in the order of fmol/min/mg protein to pmol/min/mg protein, it is assumed that RF transportation is a fast process. This is highly advantageous when using RF as a targeting moiety for diagnostic or therapeutic compounds.

Table 1. Summary of riboflavin uptake kinetics in different cell lines.

Cell Line	K_m in μM	V_{max} in pmol/min/mg Protein
Human intestinal epithelial cells (Caco-2) [46]	0.30 ± 0.03	69.97 ± 8.13
Xenopus laevis oocytes [56]	0.41 ± 0.02	0.00005 ± 0.0000007
Human liver cells (Hep G2) [57]	0.41 ± 0.08	1.19 ± 0.08
Human renal proximal tubule epithelial cells (HK-2) [47]	0.67 ± 0.21	3.35 ± 0.29
Human colonic epithelial cells (NCM460) [58]	0.14 ± 0.004	1.10 ± 0.19
Peripheral blood mononuclear cells (PBMC) [59]	0.955 ± 0.344	0.04 ± 0.02
Human trophoblast cells (BeWo) [48]	0.0013 ± 0.00068	0.01 ± 0.001
Human retinoblastoma cells (Y-79) [60]	0.019 ± 0.00037	6.98 ± 0.30
Human retinal pigment epithelial cells (ARPE-19) [61]	0.08 ± 0.014	0.45 ± 0.03
Rabbit corneal epithelial cells (rPCEC) [62]	2.05	3.99
Human embryonic kidney cells (HEK293) [38]	0.0350 ± 0.0041	0.17 ± 0.16
Human breast adenocarcinoma cells (MCF-7) [63]	0.106 ± 0.009	0.52
Human pancreatic cells (β-TC-6) [55]	0.17 ± 0.02	4.45 ± 0.16
Rat brain capillary endothelial cells (BRE4) [64]	19 ± 3	0.24 ± 0.01
Human colorectal carcinoma cells (T84) [65]	0.0532 ± 0.0216	0.36 ± 0.08

Abbreviations are defined as follows: Michaelis-Menten constant (K_m); maximum uptake rate (V_{max}).

RF internalization can be blocked by competing compounds (Table 2). To test which part of the molecular structure of RF is responsible for blocking uptake, cells were pre-treated with RF or with structural analogs (see Figure 1 for chemical structures) before exposure to RF. In pre-treatment, at least a 20-fold excess of the competing structure was used compared to RF. The pre-treatment with free RF showed that RFVTs can be saturated, reducing RF uptake. The inhibitory effect was also seen when cells were pre-treated with lumiflavin and lumichrome, both of which have an isoalloxazine ring similar to RF. The specificity of the tricyclic isoalloxazine ring to RFVT was further confirmed since bicyclic lumazine did not alter RF uptake. Moreover, pre-treatment with D-Ribose did not saturate RFVTs, indicating that the ribityl side chain of RF is not necessary for internalization. Interestingly, FMN and FAD (co-enzymes of RF) showed varying results depending on the cell line. Though in PBMC cells FMN and FAD did not significantly inhibit RF uptake, a decrease in the uptake was seen. It is likely that the amount of the competing structures was too low to significantly inhibit the uptake. On the other hand, all cells listed in Table 2 have not been tested for their expression of different RFVTs. It could be that different RFVTs have preferred affinity towards RF over FMN or FAD. Thus, blocking with FMN or FAD in the cells expressing these receptors would not be efficient.

Table 2. Effects of pre-treatment with competing structures on riboflavin uptake.

Cell Line	RF	FMN	FAD	Lumiflavin	Lumichrome	Lumazine	D-Ribose
Caco-2 [46]	+	nt	nt	+	+	-	-
Oocytes [56]	+	nt	-	+	+	-	-
Hep G2 [57]	nt	nt	nt	+	+	-	nt
HK-2 [47]	+	nt	nt	+	+	-	-
NCM460 [58]	nt	nt	nt	+	+	nt	nt
PBMC [59]	+	-	-	nt	+	nt	-
BeWo [48]	+	+	+	+	+	nt	-
Y-79 [60]	+	nt	nt	+	+	nt	nt
ARPE-19 [61]	+	nt	nt	+	+	-	nt
rPCEC [62]	+	nt	nt	+	+	nt	-
HEK293 [38]	nt	+	+	+	nt	nt	nt
β-TC-6 [55]	+	nt	nt	+	+	nt	nt
BRE4 [64]	+	+	+	+	+	nt	-

Abbreviations and symbols are defined as follows: significant uptake inhibition (+); no uptake inhibition (-); not tested (nt); riboflavin (RF); flavin mononucleotide (FMN); flavin adenine dinucleotide (FAD).

Furthermore, different inhibitory compounds have been tested to see if they affect RF internalization (Table 3). Na-K-ATPase inhibitor ouabain showed no inhibitory effect on RF uptake, proving once more that the RF internalization is not sodium-dependent. In contrast, sodium azide and 2,4 –dinitrophenol (DNP) both significantly reduced RF uptake. Sodium azide inhibits oxidative phosphorylation, whereas DNP reduces intracellular adenosine triphosphate (ATP) levels. Hence, internalization is an energy-dependent process. Moreover, the sulfhydryl group modifying agents (p-CMPS and iodoacetate) also inhibited RF internalization. This shows that sulfhydryl groups are important for uptake. Additionally, concentration-dependent inhibition by calmidazolium has been observed, indicating that RF uptake is a Ca^{2+}/calmodulin mediated pathway. In general, RF internalization seems to be sodium-independent but energy-dependent, mediated via the Ca^{2+}/calmodulin pathway.

Table 3. Effects of different inhibitory compounds on riboflavin uptake.

Cell Line	Ouabain	Sodium Azide	DNP	p-CMPS	Iodoacetate	Calmidazolium
Caco-2 [46]	nt	+	+	nt	nt	nt
Oocytes [56]	-	nt	+	+	nt	nt
Hep G2 [57]	-	+	+	+	+	+
HK-2 [47]	nt	+	+	+	+	+
NCM460 [58]	-	+	+	+	nt	+
PBMC [59]	-	nt	+	nt	-	nt
BeWo [48]	nt	+	nt	nt	nt	+
Y-79 [60]	-	+	+	nt	nt	+
ARPE-19 [61]	nt	nt	+	+	+	+
rPCEC [62]	-	+	+	nt	nt	nt
β-TC-6 [55]	nt	nt	nt	nt	nt	+
BRE4 [64]	+	+	+	nt	nt	+

Abbreviations and symbols are defined as follows: significant uptake inhibition (+); no uptake inhibition (-); not tested (nt); 2,4 –dinitrophenol (DNP); p-chloromercuriphenyl sulfonate (p-CMPS).

3. Riboflavin Targeting

Though RF has started to gain interest as a ligand for active targeting, not much research has been performed thus far. Only a few research groups have synthesized probes functionalized with RF, FAD, or FMN and tested their performance in vitro and in vivo (see Figure 3 for structures).

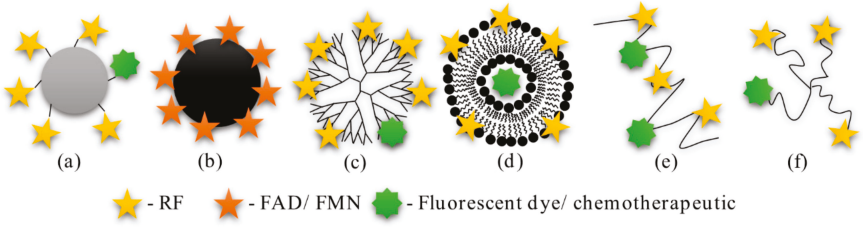

Figure 3. Probes designed to actively target RFVTs: (**a**) Bovine serum albumin-RF conjugate; (**b**) Ultrasmall superparamagnetic iron oxide nanoparticles coated with FMN/FAD; (**c**) Dendrimer-RF conjugate; (**d**) Liposome-RF conjugate; (**e**) Poly(N-(2-Hydroxypropyl)methacrylamide-RF conjugate; (**f**) 4-arm polyethylene glycol-RF conjugate.

3.1. Bioconjugates

The first RF conjugate was synthesized in the 1990s [66,67]. RF was covalently linked to bovine serum albumin (BSA) via the ribityl side chain. According to spectrophotometry, five RF molecules were attached per one BSA molecule. BSA-RF and BSA internalization were tested in vitro on human nasopharyngeal carcinoma (KB), human lung adenocarcinoma (SK-LU-1), human ovary adenocarcinoma (SK-OV), and human lung carcinoma (A549) cells [65]. Uptake of the RF conjugate was significantly higher than non-functionalized BSA in all cell lines. Surprisingly, the internalization of the conjugate was not inhibited when cells were pre-treated with an excess of RF or FMN. This is in contrast with analogous studies using other vitamins. For example, in the case of BSA-folate and BSA-biotin, strong inhibition was observed when cells were pre-treated with free vitamins [68,69]. Since other studies using RF targeted systems reported successful competitive binding experiments (see following text), it is likely that either not enough RF was used to saturate the RFVTs or BSA-RF was not taken up via an RF-mediated pathway. The latter could have been due to RF conjugation using the ribityl side chain that has been shown to reduce the binding affinity to RCP [27]. It is likely that BSA-RF could have had higher internalization than BSA due to an increase in hydrophobicity and/or size. Beyond the in vitro study, BSA-RF transport across the distal pulmonary epithelium was tested in vivo [64]. The measurements showed that a higher amount of the conjugate moved

from the trachea to blood compared to free BSA. Hence, conjugation to RF seems to increase the transcytosis of BSA through distal pulmonary epithelial cells. Nonetheless, it is unclear if this effect is specifically associated with RF and targeting of its transporters. To address this interesting finding, further experiments are required.

3.2. Ultrasmall Superparamagnetic Iron Oxide Nanoparticles

Ultrasmall superparamagnetic iron oxide nanoparticles (USPIO) have been synthesized with FAD or FMN coating for targeted diagnostic imaging [70–73]. In both cases, USPIO were synthesized via a co-precipitation method and coated with FAD or FMN via phosphate group adsorption. The co-enzymes cannot fully coat the iron particles; thus, guanosine monophosphate (GMP) was also used as a spacer to achieve stable particles. All USPIO had cores of 5 nm according to transmission electron microscopy (TEM) images (Figure 4) and hydrodynamic size of 97 nm for FMN coated [71] and 118 nm for FAD [70]. FMN/FAD coated USPIO (FLUSPIO) had r_2 relaxivities that were sufficiently high for use as magnetic resonance (MR) contrast agents and close to that of clinically approved agents.

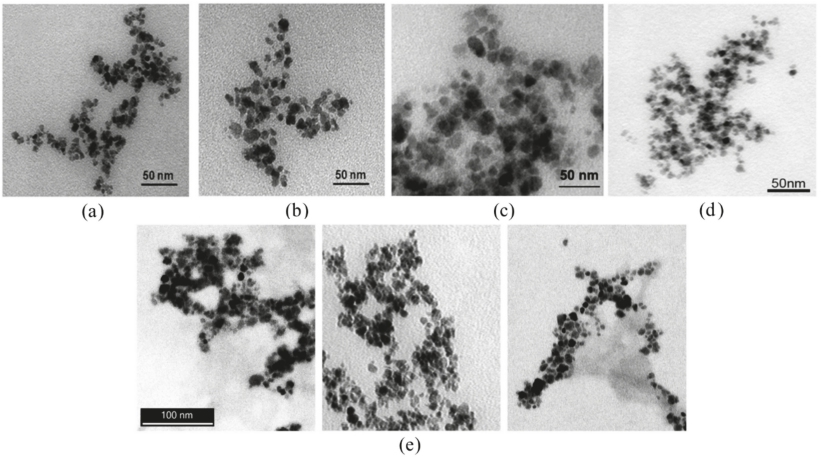

Figure 4. TEM images of different ultrasmall superparamagnetic iron oxide (USPIO) formulations: (**a**) USPIO; (**b**) FMN USPIO; (**c**) FAD USPIO; (**d**) and (**e**) different absorptive coating FMN USPIO: (**d**) GMP-FMN USPIO; (**e**) AMP-FMN USPIO, ADP-FMN USPIO, and ATP-FMN USPIO (left to right); Adapted with permission from [70–72].

The particles were further tested in vitro on LnCaP, PC3, and HUVEC. FLUSPIO did not induce toxic effects on cells in concentrations of up to 0.3 μmol Fe/mL according to Trypan blue staining, TUNEL (transferase-mediated deoxyuridine triphosphate nick end tunneling), and MTT (3-(4,5-Dimethylthiazol-2-yl)-2,5-diphenyltetrazolium bromide) assays. MRI experiments showed at least two times higher relaxation rates in cells exposed to FMN USPIO compared to those exposed to USPIO. The competitive binding experiments with FMN decreased the relaxation rates significantly, suggesting an RF-mediated uptake of FMN USPIO. Similar results were observed for USPIO coated with FAD.

In another study, instead of using GMP to produce stable FMN USPIO, ATP, adenosine diphosphate (ADP), and adenosine monophosphate (AMP) were used [73]. The new coatings produced nanoparticle clusters (Figure 4e), which had r_2 relaxivities higher than that of GMP coated FLUSPIO (Table 4). A cluster consists of a large number of small particles; thus, it is assumed that smaller particles produce higher relaxation rates due to their higher surface area. According to fluorescence measurements, AMP coated FLUSPIO had the highest amount of FMN molecules on its surface, which was likely the reason for the high cellular internalization. Furthermore, ATP, ADP, and AMP did not decrease

biocompatibility. In line with this, MR relaxometry using LNCaP, PC3, MCF-7, MLS (human ovarian serous cystadenocarcinoma), A431, and HUVECs showed higher relaxation rate changes when incubated with AMP coated FLUSPIO compared to other FLUSPIO. According to these findings, AMP coating proved to be ideal with respect to good MRI visibility and RF targeting properties. Thus, it is important to find a spacer that ensures stable particles and does not reduce the amount of targeting ligands.

Table 4. Properties of different USPIO.

USPIO formulation	Hydrodynamic Diameter	MRI r_2 Relaxivity at 3T
GMP-FMN USPIO [71]	97 nm	203 ± 1 $s^{-1}mM^{-1}$
AMP-FMN USPIO [73]	160 nm	228 ± 3 $s^{-1}mM^{-1}$
ADP-FMN USPIO [73]	168 nm	233 ± 9 $s^{-1}mM^{-1}$
ATP-FMN USPIO [73]	106 nm	259 ± 8 $s^{-1}mM^{-1}$
Resovist®[73]	72 nm	233 ± 1 $s^{-1}mM^{-1}$

Although FLUSPIO proved promising in vitro, there have been only two studies that investigated their performance in vivo. In both studies, mice bearing LnCaP tumor xenografts were used. The first study compared tumor uptake of FAD USPIO and Resovist® [70]. Instead of R2, R2* relaxation rates were determined in the in vivo experiments due to the higher sensitivity of T2*-weighted MR sequences for iron oxide nanoparticles. MRI scans showed a higher R2* relaxation rate at the tumor site after 1 and 3 h in animals injected with FAD USPIO compared to Resovist®(Figure 5a). It is important to note that FAD USPIO were only compared to Resovist®, which has a different core size and different coating that does not exactly match non-targeted USPIO. Hence, the increase in R2* could have multiple underlying causes besides the FAD coating. However, at this time, Resovist® was the only clinically approved diagnostic iron oxide nanoparticle; hence, its use as a control was justified to evaluate FAD USPIO performance against the clinical gold standard.

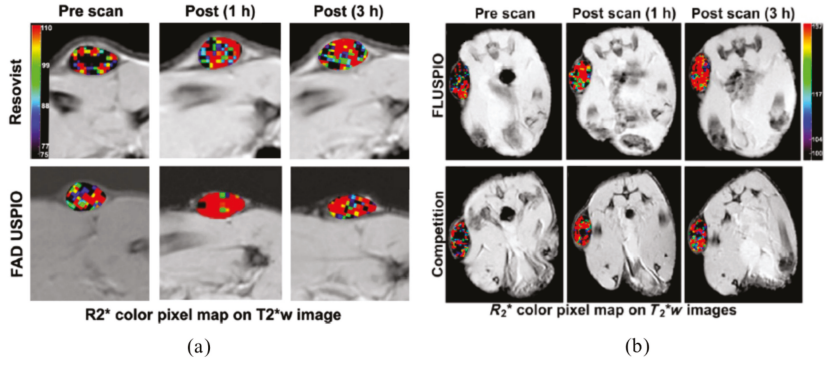

Figure 5. MRI T2 weighted images of subcutaneous right hind limb LnCaP tumors overlaid with color-coded R2* maps: (**a**) FAD USPIO show higher relaxation rates than Resovist®; (**b**) the relaxation rates of FMN competition are lower than FMN USPIO (FLUSPIO). Adapted with permission from [70,72].

Another study investigated the biodistribution and tumor uptake of FMN USPIO. Biodistribution analysis assessed by iron colorimetry showed the highest accumulation at the tumor site followed by the liver and spleen. Competitive binding of FMN USPIO after free FMN administration revealed that 1 and 3 h after injection of FMN USPIO R2*, relaxation rates of tumors were lower when the animals were pre-exposed to free FMN (Figure 5b) [72], suggesting RF-mediated FMN USPIO uptake. This goes in line with in vitro results showing RF-specific uptake of FMN USPIO by PC3 cells and HUVECs [71,72]. Further histological evaluation of the tumor tissue was performed to elucidate which

cell types in the tumors predominantly internalize FMN USPIO. Interestingly, FMN USPIO were internalized by tumor cells, endothelial cells, and macrophages. Although the uptake in macrophages and endothelial cells—to a certain degree—can be attributed to unspecific phagocytosis, enhanced uptake can also be the consequence of the upregulation of SLC52 transporters due to the enhanced metabolic activity of these cells [14,50]. In summary, FMN USPIO showed tumor specific accumulation in cancer cells and the tumor stroma, i.e., the tumor associated endothelial cells and macrophages. These results suggest that FMN is a promising diagnostic tag for diagnostic probes to simultaneously target different tumor compartments, including the cancer cells and its stroma.

3.3. Dendrimers

The first RFVT targeted drug delivery system was a fifth generation polyamidoamine (PAMAM) dendrimer functionalized with RF [74,75]. The dendrimer (diameter 5.4 nm) was covalently linked to RF via a ribityl side chain and a fluorescent dye or methotrexate (MTX). The fluorescent dendrimer was used to study uptake in KB and HeLa (human cervix adenocarcinoma) cells. FACS quantification showed a dose- and time-dependent uptake of the targeted dendrimers. The XTT assay (2,3-bis-(2-methoxy-4-nitro-5-sulfophenyl)-2H-tetrazolium-5-carboxanilide) using KB cells confirmed the time- and dose-dependent toxicity of PAMAM-RF-MTX. However, the conjugate had lower therapeutic efficacy than the free chemotherapeutic drug (IC50 values after 4 h incubation: 72 nM for the conjugate, 48 nM for MTX). The free RF and RF-PAMAM did not reduce cell viability, indicating that only MTX induced the toxic effects. Moreover, the uptake and, thus, the efficacy of PAMAM-RF-MTX was reduced using PAMAM-RF for competition. Surprisingly, competition with RF did not reduce the therapeutic efficacy of PAMAM-RF-MTX. Similar to the BSA-RF conjugate [67], it could be the case that not enough RF was used for competition. This may be particularly true when considering that, in contrast to competitively blocking with PAMAM-RF, RF may enter the cells via the transporter pathway, which is very fast and efficient so that the carrier-related transport was not significantly affected.

Furthermore, the RF-targeted dendrimer conjugate (N-10 position) was used to coat gold nanoparticles (AuNP) [76]. The AuNP were prepared by the gold (III) reduction method and had a hydrodynamic size of 30 nm according to dynamic light scattering (DLS), while atomic force microscopy (AFM) showed a 13.5 nm core diameter. The dendrimer conjugates were attached to the AuNP via gold-sulfur chemisorption and had a size of 20.5 nm measured by AFM. The uptake of AuNP-PAMAM-RF was tested in KB cells [76]. According to surface plasmon resonance (SPR) and luminescence of AuNP, the RF-targeted nanocomposite showed higher internalization into cells than the control. Moreover, the interaction of the nanocomposite with RCP was tested using UV-vis spectroscopy. The absorption peak of AuNP-PAMAM-RF decreased depending on the amount of RCP in the solution and shifted by 6 nm to the right (659 nm). In contrast, for non-targeted particles, the absorption peak shifted to the left (622 nm). The distinct different spectral trend suggested that the targeted nanocomposite had specific interactions with RCP. This interaction was further confirmed by AFM measurements of the particle size. The samples showed heterogeneity (two sizes), suggesting that different amounts of dendrimer were absorbed onto the AuNP. Despite this, AFM showed that the particles tended to increase in size when exposed to RCP, thus suggesting interactions between the gold nanocomposites and the RCP. However, as a limitation, the authors reported that AuNP-PAMAM-RF particles need further improvements to yield a homogeneous distribution of RF on the nanocomposites. Nonetheless, this is the only RF-conjugate to date that can be detected using two methods: SPR and luminescence. In conclusion, AuNP-PAMAM-RF is another promising conjugate that could be used for RF-targeted in vitro diagnostics.

Additionally, the same research group also investigated the selectivity of RCP [77,78]. Firstly, it was tested if coupling to different sites of RF changes the binding affinity towards RCP [77]. For this purpose, the PAMAM dendrimer was conjugated to RF via the isoalloxazine ring (N-3 position) or ribityl side chain (N-10 position) (see Figure 1 for isoalloxazine ring numbering). Isothermal titration calorimetry (ITC) and differential scanning calorimetry (DSC) were used to assess the binding affinity

of RCP to the dendrimers. The dissociation constant obtained from ITC measurements showed that PAMAM-RF conjugates had a higher affinity to RCP when coupled at the N-3 position than at N-10. Additionally, a higher denaturation temperature was observed for RCP when it was exposed to the dendrimers, confirming increased structural stability. Dendrimer N-3 showed a higher denaturation temperature than N-10, confirming ITC results that the N-3 dendrimer has a better affinity towards RCP. These results support the previous study [27], further confirming that changes at the N-3 position do not alter RF binding affinity to RCP.

Secondly, the dendrimers with zero, three, or five RF moieties coupled using the N-3 position were used to test if the number of targeting ligands changes, the avidity of the conjugate-RCP complex [78]. The force needed to break the bond between an AFM tip coated with one of the conjugates and the RCP-immobilized surface was measured. Non-targeted PAMAM had a weak attraction to the RCP surface, while in the case of PAMAM-RF with increasing number of RF moieties, higher forces were needed to break the bond. Thus, the study showed that increasing the amount of RF ligands on the dendrimer increases the bond strength of the conjugate-RCP complex. It is possible that at a certain number of targeting ligands the avidity starts to decrease due to steric hindrance. Thus, when designing an RF-targeted system, the number of targeting moieties should be balanced.

3.4. Liposomes

The largest structures functionalized with RF so far were liposomes [79]. Here, the RF ribityl chain was substituted by a glycerolipid moiety using a phosphate linker. The resulting RF-phospholipid was then incorporated into liposomes that were prepared by the thin film hydration method. Control and targeted liposomes had hydrodynamic diameters of 115 nm with PDI < 0.1 according to DLS. In vitro experiments showed that A431 cells preferentially internalized targeted over non-targeted liposomes. In detail, the uptake was up to 16 times higher with similar results being obtained for PC3 cells and HUVECs. Furthermore, competitive binding experiments pointed to an RF-mediated uptake. The liposomes did not reduce the viability of A431, PC3, or HUVECs after 72 h of incubation according to MTT assay, proving their biocompatibility. To assess the in vivo performance of RF-targeted liposomes, long circulating liposomes (LCL) were prepared by incorporating polyethylene glycol (PEG) spacers. The hydrodynamic diameter of the control LCL was 137 and 141 nm for targeted ones. A six times higher uptake of targeted LCL was found in PC3 cells compared to control liposomes. In vivo experiments using PC3 tumor xenografted mice indicated that control and targeted LCL had a similar biodistribution and blood half-life. However, histological analyses showed that targeted LCL underwent higher tumor cell uptake than the control ones (Figure 6). This study further confirms that RF-targeting does enhance tumor cell internalization. As liposomes have a high loading capacity and can entrap hydrophobic drugs without altering their structure, RF-targeted liposomes could be an ideal system for targeted drug delivery.

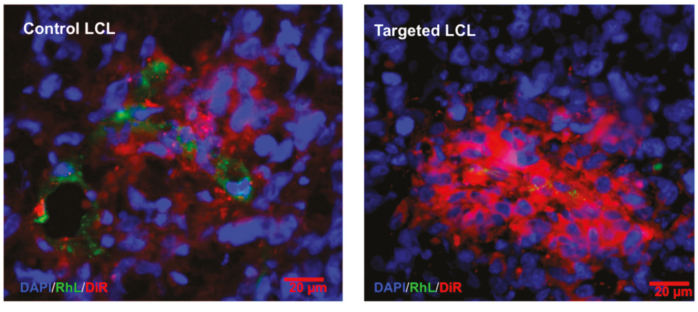

Figure 6. Fluorescence microscopy images of PC3 tumor cryosections (dissected from right hind limb) after 48 h post injection showing higher targeted LCL internalization than control. Liposomes are depicted in red, nuclei in blue, and endothelial cells in green. Adapted with permission from [79]. Copyright© 2020 American Chemical Society.

3.5. Polymers

In addition to dendrimers, other polymers have been conjugated to RF. One example is poly(N-(2-Hydroxypropyl) methacrylamide) (PHPMA), which was conjugated to folic acid (FA) or RF (via ribityl side chain) and mitomycin C (MMC) to target breast cancer [80]. It was shown that both conjugates (PHPMA-RF and PHPMA-FA) were similarly taken up by SKBR-3 cells, while MCF-7 cells predominantly internalized PHPMA-RF. The MMC-PHPMA-RF conjugate showed significantly higher cellular accumulation than free MMC and MMC-PHPMA in MCF-7 cells. However, when cells were exposed to the lysosomotropic agents monensin and primaquine, only free MMC was taken up. This further proves that RF-conjugates are internalized via an endocytic process. Additionally, the drug efficiency was tested using an MTT assay. The IC50 value of free MMC, MMC-PHPMA-RF, and PHPMA-RF were 0.05 μg/mL, 0.10 μg/mL, and 0.61 μg/mL, respectively. Hence, cytotoxicity derives mainly from the chemotherapeutic drug, and the conjugation to the polymer does not inhibit drug efficacy. Thus, the PHPMA based RF-targeted drug delivery system showed RF specific tumor cell internalization via endocytosis and therapeutic effects associated with MMC. This is the first study to show that RF-targeted drug delivery improves the therapeutic efficacy of anti-cancer drugs in vitro. These promising results encourage further research on RF-targeted drug delivery systems.

Another polymer functionalized with RF was 4-arm PEG (also known as PEGstar) [81]. One of the four arms was labeled with Cy5.5 fluorescent dye, while the other three were conjugated to RF via the N-3 position. In the study, two sizes of PEGstars were used: 10 kDa (7 nm) and 40 kDa (13 nm). The uptake experiments using A431 and PC3 cells showed higher uptake of RF-targeted polymers compared to controls, while competition experiments confirmed RF-meditated internalization. Furthermore, in vivo experiments using mice bearing PC3 or A431 tumor xenografts were performed, showing a longer blood half-life for the bigger particles (40 kDa) due to the lack of renal clearance. Computed tomography/fluorescence molecular tomography (CT/FMT) measurements indicated that 10 kDa RF-PEGstars were retained at the tumor site 3 h post injection, while control polymers dispersed. In the case of 40 kDa PEGstars, both targeted and control polymers were retained in the tumor (Figure 7a). Due to their size, small particles quickly penetrated the tissue but also rapidly redistributed into circulation, leaving only RFVT-bound and internalized particles at the tumor site. In contrast, larger particles passively accumulate at the tumor site and do not rapidly re-enter circulation. While rapid clearance is certainly necessary for a diagnostic probe, intended to display RFVT expression, maximization of overall tumor accumulation may be a necessity for most therapeutics independent of the accumulation mechanism. However, high tumor accumulation does not always mean high tumor cell uptake since the nanomedicines can be accumulated in the interstitial space. In this context, the histological evaluation revealed that targeted PEGstars of both sizes had better internalization compared to controls, clearly indicating the added value of RF-targeting (Figure 7b). Furthermore, 10 kDa RF-PEGstars were mainly internalized by tumor cells, followed by macrophages and endothelial cells, while 40 kDa ones were taken up more by macrophages. It is postulated that the larger polymer was deposited in the tumor stroma for a longer period of time, and thus internalized by macrophages to a higher extent. Nonetheless, high macrophage internalization does not mean that the larger particles would not be a promising drug delivery system; as these cells act as a reservoir of drugs, mediating their slow release towards the cancer cells [82]. In summary, this study revealed a few important facts about targeting with RF and active targeting in general. Firstly, the RF-targeting enhances internalization of the particles into tumor cells but improves tumor retention only for the very small conjugates that do not significantly benefit from EPR. Secondly, the ideal targeted system should be large enough to benefit from EPR but small enough to transit to the tumor cells, which might ideally be given for systems of antibody sizes.

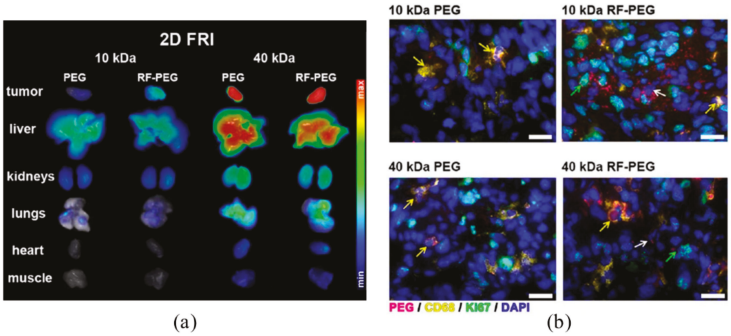

Figure 7. (**a**) Two-dimensional fluorescence reflectance images indicating PEGstar accumulation in mice bearing A431 tumors; (**b**) fluorescence microscopy images of A431 tumors showing the internalization of PEGstars. Polymers are depicted in magenta, macrophages in yellow, proliferating cells in green, and cell nuclei in blue. Adapted with permission from [81]. Copyright© 2020 American Chemical Society.

4. Conclusions and Future Perspectives

RF seems to play an important role in cancer development and progression, as its carrier protein and transporters are highly overexpressed in several cancer tissues. Thus, RFVTs and RCP have the potential to be used as biomarkers for cancer detection. Furthermore, fast and efficient RF uptake also renders it a promising targeting ligand for cancer diagnostics and therapeutics. In this context, it can be advantageous that both tumor cells and cells of the tumor microenvironment (endothelial cells and macrophages) show enhanced RF internalization. However, the exploration of this interesting pathway is in its infancy, and it is unclear why different cells upregulate different RFVTs and how this influences targeting efficacy. Additionally, the mechanism of RF internalization, depending on the size and composition of the RF-targeted diagnostics and therapeutics, require extensive investigation. Furthermore, the reviewed literature clearly indicates that diagnostic and therapeutic RF-targeted probes require different design considerations. Diagnostic RF-targeted agents should be small molecules with fast exchange kinetics between the tumor compartments and rapid elimination from the body to display the RFVT status. RF-targeted therapeutics, on the other hand, should be larger molecules that strongly accumulate via the EPR but still be small enough to penetrate the tumor tissue and benefit from the enhanced RF-mediated internalization. Thus, if these aspects are taken into consideration, RFVTs may become powerful targets for various theranostic and tumor targeted drug delivery systems.

Author Contributions: M.D. researched the data for the article and drafted the manuscript. N.D., T.L., and F.K. reviewed and edited the manuscript. All authors have read and agreed to the published version of the manuscript.

Funding: This research was supported by the Deutsche Forschungsgemeinschaft (DFG) in the framework of the Research Training Group 2375 "Tumor-targeted Drug Delivery" grant 331065168 and DFG FOR 2591 to F.K. Grant No. 321137804.

Conflicts of Interest: The authors declare no conflict of interest.

Abbreviations

A431	Human epidermoid carcinoma
A549	Human lung adenocarcinoma cells
ADP	Adenosine diphosphate
AFM	Atomic force microscope
AMP	Adenosine monophosphate
ARPE-19	Human retinal pigment epithelial cells
ATP	Adenosine triphosphate
AuNP	Gold nanoparticles
BeWo	Human trophoblast cells

BRE4	Rat brain capillary endothelial cells
BSA	Bovine serum albumin
Caco-2	Human intestinal epithelial cells
cRCP	Chicken riboflavin carrier protein
CT/FMT	Computed tomography/fluorescence molecular tomography
DNP	2,4-dinitrophenol
DSC	Differential scanning calorimetry
DU-145	Human prostate adenocarcinoma cells
EPR	Enhanced permeability and retention
FACS	Fluorescence-activated cell sorting
FAD	Flavin adenine dinucleotide
FLUSPIO	FMN/FAD coated USPIO
FMN	Flavin mononucleotide
GMP	Guanosine monophosphate
HEL293	Human embryonic kidney cells
HeLa	Human cervix adenocarcinoma cells
Hep G2	Human liver cells
HK-2	Human renal proximal tubule epithelial cells
hRCP	Human riboflavin carrier protein
HUVEC	Human umbilical vein epithelial cells
ITC	Isothermal titration calorimetry
KB	Human nasopharyngeal carcinoma cells
LCL	Long circulating liposomes
LnCaP	Human prostate adenocarcinoma cells
MCF-7	Human breast adenocarcinoma cells
MLS	Human ovarian serous cystadenocarcinoma
MMC	Mitomycin C
MR	Magnetic resonance
MRI	Magnetic resonance imaging
MTT	3-(4,5-Dimethylthiazol-2-yl)-2,5-diphenyltetrazolium bromide
MTX	Methotrexate
NCM460	Human colonic epithelial cells
PAMAM	Polyamidoamine
PBMC	Human peripheral blood mononuclear cells
PC3	Human prostate adenocarcinoma cells
p-CMPS	p-chloromercuriphenyl sulfonate
PDI	Polydispersity index
PEG	Polyethylene glycol
PHPMA	Poly(N-(2-Hydroxypropyl) methacrylamide)
pI	Isoelectric point
RCP	Riboflavin carrier protein
RF	Riboflavin
RFVT	Riboflavin transporter
rPCEC	Rabbit corneal epithelial cells
SCC	Squamous cell carcinoma
SKBR-3	Human adenocarcinoma cells
SK-LU-1	Human lung adenocarcinoma cells
SK-OV	Human ovary adenocarcinoma cells
SLC	Solute carriers
SPR	Surface plasmon resonance
T84	Human colorectal carcinoma cells
TUNEL	Transferase-mediated deoxyuridine triphosphate nick end tunneling
USPIO	Ultrasmall superparamagnetic iron oxide nanoparticles
XTT	2,3-bis-(2-methoxy-4-nitro-5-sulfophenyl)-2H-tetrazolium-5-carboxanilide
Y-79	Human retinoblastoma cells
β-TC-6	Human pancreatic cells

References

1. Golombek, S.K.; May, J.-N.; Theek, B.; Appold, L.; Drude, N.; Kiessling, F.; Lammers, T. Tumor targeting via EPR: Strategies to enhance patient responses. *Adv. Drug Deliv. Rev.* **2018**, *130*, 17–38. [CrossRef] [PubMed]
2. Muhamad, N.; Plengsuriyakarn, T.; Na-Bangchang, K. Application of active targeting nanoparticle delivery system for chemotherapeutic drugs and traditional/herbal medicines in cancer therapy: A systematic review. *Int. J. Nanomed.* **2018**, *13*, 3921–3935. [CrossRef] [PubMed]
3. Fleck, L.M. The Costs of Caring: Who Pays? Who Profits? Who Panders? *Hastings Cent. Rep.* **2006**, *36*, 13–17. [CrossRef] [PubMed]
4. Lee, L.S.; Conover, C.; Shi, C.; Whitlow, M.; Filpula, D. Prolonged Circulating Lives of Single-Chain Fv Proteins Conjugated with Polyethylene Glycol: A Comparison of Conjugation Chemistries and Compounds. *Bioconjug. Chem.* **1999**, *10*, 973–981. [CrossRef]
5. Suzuki, T.; Ikeda, K.; Tomono, T. Physicochemical and biological properties of poly(ethylene glycol)-coupled immunoglobulin G. Part II. Effect of molecular weight of poly(ethylene glycol). *J. Biomater. Sci. Polym. Ed.* **1989**, *1*, 71–84. [CrossRef]
6. Kitamura, K.; Takahashi, T.; Yamaguchi, T.; Noguchi, A.; Noguchi, A.; Takashina, K.; Tsurumi, H.; Inagake, M.; Toyokuni, T.; Hakomori, S. Chemical engineering of the monoclonal antibody A7 by polyethylene glycol for targeting cancer chemotherapy. *Cancer Res.* **1991**, *51*, 4310–4315.
7. Campbell, I.G.; Jones, T.A.; Foulkes, W.D.; Trowsdale, J. Folate-binding protein is a marker for ovarian cancer. *Cancer Res.* **1991**, *51*, 5329–5338.
8. Kalli, K.R.; Oberg, A.L.; Keeney, G.L.; Christianson, T.J.H.; Low, P.S.; Knutson, K.L.; Hartmann, L.C. Folate receptor alpha as a tumor target in epithelial ovarian cancer. *Gynecol. Oncol.* **2008**, *108*, 619–626. [CrossRef]
9. Toffoli, G.; Cernigoi, C.; Russo, A.; Gallo, A.; Bagnoli, M.; Boiocchi, M. Overexpression of folate binding protein in ovarian cancers. *Int. J. Cancer* **1997**, *74*, 193–198. [CrossRef]
10. Lutz, R.J. Targeting the folate receptor for the treatment of ovarian cancer. *Transl. Cancer Res.* **2015**, *4*, 118–126.
11. Klein, B.P. Handbook of vitamins: Nutritional, biochemical, and clinical aspects. Edited by Lawrence J. Machlin. Marcel Dekker, Inc., New York, NY. 1984. 632 pp. ISBN 0–8247-7051-X. $;9.50. *J. Pharm. Sci.* **1985**, *74*, 1024–1025. [CrossRef]
12. Tu, B.P. Biochemical Basis of Oxidative Protein Folding in the Endoplasmic Reticulum. *Science* **2000**, *290*, 1571–1574. [CrossRef]
13. Schramm, M.; Wiegmann, K.; Schramm, S.; Gluschko, A.; Herb, M.; Utermöhlen, O.; Krönke, M. Riboflavin (vitamin B2) deficiency impairs NADPH oxidase 2 (Nox2) priming and defense against Listeria monocytogenes. *Eur. J. Immunol.* **2014**, *44*, 728–741. [CrossRef] [PubMed]
14. Mazur-Bialy, A.I.; Buchala, B.; Plytycz, B. Riboflavin deprivation inhibits macrophage viability and activity – a study on the RAW 264.7 cell line. *Br. J. Nutr.* **2013**, *110*, 509–514. [CrossRef] [PubMed]
15. Sanches, S.C.; Ramalho, L.N.Z.; Mendes-Braz, M.; Terra, V.A.; Cecchini, R.; Augusto, M.J.; Ramalho, F.S. Riboflavin (vitamin B-2) reduces hepatocellular injury following liver ischaemia and reperfusion in mice. *Food Chem. Toxicol.* **2014**, *67*, 65–71. [CrossRef]
16. Liu, D.; Zempleni, J. Low activity of LSD1 elicits a pro-inflammatory gene expression profile in riboflavin-deficient human T Lymphoma Jurkat cells. *Genes Nutr.* **2014**, *9*. [CrossRef]
17. Huang, S.N.; Swaan, P.W. Involvement of a receptor-mediated component in cellular translocation of riboflavin. *J. Pharmacol. Exp. Ther.* **2000**, *294*, 117–125.
18. Powers, H.J. Riboflavin (vitamin B-2) and health. *Am. J. Clin. Nutr.* **2003**, *77*, 1352–1360. [CrossRef]
19. Jaeger, B.; Bosch, A.M. Clinical presentation and outcome of riboflavin transporter deficiency: mini review after five years of experience. *J. Inherit. Metab. Dis.* **2016**, *39*, 559–564. [CrossRef]
20. Fernandez-Banares, F.; Abad-Lacruz, A.; Xiol, X.; Gine, J.J.; Dolz, C.; Cabre, E.; Esteve, M.; Gonzalez-Huix, F.; Gassull, M.A. Vitamin status in patients with inflammatory bowel disease. *Am. J. Gastroenterol.* **1989**, *84*, 744–748.
21. Rosenthal, W.S.; Adham, N.F.; Lopez, R.; Cooperman, J.M. Riboflavin deficiency in complicated chronic alcoholism. *Am. J. Clin. Nutr.* **1973**, *26*, 858–860. [CrossRef] [PubMed]
22. Kodentsova, V.M.; Vrzhesinskaia, O.A.; Trofimenko, E.V.; Sokol'nikov, A.A.; Beketova, N.A.; Blazheevich, N.V.; Isaeva, V.A.; Aleĭnik, S.I.; Trofimenko, L.S.; Dronova, V.I. Vitamin status of children with diabetes mellitus. *Vopr. Med. Khim.* **1994**, *40*, 45–48. [PubMed]

23. Rhodes, M.B.; Bennett, N.; Feeney, R.E. The flavoprotein-apoprotein system of egg white. *J. Biol. Chem.* **1959**, *234*, 2054–2060. [PubMed]
24. Ostrowski, W.; Skarzynski, B.; Zak, Z. Isolation and properties of flavoprotein from the egg yolk. *Biochim. Biophys. Acta* **1962**, *59*, 515–517. [CrossRef]
25. Visweswariah, S.S.; Adiga, P.R. Isolation of riboflavin carrier proteins from pregnant human and umbilical cord serum: Similarities with chicken egg riboflavin carrier protein. *Biosci. Rep.* **1987**, *7*, 563–571. [CrossRef] [PubMed]
26. Nishikimi, M.; Kyogoku, Y. Flavin-Protein Interaction in Egg White Flavoprotein. *J. Biochem.* **1973**, *73*, 1233–1242. [CrossRef]
27. Choi, J.D.; McCormick, D.B. The interaction of flavins with egg white riboflavin-binding protein. *Arch. Biochem. Biophys.* **1980**, *204*, 41–51. [CrossRef]
28. Plantinga, A.; Witte, A.; Li, M.-H.; Harmon, A.; Choi, S.K.; Banaszak Holl, M.M.; Orr, B.G.; Baker, J.R.; Sinniah, K. Bioanalytical Screening of Riboflavin Antagonists for Targeted Drug Delivery—A Thermodynamic and Kinetic Study. *ACS Med. Chem. Lett.* **2011**, *2*, 363–367. [CrossRef]
29. Monaco, H.L. Crystal structure of chicken riboflavin-binding protein. *EMBO J.* **1997**, *16*, 1475–1483. [CrossRef]
30. Natraj, U.; Kumar R, A.; Kadam, P. Termination of Pregnancy in Mice with Antiserum to Chicken Riboflavin-Carrier Protein. *Biol. Reprod.* **1987**, *36*, 677–685. [CrossRef]
31. Murty, C.; Adiga, P. Pregnancy suppression by active immunization against gestation-specific riboflavin carrier protein. *Science* **1982**, *216*, 191–193. [CrossRef] [PubMed]
32. Rao, P.N.; Levine, E.; Myers, M.O.; Prakash, V.; Watson, J.; Stolier, A.; Kopicko, J.J.; Kissinger, P.; Raj, S.G.; Raj, M.H.G. Elevation of Serum Riboflavin Carrier Protein in Breast Cancer. *Cancer Epidemiol. Biomarkers Prev.* **1999**, *8*, 985–990. [PubMed]
33. Karande, A.A.; Sridhar, L.; Gopinath, K.S.; Adiga, P.R. Riboflavin carrier protein: A serum and tissue marker for breast carcinoma. *Int. J. Cancer* **2001**, *95*, 277–281. [CrossRef]
34. Rao, P.N.; Crippin, J.; Levine, E.; Hunt, J.; Baliga, S.; Balart, L.; Anthony, L.; Mulekar, M.; Raj, M.H.G. Elevation of serum riboflavin carrier protein in hepatocellular carcinoma. *Hepatol. Res.* **2006**, *35*, 83–87. [CrossRef]
35. Johnson, T.M.; Ouhtit, A.; Gaur, R.; Fernando, A.; Schwarzenberger, P.O.; Su, J.L.; Ismail, M.F.; El-Sayyad, H.I.H.; Karande, A.; Elmageed, Z.Y.A.; et al. Biochemical characterization of riboflavin carrier protein (RCP) in prostate cancer. *Front. Biosci.* **2009**, *14*, 3634–3640. [CrossRef]
36. Hediger, M.A.; Romero, M.F.; Peng, J.-B.; Rolfs, A.; Takanaga, H.; Bruford, E.A. The ABCs of solute carriers: Physiological, pathological and therapeutic implications of human membrane transport proteins. *Pflugers Arch.* **2004**, *447*, 465–468. [CrossRef]
37. Fredriksson, R.; Nordström, K.J.V.; Stephansson, O.; Hägglund, M.G.A.; Schiöth, H.B. The solute carrier (SLC) complement of the human genome: Phylogenetic classification reveals four major families. *FEBS Lett.* **2008**, *582*, 3811–3816. [CrossRef]
38. Yonezawa, A.; Masuda, S.; Katsura, T.; Inui, K. Identification and functional characterization of a novel human and rat riboflavin transporter, RFT1. *Am. J. Physiol. Cell Physiol.* **2008**, *295*, C632–C641. [CrossRef]
39. Yamamoto, S.; Inoue, K.; Ohta, K.; Fukatsu, R.; Maeda, J.; Yoshida, Y.; Yuasa, H. Identification and functional characterization of rat riboflavin transporter 2. *J. Biochem.* **2009**, *145*, 437–443. [CrossRef]
40. Yao, Y.; Yonezawa, A.; Yoshimatsu, H.; Masuda, S.; Katsura, T.; Inui, K.-I. Identification and comparative functional characterization of a new human riboflavin transporter hRFT3 expressed in the brain. *J. Nutr.* **2010**, *140*, 1220–1226. [CrossRef]
41. Moriyama, Y. Riboflavin transporter is finally identified. *J. Biochem.* **2011**, *150*, 341–343. [CrossRef] [PubMed]
42. Sabui, S.; Subramanian, V.S.; Pham, Q.; Said, H.M. Identification of transmembrane protein 237 as a novel interactor with the intestinal riboflavin transporter-3 (RFVT-3): Role in functionality and cell biology. *Am. J. Physiol. Cell Physiol.* **2019**. [CrossRef] [PubMed]
43. Yonezawa, A.; Inui, K. Novel riboflavin transporter family RFVT/SLC52: Identification, nomenclature, functional characterization and genetic diseases of RFVT/SLC52. *Mol. Asp. Med.* **2013**, *34*, 693–701. [CrossRef] [PubMed]
44. Fujimura, M.; Yamamoto, S.; Murata, T.; Yasujima, T.; Inoue, K.; Ohta, K.; Yuasa, H. Functional Characteristics of the Human Ortholog of Riboflavin Transporter 2 and Riboflavin-Responsive Expression of Its Rat Ortholog in the Small Intestine Indicate Its Involvement in Riboflavin Absorption. *J. Nutr.* **2010**, *140*, 1722–1727. [CrossRef]

45. Beztsinna, N.; Solé, M.; Taib, N.; Bestel, I. Bioengineered riboflavin in nanotechnology. *Biomaterials* **2016**, *80*, 121–133. [CrossRef] [PubMed]
46. Said, H.M.; Ma, T.Y. Mechanism of riboflavine uptake by Caco-2 human intestinal epithelial cells. *Am. J. Physiol.* **1994**, *266*, G15–G21. [CrossRef] [PubMed]
47. Kumar, C.K.; Yanagawa, N.; Ortiz, A.; Said, H.M. Mechanism and regulation of riboflavin uptake by human renal proximal tubule epithelial cell line HK-2. *Am. J. Physiol.* **1998**, *274*, F104–F110. [CrossRef] [PubMed]
48. Huang, S.N.; Swaan, P.W. Riboflavin uptake in human trophoblast-derived BeWo cell monolayers: cellular translocation and regulatory mechanisms. *J. Pharmacol. Exp. Ther.* **2001**, *298*, 264–271.
49. Foraker, A.B.; Khantwal, C.M.; Swaan, P.W. Current perspectives on the cellular uptake and trafficking of riboflavin. *Adv. Drug Deliv. Rev.* **2003**, *55*, 1467–1483. [CrossRef]
50. Bartmann, L.; Schumacher, D.; Von Stillfried, S.; Sternkopf, M.; Alampour-Rajabi, S.; van Zandvoort, M.; Kiessling, F.; Wu, Z. Evaluation of Riboflavin Transporters as Targets for Drug Delivery and Theranostics. *Front. Pharmacol.* **2019**, *10*. [CrossRef]
51. Jiang, X.-R.; Yu, X.-Y.; Fan, J.-H.; Guo, L.; Zhu, C.; Jiang, W.; Lu, S.-H. RFT2 is overexpressed in esophageal squamous cell carcinoma and promotes tumorigenesis by sustaining cell proliferation and protecting against cell death. *Cancer Lett.* **2014**, *353*, 78–86. [CrossRef] [PubMed]
52. Fu, T.; Liu, Y.; Wang, Q.; Sun, Z.; Di, H.; Fan, W.; Liu, M.; Wang, J. Overexpression of riboflavin transporter 2 contributes toward progression and invasion of glioma. *Neuroreport* **2016**, *27*, 1167–1173. [CrossRef] [PubMed]
53. Aili, A.; Hasim, A.; Kelimu, A.; Guo, X.; Mamtimin, B.; Abudula, A.; Upur, H. Association of the plasma and tissue riboflavin levels with C20orf54 expression in cervical lesions and its relationship to HPV16 infection. *PLoS ONE* **2013**, *8*, e79937. [CrossRef] [PubMed]
54. Long, L.; Pang, X.-X.; Lei, F.; Zhang, J.-S.; Wang, W.; Liao, L.-D.; Xu, X.-E.; He, J.-Z.; Wu, J.-Y.; Wu, Z.-Y.; et al. SLC52A3 expression is activated by NF-κB p65/Rel-B and serves as a prognostic biomarker in esophageal cancer. *Cell. Mol. Life Sci.* **2018**, *75*, 2643–2661. [CrossRef] [PubMed]
55. Ghosal, A.; Said, H.M. Mechanism and regulation of vitamin B2 (riboflavin) uptake by mouse and human pancreatic β-cells/islets: physiological and molecular aspects. *Am. J. Physiol. Gastrointest. Liver Physiol.* **2012**, *303*, G1052–G1058. [CrossRef]
56. Dyer, D.L.; Said, H.M. Riboflavin uptake by native Xenopus laevis oocytes. *Biochim. Biophys. Acta* **1995**, *1234*, 15–21. [CrossRef]
57. Said, H.M.; Ortiz, A.; Ma, T.Y.; McCloud, E. Riboflavin uptake by the human-derived liver cells Hep G2: Mechanism and regulation. *J. Cell. Physiol.* **1998**, *176*, 588–594. [CrossRef]
58. Said, H.M.; Ortiz, A.; Moyer, M.P.; Yanagawa, N. Riboflavin uptake by human-derived colonic epithelial NCM460 cells. *Am. J. Physiol. Cell Physiol.* **2000**, *278*, C270–C276. [CrossRef]
59. Zempleni, J.; Mock, D.M. Proliferation of Peripheral Blood Mononuclear Cells Increases Riboflavin Influx (44554). *SAGE J.* **2000**, 1. [CrossRef]
60. Kansara, V.; Pal, D.; Jain, R.; Mitra, A.K. Identification and functional characterization of riboflavin transporter in human-derived retinoblastoma cell line (Y-79): mechanisms of cellular uptake and translocation. *J. Ocul. Pharmacol. Ther.* **2005**, *21*, 275–287. [CrossRef]
61. Said, H.M.; Wang, S.; Ma, T.Y. Mechanism of riboflavin uptake by cultured human retinal pigment epithelial ARPE-19 cells: possible regulation by an intracellular Ca2+-calmodulin-mediated pathway. *J. Physiol. (Lond.)* **2005**, *566*, 369–377. [CrossRef]
62. Hariharan, S.; Janoria, K.G.; Gunda, S.; Zhu, X.; Pal, D.; Mitra, A.K. Identification and Functional Expression of a Carrier-Mediated Riboflavin Transport System on Rabbit Corneal Epithelium. *Curr. Eye Res.* **2006**, *31*, 811–824. [CrossRef]
63. Bareford, L.M.; Phelps, M.A.; Foraker, A.B.; Swaan, P.W. Intracellular Processing of Riboflavin in Human Breast Cancer Cells. *Mol. Pharm.* **2008**, *5*, 839–848. [CrossRef]
64. Patel, M.; Vadlapatla, R.K.; Pal, D.; Mitra, A.K. Molecular and functional characterization of riboflavin specific transport system in rat brain capillary endothelial cells. *Brain Res.* **2012**, *1468*, 1–10. [CrossRef]
65. Yoshimatsu, H.; Yonezawa, A.; Yao, Y.; Sugano, K.; Nakagawa, S.; Omura, T.; Matsubara, K. Functional involvement of RFVT3/ *SLC52A3* in intestinal riboflavin absorption. *Am. J. Physiol. Gastrointest. Liver Physiol.* **2014**, *306*, G102–G110. [CrossRef]

66. Wangensteen, O.D.; Bartlett, M.M.; James, J.K.; Yang, Z.F.; Low, P.S. Riboflavin-enhanced transport of serum albumin across the distal pulmonary epithelium. *Pharm. Res.* **1996**, *13*, 1861–1864. [CrossRef]
67. Holladay, S.R.; Yang, Z.; Kennedy, M.D.; Leamon, C.P.; Lee, R.J.; Jayamani, M.; Mason, T.; Low, P.S. Riboflavin-mediated delivery of a macromolecule into cultured human cells. *BBA-Gen. Subj.* **1999**, *1426*, 195–204. [CrossRef]
68. Horn, M.A.; Heinstein, P.F.; Low, P.S. Biotin-Mediated Delivery of Exogenous Macromolecules into Soybean Cells. *Plant Physiol.* **1990**, *93*, 1492–1496. [CrossRef] [PubMed]
69. Leamon, C.P.; Low, P.S. Delivery of macromolecules into living cells: a method that exploits folate receptor endocytosis. *Proc. Natl. Acad. Sci. USA* **1991**, *88*, 5572–5576. [CrossRef] [PubMed]
70. Jayapaul, J.; Arns, S.; Lederle, W.; Lammers, T.; Comba, P.; Gätjens, J.; Kiessling, F. Riboflavin carrier protein-targeted fluorescent USPIO for the assessment of vascular metabolism in tumors. *Biomaterials* **2012**, *33*, 8822–8829. [CrossRef]
71. Jayapaul, J.; Hodenius, M.; Arns, S.; Lederle, W.; Lammers, T.; Comba, P.; Kiessling, F.; Gaetjens, J. FMN-coated fluorescent iron oxide nanoparticles for RCP-mediated targeting and labeling of metabolically active cancer and endothelial cells. *Biomaterials* **2011**, *32*, 5863–5871. [CrossRef] [PubMed]
72. Jayapaul, J.; Arns, S.; Bunker, M.; Weiler, M.; Rutherford, S.; Comba, P.; Kiessling, F. In vivo evaluation of riboflavin receptor targeted fluorescent USPIO in mice with prostate cancer xenografts. *Nano. Res.* **2016**, *9*, 1319–1333. [CrossRef] [PubMed]
73. Tsvetkova, Y.; Beztsinna, N.; Jayapaul, J.; Weiler, M.; Arns, S.; Shi, Y.; Lammers, T.; Kiessling, F. Refinement of adsorptive coatings for fluorescent riboflavin-receptor-targeted iron oxide nanoparticles. *Contrast Media Mol. Imaging* **2016**, *11*, 47–54. [CrossRef] [PubMed]
74. Thomas, T.P.; Choi, S.K.; Li, M.-H.; Kotlyar, A.; Baker, J.R. Design of riboflavin-presenting PAMAM dendrimers as a new nanoplatform for cancer-targeted delivery. *Bioorg. Med. Chem. Lett.* **2010**, *20*, 5191–5194. [CrossRef] [PubMed]
75. Wong, P.T.; Sinniah, K.; Choi, S.K. Riboflavin-Conjugated Multivalent Dendrimer Platform for Cancer-Targeted Drug and Gene Delivery. In *Bioactivity of Engineered Nanoparticles*; Yan, B., Zhou, H., Gardea-Torresdey, J.L., Eds.; Springer: Singapore, 2017; pp. 145–171.
76. Witte, A.B.; Leistra, A.N.; Wong, P.T.; Bharathi, S.; Refior, K.; Smith, P.; Kaso, O.; Sinniah, K.; Choi, S.K. Atomic Force Microscopy Probing of Receptor–Nanoparticle Interactions for Riboflavin Receptor Targeted Gold–Dendrimer Nanocomposites. *J. Phys. Chem. B* **2014**, *118*, 2872–2882. [CrossRef] [PubMed]
77. Witte, A.B.; Timmer, C.M.; Gam, J.J.; Choi, S.K.; Banaszak Holl, M.M.; Orr, B.G.; Baker, J.R.; Sinniah, K. Biophysical Characterization of a Riboflavin-conjugated Dendrimer Platform for Targeted Drug Delivery. *Biomacromolecules* **2012**, *13*, 507–516. [CrossRef]
78. Leistra, A.N.; Han, J.H.; Tang, S.; Orr, B.G.; Banaszak Holl, M.M.; Choi, S.K.; Sinniah, K. Force Spectroscopy of Multivalent Binding of Riboflavin-Conjugated Dendrimers to Riboflavin Binding Protein. *J. Phys. Chem. B* **2015**, *119*, 5785–5792. [CrossRef]
79. Beztsinna, N.; Tsvetkova, Y.; Bartneck, M.; Lammers, T.; Kiessling, F.; Bestel, I. Amphiphilic Phospholipid-Based Riboflavin Derivatives for Tumor Targeting Nanomedicines. *Bioconjug. Chem.* **2016**, *27*, 2048–2061. [CrossRef]
80. Bareford, L.M.; Avaritt, B.R.; Ghandehari, H.; Nan, A.; Swaan, P.W. Riboflavin-Targeted Polymer Conjugates for Breast Tumor Delivery. *Pharm. Res.* **2013**, *30*, 1799–1812. [CrossRef]
81. Tsvetkova, Y.; Beztsinna, N.; Baues, M.; Klein, D.; Rix, A.; Golombek, S.K.; Al Rawashdeh, W.; Gremse, F.; Barz, M.; Koynov, K.; et al. Balancing Passive and Active Targeting to Different Tumor Compartments Using Riboflavin-Functionalized Polymeric Nanocarriers. *Nano. Lett.* **2017**, *17*, 4665–4674. [CrossRef]
82. Miller, M.A.; Zheng, Y.-R.; Gadde, S.; Pfirschke, C.; Zope, H.; Engblom, C.; Kohler, R.H.; Iwamoto, Y.; Yang, K.S.; Askevold, B.; et al. Tumour-associated macrophages act as a slow-release reservoir of nano-therapeutic Pt(IV) pro-drug. *Nat. Commun.* **2015**, *6*, 1–13. [CrossRef] [PubMed]

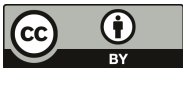

cancers

MDPI

Review

Nanodrug Delivery Systems for the Treatment of Ovarian Cancer

Jonathan M. Pantshwa, Pierre P. D. Kondiah, Yahya E. Choonara, Thashree Marimuthu and Viness Pillay *

Wits Advanced Drug Delivery Platform Research Unit, Department of Pharmacy and Pharmacology, School of Therapeutic Sciences, Faculty of Health Sciences, University of the Witwatersrand, Johannesburg, 7 York Road, Parktown 2193, South Africa; monwabisi.pantshwa@wits.ac.za (J.M.P.); pierre.kondiah@wits.ac.za (P.P.D.K.); yahya.choonara@wits.ac.za (Y.E.C.); thashree.marimuthu@wits.ac.za (T.M.)

* Correspondence: viness.pillay@wits.ac.za; Tel.: +27-11-717-2274

Received: 4 November 2019; Accepted: 13 December 2019; Published: 15 January 2020

Abstract: Despite advances achieved in medicine, chemotherapeutics still has detrimental side effects with ovarian cancer (OC), accounting for numerous deaths among females. The provision of safe, early detection and active treatment of OC remains a challenge, in spite of improvements in new antineoplastic discovery. Nanosystems have shown remarkable progress with impact in diagnosis and chemotherapy of various cancers, due to their ideal size; improved drug encapsulation within its interior core; potential to minimize drug degradation; improve in vivo drug release kinetics; and prolong blood circulation times. However, nanodrug delivery systems have few limitations regarding its accuracy of tumour targeting and the ability to provide sustained drug release. Hence, a cogent and strategic approach has focused on nanosystem functionalization with antibody-based ligands to selectively enhance cellular uptake of antineoplastics. Antibody functionalized nanosystems are (advanced) synthetic candidates, with a broad range of efficiency in specific tumour targeting, whilst leaving normal cells unaffected. This article comprehensively reviews the present status of nanosystems, with particular emphasis on nanomicelles for molecular diagnosis and treatment of OC. In addition, biomarkers of nanosystems provide important prospects as chemotherapeutic strategies to upsurge the survival rate of patients with OC.

Keywords: nanosystems; drug delivery; nanomicelles; ovarian cancer; tumour targeting; chemotherapeutics

1. Introduction

Globally, ovarian cancer (OC) is a lethal condition that accounts for millions of deaths annually in females, making this condition a major health issue [1–6]. In the last five-year survey, statistics reflected approximately 21.9 million new patients clinically diagnosed with OC on a yearly basis, with 14,270 deaths predicted in the United States every year [7]. According to the World Health Organization (WHO), OC is one of the most lethal genital malignancies in females in developing countries, with this asymptomatic disease exacerbated by lack of early diagnostic strategies and access to expensive chemotherapeutic drugs [1]. In Africa (South Africa), the Cancer Council of Southern Africa (CANSA) confirmed more than 500 cases of OC [8]. Globally, the five-year survival rate ranges from 15%–20% for the population with advanced stage ovarian cancer, even though patients undergo operative surgery and platinum chemotherapy [9].

The treatment of OC employs invasive surgery for the removal of infected ovaries, uterus, fallopian tubes, cervix and lymph nodules in the abdomen. The surgical approach is followed by external beam radiotherapy or systemic chemotherapy, depending on the stage at which the OC disease is identified. Intravenous paclitaxel and alkylating cisplatin are conventional therapeutics employed for treatment of OC with antimetabolite methotrexate also considered as a possibility. However,

conventional treatment has its own share of drawbacks, including toxicities and subsequent disease relapse, due to the development of multidrug resistance. In addition, the chemodrug is not specific for OC destruction, hence exhibiting dose cytotoxicity [10–12]. Furthermore, the long-term prognosis is usually adversative with expression and development of chemoresistant tumours. Patients undergo diverse side effects including excessive nausea, hair loss and deterioration in plasma cell counts linked with the administration of chemotherapy for OC treatment [13]. To circumvent treatment drawbacks of conventional antineoplastics, several targeted drug delivery platforms have been developed to direct antineoplastics to specific tumour sites [14].

New advances in polymeric nanotechnology—with particular emphasis on nanomicelles—provide feasible alternatives for early detection and targeted treatment of metastatic OC, thereby minimizing systemic toxicity associated with administration of chemotherapeutic drugs. The nanosystems employed as theranostics include polymeric nanoparticles, nanomicelles, nanoconjugates, as well as dendrimers [14–16].

In order to improve diagnosis and chemotherapeutic efficacy in ovarian cancer treatment, this article presents a critique of, (a) formulation of nanoparticulate delivery systems (including nanomicelles), and (b) nanoparticulate delivery systems functionalized with ligands such as antibodies to expedite specific elimination of tumours, imaging analysis and aid in decreasing drug-related side effects (Figure 1). Thus, the basics of design of these delivery systems are to improve blood circulation in vivo, polymeric biodegradability, and theranostic compatibility with adequate retention time, for nanocarrier-related therapeutics. Furthermore, the synthetic building blocks of the carrier systems are nontoxic, noninteractive with inflammatory responses, and biocompatible. Other significant properties of polymeric carrier systems are biodegradability and clearance by hepatic/ renal pathways post-drug release, with the prospect to be further traced with additional benefits in molecular imaging technologies [17].

This review thus aims to present advances in nanosytems-based molecular diagnosis and treatment of OC. A particular focus is on nanomicelles as one of the most researched nanoarchetypes for imaging/diagnosis and targeted OC treatment. The status of OC biomarkers is concise, with the integration of studies conducted on mucins and possible application in early diagnostics and management of OC. These approaches are defined to potentially identify the disease at an early stage, halt disease progression and promote recovery.

2. Current Nano-Based Drug Delivery Approaches for Ovarian Cancer Theranostic

Numerous nanodrug delivery vehicles have been developed including nanoconjugates, branched dendrimers, liposomes, nanostructured lipid formulations and polymer nanomicelles (Table 1) [18,19]. These drug delivery systems have many advantages including the promotion of therapeutic drug delivery and fulfilling several (biopharmaceutical) parameters, such as a marked increase in therapeutic impact compared to the free drug, good biodegradability and biocompatibility, nontoxic and noninflammatory characteristics, as well as future prospects in scaling-up manufacturing [20]. In chemotherapeutic systems, a nanoformulation must possess high drug-loading capacity, the ability to dissolve drugs within the inner core and selectively accumulate in tumour tissue through permeability and retention influence (passive or active targeting). Targeted chemotherapy, such as intraperitoneal implantable treatment, provides targeted therapy within the peritoneal cavity (Figure 1) [21–25]. In addition, the preparation of nanoformulations functionalized with specific ligands facilitates preferential targeting of OC tumours and ultimately increases the therapeutic effect in comparison to nonfunctionalized nanosystems [25–30].

Table 1. Outline of the distinguishable nanotherapeutic tools designed for ovarian cancer treatment [19].

Nanosystems	Polymer–Drug Conjugates	Dendrimers	Polymer Micelles	Liposomes	Solid Lipid Nanoparticles
Size	≤10 nm	2–10 nm	10–100 nm	100–200 nm	50–1000 nm
Structural characteristics	Macromolecular structure	Macromolecular Tree-like structure	Spherical Supramolecular Core shell structure	Spherical bilayer vesicle structure	Spherical, bilayer-nanocapsular structure
Carrier composition	Water-soluble polymer	Hyperbranched polymer chains	Amphiphilic di and tri-block copolymers	Phospholipid, cholesterol membrane lipids	Solid lipid emulsifier water
Drug incorporation strategy	Covalent conjugation requiring functional groups on drug and polymer	Covalent conjugation requiring functional groups on drug and polymer	Noncovalent encapsulation/ compatible with hydrophobic drugs	Noncovalent encapsulation/ compatible with hydrophilic drugs	Noncovalent encapsulation/ compatible with hydrophilic drugs
	PEG-paclitaxel & HPMA copolymer-doxorubicin—phase II trials SMANCS & CDP870 (Cimza)- Approved	Dendrimer-docetaxel & Viva gel- phase II & III trials PSMA-targeted dendrimers & Avidimer-dendrimers- Approved	CRLX-101&NKTR-102-phase II/III clinical trials Genexol- PM-Approved	SGT53-01& MCC- 46 phase I clinical trials Doxil, Ambisome & DaunoXome-Approved	SLNs with $[Gd\text{-}DTPA(H_2O)]^{2-}$ and $[Gd\text{-}DOTA(H_2O)]^{-}$ compounds preclinical trials [31]. Diazemuls & Diprivan- Approved

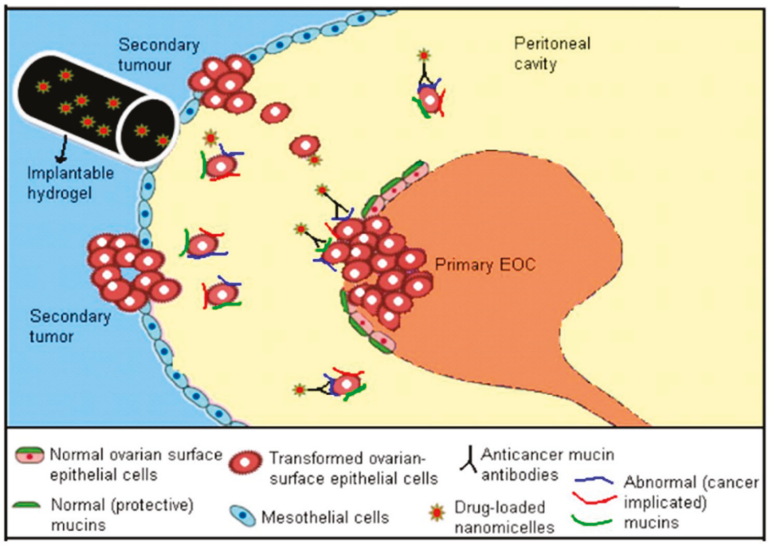

Figure 1. Illustration of the expression of cancer-associated mucins, accompanying the development of ovarian cancer and the intraperitoneal implant treatment, providing targeted therapy within the peritoneal cavity (Adapted with permission from [21].

In this context, there is a significant need to develop stable molecular biomarkers for early detection of OC [14]. Various prospective biomarkers of OC are reported. Epithelial ovarian tumours display modified cell antigens including, Human Epididymis Protein 4 (*HE4* gene), Cancer Antigen *72-4*(CA 72-4), Renal Estimated Glomerular Filtration Rate (EGFR), Soluble Mesothelin-Related Peptides (SMRP), Mesothelin, Osteopontin (OPN), Alpha-Fetoprotein (AFP), Cytotoxic T-Lymphocyte-associated Protein 4 (CTLA4), Interferon-alpha (IFNα), Kallikrein-6 (KLK6), phospholipase A2 group 2A (PLA2G2A), Erythroblastic Oncogene B2 (ErbB2), Interleukin-10 (IL-10) and Mucin-16 (MUC1–16), that differentiate cancerous cells from healthy ovarian tissue and other ordinary cells covering the

intraperitoneum [23–30]. Mucin proteins (specifically MUC16) show prospective as biomarkers and antibody functionalized micelles to provide a broad range of prospects for OC therapy [32].

Nanomicelles are synthetic nanovehicles, with high potential loading capacity for chemotherapeutics designed for site-specific ovarian tumour targeting [33–36]. A size range of a micelle between 10–100 nm promotes significant permeability, endocytosis by OC cells and decreases nonselective targeting of normal cells [37]. Nanomicelles can perforate and assemble in regions with permeated vasculatures, including tumours and inflamed tissues [37–39]. In addition, improved biocompatibility, in vivo stability, ability to incorporate a wide range of hydrophobic chemotherapeutics, as well as extended plasma circulation periods, are achieved [40,41].

3. Critical Comparison of Nanosystems to Nanomicelles for OC Treatment

Polymer–drug conjugates or prodrugs are macromolecular dispersed systems that require covalent binding of the active principle while nanoparticles on the contrary are physically attached to the active principle. Polymer–drug conjugates have low molecular weight (specific to polymer incorporation), which permits molecular targeting within the cancer cell [42,43]. Physicochemical properties of polymer–drug conjugates (pH, enzymatic-alteration, acid (H^+)-catalytic chemical reactions) are vital for drug release at a tumour site. Polymer–drug conjugates are extensively evaluated for prolonged drug release in cancer cells, tumour mass invasion, and enhancement of anti-tumour proliferation [44–46]. Therapeutics in ovarian cancer also utilize branched dendrimers formulated from several polymers and genetic DNA, however acrylamide branched nanodendrimers are usually utilized [46]. Branched dendrimers have characteristic design components including (i) peripheral surface with several potential attachment sites, (ii) the central inner core where diverse dendrons demarcate the alienated constituent stratums covering the inner core and (iii) the location for dendronic conjugation. The three fragments of branched dendrimers are modified for several uses, including drug transport and DNA delivery [47]. Polymer–drug conjugates and dendrimers have covalently bonded drug molecules to the polymeric carriers. This consecutively necessitates the association of the complex with specific biochemical processes, shielding the complex from in vivo catalytic enzymatic destruction and protonic acid-hydrolytic reactions [48–50]. Furthermore, the minute-size of these carriers (normally 10 nm), enables perforation through plasma membranes of the glomeruli [17]. Significant assemblies and differentiating properties of these delivery systems are demonstrated in Table 1, as well as in Figure 2.

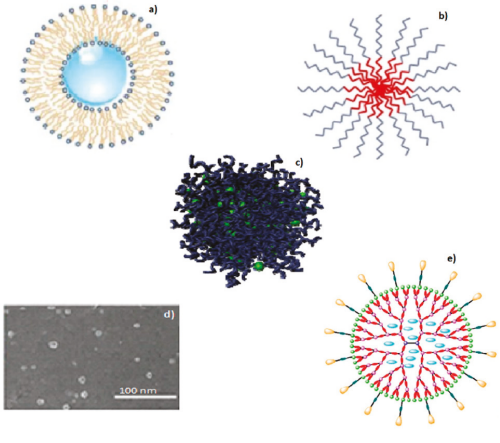

Figure 2. Schematic depicting examples of nanosized delivery systems; (**a**) liposomes, (**b**) nanomicelles, (**c**,**d**) polymer–drug conjugates, and (**e**) dendrimers, which are currently explored in detail for transport of chemotherapeutic agents (adapted with permission from (**a**) Trucillo et al. [31], (**b**) Brandta et al. [51], (**c**,**d**) Tong et al. [52], (**e**) Huang &Wu [53].

Liposomes are similar to nanomicelles due to microscopic spherical shape, consisting of a lipid bilayer, encapsulating aqueous components for hydrophobic drug incorporation. Nonpolar lipophilic drugs are incorporated within the lipid bicoating, while water-soluble drugs reside in the vesicle. Entrapment of antineoplastic therapies in lipophilic liposomes result in pharmacokinetic modifications and pharmacodynamics features, with a resultant decline in drug degradation and improved dose cytotoxicity [31,51–53]. These lipophilic nanocarriers can be utilised for specific targeting and imaging of tumour tissues; however, ligands applied to the phospholipid coating improve cellular uptake thus enabling a pronounced therapeutic effect to the targeted specific-sites [31,51–54]. Solid lipid nanoparticles (SLNs) also have similar properties to nanomicelles. On the contrary, the major challenges with liposomes include instability and difficulty in large-scale synthesis.

Poorly water-soluble drugs are encapsulated in the hydrophobic interior of SLNs, but the distribution ability is hindered by membrane destabilization. However, most liposomal and SLNs are above 90 nm in size, due to intrinsic structural parameters which significantly restrict delivery to ovarian tumour tissue. To surmount the setbacks associated with liposomes and SLNs, other nanoplatforms, including nanoemulsions, polymeric nanoparticles and polymeric nanomicelles are employed [19].

Nanoemulsions are used as templates for polymeric nanoparticle preparation. Therapeutic-loaded nanoemulsions are formed by oil-in-water (o/w) solvent evaporation techniques, employing miscible organic solvents (diethyl ether, chloroform, N, N-dimethylformamide (DMF), acetonitrile, THF). Simple liquid emulsions are either oil-suspended in an aqueous state (o/w), or water-suspended in oil (w/o). Nanoemulsions are aqueous emulsions with sizes normally between 20–200 nm. Nanoemulsions are formulated employing low-energy emulsification procedures, in which the nanosize is adjusted by the physicochemical parameters of the process [55], allowing the development of small-scale and homogeneous droplets, employing a high-energy system, in which a nanosized droplet is adjusted by the degree of the peripheral energy contribution. Among the low-energy emulsification approaches, the Phase Inversion Composition (PIC) system is highly beneficial for structures with thermo-labile composites, including therapeutics, as it can be accomplished at ambient temperature. In the PIC system, the emulsification process is activated by the variations in the voluntary amphiphilic curvature generated in emulsification, changing the constituent at stable temperatures [55].

Morphology, Composition and Mechanism of the Formation of Nanomicelles

Nanomicelles are spontaneously self-assembled or aggregated as versatile nanoparticles formed in water at certain physicochemical parameters including concentration (above Critical Nanomicelle Concentration-CNC), temperature and conductivity; employing surfactants (hydrophilic–hydrophobic polymers), with opposite affinities towards a particular solution [55]. The assembly of amphiphilic components generates the structure or shape of nanomicelles. The copolymer sequence controls the configuration of the prepared nanomicelles. Thin rod designed nanomicelles are also generated when the water-insoluble component is greater than the water-soluble component. Sphere-shaped nanomicelles are usually indicative of a longer hydrophilic component with a minor hydrophobic component, or possibly a result of equal degrees of the amphiphilic components [56]. Constituents of the prepared supramolecular structure of polymeric micelles are usually di- or tri-segment/block, or a stable copolymer (Figure 3). Poly (ethylene oxide) (PEO) forms a barrier to nanomicelles, collapsing and displaying dissolution in an aqueous solvent [33,57]. The inner central component normally possesses a biodegradable polymer such as PEO/β-amino polyesters that can be utilised as an inner core to dissolve hydrophobic pharmaceutical drugs, thus shielding loaded constituents from the aqueous environment; increasing the bioavailability and in vivo efficacy [58–60].

At low ratios in aqueous media, copolymers exist separately, however, once the molar concentration is increased, aggregation occurs [61]. The aggregates known as nanomicelles, comprises of several copolymers in a spherical arrangement [62,63]. When attachments to the polymer functional groups

are anticipated, complexes including carboxylic (COO^-) conjugate bases and amine (NH) bases are joined as the sequence terminating clusters [33].

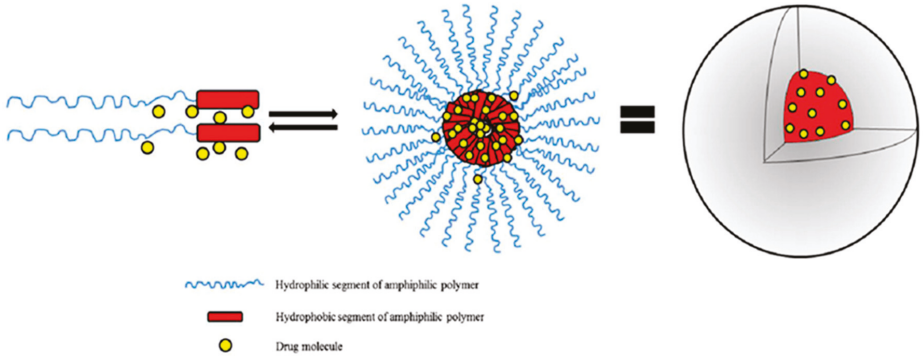

Figure 3. Schematic representation of the supramolecular structure of polymeric micelles (adapted with permission from Lu and Park [47]).

4. Classification of Nanomicelles

Nanomicelles are classified into three key distinct nanosystems i.e., colloidal nanomicelles formulated from an aggregation of polar and nonpolar molecules in an aqueous solution (amphiphilic aggregates), polyionic nanomicelles formulated from oppositely charged polymers generating an agglomeration due to electrostatic interaction, and nanomicelles originating from metal complexation [63–66].

4.1. Amphiphilic Nanomicelles

Amphiphilic colloidal nanomicelles are formed from hydrophobic interactions between the inner core and the outer shell of the surfactant molecules in a solution [60]. An active surfactant retains amphiphilic configurations, comprised of hydrophobic and hydrophilic functional groups [66]. The hydrophilic groups form the polar clusters constructed from several moieties including ionised carboxyl, conjugated sulfonate, ammonium, active hydroxyl and amides. Hydrophobic clusters are nonpolar ends, including molecular hydrocarbon chains with eight or additional carbon molecules, and can be rectilinear or separated structures. Lipophilic and hydrophilic polymers self-assemble into nanomicelles with adequate surfactant concentration. The resultant concentration of surfactant for the formation of nanomicelles is known as critical micelle concentration (CMC). Figure 4 depicts the settings of surfactant alignment on air/aqueous interface to form nanomicelles when subjected to a particular solution with opposite charge affinities to hydrophobic and hydrophilic molecules. The polar ends form the outer surface of nanomicelles with the nonpolar portions, establishes the inner central core. The quantity of drug incorporated into copolymeric nanomicelles is influenced by physicochemical parameters that result in hydrophobic interactions between the drug and the hydrophobic segment of the polymers. Hence, a consideration of physicochemical trends is an invaluable tool in the synthesis of drug loaded copolymeric nanomicelles. The amphiphilic block copolymer, Pluronic® poloxamer, generates amphiphilic nanomicelles in response to electrostatic interactions [63,67].

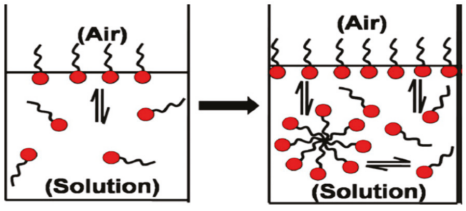

Figure 4. Schematic depiction of surfactant molecules aligning on water/air interface at pre- and post-'Critical Nanomicelle Concentration (CNC)' threshold (adapted with permission from Mukherjee et al. [68]).

4.2. Polycharged Composite Nanomicelles

Polycharged complex nanomicelles (PCCMs) are formulated by the self-assembly of oppositely charged polymers that form aggregates when distributed in an aqueous solution by hydrophilic groups, usually poly(ethylene glycol) (PEG), and are covalently attached to one of the two ionic polymers. Electrostatic interactions are the intermolecular cohesive forces of the assembled composite; with electrostatic and hydrophobic exchanges employed in formulated nanomicelle complexes. PCCMs are prepared using various synthetic methods, including common synthetic procedures and spontaneous self-assemblage or aggregation in solution. PCCMs are prepared from segment copolymers in an aqueous solution, thus circumventing associated cytotoxicity of organic solvent. These nanomicelles are stable with low CMC values—as low as 10^{-6} M. The central core of PCCMs encapsulates several therapeutics, such as hydrophilic and hydrophobic drugs employing intermolecular cohesive forces and hydrogen bond interactions. Therapeutics such as cisplatin and ionic large-scale drugs are released from PCCMs, subsequent to induction from appropriate stimuli [68].

4.3. Noncovalent Connected Polymeric Nanomicelles

These nanomicelles are prepared to employ homopolymeric material or monomer units for nanomicelle agglomeration. The inner and the outer surface are bonded at the polymer edges via specific intermolecular interactions including hydrogen bonds or metal coordinate bonds; for this reason, are known as noncovalently linked nanomicelles. Poly (4-vinylpyridine) functionalized with carboxyl-terminated polybutadiene are the mainstay of intermolecular interaction due to the formation of hydrogen linkages in a common organic solvent such as chloroform [63].

5. Surfactants Employed in Nanomicelle Targeted Platforms for Ovarian Cancer

Surfactant nanomicelles utilized for drug delivery have hydrophobic esters, including polypropylene oxide (PPO), poly(L-lactide) (PLA), poly(D,L- lactide) (PDLLA), as well as amino functional groups such as poly lactide-co-gycolide (PLGA), polycaprolactone (PCL), poly (β-amino ester), and polylactic acid (PLA) in their inner core segment for dissolving hydrophobic chemotherapeutics, as illustrated in Table 2. The hydrophobic core segment is compatible, nontoxic, biodegradable and permitted by the U.S. Food and Drug Administration (FDA) for biopharmaceutical application. On the contrary, the soluble hydrophilic corona surface of the nanomicelle used in therapeutic release is composed of poly(ethylene glycol) PEG, poly(ethylene oxide) PEO, poly N-vinyl pyrrolidone (PVP), poly N-isopropyacrylamide (PNIPAM), poly N-vinyl alcohol (PVA), and poly N-2-hydroxyproyl methacrylamide (PHPMAm), as displayed in the first section of Table 2. In this context, the surfactants self-assemble to form micelles in an aqueous solution with the central amino or ester section, which is structurally neutral/uncharged and connected to the hydrophilic corona. Protein copolymers (including drug peptide copolymers) employed in chemotherapeutic delivery enhance the accumulation at pathological sites and improve endocytotic uptake into the tumour cells. Modification of a specific sequence of the amino acid alters enzymatic functioning and the degree of immune system response [53].

Table 2. Building block copolymers employed in micelle drug transport nanosystems (adapted from Sutton et al., 2007) [69].

Copolymers	Abbreviation	Repeating Unit Structure
Corona segment		
Poly (ethylene glycol)	PEG, PEO	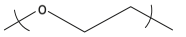
Poly (N-vinyl pyrrolidone)	PVP	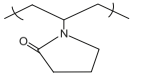
Poly (N-isopropyacrylamide	PNIPAM, NIPAM	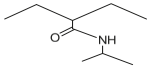
Poly (N-vinyl alcohol)	PVA	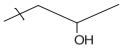
Poly (N-(2-hydroxyproyl methacrylamide)	pHPMAm	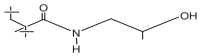
Core segment		
Polyesters Poly (propylene oxide)	PPO	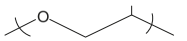
Poly esters Poly (L-lactide) Poly (D,L-lactide)	PLA, PDLLA	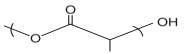
Poly (lactide-co-gycolide)	PLGA	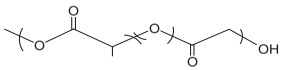
Poly (ε-caprolactone)	PCL	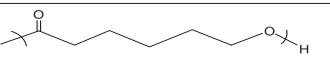
Poly(β-amino ester)		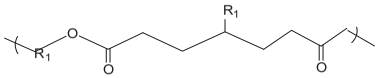
Poly(lactic acid)	PLA	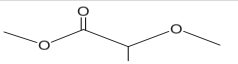

6. Preparation of Drug-Loaded Nanomicelles for Application in Ovarian Cancer

Preparation of therapeutic-loaded nanomicelles involves two major categories of therapeutic loading, reliant on the physicochemical properties of a block copolymer (Figure 5) [69]. The first category is the dissolution of co-polymer with a drug in a solution. This method is used in insoluble polymers, including Pluronics poloxamers, and necessitate the warming of the solution for nanomicelle aggregation, utilizing the dehydrated core profiling portion. This dissolution technique is also employed in preparation of PCCMs, with therapeutic polymer dissolved separately, and nanomicelle aggregates impelled by mixing of the two solutions to stabilize therapeutic–polymer ionic proportions [70,71]. The drawback of this technique is the low drug loading that occurs in nanomicelles [60,72].

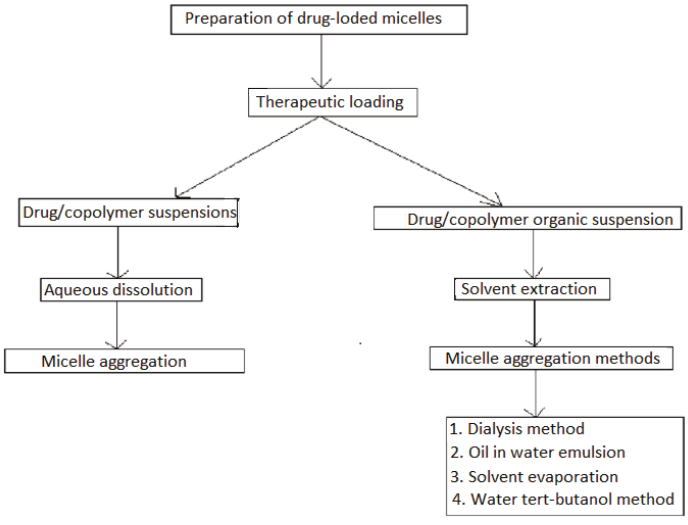

Figure 5. Commonly employed methods of drug-loaded micelle preparation.

The second method of therapeutic loading involves the surfactant, which are partially water-soluble and for which an organic solvent (such as, tert-butyl alcohol, ethyl acetic acid, methyl alcohol, toluene, dichloromethane (DCM), aprotic diethyl ether and chloroform/trichloromethane) is required to dissolve the polymer and therapeutic [73]. Nanomicelle aggregation is reliant on the liquid extraction technique. For homogenous solutions, nanomicelle formulations are extracted via a dialysis exchange method, with slow extraction of the organic solvent that activates nanomicelle aggregation. A drawback of the dialysis technique is that the dissolving of a drug–polymer involves the use of chlorinated solvents, which are toxic and thus necessitate extra time (<36 h) for the adequate encapsulation of therapeutics into the nanomicelles. Alternatively, the solvent-evaporation technique is utilized for the removal of organic solvents by air diffusion to form a polymeric film. The introduction of water to the film with heating facilitates the aggregation of drug-loaded nanomicelles. Nanomicelles synthesized from solvent-evaporation technique have increased potential of dissolving high quantities of partially soluble drugs. These methods all require sterilization and freeze-drying stabilization processes for preservation of the synthesized formulations. Figure 5 depicts the drug loading techniques for nanomicelle formulation.

The limitations in preparations of therapeutic-loaded nanomicelles are surmounted by employing improved approaches such as the tert-butanol (TBA) method, which incorporates the solution of copolymer and therapeutic liquid/TBA medium followed by freeze-drying, to form a dry powdered lyophilized cake. Stable nanomicelles spontaneously self-aggregate, upon resuspension of the lyophilized powdered polymer–therapeutic cake in an aqueous solution [74,75].

7. Applications of Nanomicelles in Ovarian Cancer

Nanomicelles are considered as prospective carriers for imaging agents and therapeutics due to their extended circulatory times, improved drug stability, specific targeting and proliferation into tumour tissue. Nanomicelles are employed as multifunctional molecular probes for identification (diagnosis), noninvasive screening and early treatment of ovarian cancer [72].

7.1. Diagnosis of Ovarian Cancer Employing Nanomicelles

Ovarian carcinoma is commonly identified in late stages due to comparative lack of early detection and diagnostic techniques in early stages [44]. The delivery and controlled release of therapeutics for site-specific targeted chemotherapy and imaging for early cancer identification are of great pertinence [76,77]. Imaging involves visualization of OC disease development, treatment efficacy and bio-distribution of therapeutics to the tumour, or investigation of molecular biomarkers [78]. Disease inspection and monitoring of therapeutic efficiency can be achieved by employing current medical visualizing modalities such as basic radiography, anatomical probes (CT scanning), ultrasound and magnetic resonance imaging (MRI) [74].

These imaging techniques can be categorized according to the energy utilized to develop visual images (heterogeneous X-ray beams, positron emissions, photon emissions), spatial specific resolution accomplished (macroscopic-, meso-scale, microscopic), or the nature of the captured information (anatomical, physiological or molecular/cellular imaging) [44,75]. However, these imaging techniques rely on a diagnosis of cancer when tumours have developed to approximately 1 cm^3, and at this stage, the malignancy has around 1 billion metastatic tumour cells [79]. Furthermore, imaging probes have low signal transmission, instability, imprecise interactions, and rapid degradation from the circulatory system [80].

Nanotherapeutic applications incorporating noninvasive tumour molecular imaging have prospects in early prognosis by increasing the precision, efficacy of chemotherapeutics, and facilitating improved infection detection [44]. If image modalities are utilized to image tumours, improved tumour intensity is assimilated with contrast nanocarrier systems. Nanoparticles have distinct techniques for molecular-targeted delivery, drug encapsulation, or improvement of pathological areal imaging. Polymeric nanoparticles, including PEG-b-poly(Lysine) copolymers have great potential in analytic molecular imaging, monitoring of cancer development or regression [44]. Small particles within nanometer range, such as gold-plated-based molecules and coated metallic quantum molecules, are the most usually employed; however, other nanoparticles and biomarkers display possibilities as potent tools for potential transmission development and therapeutic delivery in diagnosis of infected sites [44]. Various one-off administered nanomicelle-based therapeutic delivery systems for tracking and targeting of ovarian cancer are outlined in Table 3.

Table 3. Polymeric micellar systems employed for treatment and diagnosis (adapted from Kedar et al. [80]; Chen et al. [81]).

Polymer Structural Formula	Method of Synthesis	Method of Micellization	Delivered Agent	Mode of Delivery	References
PLGA-b-PPO-b-PLGA and PEG-b-PPO	Ring-opening polymerization	Dialysis method	Doxorubicin (DD)	P	[82]
Poly(ε-caprolactone)-b-PEO	Anionic ring opening polymerization	Dialysis method	Pyrene (hydrophobic fluorescent probe) (DA)	P	[83]
Poly(lactic acid)-polyurethane	Step condensation	Microphase separation method	Gliclazide (DD)	P	[84]
PMPC-b-PBMA	RAFT technology	Self-emulsion evaporation method	Paclitaxel (DD)	P	[85]
Poly(ethylene glycol-b-lactide)	Anionic ring opening polymerization	Oil-in-water emulsion method	Taxol (DD)	P	[86]
Poly(lactide-b-PEG)	Solvent polymerization	Self-emulsion solvent evaporation method	Paclitaxel (DD)	P	[87]
mPEG-b-p(HEMAm-Lac_n)	Free-radical polymerization	Rapid heating procedure	Pyrene (DA)	P	[88]
γ-Benzyl l-glutamate N-Carboxyanhydride	Polymerization	Dialysis	Adriamycin (DD)	P	[89]
Acetal-PEG-b-PLA	Ring-opening polymerization	Dialysis method	Docetaxel, ^{125} I (DD), (DA)	Tyrosine-A, tyrosyl-glutmic acid-A	[90]
COOH-PEG-b-PLGA	Polymerization	Dialysis method	Docetaxel, paclitaxel (DD)	RNA aptamer-A DNA aptamer-A	[91]
PEG-b-PCL	Free-radical polymerization	Dialysis method	Paclitaxel, rapamycin (DD)	Folate- A	[92]
PEG-b-PLLA and P(HEMA)-b-p(His)	Solvent polymerization	Dialysis method	Doxorubicin (DD)	-	[93]
P(HEMA)-b-p(His)	Solvent polymerization	Dialysis method	Doxorubicin(DD)	Folate-A	[94]
PEG-b-PLA and HEMA-co-his)-g-PLA	Anionic ring opening polymerization	Oil-in-water emulsion method	Doxorubicin, Cy 5.5 (DD), (DA)	Folate-A	[95]
PEG-b-PLA and P(NVI-co-NVP)-g-PLA	Anionic ring opening polymerization	Oil-in-water emulsion method	Doxorubicin, ^{123} I (DD), DA	Folate-A	[96]
mPEG-b-PLA and P(NIPAAm-co-MAAc)-g-PLA	Solvent polymerization	Self-emulsion solvent evaporation method	Doxorubicin, FITC (DD), DA	Galactosamine-A	[97]

Abbreviations: P-passive targeting, A-active targeting, DD-Delivered Drug & DA-Delivered Agent.

Several nanomicellar technologies have been established and are presently undergoing extensive preclinical and clinical trials for application in chemotherapeutics and diagnostic imaging of ovarian cancer. Amphiphilic block-copolymers aggregate to form dual-layered nanomicelles and are future carriers of hydrophobic treatments and diagnostic probes. Partially soluble drugs and imaging agents are encapsulated into the inner core with hydrophilic surface of amphiphilic nanomicelles, forming a stable outer shell in an aqueous solution [77].

Diagnostic modalities for three main imaging probes are radioactive metals, including indium-111 (^{111} In), and radioactive metal complexes such as ortechnetium-99 m ($^{99\,m}$ Tc), used for scintigraphy; clustered/chelated magnetic metals, including gold, for magnetic resonance imaging (MRI); and iodine for conventional X-ray computed tomography (CT). The conventional contrast agents employed in medical therapeutics are low-molecular-weight complexes composed of these chemical probes. Several diagnostically significant amphiphilic composites have been effectively integrated into nanomicelles, including diethylene-triamine penta-acetic acid (DTPA), which are chelating agents for diagnostic imaging of various nanomicellar platforms utilized in MR diagnostic imaging. Polymeric nanomicelle systems, including iodine-containing PLL-PEG nanomicelles, are employed for cancer diagnostic imaging, utilizing conventional sectional tomography (CT) imaging and Single Photon Emission Computed Tomography SPECT using gamma rays. Furthermore, to monitor nanomicelles formulations and exchanges in cancer disease, nanomicelle co-encapsulated with imaging clustered/chelated metallic groups have been employed, for example, in gold compounds, manganese oxide-loaded nanoparticles, as well as being utilized with ultrasound (US) and magnetic resonance imaging (MRI) [76]. Currently, gadolinium (Gd)-contrast medium, including Magnevist®, are medically employed where visual contrast is increased by limiting the T1 reduction period (period of high longitudinal magnetization with brighter image) of aqueous protons. Integration of Gd compound on the nanomicelles' surface upsurge the T1 reductivity and reactivity of diagnosis. The reactivity is improved by utilization of various developed architectural iron oxide nanoparticles such as surface designed Super Paramagnetic Iron Oxide Nanoparticles (SPIONS) that assemble in nanomicelle inner core and exhibit MRI reactivity at a nanomolar rate. Nanomicellar loading with therapeutics and imaging tools such as fluorescence Rhodamine and FITC probes are used for drug released imaging at specific tumour sites with distinctive designed image. Hence, nanomicelles are favourable as carriers for combinational chemotherapeutics and nanodiagnostic tools [98–100].

7.2. Treatment of Ovarian Cancer Using Nanomicelles

Nanomicelles are mainly administered intravenously (IV) and are usually exposed to several challenges of the blood circulatory system with resultant cytotoxicity before reaching the peritoneal cavity [101]. The intraperitoneal (IP) cavity is the principal site of OC disease [102]. Metastatic OC cells accountable for high mortality rate disseminate and recur at the intraperitoneal site [103]. Hence, IP nanomicellar chemotherapy is the favorable route of administration of OC treatment, with improved patient compliance as compared to intravenous (IV) treatment [104–106].

7.3. Targeting Strategies of Nanomicelles

Targeted delivery of polymeric nanomicelles loaded with chemotherapeutic agents, present many diverse advantages [107]. Targeting is usually achieved using two delivery mechanisms as depicted in Figure 6; (i) passive targeting with improved vascular permeability and absorbency effect [39], (ii) specific active receptor-mediated targeting, employing ligand functionalized-nanomicelles, including the attachment of antibodies [63].

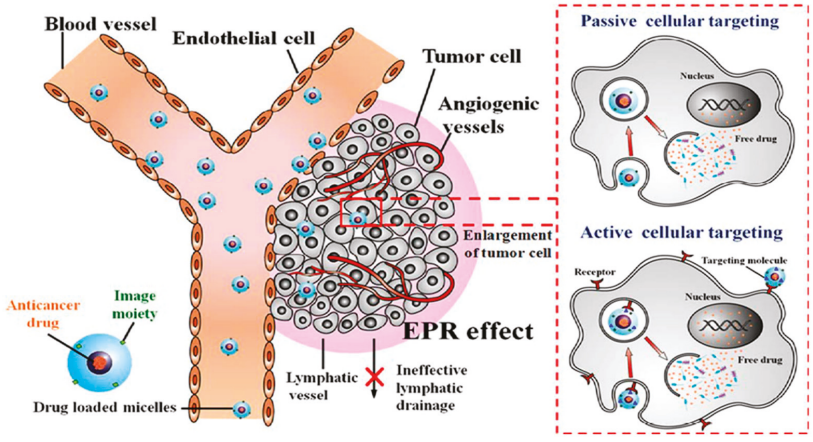

Figure 6. Schematic representation of drug loaded micelles (spheres) with imaging agents, from the administration site to the tumour tissue. After administration, micelles (10–200 nm) display specific targeting of tumour growth via passive targeting with cellular endocytotic uptake from exterior fluid to the cancer cells. Active targeting through receptor-mediated internalization is achieved by attachment of antibody ligand molecules, to the surface of micelles (Adapted with permission from Chen et al. [81]).

7.3.1. Passive Targeting by Enhanced Permeability Effect of Tumour Tubular Blood Vessels

When nonfunctionalised nanomicelles have significant continual blood circulation period and successfully accumulate in tumour tissue through the passive enhanced permeability effect (EPR), this is indicative of passive targeting [76,108]. The therapeutic payloads are distributed to the tumour extracellular matrix and dispensed into the tumour cells and tissues. EPR targeting is ascribed to pathophysiological properties of tumours that are not identified in health tissue. These properties include the architecture of leaky tumour blood vasculature, impaired lymphatic drainage scheme, and increase in formation of permeability agents [109–112]. Several passive targeting nanocarrier systems have a PEG coating for stealth and "concealment" properties, including Genexol-PM, SP1049C, NK911, Opaxio™ (formerly Xyotax™), CRLX101, ProLindac™, SPI-77 and CPT-11 [76].

7.3.2. Specific Active Receptor-Mediated Targeting

The active targeting approach involves the attachment of functional ligands to the nanomicelle surface. These ligands identify tumour-specific receptors that are overexpressed on the cancer cell plasma membranes, resulting in increased uptake and increased internalization of nanomicelles into tumour tissue via the receptor-mediated endocytosis process [113–115]. Commonly utilized affinity ligands are classified into the following categories: small unrefined molecules, nucleotides (RGD sequence), oligopeptides, sugar groups, folates, monoclonal antibodies (mAb), and nucleic DNA/RNA aptamers [116].

There are several tools that are being utilized to target particles to tumour tissue. The use of an activating ligand is a dynamic approach that is reliant on specific receptors at an attachment site. These interactions include (glycoproteins/antibody), antigens and activating attachment groups (Figure 7). The "magic bullet concept" Ehrlich hypothesized that antibody-bounded nanocarriers have progressed into a model using three components: a therapeutic, a copolymer and active functionalizing agents associated with one formulation. This targeting therapeutic strategy provides rewards, including high target specificity for the pathological/infected area and minimal toxicity to the healthy cells. Furthermore, this therapeutic strategy also improves tumour treatment, chemotherapeutics of metastatic cancer of early stage carcinoma, when the primary papillary fallopian tubes are still immature [113–115].

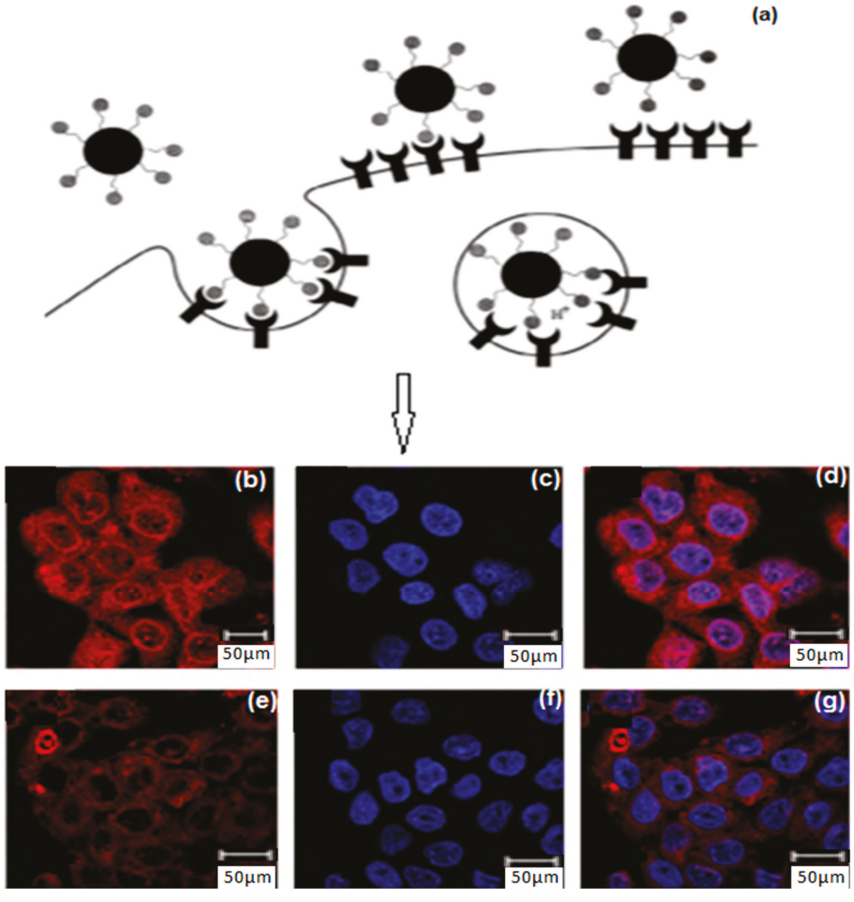

Figure 7. Schematic depiction of (**a**) active targeting, (**b**–**g**) confocal images of A431 cellular uptake incubated with cetuximab encapsulated micelles and lysotracker. The fluorescence intensity of A431 cells (**b**–**d**) treated with targeting micelles was 1.45 times higher than in cells incubated with antibody-free micelles (**e**–**g**) (Adapted with permission from Sudimack et al. [117]; Liao et al. [118].

8. Mucins as Targets for Antibodies in Chemotherapeutics

Most ovarian carcinomas are of epithelial origin and express mucins utilized as prospective diagnostics and treatment targets. Mucin glycoproteins are extracellular, glycosylated protein molecules, originating in the mucus coating and increased expression has been linked with various types of malignant pathology including OC. Currently, there are 20 identified mucins with two classifications: epithelial mucins (gelating, nongelating, film attached mucins) and lycoproteins (MUC9, MUC10, MUC18 and MUC20) [116–118]. Various research studies on the expression of mucin antigen in ovarian cancer have identified overexpression of film-attached mucins, especially MUC4, MUC5AC, and MUC16, but their biological applications are not defined. Mucin 16 (CA125) is used as a clinical biological marker in OC due to its elevated expression which results in CA125 release into the blood serum [119,120]. CA125 is a very huge cell surface mucin, first established by Robert Knapp in 1981. He identified this glycoprotein whilst exploiting identical monoclonal antibody-mAb [121]. Serum levels of CA125 are clinically utilized to diagnose OC patients on basis of regression or progression of the disease, subsequent to standard chemotherapy [122]. Moreover, abnormal mucin expression

can trigger immunity and probably cause a strong antibody response. The antibody response is symptomatic of disease expression [123]. Immunoglobulin Ig (antibodies) affiliated with mucins, can have potential application in the progression towards the detection and therapy of ovarian cancer; however, there are still few studies conducted to date [121–123].

9. Stimulus-Responsive Nanomicelles

Stimuli-responsive nanomicelles (SRM) are smart nanoparticles engineered to respond to internal/external stimuli of physical, chemical or biochemical origin, to control and release drug payloads at specific sites. SRM deliver drug payloads by structural alterations in response to the eliciting stimulus. The response presents with the degradation/disruption, polymerization or assembly of nanomicelles. The common internal stimuli in a cancer microenvironment are acidic pH, electrochemical redox potentials of the cell, and the availability of certain over-produced matrix enzymes, while external stimuli include temperature, attraction via magnetic field, light illumination (UV, visible, infrared) and ultrasound waves [95]. In this context, the formulation of nanomicelle, sensitive to external or internal stimuli is an alternative approach to targeted therapeutic release. In vitro models have provided evidence of progress for a number of stimuli-responsive approaches, however only a small proportion have been validated in animal preclinical prototypes, and also few (thermosensitive liposomes and iron oxide nanoparticles) are clinically approved by the FDA in terms of treatments and diagnostics [81].

10. Nanomicelles in Clinical Evaluations

Several therapeutic-loaded nanomicelles for chemotherapy have been evaluated for determination of toxicity and bioavailability [124]. While the impetus is on ovarian cancer, some examples of polymeric nanomicelles cited are for other types of cancer and applied for OC treatment. Preclinical evaluations and findings have revealed lots of positive data utilizing nanomicelles as therapeutic delivery systems for loading hydrophobic chemotherapeutic drugs [125]. Several micellar nanoformulations that are now under clinical evaluations are all stealth nanomicelle formulations, and specifically have a surface coating for stabilization to guarantee a compact conformational covering and protection against opsonisation by plasma proteins (Table 4) [69]. Genexol-PM micelle formulation is paclitaxel-loaded PEG-PLA micelle preparation [126]. NK012 micellar nanoformulation is also composed of a PEG coating with amino-acid repeat units, polyglutamate (PGlu) combined with antineoplastic 7-ethyl-10-hydroxy-camptothecin (SN-38) [69]. The hydrophobic PGlu component results in micelle aggregation. In vivo trials with NK012 micelle formulations validated the potency of antineoplastic action in a mice model. Recently, the accomplishments and applicability of NK012 were also screened in phase II trials in prominent breast tumour patients [69]. New paclitaxel (PTX) experimental formulations evaluated include NK105 that are composed of PEG coating and modified polyaspartate hydrophobic ration [69]. PTX drug is incorporated in the central core by hydrophobic links with the hydrophilic portion. Furthermore, a major decrease in cytotoxicity, from Cremophor EL and ethanol subsequent to primary PTX administration, was practical with NK105. In phase I trials with NK105 formulation, minor allergic reactions were identified in patients with bile duct, pancreatic, gastric, and colonic cancers compared to primary PTX treatment [69].

Table 4. Polymeric micelle-based formulations containing chemotherapeutic drugs in clinical trials.

Formulation Trade Name	Incorporated Drug	Purpose	Polymer	Particle Size (nm)	Drug Loading (%)	Phase	References
Genexol-PM	Paclitaxel	Solubilization	MPEG-PDLLA	<50	16.7	III, IV	[127]
NK-105	Paclitaxel	Targeting	PEG-P(Asp)	85	23.0	II, III	[128]
SP-1049C	Doxorubicin	Anti-MDR effect	Pluronic L61, F127	30	8.2	I, II, III	[69]
DTXL-TNP	Doxorubicin	Targeting	PLA-PEG, PLA-PEG-ACUPA	100	10	I	[129]
NC-6004	Cisplatin	Targeting	PEG-P(Glu)-Cisplatin	30	39	I, II	[130]
NC-4016	DACH-platin	Targeting	PEG-P(Glu)-DACH-platin	20–100	25	I	[131]
NK 012	SN-38	Targeting	PEG-P(Glu)-SN38	20	20.0	II	[132]
NK911	Doxorubicin	Targeting	PEG-(Asp)-Dox	40	*n*. a	II	[133]

A SP1049C phase II cancer trial in cases with advanced stomach cancer has been conducted. SP1049C has been formulated as doxorubicin (DOX)-loaded Pluronic micelles [69]. In these phase II cancer trials, SP1049C displayed to be more effective than clinical doxorubicin in therapy of various types of carcinoma [69]. SP1049C displayed superior antineoplastic action, efficiency and increased in cancer cells in several pre-clinical carcinoma models as well as doxorubicin-resistant malignancies as compared to clinical doxorubicin [69]. SP1049C formulations have been screened in phase III trials in patients with metastatic adenocarcinoma of the gastrointestinal route [69]. To minimise toxicity and increase the efficacy of cisplatin, the micellar pharmaceutical preparation NC-6004 (Nanoplatin™) was developed. The NC-6004 consists of PEG coating with poly (γ-benzyl L-glutamate)/CDDP composite [69]. A small phase I pilot showed that NC-6004 was acknowledged by carcinoma patients that were affected by colorectal carcinoma, upper oesophageal carcinoma, and lung carcinoma [69]. The Genexol-PM formulation was a micellar PTX nanoformulation formulated from PEG with polylactic acid [68,134,135]. Preclinical in vivo trials with Genexol-PM formulation exhibited a threefold increase in average dissolution time and a significantly improved antineoplastic efficacy as compared with clinical paclitaxel [69].

11. Patents in Micellar Technologies for Targeted Chemotherapeutic Drug Delivery

In a patent by Kwon and associates (2015), solubilisation of cotton gossypol (a yellow, natural phenolic aldehyde plant pigment for inhibition of various dehydrogenase enzymes) with nanomicelles was conducted. Polymeric-nanomicelles integrated chemodrugs such as gossypol, and a combination of chemodrugs were evaluated, including mixture of a platinum-derived (cisplatin-(CDDP) or carboplatin) as well as a taxane (paclitaxel (PTX) or docetaxel-(DTX)), commonly used to cure nonsmall cell-lung (NSCLC) and ovarian cancers. The nanomicelle carrier's composition enabled efficacious incorporation of the hydrophobic drugs [135–137]. Hence, this discovery provided stable and nontoxic biocompatible therapeutic formulations that potentially increased drug bioavailability. In another patent, nanomicelles encapsulating SN-38 formulation for chemotherapy of carcinoma were investigated. This development provided a nanomicelle formulation, including extended multiblock co-polymer with a SN-38 resulting from encapsulated camptothecin [61,138]. This SN-38 formulation is dominant over its camptothecin derivative since it is not reliant on stimulation by the detoxifying liver in vivo (Table 5) [138].

Bodrati in 2018 demonstrated the application of block-co-polymer nanomicelle of poly(oxyethylene)–block-poly(oxypropylene) copolymer in the administration of chemotherapeutic agents, providing noncovalent dissolvation, which minimized solubility issues [61]. Several copolymers are readily obtainable under the generic name of "poloxamers"/ "pluronics". Innovation by Hao et al. (2017) comprised of nanomicelle aggregates, composites with self-aggregated/assembled nanomicelles and methods for formulating nanomicelle aggregates and composites. Nanoformulation also included a plant prolamin proteins attached to polyethylene glycol (PEG)-coated nanomicelle [139]. This invention further derived methods for integration of drugs utilizing the conjugates of the protein nanomicelle formulation. In a patent by Rhymer (2008) micellar structures, techniques of micellar assemblies, methods of nanoimaging, approaches of chemotherapeutic delivery and life biological composites were investigated [140]. This patent presented a therapeutic technique utilizing hydrophilic, high molecular mass block copolymer for facilitation of an intraperitoneally dosed antineoplastic agent for prolonged release in the peritoneal region. The patent further described a therapeutic-loaded nanomicelle formulation, consisting of a copolymer with an exterior water-soluble moiety, a polycarboxylic acid functional group; and an anti-tumour agent attached to or incorporated in the nanomicelle. Patents in micellar technologies for antineoplastic drugs delivery are presented in Table 5.

Table 5. Micellar patents issued in the area of cancer drug delivery (Adapted and modified from Mishra et al. [138]).

Patent Type	Title	Patent No.	Chemical Formula	Action	Year	Inventor/Assignee
Micelles	C6-c18-acylated derivative of hyaluronic acid	WO2014082609 A1	(HA)-[0(C˙=O)NH-M]$_p$	AC	2014	Contipro Biotech S.R.O.
Micelles	Polymer conjugated protein micelles	EP 2678001 A2	PEG-Prolamine	AC	2014	South Dakota State University
Paclitaxel Micelle (NK105)	Micellar preparation containing sparingly water-soluble anticancer agent and novel block copolymer	09705599.0	(poly(ethylene glycol)-copoly (L-aspartic acid)	AC	2013	Nanocarrier Co. Ltd. Nippon Kayaku Co., Ltd.
Nanoplatin® (NC-6004)	Pharmaceutical composition and combined agent	098101554	(poly(ethylene glycol)-copoly (amino acid)	AC	2013	TOUDAI TLO Ltd.
DACH-Platin Micelle (NC-4016)	Coordination compound composed of diaminocyclohexane platinum (Ii) and block copolymer	2007-520209	(poly(ethylene glycol)-copoly (amino acid)	AC	2013	The University of Tokyo
Protein Micelle	Electrostatic bonding type macromolecular micelle drug carrier	EP2583563 A1	polyethylene glycol and poly(α,-β -aspartic acid)	AC	2013	TOUDAI TLO Ltd.
siRNA Micelle	Polyethylene glycol/polycation block copolymer	EP2087912 A1	PEG-PLys	AC	2013	The University of Tokyo
Sensor Linked Micelle	Active targeting polymer micelle encapsulating drug, and pharmaceutical composition	2008-539901	poly(ethylene glycol)-b-poly(2-aminoethyl methacrylate)-b-poly(styrene)	AC	2013	Nanocarrier Co. Ltd.
pH-Sensitive Micelle	Novel block copolymer used for preparing pH-responsive polymer micelles	2009-7007877	[PEG-p(Asp-Hyd-Adr)]	AC	2013	The University of Tokyo
Docetaxel Micelle	Docetaxel polymer derivative, method for producing same and use of same	2009250393	(mPEG-PDLLA)	AC	2013	Nanocarrier Co. Ltd.
Bortezomib Micelle	Pharmaceutical composition that includes block copolymer containing boronic acid compound	EP 2692777 A1	polyethylene glycol-polyglutamic acid	AC	2013	Nanocarrier Co. Ltd.
Micelles	Micelles for the solubilisation of gossypol	20120321715	Poloxamer or PEG-PCL	AC	2012	Wisconsin Alumni Research Foundation., US

Abbreviations: AC (Anticancer activity including ovarian cancer and various cancers such as lung and prostate cancer), MA Microaggregates), PEG/PEG 2000 (poly(ethylene glycol-2000), Hyaluronic acid (HA), C = O (carbonyl group), -PLys (polylysine), Asp(Aspartate), Hyd-Adr(hydrazone Adriamycin, poly-DL-lactide (PDLLA), PCL(polycaprolactone).

12. Future Recommendations

Nanomicelles are employed as drug carrier nanosystems or imaging agents. Extensive differentiation in physicochemical, pharmacological and immunological platforms is necessary prior to approval for application in humans. Antineoplastic efficacy of most chemotherapeutic nanoformulations has not advanced to an appropriate degree to evolve the formulated nanomedicines into clinical application. Thus, great research studies are conducted on optimization of physicochemical profiles of nanomicelles. Combinational chemotherapy against ovarian cancer is another approach used to enhance antineoplastic efficacy. Future trends in nanomicelle development and delivery includes circulatory computational evaluations, simulating ecosystems of the pathogens and patient-derived cell lines, induced pluripotent stem cell (iPSC) technology, three-dimensional coculture, organotypic systems, improvements in cell imaging, microfluidics, nanotechnologies and gene-editing technologies.

The main challenge is now linked with the interpretation of various productive and validated experimental findings into clinical translation. The efficacy of the therapeutics is limited due to degradation, interactions with cells, and poor tissue permeability. Furthermore, encapsulation of two or more therapeutics in a single nanocarrier system can be challenging due to different solubilities of the optimal drug combination. Nanotheranostics are therapeutics activated by a positive diagnosis of an ovarian cancer disease and will be in use in the near future for chemotherapeutics.

13. Conclusions

Novel nanomicellar technologies developed to date are focused on improving pharmacodynamics and pharmacokinetic profiles of the incorporated therapeutic agents, whilst increasing safety and compliance, to upsurge the five-year survival rate of OC patients. Nanomicellar systems have advanced as significant chemotherapeutic delivery platforms. These nanocarriers can be specifically loaded with a wide range of active drug compounds, providing a strategy to improve the bioavailability of drugs, including those abandoned due to insoluble characteristics and cytotoxicity challenges. Nanomicelles have also shown to be applicable for theranostic applications. Multipurpose polymeric nanomicelles have more attributes as therapeutic carriers, as shown by their considerable outcomes in the scope of clinical diagnosis and chemotherapeutics. These include nanomicelles attached with ligands, the enabling of specific active targeting of tumour metastasis, increased restorative effects, and reduced side effects—thus promoting more effective therapy. Although no panacea may be eminent at this time, it is anticipated that through tailored, safe, multifaceted, and rational design of nanomicelles, advanced drug delivery systems will be developed for the future treatment and diagnosis of OC.

Author Contributions: J.M.P., P.P.D.K., Y.E.C., T.M. and V.P. designed the framework and main content of the manuscript, further contributing to specific attributes on nanomedicine for ovarian chemotherapeutics. All authors have read and agreed to the published version of the manuscript.

Funding: This research was funded by National Research Foundation of South Africa.

Acknowledgments: This work was funded by the National Research Foundation (NRF) of South Africa.

Conflicts of Interest: The authors declare no conflict of interests.

References

1. Loret, N.; Denys, T.; Berx, G. The role of epithelial-to-mesenchymal plasticity in ovarian cancer progression and therapy resistance. *Cancers* **2019**, *11*, 838. [CrossRef] [PubMed]
2. Ghisoni, E.; Imbimbo, M.; Zimmermann, S.; Valabrega, G. Ovarian cancer immunotherapy: Turning up the heat. *Int. J. Mol. Sci.* **2019**, *20*, 2927. [CrossRef] [PubMed]
3. Deuster, E.; Mayr, D.; Hester, A.; Kolben, T.; Zeder-Göß, C.; Burges, A. Correlation of the aryl hydrocarbon receptor with fshr in ovarian cancer patients. *Int. J. Mol. Sci.* **2019**, *20*, 2862. [CrossRef] [PubMed]
4. Siu, K.Y.M.; Jiang, Y.; Wang, J.; Leung, T.H.Y.; Han, C.Y.; Benjamin, K. Hexokinase 2 regulates ovarian cancer cell migration, invasion and stemness via FAK/ERK1/2/MMP9/NANOG/SOX9 signaling cascades. *Cancers* **2019**, *11*, 813. [CrossRef] [PubMed]

5. Garziera, M.; Roncato, R.; Montico, M.; De Mattia, E.; Gagno, S.; Poletto, E.; Cecchin, E. New challenges in tumor mutation heterogeneity in advanced ovarian cancer by a targeted next-generation sequencing (NGS) approach. *Cells* **2019**, *8*, 584. [CrossRef]
6. Wieser, V.; Sprung, S.; Tsibulak, I.; Haybaeck, J.; Hackl, H.; Fiegl, H. Clinical impact of RANK signalling in ovarian cancer. *Cancers* **2019**, *11*, 791. [CrossRef]
7. Menyhárt, O.; Fekete, J.T.; Gyorffy, B. Gene expression indicates altered immune modulation and signaling pathway activation in ovarian cancer patients resistant to Topotecan. *Int. J. Mol. Sci.* **2019**, *20*, 2750. [CrossRef]
8. Smith, T.; Guidozzi, F. Epithelial ovarian cancer in Southern Africa. *SA J. Gynaecol. Oncol.* **2009**, *1*, 23–27. [CrossRef]
9. Erol, A.; Niemira, M.; Kretowski, A.D. Novel approaches in ovarian cancer research against heterogeneity, late diagnosis, drug resistance, and transcoelomic metastases. *Int. J. Mol. Sci.* **2019**, *20*, 2649. [CrossRef]
10. Maru, Y.; Hippo, Y. Current status of patient-derived ovarian cancer models. *Cells* **2019**, *8*, 505. [CrossRef]
11. Madariaga, A.; Lheureux, S.; Oza, A.M. Tailoring ovarian cancer treatment: Implications of BRCA1/2 mutations. *Cancers* **2019**, *11*, 416. [CrossRef]
12. Moffitt, L.; Karimnia, N.; Stephens, A.; Bilandzic, M. Therapeutic Targeting of Collective Invasion in Ovarian Cancer. *Int. J. Mol. Sci.* **2019**, *20*, 1466. [CrossRef] [PubMed]
13. Napoletano, C.; Ruscito, I.; Bellati, F.; Zizzari, I.G. Bevacizumab-based chemotherapy triggers immunological effects in responding multi-treated recurrent ovarian cancer patients by favoring the recruitment of effector t cell subsets. *J. Clin. Med.* **2019**, *8*, 380. [CrossRef] [PubMed]
14. Chishti, N.; Satveer Jagwani, S.; Dhamecha, D.; Jalalpure, S.; Dehghan, M.H. Preparation, optimization, and In Vivo Evaluation of nanoparticle-based formulation for pulmonary delivery of anticancer drug. *Medicina* **2019**, *55*, 294. [CrossRef] [PubMed]
15. Dlamini, N.G.; Basson, A.K.; Pullabhotla, V.S.R. Optimization and application of bioflocculant passivated copper nanoparticles in the wastewater treatment. *Int. J. Environ. Res. Public Health* **2019**, *16*, 2185. [CrossRef] [PubMed]
16. Cagliani, R.; Gatto, F.; Bardi, G. Protein adsorption: A feasible method for nanoparticle functionalization? *Materials* **2019**, *12*, 1991. [CrossRef]
17. Dong, X. Review on current strategies for brain drug delivery. *Theranostics* **2018**, *8*, 1481–1493. [CrossRef]
18. Basso, J.; Miranda, A.; Nunes, S.; Cova, T.; Sousa, J.; Vitorino, C.; Pais, A. Review on hydrogel-based drug delivery nanosystems for the treatment of brain tumors. *MDPI J. Gels* **2018**, *4*, 62. [CrossRef]
19. Blanco, E.; Kessinger, C.W.; Sumer, B.D.; Gao, J. Multifunctional micellar nanomedicine for cancer therapy. *Exp. Biol. Med.* **2009**, *234*, 123–131. [CrossRef]
20. Larraneta, E.; Stewart, S.; Ervine, M.; Al-Kasasbeh, R.; Donnelly, R.F. Hydrogels for hydrophobic drug delivery, classification, synthesis and applications. *J. Funct. Biomater.* **2018**, *9*, 13. [CrossRef]
21. Chirwa, N.; Pillay, V.; Choonara, Y.E.; Kumar, P.; du Toit, L. Pharmaceutical Composition. U.S. Patent 9220773 B2, 29 December 2015.
22. Vivek, R.; Thangam, R.; Kumar, S.R.; Rejeeth, C.; Kumar, G.S.; Sivasubramanian, S.; Vincent, S.; Gopi, D.; Kannan, S. HER2 targeted breast cancer therapy with switchable "off/on" multifunctional "smart" magnetic polymer core-shell nanocomposites. *ACS Appl. Mater. Interfaces* **2016**, *8*, 2262–2279. [CrossRef]
23. Fanshawe, T.R.; Power, M.; Graziadio, S.; Jones, W.; Ordonez-Mena, J.M.; Simpson, A.J.; Oxford, O. Methods for evaluation of medical prediction models, tests and biomarkers (MEMTAB) symposium. *Diagn. Progn. Res.* **2018**, *2*. [CrossRef]
24. Whitehouse, C.; Solomon, E. Current status of the molecular characterization of the ovarian cancer antigen CA125 and implications for its use in clinical screening. *Gynaecol. Oncol.* **2003**, *88*, 152–157. [CrossRef] [PubMed]
25. Yu, X.; Trase, I.; Ren, M.; Duval, K.; Guo, X.; Chen, Z. Design of nanoparticle-based carriers for targeted drug delivery. *J. Nanomater.* **2016**, *2016*, 1087250. [CrossRef] [PubMed]
26. Bhise, K.; Sau, S.; Alsaab, H.; Kashaw, S.K.; Tekade, R.K.; Iyer, A.K. Nanomedicine for cancer diagnosis and therapy, advancement, success and structure–activity relationship. *Ther. Deliv.* **2017**, *8*, 1003–1018. [CrossRef] [PubMed]

27. Luong, D.; Sau, S.; Kesharwani, P.; Iyer, A.K. Polyvalent folate-dendrimer-coated iron oxide theranostic nanoparticles for simultaneous magnetic resonance imaging and precise cancer cell targeting. *Biomacromolecules* **2017**, *18*, 1197–1209. [CrossRef]
28. Sharma, A.K.; Gothwal, A.; Kesharwani, P.; Alsaab, H.; Iyer, A.K.; Gupta, U. Dendrimer nanoarchitectures for cancer diagnosis and anticancer drug delivery. *Drug Discov. Today* **2017**, *22*, 314–326. [CrossRef]
29. Chauhan, S.C.; Singh, A.P.; Ruiz, F.; Johansson, S.L.; Jain, M.; Smith, L.M.; Batra, S.K. Aberrant expression of MUC4 in ovarian modern pathology carcinoma, diagnostic significance alone and in combination with MUC1 and MUC16 (CA125). *Mod. Pathol.* **2006**, *19*, 1386–1394. [CrossRef] [PubMed]
30. Felder, M.; Kapur, A.; Gonzalez-Bosquet, J.; Horibata, S.; Heintz, J.; Albrecht, R.; Whelan, R.J. MUC16 (CA125), tumor biomarker to cancer therapy, a work in progress. *J. Mol. Cancer* **2014**, *13*, 129. [CrossRef] [PubMed]
31. Trucillo, P.; Campardelli, R.; Reverchon, E. Supercritical CO_2 assisted liposomes formation: Optimization of the lipidic layer for an efficient hydrophilic drug loading. *J. CO_2 Util.* **2017**, *18*, 181–188. [CrossRef]
32. Kue, C.S.; Kamkaew, A.; Burgess, K.; Kiew, L.V.; Chung, L.Y.; Lee, H.B. Small molecules for active targeting in cancer. *Med. Res. Rev.* **2016**, *36*, 494–575. [CrossRef] [PubMed]
33. Fathi, M.; SimaMajidi, S.; Zangabad, P.S.; Barar, J.H.E.; Omidi, Y. Chitosan- based multifunctional nanomedicines and theranostics for targeted therapy of cancer. *Med. Res. Rev.* **2018**, *38*, 2110–2136. [CrossRef] [PubMed]
34. Larsson, M.; Huang, W.C.; Hsiao, M.H.; Wang, Y.J.; Nydén, M.; Chiou, S.H.; Liu, D.M. Biomedical applications and colloidal properties of amphiphilically modified chitosan hybrids. *Prog. Polym. Sci.* **2013**, *38*, 1307–1328. [CrossRef]
35. Chen, H.P.; Chen, M.H.; Tung, F.I.; Liu, T.Y. A novel micelle-forming material used for preparing a theranostic vehicle exhibiting enhanced in vivo therapeutic efficacy. *J. Med. Chem.* **2015**, *58*, 3704–3719. [CrossRef] [PubMed]
36. Yu, F.; Jiang, F.; Tang, X.; Wang, B. N-octyl-N-arginine-chitosan micelles for gambogic acid intravenous delivery, characterization, cell uptake, pharmacokinetics, and biodistribution. *Drug Dev. Ind. Pharm.* **2018**, *44*, 615–623. [CrossRef] [PubMed]
37. Feng, S.; Li, J.; Luo, Y.; Yin, T.; Cai, H.; Wang, Y.; Dong, Z.; Shuai, X.; Li, Z. pH-Sensitive nanomicelles for controlled and efficient drug delivery to human colorectal carcinoma lovo cells. *PLoS ONE* **2014**, *9*, e100732. [CrossRef]
38. Kobayashi, H.; Watanabe, R.; Choyke, P.L. Improving conventional enhanced permeability and retention (EPR) effects; what is the appropriate target? *Theranostics* **2014**, *4*, 81–89. [CrossRef]
39. Nakamura, Y.; Mochida, A.; Choyke, P.L.; Kobayashi, H. Nanodrug delivery, is the enhanced permeability and retention effect sufficient for curing cancer? *Bioconjug. Chem.* **2016**, *27*, 2225–2238. [CrossRef]
40. Din, F.; Aman, W.; Ullah, I.; Qureshi, O.S.; Mustapha, O.; Shafique, S.; Zeb, A. Effective use of nanocarriers as drug delivery systems for the treatment of selected tumors. *Int. J. Nanomed.* **2017**, *12*, 7291–7309. [CrossRef]
41. Sutradhar, K.B.S.; Amin, M.L. Nanotechnology in cancer drug delivery and selective targeting. *ISRN Nanotechnol.* **2014**, 939378–939389. [CrossRef]
42. Bolu, B.S.; Sanyal, M.R.; Sanyal, A. Drug delivery systems from self-assembly of dendron-polymer conjugates. *Molecules* **2018**, *23*, 1570. [CrossRef] [PubMed]
43. Macchione, M.A.; Biglione, C.; Strumia, M. Design, synthesis and architectures of hybrid nanomaterials for therapy and diagnosis applications. *Polymers* **2018**, *10*, 527. [CrossRef] [PubMed]
44. Senapati, S.; Mahanta, A.K.; Kumar, S.; Maiti, P. Controlled drug delivery vehicles for cancer treatment and their performance. *Signal Transduct. Target. Ther.* **2018**, *3*, 7. [CrossRef] [PubMed]
45. Atkinson, S.P.; Andreu, M.Z.; Vicent, M.J. Polymer therapeutics, biomarkers and new approaches for personalized cancer treatment. *J. Pers. Med* **2018**, *8*, 6.
46. Dou, X.; Wang, H.; Zhang, J.; Wang, F.; Xu, G.; Xu, H.; Xiang, S.; Fu, J.; Song, H. Aptamer—Drug conjugate, targeted delivery of doxorubicin in a HER3 aptamer-functionalized liposomal delivery system reduces cardiotoxicity. *Int. J. Nanomed.* **2018**, *13*, 763–776. [CrossRef] [PubMed]
47. Lu, Y.; Park, K. Polymeric micelles and alternative nanonized delivery vehicles for poorly soluble drugs. *Int. J. Pharm.* **2012**, *8*, 1–17. [CrossRef]
48. Wang, J.; Yang, H. Superelastic and pH-responsive degradable dendrimer cryogels prepared by cryo-aza-michael addition reaction. *Nat. Sci. Rep.* **2018**, *8*, 7155. [CrossRef]

49. Miao, T.; Wang, J.; Zeng, Y.; Liu, G.; Chen, X. Polysaccharide-based controlled release systems for therapeutics delivery and tissue engineering, from bench to bedside. *Adv. Sci.* **2018**, *5*, 1700513. [CrossRef]
50. Pelegri-O'Day, E.M.; Lin, E.; Maynard, H.D. Therapeutic protein—Polymer conjugates, advancing beyond PEGylation. *J. Am. Chem. Soc.* **2014**, *136*, 14323–14332. [CrossRef]
51. Brandta, J.V.; Piazzaa, R.D.; dos Santosa, C.C.; Vega-Chacóna, J.; Amantéaa, B.E. Synthesis and colloidal characterization of folic acid-modified PEG-b-PCL micelles for methotrexate delivery. *Colloids Surf. B Biointerfaces* **2019**, *177*, 228–234. [CrossRef]
52. Tong, R.; Yala, L.; Fan, T.M.; Cheng, J. The formulation of aptamer-coated paclitaxel-polylactide nanoconjugates and their targeting to cancer cells. *J. Biomater.* **2010**, *31*, 3043–3053. [CrossRef]
53. Huang, D.; Wu, D. Biodegradable dendrimers for drug delivery. *Mater. Sci. Eng. C* **2018**, *90*, 713–727. [CrossRef] [PubMed]
54. Lamichhane, N.; Udayakumar, T.S.; D'Souza, W.D.; Simone, M.I.I.; Charles, B.; Raghavan, S.R.; Mahmood, J.P. Liposomes: Clinical applications and potential for image-guided drug delivery. *Molecules* **2018**, *23*, 288. [CrossRef] [PubMed]
55. Fornaguera, C.; Dols-Perez, A.; Calderó, G.; García-Celma, M.J.; Camarasa, J.; Solans, C. PLGA nanoparticles prepared by nano-emulsion templating using low-energy methods as efficient nanocarriers for drug delivery across the blood-brain barrier. *J. Control. Release* **2015**, *211*, 134–143. [CrossRef] [PubMed]
56. Olusanya, T.O.B.; Ahmad, R.R.H.; Ibegbu, D.M.; Smith, J.R.; Elkordy, A.A. Liposomal drug delivery systems and anticancer drugs. *Molecules* **2018**, *23*, 907. [CrossRef]
57. Sercombe, L.; Veerati, T.; Moheimani, F.; Wu, S.Y.; Sood, A.K.; Hua, S. Advances and challenges of liposome assisted drug delivery. *Front. Pharmacol.* **2015**, *6*, 286. [CrossRef]
58. Lila, A.S.A.; Ishida, T. Liposomal delivery systems, design optimization and current applications. *Biol. Pharm. Bull.* **2017**, *40*, 1–10. [CrossRef]
59. Bhadani, A.; Kafle, A.; Koura, S.; Sakai, K.; Sakai, H.; Masahiko, A.M. Physicochemical evaluation of micellar solution and lyotropic phases formed by self-assembled aggregates of morpholinium geminis. *ACS Omega* **2017**, *2*, 5324–5334. [CrossRef]
60. Vaishya, R.D.; Khurana, V.; Patel, S.; Mitra, A.K. Controlled ocular drug delivery with nanomicelles. *Wiley Interdiscip. Rev. Nanomed. Nanobiotechnol.* **2014**, *6*, 422–437. [CrossRef]
61. Bodratti, A.M.; Alexandridis, P. Formulation of Poloxamers for Drug Delivery. *J. Funct. Biomater.* **2018**, *9*, 11. [CrossRef]
62. Aziz, Z.A.A.; Ahmad, A.; Mohd-Setapar, S.H.; Hassan, H.; Lokhat, D.; Kamal, M.A.; Ashraf, M.G. Recent advances in drug delivery of polymeric nano-micelles. *Curr. Drug Metab.* **2017**, *18*, 16–29. [CrossRef] [PubMed]
63. Simões, S.M.N.; Figueiras, A.R.; Veiga, F.; Concheiro, A.; Alvarez-Lorenzo, C. Polymeric micelles for oral drug administration enabling locoregional and systemic treatments. *Expert Opin. Drug Deliv.* **2014**, *12*, 297–318. [CrossRef] [PubMed]
64. Movassaghian, S.; Merkel, O.M.; Torchilin, V.P. Applications of polymer micelles for imaging and drug delivery. *Wiley Interdiscip. Rev. Nanomed. Nanobiotechnol.* **2015**, *7*, 691–707. [CrossRef] [PubMed]
65. Vyas, B.; Pillai, S.A.; Bahadur, A.; Bahadur, P. A comparative study on micellar and solubilizing behavior of three eo-po based star block copolymers varying in hydrophobicity and their application for the In Vitro release of anticancer drugs. *Polymers* **2018**, *10*, 76. [CrossRef]
66. Santos, M.S.; Tavares, F.W.; Biscaia, E.C. Molecular Thermodynamics of micellization, micelle size distributions and geometry transitions. *Braz. J. Chem. Eng.* **2016**, *33*, 515–523. [CrossRef]
67. Chidi, O.; Adebayo, I.V. Determination of Critical Micelle Concentration and Thermodynamic Evaluations of Micellization of GMS. *Mod. Chem. Appl.* **2018**, *6*, 2. [CrossRef]
68. Mukherjee, I.; Moulik, S.P.; Rakshit, A.K. Tensiometric determination of Gibbs surface excess and micelle point: A critical revisit. *J. Colloid Interface Sci.* **2013**, *394*, 329–336. [CrossRef]
69. Sutton, D.; Nasongkla, N.; Blanco, E.; Gao, J. Functionalized micellar systems for cancer targeted drug delivery. *Pharm. Res.* **2007**, *24*, 1029–1046. [CrossRef]
70. Nguyen, V.T.A.; De Pauw-Gillet, M.; Sandre, O.; Gauthier, M. Biocompatible polyion complex micelles synthesized from arborescent polymers. langmuir. *Am. Chem. Soc.* **2016**, *32*, 13482–13492.
71. Hussein, Y.H.A.; Youssry, M. Polymeric micelles of biodegradable diblock copolymers, enhanced encapsulation of hydrophobic drugs. *Materials* **2018**, *11*, 688. [CrossRef]

72. Ding, J.; Chen, L.; Xiao, C.; Chen, L.; Zhuang, X.; Chen, X. Noncovalent interaction-assisted polymeric micelles for controlled drug delivery. *Chem. Commun* **2014**, *50*, 11274–11290. [CrossRef] [PubMed]
73. Mandala, A.; Bisht, R.; Rupenthal, I.D.; Mitraa, A.K. Polymeric micelles for ocular drug delivery, From structural frameworks to recent preclinical studies. *J. Control. Release* **2017**, *248*, 96–116. [CrossRef] [PubMed]
74. Michalicova, P.; Mravec, F.; Peka, R.M. Fluorescence study of freeze-drying as a method for support the interactions between hyaluronic and hydrophobic species. *PLoS ONE* **2017**, *12*, e0184558. [CrossRef] [PubMed]
75. Rosenblum, D.; Josh, N.; Tao, W.; Karp, J.M.; Peer, D. Progress and challenges towards targeted delivery of cancer therapeutics. *Nat. Commun.* **2018**, *9*, 1410. [CrossRef]
76. Desai, K.G.H. Polymeric drug delivery systems for intraoral site-specific chemoprevention of oral cancer. *J. Biomed. Mater. Res. Part B* **2018**, *106*, 1383–1413. [CrossRef]
77. Hekman, M.C.H.; Boerman, O.C.; Bos, D.L.; Massuger, L.F.A.G.; Weil, S.; Grasso, L.; Rybinski, K.A.; Oosterwijk, E.; Mulders, P.F.A.; Rijpkema, M. Improved intraoperative detection of ovarian cancer by folate receptor alpha targeted dual-modality imaging. *Mol. Pharm.* **2017**, *14*, 3457–3463. [CrossRef]
78. Judy, R.P.; Keating, J.J.; DeJesus, E.M.; Jiang, J.X.; Okusanya, O.T.; Nie, S.; Singhal, S. Quantification of tumor fluorescence during intraoperative optical cancer imaging. *Sci. Rep.* **2015**, *5*, 16208. [CrossRef]
79. Jung, K.H.; Lee, K.H. Molecular imaging in the era of personalized medicine. *J. Pathol. Transl. Med.* **2015**, *49*, 5–12. [CrossRef]
80. Kedar, U.; Shidhaye, S.; Kadam, V.U. Advances in polymeric micelles for drug delivery and tumour targeting. *Nanomed. Nanotechnol. Biol. Med.* **2010**, *6*, 714–729. [CrossRef]
81. Chen, Y.; Lo, C.; Hsiue, G. Multifunctional nanomicellar systems for delivering anticancer drugs. *J. Biomed. Mater. Res. Part A* **2014**, *102*, 2024–2038. [CrossRef]
82. Harada, A.; Kataoka, K. Formation of polyion complex micelles in an aqueous milieu from a pair of oppositely-charged block copolymers with poly (ethylene glycol) segments. *Macromolecules* **1995**, *28*, 5294–5299. [CrossRef]
83. Li, Y.; Kwon, G.S. Methotrexate esters of poly (ethylene oxide)-block-poly(2-hydroxyethyl-l-aspartamide). Part I: Effects of the level of methotrexate conjugation on the stability of micelles and on drug release. *Pharm. Res.* **2000**, *17*, 607–611. [CrossRef] [PubMed]
84. Lavasanifar, A.; Samuel, J.; Kwon, G.S. Micelles self-assembled from poly (ethylene oxide)-block-poly (N-hexyl stearate l-aspartamide) by a solvent evaporation method: Effect on the solubilization and haemolytic activity of amphotericin B. *J. Control. Release* **2001**, *77*, 155–160. [CrossRef]
85. Kim, J.H.; Emoto, K.; Iijima, M.; Nagasaki, Y.; Aoyagi, T.; Okano, T.Y. Core-stabilized polymeric micelle as potential drug carrier: Increased solubilization of taxol. *Polym. Adv. Technol.* **1999**, *10*, 647–654. [CrossRef]
86. Zhiang, J.; Wu, M.; Yang, J.; Wu, Q.; Jin, Z. Anionic poly (lactic acid)-polyurethane micelles as potential biodegradable drug delivery carriers. *Colloids Surf. A* **2009**, *337*, 200–204. [CrossRef]
87. Patil, Y.B.; Toti, U.S.; Khdair, A.; Linan, M.; Panyam, J. Single-step surface functionalization of polymeric nanoparticles for targeted drug delivery. *Biomaterials* **2009**, *30*, 859–866. [CrossRef]
88. Chung, J.E.; Yokoyama, M.; Okano, T.; Yamato, M.; Aoyagi, T.; Sakurai, Y. Thermoresponsive drug delivery from polymeric micelles constructed using block copolymer of poly(N-isopropylacrylamide) and poly (butyl methacrylate). *J. Control. Release* **1999**, *62*, 115–127. [CrossRef]
89. Elliott, R.L.; Elliott, M.C.; Wang, F.; Head, J.F. Breast carcinoma and the role of iron metabolism: A cytochemical, tissue culture and ultrastructural study. *Ann. N.Y. Acad. Sci.* **1993**, *698*, 159–166. [CrossRef]
90. Yamamoto, Y.; Nagasaki, Y.; Kato, Y.; Sugiyama, Y.; Kataoka, K. Longcirculating poly (ethylene glycol)-poly (D, L-lactide) block copolymer micelles with modulated surface charge. *J. Control. Release* **2001**, *77*, 27–38. [CrossRef]
91. Guo, J.; Gao, X.; Su, L.; Xia, H.; Gu, G.; Pang, Z.; Jiang, X.; Yao, L.; Chen, J.; Chen, H. Aptamer-functionalized PEG–PLGA nanoparticles for enhanced anti-glioma drug delivery. *Biomaterials* **2011**, *32*, 8010–8020. [CrossRef]
92. Yáñez, J.; Forrest, M.; Ohgami, Y.; Kwon, G.; Davies, N. Pharmacometrics and delivery of novel nanoformulated PEG-b-poly (E-caprolactone) micelles of rapamycin. *Cancer Chemother. Pharmacol.* **2008**, *61*, 133–144. [CrossRef] [PubMed]
93. Kim, D.; Lee, E.S.; Oh, K.T.; Gao, Z.G.; Bae, Y.H. Doxorubicin-loaded polymeric micelle overcomes multidrug resistance of cancer by double-targeting folate receptor and early endosomal pH. *Small* **2008**, *4*, 2043–2050. [CrossRef] [PubMed]

94. Johnson, R.P.; Jeong, Y.I.; Choi, E.; Chung, C.W.; Kang, D.H.; Oh, S.O.; Suh, H.; Kim, I. Biocompatible poly (2-hydroxyethyl methacrylate)-bpoly (L-histidine) hybrid materials for pH-sensitive intracellular anticancer drug delivery. *Adv. Funct. Mater.* **2011**, *22*, 1058–1068. [CrossRef]
95. Tsai, H.C.; Tsai, C.H.; Lin, S.Y.; Jhang, C.R.; Chiang, Y.S.; Hsiue, G.H. Stimulated release of photosensitizers from graft and diblock micelles for photodynamic therapy. *Biomaterials* **2012**, *33*, 1827–1837. [CrossRef]
96. Lu, P.L.; Chen, Y.C.; Ou, T.W.; Chen, H.H.; Tsai, H.C.; Wen, C.J.; Lo, C.L.; Wey, S.P.; Lin, K.J.; Yen, T.C.; et al. Multifunctional hollow nanoparticles based on graft-diblock copolymers for doxorubicin delivery. *Biomaterials* **2011**, *32*, 2213–2221. [CrossRef]
97. Lin, S.Y.; Hsu, W.H.; Lo, J.M.; Tsai, H.C.; Hsiue, G.H. Novel geometry type of nanocarriers mitigated the phagocytosis for drug delivery. *J. Control. Release* **2011**, *154*, 84–92. [CrossRef] [PubMed]
98. Cholkar, K.; Patel, A.; Vadlapudi, A.D.; Ashim, K.; Mitra, A.K. Novel nanomicellar formulation approaches for anterior and posterior segment ocular drug delivery. *Recent Pat. Nanomed.* **2012**, *2*, 82–95. [CrossRef]
99. Fares, A.R.; ElMeshad, A.N.; Kassem, M.A. Enhancement of dissolution and oral bioavailability of lacidipine via pluronic P123/ F127 mixed polymeric micelles, formulation, optimization using central composite design and in vivo bioavailability study. *Drug Deliv.* **2018**, *25*, 132–142. [CrossRef]
100. Vadlapudi, A.D.; Cholkar, K.; Vadlapatla, R.K.; Mitra, A.K. Aqueous nanomicellar formulation for topical delivery of biotinylated lipid prodrug of acyclovir, formulation development and ocular biocompatibility. *J. Ocul. Pharmacol. Ther.* **2014**, *30*, 49–58. [CrossRef]
101. Lengyel, E. Ovarian cancer development and metastasis. *Am. J. Pathol.* **2010**, *177*, 1053–1064. [CrossRef]
102. Testa, U.; Petrucci, E.; Pasquini, L.; Castelli, G.; Pelosi, E. Ovarian cancers, genetic abnormalities, tumor heterogeneity and progression, clonal evolution and cancer stem cells. *Medicines* **2018**, *5*, 16. [CrossRef] [PubMed]
103. Lorenzo, G.D.; Ricci, G.; Severini, G.M.; Romano, F.; Biffi, S. Imaging and therapy of ovarian cancer, clinical application of nanoparticles and future perspectives. *Theranostics* **2018**, *8*, 16. [CrossRef] [PubMed]
104. Wright, A.A.; Cronin, A.; Milne, D.E.; Bookman, M.A.; Burger, R.A.; Cohn, D.E.; Mantia-Smaldone, G. Use and effectiveness of intraperitoneal chemotherapy for treatment of ovarian cancer. *J. Clin. Oncol.* **2015**, *33*, 2841–2847. [CrossRef] [PubMed]
105. Coward, J.I.G.; Middleton, K.; Murphy, F. New perspectives on targeted therapy in ovarian cancer. *Int. J. Women's Health* **2015**, *7*, 189–203. [CrossRef]
106. Jahangirian, H.; Lemraski, E.G.; Webster, T.J.; Moghaddam, R.; Abdollahi, Y. A review of drug delivery systems based on nanotechnology and green chemistry, green nanomedicine. *Int. J. Nanomed.* **2017**, *12*, 2957–2978. [CrossRef]
107. Fang, J.; Nakamura, H.; Maeda, H. The EPR effect, unique features of tumor blood vessels for drug delivery, factors involved, and limitations and augmentation of the effect. *Adv. Drug Deliv. Rev.* **2011**, *63*, 136–151. [CrossRef]
108. Makhmalzade, B.S.; Chavoshy, F. Polymeric micelles as cutaneous drug delivery system in normal skin and dermatological disorders. *J. Adv. Pharm. Technol. Res.* **2017**, *9*, 2–8.
109. Jahan, S.T.; Sam, M.A.; Walliser, M.; Haddadi, A. Targeted therapeutic nanoparticles, an immense promise to fight against cancer. *Hindawi J. Drug Deliv.* **2017**, *2017*, 9090325. [CrossRef]
110. Dai, L.; Liu, J.; Luo, Z.; Li, M.; Cai, K. Tumor therapy, targeted drug delivery systems. *J. Mater. Chem. B.* **2016**, *4*, 6758. [CrossRef]
111. Pillai, G. Nanomedicines for cancer therapy, an update of FDA approved and those under various stages of development. *SOJ Pharm Pharm Sci.* **2014**, *1*, 13.
112. Ljubimova, J.Y.; Sun, T.; Mashouf, L.; Ljubimov, A.V.; Israel, L.L.; Ljubimov, V.A.; Holler, E. Covalent nano delivery systems for selective imaging and treatment of brain tumours. *Adv. Drug Deliv. Rev.* **2017**, *113*, 177–200. [CrossRef] [PubMed]
113. Savla, R.; Minko, T. Nanoparticle design considerations for molecular imaging of apoptosis, diagnostic, prognostic, and therapeutic value. *Adv. Drug Deliv. Rev.* **2017**, *113*, 122–140. [CrossRef] [PubMed]
114. Estelrich, J.; Busquets, M.A.; Morán, M.C. Effect of pegylation on ligand-targeted magnetoliposomes, a missed goal. *ACS Omega* **2017**, *2*, 6544–6555. [CrossRef] [PubMed]
115. Gomes de Castro, M.A.; Ho bartner, C.; Opazo, F. Aptamers provide superior stainings of cellular receptors studied under super resolution microscopy. *PLoS ONE* **2017**, *12*, e0173050. [CrossRef] [PubMed]

116. Cha, H.; Song, K.S. Effect of MUC8 on airway Inflammation: A friend or a foe? *J. Clin. Med.* **2018**, *7*, 26. [CrossRef] [PubMed]
117. Sudimack, B.A.J.; Lee, R.J. Targeted drug delivery via the folate receptor. *J. Adv. Drug Deliv. Rev.* **2013**, *41*, 147–162. [CrossRef]
118. Liao, C.; Sun, Q.; Liang, B.; Shena, J.; Shuai, X. Targeting EGFR-overexpressing tumour cells using Cetuximab-immunomicelles loaded with doxorubicin and superparamagnetic iron oxide. *Eur. J. Radiol.* **2010**, *80*, 699–705.
119. Das, S.; Batra, S.K. Understanding the unique attributes of MUC16 (CA125), potential implications in targeted therapy. *Cancer Res.* **2015**, *75*, 4669–4674. [CrossRef]
120. Rao, T.D.; Fernández-Tejada, A.; Axelrod, A.; Rosales, N.; Yan, X.; Thapi, S.; Lewis, J.S. Antibodies against Specific MUC16 glycosylation sites inhibit ovarian cancer growth. *ACS Chem. Biol.* **2017**, *12*, 2085–2096. [CrossRef]
121. Schummer, M.; Thorpe, J.; Giraldez, M.; Bergan, L.; Tewari, M.; Urban, N. Evaluating serum markers for hormone receptor-negative breast cancer. *PLoS ONE* **2015**, *10*, e0142911. [CrossRef]
122. Kabel, A.M. Tumour markers of breast cancer: New prospective. *J. Oncol. Sci.* **2017**, *3*, 5–11.
123. Mai, B.T.; Fernandes, S.; Balakrishnan, P.B.; Pellegrino, T. Nanosystems based on magnetic nanoparticles and thermos-or ph-responsive polymers: An update and future perspectives. *Acc. Chem. Res.* **2018**, *51*, 999–1013. [CrossRef] [PubMed]
124. Naseem, S.; Bansal, N.; Logani, L.A. Recent advances in imaging technologies in dentistry. *World J. Radiol.* **2014**, *6*, 794–807.
125. Singh, A.P.; Senapati, S.; Ponnusamy, M.P.; Jain, M.; Lele, S.M.; Davis, J.S.; Batra, S.K. Clinical potential of mucins in diagnosis, prognosis, and therapy of ovarian cancer. *Lancet Oncol.* **2008**, *9*, 1076–1085. [CrossRef]
126. Bansal, K.K.; Gupta, J.; Rosling, A.; Rosenholm, J.M. Renewable poly (δ-decalactone) based block copolymer micelles as drug delivery vehicle: In Vitro and In Vivo evaluation. *Saudi Pharm. J.* **2018**, *26*, 358–368. [CrossRef]
127. Lee, K.S.; Chung, H.C.; Im, S.A.; Park, Y.H.; Kim, C.S.; Kim, S.B. Multicenter phase II trial of genexol-PM, a cremophor-free, polymeric micelle formulation of paclitaxel, in patients with metastatic breast cancer. *Breast Cancer Res. Treat.* **2008**, *108*, 241–250. [CrossRef]
128. Matsumura, Y. Poly (amino acid) micelle nanocarriers in preclinical and clinical studies. *Adv. Drug Deliv. Rev.* **2008**, *60*, 899–914. [CrossRef]
129. Hrkach, J.; Von Hoff, D.; Mukkaram, A.M.; Andrianova, E.; Auer, J.; Campbell, T. Preclinical development and clinical translation of a PSMA-targeted docetaxel nanoparticle with a differentiated pharmacological profile. *Sci. Transl. Med.* **2012**, *4*, 128ra39. [CrossRef]
130. Wilson, R.H.; Plummer, R.; Adam, J.; Eatock, M.; Boddy, A.V.; Griffin, M. Phase I and pharmacokinetic study of NC-6004, a new platinum entity of cisplatin-conjugated polymer forming micelles. *J. Clin. Oncol.* **2008**, *26*, 2573. [CrossRef]
131. Ueno, T.; Endo, K.; Hori, K.; Ozaki, N.; Tsuji, A.; Kondo, S.; Yoshizaki, T. Assessment of antitumor activity and acute peripheral neuropathy of 1,2-diaminocyclohexane platinum (II)-incorporating micelles (NC-4016). *Int. J. Nanomed.* **2014**, *9*, 3005–3012. [CrossRef]
132. Matsumura, Y.; Kataoka, K. Preclinical and clinical studies of anticancer agent-incorporating polymer micelles. *Cancer Sci.* **2009**, *100*, 572–579. [CrossRef] [PubMed]
133. Matsumura, Y.; Hamaguchi, T.; Ura, T.; Muro, K.; Yamada, Y.; Shimada, Y.; Watanabe, N. Phase I clinical trial and pharmacokinetic evaluation of NK911, a micelle-encapsulated doxorubicin. *Br. J. Cancer* **2004**, *91*, 1775–1781. [CrossRef] [PubMed]
134. Xin, Y.; Yin, M.; Zhao, L.; Meng, F.; Luo, L. Recent progress on nanoparticle-based drug delivery systems for cancer therapy. *Cancer Biol. Med.* **2017**, *14*, 228–241. [CrossRef] [PubMed]
135. Kanwal, M.; Ding, X.; Song, X.; Zhou, G.; Cao, Y. MUC16 overexpression induced by gene mutations promotes lung cancer cell growth and invasion. *Oncotarget* **2018**, *9*, 12226–12239. [CrossRef] [PubMed]
136. Kwon, G.S.; Tomoda, K.; Chiang, C.; Kozak, K.R. Examination of gossypol-pluronic micelles as potential radiosensitizers. *AAPS J.* **2015**, *17*, 1369–1375.
137. Siraj, N.; El-Zahab, B.; Hamdan, S.; Karam, T.E.; Haber, L.H.; Li, M.; Patonay, G. Fluorescence, phosphorescence, and chemiluminescence. *Anal. Chem.* **2016**, *88*, 170–202. [CrossRef] [PubMed]

138. Mishra, B.; Patel, B.B.; Tiwari, S. Colloidal nanocarriers: a review on formulation technology, types and applications toward targeted drug delivery. *Nanomedicine* **2010**, *6*, 9–24. [CrossRef]
139. Hao, J.; Tong, T.; Jin, K.; Zhuang, Q.; Han, T.; Bi, Y.; Wang, J.; Wang, X. Folic acid-functionalized drug delivery platform of resveratrol based on Pluronic 127/D-α-tocopheryl polyethylene glycol 1000 s uccinate mixed micelles. *Int. J. Nanomed.* **2017**, *12*, 2279–2292. [CrossRef]
140. Rhyner, M.N. Development of Cancer Diagnostics Using Nanoparticles and Amphiphilic Polymers. Ph.D. Thesis, Georgia Institute of Technology, Atlanta, GA, USA, 2008.

cancers

MDPI

Review

Polymeric Nanoparticles for the Treatment of Malignant Gliomas

Basant Salah Mahmoud [1,2], Ali Hamod AlAmri [1,3] and Christopher McConville [1,*]

[1] College of Medical and Dental Sciences, School of Pharmacy, University of Birmingham, Birmingham B15 2TT, UK; BSM465@student.bham.ac.uk (B.S.M.); AHA772@student.bham.ac.uk or aamri@kku.edu.sa (A.H.A.)

[2] Hormones Department, Medical Research Division, National Research Centre, El Buhouth St., Dokki, Cairo 12622, Egypt

[3] College of Pharmacy, King Khalid University, Abha 62585, Saudi Arabia

* Correspondence: C.McConville.2@bham.ac.uk

Received: 29 October 2019; Accepted: 6 January 2020; Published: 10 January 2020

Abstract: Malignant gliomas are one of the deadliest forms of brain cancer and despite advancements in treatment, patient prognosis remains poor, with an average survival of 15 months. Treatment using conventional chemotherapy does not deliver the required drug dose to the tumour site, owing to insufficient blood brain barrier (BBB) penetration, especially by hydrophilic drugs. Additionally, low molecular weight drugs cannot achieve specific accumulation in cancerous tissues and are characterized by a short circulation half-life. Nanoparticles can be designed to cross the BBB and deliver their drugs within the brain, thus improving their effectiveness for treatment when compared to administration of the free drug. The efficacy of nanoparticles can be enhanced by surface PEGylation to allow more specificity towards tumour receptors. This review will provide an overview of the different therapeutic strategies for the treatment of malignant gliomas, risk factors entailing them as well as the latest developments for brain drug delivery. It will also address the potential of polymeric nanoparticles in the treatment of malignant gliomas, including the importance of their coating and functionalization on their ability to cross the BBB and the chemistry underlying that.

Keywords: brain tumours; glioma; blood brain barrier; drug delivery; nanomedicine; polymeric nanoparticles; PEGylation

1. Introduction

In the past decade, there has been a great development in medicine and cancer treatment. However, cancer remains a challenging health issue owing to its complicated nature [1,2]. The number of cancer cases is expected to rise to 27.5 million in 2040, as stated by the American Cancer Society [1]. Among the most troublesome malignant cancers are the primary brain cancers that can rarely be cured, with a 5-year overall survival of only 35%. Gliomas count as the most common form of malignant primary brain tumours in adults [3].

The speed and ability to infiltrate and metastasize to nearby brain tissues are the main factors that determine if glioma cells are of low grade (WHO I and II) or high grade (WHO III and IV) [4]. Gliomas have the ability to infiltrate to surrounding tissue and their margins are difficult to determine. This results in conventional treatment approaches being insufficient to produce a curative outcome. Also, the difficulty in achieving successful therapeutic approaches is caused by the physical and chemical barriers that exist, hampering drugs from reaching tumour sites [5–8]. The blood brain barrier (BBB) and blood brain tumour barrier (BBTB) represent the main barriers that stop drugs from entering the brain unless they possess certain characteristics. Also, the multipotent stem cells that give rise to glioma cells, have the ability to self-renew and are responsible for glioma recurrence [9]. Efforts have

been extended towards overcoming physical hurdles by developing techniques that deliver therapeutics to the brain, however, most of these approaches are invasive and fraught with serious side effects, so curative measures should not be only be based on extending survival, but also towards improving the quality of life of patients by reducing side effects. Among the advanced therapeutic strategies is using polymeric nanoparticles for drug delivery and targeting. As will be discussed later in this review, in vitro and in vivo studies have reported promising results for drug loaded nanoparticles targeted to gliomas. Therefore, more efforts should be made towards the betterment of these nanomedicines in terms of improving their loading efficiencies, coating and ability to target gliomas.

2. High Grade Gliomas

Primary malignant brain tumours in adults are mostly gliomas, 75% of which are high grade gliomas (HGG) diagnosed in the central nervous system (CNS). The rate of incidence is 3 to 5 per 100,000 every year, afflicting mostly men. HGG can occur at any age, however, they mainly occur in the 5th and 6th decades of life [10].

Bailey and Cushing developed the seminal system for defining the morphology of glial tumours in the 1920s which is based on the glia stage of growth [11]. This system was used by the WHO in 2000 to classify Gliomas based on their morphology [12]. Gliomas were further stratified based on genetic and molecular factors that were recognized and reported by the WHO in 2016. These factors include isocitrate dehydrogenase (IDH) mutation status, the co-deletion status of 1p/19q and the mutation status of alpha thalassemia/mental retardation syndrome X-linked protein/gene (ATRX) [12]. According to the 2016 WHO classification, grade III tumours which include anaplastic astrocytoma, anaplastic oligodendroglioma and mixed anaplastic oligoastrocytoma are among HGGs, in addition to grade IV glioblastoma (GBM) [12]. GBM has the highest incident rate among HGGs with up to 60–70% of cases being a GBM. This is followed by anaplastic astrocytoma which makes up 10–15% of cases. Whereas, anaplastic oligodendrogliomas and anaplastic oligoastrocytomas have the least frequent incidence rate of only 10% [13]. Some other types of malignant gliomas, such as the WHO grade III gliomas, anaplastic ganglioglioma, anaplastic pilocytic astrocytoma and anaplastic pleomorphic xanthoastrocytoma and the grade IV gliomas, giant cell and small cell GBM, epithelioid GBM, and gliosarcoma are not very common. The main cause for HGGs is still enigmatic, with ionizing radiation only identified as a possible risk factor [14].

3. Treatment

3.1. Surgical Resection

The site, grade and morphology of the tumour will determine if complete surgical resection of the tumour can be achieved. Patients with high grade tumours require near complete resection in order to reduce the burden of the tumour and pressure inside the skull, which in turn improves the survival rate [15–18]. GBM cannot be fully cured with surgical resection as it is invasive in nature and 80% of cases result in relapse within 2 to 3 cm of the original tumour margin [19].

3.2. Radiation Treatment

Radiation therapy (RT) can be administered internally or externally and is considered the standard treatment protocol for HGGs [20]. The standard treatment using external RT involves 25 to 35 treatments on a daily basis for (5–7) weeks. Several factors control the total radiation dose to be administered which are: tumour site, grade, histology and the extent of resection [21]. A randomized trial conducted in the 1970s reported that whole brain irradiation with 60 Gy after surgical resection enhanced survival for patients suffering from HGG. This resulted in RT as being a standard therapy following tumour eradication for HGG [22]. On the other hand, studies that investigated the difference between partial and whole brain irradiation for HGG treatment proved that whole brain irradiation did not provide extra benefit compared to partial irradiation of the brain [23]. However, there was an improvement

in the delineation accuracy that was achieved employing tomography and magnetic resonance for maintaining a partial irradiation of the brain for HGG cases [24]. The developments that have occurred in imaging and RT have enabled irradiation of tumour regions with higher doses while reducing the volume of normal brain tissue exposed to irradiation. Therefore, involved field RT was granted acceptance as the standard of care for HGGs. However, the issue of RT delivery for smaller surface areas remains debatable with efforts towards targeting infiltrating tumour cells [25]. Some techniques that have been recognized for providing a more targeted irradiation towards tumour tissues include fixed field intensity modulated RT (IMRT), dynamic arc IMRT, volumetric-modulated arc therapy (VMAT) and stereotactic radiosurgery (SRS). These techniques were reported to provide a more focused approach towards affected tissues while reducing toxicity to normal tissues [26]. SRS is used to treat recurrent GBM and is used as a complementary treatment after external beam RT. However, the use of SRS for the treatment of recently diagnosed malignant gliomas is still under review [21]. Another approach for RT is interstitial RT or brachytherapy where radioactive material is implanted inside the tumour with the use of surgery. Proton therapy could also aid in targeting affected areas and may be used instead of photon irradiation [26]. RT is associated with some limitations including necrosis of normal brain tissue, neuronal damage and radiation resistance of tumour cells [19].

3.3. Chemotherapy

The chemotherapeutic drug temozolomide (TMZ) is used in combination with RT in patients with HGG in order to improve the survival rate of patients. This protocol, known as the Stupp protocol, demonstrated a median survival rate of 14.6 month compared to 12.1 months (when RT alone was administered) in a phase III clinical trial. TMZ is initially administered at a daily dose of 75 mg/m^2 for 6 weeks, with a 1-month rest period upon the completion of RT treatment. TMZ treatment begins again with a daily dose of 150 mg/m^2 for 5 days in the first month. If this dose can be withstood by the patient, a higher daily dose of 200 mg/m^2 is administered for 5 consecutive days each month until the end of the treatment period. The stupp protocol administers the TMZ therapy for 6 months following RT [27]. Synergistic effect of combined therapy using RT and adjuvant chemotherapy with TMZ continued over a 5-year follow up treatment period. Also, the inclusion of TMZ was more beneficial for patients with a methylated gene promoter that encodes O-6-methylguanine-DNA methyltransferase (MGMT). This in turn had resulted in identifying MGMT as the first biomarker in brain tumours to help anticipate the responsiveness to the TMZ treatment and selection of patients accordingly [28]. However, MGMT is unreliable for patients who do not have a methylated promoter of MGMT except for elderly GBM patients [29]. Some other chemotherapeutic drugs have shown efficacy against recurrent malignant gliomas. These drugs are methylating agents such as irinotecan or those that target the vascular endothelial growth factor such as bevacizumab. Other chemotherapy drugs such as gefitinib, erlotinib and imatinib target the epidermal and platelet-derived growth factor receptors [30].

Among the latest therapeutic approaches is a device named Optune® that received approval by the U.S. Food and Drug Administration (FDA) in October 2015. This device allows for the delivery of electric fields that enable the treatment of tumours by interrupting the division of cells causing cell death. It is used as an adjuvant therapy with TMZ following surgical resection and is the standard of care for adults that have been recently diagnosed with supratentorial GBM. The Optune® treatment regimen alongside TMZ increased survival from 4 to 7 months when compared to treatment with TMZ alone [31]. Optune® was initially approved by the FDA in 2011 as a single treatment for recurrent GBM. Optune® is alternatively used as a treatment for primary GBM after surgery and RT have been shown to be ineffective. A randomized clinical trial exhibited similar rate of survival and less side effects with a significant reduction in the infectious, gastrointestinal and hematologic complications for the Optune® treatment group compared to the standard chemotherapy group [32]. The reduced side effects and practicality of use encouraged the National Comprehensive Cancer Network (NCCN) to include Optune® as a treatment for recurrent GBM [33].

Other treatment approaches such as radioimmunotherapy, iodine-125 brachytherapy, hyperfractionation and SRS have been investigated for their ability to localise treatment and protect normal brain tissues. However, none have been shown to improve survival rates [34]. Therefore, it was concluded that chemotherapy used concomitantly and adjuvantly with RT is the standard of care in current application for GBM patients until more effective treatments become available [28].

4. Postoperative Treatment

Follow up is necessary to monitor the postoperative complications and control the disease symptoms, which include seizures, cerebral edema, turbulences in the gastrointestinal tract, osteoporosis, venous thromboembolism, dysfunction of the cognitive abilities and mood deterioration [35]. Magnetic Resonance Imaging (MRI) scans are used to monitor the size of the tumour and preformed 3 days following the surgical operation to determine how much of the tumour was eradicated. Steroids are administered to patients suffering vasogenic edema. However, treatments based on steroids are associated with adverse side effects such as myopathy [36] which affects 10% of patients with HGGs with an increased incidence rate in elderly patients that are administered corticosteroids for long time periods [37]. Also, patients become vulnerable to mental impairment, hyperglycemic and gastrointestinal complications, in addition to opportunistic bacterial infections such as *Pneumocystis jiroveci*. Dexamethasone is a more favourable corticosteroid as it is lower in activity and upon its discontinuation, myopathy can be reversed [37,38]. Patients with GBM and CNS lymphoma are more susceptible to venous thromboembolism, especially after craniotomy. Treatment using warfarin or heparin of low molecular weight is more favourable than vena cava filters in controlling the anticoagulation and reducing the complications. Levetiracetam is usually administered to patients suffering seizures due to its low toxicity and the fact that it does not interact with the chemotherapy drugs [38].

5. Prognosis

Patient prognosis remains depressing with a 15-month median survival, despite the advancements in surgical resection of the tumours [39]. Anaplastic astrocytoma afflicted patients average between 2 to 3 years survival [40]. The best prognosis is shown in cases suffering anaplastic oligodendroglioma leaving them with expected average survival of 12 to 15 years [41]. The prognostic factors involve: the extent of tumour resected, age of the patient and the Karnofsky Performance Status. Younger age and higher performance status could imply longer survival. Negative results have been linked to tumours larger than 5 to 6 cm [42]. Surgically curable tumours such as those that arise in the cerebrum or cerebellum have a better prognosis than those that arise in the brainstem or diencephalon [43].

6. Glioblastoma Multiforme

Glioblastoma multiforme (GBM) is a malignant tumour that arises in the brain and is known to be the most common form of brain tumours. It represents 16% of the tumours that originate in the brain and CNS [39]. GBM has an incidence rate of 3.2 per 100,000 population [44,45]. GBMs are mainly located in the brain but can also occur in the brain stem, cerebellum and spinal cord. Moreover, the four lobes of the brain (frontal, temporal, parietal and occipital) represent the main sites for the development of the primary gliomas, with an overall incidence rate of 61% and individual incidence rate of 25%, 20%, 13% and 3%, respectively [46]. Initially, glial cells were thought to be the only source of GBMs, however, it has been shown that several types of cells possessing the characteristics of neural stem cells, could give rise to GBMs. These cells vary in their differentiation stage where they start out as stem cells then give rise to neurons and glia. This is accompanied with changes in their phenotype, mainly caused by the variation in their signaling pathways instead of the differences in the origin of the cell type [47]. The average age in which GBMs develop is 64 [39]. Nevertheless, GBMs can develop at any age including children. Men are more likely to develop a GBM than women with a rate of 1.6 for every woman. Caucasians are also more likely to be stricken with the disease than other ethnicities [42].

GBMs can vary in their classification, for example a GBM would be classed as primary or de novo in origin if it has developed without a defined precursor. If a GBM develops from a transformed low-grade tumour it will be termed secondary. Most GBMs are primary in nature and mainly afflict the elderly, who have a poorer prognosis than their counterparts who develop secondary GBM [48]. GBMs can be further classified into four subtypes which are, classical, pro-neural, neural, and mesenchymal. Each subtype varies in its mode of development and survival [49,50]. GBMs are invasive in nature and are difficult to completely remove by surgical resection. They often exist in sensitive areas of the brain which mainly control speech, movement or the senses. The tumour cells also possess the ability to infiltrate and remain in areas that surround the brain, which leads to further disease recurrence [48].

Current Management

The current treatment regimen for GBM is the Stupp protocol which was discussed earlier as the standard of care for glioma management [28]. The main action of TMZ involves methylation of the DNA at the N7 and O6 positions on guanine which halts the DNA mismatch repair mechanism resulting in DNA nicks that halts the cell cycle at the G2-M level, causing apoptosis. However, the elevated level of MGMT activity which functions by protecting tumour cells against chemotherapeutic agents can negatively impact the TMZ response. Moreover, TMZ, is reported to be fraught with deleterious complications such as hematological issues, fatigue and susceptibility to infections [51]. Another chemotherapeutic agent used to treat GBM is the Gliadel® Wafer, which is a disc shaped 200 mg wafer made of biodegradable copolymers that contain 3.85% *w/w* of the alkylating agent bis-chloroethylnitrosourea (carmustine, also known as BCNU). Carmustine was initially approved by the FDA as a potent antineoplastic agent for the treatment of GBM by intravenous administration [52]. Gliadel® is used for local administration of carmustine, with up to 8 discs placed into the resection cavity during surgery. After treatment with Gliadel® Wafers, the median survival in a group of patients with malignant glioma (95% of which was GBM) was 42 weeks, eight patients survived one year, and four patients survived more than 18 months. Local treatment allows the chemotherapy to be concentrated at the site of the tumour while avoiding systemic side effects. However, patients suffered perioperative infections, seizures and required addition steroid treatment [53]. Moreover, the drug penetration into tissues after diffusion from the implants does not exceed 1mm which limits its efficacy [54].

In summary, the drawback of these treatments is that they are associated with serious unwanted side effects in addition to the development of resistance, limiting their efficacy. Some patients do not respond to the TMZ or BCNU, therefore, there has been a second line of drugs developed which include carboplatin, oxaliplatin, etoposide and irinotecan. Additional chemotherapeutic agents for GBM include anti-angiogenic agents like anti-VEGF monoclonal antibodies (bevacizumab), anti-FGF antibodies, monoclonal antibodies targeting EGFR (erlotinib and gefitinib) and tyrosine kinase inhibitors [19,55–57]. Despite developments in tumour diagnosis and treatment using RT and concomitant chemotherapy with TMZ, nearly all GBM patients experience tumour recurrence.

7. The Blood Brain Barrier

One of the main limitations in the systemic treatment of malignant gliomas is the presence of the BBB, which is a complex structure that comprises endothelial cells, pericytes, astroglia and perivascular mast cells and acts as a barrier to most cells, pathogens and drugs circulating in the blood. The BBB is compact in nature due to the presence of tight junctions between the endothelial cells of the vascular layer that are closely stuck together. The BBB surrounds both the brain and spinal cord capillaries and its compactness halts small molecules and ions from passing through the BBB and into the brain. The tightness of the BBB stops integral membrane proteins from moving between the apical and basolateral membranes of the cell, thus protecting the cell membrane from loss of function [58–60].

The tight junctions of the BBB have three fundamental proteins which are occludin, claudins, and junctional adhesion molecules. Occludin and claudins form the pillar of junction strands. Whereas,

when there is an immunologic response in the brain, the junctional adhesion molecules function in the transport of lymphocytes, neutrophils, and dendritic cells from the vascular system. The tight endothelial junctions and adherens junctions are made of cadherins and catenin proteins that are responsible for the adherence of the BBB endothelial cells, forming a transelectrical resistance >1500 Ω cm^2. Although the BBB acts as a physical barrier, it still regulates the transport of metabolic molecules to the brain for nutrition. Small molecules such as glucose or amino acids have specific transporters that convey them to the brain. While, macromolecules such as cytokines and neurotrophils enter the brain by receptor mediated endocytosis [61,62].

The BBB limits the passage of chemotherapeutic drugs with only low molecular weight, electrically neutral, hydrophobic drugs able to cross the BBB with a preference towards molecular weight less than 500 Da and lipophilicity expressed in log *P* as (2–3) [63]. Most chemotherapeutic drugs are large, ionically charged, hydrophilic molecules and thus cannot easily cross the BBB at the levels required for therapeutic effect, which means a large systemic dose is required. For example, irinotecan hydrochloride, which is a potent anionic chemotherapy drug, possesses a molecular weight of 623.1 Da and is hydrophilic in nature, therefore it will face difficulty crossing the BBB and accumulating in the tumour in its initial administered dose. Even if the drug crosses the BBB, it can very quickly diffuse back making it difficult to obtain constant drug levels in the brain after systemic administration.

8. Drug Delivery to the Brain

Two strategies, crossing the BBB and bypassing the BBB, are currently used for the delivery of drugs to the brain. Crossing the BBB can take place via six main pathways: paracellular transport, passive transcellular diffusion, carrier-mediated transport (CMT), receptor-mediated transcytosis (RMT), adsorptive-mediated transcytosis (AMT), and cell- mediated transport. The normal physiology of the BBB does not afford paracellular permeability [64]. However, it can take place when the BBB is compromised in CNS disorders such as GBM, which could facilitate drug delivery to the brain [65]. Transmembrane diffusion allows for the intake of most of the compounds based on their molecular weight and lipid solubility. Influx and efflux transporters facilitate mediated transport, which relies on protein carriers that bind solutes and transport them from the luminal side of the BBB to the other side of the membrane via passive or active transport mechanism [51]. Among the influx transporters are l-type amino acid transporter (LAT1), glucose transporter (GLUT1), monocarboxylate lactate transporter (MCT1), cationic amino acid transporter (CAT1), choline transporter (ChT), sodium-coupled glucose transporters (SGLTs). Influx transporters facilitate particle uptake by the BBB. Efflux transporters, on the other hand, mediate molecules exclusion form the BBB. These transporters are like p-glycoprotein (P-gp), peptide transport system-6 (PTS-6), and breast cancer resistant protein (BCRP) [66–69]. RMT involves the uptake of macromolecules by clathrin-mediated or caveolin-mediated endocytosis. This route has been previously used to deliver both free drugs and nanoparticles into the brain [70]. RMT is the route by which actively targeted drugs are internalized. Receptors expressed on the surface of cells are recognized and bound by complementary ligands coating the drug loaded nanoparticles and this complex structure enters the cell in vesicles coated with clathrin. This process is 1000 times more efficient than pinocytosis [71]. The size of clathrin-coated vesicles is determined by the size of the drug delivery vehicle which they carry [72]. Several receptors aid in transporting compounds across the BBB, such as the insulin receptor, low-density lipoprotein (LDL) receptor, transferrin receptor, neonatal Fc receptor and leptin receptor [73–77]. Whether internalization occurs by pinocytosis or RMT, the cargo is delivered to the early endosome, which is of slightly acidic pH (6–6.8). The endosome has a sorting function, where it either allows the recycling of molecules back to the plasma membrane or sends them to late endosome and lysosome for degradation [78]. Whereas, caveolin-mediated endocytosis forms caveolae which are invaginations in the plasma membrane that take the shape of small flasks that engulf large molecules and transport them internally. AMT relies on the electrostatic interaction between positively charged substances and the plasma membrane, leading to internalization of molecules followed by their transport across the BBB. This pathway could be exploited by developing drugs

or nanoparticles with positive charges or by conjugating the drug or nanoparticles with a positively charged ligand [79,80]. CMT exploits the natural mechanism involved in inflammation with drugs and nanoparticles engulfed by immune cells such as monocytes and macrophages [81,82]. In diseases such as neuroinflammation, or GBM, immune cells such as leukocytes are transported towards the brain parenchyma by chemotaxis and diapedesis processes. This process could be exploited in designing drugs or nanoparticles that can be phagocytosed by leukocytes and thus transported into the brain. The efficacy of free drugs and nanoparticles delivered by this natural mechanism, also known as the Trojan Horse mechanism has been shown to increase. This mechanism allows for larger sized particles to enter the brain, however, their larger size can result in increased toxicity [83–85]. There are a number of options for bypassing the BBB. Intracerebroventricular (ICV) administration is performed through an invasive procedure of skull penetration and drug injection directly into the brain. An implantable reservoir or a pump is used to introduce the drug through an outlet catheter. The pump allows for a constant drug supply at high concentrations. The ICV process is extremely invasive and can lead to infections and increased intracranial pressure [86]. Intracerebral/intraparenchymal administration involves the delivery of drugs directly into brain tissue either via stereotactic injection or by formulating into an implant that can be implanted during resection surgery (i.e., Gliadel®) or via stereotactic surgery. The issue with this type of delivery is that drug diffusion occurs slowly and allows drug to travel only 2 mm from the injection/implantation site [86]. Convection Enhanced Delivery (CED) is a slightly less invasive surgical procedure where catheters are placed inside the interstitial space of the brain parenchyma. A drug solution is administered into the brain under a positive pressure gradient using a pump, leading to a higher distribution volume compared to intracerebral/intraparenchymal administration [86]. This procedure is still, however, invasive in nature and could subject patients to the risk of infections, tissue injury and air bubbles. Furthermore, due to the high pressure used, the drug solution could leak into sensitive areas of the brain, such as subarachnoid space [86]. Intrathecal administration is considered one of the least invasive procedures, where drugs are injected into the subarachnoid space of the spinal cord via a lumbar puncture where they reach the CNS parenchyma in the cerebral spinal fluid [87]. However, possible side effects such as infections and adverse immune response could occur due to this technique [87]. In addition, although the ICV and intrathecal techniques can bypass the BBB and cerebrospinal fluid (CSF) hurdles, there remain the ependymal cell layer and glial cells which come in the way between the CSF and the brain parenchyma limiting the efficacy of drug diffusion to reach the brain parenchyma via these techniques [88]. Intratympanic administration employs the route of the middle ear to administer drugs, which are transported via pinocytosis, eventually reaching the brain where they bypass the labyrinthine barrier (BLB) which is similar to the BBB. This route can be suitable for therapeutics up to 1 μm size [89]. Poly(D,L-lactide-co-glycolide) (PLGA) nanoparticles were used to administer drugs via this route with promising efficacy [90]. Intranasal delivery is a non-invasive route of administration for bypassing of the BBB through spraying drugs into the nasal cavity, where they diffuse extracellularly or via convection. Another route is through olfactory sensory neuron termed intraneuronal transport or through trigeminal nerve, termed intraneuronal transport [91]. The intranasal route is beneficial in terms of being convenient to patients, allowing for rapid absorption and avoiding first pass metabolism [92]. Some other methods for crossing the BBB have been investigated, most of which are invasive in nature, such as osmotic opening of the BBB [93]. Other non-invasive methods have also been investigated, for example, the Trojan Horse technology which relies on coupling drugs to genetically engineered proteins that can cross the BBB by receptor mediated transport processes [94]. Such methods are also fraught with side effects and thus alternative more effective and less toxic methods for delivery of drugs to the brain are needed in order to improve the treatment of brain tumours [95].

9. Nanomedicine: A Non-Invasive Approach towards a Better Quality of Life

Nanotechnology has provided us with a promising tool that can be used to enhance the uptake of drugs across the BBB [96,97]. This is because nanoparticles have the ability to be loaded with

therapeutic agents and functionalized with multiple ligands that enable targeting and crossing of the BBB. In this case, the ability to cross the BBB will not be dependent on the structure of the drug, which cannot readily be altered, but on the physicochemical properties of the nanoparticles, which can be altered. Nanoparticles are proposed to perform their action in delivering drugs across BBB by concentrating the drug inside or at the surface of the BBB, which will result in a high concentration gradient between blood and brain, encouraging passive diffusion of the drug into the brain [98].

Nanoparticles have the ability to diffuse into the leaky vasculature of tumour tissues by the enhanced permeability and retention effect (EPR). This cancer-specific attribute is characterized by poor lymphatic drainage allowing the accumulation of nanoparticles to reach concentrations much higher than their concentrations in plasma [99]. The effective treatment of GBM can be accomplished by achieving three main goals: (1) Improving the ability of chemotherapeutic agents to cross the BBB, penetrate into brain tissue reaching the tumour tissue at therapeutic concentrations (2) Avoiding or reducing side effects and (3) Sustaining therapeutic concentrations of the drugs at the site of the tumour, increasing their half-life and avoiding rapid clearance [99].

10. Physicochemical Properties of Nanoparticles

The different physicochemical properties of nanoparticles such as the particle size, surface charge, hydrophobicity and coating material have an impact on the targeting process. They also impact the interaction of particles with the cell membrane and passage through biological body barriers [100]. Size is an important factor that allows transport of nanoparticles in the blood stream and enables delivery of nanoparticles to the site of the tumour. Small sized nanoparticles can easily reach the leaky blood vessels of the tumour, however, they can extravasate into the normal tissues [101]. Therefore, optimization of nanoparticles size can enhance their uptake into tumour tissues. The shape of nanoparticles is also of importance as it influences the fluid dynamics and thus particle uptake. The current trend is towards using spherical nanoparticles owing to the ease in their synthesis and application [102]. In addition, the stability of nanoparticles is affected by their surface charge which also impacts their distribution in the bloodstream. Previous studies have shown that positively charged nanoparticles could be more effective in targeting tumour vessels. However, this has been replaced by neutrally charged nanoparticles which extravasate quicker into the tumour tissue [103].

11. Nanoparticles as a Treatment for Malignant Gliomas

A range of different nanoparticle formulations have been investigated to deliver chemotherapeutic drugs to the brain. The majority of these formulations have utilized polymers that have met the strict requirements needed to be accepted for biological applications [104]. During recent years, nanoparticles for the treatment of CNS diseases such as GBM have received significant attention [105,106]. With systemic administration of free drug, a small percentage of the drug crosses the BBB with non-specific accumulation in off target tissues resulting in serious unwanted side effects. Therefore, the use of nanoparticles for delivery to the brain has the potential to increase the percentage of drug that crosses the BBB while reducing non-specific accumulation in other tissues [107,108]. For example, gadolinium-loaded nanoparticles increased the level of gadolinium 100 fold when compared to free gadolinium [109]. The manufacture of nanoparticles has improved in the last few years with optimization of drug loading, encapsulation efficiency and release profile. Furthermore, improvements in the stealth capabilities of nanoparticles have increased their protection from agglutination with proteins in the blood, enabling them to avoid being cleared from the blood by the reticuloendothelial system (RES). Nanoparticles whose surface has been modified with ligands have been used to facilitate imaging of brain tumours nanoparticles [110,111]. PEGylation of nanoparticles has been widely used in drug delivery in order to protect nanoparticles from blood protein interaction and from the RES [112,113]. Dawson et al. demonstrated that the PEGylation of nanoparticles completely prevented their interaction with proteins in the plasma. However, other studies have shown that PEGlylation does not completely prevent the interaction between proteins and nanoparticles in the blood [114].

Nanoparticles offer a non-invasive method for drug delivery to the brain. However, they need to be optimized in relation to size, release kinetics, chemical properties, while modifying their surface could improve their ability to cross the BBB as well as protecting the drug from the biological environment and enhancing drug solubility [115]. Nanoparticles for drug delivery to the brain need to meet certain essential requirements to be most effective, with reduced toxicity. The requirements include non-toxic, biodegradable, prolonged circulation period, no aggregation in the blood, good encapsulation efficiency and the ability to cross the BBB [116].

12. Routes of Administration of Nanoparticles in the Treatment of Malignant Gliomas

There are three main routes of administration for nanoparticles designed to treat brain tumours: (1) direct delivery to the brain; (2) direct systemic delivery to the brain and (3) indirect systemic delivery to the brain.

Direct delivery to the brain offers a way of bypassing the BBB by direct injection of the nanoparticles into the brain. CED has been used to infuse a nanoparticle suspension directly into brain tissue. Lollo et al. used CED to deliver 10 μL of paclitaxel-loaded lipid nanocapsules directly into the brain of mice. The results showed that the overall survival of mice treated with the lipid nanocapsules was significantly increased in comparison with mice treated with free paclitaxel [117,118]. Fourniols et al. described the direct injection of a photopolymerizable hydrogel containing TMZ-loaded micelles to the brain using a syringe to inject through an incision drilled in the skull. The TMZ-loaded micelles and injection were well tolerated while the hydrogel improved the drug release profile [119]. The major limitations of direct delivery to the brain is its invasive nature, the risk of infection and the need to control critical parameters such as pH and osmolarity which if not optimized may lead to brain damage [120]. Direct systemic delivery to the brain is where nanoparticles are directly administered into blood stream through carotid artery and transported to the brain avoiding the rest of the systemic circulation. This technique has shown improved survival compared to CED with reduced risk of brain damage [121]. Huynh et al. administered ferrociphekunol-loaded nanoparticles to the brain of GBM inflicted rats using both CED and direct systemic delivery. Direct systemic delivery provided a survival of 28 days compared to 24 days for the CED group. The results indicated that direct systemic delivery could provide a modest increase in survival when compared to direct delivery to the brain [120,122]. Indirect systemic delivery involves the delivery of nanoparticles into the systemic circulation via routes of administration that require absorption such as oral, topical, nasal, and peritoneal administration. The major advantages of oral administration are the convenience, non-invasiveness, and patient compliance. Kumar et al. administered two curcumin formulations (nanoparticles and plain suspension) orally to a rat intestinal ex-vivo model. The results showed that the bioavailability of nanoparticles formulation was 12 times greater than the plain suspension [123]. Intraperitoneal administration is widely used as an indirect systematic delivery method by injecting the drug into peritoneal tissue. It is used when administering large doses or when it is difficult to locate a vein for direct systemic delivery [124].

13. The Chemistry of Coating and Bioconjugation of Nanoparticles

Tumour tissues with their leaky vasculature allow the passive accumulation of particles from 10 to 200 nm in size by the EPR effect. However, chemotherapeutics penetration over time becomes challenging due to the increased interstitial pressure and the dense structure of the tumour tissues caused by hydrophobic regions in the brain extracellular space which block therapeutic particles, by steric hindrance, from accessing the tumour. Instead, chemotherapeutics diffuse towards the tumour edge and leak to blood vessels formed by angiogenesis. Additionally, nanoparticles are spotted by the RES as foreign particles and cleared by phagocytosis [125,126].

Advanced nanomedicine research has focused on developing stealth nanoparticles, which are designed with special coatings such as polyethylene glycol (PEG) that mask them from the RES system allowing them to circulate for longer in the bloodstream increasing tumour penetration and

physiological stability. Furthermore, the coating enables targeting of brain tumour tissues in a more specific manner than uncoated particles [127,128]. Such coated nanoparticles are chemically and physically developed using different techniques which involve grafting, coprecipitation and surface adsorption [129]. Such bioconjugation involves using coatings that are either biological in nature or synthetic but specifically designed for biological applications [130].

Nanoparticles could have their surface modified through covalent and non-covalent ligand binding Covalent binding takes place via either disulphide bonds, primary amines cross linking, primary amine-carboxylic acid reaction, maleimide-thiol reaction, aldehyde-hydrazide reaction and primary amine-free aldehyde reaction [131]. Bioconjugates are also formed by using reactive crosslinking agents or reactive groups that aid in the coupling reaction. Some secondary activating agents could act as intermediates in the coupling process that facilitate binding specific functional groups. This process is specific in nature and resembles the selection of building blocks in order to create the whole structure. Affinity molecules act as an important part in the functionalized entity and they aim at targeting biomolecules [130].

Non-covalent or physical interaction between targeting ligands and nanoparticles does not involve chemical bonds, however, it may not create as strong a binding as is the case in covalent binding [132].

The process of PEGylation could take place by coupling with linear or branched PEG molecules which provides a more stable structure with enhanced water solubility and half-life while reducing cytotoxicity and adverse immune response [133,134].

Surfactants offer a major advantage for nanoparticles by helping them penetrate the BBB as well as enhancing their uptake by tumour cells. These surfactants could be polysaccharides, poloxamers or polysorbates. A study reported that Polysorbate 80 (p80) coated polymeric nanoparticles carrying paclitaxel had enhanced uptake by GBM cells due to the coating masking them from the P-gps, which are responsible for drug resistance, as well as by allowing their penetration of the BBB [135]. Previously published studies have demonstrated the beneficial role of p80 and Poloxamer 107 as surface ligands in facilitating transport across the BBB with proven efficacy in GBM rats [70,136–138]. However, the main issue with these particles is that they could only travel through endothelial cells to neurons in close proximity with the BBB, via cell to cell processes. As a result, the parenchyma barrier of the brain tumour will remain unpenetrated. Therefore, the focus on developing nanoparticles that can exceed this hurdle is necessary for a better treatment response. Another study used a similar approach of coating their PLGA nanoparticles with two different surfactants (p80 or poloxamer 188) for the intravenous delivery of two model drugs; loperamide and doxorubicin to the brain. Good efficacy was observed in rats containing an intracranial GBM when treated with doxorubicin loaded particles, while an analgesic effect was observed in mice when treated with the loperamide loaded particles, which confirms successful transport across the BBB at therapeutic levels. On the other hand, uncoated nanoparticles used in the same study had no effect for either drugs [127].

Other targeting moieties have been investigated for the treatment of malignant gliomas. Kuo and Chen (2015) reported that using lactoferrin and folic acid as grafting ligands for PLGA nanoparticles were effective in crossing the BBB and delivering etoposide in GBM U87MG cells [139]. Lactoferrin and folic acid coated nanoparticles had aided in the permeability of etoposide by almost 2-fold as compared to the uncoated nanoparticles. This resulted in a two-fold tumour suppression by the etoposide-loaded nanoparticles when compared to the free etoposide over 48 h. Furthermore, these nanoparticles were prepared with a cationic surfactant, didodecyl dimethyl ammonium bromide (DMAB) which was previously reported to enhance the affinity of the nanoparticles to the walls of arteries allowing for their uptake via AMT [140,141]. Other studies also highlighted the role of lactoferrin and other blood proteins (transferrin, insulin and leptin) as surface ligands in traversing through the BBB by RMT [77,139,142].

Another study demonstrated that a hydrogel made of polymeric micelles coated with polyethylene glycol dimethacrylate could provide sustained release of TMZ over a 1-week period in GBM bearing mice. This study indicated a dramatic decrease in the tumour volume following treatment with

the TMZ photopolymerized hydrogel as well as increased apoptosis as compared with the other groups [119].

Dual coating of polymeric nanoparticles is also an interesting therapeutic trend. A study investigating polymeric nanoparticles with PEG and a covalently attached ligand called peptide-22 was shown to enhance BBB permeability, recognition by LDL receptor on the surface of glioma cells and increased delivery of paclitaxel [143]. The benefit of dual coating was further investigated in a study that coated PEGylated PCL nanoparticles with angiopep-2 which is a peptide that facilitates BBB permeation and drug delivery in glioma cells. This study has also employed cell penetrating peptides to allow deep permeation towards glioma cells and delivery of docetaxel which improved the rate of survival in glioma afflicted mice [144].

Another targeting protein moiety named EGFP-EGF1 was bound to polymeric nanoparticles carrying paclitaxel to form a dual coating alongside PEG aimed at targeting glioma in mice. This targeting protein has specific affinity towards tissue factor over-expressed in glioma cells therefore provided better penetration than non-fused nanoparticles. This study has reported enhanced apoptosis and necrosis and extended time of survival for mice treated with PLA-PEG-EGFP-EGF1 compared to the other groups [145].

An in vitro study using murine glioma cell lines C6 and F98 compared the cytotoxicity of etoposide loaded and unloaded PLGA nanoparticles with and without surface coatings. Their results have indicated enhanced cytotoxic effect on both glioma cell lines as compared to unloaded nanoparticles or free drug [146]. Surface coating of PLGA nanoparticles with protamine, which is a cationic protein that enhances drug transport across BBB, also significantly improved the delivery of cisplatin in bovine endothelial cells and also were cytotoxic in U87 GBM cells [147].

14. Drug-Loading of Nanoparticles

Drugs employed in the treatment of cancer can be loaded either by entrapment within, adsorption on or by covalently bonding to the nanoparticle [148]. The process of drug entrapment could take place either during or after the process of nanoparticles manufacture. Several factors, such as the solubility of the chemotherapy drug in the nanoparticles matrix, the molecular mass of the drug, the type of interaction between the drug and the nanoparticles and the functional groups on the surface of the nanoparticles influence their loading process [148].

The method of drug loading could result in drug within the core or on the surface of the nanoparticles. Drugs loaded on the surface by covalent bonding or physical adsorption as for example by electrostatic interactions between the nanoparticle and drug usually exhibit low stability and become pH liable [149,150]. Drugs entrapped within the nanoparticles usually have greater stability and tend be released over a sustained period of time.

15. Polymeric Nanoparticles for the Treatment of Malignant Gliomas

Polymeric nanoparticles are defined as submicron colloidal nanoparticles and are used as carriers for different drugs such as chemotherapeutic drugs which are either adsorbed on the surface or encapsulated within the nanoparticles [151]. There are many types of polymers which have been used in the manufacture of nanoparticles, such as poly(lactic acid) (PLA), poly(ε-caprolactone) (PCL), poly(butyl-cyanoacrylate) (PBCA), poly(glycolic acid) (PGA), PLGA and poly (amino acids). PLGA, PGA, PLA are the most extensively utilized polymers in drug delivery to the brain, because of their biocompatibility and low toxicity compared to other polymers [152]. They all degrade into lactic acid and glycolic acid that enter into the Krebs cycle where their metabolites are eliminated as carbon dioxide and water from the body [153]. Polymeric nanoparticles have advantages over other types of nanoparticles such as improved release kinetics, better compatibility with some active agents, no oxidation issues as with phospholipids and improved shelf-life [154–156]. The successful development of polymeric nanoparticles for drug delivery to the brain will require an understanding of

the molecular weight, crystallinity and stability of the polymers as well as physicochemical properties of the drug [157].

The first polymeric nanoparticles developed to deliver drugs to the brain was performed by Kreuter et al. The BBB penetration of dalargin was significantly increased by formulating it into PBCA nanoparticles [158]. In 2001, Kreuter et al. used the same dalargin-loaded PBCA nanoparticles coated with p80, to increase penetration into brain tissue. This nanoparticle formulation was utilized for the delivery of other drugs, such as doxorubicin and loperamide into the brain [70]. Calvo et al. prepared PEG-PHDCA (poly(hexadecyl cyanoacrylate)) nanoparticles which demonstrated a greater accumulation in the brain when compared to the p80 formulation, which may be due to passive diffusion or intake via macrophage [159]. The density of the PEG coating on the surface of the nanoparticles can affect the level at which they cross the BBB. Vila et al. produced PEG-PLA nanoparicles with different densities of PEG coating and demonstrated that the smaller nanoparticles with the highest density of PEG had a greater accumulation in the brain [160].

16. Targeted Polymeric Nanoparticles for the Treatment of Malignant Gliomas

The active targeting of polymeric nanoparticles via surface modification with ligands that bind to target molecules on the surface of cancer cells or other cells within the body is a significant development in nanotechnology [161]. Table 1 shows examples of developed targeted polymer nanoparticles as targeted drug delivery system for treatment of malignant gliomas. The affinity ligands bind directly to antigens that are differentially overexpressed on the plasma membrane of cells or to extracellular proteins on the target tissue [161]. Active targeting of nanoparticles can be used for either extracellular or intracellular delivery of drugs. Nanoparticles are more effective if they are targeted to intracellular sites [154,162]. For example, Alexis et al. demonstrated increased cytotoxicty of paclitaxel-loaded nanoparticles using a ligand targeted to the extracellular domain of the trans-membrane human epidermal growth factor receptor 2 (HER-2) when compred with non trageted nanoparicles. This increase in cytotoxicty was due to an increased cellular uptake by the targeted nanoparticles [163]. Studies have confirmed that enhancing cellular uptake is the most important role of using targeted nanoparticles [164,165]. Targeted nanoparticles can have either single or multi ligands attached to their surfaces. To date, most researchers have prefered to use a single ligand as multi-ligands are associated with some disadvantges, particulalry when used for penetration of the BBB and tumour cells. For example, multi-ligands influence drug release as well as the mobility of the nanoparticles. Furthermore, competitive binding and/or an interaction between ligands may reduce the targeting effeciency of the nanoparticles [166].

Transferrin receptors and low density lipoprotein receptor related protein (LRP) are known to be overexpressed on glioma cells [166]. These two receptors have been used to target polymeric nanoparticles to glioma cells by attaching the anti-transferrin and angiopep ligands to their surface. Anti-transferrin can cross the BBB through transferrin receptors while the angiopep ligand binds to LRP on the surface of glioma cells [166,171]. The transferrin receptor is the most widely characterized receptor-mediated transport system, which provides an efficient cellular uptake and is over expressed in numerous tumour cells [167]. The targeting of BBB of an in vitro model has increased 20-fold with transferrin-PLGA nanoparticles compared to non-coated PLGA nanoparticles. Chang et al. demonstrated, using an in vitro model of the BBB, that transferrin-PLGA nanoparticles had a 20 fold increase in uptake by the BBB when compared to un-coated PLGA nanoparticles. The uptake of the transferrin-PLGA nanoparticles by the BBB was by endocytosis [167]. The major disadvantages of using transferrin as a ligand for nanoparticles is the competition with endogenous transferrin for receptor binding. This may result in reducing the cellular uptake and thus the effectiveness of the nanoparticles [178]. An antibody directed against the transferrin has been used as an alternative ligand to the endogenous transferrin as it binds to an epitope of the transferrin receptor which is located at a different location from transferrin binding. Therefore, the nanoparticles have less binding competition as they do not interfere with the transferrin intake mechanism. This will increase their cellular uptake

and thus their effectivness [179]. Different antibodies such as OX26 (anti-rat TfR mAbs), R17-217 and 8D3 (both anti-mouse TfR mAbs) have been developed for enhancing brain uptake. OX26 mAbs has been shown to have a high affinity for cells that overexpress transferrin, including GBM cells [180,181]. The level of brain uptake for each of the antibodies is different. For example, the brain uptake of 8D3 mAbs was relatively high compared to R17-217 mAbs. 8D3 and R17-217 mAbs were more selective for brain than liver and kidney [182]. Rmalho et al. developed receptor mediated TMZ-loaded PLGA nanoparticles for GBM treatment functionalized with an OX26 mAbs. The cellular internalization of the OX26mAbs nanoparticles was signifcantly enhanced compared to the PLGA nanoparticles with no mAbs [176].

Table 1. Examples of developed targeted polymer nanoparticles as targeted drug delivery system for treatment of brain tumours malignant gliomas.

Polymer Type	Loaded	Size (nm)	Targeting Strategy	Targeted Site	Ref.
PLGA	Dil	90	Transferrin	Transferrin receptors	[167]
PMLA	Antisense ON	25	mAbs antisense oligonucleotides (AONs)	(proteins) laminin-411	[168]
PEG-PCL	Paclitaxel	<100	Angiopep	LRP	[169]
PEG-PLGA	Coumarin 6	125	Peptide (12 amino-acid)	Peptide	[170]
PEG-PCL	Paclitaxel Rhodamine	90	Angiopep	LRP	[171]
PLGA	Methotrexate	85	Transferrin	Transferrin receptors	[166]
PEG-PLGA	Doxorubicin	100–300	Endogenous tripeptide thiol (glutathione)	Glutathione transporters	[172]
PLGA	Loperamide	100	mAbs (8D3)	Transferrin receptors	[173]
PLGA	Curcumin	100	Magnetic guidance Peptide (T7)	Transferrin receptors	[174]
PLGA	Doxorubicin	120	Poloxamer 188	LRP	[175]
PEG-PLGA	TMZ	19	mAbs (OX26)	Transferrin receptors	[176]
PLGA	Paclitaxel	230–255	Tripeptide(RGD) Superparamac iron oxide (SPIO)	αvβ3 integrin	[177]

Another approach to enhancing the uptake of nanoparticles by the BBB is to coat them with a polymer that will facilitate cellular uptake. As discussed earlier about the role of surfactants in coating, Kreuter demonstrated that intravenously injected doxorubicin-loaded p80-coated nanoparticles had a 40% cure rate in rats with intracranially transplanted GBMs. Although not fully elucitated, he hypothesised that the most likely mechanism for transport of the nanoparticles across the BBB was endocytosis by the endothelial cells lining the brain blood capillaries. Coating the nanoparticles with p80 lead to the adsorption of apolipoprotein E from blood plasma onto the nanoparticles' surface. The particles then mimiced LDL particles and could thus interact with the LDL receptor leading to their enhanced uptake by the endothelial cells [70]. The first polymeric nanoparticles for penetration of the BBB were investigated by Schröder et al. in 1995. PBCA nanoparticle coated with p80 enhanced BBB penetration of hexapeptide dalargin-loaded nanoparticles [183]. Wohlfart et al. demonstrated, using a rat glioma model, that poloxamer 188-coated PLGA nanoparticles enabled the delivery of doxorubicin across the BBB in the therapeutically effective concentrations. The basis for their transport across the BBB was hypothesised to be adsorption of blood apolipoproteins (ApoE or ApoA-I) onto the nanoparticles surface due to the poloxamer 188 coating, followed by RMT of the nanoparticles [184]. Manlioovskaya et al. demonstrated that these same nanoparticles entered U87 human GBM cells via clathrin-mediated endocytosis. They also demonstrated that the nanoparticles released their doxorubicin via diffusion rather than by intracellular degradation [175]. These studies prove that PLGA nanoparticles coated with poloxamer 188 could improve the delivery of doxorubicin and potentially other chemotherapeutic drugs into brain tumours.

Another promising LPR ligand for delivering nanoparticles to the CNS and BBB penetration is angiopep. It is from a peptide family that is derived from aprotinin and human proteins [185]. The transcytosis capacity and parenchymal accumulation of angiopep-2 is much greater compared to

transferrin [186]. The ability of angiopep to facilitate penetration of the BBB of polymeric nanoparticles has been confirmed in a number of studies [169,187]. Xin et al. fabricated dual targeting nanoparticles to improve the drug delivery of paclitaxel to glioma cells. Angiopep-PEG-PCL nanoparticles were highly endocytosed by U87 GBM cells compared with non-targeted PEG-PCL nanoparticles. These nanoparticles have also shown higher penetration, distribution, and accumulation in 3D glioma spheroids as well as increased efficacy in U87 tumour bearing mice [169,171].

17. Challenges Associated with Nanomedicine as a Treatment for Malignant Gliomas

17.1. Reticuloendothelial System

The RES also termed the mononuclear phagocyte system (MPS), possesses cellular and noncellular components. Phagocytes could cause the clearance of nanoparticles by binding to them and triggering cytokine cascade, which causes inflammation [188]. Moreover, macromolecules such as proteins and lipids and others could attach to the surface of the nanoparticles forming a biological corona that gets recognized by the immune system and cleared from the blood stream [189]. This challenge could be overcome by surface modification of the nanoparticles that could conceal them from being recognized by the RES and allow their existence for longer periods in bloodstream. Surface modification is done using zwitterionic ligands such as cysteine, glutathione or by PEGylation [188]. In a study performed by Choi et al. using zwitterionic (cysteine) or neutral dihydrolipoic acid ((DHLA)-connected polyethylene glycol; DHLA-PEG) coatings to coat quantum dots has prevented adsorption of serum proteins and enhanced their renal clearance [190]. An in vivo study showed that using nanoparticles of PEGylated human serum albumin loaded with paclitaxel accomplished long systemic circulation of more than 96 h and enhanced accumulation in the tumour providing high efficacy against cancer and extension in the life span of animals [191]

17.2. Renal System

The main obstacle facing nanoparticles with the renal system is the process of blood filtration. Nanoparticles will follow certain routes by passing through fenestrated endothelium that has 70–100 nm pores, then they will go through the capillary endothelium and podocytes that are programmed to clear particles sized between 2 and 8 nm, whereas nanoparticles >8 nm will face difficulty crossing the glomerular filtration barrier. In addition, the fact that the glomerular basement membrane carries a negative charge, cationic nanoparticles (2–6 nm) will exhibit more renal clearance than neutral or anionic same sized nanoparticles [188]. The shape of a nanoparticle could also influence renal clearance, with enhanced clearance of rod shaped nanoparticles of size 0.8–1.2 nm diameters as reported by Ruggiero et al. [192]. Size exclusion is a major challenge that affects the overall benefit of using the nanoparticles. The solution to this problem could lie through developing nanoparticles of biodegradable materials that can break down into particles prone to renal clearance. However, this could result in premature release of the therapeutic agents before reaching their target site [193]. Therefore, in designing nanomedicines for clinical applications, it is necessary to keep the balance between formulating nanoparticles that have renal clearance to avoid long term toxicity as well as maintaining the therapeutic levels of the drugs in the plasma [188].

17.3. Blood Brain Barrier

As mentioned previously, the BBB is a barrier consisting of tight junctions that limit the entry of nanoparticles into the brain. However, nanoparticles with ligands attached have been used to pass through the BBB by the receptor mediated endocytosis [188].

17.4. Pathophysiological Barriers in Cancer

The composition and structure of the tumour extracellular matrix and its vasculature vary according to the nature of the cancer, it's position and stage, alongside personal characteristics [188].

Therefore, deep penetration of the nanoparticles could be difficult to achieve [194]. Three steps are involved in the transport of pharmaceutical agents to tumour cells. These involve flow of the nanoparticles through blood vessels, then passage through the walls of the blood vessels, eventually crossing the interstitial space to reach the tumour site. The morphological discrepancy between tumour and normal tissues affect the delivery of the therapeutic agents. The abnormal environment of tumourous tissues results in leaky vessels, abnormal blood flow, dysfunctional lymphatic vessels and vascular hyperpermeability that causes interstitial hypertension. The high pressure of the interstitial fluid and dense extracellular matrix hinder the process of diffusion [195,196]. Several strategies have been addressed to enhance drug delivery such as: (1) Normalization of tumour vasculature by using antiangiogenic agents that repair the imbalance that took place between the overexpressed proangiogenic and antiangiogenic factors in tumour tissues [196]. This approach has rapidly normalized the tumour microenvironment and reduced vessel size and vascular permeability in GBM patients after receiving cediranib as an antiangiogenic therapy [197]. In a preclinical study, surface modified nanoparticles (20–40 nm) could successfully penetrate into breast cancer tissues following vascular normalization therapy [198]. Nevertheless, normalized vasculature would not grant entry to extra large nanoparticles due to the reduced pore vessel size. In addition, vessel normalization is impermanent and requires drug administration within the normalization period [196]. (2) Normalization of tumour matrix that is mainly composed of collagen and glycosaminoglycan. The normalization process is based on degrading such components to improve nanoparticles penetration. Bacterial collagenase treatment has been administered in high collagen containing tumours such as HSTS26T sarcoma and Mu89 melanoma and has improved penetration of IgG antibodies (4.5 nm size) by two fold [199]. Also, interstitial distribution of herpes simplex virus (size 75 nm) was improved by three-fold [200]. Other strategies have been suggested to improve penetration of nanoparticles into cancerous tissues. Inhibiting growth factor-β in pancreatic adenocarcinoma was reported to enhance the penetration of polymeric nanoparticles 100 nm in size [201]. Alternatively, using multi-staged nanoparticles could enhance drug delivery in cancer. This involves using large nanoparticles that have longer half-life in the blood stream [202]. These large particles dissociate upon entry into the tumour microenvironment and release smaller nanoparticles that diffuse on a deeper level into the tumour tissue. A multistage nanoparticle system (100 nm) was engineered with a gelatin core to dissociate and release nanoparticles (10 nm) when it comes in contact with matrix metalloproteinases, for a deeper tumour penetration [203].

Designing nanoparticles that can have deep penetration into tumour tissues are under development. Additionally, smart nanoparticles are being developed that can respond to the surrounding conditions and allow a better bioavailability for treatment [204].

17.5. Multidrug Resistance

Multidrug resistance (MDR), whether hereditary or gained by long term exposure to drugs, involves discharge of drugs outside the cells leading to reduced drug concentration and efficacy inside the cell lumen. Cancer cells can be resistant to chemotherapeutic drugs causing increased toxicity of healthy cells which get exposed to drugs that get ejected by cancer cells. Some chemotherapy drugs that cancer cells are resistant to include taxanes, anthracyclines and vinca alkaloids [205]. In cancer, MDR usually comes from overexpressed P-gp which is an ATP-binding cassette (ABC) transporter that acts as an efflux pump with the ability of binding many various hydrophobic drugs [206]. Such transporter is present in several organs such as brain, liver and placenta, for example and it functions by protecting organs from toxins [207]. Some other MDR associated proteins involve MDR-associated protein-1 and the breast cancer resistance protein (BCRP) [208]. Efflux pump inhibitors such as verapamil (covera) and cyclosporine have been investigated and are emerging as first-generation antagonists [209]. Addressing MDR in cancer has involved the exploitation of nanoparticles drug delivery systems in encapsulating chemotherapy drugs. Liposomes nanoparticles encapsulating doxorubicin and verapamil have been formulated for the targeted inhibition of P-gp [210]. Furthermore, hybrid nanoparticles of lipids and co-polymers were developed and loaded with doxorubicin and GG918 to target BCRP [211]. Both

of the previously stated studies have accomplished higher cytotoxicity against leukemia and breast cancer cell lines, respectively, compared to free drug administration. PCL polymer was also employed alongside other co-polymers in the development of micelle nanoparticles of siRNA to target MDR-1 and perform silencing of the gene responsible for P-gp expression [212].

18. Clinical Transition of Polymeric Nanoparticles

Polymeric nanoparticle formulations utilizing different polymers, coatings and targeting ligands have been introduced into the clinic. As can be seen from above a wide range of different nanoparticle delivery systems have been investigated pre-clinically, which may lead to more nanoparticles reaching the clinic. Furthermore the FDA has approved a range of different routes of administration for nanoparticles, such as systemic, local, and oral administration [213]. The main route of administration used in most preclinical and clinical studies is intravenous administration due to the nanoparticles being able to reach all parts of the body giving them a high potential to influence clinical care by targeting both the primary cancer and any associated metastasis [214,215]. All of the nanoparticle formulations approved for cancer treatment are liposomal formulations. The first approved nanoparticle formulation was PEG-functionalized liposomal doxorubicin (Doxil) in 1995, and the most recently approved nanoparticle is irinotecan liposomal formulation (Onivyde) [216,217]. The majority of all approved liposomal nanoparticle formulations are not PEGylated except for Doxil and Onivyde, which have been shown to have advantages over non-PEGylated nanoparticle formulations even with their low amount of PEG [213,218]. Preclinical research performed in the 1970s, 1980s, and 1990s, using polymers as controlled release systems for drug delivery has led to a number of clinically approved products [161]. The clinical success of using polymers for controlled release, and the ability to manufacture polymeric formulations on the nanoscale have driven the research of polymeric depots away from the macro/micro scale to the nano scale [219]. A Number of PEGylated polymeric nanoparticle formulations such as SP1049C, NK911, and Genexol-PM are in early phase clinical trials for various types of cancers [220–224]. SP1049C is a pluronic polymeric micelle nanoparticle containg entrapped doxorubicin, that is currently evaluated for patients with esophagus and esophageal junction metastatic cancer in a phase II clinical trial [220]. The other two polymeric nanoparticles, K911 (doxorubicin-loaded PEG-poly(aspartic acid)) and Genexol-PM (paclitaxel-loaded PEG-PLA) are in phase II clinical trials for various cancers [221,223]. These first generation, polymeric nanoparticles have shown promising effect for various cancers with wider therapeutic windows and lower side effects. However, these nanoparticles are associated with number of limitations related to targeting, therefore targeted polymeric nanoparticles are now under preclinical and clinical investigation [161]. The first targeted polymeric nanoparticles to reach the clinic is BIND-014, which is composed of a prostate specific membrane antigen (PSMA) conjugated to a docetaxel-loaded PLGA nanoparticles [161,223]. There are only two other targeted polymeric nanoparticles currently in clinical trials, CALAA-01 (phase I), and SEL-068 (phase I) [225–227]. The synthesis of targeted nanoparticles is complex and is difficult to scale-up. The tuning of ligand density is very difficult because the target ligands attach to the surface of the pre-prepared nanoparticles through post-coupling processes. In order to achieve a high efficiency of the coupling of the ligands excessive amounts of reagents and purification techniques for removing unbound ligands are needed. These issues have lead to batch-to-batch variability and difficulty in reproducing the surface properties. Consequently, the clinical transition for targeted nanoparticles will be difficult unless they are prepared using pre-functionalized polymeric materials and minimum number of components [161,228]. However, this will require the development and registration of new polymeric excipients.

19. Conclusions

Malignant gliomas remain to be among the most aggressive forms of tumours that may not respond to most of the conventional treatments of chemotherapy and RT. This in fact is attributed to the selective nature of the BBB that prevents most particles from entry inside the brain including

therapeutics. Moreover, conventional management strategies for glioma only allow patients some extra time to survive while struggling with deleterious side effects that develop mostly from the invasiveness of the treatment approaches. Nanomedicine is a flexible and non-invasive therapeutic field that allows the design of materials with nanometer size dimensions to act as drug carriers and delivery agents crossing the BBB via targeting ligands and special coatings. Such designed nanoparticles will aim only towards receptors of interest that are overexpressed on tumour tissues, for instance, while sparing normal tissues. The promising pre-clinical data have paved the way for more nanoparticles to be introduced in the clinic. The FDA has approved various routes of administration of nanoparticles with a preference towards the intravenous route which offers advantages towards treatment of metastasized tumours. Polymeric nanoparticles are gaining more attention for the treatment of malignant gliomas owing to their biodegradable and biocompatible behaviour inside the human body and the unlimited designs and characteristics they can be manipulated into. Polymeric nanoparticles can be extra advantageous when PEGylated as discussed earlier in this review. However, further efforts are needed to optimize their size, drug loading capacity and release of hydrophilic and hydrophobic drugs, taking in consideration the different physicochemical properties of drugs and the physiological barriers that may hamper their success.

Funding: This research received no external funding.

Conflicts of Interest: The authors declare no conflict of interest.

References

1. Kaufmann, J.K.; Chiocca, E.A. Glioma virus therapies between bench and bedside. *Neuro-Oncology* **2014**, *16*, 334–351. [CrossRef]
2. Silva, C.O.; Pinho, J.O.; Lopes, J.M.; Almeida, A.J.; Gaspar, M.M.; Reis, C. Current trends in cancer nanotheranostics: Metallic, polymeric, and lipid-based systems. *Pharmaceutics* **2019**, *11*, 22. [CrossRef] [PubMed]
3. Lapointe, S.; Perry, A.; Butowski, N.A. Primary brain tumours in adults. *Lancet* **2018**, *392*, 432–446. [CrossRef]
4. Paw, I.; Carpenter, R.C.; Watabe, K.; Debinski, W.; Lo, H.-W. Mechanisms regulating glioma invasion. *Cancer Lett.* **2015**, *362*, 1–7. [CrossRef] [PubMed]
5. Cornago, M.; Garcia-Alberich, C.; Blasco-Angulo, N.; Vall-Llaura, N.; Nager, M.; Herreros, J.; Comella, J.; Sanchis, D.; Llovera, M. Histone deacetylase inhibitors promote glioma cell death by G2 checkpoint abrogation leading to mitotic catastrophe. *Cell Death Dis.* **2014**, *5*, e1435. [CrossRef] [PubMed]
6. De Boer, A.G.; Gaillard, P.J. Strategies to improve drug delivery across the blood-brain barrier. *Clin. Pharmacokinet.* **2007**, *46*, 553–576. [CrossRef]
7. Parrish, K.E.; Cen, L.; Murray, J.; Calligaris, D.; Kizilbash, S.; Mittapalli, R.K.; Carlson, B.L.; Schroeder, M.A.; Sludden, J.; Boddy, A.V. Efficacy of PARP inhibitor rucaparib in orthotopic glioblastoma xenografts is limited by ineffective drug penetration into the central nervous system. *Mol. Cancer Ther.* **2015**, *14*, 2735–2743. [CrossRef]
8. Van Tellingen, O.; Yetkin-Arik, B.; De Gooijer, M.; Wesseling, P.; Wurdinger, T.; De Vries, H. Overcoming the blood–brain tumor barrier for effective glioblastoma treatment. *Drug Resist. Updates* **2015**, *19*, 1–12. [CrossRef]
9. Binello, E.; Germano, I.M. Targeting glioma stem cells: A novel framework for brain tumors. *Cancer Sci.* **2011**, *102*, 1958–1966. [CrossRef]
10. Dolecek, T.A.; Propp, J.M.; Stroup, N.E.; Kruchko, C. CBTRUS statistical report: Primary brain and central nervous system tumors diagnosed in the United States in 2005–2009. *Neuro-Oncology* **2012**, *14*, v1–v49. [CrossRef]
11. MacKenzie, D. A classification of the tumours of the glioma group on a histogenetic basis with a correlated study of prognosis. *Can. Med. Assoc. J.* **1926**, *16*, 872.
12. Louis, D.N.; Perry, A.; Reifenberger, G.; Von Deimling, A.; Figarella-Branger, D.; Cavenee, W.K.; Ohgaki, H.; Wiestler, O.D.; Kleihues, P.; Ellison, D.W. The 2016 World Health Organization classification of tumors of the central nervous system: A summary. *Acta Neuropathol.* **2016**, *131*, 803–820. [CrossRef] [PubMed]

13. Sathornsumetee, S.; Rich, J.N.; Reardon, D.A. Diagnosis and treatment of high-grade astrocytoma. *Neurol. Clin.* **2007**, *25*, 1111–1139. [CrossRef] [PubMed]
14. Fischer, U.; Meese, E. Glioblastoma multiforme: The role of DSB repair between genotype and phenotype. *Oncogene* **2007**, *26*, 7809. [CrossRef]
15. Hess, K.R. Extent of resection as a prognostic variable in the treatment of gliomas. *J. Neuro-Oncol.* **1999**, *42*, 227–231. [CrossRef]
16. Simpson, J.; Horton, J.; Scott, C.; Curran, W.; Rubin, P.; Fischbach, J.; Isaacson, S.; Rotman, M.; Asbell, S.; Nelson, J. Influence of location and extent of surgical resection on survival of patients with glioblastoma multiforme: Results of three consecutive Radiation Therapy Oncology Group (RTOG) clinical trials. *Int. J. Radiat. Oncol. Biol. Phys.* **1993**, *26*, 239–244. [CrossRef]
17. Fadul, C.; Wood, J.; Thaler, H.; Galicich, J.; Patterson, R.; Posner, J. Morbidity and mortality of craniotomy for excision of supratentorial gliomas. *Neurology* **1988**, *38*, 1374. [CrossRef]
18. Hentschel, S.J.; Sawaya, R. Optimizing outcomes with maximal surgical resection of malignant gliomas. *Cancer Control* **2003**, *10*, 109–114. [CrossRef]
19. Iacob, G.; Dinca, E.B. Current data and strategy in glioblastoma multiforme. *J. Med. Life* **2009**, *2*, 386.
20. Van den Bent, M.; Afra, D.; De Witte, O.; Hassel, M.B.; Schraub, S.; Hoang-Xuan, K.; Malmström, P.; Collette, L.; Piérart, M.; Mirimanoff, R.; et al. Long-term efficacy of early versus delayed radiotherapy for low-grade astrocytoma and oligodendroglioma in adults: The EORTC 22845 randomised trial. *Lancet* **2005**, *366*, 985–990. [CrossRef]
21. Chandana, S.R.; Movva, S.; Arora, M.; Singh, T. Primary brain tumors in adults. *Am. Fam. Physician* **2008**, *77*, 1423–1430. [PubMed]
22. Walker, R.A. Significance of alpha-subunit HCG demonstrated in breast carcinomas by the immunoperoxidase technique. *J. Clin. Pathol.* **1978**, *31*, 245–249. [CrossRef] [PubMed]
23. Shapiro, W.R.; Green, S.B.; Burger, P.C.; Mahaley, M.S.; Selker, R.G.; VanGilder, J.C.; Robertson, J.T.; Ransohoff, J.; Mealey, J.; Strike, T.A. Randomized trial of three chemotherapy regimens and two radiotherapy regimens in postoperative treatment of malignant glioma: Brain Tumor Cooperative Group Trial 8001. *J. Neurosurg.* **1989**, *71*, 1–9. [CrossRef] [PubMed]
24. Heesters, M.; Wijrdeman, H.; Struikmans, H.; Witkamp, T.; Moerland, M. Brain tumor delineation based on CT and MR imaging. Implications for radiotherapy treatment planning. *Strahlentherapie und Onkologie* **1993**, *169*, 729–733. [PubMed]
25. Saran, R.; Robinson, B.; Abbott, K.C.; Agodoa, L.Y.; Bhave, N.; Bragg-Gresham, J.; Balkrishnan, R.; Dietrich, X.; Eckard, A.; Eggers, P.W. US renal data system 2017 annual data report: Epidemiology of kidney disease in the United States. *Am. J. Kidney Dis. Off. J. Natl. Kidney Found.* **2018**, *71*, A7. [CrossRef]
26. Scaringi, C.; Agolli, L.; Minniti, G. Technical Advances in Radiation Therapy for Brain Tumors. *Anticancer Res.* **2018**, *38*, 6041–6045. [CrossRef]
27. Stupp, R.; Mason, W.P.; Van Den Bent, M.J.; Weller, M.; Fisher, B.; Taphoorn, M.J.; Belanger, K.; Brandes, A.A.; Marosi, C.; Bogdahn, U. Radiotherapy plus concomitant and adjuvant temozolomide for glioblastoma. *N. Engl. J. Med.* **2005**, *352*, 987–996. [CrossRef]
28. Stupp, R.; Roila, F.; Group, E.G.W. Malignant glioma: ESMO clinical recommendations for diagnosis, treatment and follow-up. *Ann. Oncol.* **2009**, *20*, iv126–iv128. [CrossRef]
29. De Vleeschouwer, S.; Bergers, G. Glioblastoma: To target the tumor cell or the microenvironment. In *Glioblastoma [Internet]*; Codon Publications: Brisbane, Austrailia, 2017.
30. Stupp, R.; Hegi, M.E.; Van Den Bent, M.J.; Mason, W.P.; Weller, M.; Mirimanoff, R.O.; Cairncross, J.G.; European Organisation for Research and Treatment of Cancer; Brain Tumour and Radiotherapy Groups'; National Cancer Institute of Canada Clinical Trials Group. Changing paradigms—An update on the multidisciplinary management of malignant glioma. *Oncologist* **2006**, *11*, 165–180. [CrossRef]
31. Stupp, R.; Taillibert, S.; Kanner, A.A.; Kesari, S.; Steinberg, D.M.; Toms, S.A.; Taylor, L.P.; Lieberman, F.; Silvani, A.; Fink, K.L. Maintenance therapy with tumor-treating fields plus temozolomide vs temozolomide alone for glioblastoma: A randomized clinical trial. *JAMA* **2015**, *314*, 2535–2543. [CrossRef]
32. Stupp, R.; Wong, E.T.; Kanner, A.A.; Steinberg, D.; Engelhard, H.; Heidecke, V.; Kirson, E.D.; Taillibert, S.; Liebermann, F.; Dbalý, V. NovoTTF-100A versus physician's choice chemotherapy in recurrent glioblastoma: A randomised phase III trial of a novel treatment modality. *Eur. J. Cancer* **2012**, *48*, 2192–2202. [CrossRef] [PubMed]

33. Davis, M.E. Tumor treating fields-an emerging cancer treatment modality. *Clin. J. Oncol. Nurs.* **2013**, *17*. [CrossRef] [PubMed]
34. Barani, I.J.; Larson, D.A. Radiation therapy of glioblastoma. In *Current Understanding and Treatment of Gliomas*; Springer: New York, NY, USA, 2015; pp. 49–73.
35. Norden, A.D.; Wen, P.Y. Glioma therapy in adults. *Neurologist* **2006**, *12*, 279–292. [CrossRef] [PubMed]
36. Kostaras, X.; Cusano, F.; Kline, G.; Roa, W.; Easaw, J. Use of dexamethasone in patients with high-grade glioma: A clinical practice guideline. *Curr. Oncol.* **2014**, *21*, e493. [CrossRef] [PubMed]
37. Wen, P.Y.; Schiff, D.; Kesari, S.; Drappatz, J.; Gigas, D.C.; Doherty, L. Medical management of patients with brain tumors. *J. Neuro-Oncol.* **2006**, *80*, 313–332. [CrossRef]
38. Omuro, A.; DeAngelis, L.M. Glioblastoma and other malignant gliomas: A clinical review. *JAMA* **2013**, *310*, 1842–1850. [CrossRef]
39. Thakkar, J.P.; Dolecek, T.A.; Horbinski, C.; Ostrom, Q.T.; Lightner, D.D.; Barnholtz-Sloan, J.S.; Villano, J.L. Epidemiologic and molecular prognostic review of glioblastoma. *Cancer Epidemiol. Prev. Biomark.* **2014**, *23*, 1985–1996. [CrossRef]
40. Wick, W.; Hartmann, C.; Engel, C.; Stoffels, M.; Felsberg, J.; Stockhammer, F.; Sabel, M.C.; Koeppen, S.; Ketter, R.; Meyermann, R. NOA-04 randomized phase III trial of sequential radiochemotherapy of anaplastic glioma with procarbazine, lomustine, and vincristine or temozolomide. *J. Clin. Oncol.* **2009**, *27*, 5874. [CrossRef]
41. Cairncross, G.; Wang, M.; Shaw, E.; Jenkins, R.; Brachman, D.; Buckner, J.; Fink, K.; Souhami, L.; Laperriere, N.; Curran, W. Phase III trial of chemoradiotherapy for anaplastic oligodendroglioma: Long-term results of RTOG 9402. *J. Clin. Oncol.* **2013**, *31*, 337. [CrossRef]
42. Ellor, S.V.; Pagano-Young, T.A.; Avgeropoulos, N.G. *Glioblastoma: Background, Standard Treatment Paradigms, and Supportive Care Considerations*; SAGE Publications: Los Angeles, CA, USA, 2014.
43. Walid, M.S. Prognostic factors for long-term survival after glioblastoma. *Perm. J.* **2008**, *12*, 45. [CrossRef]
44. Ostrom, Q.T.; Gittleman, H.; Liao, P.; Rouse, C.; Chen, Y.; Dowling, J.; Wolinsky, Y.; Kruchko, C.; Barnholtz-Sloan, J. CBTRUS statistical report: Primary brain and central nervous system tumors diagnosed in the United States in 2007–2011. *Neuro-Oncology* **2014**, *16*, iv1–iv63. [CrossRef] [PubMed]
45. Ostrom, Q.T.; Gittleman, H.; Fulop, J.; Liu, M.; Blanda, R.; Kromer, C.; Wolinsky, Y.; Kruchko, C.; Barnholtz-Sloan, J.S. CBTRUS statistical report: Primary brain and central nervous system tumors diagnosed in the United States in 2008–2012. *Neuro-Oncology* **2015**, *17*, iv1–iv62. [CrossRef] [PubMed]
46. Lovely, M.P.; Stewart-Amidei, C.; Arzbaecher, J.; Bell, S.; Maher, M.E.; Maida, M.; Mogensen, K.; Nicolaseau, G. Care of the adult patient with a brain tumor. *J. Neurosci. Nurs.* **2014**, *46*, 367–369.
47. Tomasetti, C.; Li, L.; Vogelstein, B. Stem cell divisions, somatic mutations, cancer etiology, and cancer prevention. *Science* **2017**, *355*, 1330–1334. [CrossRef] [PubMed]
48. Wilson, T.A.; Karajannis, M.A.; Harter, D.H. Glioblastoma multiforme: State of the art and future therapeutics. *Surg. Neurol. Int.* **2014**, *5*, 64. [PubMed]
49. Verhaak, R.G.; Hoadley, K.A.; Purdom, E.; Wang, V.; Qi, Y.; Wilkerson, M.D.; Miller, C.R.; Ding, L.; Golub, T.; Mesirov, J.P. Integrated genomic analysis identifies clinically relevant subtypes of glioblastoma characterized by abnormalities in PDGFRA, IDH1, EGFR, and NF1. *Cancer Cell* **2010**, *17*, 98–110. [CrossRef]
50. Phillips, H.S.; Kharbanda, S.; Chen, R.; Forrest, W.F.; Soriano, R.H.; Wu, T.D.; Misra, A.; Nigro, J.M.; Colman, H.; Soroceanu, L. Molecular subclasses of high-grade glioma predict prognosis, delineate a pattern of disease progression, and resemble stages in neurogenesis. *Cancer Cell* **2006**, *9*, 157–173. [CrossRef]
51. Hart, M.G.; Garside, R.; Rogers, G.; Stein, K.; Grant, R. Temozolomide for high grade glioma. *Cochrane Database Syst. Rev.* **2013**. [CrossRef]
52. Ashby, L.S.; Smith, K.A.; Stea, B. Gliadel wafer implantation combined with standard radiotherapy and concurrent followed by adjuvant temozolomide for treatment of newly diagnosed high-grade glioma: A systematic literature review. *World J. Surg. Oncol.* **2016**, *14*, 225. [CrossRef]
53. Brem, H.; Ewend, M.G.; Piantadosi, S.; Greenhoot, J.; Burger, P.C.; Sisti, M. The safety of interstitial chemotherapy with BCNU-loaded polymer followed by radiation therapy in the treatment of newly diagnosed malignant gliomas: Phase I trial. *J. Neuro-Oncol.* **1995**, *26*, 111–123. [CrossRef]
54. Fung, L.K.; Ewend, M.G.; Sills, A.; Sipos, E.P.; Thompson, R.; Watts, M.; Colvin, O.M.; Brem, H.; Saltzman, W.M. Pharmacokinetics of interstitial delivery of carmustine, 4-hydroperoxycyclophosphamide, and paclitaxel from a biodegradable polymer implant in the monkey brain. *Cancer Res.* **1998**, *58*, 672–684. [PubMed]

55. Friedman, H.S.; Kerby, T.; Calvert, H. Temozolomide and treatment of malignant glioma. *Clin. Cancer Res.* **2000**, *6*, 2585–2597.
56. Chang, J.E.; Khuntia, D.; Robins, H.I.; Mehta, M.P. Radiotherapy and radiosensitizers in the treatment of glioblastoma multiforme. *Clin. Adv. Hematol Oncol.* **2007**, *5*, 894–902. [PubMed]
57. Scott, J.; Tsai, Y.-Y.; Chinnaiyan, P.; Yu, H.-H.M. Effectiveness of radiotherapy for elderly patients with glioblastoma. *Int. J. Radiat. Oncol. Biol. Phys.* **2011**, *81*, 206–210. [CrossRef] [PubMed]
58. Petty, M.A.; Lo, E.H. Junctional complexes of the blood–brain barrier: Permeability changes in neuroinflammation. *Prog. Neurobiol.* **2002**, *68*, 311–323. [CrossRef]
59. De Boer, A.; Breimer, D. Cytokines and blood-brain barrier permeability. In *Progress in Brain Research*; Elsevier: Amsterdam, The Netherlands, 1998; Volume 115, pp. 425–451.
60. Wahl, M.; Unterberg, A.; Baethmann, A.; Schilling, L. Mediators of blood-brain barrier dysfunction and formation of vasogenic brain edema. *J. Cereb. Blood Flow Metab.* **1988**, *8*, 621–634. [CrossRef]
61. Kastin, A.J.; Pan, W.; Maness, L.M.; Banks, W.A. Peptides crossing the blood–brain barrier: Some unusual observations. *Brain Res.* **1999**, *848*, 96–100. [CrossRef]
62. M Rabanel, J.; Aoun, V.; Elkin, I.; Mokhtar, M.; Hildgen, P. Drug-loaded nanocarriers: Passive targeting and crossing of biological barriers. *Curr. Med. Chem.* **2012**, *19*, 3070–3102. [CrossRef]
63. Habgood, M.; Begley, D.; Abbott, N. Determinants of passive drug entry into the central nervous system. *Cell. Mol. Neurobiol.* **2000**, *20*, 231–253. [CrossRef]
64. Hawkins, B.T.; Davis, T.P. The blood-brain barrier/neurovascular unit in health and disease. *Pharmacol. Rev.* **2005**, *57*, 173–185. [CrossRef]
65. Jain, K.K. Nanobiotechnology-based strategies for crossing the blood–brain barrier. *Nanomedicine* **2012**, *7*, 1225–1233. [CrossRef] [PubMed]
66. Shityakov, S.; Förster, C. In silico predictive model to determine vector-mediated transport properties for the blood–brain barrier choline transporter. *Adv. Appl. Bioinform. Chem. AABC* **2014**, *7*, 23. [CrossRef] [PubMed]
67. Yu, A.S.; Hirayama, B.A.; Timbol, G.; Liu, J.; Diez-Sampedro, A.; Kepe, V.; Satyamurthy, N.; Huang, S.-C.; Wright, E.M.; Barrio, J.R. Regional distribution of SGLT activity in rat brain in vivo. *Am. J. Physiol.-Cell Physiol.* **2012**, *304*, C240–C247. [CrossRef] [PubMed]
68. Miller, D.S. Regulation of ABC transporters blood–brain barrier: The good, the bad, and the ugly. In *Advances in Cancer Research*; Elsevier: Amsterdam, The Netherlands, 2015; Volume 125, pp. 43–70.
69. On, N.H.; Miller, D.W. Transporter-based delivery of anticancer drugs to the brain: Improving brain penetration by minimizing drug efflux at the blood-brain barrier. *Curr. Pharm. Des.* **2014**, *20*, 1499–1509. [CrossRef] [PubMed]
70. Kreuter, J. Nanoparticulate systems for brain delivery of drugs. *Adv. Drug Deliv. Rev.* **2001**, *47*, 65–81. [CrossRef]
71. Bray, D.; Levin, M.D.; Morton-Firth, C.J. Receptor clustering as a cellular mechanism to control sensitivity. *Nature* **1998**, *393*, 85. [CrossRef]
72. Ehrlich, M.; Boll, W.; Van Oijen, A.; Hariharan, R.; Chandran, K.; Nibert, M.L.; Kirchhausen, T. Endocytosis by random initiation and stabilization of clathrin-coated pits. *Cell* **2004**, *118*, 591–605. [CrossRef]
73. Giddings, S.; Chirgwin, J.; Permutt, M. Evaluation of rat insulin messenger RNA in pancreatic and extrapancreatic tissues. *Diabetologia* **1985**, *28*, 343–347. [CrossRef]
74. Skarlatos, S.; Yoshikawa, T.; Pardridge, W.M. Transport of [125I] transferrin through the rat blood-brain barrier. *Brain Res.* **1995**, *683*, 164–171. [CrossRef]
75. Zhang, Y.; Pardridge, W.M. Rapid transferrin efflux from brain to blood across the blood–brain barrier. *J. Neurochem.* **2001**, *76*, 1597–1600. [CrossRef]
76. Schlachetzki, F.; Zhu, C.; Pardridge, W.M. Expression of the neonatal Fc receptor (FcRn) at the blood–brain barrier. *J. Neurochem.* **2002**, *81*, 203–206. [CrossRef] [PubMed]
77. Golden, P.L.; Maccagnan, T.J.; Pardridge, W.M. Human blood-brain barrier leptin receptor. Binding and endocytosis in isolated human brain microvessels. *J. Clin. Investig.* **1997**, *99*, 14–18. [CrossRef] [PubMed]
78. Mellman, I. Endocytosis and molecular sorting. *Annu. Rev. Cell Dev. Biol.* **1996**, *12*, 575–625. [CrossRef] [PubMed]
79. Wang, Z.H.; Wang, Z.Y.; Sun, C.S.; Wang, C.Y.; Jiang, T.Y.; Wang, S.L. Trimethylated chitosan-conjugated PLGA nanoparticles for the delivery of drugs to the brain. *Biomaterials* **2010**, *31*, 908–915. [CrossRef]

80. Hervé, F.; Ghinea, N.; Scherrmann, J.-M. CNS delivery via adsorptive transcytosis. *AAPS J.* **2008**, *10*, 455–472. [CrossRef]
81. Batrakova, E.V.; Gendelman, H.E.; Kabanov, A.V. Cell-mediated drug delivery. *Expert Opin. Drug Deliv.* **2011**, *8*, 415–433. [CrossRef]
82. Masserini, M. Nanoparticles for brain drug delivery. *ISRN Biochem.* **2013**, *238428*. [CrossRef]
83. Jain, S.; Mishra, V.; Singh, P.; Dubey, P.; Saraf, D.; Vyas, S. RGD-anchored magnetic liposomes for monocytes/neutrophils-mediated brain targeting. *Int. J. Pharm.* **2003**, *261*, 43–55. [CrossRef]
84. Qin, J.; Chen, D.; Hu, H.; Cui, Q.; Qiao, M.; Chen, B. Surface modification of RGD-liposomes for selective drug delivery to monocytes/neutrophils in brain. *Chem. Pharm. Bull.* **2007**, *55*, 1192–1197. [CrossRef]
85. Rodrigueza, W.V.; Pritchard, P.H.; Hope, M.J. The influence of size and composition on the cholesterol mobilizing properties of liposomes in vivo. *Biochim. Biophys. Acta (BBA)-Biomembr.* **1993**, *1153*, 9–19. [CrossRef]
86. Bennewitz, M.F.; Saltzman, W.M. Nanotechnology for delivery of drugs to the brain for epilepsy. *Neurotherapeutics* **2009**, *6*, 323–336. [CrossRef] [PubMed]
87. Yi, X.; Manickam, D.S.; Brynskikh, A.; Kabanov, A.V. Agile delivery of protein therapeutics to CNS. *J. Control. Release* **2014**, *190*, 637–663. [CrossRef]
88. Blasberg, R.; Patlak, C.; Fenstermacher, J. Intrathecal chemotherapy: Brain tissue profiles after ventriculocisternal perfusion. *J. Pharm. Exp. Ther.* **1975**, *195*, 73–83.
89. Chen, G.; Zhang, X.; Yang, F.; Mu, L. Disposition of nanoparticle-based delivery system via inner ear administration. *Curr. Drug Metab.* **2010**, *11*, 886–897. [CrossRef] [PubMed]
90. Zhang, X.; Chen, G.; Wen, L.; Yang, F.; Shao, A.-l.; Li, X.; Long, W.; Mu, L. Novel multiple agents loaded PLGA nanoparticles for brain delivery via inner ear administration: In vitro and in vivo evaluation. *Eur. J. Pharm. Sci.* **2013**, *48*, 595–603. [CrossRef] [PubMed]
91. Lochhead, J.J.; Thorne, R.G. Intranasal delivery of biologics to the central nervous system. *Adv. Drug Deliv. Rev.* **2012**, *64*, 614–628. [CrossRef]
92. Zhang, T.-T.; Li, W.; Meng, G.; Wang, P.; Liao, W. Strategies for transporting nanoparticles across the blood–brain barrier. *Biomater. Sci.* **2016**, *4*, 219–229. [CrossRef]
93. Bellavance, M.-A.; Blanchette, M.; Fortin, D. Recent advances in blood–brain barrier disruption as a CNS delivery strategy. *AAPS J.* **2008**, *10*, 166–177. [CrossRef]
94. Wilson, B. Brain targeting PBCA nanoparticles and the blood–brain barrier. *Nanomedicine* **2009**, *4*, 499–502. [CrossRef]
95. Busquets, M.A.; Espargaró, A.; Sabaté, R.; Estelrich, J. Magnetic nanoparticles cross the blood-brain barrier: When physics rises to a challenge. *Nanomaterials* **2015**, *5*, 2231–2248. [CrossRef]
96. Holmes, D. The next big things are tiny. *Lancet Neurol.* **2013**, *12*, 31–32. [CrossRef]
97. Re, F.; Gregori, M.; Masserini, M. Nanotechnology for neurodegenerative disorders. *Maturitas* **2012**, *73*, 45–51. [CrossRef] [PubMed]
98. Haque, S.; Md, S.; Alam, M.I.; Sahni, J.K.; Ali, J.; Baboota, S. Nanostructure-based drug delivery systems for brain targeting. *Drug Dev. Ind. Pharm.* **2012**, *38*, 387–411. [CrossRef] [PubMed]
99. Wicki, A.; Witzigmann, D.; Balasubramanian, V.; Huwyler, J. Nanomedicine in cancer therapy: Challenges, opportunities, and clinical applications. *J. Control. Release* **2015**, *200*, 138–157. [CrossRef] [PubMed]
100. Malikmammadov, E.; Tanir, T.E.; Kiziltay, A.; Hasirci, V.; Hasirci, N. PCL and PCL-based materials in biomedical applications. *J. Biomater. Sci. Polym. Ed.* **2018**, *29*, 863–893. [CrossRef]
101. Bregoli, L.; Movia, D.; Gavigan-Imedio, J.D.; Lysaght, J.; Reynolds, J.; Prina-Mello, A. Nanomedicine applied to translational oncology: A future perspective on cancer treatment. *Nanomed. Nanotechnol. Biol. Med.* **2016**, *12*, 81–103. [CrossRef]
102. Truong, N.P.; Whittaker, M.R.; Mak, C.W.; Davis, T.P. The importance of nanoparticle shape in cancer drug delivery. *Expert Opin. Drug Deliv.* **2015**, *12*, 129–142. [CrossRef]
103. Stylianopoulos, T.; Poh, M.-Z.; Insin, N.; Bawendi, M.G.; Fukumura, D.; Munn, L.L.; Jain, R.K. Diffusion of particles in the extracellular matrix: The effect of repulsive electrostatic interactions. *Biophys. J.* **2010**, *99*, 1342–1349. [CrossRef]
104. Adabi, M.; Naghibzadeh, M.; Adabi, M.; Zarrinfard, M.A.; Esnaashari, S.S.; Seifalian, A.M.; Faridi-Majidi, R.; Tanimowo Aiyelabegan, H.; Ghanbari, H. Biocompatibility and nanostructured materials: Applications in nanomedicine. *Artif. Cells Nanomed. Biotechnol.* **2017**, *45*, 833–842. [CrossRef]

105. Wong, H.L.; Wu, X.Y.; Bendayan, R. Nanotechnological advances for the delivery of CNS therapeutics. *Adv. Drug Deliv. Rev.* **2012**, *64*, 686–700. [CrossRef]
106. Saraiva, C.; Praça, C.; Ferreira, R.; Santos, T.; Ferreira, L.; Bernardino, L. Nanoparticle-mediated brain drug delivery: Overcoming blood–brain barrier to treat neurodegenerative diseases. *J. Control. Release* **2016**, *235*, 34–47. [CrossRef] [PubMed]
107. Chapman, C.D.; Frey, W.H.; Craft, S.; Danielyan, L.; Hallschmid, M.; Schiöth, H.B.; Benedict, C. Intranasal treatment of central nervous system dysfunction in humans. *Pharm. Res.* **2013**, *30*, 2475–2484. [CrossRef] [PubMed]
108. Koo, Y.-E.L.; Reddy, G.R.; Bhojani, M.; Schneider, R.; Philbert, M.A.; Rehemtulla, A.; Ross, B.D.; Kopelman, R. Brain cancer diagnosis and therapy with nanoplatforms. *Adv. Drug Deliv. Rev.* **2006**, *58*, 1556–1577. [CrossRef] [PubMed]
109. Koffie, R.M.; Farrar, C.T.; Saidi, L.-J.; William, C.M.; Hyman, B.T.; Spires-Jones, T.L. Nanoparticles enhance brain delivery of blood–brain barrier-impermeable probes for in vivo optical and magnetic resonance imaging. *Proc. Natl. Acad. Sci. USA* **2011**, *108*, 18837–18842. [CrossRef]
110. Winer, J.L.; Kim, P.E.; Law, M.; Liu, C.Y.; Apuzzo, M.L. Visualizing the future: Enhancing neuroimaging with nanotechnology. *World Neurosurg.* **2011**, *75*, 626–637. [CrossRef]
111. Kelkar, S.S.; Reineke, T.M. Theranostics: Combining imaging and therapy. *Bioconjug. Chem.* **2011**, *22*, 1879–1903. [CrossRef]
112. Salvati, A.; Pitek, A.S.; Monopoli, M.P.; Prapainop, K.; Bombelli, F.B.; Hristov, D.R.; Kelly, P.M.; Åberg, C.; Mahon, E.; Dawson, K.A. Transferrin-functionalized nanoparticles lose their targeting capabilities when a biomolecule corona adsorbs on the surface. *Nat. Nanotechnol.* **2013**, *8*, 137. [CrossRef]
113. Hadjidemetriou, M.; Al-Ahmady, Z.; Mazza, M.; Collins, R.F.; Dawson, K.; Kostarelos, K. In vivo biomolecule corona around blood-circulating, clinically used and antibody-targeted lipid bilayer nanoscale vesicles. *ACS Nano* **2015**, *9*, 8142–8156. [CrossRef]
114. Downs, M.E.; Buch, A.; Karakatsani, M.E.; Konofagou, E.E.; Ferrera, V.P. Blood-brain barrier opening in behaving non-human primates via focused ultrasound with systemically administered microbubbles. *Sci. Rep.* **2015**, *5*, 15076. [CrossRef]
115. Meyers, J.D.; Doane, T.; Burda, C.; Basilion, J.P. Nanoparticles for imaging and treating brain cancer. *Nanomedicine* **2013**, *8*, 123–143. [CrossRef]
116. Tian, G.; Yin, W.; Jin, J.; Zhang, X.; Xing, G.; Li, S.; Gu, Z.; Zhao, Y. Engineered design of theranostic upconversion nanoparticles for tri-modal upconversion luminescence/magnetic resonance/X-ray computed tomography imaging and targeted delivery of combined anticancer drugs. *J. Mater. Chem. B* **2014**, *2*, 1379–1389. [CrossRef]
117. Lollo, G.; Vincent, M.; Ullio-Gamboa, G.; Lemaire, L.; Franconi, F.; Couez, D.; Benoit, J.-P. Development of multifunctional lipid nanocapsules for the co-delivery of paclitaxel and CpG-ODN in the treatment of glioblastoma. *Int. J. Pharm.* **2015**, *495*, 972–980. [CrossRef] [PubMed]
118. Allard, E.; Jarnet, D.; Vessières, A.; Vinchon-Petit, S.; Jaouen, G.; Benoit, J.-P.; Passirani, C. Local delivery of ferrociphenol lipid nanocapsules followed by external radiotherapy as a synergistic treatment against intracranial 9L glioma xenograft. *Pharm. Res.* **2010**, *27*, 56. [CrossRef] [PubMed]
119. Fourniols, T.; Randolph, L.D.; Staub, A.; Vanvarenberg, K.; Leprince, J.G.; Préat, V.; des Rieux, A.; Danhier, F. Temozolomide-loaded photopolymerizable PEG-DMA-based hydrogel for the treatment of glioblastoma. *J. Control. Release* **2015**, *210*, 95–104. [CrossRef]
120. Huynh, N.T.; Passirani, C.; Allard-Vannier, E.; Lemaire, L.; Roux, J.; Garcion, E.; Vessieres, A.; Benoit, J.-P. Administration-dependent efficacy of ferrociphenol lipid nanocapsules for the treatment of intracranial 9L rat gliosarcoma. *Int. J. Pharm.* **2012**, *423*, 55–62. [CrossRef]
121. Laine, A.-L.; Huynh, N.T.; Clavreul, A.; Balzeau, J.; Béjaud, J.; Vessieres, A.; Benoit, J.-P.; Eyer, J.; Passirani, C. Brain tumour targeting strategies via coated ferrociphenol lipid nanocapsules. *Eur. J. Pharm. Biopharm.* **2012**, *81*, 690–693. [CrossRef]
122. Huynh, N.T.; Morille, M.; Bejaud, J.; Legras, P.; Vessieres, A.; Jaouen, G.; Benoit, J.-P.; Passirani, C. Treatment of 9L gliosarcoma in rats by ferrociphenol-loaded lipid nanocapsules based on a passive targeting strategy via the EPR effect. *Pharm. Res.* **2011**, *28*, 3189–3198. [CrossRef]
123. Kumar, A.; Ahuja, A.; Ali, J.; Baboota, S. Curcumin-loaded lipid nanocarrier for improving bioavailability, stability and cytotoxicity against malignant glioma cells. *Drug Deliv.* **2016**, *23*, 214–229. [CrossRef]

124. Verreault, M.; Wehbe, M.; Strutt, D.; Masin, D.; Anantha, M.; Walker, D.; Chu, F.; Backstrom, I.; Kalra, J.; Waterhouse, D. Determination of an optimal dosing schedule for combining Irinophore C™ and temozolomide in an orthotopic model of glioblastoma. *J. Control. Release* **2015**, *220*, 348–357. [CrossRef]
125. G Gritsenko, P.; Ilina, O.; Friedl, P. Interstitial guidance of cancer invasion. *J. Pathol.* **2012**, *226*, 185–199. [CrossRef]
126. Pluen, A.; Boucher, Y.; Ramanujan, S.; McKee, T.D.; Gohongi, T.; di Tomaso, E.; Brown, E.B.; Izumi, Y.; Campbell, R.B.; Berk, D.A. Role of tumor–host interactions in interstitial diffusion of macromolecules: Cranial vs. subcutaneous tumors. *Proc. Natl. Acad. Sci. USA* **2001**, *98*, 4628–4633. [CrossRef] [PubMed]
127. Gelperina, S.; Maksimenko, O.; Khalansky, A.; Vanchugova, L.; Shipulo, E.; Abbasova, K.; Berdiev, R.; Wohlfart, S.; Chepurnova, N.; Kreuter, J. Drug delivery to the brain using surfactant-coated poly (lactide-co-glycolide) nanoparticles: Influence of the formulation parameters. *Eur. J. Pharm. Biopharm.* **2010**, *74*, 157–163. [CrossRef]
128. Garcia-Garcia, E.; Andrieux, K.; Gil, S.; Couvreur, P. Colloidal carriers and blood–brain barrier (BBB) translocation: A way to deliver drugs to the brain? *Int. J. Pharm.* **2005**, *298*, 274–292. [CrossRef] [PubMed]
129. Esmaeili, F.; Ghahremani, M.H.; Esmaeili, B.; Khoshayand, M.R.; Atyabi, F.; Dinarvand, R. PLGA nanoparticles of different surface properties: Preparation and evaluation of their body distribution. *Int. J. Pharm.* **2008**, *349*, 249–255. [CrossRef] [PubMed]
130. Hermanson, G.T. *Bioconjugate Techniques*; Academic press: Cambridge, MA, USA, 2013.
131. Nobs, L.; Buchegger, F.; Gurny, R.; Allémann, E. Current methods for attaching targeting ligands to liposomes and nanoparticles. *J. Pharm. Sci.* **2004**, *93*, 1980–1992. [CrossRef] [PubMed]
132. Koo, B.-K.; Lim, H.-S.; Song, R.; Yoon, M.-J.; Yoon, K.-J.; Moon, J.-S.; Kim, Y.-W.; Kwon, M.-c.; Yoo, K.-W.; Kong, M.-P. Mind bomb 1 is essential for generating functional Notch ligands to activate Notch. *Development* **2005**, *132*, 3459–3470. [CrossRef]
133. Webster, R.; Didier, E.; Harris, P.; Siegel, N.; Stadler, J.; Tilbury, L.; Smith, D. PEGylated proteins: Evaluation of their safety in the absence of definitive metabolism studies. *Drug Metab. Dispos.* **2007**, *35*, 9–16. [CrossRef]
134. Jevševar, S.; Kunstelj, M.; Porekar, V.G. PEGylation of therapeutic proteins. *Biotechnol. J. Healthc. Nutr. Technol.* **2010**, *5*, 113–128.
135. Koziara, J.M.; Lockman, P.R.; Allen, D.D.; Mumper, R.J. Paclitaxel nanoparticles for the potential treatment of brain tumors. *J. Control. Release* **2004**, *99*, 259–269. [CrossRef]
136. Petri, B.; Bootz, A.; Khalansky, A.; Hekmatara, T.; Müller, R.; Uhl, R.; Kreuter, J.; Gelperina, S. Chemotherapy of brain tumour using doxorubicin bound to surfactant-coated poly (butyl cyanoacrylate) nanoparticles: Revisiting the role of surfactants. *J. Control. Release* **2007**, *117*, 51–58. [CrossRef]
137. Steiniger, S.C.; Kreuter, J.; Khalansky, A.S.; Skidan, I.N.; Bobruskin, A.I.; Smirnova, Z.S.; Severin, S.E.; Uhl, R.; Kock, M.; Geiger, K.D. Chemotherapy of glioblastoma in rats using doxorubicin-loaded nanoparticles. *Int. J. Cancer* **2004**, *109*, 759–767. [CrossRef] [PubMed]
138. Hekmatara, T.; Bernreuther, C.; Khalansky, A.; Theisen, A.; Weissenberger, J.; Matschke, J.; Gelperina, S.; Kreuter, J.; Glatzel, M. Efficient systemic therapy of rat glioblastoma by nanoparticle-bound doxorubicin is due to antiangiogenic effects. *Clin. Neuropathol.* **2009**, *28*, 153–164. [CrossRef] [PubMed]
139. Kuo, Y.-C.; Chen, Y.-C. Targeting delivery of etoposide to inhibit the growth of human glioblastoma multiforme using lactoferrin-and folic acid-grafted poly (lactide-co-glycolide) nanoparticles. *International J. Pharm.* **2015**, *479*, 138–149. [CrossRef] [PubMed]
140. Labhasetwar, V.; Song, C.; Humphrey, W.; Shebuski, R.; Levy, R.J. Arterial uptake of biodegradable nanoparticles: Effect of surface modifications. *J. Pharm. Sci.* **1998**, *87*, 1229–1234. [CrossRef]
141. Zhang, D.; Mehler, M.F.; Song, Q.; Kessler, J.A. Development of bone morphogenetic protein receptors in the nervous system and possible roles in regulating trkC expression. *J. Neurosci.* **1998**, *18*, 3314–3326. [CrossRef]
142. Huang, R.; Ke, W.; Han, L.; Liu, Y.; Shao, K.; Ye, L.; Lou, J.; Jiang, C.; Pei, Y. Brain-targeting mechanisms of lactoferrin-modified DNA-loaded nanoparticles. *J. Cereb. Blood Flow Metab.* **2009**, *29*, 1914–1923. [CrossRef]
143. Zhang, B.; Sun, X.; Mei, H.; Wang, Y.; Liao, Z.; Chen, J.; Zhang, Q.; Hu, Y.; Pang, Z.; Jiang, X. LDLR-mediated peptide-22-conjugated nanoparticles for dual-targeting therapy of brain glioma. *Biomaterials* **2013**, *34*, 9171–9182. [CrossRef]
144. Gao, H.; Zhang, S.; Cao, S.; Yang, Z.; Pang, Z.; Jiang, X. Angiopep-2 and activatable cell-penetrating peptide dual-functionalized nanoparticles for systemic glioma-targeting delivery. *Mol. Pharm.* **2014**, *11*, 2755–2763. [CrossRef]

145. Zhang, B.; Wang, H.; Liao, Z.; Wang, Y.; Hu, Y.; Yang, J.; Shen, S.; Chen, J.; Mei, H.; Shi, W. EGFP–EGF1-conjugated nanoparticles for targeting both neovascular and glioma cells in therapy of brain glioma. *Biomaterials* **2014**, *35*, 4133–4145. [CrossRef]
146. Callewaert, M.; Dukic, S.; Van Gulick, L.; Vittier, M.; Gafa, V.; Andry, M.C.; Molinari, M.; Roullin, V.G. Etoposide encapsulation in surface-modified poly (lactide-co-glycolide) nanoparticles strongly enhances glioma antitumor efficiency. *J. Biomed. Mater. Res. Part A* **2013**, *101*, 1319–1327. [CrossRef]
147. Dhami, N.K.; Pandey, R.S.; Jain, U.K.; Chandra, R.; Madan, J. Non-aggregated protamine-coated poly (lactide-co-glycolide) nanoparticles of cisplatin crossed blood–brain barrier, enhanced drug delivery and improved therapeutic index in glioblastoma cells: In vitro studies. *J. Microencapsul.* **2014**, *31*, 685–693. [CrossRef]
148. Peer, D.; Karp, J.M.; Hong, S.; Farokhzad, O.C.; Margalit, R.; Langer, R. Nanocarriers as an emerging platform for cancer therapy. *Nat. Nanotechnol.* **2007**, *2*, 751. [CrossRef]
149. Liu, Z.; Robinson, J.T.; Tabakman, S.M.; Yang, K.; Dai, H. Carbon materials for drug delivery & cancer therapy. *Mater. Today* **2011**, *14*, 316–323.
150. West, K.R.; Otto, S. Reversible covalent chemistry in drug delivery. *Curr. Drug Discov. Technol.* **2005**, *2*, 123–160. [CrossRef] [PubMed]
151. Reis, C.P.; Neufeld, R.J.; Ribeiro, A.J.; Veiga, F. Nanoencapsulation I. Methods for preparation of drug-loaded polymeric nanoparticles. *Nanomed. Nanotechnol. Biol. Med.* **2006**, *2*, 8–21. [CrossRef] [PubMed]
152. Béduneau, A.; Saulnier, P.; Benoit, J.-P. Active targeting of brain tumors using nanocarriers. *Biomaterials* **2007**, *28*, 4947–4967. [CrossRef]
153. Crotts, G.; Park, T.G. Protein delivery from poly (lactic-co-glycolic acid) biodegradable microspheres: Release kinetics and stability issues. *J. Microencapsul.* **1998**, *15*, 699–713. [CrossRef] [PubMed]
154. Shi, J.; Xiao, Z.; Kamaly, N.; Farokhzad, O.C. Self-assembled targeted nanoparticles: Evolution of technologies and bench to bedside translation. *Acc. Chem. Res.* **2011**, *44*, 1123–1134. [CrossRef]
155. Davis, M.E. The first targeted delivery of siRNA in humans via a self-assembling, cyclodextrin polymer-based nanoparticle: From concept to clinic. *Mol. Pharm.* **2009**, *6*, 659–668. [CrossRef]
156. Drummond, D.C.; Meyer, O.; Hong, K.; Kirpotin, D.B.; Papahadjopoulos, D. Optimizing liposomes for delivery of chemotherapeutic agents to solid tumors. *Pharm. Rev.* **1999**, *51*, 691–744.
157. Masood, F. Polymeric nanoparticles for targeted drug delivery system for cancer therapy. *Mater. Sci. Eng. C* **2016**, *60*, 569–578. [CrossRef] [PubMed]
158. Kreuter, J.; Alyautdin, R.N.; Kharkevich, D.A.; Ivanov, A.A. Passage of peptides through the blood-brain barrier with colloidal polymer particles (nanoparticles). *Brain Res.* **1995**, *674*, 171–174. [CrossRef]
159. Calvo, P.; Gouritin, B.; Chacun, H.; Desmaële, D.; D'Angelo, J.; Noel, J.-P.; Georgin, D.; Fattal, E.; Andreux, J.P.; Couvreur, P. Long-circulating PEGylated polycyanoacrylate nanoparticles as new drug carrier for brain delivery. *Pharm. Res.* **2001**, *18*, 1157–1166. [CrossRef] [PubMed]
160. Gao, X.; Tao, W.; Lu, W.; Zhang, Q.; Zhang, Y.; Jiang, X.; Fu, S. Lectin-conjugated PEG–PLA nanoparticles: Preparation and brain delivery after intranasal administration. *Biomaterials* **2006**, *27*, 3482–3490. [CrossRef] [PubMed]
161. Kamaly, N.; Xiao, Z.; Valencia, P.M.; Radovic-Moreno, A.F.; Farokhzad, O.C. Targeted polymeric therapeutic nanoparticles: Design, development and clinical translation. *Chem. Soc. Rev.* **2012**, *41*, 2971–3010. [CrossRef]
162. Sugano, M.; Egilmez, N.K.; Yokota, S.J.; Chen, F.-A.; Harding, J.; Huang, S.K.; Bankert, R.B. Antibody targeting of doxorubicin-loaded liposomes suppresses the growth and metastatic spread of established human lung tumor xenografts in severe combined immunodeficient mice. *Cancer Res.* **2000**, *60*, 6942–6949.
163. Alexis, F.; Pridgen, E.; Molnar, L.K.; Farokhzad, O.C. Factors affecting the clearance and biodistribution of polymeric nanoparticles. *Mol. Pharm.* **2008**, *5*, 505–515. [CrossRef]
164. Kirpotin, D.B.; Drummond, D.C.; Shao, Y.; Shalaby, M.R.; Hong, K.; Nielsen, U.B.; Marks, J.D.; Benz, C.C.; Park, J.W. Antibody targeting of long-circulating lipidic nanoparticles does not increase tumor localization but does increase internalization in animal models. *Cancer Res.* **2006**, *66*, 6732–6740. [CrossRef]
165. Bartlett, D.W.; Su, H.; Hildebrandt, I.J.; Weber, W.A.; Davis, M.E. Impact of tumor-specific targeting on the biodistribution and efficacy of siRNA nanoparticles measured by multimodality in vivo imaging. *Proc. Natl. Acad. Sci. USA* **2007**, *104*, 15549–15554. [CrossRef]

166. Jain, A.; Jain, A.; Garg, N.K.; Tyagi, R.K.; Singh, B.; Katare, O.P.; Webster, T.J.; Soni, V. Surface engineered polymeric nanocarriers mediate the delivery of transferrin–methotrexate conjugates for an improved understanding of brain cancer. *Acta Biomater.* **2015**, *24*, 140–151. [CrossRef]
167. Chang, J.; Jallouli, Y.; Kroubi, M.; Yuan, X.-B.; Feng, W.; Kang, C.-S.; Pu, P.-Y.; Betbeder, D. Characterization of endocytosis of transferrin-coated PLGA nanoparticles by the blood–brain barrier. *Int. J. Pharm.* **2009**, *379*, 285–292. [CrossRef]
168. Ding, H.; Inoue, S.; Ljubimov, A.V.; Patil, R.; Portilla-Arias, J.; Hu, J.; Konda, B.; Wawrowsky, K.A.; Fujita, M.; Karabalin, N. Inhibition of brain tumor growth by intravenous poly (β-L-malic acid) nanobioconjugate with pH-dependent drug release. *Proc. Natl. Acad. Sci. USA* **2010**, *107*, 18143–18148. [CrossRef] [PubMed]
169. Xin, H.; Jiang, X.; Gu, J.; Sha, X.; Chen, L.; Law, K.; Chen, Y.; Wang, X.; Jiang, Y.; Fang, X. Angiopep-conjugated poly (ethylene glycol)-co-poly (ε-caprolactone) nanoparticles as dual-targeting drug delivery system for brain glioma. *Biomaterials* **2011**, *32*, 4293–4305. [CrossRef] [PubMed]
170. Li, J.; Feng, L.; Fan, L.; Zha, Y.; Guo, L.; Zhang, Q.; Chen, J.; Pang, Z.; Wang, Y.; Jiang, X. Targeting the brain with PEG–PLGA nanoparticles modified with phage-displayed peptides. *Biomaterials* **2011**, *32*, 4943–4950. [CrossRef] [PubMed]
171. Xin, H.; Sha, X.; Jiang, X.; Zhang, W.; Chen, L.; Fang, X. Anti-glioblastoma efficacy and safety of paclitaxel-loading Angiopep-conjugated dual targeting PEG-PCL nanoparticles. *Biomaterials* **2012**, *33*, 8167–8176. [CrossRef] [PubMed]
172. Geldenhuys, W.; Wehrung, D.; Groshev, A.; Hirani, A.; Sutariya, V. Brain-targeted delivery of doxorubicin using glutathione-coated nanoparticles for brain cancers. *Pharm. Dev. Technol.* **2015**, *20*, 497–506. [CrossRef]
173. Fornaguera, C.; Dols-Perez, A.; Caldero, G.; Garcia-Celma, M.; Camarasa, J.; Solans, C. PLGA nanoparticles prepared by nano-emulsion templating using low-energy methods as efficient nanocarriers for drug delivery across the blood–brain barrier. *J. Control. Release* **2015**, *211*, 134–143. [CrossRef]
174. Cui, Y.; Zhang, M.; Zeng, F.; Jin, H.; Xu, Q.; Huang, Y. Dual-targeting magnetic PLGA nanoparticles for codelivery of paclitaxel and curcumin for brain tumor therapy. *ACS Appl. Mater. Interfaces* **2016**, *8*, 32159–32169. [CrossRef]
175. Malinovskaya, Y.; Melnikov, P.; Baklaushev, V.; Gabashvili, A.; Osipova, N.; Mantrov, S.; Ermolenko, Y.; Maksimenko, O.; Gorshkova, M.; Balabanyan, V. Delivery of doxorubicin-loaded PLGA nanoparticles into U87 human glioblastoma cells. *Int. J. Pharm.* **2017**, *524*, 77–90. [CrossRef] [PubMed]
176. Ramalho, M.; Sevin, E.; Gosselet, F.; Lima, J.; Coelho, M.; Loureiro, J.; Pereira, M. Receptor-mediated PLGA nanoparticles for glioblastoma multiforme treatment. *Int. J. Pharm.* **2018**, *545*, 84–92. [CrossRef]
177. Ganipineni, L.P.; Ucakar, B.; Joudiou, N.; Riva, R.; Jérôme, C.; Gallez, B.; Danhier, F.; Préat, V. Paclitaxel-loaded multifunctional nanoparticles for the targeted treatment of glioblastoma. *J. Drug Target.* **2019**, *27*, 614–623. [CrossRef] [PubMed]
178. Georgieva, J.; Hoekstra, D.; Zuhorn, I. Smuggling drugs into the brain: An overview of ligands targeting transcytosis for drug delivery across the blood–brain barrier. *Pharmaceutics* **2014**, *6*, 557–583. [CrossRef] [PubMed]
179. Chen, Y.; Liu, L. Modern methods for delivery of drugs across the blood–brain barrier. *Adv. Drug Deliv. Rev.* **2012**, *64*, 640–665. [CrossRef] [PubMed]
180. Loureiro, J.A.; Gomes, B.; Coelho, M.A.; Carmo Pereira, M.d.; Rocha, S. Targeting nanoparticles across the blood–brain barrier with monoclonal antibodies. *Nanomedicine* **2014**, *9*, 709–722. [CrossRef]
181. Calzolari, A.; Larocca, L.M.; Deaglio, S.; Finisguerra, V.; Boe, A.; Raggi, C.; Ricci-Vitani, L.; Pierconti, F.; Malavasi, F.; De Maria, R. Transferrin receptor 2 is frequently and highly expressed in glioblastomas. *Transl. Oncol.* **2010**, *3*, 123. [CrossRef]
182. Lee, H.J.; Engelhardt, B.; Lesley, J.; Bickel, U.; Pardridge, W.M. Targeting rat anti-mouse transferrin receptor monoclonal antibodies through blood-brain barrier in mouse. *J. Pharm. Exp. Ther.* **2000**, *292*, 1048–1052.
183. Schröder, U.; Sabel, B.A. Nanoparticles, a drug carrier system to pass the blood-brain barrier, permit central analgesic effects of iv dalargin injections. *Brain Res.* **1996**, *710*, 121–124. [CrossRef]
184. Wohlfart, S.; Khalansky, A.S.; Gelperina, S.; Maksimenko, O.; Bernreuther, C.; Glatzel, M.; Kreuter, J. Efficient chemotherapy of rat glioblastoma using doxorubicin-loaded PLGA nanoparticles with different stabilizers. *PLoS ONE* **2011**, *6*, e19121. [CrossRef]

185. Demeule, M.; Regina, A.; Che, C.; Poirier, J.; Nguyen, T.; Gabathuler, R.; Castaigne, J.-P.; Beliveau, R. Identification and design of peptides as a new drug delivery system for the brain. *J. Pharm. Exp. Ther.* **2008**, *324*, 1064–1072. [CrossRef]
186. Demeule, M.; Currie, J.C.; Bertrand, Y.; Ché, C.; Nguyen, T.; Régina, A.; Gabathuler, R.; Castaigne, J.P.; Béliveau, R. Involvement of the low-density lipoprotein receptor-related protein in the transcytosis of the brain delivery vector Angiopep-2. *J. Neurochem.* **2008**, *106*, 1534–1544. [CrossRef]
187. Shao, K.; Huang, R.; Li, J.; Han, L.; Ye, L.; Lou, J.; Jiang, C. Angiopep-2 modified PE-PEG based polymeric micelles for amphotericin B delivery targeted to the brain. *J. Control. Release* **2010**, *147*, 118–126. [CrossRef] [PubMed]
188. von Roemeling, C.; Jiang, W.; Chan, C.K.; Weissman, I.L.; Kim, B.Y. Breaking down the barriers to precision cancer nanomedicine. *Trends Biotechnol.* **2017**, *35*, 159–171. [CrossRef] [PubMed]
189. Miele, E.; Spinelli, G.P.; Miele, E.; Tomao, F.; Tomao, S. Albumin-bound formulation of paclitaxel (Abraxane®ABI-007) in the treatment of breast cancer. *Int. J. Nanomed.* **2009**, *4*, 99.
190. Choi, H.S.; Liu, W.; Misra, P.; Tanaka, E.; Zimmer, J.P.; Ipe, B.I.; Bawendi, M.G.; Frangioni, J.V. Renal clearance of quantum dots. *Nat. Biotechnol.* **2007**, *25*, 1165. [CrossRef] [PubMed]
191. Lee, J.E.; Kim, M.G.; Jang, Y.L.; Lee, M.S.; Kim, N.W.; Yin, Y.; Lee, J.H.; Lim, S.Y.; Park, J.W.; Kim, J. Self-assembled PEGylated albumin nanoparticles (SPAN) as a platform for cancer chemotherapy and imaging. *Drug Deliv.* **2018**, *25*, 1570–1578. [CrossRef]
192. Ruggiero, A.; Villa, C.H.; Bander, E.; Rey, D.A.; Bergkvist, M.; Batt, C.A.; Manova-Todorova, K.; Deen, W.M.; Scheinberg, D.A.; McDevitt, M.R. Paradoxical glomerular filtration of carbon nanotubes. *Proc. Natl. Acad. Sci. USA* **2010**, *107*, 12369–12374. [CrossRef]
193. Liu, J.; Yu, M.; Zhou, C.; Yang, S.; Ning, X.; Zheng, J. Passive tumor targeting of renal-clearable luminescent gold nanoparticles: Long tumor retention and fast normal tissue clearance. *J. Am. Chem. Soc.* **2013**, *135*, 4978–4981. [CrossRef]
194. Blanco, E.; Shen, H.; Ferrari, M. Principles of nanoparticle design for overcoming biological barriers to drug delivery. *Nat. Biotechnol.* **2015**, *33*, 941. [CrossRef]
195. Boucher, Y.; Baxter, L.T.; Jain, R.K. Interstitial pressure gradients in tissue-isolated and subcutaneous tumors: Implications for therapy. *Cancer Res.* **1990**, *50*, 4478–4484.
196. Jain, R.K. Normalization of tumor vasculature: An emerging concept in antiangiogenic therapy. *Science* **2005**, *307*, 58–62. [CrossRef]
197. Batchelor, T.T.; Sorensen, A.G.; di Tomaso, E.; Zhang, W.-T.; Duda, D.G.; Cohen, K.S.; Kozak, K.R.; Cahill, D.P.; Chen, P.-J.; Zhu, M. AZD2171, a pan-VEGF receptor tyrosine kinase inhibitor, normalizes tumor vasculature and alleviates edema in glioblastoma patients. *Cancer Cell* **2007**, *11*, 83–95. [CrossRef] [PubMed]
198. Jiang, W.; Huang, Y.; An, Y.; Kim, B.Y. Remodeling tumor vasculature to enhance delivery of intermediate-sized nanoparticles. *ACS Nano* **2015**, *9*, 8689–8696. [CrossRef] [PubMed]
199. Alexandrakis, G.; Brown, E.B.; Tong, R.T.; McKee, T.D.; Campbell, R.B.; Boucher, Y.; Jain, R.K. Two-photon fluorescence correlation microscopy reveals the two-phase nature of transport in tumors. *Nat. Med.* **2004**, *10*, 203. [CrossRef] [PubMed]
200. McKee, T.D.; Grandi, P.; Mok, W.; Alexandrakis, G.; Insin, N.; Zimmer, J.P.; Bawendi, M.G.; Boucher, Y.; Breakefield, X.O.; Jain, R.K. Degradation of fibrillar collagen in a human melanoma xenograft improves the efficacy of an oncolytic herpes simplex virus vector. *Cancer Res.* **2006**, *66*, 2509–2513. [CrossRef]
201. Cabral, H.; Matsumoto, Y.; Mizuno, K.; Chen, Q.; Murakami, M.; Kimura, M.; Terada, Y.; Kano, M.; Miyazono, K.; Uesaka, M. Accumulation of sub-100 nm polymeric micelles in poorly permeable tumours depends on size. *Nat. Nanotechnol.* **2011**, *6*, 815. [CrossRef]
202. Ferrari, M. Frontiers in cancer nanomedicine: Directing mass transport through biological barriers. *Trends Biotechnol.* **2010**, *28*, 181–188. [CrossRef]
203. Wong, C.; Stylianopoulos, T.; Cui, J.; Martin, J.; Chauhan, V.P.; Jiang, W.; Popović, Z.; Jain, R.K.; Bawendi, M.G.; Fukumura, D. Multistage nanoparticle delivery system for deep penetration into tumor tissue. *Proc. Natl. Acad. Sci. USA* **2011**, *108*, 2426–2431. [CrossRef]
204. Huang, C.-F.; Yao, G.-H.; Liang, R.-P.; Qiu, J.-D. Graphene oxide and dextran capped gold nanoparticles based surface plasmon resonance sensor for sensitive detection of concanavalin A. *Biosens. Bioelectron.* **2013**, *50*, 305–310. [CrossRef]

205. Szakács, G.; Paterson, J.K.; Ludwig, J.A.; Booth-Genthe, C.; Gottesman, M.M. Targeting multidrug resistance in cancer. *Nat. Rev. Drug Discov.* **2006**, *5*, 219. [CrossRef]
206. Aller, S.G.; Yu, J.; Ward, A.; Weng, Y.; Chittaboina, S.; Zhuo, R.; Harrell, P.M.; Trinh, Y.T.; Zhang, Q.; Urbatsch, I.L. Structure of P-glycoprotein reveals a molecular basis for poly-specific drug binding. *Science* **2009**, *323*, 1718–1722. [CrossRef]
207. Gottesman, M.M.; Fojo, T.; Bates, S.E. Multidrug resistance in cancer: Role of ATP–dependent transporters. *Nat. Rev. Cancer* **2002**, *2*, 48. [CrossRef] [PubMed]
208. Fletcher, J.I.; Haber, M.; Henderson, M.J.; Norris, M.D. ABC transporters in cancer: More than just drug efflux pumps. *Nat. Rev. Cancer* **2010**, *10*, 147. [CrossRef]
209. Dean, M.; Fojo, T.; Bates, S. Tumour stem cells and drug resistance. *Nat. Rev. Cancer* **2005**, *5*, 275. [CrossRef]
210. Wu, J.; Lee, A.; Lu, Y.; Lee, R.J. Vascular targeting of doxorubicin using cationic liposomes. *Int. J. Pharm.* **2007**, *337*, 329–335. [CrossRef] [PubMed]
211. Wong, H.L.; Bendayan, R.; Rauth, A.M.; Xue, H.Y.; Babakhanian, K.; Wu, X.Y. A mechanistic study of enhanced doxorubicin uptake and retention in multidrug resistant breast cancer cells using a polymer-lipid hybrid nanoparticle system. *J. Pharm. Exp. Ther.* **2006**, *317*, 1372–1381. [CrossRef] [PubMed]
212. Xiong, X.-B.; Lavasanifar, A. Traceable multifunctional micellar nanocarriers for cancer-targeted co-delivery of MDR-1 siRNA and doxorubicin. *ACS Nano* **2011**, *5*, 5202–5213. [CrossRef] [PubMed]
213. Anselmo, A.C.; Mitragotri, S. Nanoparticles in the clinic. *Bioeng. Transl. Med.* **2016**, *1*, 10–29. [CrossRef] [PubMed]
214. Dobrovolskaia, M.A.; Aggarwal, P.; Hall, J.B.; McNeil, S.E. Preclinical studies to understand nanoparticle interaction with the immune system and its potential effects on nanoparticle biodistribution. *Mol. Pharm.* **2008**, *5*, 487–495. [CrossRef]
215. Moghimi, S.M.; Hunter, A.C.; Murray, J.C. Long-circulating and target-specific nanoparticles: Theory to practice. *Pharm. Rev.* **2001**, *53*, 283–318.
216. Barenholz, Y.C. Doxil®—The first FDA-approved nano-drug: Lessons learned. *J. Control. Release* **2012**, *160*, 117–134. [CrossRef]
217. Carnevale, J.; Ko, A.H. MM-398 (nanoliposomal irinotecan): Emergence of a novel therapy for the treatment of advanced pancreatic cancer. *Future Oncol.* **2016**, *12*, 453–464. [CrossRef] [PubMed]
218. Chang, T.; Shiah, H.; Yang, C.; Yeh, K.; Cheng, A.; Shen, B.; Wang, Y.; Yeh, C.; Chiang, N.; Chang, J.-Y. Phase I study of nanoliposomal irinotecan (PEP02) in advanced solid tumor patients. *Cancer Chemother. Pharmacol.* **2015**, *75*, 579–586. [CrossRef] [PubMed]
219. Kreuter, J. Nanoparticles and nanocapsules—New dosage forms in the nanometer size range. *Pharm. Acta Helv.* **1978**, *53*, 33–39.
220. Valle, J.W.; Armstrong, A.; Newman, C.; Alakhov, V.; Pietrzynski, G.; Brewer, J.; Campbell, S.; Corrie, P.; Rowinsky, E.K.; Ranson, M. A phase 2 study of SP1049C, doxorubicin in P-glycoprotein-targeting pluronics, in patients with advanced adenocarcinoma of the esophagus and gastroesophageal junction. *Investig. New Drugs* **2011**, *29*, 1029–1037. [CrossRef] [PubMed]
221. Andrade, F.; Almeida, A.; Rafael, D.; Schwartz, S.; Sarmento, B. Micellar-Based Nanoparticles for Cancer Therapy and Bioimaging. In *Nanooncology*; Springer: New York, NY, USA, 2018; pp. 211–238.
222. Matsumura, Y.; Hamaguchi, T.; Ura, T.; Muro, K.; Yamada, Y.; Shimada, Y.; Shirao, K.; Okusaka, T.; Ueno, H.; Ikeda, M. Phase I clinical trial and pharmacokinetic evaluation of NK911, a micelle-encapsulated doxorubicin. *Br. J. Cancer* **2004**, *91*, 1775. [CrossRef] [PubMed]
223. Ahn, H.K.; Jung, M.; Sym, S.J.; Shin, D.B.; Kang, S.M.; Kyung, S.Y.; Park, J.-W.; Jeong, S.H.; Cho, E.K. A phase II trial of Cremorphor EL-free paclitaxel (Genexol-PM) and gemcitabine in patients with advanced non-small cell lung cancer. *Cancer Chemother. Pharmacol.* **2014**, *74*, 277–282. [CrossRef]
224. Kim, T.-Y.; Kim, D.-W.; Chung, J.-Y.; Shin, S.G.; Kim, S.-C.; Heo, D.S.; Kim, N.K.; Bang, Y.-J. Phase I and pharmacokinetic study of Genexol-PM, a cremophor-free, polymeric micelle-formulated paclitaxel, in patients with advanced malignancies. *Clin. Cancer Res.* **2004**, *10*, 3708–3716. [CrossRef]
225. Autio, K.A.; Dreicer, R.; Anderson, J.; Garcia, J.A.; Alva, A.; Hart, L.L.; Milowsky, M.I.; Posadas, E.M.; Ryan, C.J.; Graf, R.P. Safety and efficacy of BIND-014, a docetaxel nanoparticle targeting prostate-specific membrane antigen for patients with metastatic castration-resistant prostate cancer: A phase 2 clinical trial. *JAMA Oncol.* **2018**, *4*, 1344–1351. [CrossRef]

226. Chakraborty, C.; Sharma, A.R.; Sharma, G.; Doss, C.G.P.; Lee, S.-S. Therapeutic miRNA and siRNA: Moving from bench to clinic as next generation medicine. *Mol. Therapy-Nucleic Acids* **2017**, *8*, 132–143. [CrossRef]
227. Giri, V.P.; Kanodia, S.; Giri, O.P.; Sumit, K. Anti-nicotine vaccine: Current status. *Int. J. Basic Clin. Pharm.* **2017**, *4*, 1309–1313. [CrossRef]
228. Gu, F.; Zhang, L.; Teply, B.A.; Mann, N.; Wang, A.; Radovic-Moreno, A.F.; Langer, R.; Farokhzad, O.C. Precise engineering of targeted nanoparticles by using self-assembled biointegrated block copolymers. *Proc. Natl. Acad. Sci. USA* **2008**, *105*, 2586–2591. [CrossRef] [PubMed]

cancers

MDPI

Review

Exploiting Current Understanding of Hypoxia Mediated Tumour Progression for Nanotherapeutic Development

Jie Feng †, Niall M. Byrne †, Wafa Al Jamal and Jonathan A. Coulter *

School of Pharmacy, Queens University Belfast, Lisburn Road, Belfast BT9 7BL, UK; jfeng09@qub.ac.uk (J.F.); n.byrne@qub.ac.uk (N.M.B.); w.al-jamal@qub.ac.uk (W.A.J.)

* Correspondence: j.coulter@qub.ac.uk

† These authors contributed equally to this work.

Received: 30 October 2019; Accepted: 7 December 2019; Published: 11 December 2019

Abstract: Hypoxia is one of the most common phenotypes of malignant tumours. Hypoxia leads to the increased activity of hypoxia-inducible factors (HIFs), which regulate the expression of genes controlling a raft of pro-tumour phenotypes. These include maintenance of the cancer stem cell compartment, epithelial-mesenchymal transition (EMT), angiogenesis, immunosuppression, and metabolic reprogramming. Hypoxia can also contribute to the tumour progression in a HIF-independent manner via the activation of a complex signalling network pathway, including JAK-STAT, RhoA/ROCK, NF-κB and PI3/AKT. Recent studies suggest that nanotherapeutics offer a unique opportunity to target the hypoxic microenvironment, enhancing the therapeutic window of conventional therapeutics. In this review, we summarise recent advances in understanding the impact of hypoxia on tumour progression, while outlining possible nanotherapeutic approaches for overcoming hypoxia-mediated resistance.

Keywords: angiogenesis; epithelial-to-mesenchymal transition; hypoxia; immunosuppression; metabolism; nanoparticle; nanotherapeutics; tumour microenvironment

1. Introduction

The hostile microenvironment within a solid tumour is increasingly recognized as a major impediment to effective cancer therapy [1]. Hypoxia, a hallmark of malignancy, is one of the most typical and important features of the tumour microenvironment (TME), caused by the imbalance between oxygen supply and consumption by cancer and stromal cells [2,3]. Failure of the local environment to overcome this deficit due to the aberrant vascular architecture results in tumour hypoxia. Hypoxia has been shown to contribute to malignant progression and treatment failure, in particular, resistance to radiotherapy.

1.1. Defining Tumour Hypoxia

Since the development of the oxygen electrode, direct measurements of tissue oxygenation has revealed considerable heterogeneity in oxygen concentration in normal and pathological tissue. Physiological hypoxia is typically defined as ≤2% O_2 (15 mmHg), while pathological hypoxia defined as ≤1% O_2 and radiobiological hypoxia as ≤0.4% [3]. Hypoxia is classified as perfusion-limited (acute) hypoxia or diffusion-limited (chronic) hypoxia [4]. Perfusion-limited hypoxia is often caused by the structural and functional abnormality of tumour microvasculature, characterized by an immature endothelial cell lining and basement membrane, disorganized vascular network and wide intercellular spaces. These structural abnormalities lead to the rapid oxygen fluctuations between hypoxia, anoxia and reoxygenation [4]. The lifetime of perfusion related hypoxia ranges from less than a minute to

several hours in experimental tumours [5]. In contrast, diffusion-limited hypoxia is mainly due to an increase in diffusion distance, attributed to a rapidly expanding tumour. Tumour cells are often far from nutritive blood vessels, where most of the accessible molecular oxygen is consumed by proliferating cells before diffusion to deep tumour layers occurs. This results in the development of a hypoxic tumour core [6].These two forms of tumour hypoxia often overlap spatio-temporally, influencing the interaction between cancer, stromal and immune host cells. Additionally, tissue oxygenation may also be perturbed by anaemia, which can often occur following chemotherapy, radiotherapy, blood loss and low haemoglobin levels [7].

1.2. Implications of Tumour Hypoxia and Nanotherapeutic Opportunities

It has previously been suggested that up to 60% of solid tumours contain hypoxic or anoxic regions, conferring major implications for chemo- and radiotherapy [8]. Biologically, hypoxia can trigger proteomic alterations within neoplastic and stromal cells, further promoting malignant progression and poor survival. Furthermore, hypoxia is the leading cause of treatment failure for radiotherapy and photodynamic therapy since both approaches rely on the creation of reactive oxygen species. For chemotherapy, solid tumour hypoxia is associated with elevated HIF gene expression, promoting double-strand DNA repair and subsequently, chemo-resistance [9]. Hypoxia is also a potential barrier to immunotherapy. Several studies suggest that the recruitment of immunosuppressive cells within hypoxic regions promote immune suppression. Furthermore, hypoxia-driven adaptive mechanisms diminish the immune cell response via expression of immune check-point molecules such as PDL-1 (programmed death ligand-1) and HLA-G (human leukocyte antigen G), altering both tumour metabolism and metabolite formation [10]. Nanotherapeutics offer a unique approach to exploit the physiological and pathophysiological response to hypoxia within the TME. Interest in the use of nanoparticles (NPs) for biological applications, including enhanced drug delivery, diagnostic imaging and as radiosensitisers, has increased over the last 25 years [11,12].

1.3. Scope of the Review

In this review, we summarise recent advances relating to the biological consequence and therapeutic efficacy of tumour hypoxia [13,14]. We outline the negative impact of tumour hypoxia on the propagation of cancer stem cells, malignant progression, metastasis immunosuppression and metabolic reprogramming. We also consider the use of nanoparticles to manipulate hypoxia-induced features of the TME for therapeutic gain (Figure 1).

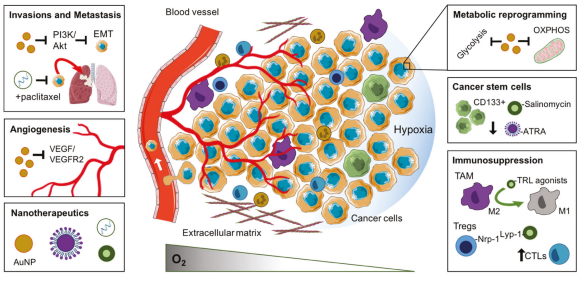

Figure 1. Nanotherapeutic approaches to exploit the hypoxic tumour microenvironment. The response of the tumour microenvironment to reduced oxygenation, including cancer stem cell enrichment, angiogenesis, invasion and metastasis, metabolic reprogramming and immunosuppression, and the nanotherapeutic approaches to exploit or manipulate these features. Abbreviations: AuNP, gold nanoparticle; CTL, cytotoxic T lymphocyte; EMT, epithelial to mesenchymal transition; MDSCs, myeloid-derived suppressor cells; OXPHOS, oxidative phosphorylation; TAM, tumour-associated macrophage.

2. Biological Response and Therapeutic Opportunities of Tumour Hypoxia

The presence of hypoxia strongly correlates with an aggressive tumour phenotype, therapeutic resistance and poor patient survival. Initially, we outline the mechanisms by which hypoxia promotes an aggressive tumour phenotype, and discuss the treatment opportunities that may exist using nanotherapeutic strategies (Table 1). The full biological response and therapeutic implications to hypoxia are extensive and well beyond the limits of this review paper. As such, we will review only recent discoveries related to the cellular response of hypoxia-driven malignant progression and resistance, which have been summarised in Figure 2.

Table 1. Summary of nanotherapeutic strategies to overcome hypoxia-mediated progression.

Nanoparticle Formulation	Drug/Therapeutic	Targeting Moiety	Target	Indications and Measured Benefit	Ref.
			2.1 Enrichment and propagation of cancer stem cells		
PLGA	Salinomycin	CD133 aptamer	CD133 receptor	Selectively kill $CD133^+$ osteosarcoma cells et and in vivo and reduce tumoursphere formation and the percentage of Sao-2 $CD133^+$ cells	[15]
PLGA-PEG	Salinomycin	CD133 Antibody	CD133 receptor	Reduction in the percentage of $CD133^+$ ovarian cancer cells. 2.5- fold decrease in PA-1tumor sphere number compared to the saline control	[16]
Lipid polymers	Salinomycin	CD133 and EGFR aptamer	CD133 receptor EGFR	Targeting both osteosarcoma CSCs and cancer cells with high specificity, 90% decrease in tumour volume	[17]
Lipid polymers	ATRA	CD133 aptamer	CD133 receptor	Osteosarcoma tumour volume inhibitory rate for the ATRA-PLNP-CD133 treated group was 81.1%	[18]
Hyaluronic acid and styrene-maleic acid Nano micelle	Curcumin	Hyaluronic acid	CD44 receptor	Marked inhibition of NF-κB signalling and significant reduction in CD44+ expression cells in pancreatic cancer cells	[19]
Pluronic f127	Doxorubicin	Chitosan	CD44 receptor	Increased the toxicity of doxorubicin (Dox)by six times compared to free Dox in eliminating CD44+ CSC-like cells in MCF-7 breast cancer (BCa) cells.	[20]
Liposome	Salinomycin Doxorubicin			A significant decrease in liver cancer stem cells in vivo (HepG2, HepG2-TS cells)	[21]
PLGA	Salinomycin Paclitaxel	Hyaluronic acid	CD44 receptor	A significant reduction in CD44+ cells in Breast cancer, MCF-7 and MDA-MB-231 cells	[22]
PEG-PLA	Doxorubicin ATRA			Induced differentiation of CSCs and sensitized cells toward DOX treatment. Combinatory treatment significantly reduces MDA-MB-231 tumour growth in vivo.	[23]
Mesoporous silica	Cisplatin, 5-fluoroucail, paclitaxel	siRNA	ABCG2	Downregulation of ABCG2 significantly enhanced the drug-induced apoptosis and inhibited Hep-2 (laryngeal) tumour growth in vivo.	[24]
PLGA	Paclitaxel	Wedelolactone	SOX-2, ABCG2	Wedelolactone treatment sensitizes MDA-MB-231 BCa cells to the effects of paclitaxel and significantly reduced the ALDH+ breast cancer CSCs and suppressed the tumour growth	[25]
Silica	γ-secretase inhibitor		Notch signalling	Breast cancer, MDA-MB-231 cells. Reduce ALDH side population in CAM model and suppressed tumor growth in vivo	[26]
			2.2 Invasion and Metastasis		
AuNPs			MAPK signalling	Inhibited the proliferation of SKOV3 (ovarian) cancer cells and delayed the tumoral and metastases growth by reversing EMT and inhibition of MAPK signalling	[27]
PEI coated SPIONs			Src kinase, miR-21, MMP2	Reduced the invadosome intensity and decreased the ability of Pan02 (pancreatic cancer) cells to invade through basement membrane.	[28]
FA-PEG-PEI-SPIONs		miR-125b-5p	JAK-STAT, Wnt/β-Catenin	Inhibited the invasion, migration, and growth of HCC HUH7 and HCCLM3 cells	[29]
Zinc arsenite			SHP-1/JAK-STAT	Inhibit tumour growth of HCC xenografts by 2.2-fold and metastasis by 3.5-fold as compare free arsenic trioxide-based NPs	[30]
PEG-AuNPs			PI3/AKT	Supressed tumour growth and decrease sphere formation of glioblastoma and lung adenocarcinoma A549 cells	[31]
Hyaluronic acid conjugated NPs	cisplatin	siRNA	Snail, Twist	Knockdown Twist and reversed chemoresistance to reduce tumour growth and metastasis of Ovarian cancer, F2 and Ovacar 8 cells in vivo	[32]
Amphiphilic polymers	paclitaxel	siRNA	Snail, Twist	Inhibited tumour growth and metastasis of 4T1 tumours in vivo simultaneously	[33]

Table 1. *Cont.*

Nanoparticle Formulation	Drug/Therapeutic	Targeting Moiety	Target	Indications and Measured Benefit	Ref.
			2.3 Angiogenesis		
AuNPs			VEGF, bFGF	inhibited endothelial /fibroblast cell proliferation & angiogenesis in an ovarian cancer model in vivo	[34]
AuNPs			EMT, MMP-2	Facilitated tumour vasculature normalization, increased blood perfusion and alleviate tumour hypoxia in a model of lung cancer (B16F10) in vivo	[35]
AuNPs			Anterior gradient 2 (AGR2)	Reduced vessel density, tumour volume and increased the pericyte coverage in metastatic CRC model (SW620) in vivo	[36]
AuNPs		RGD	αvβ3	Induced tumour vascular disruption and improved the therapeutic outcome of radiotherapy of Panc-1 pancreatic tumours in vivo	[37]
AuNPs		RGD	αvβ3	Reduced breast cancer (MDA-MB-231) cell viability and increased DNA damage compared to radiation alone in vitro.	[38]
			2.4 Immunosuppression		
β-cyclodextrin	TLR7/8 agonist (R848)	Cyclodextrin	Engulfed by TAMs	Remodelled TME from M2 to M1 phenotype. Improved anti-PD-1 response rates in murine colon cancer models	[39]
PLGA	TRL9 agonist	Galactose	MGL—TAMs	Reprogrammed TAMs from M2-M1, suppressed melanoma tumour growth and increased CTL infiltration in vivo	[40]
PLGA	PI3K-γ inhibitor (IPI-549)	AEAA	Sigma-1 receptor—TME	Reduced MDSC proportion and decreased tumour growth in pancreatic tumour model in vivo	[41]
Magnetic zinc-doped iron oxide			MDSC	Repolarise MDSCs from immunosuppressive to pro-inflammatory when combined with Rad.	[42]
PLGA	Tyrosine kinase inhibitor (Imatinib)	Lyp-1	Nrp-1—Tregs	Enhanced tumour inhibition and survival of murine melanoma tumours when combined with immune checkpoint inhibitor	[43]
PLGA	Anti-PD-L1 & ICG	MMP-2 sensitive property	MMP-2—TME	Increased CTL tumour infiltration. Suppressed tumour growth and lung metastasis in 4T1 breast cancer model	[44]
			2.5 Metabolic reprogramming		
AuNPs	3-BPP		HK2 (mitochondria)	Suppressed tumour cell glycolysis and OXPHOS in prostate cells in vitro	[45]
PLGA	Atovaquone + Veterporfin		Complex III (mitochondria)	Improved intratumoural oxygenation and anti-tumour response to PDT in 4T1 tumour bearing mice	[46]
Gelatin	Atovaquone + ICG		Complex III (mitochondria)	Improved intratumoural oxygenation and anti-tumour response to PDT in HeLa xenografts	[47]
PEG-PCL	Metformin + IR780		Complex I (mitochondria)	Decreased endogenous oxygen consumption in gastric cancer cells in vitro. Improved PDT and PTT in vivo	[48]
Tungsten oxide ($W_{18}O_{49}$)	Metformin		Complex I (mitochondria)	Lowered OCR and inhibit tumour growth in Raji-lymphoma-bearing mice	[49]

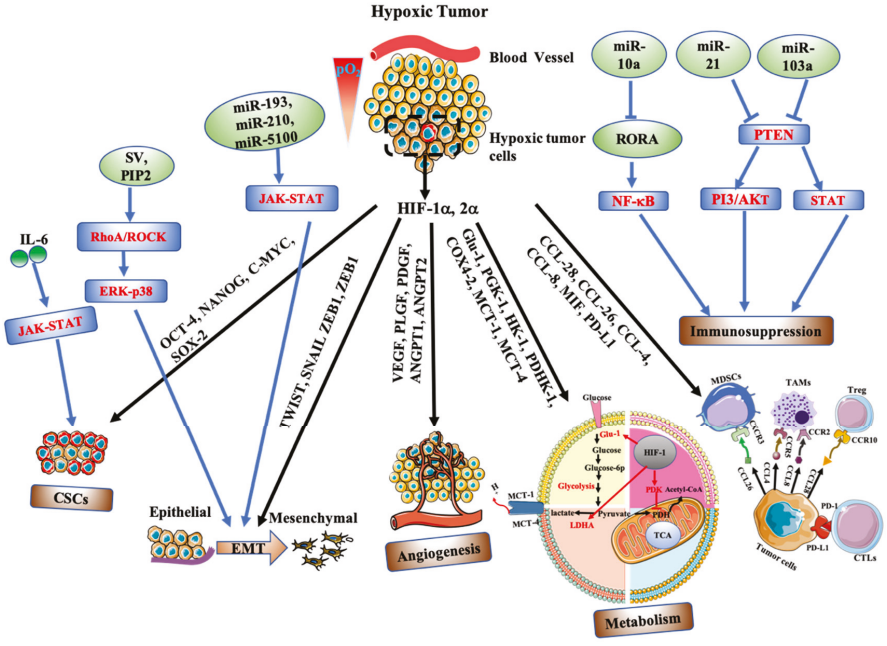

Figure 2. Hypoxia regulates tumour progression via various mechanisms, including HIF independent (blue arrow) and HIF-dependent manner (black arrow). Intratumoural hypoxia causes overexpression of HIF-1α and HIF-2α, leading to transactivation of multiple target genes outlined above. These regulate the cellular response to CSCs maintenance, EMT induction, angiogenesis, metabolic reprogramming, and immunosuppression. Tumour progression is also influenced by numerous HIF-independent factors including miRNA expression and cytokine release, activating various pro-tumour signalling pathways. Abbreviations: IL-6, interleukin 6; SV, supervillain; PIP2, phosphatidylinositol (4,5) biphosphate; RORA, RAR-related orphan receptor; MDSCs, myeloid-derived suppressor cells; TAMs, tumour-associated macrophages; Treg, regulatory T cells; CTLs, cytotoxic T lymphocytes.

2.1. Enrichment and Propagation of Cancer Stem Cells

Cancer stem cells (CSCs) or tumour initiating cells are a small subpopulation of cells which share progenitor-like characteristics including self-renewal, tumour initiation and multi-lineage differentiation. Furthermore, tumour hypoxia has been directly correlated with metastatic potential and treatment resistance. CSCs can induce cell cycle arrest, conferring resistance to both chemo- and radiotherapy. Post-treatment, surviving CSCs are released from dormancy driving repopulation and dissemination. Therefore, a deep understanding of the influence of hypoxia in CSCs biology is central to the development of future therapeutic approaches.

The CSCs model is driven by many key regulatory factors including genetic diversity, epigenetics and the TME. Recent evidence points to the influence of the microenvironment on cell plasticity and differentiation. Tumour hypoxia is a key environmental stress associated with CSC self-renewal, epithelial-to-mesenchymal transition (EMT) and treatment resistance. Hypoxia expands the CSCs population through several molecular mechanisms. Hypoxia mediated epigenetics act as a possible driving force for promoting cancer stemness. These epigenetic factors include DNA methylation, histone modification, chromatin remodelling and microRNA expression. Kang et al. (2019) identified hypoxia as a key driver of cancer stemness and EMT in multiple lung cancer models, driven by a decrease in E-cadherin and a corresponding increase in the mesenchymal markers fibronectin, vimentin, α-SMA, slug and ZEB1 [50]. Additionally, significant activation of the CSC marker CXCR4 was reported.

The impact of CXCR4 was demonstrated following the induction of strong CXCR4 immunoreactivity following the intratumoural injection of hypoxic cells. Furthermore, methylation-specific PCR and sequencing data further confirmed a decrease in CXCR4 promoter methylation under hypoxia, thus promoting CXCR4 expression and the acquisition of CSC-like properties. Prasad et al. (2017) investigated the role of hypoxia in regulating stemness in an aggressive glioblastoma tumour model [51]. The authors reported hypoxia-mediated self-renewal of A172 cells through elevated neurosphere formation. Furthermore, at the molecular level, OCT-4, NANOG, SOX-2 and Stat3 gene and protein expression were highly upregulated following chronic hypoxia (Figure 2). Importantly, hypoxia was shown to reduce 5-methyltosine (5-mC) expression by at least three-fold at all OCT-4 regulatory regions (OA, OB, OC), and within the promoter region of NANOG. Furthermore, a concomitant enrichment of 5-hydroxymethylcytosine (5-hmC) at OCT-4 regions (OA (2.5-fold), OB (4.6-fold)), together with a significant reduction of H3K27me3 methylation confirmed hypoxia-meditated regulation of stem associated genes. N6-methyladenosine (m6A) modification has recently been identified as an important regulator of stem cell pluripotency. Zhang et al. (2016) showed that hypoxia induced HIF-1α and HIF-2α dependent expression of AlkB homolog 5 (ALKBH5) [52], a m6A demethylase in breast cancer models. This resulted in demethylation at m6A residues within the 3'-UTR of NANOG, upregulating functional NANOG protein and contributing to breast CSC enrichment.

The influence of hypoxia on cell cycle progression in glioma CSCs has been demonstrated by Li et al. (2013) [53]. Cells maintained in 1% O_2 for 48 h significantly increased G_0/G_1 accumulation with a corresponding reduction in G_2/M cells, indicating elevated quiescence. This phenotype corresponded with elevated OCT-4 and SOX-2 and reduced expression of GFAP, a marker of stem cell differentiation, implying that hypoxia stemness is primarily attributed to dedifferentiation. Hypoxia has also been shown to promote dedifferentiation of mature glioma cells into stem-like glioma stem cells (GSCs). Hypoxia induced single differentiated CD133-/CD15-/NESTIN- glioma cells into viable neurospheres through elevated expression of critical genes including SOX-2, OCT-4, KLF-4, NANOG, CD133, CD15, NESTIN and ABCG2 [54]. Interestingly, hypoxia induced CSC enrichment also resulted in increased tumourgenicity and mortality in vivo. At the molecular level, higher levels of HIF-1α were measured in both neurosphere and tumour samples, with the importance of HIF-1α further illustrated through interference experiments, potently suppressing neurosphere formation and stem cell marker expression (CD133, CD15 and NESTIN).

Recent mechanistic evidence supported the CSC maintenance function of hypoxia stimulated JAK-STAT signalling in breast cancer models [55]. Conditioned medium (CM) from hypoxic estrogen receptor (ER-α) positive tumour cells enriched the fraction of CSCs compared to normal growth conditions. Conversely, conditioned medium from ERα -negative tumour cells decreases the CSC subpopulations. The authors reported that JAK-STAT signalling activity regulates the contrasting secretome of ERα positive and ERα negative breast cancer cells, through differential cytokine (IL6, IL12RB2) secretion dependent on estrogen receptor status, acting as a key regulator of JAK-STAT phosphorylation (Figure 2).

Nanotherapeutic Approaches to Target Cancer Stem Cells

Targeting CSCs is of particular interest, given their purported therapeutic resistance and capacity for tumour repopulation following treatment. ALDH, CD44, CD133 and other cell surface markers outlined above have frequently been used as putative CSC markers. In addition, CSCs are dependent on cell signalling pathways including Wnt and Notch, which may act as therapeutic drug targets for intervention [56,57]. A number of therapeutic agents that have effects on eliminating or inhibiting CSCs have been proposed and confirmed, including, doxorubicin, paclitaxel, salinomycin, curcumin and all-trans retinoic acid. However, most of the agents have characteristics limiting their effective application in vivo, including poor solubility, low specificity, poor stability, and short circulation time. Nanotechnology drug delivery approaches hold significant potential for tackling these limitations. A series of therapeutic agents have been loaded into CD133 or CD44 functionalized

nanosystems, demonstrating an increased efficacy for eliminating CSC populations both in vitro and in vivo. Doxorubicin, a widely used clinical agent, was loaded into chitosan decorated NPs, with the nanoformulation exhibiting six-fold increased cytotoxicity over free doxorubicin. Importantly, this approach was shown to eliminate CD44+ CSCs-like cells leading to a significant reduction in tumour growth [20].

All-trans retinoic acid (ATRA), an active metabolite of vitamin A, has shown therapeutic efficacy in modulating CSC subpopulations, evidenced by reductions in the CSC markers CD44 and ALDH in gastric carcinoma models in vitro and in vivo and the attenuation of CSC-like properties in ALDH-high expressing ovarian CSCs [58,59]. When ATRA was incorporated into lipid-polymer NPs conjugated with CD133 aptamers, increased targeting and therapeutic efficacy against osteosarcoma CSCs was reported over ATRA alone (tumour volume inhibitory rates of 81.1% and 44.3%, respectively) [18]. Salinomycin, a polyether ionophore antibiotic, has also shown potential in killing CSCs. Poly (lactic-co-glycolic acid) NPs conjugated with CD133 aptamers, specifically delivered salinomycin to CD133+ Saos-2 CSCs significantly attenuating osteosarcoma tumour growth in comparison to salinomycin-only treatment (7.1-fold increase in tumour growth over 60 days in comparison to 17.4-fold increase) as well as reducing the frequency of CD133+ cells in vivo [15]. Similar observations have been shown in models of ovarian cancer in vivo, and in models of osteosarcoma following dual targeting with CD133 and EGFR aptamers [16,17]. Curcumin, a well-known dietary polyphenol derived from the rhizomes of turmeric, has shown excellent therapeutic efficacy against CSCs through the suppression of both CSC self-renewal pathways (Wnt/β-catenin, hedgehog (Hh), and Notch) and specific microRNA involved in the acquisition of EMT [60]. Furthermore, curcumin loaded CD44+ targeting nanomicelles resulted in the potent suppression of pro-tumour NF-κB signalling [19]. The inhibition of Notch signalling using γ-secretase inhibitors has been shown to slow tumour growth using xenograft models of medulloblastoma and by reducing CSC (CD133+) subpopulations [61]. However, inhibiting key CSC signalling pathways may inadvertently affect normal stem cell function. Targeted inhibition of Notch signalling in breast CSCs was achieved using a γ-secretase inhibitor loaded on a glucose-functionalised mesoporous silica nanoparticle. These co-functionalised NPs successfully reduced the MDA-MB-231 CSC ALDH side-population in a chick embryo chorioallantoic membrane (CAM) model, reducing tumour growth in vivo [26].

The combination of chemotherapy agents and salinomycin or ATRA has also received increased attention due to an enhanced synergy achieved through eradicating both terminally differentiated tumour cells and CSCs (Figure 1). For example, Gong et al. (2016) reported that a nanoliposome delivery system co-delivering salinomycin and doxorubicin possessed the best tumour inhibitory rate, significantly reducing the percentage of liver CSCs in vivo [21]. A similar study reported that co-delivery of salinomycin and paclitaxel using hyaluronic acid decorated poly (lactic-co-glycolic acid) NPs showed the highest cytotoxicity against CD44+ breast CSCs compared to salinomycin or paclitaxel used as monotherapies [22]. Sun et al. (2015) also reported that co-delivery of ATRA and doxorubicin in a nanoparticle formulation effectively delivered the agents to both non-CSCs and CSCs, forcing CSC differentiation into a more treatment sensitive phenotype, with the effect of markedly suppressing tumour growth [23].

Recently, ATP-binding cassette subfamily G member 2 (ABCG2), a member of the ABC transporter family, has also been recognized as a promising target for CSCs. ABCG2 has been proposed as the main driver contributing to a subpopulation of slow-cycling CSCs, endowed with enhanced tumourigenic potential and multidrug resistance [62]. Targeting and suppressing ABCG2 function, therefore, represents a sensible strategy to sensitise CSCs populations to chemotherapy. For example, Qi et al. (2015) loaded NPs with siRNA targeting ABCG2 and a chemotherapeutic (cisplatin, 5-fluoroucail or paclitaxel) for the treatment of CD133+ laryngeal carcinoma. The authors reported that the downregulation of ABCG2 significantly enhanced chemotherapeutic drug-induced apoptosis, leading to superior control of tumour growth [24]. Similarly, co-delivery of wedelolatone (Wdl) and paclitaxel incorporated within

PLGA NPs downregulated the ABCG2 and SOX-2 expression, sensitising tumour cells to paclitaxel treatment, and reducing the overall percentage of ALDH+ CSCs in vitro and in solid tumours [25].

2.2. Invasions and Metastasis

Malignant tumours frequently exhibit hypoxia and nutrient deprivation, closely correlated with therapeutic treatment resistance and tumour relapse. Despite significant advances in the treatment of metastatic disease, the underlying mechanisms of metastasis are less well developed. Growing evidence indicates that the hypoxic microenvironment promotes tumour progression by triggering a series of transcriptional responses that regulate migration, invasion, cell proliferation, angiogenesis and cell metabolism, ultimately contributing to an aggressive tumour phenotype [63,64].

Metastasis is a complicated process comprised of a series of highly regulated steps where tumour cells gain more invasive properties. It begins with a change in tumour plasticity, through a process called epithelial-mesenchymal transition (EMT), where epithelial cells lose cell–cell adherence, endowing tumour cells with an enhanced migratory and invasive potential [65]. A critical hallmark of EMT is the repression of E-cadherin expression and the upregulation of associated mesenchymal genes. This transformation results in the disruption of cell–cell adhesion and cell polarity. Hypoxia can induce EMT and invasion via the regulation of EMT-associated transcriptional factors including TWIST, SNAIL, ZEB1, ZEB2 (Figure 2) [66,67]. Pancreatic cancer cells display enhanced cell proliferation and EMT under hypoxic conditions, mediated through an upregulation of HIF-1α and TWIST, corresponding with a dramatic decrease in the expression of E-cadherin and p16Ink4A (p16). However, knockdown of HIF-1α was shown to mask the effect of TWIST overexpression, hypoxia-induced EMT and proliferation through HIF-1α /TWIST signalling, indicating the dominant nature of HIF-1α expression [68].

EMT induction is also controlled by other regulatory mechanisms, with recent studies reporting the influence of specific miRNAs. MicroRNAs suppress protein expression through a combination of mRNA destabilisation and translational repression. Recent reports have shown that hypoxia alters miRNA expression including exosome derived miR-193a-3p, miR-210-3p and miR-5100 (released from hypoxic bone marrow-derived mesenchymal stem cells), promoting epithelial cancer cell invasion and lung metastasis through JAK-STAT overactivation (Figure 2) [69]. Similarly, hypoxia was shown to upregulate miR-210-5P and miR-210-3p [70], upstream precursors N-cadherin, Twist, MMP-2 in hepatoma cell models. Inhibition of miR-210-5P and miR-210-3p suppressed EMT induction and cell progression, indicating that hypoxia-induced miR-210-5p and miR-210 3p are important regulators of a hypoxia-induced metastatic phenotype. Hypoxia-regulated expression of miR-310a-3p has also been shown to push macrophage differentiation towards an M2 phenotype in a HIF-1α or HIF-2α dependent manner [71]. Importantly, invasion and migration potential appeared to be significantly enhanced in macrophages exposed to miR-301a-3p loaded exosomes, providing a mechanism by which hypoxia can stimulate immune cell-mediated tumour progression.

Exosome liberated miR-310a-30p is understood to polarize macrophages into an M2 phenotype via the activation of PTEN/P13Kγ signalling, favouring the malignant properties of tumour cells, due in part to the expression of the anti-inflammatory cytokine (IL-10) and arginase-1 (Arg1) [72]. Additionally, hypoxia can stimulate EMT through a number of other cell-signalling pathways which include RhoA/ROCK-ERK/P38, PI3/Akt. Kaneka et al. (2016) showed that hypoxia treatment induced cell invasion, migration and EMT using oral squamous cell carcinoma (OSCC) cell lines [73]. The authors reported that overexpression of HIF-1α triggers PI3/Akt signalling and the subsequent phosphorylation of GSK3-β (p-GSK3-β). Conversely, inhibition of PI3/Akt signalling led to reduced phosphorylation of GSK3-β and Akt, suppressing EMT induction. These data suggest that hypoxia-induced pGSK3-β is an important regulator in the invasion and metastasis of OSCC. Additionally, supervillin (SV), a protein with two recognised isoforms (SV4 and SV5) was also shown to be upregulated in HCC tumour models under hypoxic conditions, with elevated SV4 and SV5 levels associated with enhanced cell migration and reorganization of the action cytoskeleton, thus promoting EMT [74]. RhoA/Rock and MAPK/ERK/p38 signalling were identified as companion proteins involved in supervillin-driven

HCC migration and invasion. Perhaps more importantly, ERK/p38 phosphorylation is downstream of RhoA/ROCK activation. Therefore, it could be suggested that supervillain-induced EMT is mainly mediated through the RhoA/ROCK and ERK/p38 pathways. Similar results were reported by Huang et al. (2019) in hepatocellular carcinoma models, where the induction of EMT due to actin cytoskeleton remodelling was controlled by the negative regulation of CAPZA1 (capping actin protein of muscle Z-line alpha subunit 1; Figure 2) [75]. As such, the downregulation of CAPZA1 promoted cell invasion, migration and the induction of EMT. CAPZA1 regulation in actin remodelling was primarily mediated via the interaction between CAPZA1 and phosphatidylinositol (4,5) bisphosphate (PIP2), in which the combination of PIP2 and CAPZA1 would lead to CAPZA1 depletion and a subsequent increase in F-actin levels. The authors reported that levels of PIP2 under hypoxia could be modulated by HIF-1α/RhoA/Rock1 signalling, in which hypoxia treatment led to the increased expression of HIF-1α, RhoA and Rock1, hence resulting in elevated PIP2 levels and subsequent actin cytoskeleton remodelling.

Targeting EMT and Metastatic Progression with Nanoparticle Formulations

As outlined above, the ability of cancer cells to invade local tissue and spread to distant sites is a critical step in disease progression, often accompanied by a poorer clinical prognosis. EMT is the proposed mechanism by which cells acquire the properties necessary for invasion and migration. Intrinsic properties of NPs have the potential to inhibit cancer progression through the regulation of EMT. For example, Arvizao et al. (2013) reported that gold NP (AuNP) treatment can delay tumour metastases through the inhibition of MAPK signalling and EMT reversal. They found that unmodified AuNPs not only downregulated the phosphorylation of MAPK but also reversed EMT by downregulating Snail, N-Cadherin, Vimentin [27]. Polyethylenimine coated superparamagnetic iron NPs (SPIONs) are proven to inhibit tumour cell migration and invasion through the inhibition of Src kinase activity and downregulation of MT1-MMP and MMP2 matrix-metalloproteinases. In addition, SPIONs treatment can downregulate miR-21, upregulating cell migration inhibitors PTEN, PDCD4 and sproutyl-1 [28].

Targeting metastatic signalling pathways involving EMT induction represents another approach for inhibiting metastasis [76]. PEGylated AuNPs combined with cold plasma, were proven to inhibit glioblastoma cell proliferation in vitro by blocking PI3K/Akt signalling (Figure 1). In addition, co-treatment of glioma xenografts suppressed tumour growth and mesenchymal markers expression including N-Cad, Zeb-1 and Slug, while increasing the epithelial cell marker E-cadherin; suggesting a reversal of EMT [31]. The aberrant activation of JAK-STAT signalling confers malignant properties to cancer cells, including EMT induction and malignant progression [77]. Inhibition of JAK-STAT signalling has been shown to reduce cancer proliferation and metastasis. Guo et al. (2019) loaded miR-125-5p into a folate acid coated Fa-polyethyleneglycol (PEG)–g-polyetherimide (PEI) superparamagnetic iron oxide nanocarrier (SPIONs), evaluating its therapeutic effect against hepatocellular carcinoma (HCC). The authors reported that the miR-125-5p loaded nanomedicine effectively inhibited the EMT potential of HCC cells via the inhibition of STAT and the inactivation of Wnt/β-Catenin, inhibiting tumour growth in HCC-bearing mice [29]. Similar work by Huang et al. (2019) demonstrated that silica-coated zinc arsenite NPs (ZnAs@SiO_2 NPs) significantly inhibited the proliferation, migration and invasion of HCC cell lines, attenuating in vivo tumour growth by 2.2-fold in comparison to NP-only control, mediated through the upregulation of SH2-containing protein tyrosine phosphatase 1 (SHP-1) and the corresponding suppression of JAK2/STAT3 signalling [30].

Hypoxia exposure leads to an increase in TWIST expression. Hyaluronic-acid conjugated mesoporous silica nanoparticles (MSN-HAs) loaded with TWIST siRNA successfully suppressed TWIST expression in vitro, subsequently reducing the tumour burden in a model of epithelial ovarian cancer in vivo [33]. Furthermore, amphiphilic polymer-based nanoparticles loaded with siRNAs against SNAIL and TWIST, and used in combination with the chemotherapeutic paclitaxel, inhibited tumour growth and metastasis of the 4T1 breast cancer model in vivo, while siRNA alone exhibited

only modest benefits (Figure 1) [32]. Therefore, co-delivery of EMT targeted molecules loaded on nanoparticles may provide enhanced metastatic inhibition.

2.3. Angiogenesis

Abnormal angiogenesis is a common feature of tumour malignant progression, where rapid growing tumours outstrip oxygen supply, yielding a hypoxic tumour mass. Consequently, hypoxia induces the formation of new blood vessels in an attempt to ameliorate oxygen depletion stress. Hypoxia and HIF-1 expression trigger an imbalance between pro- and anti-angiogenic factors and cytokines modulating gene expression involved in the angiogenetic response [78,79]. This typically includes the activation of angiogenic genes and receptors such as VEGF (vascular endothelial growth factor), PLGF (placental growth factor), PDGFB (platelet-derived factor) and integrins among others (Figure 2) [80]. Integrins, particularly alpha v beta 3 ($\alpha v\beta 3$), have been shown to be upregulated within the TME, expressed on both tumour cells and the vasculature [81]. Hypoxia ($1\%O_2$) has been shown to upregulate αv expression in human microvascular endothelial (HMEC-1) cells in vitro. Furthermore, knockdown of HIF-1α was shown to inhibit hypoxia stimulated β3-integrin expression, suggesting induction of β3-integrin is HIF-dependent [82]. The effect of HIF-1α on the angiogenic potential of small cell lung cancer (SCLC) significantly upregulated the expression of pro-angiogenic genes including VEGF-A, TNFA1P6, PDGFC, FN1, MMP 28 and MMP14 [83]. Myocyte enhancer factor 2D (MEF2D) has also been proven to play a central role in tumour angiogenesis [84]. MEF2D expression positively correlated with colorectal tumour angiogenesis, through the induction of pro-angiogenic factors including PDGF-BB, PDGF-C, PLGF, milk fat globule factor (MFG)-E8, and tumour necrosis factor superfamily member (TNFRSF). Furthermore, it was observed that MEF2D is a downstream effector of HIF-1α transcriptional activity.

As with EMT, exosomal miRNA has also been proven to promote angiogenesis. Matsuura et al. (2019) compared the angiogenic activity of HUVEC cells co-cultured with exosomes derived from hepatocarcinoma cells cultured under variable oxygen tensions [85]. Harvested exosomes collected under hypoxic stress displayed enhanced tubule formation in HUVECs cells, mediated through miR-155 upregulation. Conversely, miR-155 knockdown attenuated tubule formation, implying that exosomal miR-155 regulates angiogenic potential. Similarly, Hsu et al. (2017) demonstrated that exosomal miR-23a derived from lung cancer was significantly upregulated by hypoxia [86]. Exosomal miR-23a suppressed prolyl-hydroxylase 1 and 2 (PHD 1 and 2) and inhibited tight junction protein ZO-1, with the effect of increased vascular permeability and tumour cell transendothelial migration, effects reversed in knockout experiments.

Overcoming Hypoxia-Driven Angiogenesis Using Nanoparticles

Angiogenesis modulating strategies have largely focused on either inhibiting, disrupting or normalising the aberrant tumour vasculature. In this context, nanoparticles are at an advantage as they may exploit the leaky and aberrant vascular architecture of the TME, accumulating within tumour tissue via the enhanced permeability and retention (EPR) effect [87]. Interestingly, gold NPs (AuNPs) have been shown to have intrinsic anti-angiogenic effects in vivo, likely through inhibition of the VEGF/VEGFR2 signalling pathway (Figure 1) [34,88,89]. Evidence from an in vivo melanoma model has shown that AuNPs could normalise tumour vasculature, alleviate tumour hypoxia and reduce metastatic spread to the lungs (20% of AuNP-treated tumour-bearing animals developed metastasis in comparison to 66.7% of control-treated) [35]. However, the anti-angiogenic potential of AuNPs appears to be transient: In a xenograft model of colorectal cancer (CRC), AuNPs treatment reduced vessel density and increased pericyte coverage concomitant with vascular normalization and improvements in tumour hypoxia until day 9 of treatment, after which these improvements were lost [36]. This suggests that AuNPs may provide a therapeutic window of vascular normalisation, in which chemotherapy and radiotherapy could be more effectively utilised.

Of note, only 0.7% of systemically administered nanoparticles reach their intended site of the solid tumour [90]. Furthermore, the "passive targeting" approaches afforded by the EPR effect does not appear to be meaningfully replicated clinically, likely attributed to the considerable heterogeneity of the TME and metabolic differences of pre-clinical tumour models [91]. Therefore, tumour-targeted approaches are required to increase specificity. Integrins have become attractive anti-angiogenic targets given their role in tumour vascularisation [92]. In models of normal angiogenesis, liposome NPs functionalised with the αvβ3-integrin targeting peptide Arg-Gly-Asp (RGD) encapsulating doxorubicin exhibited potent antiangiogenic properties in vivo, inhibiting angiogenesis by up to 70% compared to controls [93]. In pre-clinical models, the co-functionalisation of AuNPs with RGD induced specific vascular damage in pancreatic tumour xenografts when coupled with image-guided radiation therapy [37]. Furthermore, RGD-functionalised AuNPs have also been shown to reduce MDA-MB-231 breast cancer cell invasiveness following radiotherapy in vitro [38]. Functionalisation of nanoparticles with other integrin targeting peptides such as the αvβ1-targeted ATN-161, which has been shown to reduce tumour microvessels by almost 50% in pre-clinical murine models of colon cancer when combined with 5-fluoroucail infusion, may improve vascular targeting and TME anti-angiogenic strategies [94].

2.4. Immunosuppression

A critical event in malignant tumour progression is the ability for tumour cells to acquire immunosuppression. Tumour hypoxia has been reported to promote an immunosuppressive microenvironment by recruiting regulatory T cells (Tregs), myeloid-derived suppressor cells (MDSCs) and tumour associated macrophages (TAMs) [95,96]. Tregs are an important stromal cell population that support tumour progression by immune evasion. Tumour hypoxia has been implicated in promoting the generation and the recruitment of Tregs via the production of TGF-β and chemokine ligand 28 (CCL28) (Figure 2). Treg recruitment and CCL28 expression were shown to be significantly upregulated under hypoxic conditions. In a xenograft model of liver cancer, CCL28 upregulation promoted tumour growth and Treg recruitment in vivo in a HIF-1α dependent manner. While knocking down of CCL28 could reverse hypoxia-induced recruitment, overexpression or knockdown of CCL28 did not pose any effect on colony formation or cell proliferation, indicating that CCL-28 most likely exerts its oncogenic role in a non-cell autonomous manner by recruiting Tregs [97].

Severe hypoxia has been observed in the colon of mice suffering from colitis-associated colon cancer (CAC), accompanied by reduced T cell CD4+ effector cell differentiation and the enhanced activity of suppressive Tregs. Furthermore, downregulation of pro-inflammatory cytokines (IL-2, IL-17, IFN-γ, and IL-9) and upregulation of the anti-inflammatory cytokine IL-10 was detected in CD4+ T cells stimulated under hypoxic conditions. Furthermore, the proportion of IFN-γ producing Th1 cells were significantly decreased under hypoxia. It is interesting to note that there is only a slight expression of PD-1 by CD4+Foxp-T cells in the colon of mice suffering from CAC compared to healthy control mice after stimulation under hypoxia. In contrast, significant upregulation of PD-1 in CD4+Foxp+ Tregs occurred following CAC hypoxic exposure. This indicates that hypoxia enhanced Tregs mediate immunosuppression rather than T-cell exhaustion dominating [98].

MDSCs represent another type of immune suppressor in the TME which has been proven to confer a negative impact on T-cell and NK cells. Hypoxia-promoted secretion of glioma-derived exosomes (GDEs) can be endocytosed by murine MDSCs. These hypoxia stimulated GDEs resulted in an enhanced ability to induce MDSCs activation and expansion compared to normoxic stimulated cells. This effect was mediated by targeting RAR-related orphan receptor alpha (RORA) and phosphatase and tensin homolog (PTEN) via miR-10a and miR-21 in GDEs (Figure 2) [99]. In addition, hypoxia has been reported to stimulate the migration of CD11b+Gr-1+ myeloid cells via the secretion of macrophage migration inhibitory factor (MIF) and interleukin-6 (IL-6) by head and neck squamous carcinoma (HNSCC). HIF-1α/2α dependent MIF and IL-6 regulate the chemotaxis, differentiation and pro-angiogenic function of CD11b+Gr-1+ myeloid cells. This is mediated through the binding of

CD74/CXCR4, CD74/CXCR2 and subsequent activation of MAPK and PI3K/AKT signalling pathways. Knockdown of HIF-1α/2α fails to inhibit the migration of CD11b+Gr-1+ myeloid cells due to the compensatory effect of NF-κB under hypoxic condition, whereas dual blockade of HIF-1α/2α and NF-κB successfully inhibited this effect [100].

Hypoxia also serves as an important driver of MDSCs recruitment. In a model of hepatocellular carcinoma (HCC), HIF-1α upregulated the expression of chemokine (C-C motif) ligand 26 (CCL-26) in cancer cells, recruiting chemokine (C-X3-C motif) receptor 1 (CX3CR1) expressing-MDSCs to primary tumours and promoting HCC tumour growth. Furthermore, inhibition of CCL-26 by the HIF inhibitor digoxin or through the blockade of CX3CR1 using a neutralizing antibody suppressed MDSC recruitment and tumour growth [101]. Hypoxia can also directly promote the accumulation of MDSCs. Upregulation of ectonucleoside triphosphate diphohydrolase (ENTPD2) in HCC cell lines by hypoxia and HIF-1α, contributed to HCC tumour growth and MDSC accumulation. This effect was mediated by the prevention of MDSCs differentiation via the conversion of extracellular ATP to 5'-AMP by ENTPD2. As such, knockdown or inhibition of ENTP2 suppressed tumour growth, enhancing the efficacy of immune checkpoint inhibitors [102].

TAMs are one of the most abundant forms of immune cell populations within the TME, emerging as an important regulator in fostering malignancy, cancer progression and therapeutic resistance [103]. Tumour hypoxia has been proven to enhance TAM recruitment and infiltration via the hypoxia-induced secretion of chemokines (CCL-4, CCL-8,) and metabolites (lipoxygenase metabolites; Figure 2). Hypoxia and secreted macrophage soluble factors promote glioblastoma (GBM) invasiveness, though enhanced matrix metalloproteinase (MMP)-9 activity, promoting CCL4-CCR5 signalling between TAMs and U87 GBM tumour cells [104].

Macrophages can also undergo phenotypic changes and different forms of activation depending on the signal. Typically, classically activated macrophages are stimulated by T helper 1 (Th1) cytokines (TNF-α, IFN-γ) as well as microbial cell wall components. Indeed, the classical M1 macrophage phenotype is known to possess potential antibacterial and anti-inflammatory activity through the secretion of reactive oxygen species and nitrogen intermediates, thereby counteracting cancer progression. An alternative M2 macrophage immunosuppressive phenotype is stimulated by Th2 cytokines (IL-4, IL-13) and other cytokines, which are responsible for blocking Th1 response and promote angiogenesis and cell proliferating. Tumour hypoxia has been indicated to play a pivotal role in the phenotypical control of TAMs [105].

Hypoxia-induced extracellular vesicle (EV) miR-103a from lung cancer cells increased M2-type polarization, mediated by suppressed PTEN activity and the subsequent activation of the PI3/AKT and STAT pathway. Inhibition of miR-103a led to a decrease in hypoxia-induced M2-type polarization, while macrophages treated with EV miR-103a further enhanced cancer progression and tumour angiogenesis [106]. In addition, hypoxic-conditioned medium can push macrophages towards an M2 phenotype, mediated through the upregulation of neuropilin-1 (Nrp-1). Inhibition of Nrp-1 expression with siRNA can reduce the recruitment of macrophages and partially reversed the effect of hypoxia on the induction of the M2 phenotype [107].

Tumour derived exosomes enriched in immunosuppressive proteins including the chemokines/chemoattractant (CSF-1), monocyte chemoattractant protein-1/C-C chemokine 2 (MCP-1/CCL-2), and TGF-β, are also enhanced during hypoxia, leading to the macrophage recruitment and M2-like polarization both in vitro and in vivo [108]. Furthermore, hypoxia-induced exosomes can enhance oxidative phosphorylation in bone marrow. This occurs via the transfer of let-7a miRNA and subsequent suppression of insulin-Akt-mTOR pathway, resulting in the metabolic reprogramming of infiltrating monocytic macrophages. Hypoxia also inhibits T-cell anti-tumour functions through the accumulation of extracellular adenosine, induced through the increased expression of ectonucleotidase CD73 and CD39, both of which are products of HIF target genes [109,110]. Accumulated adenosine in the TME acts as a negative regulator of the anti-tumour T cell response, in which the binding of adenosine to A2AR triggers T-cell apoptosis, contributing to tumour immune evasion [111].

Upregulation of negative immune checkpoint molecule of programmed death ligand (PD-L1) in tumour cells, macrophages and dendritic cells under hypoxia, can initiate the interactions between PD-L1 and cell surface checkpoint receptor programmed cell death-1 (PD-1) expressed on effector T cells, resulting in the increased apoptosis of cytotoxic T lymphocytes (CTLs) and subsequent downregulation of T-cell antitumour reactivity. Increased PD-L1 and HIF target genes (CAIX and GLUT1) expression have been observed in a renal cell carcinoma (RCC) model possessing a VHL mutation. Furthermore, there is almost no PD-L1 expression in the presence of pVHL or absence of HIF-2α, indicating that PD-L1 expression is specifically regulated by the pVHL/HIF-2α axis in RCC [112]. Hypoxia exposure of DU145 and MDA-MB-231 cells led to the upregulation of PD-L1 expression in a HIF-1α dependent manner, where HIF-1α suppression led to a reduction in PD-L1 mRNA and cell surface protein in human prostate and murine melanoma cells. Furthermore, hypoxia induced resistance to CTL-mediated lysis in B16-OVA cells, which was abolished following a knockdown either HIF-1α or PD-L1 [113].

Reprogramming the Immunosuppressive TME with Nanotherapeutics

Immunotherapy has revolutionised cancer treatment. Immune checkpoint inhibitors, including those to PD-1, PD-L1 and CTL antigen 4 (CTLA-4), have now been approved for a number of cancers [114]. However, tumour immune evasion represents a major hurdle for the success of these therapeutics, which is potentiated during hypoxia as detailed above. Targeted approaches which temporally or spatially control the hypoxia-induced immune responses within the TME are essential, given that off-target and adverse effects may occur following manipulation of the immune system [115]. The use of nanotherapeutics as drug delivery approaches are now being considered to specifically modulate the immunosuppressive microenvironment of the tumour while sparing systemic immune modulation to induce an anti-tumour immune response [116].

Given their high plasticity, reprogramming or repolarisation of TAMs from an immunosuppressive M2-like phenotype to an anti-tumourigenic M1-like phenotype is an attractive approach. Furthermore, as these cells readily internalise particles, nanoparticles may be used to deliver agents directly to these cells. β-cyclodextrin nanoparticles loaded with the toll-like receptor (TLR) 7 and 8 agonist R848 were selectively delivered to TAMs in vivo, altering the TME phenotype to that of an M1 (Figure 1). Furthermore, when combined with the immune checkpoint inhibitor anti-PD-1, NPs significantly improved immunotherapy response rates, with complete tumour regression observed in almost 30% of CRC-bearing mice [39]. In another study, TAM reprogramming from an M2 to an M1 phenotype was also performed using baicalin-loaded PLGA nanoparticles containing a TLR 9 agonist and an antigenic peptide (HgP) to activate immune cells and promote anti-tumour immunity. NPs were further entrapped in a galactose-modified erythrocyte coating to increase biocompatibility and TAM targeting, the macrophage galactose-type lectin (MGL; CD301) receptor is expressed on myeloid antigen-presenting cells including macrophages. These biomimetic NPs also suppressed melanoma growth in vivo and increased the infiltration of CD8+ T cells into the TME [40].

Targeting the MDSC compartment may be another approach for improving immune tolerance within the TME. As mentioned above, PI3K signalling is crucial in the functioning of myeloid suppressor cells in response to chemokines, particularly the PI3K-γ isoform. PLGA NPs have been developed to incorporate the PI3K-γ inhibitor IPI-549, and co-functionalised to target the TME with aminoethyl anisamide (AEAA), a ligand for sigma-1 receptor which is overexpressed in a number of tumour types including pancreatic adenocarcinoma. IPI-549 loaded NPs significantly reduced both MDSC and tumour associated B cell proportions in KPC pancreatic tumour-bearing mice while also inhibiting tumour growth in comparison to free-IPI-549 [41]. An alternative approach, to repolarise MDSCs away from an immunosuppressive phenotype, has also been demonstrated in a glioma model in vivo. When combined with radiotherapy, magnetic zinc-doped iron oxide nanoparticles modified with polyethylenimine had the potential to reprogram MDSCs in the TME following intratumoural injection [42].

Lyp-1, a Nrp-1-binding peptide, homes to lymphatics, TAMs and tumour cells, particularly those within hypoxic regions of the tumour [117]. Lyp-1 conjugation has been shown to increase cellular uptake of PEG-PLGA (Poly (lactic-co-glycolic acid)) nanoparticles in lymphatic metastatic tumours in vivo [118]. Of particular interest, Lyp-1 may be used to target Nrp-1 expressing Tregs. Nanoparticles modified with the more potent truncated tLyp-1 peptide reduced immunosuppressive Tregs in the TME of murine B16/BL6 melanoma tumours in vivo, while activating intratumoural CD8+ T cells when combined with an anti-CTLA-4 immunotherapeutic (Figure 1). This approach also enhanced tumour inhibition and survival [43]. Limited infiltration and activation of CTLs, through Treg-mediated suppression, is another characteristic of the immunosuppressive TME. Recently, TME-activated nanoparticles conjugated with antibodies against PD-L1 have been co-loaded with the photosensitiser indocyanine green (ICG). Photodynamic therapy (PDT) combining ICG treatment with near-infrared (NIR) irradiation induced the generation of ROS, promoting intratumoral CTL infiltration. Furthermore, this nanoparticle and NIR combination therapy suppressed tumour growth and lung metastasis in the 4T1 murine mammary cancer model [44]. Interestingly, αvβ3-integrin (discussed in Section 2.3) has been shown to be a regulator of PD-L1, with αvβ3-integrin depleted tumour cells exhibiting reduced PD-L1 expression and increased CD8+ T cell infiltration in vivo. Furthermore, αvβ3-integrin blockade could prime tumours to anti-PD-1 therapy [119]. Therefore, effective functionalisation of nanoparticles to target and subsequently manipulate immune signalling or cells of the TME including Tregs and TAMs, may overcome the hypoxia-driven immunosuppression and also allow greater sensitising to immunotherapeutic strategies.

2.5. Metabolic Reprogramming

Molecular oxygen is a critical component of mitochondrial ATP production. However, tumour cells often forgo oxidative phosphorylation (OXPHOS) in the mitochondria in favour of increased glycolysis, even in the presence of oxygen. This aerobic glycolysis phenomenon in tumour cells is often known as the "Warburg effect", following observations of Otto Warburg in the early twentieth century [120,121]. This metabolic transformation of cells can be enhanced by tumour hypoxia. HIF-1α has been reported to induce multiple changes in gene expression that mediate the switch from OXPHOS to glycolytic metabolism. These include the upregulation of glucose transporter-1 (Glu-1) and key glycolytic enzymes, such as lactate dehydrogenase A (LDHA), phosphoglycerate kinase 1 (PGK-1) and the hexokinase family of proteins (HK-1 and HK-II), resulting in enhanced glycolytic flux in order to meet cellular demands (extensively reviewed in [66]). Interestingly, bone marrow adipocytes have been shown to promote the Warburg effect in metastatic prostate cancer cells [122], which could be reversed following knockdown of HIF-1α. Furthermore, inhibition of HIF-1α hydroxylation and degradation via EV transmission of HIF-1α stabilising long noncoding RNA (HISLA) from TAMs has also been shown to enhance aerobic glycolysis and apoptotic resistance of breast cancer cells [123].

In addition to increasing the glycolytic activity, hypoxia can also suppress the production of mitochondrial ROS by uncoupling glycolysis and OXPHOS via the upregulation of pyruvate dehydrogenase kinase-1 (PDK-1). Hypoxia-induced PDK-1 expression can block the conversion of pyruvate to acetyl-CoA, hereby preventing ATP production via the TCA cycle, attenuating ROS production, which in turn protects cancer cells from hypoxia-induced apoptosis [124]. Hypoxia-induced expression of PDK-1 has also been shown in pancreatic cells to reduce pyruvate dehydrogenase (PDH) activity through phosphorylation of the E1α subunit at serine 232 [125]. More importantly, a clinical cohort of head and neck squamous cell carcinoma biopsies has shown that patients with phosphorylated E1α or expression of PDK-1 tend to experience a poorer clinical outcome.

Hypoxia attenuation of metabolism may also occur through modulating the function of the electron transport chain via the downregulation of cytochrome-c oxidase (COX, complex IV). HIF-1α have been shown to activate the transcription of genes encoding COX4-2 and the mitochondrial protease LON, leading to the degradation of the COX4-1 subunit, aiding in better adaption to hypoxia with reduced ROS production [126]. Hypoxia has also been shown to modulate monocaroboxylate

transport expression (MCT), a group of transmembrane proteins responsible for the regulation of lactate metabolism. Hypoxia-induced MCT-1 plasma membrane expression, both in vitro and in vivo, can promote the glycolytic phenotype of glioblastomas. In addition, inhibition of MCT-1 significantly reduced lactate production, cell proliferation and invasion [127]. Furthermore, HIF-1α knockdown in the SW48 CRC cell line has also been shown to reduce MCT-4 expression in vitro [128], indicating that MCTs could be potentially acted on as therapeutic targets.

Nanotherapeutics to Target or Overcome Metabolic Reprogramming

The metabolic transformation of tumour cells to favour glycolysis over OXPHOS represents a promising therapeutic target that may be exploited by nanoparticles. Among the hexokinase family of proteins, HK-2, which catalyses the phosphorylation of glucose, is frequently overexpressed in tumour cells [129]. As a result, inhibitors to HK-2, including 3-bromopyruvate (3-BP), have been utilised to inhibit glycolysis and subsequently induce cell growth arrest [130]. However, the potential for off-target effects means that clinical applications have been limited. AuNPs targeted to the mitochondria and functionalised with 3-BP were able to suppress tumour cell glycolysis, in addition to reducing mitochondrial OXPHOS in PC3 and DU145 prostate cancer cells in vitro (Figure 1). Furthermore, the anti-cancer potential of these AuNPs was potentiated in tumour cells when combined with laser irradiation in comparison to normal hMSC cells, which displayed no significant toxicity following treatment [45]. MCT-4 is upregulated due to the high rate of glycolysis, which is responsible for lactate/H^+ across the cell membrane and the induction of an acidic tumour microenvironment [131]. Targeting MCT-4 represents another promising approach for modulating glycolysis. For example, Liu et al. (2018) loaded the amorphous iron oxide NPs with siRNA targeting MCT-4 for the treatment of prostate cancer [132]; the author found that significant suppression of MCT-4 expression and enhanced Fenton-like reaction-induced oxidative damages were seen both in vitro and in vivo, leading to a significant inhibition in tumour growth.

An alternative approach to overcome hypoxia-driven metabolic reprogramming within the TME is to alleviate tumour hypoxia by reducing the oxygen consumption (OC) within cells. To this end, a limited number of therapeutics have been identified with the potential to reduce the OC in tumour cells including the anti-malarial atovaquone and the anti-diabetic metformin. Atovaquone has been shown to reduce the OC by more than 80% in a number of tumour cells in vitro, and could abolish hypoxia in xenograft models of head and neck cancer and colon cancer after seven days of treatment, by inhibiting mitochondrial complex III. This was also associated with an improved radiation tumour growth response in vivo (growth delay of 13.2 days between control and atovaquone irradiation groups) [133]. NPs formulations containing atovaquone have previously been developed as long-acting chemoprophylaxis for malaria in pre-clinical models [134], and to improve the bioavailability of the drug [135]. More recently, co-functionalised NPs have been developed encapsulating atovaquone with either the photosensitiser veterporfin or ICG to improve PDT responses in 4T1 mammary tumour-bearing and HeLa cervical adenocarcinoma-bearing animals in vivo, by increasing intratumoural oxygenation resulting in greater anti-tumour effects [46,47].

Conversely, the anti-diabetic metformin has been shown to reduce OC by inhibiting complex I in the mitochondrial electron transport chain, leading to improvements in tumour oxygenation and radiation responses in models of colon cancer in vivo [136]. PEG-PCL (poly(ε-caprolactone)) liposome NPs containing metformin and a photosensitizer (IR780) have also been shown to decrease endogenous OC in gastric cancer cells in vitro and increase ROS generation. In vivo, these co-functionalised NPs could overcome hypoxia and improve PDT and photothermal therapy (PPT) to attenuate tumour growth [48]. Tungsten oxide NPs including $W_{18}O_{49}$ have been used as effective PDT and PPT agents due to their ability to generate ROS and produce heat when combined with NIR laser irradiation [137]. However, this effect may be limited by hypoxia, as such the development of platelet membrane NPs co-loaded with metformin and $W_{18}O_{49}$ have been shown to improve responses to PDT and PPT in vitro

by reducing the OC in tumour cells, and significantly inhibiting tumour growth and increasing TUNEL staining (a measure of tumour apoptosis) in Raji-lymphoma xenografts [49].

3. Conclusions and Future Perspectives

Tumour hypoxia is a critical feature of the TME, contributing to disease progression and resistance to chemo and radiotherapy. The response to tumour hypoxia is mainly driven by oxygen-dependent HIFs that enable tumour progression. However, a complete understanding of the mechanisms driving the response to hypoxia within the TME remains elusive. Hypoxia has effects not only on tumour cells and on the maintenance of CSCs, but also on those cells of the surrounding stroma, driving angiogenesis, malignant progression, immunosuppression and aiding in metabolic reprogramming (Figure 2). Despite the fact that nanotherapeutics hold real potential for targeting these physiological and pathological responses to hypoxia in the TME (summarised in Table 1), most of these hypoxic based nanotherapeutics remain at a preliminary stage of development.

Significant barriers to the translation of NPs include sufficient tumour penetration, stability and potential systemic toxicity. However, meaningful achievements have been made to improve nanomedicine delivery and retention in solid tumours through smart nanoparticle design and TME modification. Development of self-recognition biomimetic nanodelivery systems have shown great potential in increasing the circulation and biocompatibility of nanoparticles within the host organism; this includes coating NPs with an erythrocyte or cancer cell membrane. Alternatively, enhanced tumour penetration could be achieved through the use of circulating monocytes or macrophages [138]. Tumour pre-treatments with radiation therapy or mild hyperthermia represent another promising approach for improving nanoparticle deposition and intratumoural distribution [139]. Furthermore, given that the EPR effect has been shown to be not recapitulated clinically, approaches that improve the distribution of NPs into hypoxic regions of the TME are required. Vascular normalisation or ECM modification is one approach that has been shown to increase the intratumoural accumulation and distribution of nanomedicine in preclinical models, which may also improve tissue oxygenation alleviating hypoxia within the TME [140–142]. However, alternative approaches to improve tissue penetration may be afforded by direct intratumoural administration of NPs.

Future research efforts and clinical translation of nanotherapeutics will require a detailed understanding of the molecular nature of the hypoxic TME to optimise treatment combinations. This approach will undoubtedly facilitate the development of more promising nanotherapeutic platforms for the future treatment of hypoxic tumours that are not only targeted towards tumour cells, but have dual-targeting effects on cells of the TME in addition to augmenting intratumoural oxygenation.

Author Contributions: Conceptualisation, J.F. and J.A.C.; writing—original draft preparation, J.F. and N.M.B., writing and editing, J.F., N.M.B., W.A.J. and J.A.C.

Funding: This research received no external funding.

Conflicts of Interest: The authors declare no conflicts of interest.

References

1. Horsman, M.R.; Vaupel, P. Pathophysiological basis for the formation of the tumor microenvironment. *Front. Oncol.* **2016**, *6*, 66. [CrossRef]
2. Hockel, M.; Vaupel, P. Tumor hypoxia: Definitions and current clinical, biologic, and molecular aspects. *J. Natl. Cancer Inst.* **2001**, *93*, 266–276. [CrossRef] [PubMed]
3. McKeown, S.R. Defining normoxia, physoxia and hypoxia in tumours—Implications for treatment response. *Br. J. Radiol.* **2014**, *87*, 20130676. [CrossRef]
4. Vaupel, P.; Harrison, L. Tumor hypoxia: Causative factors, compensatory mechanisms, and cellular response. *Oncologist* **2004**, *9*, 4–9. [CrossRef] [PubMed]
5. Dewhirst, M.W. Concepts of oxygen transport at the microcirculatory level. In *Seminars in Radiation Oncology*; Elsevier: Amsterdam, The Netherlands, 1998; Volume 8, pp. 143–150.

6. Durand, R.E.; Sham, E. The lifetime of hypoxic human tumor cells. *Int. J. Radiat. Oncol. Biol. Phys.* **1998**, *42*, 711–715. [CrossRef]
7. Dubsky, P.; Sevelda, P.; Jakesz, R.; Hausmaninger, H.; Samonigg, H.; Seifert, M.; Denison, U.; Mlineritsch, B.; Steger, G.; Kwasny, W. Anemia is a significant prognostic factor in local relapse-free survival of premenopausal primary breast cancer patients receiving adjuvant cyclophosphamide/methotrexate/5-fluorouracil chemotherapy. *Clin. Cancer Res.* **2008**, *14*, 2082–2087. [CrossRef] [PubMed]
8. Vaupel, P.; Mayer, A. Hypoxia in cancer: Significance and impact on clinical outcome. *Cancer Metastasis Rev.* **2007**, *26*, 225–239. [CrossRef]
9. Plavetić, D.; Plavetić, N.D.; Barić, M.B.; Bradić, L.B.; Kulić, A.N.A.; Pleština, S. Hypoxia in solid tumors: Biological responses to hypoxia and implications on therapy and prognosis. *Period. Biol.* **2014**, *116*, 361–364.
10. Li, Y.; Patel, S.P.; Roszik, J.; Qin, Y. Hypoxia-driven immunosuppressive metabolites in the tumor microenvironment: New approaches for combinational immunotherapy. *Front. Immunol.* **2018**, *9*, 1591. [CrossRef]
11. Prasad, M.; Lambe, U.P.; Brar, B.; Shah, I.; Manimegalai, J.; Ranjan, K.; Rao, R.; Kumar, S.; Mahant, S.; Khurana, S.K.; et al. Nanotherapeutics: An insight into healthcare and multi-dimensional applications in medical sector of the modern world. *Biomed. Pharmacother.* **2018**, *97*, 1521–1537. [CrossRef]
12. Thakor, A.S.; Jokerst, J.V.; Ghanouni, P.; Campbell, J.L.; Mittra, E.; Gambhir, S.S. Clinically Approved Nanoparticle Imaging Agents. *J. Nucl. Med.* **2016**, *57*, 1833–1837. [CrossRef] [PubMed]
13. Province, P.; Griguer, C.E.; Han, X.; Shaykh, H.F. Hypoxia, angiogenesis and mechanisms for invasion of malignant gliomas. In *Evolution of the Molecular Biology of Brain Tumors and the Therapeutic Implications*; IntechOpen: London, UK, 2013.
14. Qiu, G.-Z.; Jin, M.-Z.; Dai, J.-X.; Sun, W.; Feng, J.-H.; Jin, W.-L. Reprogramming of the tumor in the hypoxic niche: The emerging concept and associated therapeutic strategies. *Trends Pharmacol. Sci.* **2017**, *38*, 669–686. [CrossRef] [PubMed]
15. Ni, M.; Xiong, M.; Zhang, X.; Cai, G.; Chen, H.; Zeng, Q.; Yu, Z. Poly(lactic-co-glycolic acid) nanoparticles conjugated with CD133 aptamers for targeted salinomycin delivery to CD133+ osteosarcoma cancer stem cells. *Int. J. Nanomed.* **2015**, *10*, 2537–2554.
16. Mi, Y.; Huang, Y.; Deng, J. The enhanced delivery of salinomycin to CD133+ ovarian cancer stem cells through CD133 antibody conjugation with poly (lactic-co-glycolic acid)-poly (ethylene glycol) nanoparticles. *Oncol. Lett.* **2018**, *15*, 6611–6621. [CrossRef]
17. Chen, F.; Zeng, Y.; Qi, X.; Chen, Y.; Ge, Z.; Jiang, Z.; Zhang, X.; Dong, Y.; Chen, H.; Yu, Z. Targeted salinomycin delivery with EGFR and CD133 aptamers based dual-ligand lipid-polymer nanoparticles to both osteosarcoma cells and cancer stem cells. *Nanomed. Nanotechnol. Biol. Med.* **2018**, *14*, 2115–2127. [CrossRef]
18. Gui, K.; Zhang, X.; Chen, F.; Ge, Z.; Zhang, S.; Qi, X.; Sun, J.; Yu, Z. Lipid-polymer nanoparticles with CD133 aptamers for targeted delivery of all-trans retinoic acid to osteosarcoma initiating cells. *Biomed. Pharmacother.* **2019**, *111*, 751–764. [CrossRef]
19. Kesharwani, P.; Banerjee, S.; Padhye, S.; Sarkar, F.H.; Iyer, A.K. Hyaluronic acid engineered nanomicelles loaded with 3, 4-difluorobenzylidene curcumin for targeted killing of CD44+ stem-like pancreatic cancer cells. *Biomacromolecules* **2015**, *16*, 3042–3053. [CrossRef]
20. Rao, W.; Wang, H.; Han, J.; Zhao, S.; Dumbleton, J.; Agarwal, P.; Zhang, W.; Zhao, G.; Yu, J.; Zynger, D.L.; et al. Chitosan-decorated doxorubicin-encapsulated nanoparticle targets and eliminates tumor reinitiating cancer stem-like cells. *ACS Nano* **2015**, *9*, 5725–5740. [CrossRef]
21. Gong, Z.; Chen, D.; Xie, F.; Liu, J.; Zhang, H.; Zou, H.; Yu, Y.; Chen, Y.; Sun, Z.; Wang, X.; et al. Codelivery of salinomycin and doxorubicin using nanoliposomes for targeting both liver cancer cells and cancer stem cells. *Nanomedicine* **2016**, *11*, 2565–2579. [CrossRef]
22. Muntimadugu, E.; Kumar, R.; Saladi, S.; Rafeeqi, T.A.; Khan, W. CD44 targeted chemotherapy for co-eradication of breast cancer stem cells and cancer cells using polymeric nanoparticles of salinomycin and paclitaxel. *Colloids Surf. B Biointerfaces* **2016**, *143*, 532–546. [CrossRef]
23. Sun, R.; Liu, Y.; Li, S.-Y.; Shen, S.; Du, X.-J.; Xu, C.-F.; Cao, Z.-T.; Bao, Y.; Zhu, Y.-H.; Li, Y.-P.; et al. Co-delivery of all-trans-retinoic acid and doxorubicin for cancer therapy with synergistic inhibition of cancer stem cells. *Biomaterials* **2015**, *37*, 405–414. [CrossRef] [PubMed]

24. Qi, X.; Yu, D.; Jia, B.; Jin, C.; Liu, X.; Zhao, X.; Zhang, G. Targeting $CD133^{+}$ laryngeal carcinoma cells with chemotherapeutic drugs and siRNA against ABCG2 mediated by thermo/pH-sensitive mesoporous silica nanoparticles. *Tumor Biol.* **2016**, *37*, 2209–2217. [CrossRef] [PubMed]
25. Das, S.; Mukherjee, P.; Chatterjee, R.; Jamal, Z.; Chatterji, U. Enhancing Chemosensitivity of Breast Cancer Stem Cells by Downregulating SOX2 and ABCG2 Using Wedelolactone-encapsulated Nanoparticles. *Mol. Cancer Ther.* **2019**, *18*, 680–692. [CrossRef]
26. Mamaeva, V.; Niemi, R.; Beck, M.; Ozliseli, E.; Desai, D.; Landor, S.; Gronroos, T.; Kronqvist, P.; Pettersen, I.K.; McCormack, E.; et al. Inhibiting Notch Activity in Breast Cancer Stem Cells by Glucose Functionalized Nanoparticles Carrying gamma-secretase Inhibitors. *Mol. Ther.* **2016**, *24*, 926–936. [CrossRef] [PubMed]
27. Arvizo, R.R.; Saha, S.; Wang, E.; Robertson, J.D.; Bhattacharya, R.; Mukherjee, P. Inhibition of tumor growth and metastasis by a self-therapeutic nanoparticle. *Proc. Natl. Acad. Sci. USA* **2013**, *110*, 6700–6705. [CrossRef] [PubMed]
28. Mulens-Arias, V.; Rojas, J.M.; Pérez-Yagüe, S.; del Puerto Morales, M.; Barber, D.F. Polyethylenimine-coated SPION exhibits potential intrinsic anti-metastatic properties inhibiting migration and invasion of pancreatic tumor cells. *J. Control. Release* **2015**, *216*, 78–92. [CrossRef] [PubMed]
29. Guo, R.; Wu, Z.; Wang, J.; Li, Q.; Shen, S.; Wang, W.; Zhou, L.; Wang, W.; Cao, Z.; Guo, Y. Development of a Non-Coding-RNA-based EMT/CSC Inhibitory Nanomedicine for In Vivo Treatment and Monitoring of HCC. *Adv. Sci.* **2019**, *6*, 1801885. [CrossRef]
30. Huang, Y.; Zhou, B.; Luo, H.; Mao, J.; Huang, Y.; Zhang, K.; Mei, C.; Yan, Y.; Jin, H.; Gao, J. ZnAs@ SiO_2 nanoparticles as a potential anti-tumor drug for targeting stemness and epithelial-mesenchymal transition in hepatocellular carcinoma via SHP-1/JAK2/STAT3 signaling. *Theranostics* **2019**, *9*, 4391. [CrossRef]
31. Kaushik, N.K.; Kaushik, N.; Yoo, K.C.; Uddin, N.; Kim, J.S.; Lee, S.J.; Choi, E.H. Low doses of PEG-coated gold nanoparticles sensitize solid tumors to cold plasma by blocking the PI3K/AKT-driven signaling axis to suppress cellular transformation by inhibiting growth and EMT. *Biomaterials* **2016**, *87*, 118–130. [CrossRef]
32. Tang, S.; Yin, Q.; Su, J.; Sun, H.; Meng, Q.; Chen, Y.; Chen, L.; Huang, Y.; Gu, W.; Xu, M.; et al. Inhibition of metastasis and growth of breast cancer by pH-sensitive poly (beta-amino ester) nanoparticles co-delivering two siRNA and paclitaxel. *Biomaterials* **2015**, *48*, 1–15. [CrossRef]
33. Shahin, S.A.; Wang, R.; Simargi, S.I.; Contreras, A.; Parra Echavarria, L.; Qu, L.; Wen, W.; Dellinger, T.; Unternaehrer, J.; Tamanoi, F.; et al. Hyaluronic acid conjugated nanoparticle delivery of siRNA against TWIST reduces tumor burden and enhances sensitivity to cisplatin in ovarian cancer. *Nanomedicine* **2018**, *14*, 1381–1394. [CrossRef] [PubMed]
34. Mukherjee, P.; Bhattacharya, R.; Wang, P.; Wang, L.; Basu, S.; Nagy, J.A.; Atala, A.; Mukhopadhyay, D.; Soker, S. Antiangiogenic properties of gold nanoparticles. *Clin. Cancer Res.* **2005**, *11*, 3530–3534. [CrossRef] [PubMed]
35. Li, W.; Li, X.; Liu, S.; Yang, W.; Pan, F.; Yang, X.Y.; Du, B.; Qin, L.; Pan, Y. Gold nanoparticles attenuate metastasis by tumor vasculature normalization and epithelial-mesenchymal transition inhibition. *Int. J. Nanomed.* **2017**, *12*, 3509–3520. [CrossRef] [PubMed]
36. Pan, F.; Li, W.; Yang, W.; Yang, X.Y.; Liu, S.; Li, X.; Zhao, X.; Ding, H.; Qin, L.; Pan, Y. Anterior gradient 2 as a supervisory marker for tumor vessel normalization induced by anti-angiogenic treatment. *Oncol. Lett.* **2018**, *16*, 3083–3091. [CrossRef] [PubMed]
37. Kunjachan, S.; Detappe, A.; Kumar, R.; Ireland, T.; Cameron, L.; Biancur, D.E.; Motto-Ros, V.; Sancey, L.; Sridhar, S.; Makrigiorgos, G.M.; et al. Nanoparticle mediated tumor vascular disruption: A novel strategy in radiation therapy. *Nano Lett.* **2015**, *15*, 7488–7496. [CrossRef]
38. Wu, P.; Onodera, Y.; Ichikawa, Y.; Rankin, E.B.; Giaccia, A.J.; Watanabe, Y.; Qian, W.; Hashimoto, T.; Shirato, H.; Nam, J.-M. Targeting integrins with RGD-conjugated gold nanoparticles in radiotherapy decreases the invasive activity of breast cancer cells. *Int. J. Nanomed.* **2017**, *12*, 5069–5085. [CrossRef]
39. Rodell, C.B.; Arlauckas, S.P.; Cuccarese, M.F.; Garris, C.S.; Li, R.; Ahmed, M.S.; Kohler, R.H.; Pittet, M.J.; Weissleder, R. TLR7/8-agonist-loaded nanoparticles promote the polarization of tumour-associated macrophages to enhance cancer immunotherapy. *Nat. Biomed. Eng.* **2018**, *2*, 578–588. [CrossRef]
40. Han, S.; Wang, W.; Wang, S.; Wang, S.; Ju, R.; Pan, Z.; Yang, T.; Zhang, G.; Wang, H.; Wang, L. Multifunctional biomimetic nanoparticles loading baicalin for polarizing tumor-associated macrophages. *Nanoscale* **2019**, *11*, 20206–20220. [CrossRef]

41. Zhang, X.; Shen, L.; Liu, Q.; Hou, L.; Huang, L. Inhibiting PI3 kinase-γ in both myeloid and plasma cells remodels the suppressive tumor microenvironment in desmoplastic tumors. *J. Control. Release* **2019**, *309*, 173–180. [CrossRef]
42. Wu, C.; Muroski, M.E.; Miska, J.; Lee-Chang, C.; Shen, Y.; Rashidi, A.; Zhang, P.; Xiao, T.; Han, Y.; Lopez-Rosas, A.; et al. Repolarization of myeloid derived suppressor cells via magnetic nanoparticles to promote radiotherapy for glioma treatment. *Nanomed. Nanotechnol. Biol. Med.* **2019**, *16*, 126–137. [CrossRef]
43. Ou, W.; Thapa, R.K.; Jiang, L.; Soe, Z.C.; Gautam, M.; Chang, J.H.; Jeong, J.H.; Ku, S.K.; Choi, H.G.; Yong, C.S.; et al. Regulatory T cell-targeted hybrid nanoparticles combined with immuno-checkpoint blockage for cancer immunotherapy. *J. Control. Release* **2018**, *281*, 84–96. [CrossRef] [PubMed]
44. Wang, D.; Wang, T.; Yu, H.; Feng, B.; Zhou, L.; Zhou, F.; Hou, B.; Zhang, H.; Luo, M.; Li, Y. Engineering nanoparticles to locally activate T cells in the tumor microenvironment. *Sci. Immunol.* **2019**, *4*, eaau6584. [CrossRef] [PubMed]
45. Marrache, S.; Dhar, S. The energy blocker inside the power house: Mitochondria targeted delivery of 3-bromopyruvate. *Chem. Sci.* **2015**, *6*, 1832–1845. [CrossRef] [PubMed]
46. Fan, Y.; Zhou, T.; Cui, P.; He, Y.; Chang, X.; Xing, L.; Jiang, H. Modulation of Intracellular Oxygen Pressure by Dual-Drug Nanoparticles to Enhance Photodynamic Therapy. *Adv. Funct. Mater.* **2019**, *29*, 1806708. [CrossRef]
47. Xia, D.; Xu, P.; Luo, X.; Zhu, J.; Gu, H.; Huo, D.; Hu, Y. Overcoming Hypoxia by Multistage Nanoparticle Delivery System to Inhibit Mitochondrial Respiration for Photodynamic Therapy. *Adv. Funct. Mater.* **2019**, *29*, 1807294. [CrossRef]
48. Yang, Z.; Wang, J.; Liu, S.; Li, X.; Miao, L.; Yang, B.; Zhang, C.; He, J.; Ai, S.; Guan, W. Defeating relapsed and refractory malignancies through a nano-enabled mitochondria-mediated respiratory inhibition and damage pathway. *Biomaterials* **2019**, *229*, 119580. [CrossRef]
49. Zuo, H.; Tao, J.; Shi, H.; He, J.; Zhou, Z.; Zhang, C. Platelet-mimicking nanoparticles co-loaded with W18O49 and metformin alleviate tumor hypoxia for enhanced photodynamic therapy and photothermal therapy. *Acta Biomater.* **2018**, *80*, 296–307. [CrossRef]
50. Kang, N.; Choi, S.Y.; Kim, B.N.; Yeo, C.D.; Park, C.K.; Kim, Y.K.; Kim, T.-J.; Lee, S.-B.; Lee, S.H.; Park, J.Y.; et al. Hypoxia-induced cancer stemness acquisition is associated with CXCR4 activation by its aberrant promoter demethylation. *BMC Cancer* **2019**, *19*, 148. [CrossRef]
51. Prasad, P.; Mittal, S.A.; Chongtham, J.; Mohanty, S.; Srivastava, T. Hypoxia-Mediated Epigenetic Regulation of Stemness in Brain Tumor Cells. *Stem Cells* **2017**, *35*, 1468–1478. [CrossRef]
52. Zhang, C.; Samanta, D.; Lu, H.; Bullen, J.W.; Zhang, H.; Chen, I.; He, X.; Semenza, G.L. Hypoxia induces the breast cancer stem cell phenotype by HIF-dependent and ALKBH5-mediated m6A-demethylation of NANOG mRNA. *Proc. Natl. Acad. Sci. USA* **2016**, *113*, E2047–E2056. [CrossRef]
53. Li, P.; Zhou, C.; Xu, L.; Xiao, H. Hypoxia enhances stemness of cancer stem cells in glioblastoma: An in vitro study. *Int. J. Med. Sci.* **2013**, *10*, 399. [CrossRef] [PubMed]
54. Wang, P.; Lan, C.; Xiong, S.; Zhao, X.; Shan, Y.; Hu, R.; Wan, W.; Yu, S.; Liao, B.; Li, G.; et al. HIF1α regulates single differentiated glioma cell dedifferentiation to stem-like cell phenotypes with high tumorigenic potential under hypoxia. *Oncotarget* **2017**, *8*, 28074. [PubMed]
55. Jacobsson, H.; Harrison, H.; Hughes, É.; Persson, E.; Rhost, S.; Fitzpatrick, P.; Gustafsson, A.; Andersson, D.; Gregersson, P.; Magnusson, Y.; et al. Hypoxia-induced secretion stimulates breast cancer stem cell regulatory signalling pathways. *Mol. Oncol.* **2019**, *13*, 1693–1705. [CrossRef] [PubMed]
56. Batlle, E.; Clevers, H. Cancer stem cells revisited. *Nat. Med.* **2017**, *23*, 1124–1134. [CrossRef] [PubMed]
57. Asghari, F.; Khademi, R.; Esmaeili Ranjbar, F.; Veisi Malekshahi, Z.; Faridi Majidi, R. Application of Nanotechnology in Targeting of Cancer Stem Cells: A Review. *Int. J. Stem Cells* **2019**, *12*, 227–239. [CrossRef] [PubMed]
58. Nguyen, P.H.; Giraud, J.; Staedel, C.; Chambonnier, L.; Dubus, P.; Chevret, E.; Boeuf, H.; Gauthereau, X.; Rousseau, B.; Fevre, M.; et al. All-trans retinoic acid targets gastric cancer stem cells and inhibits patient-derived gastric carcinoma tumor growth. *Oncogene* **2016**, *35*, 5619–5628. [CrossRef]
59. Kim, D.; Choi, B.H.; Ryoo, I.G.; Kwak, M.K. High NRF2 level mediates cancer stem cell-like properties of aldehyde dehydrogenase (ALDH)-high ovarian cancer cells: Inhibitory role of all-trans retinoic acid in ALDH/NRF2 signaling. *Cell Death Dis.* **2018**, *9*, 896. [CrossRef]

60. Li, Y.; Zhang, T. Targeting cancer stem cells by curcumin and clinical applications. *Cancer Lett.* **2014**, *346*, 197–205. [CrossRef]
61. Fan, X.; Matsui, W.; Khaki, L.; Stearns, D.; Chun, J.; Li, Y.M.; Eberhart, C.G. Notch pathway inhibition depletes stem-like cells and blocks engraftment in embryonal brain tumors. *Cancer Res.* **2006**, *66*, 7445–7452. [CrossRef]
62. Begicevic, R.-R.; Falasca, M. ABC transporters in cancer stem cells: Beyond chemoresistance. *Int. J. Mol. Sci.* **2017**, *18*, 2362. [CrossRef]
63. Muz, B.; de la Puente, P.; Azab, F.; Azab, A.K. The role of hypoxia in cancer progression, angiogenesis, metastasis, and resistance to therapy. *Hypoxia* **2015**, *3*, 83. [CrossRef] [PubMed]
64. Rankin, E.B.; Giaccia, A.J. Hypoxic control of metastasis. *Science* **2016**, *352*, 175–180. [CrossRef] [PubMed]
65. Suarez-Carmona, M.; Lesage, J.; Cataldo, D.; Gilles, C. EMT and inflammation: Inseparable actors of cancer progression. *Mol. Oncol.* **2017**, *11*, 805–823. [CrossRef] [PubMed]
66. Schito, L.; Semenza, G.L. Hypoxia-inducible factors: Master regulators of cancer progression. *Trends Cancer* **2016**, *2*, 758–770. [CrossRef] [PubMed]
67. Shibue, T.; Weinberg, R.A. EMT, CSCs, and drug resistance: The mechanistic link and clinical implications. *Nat. Rev. Clin. Oncol.* **2017**, *14*, 611. [CrossRef] [PubMed]
68. Chen, S.; Chen, J.; Zhang, J.; Chen, H.; Yan, M.; Huang, L.; Tian, Y.; Chen, Y.; Wang, Y. Hypoxia induces TWIST-activated epithelial–mesenchymal transition and proliferation of pancreatic cancer cells in vitro and in nude mice. *Cancer Lett.* **2016**, *383*, 73–84. [CrossRef]
69. Zhang, X.; Sai, B.; Wang, F.; Wang, L.; Wang, Y.; Zheng, L.; Li, G.; Tang, J.; Xiang, J. Hypoxic BMSC-derived exosomal miRNAs promote metastasis of lung cancer cells via STAT3-induced EMT. *Mol. Cancer* **2019**, *18*, 40. [CrossRef]
70. Li, X.; Wu, H.; Wu, M.; Feng, Y.; Wu, S.; Shen, X.; He, J.; Luo, X. Hypoxia-related miR-210-5p and miR-210-3p regulate hypoxia-induced migration and epithelial-mesenchymal transition in hepatoma cells. *Int. J. Clin. Exp. Med.* **2019**, *12*, 5096–5104.
71. Wang, X.; Luo, G.; Zhang, K.; Cao, J.; Huang, C.; Jiang, T.; Liu, B.; Su, L.; Qiu, Z. Hypoxic tumor-derived exosomal miR-301a mediates M2 macrophage polarization via PTEN/PI3Kγ to promote pancreatic cancer metastasis. *Cancer Res.* **2018**, *78*, 4586–4598. [CrossRef]
72. Wang, J.; Cao, Z.; Zhang, X.-M.; Nakamura, M.; Sun, M.; Hartman, J.; Harris, R.A.; Sun, Y.; Cao, Y. Novel mechanism of macrophage-mediated metastasis revealed in a zebrafish model of tumor development. *Cancer Res.* **2015**, *75*, 306–315. [CrossRef]
73. Kaneko, T.; Dehari, H.; Sasaki, T.; Igarashi, T.; Ogi, K.; Okamoto, J.; Kawata, M.; Kobayashi, J.; Miyazaki, A.; Nakamori, K.; et al. Hypoxia-induced epithelial-mesenchymal transition is regulated by phosphorylation of GSK3-β via PI3 K/Akt signaling in oral squamous cell carcinoma. *Oral Surg. Oral Med. Oral Pathol. Oral Radiol.* **2016**, *122*, 719–730. [CrossRef] [PubMed]
74. Chen, X.; Zhang, S.; Wang, Z.; Wang, F.; Cao, X.; Wu, Q.; Zhao, C.; Ma, H.; Ye, F.; Wang, H. Supervillin promotes epithelial-mesenchymal transition and metastasis of hepatocellular carcinoma in hypoxia via activation of the RhoA/ROCK-ERK/p38 pathway. *J. Exp. Clin. Cancer Res.* **2018**, *37*, 128. [CrossRef] [PubMed]
75. Huang, D.; Cao, L.; Xiao, L.; Song, J.; Zhang, Y.; Zheng, P.; Zheng, S. Hypoxia induces actin cytoskeleton remodeling by regulating the binding of CAPZA1 to F-actin via PIP2 to drive EMT in hepatocellular carcinoma. *Cancer Lett.* **2019**, *448*, 117–127. [CrossRef] [PubMed]
76. Gonciar, D.; Mocan, T.; Matea, C.T.; Zdrehus, C.; Mosteanu, O.; Mocan, L.; Pop, T. Nanotechnology in metastatic cancer treatment: Current Achievements and Future Research Trends. *J. Cancer* **2019**, *10*, 1358–1369. [CrossRef] [PubMed]
77. Thomas, S.J.; Snowden, J.A.; Zeidler, M.P.; Danson, S.J. The role of JAK/STAT signalling in the pathogenesis, prognosis and treatment of solid tumours. *Br. J. Cancer* **2015**, *113*, 365. [CrossRef]
78. Rey, S.; Semenza, G.L. Hypoxia-inducible factor-1-dependent mechanisms of vascularization and vascular remodelling. *Cardiovasc. Res.* **2010**, *86*, 236–242. [CrossRef]
79. Yang, Y.; Sun, M.; Wang, L.; Jiao, B. HIFs, angiogenesis, and cancer. *J. Cell. Biochem.* **2013**, *114*, 967–974. [CrossRef]
80. Zimna, A.; Kurpisz, M. Hypoxia-inducible factor-1 in physiological and pathophysiological angiogenesis: Applications and therapies. *BioMed Res. Int.* **2015**, *2015*. [CrossRef]

81. Zheng, D.-Q.; Woodard, A.S.; Fornaro, M.; Tallini, G.; Languino, L.R. Prostatic Carcinoma Cell Migration via αvβ3Integrin Is Modulated by a Focal Adhesion Kinase Pathway. *Cancer Res.* **1999**, *59*, 1655–1664.
82. Befani, C.; Liakos, P. Hypoxia upregulates integrin gene expression in microvascular endothelial cells and promotes their migration and capillary-like tube formation. *Cell Biol. Int.* **2017**, *41*, 769–778. [CrossRef]
83. Wan, J.; Chai, H.; Yu, Z.; Ge, W.; Kang, N.; Xia, W.; Che, Y. HIF-1α effects on angiogenic potential in human small cell lung carcinoma. *J. Exp. Clin. Cancer Res.* **2011**, *30*, 77. [CrossRef] [PubMed]
84. Xiang, J.; Sun, H.; Su, L.; Liu, L.; Shan, J.; Shen, J.; Yang, Z.; Chen, J.; Zhong, X.; Avila, M.A.; et al. Myocyte enhancer factor 2D promotes colorectal cancer angiogenesis downstream of hypoxia-inducible factor 1α. *Cancer Lett.* **2017**, *400*, 117–126. [CrossRef] [PubMed]
85. Matsuura, Y.; Wada, H.; Eguchi, H.; Gotoh, K.; Kobayashi, S.; Kinoshita, M.; Kubo, M.; Hayashi, K.; Iwagami, Y.; Yamada, D.; et al. Exosomal miR-155 Derived from Hepatocellular Carcinoma Cells Under Hypoxia Promotes Angiogenesis in Endothelial Cells. *Dig. Dis. Sci.* **2019**, *64*, 792–802. [CrossRef] [PubMed]
86. Hsu, Y.L.; Hung, J.Y.; Chang, W.A.; Lin, Y.S.; Pan, Y.C.; Tsai, P.H.; Wu, C.Y.; Kuo, P.L. Hypoxic lung cancer-secreted exosomal miR-23a increased angiogenesis and vascular permeability by targeting prolyl hydroxylase and tight junction protein ZO-1. *Oncogene* **2017**, *36*, 4929. [CrossRef]
87. Chen, Q.; Liu, G.; Liu, S.; Su, H.; Wang, Y.; Li, J.; Luo, C. Remodeling the Tumor Microenvironment with Emerging Nanotherapeutics. *Trends Pharm. Sci.* **2018**, *39*, 59–74. [CrossRef]
88. Pan, Y.; Wu, Q.; Qin, L.; Cai, J.; Du, B. Gold nanoparticles inhibit VEGF165-induced migration and tube formation of endothelial cells via the Akt pathway. *BioMed Res. Int.* **2014**, *2014*, 418624. [CrossRef]
89. Darweesh, R.S.; Ayoub, N.M.; Nazzal, S. Gold nanoparticles and angiogenesis: Molecular mechanisms and biomedical applications. *Int. J. Nanomed.* **2019**, *14*, 7643–7663. [CrossRef]
90. Wilhelm, S.; Tavares, A.J.; Dai, Q.; Ohta, S.; Audet, J.; Dvorak, H.F.; Chan, W.C.W. Analysis of nanoparticle delivery to tumours. *Nat. Rev. Mater.* **2016**, *1*, 16014. [CrossRef]
91. Danhier, F. To exploit the tumor microenvironment: Since the EPR effect fails in the clinic, what is the future of nanomedicine? *J. Control. Release* **2016**, *244*, 108–121. [CrossRef]
92. Rocha, L.A.; Learmonth, D.A.; Sousa, R.A.; Salgado, A.J. alphavbeta3 and alpha5beta1 integrin-specific ligands: From tumor angiogenesis inhibitors to vascularization promoters in regenerative medicine? *Biotechnol. Adv.* **2018**, *36*, 208–227. [CrossRef]
93. Murphy, E.A.; Majeti, B.K.; Barnes, L.A.; Makale, M.; Weis, S.M.; Lutu-Fuga, K.; Wrasidlo, W.; Cheresh, D.A. Nanoparticle-mediated drug delivery to tumor vasculature suppresses metastasis. *Proc. Natl. Acad. Sci. USA* **2008**, *105*, 9343–9348. [CrossRef] [PubMed]
94. Stoeltzing, O.; Liu, W.; Reinmuth, N.; Fan, F.; Parry, G.C.; Parikh, A.A.; McCarty, M.F.; Bucana, C.D.; Mazar, A.P.; Ellis, L.M. Inhibition of integrin α5β1 function with a small peptide (ATN-161) plus continuous 5-FU infusion reduces colorectal liver metastases and improves survival in mice. *Int. J. Cancer* **2003**, *104*, 496–503. [CrossRef] [PubMed]
95. Chouaib, S.; Umansky, V.; Kieda, C. The role of hypoxia in shaping the recruitment of proangiogenic and immunosuppressive cells in the tumor microenvironment. *Contemp. Oncol.* **2018**, *22*, 7. [CrossRef] [PubMed]
96. Noman, M.Z.; Hasmim, M.; Messai, Y.; Terry, S.; Kieda, C.; Janji, B.; Chouaib, S. Hypoxia: A key player in antitumor immune response. A review in the theme: Cellular responses to hypoxia. *Am. J. Physiol. Cell Physiol.* **2015**, *309*, C569–C579. [CrossRef]
97. Ren, L.; Yu, Y.; Wang, L.; Zhu, Z.; Lu, R.; Yao, Z. Hypoxia-induced CCL28 promotes recruitment of regulatory T cells and tumor growth in liver cancer. *Oncotarget* **2016**, *7*, 75763. [CrossRef]
98. Westendorf, A.M.; Skibbe, K.; Adamczyk, A.; Buer, J.; Geffers, R.; Hansen, W.; Pastille, E.; Jendrossek, V. Hypoxia enhances immunosuppression by inhibiting CD4+ effector T cell function and promoting Treg activity. *Cell. Physiol. Biochem.* **2017**, *41*, 1271–1284. [CrossRef]
99. Guo, X.; Qiu, W.; Liu, Q.; Qian, M.; Wang, S.; Zhang, Z.; Gao, X.; Chen, Z.; Xue, H.; Li, G. Immunosuppressive effects of hypoxia-induced glioma exosomes through myeloid-derived suppressor cells via the miR-10a/Rora and miR-21/Pten pathways. *Oncogene* **2018**, *37*, 4239. [CrossRef]
100. Zhu, G.; Tang, Y.; Geng, N.; Zheng, M.; Jiang, J.; Li, L.; Li, K.; Lei, Z.; Chen, W.; Fan, Y.; et al. HIF-α/MIF and NF-κB/IL-6 axes contribute to the recruitment of CD11b+ Gr-1+ myeloid cells in hypoxic microenvironment of HNSCC. *Neoplasia* **2014**, *16*, 168. [CrossRef]

101. Chiu, D.K.; Xu, I.M.; Lai, R.K.; Tse, A.P.; Wei, L.L.; Koh, H.; Li, L.L.; Lee, D.; Lo, R.C.; Wong, C.; et al. Hypoxia induces myeloid-derived suppressor cell recruitment to hepatocellular carcinoma through chemokine (C-C motif) ligand 26. *Hepatology* **2016**, *64*, 797–813. [CrossRef]
102. Chiu, D.K.-C.; Tse, A.P.-W.; Xu, I.M.-J.; Di Cui, J.; Lai, R.K.-H.; Li, L.L.; Koh, H.-Y.; Tsang, F.H.-C.; Wei, L.L.; Wong, C.-M.; et al. Hypoxia inducible factor HIF-1 promotes myeloid-derived suppressor cells accumulation through ENTPD2/CD39L1 in hepatocellular carcinoma. *Nat. Commun.* **2017**, *8*, 517. [CrossRef]
103. Yang, L.; Zhang, Y. Tumor-associated macrophages: From basic research to clinical application. *J. Hematol. Oncol.* **2017**, *10*, 58. [CrossRef] [PubMed]
104. Wang, Y.; Liu, T.; Yang, N.; Xu, S.; Li, X.; Wang, D. Hypoxia and macrophages promote glioblastoma invasion by the CCL4-CCR5 axis. *Oncol. Rep.* **2016**, *36*, 3522–3528. [CrossRef] [PubMed]
105. Muraille, E.; Leo, O.; Moser, M. TH1/TH2 paradigm extended: Macrophage polarization as an unappreciated pathogen-driven escape mechanism? *Front. Immunol.* **2014**, *5*, 603. [CrossRef] [PubMed]
106. Hsu, Y.-L.; Hung, J.-Y.; Chang, W.-A.; Jian, S.-F.; Lin, Y.-S.; Pan, Y.-C.; Wu, C.-Y.; Kuo, P.-L. Hypoxic lung-Cancer-derived extracellular vesicle MicroRNA-103a increases the oncogenic effects of macrophages by targeting PTEN. *Mol. Ther.* **2018**, *26*, 568–581. [CrossRef]
107. Chen, X.; Wu, S.; Yan, R.; Fan, L.; Yu, L.; Zhang, Y.; Wei, W.; Zhou, C.; Wu, X.; Zhong, M.; et al. The role of the hypoxia-Nrp-1 axis in the activation of M2-like tumor-associated macrophages in the tumor microenvironment of cervical cancer. *Mol. Carcinog.* **2019**, *58*, 388–397. [CrossRef]
108. Park, J.E.; Dutta, B.; Tse, S.W.; Gupta, N.; Tan, C.F.; Low, J.K.; Yeoh, K.W.; Kon, O.L.; Tam, J.P.; Sze, S.K. Hypoxia-induced tumor exosomes promote M2-like macrophage polarization of infiltrating myeloid cells and microRNA-mediated metabolic shift. *Oncogene* **2019**, *1*, 5158–5173. [CrossRef]
109. Deaglio, S.; Dwyer, K.M.; Gao, W.; Friedman, D.; Usheva, A.; Erat, A.; Chen, J.-F.; Enjyoji, K.; Linden, J.; Oukka, M. Adenosine generation catalyzed by CD39 and CD73 expressed on regulatory T cells mediates immune suppression. *J. Exp. Med.* **2007**, *204*, 1257–1265. [CrossRef]
110. Li, J.; Wang, L.; Chen, X.; Li, L.; Li, Y.; Ping, Y.; Huang, L.; Yue, D.; Zhang, Z.; Wang, F.; et al. CD39/CD73 upregulation on myeloid-derived suppressor cells via TGF-β-mTOR-HIF-1 signaling in patients with non-small cell lung cancer. *Oncoimmunology* **2017**, *6*, e1320011. [CrossRef]
111. Sitkovsky, M.V.; Kjaergaard, J.; Lukashev, D.; Ohta, A. Hypoxia-adenosinergic immunosuppression: Tumor protection by T regulatory cells and cancerous tissue hypoxia. *Clin. Cancer Res.* **2008**, *14*, 5947–5952. [CrossRef]
112. Ruf, M.; Moch, H.; Schraml, P. PD-L1 expression is regulated by hypoxia inducible factor in clear cell renal cell carcinoma. *Int. J. Cancer* **2016**, *139*, 396–403. [CrossRef]
113. Barsoum, I.B.; Smallwood, C.A.; Siemens, D.R.; Graham, C.H. A mechanism of hypoxia-mediated escape from adaptive immunity in cancer cells. *Cancer Res.* **2014**, *74*, 665–674. [CrossRef]
114. Darvin, P.; Toor, S.M.; Sasidharan Nair, V.; Elkord, E. Immune checkpoint inhibitors: Recent progress and potential biomarkers. *Exp. Mol. Med.* **2018**, *50*, 165. [CrossRef]
115. Riley, R.S.; June, C.H.; Langer, R.; Mitchell, M.J. Delivery technologies for cancer immunotherapy. *Nat. Rev. Drug Discov.* **2019**, *18*, 175–196. [CrossRef]
116. Goldberg, M.S. Improving cancer immunotherapy through nanotechnology. *Nat. Rev. Cancer* **2019**, *19*, 587–602. [CrossRef]
117. Laakkonen, P.; Åkerman, M.E.; Biliran, H.; Yang, M.; Ferrer, F.; Karpanen, T.; Hoffman, R.M.; Ruoslahti, E. Antitumor activity of a homing peptide that targets tumor lymphatics and tumor cells. *Proc. Natl. Acad. Sci. USA* **2004**, *101*, 9381–9386. [CrossRef]
118. Luo, G.; Yu, X.; Jin, C.; Yang, F.; Fu, D.; Long, J.; Xu, J.; Zhan, C.; Lu, W. LyP-1-conjugated nanoparticles for targeting drug delivery to lymphatic metastatic tumors. *Int. J. Pharm.* **2010**, *385*, 150–156. [CrossRef]
119. Vannini, A.; Leoni, V.; Barboni, C.; Sanapo, M.; Zaghini, A.; Malatesta, P.; Campadelli-Fiume, G.; Gianni, T. αvβ3-integrin regulates PD-L1 expression and is involved in cancer immune evasion. *Proc. Natl. Acad. Sci. USA* **2019**, *116*, 20141–20150. [CrossRef]

120. Warburg, O.; Wind, F.; Negelein, E. The metabolism of tumors in the body. *J. Gen. Physiol.* **1927**, *8*, 519–530. [CrossRef]
121. Warburg, O. On the origin of cancer cells. *Science* **1956**, *123*, 309–314. [CrossRef]
122. Diedrich, J.D.; Rajagurubandara, E.; Herroon, M.K.; Mahapatra, G.; Hüttemann, M.; Podgorski, I. Bone marrow adipocytes promote the Warburg phenotype in metastatic prostate tumors via HIF-1α activation. *Oncotarget* **2016**, *7*, 64854. [CrossRef]
123. Chen, F.; Chen, J.; Yang, L.; Liu, J.; Zhang, X.; Zhang, Y.; Tu, Q.; Yin, D.; Lin, D.; Wong, P.-P.; et al. Extracellular vesicle-packaged HIF-1α-stabilizing lncRNA from tumour-associated macrophages regulates aerobic glycolysis of breast cancer cells. *Nat. Cell Biol.* **2019**, *21*, 498. [CrossRef]
124. Xie, H.; Simon, M.C. Oxygen availability and metabolic reprogramming in cancer. *J. Biol. Chem.* **2017**, *292*, 16825–16832. [CrossRef]
125. Golias, T.; Papandreou, I.; Sun, R.; Kumar, B.; Brown, N.V.; Swanson, B.J.; Pai, R.; Jaitin, D.; Le, Q.-T.; Teknos, T.N.; et al. Hypoxic repression of pyruvate dehydrogenase activity is necessary for metabolic reprogramming and growth of model tumours. *Sci. Rep.* **2016**, *6*, 31146. [CrossRef] [PubMed]
126. Eales, K.L.; Hollinshead, K.E.R.; Tennant, D.A. Hypoxia and metabolic adaptation of cancer cells. *Oncogenesis* **2016**, *5*, e190. [CrossRef] [PubMed]
127. Miranda-Gonçalves, V.; Granja, S.; Martinho, O.; Honavar, M.; Pojo, M.; Costa, B.M.; Pires, M.M.; Pinheiro, C.; Cordeiro, M.; Bebiano, G.; et al. Hypoxia-mediated upregulation of MCT1 expression supports the glycolytic phenotype of glioblastomas. *Oncotarget* **2016**, *7*, 46335. [CrossRef] [PubMed]
128. Kim, H.K.; Lee, I.; Bang, H.; Kim, H.C.; Lee, W.Y.; Yun, S.H.; Lee, J.; Lee, S.J.; Park, Y.S.; Kim, K.-M. MCT4 expression is a potential therapeutic target in colorectal cancer with peritoneal carcinomatosis. *Mol. Cancer Ther.* **2018**, *17*, 838–848. [CrossRef]
129. Shinohara, Y.; Yamamoto, K.; Kogure, K.; Ichihara, J.; Terada, H. Steady state transcript levels of the type II hexokinase and type 1 glucose transporter in human tumor cell lines. *Cancer Lett.* **1994**, *82*, 27–32. [CrossRef]
130. Fan, T.; Sun, G.; Sun, X.; Zhao, L.; Zhong, R.; Peng, Y. Tumor energy metabolism and potential of 3-Bromopyruvate as an inhibitor of aerobic glycolysis: Implications in tumor treatment. *Cancers* **2019**, *11*, 317. [CrossRef]
131. Halestrap, A.P. Monocarboxylic acid transport. *Compr. Physiol.* **2011**, *3*, 1611–1643.
132. Liu, Y.; Ji, X.; Tong, W.W.L.; Askhatova, D.; Yang, T.; Cheng, H.; Wang, Y.; Shi, J. Engineering multifunctional RNAi nanomedicine to concurrently target cancer hallmarks for combinatorial therapy. *Angew. Chem. Int. Ed.* **2018**, *57*, 1510–1513. [CrossRef]
133. Ashton, T.M.; Fokas, E.; Kunz-Schughart, L.A.; Folkes, L.K.; Anbalagan, S.; Huether, M.; Kelly, C.J.; Pirovano, G.; Buffa, F.M.; Hammond, E.M.; et al. The anti-malarial atovaquone increases radiosensitivity by alleviating tumour hypoxia. *Nat. Commun.* **2016**, *7*, 12308. [CrossRef]
134. Bakshi, R.P.; Tatham, L.M.; Savage, A.C.; Tripathi, A.K.; Mlambo, G.; Ippolito, M.M.; Nenortas, E.; Rannard, S.P.; Owen, A.; Shapiro, T.A. Long-acting injectable atovaquone nanomedicines for malaria prophylaxis. *Nat. Commun.* **2018**, *9*, 315. [CrossRef]
135. Calvo, J.; Lavandera, J.L.; Agüeros, M.; Irache, J.M. Cyclodextrin/poly (anhydride) nanoparticles as drug carriers for the oral delivery of atovaquone. *Biomed. Microdevices* **2011**, *13*, 1015–1025. [CrossRef]
136. Zannella, V.E.; Dal Pra, A.; Muaddi, H.; McKee, T.D.; Stapleton, S.; Sykes, J.; Glicksman, R.; Chaib, S.; Zamiara, P.; Milosevic, M. Reprogramming metabolism with metformin improves tumor oxygenation and radiotherapy response. *Clin. Cancer Res.* **2013**, *19*, 6741–6750. [CrossRef]
137. Qiu, J.; Xiao, Q.; Zheng, X.; Zhang, L.; Xing, H.; Ni, D.; Liu, Y.; Zhang, S.; Ren, Q.; Hua, Y.; et al. Single W18O49 nanowires: A multifunctional nanoplatform for computed tomography imaging and photothermal/photodynamic/radiation synergistic cancer therapy. *Nano Res.* **2015**, *8*, 3580–3590. [CrossRef]
138. Si, J.; Shao, S.; Shen, Y.; Wang, K. Macrophages as active nanocarriers for targeted early and adjuvant cancer chemotherapy. *Small* **2016**, *12*, 5108–5119. [CrossRef]
139. Overchuk, M.; Zheng, G. Overcoming obstacles in the tumor microenvironment: Recent advancements in nanoparticle delivery for cancer theranostics. *Biomaterials* **2018**, *156*, 217–237. [CrossRef]
140. Li, W.; Quan, Y.-Y.; Li, Y.; Lu, L.; Cui, M. Monitoring of tumor vascular normalization: The key points from basic research to clinical application. *Cancer Manag. Res.* **2018**, *10*, 4163. [CrossRef]

141. Chen, Y.; Liu, X.; Yuan, H.; Yang, Z.; von Roemeling, C.A.; Qie, Y.; Zhao, H.; Wang, Y.; Jiang, W.; Kim, B.Y.S. Therapeutic Remodeling of the Tumor Microenvironment Enhances Nanoparticle Delivery. *Adv. Sci.* **2019**, *6*, 1802070. [CrossRef]
142. Zhang, B.; Hu, Y.; Pang, Z. Modulating the tumor microenvironment to enhance tumor nanomedicine delivery. *Front. Pharmacol.* **2017**, *8*, 952. [CrossRef]

cancers

MDPI

Review

Engineered Extracellular Vesicles as a Reliable Tool in Cancer Nanomedicine

Francesca Susa †, Tania Limongi †, Bianca Dumontel, Veronica Vighetto and Valentina Cauda *

Department of Applied Science and Technology, Politecnico di Torino, Corso Duca degli Abruzzi 24, 10129 Turin, Italy; francesca.susa@polito.it (F.S.); tania.limongi@polito.it (T.L.); bianca.dumontel@polito.it (B.D.); veronica.vighetto@polito.it (V.V.)

* Correspondence: valentina.cauda@polito.it

† Equal contribution.

Received: 14 November 2019; Accepted: 4 December 2019; Published: 9 December 2019

Abstract: Fast diagnosis and more efficient therapies for cancer surely represent one of the huge tasks for the worldwide researchers' and clinicians' community. In the last two decades, our understanding of the biology and molecular pathology of cancer mechanisms, coupled with the continuous development of the material science and technological compounds, have successfully improved nanomedicine applications in oncology. This review argues on nanomedicine application of engineered extracellular vesicles (EVs) in oncology. All the most innovative processes of EVs engineering are discussed together with the related degree of applicability for each one of them in cancer nanomedicines.

Keywords: extracellular vesicles; exosomes; chemico-physical functionalization; loading; cancer; nanomedicine; translational medicine; nanotechnology: bioengineering

1. Introduction

The latest literature reports underline that extracellular vesicles (EVs), released by prokaryotic and eukaryotes cells into the extracellular surroundings, are the main drivers of the intracellular communication, not only in physiological but also under pathological conditions [1–9].

The International Society for Extracellular Vesicles (ISEV) defines EVs generally as lipid bilayer-delimited particles released from cells and unable to replicate [10]. Agreement has not yet been reached on the specific markers for defining EVs subtypes, such as exosomes and ectosomes, originated from the endosome and the plasma membrane, respectively. Researchers are advised to contemplate the use of operational terms for EV subtype definition, referring to EVs' physical characteristics such as size (<100 nm for "small EVs", and > 200 nm for "medium/large EVs"), density, biochemical composition (tetraspanin/Annexin presence, etc.) and reference to condition or tissue/cell biogenesis (podocyte EVs, cardiosomes and prosatosomes, large oncosomes, apoptotic bodies) [10–12]. More in general, referring to their dimension and biogenesis' mechanisms, EVs can be grouped into three broad categories: apoptotic bodies, ectosomes and exosomes [13,14].

Apoptotic bodies (ApoBDs) are typically 1–5 μm EVs released as cells' blebs during the apoptotic process. They contain cytoplasm, organelles and often also nuclear fragment, lipids, proteins [15] and a high amounts of phosphatidylserine [16].

Ectosomes and exosomes formation rests on confined microdomains assembled in the plasma membrane for ectosomes and in the endocytic membrane system for exosomes [17]. Ectosomes (100–500 nm diameter) are larger than exosomes (30–150 nm diameter) and both their cargoes and membranes composition partially differ from each other. Exosomes originate from the endosomal compartment inside multivesicular bodies and they are released by the fusion with the plasma membrane. Exosomes' membranes are rich in tetraspanins (CD9, CD63, CD81, CD82 and CD151) [18],

sphingomyelin, cholesterol [19] and adhesion molecule (ICAM-1), while the ectosomes' ones are characterized by plentiful of glycoproteins, receptors and metallo proteinases [17,20].

Oncosomes are exceptionally large ectosomes, typical of advanced cancers containing active molecules involved in the metabolic pathways promoting tumoral cell survival and growth [21].

Starting from the key role that the tumor microenvironment plays in cancer establishment and progression, it is easy to understand how the EVs have an active part in influencing processes as pre-metastatic niche development, oncogenic transfer, and immune modulation [22,23].

Tumor-derived EVs, by carrying chemokines, are able to induce white blood cells' chemotactic response [24]. Tumor-derived exosomes promote inflammation compromising natural immunity and reprogramming T cells [25], while ApoBDs join in the horizontal oncogenes transfer thanks to the nuclear material that comes out from the dying cells by which they were produced [26].

Since EVs have an active role in the tumoral intercellular communication and signal transduction systems, it spontaneously comes out to consider their applications as biomarkers and therapeutic agents in oncology.

It actually results very interesting to observe how an advanced Web of Science search (carried out on the 26th September 2019 at the all databases level) for the terms 'extracellular vesicles cancer' and 'extracellular vesicles cancer nanomedicine' has clearly shown an incredible increase in the number of publications in the last five years (Figure 1). A further more detailed analysis was carried out on these results and considered the percentages of the papers' distribution in the various research areas. It revealed that, by adding the term 'nanomedicine' to the query, the percentage of papers in the section 'Science technology other topics' increases from the 25% to the 85%, thus demonstrating the current interdisciplinary research trend of this topic.

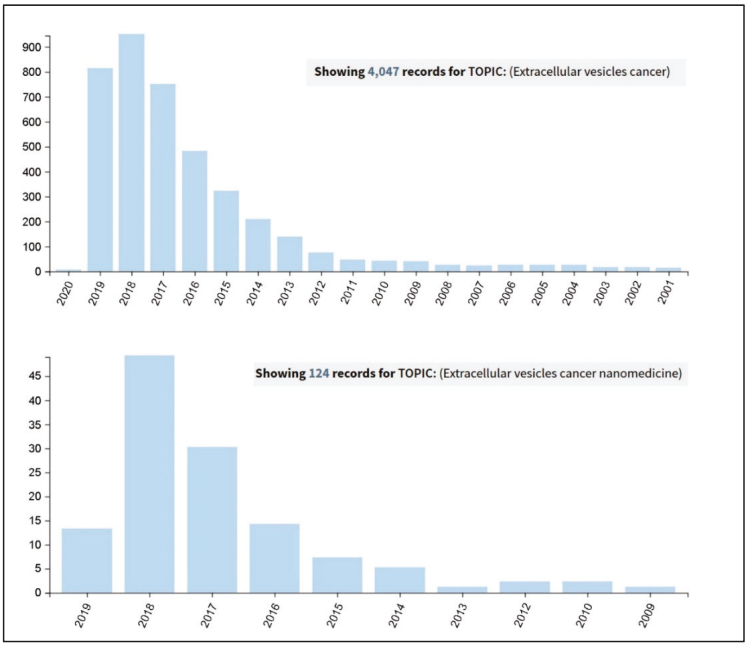

Figure 1. Results coming out from a Web of Science search carried out on the 26th September 2019, at the all databases level, for the terms 'extracellular vesicles cancer' (upper panel) and 'extracellular vesicles cancer nanomedicine' (lower panel).

Current trends refer to EVs as successfully non-invasive diagnostic and prognostic biomarkers: actually their membrane proteins, their lipid fingerprint (reflecting the protein and lipidic content of the parent cells at the moment of their formation) and micro RNA load can be easily screened in blood, urine and in other biological fluids [20,26,27].

Regarding EVs' application as cancer therapeutics, it basically differs from conventional approaches, i.e., molecular targeting drugs and chemotherapy. Referring to native EVs, a huge number of in vivo and in vitro studies have been reported [28–34]. In details, three main approaches in cancer treatment through native EVs can be identified: the inhibition of EVs production [35–37], the eradication of circulating EVs, and finally the reduction of EV uptake [38,39].

EVs are usually biocompatible, low immunogenic and non-cytotoxic, with a high loading ability, long life span in circulation and the capacity to cross barriers, i.e., the cytoplasmic and the blood brain barriers, making them suitable for drug delivery applications [40,41]. Furthermore, EVs are internalized 10 times more than liposomes of similar size in cancer cells, showing a higher specificity towards tumoral cells [42] and, thanks to their dimensions, they can also exploit the enhanced retention and permeability effect to accumulate in the cancerous tissues and reach easily the bulk of a solid tumor [43]. The research on EVs is making great strides in cancer medicine and there are already 136 clinical trials on exosomes and 36 on EVs listed on "www.clinicaltrials.gov" both for therapy and diagnosis. Given these premises, EVs can be considered promising tools for the development of new engineered devices for therapeutic and diagnostic applications. Starting from scalable, reproducible and well standardized EVs isolation procedures, it is possible to obtain highly purified products ready for further microscopic, immunological characterizations or for cryopreservation treatments able to guarantee the stability and integrity necessary for long-term storage or subsequent modifications. Otherwise, these modifications can be carried out directly by engineering the parent cells before the isolation, to obtain already loaded or functionalized EVs (Figure 2).

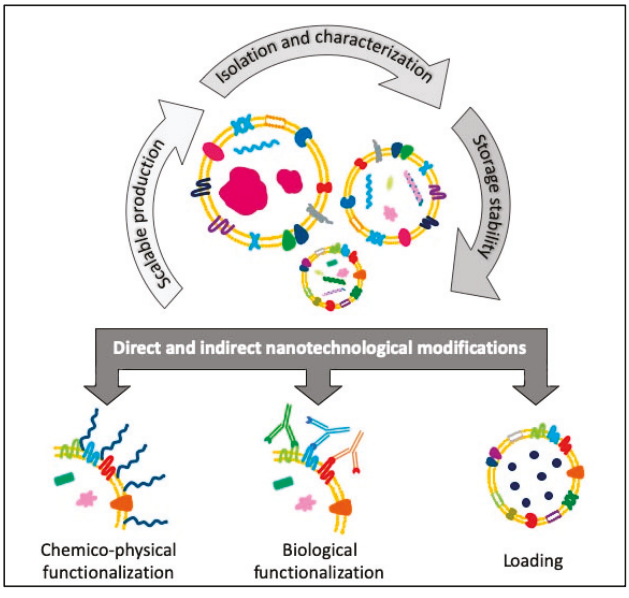

Figure 2. Schematic view of the flow of the different steps concerning the direct and indirect engineering of extracellular vesicles (EVs) for cancer diagnosis and therapy applications.

In this review we summarize the last studies about the direct and indirect engineering of EVs. The first one takes place immediately after the isolation or thawing steps, by means of membrane

permeabilization, surface functionalization or loading strategy. The second engineering method, i.e., the indirect one, happens when the engineering process is applied through molecular or genetic strategies on the parent cell that will secrete the vesicles.

2. EVs' Post Isolation Direct Engineering

2.1. Chemico-Physical Functionalization

Post-isolation modification techniques, enabling the functionalization of the EVs surface with specific moieties, improve their targeting abilities and biodistribution, allowing their in vivo and in vitro tracking.

The methods for the direct engineering of EVs surfaces can be essentially divided in covalent and non-covalent chemical modifications. In the first case, chemical reactions are performed between functionalizing molecules or chemical linker and the amine groups, which are reactive functional units widely expressed on exosomes' surfaces [44]. Even if EVs, as non-living entities, have major advantages with respect to cells regarding reagents and reaction conditions, these must be carefully controlled and optimized in order to avoid vesicles disruption, denaturation and aggregation due to the use of inappropriate temperature, pressure, and/or osmolarity [16].

The non-covalent approaches, instead, refer to membrane modifications by milder reactions, based on electrostatic interactions and receptor-ligand binding as well as lipid-conjugated compounds post-insertion into the EVs' lipid bilayer [44].

Fluorescent and magnetic labeling represent a couple of the main results of the research on EV surface modifications [44]. In fact, tracing the cellular trafficking of autologous exosomes or their biodistribution and pharmacokinetics is essential to investigate their possible diagnostic and therapeutic applications [45].

EVs can be efficiently labelled after their isolation with organic fluorescent dyes. This class of dyes is widely used for in vivo and in vitro imaging [45] and includes a variety of fluorophore-conjugates. These are able to selectively interact with different components of EVs, like RNA and DNA contained inside them [46] or directly with their lipid bilayer [47,48] or with the amine groups of surface proteins by covalent bonds [49].

Click-chemistry is successfully used for the functionalization of exosomes with fluorescent, radioactive and magnetic resonance imaging (MRI) agents for precise in vivo exosomes tracking [50]. In particular, exosomes are chemically modified with terminal alkyne groups by cross-linking the amine groups of exosomal membrane and the carboxyl group of 4-pentynoic acid using carbodiimide activation. In a second step, the inserted alkyne terminal groups are reacted with azide-fluor 545 to form a triazole linkage, according to the typical click-chemistry reaction [51]. In this way the number of cross-linked alkyne groups is controlled in order to avoid the overmodification of exosomal membrane proteins. With a standard calibration curve, it is estimated that approximately 1.5 alkyne modifications are made for every 150 kDa of exosomal protein [50], ensuring the preservation of size of exosomes and their capability of interaction with recipient cells.

The modification with polyethylene glycol (PEG) is a common approach used to prevent opsonization and extend the circulation half-life of liposomes and synthetic nanoparticles (NPs), it has also been successfully transferred to EVs. PEGylation of EVs results in a significant increase in circulation time after intravenous injection in mice, from 10 min for unmodified EVs to 60 min or even 240 min for PEG-functionalized exosomes. The decoration of EVs membrane is obtained, at 40 °C, by a post-insertion mechanism, combining PEG-phospholipids micelles (i.e., 1,2-dimyristoyl-sn-glycero-3-phosphoethanolamine (DMPE)-PEG) with EVs extracted from mouse neuroblastoma cells, maximizing the moieties incorporation while preserving EVs characteristics [52].

While opportunely minimizing the recognition by mononuclear phagocytic system, the PEG corona strongly reduces the EVs-cell interaction in vitro [52]. The further functionalization of distal end of PEG chain with appropriate targeting ligands, as already described for synthetic particles [53], can

easily overcome this drawback and create a promising tool for drug delivery with stealth properties and targeting abilities. A very recent study [54] described how modify EVs' surface with the active targeting ligand mannose. Exosomes' surface was successfully modified with PEG, avoiding particle aggregation, through the incorporation of 1,2-distearoyl-sn-glycero-3-phosphoethanolamine (DSPE) into the lipid layer of the exosome. For targeting purposes, the PEG's distal end, functionalized with amine groups, was further conjugated with mannose-isothiocyanate, guaranteeing a better accumulation of functional exosomes in lymph-nodes [54].

Exosomes loaded with paclitaxel (PTX) are modified with aminoethyl anisamide-polyethylene glycol (AA-PEG) as targeting ligand toward sigma receptor, overexpressed by lung cancer cells [55]. The AA-PEG complex has been inserted in exosomal membrane conjugated with DSPE lipid by using a process that includes sonication and incubation steps, already developed by the same laboratory for the drug loading [56]. The in vitro and in vivo uptake tests, confirmed that AA-PEG exosomes are taken up in much higher quantities than non-vectorized ones. Furthermore, the in vitro uptake of PEGylated exosomes without targeting moiety is lower than that of unmodified exosomes, probably due to the PEG chains blocking interaction of exosomal surface proteins [55].

The same principle of post-insertion of a lipid linked with a molecule able to provide a conjugation site for targeting ligands is used to functionalize exosomes membranes with folate and two RNA aptamers, specific for typical cancer receptors (i.e., prostate-specific membrane antigen (PSMA) RNA aptamer, and epidermal growth-factor receptor (EGFR) RNA aptamer) [57]. A cholesterol-triethylene glycol (TEG) is conjugated with the engineered packaging RNA-three-ways junction (pRNA-3WJ), exploiting the spontaneous insertion of the cholesterol via its hydrophobic moiety into the lipidic bilayer and thus able to anchor the 3WJ into the EVs membrane. The particular spatial conformation of the conjugate, with the cholesterol specifically placed on the arrow tail of the 3WJ, prevented the RNA ligand from trafficking into the EVs, ensuring an oriented surface display of targeting ligands for cancer receptor binding [57].

Enhancement of exosomes' therapeutic ability has been also obtained by an electrostatic interaction of original exosomes and cationized pullulan [58]. Nakase et al. used cationic lipids to increase the exosomal surface charge and help the interaction between EVs and target cells [59]. The membrane charge modification is obtained by the use of lipofectamine (LTX), a commercially available transfection reagent containing cationic lipids, which adsorbs on the exosomes surface and can help the interaction with negatively charged cells surface. The positive charge conferred from cationic lipids is also exploited to functionalize the exosomes surface with a negative charged pH-sensitive fusogenic peptide, GALA, able to guarantee an effective intracellular fusion of exosomal and endosomal membranes and the subsequent cytosolic release of the exosomal contents [60], fundamental for efficient therapeutic applications. This double membrane functionalization, based on electrostatic interactions and GALA peptide, provides an enhanced cellular uptake and the cytosolic release of artificially encapsulated cargo in the treatment of cancerous Hela cells in vitro [59].

It is well known that glycosylation has an important role in different biological function of EVs, like in the cargo proteins recruitment [61] and in the cellular recognition and uptake [62]. Recent glycomic analyses [63], performed by lectin microarray technology on EVs derived from different biological sources, reveal both enrichment and exclusion of glycan epitopes with respect to the membranes of their parental cells. In general lectin analyses reveal that EVs are enriched in high mannose, complex N-linked glycan, poly N-acetyllactosamine epitopes and in α-2,6 sialic acid [63], which is certainly involved in exosomes-cells interaction, thanks to sialic acid-recognizing lectins present on cell surfaces [64].

Furthermore, alteration in glycosylation pattern has been associated with different pathologies, including cancer [65], in which glycan changes took a variety of forms, i.e., loss or excessive expression of certain glycans, increased expression of incomplete or truncated glycans and, less commonly, appearance of novel glycans [66]. These changes are non-random, but closely correlated with malignant

transformation and progression [66], making glycan structures valuable targets for anti-tumoral diagnostic and therapeutic strategies.

Direct manipulation of glycosylation could be used to modify the surface of EVs in order to obtain enhanced delivery or specific targeting to selected tissues for therapeutic purposes. In a recent study, modified EVs are produced by treating them with an enzyme (neuraminidase) able to digest the glycoproteins' terminal sialic acid residues [67]. The glycosidase treatment produces different in vivo biodistribution, causing for example a better accumulation in axillary lymph nodes of modified EVs compared to untreated ones, suggesting their valuable application as drug carriers when the lymphatic system is targeted [67].

A similar enzymatic treatment with a pan-sialic acid hydrolase is performed to reduce the expression of immune inhibitory sialic acids on glioblastoma-derived EVs [68]. Lectin-binding analyses confirmed that surface glycoconjugates of glioblastoma-derived EVs are dominated by immune inhibitory sialic acid-capped N-glycans and complex bi-antennary glycans [69].

Thus, manipulation of surface glycosylation combined with the insertion of a high affinity ligand for DC-specific ICAM-3-grabbing non-integrin (DC-SIGN) receptor leads to an enhanced internalization of glioblastoma-derived EVs in dendritic cells for the triggering of an efficient anti-tumor immune response [68].

Another valuable application of protein glycoengineering could be found in the stabilization of targeting peptides fused to exosomal membrane protein. It was demonstrated that peptides expressed on the N-terminus of lysosome-associated membrane glycoprotein 2b (Lamp2b) could be degraded during exosomes biogenesis by endosomal proteases [70]. The inclusion of a glycosylation motif to the N-terminus of the fusion protein efficiently protects the targeting peptide from proteolysis, enhancing its expression in exosomes membrane while preserving the peptide-target interactions [70].

Other post-isolation functionalization techniques involve biological molecules as receptors or antigens. A33 antigen has been proven to be overexpressed in colorectal cancer cells, demonstrating to be a novel target as immunotherapeutic agent for cancer therapy even in clinical trials (NCT00003360, NCT00199862 and NCT00291486). EVs isolated from colorectal cancer cell line present the A33 antigen on their surface. These EVs are loaded with doxorubicin and functionalized with superparamagnetic iron oxide nanoparticles (SPIONs) coated with high-density A33 antibodies, forming a complex with antitumor activity towards colorectal cancer with reduced systemic toxicity [71].

EVs have been post-extraction engineered also for the treatment of glioblastoma multiforme. Methotrexate-loaded EVs were functionalized with the pro-apoptotic peptide KLA, and the targeted peptide, low-density lipoprotein (LDL), to target the LDL receptor overexpressed on the blood brain barrier and glioblastoma cells [72]. A summary of the post-extraction chemico-physical modifications of EVs is presented in Table 1.

Table 1. EVs' post isolation engineering: direct chemico-physical functionalizations.

EVs Type	Nanotechnological Modification	Application	Reference
Exosomes from 4T1, MCF-7 and PC3 cells	Labeling with DiR [a]	In vivo fluorescence imaging of tumor-derived exosomes	[47]
Exosomes from 4T1 cells	Surface conjugation with azide-fluor545 by click chemistry	In vitro fluorescence imaging	[50]
Exosomes from PC12 cells	Labeling of exosomes proteins with TAMRA-NHS [b]	In vitro fluorescence imaging	[49]
Exosomes from fetal bovine serum	PEGylation by post-insertion of DSPE-PEG-mannose or chemical conjugation of NHS-PEG	Stealth and targeted Exosomes for elevated uptake in DCs	[54]
Exosomes from embryonic stem cells	DSPE-PEG-c(RGDyK)	Targeting glioblastoma, lung cancer and prostate cancer cells	[73]
Exosomes from RAW 264.7 cells	Post-insertion of DSPE-PEG-AA	Stealth and targeted exosomes for the in vitro and in vivo treatment of lung cancer	[55]
EVs from Neuro2A cells	Post-insertion of DMPE-PEG-EGa1 nanobody	Stealth and targeted EVs for the in vitro and in vivo treatment of cancer cells	[52]
EVs from HEK 293T cells	Post-insertion of cholesterolTEG-pRNA3WJ-targeting ligands	Targeted EVs for the in vivo treatment of breast, prostate and colorectal cancer	[57]
Exosomes from MSCs	Chemical functionalization with cationized pullulan	Targeted exosomes for the in vitro and in vivo treatment of liver injury	[74]
EVs from MLP29 cells	Modification of EVs surface glycosylation by neuraminidase	Modification of EVs glycosylation for altered in vivo biodistribution	[67]
EVs from U87 and GBM8 cells	Enzymatic modification of EVs surface glycosylation and insertion of targeting ligand to DC-SIGN	Modification of EVs glycosylation and insertion of targeting ligand for improved uptake in DCs	[68]
Exosomes from Hela cells	Hexadecaarginine (R16) peptide, an arginine-rich cell-penetrating peptide	Activation of the macropinocytosis pathway, affecting cellular uptake of EVs	[75]
Exosomes from HeLa cells	Modification with LTX and GALA peptide via electrostatic interactions	Charge modified exosomes for enhanced cellular uptake and in vitro cytosolic release	[59]
Exosomes from transfected HEK 293T	Glycosylation of targeting-peptide-Lamp2b fusion proteins	Stabilization of targeting peptide-Lamp2b fusion protein with glycosylation motif	[70]
Exosomes from human colorectal carcinoma	Fe_3O_4 Superparamagnetic nanoparticles with high density A33 antibody	Antiproliferative effect in colorectal cancer	[71]
Extracellular vesicles from fibroblasts	Apoptotic peptide Lys-Leu-Ala (KLA) or LDL	Extravasation across BBB and target glioblastoma multiforme	[72]
Exosomes from bovine milk	Folic acid	Human lung and breast cancer reduction	[41]
Plasma membrane vesicles	Bond of the EGF ligand to the transmembrane domain of transferrin receptor	Target EGFR-expressing cancers	[76]
Exosomes-like nanoparticles from grapefruit	Inflammatory related receptor enriched membranes of activated leukocytes	Target inflammatory tumor tissues	[77]

Acronym legend: [a] DiR: DiIC18(7) (1,1′-dioctadecyl-3,3,3′,3′-tetramethylindotricarbocyanine Iodide); [b] TAMRA-NHS: carboxytetramethylrhodamine succinimidyl ester.

2.2. *Loading Nanotechnological Modification into EVs*

EVs can be successfully engineered acting as vehicles to transport different types of cargo such as drugs, active molecules, nucleic acids and nanoparticles for imaging, tracking or therapeutic purposes in cancer biology or medicine [78,79].

As widely reported in the literature [16,80], several methods are used to incorporate cargoes inside EVs. Exogenous methods for loading EVs require the isolation of the vesicles at first, and their successively loading according to different procedures.

One of the simplest way is to co-incubate the EVs with the desired content, which will penetrate into the vesicle membrane due to the different gradient of its concentration between the two sides of the EVs membrane [81,82]. In particular, in the case of hydrophobic compounds, the internalization could be reached by a simple passive diffusion process. The lipidic membrane presents a hydrophobic region completely separated from the intra and the extra cellular region, thus incubation with high concentration of drugs, such as doxorubicin, paclitaxel or imatinib, generates EVs loaded with therapeutics molecules [47,83,84]. This strategy requires minimal manipulations and allows the loading of a high amount of molecules [85].

Otherwise, the loading of hydrophilic molecules inside the intraluminal space requires the mechanical or chemical disruption of the lipid envelope. Electroporation is based on the application of an electric field to the EVs solution to create nanosized pores in the vesicles' phospholipidic membrane, enabling the diffusion of the desired drug [59,79,86], small interfering DNA (siRNA) [87,88], DNA [89] or NPs [90], maintaining the biological activity of the cargo. However, electroporation can change the physical characteristics of EVs and it is applicable only to small molecules, which can also aggregate and stick on the EVs' surface [85].

A sequence of freeze-thawing cycles of the EVs, which leads to the disruption of their membranes, can be used as exogenous method of loading. Membrane fractures or deformations, due to the ice-crystals formation, induce the encapsulation of relatively bulky molecules [91] such as proteins [92] and nanoparticles [93] without affecting their biological activity.

Another method of loading hydrophilic compounds inside EVs is sonication: vesicles and exogenous molecules can be mixed together and exposed to ultrasound. By disrupting the lipid membranes, the incorporation of the molecules inside the EVs occurs while the membrane is auto reconstructing [94]. This method prevents the aggregation of sensitive cargoes such as siRNA [95]. Nevertheless, both sonication and freeze-thawing methods cause a significant increase in the size of EVs, indicating that their morphofunctional characteristics could be in some way compromised [56,92,96].

EVs and cargo molecules can be also incubated together and then extruded through the use of a syringe-based lipid extruder. The process disrupts the vesicle membrane allowing the mixing of the different components in solution [97]. This method is recognized as the most efficient loading technique for water soluble cargoes such as many anticancer drugs and catalase are [98,99].

EVs' membranes permeabilization can be achieved also through chemicals stimuli: detergents like saponin can dissolve cholesterol forming pores in the membrane, altering its permeability and allowing the cargo penetration inside the vesicles [97,100].

The possibility of being packaged in extracellular vesicles could represent a great plus in oncology also for a wide range of just Food and Drug Administration (FDA)-approved drugs. Paclitaxel (PTX) is a potent chemotherapeutic agent, used in multi drug resistant (MDR) cancer treatments. Its encapsulation into EVs has been largely studied to increase the efficiency of cargo release and the preferential accumulation into cancer cells, suggesting the possibility to obtain a higher targeting specificity [47,56,101]. PTX encapsulated in endothelial cell-derived exosomes has the ability to cross the BBB and be released in brain tumors in vivo [81]. PTX can be also encapsulated in milk-derived EVs which improve the efficacy of the drug and decrease the immunologic toxicity [41,102].

Doxorubicin (DOX) is an antineoplastic drug used for the treatment of different cancers, such as breast cancer, leukemia, lymphoma. Its cardiotoxicity, limits its applications and its maximum tolerated dose, thus a delivery vehicle is needed to improve DOX biodistribution. A wide number of studies have been done on the encapsulation of doxorubicin in EVs [83,103,104]. The efficiency of the EVs-DOX nanoconstruct has been validated both in vitro and in vivo, as vehicle for a targeting delivery of the drug to breast cancer cells, reducing the relative side effects [79,105,106]. The encapsulation in EVs drastically reduced the in vivo cardiotoxicity of free DOX and the accumulation of the drug in cardiac tissues is diminished of approximatively the 40%, without affecting the efficacy of DOX towards cancerous cells [107].

Curcumin is another drug widely used in clinics with a variety of applications, due to its antioxidant and anti-inflammatory properties [108]. While curcumin does not show any antitumor properties when administered via dietary, it reveals a significant inhibition of tumor growth in vivo when loaded into exosome [109]. Another property of curcumin, loaded in EVs, is the partial reversal inhibition of NK cell tumor cytotoxicity in breast tumor cells, supporting the anti-cancer behavior of this bio-system [110]. The safety and efficacy of this system has been largely confirmed, leading to clinical trials. From 2011 plant exosomes have been used to deliver curcumin in clinical trial (NCT01294072) to treat colon cancer tissue.

Another category of cargo is composed by biomolecules as siRNA, miRNA (microRNA or miR): siRNAs are considered as promising anticancer treatment, owing to the ability to modulate oncogene expression levels [111]. Challenges in the use of RNAs are their rapid clearance into the blood stream and its inability to cross cell membrane. In this contest EVs could represent are a promising vehicle to deliver therapeutic RNA, due to their carrying ability and to their affinity with cell's membrane.

Considering the various types of materials that can be loaded into the vesicles with the techniques described above, we can assert that NPs can be finely tuned for a wide number of applications through a strict control of physical and chemical parameters [112]. However, when administered into the body, they could face some problems such as opsonization and/or aggregation [113,114].

The first phenomenon could lead to their recognition and elimination by the immune system, while the second one could cause deleterious effects, such as thrombosis and accumulation in off-target organs as liver, spleen and kidney. The shielding of NPs with EVs can thus potentially help to overcome these drawbacks: the biomimetic coating can prevent or reduce the aspecific interaction with proteins and, if further functionalized with targeting molecules, can avoid NPs' accumulation in undesired tissues and organs [115–117].

Internalization of gold NPs into exosome has been largely studied for different purposes, such as therapeutic and diagnostic ones [78]. The combination of gold NPs loaded with doxorubicin and encapsulated in EVs decreases drug's toxicity increasing its delivery to the cancer cells [118].

Metal-organic frameworks (MOF) NPs have recently emerged as valuable nanocarriers, due to their biocompatibility and high loading efficiency. However, cargo leakages and degradation before they reach their target cells must be avoided, and a biomimetic shield sometimes solves these problems. The encapsulation of MOF NPs inside exosomes, achieved by simple incubation, allows the delivery of the anticancer drug as suberoyl bishydroxamic acid [82] or the protein gelonin [119] able to target cancer cells, avoiding the premature cargo leakage and the degradation caused by the protease enzymes.

Another class of NPs broadly used in the biomedical field is the iron oxide one and, more specifically, SPIONs are known for their magnetic, imaging, and heating capabilities. Literature refers to EVs loaded with iron oxide nanoparticles and a clinical photosensitizer molecule (Foscan) used as biocamouflaged agents for photodynamic therapy, magnetic resonance imaging, magnetic manipulation, and hyperthermia [120]. Gold-iron oxide NPs covered with tumor cell-derived EVs are successfully indicated for theranostic applications, as they result suitable for both magnetic resonance imaging and photothermal treatment at the same time [121].

A new nanoconstruct exploits the peculiar features of zinc oxide NPs (ZnO NPs) to treat cancer without the addition of drugs. Zinc oxide NPs encapsulated inside the EVs can be efficiently internalized by cancer cells causing their apoptosis [122]. A summary of cargo-loaded EVs with the related bibliographic references is provided in Table 2.

Table 2. Direct loading nanotechnological modification of EVs.

EVs Type	Nanotechnological Modification	Application	Loading Method	Reference
Exosomes from mesenchymal stem cells	Glucose-coated gold nanoparticles (NPs)	In vivo neuroimaging	Co-incubation	[78]
Exosome from lung cancer or fibroblasts	Gold NPs and doxorubicin	Lung cancer treatment	Co-incubation	[118]
EVs from breast adenocarcinoma	MOF NPs. NPs matrix contained gelonin	Inhibit adenocarcinoma growth	Sonication and extrusion	[119]
Exosomes from Hela cells	MOF NPs	Hela cells	Co-incubation	[82]
EVs from KB cells	ZnO NPs	Cytotoxic effect against KB cells	Co-incubation	[122]
EVs from endothelial, cancer and stem cell lines	Porphyrins	To improve photodynamic therapy	Electroporation, extrusion, saponin-assisted and dialysis	[97]
Exosomes from embryonic stem cells	Paclitaxel	Glioma therapy	Co-incubation	[73]
Milk-derived exosomes		To reduce paclitaxel's side effects	Co-incubation	[102]
Exosomes from macrophages		To overcome MDR in cancer cells	Co-incubation, electroporation and sonication	[56]
Exosomes from brain cell lines		To treat brain tumor	Co-incubation	[81]
EVs from prostatic cancer		Cytotoxic effect against prostate cancer	Co-incubation	[83]
Exosomes from human colorectal carcinoma	Doxorubicin	Antiproliferative effect in colorectal cancer	Dialysis	[71]
Exosomes from breast cancer		To treat breast and ovarian cancer	Electroporation	[106]
Exosomes from breast cancer		To reduce cardiotoxicity of doxorubicin	Electroporation	[107]
Exosomes from 4T1, MCF-7, and PC3 cell line		Breast cancer	Co-incubation	[47]
Exosomes from mouse immature dendritic cells		For targeted delivery of chemotherapeutic	Electroporation	[79]
Milk-derived exosomes	Curcumin	Cervical cancer	Co-incubation	[109]
Exosomes from lymphoma cells		Activate myeloid cells in vivo	Co-incubation	[123]
Plant exosomes		Colon cancer		NCT01294072
Milk-derived exosomes	Paclitaxel, Docetaxel, Withaferin A and curcumin	Targeting and therapy of lung cancer cells	Co-incubation	[41]
Milk-derived exosomes	Celastrol	Inhibition of Hsp90 and NF-κB [a] activation pathways in lung cancer	Co-incubation	[124]
EVs from lung cancer	Oncolytic adenovirus and paclitaxel	Enhance immunogenicity in lung cancer	Co-incubation	[125]
Exosomes from HEK 293 cells	siRNA	Efficient delivery of siRNA in cancer cells	Electroporation	[126]
Exosomes from HEK 293 cells	Polo-like kinase 1 (PLK-1) siRNA	Silencing PLK-1 gene in bladder cancer cells	Electroporation	[127]
Exosomes from HEK 293 and MCF-7 cells	siRNA, miRNA and ssDNA [b]	Oncogene knockdown	Sonication	[95]
Plasma-derived EVs	miRNA cel-39	Promote apoptosis of hepatocellular carcinoma	Electroporation	[128]

Acronym legend: [a] NF-κB: nuclear factor kappa-light-chain-enhancer of activated B cells; [b] ssDNA: single stranded DNA.

3. EVs' Indirect Nanotechnological Modification through Parent Cells' Engineering

A frequently applied method to modify EVs in vitro, i.e., loading cargo molecules or accomplishing membrane functionalization, is through the engineering of parent cells. Cell engineering methods, such as genetic and metabolic modification and exogenous delivery, can alter the surface expression and cargo content of newly-produced EVs and thus enhance their biocompatibility, targeting and therapeutic abilities [129].

3.1. Indirect Surface Functionalization

EVs' membrane is a complex structure constituted by phospholipids and membrane proteins. Since the membrane is the first point of contact with the cell, tuning its composition strongly improves the targeting ability and enhances the therapeutic ability of EVs [85].

This approach can be employed for the non-invasive monitoring of EVs in vivo exploiting the fluorescence of some binding molecules. Molecular imaging allows a quantification of the EVs biodistribution and, eventually, a therapeutic effect over the time. For instance, pancreatic cell lines that stably expresses the green fluorescent protein (GFP) linked to CD63 can produce exosomes consistently positive to GFP [130–132]. Another effective labelling strategy for EVs is the incorporation of an azido-sugar in the glycans through a combined metabolic glycan labelling click chemistry reaction. Tetraacetylated N-azidoacetyl-D-mannosamine (Ac4ManNAz) is placed in culture with the parent cells, spontaneously incorporated into glycans and uniformly redistributed on their EVs. The azido-EVs are then labeled with azadibenzylcyclooctyne (ADIBO)-fluorescent dyes by a bioorthogonal click reaction [133]. Exploiting the principle of bioluminescence for tracking EVs, in vivo Gaussian Luciferase (Gluc) is linked to a transmembrane domain of a platelet-derived growth factor receptor [134,135], or a lactadherin [136,137]. Gluc is the only naturally-produced luciferase that can emit flash of bioluminescence in the presence of oxygen as cofactor for the reaction. After the engineering of parent cells with Gluc, the produced EVs are extracted and, when administered systemically, they can be tracked in vivo thanks to their bioluminescence [134,135]. The cellular transgene expression into the parent cell allows the expression of the candidate protein or peptide in the released EVs. The coding sequence of the desired ligand is inserted by a gene transfer vector (i.e., lentivirus) between the signal peptide and the N-terminus of the mature peptide of a transmembrane protein. In this way, the parent cells can generate EVs with the peptide of interest on their surface [129]. The candidate protein or peptide, after the transfection in the parent cells, fuses with EVs membrane proteins such as Lamp2b and tetraspanins CD63 and CD9 [43], thus the produced EVs display the just-engineered molecule on their surface. For instance, dendritic cells can be engineered to express a protein composed by Lamp2b and αv integrin-specific iRGD peptide in order to secrete iRGD peptide-EVs. This functionalization considerably increases the delivery of doxorubicin to αv integrin-positive breast cancer cells in vitro [79]. The transfection can occur by using plasmid vectors. A plasmid vector encoding streptavidin (which binds to biotin with high affinity) and lactadherin (an exosome-tropic protein) fusion protein allow to obtain streptavidin-lactadherin-modified exosomes that are mixed with the biotinylated pH-sensitive fusogenic GALA peptide exerting a lytic activity in acid environment [138]. Lentiviral vector bearing LAMP2b-Designed ankyrin repeat protein (DARPin) G3 chimeric gene or herpes simplex virus with plasmid pACgp67B-HER2m, containing the anti-human epidermal growth factor receptor 2 (HER2) scFv (ML39) antibody DNA sequence, are used to engineer HEK-293T cells. EVs isolated from transfected cells can bind specifically to HER2/Neu in adenocarcinoma cell lines [139,140]. Human carcinoembryonic antigen or human HER2/neu can be also inserted into the mouse lactadherin expression plasmid p6mLC1C2 and transfected into dendritic cells, enhancing the production of functionalized EVs to target breast cancer cells [141]. Similarly, prostate-specific antigen and prostatic acid phosphatase linked to the C1C2 domain of lactadherin produce EVs that specifically target prostate cancer cells [142]. In another study, an anti-epidermal growth factor receptor (EGFR) nanobodies with anchor signal peptide glycosylphosphatidylinositol (GPI) fusion protein are transfected to parent cells in order to generate EVs with this functionalization. These EVs show a significantly improved targeting ability towards EGFR-positive tumor cells [143].

An alternative strategy is the hydrophobic insertion used to functionalize the EVs' membranes by exploiting the phospholipid composition of plasma membranes. Amphiphilic molecule DSPE-PEG, FDA approved for medical applications, can self-assemble in the phospholipid bilayer [144]. Based on this consideration, if DSPE-PEG is bound to the molecule of interest, it can be incorporated inside the cell membrane, making it overexpresses the molecule on its surface and producing EVs with the desired functionalization. The most frequently used molecules are biotin and folate: the first one binds

selectively with streptavidin, used for further functionalization, and the second one targets specific cancer cells [86,145–147]. In addition to folate, also other binding sites can be created on EVs using this approach, for example by adding the RGD sequence or sulfhydryl groups [148].

A summary of EVs 'surface functionalization nanotechnological modification through parent cells' engineering with the related bibliographic references is reported in Table 3.

Table 3. EVs' Surface functionalization by parent cells' engineering.

EVs Type	Nanotechnological Modification	Application	Reference
Exosomes from breast cancer	Ac4ManNAz labeled with ADIBO-fluorescent dyes	Breast cancer imaging	[133]
Exosomes from melanoma	Gaussian Luciferase	Biodistribution and tumor targeting	[137]
Exosomes from HEK 293T	Gaussian Luciferase	Biodistribution and tumor targeting	[134,135]
Exosomes from melanoma	Gaussian Luciferase	Biodistribution and tumor targeting	[136]
Exosomes from HEK 293T	Alexa Fluor 680-Streptavidin	Biodistribution and tumor targeting	[135]
Exosomes from different cell lines	GFP	Monitoring and tracking of exosomes uptake in different types of cancer	[130–132,149]
EVs from HEK 293T	Palmitoylation signal genetically fused in-frame to the N terminus of enhanced green fluorescence protein (EGFP) and tandem dimer Tomato (tdTomato)	Monitoring the uptake by cancer cells	[150]
Exosomes from macrophage	Arginyl–glycyl–aspartic acid (RGD)-functionalized DSPE-PEG (DSPE-PEG-RGD), sulfhydryl-functionalized DSPE-PEG (DSPE-PEG-SH) and folic acid	Targeting Hela cells	[148]
EVs from squamous cell carcinoma	DSPE-PEG-Biotin and folate	Targeting breast cancer for diagnosis and therapy	[145]
Exosomes from HUVEC	DSPE-PEG-biotin	Targeting hepatocellular carcinoma	[147]
EVs from macrophage	DSPE-PEG-Biotin and folate	Targeting Hela cells	[86]
EVs from HUVEC	DSPE-PEG-Biotin	Targeting melanoma	[146]
Exosomes from HEK 293T	DARPins	Targeting HER-2 over-expressing cancer cells (breast, ovarian and gastric cancers)	[139]
Exosomes from HEK 293	Anti-HER2 scFv antibody (ML39)	Inhibit the growth of HER2 positive breast cancer	[140]
Exosomes from murine melanoma	Streptavidin-lactadherin fusion protein linked with biotinylated pH-sensitive fusogenic GALA peptide	Cancer immunotherapy	[138]
Extracellular vesicles from murine neural stem cells	Anti-EGFR fused to GPI anchor signal peptides	Targeting of Hela cells	[143]
Exosomes from dendritic cells	Lamp2b fused with iRGD (CRGDKGPDC) targeting peptide for αv integrin	Targeting breast cancer	[79]
Exosomes from dendritic cells	Carcinoembryonic antigen or HER2 linked to the C1C2 domain of lactadherin	Targeting breast cancer	[141]
Exosomes from HEK 293F cells	Prostate-specific antigen, and prostatic acid phosphatase linked to the C1C2 domain of lactadherin	Targeting prostate cancer	[142]
Exosomes from fibrosarcoma cells	Chicken egg ovalbumin by fusing it to the C1C2 domain of the lactadherin	In vivo fibrosarcoma. More efficient antitumor immune response	[151,152]
Exosomes from dendritic cell line	C1C2 domain of lactadherin is fused to soluble proteins or extracellular domain of membrane proteins	Generate antibodies against tumor biomarkers	[153]
	Transmembrane protein HLA-A2 [a]		

Acronym legend: [a] HLA-A2: Human leukocyte antigen A2.

3.2. Indirect Loading

Genetically engineered parent cells allow the production of pre-loaded EVs. This approach enhances the loading efficiency of molecules inside the EVs compared to the post-isolation techniques, minimizing the impairment of the structures or of the biological activity of both cargoes and carriers [44]. Some reports demonstrate the successful internalization of miRNA, siRNA [84,154] and nanoparticles [155] inside EVs produced from engineered parental cells. Furthermore, cells can be transfected with short RNA-encoding plasmid DNA (pDNA) in order to generate EVs enriched with target RNA [121,156]. The efficiency of cargo uptake inside EVs strongly depends on its high concentration inside the parent cells, because only a small amount is released as packed in the EVs [85]. Loading proteins inside the EVs can be accomplished by transfecting the parent cell with a vector containing the gene which codifies the specific protein. Proteins encoded by the transfected gene are synthesized by the cells and then secreted enveloped in EVs. Despite the apparent simplicity of this approach, many aspects need to be considered. The expression of cytotoxic proteins can inhibit the growth of the parent cells or induce their apoptosis. Furthermore, impaired biological reactions and interactions can obstacle the production of EVs ability [40].

Viruses are often used for the transfection of genetic materials or molecules inside the parent cells in vitro. Different kind of viruses are employed, but the most used is lentivirus because of its transfection ability and safety. Generally, the transfection of parent cells has the aim to overexpress a particular therapeutic or anticancer molecule in order to secrete it as enveloped inside EVs. For example, EVs-enriched human MUC1 (hMUC1) injected intra-dermally suppress the growth of hMUC1-expressing tumor [157]. Similarly, tumor necrosis factor (TNF)-related apoptosis-inducing ligand (TRAIL), a widely tested anticancer protein, causes the apoptosis of transformed or tumoral cells, but not of the normal ones. Due to its therapeutic efficacy, it has been encapsulated in EVs to overcome the shortcomings of a poor pharmacokinetic profile and the tumor resistance to drug [158,159]. Target proteins can also be delivered inside the parent cell by fusion with constitutive proteins of EVs, such as CD63, to improve the specificity of the protein loaded inside EVs [160]. Nef/E7 DNA vector expressing Nef exosome-anchoring protein combined with HPV-E7 is delivered to parent cells to make them able to generate immunogenic EVs containing the Nef-E7 fusion protein to elicit an efficient anti-E7 cytotoxic T lymphocyte immune response for cancer therapy [161]. Another strategy to incorporate proteins of interest inside EVs is pseudotyping, which packages viral RNAs or DNAs with the envelope proteins from another virus. The G glycoprotein of the vesicular stomatitis virus glycoprotein (VSVG) is frequently used for this purpose because of its efficacy in transduction and broad tropism. The selected protein is fused with VSVG and transfected into different parent cell lines [162]. This method can be further developed by adding to VSVG cell-recognizing peptides for targeting or engineered therapeutic antibodies, such as anti-CD19 chimeric antigen receptors, that target specific suppressors of cytotoxic T cells for cancer therapy [163]. A novel method, called EXPLORs (exosomes for protein loading via optically reversible protein-protein interactions), allows the loading of cargo proteins inside EVs through endogenous biogenesis processes, delivering soluble proteins into the cytosol via controlled, reversible protein-protein interactions. For this purpose, a photoreceptor cryptochrome 2 (CRY2) and CRY-interacting basic-helix-loop-helix 1 (CIB1) protein module, which regulates the floral initiation of Arabidopsis thaliana via blue light-dependent phosphorylation, are selected. Then, a transient docking of CRY2-conjugated cargo proteins is induced by introducing CIBN (a truncated version of CIB1) conjugated with an exosome-associated tetraspanin protein CD9 and by blue light illumination. After the release of the EVs with the cargo proteins linked to tetraspanins from the parent cell, they can be detached from CD9-conjugated CIBN by the removal of the illumination source, releasing them into the intraluminal space of the EVs [164].

The strategies described above to load EVs with proteins by engineering of the parent cells can be applied also in the case of nucleic acids. For instance, to reverse the chemoresistance to cisplatin-refractory gastric cancer, human embryonic kidney 293T (HEK-293T) cells are transfected with anti-miR-214 and the produced vesicles are administered systemically in combination with

cisplatin, injected intraperitoneally, to overcome the in vitro and in vivo drug-resistance [165]. EVs produced by miR-134 or anti-miR-21 transfected mammary carcinoma cells have the ability to reduce the cellular proliferation and migration and to enhance the apoptosis in breast cancers [121,166]. miR-122 is essential to tune the chemosensitivity of hepatocellular carcinoma cells. Its effective delivery is accomplished by transfecting adipose-derived mesenchymal stem cells in order to produce EVs already loaded with miR-122 [167]. EVs from mesenchymal stem cells transfected with miR-146b expressing plasmid silence the EGFR and significantly decrease glioma growth [168], while EVs loaded with miR-143 inhibit the migration ability of osteosarcoma cells [169]. Mesenchymal stem cells can be loaded with anti-miR-9 to produce anti-miR-9 EVs. Anti-miR-9 delivered to cancer cells can reverse the expression of P-glycoprotein, involved in the chemoresistance, to enhance the efficacy of the temozolomide in otherwise resistant glioblastomas [170]. HEK-293T cell line can be genetically engineered to overexpress a suicide gene mRNA and protein-cytosine deaminase fused to uracil phosphoribosyltransferase in their microvesicles. They can transfer the therapeutic mRNA/protein to schwannoma cancer cells, achieving the inhibition of tumor growth [171]. Prostate cancer cell line is incubated with spherical nucleic acids (SNA), which are a new type of therapeutic agent composed by a core of gold nanoparticle with a dense shell of highly oriented nucleotides. The secreted EVs display a potent gene knockdown, when internalized in cancer cell, due to the presence of the anti-miR-21 [155]. EVs overexpressing hepatocyte growth factor (HGF) siRNA drastically reduced HGF and vascular endothelial growth factor (VEGF) expression in gastric cancer [172]. EVs delivery of siRNA against RAD51 and RAD52 causes an inhibition of proliferation and a massive reproductive cell death in human breast cancer cells [173].

The previously described method EXPLOR can be also used for the encapsulation of peptides inside cells, in particular of miR-21 sponges inside HEK-293T cells. The EVs produced are then loaded with this nucleic acid, which is an inhibitor of miR-21, overexpressed in most cancer types, and reduces the tumor progression and metastasis. After the collection of EVs loaded with miR-21 sponges, EVs are functionalized with cholesterol-AS411 aptamers exploiting the interaction with lipids of EVs' membrane. The expression of AS1411 on EVs allows the targeting of leukemia cells for the interaction with nucleolin, overexpressed by these cancer lines. miR-21 sponges can inhibit miR-21 functions, triggering leukemia cells' apoptosis [174].

Engineering the donor cells in order to make them produce already loaded EVs is possible also in the case of chemotherapeutic drugs and nanoparticles, as resumed in Table 4. For example, mesenchymal stromal cells are cultured for 24 h with paclitaxel and, after a change of media, cells are left to produce EVs with Paclitaxel for 48 h. These EVs can be used in the treatment of human pancreatic adenocarcinoma and they demonstrate a strong antiproliferative activity [101]. A melanoma cell line is engineered to produced EVs loaded with both survivin T34A and gemcitabine. Loaded EVs are collected and administered to pancreatic adenocarcinoma cells. The presence of survivin-T34A, which targets and inhibits survivin, an inhibitor of apoptosis, enhances the toxic effect of the Gemcitabine with lower dosages [175]. Different cell lines are incubated with methotrexate or doxorubicin and then irradiated with ultraviolet light to induce cells apoptosis. The produced ApoBDs, as delivery vehicles of chemotherapeutic drugs, exert a strong cytotoxic effect and inhibit the drug efflux from cancer cells [176]. A hybrid approach between drugs and nanoparticles involves the co-incubation of macrophages with both iron oxide NPs and a photosensitizer called m-THPC. The produced EVs containing both the two cargoes stabilize the strong hydrophobic photosensitizer drug and are injected into a mouse model. The drug allows the photodynamic therapy on cancer cells, while nanoparticles, responsive to magnetic fields, can be tracked with magnetic resonance imaging and used for hyperthermia treatments [177]. A further experiment, carried out by the previous research groups, besides the iron oxide nanoparticles, includes also a chemotherapeutic agent (doxorubicin), tissue-plasminogen activator (t-PA) and two photosensitizers (disulfonated tetraphenylchlorin-TPCS2a and 5,10,15,20-tetra(*m*-hydroxyphenyl)chlorin-mTHPC) to better enhance the antitumor ability of the produced EVs [178]. The delivery of compounds to parent cells can

be difficult, especially in presence of hydrophobic molecules. For this reason, in the case of the hydrophobic photosensitizer zinc phthalocyanine, it is encapsulated in liposomes and they are used to treat the parent cells. The hydrophobic compound is secreted from the parent cells by incorporation in the EVs and then transferred to adjacent cells. This approach allows to significantly penetrates spheroids and in vivo solid tumors, enhancing the efficacy of the therapy [179]. The same procedure can be followed also for other molecule, both hydrophobic or hydrophilic, including fluorophores such as 1,1′-dioctadecyl-3,3,3′,3′-tetramethylindodicarbocyanine perchlorate (DiD) and carboxy-fluorescein, drugs (paclitaxel and tirapazamine), lipids and bio-orthogonal chemicals [180]. A similar approach is used also to incorporate nanoparticles inside EVs. Hollow-gold nanoparticles were shielded with a PEG functionalization and then incubated with human placental mesenchymal stem cells. After the uptake, the cells produced EVs loaded with hollow-gold nanoparticles. These EVs allowed to track the cell-cell communication and also perform the optical hyperthermia for cancer therapy [181].

Table 4. Nanotechnological modification of EVs' loading through parent cell engineering.

EVs Type	Nanotechnological Modification	Application	Reference
Human placental mesenchymal stem cells	Hollow gold NPs	Hyperthermia therapy against different type of cancer	[181]
Exosomes from hepatocellular carcinoma	Porous silicon NPs loaded with doxorubicin	Decreased the expression of multidrug-resistant protein P-glycoprotein	[182]
EVs from mesenchymal stem cells	SPIONs	Therapy against leukemia	[183]
EVs from HUVEC	Iron oxide NPs and clinical photosensitizer (Foscan)	Phototoxicity against prostate adenocarcinoma cells	[120]
Extracellular vesicles from human macrophages	Iron oxide nanoparticles and m-THPC photosensitizer	Theranostic approach against cervical and prostate cancer	[177]
Microvesicles from different cancer cell lines	A hydrophobic photosensitizer zinc phthalocyanine encapsulated in liposomes	Photodynamic therapy for different cancer cell lines	[179]
Microvesicles from human macrophages	Doxorubicin, tissue-plasminogen activator and two photosensitizers	Targeting and therapy of ovarian and prostate cancers	[178]
Exosomes from mesenchyme stromal cells	Paclitaxel	Treatment of pancreatic cancer	[101]
Exosomes from melanoma cell line	Survivin-T34A and Gemcitabine	Treatment of pancreatic adenocarcinoma	[175]
Apoptotic bodies from tumoral cells	Doxorubicin or Metotrexate	Tumor cells killing with reduce side effects	[176] NCT01854866
Exosomes from breast cancer	Curcumin	Reverse inhibition of NK cell tumor cytotoxicity in breast cancer	[110]
Exosomes from HEK 293	P53 gene	Transfer p53 gene to p53-deficient cells	[184]
Exosomes from HEK 293T	miR-21 sponges	Therapy for leukemia cells	[174]
Extracellular vesicles from breast cancer	Anti-miR-21	Theranostic method for breast cancer	[121]
Exosomes from HEK 293T	Inhibitor of miR-214	Reverse chemoresistance to cisplatin in gastric cancer	[165]
Exosomes from prostate cancer cells	Anti-miR-21 spherical nucleic acid	Prostate cancer	[155]
Exosomes from mammary carcinomas	miR-134	Increase sensitivity of breast cancers to chemotherapeutic drugs	[166]
Exosomes from mesenchyme stem cells	miR-122	Increase sensitivity of hepatocellular carcinoma to chemotherapeutic drugs	[167]
Exosomes from mesenchymal stem cells	miR-143	Inhibit migration of osteosarcoma cells	[169]
Exosomes from mesenchymal stem cells	anti-miR-9	Increase sensitivity of glioblastoma multiforme to chemotherapeutic drugs	[170]
Exosomes from mesenchyme stem cells	miR-146b	Inhibit glioma growth	[168]

Table 4. *Cont.*

EVs Type	Nanotechnological Modification	Application	Reference
Microvesicles from HEK 293T	Suicide gene mRNA and protein-cytosine deaminase fused to uracil phosphoribosyltransferase	Inhibit schwannoma tumor growth	[171]
Exosomes from HEK 293T	HGF siRNA	Inhibition of tumor growth and angiogenesis in gastric cancer	[172]
Exosomes from breast cancer cells	RAD51 and RAD52 siRNA	Gene therapy against breast cancer	[173]
Extracellular vesicles from mesenchymal stem cells	TNF-related apoptosis-inducing ligand (TRAIL)	Lung, breast, kidney cancer, pleural mesothelioma and neuroblastoma	[158]
Exosomes from chronic myelogenous leukemia cells	TNF-related apoptosis-inducing ligand (TRAIL)	Enhance apoptosis in lymphoma	[159]
Exosomes from HEK 293T	VSVG	Glioblastoma and liver cancer cells	[162]
Exosomes from lymphoblast	Nef-E7 fusion protein	T lymphocytes immune response	[161]
Exosomes from two mouse cell lines	Human MUC1 tumor antigen	Generate immune response against tumor	[157]
Microvesicles from different cancer cell lines	DiD, carboxyfluorescein, paclitaxel, tirapazamine encapsulated in fusogenic liposomes	The same cancer cell lines used to produce microvesicles	[180]

The engineering of parent cells can also be addressed to obtain EVs loaded with molecules, such as drugs or nucleic acids, and with a specific surface functionalization (as summarized in Table 5). HEK-293T cells engineered to express Lamp2b protein, fused with a fragment of interleukin 3 (IL-3), and then incubated with Imatinib or BCR-ABL siRNA, can produce EVs loaded with the desired cargoes and expressing the IL-3 fragment on their surface. The IL-3 receptor is overexpressed in chronic myeloid leukemia and acute myeloid leukemia blasts and almost absent in hematopoietic stem cells. Exploiting this characteristic, IL-3 expressing EVs can target these cancerous cells and overcome the drug resistance to imatinib or deliver functional BCR-ABL siRNA towards imatinib-resistant cells [84]. The cell line used above can be also transfected with pDisplay vector encoding GE11 peptide or EGF, and with let-7a miRNA. The harvested EVs are functionalized with the peptide on their surface and loaded with the miRNA. Then, EVs are injected intravenously and their surface functionalization allows the specific targeting of EGFR-expressing cancer tissues, such as breast cancer. The tumor suppressor let-7a is delivered to the tumor and reduce the expression of RAS and HMGA2 inhibiting the malignant growth of cancer cells [154]. In another study, adeno-associated virus (AAV) is used as viral vector for transfection. It is broadly used for gene therapy in human, thanks to its safety profile, but it has some limitations, such as off-target gene delivery (to liver for example) and low transfection of target cells. For this reason, by transfecting the parent cells with AAV, capsids associate with the membrane and the interior part of the newly-produced EVs (called vexosomes). Harvested vexosomes show to be more resistant to anti-AAV antibodies if compared to naked AAV and they can efficiently transduce cells, enhancing gene transfer. Furthermore, parent cells are also engineered to express a transmembrane receptor on the microvesicle surface, i.e., biotin acceptor peptide-transmembrane domain (BAP-TM) receptor, allowing the specific targeting of glioblastoma cells [185]. Gene engineering method is applied to HEK-293T cell line to functionalize the CD9 tetraspanin with the RNA-binding protein HuR and then, they are modified with miR-155 or the clustered regularly interspaced short palindromic repeats (CRISPR)/Cas9 system. The produced EVs are effectively enriched by the above mentioned RNAs and in future these nanoconstructs need to be evaluated in some diseases such as liver cancer [186].

Table 5. EVs' indirect modifications through combined loading and surface parent cells engineering.

EVs Type	Nanotechnological Modification	Application	Reference
Exosomes from HEK 293T	Functionalization: CD9-HuR Load: miR-155 or CRISPR/Cas9	Targeting and therapy of liver cancer	[186]
Exosomes from HEK 293T	Functionalization: Lamp2b, fused to a fragment of IL-3 Load: Imatinib or BCR-ABL siRNA	Inhibition of chronic myeloid leukemia growth	[84]
Exosomes from HEK 293T	Functionalization: GE 11 peptide Load: let-7a miRNA	Targeting and therapy of EGFR-expressing cancer tissues	[154]
Exosomes from HEK 293T cells	Functionalization: BAP-TM receptor and biotin ligase BirA Load: viral capside	Gene therapy against glioma	[185]

4. Conclusions and Future Outlook

Nanotechnology-modified EVs are promising tools for the next generation of nanomedicine for both diagnostic and therapeutic purposes with non-cytotoxic effects and a low immunogenic profiles.

In the present review, we have reported how nanoengineered EVs may be obtained either by direct post-extraction modification or by the indirect nanotechnological modification through the engineering of the parental cells producing them. From the therapeutic point of view, targeted EVs can promote the efficacy in cargo transportation toward a target cell or tissue, while also reducing off-target delivery. EVs can be loaded with very different therapeutic cargos, including both hydrophilic and hydrophobic drugs, nucleic acids like miRNA, siRNA, and recombinant proteins, or even solid-state nanoparticles. Various strategies are also available for their surface functionalization, in view of modulating the EV innate homing capabilities or refine specific targets.

Despite the advances outlined in this review, many challenges still have to be overcome to render EVs an effective and clinically-approved nanomedicine approach. First of all, achieving large-scale production of EVs for clinical use is a major challenge. In addition, a careful study on the purification processes, potentially based on immune-selection and isolation, is surely required in order to achieve high purity of the nano-engineered EVs and remove all the eventual reaction by-products or uncoupled molecules, cargos or nanoparticles after the EVs modification. Furthermore, more systematic in vivo studies are required to gain information about the re-engineered EVs toxicology, biodistribution, pharmacodynamics and pharmacokinetics.

Finally, the complex structure, the variable composition and functional activity of secreted EVs can impair their pharmaceutical approval, preventing their systematic clinical use. A potential alternative can be envisioned in the development of biomimetics EVs, thus assembled using clinical-grade and purified synthetic lipids and the necessary proteins under controlled GMP procedures to mimic the naturally-secreted ones. Strikingly, such biomimetic nanotools will not suffer from large-scale production limitations and variable compositions and can be ideal for the incorporation of many and different molecules or nanoparticles with biomodulatory, cytotoxic, anti-proliferative and imaging capabilities. Such re-engineering of EVs would thus allow novel non-immunogenic, highly stable, hemocompatible nanoplatforms, with customizable targeting and drug delivery abilities.

However, possible drawbacks in terms of manufacture reproducibility and high cost can come against this vision. Furthermore, the precise components of natural exosomes, that are the key for obtaining efficient cell homing, therapeutic delivery and biomarker signature, are still under study and at the infancy of knowledge.

More in general, it is thus clear that the way to efficiently obtain highly purified, well-characterized and reproducible nano-engineered EVs is still a long way. The fulfillment of these objectives will allow high performances in terms of targeting, therapeutic and diagnostic abilities, avoiding any potential side effects. Furthermore, achieving the above-mentioned vision will be the starting point of the subsequent industrial development of these novel nano-engineered EVs, including scaling up

and quality control of production, rigorous pharmacokinetic and toxicological studies and, eventually, clinical testing.

Author Contributions: Conceptualization, T.L.; Resources, V.C.; Literature Search: F.S., T.L., B.D., V.V.; Writing-Original Draft Preparation, F.S., T.L., B.D., V.V.; Writing-Review & Editing, T.L. and V.C.; Project Administration, V.C.; Funding Acquisition, V.C. All authors have given approval to the final version of the manuscript.

Funding: This work has received funding from the European Research Council (ERC) under the European Union's Horizon 2020 research and innovation program (Grant Agreement No 678151—Project Acronym "TROJANANOHORSE"—ERC starting Grant).

Conflicts of Interest: There are no conflicts to declare.

References

1. D'Anca, M.; Fenoglio, C.; Serpente, M.; Arosio, B.; Cesari, M.; Scarpini, E.A.; Galimberti, D. Exosome determinants of physiological aging and age-related neurodegenerative diseases. *Front. Aging Neurosci.* **2019**, *11*, 232. [CrossRef] [PubMed]
2. Giusti, I.; Di Francesco, M.; D'Ascenzo, S.; Palmerini, M.G.; Macchiarelli, G.; Carta, G.; Dolo, V. Ovarian cancer-derived extracellular vesicles affect normal human fibroblast behavior. *Cancer Biol. Ther.* **2018**, *19*, 722–734. [CrossRef] [PubMed]
3. Ilaria, G.; Marianna Di, F.; Vincenza, D. Extracellular vesicles in glioblastoma: Role in biological processes and in therapeutic applications. *Curr. Cancer Drug Targets* **2017**, *17*, 221–235. [CrossRef]
4. Palumbo, P.; Lombardi, F.; Augello, F.R.; Giusti, I.; Luzzi, S.; Dolo, V.; Cifone, M.G.; Cinque, B. NOS_2 inhibitor 1400W induces autophagic flux and influences extracellular vesicle profile in human glioblastoma U87MG cell line. *Int. J. Mol. Sci.* **2019**, *20*, 3010. [CrossRef] [PubMed]
5. Rome, S.; Forterre, A.; Mizgier, M.L.; Bouzakri, K. Skeletal muscle-released extracellular vesicles: State of the art. *Front. Physiol.* **2019**, *10*, 929. [CrossRef] [PubMed]
6. Ruivo, C.F.; Adem, B.; Silva, M.; Melo, S.A. The biology of cancer exosomes: Insights and new perspectives. *Cancer Res.* **2017**, *77*, 6480. [CrossRef] [PubMed]
7. Rybak, K.; Robatzek, S. Functions of extracellular vesicles in immunity and virulence. *Plant Physiol.* **2019**, *179*, 1236–1247. [CrossRef]
8. Yamamoto, T.; Kosaka, N.; Ochiya, T. Latest advances in extracellular vesicles: From bench to bedside. *Sci. Technol. Adv. Mater.* **2019**, *20*, 746–757. [CrossRef]
9. Yang, J.; Dang, G.; Lü, S.; Liu, H.; Ma, X.; Han, L.; Deng, J.; Miao, Y.; Li, X.; Shao, F.; et al. T-cell-derived extracellular vesicles regulate B-cell IgG production via pyruvate kinase muscle isozyme 2. *FASEB J.* **2019**, *33*. [CrossRef]
10. Théry, C.; Witwer, K.W.; Aikawa, E.; Alcaraz, M.J.; Anderson, J.D.; Andriantsitohaina, R.; Antoniou, A.; Arab, T.; Archer, F.; Atkin-Smith, G.K.; et al. Minimal information for studies of extracellular vesicles 2018 (MISEV2018): A position statement of the International Society for Extracellular Vesicles and update of the MISEV2014 guidelines. *J. Extracell. Vesicles* **2018**, *7*, 1535750. [CrossRef]
11. Witwer, K.W.; Théry, C. Extracellular vesicles or exosomes? On primacy, precision, and popularity influencing a choice of nomenclature. *J. Extracell. Vesicles* **2019**, *8*, 1648167. [CrossRef] [PubMed]
12. Willms, E.; Cabañas, C.; Mäger, I.; Wood, M.J.A.; Vader, P. Extracellular vesicle heterogeneity: Subpopulations, isolation techniques, and diverse functions in cancer progression. *Front. Immunol.* **2018**, *9*, 738. [CrossRef] [PubMed]
13. Van Niel, G.; D'Angelo, G.; Raposo, G. Shedding light on the cell biology of extracellular vesicles. *Nat. Rev. Mol. Cell Biol.* **2018**, *19*, 213. [CrossRef] [PubMed]
14. Caruso, S.; Poon, I.K.H. Apoptotic cell-derived extracellular vesicles: More than just debris. *Front. Immunol.* **2018**, *9*, 1486. [CrossRef] [PubMed]
15. Hauser, P.; Wang, S.; Didenko, V.V. Apoptotic bodies: Selective detection in extracellular vesicles. In *Signal Transduction Immunohistochemistry: Methods and Protocols*; Kalyuzhny, A.E., Ed.; Springer New York: New York, NY, USA, 2017; pp. 193–200. [CrossRef]
16. Antimisiaris, S.G.; Mourtas, S.; Marazioti, A. Exosomes and exosome-inspired vesicles for targeted drug delivery. *Pharmaceutics* **2018**, *10*, 218. [CrossRef]

17. Meldolesi, J. Exosomes and ectosomes in intercellular communication. *Curr. Biol.* **2018**, *28*, R435–R444. [CrossRef]
18. Théry, C.; Zitvogel, L.; Amigorena, S. Exosomes: Composition, biogenesis and function. *Nat. Rev. Immunol.* **2002**, *2*, 569–579. [CrossRef]
19. Kalra, H.; Drummen, G.P.C.; Mathivanan, S. Focus on extracellular vesicles: Introducing the next small big thing. *Int. J. Mol. Sci.* **2016**, *17*, 170. [CrossRef]
20. He, C.; Zheng, S.; Luo, Y.; Wang, B. Exosome theranostics: Biology and translational medicine. *Theranostics* **2018**, *8*, 237–255. [CrossRef]
21. Jaiswal, R.; Sedger, L.M. Intercellular vesicular transfer by exosomes, microparticles and oncosomes—Implications for cancer biology and treatments. *Front. Oncol.* **2019**, *9*, 125. [CrossRef]
22. Maacha, S.; Bhat, A.A.; Jimenez, L.; Raza, A.; Haris, M.; Uddin, S.; Grivel, J.-C. Extracellular vesicles-mediated intercellular communication: Roles in the tumor microenvironment and anti-cancer drug resistance. *Mol. Cancer* **2019**, *18*, 55. [CrossRef] [PubMed]
23. Han, L.; Lam, E.W.F.; Sun, Y. Extracellular vesicles in the tumor microenvironment: Old stories, but new tales. *Mol. Cancer* **2019**, *18*, 59. [CrossRef] [PubMed]
24. Sung, B.H.; Weaver, A.M. Exosome secretion promotes chemotaxis of cancer cells. *Cell Adh. Migr.* **2017**, *11*, 187–195. [CrossRef] [PubMed]
25. Gao, L.; Wang, L.; Dai, T.; Jin, K.; Zhang, Z.; Wang, S.; Xie, F.; Fang, P.; Yang, B.; Huang, H.; et al. Tumor-derived exosomes antagonize innate antiviral immunity. *Nat. Immunol.* **2018**, *19*, 233–245. [CrossRef] [PubMed]
26. Choi, D.; Lee, T.H.; Spinelli, C.; Chennakrishnaiah, S.; D'Asti, E.; Rak, J. Extracellular vesicle communication pathways as regulatory targets of oncogenic transformation. *Semin. Cell Dev. Biol.* **2017**, *67*, 11–22. [CrossRef]
27. Tirinato, L.; Pagliari, F.; Limongi, T.; Marini, M.; Falqui, A.; Seco, J.; Candeloro, P.; Liberale, C.; Di Fabrizio, E. An overview of lipid droplets in cancer and cancer stem cells. *Stem Cells Int.* **2017**, *2017*, 1656053. [CrossRef]
28. Romagnoli, G.G.; Zelante, B.B.; Toniolo, P.A.; Migliori, I.K.; Barbuto, J.A.M. Dendritic cell-derived exosomes may be a tool for cancer immunotherapy by converting tumor cells into immunogenic targets. *Front. Immunol.* **2015**, *5*. [CrossRef]
29. Pitt, J.M.; André, F.; Amigorena, S.; Soria, J.-C.; Eggermont, A.; Kroemer, G.; Zitvogel, L. Dendritic cell-derived exosomes for cancer therapy. *J. Clin. Investig.* **2016**, *126*, 1224–1232. [CrossRef]
30. Markov, O.; Oshchepkova, A.; Mironova, N. Immunotherapy based on dendritic cell-targeted/-derived extracellular vesicles—A novel strategy for enhancement of the anti-tumor immune response. *Front. Pharmacol.* **2019**, *10*, 1152. [CrossRef]
31. Munich, S.; Sobo-Vujanovic, A.; Buchser, W.J.; Beer-Stolz, D.; Vujanovic, N.L. Dendritic cell exosomes directly kill tumor cells and activate natural killer cells via TNF superfamily ligands. *Oncoimmunology* **2012**, *1*, 1074–1083. [CrossRef]
32. Viaud, S.; Théry, C.; Ploix, S.; Tursz, T.; Lapierre, V.; Lantz, O.; Zitvogel, L.; Chaput, N. Dendritic cell-derived exosomes for cancer immunotherapy: What's next? *Cancer Res.* **2010**, *70*, 1281. [CrossRef] [PubMed]
33. Zhang, B.; Yin, Y.; Lai, R.C.; Lim, S.K. Immunotherapeutic potential of extracellular vesicles. *Front. Immunol.* **2014**, *5*, 518. [CrossRef] [PubMed]
34. Syn, N.L.; Wang, L.; Chow, E.K.-H.; Lim, C.T.; Goh, B.-C. Exosomes in cancer nanomedicine and immunotherapy: Prospects and challenges. *Trends Biotechnol.* **2017**, *35*, 665–676. [CrossRef] [PubMed]
35. Yokoi, A.; Yoshioka, Y.; Yamamoto, Y.; Ishikawa, M.; Ikeda, S.-I.; Kato, T.; Kiyono, T.; Takeshita, F.; Kajiyama, H.; Kikkawa, F.; et al. Malignant extracellular vesicles carrying MMP1 mRNA facilitate peritoneal dissemination in ovarian cancer. *Nat. Commun.* **2017**, *8*, 14470. [CrossRef]
36. Ostrowski, M.; Carmo, N.B.; Krumeich, S.; Fanget, I.; Raposo, G.; Savina, A.; Moita, C.F.; Schauer, K.; Hume, A.N.; Freitas, R.P.; et al. Rab27a and Rab27b control different steps of the exosome secretion pathway. *Nat. Cell Biol.* **2010**, *12*, 19–30. [CrossRef]
37. Baietti, M.F.; Zhang, Z.; Mortier, E.; Melchior, A.; Degeest, G.; Geeraerts, A.; Ivarsson, Y.; Depoortere, F.; Coomans, C.; Vermeiren, E.; et al. Syndecan–syntenin–ALIX regulates the biogenesis of exosomes. *Nat. Cell Biol.* **2012**, *14*, 677–685. [CrossRef]
38. Khawar, M.B.; Abbasi, M.H.; Siddique, Z.; Arif, A.; Sheikh, N. An update on novel therapeutic warfronts of extracellular vesicles (EVs) in cancer treatment: Where we are standing right now and where to go in the future. *Oxid. Med. Cell Longev.* **2019**, *2019*, 9702562. [CrossRef]

39. Kosaka, N.; Yoshioka, Y.; Fujita, Y.; Ochiya, T. Versatile roles of extracellular vesicles in cancer. *J. Clin. Investig.* **2016**, *126*, 1163–1172. [CrossRef]
40. Liu, C.; Su, C. Design strategies and application progress of therapeutic exosomes. *Theranostics* **2019**, *9*, 1015–1028. [CrossRef]
41. Munagala, R.; Aqil, F.; Jeyabalan, J.; Gupta, R.C. Bovine milk-derived exosomes for drug delivery. *Cancer Lett.* **2016**, *371*, 48–61. [CrossRef]
42. Smyth, T.J.; Redzic, J.S.; Graner, M.W.; Anchordoquy, T.J. Examination of the specificity of tumor cell derived exosomes with tumor cells in vitro. *Biochim. Biophys. Acta* **2014**, *1838*, 2954–2965. [CrossRef] [PubMed]
43. Wang, J.; Zheng, Y.; Zhao, M. Exosome-based cancer therapy: Implication for targeting cancer stem cells. *Front. Pharmacol.* **2017**, *7*, 533. [CrossRef] [PubMed]
44. Armstrong, J.P.; Holme, M.N.; Stevens, M.M. Re-engineering extracellular vesicles as smart nanoscale therapeutics. *ACS Nano* **2017**, *11*, 69–83. [CrossRef] [PubMed]
45. Shen, L.-M.; Quan, L.; Liu, J. Tracking exosomes in vitro and in vivo to elucidate their physiological functions: Implications for diagnostic and therapeutic nanocarriers. *ACS Appl. Nano Mater.* **2018**, *1*, 2438–2448. [CrossRef]
46. Chiba, M.; Kubota, S.; Sato, K.; Monzen, S. Exosomes released from pancreatic cancer cells enhance angiogenic activities via dynamin-dependent endocytosis in endothelial cells in vitro. *Sci. Rep.* **2018**, *8*, 11972. [CrossRef] [PubMed]
47. Smyth, T.; Kullberg, M.; Malik, N.; Smith-Jones, P.; Graner, M.W.; Anchordoquy, T.J. Biodistribution and delivery efficiency of unmodified tumor-derived exosomes. *J. Control. Release* **2015**, *199*, 145–155. [CrossRef] [PubMed]
48. Franzen, C.A.; Simms, P.E.; Van Huis, A.F.; Foreman, K.E.; Kuo, P.C.; Gupta, G.N. Characterization of uptake and internalization of exosomes by bladder cancer cells. *Biomed. Res. Int.* **2014**, *2014*, 619829. [CrossRef]
49. Tian, T.; Wang, Y.; Wang, H.; Zhu, Z.; Xiao, Z. Visualizing of the cellular uptake and intracellular trafficking of exosomes by live-cell microscopy. *J. Cell. Biochem.* **2010**, *111*, 488–496. [CrossRef]
50. Smyth, T.; Petrova, K.; Payton, N.M.; Persaud, I.; Redzic, J.S.; Graner, M.W.; Smith-Jones, P.; Anchordoquy, T.J. Surface functionalization of exosomes using click chemistry. *Bioconjug. Chem.* **2014**, *25*, 1777–1784. [CrossRef]
51. Hein, C.D.; Liu, X.-M.; Wang, D. Click chemistry, a powerful tool for pharmaceutical sciences. *Pharmacol. Res.* **2008**, *25*, 2216–2230. [CrossRef]
52. Kooijmans, S.A.A.; Fliervoet, L.A.L.; van der Meel, R.; Fens, M.; Heijnen, H.F.G.; van Bergen En Henegouwen, P.M.P.; Vader, P.; Schiffelers, R.M. PEGylated and targeted extracellular vesicles display enhanced cell specificity and circulation time. *J. Control. Release* **2016**, *224*, 77–85. [CrossRef] [PubMed]
53. Allen, T.M.; Sapra, P.; Moase, E. Use of the post-insertion method for the formation of ligand-coupled liposomes. *Cell. Mol. Biol. Lett.* **2002**, *7*, 889–894. [PubMed]
54. Choi, E.S.; Song, J.; Kang, Y.Y.; Mok, H. Mannose-modified serum exosomes for the elevated uptake to murine dendritic cells and lymphatic accumulation. *Macromol. Biosci.* **2019**, *19*, e1900042. [CrossRef]
55. Kim, M.S.; Haney, M.J.; Zhao, Y.; Yuan, D.; Deygen, I.; Klyachko, N.L.; Kabanov, A.V.; Batrakova, E.V. Engineering macrophage-derived exosomes for targeted paclitaxel delivery to pulmonary metastases: In vitro and in vivo evaluations. *Nanomedicine* **2018**, *14*, 195–204. [CrossRef] [PubMed]
56. Kim, M.S.; Haney, M.J.; Zhao, Y.; Mahajan, V.; Deygen, I.; Klyachko, N.L.; Inskoe, E.; Piroyan, A.; Sokolsky, M.; Okolie, O.; et al. Development of exosome-encapsulated paclitaxel to overcome MDR in cancer cells. *Nanomed. Nanotechnol. Biol. Med.* **2016**, *12*, 655–664. [CrossRef] [PubMed]
57. Pi, F.; Binzel, D.W.; Lee, T.J.; Li, Z.; Sun, M.; Rychahou, P.; Li, H.; Haque, F.; Wang, S.; Croce, C.M.; et al. Nanoparticle orientation to control RNA loading and ligand display on extracellular vesicles for cancer regression. *Nat. Nanotechnol.* **2018**, *13*, 82–89. [CrossRef]
58. Jo, J.; Okazaki, A.; Nagane, K.; Yamamoto, M.; Tabata, Y. Preparation of cationized polysaccharides as gene transfection carrier for bone marrow-derived mesenchymal stem cells. *J. Biomater. Sci. Polym. Ed.* **2010**, *21*, 185–204. [CrossRef]
59. Nakase, I.; Futaki, S. Combined treatment with a pH-sensitive fusogenic peptide and cationic lipids achieves enhanced cytosolic delivery of exosomes. *Sci. Rep.* **2015**, *5*, 10112. [CrossRef]
60. Nakase, I.; Kogure, K.; Harashima, H.; Futaki, S. Application of a fusiogenic peptide GALA for intracellular delivery. *Methods Mol. Biol. (Clifton, NJ)* **2011**, *683*, 525–533. [CrossRef]

61. Liang, Y.; Eng, W.S.; Colquhoun, D.R.; Dinglasan, R.R.; Graham, D.R.; Mahal, L.K. Complex N-linked glycans serve as a determinant for exosome/microvesicle cargo recruitment. *J. Biol. Chem.* **2014**, *289*, 32526–32537. [CrossRef]
62. Williams, C.; Pazos, R.; Royo, F.; González, E.; Roura-Ferrer, M.; Martinez, A.; Gamiz, J.; Reichardt, N.-C.; Falcón-Pérez, J.M. Assessing the role of surface glycans of extracellular vesicles on cellular uptake. *Sci. Rep.* **2019**, *9*, 11920. [CrossRef] [PubMed]
63. Batista, B.S.; Eng, W.S.; Pilobello, K.T.; Hendricks-Munoz, K.D.; Mahal, L.K. Identification of a conserved glycan signature for microvesicles. *J. Proteome Res.* **2011**, *10*, 4624–4633. [CrossRef] [PubMed]
64. Shimoda, A.; Tahara, Y.; Sawada, S.I.; Sasaki, Y.; Akiyoshi, K. Glycan profiling analysis using evanescent-field fluorescence-assisted lectin array: Importance of sugar recognition for cellular uptake of exosomes from mesenchymal stem cells. *Biochem. Biophys. Res. Commun.* **2017**, *491*, 701–707. [CrossRef] [PubMed]
65. Rodrigues, J.G.; Balmana, M.; Macedo, J.A.; Pocas, J.; Fernandes, A.; de-Freitas-Junior, J.C.M.; Pinho, S.S.; Gomes, J.; Magalhaes, A.; Gomes, C.; et al. Glycosylation in cancer: Selected roles in tumour progression, immune modulation and metastasis. *Cell. Immunol.* **2018**, *333*, 46–57. [CrossRef]
66. Varki, A.; Kannagi, E.; Toole, B.; Stanley, P. Glycosylation changes in cancer. In *Essentials of Glycobiology*, 3rd ed.; Cold Spring Harbor Laboratory Press: Cold Spring Harbor, NY, USA, 2017. [CrossRef]
67. Royo, F.; Cossio, U.; Ruiz de Angulo, A.; Llop, J.; Falcon-Perez, J.M. Modification of the glycosylation of extracellular vesicles alters their biodistribution in mice. *Nanoscale* **2019**, *11*, 1531–1537. [CrossRef]
68. Dusoswa, S.A.; Horrevorts, S.K.; Ambrosini, M.; Kalay, H.; Paauw, N.J.; Nieuwland, R.; Pegtel, M.D.; Würdinger, T.; Van Kooyk, Y.; Garcia-Vallejo, J.J. Glycan modification of glioblastoma-derived extracellular vesicles enhances receptor-mediated targeting of dendritic cells. *J. Extracell. Vesicles* **2019**, *8*, 1648995. [CrossRef]
69. Santegoets, K.C.M.; Gielen, P.R.; Büll, C.; Schulte, B.M.; Kers-Rebel, E.D.; Küsters, B.; Bossman, S.A.J.F.H.; ter Laan, M.; Wesseling, P.; Adema, G.J. Expression profiling of immune inhibitory Siglecs and their ligands in patients with glioma. *Cancer Immunol. Immunother.* **2019**, *68*, 937–949. [CrossRef]
70. Hung, M.E.; Leonard, J.N. Stabilization of exosome-targeting peptides via engineered glycosylation. *J. Biol. Chem.* **2015**, *290*, 8166–8172. [CrossRef]
71. Li, Y.; Gao, Y.; Gong, C.; Wang, Z.; Xia, Q.; Gu, F.; Hu, C.; Zhang, L.; Guo, H.; Gao, S. A33 antibody-functionalized exosomes for targeted delivery of doxorubicin against colorectal cancer. *Nanomed. Nanotechnol. Biol. Med.* **2018**, *14*, 1973–1985. [CrossRef]
72. Ye, Z.; Zhang, T.; He, W.; Jin, H.; Liu, C.; Yang, Z.; Ren, J. Methotrexate-loaded extracellular vesicles functionalized with therapeutic and targeted peptides for the treatment of glioblastoma multiforme. *ACS Appl. Mater. Interfaces* **2018**, *10*, 12341–12350. [CrossRef]
73. Zhu, Q.; Ling, X.; Yang, Y.; Zhang, J.; Li, Q.; Niu, X.; Hu, G.; Chen, B.; Li, H.; Wang, Y.; et al. Embryonic stem cells-derived exosomes endowed with targeting properties as chemotherapeutics delivery vehicles for glioblastoma therapy. *Adv. Sci.* **2019**, *6*, 1801899. [CrossRef] [PubMed]
74. Tamura, R.; Uemoto, S.; Tabata, Y. Augmented liver targeting of exosomes by surface modification with cationized pullulan. *Acta Biomater.* **2017**, *57*, 274–284. [CrossRef] [PubMed]
75. Nakase, I.; Noguchi, K.; Aoki, A.; Takatani-Nakase, T.; Fujii, I.; Futaki, S. Arginine-rich cell-penetrating peptide-modified extracellular vesicles for active macropinocytosis induction and efficient intracellular delivery. *Sci. Rep.* **2017**, *7*, 1991. [CrossRef] [PubMed]
76. Zhao, C.; Busch, D.J.; Vershel, C.P.; Stachowiak, J.C. Multifunctional transmembrane protein ligands for cell-specific targeting of plasma membrane-derived vesicles. *Small* **2016**, *12*, 3837–3848. [CrossRef] [PubMed]
77. Wang, Q.; Ren, Y.; Mu, J.; Egilmez, N.K.; Zhuang, X.; Deng, Z.; Zhang, L.; Yan, J.; Miller, D.; Zhang, H.-G. Grapefruit-derived nanovectors use an activated leukocyte trafficking pathway to deliver therapeutic agents to inflammatory tumor sites. *Cancer Res.* **2015**, *75*, 2520–2529. [CrossRef] [PubMed]
78. Betzer, O.; Perets, N.; Angel, A.; Motiei, M.; Sadan, T.; Yadid, G.; Offen, D.; Popovtzer, R. In vivo neuroimaging of exosomes using gold nanoparticles. *ACS Nano* **2017**, *11*, 10883–10893. [CrossRef]
79. Tian, Y.; Li, S.; Song, J.; Ji, T.; Zhu, M.; Anderson, G.J.; Wei, J.; Nie, G. A doxorubicin delivery platform using engineered natural membrane vesicle exosomes for targeted tumor therapy. *Biomaterials* **2014**, *35*, 2383–2390. [CrossRef]
80. Bunggulawa, E.J.; Wang, W.; Yin, T.; Wang, N.; Durkan, C.; Wang, Y.; Wang, G. Recent advancements in the use of exosomes as drug delivery systems. *J. Nanobiotechnol.* **2018**, *16*, 81. [CrossRef]

81. Yang, T.; Martin, P.; Fogarty, B.; Brown, A.; Schurman, K.; Phipps, R.; Yin, V.P.; Lockman, P.; Bai, S. Exosome delivered anticancer drugs across the blood-brain barrier for brain cancer therapy in danio rerio. *Pharmacol. Res.* **2015**, *32*, 2003–2014. [CrossRef]
82. Illes, B.; Hirschle, P.; Barnert, S.; Cauda, V.; Engelke, H. Exosome-coated metal–organic framework nanoparticles: An efficient drug delivery platform. *Chem. Mater.* **2017**, *29*. [CrossRef]
83. Saari, H.; Lázaro-Ibáñez, E.; Viitala, T.; Vuorimaa-Laukkanen, E.; Siljander, P.; Yliperttula, M. Microvesicle- and exosome-mediated drug delivery enhances the cytotoxicity of Paclitaxel in autologous prostate cancer cells. *J. Control. Release* **2015**, *220*, 727–737. [CrossRef] [PubMed]
84. Bellavia, D.; Raimondo, S.; Calabrese, G.; Forte, S.; Cristaldi, M.; Patinella, A.; Memeo, L.; Manno, M.; Raccosta, S.; Diana, P.; et al. Interleukin 3-receptor targeted exosomes inhibit in vitro and in vivo Chronic Myelogenous Leukemia cell growth. *Theranostics* **2017**, *7*, 1333–1345. [CrossRef] [PubMed]
85. Kim, H.; Kim, D.; Nam, H.; Moon, S.; Kwon, Y.J.; Lee, J.B. Engineered extracellular vesicles and their mimetics for clinical translation. *Methods* **2019**, *19*, 30221-x. [CrossRef] [PubMed]
86. Zhang, W.; Yu, Z.-L.; Wu, M.; Ren, J.-G.; Xia, H.-F.; Sa, G.-L.; Zhu, J.-Y.; Pang, D.-W.; Zhao, Y.-F.; Chen, G. Magnetic and folate functionalization enables rapid isolation and enhanced tumor-targeting of cell-derived microvesicles. *ACS Nano* **2017**, *11*, 277–290. [CrossRef] [PubMed]
87. Alvarez-Erviti, L.; Seow, Y.; Yin, H.; Betts, C.; Lakhal, S.; Wood, M.J.A. Delivery of siRNA to the mouse brain by systemic injection of targeted exosomes. *Nat. Biotechnol.* **2011**, *29*, 341–345. [CrossRef]
88. Wahlgren, J.; Karlson, T.D.L.; Brisslert, M.; Vaziri Sani, F.; Telemo, E.; Sunnerhagen, P.; Valadi, H. Plasma exosomes can deliver exogenous short interfering RNA to monocytes and lymphocytes. *Nucleic Acids Res.* **2012**, *40*, e130. [CrossRef]
89. Lamichhane, T.N.; Raiker, R.S.; Jay, S.M. Exogenous DNA loading into extracellular vesicles via electroporation is size-dependent and enables limited gene delivery. *Mol. Pharmacol.* **2015**, *12*, 3650–3657. [CrossRef]
90. Hood, J.L.; Scott, M.J.; Wickline, S.A. Maximizing exosome colloidal stability following electroporation. *Anal. Biochem* **2014**, *448*, 41–49. [CrossRef]
91. Sato, Y.T.; Umezaki, K.; Sawada, S.; Mukai, S.-A.; Sasaki, Y.; Harada, N.; Shiku, H.; Akiyoshi, K. Engineering hybrid exosomes by membrane fusion with liposomes. *Sci. Rep.* **2016**, *6*, 21933. [CrossRef]
92. Haney, M.J.; Klyachko, N.L.; Harrison, E.B.; Zhao, Y.; Kabanov, A.V.; Batrakova, E.V. TPP1 Delivery to lysosomes with extracellular vesicles and their enhanced brain distribution in the animal model of batten disease. *Adv. Healthc. Mater.* **2019**, *8*, 1801271. [CrossRef]
93. Khongkow, M.; Yata, T.; Boonrungsiman, S.; Ruktanonchai, U.R.; Graham, D.; Namdee, K. Surface modification of gold nanoparticles with neuron-targeted exosome for enhanced blood-brain barrier penetration. *Sci. Rep.* **2019**, *9*, 8278. [CrossRef] [PubMed]
94. Jiang, X.-C.; Gao, J.-Q. Exosomes as novel bio-carriers for gene and drug delivery. *Int. J. Pharmacol.* **2017**, *521*, 167–175. [CrossRef] [PubMed]
95. Lamichhane, T.N.; Jeyaram, A.; Patel, D.B.; Parajuli, B.; Livingston, N.K.; Arumugasaamy, N.; Schardt, J.S.; Jay, S.M. Oncogene knockdown via active loading of small RNAs into extracellular vesicles by sonication. *Cell. Mol. Bioeng.* **2016**, *9*, 315–324. [CrossRef] [PubMed]
96. Haney, M.J.; Klyachko, N.L.; Zhao, Y.; Gupta, R.; Plotnikova, E.G.; He, Z.; Patel, T.; Piroyan, A.; Sokolsky, M.; Kabanov, A.V.; et al. Exosomes as drug delivery vehicles for Parkinson's disease therapy. *J. Control. Release* **2015**, *207*, 18–30. [CrossRef] [PubMed]
97. Fuhrmann, G.; Serio, A.; Mazo, M.; Nair, R.; Stevens, M.M. Active loading into extracellular vesicles significantly improves the cellular uptake and photodynamic effect of porphyrins. *J. Control. Release* **2015**, *205*, 35–44. [CrossRef]
98. Zhang, D.; Qin, X.; Wu, T.; Qiao, Q.; Song, Q.; Zhang, Z. Extracellular vesicles based self-grown gold nanopopcorn for combinatorial chemo-photothermal therapy. *Biomaterials* **2019**, *197*, 220–228. [CrossRef]
99. Ha, D.; Yang, N.; Nadithe, V. Exosomes as therapeutic drug carriers and delivery vehicles across biological membranes: Current perspectives and future challenges. *Acta Pharm. Sin. B* **2016**, *6*, 287–296. [CrossRef]
100. Podolak, I.; Galanty, A.; Sobolewska, D. Saponins as cytotoxic agents: A review. *Phytochem. Rev.* **2010**, *9*, 425–474. [CrossRef]
101. Pascucci, L.; Coccè, V.; Bonomi, A.; Ami, D.; Ceccarelli, P.; Ciusani, E.; Viganò, L.; Locatelli, A.; Sisto, F.; Doglia, S.M.; et al. Paclitaxel is incorporated by mesenchymal stromal cells and released in exosomes that inhibit in vitro tumor growth: A new approach for drug delivery. *J. Control. Release* **2014**, *192*, 262–270. [CrossRef]

102. Agrawal, A.K.; Aqil, F.; Jeyabalan, J.; Spencer, W.A.; Beck, J.; Gachuki, B.W.; Alhakeem, S.S.; Oben, K.; Munagala, R.; Bondada, S.; et al. Milk-derived exosomes for oral delivery of paclitaxel. *Nanomed. Nanotechnol. Biol. Med.* **2017**, *13*, 1627–1636. [CrossRef]
103. Aubertin, K.; Silva, A.K.A.; Luciani, N.; Espinosa, A.; Djemat, A.; Charue, D.; Gallet, F.; Blanc-Brude, O.; Wilhelm, C. Massive release of extracellular vesicles from cancer cells after photodynamic treatment or chemotherapy. *Sci. Rep.* **2016**, *6*, 35376. [CrossRef] [PubMed]
104. Goh, W.J.; Lee, C.K.; Zou, S.; Woon, E.C.; Czarny, B.; Pastorin, G. Doxorubicin-loaded cell-derived nanovesicles: An alternative targeted approach for anti-tumor therapy. *Int. J. Nanomed.* **2017**, *12*, 2759–2767. [CrossRef] [PubMed]
105. Yoneda, A.; Lendorf, M.E.; Couchman, J.R.; Multhaupt, H.A.B. Breast and ovarian cancers: A survey and possible roles for the cell surface heparan sulfate proteoglycans. *J. Histochem. Cytochem.* **2012**, *60*, 9–21. [CrossRef] [PubMed]
106. Hadla, M.; Palazzolo, S.; Corona, G.; Caligiuri, I.; Canzonieri, V.; Toffoli, G.; Rizzolio, F. Exosomes increase the therapeutic index of doxorubicin in breast and ovarian cancer mouse models. *Nanomedicine* **2016**, *11*, 2431–2441. [CrossRef] [PubMed]
107. Toffoli, G.; Hadla, M.; Corona, G.; Caligiuri, I.; Palazzolo, S.; Semeraro, S.; Gamini, A.; Canzonieri, V.; Rizzolio, F. Exosomal doxorubicin reduces the cardiac toxicity of doxorubicin. *Nanomedicine* **2015**, *10*, 2963–2971. [CrossRef] [PubMed]
108. Hewlings, S.J.; Kalman, D.S. Curcumin: A review of its' effects on human health. *Foods* **2017**, *6*, 92. [CrossRef]
109. Aqil, F.; Munagala, R.; Jeyabalan, J.; Agrawal, A.K.; Gupta, R. Exosomes for the enhanced tissue bioavailability and efficacy of curcumin. *AAPS J.* **2017**, *19*, 1691–1702. [CrossRef]
110. Zhang, H.-G.; Kim, H.; Liu, C.; Yu, S.; Wang, J.; Grizzle, W.E.; Kimberly, R.P.; Barnes, S. Curcumin reverses breast tumor exosomes mediated immune suppression of NK cell tumor cytotoxicity. *Biochim. Biophys. Acta* **2007**, *1773*, 1116–1123. [CrossRef]
111. Farooqi, A.A.; Rehman, Z.U.; Muntane, J. Antisense therapeutics in oncology: Current status. *OncoTargets Ther.* **2014**, *7*, 2035–2042. [CrossRef]
112. Brazzale, C.; Canaparo, R.; Racca, L.; Foglietta, F.; Durando, G.; Fantozzi, R.; Caliceti, P.; Salmaso, S.; Serpe, L. Enhanced selective sonosensitizing efficacy of ultrasound-based anticancer treatment by targeted gold nanoparticles. *Nanomedicine* **2016**, *11*, 3053–3070. [CrossRef]
113. Limongi, T.; Canta, M.; Racca, L.; Ancona, A.; Tritta, S.; Vighetto, V.; Cauda, V. Improving dispersal of therapeutic nanoparticles in the human body. *Nanomedicine* **2019**, *14*, 797–801. [CrossRef] [PubMed]
114. Zhang, L.; Gu, F.X.; Chan, J.M.; Wang, A.Z.; Langer, R.S.; Farokhzad, O.C. Nanoparticles in medicine: Therapeutic applications and developments. *Clin. Pharmacol. Ther.* **2008**, *83*, 761–769. [CrossRef] [PubMed]
115. Vogt, S.; Stadlmayr, G.; Grillari, J.; Rüker, F.; Wozniak-Knopp, G. Engineering of surface proteins in extracellular vesicles for tissue-specific targeting. *Curr. Top. Biochem. Eng.* **2019**. [CrossRef]
116. Van Meer, G.; Voelker, D.R.; Feigenson, G.W. Membrane lipids: Where they are and how they behave. *Nat. Rev. Mol. Cell Biol.* **2008**, *9*, 112–124. [CrossRef]
117. Barile, L.; Vassalli, G. Exosomes: Therapy delivery tools and biomarkers of diseases. *Pharmacol. Ther.* **2017**, *174*, 63–78. [CrossRef]
118. Srivastava, A.; Amreddy, N.; Babu, A.; Panneerselvam, J.; Mehta, M.; Muralidharan, R.; Chen, A.; Zhao, Y.D.; Razaq, M.; Riedinger, N.; et al. Nanosomes carrying doxorubicin exhibit potent anticancer activity against human lung cancer cells. *Sci. Rep.* **2016**, *6*, 38541. [CrossRef]
119. Cheng, G.; Li, W.; Ha, L.; Han, X.; Hao, S.; Wan, Y.; Wang, Z.; Dong, F.; Zou, X.; Mao, Y.; et al. Self-assembly of extracellular vesicle-like metal–organic framework nanoparticles for protection and intracellular delivery of biofunctional proteins. *J. Am. Chem. Soc.* **2018**, *140*, 7282–7291. [CrossRef]
120. Piffoux, M.; Silva, A.K.A.; Lugagne, J.-B.; Hersen, P.; Wilhelm, C.; Gazeau, F. Extracellular vesicle production loaded with nanoparticles and drugs in a trade-off between loading, yield and purity: Towards a personalized drug delivery system. *Adv. Biosyst.* **2017**, *1*, 1700044. [CrossRef]
121. Bose, R.J.C.; Uday Kumar, S.; Zeng, Y.; Afjei, R.; Robinson, E.; Lau, K.; Bermudez, A.; Habte, F.; Pitteri, S.J.; Sinclair, R.; et al. Tumor cell-derived extracellular vesicle-coated nanocarriers: An efficient theranostic platform for the cancer-specific delivery of Anti-miR-21 and imaging agents. *ACS Nano* **2018**, *12*, 10817–10832. [CrossRef]

122. Dumontel, B.; Susa, F.; Limongi, T.; Canta, M.; Racca, L.; Chiodoni, A.; Garino, N.; Chiabotto, G.; Centomo, M.L.; Pignochino, Y.; et al. ZnO nanocrystals shuttled by extracellular vesicles as effective Trojan nano-horses against cancer cells. *Nanomedicine* **2019**, *14*. [CrossRef]
123. Sun, D.; Zhuang, X.; Xiang, X.; Liu, Y.; Zhang, S.; Liu, C.; Barnes, S.; Grizzle, W.; Miller, D.; Zhang, H.-G. A novel nanoparticle drug delivery system: The anti-inflammatory activity of curcumin is enhanced when encapsulated in exosomes. *Mol. Ther.* **2010**, *18*, 1606–1614. [CrossRef] [PubMed]
124. Aqil, F.; Kausar, H.; Agrawal, A.K.; Jeyabalan, J.; Kyakulaga, A.-H.; Munagala, R.; Gupta, R. Exosomal formulation enhances therapeutic response of celastrol against lung cancer. *Exp. Mol. Pathol.* **2016**, *101*, 12–21. [CrossRef] [PubMed]
125. Garofalo, M.; Villa, A.; Rizzi, N.; Kuryk, L.; Rinner, B.; Cerullo, V.; Yliperttula, M.; Mazzaferro, V.; Ciana, P. Extracellular vesicles enhance the targeted delivery of immunogenic oncolytic adenovirus and paclitaxel in immunocompetent mice. *J. Control. Release* **2019**, *294*, 165–175. [CrossRef] [PubMed]
126. Faruqu, F.N.; Wang, J.T.; Xu, L.; McNickle, L.; Chong, E.M.; Walters, A.; Gurney, M.; Clayton, A.; Smyth, L.A.; Hider, R.; et al. Membrane radiolabelling of exosomes for comparative biodistribution analysis in immunocompetent and immunodeficient mice—A novel and universal approach. *Theranostics* **2019**, *9*, 1666–1682. [CrossRef]
127. Greco, K.A.; Franzen, C.A.; Foreman, K.E.; Flanigan, R.C.; Kuo, P.C.; Gupta, G.N. PLK-1 Silencing in bladder cancer by siRNA delivered with exosomes. *Urology* **2016**, *91*, 241.e1–241.e7. [CrossRef]
128. Pomatto, M.A.C.; Bussolati, B.; D'Antico, S.; Ghiotto, S.; Tetta, C.; Brizzi, M.F.; Camussi, G. Improved loading of plasma-derived extracellular vesicles to encapsulate antitumor miRNAs. *Mol. Ther. Methods Clin. Dev.* **2019**, *13*, 133–144. [CrossRef]
129. Mentkowski, K.I.; Snitzer, J.D.; Rusnak, S.; Lang, J.K. Therapeutic potential of engineered extracellular vesicles. *AAPS J.* **2018**, *20*, 50. [CrossRef]
130. Zomer, A.; Maynard, C.; Verweij, F.J.; Kamermans, A.; Schäfer, R.; Beerling, E.; Schiffelers, R.M.; de Wit, E.; Berenguer, J.; Ellenbroek, S.I.J.; et al. In vivo imaging reveals extracellular vesicle-mediated phenocopying of metastatic behavior. *Cell* **2015**, *161*, 1046–1057. [CrossRef]
131. Hoffman, R.M. Stromal-cell and cancer-cell exosomes leading the metastatic exodus for the promised niche. *Breast Cancer Res.* **2013**, *15*, 310. [CrossRef]
132. Melo, S.A.; Luecke, L.B.; Kahlert, C.; Fernandez, A.F.; Gammon, S.T.; Kaye, J.; LeBleu, V.S.; Mittendorf, E.A.; Weitz, J.; Rahbari, N.; et al. Glypican-1 identifies cancer exosomes and detects early pancreatic cancer. *Nature* **2015**, *523*, 177. [CrossRef]
133. Lee, T.S.; Kim, Y.; Zhang, W.; Song, I.H.; Tung, C.-H. Facile metabolic glycan labeling strategy for exosome tracking. *Biochim. Biophys. Acta* **2018**, *1862*, 1091–1100. [CrossRef] [PubMed]
134. Lai, C.P.; Tannous, B.A.; Breakefield, X.O. Noninvasive in vivo monitoring of extracellular vesicles. In *Bioluminescent Imaging: Methods and Protocols*; Badr, C.E., Ed.; Humana Press: Totowa, NJ, USA, 2014; pp. 249–258. [CrossRef]
135. Lai, C.P.; Mardini, O.; Ericsson, M.; Prabhakar, S.; Maguire, C.; Chen, J.W.; Tannous, B.A.; Breakefield, X.O. Dynamic biodistribution of extracellular vesicles in vivo using a multimodal imaging reporter. *ACS Nano* **2014**, *8*, 483–494. [CrossRef] [PubMed]
136. Takahashi, Y.; Nishikawa, M.; Shinotsuka, H.; Matsui, Y.; Ohara, S.; Imai, T.; Takakura, Y. Visualization and in vivo tracking of the exosomes of murine melanoma B16-BL6 cells in mice after intravenous injection. *J. Biotechnol.* **2013**, *165*, 77–84. [CrossRef] [PubMed]
137. Imai, T.; Takahashi, Y.; Nishikawa, M.; Kato, K.; Morishita, M.; Yamashita, T.; Matsumoto, A.; Charoenviriyakul, C.; Takakura, Y. Macrophage-dependent clearance of systemically administered B16BL6-derived exosomes from the blood circulation in mice. *J. Extracell. Vesicles* **2015**, *4*, 26238. [CrossRef] [PubMed]
138. Morishita, M.; Takahashi, Y.; Nishikawa, M.; Ariizumi, R.; Takakura, Y. Enhanced class I tumor antigen presentation via cytosolic delivery of exosomal cargos by tumor-cell-derived exosomes displaying a pH-sensitive fusogenic peptide. *Mol. Pharmacol.* **2017**, *14*, 4079–4086. [CrossRef] [PubMed]
139. Limoni, S.K.; Moghadam, M.F.; Moazzeni, S.M.; Gomari, H.; Salimi, F. Engineered exosomes for targeted transfer of siRNA to HER2 positive breast cancer cells. *Appl. Biochem. Biotechnol.* **2019**, *187*, 352–364. [CrossRef] [PubMed]

140. Wang, J.-H.; Forterre, A.V.; Zhao, J.; Frimannsson, D.O.; Delcayre, A.; Antes, T.J.; Efron, B.; Jeffrey, S.S.; Pegram, M.D.; Matin, A.C. Anti-HER2 scFv-directed extracellular vesicle-mediated mRNA-based gene delivery inhibits growth of HER2-positive human breast tumor xenografts by prodrug activation. *Mol. Cancer Ther.* **2018**, *17*, 1133–1142. [CrossRef]
141. Hartman, Z.C.; Wei, J.; Glass, O.K.; Guo, H.; Lei, G.; Yang, X.-Y.; Osada, T.; Hobeika, A.; Delcayre, A.; Le Pecq, J.-B.; et al. Increasing vaccine potency through exosome antigen targeting. *Vaccine* **2011**, *29*, 9361–9367. [CrossRef]
142. Rountree, R.B.; Mandl, S.J.; Nachtwey, J.M.; Dalpozzo, K.; Do, L.; Lombardo, J.R.; Schoonmaker, P.L.; Brinkmann, K.; Dirmeier, U.; Laus, R.; et al. Exosome targeting of tumor antigens expressed by cancer vaccines can improve antigen immunogenicity and therapeutic efficacy. *Cancer Res.* **2011**, *71*, 5235. [CrossRef]
143. Kooijmans, S.A.A.; Aleza, C.G.; Roffler, S.R.; van Solinge, W.W.; Vader, P.; Schiffelers, R.M. Display of GPI-anchored anti-EGFR nanobodies on extracellular vesicles promotes tumour cell targeting. *J. Extracell. Vesicles* **2016**, *5*, 31053. [CrossRef]
144. Yamamoto, T.; Teramura, Y.; Itagaki, T.; Arima, Y.; Iwata, H. Interaction of poly(ethylene glycol)-conjugated phospholipids with supported lipid membranes and their influence on protein adsorption. *Sci. Technol. Adv. Mater.* **2016**, *17*, 677–684. [CrossRef] [PubMed]
145. Zhu, L.; Dong, D.; Yu, Z.-L.; Zhao, Y.-F.; Pang, D.-W.; Zhang, Z.-L. Folate-engineered microvesicles for enhanced target and synergistic therapy toward breast cancer. *ACS Appl. Mater. Interfaces* **2017**, *9*, 5100–5108. [CrossRef] [PubMed]
146. Chen, G.; Zhu, J.-Y.; Zhang, Z.-L.; Zhang, W.; Ren, J.-G.; Wu, M.; Hong, Z.-Y.; Lv, C.; Pang, D.-W.; Zhao, Y.-F. Transformation of cell-derived microparticles into quantum-dot-labeled nanovectors for antitumor siRNA delivery. *Angew. Chem. Int. Ed.* **2015**, *54*, 1036–1040. [CrossRef] [PubMed]
147. Wang, J.; Li, W.; Zhang, L.; Ban, L.; Chen, P.; Du, W.; Feng, X.; Liu, B.-F. Chemically edited exosomes with dual ligand purified by microfluidic device for active targeted drug delivery to tumor cells. *ACS Appl. Mater. Interfaces* **2017**, *9*, 27441–27452. [CrossRef]
148. Wang, J.; Dong, Y.; Li, Y.; Li, W.; Cheng, K.; Qian, Y.; Xu, G.; Zhang, X.; Hu, L.; Chen, P.; et al. Designer exosomes for active targeted chemo-photothermal synergistic tumor therapy. *Adv. Funct. Mater.* **2018**, *28*, 1707360. [CrossRef]
149. Suetsugu, A.; Honma, K.; Saji, S.; Moriwaki, H.; Ochiya, T.; Hoffman, R.M. Imaging exosome transfer from breast cancer cells to stroma at metastatic sites in orthotopic nude-mouse models. *Adv. Drug Deliv. Rev.* **2013**, *65*, 383–390. [CrossRef]
150. Lai, C.P.; Kim, E.Y.; Badr, C.E.; Weissleder, R.; Mempel, T.R.; Tannous, B.A.; Breakefield, X.O. Visualization and tracking of tumour extracellular vesicle delivery and RNA translation using multiplexed reporters. *Nat. Commun.* **2015**, *6*, 7029. [CrossRef]
151. Zeelenberg, I.S.; Ostrowski, M.; Krumeich, S.; Bobrie, A.; Jancic, C.; Boissonnas, A.; Delcayre, A.; Le Pecq, J.-B.; Combadière, B.; Amigorena, S.; et al. Targeting tumor antigens to secreted membrane vesicles in vivo induces efficient antitumor immune responses. *Cancer Res.* **2008**, *68*, 1228. [CrossRef]
152. Zeelenberg, I.S.; van Maren, W.W.C.; Boissonnas, A.; Van Hout-Kuijer, M.A.; Den Brok, M.H.M.G.M.; Wagenaars, J.A.L.; van der Schaaf, A.; Jansen, E.J.R.; Amigorena, S.; Théry, C.; et al. Antigen localization controls T cell-mediated tumor immunity. *J. Immunol.* **2011**, *187*, 1281. [CrossRef]
153. Delcayre, A.; Estelles, A.; Sperinde, J.; Roulon, T.; Paz, P.; Aguilar, B.; Villanueva, J.; Khine, S.; Le Pecq, J.-B. Exosome display technology: Applications to the development of new diagnostics and therapeutics. *Blood Cells Mol. Dis.* **2005**, *35*, 158–168. [CrossRef]
154. Ohno, S.-I.; Takanashi, M.; Sudo, K.; Ueda, S.; Ishikawa, A.; Matsuyama, N.; Fujita, K.; Mizutani, T.; Ohgi, T.; Ochiya, T.; et al. Systemically injected exosomes targeted to EGFR deliver antitumor microRNA to breast cancer cells. *Mol. Ther.* **2013**, *21*, 185–191. [CrossRef] [PubMed]
155. Alhasan, A.H.; Patel, P.C.; Choi, C.H.J.; Mirkin, C.A. Exosome encased spherical nucleic acid gold nanoparticle conjugates as potent microRNA regulation agents. *Small* **2014**, *10*, 186–192. [CrossRef] [PubMed]
156. Tao, S.-C.; Yuan, T.; Zhang, Y.-L.; Yin, W.-J.; Guo, S.-C.; Zhang, C.-Q. Exosomes derived from miR-140-5p-overexpressing human synovial mesenchymal stem cells enhance cartilage tissue regeneration and prevent osteoarthritis of the knee in a rat model. *Theranostics* **2017**, *7*, 180–195. [CrossRef]

157. Cho, J.-A.; Yeo, D.-J.; Son, H.-Y.; Kim, H.-W.; Jung, D.-S.; Ko, J.-K.; Koh, J.S.; Kim, Y.-N.; Kim, C.-W. Exosomes: A new delivery system for tumor antigens in cancer immunotherapy. *Int. J. Cancer* **2005**, *114*, 613–622. [CrossRef] [PubMed]
158. Yuan, Z.; Kolluri, K.K.; Gowers, K.H.C.; Janes, S.M. TRAIL delivery by MSC-derived extracellular vesicles is an effective anticancer therapy. *J. Extracell. Vesicles* **2017**, *6*, 1265291. [CrossRef] [PubMed]
159. Rivoltini, L.; Chiodoni, C.; Squarcina, P.; Tortoreto, M.; Villa, A.; Vergani, B.; Bürdek, M.; Botti, L.; Arioli, I.; Cova, A.; et al. TNF-related apoptosis-inducing ligand (TRAIL)-armed exosomes deliver proapoptotic signals to tumor site. *Clin. Cancer Res.* **2016**, *22*, 3499. [CrossRef]
160. Yang, Y.; Hong, Y.; Cho, E.; Kim, G.B.; Kim, I.-S. Extracellular vesicles as a platform for membrane-associated therapeutic protein delivery. *J. Extracell. Vesicles* **2018**, *7*, 1440131. [CrossRef]
161. Di Bonito, P.; Chiozzini, C.; Arenaccio, C.; Anticoli, S.; Manfredi, F.; Olivetta, E.; Ferrantelli, F.; Falcone, E.; Ruggieri, A.; Federico, M. Antitumor HPV E7-specific CTL activity elicited by in vivo engineered exosomes produced through DNA inoculation. *Int. J. Nanomed.* **2017**, *12*, 4579–4591. [CrossRef]
162. Meyer, C.; Losacco, J.; Stickney, Z.; Li, L.; Marriott, G.; Lu, B. Pseudotyping exosomes for enhanced protein delivery in mammalian cells. *Int. J. Nanomed.* **2017**, *12*, 3153–3170. [CrossRef]
163. Kochenderfer, J.N.; Rosenberg, S.A. Treating B-cell cancer with T cells expressing anti-CD19 chimeric antigen receptors. *Nat. Rev. Clin. Oncol.* **2013**, *10*, 267–276. [CrossRef]
164. Yim, N.; Ryu, S.-W.; Choi, K.; Lee, K.R.; Lee, S.; Choi, H.; Kim, J.; Shaker, M.R.; Sun, W.; Park, J.-H.; et al. Exosome engineering for efficient intracellular delivery of soluble proteins using optically reversible protein–protein interaction module. *Nat. Commun.* **2016**, *7*, 12277. [CrossRef] [PubMed]
165. Wang, X.; Zhang, H.; Bai, M.; Ning, T.; Ge, S.; Deng, T.; Liu, R.; Zhang, L.; Ying, G.; Ba, Y. Exosomes serve as nanoparticles to deliver anti-miR-214 to reverse chemoresistance to cisplatin in gastric cancer. *Mol. Ther.* **2018**, *26*, 774–783. [CrossRef] [PubMed]
166. O'Brien, K.; Lowry, M.C.; Corcoran, C.; Martinez, V.G.; Daly, M.; Rani, S.; Gallagher, W.M.; Radomski, M.W.; MacLeod, R.A.F.; O'Driscoll, L. MiR-134 in extracellular vesicles reduces triple-negative breast cancer aggression and increases drug sensitivity. *Oncotarget* **2015**, *6*, 32774–32789. [CrossRef] [PubMed]
167. Lou, G.; Song, X.; Yang, F.; Wu, S.; Wang, J.; Chen, Z.; Liu, Y. Exosomes derived from miR-122-modified adipose tissue-derived MSCs increase chemosensitivity of hepatocellular carcinoma. *J. Hematol. Oncol.* **2015**, *8*, 122. [CrossRef] [PubMed]
168. Katakowski, M.; Buller, B.; Zheng, X.; Lu, Y.; Rogers, T.; Osobamiro, O.; Shu, W.; Jiang, F.; Chopp, M. Exosomes from marrow stromal cells expressing miR-146b inhibit glioma growth. *Cancer Lett.* **2013**, *335*, 201–204. [CrossRef] [PubMed]
169. Shimbo, K.; Miyaki, S.; Ishitobi, H.; Kato, Y.; Kubo, T.; Shimose, S.; Ochi, M. Exosome-formed synthetic microRNA-143 is transferred to osteosarcoma cells and inhibits their migration. *Biochem. Biophys. Res. Commun.* **2014**, *445*, 381–387. [CrossRef]
170. Munoz, J.L.; Bliss, S.A.; Greco, S.J.; Ramkissoon, S.H.; Ligon, K.L.; Rameshwar, P. Delivery of functional anti-miR-9 by mesenchymal stem cell-derived exosomes to glioblastoma multiforme cells conferred chemosensitivity. *Mol. Ther. Nucleic Acids* **2013**, *2*, e126. [CrossRef]
171. Mizrak, A.; Bolukbasi, M.F.; Ozdener, G.B.; Brenner, G.J.; Madlener, S.; Erkan, E.P.; Ströbel, T.; Breakefield, X.O.; Saydam, O. Genetically engineered microvesicles carrying suicide mRNA/protein inhibit schwannoma tumor growth. *Mol. Ther.* **2013**, *21*, 101–108. [CrossRef]
172. Zhang, H.; Wang, Y.; Bai, M.; Wang, J.; Zhu, K.; Liu, R.; Ge, S.; Li, J.; Ning, T.; Deng, T.; et al. Exosomes serve as nanoparticles to suppress tumor growth and angiogenesis in gastric cancer by delivering hepatocyte growth factor siRNA. *Cancer Sci.* **2018**, *109*, 629–641. [CrossRef]
173. Shtam, T.A.; Kovalev, R.A.; Varfolomeeva, E.Y.; Makarov, E.M.; Kil, Y.V.; Filatov, M.V. Exosomes are natural carriers of exogenous siRNA to human cells in vitro. *Cell Commun. Signal.* **2013**, *11*, 88. [CrossRef]
174. Huang, L.; Gu, N.; Zhang, X.-E.; Wang, D.-B. Light-inducible exosome-based vehicle for endogenous RNA loading and delivery to leukemia cells. *Adv. Funct. Mater.* **2019**, *29*, 1807189. [CrossRef]
175. Aspe, J.R.; Diaz Osterman, C.J.; Jutzy, J.M.S.; Deshields, S.; Whang, S.; Wall, N.R. Enhancement of Gemcitabine sensitivity in pancreatic adenocarcinoma by novel exosome-mediated delivery of the Survivin-T34A mutant. *J. Extracell. Vesicles* **2014**, *3*. [CrossRef]
176. Tang, K.; Zhang, Y.; Zhang, H.; Xu, P.; Liu, J.; Ma, J.; Lv, M.; Li, D.; Katirai, F.; Shen, G.-X.; et al. Delivery of chemotherapeutic drugs in tumour cell-derived microparticles. *Nat. Commun.* **2012**, *3*, 1282. [CrossRef]

177. Silva, A.K.A.; Kolosnjaj-Tabi, J.; Bonneau, S.; Marangon, I.; Boggetto, N.; Aubertin, K.; Clément, O.; Bureau, M.F.; Luciani, N.; Gazeau, F.; et al. Magnetic and photoresponsive theranosomes: Translating cell-released vesicles into smart nanovectors for cancer therapy. *ACS Nano* **2013**, *7*, 4954–4966. [CrossRef]
178. Silva, A.K.A.; Luciani, N.; Gazeau, F.; Aubertin, K.; Bonneau, S.; Chauvierre, C.; Letourneur, D.; Wilhelm, C. Combining magnetic nanoparticles with cell derived microvesicles for drug loading and targeting. *Nanomed. Nanotechnol. Biol. Med.* **2015**, *11*, 645–655. [CrossRef]
179. Lee, J.; Kim, J.; Jeong, M.; Lee, H.; Goh, U.; Kim, H.; Kim, B.; Park, J.-H. Liposome-based engineering of cells to package hydrophobic compounds in membrane vesicles for tumor penetration. *Nano Lett.* **2015**, *15*, 2938–2944. [CrossRef]
180. Lee, J.; Lee, H.; Goh, U.; Kim, J.; Jeong, M.; Lee, J.; Park, J.-H. Cellular engineering with membrane fusogenic liposomes to produce functionalized extracellular vesicles. *ACS Appl. Mater. Interfaces* **2016**, *8*, 6790–6795. [CrossRef]
181. Sancho-Albero, M.; Navascués, N.; Mendoza, G.; Sebastián, V.; Arruebo, M.; Martín-Duque, P.; Santamaría, J. Exosome origin determines cell targeting and the transfer of therapeutic nanoparticles towards target cells. *J. Nanobiotechnol.* **2019**, *17*, 16. [CrossRef]
182. Yong, T.; Zhang, X.; Bie, N.; Zhang, H.; Zhang, X.; Li, F.; Hakeem, A.; Hu, J.; Gan, L.; Santos, H.A.; et al. Tumor exosome-based nanoparticles are efficient drug carriers for chemotherapy. *Nat. Commun.* **2019**, *10*, 3838. [CrossRef]
183. Mulens-Arias, V.; Nicolas-Boluda, A.; Brun, A.; Gazeau, F. Theranostic iron oxide nanoparticle cargo defines extracellular vesicle-dependent modulation of macrophage activation and migratory behavior. *Adv. Biosyst.* **2018**, *2*. [CrossRef]
184. Burdakov, V.S.; Kovalev, R.A.; Pantina, R.A.; Varfolomeeva, E.Y.; Makarov, E.M.; Filatov, M.V. Exosomes transfer p53 between cells and can suppress growth and proliferation of p53-negative cells. *Cell Tissue Biol.* **2018**, *12*, 20–26. [CrossRef]
185. Maguire, C.A.; Balaj, L.; Sivaraman, S.; Crommentuijn, M.H.W.; Ericsson, M.; Mincheva-Nilsson, L.; Baranov, V.; Gianni, D.; Tannous, B.A.; Sena-Esteves, M.; et al. Microvesicle-associated AAV vector as a novel gene delivery system. *Mol. Ther.* **2012**, *20*, 960–971. [CrossRef]
186. Li, Z.; Zhou, X.; Wei, M.; Gao, X.; Zhao, L.; Shi, R.; Sun, W.; Duan, Y.; Yang, G.; Yuan, L. In vitro and in vivo RNA inhibition by CD9-HuR functionalized exosomes encapsulated with miRNA or CRISPR/dCas9. *Nano Lett.* **2019**, *19*, 19–28. [CrossRef]

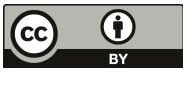

cancers

MDPI

Review

Multifunctional Magnetic Nanowires: Design, Fabrication, and Future Prospects as Cancer Therapeutics

Abu Bakr A. Nana, Thashree Marimuthu, Pierre P. D. Kondiah, Yahya E. Choonara, Lisa C. Du Toit and Viness Pillay *

Wits Advanced Drug Delivery Platform Research Unit, Department of Pharmacy and Pharmacology, School of Therapeutic Sciences, University of the Witwatersrand, Johannesburg, 7 York Road, Parktown 2193, South Africa; abubakr.nana@gmail.com (A.B.A.N.); thashree.marimuthu@wits.ac.za (T.M.); pierre.kondiah@wits.ac.za (P.P.D.K.); yahya.choonara@wits.ac.za (Y.E.C.); lisa.dutoit1@wits.ac.za (L.C.D.T.)
* Correspondence: viness.pillay@wits.ac.za; Tel.: +27-11-717-2274

Received: 5 November 2019; Accepted: 25 November 2019; Published: 6 December 2019

Abstract: Traditional cancer therapeutics are limited by factors such as multi-drug resistance and a plethora of adverse effect. These limitations need to be overcome for the progression of cancer treatment. In order to overcome these limitations, multifunctional nanosystems have recently been introduced into the market. The employment of multifunctional nanosystems provide for the enhancement of treatment efficacy and therapeutic effect as well as a decrease in drug toxicity. However, in addition to these effects, magnetic nanowires bring specific advantages over traditional nanoparticles in multifunctional systems in terms of the formulation and application into a therapeutic system. The most significant of which is its larger surface area, larger net magnetic moment compared to nanoparticles, and interaction under a magnetic field. This results in magnetic nanowires producing a greater drug delivery and therapeutic platform with specific regard to magnetic drug targeting, magnetic hyperthermia, and magnetic actuation. This, in turn, increases the potential of magnetic nanowires for decreasing adverse effects and improving patient therapeutic outcomes. This review focuses on the design, fabrication, and future potential of multifunctional magnetic nanowire systems with the emphasis on improving patient chemotherapeutic outcomes.

Keywords: magnetic nanowires; cancer; magnetic hyperthermia; magnetic actuation; magnetic drug targeting

1. Introduction

Cancer is amongst the most pernicious diseases known, due to the high mortality and incidence rates reported [1]. Traditional treatment such as chemotherapy, radiation therapy, and surgery has provided successful treatment and control of cancer to a certain extent [2]. However, each approach comes with its own difficulties, notably being invasive or unspecific in its killing effect leading to grave adverse effects. Alternative therapies such as carbon ion therapy and proton therapy are more specific and carries a lower side effect risk when compared to X-ray radiotherapy. The limitation of these therapies is that they require specialized equipment and personnel, thus resulting in high cost and constrained treatment accessibility [3]. Chemotherapy, when looked at in isolation, has further shortcomings such as short half-life, acquired drug resistance, nonspecific bio-distribution in cells and tissues, rapid metabolism, and excretion. This leads to a low therapeutic index due to the destruction of healthy cells and potent toxicity [1].

Multifunctional nanosystems has been of recent interest in anti-cancer-therapy for the purpose of developing safe, effective, and efficacious drug delivery systems, due to the potential of overcoming

the disadvantages of traditional strategies. Amongst the most promising multifunctional nanosystems include the use of magnetic drug targeting, actuation, or hyperthermia in amalgamation with triggered drug release strategies as well as their combination with diagnostic methods such as magnetic resonance imaging and fluorescence imaging. This can lead to a theranostic approach personalizing cancer treatment for patients. Amongst the various nanoparticles and nanocarriers that multifunctional nanosystems are comprised of, nanowires (NWs) are of key interest due to their shape anisotropy and large surface area. Figure 1 shows a NW system, in which stimuli release the drug in the presence of a decreased pH after cellular internalization.

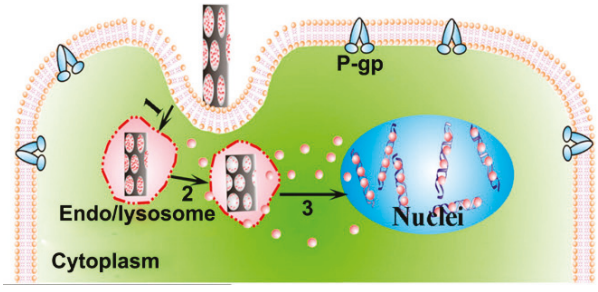

Figure 1. Schematic showing doxorubicin loaded nanowires being internalized into the cytoplasm and releasing the drug from the pH stimuli from the endo/lysosome. Where P-gp is P-glycoprotein. Adapted with permission from Peng et al. [4].

NWs have widespread applications in various fields including drug delivery [5], sensors [6], biomedicine [7], water purification [8], magnetic storage [9], and electronics [10]. NW application in drug delivery includes the use in both targeted drug delivery systems such as magnetically responsive platforms [11,12] and triggered release systems such as pH responsive systems [13]. NWs are also used to induce non-chemotoxic cell death by using magnetic actuation and induced localized hyperthermia in the presence of an alternating magnetic field.

NW are structurally characterized as one-dimensional geometry, involving large lengths reaching micrometer range and small diameters in the nano-range (~10–200 nm). Their length-to-diameter ratio (aspect ratio) is usually large [14], which differentiates them from nanorods.

These intrinsic properties of NW provide specific advantages in terms of drug delivery, which is of particular interest with regards to cancer therapeutics, such as a large surface-area-to-volume ratio and increased biocompatibility by its ability to camouflage and be coated with various biocompatible and biodegradable coatings (biopolymers and semi-synthetic polymers) increasing its solubility, stability, and its ability to be functionalized. NWs therefore provide an efficient platform for drug delivery systems to be based on. The large surface-area-to-volume ratio allows for greater drug loading and attachment of targeting molecules while the small diameters provide the ability to pass through narrow capillaries [15]. With regards to magnetically responsive NW, the elongated shape brings inherent advantages that can be exploited. Their anisotropic magnetic and physical properties allow for easy magnetization, greater magnetic moments when compared to spherical particles, and NWs also have large remnant magnetization. The large remnant magnetization intensifies the effectiveness and range of the magnetic interactions due to its favorable energy configuration [16], which results in magnetic navigation being able to be carried out at deeper locations inside the body [17].

There are multiple fabrication methods for synthesizing NWs. These include chemical methods, physical methods, electrodeposition, and electroless deposition [18], which use both the bottom-up and top-down approaches. In the top-down approach, which is a subtractive technique, material is carved of a larger starting material block, revealing the NW. On the other hand, the bottom-up approach is an additive-type synthesis in which smaller particles are bound together to synthesize the NW [19].

This review will focus on design of multifunctional systems of magnetic NW, including the fabrication methods of magnetic NW; strategies and application of magnetic NW-based nanosystems for cancer therapeutics; characterization of the magnetic NW nanosystems including toxicity, cell internalization, drug loading, and release; and critical evaluation of the performance for NW-based multifunctional nanosystems, for improved therapeutic outcomes.

2. Considerations and Applications of Magnetic Nanowires for Cancer Therapeutics

In order to design effective cancer therapeutic systems, the applications of the magnetic NW must be tailored to achieve in the appropriate microenvironment of the targeted cancer, which the therapeutic system is designed for. Thereafter, the most appropriate applications of magnetic NW must be synergistically combined to validate the rational of incorporating the NW into a multifunctional system. Below, the general considerations of tumor microenvironment will be discussed as well as the applications of magnetic NW in a therapeutic system.

2.1. Considerations of the Microenvironment of Cancerous Tissue for the Design of Magnetic Nanowire Therapeutic Systems

Tumor microenvironments play an important role in the biological impact of nanosystems as well their distribution [20]. For nanosystems to be efficacious for cancer therapeutics, it needs to attain a homogenous distribution intratumorally, however nanosystems need to overcome the tumor microenvironment's barriers, which are summarized by Fernandez and co-workers [21]. Although the enhanced permeability and retention effect promotes extravasation of nanosystems intratumorally, they must first overcome the high interstitial pressure, abnormal tumor vasculature, and dense stroma, so that they may be efficacious. Explicit pathophysiological conditions of the targeted tumor, such as functional proteins and levels of amino acids, as well as endogenous factors of the tumor microenvironment must be considered in the design of optimal-nanosystems. These factors include acidosis, hypoxia, hyperthermia, oxidative stress, enzyme activity, redox potential, and high interstitial fluid pressure. However, these factors can also be exploited in the drug delivery design of nanosystems. For instance, nanosystems can be designed to take advantage of the tumor acidic environment, which differs from physiological pH to initiate drug release. This can be achieved by bonding the drug to the nanosystems using acid hydrolysis sensitive covalent bonds [22]. Active targeting can also be achieved using pathophysiological conditions of the targeted tumor. This is accomplished by binding specific antibodies that bind to receptors expressed on the tumor cell such as attaching anti-Her2/neu antibody to the nanosystem, which binds to Her2/neu receptors on the tumor cell membrane. Aptamers and ligands can also be used in a similar regard [23]. A promising potential application of magnetic NW drug delivery systems is the attachment of Wnt inhibitors. Traditionally, Wnt inhibitors are restricted by high toxicity and inefficient drug delivery systems [24]. However, these limitations can be overcome by a targeted and stimuli-release drug delivery system, which nanotechnology, and in particular magnetic NWs, can achieve [24].

2.2. Cancer Therapeutic Applications Employing Magnetic Nanowires

Nanocarriers have been greatly reviewed and have shown to have great therapeutic benefits. These advantages include the ability to increase the permeation of drugs across the epithelial lining of the gut wall, half-life, and solubility of hydrophobic drugs. Nanosystems, on the other hand, are favored due to its ability to overcome the limitations of conventional therapy. For example, being able to selectively release drug, increase accumulation in the target organ, and design a targeting ability within the nanosystems. Nanosystems also have the capability to perform multiple roles, such as theranostics, measuring dose response, and drug efficacy.

NWs can be integrated into such multifaceted drug delivery systems coalescing the inherent properties of NW and the efficacy of nanosystems, producing an advanced, modifiable, and functionalizable platform for drug delivery. These platforms are most commonly in a hybrid

inorganic-polymer NW orientation or synthesized as a silicon core. The NW being the inorganic core while the surface coatings bring about a variety of biomedical properties. These surface coatings use various stimuli to illicit responses in a way that allows the systems to become targeted, selective, and stimulate drug release in order to increase therapeutic outcomes and decrease adverse effects of therapy.

This combination is effective in the development of drug delivery platforms for cancer treatment due to the unique merits it provides. It can enhance therapeutic effects by combating multiple drug resistance in cancers or provide a synergistic combination of therapeutic effects. This combination also allows for the accumulation of drug at the targeted tumor sites, thus reducing adverse effects of treatment [25–28].

2.2.1. The Application of Magnetic Nanowires as Magnetic Drug Targeting Agents in Cancer Therapeutics

Drug accumulation at specific tumor sites can be achieved when an external magnetic field is used to draw out and trap magnetically active, drug-loaded nanoparticles from the circulatory system. It is promising for its potential of increasing the saturation of drug at the required site while decreasing the saturation in healthy tissue. Thus, reducing adverse effects and increasing therapeutic outcomes. Magnetic targeting is thus dependent on two factors, a nanocarrier that is magnetically responsive and a magnetic field gradient [29]. Magnet systems employed in magnetic targeting fall into two classes, the use of an external magnet and the combination of an external magnet with an implanted magnet near the target area [29]. Magnetic NW systems that are delivered into the blood stream must overcome the viscous drag force of the blood stream. Therefore, the magnetic NW systems will potentially be captured from the capillary blood flow by the external magnet to the target area. The large magnetic moments of magnetic NW reduce the field gradient required to capture the NW [17]. To provide the magnetic field and magnetic field gradient, there are currently two categories of magnet systems; static field magnet systems and varying field magnet systems. Static field magnet systems are low cost, convenient, and simple but lack targeting accuracy, while varying field magnet systems have high targeting accuracy, which make it possible for employing three dimensional (3-D) precise targeting but are energy consuming and require complex hardware systems and exact calculations [30].

Magnetic NWs have an inherent advantage over spherical nanoparticles such as superparamagnetic iron oxide nanoparticles, as the anisotropy of NW allow for deeper tumors to be targeted and have a higher drug loading capacity [12,31]. Pondman et al. created an iron-palladium (FePd) NW system functionalized with oleic acid. This resulted in non-immunotoxic, non-cytotoxic delivery platform granted, unsuccessful in accumulating the NW at the target site in pilot studies. Their FePd NW dimensions were 1.9 ± 0.3 μm in length and 88 ± 15 nm in diameter resulting in an aspect ratio of 22. When a magnetic field was applied to the NW inside the template in three different directions, 0°, 45°, and 90° to the NW direction, the wires showed remanence in all three directions and when tested in random orientations, provided a saturation magnetization (Ms) ± 80 $A.m^2/kg$ and a remnant magnetization (MR) ± 25 $A.m^2/kg$ [17]. Pondman and co-workers performed in vivo studies using Their FePd NW on rats. No negative reactions were shown after intravenous administration with no FePd NW found in the kidneys and liver. The studies suggested a high circulation time due to the immune response and first pass filtration of the kidneys not removing the FePd NW system. However, they were not able to prove significant localization of their NW system at target site. This was likely caused by the removal of blood from the rat in the fixation process [17]. Alsharif et al. iron (Fe) NW with an aspect ratio of 75 had a Fe_2O_3 layer surrounding the Fe NW and provided much larger Ms and MR of 427 $A.m^2/kg$ and 388 $A.m^2/kg$, respectively. This confirmed its permanent magnetic properties and is indicative of its greater potential as a magnetic targeting agent when compared to the FePd NW. However, the Fe NWs will have a greater degree of aggregation, which will need to be overcome in order to be effective and safe as a drug delivery system [32]. The magnetic properties of the cobalt (Co) NW and functionalized Co NW of Zhu et al. was not characterized by a magnetometer. However, its

potential for providing targeted chemotherapy was shown by suspending the Co NW, GO-Co NW, and GO-PEG-Co NW in polyvinyl alcohol (PVA) solution (where GO is graphene oxide and PEG is polyethylene glycol) and placed near an external magnet. This resulted in each group being attracted to the external magnet within one minute [33].

2.2.2. The Application of Magnetic Nanowires as Hyperthermic Agents in Cancer Therapeutics

The use of NW as hyperthermic agents is promising due to its ability to be optimally structured to provide thermal response to stimuli such as low-frequency alternating magnetic fields and of near-infrared irradiation [34]. Hyperthermia involves the energy insertion into malignant tumors resulting in the death of the cancer cells. It can be characterized into three states; diathermy (greater than 41 °C), apoptosis (between 42 °C and 46 °C), and thermoablation (greater than 46 °C). Diathermy stimulates tumor growth, apoptosis is the ideal range for cancer cell destruction, while thermoablation stimulates heat-induced necrosis [35].

There are two modes of inducing magnetic hyperthermia in the presence of an alternating magnetic field. These are the Brownian relaxation mechanism and the Néel relaxation mechanism [36]. The Brownian mechanism involves the NW rotation-vibration towards the direction of the external magnetic field. This results in a mechanical friction caused by the magnetic NW in its suspended medium, inducing the hyperthermia. The Néel mechanism involves the rotation of the magnetic moment within the NW in an external magnetic field. Néel's mechanism therefore induces hyperthermia by the "internal friction" caused by the magnetic moment movement. The Néel mechanism provides a more specific cell death mechanism as it induces minor mechanical damage to cells when compared to the Brownian mechanism, which is non-selective in its mechanical damage of cell membranes. In addition, heat induced in terms of hysteresis losses is dependent on the particular reversal mechanism. This is usually mediated by the nucleation and propagation of a magnetic domain wall. The domain wall is dependent on both the specific materials and geometry and can be of two types, vortex or transverse domain wall. The domain wall dynamics influences the heating performance of the NW and creates a certain maximum frequency in which a heating response is elicited [37]. Magnetic heating has strong dependence on the magnetic properties of the magnetic NW [38]. Specific absorption rate, which is used to quantify the heating efficiency, is increased when an alternating magnetic field equal to or lower than the coercive field is applied. Therefore, metallic NWs such as Nickel (Ni) and Fe have greater heating power when compared to Co due to their coersivity. The coercive field is also influenced by the geometry of the NW. Consequently, the heating efficiency of thicker NW will be greater than that of thinner NW and longer NW will be greater than shorter NW [38,39].

The recommended frequencies of electromagnetic fields lie between 50 kHz $< f <$ 1 MHz as physiological responses such as muscle (skeletal and peripheral) and cardiac stimulation occur with increasing frequencies [40]. Choi et al. produced Ni NWs and successfully induced hyperthermia in HEK-293 cells. This was achieved using radio frequency (RF) electromagnetic fields. The Ni NW was internalized by the cells and after the application of a RF of 810 MHz [41]. Lin and coworkers fabricated Fe NW with a coercive force of about 9.7 Oe. This provided a high saturated heating temperature of 73.8 °C at a concentration of 500 ppm. During their cytotoxicity studies investigating hyperthermia derived from Fe NW, they revealed a mortality rate of 80% for EMT-6 cells. This highlights the feasibility of using Fe NW in hyperthermia therapy [36]. Alonso et al. synthesized FeCo NW to study their potential in magnetic hyperthermia. They found that the Specific absorption rate increased with an increase in length and obtained remarkable specific absorption rate values of ~1500 W/g [39]. Hopkins et al. produced Ni-gold (Au) core-shell NW and for RF initiated hyperthermia for thermotherapy. During in vivo, the NiAu core-shell NW was intratumorally injected into the mice. A RF of 950 MHz and power of 10 W was then applied for 30 min with the mice under injectable anesthesia with a second and third treatment carried out at day 20 and day 30, respectively, after the first treatment. This resulted in significant damage to the malignant solid tumor on the mice [42].

2.2.3. The Application of Magnetic Nanowires as Magnetic Actuation Agents in Cancer Therapeutics

Magnetic NW can induce cell death without a heat dependent mechanism in a magneto-mechanical process as depicted in Figure 2 [43,44]. The first study of magnetic actuation induced cytotoxic effects arising from alternating magnetic fields at low frequencies was studied by Zablotskii and colleagues [45]. They applied a high-gradient magnetic field with a low frequency (1–10 Hz) as well as mechanical vibration on incubated mesenchymal stem cells. Their results suggested that both the mechanical vibration and alternating magnetic field played an active role in the F-actin remodeling and succeeding down-regulation of the audiogenic genes adiponectin AP2 and PPARγ.

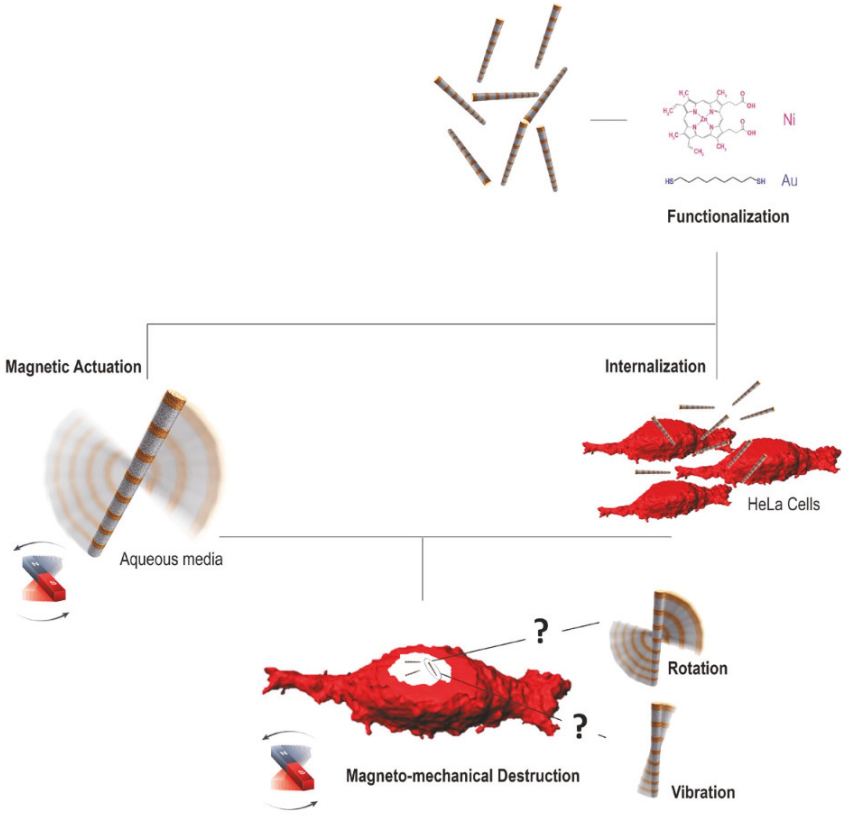

Figure 2. Diagram showing proposed mechanism of action for magnetic actuation stimulating a magneto-mechanical cell death in the presence of an alternating magnetic field. Adapted with permission from [46].

This mechanism was later applied to a more cancer therapeutic approach by researchers. The exemplary study of Contreras and co-workers exhibited the use of Ni NW for a non-chemotoxic approach to cancer cell death. They fabricated Ni NWs with a length 4.1 ± 1.4 μm and a diameter of 30 to 40 nm. The Ms value measured was 46.7 $A.m^2/kg$, which is lower than the reported literature value for bulk Ni, which is 54.3 $A.m^2/kg$ [47]. This phenomenon was associated with the surface oxidation of the Ni NW according to Contreras and co-workers. When comparing the array Ni NW to a single Ni NW, the Ms increased to 47.4 $A.m^2/kg$ as the single Ni NW acts as a permanent magnet and is free from magnetostatic interactions, which the array experiences and thus show single domain properties [48]. The behavior of magnetic NW is administrated by its magnetization in the presence of an alternating

magnetic field. In the case of Ni NW, it is determined by the shape anisotropy and the NW axis (magnetic easy axis) [44,49]. This results in the Ni NW to produce a torque when trying to align their magnetic moment with the alternating magnetic field. This mechanism is applicable for all magnetic NW with the same characteristic. Therefore, when the NWs are exposed to an alternating magnetic field, they will experience torque, while trying to align the magnetic moment with the field. This torque results in a force being applied on the cell, which leads to its death in the presence of an alternating magnetic field as shown in Figure 2. Serrà et al. fabricated a multi-component Au/Ni–nickel oxide (NiO) NW using pulsed potentiostatic electrodeposition. They incubated the NW with HeLa cells for 24 h, after which 70% of the NW were internalized. They observed 24% cell death after an alternating magnetic field of 14 and 35 mT and 20 Hz was applied for 15 min. The segmentation of the NW assisted in tailoring the MR, which in turn decreased the NW agglomeration, and the observed cell death was not induced by magneto-mechanical effect due to the lower MR, but rather it was associated with the NW vibration, which further highlights the association of magnetization and NW behavior [46].

Specific loss power (heat produced) frequency dependence is linear for ferromagnetic particles [50]. Therefore, in order to produce the heat required for thermoablation, the amplitude of the alternating magnetic field necessary is ~10 kA/m and around 100 kHz frequency is required [51,52]. Magnetic actuation cell deaths were induced at ranges largely below those thresholds. The Fe NW systems of Martínez-Banderas and co-workers used a 1 mT, 10 Hz alternating magnetic field to induce cell death while Contreras and co-workers used alternating magnetic fields of 0.5 mT and 0.1, 1, and 10 Hz to induce cell death. This low amplitude and frequency requirement translate into lower cost of magnetic actuation cancer treatment and increased safety of patients by reducing the risk of thermoablation [43].

This principle of inducing magneto-mechanical cell death by magnetic actuation can be applied to cancer therapeutics to induce non-chemotoxic destruction to a malignant tumor. The advantage of this is that it not only can reduce or eliminate chemotherapeutic side effects, it can also be used as an alternative cell killing mechanism in multi-drug resistant cancer.

2.3. Magnetic Multifunctional Nanowire Systems in Cancer Therapeutics

The core principle behind formulating NW systems using a magnetic core is magnetic navigation [17,53,54]. The ability to localize a delivery system using a non-invasive and relatively safe force is highly remunerative in cancer therapy, as it allows the progression from the limitations of traditional cancer chemotherapy by allowing therapeutic effects to be directly targeted at the tumor site, thus reducing secondary effects. In addition to magnetic navigation, magnetic wires are used for inducing cell death by magneto-mechanical means using magnetic actuation [43] and induced local hyperthermia [55] by applying a low- and high-frequency alternating magnetic field, respectively.

Magnetic NW cores are functionalized by their surface modifications. These modifications alter the pharmacokinetics of the magnetic NW systems, adjust the cytotoxicity, allow for attachments of biomolecules such as ligands, and allow for the conjugation or entrapment of drugs [56]. Surface modifications are also used to input a responsive behavior to the system usually to provide effects such as triggered drug release or hyperthermia. The stimuli used to initiate such behavior include a change in pH and radiation. The coalescence of the magnetic NW and stimuli-responsive surface coatings create multifunctional magnetic NW systems that have potential advantages over traditional cancer therapy. Figure 3a depicts Co NWs while Figure 3b,c depict Co NWs with surface modifications that were designed to increase the biocompatibility, enable drug loading using electrostatic means, and provide photothermal responsiveness from a stimulus (near-infrared irradiation).

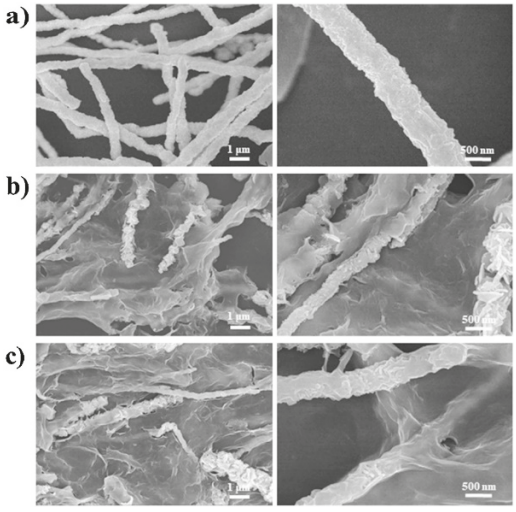

Figure 3. (**a**) Microscopy of unfunctionalized Co nanowires (NWs) portraying a rough morphology. (**b**) Microscopy of stimuli responsive graphene oxide (GO) functionalized Co NW. (**c**) Microscopy of GO-polyethylene glycol (PEG)-functionalized Co NW. Reproduced with permission from [33].

2.3.1. The Use of Magnetic Nanowire Magnetic-Chemo-Photothermal Systems in Cancer Therapeutics

The use of a multifunctional system that is magnetically targeted to deliver a chemotherapeutic load to the tumor site, in addition to inducing a local hyperthermia in the tumor to induce cell death in synergy to the chemotherapeutic drug, is advantageous for the following reasons; it decreases drug adverse and side effects, enhances the efficacy of tumor destruction, and can potentially be used to combat multi-drug resistance in chemotherapy. This approach was explored by Zhu et al. [33]. They built this multifunctional nanowire system on Co nanowires treated with GO and PEG, which provided the desired responsiveness to pH, magnetic fields, and near-infrared irradiation. A template-free reduction method was used to synthesize the CO NWs in the presence of a magnetic field. This produced unordered, irregular, and rough NWs on which the PEG and GO were coated. Three different groups were produced, namely Co NWs, Co NWs-GO, and Co NWs-GO-PEG, and were characterized by their drug loading ability, toxicity magnetic, and photothermal properties, which are discussed in the relevant sections below. They produced a system that can potentially be magnetically targeted to a tumor site, thereafter release the loaded drug due to the combined decrease in PH at the tumor site, and an application of near-infrared irradiation, which both stimulates drug release and local hyperthermia; thus, inducing cell death by both the drug and the local temperature increase. This is a promising model; however, further studies need to be carried out to determine the in vitro and in vivo magnetic targeting ability so that this system can be phased into clinical trials.

2.3.2. The Use of Magnetic Nanowire Magnetic Actuation-Chemotherapeutic Systems in Cancer Therapeutics

Martínez-Banderas et al. conducted a study, which used the combined chemotherapeutic effects of doxorubicin (DOX) and mechanical disturbances, induced by a low-frequency alternating magnetic field, of their magnetic NWs to prompt cancer cell death. Their system was built upon Fe NWs with an average length of 6.4 ± 1.3 μm and a diameter of 30 to 40 nm. The Fe NW were coated with bovine serum albumin (BSA) and (3-aminopropyl) triethoxysilane (APTES) independently and additionally functionalized with DOX. The Fe NW were synthesized using electrodeposition and formed NWs of a monocrystaline nature. An interesting aspect of these Fe NWs was that it was found to have a

4–10 nm thick layer of iron oxide on its surface (monocrystaline Fe NW surface oxide layer caps at 10 nm) [57] as compared to completely oxidized, which occur to polycrystalline Fe NW over time. This ensures that an Fe core will remain. The oxidation most likely occurred when dissolving the template in sodium hydroxide (NaOH) as the NaOH provides very good oxidizing conditions for Fe. The Fe oxide interphase is important for two reasons. The first being that the remnant magnetizations and magnetic saturation depend on the oxide thickness. The second being it provides a site for the covalent attachment of surface coating. Martínez-Banderas and colleagues thus created a system in which cell death was caused by the cytotoxic effect of DOX and structural damage to the cells by the magneto-mechanical disturbances as shown when tested on MDA-MB-231 cells [11,58].

2.3.3. The Use of Magnetic Nanowire as a Theranostics System in Cancer

It is important to note the role of magnetic NW in theranostics, a paradigm shift promoting personalization of treatment through the combination of diagnostics and therapeutics. The role of magnetic NW platforms in therapeutics encompasses targeted and triggered release drug delivery, photothermal therapy, and magnetic actuation systems as discussed above [59]. In terms of diagnostics, the large surface area of NW increases the efficacy of fluorescence labelling while in terms of magnetic NW, it increases the magnetic moment, making it attractive in fluorescence imaging and magnetic resonance imaging (MRI), respectively. Contrast agents for MRI are grouped into two categories, namely T_1 and T_2. The distinguishing factor between T_1 and T_2 agents is that T_1 is based on longitudinal magnetization recovery while T_2 is based on transverse magnetization decay [60]. In this regard, Fe and Ni NW have been shown to be useful T_2 contrast agents with Ni NW being comparable to commercial agents [61,62]. The effectiveness of NW in both therapeutics and diagnostics makes NW and magnetic NW an attractive prospect for designing theranostics systems for cancer.

3. NW Fabrication and Synthesis of Magnetic Nanowire Drug Delivery Systems

3.1. Fabrication Methods of Magnetic Nanowires

There are two main approach strategies for the fabrication of NW. Namely, the bottom-up and top-down approaches. The bottom-up approach involves the spontaneous assembly of small substrates (atoms or molecules) into the desired nanostructure while the top-down approach involves the breakdown of a suitable starting material until the desired nanostructure is formed [63].

A common top-down technique is lithography. Lithography is further divided into various techniques including photolithography and electron beam lithography. The main principle of these techniques is that a pattern is engraved onto an underlying substrate and the desired material is transferred onto the pattern. Therefore, these techniques are a hybrid of the top-down and bottom-up approaches.

These techniques have the advantage of easily being scaled up and can be used for the production of one- and two-dimensional particles that has at least one lateral dimension in the nanoscale range, however the resolution achieved is low and has etching and coating constraints, thus making it impractical for the use in drug delivery [63,64].

Bottom-up techniques enable the synthesis of complex structures such as non-straight vertical structures, structures made up of multiple components, and structures that have changes in the chemical composition. The main advantage provided by bottom-up techniques is the ability to synthesize structures with high aspect ratios. Bottom-up techniques employ chemical [33,65], physical [66], and electrochemical [67] methods to produce nanowires.

The NW fabrication techniques are summarized in Table 1, noting the advantages and disadvantages of each while selected fabrication techniques of promising methods used for the NW synthesis in drug delivery are discussed in further detail below, further highlighting the advantages and disadvantages of the technique and evaluating the potential for each technique to advance drug delivery.

Table 1. Overview of fabrication techniques applied for the synthesis of magnetic NWs.

Fabrication Technique	Top-Down/Bottom-Up	Magnetic NW Composition Achievable by This Technique	Remarks on Technique	References
electrodeposition	bottom-up	Fe and Fe-based compounds Co and Co-based compounds Ni and Ni-based compounds	Cost effective enables synthesis of accurate dimensions and complex structure Individualistic growth on non-planar surfaces	[68–70]
atomic Layer deposition	bottom-up	Fe and Fe oxides Co and Co oxides Ni and Ni oxides	Cost effective enables complex structure synthesis Slow deposition rate	[70,71]
chemical vapor deposition	bottom-up	single-crystalline Ni and Ni alloys single-crystalline Co and Co alloys single-crystalline Fe and Fe alloys	Cost effective enables complex structure synthesis Difficult to deposit multicomponent constituents	[70,72]
pulsed laser deposition	bottom-up	Fe and Fe oxides Co and Co oxides Ni and Ni oxides	Cost effective enables complex structure synthesis Difficult to control dimensions of NW	[70,73]
Focused Electron Beam Induced Deposition	bottom-up	Fe deposits Co deposits	Cost effective enables complex structure synthesis Lack of control in final composition of NW	[70,74]
Chemical reduction	bottom-up	Fe and Fe-based materials Ni and Ni-based compounds	Cost effective Difficult to control NW dimensions and morphology	[70,75]
Solvothermal	bottom-up	Co and Co-based compounds Ni and Ni-based compounds Fe and Fe-based compounds	Difficult to control NW dimensions and morphology Requires high temperatures and pressures	[70,75]
Hydrothermal	bottom-up	Fe and Fe-based compounds Co and Co-based compounds Ni and Ni-based compounds	One step synthesis Difficult to control NW dimensions and morphology	[70,75]
Sol-Gel	bottom-up	Fe and Fe-based compounds Co and Co-based compounds Ni and Ni-based compounds	Cost effective scalable Can form defects in products	[70,76]
Lithography Techniques	top-down	Fe and Fe-based compounds Co and Co-based compounds Ni and Ni-based compounds	Flexible in designing nanoparticles low resolution high cost	[70,77]

3.1.1. Electrodeposition of Magnetic Nanowires

A very convenient and common method for nanoparticle synthesis is electrodeposition. It was traditionally used as a conventional surface modification method for adjustments of surface morphology and characteristics and can be used to fabricate nanoparticles of single or multiple composition [78–81]. Electrodeposition is the formation and deposition of solids through electrochemical reactions. These solids are usually formed by the reduction of an electroactive species contained in an electrolyte by applying a potential. This distinguishes it from electroless deposition in which a reducing agent replaces the applied potential [82].

A further distinction can be made in the electrodeposition of NW; deposition using templates and template-less deposition [70]. There are two types of templates, soft templates and hard templates. Soft templates are non-rigid structures that are used to control the direction of growth and therefore resultant shapes of nanoparticles produced. Soft templates include surfactant aggregates, micelles, and co-block polymers, and can be used to generate porosity and texture control of the resultant NW. The downside of soft templates is that the baths containing the soft templates usually express a low conductivity, which in turn hinders the electrodeposition process. Hard templates are rigid structures that are conductive on one end and regulate the size and shape of the synthesized nanoparticles by the shape of the template itself. The pioneering work of Possin first demonstrated this principle of fabricating small diameter NW in porous membranes [83]. Hard templates are extremely versatile, convenient, and are recurrently used in the synthesis of NW. The most common hard templates are anodized alumina, polycarbonate membranes, and mesoporous materials [84]. Hard templates allow for the synthesis of freestanding NW as well as both orientated and non-orientated NW. They also facilitate the synthesis of complex one-dimensional NW [70]. The downside of using hard templates include the removal of the template as it can affect the NW, diffusion of the electroactive species through the narrow diameter pore channels, difficulty in upscaling due to the difficulty of producing large templates with homogenous pore distribution (with small pore diameters), and the difficulty of producing templates with uniform pore diameters. When no physical template is used for controlling the morphology and shape of the produced nanoparticle, deposition rates are used in its place. Control of deposition rates is achieved by the modification of current density concentration of the electroactive species, temperature, and applied potentials.

Electrodeposition therefore has the potential of producing NW for effective drug delivery systems as precise control of the NW dimensions can be achieved, which is essential for positive cell interaction, control of magnetic ability, and drug loading. This technique can produce a variety of non-toxic, biocompatible NW including iron oxide, iron, and iron–palladium NWs, as well as segmented NWs in a convenient, scalable, and reproducible way; thus, providing a stable platform in which drug delivery systems can be engineered onto while keeping the inherent benefits of a NW for multifunctional systems.

3.1.2. Pulsed Laser Deposition of Magnetic Nanowires

Another common and valued growth mechanism for the synthesis of nanowires is pulsed laser deposition (PLD) [85–88]. A pulsated high-powered laser beam is used to excite the surface energies of a target substrate in a controlled atmosphere producing an ejected plume. The vapor is then deposited onto a sample stage producing thin films or nanoparticles with the same composition as the target. PLD allows for synthesis of nanoparticles with a monocrystalline nature, high purity, and low defects to be synthesized. Other advantages of PLD is that it has a fast production rate and it is scalable.

Shkurmanov and co-workers studied the growth of zinc oxide (ZnO) nanowires via PLD in order to understand the mechanism in which the nanowires are formed [89]. They observed that the NW growth was non-linear and can be explained in terms of the number of laser pulses applied and its interaction with four distinct flows of particles. The first flow forms the nuclei in which the NW will grow from, while the second flow is responsible for the vertical growth of the nanowire. The third flow was found to cause a backflow and decreased the length of the NW. Lastly, the fourth flow was

responsible for the lateral growth of the NW. This proved that geometric parameters can be controlled when using PLD.

An exemplary study of Nikov et al. paved the way for the formation of magnetic NW using PLD by employing the aid of a magnetic field [87]. This study provided a simple method of producing magnetic NWs, which increases its industrial value. This method also produces NWs composed of smaller nanoparticles. This property can be exploited to potentially positively affect drug loading capabilities of drug delivery systems. Furthermore, Nikov and co-workers used this method to fabricated iron oxide NW [90]. This study further demonstrated that the pressure and surrounding gas can be used to manipulate the type of oxide formed. Another interesting effect of the magnetic field is that it allowed the deposition of the iron oxides in arranged nanowire structures at a low pressure and a target substrate distance of 40 mm.

PLD provides an effective method of producing NW arrays, which are especially promising in implantable and transdermal drug delivery systems. It excels in producing NW composed of magnetic materials, which is a property that can be exploited in the development and commercialization of multifunctional drug delivery systems.

3.1.3. Other Synthesis Techniques of Magnetic Nanowires

There are various other fabrication techniques in which NWs can be synthesized. However, the most promising fabrication technique is electrodeposition due to its precise dimension control. These techniques are commented on in Table 1 and include atomic layer deposition, chemical vapor deposition, pulsed laser deposition, focused electron beam induced deposition, chemical reduction, solvothermal, hydrothermal, sol-gel, and lithography techniques such as photolithography and electron beam lithography.

3.2. Magnetic Properties and Advantages of Nanowires in Drug Delivery Systems

NW are synthesized from both magnetic and non-magnetic substrates. Both NW and magnetic NW offer potential advantages over nanoparticles and magnetic nanoparticles due to their larger surface area to volume ratio (high aspect ratio), which allows for greater drug loading, increased attachment sites, for decorations such as proteins, peptides, and polymers, and increased binding to cells. Magnetic NW have greater advantages when compared to magnetic nanoparticles due to their strong shape anisotropy and energetically favorable magnetization. They provide greater magnetic moments and in the presence of an alternating magnetic field, can either provide mechanical motion by aligning to the magnetic moment with an applied low-frequency alternating magnetic field or induce a local hyperthermia at a high-frequency (~100 kHz) alternating magnetic field [11].

The most frequently used materials for synthesizing the magnetic components of magnetic NWs for drug delivery systems are Fe, Ni, Co, as well as their compounds and alloys. Magnetic NWs display specific advantages when compared to spiracle and other nanoparticles as well. The increased aspect ratio of ferromagnetic NWs provides stronger magnetic moments per unit volume and large remnant magnetizations without decreasing the mobility of the nanoparticles. The larger remnant magnetization allows the NW to be used in low-field environments, which in turn translates into NWs being able to target deeper tissues with smaller and weaker magnets as the geometry of NWs has an increasing effect on force applied by the magnetic field. NWs with aspect ratios greater than three show larger magnetic dipoles when compared same volume spherical nanoparticles [12]. This results in the potential of a more efficient magnetic system to be designed for magnetic drug targeting for cancer therapeutics.

3.3. Stabilization and Functionalization of the Magnetic Nanowires

The surface area of NWs are decorated with coatings mainly for three intended purposes: To increase the biocompatibility of the NW, stabilize the NW (prevent NW agglomeration), and to functionalize the NW in order to tailor the NW to excel in the niche of interest [43].

The work by Zhu et al. used a coating of PEG and GO to both stabilize and functionalize their Co NW, thereby increasing its drug loading capacity and biocompatibility. Both the PEG and GO were attached to the Co NW by electrostatic adsorption using an ultrasonic dispersion method. The GO played a dual role; to enhance the photothermal therapy efficacy, as it is a known photothermal agent, and to provide attachment points for the loaded drug (Doxorubicin) [33]. When irradiated with a 808 nm laser for six minutes, the Co NW and GO-functionalized CO NW heated to a temperature of 39.1 °C and 40.6 °C, respectively, indicating the ability of GO to improve the excellent photothermal effect of Co NW.

Magnetic NWs can also be functionalized by the attachment of antibodies to target specific cells, thus increasing its selectivity. Contreras et al. successfully functionalized their Ni NWs with EGFR antibody (ab62 abcam®). This was achieved by first modifying the antibody with N-Succinimidyl S-acetyl thioacetate. Thereafter, it was further modified to introduce sulfhydryl groups so that it could attach to the Ni NW [91].

The NW system of Martínez-Banderas and research group was tested with three distinct coatings, BSA, APTES, and APTES-PEG. The BSA and APTES were covalently bonded to the surface Fe_2O_3 interphase of the Fe NW while they functionalized APTES with PEG by activating the APTES with sulfhydryl groups and the reacting with the thiol group in thiol-PEG, thus achieving disulfide bonds. The three coatings were compared using MDA-MB-231 breast cancer cells, which were incubated with the coated Fe NW and added cyanide Fe salt. Bright field imaging was used to determine the distribution, size, and morphology of the Fe NW agglomerates. All three coatings reduced the size of the agglomerates, thus ensuring a greater homogeneity of the Fe NW distribution across the sample. APTES-PEG had the least efficacy of this effect [11]. Figure 4A,B depicts the transmission electron microscopy image of the APTES-NW and BSA-NW respectively, visualizing the coating on the NW.

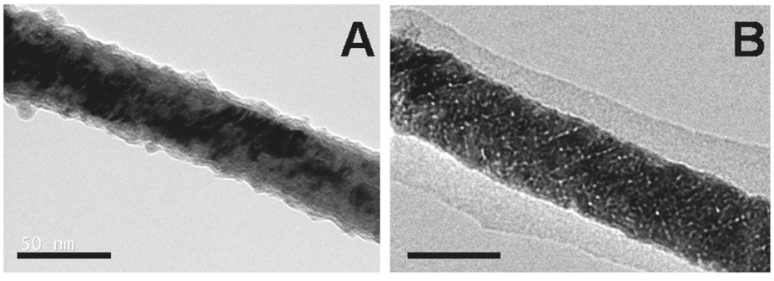

Figure 4. Figure showing surface modifications on magnetic NW for stabilization. (**A**) (3-aminopropyl) triethoxysilane (APTES)-coated Fe NW. (**B**) Bovine serum albumin (BSA)-coated Fe NW. Reproduced with permission from [11]. Scale bars: 50 nm.

Contreras and co-workers did not stabilize their Ni NWs with any coating, which thus caused the aggregation of the Ni NW. The Ni NW zeta potential was measured to be a low value of −15.1 mV [92]. This value infers a weak electrostatic repulsive force which correlates with Contreras' observation of released Ni NW aggregating. This study highlights the efficacy of surface coatings to stabilize NW in terms of aggregation of the NW. Preventing the NW tendency to aggregate is essential as particle aggregates in the bloodstream can cause an embolism, while in tissue it can cause heterogeneous cytotoxic activity. Martínez-Banderas and research group managed to reduce the aggregation of Fe NWs, which is known to have higher remnant magnetization, which makes it inherently unstable. The stability of the Ni NW can be increased with surface modification such as coating with charged polymers or non-magnetic metal such as Au. The increase in magnetic NW stability increases its desirability in drug delivery as it will allow for safer therapy a formulation with a longer shelf life.

Stabilizing NW is therefore indispensable in the design and formulation of NW drug delivery systems as it prevents the aggregation of magnetic cored NW caused by their remnant magnetization.

This, in turn, reduces the probability of mechanical obstruction in the circulatory system caused by NW aggregation. Therefore, NW coatings allow for the optimal design of multifunctional systems, which is essential in potentially improving cancer therapeutic outcomes.

3.4. Chemotherapeutic Drug Loading and Release of Magnetic Nanowire Systems

Large surface area has a positive influence on the drug loading capacity of nanosystems. Thus, NW morphology has a direct impact on drug loading capacity. Although NWs inherently have large surface areas, their surface area can be increased further by changing their morphology to include rough surfaces [93,94] or by synthesizing porous NWs [95,96]. Guo and co-workers achieved a high drug loading of 2000 mg/g using porous NW while Zhu and co-workers achieved a high drug loading capacity of 992.91 mg/g with their Co NW, which had a rough morphology. The GO in the functionalized Co NW of Zhu and research group provided attachment points for DOX or other therapeutic agents as it is decorated with many functional groups on its surface such as hydroxide radicals. In the case of DOX, it is hypothesized that it is also able to absorb directly onto the GO via π-π interactions. Their NW system also exhibited a higher drug release profile in acidic environments and after near infrared radiation when compared to the control [33]. The decrease in PH made the DOX more hydrophilic and soluble due to the protonation of the NH_2 group on it, thus causing the release from the Co NW-GO. They also proved a direct correlation between drug release and laser power intensity.

The BSA and APTES coated Fe NW of Martínez-Banderas and colleagues were functionalized using PH responsive covalent bonds. This was achieved by introducing free thiol groups to the coated Fe NW by reacting 2-IT and amine groups on the coated Fe NW. The free thiol groups were then reacted to the maleimide group of a DOX derivative (5-Maleimidovaleroyl) hydrazone of Doxorubicin in order to attach it. This yielded low loading capacities of 50 μmol DOX/g Fe (27 mg/g) for the DOX-APTES-Fe NW and 25 μmol DOX/g Fe (13.6 mg/g) in the case of DOX-BSA-Fe NW [11]. The low loading was due to the relatively smooth surface of the Fe NW, highlighting the importance of morphology on drug loading.

4. Cellular Interactions and Toxicity Between Magnetic Nanowires and Cells

4.1. Cellular Internalization of Magnetic Nanowires

Cellular internalization of NW supports the NW utilization and efficacy. There are three main potential uptake mechanisms for nanoparticles; receptor-mediated endocytosis, pinocytosis, and phagocytosis [97]. NW suffers an inherent disadvantage when compared to spherical nanoparticles in terms of cell internalization. It is speculated that the different curvatures between the two shapes has a direct effect on cell binding. When the longitudinal axis of NW is bound to the cell membrane, the larger surface contact area blocks available membrane receptors, thus reducing cell internalization. There are many factors that govern cell internalization of nanoparticles besides shape. These are extensively discussed in a review conducted by Murugan et al. of the Wits Advanced Drug Delivery Platform, South Africa [98]. Briefly, in order to design smart nanosystems, an understanding of physicochemical properties is essential. Other determinant factors in terms of cell internalization include uptake pathways and interaction of the nanoparticles with receptors. Neutral and cationic nanoparticles have higher transport efficiency into the cells when compared to negatively charged nanoparticles [99,100]. This phenomenon is the result of anionic particles having smaller binding efficiency to cell surfaces when compared to cationic and neutral particles, leading to a reduction in membrane-wrapping phenomena resulting in a decrease in cellular internalization [99,101,102]. Hydrophilic outer protective layers increase circulation time while nanoparticles functionalized with proteins or peptides directly increase cellular uptake by localizing the nanoparticle at the targeted site, receptor-mediated endocytic pathways, and direct cell penetration. Nanoparticle size also plays an

important role in cellular uptake; 95–200 nm is the ideal size according to the literature for increased cellular uptake [103]. In terms of NWs, high aspect ratio NWs can also be internalized [104].

Fe NW also have good cell internalization as shown by [105] and further demonstrated by Martínez-Banderas and co-workers. Martínez-Banderas and co-workers had a total cell internalization for their APTES-Fe NW and BSA-Fe NW of 19% and 15%, respectively. These values were determined using Inductively Coupled Plasma Mass Spectrometry (ICP-MS) measurements on their incubated cells with the coated Fe NWs. The results yielded no significant difference for the APTES-Fe NW and BSA-Fe NWs in the cellular internalization [11]. Figure 5A,B shows the cellular uptake using HeLa cells of uncoated, positively charged, non-uniformly sized Fe NWs of Song and co-workers. The weakly negatively charged Ni NW of Contreras and research group also had a high affinity to cell internalization. Similar results were achieved for other Ni NWs, including those with large lengths [106]. The cellular uptake of FePd NW of Guo and co-workers was studied on RAW264.7 and HeLa cells. Both cell lines took up both single NW and NW clusters with RAW264.7 cells having greater cell internalization, suggesting rapid removal from blood stream.

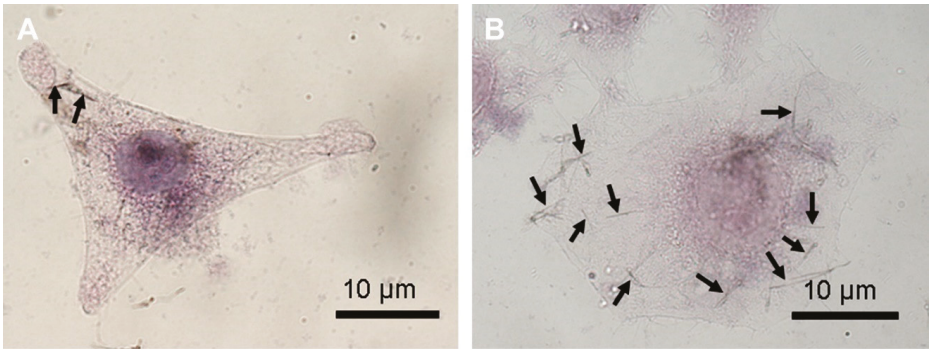

Figure 5. Cellular internalization and accumulation of magnetic NW into cells. (**A**,**B**) Internalized Fe NW in HeLa cells. Adapted with permission from [105]. Scales bars: 10 μm.

4.2. Cellular Toxicity of Magnetic Nanowires and Drug Loaded Magnetic Nanowires

Toxicity is important when designing nanosystems. The coatings used in NW systems are usually well-known biocompatible molecules used to counter the toxicity of toxic inorganic NW. Common NWs used in NW systems are silicon, Au, silver, Co, Fe, and Ni, amongst which Co, Fe, and Ni and their compounds produce magnetic NWs. From these, Co and Ni are the most toxic while Fe and silicon are deemed biocompatible. However, in comparison to Fe NW, a large number of studies have been conducted on Ni NW despite Ni's known cytotoxicity, carcinogenicity, and genotoxicity [107,108], and the literature reveals that Fe is less toxic. The reason for this is that the large remnant magnetization of Fe NWs causes stronger aggregation and thus limits its use in the single NW form. Metal alloys are also used to synthesize NWs, such as iron palladium (FePd) NWs. FePd NWs are non-toxic and do not readily undergo oxidation [17,109]. Si NWs are also known to be non-toxic, have high biocompatibility, improve hydrophilicity, and can be made magnetic by decorating with Fe oxide nanoparticles. In terms of the effect of the NW length on cellular toxicity, Donaldson et al. reviewed the effect of fiber like particles and found that longer fibers were more toxic then shorter fibers [110]. However, Song et al. showed that at the same concentration, Fe NWs of shorter lengths (2 μm) were more toxic then longer lengths (5 μm) of Fe NWs [105]. According to Song et al., this was attributed to smaller size particles having greater cellular internalization [111].

The toxicity of magnetic NW can be altered by surface modifications of the NW. Zhu et al. conducted biocompatibility tests of their GO and PEG decorated Co NW by determining its cytotoxicity using 3T3 and 4T1 cells and hemocompatibility by determining if the Co NWs, Co NWs-GO, and

Co NWs-GO-PEG caused thrombosis or hemolysis. The Co NW itself was found to be very toxic. However, the addition of GO and PEG decreased the cytotoxicity of the system to a great extent. The cell viability of 3T3 and 4T1 cells after culturing with the NW was 35% and 32%, respectively, for the Co NW, while it increased to 96% and 89%, respectively, for the Co NWs-GO-PEG for both at 50 μg/mL concentration. Their results also show no significant difference in the thrombosis time and did not cause hemolysis [33].

Applying an alternating magnetic field to magnetic NW while it is incubated with cells increases the toxicity of the NW. When incubating their Ni NW with HCT116 cells, Contreras and co-workers measured no significant drop in cell viability using 2.4 μg/mL of Ni NW without the presence of an alternating magnetic field, while at a concentration of 12 μg/mL, the cell viability dropped to slightly below 90%. When an alternating magnetic field is applied at 1 Hz, 0.5 mT for 1 h, the cell viability for 2.4 μg/mL drops to around 75% while using a concentration of 12 μg/mL causes the cell viability to drop to slightly below 70%. This shows that higher concentrations of magnetic NWs have a greater effect at inducing cell death [43].

The cellular toxicity of magnetic NWs increases when functionalized with cytotoxic agents both with and without the presence of an alternating magnetic field. Martínez-Banderas and co-workers conducted cell studies for their Fe NW systems using Alamar Blue assay and MDA-MB-231 cells to determine their systems ability to induce cell death in cancer by combining the cytotoxicity of DOX and the mechanical motion provided by the low-frequency alternating magnetic field. Their results showed that alternating magnetic field without the Fe NW systems had no effect on the cell viability and cytotoxicity of DOX. The coated Fe NW systems without the alternating magnetic field present had no significant decrease in the cell viability, which is testament to its biocompatibility while when in the presence of an alternating magnetic field produced a significant decrease in cell viability of 23% and 28% for the and APTES- Fe NW (26 μg of Fe/mL) and BSA-Fe NW (28 μg of Fe/mL), respectively, showing possible cancer cell death by Magnetic actuation. For the DOX-Fe NW systems, they showed a decrease in cell viability of 54% and 58% for DOX-APTES-Fe NW (26 μg of Fe/mL, 1.3 μM DOX) and DOX-BSA-Fe NW (28 μg of Fe/mL, 0.73 μM DOX), which is indicative of their selective intracellular drug release and the efficacy of Fe NW as nanocarriers. The addition of an alternating magnetic field to the DOX loaded Fe NW systems yielded a further 10% and 8% reduction in cell viability for DOX-APTES-Fe NW (26 μg of Fe/mL, 1.3 μM DOX) and DOX-BSA-Fe NW (28 μg of Fe/mL, 0.73 μM DOX), respectively, showing a weak additive effect instead of a synergistic effect for the combination of chemotherapy and magneto-mechanically induced cancer cell death [11].

It is interesting to note that although the BSA-Fe NWs had a lower drug loading capacity compared to APTES-Fe NWs, their efficacy in cytotoxic activity was similar. This was attributed, according to Martínez-Banderas and research group, to the greater cell internalization of the BSA-Fe NWs. Another point of interest is that NW can be used for the separation of biomolecules, their purification, and manipulation, which is applicable in the development of biosensors. This technology can lead to the ability to effectively detect circulating tumor cells leading to a better prognosis for cancer patients [112].

4.3. Cellular Degradation of Magnetic Nanowires

Understanding carrier degradation or metabolism is important in nanoparticle drug delivery to ensure high therapeutic efficacy [113]. The innovative work by Safi et al. revealed that cells are able to degrade NWs as well as decrease the size of the aggregates with their remains found directly dispersed in the cytosol or in vesicular compartments. Singular NWs, on the other hand, were found in endosomal compartments only [114]. Fe NWs and Ni NWs have oxidized surfaces and continue to be oxidized, degraded, and dissolved intracellularly by the lysosomal compartments. Perez et al. reported that ~2% of the Ni NWs dose was dissolved intracellularly after 71 h [115] and Fe experienced the same fate with the lysosomes without cytotoxic contribution. The fate of both the degraded and non-degraded NWs is potentially renal clearance. High aspect ratio nanoparticles have been found to

be renally clearable with high efficiency of elimination. This is caused by the flow orientation of high aspect ratio nanoparticles, which aligns the long axis of the nanoparticle to point to the glomerular capillary pore openings [116].

5. Conclusions and Future Prospects

The application of magnetic NW has great potential for improving therapeutic outcomes for cancer therapy. They provide the benefits of traditional nanoparticles in addition to the inherent advantages of NW, thus making NW an ideal platform to build multifunctional nanosystems upon. However, the full potential of magnetic NW in drug has yet to be reached as further applications and functionalizations that can be molded onto the versatile magnetic NW platform such as Wnt inhibitor delivery systems, attachment of ligands in order to increase the selectivity, and a theranostic system that includes the attachment of fluorescent compounds, chemotherapeutic drugs, and modifications that increase cancer cell selectivity, require further research. Effective in vivo studies for multifunctional NW nanosystems is essential for the progression of this technology into the pre-clinical phase. The magnetic applications of NWs such as magnetic hyperthermia, magnetic actuation, and magnetic drug targeting has shown great potential for improving cancer therapeutics and therefore requires further research to optimize an efficacious multifunctional therapeutic system that will better the prognosis and increase the quality of life for cancer patients. Improvements can be made in tumor targeting so that magnetic NW can be accumulated into the tumor using a three-dimensional targeting model. The control of temperature change needs to be studied and optimized in in vivo studies.

Author Contributions: The manuscript was completed through contributions from all authors; A.B.A.N., T.M., P.P.D.K., Y.E.C., L.C.D.T., V.P., from framework design and manuscript content to manuscript optimization. All authors approved the final submission.

Funding: This work was supported by the National Research Foundation (NRF) of South Africa.

Conflicts of Interest: The authors declare no conflicts of interest.

References

1. Wang, Y.; Zhao, R.; Wang, S.; Liu, Z.; Tang, R. In vivo Dual-Targeted Chemotherapy of Drug Resistant Cancer by Rationally Designed Nanocarrier. *Biomaterials* **2016**, *75*, 71–81. [CrossRef] [PubMed]
2. Pan, Y.; Xue, P.; Liu, S.; Zhang, L.; Guan, Q.; Zhu, J.; Tian, X. Metal-Based Hybrid Nanoparticles as Radiosensitizers in Cancer Therapy. *Colloid Interface Sci. Commun.* **2018**, *23*, 45–51. [CrossRef]
3. Rackwitz, T.; Debus, J. Clinical Applications of Proton and Carbon Ion Therapy. *Semin. Oncol.* **2019**, *46*, 226–232. [CrossRef] [PubMed]
4. Peng, F.; Su, Y.; Ji, X.; Zhong, Y.; Wei, X.; He, Y. Doxorubicin-Loaded Silicon Nanowires for the Treatment of Drug-Resistant Cancer Cells. *Biomaterials* **2014**, *35*, 5188–5195. [CrossRef] [PubMed]
5. Chen, X.-Z.; Hoop, M.; Shamsudhin, N.; Huang, T.; Özkale, B.; Li, Q.; Siringil, E.; Mushtaq, F.; Di Tizio, L.; Nelson, B.J.; et al. Hybrid Magnetoelectric Nanowires for Nanorobotic Applications: Fabrication, Magnetoelectric Coupling, and Magnetically Assisted in Vitro Targeted Drug Delivery. *Adv. Mater.* **2017**, *29*, 1605458. [CrossRef] [PubMed]
6. Doucey, M.-A.; Carrara, S. Nanowire Sensors in Cancer. *Trends Biotechnol.* **2019**, *37*, 86–99. [CrossRef] [PubMed]
7. Jones, R.S.; Draheim, R.R.; Roldo, M. Silver Nanowires: Synthesis, Antibacterial Activity and Biomedical Applications. *Appl. Sci.* **2018**, *8*, 673. [CrossRef]
8. Wang, Z.; Wu, A.; Colombi Ciacchi, L.; Wei, G. Recent Advances in Nanoporous Membranes for Water Purification. *Nanomaterials* **2018**, *8*, 65. [CrossRef]
9. Irshad, I.; Ahmad, F.; Mohammed, N. A Review on Nanowires as an Alternative High Density Magnetic Storage Media. *AIP Conf. Proc.* **2012**, *1482*, 625–632. [CrossRef]
10. Bayrak, T.; Jagtap, N.S.; Erbe, A. Review of the Electrical Characterization of Metallic Nanowires on DNA Templates. *Int. J. Mol. Sci.* **2018**, *19*, 3019. [CrossRef]

11. Martínez-Banderas, A.I.; Aires, A.; Teran, F.J.; Perez, J.E.; Cadenas, J.F.; Alsharif, N.; Ravasi, T.; Cortajarena, A.L.; Kosel, J. Functionalized Magnetic Nanowires for Chemical and Magneto-Mechanical Induction of Cancer Cell Death. *Sci. Rep.* **2016**, *6*, 35786. Available online: https://www.nature.com/articles/srep35786#supplementary-information (accessed on 12 August 2019). [CrossRef] [PubMed]
12. Heidarshenas, B.; Wei, H.; Ali Moghimi, Z.; Hussain, G.; Baniasadi, F.; Naghieh, G. Nanowires in Magnetic Drug Targeting. *Mater. Sci. Eng. Int. J.* **2019**, *3*, 3–9. [CrossRef]
13. Esteban-Fernández de Ávila, B.; Ramírez-Herrera, D.E.; Campuzano, S.; Angsantikul, P.; Zhang, L.; Wang, J. Nanomotor-Enabled Ph-Responsive Intracellular Delivery of Caspase-3: Toward Rapid Cell Apoptosis. *ACS Nano* **2017**, *11*, 5367–5374. [CrossRef] [PubMed]
14. Assunção-Silva, R.C.; Gomes, E.D.; Silva, N.A.; Salgado, A.J. Chapter 8-Nanoengineered Biomaterials for Spinal Cord Regeneration. In *Nanoengineered Biomaterials for Regenerative Medicine*; Mozafari, M., Rajadas, J., Kaplan, D., Eds.; Elsevier: Boston, MA, USA, 2019; pp. 167–185. [CrossRef]
15. Pondman, K.; Maijenburg, W.; Celikkol, B.; Pathan, A.A.; Kishore, U.; Ten Haken, B.; Ten Elshof, A. Au Coated Ni Nanowires with Tuneable Dimensions for Biomedical Applications. *J. Mater. Chem.* **2013**, *1*, 6129–6136. [CrossRef]
16. Lisjak, D.; Mertelj, A. Anisotropic Magnetic Nanoparticles: A Review of Their Properties, Syntheses and Potential Applications. *Prog. Mater. Sci.* **2018**, *95*, 286–328. [CrossRef]
17. Pondman, K.M.; Bunt, N.D.; Maijenburg, A.W.; van Wezel, R.J.A.; Kishore, U.; Abelmann, L.; ten Elshof, J.E.; ten Haken, B. Magnetic Drug Delivery with Fepd Nanowires. *J. Magn. Magn. Mater.* **2015**, *380*, 299–306. [CrossRef]
18. Banerjee, S.; Dan, A.; Chakravorty, D. Review Synthesis of Conducting Nanowires. *J. Mater. Sci.* **2002**, *37*, 4261–4271. [CrossRef]
19. Biswas, A.; Bayer, I.S.; Biris, A.S.; Wang, T.; Dervishi, E.; Faupel, F. Advances in Top–Down and Bottom–up Surface Nanofabrication: Techniques, Applications & Future Prospects. *Adv. Colloid Interface Sci.* **2012**, *170*, 2–27. [CrossRef]
20. Mu, Q.; Yan, B. Editorial: Nanoparticles in Cancer Therapy-Novel Concepts, Mechanisms, and Applications. *Front. Pharmacol.* **2019**, *9*. [CrossRef]
21. Fernandes, C.; Suares, D.; Yergeri, M.C. Tumor Microenvironment Targeted Nanotherapy. *Front. Pharmacol.* **2018**, *9*. [CrossRef]
22. Latorre, A.; Couleaud, P.; Aires, A.; Cortajarena, A.L.; Somoza, Á. Multifunctionalization of Magnetic Nanoparticles for Controlled Drug Release: A General Approach. *Eur. J. Med. Chem.* **2014**, *82*, 355–362. [CrossRef] [PubMed]
23. Hoosen, Y.; Pradeep, P.; Kumar, P.; du Toit, L.C.; Choonara, Y.E.; Pillay, V. Nanotechnology and Glycosaminoglycans: Paving the Way Forward for Ovarian Cancer Intervention. *Int. J. Mol. Sci.* **2018**, *19*, 731. [CrossRef] [PubMed]
24. Qin, W.; Zheng, Y.; Qian, B.-Z.; Zhao, M. Prostate Cancer Stem Cells and Nanotechnology: A Focus on Wnt Signaling. *Front. Pharmacol.* **2017**, *8*, 153. [CrossRef] [PubMed]
25. Guo, D.; Ji, X.; Wang, H.; Bin, S.; Chu, B.; Shi, Y.; Su, Y.; He, Y. Silicon Nanowire-Based Multifunctional Platform for Chemo-Photothermal Synergistic Cancer Therapy. *J. Mater. Chem. B* **2018**, *6*, 3876–3883. [CrossRef]
26. Tan, H.; Huang, Y.; Xu, J.; Chen, B.; Zhang, P.; Ye, Z.; Liang, S.; Xiao, L.; Liu, Z. Spider Toxin Peptide Lycosin-I Functionalized Gold Nanoparticles for in Vivo Tumor Targeting and Therapy. *Theranostics* **2017**, *7*, 3168–3178. [CrossRef] [PubMed]
27. Chen, C.-W.; Syu, W.-J.; Huang, T.-C.; Lee, Y.-C.; Hsiao, J.-K.; Huang, K.-Y.; Yu, H.-P.; Liao, M.-Y.; Lai, P.-S. Encapsulation of Au/Fe_3o_4 Nanoparticles into a Polymer Nanoarchitecture with Combined near Infrared-Triggered Chemo-Photothermal Therapy Based on Intracellular Secondary Protein Understanding. *J. Mater. Chem. B* **2017**, *5*, 5774–5782. [CrossRef]
28. Li, T.; Liu, H.; Xi, G.; Pang, Y.; Wu, L.; Wang, X.; Chen, T. One-Step Reduction and Peiylation of Pegylated Nanographene Oxide for Highly Efficient Chemo-Photothermal Therapy. *J. Mater. Chem. B* **2016**, *4*, 2972–2983. [CrossRef]
29. Sensenig, R.; Sapir, Y.; MacDonald, C.; Cohen, S.; Polyak, B. Magnetic Nanoparticle-Based Approaches to Locally Target Therapy and Enhance Tissue Regeneration in Vivo. *Nanomedicine* **2012**, *7*, 1425–1442. [CrossRef]

30. Liu, Y.-L.; Chen, D.; Shang, P.; Yin, D.-C. A Review of Magnet Systems for Targeted Drug Delivery. *J. Control. Release* **2019**, *302*, 90–104. [CrossRef]
31. Shen, S.; Wu, Y.; Liu, Y.; Wu, D. High Drug-Loading Nanomedicines: Progress, Current Status, and Prospects. *Int. J. Nanomed.* **2017**, *12*, 4085–4109. [CrossRef]
32. Alsharif, N.; Martinez Banderas, A.; Merzaban, J.; Ravasi, T.; Kosel, J. Biofunctionalizing Magnetic Nanowires toward Targeting and Killing Leukemia Cancer Cells. *IEEE Trans. Magn.* **2018**, *55*, 1–5. [CrossRef]
33. Zhu, H.; Deng, J.; Yang, Y.; Li, Y.; Shi, J.; Zhao, J.; Deng, Y.; Chen, X.; Yang, W. Cobalt Nanowire-Based Multifunctional Platform for Targeted Chemo-Photothermal Synergistic Cancer Therapy. *Colloids Surf. B* **2019**, *180*, 401–410. [CrossRef] [PubMed]
34. Su, Y.; Wei, X.; Peng, F.; Zhong, Y.; Lu, Y.; Su, S.; Xu, T.; Lee, S.-T.; He, Y. Gold Nanoparticles-Decorated Silicon Nanowires as Highly Efficient near-Infrared Hyperthermia Agents for Cancer Cells Destruction. *Nano Lett.* **2012**, *12*, 1845–1850. [CrossRef] [PubMed]
35. Egolf, P.W.; Shamsudhin, N.; Pané, S.; Vuarnoz, D.; Pokki, J.; Pawlowski, A.-G.; Tsague, P.; Marco, B.; Bovy, W.; Tucev, S.; et al. Hyperthermia with Rotating Magnetic Nanowires Inducing Heat into Tumor by Fluid Friction. *J. Appl. Phys.* **2016**, *120*, 064304. [CrossRef]
36. Lin, W.-S.; Lin, H.-M.; Chen, H.-H.; Hwu, Y.-K.; Chiou, Y.-J. Shape Effects of Iron Nanowires on Hyperthermia Treatment. *J. Nanomater.* **2013**, *2013*, 9. [CrossRef]
37. Fernandez-Roldan, J.A.; Serantes, D.; del Real, R.P.; Vazquez, M.; Chubykalo-Fesenko, O. Micromagnetic Evaluation of the Dissipated Heat in Cylindrical Magnetic Nanowires. *Appl. Phys. Lett.* **2018**, *112*, 212402. [CrossRef]
38. Contreras, M.F.; Zaher, A.; Perez, J.E.; Ravasi, T.; Kosel, J. Magnetic Nanowires and Hyperthermia: How Geometry and Material Affect Heat Production Efficiency. In Proceedings of the 2015 IEEE International Magnetics Conference (INTERMAG), Beijing, China, 11–15 May 2015.
39. Alonso, J.; Khurshid, H.; Sankar, V.; Nemati, Z.; Phan, M.H.; Garayo, E.; García, J.A.; Srikanth, H. Feco Nanowires with Enhanced Heating Powers and Controllable Dimensions for Magnetic Hyperthermia. *J. Appl. Phys.* **2015**, *117*, 17D113. [CrossRef]
40. Spirou, S.V.; Basini, M.; Lascialfari, A.; Sangregorio, C.; Innocenti, C. Magnetic Hyperthermia and Radiation Therapy: Radiobiological Principles and Current Practice. *Nanomaterials* **2018**, *8*, 401. [CrossRef]
41. Choi, D.S.; Park, J.; Kim, S.; Gracias, D.H.; Cho, M.K.; Kim, Y.K.; Fung, A.; Lee, S.E.; Chen, Y.; Khanal, S.; et al. Hyperthermia with Magnetic Nanowires for Inactivating Living Cells. *J. Nanosci. Nanotechnol.* **2008**, *8*, 2323–2327. [CrossRef]
42. Hopkins, X.; Gill, W.A.; Kringel, R.; Wang, G.; Hass, J.; Acharya, S.; Park, J.; Jeon, I.T.; An, B.H.; Lee, J.S.; et al. Radio Frequency-Mediated Local Thermotherapy for Destruction of Pancreatic Tumors Using Ni–Au Core–Shell Nanowires. *Nanotechnology* **2016**, *28*, 03LT01. [CrossRef]
43. Contreras, M.F.; Sougrat, R.; Zaher, A.; Ravasi, T.; Kosel, J. Non-Chemotoxic Induction of Cancer Cell Death Using Magnetic Nanowires. *Int. J. Nanomed.* **2015**, *10*, 2141–2153. [CrossRef] [PubMed]
44. Fung, A.; Kapadia, V.; Pierstorff, E.; Ho, D.; Chen, Y. Induction of Cell Death by Magnetic Actuation of Nickel Nanowires Internalized by Fibroblasts. *J. Phys. Chem. C* **2008**, *112*. [CrossRef]
45. Zablotskii, V.; Lunov, O.; Novotna, B.; Churpita, O.; Trosan, P.; Holan, V.; Syková, E.; Dejneka, A.; Kubinova, S. Down-Regulation of Adipogenesis of Mesenchymal Stem Cells by Oscillating High-Gradient Magnetic Fields and Mechanical Vibration. *Appl. Phys. Lett.* **2014**, *105*, 103702. [CrossRef]
46. Serrà, A.; Vázquez-Mariño, G.; García-Torres, J.; Bosch, M.; Vallés, E. Magnetic Actuation of Multifunctional Nanorobotic Platforms to Induce Cancer Cell Death. *Adv. Biosyst.* **2018**, *2*, 1700220. [CrossRef]
47. Nielsch, K.; Wehrspohn, R.; Barthel, J.; Gosele, U.; Fischer, S.; Kronmüller, H. Hexagonally Ordered 100 Nm Period Nickel Nanowire Arrays. *Appl. Phys. Lett.* **2001**, *79*, 1360–1362. [CrossRef]
48. Vega, V.; Böhnert, T.; Martens, S.; Waleczek, M.; Moreno, J.; Görlitz, D.; Prida, V.; Nielsch, K. Tuning the Magnetic Anisotropy of Coni Nanowires: Comparison between Single Nanowires and Nanowire Arrays in Hard-Anodic Aluminum Oxide Membranes. *Nanotechnology* **2012**, *23*, 465709. [CrossRef]
49. Ferré, R.; Ounadjela, K.; George, J.M.; Piraux, L.; Dubois, S. Magnetization Processes in Nickel and Cobalt Electrodeposited Nanowires. *Phys. Rev. B* **1997**, *56*, 14066–14075. [CrossRef]
50. Hergt, R.; Dutz, S.; Müller, R.; Zeisberger, M. Magnetic Particle Hyperthermia: Nanoparticle Magnetism and Materials Development for Cancer Therapy. *J. Phys. Condens. Matter* **2006**, *18*, S2919. [CrossRef]

51. Glöckl, G.; Hergt, R.; Zeisberger, M.; Dutz, S.; Nagel, S.; Weitschies, W. The Effect of Field Parameters, Nanoparticle Properties and Immobilization on the Specific Heating Power in Magnetic Particle Hyperthermia. *J. Phys.* **2006**, *18*, S2935. [CrossRef]
52. Kossatz, S.; Grandke, J.; Couleaud, P.; Latorre, A.; Aires, A.; Crosbie-Staunton, K.; Ludwig, R.; Dahring, H.; Ettelt, V.; Lazaro-Carrillo, A.; et al. Efficient Treatment of Breast Cancer Xenografts with Multifunctionalized Iron Oxide Nanoparticles Combining Magnetic Hyperthermia and Anti-Cancer Drug Delivery. *Breast Cancer Res.* **2015**, *17*, 66. [CrossRef]
53. Gao, W.; Kagan, D.; Pak, O.S.; Clawson, C.; Campuzano, S.; Chuluun-Erdene, E.; Shipton, E.; Fullerton, E.E.; Zhang, L.; Lauga, E.; et al. Cargo-Towing Fuel-Free Magnetic Nanoswimmers for Targeted Drug Delivery. *Small* **2012**, *8*, 460–467. [CrossRef]
54. Gao, W.; de Ávila, B.E.-F.; Zhang, L.; Wang, J. Targeting and Isolation of Cancer Cells Using Micro/Nanomotors. *Adv. Drug Deliv. Rev.* **2018**, *125*, 94–101. [CrossRef]
55. Liu, X.L.; Fan, H.M. Innovative Magnetic Nanoparticle Platform for Magnetic Resonance Imaging and Magnetic Fluid Hyperthermia Applications. *Curr. Opin. Chem. Eng.* **2014**, *4*, 38–46. [CrossRef]
56. Bose, R.J.C.; Lee, S.-H.; Park, H. Biofunctionalized Nanoparticles: An Emerging Drug Delivery Platform for Various Disease Treatments. *Drug Discov. Today* **2016**, *21*, 1303–1312. [CrossRef]
57. Ivanov, Y.P.; Alfadhel, A.; Alnassar, M.; Perez, J.E.; Vazquez, M.; Chuvilin, A.; Kosel, J. Tunable Magnetic Nanowires for Biomedical and Harsh Environment Applications. *Sci. Rep.* **2016**, *6*, 24189. [CrossRef]
58. Martinez Banderas, A. *A Combined Chemical and Magneto-Mechanical Induction of Cancer Cell Death by the Use of Functionalized Magnetic Iron Nanowires*; King Abdullah University of Science and Technology: Thuwal, Saudi Arabia, 2016.
59. Sneider, A.; VanDyke, D.; Paliwal, S.; Rai, P. Remotely Triggered Nano-Theranostics for Cancer Applications. *Nanotheranostics* **2017**, *1*, 1. [CrossRef]
60. Lee, N.; Hyeon, T. Designed Synthesis of Uniformly Sized Iron Oxide Nanoparticles for Efficient Magnetic Resonance Imaging Contrast Agents. *Chem. Soc. Rev.* **2012**, *41*, 2575–2589. [CrossRef]
61. Shore, D.; Pailloux, S.L.; Zhang, J.; Gage, T.; Flannigan, D.J.; Garwood, M.; Pierre, V.C.; Stadler, B.J.H. Electrodeposited Fe and Fe–Au Nanowires as Mri Contrast Agents. *Chem. Commun.* **2016**, *52*, 12634–12637. [CrossRef]
62. Bañobre-López, M.; Bran, C.; Rodríguez-Abreu, C.; Gallo, J.; Vázquez, M.; Rivas, J. A Colloidally Stable Water Dispersion of Ni Nanowires as an Efficient T2-Mri Contrast Agent. *J. Mater. Chem. B* **2017**, *5*, 3338–3347. [CrossRef]
63. Staňo, M.; Fruchart, O. Chapter 3-Magnetic Nanowires and Nanotubes. In *Handbook of Magnetic Materials*; Brück, E., Ed.; Elsevier: Boston, MA, USA, 2018; Volume 27, pp. 155–267.
64. Sumanth Kumar, D.; Jai Kumar, B.; Mahesh, H.M. Chapter 3-Quantum Nanostructures (Qds): An Overview. In *Synthesis of Inorganic Nanomaterials*; Mohan Bhagyaraj, S., Oluwafemi, O.S., Kalarikkal, N., Thomas, S., Eds.; Woodhead Publishing: Sawston, UK, 2018; pp. 59–88. [CrossRef]
65. Li, X.; Sun, L.; Wang, H.; Xie, K.; Long, Q.; Lai, X.; Liao, L. Synthesis of Cobalt Nanowires in Aqueous Solution under an External Magnetic Field. *Beilstein J. Nanotechnol.* **2016**, *7*, 990–994. [CrossRef]
66. Zhao, Z.-J.; Hwang, S.H.; Jeon, S.; Jung, J.-Y.; Lee, J.; Choi, D.-G.; Choi, J.-H.; Park, S.-H.; Jeong, J.-H. Effects of Polymer Surface Energy on Morphology and Properties of Silver Nanowire Fabricated Via Nanoimprint and E-Beam Evaporation. *Appl. Surf. Sci.* **2017**, *420*, 429–438. [CrossRef]
67. Datta, A.; Sangle, A.; Hardingham, N.; Cooper, C.; Kraan, M.; Ritchie, D.; Narayan, V.; Kar-Narayan, S. Structure and Thermoelectric Properties of Bi2−Xsbxte3 Nanowires Grown in Flexible Nanoporous Polycarbonate Templates. *Materials* **2017**, *10*, 553. [CrossRef]
68. DeMeo, D.; Macnaughton, S.; Sonkusale, S.; Vandervelde, T. Electrodeposited Copper Oxide and Zinc Oxide Core-Shell Nanowire Photovoltaic Cells. In *Nanowires-Implementations and Applications*; Hashim, A., Ed.; IntechOpen: London, UK, 2011. [CrossRef]
69. Yu, Y.; Li, J.; Wang, J.; Wu, X.; Yu, C.; Xu, T.; Chang, B.; Sun, H.; Arandiyan, H. Orientation Growth and Magnetic Properties of Electrochemical Deposited Nickel Nanowire Arrays. *Catalysts* **2019**, *9*, 152. [CrossRef]
70. Serrà, A.; Vallés, E. Advanced Electrochemical Synthesis of Multicomponent Metallic Nanorods and Nanowires: Fundamentals and Applications. *Appl. Mater. Today* **2018**, *12*, 207–234. [CrossRef]
71. Oviroh, P.O.; Akbarzadeh, R.; Pan, D.; Coetzee, R.A.M.; Jen, T.-C. New Development of Atomic Layer Deposition: Processes, Methods and Applications. *Sci. Technol. Adv. Mater.* **2019**, *20*, 465–496. [CrossRef]

72. Martín-Palma, R.J.; Lakhtakia, A. Chapter 15-Vapor-Deposition Techniques. In *Engineered Biomimicry*; Lakhtakia, A., Martín-Palma, R.J., Eds.; Elsevier: Boston, MA, USA, 2013; pp. 383–398. [CrossRef]
73. Parasuraman, K.; Raghunathan, V. Status of Pulsed Laser Deposition: Challenges and Opportunities. *Surf. Eng.* **2006**, *22*, 81–83. [CrossRef]
74. De Teresa, J.; Fernández-Pacheco, A.; Córdoba, R.; Serrano-Ramón, L.; Sangiao, S.; Ibarra, M. Review of Magnetic Nanostructures Grown by Focused Electron Beam Induced Deposition (Febid). *J. Phys. D* **2016**, *49*, 243003. [CrossRef]
75. Nguyen, D.M.; Bich, H.N.; Hai Anh, P.D.; Ai-Le, P.H.; Bui, Q.B. Vertical Copper Oxide Nanowire Arrays Attached Three-Dimensional Macroporous Framework as a Self-Supported Sensor for Sensitive Hydrogen Peroxide Detection. *Arab. J. Chem.* **2019**. [CrossRef]
76. Pirouzfar, A.; Seyyed Ebrahimi, S.A. Optimization of Sol–Gel Synthesis of $Cofe_2o_4$ Nanowires Using Template Assisted Vacuum Suction Method. *J. Magn. Magn. Mater.* **2014**, *370*, 1–5. [CrossRef]
77. Hamdana, G.; Südkamp, T.; Descoins, M.; Mangelinck, D.; Caccamo, L.; Bertke, M.; Wasisto, H.S.; Bracht, H.; Peiner, E. Towards Fabrication of 3d Isotopically Modulated Vertical Silicon Nanowires in Selective Areas by Nanosphere Lithography. *Microelectron. Eng.* **2017**, *179*, 74–82. [CrossRef]
78. Ferreira, J.M.; Souza, K.P.; Queiroz, F.M.; Costa, I.; Tomachuk, C.R. Electrochemical and Chemical Characterization of Electrodeposited Zinc Surface Exposed to New Surface Treatments. *Surf. Coat. Technol.* **2016**, *294*, 36–46. [CrossRef]
79. Loto, C.A. Electroless Nickel Plating–A Review. *Silicon* **2016**, *8*, 177–186. [CrossRef]
80. Asadian, E.; Ghalkhani, M.; Shahrokhian, S. Electrochemical Sensing Based on Carbon Nanoparticles: A Review. *Sens. Actuators B* **2019**, *293*, 183–209. [CrossRef]
81. Jamkhande, P.G.; Ghule, N.W.; Bamer, A.H.; Kalaskar, M.G. Metal Nanoparticles Synthesis: An Overview on Methods of Preparation, Advantages and Disadvantages, and Applications. *J. Drug Deliv. Sci. Technol.* **2019**, *53*, 101174. [CrossRef]
82. Ghosh, S. Electroless Copper Deposition: A Critical Review. *Thin Solid Films* **2019**, *669*, 641–658. [CrossRef]
83. Possin, G.E. A Method for Forming Very Small Diameter Wires. *Rev. Sci. Instrum.* **1970**, *41*, 772–774. [CrossRef]
84. Pérez-Page, M.; Yu, E.; Li, J.; Rahman, M.; Dryden, D.M.; Vidu, R.; Stroeve, P. Template-Based Syntheses for Shape Controlled Nanostructures. *Adv. Colloid Interface Sci.* **2016**, *234*, 51–79. [CrossRef]
85. Gontad, F.; Caricato, A.P.; Cesaria, M.; Resta, V.; Taurino, A.; Colombelli, A.; Leo, C.; Klini, A.; Manousaki, A.; Convertino, A.; et al. Decoration of Silica Nanowires with Gold Nanoparticles through Ultra-Short Pulsed Laser Deposition. *Appl. Surf. Sci.* **2017**, *418*, 430–436. [CrossRef]
86. Li, H.; Guan, L.; Xu, Z.; Zhao, Y.; Sun, J.; Wu, J.; Xu, N. Synthesis and Characterization of Amorphous Sio_2 Nanowires Via Pulsed Laser Deposition Accompanied by N2 Annealing. *Appl. Surf. Sci.* **2016**, *389*, 705–712. [CrossRef]
87. Nikov, R.G.; Dikovska, A.O.; Atanasova, G.B.; Avdeev, G.V.; Nedyalkov, N.N. Magnetic-Field-Assisted Formation of Oriented Nanowires Produced by Pld in Open Air. *Appl. Surf. Sci.* **2018**, *458*, 273–280. [CrossRef]
88. Qiu, Z.; Gong, H.; Yang, X.; Zhang, Z.; Han, J.; Cao, B.; Nakamura, D.; Okada, T. Phosphorus Concentration Dependent Microstructure and Optical Property of Zno Nanowires Grown by High-Pressure Pulsed Laser Deposition. *J. Phys. Chem. C* **2015**, *119*, 4371–4378. [CrossRef]
89. Shkurmanov, A.; Sturm, C.; Hochmuth, H.; Grundmann, M. Growth Kinetics of Ultrathin Zno Nanowires Grown by Pulsed Laser Deposition. *Procedia Eng.* **2016**, *168*, 1156–1159. [CrossRef]
90. Nikov, R.G.; Dikovska, A.O.; Avdeev, G.V.; Amoruso, S.; Ausanio, G.; Nedyalkov, N.N. Pld Fabrication of Oriented Nanowires in Magnetic Field. *Appl. Surf. Sci.* **2019**, *471*, 368–374. [CrossRef]
91. Contreras, M.F.; Ravasi, T.; Kosel, J. Targeted Cancer Cell Death Induced by Induced by Biofunctionalized Magnetic Nanowires. In Proceedings of the 2nd Middle East Conference on Biomedical Engineering, Doha, Qatar, 17–20 February 2014.
92. Sun, D. Effect of Zeta Potential and Particle Size on the Stability of Sio_2 Nanospheres as Carrier for Ultrasound Imaging Contrast Agents. *Int. J. Electrochem. Sci.* **2016**, *11*, 8520–8529. [CrossRef]
93. Hussain, M.; Xie, J.; Hou, Z.; Shezad, K.; Xu, J.; Wang, K.; Gao, Y.; Shen, L.; Zhu, J. Regulation of Drug Release by Tuning Surface Textures of Biodegradable Polymer Microparticles. *ACS Appl. Mater. Interfaces* **2017**, *9*, 14391–14400. [CrossRef]

94. Zhang, H.; Xu, H.; Wu, M.; Yufang, Z.; Wang, D.; Jiao, Z. A Soft–Hard Template Approach Towards Hollow Mesoporous Silica Nanoparticles with Rough Surfaces for Controlled Drug Delivery and Protein Adsorption. *J. Mater. Chem. B* **2015**, *3*. [CrossRef]
95. Peng, F.; Su, Y.; Wei, X.; Lu, Y.; Zhou, Y.; Zhong, Y.; Lee, S.-T.; He, Y. Silicon-Nanowire-Based Nanocarriers with Ultrahigh Drug-Loading Capacity for in Vitro and in Vivo Cancer Therapy. *Angew. Chem. Int. Ed. Commun.* **2013**, *52*, 1457–1461. [CrossRef]
96. Wang, J.; Kumeria, T.; Bezem, M.T.; Wang, J.; Sailor, M.J. Self-Reporting Photoluminescent Porous Silicon Microparticles for Drug Delivery. *ACS Appl. Mater. Interfaces* **2018**, *10*, 3200–3209. [CrossRef]
97. Lorenz, M.R.; Holzapfel, V.; Musyanovych, A.; Nothelfer, K.; Walther, P.; Frank, H.; Landfester, K.; Schrezenmeier, H.; Mailänder, V. Uptake of Functionalized, Fluorescent-Labeled Polymeric Particles in Different Cell Lines and Stem Cells. *Biomaterials* **2006**, *27*, 2820–2828. [CrossRef]
98. Murugan, K.; Choonara, Y.E.; Kumar, P.; Bijukumar, D.; du Toit, L.C.; Pillay, V. Parameters and Characteristics Governing Cellular Internalization and Trans-Barrier Trafficking of Nanostructures. *Int. J. Nanomed.* **2015**, *10*, 2191–2206. [CrossRef]
99. Chithrani, B.D.; Ghazani, A.A.; Chan, W.C. Determining the Size and Shape Dependence of Gold Nanoparticle Uptake into Mammalian Cells. *Nano Lett.* **2006**, *6*, 662–668. [CrossRef]
100. Frohlich, E. The Role of Surface Charge in Cellular Uptake and Cytotoxicity of Medical Nanoparticles. *Int. J. Nanomed.* **2012**, *7*, 5577–5591. [CrossRef]
101. Behzadi, S.; Serpooshan, V.; Hamaly, M.; Alkawareek, M.; Dreaden, E.; Brown, D.; Alkilany, A.; Farokhzad, O.; Mahmoudi, M. Cellular Uptake of Nanoparticles: Journey inside the Cell. *Chem. Soc. Rev.* **2017**, *46*. [CrossRef]
102. Panzarini, E.; Mariano, S.; Carata, E.; Mura, F.; Rossi, M.; Dini, L. Intracellular transport of silver and gold nanoparticles and biological responses: An update. *Int. J. Mol. Sci.* **2018**, *19*, e1305. [CrossRef]
103. Awaad, A.; Nakamura, M.; Ishimura, K. Imaging of Size-Dependent Uptake and Identification of Novel Pathways in Mouse Peyer's Patches Using Fluorescent Organosilica Particles. *Nanomedicine* **2012**, *8*, 627–636. [CrossRef]
104. Prina-Mello, A.; Diao, Z.; Coey, J.M.D. Internalization of Ferromagnetic Nanowires by Different Living Cells. *J. Nanobiotechnol.* **2006**, *4*, 9. [CrossRef]
105. Song, M.M.; Song, W.J.; Bi, H.; Wang, J.; Wu, W.L.; Sun, J.; Yu, M. Cytotoxicity and Cellular Uptake of Iron Nanowires. *Biomaterials* **2010**, *31*, 1509–1517. [CrossRef]
106. Choi, D.; Fung, A.; Moon, H.; Ho, D.; Chen, Y.; Kan, E.; Rheem, Y.; Yoo, B.; Myung, N. Transport of Living Cells with Magnetically Assembled Nanowires. *Biomed. Microdevices* **2007**, *9*, 143–148. [CrossRef]
107. Poland, C.A.; Byrne, F.; Cho, W.S.; Prina-Mello, A.; Murphy, F.A.; Davies, G.L.; Coey, J.M.; Gounko, Y.; Duffin, R.; Volkov, Y.; et al. Length-Dependent Pathogenic Effects of Nickel Nanowires in the Lungs and the Peritoneal Cavity. *Nanotoxicology* **2012**, *6*, 899–911. [CrossRef]
108. Wong, P.K. Mutagenicity of Heavy Metals. *Bull. Environ. Contam. Toxicol.* **1988**, *40*, 597–603. [CrossRef]
109. Žužek Rožman, K.; Pečko, D.; Šturm, S.; Maver, U.; Nadrah, P.; Bele, M.; Kobe, S. Electrochemical Synthesis and Characterization of Fe70pd30 Nanotubes for Drug-Delivery Applications. *Mater. Chem. Phys.* **2012**, *133*, 218–224. [CrossRef]
110. Donaldson, K.; Tran, C.L. An Introduction to the Short-Term Toxicology of Respirable Industrial Fibres. *Mutat. Res. Fundam. Mol. Mech. Mutagenesis* **2004**, *553*, 5–9. [CrossRef]
111. Magrez, A.; Kasas, S.; Salicio, V.; Pasquier, N.; Seo, J.W.; Celio, M.; Catsicas, S.; Schwaller, B.; Forro, L. Cellular Toxicity of Carbon-Based Nanomaterials. *Nano Lett.* **2006**, *6*, 1121–1125. [CrossRef]
112. Rahong, S.; Yasui, T.; Kaji, N.; Baba, Y. Recent Developments in Nanowires for Bio-Applications from Molecular to Cellular Levels. *Lab Chip* **2016**, *16*, 1126–1138. [CrossRef]
113. Jahangirian, H.; Kalantari, K.; Izadiyan, Z.; Rafiee-Moghaddam, R.; Shameli, K.; Webster, T.J. A Review of Small Molecules and Drug Delivery Applications Using Gold and Iron Nanoparticles. *Int. J. Nanomed.* **2019**, *14*, 1633–1657. [CrossRef]
114. Safi, M.; Yan, M.; Guedeau-Boudeville, M.-A.; Conjeaud, H.; Garnier-Thibaud, V.; Boggetto, N.; Baeza-Squiban, A.; Niedergang, F.; Averbeck, D.; Berret, J.-F. Interactions between Magnetic Nanowires and Living Cells: Uptake, Toxicity, and Degradation. *ACS Nano* **2011**, *5*, 5354–5364. [CrossRef]

115. Perez, J.E.; Contreras, M.F.; Vilanova, E.; Felix, L.P.; Margineanu, M.B.; Luongo, G.; Porter, A.E.; Dunlop, I.E.; Ravasi, T.; Kosel, J. Cytotoxicity and Intracellular Dissolution of Nickel Nanowires. *Nanotoxicology* **2016**, *10*, 871–880. [CrossRef]
116. Liu, J.; Yu, M.; Zhou, C.; Zheng, J. Renal Clearable Inorganic Nanoparticles: A New Frontier of Bionanotechnology. *Mater. Today* **2013**, *16*, 477–486. [CrossRef]

cancers

MDPI

Review

Thirty Years of Cancer Nanomedicine: Success, Frustration, and Hope

Lucia Salvioni [1,†], Maria Antonietta Rizzuto [1,†], Jessica Armida Bertolini [1], Laura Pandolfi [2], Miriam Colombo [1] and Davide Prosperi [1,3,*]

[1] Department of Biotecnology and Bioscience, University of Milano-Bicocca, piazza della Scienza 2, 20126 Milano, Italy; lucia.salvioni@unimib.it (L.S.); maria.rizzuto@unimib.it (M.A.R.); jessica.bertolini@unimib.it (J.A.B.); miriam.colombo@unimib.it (M.C.)

[2] Unit of Respiratory Diseases, IRCCS Policlinico San Matteo Foundation, 27100 Pavia, Italy; l.pandolfi@smatteo.pv.it

[3] Nanomedicine Laboratory, ICS Maugeri, via S. Maugeri 10, 27100 Pavia, Italy

* Correspondence: davide.prosperi@unimib.it

† These authors contributed equally to this paper.

Received: 31 October 2019; Accepted: 22 November 2019; Published: 25 November 2019

Abstract: Starting with the enhanced permeability and retention (EPR) effect discovery, nanomedicine has gained a crucial role in cancer treatment. The advances in the field have led to the approval of nanodrugs with improved safety profile and still inspire the ongoing investigations. However, several restrictions, such as high manufacturing costs, technical challenges, and effectiveness below expectations, raised skeptical opinions within the scientific community about the clinical relevance of nanomedicine. In this review, we aim to give an overall vision of the current hurdles encountered by nanotherapeutics along with their design, development, and translation, and we offer a prospective view on possible strategies to overcome such limitations.

Keywords: cancer nanomedicine; EPR effect; tumor microenvironment; nanoparticles; nano–bio interactions; clinical translation

1. Introduction

Nanomedicine is an emerging key technology of the 21st century. Although the fundamental concept of a new era of nanotechnology dates back to 1959 with the renowned visionary speech of Richard Feynman at Caltech [1], the optimistic expectation that nanoparticles and other nanoscale tools could be successfully exploited to improve the diagnosis and pharmacological treatment of several human diseases was only first established in the 1990s [2]. During the last three decades, we have witnessed impressive advances in the field, and our scientific understanding of the mechanisms regulating matter organization and interaction with biological systems at the nanoscale has progressed significantly. Nanomedicine, taking advantage of the use of engineered particles having size typically ranging from 1 to 100 nm, aims to exploit nanotechnology for several biomedical applications, mainly disease treatment, diagnosis, and molecular imaging, as well as regenerative medicine and tissue engineering. From the beginning, nanomedicine has been frequently associated with the use of nanoparticles in oncology [3].

In 1986, Maeda and coworkers observed a substantial accumulation of macromolecules in the tumor tissue attributable to a hyperpermeable neovasculature and compromised lymphatic drainage [4]. In principle, the fenestrated endothelial wall in proximity to tumor tissues represents a sort of privileged gate giving selective access to particles in the sub-micrometer scale. Since then, the so-called enhanced permeability and retention (EPR) effect has been validated for particles up to 400–600 nm [5], becoming the pillar of the research in cancer

nanomedicine [6]. The general purpose was to improve the performance of chemotherapeutics, both in terms of efficacy and safety. These efforts resulted in the approval of several innovative nanodrugs and still inspire ongoing investigations [7]. However, after 30 years of exciting discoveries, together with the progress in clinical exploitation, several challenges and limitations are now emerging. Notably, nanomedicine-based treatments often resulted in the lack of, or the limited gain in, overall patient survival [8]. For instance, the first approved PEGylated liposomal doxorubicin formulations (Doxil®, Baxter Healthcare CorporationDeerfield, IL, USA and Caelyx®, Janssen Pharmaceutica NV, Turnhoutseweg, Beerse, Belgium) showed improvements in safety but not in efficacy compared to the standard therapies [9]. Moreover, although all the attempts to develop advanced nanosized drug delivery systems (DDSs) alternative to the conventional approved liposomal formulations, their clinical translation has been frequently hampered by several technical and cost challenges. Therefore, a serious skepticism towards the use of pharmacological nanocarriers (NCs) is growing in the scientific community [10–12].

However, such uncertainty seems to be somewhat overestimated. Indeed, the mentioned limitations highlight the poor understanding of tumor biology as a consequence of the incomplete predictability of the available preclinical models and the large heterogenicity in the patient population. Particularly, the relevance of the EPR effect, which was acknowledged as the "royal gate" in the DDS field, should be now reconsidered in the light of the inter- and intra-patient variability [13]. Additionally, deeper comprehension of the nano–bio interactions may point out new perspectives as well as indicate the most promising approaches to be pursued. Indeed, besides ameliorating the delivery of small chemotherapeutic agents to the tumor cells, new strategies are currently under investigation, including the possibility of exploiting nanoparticles for biologics administration and targeting or activating cellular populations different from the cancer cells (e.g., improving the immunotherapy efficacy) [13,14].

This review aims to disclose the current hurdles encountered in the clinical translation of nanotherapeutics that have been validated at the laboratory level, focusing on the products' development as well as their biological fate after in vivo administration. We also discuss the nanomedicine impact in the oncology field and propose innovative strategies for maximizing their performance.

2. State of the Art in Nanomedicine Research

The main purpose of this section is to give a general picture of the biological processes in which the NCs are involved, once administered in vivo, as well as their clinical implications. However, it is worth mentioning that the NCs' fate and therapeutic outcome is strongly affected by their particular chemical composition and other specific structural features, including surface properties (e.g., charge and hydrophilic to hydrophobic ratio), general physical characteristics (e.g., size, shape, and stiffness) and functionalization (Figure 1).

2.1. Protein Corona

One of the main issues relating to the clinical translation of NCs is represented by the lack of comprehensive knowledge about the interaction between NCs and biological fluids. In particular, the high protein concentration of the physiological environment greatly affects the NCs' biological behavior. Indeed, in response to the characteristics of the administered nanoparticles, endogenous proteins promptly adsorb on the surface, creating the so-called protein corona (PC). As established by several groups, this layer is highly dynamic, and its composition is strongly influenced by the biological milieu [15,16]. The protein adsorption impacts particle size, stability, surface properties, and defines the NCs' biological identity and, therefore, their fate [13]. For instance, binding with opsonins (e.g., IgGs and complement proteins), as well as some conformational changes in the attached proteins, trigger NCs uptake by the mononuclear phagocyte system (MPS) [17]. Although in early studies, the PC relevance was confined to some undesirable effects, including NCs clearance and activation of

the immune system, it is now believed that in several circumstances, PC also dictates the cellular uptake and intracellular localization of NCs [17–19]. While most studies involving nanoparticles as DDSs were originally intended to discourage the protein adsorption by surface coating with hydrophilic polymers (e.g., polyethylene glycol, PEG; zwitterions; carbohydrates; etc.), more recently, some innovative strategies have attempted to benefit from these spontaneous interactions. Such strategies may be accomplished by promoting the adsorption in vivo or by decorating in vitro the NCs surface with specific proteins, which decrease the MPS uptake and/or preferentially lead to a targeted delivery [20]. A recent example of the latter approach was the regulation of the PC formation by precoating the NCs with a HER2 affibody–glutathione–S–transferase fusion protein. This study demonstrated that the formation of a protein shield reduces the adsorption of serum proteins maintaining the selective targeting ability of the targeting molecule [21].

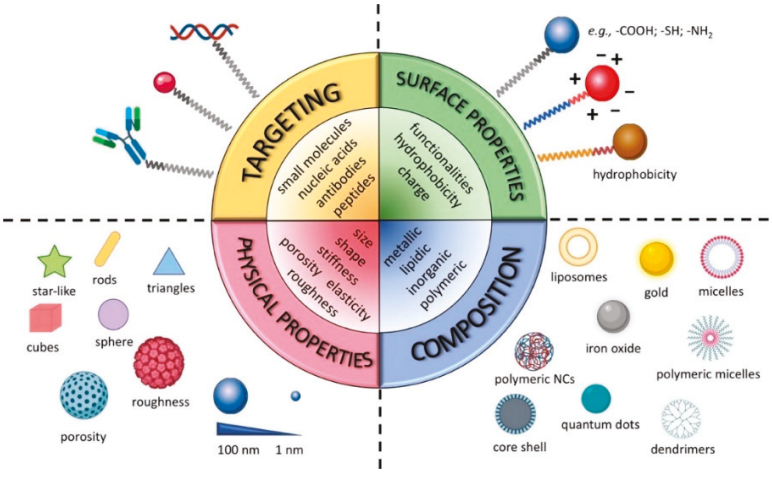

Figure 1. Tunable physical and chemical properties of nanocarriers (NCs).

Considering the multitude of processes in which the PC is directly involved, it is of paramount importance to better understand the driving forces that lead to the PC formation and how it can be manipulated to predict the NCs' fate after their administration in vivo. Nowadays, despite many efforts, a validated model to mimic the in vivo PC generation, as well as an affordable characterization method, are still missing.

2.2. Pharmacokinetics and Biodistribution

Several parameters affect the pharmacokinetics and biodistribution of NCs, including the administration route and NCs' features, such as size, shape, surface, and mechanical properties. After systemic administration, the major clearance organs are lungs, liver, spleen, kidneys; the relationships between the biodistribution in such organs and the NCs properties are reported in Table 1. In general, for particles above the renal threshold (size > 5.5 nm) [22], the elimination is performed by tissue-resident macrophages, monocytes, and dendritic cells belonging to the MPS, although the role of endothelial cells has been recently reconsidered [23,24].

Table 1. Properties-dependent clearance of nanocarriers (NCs).

	Biodistribution Profiles in Clearance Organs
SIZE	Renal excretion is particularly relevant for NCs below the threshold value (ca. 5.5 nm) [25]. MPS clearance is operated by liver>spleen>lung phagocytes. However, the spleen and lung fraction increase with the particle size: NCs > 150 nm are more prone to splenic filtration, while lung accumulation is particularly promoted when the NCs size is close to the micromillimeter range, or they aggregate [26,27].
SURFACE CHARGE	It is generally accepted that positively charged NCs are more rapidly sequestered by MPS than negative and neutral NCs due to the highly-dense coating of serum proteins formed on the administration [27]. However, the surface hydrophobicity, as well as the charge density, strongly influences the elimination rate [28].
SHAPE	NCs' shape determines the movement in blood circulation and the organ-specific biodistribution [25]. Spherical NCs presented the longest circulation time, while rod-, disc-, cage- particles exhibited an increased splenic and hepatic accumulation compared with spherical counterparts [29].
STIFFNESS	Due to the intrinsic deformability, soft NCs have prolonged circulation lifetimes and reduced splenic accumulation when compared with rigid NCs [30].

As already mentioned, several strategies have been developed to escape the MPS recognition, and the most established exploits antifouling polymer grafting (e.g., PEG) onto NCs surface. Thus, some clinical products (i.e., Doxil® and Onivyde®, Les Laboratoires Servier Industrie, Route de Saran, Gidy, France) take advantage of PEGylation to facilitate the immunoevasion. However, the steric barrier created by this polymer does not specifically prevent the interaction with the MPS. Additionally, in some patients, phenomena such as complement activation, infusion reactions, and the production of PEG antibodies have been observed [31–33]. Alternative and more effective strategies are currently under investigation, including the functionalization with CD47 self-peptide and the use of engineered extracellular vesicles or cell membrane-coated particles [34,35]. All these approaches are intended to prolong the circulation time of NCs, although the extended half-life is not always associated with an improvement in the tumor accumulation. In this context, the drug release kinetics (Section 2.5), along with target accessibility (Section 2.3), have been demonstrated to significantly contribute to the treatment response.

2.3. Tumor-Specific Accumulation

A tumor mass consists of proliferating cancer cells and stromal cells (i.e., fibroblasts, immune, and perivascular cells), supplied with a dense extracellular matrix (ECM) and a tortuous and chaotic blood vessels' network. The architecture and properties of this organ-like entity are illustrated in Figure 2. In addition to cancer onset and progression, the so-called tumor microenvironment (TME) is closely involved in tumor resistance to treatments [36,37]. The understanding of tumor biology is of utmost importance in nanomedicine also because TME was clearly demonstrated to minimize the NCs' efficacy by opposing several barriers. First of all, the nanocomplex extravasation is required and generally associated with the EPR effect that characterizes the tumor region [38]. Actually, the discontinuous and fenestrated blood vessels, together with the poor lymphatic drainage, led to optimistic over-expectations in nanomedicine. However, differently from the experimental confirmations achieved from preclinical models, increasing evidence suggests that the great variability in the extent of the EPR effect can be found both among patients and tumor types [39]. Moreover, recent studies revealed that, besides the leaky blood vessels, endothelial transcytosis, as well as vascular bursts, enhance tumor permeability [40,41].

Once extravasated, NCs are expected to homogeneously distribute within the tumor area, but tissue penetration is strongly hampered by several obstructing factors, including the elevated interstitial fluid

pressure (IFP) caused by inefficient lymphatic drainage and blood vessel compression, and solid stress associated with high cellular density and excessive production of ECM [6]. These factors restrict the NC action to the cells located in the perivascular space, hiding the more resistant cells placed in the hypoxia regions.

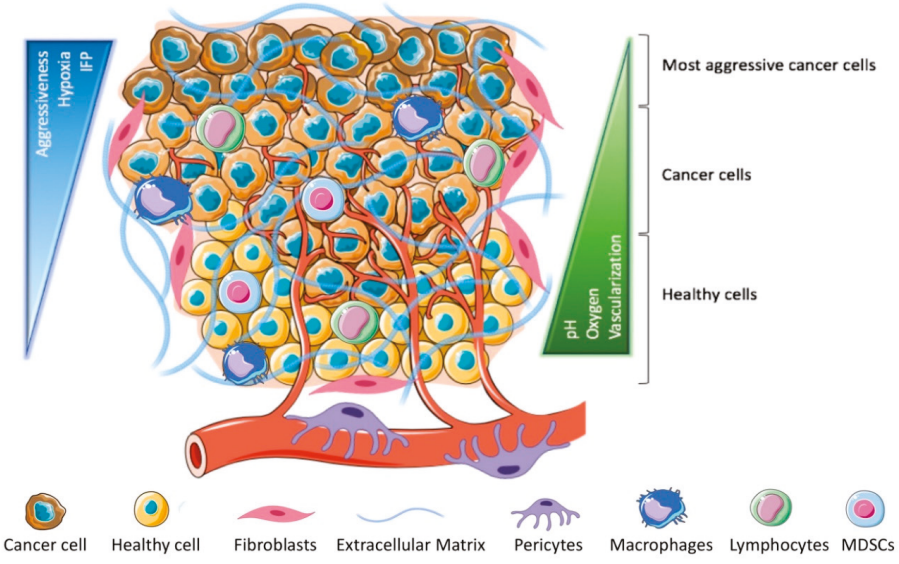

Figure 2. Tumor microenvironment. Tumor tissue is characterized by a high cellular density that hampers oxygen and nutrient perfusion. Accordingly, cancer cells are genetically and epigenetically heterogeneous, and those located far from the blood vessels: (1) favor an anaerobic metabolism that leads to the environment acidification; (2) are more resistant to pharmacological treatments because of their low division rate and genetic instability [42]. Fibroblasts and pericytes are responsible for tissue remodeling, while the immunosuppressive milieu hinders immune cell activity. NCs extravasation and penetration are mainly limited by solid stress and high interstitial fluid pressure, which in certain areas may reach values close to the aortic pressure [43].

Therefore, the tumor accumulation can be considered as the major hurdle to the clinical translation and application of nanosized DDSs. For this reason, the TME modulation and the patient stratification have been recently proposed as strategies to improve the nanodrugs' performance, as discussed below. In addition, an exhaustive understanding of the factors that guide the tissue penetration is extremely urgent. Size, shape, and surface chemistry have been identified as the major characteristics responsible for NCs diffusion inside the tumor mass [44,45]. Beside some universally accepted correlation, such as the inverse proportion between NC size and penetration ability, there are still controversial opinions about the impact of surface charge [46,47]. The functionalization of the NC surface with tissue and cell-penetrating peptides, such as the iRGD peptide, is a promising strategy to increase vascular and tissue permeability. Specifically, iRGD interacts with α_v integrins on the endothelium, stimulating a proteolytic cleavage, and the subsequent binding of the released C-end-R peptide with neuropilin-1, ensuring both the tumor homing and tissue penetration [48]. Recent concerns about possible non-specific interactions of iRGD that might reduce the target accumulation of NCs could be overcome by triggering the penetrating peptide exposure in the TME following specific stimuli [49]. Another common approach to minimize the interaction between NCs and the ECM is surface PEGylation, as has been demonstrated in different tumor models, such as orthotopic brain and lung cancers [50,51]. However, a dense PEG

layer may discourage interaction with target cells. Hence, the NC properties should be carefully optimized to balance their diffusion and target recognition capabilities.

2.4. Cellular Internalization

An effective cellular uptake has an impact on the therapeutic response, as many drugs are directed towards intracellular targets. Notably, an enhanced internalization is crucial for improving the activity of both biologics and small molecules, as it allows poor cellular permeability to be overcome, and the multidrug efflux transporters to be bypassed, respectively [52,53]. The most common approach to increase the NCs uptake is "active" (i.e., molecular) targeting. This strategy aims at improving the selectivity of NCs toward the target cells by decorating their surface with affinity ligands that recognize receptors specifically overexpressed on tumor vasculature or tumor cells [54]. However, the molecular forces that drive ligand–receptor binding only extend over 0.3–0.5 nm [55]. Thus, to promote tumor retention and increase cellular uptake, an efficient NC extravasation is needed [12]. It should be noted that the NC functionalization is expected to alter their physical–chemical properties, affecting the MPS uptake as well as the intratumoral penetration [31]. Moreover, the targeting receptor should be carefully selected, taking into account its preferential tumor expression compared to normal tissues and immune cells, as well as its capability to internalize the NCs upon interaction. A big concern for active targeting success is posed by cancer cell heterogeneity: indeed, it is well known that the cancer cells' epigenetic diversity leads to different expression levels of the targeting receptor [10]. On the other hand, cellular internalization is performed by receptor-mediated endocytosis, which usually leads to NC degradation. In this context, for all the therapeutics that are susceptible to lysosomal digestion (e.g., biologics), an efficient endosomal escape is essential to preserve drug efficacy [56]. Different strategies have been proposed to promote this event, such as membrane fusion, osmotic rupture, particle swelling, and membrane destabilization [57]. Despite these efforts, the proportion of NCs that actually perform the endosomal escape remains extremely low, and thus, more efficient or alternative approaches are demanded [58]. For instance, Rotello and coworkers proposed an endosomal-free cytosolic delivery based on the direct fusion between the nanoassemblies and the plasma membrane [59], whereas Gong and colleagues have recently developed a polymeric coating, termed nanocapsule, with an improved endosomal escape compared with commercial agents [60]. All these concerns underline that, although targeted nanomedicine was proposed as a magic bullet for cancer treatment, its clinical relevance still needs to be validated. Indeed, despite the superiority of the active over the merely passive targeting demonstrated in preclinical models, at present, none of these nanodrugs have been approved [8]. Therefore, increased awareness of the molecular mechanisms governing active targeting is imperative, considering that common belief on nanoparticle-biosystem interactions do not always allow for reliable predictions. For instance, as demonstrated by Colombo et al., maximizing the number of targeting moieties on the NC is indeed expected to improve the molecular targeting in vitro but does not necessarily result in superior therapeutic performance in vivo [61].

2.5. Drug Delivery and Release

In a drug delivery framework, the nanoformulation is intended to enhance the drug protection and permeability, to extend the therapeutic agent half-life, to improve the drug solubility and/or increase its therapeutic index [62]. As already stressed above, different types of drugs, including both small molecules and biologics, can benefit from nanoscale DDSs in enhancing their therapeutic efficacy. Indeed, NCs may broaden the spectra of the administered drugs when they are small molecules, whereas they may overcome the drawbacks associated with large, hydrophilic, and delicate biological molecules improving their availability or helping them to cross the biological barriers [63,64]. However, it is worth mentioning that the release performance of these DDSs should be carefully investigated, and the NCs' design possibly optimized. Especially for long-circulating NCs, minimizing the premature drug release is fundamental to improve its therapeutic outcome [65].

Additionally, new nanoparticle-based classes of DDSs have been recently developed to precisely control the drug release in response to specific conditions, such as the stimuli-responsive NCs that will be discussed further below (Section 5.1.2) [13,43].

3. Controversies Around Clinical Translation of Cancer Nanomedicines

The first nanomedicine that received clinical approval was the PEGylated liposomal formulation of doxorubicin in 1995 (Doxil®/Caelyx®). Since then, 15 nanodrugs have been developed and tested for cancer treatment and have entered the market (Table 2). Doxil®/Caelyx®, together with the albumin-based formulation of paclitaxel (commercialized by Celgene corporation under the Abraxane®, Summit, NJ, USA trademark), currently represents the top-selling nanomedicines in 2018, accounting for $252 M and $950 M, respectively [8]. The liposomal doxorubicin formulations demonstrated a different drug distribution compared to standard treatments, limiting the cardiotoxicity induced by anthracyclines [66]. The new therapeutic index achieved broadened the spectrum of treatable candidates and improved patient compliance. In turn, Abraxane® strongly enhanced paclitaxel tolerance, allowing drug administration without the use of toxic solubilizing surfactants (e.g., castor oil—cremophor EL®). Notably, clinical studies have demonstrated a significant increase in the maximum tolerated dose as well as shorter infusion time of Abraxane® compared to a cremophor EL®-based formulation [67].

Table 2. Clinically approved cancer nanomedicines [8,31].

Product Name	Composition	Indications	First Approval
Doxil/Caelyx	PEGylated liposomal doxorubicin	Myeloma, Kaposi's sarcoma, breast, and ovarian cancer	Approved in the US (1995)
DaunoXome	liposomal daunorubicin	Kaposi's sarcoma	Approved in the US (1996)
Myocet	liposomal doxorubicin	Breast cancer	Approved in Europe/Canada (2000)
Abraxane	albumin-bound paclitaxel	Breast, non-small-cell lung, and pancreatic cancer	Approved in the US (2005)
Lipusu	liposomal paclitaxel	Breast and non-small-cell lung cancer	Approved in China (2006)
Oncaspar	L-asparaginase conjugate	Acute lymphoblastic leukemia	Approved in the US (2006)
DepoCyt	liposomal cytarabine	Lymphoma, Leukemia	Approved in the US (1999)
Genexol-PM	paclitaxel micellar	Breast, non-small-cell lung, ovarian, and gastric cancer	Approved in Korea (2007)
Mepact	liposomal mifamurtide	Osteogenic sarcoma	Approved in Europe (2009)
NanoTherm	Iron oxide nanoparticles	Brain tumors	Approved in Europe (2011)
Marqibo	Liposomal vincristine sulfate	Acute lymphoblastic leukemia	Approved in the US (2012)
ONIVYDE	liposomal irinotecan	Advanced pancreatic cancer	Approved in the US (2015)
DHP107	paclitaxel lipid nanoparticles (oral administration)	Gastric cancer	Approved in Korea (2016)
Vyxeos	liposomal daunorubicin and cytarabine	High-risk acute myeloid leukemia	Approved in the US (2017)
Apealea	paclitaxel micellar	Ovarian, peritoneal, and fallopian tube cancer	Approved in Europe (2018)
Hensify	hafnium oxide nanoparticles	Locally-advanced soft tissue sarcoma	Approved in Europe (2019)

However, despite the important advantage of these nanomedicines in terms of safety, the treatment efficacy did not increase as expected. So far, most approved nanodrugs exhibited only a moderate impact on overall survival as compared to relevant standard therapies [8]. Among the nano-based products under clinical investigation, some of them aim to ameliorate the cancer treatment performance by means of active targeting (e.g., BIND-014) and stimuli-responsive drug release (e.g., ThermoDox) [68,69]. Nevertheless, the low efficacy still represents the main hurdle to the nanodrugs' clinical translation. In particular, among the 94% successful phase I trials, only 14% concluded phase III with positive outcomes [8]. This disappointing efficacy is likely due to multiple factors, such as an incomplete knowledge about the nano–bio interactions (Section 2) and poor reliability of the existing preclinical models. Lack of reliable disease models is particularly disappointing, as mouse tumor models fail to recapitulate the complexity of human tumors mainly because of their large size, the limited cancer cell heterogenicity, the exaggerated EPR effect, and general immunodeficiency [70].

Additional drivers behind the modest clinical translation of nanomedicines are technical and cost challenges in product manufacturing and scale-up. Several clinical trials were terminated or delayed due to unaffordable financial burdens. Indeed, the development of next-generation products other than the conventional liposomal formulations requires huge investments and poses serious issues about the process reproducibility [8,9]. Overall, the large pharma companies, the only entities that can afford such a prohibitive expense, are discouraged from supporting the clinical investigation because of the low perceived success chances. Therefore, it is of utmost relevance to consider that product clinical outcomes and funding availability are closely related since pharmaceutical companies and the healthcare system are more prone to invest if the improvement in treatment efficacy is significant [8].

4. Is It Still Reasonable to Invest in Cancer Nanomedicine?

As already mentioned, nanotechnology has attracted great interest in cancer treatment due to the unique physiochemical properties of nanostructures that can be exploited for diagnostic and therapeutic purposes. Searching "Nanoparticles" on Scopus.com, a publication peak is notable in 2018 with 57,434 documents (Figure 3A) and 22.7% (16,395 documents) of them related to cancer treatment and diagnosis. However, focusing on the subject area (Figure 3B), most of these works were reported in materials and chemistry-related journals, whereas only 17.3% were published in journals referring to the medical research area (including pharmacology, toxicology, and pharmaceutics; medicine; immunology and microbiology).

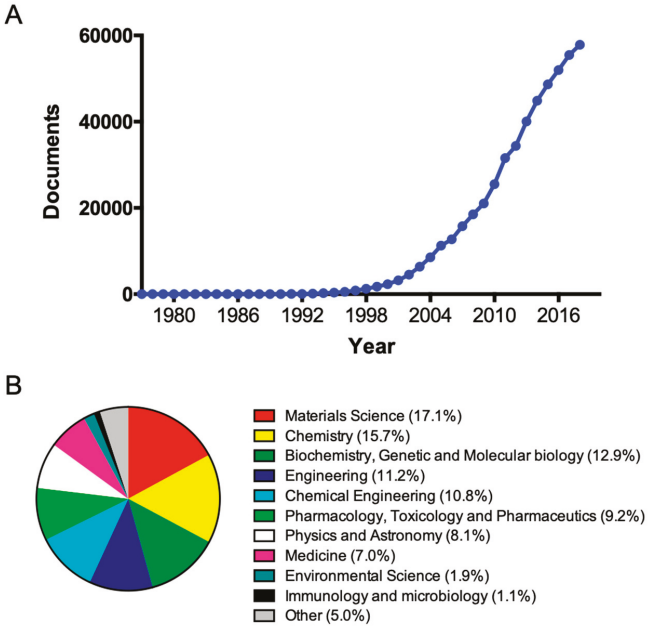

Figure 3. (**A**) Publication peak of "nanoparticles" related papers; (**B**) Subject areas of "nanoparticles + cancer" papers. Elaborated data are derived from the Scopus research tool.

Such publication distribution corroborates the assumption that cancer nanomedicine is more focused on a "formulation-driven" rather than a "disease-driven" approach. Many researchers have pointed out that this one, together with overgeneralizing drug-targeting/delivery concepts and overselling preclinical studies, are the main causes of the suboptimal clinical translation of cancer nanomedicine [71]. In fact, even if the cancer nanomedicine research comprises different types of materials used for synthesizing NCs, only lipidic, one protein-based, a few polymeric and inorganic

nanovehicles have been approved for marketing (Table 2) [72]. These considerations highlight the current limitation of nanomedicine in cancer treatment, leading the scientific community to ask if it is still reasonable to continue to invest in this field. As it can be inferred by Section 2 of this review, ready after administration NCs have to face many hurdles that can reduce therapeutic/targeting/accumulation efficiency. However, it is worth mentioning that both successes and failures have contributed to change the focus of studies to better understand the interaction between NCs and numerous cancer biological mechanisms, triggering new discoveries and future ambitions [9,13,73]. To make some examples, the emerging concerns regarding the real efficacy of the EPR effect in humans forced scientists to go in-depth in defining human TME characteristics to develop NCs with different size, shape, and surface properties to increase their penetration into the tumor mass [13]. Otherwise, the modulation of TME components (e.g., vasculature, ECM) is another interesting point of view to improve the delivery of nanomedicine to solid tumors [12,74].

Another crucial step in cancer nanomedicine is the relationship between the treatment efficacy and the immune system response. This vast branch of nanomedicine offered the opportunity to understand that (1) the available animal models are largely unsuitable, because usually scientists make use of immunodeficient mice, and (2) NCs can be sequestered or opsonized by immune cells [75,76]. In particular, tumor-associated macrophages (TAMs) are one of the primary biological barriers in cancer tissue invariably encountered by NCs, so that scientists tried to exploit this "disadvantage" using TAMs as a reservoir of nanovehicles, to increase the site-specific drug release [13,77]. Another interesting progress is the design of NCs that can avoid phagocytosis through the modification of their surfaces (e.g., with CD47) [78] or that can modulate the polarization and activity of macrophages [79,80]. In addition, studies about the numerous molecular targets found to develop specific active targeted NCs brought huge knowledge. Even if the real efficacy of active targeting in cancer affected patients is still in debate, this kind of approach allowed improvement in the awareness about the molecular characteristics of different cancer types [10,72,81]. Moreover, the evidence that NCs could be entrapped inside endosomes and/or lysosomes led the scientists to study this mechanism developing NCs able to reach the cell cytosol by clever strategies, including direct fusion with the plasma membrane [59] or by performing enhanced endosomal escape [82–84]. The use of engineered NCs can bring other opportunities, such as the encapsulation of poorly soluble drugs [85–87], as well as the delivery of biologics improving their bioavailability, permeability, and stability in the biological environment [53,72]. Thanks to NCs, it is possible to use drugs already accepted by clinical trials, opening the chance to administer them by different routes (i.e., topic [88], oral [89], and inhalation [90] rather than intravenous). This is a relevant point in locally administered therapies because this approach could re-establish the importance of active targeting by decreasing the number of physical and biological barriers that NCs need to overcome.

All these observations justify the ongoing enthusiasm which believes in nanomedicine that will lead to further investment in this field regardless of the unsatisfactory success rate hitherto achieved. However, it is urgent to reduce the gap between the huge number of published papers and the poor clinical outcome of these technologies. First, a sincere effort in the establishment of more clinically relevant models is required. In this context, 3D cultures (e.g., organoids and spheroids) have been proposed as an alternative to 2D cultures for in vitro purposes [91,92], whereas innovative in vivo models, such as patient-derived xenografts and genetically engineered mice, aim to recapitulate the complexity of human tumors [93]. Interestingly, the chicken chorioallantoic membrane (CAM) is emerging as a less time-consuming and a cost-effective alternative to the conventional mouse models [94]. Moreover, it is equally necessary to improve the research data collection to make them as informative as possible. In this regard, Caruso et al. suggested standardization of bio–nano experimental investigations [95], although, among the scientific community, the debate about aspects that need to be improved is still open [96]. Finally, other key points have been suggested by the European Technology Platform for Nanomedicine (ETPN) Agenda to ameliorate the clinical translation: (1) to change from a "formulation-driven" to a "disease-driven" approach considering the influence of tumor

pathophysiology in the clinical outcome and/or focusing on unmet medical needs; (2) to facilitate and increase the dialogue between all the scientific disciplines that play a role in cancer nanomedicine; (3) to consider the balance between benefit for patients and cost constraints for the healthcare system; and (4) to sustain competitiveness of the healthcare economy at the global market [73].

5. Outlook on Future Strategies

Many factors still limit nanomedicine clinical translation and application. However, the presence of several currently active research areas demonstrates that there is still a lot of interest in filling this gap. Accordingly, this section aims to discuss the most promising strategies.

5.1. Strategies to Enhance Tumor Accumulation

Among the above-mentioned issues that hampered the clinical translations of nanomedicines, including overcoming biological barriers, increasing bioavailability, and circulation time of nanodrugs, improving active targeting, etc., enhancing tumor accumulation remains a primary objective. The following approaches are envisioned to allow researchers to step forward.

5.1.1. Priming of the TME

Since several barriers in the TME prevent the nanomedicines delivery, many attempts, extensively reviewed elsewhere [97–99], have been made to improve the EPR effect by lowering the solid stress as well as the IFP. Among them, the normalization of the abnormal tumor vasculature aims to restore a more physiological condition, reducing the vessel leakiness, strengthening the structure of the basement membrane, and improving the coverage of pericytes. Although anti-angiogenic therapy may appear to prevent the tumor accumulation, it has been demonstrated that the vasculature is still permeable to relatively small NCs (20–40 nm), and the significant reduction in the IFP causes increased tumor retention [100,101]. The normalization process is usually achieved by inhibiting pro-angiogenic effectors, such as the VEGF (e.g., through bevacizumab) or PDGF (e.g., using imatinib) [100,101]. Another reported approach is the reduction of solid stress by inducing the tumor cells' apoptosis. Indeed, the rapid cancer cell proliferation causes a compression of lymphatic and blood vessels promoting hypoxia, inflammation, immunosuppression, and metastasis, also representing an obstacle for drug penetration [102]. In this context, it has been observed that paclitaxel tumor priming reduces cell density and IFP, improving the penetration of several NCs, as observed for doxorubicin-loaded liposomes and lipid siRNA complexes [103–105]. Furthermore, ECM degradation has been proposed to alleviate solid stress and enhance NCs intratumoral accumulation. Notably, the use of collagenases, relaxin, and hyaluronidases have been explored for this purpose, and their association with chemotherapeutics is already under clinical trials [106–108]. Although efficient in promoting the tumor accumulation, the clinical application of such strategies is hampered by safety concerns, high costs, and the intrinsic instability of biologic drugs. To tackle these limitations, delivery improvement of these agents and/or the use of alternative cost-effective and well-tolerated small molecules (e.g., the already available Celecoxib) are under investigation [109]. Additionally, another relevant drawback of TME alteration is the possible promotion of tumor progression and invasiveness [31].

In addition to all the above, NCs biodistribution can be ameliorated by interfering with the MPS activity. Notably, tumor homing can be improved by saturating the main clearance organs with decoy NCs or by inhibiting the MPS uptake. Indeed, considering the negligible fraction of NCs that reach the tumor after administration, even small changes in clearance organs accumulation could significantly affect the therapeutic outcome [31,110–112].

5.1.2. Nanocarriers Engineering

In addition to tumor priming, NC engineering may represent a valid strategy for improving nanomedicine performance. Among the reported approaches, stimuli-responsive NCs play a prominent role. These nanoformulations exploit specific endogenous or exogenous stimuli that trigger drug

release, specifically within the tumor tissue. In the first case, NCs responsive to acidic pH, hypoxic environment [113–115], overexpression of tissue remodeling enzymes (e.g., MMP2-9) [116] or the high intracellular concentration of glutathione demonstrated an increase in the cargo therapeutic efficacy and safety [117]. On the other hand, magnetic, thermo-, electric-, light- and ultrasound-sensitive materials may be employed for nanodrugs development to promote the intratumoral drug delivery [118–120]. In this context, several products, such as thermosensitive liposomes (Thermodox), enzyme activated polymeric NCs (Opaxio), as well as magnetic nanoparticles (MTC-Dox), are currently under clinical investigation or approved [43]. Moreover, the combination of different stimuli has recently been proposed to further improve the efficacy of nanoscale DDSs for cancer treatment [43]. In general, the concept of multifunctional vectors is slowly establishing together with a wider comprehension of nano–bio interactions. In particular, novel systems capable of modifying their proprieties in a spatiotemporal way (multistage DDSs) have been developed. For instance, relatively big NCs (<200 nm) can respond to specific stimuli releasing small particles (5–15 nm) able to deeply penetrate into the tumor tissue [121,122]. Alternatively, in multi-layered NCs, the external shell (e.g., PEGylated responsive materials) is expected to change in proximity to a tumor, exposing the hidden penetrating peptides or targeting agents [123–125]. Despite the interesting results, it remains questionable whether increasing the complexity of NCs could excessively hinder their clinical translation. In light of the above consideration, another option may be using nature-inspired NCs composed of biological materials, such as proteins (e.g., albumin, lipoproteins, ferritin) or cellular-derived membranes (e.g., cancer cells, platelets, erythrocytes, and leukocytes) [126]. These materials are generally well-tolerated, less recognized by MPS, and are eventually able to increase tumor targeting. For instance, ferritin-based NCs showed an intrinsic tumor homing as well as an improved performance compared to the liposomal formulation, when loaded with doxorubicin [127]. Another pioneering approach exploited the use of engineered leukocytes membrane to enhance the NCs' accumulation in the proximity of inflamed tumor tissues [128].

5.1.3. Optimizing the Administration Route

Currently, most of the nanomedicines are intravenously injected, but to increase the NCs potential and adopt a more "disease-driven" approach, alternative administration routes might be considered. For instance, the local administration of drug-loaded NCs could perform better than the systemic one because it could reduce the off-target toxicity as well as increase the tumor accumulation bypassing the physiological barriers [54]. This strategy is particularly recommended for non-metastatic tumors or when surgery is contraindicated [54]. As recently reviewed, for lung cancer therapy, the pulmonary route has been explored to improve drug delivery [129]. The local administration proved to be effective even in glioma models where drug-loaded NCs could show a safer toxicity profile compared to the free molecule [50]. Furthermore, some clinically approved products take advantage of local administration: Hensify® (Nanobiotix, Rue de Wattignies, Paris, France) enhances the performance of radiotherapy in advanced soft tissue sarcoma, whereas intracranially injected iron oxide nanoparticles (Nanotherm®) efficiently induced hyperthermia in glioblastoma treatment [130,131]. In addition, non-conventional systemic administration routes may be investigated to specifically accumulate drugs to cellular or tissue targets. Particularly, non-invasive intranasal administration may be exploited for the nose-to-brain delivery, circumventing the first passage in the liver and the blood–brain barrier, thus increasing the fraction of drug at the target site [132,133]. On the other hand, intraperitoneally injection proved to be effective in targeting circulating macrophages, which, once repolarized, exhibited inherent tumor tropism [134]. Finally, as demonstrated by the recent approval of DHP107 (Liporaxel®, DAE HWA Pharm, Seoul, Korea) the oral route has been investigated for increasing patient compliance and reduce the therapy costs [135].

5.2. Nanoimmunology and New Targets

Although classical nanotherapies are directed towards cancer cells, innovative approaches rely on targeting alternative cellular components. Considering the increasing role of cancer immunotherapy, not surprisingly, most of these new targets belong to the immune system. As extensively reviewed, many approaches have been investigated to ameliorate the impact of cancer immunotherapy through the use of nanomedicine [14,136,137]. Here we focus on those that directly modulate the activity of particular cellular mediators, such as tumor-associated macrophages (TAMs), myeloid-derived suppressor cells (MDSCs) and regulatory T cells (Treg) [138]. TAMs are usually characterized by a high M2/M1 ratio, leading to an immunosuppressive environment that promotes tumor progression [139]. The three main strategies, which target TAMs are (1) repolarization of M2 in M1; (2) abolishment of macrophage recruitment via cytokines inhibition; (3) eradication of M2 cells [138,140]. Notably, the selectivity towards M2 can be achieved by targeting the overexpressed mannose receptor [141]. Moreover, the targeting of CD44, along with the intraperitoneal injection, leads to the macrophage-specific delivery exploitable for the repolarization strategy [134].

Other currently investigated targets are the MDSCs, immature cells that contribute to tumor progression by releasing immunosuppressive cytokines [138]. Nanomedicine aims to promote their differentiation into mature cells [142,143], as well as interfere with MDSCs accumulation/activity, by improving the drug delivery [144].

Similarly, Tregs mediate the immunosuppression by inhibiting the activation and expansion of effector T cells, and their downregulation could be ameliorated by the use of NCs. In particular, Tregs can be actively targeted by using their specific markers, such as glucocorticoid-induced Tumor Necrosis Factor Receptor-related protein (GITR), or neuropilin-1 receptor by binding of tLyp1 peptide [145,146]. However, this therapeutic strategy needs to be further validated because Tregs instability could be associated with the onset of autoimmune disorders [147].

In addition to immune cells, cancer-associated fibroblasts (CAFs) have been recently identified as candidates for antitumoral therapies because they are responsible for both immunosuppression and TME reorganization [148,149]. Alternatively, the TME can be directly modulated by NCs. Indeed, the reduction of tumor hypoxia, the restoration of physiological pH, and the inhibition of immunosuppressive soluble mediators impair the tumor progression improving the outcome of current therapies [150].

5.3. Companion Diagnostic

A promising strategy to improve nanomedicine efficacy is the companion diagnostic, which refers to a stratification of patients based on tumor characteristics. Different strategies are currently under investigation based on the use of biomarker profiles and imaging data. The first aims to identify circulating proteins associated with the TME and positively correlated to the EPR effect. For instance, the ratio of MMP9 to the tissue inhibitor of metalloproteinase 1, the collagen content in the capillary walls, and some angiogenesis markers have been shown to predict the EPR entity [13]. On the other hand, radio-labeled and ferumoxytol-loaded NCs have been adopted to monitor their biodistribution by non-invasive techniques (e.g., Single Photon Emission Computed Tomography or Photon Emission Tomography and magnetic resonance imaging, respectively) [13]. The final goal is selecting patients that present the highest probability to positively respond to a specific therapeutic treatment [31]. However, to reach a real utility in clinics, these approaches need to be further validated by accurate correlative studies, defining a clear set of parameters and criteria able to predict the therapeutic outcome [9].

6. Conclusions

The unique attributes of nanoparticles allow clinicians of the 21st century to design innovative therapeutic strategies for use as monotherapies or to be combined with existing chemotherapeutic

treatments or conventional radiotherapy. The recent advances achieved by researchers in the development of tumor-targeting NCs together with a faster data collection deriving from the study of their communication with the biological milieu has generated optimistic expectations for the rapid translation of this basic research into the clinical practice with immediate benefits for oncology patients. However, only a few nanodrugs have actually reached the marketplace and are now approved by the FDA or EMA for specific cancer treatments. This transitory failure has raised some criticisms on the real effectiveness of nanomedicine so that the huge amount of resources dedicated to the research in this field in the last decade has been questioned. This review highlights the main challenges that the scientific community, assisted by the health system and industry, should face in a virtuous joint effort aimed to bring the new discoveries to an established practice that would allow the regulatory bodies to accelerate the process toward the bedside (Section 4). A well-standardized toolkit for the physicochemical, pharmacological, and immunological characterization of all newly developed nanodrugs should be defined before they can be approved for use in humans. The distribution of nanoparticle size, uniformity, surface coating, colloidal stability, and reproducibility from batch to batch also needs to be accurately regulated. Recently, attempts to overcome such barriers to the progression of nanooncology have suggested the definition of a "minimum information standard" for experimental protocols associated with the investigation of the nano–bio interface, leading to the so-called MIRIBEL (minimum information reporting in bio–nano-interaction) paradigm [95]. The collection of three standard categories should be satisfied to fulfill the minimal requirement for good practice in nanomedicine, including appropriate material characterization, biological characterization, and details of experimental protocols. Furthermore, standardized assays for the assessment of short-term and long-term toxicity of nanoparticles will also need to be defined in 2D/3D cell cultures and animal models before approval for clinical trials. Eventually, the cross-fertilization of nanotechnology with recent progress in advanced immunotherapies, together with a renowned knowledge of the impact of environmental factors (e.g., microbiota) on cancer, is expected to trigger a new spur in nanomedicine discovery [151,152]. This entails that nanomedicine researches in the future will be invited to move from a limited "formulation-driven" approach to a preferential "disease-driven" setting, leading to a new era of nanooncology.

Author Contributions: The manuscript was written with the contribution of all the authors. L.S. and M.A.R. organized the collected materials. D.P. critically supervised the work.

Funding: This work has been supported by the project "Development of a biotechnological nanoparticle platform for the delivery of antitumor therapies using Patient Derived-Organoid library of breast cancer" funded by the MIUR Progetti di Ricerca di Rilevante Interesse Nazionale (PRIN) Bando 2017—grant 2017E3A2NR. This research received also funding from AIRC under IG 2018-ID. 21565 project—P.I. Prosperi Davide, and Direzione Generale Ricerca, Innovazione, Università, Export e Internazionalizzazione of the Regione Lombardia.

Conflicts of Interest: The authors declare no conflict of interest.

References

1. Feynman, R.P. There's Plenty of Room at the Bottom. *Eng. Sci.* **1960**, *23*, 22–36. Available online: http://www.richardfeynman.com/ (accessed on 22 November 2019).
2. Tibbals, H.F. *Medical Nanotechnology and Nanomedicine*, 1st ed.; CRC Press: Boca Raton, FL, USA, 2011.
3. Etheridge, M.L.; Campbell, S.A.; Erdman, A.G.; Haynes, C.L.; Wolf, S.M.; McCullough, J. The big picture on nanomedicine: The state of investigational and approved nanoedicine products. *Nanomed. Nanotechnol. Biol. Med.* **2013**, *9*, 1–14. [CrossRef] [PubMed]
4. Matsumura, Y.; Maeda, H. A new concept for macromolecular therapeutics in cancer chemotherapy: Mechanism of tumoritropic accumulation of proteins and the antitumor agent smancs. *Cancer Res.* **1986**, *12*, 6387–6392.
5. Yuan, F.; Dellian, M.; Fukumura, D.; Leunig, M.; Berk, D.A.; Torchilin, V.P.; Jain, R.K. Vascular permeability in a human tumor xenograft: Molecular size dependence and cutoff size. *Cancer Res.* **1995**, *55*, 3752–3756. [PubMed]

6. Nakamura, Y.; Mochida, A.; Choyke, P.L.; Kobayashi, H. Nanodrug Delivery: Is the Enhanced Permeability and Retention Effect Sufficient for Curing Cancer? *Bioconjug. Chem.* **2016**, *27*, 2225–2238. [CrossRef] [PubMed]
7. Wang, A.Z.; Langer, R.; Farokhzad, O.C. Nanoparticle Delivery of Cancer Drugs. *Annu. Rev. Med.* **2012**, *63*, 185–198. [CrossRef]
8. He, H.; Liu, L.; Morin, E.E.; Liu, M.; Schwendeman, A. Survey of Clinical Translation of Cancer Nanomedicines-Lessons Learned from Successes and Failures. *Acc. Chem. Res.* **2019**, *52*, 2445–2461. [CrossRef]
9. Hare, J.I.; Lammers, T.; Ashford, M.B.; Puri, S.; Storm, G.; Barry, S.T. Challenges and strategies in anti-cancer nanomedicine development: An industry perspective. *Adv. Drug Deliv. Rev.* **2017**, *108*, 25–38. [CrossRef]
10. Youn, Y.S.; Bae, Y.H. Perspectives on the past, present, and future of cancer nanomedicine. *Adv. Drug Deliv. Rev.* **2018**, *130*, 3–11. [CrossRef]
11. Wilhelm, S.; Anthony, J.; Tavares, A.J.; Dai, Q.; Ohta, S.; Audet, J.; Dvorak, H.F.; Chan, W.C.W. Analysis of nanoparticle delivery to tumours. *Nat. Rev. Mater.* **2016**, *1*, 16014. [CrossRef]
12. Danhier, F. To exploit the tumor microenvironment: Since the EPR effect fails in the clinic, what is the future of nanomedicine? *J. Control. Release* **2016**, *244*, 108–121. [CrossRef] [PubMed]
13. Shi, J.; Kantoff, P.W.; Wooster, R.; Farokhzad, O.C. Cancer nanomedicine: Progress, challenges and opportunities. *Nat. Rev. Cancer* **2017**, *17*, 20–37. [CrossRef] [PubMed]
14. Shi, Y.; Lammers, T. Combining Nanomedicine and Immunotherapy. *Acc. Chem. Res.* **2019**, *52*, 1543–1554. [CrossRef] [PubMed]
15. Tenzer, S.; Docter, D.; Kuharev, J.; Musyanovych, A.; Fetz, V.; Hecht, R.; Schlenk, F.; Fischer, D.; Kiouptsi, K.; Reinhardt, C.; et al. Rapid formation of plasma protein corona critically affects nanoparticle pathophysiology. *Nat. Nanotechnol.* **2013**, *8*, 772–781. [CrossRef]
16. Docter, D.; Westmeier, D.; Markiewicz, M.; Stolte, S.; Knauer, S.K.; Stauber, R.H. The nanoparticle biomolecule corona: Lessons learned-challenge accepted? *Chem. Soc. Rev.* **2015**, *44*, 6094–6121. [CrossRef]
17. Caracciolo, G.; Farokhzad, O.C.; Mahmoudi, M. Biological Identity of Nanoparticles In Vivo: Clinical Implications of the Protein Corona. *Trends Biotechnol.* **2017**, *35*, 257–264. [CrossRef]
18. Ritz, S.; Schöttler, S.; Kotman, N.; Baier, G.; Musyanovych, A.; Kuharev, J.; Landfester, K.; Schild, H.; Jahn, O.; Tenzer, S.; et al. Protein Corona of Nanoparticles: Distinct Proteins Regulate the Cellular Uptake. *Biomacromolecules* **2015**, *16*, 1311–1321. [CrossRef]
19. Ding, L.; Yao, C.; Yin, X.; Li, C.; Huang, Y.; Wu, M.; Wang, B.; Guo, X.; Wang, Y.; Wu, M. Size, Shape, and Protein Corona Determine Cellular Uptake and Removal Mechanisms of Gold Nanoparticles. *Small* **2018**, *14*, 1801451. [CrossRef]
20. Nguyen, V.H.; Lee, B. Protein corona: A new approach for nanomedicine design. *Int. J. Nanomed.* **2017**, *12*, 3137–3151. [CrossRef]
21. Oh, J.Y.; Kim, H.S.; Palanikumar, L.; Go, E.M.; Jana, B.; Park, S.A.; Kim, H.Y.; Kim, K.; Seo, J.K.; Kwak, S.K.; et al. Cloaking nanoparticles with protein corona shield for targeted drug delivery. *Nat. Commun.* **2018**, *9*, 4548. [CrossRef]
22. Choi, H.S.; Liu, W.; Misra, P.; Tanaka, E.; Zimmer, J.P.; Itty Ipe, B.; Bawendi, M.G.; Frangioni, J.V. Renal clearance of nanoparticles. *Nat. Biotechnol.* **2007**, *25*, 1165–1170. [CrossRef] [PubMed]
23. Rizzuto, M.; Salvioni, L.; Rotem, R.; Colombo, M.; Zanoni, I.; Granucci, F.; Prosperi, D. Are nanotechnological approaches the future of treating inflammatory diseases? *Nanomedicine* **2019**, *14*, 2379–2390. [CrossRef] [PubMed]
24. Campbell, F.; Bos, F.L.; Sieber, S.; Arias-Alpizar, G.; Koch, B.E.; Huwyler, J.; Kros, A.; Bussmann, J. Directing Nanoparticle Biodistribution through Evasion and Exploitation of Stab2-Dependent Nanoparticle Uptake. *ACS Nano* **2018**, *12*, 2138–2150. [CrossRef] [PubMed]
25. Wei, Y.; Quan, L.; Zhou, C.; Zhan, Q. Factors relating to the biodistribution & clearance of nanoparticles & their effects on in vivo application. *Nanomedicine* **2018**, *13*, 1495–1512. [CrossRef] [PubMed]
26. Pérez-Campaña, C.; Gómez-Vallejo, V.; Puigivila, M.; Martín, A.; Calvo-Fernández, T.; Moya, S.E.; Ziolo, R.F.; Reese, T.; Llop, J. Biodistribution of different sized nanoparticles assessed by positron emission tomography: A general strategy for direct activation of metal oxide particles. *ACS Nano* **2013**, *7*, 3498–3505. [CrossRef] [PubMed]

27. Li, S.D.; Huang, L. Pharmacokinetics and Biodistribution of Nanoparticles. *Mol. Pharm.* **2008**, *5*, 496–504. [CrossRef]
28. Duan, X.; Li, Y. Physicochemical characteristics of nanoparticles affect circulation, biodistribution, cellular internalization, and trafficking. *Small* **2013**, *9*, 1521–1532. [CrossRef]
29. Black, K.C.; Wang, Y.; Luehmann, H.P.; Cai, X.; Xing, W.; Pang, B.; Zhao, Y.; Cutler, C.S.; Wang, L.V.; Liu, Y.; et al. Radioactive 198Au-doped nanostructures with different shapes for in vivo analyses of their biodistribution, tumor uptake, and intratumoral distribution. *ACS Nano* **2014**, *8*, 4385–4394. [CrossRef]
30. Zhang, L.; Cao, Z.; Li, Y.; Ella-Menye, J.R.; Bai, T.; Jiang, S. Softer Zwitterionic Nanogels for Longer Circulation and Lower Splenic accumulation. *ACS Nano* **2012**, *6*, 6681–6686. [CrossRef]
31. Wolfram, J.; Ferrari, M. Clinical cancer nanomedicine. *Nano Today* **2019**, *25*, 85–98. [CrossRef]
32. Moghimi, S.M.; Andersena, A.J.; Hashemia, S.H.; Lettiero, B.; Ahmadvanda, D.; Hunterb, A.C.; Andresenc, T.L.; Hamadd, I.; Szebenie, J. Complement activation cascade triggered by PEG–PL engineered nanomedicines and carbon nanotubes: The challenges ahead. *J. Control. Release* **2010**, *146*, 175–181. [CrossRef] [PubMed]
33. Marina, N.M.; Cochrane, D.; Harney, E.; Zomorodi, K.; Blaney, S.; Winick, N.; Bernstein, M.; Link, M.P. Dose escalation and pharmacokinetics of pegylated liposomal doxorubicin (Doxil) in children with solid tumors: A pediatric oncology group study. *Clin. Cancer Res.* **2002**, *8*, 413–418. [PubMed]
34. Rodriguez, P.L.; Harada, T.; Christian, D.A.; Pantano, D.A.; Tsai, R.K.; Discher, D.E. Minimal "Self" peptides that inhibit phagocytic clearance and enhance delivery of nanoparticles. *Science* **2013**, *339*, 971–975. [CrossRef] [PubMed]
35. Parodi, A.; Molinaro, R.; Sushnitha, M.; Evangelopoulos, M.; Martinez, J.O.; Arrighetti, N.; Corbo, C.; Tasciotti, E. Bio-inspired engineering of cell- and virus-like nanoparticles for drug delivery. *Biomaterials* **2017**, *147*, 155–168. [CrossRef] [PubMed]
36. Junttila, M.R.; de Sauvage, F.J. Influence of tumour micro-environment heterogeneity on therapeutic response. *Nature* **2013**, *501*, 346–354. [CrossRef] [PubMed]
37. Quail, D.F.; Joyce, J.A. Microenvironmental regulation of tumor progression and metastasis. *Nat. Med.* **2013**, *19*, 1423–1437. [CrossRef] [PubMed]
38. Maeda, H. Enhanced Permeability and Retention (EPR) Efect: Basis for Drug Targeting to Tumor. In *Biomedical Aspects of Drug Targeting*; Muzykantov, V., Torchilin, V., Eds.; Springer: Boston, MA, USA, 2002; pp. 211–228.
39. Natfji, A.A.; Ravishankar, D.; Osborn, H.M.I.; Greco, F. Parameters Affecting the Enhanced Permeability and Retention Effect: The Need for Patient Selection. *J. Pharm. Sci.* **2017**, *106*, 3179–3187. [CrossRef]
40. Moghimi, S.M.; Simberg, D. Nanoparticle transport pathways into tumors. *J. Nanopart. Res.* **2018**, *20*, 169. [CrossRef]
41. Matsumoto, Y.; Nichols, J.W.; Toh, K.; Nomoto, T.; Cabral, H.; Miura, Y.; Christie, R.J.; Yamada, N.; Ogura, T.; Kano, M.R.; et al. Vascular bursts enhance permeability of tumour blood vessels and improve nanoparticle delivery. *Nat. Nanotechnol.* **2016**, *11*, 533–538. [CrossRef]
42. Nicolas-Boluda, A.; Silva, A.K.A.; Fournel, S.; Gazeau, F. Physical oncology: New targets for nanomedicine. *Biomaterials* **2018**, *150*, 87–99. [CrossRef]
43. El-Sawy, H.S.; Al-Abd, A.M.; Ahmed, T.A.; El-Say, K.M.; Torchilin, V.P. Stimuli-Responsive Nano-Architecture Drug-Delivery Systems to Solid Tumor Micromilieu: Past, Present, and Future Perspectives. *ACS Nano* **2018**, *12*, 10636–10664. [CrossRef] [PubMed]
44. Sun, Q.; Ojha, T.; Kiessling, F.; Lammers, T.; Yang Shi, Y. Enhancing Tumor Penetration of Nanomedicines. *Biomacromolecules* **2017**, *185*, 1449–1459. [CrossRef] [PubMed]
45. Zhang, Y.R.; Lin, R.; Li, H.J.; He, W.L.; Du, J.Z.; Wang, J. Strategies to improve tumor penetration of nanomedicines through nanoparticle design. *Wiley Interdiscip. Rev. Nanomed. Nanobiotechnol.* **2019**, *11*, e1519. [CrossRef]
46. Han, D.; Qi, H.; Huang, K.; Li, X.; Zhan, Q.; Zhao, J.; Xin Hou, X.; Xianjin Yang, X.; Kang, C.; Yuan, X. The effects of surface charge on the intra-tumor penetration of drug delivery vehicles with tumor progression. *J. Mater. Chem. B* **2018**, *6*, 3331–3339. [CrossRef]
47. Stylianopoulos, T.; Poh, M.; Insin, N.; Bawendi, M.G.; Fukumura, D.; Munn, L.L.; Jain, R.K. Diffusion of Particles in the Extracellular Matrix: The Effect of Repulsive Electrostatic Interactions. *Biophys. J.* **2010**, *99*, 1342–1349. [CrossRef]

48. Wang, Y.; Xie, Y.; Li, J.; Peng, Z.; Sheinin, Y.; Zhou, J.; David Oupický, D. Tumor-Penetrating Nanoparticles for Enhanced Anticancer Activity of Combined Photodynamic and Hypoxia-Activated Therapy. *ACS Nano* **2017**, *11*, 2227–2238. [CrossRef]
49. Ding, Y.; Jinjian Liu, J.; Zhang, Y.; Li, X.; Ou, H.; Cheng, T.; Ma, L.; An, Y.; Liu, J.; Huang, F.; et al. A novel strategy based on a ligand-switchable nanoparticle delivery system for deep tumor penetration. *Nanoscale Horiz.* **2019**, *4*, 658–666. [CrossRef]
50. Zhang, C.; Nance, E.A.; Mastorakos, P.; Chisholm, J.; Berry, S.; Eberharth, C.; Tyler, B.; Brem, H.; Suk, J.S.; Hanes, J. Convection enhanced delivery of cisplatin-loaded brain penetrating nanoparticles cures malignant glioma in rats. *J. Control. Release* **2017**, *263*, 112–119. [CrossRef]
51. Huang, X.; Chisholm, J.; Zhuang, J.; Xiao, Y.; Duncan, G.; Chen, X.; Suk, J.S.; Hanes, J. Protein nanocages that penetrate airway mucus and tumor tissue. *Proc. Natl. Acad. Sci. USA* **2017**, *114*, E6595–E6602. [CrossRef]
52. Bellini, M.; Mazzucchelli, S.; Galbiati, E.; Sommaruga, S.; Fiandra, L.; Truffi, M.; Rizzuto, M.A.; Colombo, M.; Tortora, P.; Corsi, F.; et al. Protein nanocages for self-triggered nuclear delivery of DNA-targeted chemotherapeutics in Cancer Cells. *J. Control. Release* **2014**, *196*, 184–196. [CrossRef] [PubMed]
53. Wahilich, J.; Desai, A.; Greco, F.; Hill, K.; Jones, A.T.; Mrsny, R.J.; Pasut, G.; Perrie, Y.; Seib, F.P.; Seymour, L.W.; et al. Nanomedicines for the Delivery of Biologics. *Pharmaceutics* **2019**, *11*, 210. [CrossRef]
54. Rosenblum, D.; Joshi, N.; Tao, W.; Karp, J.M.; Peer, D. Progress and challenges towards targeted delivery of cancer therapeutics. *Nat. Commun.* **2018**, *9*, 1410. [CrossRef]
55. Du, X.; Li, Y.; Xia, Y.L.; Ai, S.M.; Liang, J.; Sang, P.; Ji, X.L.; Liu, S.Q. Insights into Protein-Ligand Interactions: Mechanisms, Models, and Methods. *Int. J. Mol. Sci.* **2016**, *17*, 144. [CrossRef]
56. Selby, L.I.; Cortez-Jugo, C.M.; Such, G.K.; Johnston, A.P.R. Nanoescapology: Progress toward understanding the endosomal escape of polymericnanoparticles. *Wiley Interdiscip. Rev. Nanomed. Nanobiotechnol.* **2017**, *9*, 1452. [CrossRef]
57. Smith, S.A.; Selby, L.I.; Johnston, A.P.R.; Such, G.K. The Endosomal Escape of Nanoparticles: Toward More Efficient Cellular Delivery. *Bioconjug. Chem.* **2019**, *30*, 263–272. [CrossRef] [PubMed]
58. Vermeulen, L.M.P.; Brans, T.; Samal, S.K.; Dubruel, P.; Demeester, J.; De Smedt, S.C.; Remaut, K.; Braeckmans, K. Endosomal Size and Membrane Leakiness Influence Proton Sponge-Based Rupture of Endosomal Vesicles. *ACS Nano* **2018**, *12*, 2332–2345. [CrossRef] [PubMed]
59. Mout, R.; Ray, M.; Yesilbag Tonga, G.; Lee, Y.W.; Tay, T.; Sasaki, K.; Rotello, V.M. Direct Cytosolic Delivery of CRISPR/Cas9-Ribonucleoprotein for Efficient Gene Editing. *ACS Nano* **2017**, *11*, 2452–2458. [CrossRef] [PubMed]
60. Chen, G.; Abdeen, A.A.; Wang, Y.; Shahi, P.K.; Robertson, S.; Xie, R.; Suzuki, M.; Pattnaik, B.R.; Saha, K.; Gong, S. A biodegradable nanocapsule delivers a Cas9 ribonucleoprotein complex for in vivo genome editing. *Nat. Nanotechnol.* **2019**, *14*, 974–980. [CrossRef] [PubMed]
61. Colombo, M.; Fiandra, L.; Alessio, G.; Mazzucchelli, S.; Nebuloni, M.; De Palma, C.; Kantner, K.; Pelaz, B.; Rotem, R.; Corsi, F.; et al. Tumour homing and therapeutic effect of colloidal nanoparticles depend on the number of attached antibodies. *Nat. Commun.* **2016**, *7*, 13818. [CrossRef]
62. Prosperi, D.; Colombo, M.; Zanoni, I.; Granucci, F. Drug nanocarriers to treat autoimmunity and chronic inflammatory diseases. *Semin. Immunol.* **2017**, *34*, 61–67. [CrossRef]
63. Mitragotri, S.; Burke, P.A.; Langer, R. Overcoming the challenges in administering biopharmaceuticals: Formulation and delivery strategies. *Nat. Rev. Drug Discov.* **2014**, *13*, 655–672. [CrossRef]
64. Chen, Z.G. Small-molecule delivery by nanoparticles for anticancer therapy. *Trends Mol. Med.* **2010**, *16*, 594–602. [CrossRef]
65. Wu, J.; Yuan, J.; Ye, B.; Wu, Y.; Xu, Z.; Chen, J.; Chen, J. Dual-Responsive Core Crosslinking Glycopolymer-Drug Conjugates Nanoparticles for Precise Hepatocarcinoma Therapy. *Front. Pharmacol.* **2018**, *9*, 663. [CrossRef]
66. Soloman, R.; Gabizon, A. Clinical pharmacology of liposomal anthracyclines: Focus on pegylated liposomal Doxorubicin. *Clin. Lymphoma Myeloma* **2008**, *8*, 21–32. [CrossRef] [PubMed]
67. Stinchcombe, T.E. Nanoparticle albumin-bound paclitaxel: A novel Cremphor-EL®-free formulation of paclitaxel. *Nanomedicine* **2007**, *2*. [CrossRef] [PubMed]
68. Autio, K.A.; Dreicer, R.; Anderson, J.; Garcia, J.A.; Alva, A.; Hart, L.L.; Milowsky, M.I.; Posadas, E.M.; Ryan, C.J.; Graf, R.P.; et al. Safety and Efficacy of BIND-014, a Docetaxel Nanoparticle Targeting Prostate-Specific Membrane Antigen for Patients With Metastatic Castration-Resistant Prostate Cancer: A Phase 2 Clinical Trial. *JAMA Oncol.* **2018**, *4*, 1344–1351. [CrossRef] [PubMed]

69. Lyon, P.C.; Griffiths, L.F.; Lee, J.; Chung, D.; Carlisle, R.; Wu, F.; Middleton, M.R.; Gleeson, F.V.; Coussios, C.C. Clinical trial protocol for TARDOX: A phase I study to investigate the feasibility of targeted release of lyso-thermosensitive liposomal doxorubicin (ThermoDox®) using focused ultrasound in patients with liver tumours. *J. Ther. Ultrasound* **2017**, *5*, 28. [CrossRef] [PubMed]
70. Lammers, T.; Kiessling, F.; Hennink, W.E.; Storm, G. Drug targeting to tumors: Principles, pitfalls and (pre-) clinical progress. *J. Control. Release* **2012**, *161*, 175–187. [CrossRef]
71. Van Der Meel, R.; Lammers, T.; Hennink, W.E. Cancer nanomedicines: Oversold or underappreciated? *Expert Opin. Drug Deliv.* **2017**, *14*, 1–5. [CrossRef]
72. Hua, S.; de Matos, M.B.C.; Metselaar, J.M.; Storm, G. Current Trends and Challenges in the Clinical Translation of Nanoparticulate Nanomedicines: Pathways for Translational Development and Commercialization. *Front. Pharmacol.* **2018**, *9*, 790. [CrossRef]
73. Strategic Research and Innovation Agenda for Nanomedicine 2016–2030. Available online: https://etp-nanomedicine.eu/about-nanomedicine/strategic-research-and-innovation-agenda/ (accessed on 31 October 2019).
74. Chen, Y.; Liu, X.; Yuan, H.; Yang, Z.; von Roemeling, C.A.; Qie, Y.; Zhao, H.; Wang, Y.; Jiang, W.; Kim, B.Y.S. Therapeutic Remodeling of the Tumor Microenvironment Enhances Nanoparticle Delivery. *Adv. Sci.* **2019**, *6*, 1802070. [CrossRef] [PubMed]
75. Fadeel, B. Hide and Seek: Nanomaterial Interactions with the Immune System. *Front. Immunol.* **2019**, *10*, 133. [CrossRef] [PubMed]
76. Reichel, D.; Tripathi, M.; Perez, J.M. Biological Effects of Nanoparticles on Macrophage Polarization in the Tumor Microenvironment. *Nanotheranostics* **2019**, *3*, 66–88. [CrossRef] [PubMed]
77. Miller, M.A.; Zheng, Y.R.; Gadde, S.; Pfirschke, C.; Zope, H.; Engblom, C.; Kohler, R.H.; Iwamoto, Y.; Yang, K.S.; Askevold, B.; et al. Tumour-associated macrophages act as a slow-release reservoir of nano-therapeutic Pt(IV) pro-drug. *Nat. Commun.* **2015**, *6*, 8692. [CrossRef]
78. Qie, Y.; Yuan, H.; von Roemeling, C.A.; Chen, Y.; Liu, X.; Shih, K.D.; Knight, J.A.; Tun, H.W.; Wharen, R.E.; Jiang, W.; et al. Surface modification of nanoparticles enables selective evasion of phagocytic clearance bydistinct macrophage phenotypes. *Sci. Rep.* **2016**, *6*, 26269. [CrossRef]
79. Zhang, F.; Parayath, N.N.; Ene, C.I.; Stephan, S.B.; Koehne, A.L.; Coon, M.E.; Holland, E.C.; Stephan, M.T. Genetic programming of macrophages to perform anti-tumor functions using targeted mRNA nanocarriers. *Nat. Commun.* **2019**, *10*, 3974. [CrossRef]
80. Chen, L.; Ma, X.; Dang, M.; Dong, H.; Hu, H.; Su, X.; Liu, W.; Wang, Q.; Mou, Y.; Teng, Z. Simultaneous T Cell Activation and Macrophage Polarization to Promote Potent Tumor Suppression by Iron Oxide-Embedded Large-Pore Mesoporous Organosilica Core-Shell Nanospheres. *Adv. Healthc. Mater.* **2019**, *8*, 1900039. [CrossRef]
81. Kwon, I.K.; Lee, S.C.; Han, B.; Park, K. Analysis on the current status of targeted drug delivery to tumors. *J. Control. Release* **2012**, *164*, 108–114. [CrossRef]
82. Fortuni, B.; Inose, T.; Ricci, M.; Fujita, Y.; Van Zundert, I.; Masuhara, A.; Fron, E.; Mizuno, H.; Latterini, L.; Rocha, S.; et al. Polymeric Engineering of Nanoparticles for Highly Efficient Multifunctional Drug Delivery Systems. *Sci. Rep.* **2019**, *9*, 2666. [CrossRef]
83. Huang, J.L.; Chen, H.Z.; Gao, X.L. Lipid-coated calcium phosphate nanoparticle and beyond: A versatile platform for drug delivery. *J. Drug Target* **2018**, *26*, 398–406. [CrossRef]
84. Maugeri, M.; Nawaz, M.; Papadimitriou, A.; Angerfors, A.; Camponeschi, A.; Na, M.; Hölttä, M.; Skantze, P.; Johansson, S.; Sundqvist, M.; et al. Linkage between endosomal escape of LNP-mRNA and loading into EVs for transport to other cells. *Nat. Commun.* **2019**, *10*, 4333. [CrossRef] [PubMed]
85. Pandolfi, L.; Bellini, M.; Vanna, R.; Morasso, C.; Zago, A.; Carcano, S.; Avvakumova, S.; Bertolini, J.A.; Rizzuto, M.A.; Colombo, M.; et al. H-Ferritin Enriches the Curcumin Uptake and Improves the Therapeutic Efficacy in Triple Negative Breast Cancer Cells. *Biomacromolecules* **2017**, *18*, 3318–3330. [CrossRef] [PubMed]
86. Verderio, P.; Pandolfi, L.; Mazzucchelli, S.; Marinozzi, M.R.; Vanna, R.; Gramatica, F.; Corsi, F.; Colombo, M.; Morasso, C.; Prosperi, D. Antiproliferative effect of ASC-J9 delivered by PLGA nanoparticles against estrogen-dependentbreast cancer cells. *Mol. Pharm.* **2014**, *11*, 2864–2875. [CrossRef] [PubMed]
87. Chu, P.Y.; Tsai, S.C.; Ko, H.Y.; Wu, C.C.; Lin, Y.H. Co-Delivery of Natural Compounds with a Dual-Targeted Nanoparticle Delivery System for Improving Synergistic Therapy in an Orthotopic Tumor Model. *ACS Appl. Mater. Interfaces* **2019**, *11*, 23880–23892. [CrossRef]

88. Musazzi, U.M.; Santini, B.; Selmin, F.; Marini, V.; Corsi, F.; Allevi, R.; Ferretti, A.M.; Prosperi, D.; Cilurzo, F.; Colombo, M.; et al. Impact of semi-solid formulations on skin penetration of iron oxide nanoparticles. *J. Nanobiotechnol.* **2017**, *15*, 14. [CrossRef]
89. Salvioni, L.; Fiandra, L.; Del Curto, M.D.; Mazzucchelli, S.; Allevi, R.; Truffi, M.; Sorrentino, L.; Santini, B.; Cerea, M.; Palugan, L.; et al. Oral delivery of insulin via polyethylene imine-based nanoparticles for colonic release allows glycemic control in diabetic rats. *Pharmacol. Res.* **2016**, *110*, 122–130. [CrossRef]
90. Codullo, V.; Cova, E.; Pandolfi, L.; Breda, S.; Morosini, M.; Frangipane, V.; Malatesta, M.; Calderan, L.; Cagnone, M.; Pacini, C.; et al. Imatinib-loaded gold nanoparticles inhibit proliferation of fibroblasts and macrophages from systemic sclerosis patients and ameliorate experimental bleomycin-induced lung fibrosis. *J. Control. Release* **2019**, *310*, 198–208. [CrossRef]
91. Ferreira, L.P.; Gaspar, V.M.; Mano, J.F. Design of spherically structured 3D in vitro tumor models -Advances and prospects. *Acta Biomater.* **2018**, *75*, 11–34. [CrossRef]
92. Weeber, F.; Ooft, S.N.; Dijkstra, K.K.; Voest, E.E. Tumor Organoids as a Pre-clinical Cancer Model for Drug Discovery. *Cell Chem. Biol.* **2017**, *24*, 1092–1100. [CrossRef]
93. Day, C.; Merlino, G.; Van Dyke, T. Preclinical Mouse Cancer Models: A Maze of Opportunities and Challenges. *Cell* **2015**, *163*, 39–53. [CrossRef]
94. Vu, B.T.; Shahin, S.A.; Croissant, J.; Fatieiev, Y.; Matsumoto, K.; Le-Hoang Doan, T.; Yik, T.; Simargi, S.; Conteras, A.; Ratliff, L.; et al. Chick chorioallantoic membrane assay as an in vivo model to study the effect of nanoparticle-based anticancer drugs in ovarian cancer. *Sci. Rep.* **2018**, *8*, 8524. [CrossRef]
95. Faria, M.; Björnmalm, M.; Thurecht, K.J.; Kent, S.J.; Parton, R.G.; Kavallaris, M.; Johnston, A.P.R.; Gooding, J.J.; Corrie, S.R.; Boyd, B.J.; et al. Minimum information reporting in bio-nano experimental literature. *Nat. Nanotechnol.* **2018**, *13*, 777–785. [CrossRef] [PubMed]
96. Leong, H.S.; Butler, K.S.; Brinker, C.J.; Azzawi, M.; Conlan, S.; Dufés, C.; Owen, A.; Rannard, S.; Scott, C.; Chen, C.; et al. On the issue of transparency and reproducibility in nanomedicine. *Nat. Nanotechnol.* **2019**, *14*, 629–635. [CrossRef] [PubMed]
97. Zhang, B.; Hu, Y.; Pang, Z. Modulating the Tumor Microenvironment to Enhance Tumor Nanomedicine Delivery. *Front. Pharmacol.* **2017**, *8*, 952. [CrossRef] [PubMed]
98. Chauhan, V.P.; Jain, R.K. Strategies for advancing cancer nanomedicine. *Nat. Mater.* **2013**, *12*, 958–962. [CrossRef] [PubMed]
99. Khawar, I.A.; Kim, J.H.; Kuh, H.J. Improving drug delivery to solid tumors: Priming the tumor microenvironment. *J. Control. Release* **2015**, *201*, 78–89. [CrossRef] [PubMed]
100. Chauhan, V.P.; Stylianopoulos, T.; Martin, J.D.; Popović, Z.; Chen, O.; Kamoun, W.S.; Bawendi, M.G.; Fukumura, D.; Jain, R.K. Normalization of tumour blood vessels improves the delivery of nanomedicines in a size-dependent manner. *Nat. Nanotechnol.* **2012**, *7*, 383–388. [CrossRef]
101. Zhang, B.; Shi, W.; Jiang, T.; Wang, L.; Mei, H.; Lu, H.; Hu, Y.; Pang, Z. Optimization of the tumor microenvironment and nanomedicine properties simultaneously to improve tumor therapy. *Oncotarget* **2016**, *7*, 62607–62618. [CrossRef]
102. Stylianopoulos, T.; Martin, J.D.; Chauhan, V.P.; Jain, S.R.; Diop-Frimpong, B.; Bardeesy, N.; Smith, B.L.; Ferrone, C.R.; Hornicek, F.J.; Boucher, Y.; et al. Causes, consequences, and remedies for growth-induced solid stress in murine and human tumors. *Proc. Natl. Acad. Sci. USA* **2012**, *109*, 15101–15108. [CrossRef]
103. Lu, D.; Wientjes, M.G.; Lu, Z.; Au, J.L. Tumor priming enhances delivery and efficacy of nanomedicines. *J. Pharmacol. Exp. Ther.* **2007**, *322*, 80–88. [CrossRef]
104. Yu, Q.; Qiu, Y.; Chen, X.; Wang, X.; Mei, L.; Wu, H.; Liu, K.; Liu, Y.; Li, M.; Zhang, Z.; et al. Chemotherapy priming of the Pancreatic Tumor Microenvironment Promotes Delivery and Anti-Metastasis Efficacy of Intravenous Low-Molecular-Weight Heparin-Coated Lipid-siRNA Complex. *Theranostics* **2019**, *9*, 355–368. [CrossRef] [PubMed]
105. Wang, J.; Lu, Z.; Wang, J.; Cui, M.; Yeung, B.Z.; Cole, D.J.; Wientjes, M.G.; Au, J.L. Paclitaxel tumor priming promotes delivery and transfection of intravenous lipid-siRNA in pancreatic tumors. *J. Control. Release* **2015**, *216*, 103–110. [CrossRef] [PubMed]
106. Zinger, A.; Koren, L.; Adir, O.; Poley, M.; Alyan, M.; Yaari, Z.; Noor, N.; Krinsky, N.; Simon, A.; Gibori, H.; et al. Collagenase Nanoparticles Enhance the Penetration of Drugs into Pancreatic Tumors. *ACS Nano* **2019**, *13*, 11008–11021. [CrossRef] [PubMed]

107. Mardhian, D.F.; Storm, G.; Bansal, R.; Prakash, J. Nano-targeted relaxin impairs fibrosis and tumor growth in pancreatic cancer and improves the efficacy of gemcitabine in vivo. *J. Control. Release* **2018**, *290*, 1–10. [CrossRef] [PubMed]
108. Wong, K.M.; Horton, K.J.; Coveler, A.L.; Hingorani, S.R.; Harris, W.P. Targeting the Tumor Stroma: The Biology and Clinical Development of Pegylated Recombinant Human Hyaluronidase (PEGPH20). *Curr. Oncol. Rep.* **2017**, *19*, 47. [CrossRef] [PubMed]
109. Zhang, B.; Jin, K.; Jiang, T.; Wang, L.; Shen, S.; Luo, Z.; Tuo, Y.; Liu, X.; Hu, Y.; Pang, Z. Celecoxib normalizes the tumor microenvironment and enhances small nanotherapeutics delivery to A549 tumors in nude mice. *Sci. Rep.* **2017**, *7*, 10071. [CrossRef]
110. Diagaradjane, P.; Deorukhkar, A.; Gelovani, J.G.; Maru, D.M.; Krishnan, S. Gadolinium chloride augments tumor-specific imaging of targeted quantum dots in vivo. *ACS Nano* **2010**, *4*, 4131–4141. [CrossRef]
111. Liu, T.; Choi, H.; Zhou, R.; Chen, I.W. RES blockade: A strategy for boosting efficiency of nanoparticle drug. *Nano Today* **2015**, *10*, 11–21. [CrossRef]
112. Wolfram, J.; Nizzero, S.; Liu, H.; Li, F.; Zhang, G.; Li, Z.; Shen, H.; Blanco, E.; Ferrari, M. A chloroquine-induced macrophage-preconditioning strategy for improved nanodelivery. *Sci. Rep.* **2017**, *7*, 13738. [CrossRef]
113. Wu, W.; Luo, L.; Wang, Y.; Wu, Q.; Dai, H.B.; Li, J.S.; Durkan, C.; Wang, N.; Wang, G.X. Endogenous pH-responsive nanoparticles with programmable size changes for targeted tumor therapy and imaging applications. *Theranostics* **2018**, *8*, 3038–3058. [CrossRef]
114. Kulkarni, P.; Haldar, M.K.; You, S.; Choi, Y.; Mallik, S. Hypoxia-Responsive Polymersomes for Drug Delivery to Hypoxic Pancreatic Cancer Cells. *Biomacromolecules* **2016**, *17*, 2507–2513. [CrossRef] [PubMed]
115. Ahmad, Z.; Lv, S.; Tang, Z.; Shah, A.; Chen, X. Methoxy Poly (Ethylene Glycol)-Block-Poly (Glutamic Acid)-Graft-6-(2-Nitroimidazole) Hexyl Amine Nanoparticles for Potential Hypoxia-Responsive Delivery of Doxorubicin. *J. Biomater. Sci. Polym. Ed.* **2016**, *27*, 40–54. [CrossRef] [PubMed]
116. Cathcart, J.; Pulkoski-Gross, A.; Cao, J. Targeting Matrix Metalloproteinases in Cancer: Bringing New Life to Old Ideas. *Genes. Dis.* **2015**, *2*, 26–34. [CrossRef] [PubMed]
117. Mura, S.; Nicolas, J.; Couvreur, P. Stimuli-Responsive Nanocarriers for Drug Delivery. *Nat. Mater.* **2013**, *12*, 991–1003. [CrossRef] [PubMed]
118. Wu, M.; Huang, S. Magnetic Nanoparticles in Cancer Diagnosis, Drug Delivery and Treatment. *Mol. Clin. Oncol.* **2017**, *7*, 738–746. [CrossRef]
119. Jiang, J.; Tong, X.; Morris, D.; Zhao, Y. Toward Photocontrolled Release Using Light-Dissociable Block Copolymer Micelles. *Macromolecules* **2006**, *39*, 4633–4640. [CrossRef]
120. Rapoport, N.Y.; Kennedy, A.M.; Shea, J.E.; Scaife, C.L.; Nam, K.H. Controlled and targeted tumor chemotherapy by ultrasound-activated nanoemulsions/microbubbles. *J. Control. Release* **2009**, *138*, 268–276. [CrossRef]
121. Kim, J.; Jo, C.; Lim, W.G.; Jung, S.; Lee, Y.M.; Lim, J.; Lee, H.; Lee, J.; Kim, W.J. Programmed Nanoparticle-Loaded Nanoparticles for Deep-Penetrating 3D Cancer Therapy. *Adv. Mater.* **2018**, *30*, 1707557. [CrossRef]
122. Li, H.J.; Du, J.Z.; Liu, J.; Du, X.J.; Shen, S.; Zhu, Y.H.; Wang, X.; Ye, X.; Nie, S.; Wang, J. Smart Superstructures with Ultrahigh pH-Sensitivity for Targeting Acidic Tumor Microenvironment: Instantaneous Size Switching and Improved Tumor Penetration. *ACS Nano* **2016**, *10*, 6753–6761. [CrossRef]
123. Zhu, L.; Wang, T.; Perche, F.; Taigind, A.; Torchilin, V.P. Enhanced anticancer activity of nanopreparation containing an MMP2-sensitive PEG-drug conjugate and cell-penetrating moiety. *Proc. Natl. Acad. Sci. USA* **2013**, *110*, 17047–17052. [CrossRef]
124. Xu, X.; Saw, P.E.; Tao, W.; Li, Y.; Ji, X.; Yu, M.; Mahmoudi, M.; Rasmussen, J.; Ayyash, D.; Zhou, Y.; et al. Tumor Microenvironment-Responsive Multistaged Nanoplatform for Systemic RNAi and Cancer Therapy. *Nano Lett.* **2017**, *17*, 4427–4435. [CrossRef] [PubMed]
125. Li, L.; Sun, W.; Zhong, J.; Yang, Q.; Zhu, X.; Zhou, Z.; Zhang, Z.; Huang, Y. Multistage Nanovehicle Delivery System Based on Stepwise Size Reduction and Charge Reversal for Programmed Nuclear Targeting of Systemically Administered Anticancer Drugs. *Adv. Funct. Mater.* **2015**, *25*, 4101–4113. [CrossRef]
126. Li, B.; Wang, F.; Gui, L.; He, Q.; Yao, Y.; Chen, H. The potential of biomimetic nanoparticles for tumor-targeted drug delivery. *Nanomedicine* **2018**, *13*, 2099–2118. [CrossRef] [PubMed]

127. Mazzucchelli, S.; Bellini, M.; Fiandra, L.; Truffi, M.; Rizzuto, M.A.; Sorrentino, L.; Longhi, E.; Nebuloni, M.; Prosperi, D.; Corsi, F. Nanometronomic treatment of 4T1 breast cancer with nanocaged doxorubicin prevents drug resistance and circumvents cardiotoxicity. *Oncotarget* **2017**, *8*, 8383–8396. [CrossRef]
128. Martinez, J.O.; Molinaro, R.; Hartman, K.A.; Boada, C.; Sukhovershin, R.; De Rosa, E.; Kirui, D.; Zhang, S.; Evangelopoulos, M.; Carter, A.M.; et al. Biomimetic nanoparticles with enhanced affinity towards activated endothelium as versatile tools for theranostic drug delivery. *Theranostics* **2018**, *8*, 1131–1145. [CrossRef]
129. Abdelaziz, H.M.; Gaber, M.; Abd-Elwakil, M.M.; Mabrouk, M.T.; Elgohary, M.M.; Kamel, N.M.; Kabary, D.M.; Freag, M.S.; Samaha, M.W.; Mortada, S.M.; et al. Inhalable particulate drug delivery systems for lung cancer therapy: Nanoparticles, microparticles, nanocomposites and nanoaggregates. *J. Control. Release* **2018**, *269*, 374–392. [CrossRef]
130. Nanobiotix Announces First Ever Radioenhancer to Receive European Market Approval. Available online: https://www.globenewswire.com/news-release/2019/04/04/1797273/0/en/Nanobiotix-Announces-First-Ever-Radioenhancer-to-Receive-European-Market-Approval.html (accessed on 19 November 2019).
131. The Nanotherm® Therapy. Available online: https://www.magforce.com/en/home/our_therapy/ (accessed on 19 November 2019).
132. Sekerdag, E.; Lüle, S.; Bozdağ Pehlivan, S.; Öztürk, N.; Kara, A.; Kaffashi, A.; Vural, I.; Işıkay, I.; Yavuz, B.; Oguz, K.K.; et al. A potential non-invasive glioblastoma treatment: Nose-to-brain delivery of farnesylthiosalicylic acid incorporated hybrid nanoparticles. *J. Control. Release* **2017**, *261*, 187–198. [CrossRef]
133. Chu, L.; Wang, A.; Ni, L.; Yan, X.; Song, Y.; Zhao, M.; Sun, K.; Mu, H.; Liu, S.; Wu, Z.; et al. Nose-to-brain delivery of temozolomide-loaded PLGA nanoparticles functionalized with anti-EPHA3 for glioblastoma targeting. *Drug Deliv.* **2018**, *25*, 1634–1641. [CrossRef]
134. Parayath, N.N.; Parikh, A.; Amiji, M.M. Repolarization of Tumor-Associated Macrophages in a Genetically Engineered Nonsmall Cell Lung Cancer Model by Intraperitoneal Administration of Hyaluronic Acid-Based Nanoparticles Encapsulating MicroRNA-125b. *Nano Lett.* **2018**, *18*, 3571–3579. [CrossRef]
135. Jang, Y.; Chung, H.J.; Hong, J.W.; Yun, C.W.; Chung, H. Absorption mechanism of DHP107, an oral paclitaxel formulation that forms a hydrated lipidic sponge phase. *Acta Pharmacol. Sin.* **2017**, *38*, 133–145. [CrossRef]
136. Song, W.; Musetti, S.N.; Huang, L. Nanomaterials for cancer immunotherapy. *Biomaterials* **2017**, *148*, 16–30. [CrossRef]
137. Musetti, S.; Huang, L. Nanoparticle-Mediated Remodeling of the Tumor Microenvironment to Enhance Immunotherapy. *ACS Nano* **2018**, *12*, 11740–11755. [CrossRef]
138. Huai, Y.; Hossen, M.N.; Wilhelm, S.; Bhattacharya, R.; Mukherjee, P. Nanoparticle Interactions with the Tumor Microenvironment. *Bioconjug. Chem.* **2019**, *30*, 2247–2263. [CrossRef] [PubMed]
139. Zhang, M.; He, Y.; Sun, X.; Li, Q.; Wang, W.; Zhao, A.; Di, W. A high M1/M2 ratio of tumor-associated macrophages is associated with extended survival in ovarian cancer patients. *J. Ovarian Res.* **2014**, *7*, 19. [CrossRef] [PubMed]
140. Song, M.; Liu, T.; Shi, C.; Zhang, X.; Chen, X. Bioconjugated Manganese Dioxide Nanoparticles Enhance Chemotherapy Response by Priming Tumor-Associated Macrophages toward M1-like Phenotype and Attenuating Tumor Hypoxia. *ACS Nano* **2016**, *10*, 633–647. [CrossRef] [PubMed]
141. Zhu, S.; Niu, M.; O'Mary, H.; Cui, Z. Targeting of tumor-associated macrophages made possible by PEG-sheddable, mannose-modified nanoparticles. *Mol. Pharm.* **2013**, *10*, 3525–3530. [CrossRef]
142. Kong, M.; Tang, J.; Qiao, Q.; Wu, T.; Qi, Y.; Tan, S.; Gao, X.; Zhang, Z. Biodegradable Hollow Mesoporous Silica Nanoparticles for Regulating Tumor Microenvironment and Enhancing Antitumor Efficiency. *Theranostics* **2017**, *7*, 3276–3292. [CrossRef]
143. Kourtis, I.C.; Hirosue, S.; de Titta, A.; Kontos, S.; Stegmann, T.; Hubbell, J.A.; Swartz, M.A. Peripherally administered nanoparticles target monocytic myeloid cells, secondary lymphoid organs and tumors in mice. *PLoS ONE* **2013**, *8*, e61646. [CrossRef]
144. Sasso, M.S.; Lollo, G.; Pitorre, M.; Solito, S.; Pinton, L.; Valpione, S.; Bastiat, G.; Mandruzzato, S.; Bronte, V.; Marigo, I.; et al. Low dose gemcitabine-loaded lipid nanocapsules target monocytic myeloid-derived suppressor cells and potentiate cancer immunotherapy. *Biomaterials* **2016**, *96*, 47–62. [CrossRef]
145. Ou, W.; Jiang, L.; Thapa, R.K.; Soe, Z.C.; Poudel, K.; Chang, J.H.; Ku, S.K.; Choi, H.G.; Yong, C.S.; Kim, J.O. Combination of NIR therapy and regulatory T cell modulation using layer-by-layer hybrid nanoparticles for effective cancer photoimmunotherapy. *Theranostics* **2018**, *8*, 4574–4590. [CrossRef]

146. Ou, W.; Thapa, R.K.; Jiang, L.; Soe, Z.C.; Gautam, M.; Chang, J.H.; Jeong, J.H.; Ku, S.K.; Choi, H.G.; Yong, C.S.; et al. Regulatory T cell-targeted hybrid nanoparticles combined with immuno-checkpoint blockage for cancer immunotherapy. *J. Control. Release* **2018**, *281*, 84–96. [CrossRef]
147. Dominguez-Villar, M.; Hafler, D.A. Regulatory T cells in autoimmune disease. *Nat. Immunol.* **2018**, *19*, 665–673. [CrossRef] [PubMed]
148. Chen, X.; Song, E. Turning foes to friends: Targeting cancer-associated fibroblasts. *Nat. Rev. Drug Discov.* **2019**, *18*, 99–115. [CrossRef]
149. Truffi, M.; Mazzucchelli, S.; Bonizzi, A.; Sorrentino, L.; Allevi, R.; Vanna, R.; Morasso, C.; Corsi, F. Nano-Strategies to Target Breast Cancer-Associated Fibroblasts: Rearranging the Tumor Microenvironment to Achieve Antitumor Efficacy. *Int. J. Mol. Sci.* **2019**, *20*, 1263. [CrossRef] [PubMed]
150. Liu, J.; Chen, G.; Feng, L.; Liu, Z. Nanomedicine for tumor microenvironment modulation and cancer treatment enhancement. *Nano Today* **2018**, *21*, 55–73. [CrossRef]
151. Wang, D.; Wang, T.; Yu, H.; Feng, B.; Zhou, L.; Zhou, F.; Hou, B.; Zhang, H.; Luo, M.; Li, Y. Engineering nanoparticles to locally activate T cells in the tumor microenvironment. *Sci. Immunol.* **2019**, *4*, eaau6584. [CrossRef] [PubMed]
152. Tadokoro, Y.; Hoshii, T.; Yamazaki, S.; Eto, K.; Ema, H.; Kobayashi, M.; Ueno, M.; Ohta, K.; Arai, Y.; Hara, E.; et al. Spred1 Safeguards Hematopoietic Homeostasis against Diet-Induced Systemic Stress. *Cell Stem Cell* **2018**, *22*, 713–725. [CrossRef]

cancers

MDPI

Review

Cancer Cell Membrane-Coated Nanoparticles for Cancer Management

Jenna C. Harris [1], Mackenzie A. Scully [2] and Emily S. Day [1,2,3,*]

1 Materials Science and Engineering, University of Delaware, Newark, DE 19716, USA; harrisj@udel.edu
2 Biomedical Engineering, University of Delaware, Newark, DE 19716, USA; mkscully@udel.edu
3 Helen F. Graham Cancer Center and Research Institute, Newark, DE 19713, USA
* Correspondence: emilyday@udel.edu; Tel.: +1-302-831-8050

Received: 28 October 2019; Accepted: 18 November 2019; Published: 21 November 2019

Abstract: Cancer is a global health problem in need of transformative treatment solutions for improved patient outcomes. Many conventional treatments prove ineffective and produce undesirable side effects because they are incapable of targeting only cancer cells within tumors and metastases post administration. There is a desperate need for targeted therapies that can maximize treatment success and minimize toxicity. Nanoparticles (NPs) with tunable physicochemical properties have potential to meet the need for high precision cancer therapies. At the forefront of nanomedicine is biomimetic nanotechnology, which hides NPs from the immune system and provides superior targeting capabilities by cloaking NPs in cell-derived membranes. Cancer cell membranes expressing "markers of self" and "self-recognition molecules" can be removed from cancer cells and wrapped around a variety of NPs, providing homotypic targeting and circumventing the challenge of synthetically replicating natural cell surfaces. Compared to unwrapped NPs, cancer cell membrane-wrapped NPs (CCNPs) provide reduced accumulation in healthy tissues and higher accumulation in tumors and metastases. The unique biointerfacing capabilities of CCNPs enable their use as targeted nanovehicles for enhanced drug delivery, localized phototherapy, intensified imaging, or more potent immunotherapy. This review summarizes the state-of-the-art in CCNP technology and provides insight to the path forward for clinical implementation.

Keywords: biomimetic; nanocarrier; membrane-wrapped; cancer; targeted delivery; drug delivery; immunotherapy; photothermal therapy; photodynamic therapy; imaging

1. Introduction to Cancer and Nanomedicine

Cancer is a devastating global public health problem in desperate need of transformative solutions. It is the second leading cause of death in the United States and predicted to take 1700 lives per day in 2019 [1]. There is approximately a 37% chance a person will be diagnosed with cancer in their lifetime [1]. These alarming statistics indicate a critical need for technologies that can improve the early diagnosis and effective treatment of cancer.

Conventional methods to treat cancer involve the surgical resection of tumors followed or preceded by aggressive chemotherapy and localized radiotherapy [2,3]. However, if tumors are non-resectable or metastasized, chemotherapy is the only therapeutic resolution to attempt to control the size and spread of the cancer [3]. Despite being the main clinical strategy, cytotoxic chemotherapeutics are incapable of targeting only cancer cells post-systemic administration [3,4]. Only a small fraction of drugs will accumulate in the desired tumor regions and metastatic lesions before being cleared from the body or entering non-targeted tissues [2,3,5]. Consequently, adverse side effects to healthy tissues limit the dosage of free drugs that can be administered, which reduces efficacy [6,7]. Further, due to the heterogeneous nature of tumors, which contain multiple cellular phenotypes, clinical practice and exploratory studies have shown that treatment regimens that employ only a single therapeutic agent

are incapable of eliminating whole tumors and are even less effective in reducing and preventing metastasis [6]. There is a need for multimodal and synergistic cancer therapies that can improve patient outcomes [6,7].

Nanotechnology offers the opportunity to create nanovehicles that can carry either single or multiple therapeutic cargos, as well as contrast agents, to tumors for improved treatment and imaging. Nanoparticles (NPs) can be "smart designed" for enhanced drug delivery, phototherapy, vaccination, immunotherapy, and imaging [6,8]. Additionally, NPs can be synthesized with diverse physicochemical and surface properties that can be tailored to enhance cellular and molecular delivery, increase circulation times, facilitate crossing of biological barriers, and control cargo release [7–9]. Some nanomaterials can be designed with inherent optical or chemical properties that can be harnessed to enable stimuli-responsive therapy [10]. Nanovehicles can also be designed to integrate multiple therapeutic modalities in a single system to overcome the barriers experienced by cancer monotherapies [6].

The tumor microenvironment is characterized by leaky tumor vasculature and poor lymphatic drainage [3,8,9]. All systemically administered nanovehicles exploit this tumor pathophysiology to passively accumulate and be retained in tumor tissue; this is known as the enhanced permeability and retention (EPR) effect [4,11–14]. However, for NPs to utilize the EPR effect, they must first navigate the bloodstream, where they will be exposed to various proteins that may alter their surface chemistry. When NPs are coated with opsonin proteins, they are rapidly cleared by tissue resident macrophages of the liver and spleen, which limits their tumor delivery. For nanovehicles to efficiently enter tumors and be effective, they must evade detection by the immune system to exhibit long circulation, and protect their cargo from degradation or premature release [3,4,15]. Historically, NPs have been decorated with surface modifications, such as polyethylene glycol (PEG), to decrease their rapid opsonization and phagocytosis and increase their anti-tumor efficacy [3,4,7,16–19]. However, PEG-functionalized NPs can induce an "anti-PEG" immunological response and PEG does not impart NPs with cell-specific binding capabilities [3,16]. Additionally, PEGylated NPs are still cleared from the body, necessitating the use of more diverse and effective coatings. Researchers have coated NPs with ligands designed to enhance their cell-specific internalization via receptor-mediated processes to increase tumor retention and reduce off-target effects [17,18,20,21]. Still, there is substantial room for improvement.

While ligand-targeted NP delivery to desired tumor cells is often depicted as a straightforward and easily accomplished task, it is extremely challenging to achieve this goal [21]. In part, this is due to the immense diversity in the abundance, variety, and complexity of proteins found on cancer cell membranes that might be targeted by NPs [3,10,22]. In addition to choosing the right molecule or combination of molecules to target, researchers must also carefully select the conjugation chemistry for ligand attachment to NPs [17,23]. Ligands that are too densely packed on an NP surface can cause a non-cooperative effect on target receptor binding, increased uptake by immune cells, and nonspecific binding to perivascular cells after extravasation [21,23,24]. This limits the NPs' success due to low circulation time, early clearance from the body, and unwanted immune responses [16,18,19]. Further, serum proteins and opsonins can quickly coat ligand-targeted NPs in the bloodstream, rendering the targeting agents ineffective and increasing the rate of NP clearance from the body. These shortcomings create a need for surface modifications that can better disguise nanovehicles from the immune system, prolong circulation time, and provide enhanced targeting and cell internalization capabilities.

Biomimetic nanotechnology harnesses the unique biological makeup of cell membranes and combines it with the flexibility of NP substrates and a wide range of payloads to improve targeted delivery. The general concept is to wrap NPs with cell-derived membranes that provide the complex biological entities found on natural cell membranes (Figure 1), which are nearly impossible to synthetically replicate via ligand attachments [22,25,26]. Since cell membranes contain both "markers of self" and "self-recognition molecules", NPs wrapped in cell membranes can avoid immune recognition to maximally accumulate in tumors. Cell membrane coating technology was first introduced as a method to prolong NP circulation by using red blood cell (RBC) membranes to provide "stealth"

properties to synthetic NPs [27]. It was shown that RBC-coated NPs exhibited a circulation half-life of 39.6 hours, substantially improved versus the 15.8-hour half-life of PEGylated NPs [27]. The field of cell membrane coating nanotechnology has since exploded with variations on this design [15,28–32]. Currently, cell membrane coating technology has been applied with many cell types, including platelets, leukocytes, cancer cells, stem cells, and more [33–39]. Cell membrane coatings have also been wrapped around a variety of materials, ranging from polymers to metals, to enhance their biointerfacing capabilities [2,8,22,40]. The two main advantages obtained from cell membrane wrapping are (1) reduced nonspecific uptake and (2) higher levels of specific targeting compared to non-wrapped NPs [2,25]. Notably, the hydrophobicity, charge, size, and structure of the core nanovehicles can be tailored to load desired cargoes within the interior without inhibiting the stealth or targeting properties of the membrane coating exterior [10]. Accordingly, cell membrane-coated NPs prove superior to previous NP synthesis techniques that have tried to reverse-engineer biological functions and interactions with limited success [3,4,41].

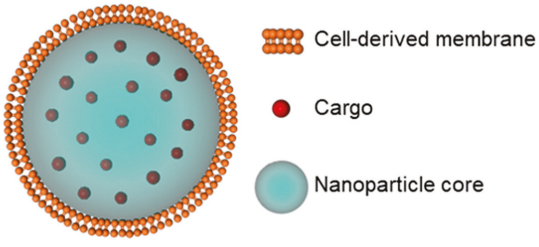

Figure 1. Scheme depicting the components of a representative membrane-wrapped nanoparticle.

Cancer cell membranes are the ideal candidate to wrap around NPs for oncological applications [8,22]. Cancer cells are robust and easy to culture in large volumes in vitro for mass membrane collection and also possess the unique ability to self-target homologous cells (also known as homotypic targeting), unlike most other membrane donors [8,9,40,42]. This unique ability translates to cancer cell membrane-wrapped NPs (CCNPs), which retain the ability to homotypically target primary tumors and metastatic nodules [40,42–45] (Figure 2). Additionally, CCNPs display unprecedented binding and selective uptake in tumor cells matched to those from which they were derived, as well as have reduced immune clearance after systemic administration compared to non-coated NPs [22,40,42,44,46,47]. These unique properties enable CCNPs to be used as nanovehicles for enhanced chemotherapeutic drug delivery, localized phototherapy, intensified tumor imaging, or potent immune modulation.

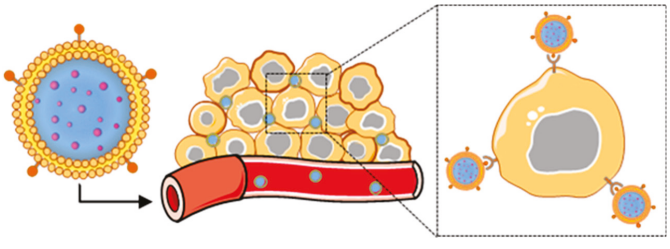

Figure 2. Scheme depicting the delivery of cancer cell membrane-wrapped nanoparticles (CCNPs) to tumors. Upon systemic administration, CCNPs exhibit long circulation due to the presence of "markers of self" on the membrane surface that minimize immune recognition. Additionally, CCNP membranes contain "self-recognition" molecules that allow the NPs to bind homotypic tumor cells after escaping from tumor vessels.

In the following sections, we describe the synthesis and characterization of CCNPs and the different types of treatments these unique NPs can accomplish. We also provide a forward-looking perspective on the challenges to be addressed as this technology progresses from the laboratory setting to the clinic.

2. Cancer Cell Membrane-Wrapped Nanovehicles

2.1. Multi-step Synthesis of Cell Membrane-Wrapped Nanovehicles

The synthesis of cell membrane-coated nanovehicles involves three steps: (1) membrane extraction from source cells, (2) fabrication of the nanoparticulate core, and (3) fusion of the membranes and nanoparticulate cores to form core-shell membrane-wrapped NPs (Figure 3). Below, each step is described in detail.

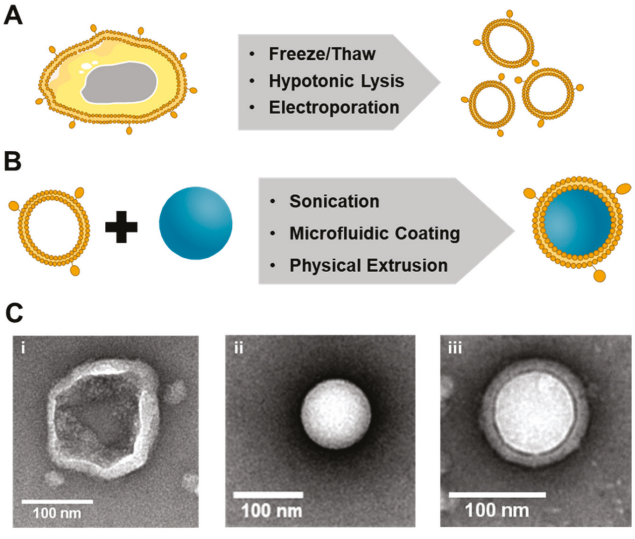

Figure 3. Illustration of the synthesis of membrane-wrapped nanoparticles. (**A**) Cell membranes can be extracted from their source cells by applying one of three methods. (**B**) Membranes can be wrapped around different types of nanoparticles using one of the three membrane–core fusion methods. (**C**) Transmission electron microscopy images of a (i) 4T1 breast cancer cell membrane vesicle, (ii) bare poly(lactic-co-glycolic acid) (PLGA) nanoparticle, and (iii) 4T1 cancer-cell membrane-wrapped PLGA nanoparticle prepared by the authors using the hypotonic lysis method depicted in (A) and the physical extrusion method depicted in (B).

2.1.1. Membrane Extraction

At its most basic level, membrane extraction requires that internal cell components are removed while leaving the functional components of the membrane intact. This membrane extraction procedure requires large volumes of cells to be harvested from culture dishes or blood and tissue samples [8,22,31,48,49]. This process has been accomplished in many ways including freeze–thaw cycling [36,48,50], electroporation [51], and osmosis-based lysis coupled with physical homogenization [22,48] (Figure 3A). For freeze–thaw techniques, cells are frozen at −80 °C and thawed at either room temperature or 37 °C in repeated cycles. These cycles cause damage to cell membranes due to breakage of ice crystals, which leads to the removal of the cytosol and retention of the membranes. This technique is most appropriate for non-nucleated cells, such as RBCs or platelets, since the freeze steps can potentially cause damage such as loss of membrane structure, reduced protein stability, and consequent protein unfolding and reduced membrane function [10,36,48].

Electroporation lyses cells by exposing them to strong electric fields, causing temporary loss of semi-permeability, and pore formation in the cell membrane, releasing intracellular components [51]. Consequently, electroporation disruption of membranes results in irreversible deterioration of structural integrity, denaturation of membrane proteins, and loss of lipid asymmetry. Therefore, care must be taken when designing the experimental set-up of electroporation as conditions that are too harsh can cause loss of natural membrane potential [51,52].

The most popular method to extract cancer cell membranes involves osmosis-based cell lysis with a mild hypotonic solution, followed by mechanical membrane disruption with a homogenizer [48]. Discontinuous gradient centrifugation removes intracellular biomacromolecules, intracellular vesicles, and nuclei, and the membrane-rich fraction is washed with isotonic buffers to obtain membrane vesicles [23,53]. These vesicles can then be further sonicated or extruded through polycarbonate membranes to produce vesicles of the desired size [48]. Cancer cells require milder lysis conditions and greater ultracentrifugation speeds compared to non-nucleated cells. The differences in osmosis-based membrane extraction methods deviate between cell types due to eukaryotic cells' phospholipid bilayer fluidity and smaller cell size [10].

2.1.2. Selection of Nanoparticle Core

As a variety of NP core designs may be utilized to produce CCNPs, depending on the intended application, it is unwarranted to describe any one specific NP synthesis here. The main criterion, independent of core material, is that the NPs have a negative zeta potential. This will facilitate proper orientation of the membrane around the NP owing to electrostatic repulsion between the NP surface and negative extracellular membrane components [27]. To date, the types of synthetic NPs that have been wrapped with cell-derived membranes for cancer therapies include nanocrystals [54], nanocages [42], mineral-based or mesoporous silica [35,49,55–58], polymeric cores [30,40,45,59–64], organic and inorganic metal frameworks [44,51,65–67], protein cores [68,69], and gold-based or magnetic nanoparticles [70–72] (Figure 4, Table 1). Poly(lactic-co-glycolic) acid (PLGA) is one of the most widely used NP cores due to its biodegradability, FDA approval, and ability to encapsulate many products [17–19]. Metallic-based NPs have also been widely used because they can aid in imaging and thus provide multiple functions [32,61,65,71,72]. Overall, the composition of the nanovehicle core is an important consideration when designing CCNPs as it dictates the release and efficacy of the cargo once it has been guided to the desired cells by the membrane coating.

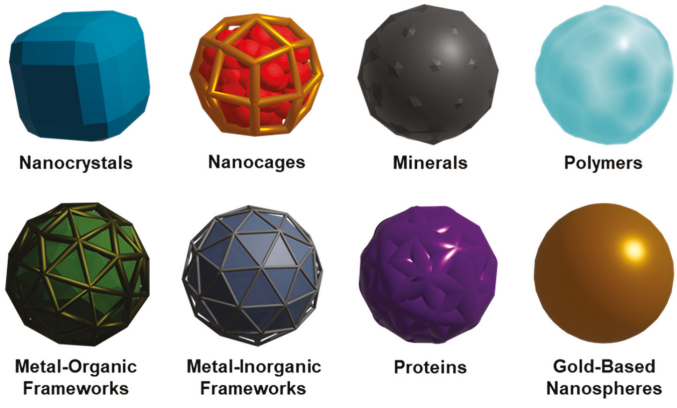

Figure 4. Summary of various nanoparticle formulations that have been wrapped with cell-derived membranes to enable cancer treatment and imaging.

Table 1. Breakdown of cancer cell membrane-wrapped nanovehicles mentioned in the text and their purposes.

Membrane Source	Core NP Material	Cargo Loaded	Particle Purpose (Besides Homotypic Targeting)	Year	Ref.
4T1	poly(caprolactone); Pluronic F-68	paclitaxel	drug delivery	2016	[40]
4T1	gold nanocages	doxorubicin	PTT; hyperthermia-triggered drug release	2017	[42]
4T1	poly(cyclopentadithiophene-*alt*-benzothiadiazole)		PTT; PDT; PA imaging	2018	[61]
4T1	PCN-224	tirapazamine	PDT; drug delivery	2017	[73]
MDA-MB-435	Ln-doped upconversion nanocrystal		FL imaging	2016	[54]
MDA-MB-435	PLGA	DiD fluorophore	FL imaging	2014	[45]
Luciferase- expressing MDA-MB-231	PLGA		FL imaging	2019	[43]
MCF-7 [1]	PLGA	indocyanine green	PTT; PA/FL imaging	2016	[74]
MCF-7 [1]	PLGA	doxorubicin; hemoglobin	PDT; drug delivery	2017	[63]
MCF-7 [2]	melanin		PTT; PA imaging	2019	[68]
B16-F10 [2]	hollow copper sulfide	doxorubicin	drug delivery	2018	[57]
B16-F10	mesoporous silica	glucose oxidase	immunotherapy; starvation therapy	2019	[55]
B16-F10	hollow manganese dioxide	chlorin e6; glucose oxidase	PDT; starvation therapy	2019	[67]
B16-F10	PLGA	CpG 1826	Immunotherapy [4]	2017	[75]
B16-F10	PLGA	monophosphoryl lipid A	Immunotherapy [4]	2014	[45]
B16-OVA [3]	PLGA	imiquimod	Immunotherapy [4]	2018	[64]
HeLa	iron oxide	doxorubicin	drug delivery	2016	[44]
HeLa	PLGA	doxorubicin; siRNA	drug delivery	2019	[46]
HeLa		doxorubicin; indocyanine green	PTT; drug delivery (carrier free)	2018	[76]
HepG2	PLGA	doxorubicin	drug delivery	2019	[62]

Table 1. *Cont.*

Membrane Source	Core NP Material	Cargo Loaded	Particle Purpose (Besides Homotypic Targeting)	Year	Ref.
H22	iron oxide	doxorubicin	drug delivery	2016	[44]
SMMC-7721	superparamagnetic iron oxide	chlorin e6	PDT; MR/NIR imaging	2018	[72]
UM-SCC-7	iron oxide	doxorubicin	drug delivery	2016	[44]
CAL 27	Ln-doped upconversion nanocrystal		FL imaging	2016	[54]
LNCaP-Al	mesoporous silica	doxorubicin; calcium carbonate	drug delivery; pH sensitive release	2019	[56]
DU 145	Ln-doped upconversion nanocrystal		FL imaging	2016	[54]
U87	PLGA		Immunotherapy [4]	2019	[43]
HCT 116	Ln-doped upconversion nanocrystal		FL imaging	2016	[54]

[1] Membranes were mixed with PEGylated phospholipid (DSPE-PEG) before coating; [2] Membranes were mixed with red blood cell membranes before coating; [3] Membranes were modified with mannose after coating; [4] Particles were not used for homotypic targeting; Note: Murine mammary (4T1), human mammary (MDA-MB-435, MDA-MB-231, MCF-7), murine melanoma (B16-F10, B16-OVA), human cervical (HeLa), human hepatocellular (HepG2, H22, SMMC-7721), human squamous (UM-SCC-7, CAL 27), human prostate (LNCaP-Al, DU 145), human glioma (U87), human colorectal (HCT 116).

2.1.3. Fusion of Membrane Vesicles with Nanoparticle Cores

Methods of coating NPs with membranes can be divided into three generalized strategies: physical extrusion, sonication, and microfluidic coating (Figure 3B). All of these methods take advantage of electrostatic interactions between the nanoparticulate core and membrane components to form a stable and energetically favorable core-shell structure with the right-side-out membrane topological orientation [27,36,48]. In physical extrusion, nanovehicles and membrane vesicles are co-extruded through a porous membrane, similar to how membrane vesicles are formed by mechanical extrusion [27]. The force provided by the extrusion disrupts the membrane structure and enables it to reform around the NP cores [27,48]. A representative transmission electron micrograph of a CCNP prepared by extrusion in the authors' lab is shown in Figure 3C. Here, the CCNP is composed of a PLGA core surrounded by a membrane derived from a 4T1 mouse breast cancer cell. In the authors' experience, the extrusion method is very robust in terms of reproducibility and creating CCNPs with consistent characteristics (size, zeta potential, membrane thickness, etc.). In sonication-based methods, nanovehicles and membranes are again combined, and ultrasonic energy provides disruptive forces that result in spontaneous formation of core-shell nanostructures [53,59]. This technique has the added benefit of losing less material than physical extrusion. Lastly, a relatively new approach to enable membrane coating is to employ microfluidics. This fabrication technique combines rapid mixing of NPs and membrane vesicles with electroporation and has successfully been used to coat RBC membranes around magnetic NPs [51]. For this strategy to be successful, the process pulse voltage, duration, and flow velocity all have to be optimized, making it a potentially more difficult method to attempt for those not already familiar with microfluidics.

2.2. Characterization of Membrane-Coated Nanoparticles

It is critical to compare various features between bare and wrapped NPs to confirm complete membrane wrapping. Successful wrapping can be validated by observing a 10–20 nanometer increase in particle size after wrapping, equating to the thickness of the membrane layer. This can be measured by dynamic light scattering (DLS), transmission electron microscopy (TEM) (Figure 3C), or nanoparticle tracking analysis (NTA). Analysis of the NPs' zeta potential, or surface charge, can also be used to confirm membrane wrapping. The final charge of the CCNPs must be similar to that of the membrane vesicles used to prepare them, as the bare NPs inherit the surface charge of the membranes after successful wrapping. To further confirm successful membrane wrapping and the removal of intracellular components, Western blotting and SDS-PAGE can be performed to identify the main protein components of whole cell lysate, membrane lysate, and membrane-wrapped NPs. Membrane-wrapped NPs should share nearly identical protein content to the membrane lysate, but lack the nuclear and mitochondrial components of the whole cell lysate. Individual membrane surface markers can also be identified and their intensity compared between samples to confirm their successful translocation onto NPs from source cells during membrane wrapping. For example, Fang et al. showed by Western blotting that CCNPs prepared by physically extruding PLGA NPs with B16-F10 mouse melanoma membranes collected by hypotonic lysis were positive for the membrane markers pan-cadherin, Na^+/K^+-ATPase, and gp100, but lacked the intracellular markers histone H3, cytochrome c oxidase, and glyceraldehyde 3-phosphate dehydrogenase [45]. These data indicate that the preparation of CCNPs by hypotonic membrane lysis followed by physical extrusion with core NPs offers excellent preservation of the components of the original cell membrane. In the future, researchers utilizing other methods to prepare CCNPs should perform similar analyses to reveal which method imparts CCNPs with the greatest resemblance to their source cells.

3. Applications of Membrane-Wrapped Nanoparticles in Cancer

3.1. Drug Delivery

Cancer drug delivery is one field in which membrane-wrapped nanovehicles, and CCNPs in particular, have substantial potential to improve the state-of-the-art. Encapsulating drug cargo within nanocarriers that offer tailorable control of release kinetics, such as polymer-based cores, can dramatically improve bioavailability, and tumor-specific delivery can be further enhanced by coating these vehicles with cancer cell membranes [17–19]. Moreover, synthetic NPs' physicochemical properties can be modified for sustainable or triggered cargo release, resulting in less systemic toxicity than freely delivered cargo [4,22,47,77]. As an extra benefit, membrane coatings can provide an additional decrease in premature drug release by slowing diffusion and allowing nanovehicles to accumulate in tumors before too much drug is lost [10,22]. Increasing the ratio of drug that reaches tumors versus normal tissue is critical to maximize therapeutic effects and safety.

Doxorubicin (DOX) is a commonly used chemotherapeutic that intercalates into DNA to yield topoisomerase II-mediated DNA damage followed by cell death [78]. DOX has been used clinically to treat many cancers, including breast cancer, ovarian cancer, and various lymphomas and leukemias [78]. Several researchers have shown that encapsulating DOX in membrane-wrapped NPs is advantageous compared to freely delivered DOX [56,62,63]. For example, Xu et al. developed PLGA-DOX NPs wrapped in membranes derived from HepG2 hepatocarcinoma cells and showed these NPs could deliver an effective drug payload to Hep2G tumors in mice [62]. Additionally, the CCNPs exhibited less systemic toxicity than freely delivered DOX. This was attributed to enhanced DOX accumulation at the tumor site (and less accumulation at off-target sites) due to lack of premature release from the particles [62]. Another chemotherapeutic small molecule, paclitaxel (PTX), which is clinically used to treat AIDS-related Kaposi sarcoma, breast, non-small cell lung, and ovarian cancers [79–85], has been explored in conjugation with membrane-wrapped NPs. In one study, PTX was loaded into poly(caprolactone) (PCL) and pluronic copolymer F68 cores that were wrapped with 4T1 mouse mammary breast cancer cell membranes [40]. The homotypic targeting and drug delivery capabilities of these cancer cell membrane-wrapped PTX-loaded polymeric nanoparticles (CPPNs) were explored in a highly metastatic 4T1 in vivo tumor model. CPPNs remarkably targeted and inhibited the growth of homotypic 4T1 primary tumors and metastatic nodules in orthotopic mammary tumor models and in blood-vessel-metastasis mouse models, with 6.5-fold fewer metastatic nodules than unwrapped PPNs [40]. The intact 4T1 cell membrane wrapping decreased phagocytic uptake and increased blood-circulation time to increase the antitumor effect of the drug payload.

In addition to single drugs, multiple cargoes with synergistic actions can be encapsulated in CCNPs. This ensures the cargos are delivered to the same cells within tumor sites for improved anticancer effects. This was demonstrated with PLGA cores that were loaded with hemoglobin (Hb) and DOX and coated with MCF-7 human breast cancer cell membranes with a PEGylated phospholipid to overcome hypoxia-induced chemoresistance [63]. By suppressing the expression of hypoxia-inducible factor-1α, multidrug resistance gene 1, and P-glycoprotein, the biomimetic oxygen nanocarriers were able to perform safe and highly efficient O2-interfered chemotherapy by reducing the exocytosis of DOX. Simultaneously, the system achieved higher tumor specificity and lower DOX toxicity due to the cancer cell adhesion molecules retained on the NP surface [63]. This was an excellent demonstration of the potential for CCNPs to achieve multi-therapeutic delivery. In a similar approach, Chen et al. developed CCNPs to deliver DOX in combination with small interfering RNA (siRNA) against PD-L1, a gene that is overexpressed on tumor cells and whose inhibition could lead to an increased anti-tumor immune response [46]. Here, both cargos were loaded into PLGA NP cores and homotypic targeting was achieved by wrapping the NPs with HeLa cervical cancer cell membranes [46]. The CCNPs exhibited preferential uptake by HeLa cells versus non-targeted MDA-MB-231 breast cancer cells, and were able to suppress PD-L1 expression and reduce cell viability. Future studies are necessary to evaluate the impact of this system in vivo.

CCNPs that incorporate stimuli-responsive features have also been designed to take advantage of the acidic tumor microenvironment as a trigger for localized drug release [63]. In one example, mesoporous silica nanoparticle (MSN) cores were used to encapsulate DOX with the addition of a unique CaCO3 interlayer [56]. The interlayer acted as sheddable pH-sensitive gatekeeper to allow drug release only in the acidic tumor microenvironment. MSNs were wrapped with LNCaP-AI prostate cancer cell membranes (MSN/DOX@CaCO3@CM) to improve the colloidal stability and tumor accumulation of the system. In comparison to free DOX, MSN/DOX@CaCO3@CM NPs exhibited increased cell uptake and induced higher rates of apoptotic death in prostate cancer cells. In vivo experiments demonstrated that the NPs had remarkable antitumor effects and suppressed tumor growth [56]. Overall, this study demonstrated that coupling the increased localization of CCNPs in tumor microenvironments with pH-stimulated release of chemotherapeutic drugs is a potent strategy to enhance therapeutic ratios.

Importantly, across various platforms, it has been shown that cancer cell membrane coatings do not negatively interfere with drug loading inside NPs. As demonstrated by the examples discussed, there is great promise in the field for CCNPs to enhance drug delivery to desired sites to improve safety and efficacy. This opens the door for the development of many new treatment strategies.

3.2. Photothermal and Photodynamic Therapy

While some NPs exploit features of the tumor microenvironment such as low pH or presence of specific enzymes to enable stimuli-responsive drug release and high precision therapy, another route to enable site-specific treatment of tumors is to utilize nanomaterials that are inactive until they are triggered with externally applied light. The two main examples of this are photothermal therapy (PTT) and photodynamic therapy (PDT), and both have recently been explored in conjugation with membrane-wrapped NPs. In photothermal therapy, NPs with unique optical properties are delivered into tumors, which are then irradiated with near-infrared light that causes the NPs to produce heat capable of thermally damaging cancer cells [86–92]. Similarly, in PDT, photosensitizers are delivered into tumors, and subsequent irradiation of the tumor causes the photosensitizer to transfer the absorbed energy to adjacent tissue oxygen molecules, producing toxic singlet oxygen that destroys cancer cells [89]. While there are some examples of membrane-wrapped NPs being used strictly for PTT or PDT to treat cancer [70,93–98], these singular treatments use non-cancer cell membranes. When cancer cell membranes are used for wrapping, they are commonly studied in combination with other therapeutic strategies, such as drug delivery. Some accomplishments in this field are summarized below.

3.2.1. Combination Photothermal Therapy and Chemotherapy

Combining PTT with chemotherapy offers many advantages versus either treatment alone. Several studies have shown that PTT can elevate drug delivery into tumors or into cancer cells by increasing vascular permeability and cancer cell membrane permeability [86,99]. Additionally, PTT alone is best suited for primary tumors, as it cannot be readily applied to disseminated metastatic tumors. Combining PTT with chemotherapy offers a way to treat both primary tumors and metastatic lesions. Further, there is some evidence that under the right conditions, combined PTT and chemotherapy can lead to anti-cancer immune responses that maximize the duration of response [100]. Given these advantages, researchers have explored the co-delivery of photothermal agents and cytotoxic drugs to cancer using CCNPs.

Combination PTT and chemotherapy mediated by CCNPs has been most widely explored using DOX as the chemotherapeutic agent [42,57,76]. In all cases, the DOX had improved tumor delivery due to the cancer cell membrane coating of the system and DOX was able to act successfully in combination with PTT to decrease tumor growth. In one study that co-loaded DOX and indocyanine green (ICG) photothermal agents in membrane-wrapped NPs, DOX was delivered in a "bomb-like" manner to the tumor surroundings [76]. This was due to the HeLa cervical cancer cell membrane wrapped around the

cargo being disrupted by PTT, which led to enhanced chemo-PTT efficacy [76]. In an unusual case of using multiple types of membranes to coat NPs, RBC and B16-F10 mouse melanoma membranes were mixed to create a hybrid membrane that provided increased immune evasion and tumor targeting, respectively. The membranes were wrapped around DOX-loaded copper sulfide NPs, and these NPs exhibited synergistic effects with close to 100% tumor growth inhibition [57]. Lastly, when DOX was loaded into the core of gold nanocages, the hyperthermia induced-release of DOX in the targeted cells inhibited the growth of both primary tumors and metastatic nodules in a highly metastatic 4T1 mouse mammary tumor model [42]. These findings demonstrate the immense potential of combining PTT with chemotherapy using CCNPs.

3.2.2. Photodynamic Therapy Combined with Chemotherapy or Starvation Therapy

The benefits of combining chemotherapy with PDT include having reactive oxygen species (ROS) available to initiate drug release and promote intracellular drug delivery, as well inducing hypoxia in the tumor region for activating encapsulated drugs [6]. Conversely, a limitation of PDT is that it relies on tumor oxygen, and is therefore not effective in hypoxic tumor regions. By combining PDT with drugs that are not hindered by hypoxia, more thorough tumor treatment can be achieved. In one example of dual PDT/chemotherapy, a porphyrinic metal organic framework (a PDT photosensitizer) was combined with tirapazamine (TPZ, a bioreactive chemotherapeutic) [73]. These agents were wrapped in membranes derived from 4T1 breast cancer cells, and the resultant NPs were delivered to mice bearing orthotopic 4T1 breast cancer tumors. Following irradiation, the porphyrinic metal organic frameworks produced ROS, leading to local hypoxia within the tumors, which accelerated the activation of TPZ for an enhanced chemotherapeutic effect. Because the treatment was activated only in the presence of light at the tumor site, negligible side effects were observed [73].

Besides being combined with chemotherapy, PDT has also been combined with starvation therapy. In starvation therapy, glucose oxidase (GOx) is delivered to tumors. GOx will transform glucose into gluconic acid and hydrogen peroxide, starving the cells of glucose, a vital nutrient for tumor growth. In one example, a cascade reaction system made of hollow manganese dioxide (MnO_2) NPs encapsulating a photosensitizer and coated with GOx were wrapped in B16-F10 cancer cell membranes [67]. Once delivered to tumors, the MnO_2 reactors were irradiated for continuous oxygen generation, supported by the conversion of glucose to singlet oxygen. This system has potential to solve hypoxia issues in tumors and promote starvation. Starvation therapy mediated by membrane-wrapped NPs has also been explored without PDT [55]. In this study, GOx-loaded membrane-wrapped mesoporous silica NPs were combined with PD-1 antibody treatment and shown to be more effective at stimulating an anti-cancer immune response than the single therapies, resulting in better cancer ablation. The above examples demonstrate that CCNPs have the ability to target tumor cells throughout the body and enable PTT or PDT in combination with chemotherapy or starvation therapy. These combinatorial delivery systems are more effective than monotherapies and offer extremely high precision treatment of tumors since they are activated only when light and NPs are combined at the tumor site. Continued development of these platforms will likely yield impressive results against a variety of tumor types.

3.3. Tumor Imaging

In many cases, it is desirable to monitor the accumulation of membrane-wrapped NPs within tumors, as this can guide and inform drug delivery, PDT, and PTT [44,61,72,74]. Most NP cores that enable imaging with high contrast are metallic-based, such as iron oxide or lanthanide-doped nanocrystals, but development of organic or polymer-based nanoparticles as imaging agents has also been explored [44,54,72,74].

In a study whose sole purpose was to view homologous targeting of upconversion nanoprobes (UCNPs), researchers used multiple types of cancer cell membranes (breast, prostate, colorectal, and squamous cell cancer) to prepare corresponding batches of wrapped lanthanide-doped nanocrystals [54]. These NPs could convert near-infrared (NIR) light into visible light, providing high signal-to-noise ratio. The specificity of homotypic membrane-mediated targeting was beautifully exhibited when mice bearing MDA-MB-435 breast cancer tumors were separately treated with each type of membrane-wrapped UCNPs, as only UCNPs wrapped in membranes derived from MDA-MB-435 cells exhibited notable tumor retention. This indicates that while the cancer-membrane-wrapped NPs possess the same immune evasion potential as RBC-wrapped NPs, mismatch of the donor membranes and host tumor cells leads to little tumor targeting. In a similar study, researchers developed magnetic iron oxide NPs loaded with DOX-HCl and coated them in either UM-SCC-7 squamous cell carcinoma or H22 hepatocellular carcinoma membranes [44]. The team used magnetic resonance imaging to show in mice bearing each type of tumor that the particles could bypass the heterologous tumor and preferentially target their homotypic tumor (Figure 5). Future research could evaluate the degree of mismatch that is acceptable when preparing CCNPs to maintain homotypic binding. While both of these studies used cells derived from different tumor types to demonstrate that homotypic binding requires membrane:tumor matching, it would be interesting to investigate if membranes derived from cancer cells that are from the same tissue but exhibit different biomarkers can provide targeted delivery.

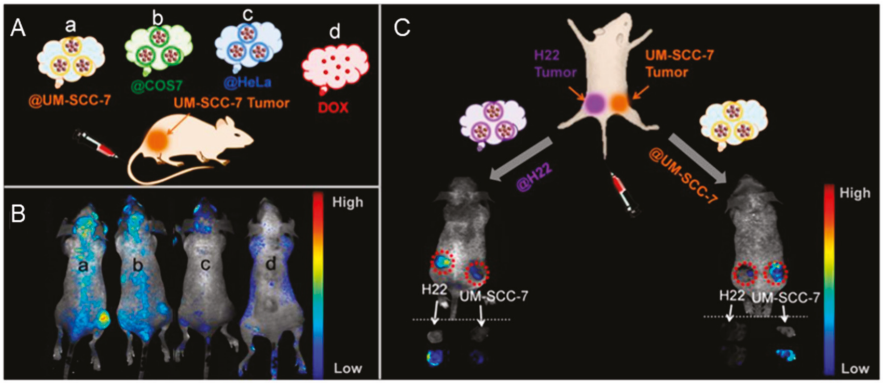

Figure 5. Demonstration of homotypic tumor targeting by CCNPs. (**A**) Illustration of experimental design for data shown in (**B**). Mice bearing human squamous carcinoma (UM-SCC-7) tumors were treated with doxorubicin (DOX) alone or with DOX and magnetic iron oxide nanoparticles that were wrapped with membranes derived from three different sources (COS7 monkey kidney cells, HeLa cervical cancer cells, or homotypic UM-SCC-7 squamous carcinoma cells). (**B**) In vivo fluorescence images of mice bearing UM-SCC-7 tumors 24 hours post-injection with membrane-wrapped nanoparticles prepared with (**a**) UM-SCC-7, (**b**) COS7, or (**c**) HeLa membranes as described in A, or post-injection with (**d**) DOX at an equivalent DOX dosage. The highest tumor accumulation is observed for homotypic membrane-wrapped nanoparticles. (**C**) Illustration of the dual tumor-bearing mouse model in which one flank harbored a hepatocellular carcinoma (H22) tumor and the other harbored a UM-SCC-7 tumor. The animals were injected with membrane-wrapped NPs designed to homotypically target one tumor or the other. Twelve hours post-injection, in vivo fluorescence images and ex vivo images of tumors were acquired. Both types of membrane-wrapped nanoparticles evaluated exhibited preferential accumulation in homotypic tumors (matched to the source membrane) versus heterotypic tumors with membrane mismatch. Reprinted (adapted) with permission from Reference [44]: Zhu, J.Y.; Zheng, D.W.; Zhang, M.K.; et al. *Nano Lett.* **2016**, *16*, 5895–5901. Copyright (2016) American Chemical Society.

Membrane-wrapped NPs that incorporate both contrast agents and photoactive agents have also been used for tumor imaging and phototherapies. In one study, ICG-loaded NPs wrapped with

MCF-7-PEG fused membranes exhibited a PTT response, but also had fluorescence and photoacoustic (PA) imaging capabilities [74]. PEG incorporation in this system diminished non-specific binding of serum proteins and helped stop aggregation and opsonization leading to phagocytosis in vivo. This particle formulation ablated tumors after a single dose and laser irradiation, and provided high spatial resolution imaging of the tumor microstructure through PA imaging of the ICG signal in and around tumor microvesicles. In another study, MCF-7 membranes were fused with RBC membranes to coat melanin nanoparticles [68]. The biocompatible melanin core provided both PTT and PA imaging and the size dependence of the particles for optimal PTT and PA imaging were explored to find the balance between the two.

Similarly, dual-modal imaging has been used with PDT by loading photosensitizers into magnetic nanobeads to target hepatocellular carcinoma [72]. Both near-infrared (NIR) fluorescence imaging and magnetic resonance (MR) imaging could be accomplished with this system, with NIR enabled by the loaded chlorin e6 (Ce6) photosensitizers that also provided PDT capabilities, and MR provided by the superparamagnetic iron oxide nanostructures. In an even more complex system, multimodal cancer phototheranostics were explored for the early diagnosis and precision therapy of cancer [61]. Here, organic, multimodal, NIR-semiconducting polymer NPs were produced, generating NIR and PA signals for imaging, as well as singlet oxygen and cytotoxic heat for combinatorial PDT-PTT effects. These NPs were coated in either activated fibroblast membranes or 4T1 cancer cell membranes, where interestingly, the fibroblast-coated NPs performed better than their cancer cell membrane-coated counterparts [61]. Although the 4T1 membrane NPs targeted cancer cells, they were limited by the abundance of cancer-associated fibroblasts in the tumor environments, making their accumulation only marginally higher than non-targeted particles. The activated fibroblast-coated NPs, in contrast, exhibited heightened tumor accumulation through their homotypic targeting of cancer-associated fibroblasts at the tumor site.

3.4. Immune Stimulation

There is growing interest in the field of oncology in using technologies to stimulate the body's immune system to attack tumor cells. Immunotherapy can be applied as either a cancer treatment or as a preventative cancer vaccination, and is advantageous over cytotoxic agents because of its high specificity and low toxicity [2,6,18,75,101–106]. Effective immune stimulation typically requires that both adjuvants and tumor antigens be delivered to the body. One advantage of CCNPs is that their membrane coatings carry a full array of cancer cell membrane antigens that can stimulate an anticancer immune response. Thus, combining CCNPs with adjuvant technologies is a promising strategy to elicit robust anti-tumor responses. In the following sections, it is assumed readers have a basic familiarity with cancer immunotherapy. For detailed reviews, we refer the readers to recent publications [102,105–110].

Exploring the immune stimulatory capabilities of membrane-wrapped NPs, Fang et al. prepared PLGA NPs wrapped in B16-F10 melanoma or MDA-MB-435 human breast cancer membranes and utilized these NPs to deliver antigens to source tumor cells and antigen presenting cells (APCs) [45]. The CCNPs enhanced source cell-specific binding and uptake compared to RBC-wrapped NPs and bare NPs. They also successfully delivered membrane-bound tumor-associated antigens to APCs. However, this was insufficient to induce dendritic cell maturation due to the limited immunogenicity of syngeneic cancer cell membrane material. To overcome this issue, the team incorporated monophosphoryl lipid A (MPLA), an immunoadjuvant lipopolysaccharide derivative that binds to toll-like receptor 4 (TLR-4), into the CCNPs, and this significantly increased the APC maturation to promote an anticancer immune response [45]. In a similar approach, Kroll et al. developed B16-F10 melanoma membrane-wrapped PLGA NPs loaded with CpG oligodeoxynucleotide 1826 (CpG), a nucleic acid-based immunological adjuvant known to trigger APC maturation, and tested these in combination with a CTLA4 and anti-PD-1 checkpoint blockade cocktail [75]. The nanovehicles simultaneously delivered syngeneic cancer antigens with a powerful immunological adjuvant to

promote antigen presentation. When applied separately in vivo, the CpG-CCNPs or checkpoint blockade cocktail did not significantly impair the growth of B16-F10 tumors. However, when combined, the systems synergistically promoted a strong antitumor response and modulated various aspects of the immune system [75]. Together, both of these studies indicate the potential for CCNPs to trigger superior anti-cancer immune responses by enabling codelivery of tumor antigens and adjuvants.

As the field matures, researchers will continue to design new ways to enhance immunotherapy mediated by CCNPs. Yang et al. recently showed that CCNP delivery to dendritic cells (DCs) could be enhanced by modifying CCNPs with mannose (which binds receptors on DCs) through lipid anchors [64]. The CCNPs consisted of PLGA cores encapsulating R837, an agonist against toll-like receptor 7 (TLR-7), wrapped with B16-OVA melanoma cancer cells and functionalized with mannose. The mannose-modified nanovaccine exhibited impressive DC uptake, triggering DC maturation. It also successfully traveled to draining lymph nodes post-transdermal injection and facilitated potent tumor-specific immune responses [64]. In another unique nanovaccine design, melanoma cell membrane fractions were coated onto PLGA NPs and their ability to effect fibroblast-mediated invasion, change experimental metastasis, and induce an immune response in immunocompetent mice was evaluated [43]. The nanovaccine successfully inhibited cancer cell migration toward fibroblasts, significantly decreased metastatic burden, and increased cytotoxic T lymphocytes, indicating membrane-wrapped nanovaccines not only show potential as antigen delivery vehicles for primary tumor elimination, but also as metastasis inhibitors.

In summary, CCNPs have great potential as either prophylactic vaccines to protect patients from tumor cell challenges or as therapeutic agents to shrink tumors by inducing anti-cancer immune responses. It is observed that tumor antigen presentation from the membrane coating alone, even in highly immunogenic contexts, may not be powerful enough to overcome the immunosuppressive tumor microenvironment. Therefore, technologies must be combined with adjuvants, immune checkpoint blockade therapies, or other approaches to achieve optimal anti-cancer effects. Nevertheless, the biocompatible nature of CCNPs makes them promising as personalized therapies to induce cancer-specific immune responses for individual cancer patients.

4. Challenges and Path Forward

While many of the described successes of CCNP systems are extremely encouraging, there are still many challenges to address before these technologies become commercially available. One potential issue is the need for patient education, as concern may develop over having cancer cell-derived material injected into the body. Although patients who already have cancer may be willing to overlook this concern if it provides a chance to eradicate their disease, healthy patients who are at-risk for certain types of cancer and wish to use this technology as a preventative vaccine may be less receptive. In addition to educating the population, stringent testing and procedures will have to be developed to ensure that the membrane coatings are pure (lacking any internal component of the source cells) and do not contain any molecules that might promote cancer growth. As the development of membrane-wrapped NPs is already becoming more mature, with proper tests this should not be an issue and this hurdle could be feasibly overcome.

One of the biggest draws of using cell membranes to coat NPs is the ability to have a personalized treatment. NPs coated with membranes derived from a patient's own cells should be able to evade unwanted immune responses that can occur when foreign material is introduced to the body. However, the feasibility of creating CCNPs for each individual patient is a significant question. Preparing patient-specific CCNPs will require strict quality control and regulatory methods. Additionally, while biopsy samples could be used to create CCNPs for patients with existing tumors, the production of CCNPs for prophylactic vaccination will require a different approach. Donor cells could possibly be used, but immunostimulatory issues may arise. One way this could be mitigated is by preparing particles with mixed membrane coatings, as several studies have shown this can imbue the NPs with properties of both membranes [57,68,111]. In this case, donor cancer cell membranes

could be mixed with RBC or platelet membranes from the patient, lessening the portion of foreign membrane material to minimize an immune response. This strategy needs to be explored in many models in order to validate its use. An additional consideration for the use of CCNPs in a prophylactic setting is the need to define the appropriate patient population based on genetic testing or family history of specific cancers. However, if the concerns mentioned here can be sufficiently addressed, the potential impact of CCNPs for personalized cancer therapy is vast.

Lastly, for CCNPs to be successful in the clinic, methods for manufacturing scale-up need to be developed. Particle replication on a small laboratory scale is already difficult due to the complex biological components involved and concerns of batch to batch consistency need to be addressed. One of the largest hurdles in scaling up the process is the need for large quantities of membranes. This requires millions, if not billions, of cells, and the facilities to grow them. Besides producing the necessary amount of membrane material, the scaling up of the NP cores is another concern, especially if the design is more complex or a multi-component system. The more complicated a nanotherapy fabrication is, the more difficult it is to create reproducible and identical particles at large scale. Finally, the assembly of how membrane vesicles are fused with NP cores could be difficult to replicate at a large scale. In short, the more steps to the process, the more difficult it will be to produce commercial quantities of high-quality material. This must be addressed before membrane-wrapped NP technologies can reach clinical trials or achieve FDA approval.

5. Conclusions

This review has highlighted the current state-of-the-art in developing CCNPs for the management of cancer. CCNPs have immense potential as tools to improve the imaging and treatment of tumors, but they also face substantial challenges in translating to the clinic. The future of the field lies in solving these issues or working around them to deliver specific, personalized therapy to single patients. While difficult to accomplish, the chance of eradicating even a single type of cancer, whether by therapy or vaccine, will continue to drive the many paths of research surrounding CCNPs described in this Review.

Author Contributions: Conceptualization, M.A.S., J.C.H., and E.S.D.; investigation, M.A.S. and J.C.H.; resources, E.S.D.; writing—original draft preparation, M.A.S. and J.C.H.; writing—review and editing, M.A.S., J.C.H., and E.S.D.; supervision, E.S.D.; project administration, E.S.D.; funding acquisition, E.S.D.

Funding: Funding for this research was provided by the National Science Foundation under award number DMR-1752009.

Conflicts of Interest: The authors declare no conflict of interest. The funders had no role in the design of the study; in the collection, analyses, or interpretation of data; in the writing of the manuscript, or in the decision to publish the results.

References

1. Jemal, A.; Siegel, R.; Ward, E.; Murray, T.; Xu, J.; Thun, M.J. Cancer Statistics, 2019. CA. *Cancer J. Clin.* **2019**, *57*, 43–66. [CrossRef] [PubMed]
2. Lang, T.; Yin, Q.; Li, Y. Progress of Cell-Derived Biomimetic Drug Delivery Systems for Cancer Therapy. *Adv. Ther.* **2018**, *1*, 1800053. [CrossRef]
3. Steichen, S.D.; Caldorera-Moore, M.; Peppas, N.A. A review of current nanoparticle and targeting moieties for the delivery of cancer therapeutics. *Eur. J. Pharm. Sci.* **2013**, *48*, 416–427. [CrossRef] [PubMed]
4. Sun, T.; Zhang, Y.S.; Pang, B.; Hyun, D.C.; Yang, M.; Xia, Y. Engineered nanoparticles for drug delivery in cancer therapy. *Angew. Chem. Int. Ed.* **2014**, *53*, 12320–12364.
5. Albanese, A.; Tang, P.S.; Chan, W.C.W. The Effect of Nanoparticle Size, Shape, and Surface Chemistry on Biological Systems. *Annu. Rev. Biomed. Eng.* **2012**. [CrossRef]
6. Fan, W.; Yung, B.; Huang, P.; Chen, X. Nanotechnology for Multimodal Synergistic Cancer Therapy. *Chem. Rev.* **2017**, *117*, 13566–13638. [CrossRef]

7. Kim, K.Y. Nanotechnology platforms and physiological challenges for cancer therapeutics. *Nanomed. Nanotechnol. Biol. Med.* **2007**, *3*, 103–110. [CrossRef]
8. Vijayan, V.; Uthaman, S.; Park, I.K. Cell membrane-camouflaged nanoparticles: A promising biomimetic strategy for cancer theragnostics. *Polymers (Basel)* **2018**, *10*, 983. [CrossRef]
9. Shi, J.; Kantoff, P.W.; Wooster, R.; Farokhzad, O.C. Cancer nanomedicine: Progress, challenges and opportunities. *Nat. Rev. Cancer* **2017**, *17*, 20–37.
10. Thanuja, M.Y.; Anupama, C.; Ranganath, S.H. Bioengineered cellular and cell membrane-derived vehicles for actively targeted drug delivery: So near and yet so far. *Adv. Drug Deliv. Rev.* **2018**, *132*, 57–80. [CrossRef]
11. Matsumara, Y.; Maeda, H. A New Concept for Macromolecular Therapeutics in Cancer Chemotherapy: Mechanism of Tumoritropic Accumulation of Proteins and the Antitumor Agent Smancs A New Concept for Macromolecular Therapeutics in Cancer Chemotherapy: Mechanism of Tumoritropic Accum. *Cancer Res.* **1987**, *46*, 6387–6392.
12. Bertrand, N.; Wu, J.; Xu, X.; Kamaly, N.; Frakhzad, O.C. Cancer Nanotechnology: The impact of passive and active targeting in the era of modern cancer biology. *Adv. Drug Deliv. Rev.* **2014**, *66*, 2–25. [CrossRef] [PubMed]
13. Gerlowski, L.E.; Jain, R.K. Microvascular permeability of normal and neoplastic tissues. *Microvasc. Res.* **1986**, *31*, 288–305. [CrossRef]
14. Maeda, H. Toward a full understanding of the EPR effect in primary and metastatic tumors as well as issues related to its heterogeneity. *Adv. Drug Deliv. Rev.* **2015**, *91*, 3–6. [CrossRef]
15. Rao, L.; Bu, L.L.; Xu, J.H.; Cai, B.; Yu, G.T.; Yu, X.; He, Z.; Huang, Q.; Li, A.; Guo, S.S.; et al. Red Blood Cell Membrane as a Biomimetic Nanocoating for Prolonged Circulation Time and Reduced Accelerated Blood Clearance. *Small* **2015**, *11*, 6225–6236. [CrossRef]
16. Verhoef, J.J.F.; Anchordoquy, T.J. Questioning the use of PEGylation for drug delivery. *Drug Deliv. Transl. Res.* **2013**, *3*, 499–503. [CrossRef]
17. Kumari, A.; Yadav, S.K.; Yadav, S.C. Biodegradable polymeric nanoparticles based drug delivery systems. *Colloids Surfaces B Biointerfaces* **2010**, *75*, 1–18. [CrossRef]
18. Danhier, F.; Ansorena, E.; Silva, J.M.; Coco, R.; Le Breton, A.; Préat, V. PLGA-based nanoparticles: An overview of biomedical applications. *J. Control. Release* **2012**, *161*, 505–522. [CrossRef]
19. Vasir, J.K.; Labhasetwar, V. Biodegradable nanoparticles for cytosolic delivery of therapeutics. *Adv. Drug Deliv. Rev.* **2008**, *59*, 718–728. [CrossRef]
20. Astete, C.E.; Sabilov, C.M. Synthesis and characterization of PLGA nanoparticles. *J. Mater. Sci. Mater. Electron.* **2011**, *22*, 1761–1765. [CrossRef]
21. Valcourt, D.M.; Harris, J.; Riley, R.S.; Dang, M.; Wang, J.; Day, E.S. Advances in targeted nanotherapeutics: From bioconjugation to biomimicry. *Nano Res.* **2018**, *11*, 4999–5016. [CrossRef]
22. Fang, R.H.; Kroll, A.V.; Gao, W.; Zhang, L. Cell Membrane Coating Nanotechnology. *Adv. Mater.* **2018**, *30*, 1–34. [CrossRef] [PubMed]
23. Fang, R.H.; Jiang, Y.; Fang, J.C.; Zhang, L. Cell membrane-derived nanomaterials for biomedical applications. *Biomaterials* **2018**, *128*, 69–83. [CrossRef] [PubMed]
24. Luk, B.T.; Zhang, L. Cell Membrane-Camouflaged Nanoparticles for Drug Delivery. *J. Control. Release* **2016**, *25*, 289–313. [CrossRef] [PubMed]
25. Kroll, A.V.; Fang, R.H.; Zhang, L. Biointerfacing and applications of cell membrane-coated nanoparticles. *Bioconjug. Chem.* **2017**, *28*, 23–32. [CrossRef] [PubMed]
26. Li, R.; He, Y.; Zhang, S.; Qin, J.; Wang, J. Cell membrane-based nanoparticles: A new biomimetic platform for tumor diagnosis and treatment. *Acta Pharm. Sin. B* **2018**, *8*, 14–22. [CrossRef]
27. Hu, C.-M.J.; Zhang, L.; Aryal, S.; Cheung, C.; Fang, R.H.; Zhang, L. Erythrocyte membrane-camouflaged polymeric nanoparticles as a biomimetic delivery platform. *Proc. Natl. Acad. Sci. USA* **2011**, *108*, 10980–10985. [CrossRef]
28. Aryal, S.; Hu, C.-M.J.; Fang, R.H.; Dehaini, D.; Carpenter, C.; Zhang, D.-E.; Zhang, L. Erythrocyte membrane-cloaked polymeric nanoparticles for controlled drug loading and release. *Nanomedicine* **2013**, *8*, 1271–1280. [CrossRef]
29. Piao, J.G.; Wang, L.; Gao, F.; You, Y.Z.; Xiong, Y.; Yang, L. Erythrocyte membrane is an alternative coating to polyethylene glycol for prolonging the circulation lifetime of gold nanocages for photothermal therapy. *ACS Nano* **2014**, *8*, 10414–10425. [CrossRef]

30. Guo, Y.; Wang, D.; Song, Q.; Wu, T.; Zhuang, X.; Bao, Y.; Kong, M.; Qi, Y.; Tan, S.; Zhang, Z. Erythrocyte Membrane-Enveloped Polymeric Nanoparticles as Nanovaccine for Induction of Antitumor Immunity against Melanoma. *ACS Nano* **2015**, *9*, 6918–6933. [CrossRef]
31. Su, J.; Sun, H.; Meng, Q.; Zhang, P.; Yin, Q.; Li, Y. Enhanced blood suspensibility and laser-Activated tumor-specific drug release of theranostic mesoporous silica nanoparticles by functionalizing with erythrocyte membranes. *Theranostics* **2017**, *7*, 523–537. [CrossRef] [PubMed]
32. Ren, X.; Zheng, R.; Fang, X.; Wang, X.; Zhang, X.; Yang, W.; Sha, X. Red blood cell membrane camouflaged magnetic nanoclusters for imaging-guided photothermal therapy. *Biomaterials* **2016**, *92*, 13–24. [CrossRef] [PubMed]
33. Parodi, A.; Quattrocchi, N.; Van De Ven, A.L.; Chiappini, C.; Evangelopoulos, M.; Martinez, J.O.; Brown, B.S.; Khaled, S.Z.; Yazdi, I.K.; Enzo, M.V.; et al. Synthetic nanoparticles functionalized with biomimetic leukocyte membranes possess cell-like functions. *Nat. Nanotechnol.* **2013**, *8*, 61–68. [CrossRef] [PubMed]
34. Hu, Q.; Sun, W.; Qian, C.; Wang, C.; Bomba, H.N.; Gu, Z. Anticancer platelet-mimicking nanovehicles. *Adv. Mater.* **2016**, *27*, 7043–7050. [CrossRef] [PubMed]
35. Xuan, M.; Shao, J.; Dai, L.; He, Q.; Li, J. Macrophage Cell Membrane Camouflaged Mesoporous Silica Nanocapsules for In Vivo Cancer Therapy. *Adv. Healthc. Mater.* **2015**, *4*, 1645–1652. [CrossRef] [PubMed]
36. Hu, C.J.; Fang, R.; Wang, K.; Luk, B.T.; Thamphiwatana, S.; Dehaini, D.; Nguyen, P.; Angsantikul, P.; Wen, C.H.; Kroll, A.V.; et al. Nanoparticle biointerfacing via platelet membrane cloaking. *Nature* **2016**, *526*, 118–121. [CrossRef]
37. Zhang, Q.; Dehaini, D.; Zhang, Y.; Zhou, J.; Chen, X.; Zhang, L.; Fang, R.H.; Gao, W.; Zhang, L. Neutrophil membrane-coated nanoparticles inhibit synovial inflammation and alleviate joint damage in inflammatory arthritis. *Nat. Nanotechnol.* **2018**, *13*, 1182–1190. [CrossRef]
38. Rao, L.; Bu, L.L.; Ma, L.; Wang, W.; Liu, H.; Wan, D.; Liu, J.F.; Li, A.; Guo, S.S.; Zhang, L.; et al. Platelet-Facilitated Photothermal Therapy of Head and Neck Squamous Cell Carcinoma. *Angew. Chem. Int. Ed.* **2018**, *57*, 986–991. [CrossRef]
39. Hu, Q.; Sun, W.; Qian, C.; Bomba, H.N.; Xin, H.; Gu, Z. Relay Drug Delivery for Amplifying Targeting Signal and Enhancing Anticancer Efficacy. *Adv. Mater.* **2017**, *29*. [CrossRef]
40. Sun, H.; Su, J.; Meng, Q.; Yin, Q.; Chen, L.; Gu, W.; Zhang, P.; Zhang, Z.; Yu, H.; Wang, S.; et al. Cancer-Cell-Biomimetic Nanoparticles for Targeted Therapy of Homotypic Tumors. *Adv. Mater.* **2016**, *28*, 9581–9588. [CrossRef]
41. Dehaini, D.; Fang, R.H.; Zhang, L. Biomimetic strategies for targeted nanoparticle delivery. *Bioeng. Transl. Med.* **2016**, *1*, 30–46. [CrossRef] [PubMed]
42. Sun, H.; Su, J.; Meng, Q.; Yin, Q.; Chen, L.; Gu, W.; Zhang, Z.; Yu, H.; Zhang, P.; Wang, S.; et al. Cancer Cell Membrane-Coated Gold Nanocages with Hyperthermia-Triggered Drug Release and Homotypic Target Inhibit Growth and Metastasis of Breast Cancer. *Adv. Funct. Mater.* **2017**, *27*. [CrossRef]
43. Jin, J.; Krishnamachary, B.; Barnett, J.D.; Chatterjee, S.; Chang, D.; Mironchik, Y.; Wildes, F.; Jaffee, E.M.; Nimmagadda, S.; Bhujwalla, Z.M. Human Cancer Cell Membrane-Coated Biomimetic Nanoparticles Reduce Fibroblast-Mediated Invasion and Metastasis and Induce T-Cells. *ACS Appl. Mater. Interfaces* **2019**, *11*, 7850–7861. [CrossRef] [PubMed]
44. Zhu, J.Y.; Zheng, D.W.; Zhang, M.K.; Yu, W.Y.; Qiu, W.X.; Hu, J.J.; Feng, J.; Zhang, X.Z. Preferential Cancer Cell Self-Recognition and Tumor Self-Targeting by Coating Nanoparticles with Homotypic Cancer Cell Membranes. *Nano Lett.* **2016**, *16*, 5895–5901. [CrossRef] [PubMed]
45. Fang, R.H.; Hu, C.M.J.; Luk, B.T.; Gao, W.; Copp, J.A.; Tai, Y.; O'Connor, D.E.; Zhang, L. Cancer cell membrane-coated nanoparticles for anticancer vaccination and drug delivery. *Nano Lett.* **2014**, *14*, 2181–2188. [CrossRef] [PubMed]
46. Chen, M.; Chen, M.; He, J. Cancer cell membrane cloaking nanoparticles for targeted co-delivery of doxorubicin and PD-L1 siRNA. *Artif. Cells Nanomed. Biotechnol.* **2019**, *47*, 1635–1641. [CrossRef] [PubMed]
47. Luk, B.T.; Zhang, L. Cell membrane-camouflaged nanoparticles for drug delivery. *J. Control. Release* **2015**, *220*, 600–607. [CrossRef]
48. Zhai, Y.; Su, J.; Ran, W.; Zhang, P.; Yin, Q.; Zhang, Z.; Yu, H.; Li, Y. Preparation and application of cell membrane-camouflaged nanoparticles for cancer therapy. *Theranostics* **2017**, *7*, 2575–2592. [CrossRef]

49. Chen, W.; Zeng, K.; Liu, H.; Ouyang, J.; Wang, L.; Liu, Y.; Wang, H.; Deng, L.; Liu, Y.N. Cell Membrane Camouflaged Hollow Prussian Blue Nanoparticles for Synergistic Photothermal-/Chemotherapy of Cancer. *Adv. Funct. Mater.* **2017**, *27*. [CrossRef]
50. Xia, Q.; Zhang, Y.; Li, Z.; Hou, X.; Feng, N. Red blood cell membrane-camouflaged nanoparticles: A novel drug delivery system for antitumor application. *Acta Pharm. Sin. B* **2019**. [CrossRef]
51. Rao, L.; Cai, B.; Bu, L.L.; Liao, Q.Q.; Guo, S.S.; Zhao, X.Z.; Dong, W.F.; Liu, W. Microfluidic Electroporation-Facilitated Synthesis of Erythrocyte Membrane-Coated Magnetic Nanoparticles for Enhanced Imaging-Guided Cancer Therapy. *ACS Nano* **2017**, *11*, 3496–3505. [CrossRef] [PubMed]
52. Tsong, T.Y. Electroporation of cell membranes. *Biophys. J.* **1991**, *60*, 297–306. [CrossRef]
53. Fan, Z.; Zhou, H.; Li, P.Y.; Speer, J.E.; Cheng, H. Structural elucidation of cell membrane-derived nanoparticles using molecular probes. *J. Mater. Chem. B* **2014**, *2*, 8231–8238. [CrossRef]
54. Rao, L.; Bu, L.L.; Cai, B.; Xu, J.H.; Li, A.; Zhang, W.F.; Sun, Z.J.; Guo, S.S.; Liu, W.; Wang, T.H.; et al. Cancer Cell Membrane-Coated Upconversion Nanoprobes for Highly Specific Tumor Imaging. *Adv. Mater.* **2016**, *28*, 3460–3466. [CrossRef] [PubMed]
55. Xie, W.; Deng, W.W.; Zan, M.; Rao, L.; Yu, G.T.; Zhu, D.M.; Wu, W.T.; Chen, B.; Ji, L.W.; Chen, L.; et al. Cancer Cell Membrane Camouflaged Nanoparticles to Realize Starvation Therapy Together with Checkpoint Blockades for Enhancing Cancer Therapy. *ACS Nano* **2019**, *13*, 2849–2857. [CrossRef]
56. Liu, C.M.; Chen, G.B.; Chen, H.H.; Zhang, J.B.; Li, H.Z.; Sheng, M.X.; Weng, W.B.; Guo, S.M. Cancer cell membrane-cloaked mesoporous silica nanoparticles with a pH-sensitive gatekeeper for cancer treatment. *Colloids Surfaces B Biointerfaces* **2019**, *175*, 477–486. [CrossRef]
57. Wang, D.; Dong, H.; Li, M.; Cao, Y.; Yang, F.; Zhang, K.; Dai, W.; Wang, C.; Zhang, X. Erythrocyte-Cancer Hybrid Membrane Camouflaged Hollow Copper Sulfide Nanoparticles for Prolonged Circulation Life and Homotypic-Targeting Photothermal/Chemotherapy of Melanoma. *ACS Nano* **2018**, *12*, 5241–5252. [CrossRef]
58. Rao, L.; Meng, Q.F.; Huang, Q.; Liu, P.; Bu, L.L.; Kondamareddy, K.K.; Guo, S.S.; Liu, W.; Zhao, X.Z. Photocatalytic Degradation of Cell Membrane Coatings for Controlled Drug Release. *Adv. Healthc. Mater.* **2016**, *5*, 1420–1427. [CrossRef]
59. Copp, J.A.; Fang, R.H.; Luk, B.T.; Hu, C.-M.J.; Gao, W.; Zhang, K.; Zhang, L. Clearance of pathological antibodies using biomimetic nanoparticles. *Proc. Natl. Acad. Sci. USA* **2014**, *111*, 13481–13486. [CrossRef]
60. Zhou, H.; Fan, Z.; Lemons, P.K.; Cheng, H. A facile approach to functionalize cell membrane-coated nanoparticles. *Theranostics* **2016**, *6*, 1012–1022. [CrossRef]
61. Li, J.; Zhen, X.; Lyu, Y.; Jiang, Y.; Huang, J.; Pu, K. Cell Membrane Coated Semiconducting Polymer Nanoparticles for Enhanced Multimodal Cancer Phototheranostics. *ACS Nano* **2018**, *12*, 8520–8530. [CrossRef] [PubMed]
62. Xu, L.; Wu, S.; Wang, J. Cancer cell membrane–coated nanocarriers for homologous target inhibiting the growth of hepatocellular carcinoma. *J. Bioact. Compat. Polym.* **2019**, *34*, 58–71. [CrossRef]
63. Tian, H.; Luo, Z.; Liu, L.; Zheng, M.; Chen, Z.; Ma, A.; Liang, R.; Han, Z.; Lu, C.; Cai, L. Cancer Cell Membrane-Biomimetic Oxygen Nanocarrier for Breaking Hypoxia-Induced Chemoresistance. *Adv. Funct. Mater.* **2017**, *27*, 1–7. [CrossRef]
64. Yang, R.; Xu, J.; Xu, L.; Sun, X.; Chen, Q.; Zhao, Y.; Peng, R.; Liu, Z. Cancer Cell Membrane-Coated Adjuvant Nanoparticles with Mannose Modification for Effective Anticancer Vaccination. *ACS Nano* **2018**, *12*, 5121–5129. [CrossRef]
65. Yu, G.T.; Rao, L.; Wu, H.; Yang, L.L.; Bu, L.L.; Deng, W.W.; Wu, L.; Nan, X.; Zhang, W.F.; Zhao, X.Z.; et al. Myeloid-Derived Suppressor Cell Membrane-Coated Magnetic Nanoparticles for Cancer Theranostics by Inducing Macrophage Polarization and Synergizing Immunogenic Cell Death. *Adv. Funct. Mater.* **2018**, *28*, 1–9. [CrossRef]
66. Song, Q.; Yin, Y.; Shang, L.; Wu, T.; Zhang, D.; Kong, M.; Zhao, Y.; He, Y.; Tan, S.; Guo, Y.; et al. Tumor Microenvironment Responsive Nanogel for the Combinatorial Antitumor Effect of Chemotherapy and Immunotherapy. *Nano Lett.* **2017**, *17*, 6366–6375. [CrossRef]
67. Pan, W.; Ge, Y.; Yu, Z.; Zhou, P.; Cui, B.; Li, N.; Tang, B. A cancer cell membrane-encapsulated MnO_2 nanoreactor for combined photodynamic-starvation therapy. *Chem. Commun.* **2019**, *55*, 5115–5118. [CrossRef]
68. Jiang, Q.; Liu, Y.; Guo, R.; Yao, X.; Sung, S.; Pang, Z.; Yang, W. Erythrocyte-cancer hybrid membrane-camouflaged melanin nanoparticles for enhancing photothermal therapy efficacy in tumors. *Biomaterials* **2019**, *192*, 292–308. [CrossRef]

69. Gao, L.; Han, L.; Ding, X.; Xu, J.; Wang, J.; Zhu, J.; Lu, W.; Sun, J.; Yu, L.; Yan, Z.; et al. An effective intracellular delivery system of monoclonal antibody for treatment of tumors: Erythrocyte membrane-coated self-associated antibody nanoparticles. *Nanotechnology* **2017**, *28*. [CrossRef]
70. Gao, W.; Hu, C.M.J.; Fang, R.H.; Luk, B.T.; Su, J.; Zhang, L. Surface Functionalization of Gold Nanoparticles with Red Blood Cell Membranes. *Adv. Mater.* **2014**, *25*, 3549–3553. [CrossRef]
71. Hirsch, L.R.; Stafford, R.J.; Bankson, J.A.; Sershen, S.R.; Rivera, B.; Price, R.E.; Hazle, J.D.; Halas, N.J.; West, J.L. Nanoshell-mediated near-infrared thermal therapy of tumors under magnetic resonance guidance. *Proc. Natl. Acad. Sci. USA* **2003**. [CrossRef] [PubMed]
72. Li, J.; Wang, X.; Zheng, D.; Lin, X.; Wei, Z.; Zhang, D.; Li, Z.; Zhang, Y.; Wu, M.; Liu, X. Cancer cell membrane-coated magnetic nanoparticles for MR/NIR fluorescence dual-modal imaging and photodynamic therapy. *Biomater. Sci.* **2018**, *6*, 1834–1845. [CrossRef] [PubMed]
73. Li, S.Y.; Cheng, H.; Qiu, W.X.; Zhang, L.; Wan, S.S.; Zeng, J.Y.; Zhang, X.Z. Cancer cell membrane-coated biomimetic platform for tumor targeted photodynamic therapy and hypoxia-amplified bioreductive therapy. *Biomaterials* **2017**, *142*, 149–161. [CrossRef] [PubMed]
74. Chen, Z.; Zhao, P.; Luo, Z.; Zheng, M.; Tian, H.; Gong, P.; Gao, G.; Pan, H.; Liu, L.; Ma, A.; et al. Cancer Cell Membrane-Biomimetic Nanoparticles for Homologous-Targeting Dual-Modal Imaging and Photothermal Therapy. *ACS Nano* **2016**, *10*, 10049–10057. [CrossRef] [PubMed]
75. Kroll, A.V.; Fang, R.H.; Jiang, Y.; Zhou, J.; Wei, X.; Yu, C.L.; Gao, J.; Luk, B.T.; Dehaini, D.; Gao, W.; et al. Nanoparticulate Delivery of Cancer Cell Membrane Elicits Multiantigenic Antitumor Immunity. *Adv. Mater.* **2017**, *29*, 1–9. [CrossRef] [PubMed]
76. Zhang, N.; Li, M.; Sun, X.; Jia, H.; Liu, W. NIR-responsive cancer cytomembrane-cloaked carrier-free nanosystems for highly efficient and self-targeted tumor drug delivery. *Biomaterials* **2018**, *159*, 25–36. [CrossRef] [PubMed]
77. Astete, C.E.; Sabliov, C.M. Synthesis and characterization of PLGA nanoparticles. *J. Biomater. Sci. Polym. Ed.* **2006**, *17*, 247–289. [CrossRef]
78. Lovitt, C.J.; Shelper, T.B.; Avery, V.M. Doxorubicin resistance in breast cancer cells is mediated by extracellular matrix proteins. *BMC Cancer* **2018**, *18*, 1–11. [CrossRef]
79. Herbst, R.S.; Giaccone, G.; Schiller, J.H.; Natale, R.B.; Miller, V.; Manegold, C.; Scagliotti, G.; Rosell, R.; Oliff, I.; Reeves, J.A.; et al. Gefitinib in combination with paclitaxel and carboplatin in advanced non-small-cell lung cancer: A phase III trial—INTACT 2. *J. Clin. Oncol.* **2004**, *22*, 785–794. [CrossRef]
80. Miller, K.; Wang, M.; Gralow, J.; Dickler, M.; Cobleigh, M.; Perez, E.A.; Shenkier, T.; Cella, D.; Davidson, N.E. Paclitaxel plus bevacizumab versus paclitaxel alone for metastatic breast cancer. *N. Engl. J. Med.* **2007**, *357*, 2666–2676. [CrossRef]
81. Dezube, B.J.; Pantanowitz, L.; Aboulafia, D.M. Management of AIDS-Related Kaposi Sarcoma: Advances in Target Discovery and Treatment. *AIDS Read.* **2004**, 1–8.
82. Armstrong, D.K.; Bundy, B.; Wenzel, L.; Huang, H.Q.; Baergen, R.; Lele, S.; Copeland, L.J.; Walker, J.L.; Burger, R.A.; Mackey, D. Intraperitoneal cisplatin and paclitaxel in ovarian cancer. *N. Engl. J. Med.* **2006**, *354*, 34–43. [CrossRef] [PubMed]
83. Johnson, D.H.; Fehrenbacher, L.; Novotny, W.F.; Herbst, R.S.; Nemunaitis, J.J.; Jablons, D.M.; Langer, C.J.; DeVore, R.F.; Gaudreault, J.; Damico, L.A.; et al. Randomized phase II trial comparing bevacizumab plus carboplatin and paclitaxel with carboplatin and paclitaxel alone in previously untreated locally advanced or metastatic non-small-cell lung cancer. *J. Clin. Oncol.* **2004**, *22*, 2184–2191. [CrossRef] [PubMed]
84. du Bois, A.; Luck, H.-J.; Meier, W.; Adams, H.-P.; Mobus, V.; Costa, S.; Bauknecht, T.; Richter, B.; Warm, M.; Schroder, W.; et al. A Randomized Clinical Trial of Cisplatin/Paclitaxel Versus Carboplatin/Paclitaxel as First-Line Treatment of Ovarian Cancer. *J. Natl. Cancer Inst.* **2003**, *95*, 1320–1329. [CrossRef]
85. Sparano, J.A.; Wang, M.; Martino, S.; Jones, V.; Perez, E.A.; Sapher, T.; Wolff, A.; Sledge, G.W.; Wood, W.C.; Davidson, N.E. Weekly Paclitaxel in the Adjuvant Treatment of Breast Cancer. *N. Engl. J. Med.* **2008**, *358*, 1663–1671. [CrossRef]
86. Fay, B.L.; Melamed, J.R.; Day, E.S. Nanoshell-mediated photothermal therapy can enhance chemotherapy in inflammatory breast cancer cells. *Int. J. Nanomed.* **2015**, *10*, 6931–6941.
87. Valcourt, D.M.; Dang, M.N.; Day, E.S. IR820-loaded PLGA nanoparticles for photothermal therapy of triple-negative breast cancer. *J. Biomed. Mater. Res* **2019**, *107*, 1702–1712. [CrossRef]

88. Riley, R.S.; Day, E.S. Gold nanoparticle-mediated photothermal therapy: Applications and opportunities for multimodal cancer treatment. *Wiley Interdiscip. Rev. Nanomed. Nanobiotechnol.* **2017**, *9*. [CrossRef]
89. Riley, R.S.; O'sullivan, R.K.; Potocny, A.M.; Rosenthal, J.; Day, E.S. Evaluating nanoshells and a potent biladiene photosensitizer for dual photothermal and photodynamic therapy of triple negative breast cancer cells. *Nanomaterials* **2018**, *8*, 658. [CrossRef]
90. Day, E.S.; Thompson, P.A.; Zhang, L.; Lewinski, N.A.; Ahmed, N.; Drezek, R.A.; Blaney, S.M.; West, J.L. Nanoshell-mediated photothermal therapy improves survival in a murine glioma model. *J. Neurooncol.* **2011**, *104*, 55–63. [CrossRef]
91. Day, E.S.; Zhang, L.; Thompson, P.A.; Zawaski, J.A.; Kaffes, C.C.; Gaber, M.W.; Blaney, S.M.; West, J.L. Vascular-targeted photothermal therapy of an orthotopic murine glioma model. *Nanomedicine* **2012**, *7*, 1133–1148. [CrossRef] [PubMed]
92. Melamed, J.R.; Edelstein, R.S.; Day, E.S. Elucidating the fundamental mechanisms of cell death triggered by photothermal therapy. *ACS Nano* **2015**, *9*, 6–11. [CrossRef] [PubMed]
93. Hu, C.-M.J.; Fang, R.H.; Luk, B.T.; Chen, K.N.H.; Carpenter, C.; Gao, W.; Zhang, K.; Zhang, L. 'Marker-of-self' functionalization of nanoscale particles through a top-down cellular membrane coating approach. *Nanoscale* **2013**, *5*, 2664. [CrossRef] [PubMed]
94. Gao, C.; Lin, Z.; Wu, Z.; Lin, X.; He, Q. Stem-Cell-Membrane Camouflaging on Near-Infrared Photoactivated Upconversion Nanoarchitectures for in Vivo Remote-Controlled Photodynamic Therapy. *ACS Appl. Mater. Interfaces* **2016**, *8*, 34252–34260. [CrossRef]
95. Xuan, M.; Shao, J.; Dai, L.; Li, J.; He, Q. Macrophage Cell Membrane Camouflaged Au Nanoshells for in Vivo Prolonged Circulation Life and Enhanced Cancer Photothermal Therapy. *ACS Appl. Mater. Interfaces* **2016**, *8*, 9610–9618. [CrossRef]
96. Liu, W.L.; Liu, T.; Zou, M.Z.; Yu, W.Y.; Li, C.X.; He, Z.Y.; Zhang, M.K.; Liu, M.D.; Li, Z.H.; Feng, J.; et al. Aggressive Man-Made Red Blood Cells for Hypoxia-Resistant Photodynamic Therapy. *Adv. Mater.* **2018**, *30*, 1–10. [CrossRef]
97. Xuan, M.; Shao, J.; Zhao, J.; Li, Q.; Dai, L.; Li, J. Magnetic Mesoporous Silica Nanoparticles Cloaked by Red Blood Cell Membranes: Applications in Cancer Therapy. *Angew. Chem. Int. Ed.* **2018**, *57*, 6049–6053. [CrossRef]
98. Zhen, X.; Cheng, P.; Pu, K. Recent Advances in Cell Membrane–Camouflaged Nanoparticles for Cancer Phototherapy. *Small* **2019**, *15*, 1–19. [CrossRef]
99. Park, J.H.; Von Maltzahn, G.; Xu, M.J.; Fogal, V.; Kotamraju, V.R.; Ruoslahti, E.; Bhatia, S.N.; Sailor, M.J. Cooperative nanomaterial system to sensitize, target, and treat tumors. *Proc. Natl. Acad. Sci. USA* **2010**, *107*, 981–986. [CrossRef]
100. Nam, J.; Son, S.; Ochyl, L.J.; Kuai, R.; Schwendeman, A.; Moon, J.J. Chemo-photothermal therapy combination elicits anti-tumor immunity against advanced metastatic cancer. *Nat. Commun.* **2018**. [CrossRef]
101. Wang, C.; Ye, Y.; Hu, Q.; Bellotti, A.; Gu, Z. Tailoring Biomaterials for Cancer Immunotherapy: Emerging Trends and Future Outlook. *Adv. Mater.* **2017**, *29*, 1–24. [CrossRef] [PubMed]
102. Finn, O.J. Cancer vaccines: Between the idea and the reality. *Nat. Rev. Immunol.* **2003**, *3*, 630–641. [CrossRef] [PubMed]
103. Wilhelm, S.; Tavares, A.J.; Dai, Q.; Ohta, S.; Audet, J.; Dvorak, H.F.; Chan, W.C.W. Analysis of nanoparticle delivery to tumours. *Nat. Rev. Mater.* **2016**, *1*, 1–12. [CrossRef]
104. Gubin, M.M.; Zhang, X.; Schuster, H.; Caron, E.; Ward, J.P.; Noguchi, T.; Ivanova, Y.; Hundal, J.; Arthur, C.D.; Krebber, W.J.; et al. Checkpoint blockade cancer immunotherapy targets tumour-specific mutant antigens. *Nature* **2014**, *515*, 577–581. [CrossRef]
105. Pardoll, D.M. The blockade of immune checkpoints in cancer immunotherapy. *Nat. Rev. Cancer* **2012**, *12*, 252–264. [CrossRef]
106. Kirkwood, J.M.; Butterfield, L.H.; Tarhini, A.A.; Zarour, H.; Kalinski, P.; Ferrone, S. Immunotherapy of Cancer in 2012. *CA Cancer J. Clin.* **2012**, *62*, 309–335. [CrossRef]
107. Schumacher, T.N.; Schreiber, R.D. Neoantigens in cancer immunotherapy. *Science* **2015**, *348*, 69–74. [CrossRef]
108. Ribas, A.; Wolchok, J.D. Cancer immunotherapy using checkpoint blockade. *Science* **2018**, *359*, 1350–1355. [CrossRef]
109. Mellman, I.; Coukos, G.; Dranoff, G. Cancer immunotherapy comes of age. *Nature* **2011**, *480*, 480–489. [CrossRef]

110. Couzin-Frankel, J. Cancer immunotherapy. *Science* **2013**, *342*, 1432–1433. [CrossRef]
111. Dehaini, D.; Wei, X.; Fang, R.H.; Masson, S.; Angsantikul, P.; Luk, B.T.; Zhang, Y.; Ying, M.; Jiang, Y.; Kroll, A.V.; et al. Erythrocyte–Platelet Hybrid Membrane Coating for Enhanced Nanoparticle Functionalization. *Adv. Mater.* **2017**, *29*, 1–8. [CrossRef] [PubMed]

cancers

MDPI

Review

Targeting Integrins in Cancer Nanomedicine: Applications in Cancer Diagnosis and Therapy

Ping-Hsiu Wu [1], Abayomi Emmanuel Opadele [2], Yasuhito Onodera [1,3,*] and Jin-Min Nam [1,*]

[1] Global Station for Quantum Medical Science and Engineering, Global Institution for Collaborative Research and Education (GI-CoRE), Hokkaido University, Sapporo 060-8638, Hokkaido, Japan; phwu@pop.med.hokudai.ac.jp

[2] Molecular and Cellular Dynamics Research, Graduate School of Biomedical Science and Engineering, Hokkaido University, Sapporo 060-8638, Hokkaido, Japan; abayomiopadele@gmail.com

[3] Department of Molecular Biology, Faculty of Medicine, Hokkaido University, Sapporo 060-8638, Hokkaido, Japan

* Correspondence: yonodera@med.hokudai.ac.jp (Y.O.); jinmini@med.hokudai.ac.jp (J.-M.N.); Tel.: +81-11-706-5045 (Y.O.); +81-11-706-5076 (J.-M.N.); Fax: +81-11-706-7005 (J.-M.N.)

Received: 18 October 2019; Accepted: 12 November 2019; Published: 13 November 2019

Abstract: Due to advancements in nanotechnology, the application of nanosized materials (nanomaterials) in cancer diagnostics and therapeutics has become a leading area in cancer research. The decoration of nanomaterial surfaces with biological ligands is a major strategy for directing the actions of nanomaterials specifically to cancer cells. These ligands can bind to specific receptors on the cell surface and enable nanomaterials to actively target cancer cells. Integrins are one of the cell surface receptors that regulate the communication between cells and their microenvironment. Several integrins are overexpressed in many types of cancer cells and the tumor microvasculature and function in the mediation of various cellular events. Therefore, the surface modification of nanomaterials with integrin-specific ligands not only increases their binding affinity to cancer cells but also enhances the cellular uptake of nanomaterials through the intracellular trafficking of integrins. Moreover, the integrin-specific ligands themselves interfere with cancer migration and invasion by interacting with integrins, and this finding provides a novel direction for new treatment approaches in cancer nanomedicine. This article reviews the integrin-specific ligands that have been used in cancer nanomedicine and provides an overview of the recent progress in cancer diagnostics and therapeutic strategies involving the use of integrin-targeted nanomaterials.

Keywords: nanomedicine; nanoparticles; integrin; RGD peptide; active targeting; cancer diagnosis; drug delivery; radiotherapy; hyperthermia therapy

1. Introduction

1.1. Cancer Nanomedicine

An increasing number of nanotechnologies have been applied to the screening, diagnosis, and treatment of cancer in the field of cancer nanomedicine. Since the first nanomedical cancer drug Doxil (liposomal doxorubicin) received approval by the food and drug administration of America (FDA) in 1995 [1], the number of new applications in cancer nanomedicine has increased. Compared with conventional cancer interventions, nanomedicine, which involves the nanoscale application of highly specific medical interventions, has unique features. For example, nanomedicine offers the ability to specifically target and greatly enhance the detection of tumors [2,3]. In cancer treatment, nanomedicine not only improves the therapeutic indexes of traditional medications but also provides innovative concepts for new treatment approaches [4]. Those appealing advantages have incentivized

more scientists to undertake research in cancer nanomedicine, and these studies have contributed to the development of promising treatments for overcoming cancer in the future.

1.2. Characterization of Nanoparticles

To produce nanomedical agents for cancer diagnosis or treatment, scientists first select the nanoparticle (NP) platform on the basis of the therapeutic approach. The main structure of NP platforms can be divided into organic and inorganic materials. Organic NPs, such as liposomes [1], polymeric NPs [5], dendrimers [6], viral NPs [7], and exosomes [8], are usually used for drug delivery or gene therapy, and inorganic NPs include carbon-based NPs [9], metal-based NPs [10], mesoporous silica [11] and quantum dots (QDs) [12]. Over the last few decades, these NPs have become increasingly advanced with new designs and applications, such as functionalization for achieving stimuli-responsive effects [13]. For example, Gao et al. used inorganic NPs to induce heat after exogenous stimulation to trigger the release of cytotoxic agents [14]. In addition, due to their unique physical properties, inorganic NPs, such as metal-based NPs, can be used in innovative approaches, including the enhancement of radiotherapy [15] and the induction of hyperthermia in cancer cells [16].

Subsequently, the delivery of NPs is considered, and there are two major approaches for transporting NPs to cancer cells: passive targeting and active targeting (Figure 1). By leveraging the pathophysiological processes in cancer (for example, leaky tumor vasculature, poor lymphatic drainage, and tumor microenvironment interactions), NPs can take advantage of the enhanced permeability and retention (EPR) effects to accumulate around tumoral tissue, and this process is called passive targeting [17]. The first-generation nanomedicine drugs, such as Doxil, Myocet (non-polyethylene glycosylated (PEGylated) liposomal doxorubicin) and DaunoXome (non-PEGylated liposomal daunorubicin), are EPR effect-based nanomedical drugs that have already been routinely used for treating patients [18]. However, the use of NPs through only passive targeting does not achieve the best therapeutic effects because the EPR effect applies not only to tumors but also to some normal tissues [19,20], such as hepatic or splenic tissue with fenestrated blood vessels, and leads to unexpected NP accumulation in these normal tissues. In addition, solid tumor tissues are heterogeneous neoplasms composed of different types of cells, including cancer cells, mesenchymal cells, endovascular cells, and immune cells [21]. This heterogeneity of tumoral tissue limits the ability of delivering NPs specifically to tumor cells.

To enhance the accumulation of NPs in cancer cells, scientists decorate NPs with targeting ligands that recognize specific receptors on the tumor cell surface, and this approach is called active targeting [22]. Active targeting effectively increases not only the tumor uptake of NPs independent of the EPR effect but also the ability of NPs to cross physiological barriers, such as the intestinal mucosa [23] or the blood–brain barrier [24]. Selecting the appropriate targeting ligand is critical for optimizing the efficiency of active targeting. Representative ligands used for the active targeting of NPs include antibodies, peptides, nucleic acids, sugars, and/or other small molecules [25]. In the past, antibodies have generally been selected as targeting moieties for use in nanomedicine due to their high specificity and wide availability [26]. However, the clinical use of antibody-based NPs is limited by certain features of the antibodies, such as the large size of antibodies, which impedes the effectiveness of surface conjugation [27], or the immunogenicity of antibodies, which leads to high clearance from the blood [28]. In addition, the easy degradation of antibodies during environmental changes (temperature, pH level, photostability, oxidation, etc.) is also a problem [29]. Peptides with smaller molecular sizes and simple three-dimensional structures do not have the disadvantages of antibody-based NPs. In addition, the synthesis of peptides is relatively simple and inexpensive compared with the production and cost of antibodies, which facilitates their translation to the clinic.

Research on nucleic acids is relatively more recent than that on peptides, and the lack of safety data and clinical reports on nucleic acids limits their application [30]. Sugars (such as saccharides, oligosaccharides, and polysaccharides) are larger than peptides, which affects their application for NP modification. Compared with other small-molecule agents, peptides are more specific to their targets

because they are derived from linear protein sequences [31]. Therefore, peptides that can specifically bind to surface receptors on cancer cells, particularly integrin-targeted peptides, have attracted extensive attention.

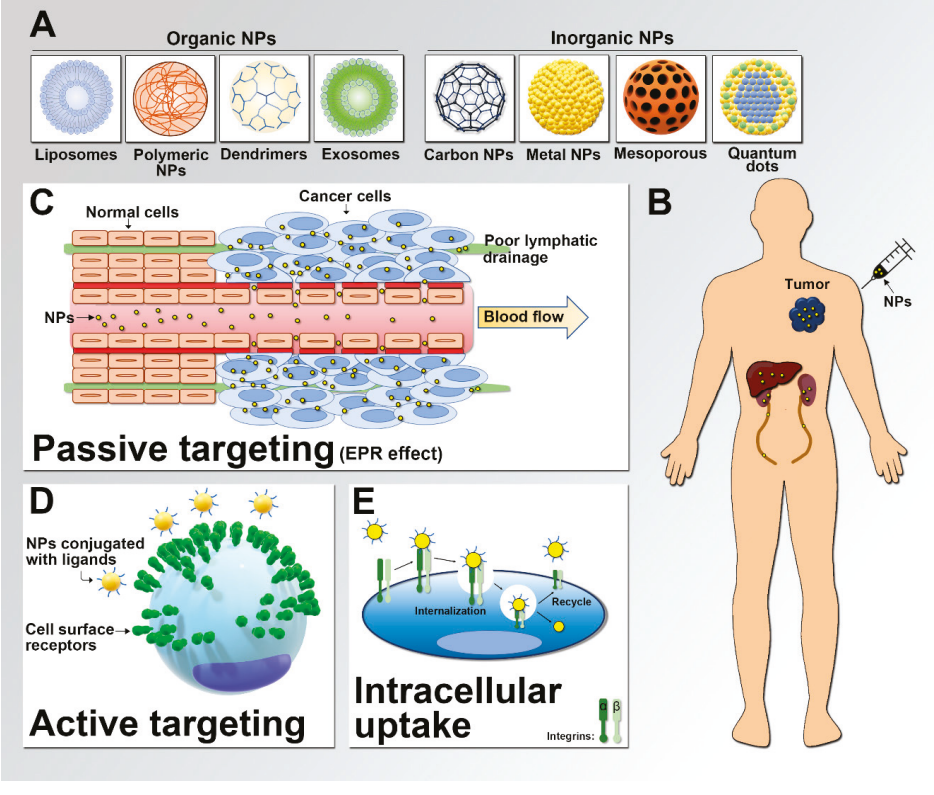

Figure 1. Uptake of nanoparticles (NPs). (**A**) Representative NPs used for cancer nanomedicine. (**B**) Accumulation of NPs in the human body. The organs that typically show the highest NP accumulation are the liver and kidney. (**C**) Schematic of passive targeting (enhanced permeability and retention (EPR) effects). NPs preferentially accumulate within tumors due to their leaky vasculature and poor lymphatic drainage. (**D**) Schematic of the active targeting of NPs conjugated with specific ligands that target surface receptors on cancer cells. (**E**) Schematic of intracellular uptake. This figure shows an example of the internalization of integrin-targeted NPs by cells through endocytosis after binding to integrins.

1.3. Integrins in Cancer Nanomedicine

Integrins constitute a family of cell surface receptors that mainly facilitate cell-to-extracellular matrix (ECM) adhesion. Each integrin belonging to this family of heterodimeric transmembrane receptors is composed of an α subunit and a β subunit. Mammals have 18 α-subunits and eight β-subunits, and these subunits form 24 different integrins [32]. Various integrins play two major functions: attaching the cell body to the ECM and receiving signals transduced from the ECM. The extracellular domain of these integrins shows strong affinity for ECM proteins, including fibronectin, vitronectin, collagen, and laminin. After binding to ECM and clustering, these integrins also activate signal transduction pathways that mediate cellular signals related to cell growth, survival, division, and migration [33]. In contrast, the overexpression of certain integrins has been observed in highly

malignant cancer cells (Table 1) and plays an important role in malignant properties, including cancer progression [34], invasion/metastasis [34], tumor angiogenesis [35], and even resistance to conventional cancer therapy [36,37]. These facts suggest that targeting integrins overexpressed in cancer cells is a feasible strategy for use in cancer nanomedicine.

Table 1. Arg-Gly-Asp (RGD) peptide-binding integrins in cancer cells.

Integrin	Binding Ligands	Specific Functions in Cancers	Associated Cancers (Detected in Clinical Studies)
α5β1	Fibronectin	Increases tumor progression [38] Increases cancer invasion [39] Mediates resistance to radiotherapy [36]	Head and neck cancer [40,41]
	Vitronectin		Non-small cell lung cancer [42]
	Fibrinogen		Breast cancer [43]
	Osteopontin		Prostate cancer [44]
			Ovarian cancer [45]
			Melanoma [46]
αvβ3	Fibronectin	Increases tumor progression [47] Increases lymph node metastasis [48] Increases bone metastasis [49] Is involved in cancer immune evasion [50]	Glioma [51]
	Vitronectin		Head and neck cancer [40]
	Fibrinogen		Non-small cell lung cancer [52]
	Osteopontin		Lung cancer brain metastases [53]
	Tenascin		
	Thyroid hormone T4		Gastric cancer [54]
			Pancreatic cancer [48]
			Prostate cancer [55]
			Melanoma [46]
αvβ5	Fibronectin	Increases tumor progression [56] Is involved in glioma invasion [57]	Lung cancer brain metastases [53]
	Vitronectin		Non-small cell lung cancer [52]
	Fibrinogen		Gastric cancer [54]
	Osteopontin		Prostate cancer [55]
αvβ6	Fibronectin	Promotes hepatic tumorigenesis [58] Increases tumor progression [59] Increases lymph node metastasis [60] Mediates resistance to chemotherapy [61]	Head and neck cancer [62]
	Vitronectin		Non-small cell lung cancer [63]
	Fibrinogen		Breast cancer [64]
	Osteopontin		Lung cancer brain metastases [62]
	Tenascin		Gastric cancer [65]
			Pancreatic cancer [55]
			Colon cancer [66]
			Endometrial cancer [67]
			Ovarian cancer [68]
			Basal cell carcinoma [69]
αvβ8	Fibronectin	Is involved in cancer immune evasion [70] Mediates resistance to chemo- and radiotherapy [71]	Head and neck cancer [72]
	Vitronectin Fibrinogen		Non-small cell lung cancer [52]
	Osteopontin		Prostate cancer [55]

The Arg-Gly-Asp (RGD) peptide is the most representative binding motif involved in the interactions of ECM proteins with integrins [73]. Since the RGD peptide was first discovered in 1984 [74], studies on integrin-targeted peptides in cancer diagnosis and treatment have become popular [75]. Interestingly, some of the artificial integrin-targeted peptide mimics act as antagonists that can inhibit integrin-mediated functions [76,77]. Through modification with integrin-targeted peptides, these NPs have been shown to exhibit not only high affinity to integrin-overexpressing cancer cells but also potential efficacy to suppress cancer progression through the inhibition of integrin-mediated functions [78,79].

In addition to the above-described features, the intercellular uptake and trafficking of integrins constitute another process that might be related to the efficacy of NPs. After binding to ECM ligands, integrins trigger 'outside-in' signals that promote downstream signaling to regulate the above-described cell behaviors [80]. Consequently, ligand-bound integrins are internalized by cells for focal adhesion turnover mainly by clathrin-mediated endocytosis and then transported to late endosomes or lysosomes [81]. In the acidic environment of late endosomes or lysosomes, some integrins are detached from the binding ligands, and the unbound free integrins are recycled back to the plasma membrane [80,82]. Incidentally, the required factors for regulating the recycling of integrins back to the plasma membrane are specifically upregulated in cancer cells and thus related to cancer progression [80,82]. Due to these characteristics (endocytosis and recycling of integrins), the integrin-targeted NPs are able to interact with integrins on the cell surface and are effectively internalized by the cancer cells together with the ligand [83], and some of these NPs accumulate in late endosomes and lysosomes [78].

2. Ligands Used in Integrin-Targeted NPs

By modification with integrin-targeted ligands on their surface, NPs can specifically target integrin-expressing cancer cells. As described above, the RGD motif is the first-discovered and the most widely studied integrin-targeted ligand [74] and can be recognized by integrins that are important for cancer progression and metastasis, including αvβ3-, αvβ5-, αvβ6-, αvβ8-, and α5β1-integrins [73]. In addition to the RGD motif, several non-RGD motifs have also been found to serve as specific integrin-target ligands and have characteristics that differ from those of RGD motifs (see below).

2.1. RGD-Based Integrin-Targeted Ligands

The RGD sequence has been found in many ECM proteins, including fibronectin [74], vitronectin [84], von Willebrand factor [85], osteopontin [86], and laminin [87]. The RGD-containing peptides can generally be divided into those with linear and those with cyclic structures. The cyclic RGD (cRGD) peptides display higher activity than the linear RGD peptides due to a less flexible conformational structure that resists proteolysis [88,89]. To enhance the biological properties and pharmacokinetics of RGD peptides, including their affinity, various strategies have been used to modify the structure of RGD peptides, such as altering their structure [90] and the stereochemical configuration of the constituent amino acids [91], introducing other amino acids to flank the RGD sequence [92], and *N*-methylation [93,94]. The modification of NPs with RGD peptides could increase their binding affinity to specific integrins. For example, Maltsev et al. transformed the long binding helix of an RGD ligand to an enzymatically stable cyclic peptide endowed with subnanomolar binding affinity toward the αvβ6-integrin receptor [90], and the resulting molecule could be used for intraoperative cytological assessment of bony resection margins in patients with head and neck cancer [95]. Cilengitide (Merck, Germany), an *N*-methylated cRGDfV derivative [c(RGDfNMeVal)], is a very potent antagonist of αvβ3-, αvβ5-, and α5β1-integrins [96]. Compared with other compounds, Cilengitide exhibits significantly higher binding affinity for these integrins [97]. Although Cilengitide failed to improve the treatment outcomes of glioblastoma multiforme in phase III clinical trials [98], NPs modified with Cilengitide show promising results in preclinical research [99]. Other well-known RGD peptides include cRGDfV [91] (the parent peptide of Cilengitide), cRGDfK [100], and RGD4C (ACDCRGDCFCG) [101].

In addition, iRGD (CRGDK/RGPD/EC), a relatively new compound, was produced to induce a multistep tumor-targeting process that differs from that of the other RGD peptides [102]. After binding to αv-integrins, iRGD is cleaved by a protease to expose the binding motif for neuropilin-1. Consequently, the iRGD-conjugated material is transferred from the integrins to neuropilin-1 and deeply penetrates into the tumor. This unique delivery method has been used in ongoing research in the field of cancer nanomedicine [103].

2.2. Non-RGD Integrin-Targeted Ligands

In addition to the RGD peptide, the Asp-Gly-Arg (NGR) peptide is an integrin-binding motif found in fibronectin [104]. On the basis of the structure of the NGR peptide, another peptide motif, isoDGR, which is found in fibronectin, was produced by in situ rearrangement to convert asparagine into iso-aspartate [105]. A survey of the binding affinity of integrin-targeted ligands to integrins revealed that the compound c(phgisoDGRk), which contains isoDGR, shows high affinity to αvβ6-, αvβ8-, and α5β1-integrins [97]. Several groups have used isoDGR ligands to modify NPs to target integrins [106,107]. Another non-RGD pentapeptide derived from the synergy domain of fibronectin is Ac-PHSCN-NH_2, which was clinically developed under the trade name ATN-161 for the treatment of several solid tumors [36,108] due to its high affinity for α5β1-integrin and relatively lower affinity for αvβ3- and αvβ5-integrins [109]. Other integrin-targeted peptidomimetics, including SCH221153 (αvβ3- and αvβ5-integrin specific), BCH-15046 (αvβ3-, αvβ5-, and α5β1-integrin specific), SJ749 (α5β1-integrin specific), JSM6427 (α5β1-integrin specific), and A20FMDV2 (αvβ6-integrin specific), have been developed, and these have shown anticancer activities in preclinical models and when used on NPs [110,111].

In addition to the ECM-related peptides, tetraiodothyroacetic acid (tetrac), a thyroid hormone analog, has recently been used as an αvβ3-integrin-targeted ligand. Thyroid hormones induce tumor growth and angiogenesis via αvβ3-integrin [112,113]. On the basis of this concept, researchers have used tetrac to manufacture integrin-targeted NPs, which have recently shown promising results in preclinical studies [114,115].

3. Applications of NPs in Cancer Diagnosis

NPs have a wide range of applications, particularly in the field of molecular imaging. The introduction of molecular imaging to cancer diagnosis has provided a new approach for understanding tumor characteristics without depending on invasive diagnostic procedures [116]. Kircher et al. [117] defined molecular imaging as the noninvasive imaging of cellular and subcellular events. The advent of nanotechnology has led to the use of NPs in cancer diagnosis, and this targeted molecular imaging method offers a better approach for detecting cancer cells.

NPs with conjugated integrin-targeted ligands can be used to obtain images of integrins [118–121], which are overexpressed in many cancer cells and angiogenic vessels, as previously described. Among the advantages of imaging integrins, the following are specific to clinical cancer diagnosis: (i) the imaged integrins can be used to identify integrin-overexpressing tumors, which represent highly invasive or high-grade tumor disease for which a precise personalized cancer treatment can be applied; (ii) tumor imaging can lead to the early detection of metastatic disease; and (iii) the imaging of tumors can reveal tumor neoangiogenic activity that requires antiangiogenic therapies. The composition of the integrin-targeted NPs is an important factor for obtaining precise and useful integrin images. In addition, selecting the appropriate diagnostic tool for imaging integrins is another important issue to consider. Several imaging modalities have been employed for accurate cancer diagnoses, but different studies have shown that positron emission tomography (PET) imaging [2], magnetic resonance imaging (MRI) [122], fluorescence reflectance imaging (FRI) [123], and fluorescence molecular tomography (FMT) [3] are particularly effective methods for imaging integrin-targeted NPs due to their high spatial resolution and ability to capture images in real time.

In this section, we review the representative means for fabricating and characterizing integrin-targeted NPs for use in cancer diagnosis and then describe the associated techniques.

3.1. Fabrication of Integrin-Targeted NPs for Cancer Diagnosis

To obtain highly precise images of integrins targeted by NPs, several factors should be considered. Montet et al. [123] used cRGD-conjugated fluorescence-based NPs to detect integrin-expressing cancer cells in tumor-bearing mice through MRI, FRI, and FMT images. These researchers suggested that (i) the expression level of integrins in tumor cells, (ii) the pharmacokinetics of NPs (which should have a sufficient half-life in blood to slowly escape from the vasculature over a long circulation time), and (iii) the vascularized nature of tumors (through which NPs enter the cancer cells efficiently) are the factors that influence RGD-conjugated NPs to allow the efficient imaging of integrins.

In addition to the detection of integrin-expressing cancer cells at their site of origin, NPs can be used for the early detection of metastatic cancer cells, which makes NPs attractive for use in cancer diagnosis. A significant proportion of deaths result from cancer metastases [124]. Several studies have suggested that early metastatic cancer cells can be targeted with NPs [125,126], although the targeting of metastatic cancers with nano-objects, which have a relatively small size and low vascularization, has proven to be a Herculean task. To achieve this goal, Peiris et al. fabricated chain-shaped NPs with c(RGDfC) conjugated on their surfaces for tumoral vascular targeting [3]. Nanochain technology was deployed to fabricate four iron oxide nanospheres [127] that were then fused with cRGD to create chain-shaped NPs, and the resulting NPs were linearly assembled via chemical reaction [128]. Due to the high metastatic potential of 4T1 breast cancer cell lines [129], Peiris et al. used 4T1 tumor-bearing mice to evaluate the uptake of the NPs by metastatic cancer cells [3]. These researchers reported that the cRGD-conjugated chain-shaped NPs have the potential to detect metastatic tumors in addition to primary tumors.

Similarly, another study fabricated RGD peptides with green fluorescent zinc oxide nanowires (ZnO-NWs) [130]. Zinc oxide is a biocompatible multifunctional material with excellent piezoelectric and pyroelectric properties that can be used as a medical fluorescent material [131,132]. In addition, the low toxicity and biodegradable properties of nanomaterials in the human body are also important features of ZnO and make it a great candidate for use in cancer nanomedicine [133]. To produce compact and useful ZnO-based NPs for cancer diagnosis, Hong et al. synthesized specific green fluorescent ZnO-NWs and further conjugated ZnO-NWs with the c(RGDyK) peptide to target αvβ3-integrin [130]. These researchers demonstrated the usefulness of ZnO-NWs for the cancer-targeted optical imaging of U87MG human glioblastoma cells with high αvβ3-integrin expression. However, αvβ3-integrin-negative cells, such as MCF-7 human breast cancer cells, did not show fluorescence signals.

Biocompatible QDs conjugated with RGD peptides have also been considered nanomaterials for detecting the tumor vasculature [134]. The introduction of QDs for biological and optical imaging was largely based on the ability to deliver these nanosized objects to cancer cells [134,135]. In fact, Cai Weibo et al. reported the use of QDs conjugated with the RGD peptide (QD705) for imaging the αvβ3-integrin-positive tumor vasculature in living mice [134]. The study also reported that during angiogenesis, the overexpression of αvβ3-integrin was detected in the tumor vasculature, and this observation paved the way for using QDs for optical integrin-targeted imaging in cancer diagnosis. Similarly, Smith et al. investigated the tumor neovasculature in mice by conjugating the QDs with RGD peptide, which bind to luminal endothelial cells, to capture images of αvβ3-integrin [136]. These researchers revealed that QDs bind aggregately rather than individually, which indicates the unexpected distribution pattern of αvβ3-integrin in the tumor neovasculature. However, the challenge of using QDs is that their large size causes them to be retained in the vascular system, which could restrict their exudation from the blood vessels and lead to diffusion to cells distant from the vessels. It has been reported that these effects could potentially induce toxicity to normal tissues and thus reduce the imaging efficiency and sensitivity of QDs [137]. To correct this anomaly, an ultra-small sized

luminescent silver sulfide (Ag_2S) NP was developed, and the resulting Ag_2S QDs induced negligible toxicity in tissues [138]. In contrast, Lin et al. synthesized ultrasmall superparamagnetic iron oxide NPs (USIO-NPs) using a coprecipitation method and conjugated the USIO-NPs with RGD peptides to target integrins [139]. Their study further revealed that RGD-conjugated USIO-NPs have the potential to differentiate human cancer tumors and cells with different integrin expression levels, such as MCF-7, A549, HT-29, and HT-1080 cells [139].

3.2. Techniques for Imaging Integrin-Targeted NPs

As described above, PET [2], MRI [122], FRI [123], and FMT [3], among others, have proven to be effective methods for imaging integrin-targeted NPs. With the aid of a small-animal PET system, tumor imaging has been performed with iodine-124 dimeric cyclic RGDyk upconversion nanophosphors [^{124}I-(cRGDyk)$_2$-UCNPs] in a U87MG tumor model [2]. Images of αvβ3-integrin were taken after the administration of a conjugated radionuclide during PET scanning, which lasted for approximately 1 h.

In contrast, MRI technology is considered an effective imaging modality due to its high spatial resolution and its non-reliance on ionizing radiation (IR). In fact, Vargas et al. suggested that diffusion-weighted MRI can be used to detect aggressiveness in certain malignancies [140]. Goswami et al. conjugated cRGD peptides to a vertex-differentiated contrast agent, [closo-B12]$^{2-}$ (CA-12), and investigated its ability to target αvβ3-integrin following in vivo MRI analysis [122]. The study confirmed the ability of cRGD-conjugated CA-12 to selectively target αvβ3-integrin while inducing negligible toxicity in the site injected with the contrast agent. This kind of study might improve MRI by overcoming its low specificity in several situations (such as the false-positive rate of 10% for breast cancer [141]) and are thus likely to have a significant impact on cancer diagnosis in the future.

Additionally, optical imaging is considered a suitable preference for imaging cellular and molecular processes due to its high sensitivity. In further prospective research, Akers et al. [142] reported that for imaging αvβ3-integrins, RGD-conjugated NPs can be used to delineate tumor-induced angiogenesis by optical imaging. They suggested that when developing new molecular agents for cancer imaging, the animal model selected might influence the outcome. The use of multiple animal models is important for assessing the robustness of these molecular agents with high tumor-to-surrounding tissue contrast.

4. Applications in Cancer Treatment

4.1. Drug Delivery

A conventional method of treating cancer involves chemotherapy. However, systemic toxicity, severe side effects, and the inability to achieve sufficient drug accumulation in the tumor remain the current challenges associated with the use of chemotherapeutic agents [143,144]. To overcome these challenges, Tian et al. suggested that innocuous, tissue-specific, and noninflammatory (i.e., avoiding the induction of side effects caused by innate immune activation) delivery technologies should be developed and translated into clinical practice for cancer therapy [145]. Further studies revealed that with the aid of nanotechnology, specifically designed NPs, which act as delivery vehicles, can control therapeutic processes in cancer therapy [146,147]. In fact, several studies on the use of ligand-mediated "smart drug delivery systems" have revealed that therapeutic agents can be more specifically transported to tumor sites by targeting αvβ3-integrins on cancer cells, and these types of agents have proven to be efficient in a cancer therapy regime [148–151]. Several typical chemotherapeutic agents, such as doxorubicin [145,152–154], cisplatin [149], and paclitaxel [155–157], have been combined with RGD-conjugated NPs to target integrin-overexpressing tumors.

Doxorubicin is an important cancer therapeutic agent that is currently used as the standard treatment for many neoplastic diseases. However, it has also been reported that the dose-dependent cardiac toxicity of this agent, which leads to cardiomyopathy, has limited its clinical use [158]. To overcome the short biological half-life and adverse effects of doxorubicin, polymer-based NPs conjugated with RGD peptides were developed to deliver doxorubicin directly to a tumor

site [159–162]. Moreover, a similar study using RGD-conjugated polymer-based NPs further modified these NPs with organelle-targeting ligands [163]. In the study, the NPs that targeted the nucleus, which were achieved with RGD4C-PEO-b-P(CL-Hyd-DOX) (RGD ligand poly(ethylene oxide)-block-poly(ε-caprolactone) with doxorubicin conjugated to the core using pH-sensitive hydrazone bonds), induced the highest cytotoxic response in doxorubicin-sensitive cancer cells, and the mitochondrion-targeted NPs, which were obtained with RGD4C-PEO-b-P(CL-Ami-DOX) (RGD ligand poly(ethylene oxide)-block-poly(ε-caprolactone) with doxorubicin conjugated to the core using stable amide bonds), induced the highest cytotoxic response in doxorubicin-resistant cancer cells [163]. In addition to polymer-based NPs, Tian et al. manufactured iRGD-conjugated exosomes (iRGD-Exos) by engineering immature murine dendritic cells with the aim of producing drug-carrier NPs that induce low inflammatory and toxicity [145]. The iRGD-Exos were loaded with doxorubicin by electroporation to create iRGD-Exos-Dox. Compared with doxorubicin alone or Exos-Dox without iRGD conjugation, iRGD-Exos-Dox exerted a superior cytotoxic effect in αv-integrin-positive breast cancer cells in both in vitro and in vivo experiments. The study suggests a possible clinical approach for using an integrin-targeted exosome-based drug delivery system for the treatment of tumor disease [145].

In addition to doxorubicin, cisplatin is a widely used anticancer drug [164]. It has been estimated that only a small proportion (only 1% or less) of the Pt(II) compound cisplatin is delivered to the cells and binds to DNA, whereas a significant proportion (approximately 90%) is targeted toward proteins and low-molecular weight biomolecules [165,166]. To overcome this disparity, a novel method was developed to convert Pt(IV) complexes into prodrugs that can be intracellularly activated by reduction to generate Pt(II), and as a result, a large fraction of platinum can be delivered to the cancerous cells [166]. Graf et al. [149] synthesized a polymeric NP system that consists of an encapsulated Pt(IV) prodrug and cRGD peptides targeted to αvβ3-integrin on cancer cells and performed in vitro tests. Their results revealed that the synthesized NPs exhibited enhanced cytotoxicity compared with cisplatin administered at its conventional dosage in prostate and breast cancer cell lines.

Other chemotherapeutic drugs, such as paclitaxel, which has the trade names Taxol and Abraxane [155,156]; cetuximab, which is also known as Erbitux [167]; and temozolomide, which is an oral alkylating chemotherapeutic drug [168], have shown strategic promise in cancer therapy when loaded onto integrin-targeted NPs, which has resulted in an improved treatment efficacy.

Different therapeutic agents induce cytotoxic effects in cancer cells via different mechanisms and thereby produce drug resistance in different ways [169]. Hence, the simultaneous combination of different chemotherapeutic agents for the treatment of tumor disease has been used to improve the therapeutic outcomes. However, the therapeutic outcomes of combination chemotherapy remain unsatisfactory due to discrepancies in tumor uptake and their different pharmacokinetic profiles [170]. These obstacles can be overcome by nanomedicine. Several studies used integrin-targeted NPs and loaded them with two different therapeutic agents. For example, some researchers loaded topotecan (TPT) and quercetin (QT) on mesoporous silica NPs for the treatment of integrin-expressing breast cancer cells [171], another group loaded paclitaxel and cisplatin onto RGD-conjugated lipid-polymer NPs for the treatment of lung tumor [172], and another study combined doxorubicin with c-Myc small interfering RNA (siRNA) and loaded these onto RGD-conjugated NPs [173]. These new-generation NP-based drugs provide a promising future for improving chemotherapy.

4.2. Radiotherapy, Hyperthermia Therapy, and Photodynamic Therapy

In addition to serving as drug delivery carriers, NPs have other applications, such as enhancers or producers of therapeutic effects by themselves. These types of NPs are mainly metal-based NPs, which can cause greater damage directly in cancer cells following external excitation. In this section, we discuss the application of integrin-targeted NPs in radiotherapy, photothermal therapy (PTT), magnetic hyperthermia therapy (MHT), and photodynamic therapy (PDT).

4.2.1. Radiotherapy

Radiotherapy is one of the standard and effective cancer therapies based on IR. Over the last decades, clinical and in vitro studies have revealed that elements with a high atomic number (Z) can enhance the external radiation effect [174,175]. The application of IR to high-Z material generates several types of emissions, including scattered X-rays/photons, photoelectrons, Compton electrons, Auger electrons, and fluorescence photons, which can enhance the radiation effect in the area around the high-Z material [176]. With recent advances in nanomedicine, the application of high-Z metals as radiosensitizers has attracted the interest of researchers in radiation oncology. Among the high-Z metals, gold (Au, Z = 79) is the element most often used as an NP platform. Gold NPs (AuNPs) possess several advantages over other materials: (i) good biocompatibility, as indicated by the ease with which AuNPs enter the human body without inducing harmful effects [177]; (ii) the straightforward nature of the synthesis of different-sized AuNPs [178]; and (iii) the easy functionalization of AuNPs by conjugating ligands to its surface [179]. These characteristics have inspired individuals to conjugate integrin-targeted ligands to the surface of AuNPs, which illustrates the concept of "targeted radiosensitizers". We have reported the radiosensitizing effects of RGD-conjugated polyethylene-glycosylated AuNPs (RGD/P-AuNPs) on integrin-overexpressing breast cancer cells [78]. Our study showed that RGD/P-AuNPs are efficaciously internalized into integrin-overexpressing cancer cells subjected to an increase in radiation-induced DNA damage. Interestingly, the IR-induced invasiveness [180] was also suppressed by the RGD/P-AuNPs [78]. Several studies have revealed that some cancer cells that survive radiotherapy might exhibit enhanced invasiveness (IR-enhanced invasiveness) [181,182] or acquire an invasive phenotype [183], which might lead to a higher proportion of distal recurrences after radiotherapy. Because integrins play important roles in cancer invasion and migration [184], it is not surprising that integrin-targeted NPs may influence the IR-induced invasiveness of cancer cells. However, although invasion is an important hallmark of cancer cells [185], most studies on nanomedicine have not focused on the effect of cancer invasion after integrin-targeted NP treatment. Hence, the evaluation of cancer cell invasiveness in studies on integrin-targeted NPs would provide important and useful information for researchers in the field of cancer biology and nanomedicine. Consistent with our in vitro study, an in vivo study performed by Liang et al. [186] demonstrated the capacity of RGD-conjugated AuNPs to increase the therapeutic effect of IR. These researchers produced c(RGDyC)-AuNPs and reported that c(RGDyC)-AuNPs are more highly accumulated in tumors compared with non-RGD-conjugated AuNPs. Their results also showed that the use of c(RGDyC)-AuNPs followed by radiotherapy effectively reduces the tumor size. In addition to conventional X-ray irradiation, Enferadia et al. [187] used protons (particle radiotherapy) combined with c(RGDfK)-conjugated ultrasmall AuNPs (1.8-nm diameter) in a murine glioma cell model and compared the results with those obtained with kilovolt and megavolt X-ray therapy. Their results showed that the c(RGDfK)-AuNPs enhanced the efficacy of all the combined treatments, but no obvious differences were found between the different radiation modalities.

In addition to sensitizing cells to external IR treatment, another approach is the conjugation of radiolabeled peptides to AuNPs. Vilchis-Juárez et al. produced c[RGDfK(C)] conjugated-^{177}Lu-Labeled AuNPs (^{177}Lu-AuNP-RGD) and validated their therapeutic effect in glioma-bearing mice [188]. Their results showed that Lu-AuNP-RGD delivered the most highly absorbed tumor radiation dose in tumor cells compared to that of Lu-AuNPs or Lu-RGD. The uptake of Lu-AuNP-RGD by nontargeted organs was low in the treated mice. As described above, the therapeutic efficacy of both external radiotherapy and radioactive treatment can be enhanced by integrin-targeted AuNPs.

4.2.2. Hyperthermia Therapy

Hyperthermia therapy (also known as thermotherapy) generally described the use of heat (i.e., a temperature higher than the normal body temperature (>37 °C)) to treat disease [189]. The use of hyperthermia as a method for treating cancer has a long history, dating back to approximately 3000 B.C. in ancient Egypt [190]. The temperature used in hyperthermia cancer treatments can be categorized as

nonlethal (39 to 42 °C) or lethal (>42 °C). At a nonlethal temperature, tumor oxygenation is improved, which makes cancer cells more sensitive to radiotherapy or chemotherapy [191]. At lethal temperatures, cancer cells are more greatly damaged than normal cells because heat cannot be readily dissipated by the circulating blood in tumor tissue [192]. Although hyperthermia research continues to improve adjuvant or direct therapy, the means of heating tumor tissue to an effective temperature remains a critical problem. Conventional external heat sources, such as microwave or ultrasound, have limited by their inability to conduct heat to a high depth in tumor tissues [193]. With the advancement of nanomedicine, several metal NPs were found to have a high capacity to induce heat through energy transduction [194]. This phenomenon introduced the "inside-out" hyperthermia therapy because the heat source, an NP, is placed in the cancer cells. According to their different trigger approaches, these types of therapy can be generally identified as PTT and MHT. Photothermal therapy usually utilizes external near-infrared (NIR) radiation (wavelength from 750 to 2500 nm) to irradiate the light-absorbing NPs that accumulate in cancer cells. The absorption and scattering of NIR radiation in the human body are minimal but can increase the temperature of light-absorbing NPs to higher than 42 °C [195]. The most characterized light-absorbing NP platform is based on AuNPs due to their incomparable absorbance of NIR radiation [196]. Several studies have shown promising results regarding the use of cRGD-conjugated AuNPs in PTT for the treatment of breast cancer cells [197], melanoma cells [198], and human glioma cell-bearing mice [199]. In addition to AuNPs, NPs of copper sulfide (CuS) also show good photothermal properties and can thus be used in PTT. A study used cRGD-conjugated CuS NPs to treat human gastric tumor cell-bearing mice by PTT, and the results showed that cRGD-CuS NPs selectively entered primary and lymph node metastatic tumor cells to treat cancer without obvious side effects [200]. In addition to using the hyperthermia effect of Cu to kill cancer cells, novel Cu-based NPs were recently developed to induce cancer cell cytotoxicity using another approach [14]. Vinyl azide, a cytotoxicity agent, is encapsulated into c(RGDfE)-conjugated hollow copper sulfide NPs. Upon NIR irradiation, the local temperature increases to trigger the vinyl azide to rapidly release N_2 bubbles, and these N_2 bubbles instantly explode to destroy the neovasculature that expresses $\alpha v\beta 3$-integrin and further induce necrosis of the surrounding tumor cells. This notion, which was inspired by PTT, provides a novel approach in cancer nanomedicine for the future development of more effective therapies.

In contrast to PTT, MHT utilizes an alternating magnetic field (AMF) instead of irradiating light to generate heat in magnetic NPs. Iron oxide NPs (or ferrite NPs) are the most studied magnetic NPs to date. A study showed that cRGD-conjugated iron oxide NPs can be used for tumor detection by MRI and induce MHT to treat cancer cells [201]. However, although MHT is the oldest and best-known external localized heat therapy, the use of AMF is complicated, and the heating efficacy of MHT is unclear compared with that of PTT, the application of MHT faces challenges. A study used RGD peptide-conjugated magnetosomes (synthesized by magnetotactic bacteria, which show efficacy for MHT) to treat human prostatic and uterine cancer cells by PHT and MHT excitation, respectively [202], and their results showed that PHT was much more efficient than MHT in both cellular and in vivo models. Therefore, identification of the appropriate approaches for inducing hyperthermia therapy should be carefully considered.

Although the use of hyperthermia as the single cancer treatment modality still faces many challenges [192], recent studies have yielded promising results from the combination of hyperthermia with other treatment modalities, such as chemotherapy [203], radiotherapy [204], and immunotherapy [205]. With the assistance of integrin-targeted NPs, the application of hyperthermia to increase the therapeutic efficacy of other treatments might become more feasible and can possibly improve cancer therapy.

4.2.3. Photodynamic Therapy

Photodynamic therapy (PDT) for cancer deploys the use of photosensitizing agents that are injected into the bloodstream and transmitted to cancerous cells and thereby expose a tumor

to a wavelength of light that causes the direct killing of cancer cells or shrinkage of the tumor volume [206,207]. To specifically deliver photosensitizing agents into cancer cells, several studies have used integrin-targeting NPs as carriers. Wang et al. conjugated carboxyl functionalized iron oxide NPs with a fibronectin-mimetic peptide (PR_b, [KSSPHSRN(SG)$_5$RGDSP]) [208], which contains RGD and another fibronectin sequence, Pro-His-Ser-Arg-Asn (PHSRN) [209], that binds integrins. The study revealed that the combination of a second-generation photosensitizing agent, Pc 4, with these RGD-conjugated iron oxide NPs showed promising advantages compared with ordinary Pc 4 in the treatment of head and neck cancer. In addition, the combination of Pc 4 with these NPs also improved the MRI contrast [208]. Li et al. used c[RGDfK(Ac-SCH$_2$CO)] peptides conjugated with albumin-based NPs with a photosensitizer IRDye 700DX to treat ovarian cancer in three dimensional (3D) culture, and the results showed a significant cytotoxic effect in cancer cells [210]. Other studies have also shown promising results regarding the use of integrin-targeted NPs to deliver photosensitizing agents to cancer cells [211–213].

5. Issues of Integrin-Targeted NPs

The modification of NPs with integrin-targeted ligands has become a useful practice in cancer nanomedicine, but several issues remain to be considered. For example, integrin-targeted NPs might have a lower efficacy for the treatment of low-integrin-expressing cancer cells. To overcome this problem, some groups have attempted to mix different ligands to enhance the targeting ability of the NPs; for example, some researchers have conjugated RGD and folate (to target the folate receptor, which is overexpressed in many tumor cells) together [214] or have used an anti-vascular endothelial growth factor (VEGF) aptamer together with RGD on NPs [215]. Another problem is the localization of AuNPs in cells. As described above, integrin-targeted NPs mainly accumulate in late endosomes and lysosomes [78]. This localization suggests that NPs appear to work in lysosomes, but in some situations, the function of the lysosomes might decrease NP efficacy. For example, some studies have used NPs to deliver siRNA into cancer cells for gene therapy, but the siRNA might be digested in lysosomes [216]. To overcome this problem, several strategies for facilitating endosome escape, such as ion pair formation, the "proton sponge effect", destabilization of the endosome membrane, and the hydrophobic modification of the NPs, have been researched [217]. These types of efforts might compensate for the shortage of integrin-targeted peptides and achieve the goal of using NPs to reach the anticipated goals.

6. Conclusions

The use of integrin-targeted NPs significantly improves the efficacy of cancer nanomedicine. The benefit of these integrin-targeted NPs has been comprehensively examined in various applications of cancer nanomedicine. We believe that the use of integrin-targeted NPs will be widely used in the future in clinical settings, where they will improve the efficacy of cancer diagnosis and treatment.

Author Contributions: Conceptualization, P.-H.W. and J.-M.N.; writing—original draft preparation, P.-H.W. and A.E.O.; writing—review and editing P.-H.W., Y.O., and J.-M.N.; and preparation of figures and tables, P.-H.W. All the authors read and approved the final manuscript.

Funding: This research was supported in part by the Global Station for Quantum Medical Science and Engineering (GSQ), Global Institution for Collaborative Research and Education (GI-CoRE) at Hokkaido University and a Grant-in-Aid from Scientific Research (C) to J.-M.N.

Acknowledgments: We would like to thank Chou Chih-An for critically reading the manuscript.

Conflicts of Interest: The authors declare no conflict of interest.

List of Abbreviations

AuNPs	**Gold NPs**
3D	three dimensional
CA-12	$[closo\text{-}B12]^{2-}$
cRGD	Cyclic RGD
ECM	Extracellular matrix
EPR	Enhanced permeability and retention
Exos	Exosome
FDA	The food and drug administration of America
FMT	Fluorescence molecular tomography
FRI	Fluorescence reflectance imaging
IR	Ionizing radiation
Lu-AuNP-RGD	RGD conjugated-^{177}Lu-Labeled AuNPs
MHT	Magnetic hyperthermia therapy
MRI	Magnetic resonance imaging
NIR	Near-infrared
NP	Nanoparticle
PDT	Photodynamic therapy
PET	Positron emission tomography
PEGylated	polyethylene glycosylated
PHSRN	Pro-His-Ser-Arg-Asn
PTT	Photothermal therapy
QDs	Quantum dots
QT	Quercetin
RGD	Arg-Gly-Asp
RGD/P-AuNPs	RGD-conjugated polyethylene-glycosylated AuNPs
siRNA	Small interfering RNA
Tetrac	Tetraiodothyroacetic acid
TPT	Topotecan
USIO-NPs	Ultrasmall superparamagnetic iron oxide NPs
VEGF	Vascular endothelial growth factor
Z	Atomic number
ZnO-NWs	Zinc oxide nanowires

References

1. Barenholz, Y. Doxil(R)—The first FDA-approved nano-drug: Lessons learned. *J. Control. Release* **2012**, *160*, 117–134. [CrossRef] [PubMed]
2. Lee, J.; Lee, T.S.; Ryu, J.; Hong, S.; Kang, M.; Im, K.; Kang, J.H.; Lim, S.M.; Park, S.; Song, R. RGD peptide-conjugated multimodal NaGdF4:Yb3+/Er3+ nanophosphors for upconversion luminescence, MR, and PET imaging of tumor angiogenesis. *J. Nucl. Med.* **2013**, *54*, 96–103. [CrossRef] [PubMed]
3. Peiris, P.M.; Toy, R.; Doolittle, E.; Pansky, J.; Abramowski, A.; Tam, M.; Vicente, P.; Tran, E.; Hayden, E.; Camann, A.; et al. Imaging metastasis using an integrin-targeting chain-shaped nanoparticle. *ACS Nano* **2012**, *6*, 8783–8795. [CrossRef] [PubMed]
4. Shi, J.; Kantoff, P.W.; Wooster, R.; Farokhzad, O.C. Cancer nanomedicine: Progress, challenges and opportunities. *Nat. Rev. Cancer* **2017**, *17*, 20–37. [CrossRef] [PubMed]
5. Eliasof, S.; Lazarus, D.; Peters, C.G.; Case, R.I.; Cole, R.O.; Hwang, J.; Schluep, T.; Chao, J.; Lin, J.; Yen, Y.; et al. Correlating preclinical animal studies and human clinical trials of a multifunctional, polymeric nanoparticle. *Proc. Natl. Acad. Sci. USA* **2013**, *110*, 15127–15132. [CrossRef] [PubMed]
6. Kim, Y.; Park, E.J.; Na, D.H. Recent progress in dendrimer-based nanomedicine development. *Arch. Pharm. Res.* **2018**, *41*, 571–582. [CrossRef]
7. Czapar, A.E.; Zheng, Y.R.; Riddell, I.A.; Shukla, S.; Awuah, S.G.; Lippard, S.J.; Steinmetz, N.F. Tobacco mosaic virus delivery of phenanthriplatin for cancer therapy. *ACS Nano* **2016**, *10*, 4119–4126. [CrossRef]

8. Liu, C.; Su, C. Design strategies and application progress of therapeutic exosomes. *Theranostics* **2019**, *9*, 1015–1028. [CrossRef]
9. Cha, C.; Shin, S.R.; Annabi, N.; Dokmeci, M.R.; Khademhosseini, A. Carbon-based nanomaterials: Multifunctional materials for biomedical engineering. *ACS Nano* **2013**, *7*, 2891–2897. [CrossRef]
10. Sweet, M.J.; Chesser, A.; Singleton, I. Review: Metal-based nanoparticles; size, function, and areas for advancement in applied microbiology. *Adv. Appl. Microbiol.* **2012**, *80*, 113–142.
11. Martinez-Carmona, M.; Colilla, M.; Vallet-Regi, M. Smart mesoporous nanomaterials for antitumor therapy. *Nanomaterials* **2015**, *5*, 1906–1937. [CrossRef] [PubMed]
12. Fang, M.; Peng, C.W.; Pang, D.W.; Li, Y. Quantum dots for cancer research: Current status, remaining issues, and future perspectives. *Cancer Biol. Med.* **2012**, *9*, 151–163. [PubMed]
13. Mura, S.; Nicolas, J.; Couvreur, P. Stimuli-responsive nanocarriers for drug delivery. *Nat. Mater.* **2013**, *12*, 991–1003. [CrossRef] [PubMed]
14. Gao, W.; Li, S.; Liu, Z.; Sun, Y.; Cao, W.; Tong, L.; Cui, G.; Tang, B. Targeting and destroying tumor vasculature with a near-infrared laser-activated "nanobomb" for efficient tumor ablation. *Biomaterials* **2017**, *139*, 1–11. [CrossRef] [PubMed]
15. Retif, P.; Pinel, S.; Toussaint, M.; Frochot, C.; Chouikrat, R.; Bastogne, T.; Barberi-Heyob, M. Nanoparticles for radiation therapy enhancement: The key parameters. *Theranostics* **2015**, *5*, 1030–1044. [CrossRef] [PubMed]
16. Sohail, A.; Ahmad, Z.; Beg, O.A.; Arshad, S.; Sherin, L. A review on hyperthermia via nanoparticle-mediated therapy. *Bull. Cancer* **2017**, *104*, 452–461. [CrossRef]
17. Greish, K. Enhanced permeability and retention (EPR) effect for anticancer nanomedicine drug targeting. *Methods Mol. Biol.* **2010**, *624*, 25–37.
18. Jain, R.K.; Stylianopoulos, T. Delivering nanomedicine to solid tumors. *Nat. Rev. Clin. Oncol.* **2010**, *7*, 653–664. [CrossRef]
19. Zhang, Y.N.; Poon, W.; Tavares, A.J.; McGilvray, I.D.; Chan, W.C.W. Nanoparticle-liver interactions: Cellular uptake and hepatobiliary elimination. *J. Control. Release* **2016**, *240*, 332–348. [CrossRef]
20. Gref, R.; Minamitake, Y.; Peracchia, M.T.; Trubetskoy, V.; Torchilin, V.; Langer, R. Biodegradable long-circulating polymeric nanospheres. *Science* **1994**, *263*, 1600–1603. [CrossRef]
21. Egeblad, M.; Nakasone, E.S.; Werb, Z. Tumors as organs: Complex tissues that interface with the entire organism. *Dev. Cell* **2010**, *18*, 884–901. [CrossRef] [PubMed]
22. Bertrand, N.; Wu, J.; Xu, X.; Kamaly, N.; Farokhzad, O.C. Cancer nanotechnology: The impact of passive and active targeting in the era of modern cancer biology. *Adv. Drug Deliv. Rev.* **2014**, *66*, 2–25. [CrossRef] [PubMed]
23. Pridgen, E.M.; Alexis, F.; Kuo, T.T.; Levy-Nissenbaum, E.; Karnik, R.; Blumberg, R.S.; Langer, R.; Farokhzad, O.C. Transepithelial transport of Fc-targeted nanoparticles by the neonatal fc receptor for oral delivery. *Sci. Transl. Med.* **2013**, *5*, 213ra167. [CrossRef] [PubMed]
24. Cheng, Y.; Morshed, R.A.; Auffinger, B.; Tobias, A.L.; Lesniak, M.S. Multifunctional nanoparticles for brain tumor imaging and therapy. *Adv. Drug Deliv. Rev.* **2014**, *66*, 42–57. [CrossRef]
25. Muhamad, N.; Plengsuriyakarn, T.; Na-Bangchang, K. Application of active targeting nanoparticle delivery system for chemotherapeutic drugs and traditional/herbal medicines in cancer therapy: A systematic review. *Int. J. Nanomed.* **2018**, *13*, 3921–3935. [CrossRef]
26. Allen, T.M. Ligand-targeted therapeutics in anticancer therapy. *Nat. Rev. Cancer* **2002**, *2*, 750–763. [CrossRef]
27. Wang, Y.; Dossey, A.M.; Froude, J.W., 2nd; Lubitz, S.; Tzur, D.; Semenchenko, V.; Wishart, D.S. PSA fluoroimmunoassays using anti-PSA ScFv and quantum-dot conjugates. *Nanomedicine* **2008**, *3*, 475–483. [CrossRef]
28. Hwang, W.Y.; Foote, J. Immunogenicity of engineered antibodies. *Methods* **2005**, *36*, 3–10. [CrossRef]
29. Nowak, C.; Cheung, J.K.; Dellatore, S.M.; Katiyar, A.; Bhat, R.; Sun, J.; Ponniah, G.; Neill, A.; Mason, B.; Beck, A.; et al. Forced degradation of recombinant monoclonal antibodies: A practical guide. *MAbs* **2017**, *9*, 1217–1230. [CrossRef]
30. Zhou, J.; Rossi, J. Aptamers as targeted therapeutics: Current potential and challenges. *Nat. Rev. Drug Discov.* **2017**, *16*, 181–202. [CrossRef]
31. Cirillo, D.; Pentimalli, F.; Giordano, A. Peptides or small molecules? Different approaches to develop more effective CDK inhibitors. *Curr. Med. Chem.* **2011**, *18*, 2854–2866. [CrossRef] [PubMed]
32. Barczyk, M.; Carracedo, S.; Gullberg, D. Integrins. *Cell Tissue Res.* **2010**, *339*, 269–280. [CrossRef] [PubMed]

33. Cabodi, S.; Di Stefano, P.; Leal Mdel, P.; Tinnirello, A.; Bisaro, B.; Morello, V.; Damiano, L.; Aramu, S.; Repetto, D.; Tornillo, G.; et al. Integrins and signal transduction. *Adv. Exp. Med. Biol.* **2010**, *674*, 43–54. [PubMed]
34. Hamidi, H.; Ivaska, J. Every step of the way: Integrins in cancer progression and metastasis. *Nat. Rev. Cancer* **2018**, *18*, 533–548. [CrossRef]
35. Mahabeleshwar, G.H.; Feng, W.; Reddy, K.; Plow, E.F.; Byzova, T.V. Mechanisms of integrin-vascular endothelial growth factor receptor cross-activation in angiogenesis. *Circ. Res.* **2007**, *101*, 570–580. [CrossRef]
36. Nam, J.M.; Onodera, Y.; Bissell, M.J.; Park, C.C. Breast cancer cells in three-dimensional culture display an enhanced radioresponse after coordinate targeting of integrin alpha5beta1 and fibronectin. *Cancer Res.* **2010**, *70*, 5238–5248. [CrossRef]
37. Xu, Z.; Zou, L.; Ma, G.; Wu, X.; Huang, F.; Feng, T.; Li, S.; Lin, Q.; He, X.; Liu, Z.; et al. Integrin beta1 is a critical effector in promoting metastasis and chemo-resistance of esophageal squamous cell carcinoma. *Am. J. Cancer Res.* **2017**, *7*, 531–542.
38. Roman, J.; Ritzenthaler, J.D.; Roser-Page, S.; Sun, X.; Han, S. Alpha5beta1-integrin expression is essential for tumor progression in experimental lung cancer. *Am. J. Respir. Cell Mol. Biol.* **2010**, *43*, 684–691. [CrossRef]
39. Mierke, C.T.; Frey, B.; Fellner, M.; Herrmann, M.; Fabry, B. Integrin alpha5beta1 facilitates cancer cell invasion through enhanced contractile forces. *J. Cell Sci.* **2011**, *124*, 369–383. [CrossRef]
40. Fabricius, E.M.; Wildner, G.P.; Kruse-Boitschenko, U.; Hoffmeister, B.; Goodman, S.L.; Raguse, J.D. Immunohistochemical analysis of integrins alphavbeta3, alphavbeta5 and alpha5beta1, and their ligands, fibrinogen, fibronectin, osteopontin and vitronectin, in frozen sections of human oral head and neck squamous cell carcinomas. *Exp. Ther. Med.* **2011**, *2*, 9–19. [CrossRef]
41. Hong, Y.M.; Gan, W.G.; Xu, Z.H. Significance of the expression of integrin beta1, VEGF and MVD in hypopharyngeal squamous cell carcinoma. *Genet. Mol. Res.* **2014**, *13*, 6455–6465. [CrossRef] [PubMed]
42. Adachi, M.; Taki, T.; Higashiyama, M.; Kohno, N.; Inufusa, H.; Miyake, M. Significance of integrin alpha5 gene expression as a prognostic factor in node-negative non-small cell lung cancer. *Clin. Cancer Res.* **2000**, *6*, 96–101. [PubMed]
43. Dos Santos, P.B.; Zanetti, J.S.; Ribeiro-Silva, A.; Beltrao, E.I. Beta 1 integrin predicts survival in breast cancer: A clinicopathological and immunohistochemical study. *Diagn. Pathol.* **2012**, *7*, 104. [CrossRef] [PubMed]
44. Pontes-Junior, J.; Reis, S.T.; Bernardes, F.S.; Oliveira, L.C.; Barros, E.A.; Dall'Oglio, M.F.; Timosczuk, L.M.; Ribeiro-Filho, L.A.; Srougi, M.; Leite, K.R. Correlation between beta1 integrin expression and prognosis in clinically localized prostate cancer. *Int. Braz. J. Urol.* **2013**, *39*, 335–342. [CrossRef] [PubMed]
45. Sawada, K.; Mitra, A.K.; Radjabi, A.R.; Bhaskar, V.; Kistner, E.O.; Tretiakova, M.; Jagadeeswaran, S.; Montag, A.; Becker, A.; Kenny, H.A.; et al. Loss of E-cadherin promotes ovarian cancer metastasis via alpha 5-integrin, which is a therapeutic target. *Cancer Res.* **2008**, *68*, 2329–2339. [CrossRef]
46. Danen, E.H.; Ten Berge, P.J.; Van Muijen, G.N.; Van 't Hof-Grootenboer, A.E.; Brocker, E.B.; Ruiter, D.J. Emergence of alpha 5 beta 1 fibronectin- and alpha v beta 3 vitronectin-receptor expression in melanocytic tumour progression. *Histopathology* **1994**, *24*, 249–256. [CrossRef]
47. Cooper, C.R.; Chay, C.H.; Pienta, K.J. The role of alpha(v)beta(3) in prostate cancer progression. *Neoplasia* **2002**, *4*, 191–194. [CrossRef]
48. Hosotani, R.; Kawaguchi, M.; Masui, T.; Koshiba, T.; Ida, J.; Fujimoto, K.; Wada, M.; Doi, R.; Imamura, M. Expression of integrin alphaVbeta3 in pancreatic carcinoma: Relation to MMP-2 activation and lymph node metastasis. *Pancreas* **2002**, *25*, e30–e35. [CrossRef]
49. McCabe, N.P.; De, S.; Vasanji, A.; Brainard, J.; Byzova, T.V. Prostate cancer specific integrin alphavbeta3 modulates bone metastatic growth and tissue remodeling. *Oncogene* **2007**, *26*, 6238–6243. [CrossRef]
50. Vannini, A.; Leoni, V.; Barboni, C.; Sanapo, M.; Zaghini, A.; Malatesta, P.; Campadelli-Fiume, G.; Gianni, T. alphavbeta3-integrin regulates PD-L1 expression and is involved in cancer immune evasion. *Proc. Natl. Acad. Sci. USA* **2019**, *116*, 20141–20150. [CrossRef]
51. Schnell, O.; Krebs, B.; Wagner, E.; Romagna, A.; Beer, A.J.; Grau, S.J.; Thon, N.; Goetz, C.; Kretzschmar, H.A.; Tonn, J.C.; et al. Expression of integrin alphavbeta3 in gliomas correlates with tumor grade and is not restricted to tumor vasculature. *Brain Pathol.* **2008**, *18*, 378–386. [CrossRef] [PubMed]
52. Boger, C.; Kalthoff, H.; Goodman, S.L.; Behrens, H.M.; Rocken, C. Integrins and their ligands are expressed in non-small cell lung cancer but not correlated with parameters of disease progression. *Virchows Arch.* **2014**, *464*, 69–78. [CrossRef] [PubMed]

53. Berghoff, A.S.; Kovanda, A.K.; Melchardt, T.; Bartsch, R.; Hainfellner, J.A.; Sipos, B.; Schittenhelm, J.; Zielinski, C.C.; Widhalm, G.; Dieckmann, K.; et al. Alphavbeta3, alphavbeta5 and alphavbeta6 integrins in brain metastases of lung cancer. *Clin. Exp. Metastasis* **2014**, *31*, 841–851. [CrossRef] [PubMed]
54. Boger, C.; Warneke, V.S.; Behrens, H.M.; Kalthoff, H.; Goodman, S.L.; Becker, T.; Rocken, C. Integrins alphavbeta3 and alphavbeta5 as prognostic, diagnostic, and therapeutic targets in gastric cancer. *Gastric Cancer* **2015**, *18*, 784–795. [CrossRef]
55. Hess, K.; Boger, C.; Behrens, H.M.; Rocken, C. Correlation between the expression of integrins in prostate cancer and clinical outcome in 1284 patients. *Ann. Diagn. Pathol.* **2014**, *18*, 343–350. [CrossRef]
56. Cao, Q.; Chen, X.; Wu, X.; Liao, R.; Huang, P.; Tan, Y.; Wang, L.; Ren, G.; Huang, J.; Dong, C. Inhibition of UGT8 suppresses basal-like breast cancer progression by attenuating sulfatide-alphaVbeta5 axis. *J. Exp. Med.* **2018**, *215*, 1679–1692. [CrossRef]
57. Bello, L.; Francolini, M.; Marthyn, P.; Zhang, J.; Carroll, R.S.; Nikas, D.C.; Strasser, J.F.; Villani, R.; Cheresh, D.A.; Black, P.M. Alpha(v)beta3 and alpha(v)beta5 integrin expression in glioma periphery. *Neurosurgery* **2001**, *49*, 380–389.
58. Peng, Z.W.; Ikenaga, N.; Liu, S.B.; Sverdlov, D.Y.; Vaid, K.A.; Dixit, R.; Weinreb, P.H.; Violette, S.; Sheppard, D.; Schuppan, D.; et al. Integrin alphavbeta6 critically regulates hepatic progenitor cell function and promotes ductular reaction, fibrosis, and tumorigenesis. *Hepatology* **2016**, *63*, 217–232. [CrossRef]
59. Ahmed, N.; Niu, J.; Dorahy, D.J.; Gu, X.; Andrews, S.; Meldrum, C.J.; Scott, R.J.; Baker, M.S.; Macreadie, I.G.; Agrez, M.V. Direct integrin alphavbeta6-ERK binding: Implications for tumour growth. *Oncogene* **2002**, *21*, 1370–1380. [CrossRef]
60. Li, Z.; Biswas, S.; Liang, B.; Zou, X.; Shan, L.; Li, Y.; Fang, R.; Niu, J. Integrin beta6 serves as an immunohistochemical marker for lymph node metastasis and promotes cell invasiveness in cholangiocarcinoma. *Sci. Rep.* **2016**, *6*, 30081. [CrossRef]
61. Liu, S.; Wang, J.; Niu, W.; Liu, E.; Wang, J.; Peng, C.; Lin, P.; Wang, B.; Khan, A.Q.; Gao, H.; et al. The beta6-integrin-ERK/MAP kinase pathway contributes to chemo resistance in colon cancer. *Cancer Lett.* **2013**, *328*, 325–334. [CrossRef]
62. Impola, U.; Uitto, V.J.; Hietanen, J.; Hakkinen, L.; Zhang, L.; Larjava, H.; Isaka, K.; Saarialho-Kere, U. Differential expression of matrilysin-1 (MMP-7), 92 kD gelatinase (MMP-9), and metalloelastase (MMP-12) in oral verrucous and squamous cell cancer. *J. Pathol.* **2004**, *202*, 14–22. [CrossRef]
63. Elayadi, A.N.; Samli, K.N.; Prudkin, L.; Liu, Y.H.; Bian, A.; Xie, X.J.; Wistuba, I.I.; Roth, J.A.; McGuire, M.J.; Brown, K.C. A peptide selected by biopanning identifies the integrin alphavbeta6 as a prognostic biomarker for nonsmall cell lung cancer. *Cancer Res.* **2007**, *67*, 5889–5895. [CrossRef]
64. Moore, K.M.; Thomas, G.J.; Duffy, S.W.; Warwick, J.; Gabe, R.; Chou, P.; Ellis, I.O.; Green, A.R.; Haider, S.; Brouilette, K.; et al. Therapeutic targeting of integrin alphavbeta6 in breast cancer. *J. Natl. Cancer Inst.* **2014**, *106*. [CrossRef]
65. Zhang, Z.Y.; Xu, K.S.; Wang, J.S.; Yang, G.Y.; Wang, W.; Wang, J.Y.; Niu, W.B.; Liu, E.Y.; Mi, Y.T.; Niu, J. Integrin alphanvbeta6 acts as a prognostic indicator in gastric carcinoma. *Clin. Oncol. (R. Coll. Radiol.)* **2008**, *20*, 61–66. [CrossRef]
66. Yang, G.Y.; Guo, S.; Dong, C.Y.; Wang, X.Q.; Hu, B.Y.; Liu, Y.F.; Chen, Y.W.; Niu, J.; Dong, J.H. Integrin alphavbeta6 sustains and promotes tumor invasive growth in colon cancer progression. *World J. Gastroenterol.* **2015**, *21*, 7457–7467. [CrossRef]
67. Hecht, J.L.; Dolinski, B.M.; Gardner, H.A.; Violette, S.M.; Weinreb, P.H. Overexpression of the alphavbeta6 integrin in endometrial cancer. *Appl. Immunohistochem. Mol. Morphol.* **2008**, *16*, 543–547. [CrossRef]
68. Ahmed, N.; Riley, C.; Rice, G.E.; Quinn, M.A.; Baker, M.S. Alpha(v)beta(6) integrin-A marker for the malignant potential of epithelial ovarian cancer. *J. Histochem. Cytochem.* **2002**, *50*, 1371–1380. [CrossRef]
69. Marsh, D.; Dickinson, S.; Neill, G.W.; Marshall, J.F.; Hart, I.R.; Thomas, G.J. Alpha vbeta 6 Integrin promotes the invasion of morphoeic basal cell carcinoma through stromal modulation. *Cancer Res.* **2008**, *68*, 3295–3303. [CrossRef]
70. Takasaka, N.; Seed, R.I.; Cormier, A.; Bondesson, A.J.; Lou, J.; Elattma, A.; Ito, S.; Yanagisawa, H.; Hashimoto, M.; Ma, R.; et al. Integrin alphavbeta8-expressing tumor cells evade host immunity by regulating TGF-beta activation in immune cells. *JCI Insight* **2018**, *3*, e122591. [CrossRef]
71. Jin, S.; Lee, W.C.; Aust, D.; Pilarsky, C.; Cordes, N. Beta8 integrin mediates pancreatic cancer cell radiochemoresistance. *Mol. Cancer Res.* **2019**, *17*, 2126–2138. [CrossRef]

72. Hayashido, Y.; Kitano, H.; Sakaue, T.; Fujii, T.; Suematsu, M.; Sakurai, S.; Okamoto, T. Overexpression of integrin alphav facilitates proliferation and invasion of oral squamous cell carcinoma cells via MEK/ERK signaling pathway that is activated by interaction of integrin alphavbeta8 with type collagen. *Int. J. Oncol.* **2014**, *45*, 1875–1882. [CrossRef]
73. Nieberler, M.; Reuning, U.; Reichart, F.; Notni, J.; Wester, H.J.; Schwaiger, M.; Weinmuller, M.; Rader, A.; Steiger, K.; Kessler, H. Exploring the role of RGD-recognizing integrins in cancer. *Cancers* **2017**, *9*, 116. [CrossRef]
74. Pierschbacher, M.D.; Ruoslahti, E. Cell attachment activity of fibronectin can be duplicated by small synthetic fragments of the molecule. *Nature* **1984**, *309*, 30–33. [CrossRef]
75. Boohaker, R.J.; Lee, M.W.; Vishnubhotla, P.; Perez, J.M.; Khaled, A.R. The use of therapeutic peptides to target and to kill cancer cells. *Curr. Med. Chem.* **2012**, *19*, 3794–3804. [CrossRef]
76. Russo, M.A.; Paolillo, M.; Sanchez-Hernandez, Y.; Curti, D.; Ciusani, E.; Serra, M.; Colombo, L.; Schinelli, S. A small-molecule RGD-integrin antagonist inhibits cell adhesion, cell migration and induces anoikis in glioblastoma cells. *Int. J. Oncol.* **2013**, *42*, 83–92. [CrossRef]
77. Desgrosellier, J.S.; Cheresh, D.A. Integrins in cancer: Biological implications and therapeutic opportunities. *Nat. Rev. Cancer* **2010**, *10*, 9–22. [CrossRef]
78. Wu, P.H.; Onodera, Y.; Ichikawa, Y.; Rankin, E.B.; Giaccia, A.J.; Watanabe, Y.; Qian, W.; Hashimoto, T.; Shirato, H.; Nam, J.M. Targeting integrins with RGD-conjugated gold nanoparticles in radiotherapy decreases the invasive activity of breast cancer cells. *Int. J. Nanomed.* **2017**, *12*, 5069–5085. [CrossRef]
79. Ali, M.R.K.; Wu, Y.; Tang, Y.; Xiao, H.; Chen, K.; Han, T.; Fang, N.; Wu, R.; El-Sayed, M.A. Targeting cancer cell integrins using gold nanorods in photothermal therapy inhibits migration through affecting cytoskeletal proteins. *Proc. Natl. Acad. Sci. USA* **2017**, *114*, E5655–E5663. [CrossRef]
80. Onodera, Y.; Nam, J.M.; Sabe, H. Intracellular trafficking of integrins in cancer cells. *Pharmacol. Ther.* **2013**, *140*, 1–9. [CrossRef]
81. Ezratty, E.J.; Bertaux, C.; Marcantonio, E.E.; Gundersen, G.G. Clathrin mediates integrin endocytosis for focal adhesion disassembly in migrating cells. *J. Cell Biol.* **2009**, *187*, 733–747. [CrossRef]
82. Dozynkiewicz, M.A.; Jamieson, N.B.; Macpherson, I.; Grindlay, J.; van den Berghe, P.V.; von Thun, A.; Morton, J.P.; Gourley, C.; Timpson, P.; Nixon, C.; et al. Rab25 and CLIC3 collaborate to promote integrin recycling from late endosomes/lysosomes and drive cancer progression. *Dev. Cell* **2012**, *22*, 131–145. [CrossRef]
83. Danhier, F.; Pourcelle, V.; Marchand-Brynaert, J.; Jerome, C.; Feron, O.; Preat, V. Targeting of tumor endothelium by RGD-grafted PLGA-nanoparticles. *Methods Enzymol.* **2012**, *508*, 157–175.
84. Suzuki, S.; Oldberg, A.; Hayman, E.G.; Pierschbacher, M.D.; Ruoslahti, E. Complete amino acid sequence of human vitronectin deduced from cDNA. Similarity of cell attachment sites in vitronectin and fibronectin. *Embo J.* **1985**, *4*, 2519–2524. [CrossRef]
85. Plow, E.F.; Pierschbacher, M.D.; Ruoslahti, E.; Marguerie, G.A.; Ginsberg, M.H. The effect of Arg-Gly-Asp-containing peptides on fibrinogen and von Willebrand factor binding to platelets. *Proc. Natl. Acad. Sci. USA* **1985**, *82*, 8057–8061.
86. Oldberg, A.; Franzen, A.; Heinegard, D. Cloning and sequence analysis of rat bone sialoprotein (osteopontin) cDNA reveals an Arg-Gly-Asp cell-binding sequence. *Proc. Natl. Acad. Sci. USA* **1986**, *83*, 8819–8823. [CrossRef]
87. Grant, D.S.; Tashiro, K.; Segui-Real, B.; Yamada, Y.; Martin, G.R.; Kleinman, H.K. Two different laminin domains mediate the differentiation of human endothelial cells into capillary-like structures in vitro. *Cell* **1989**, *58*, 933–943. [CrossRef]
88. Verrier, S.; Pallu, S.; Bareille, R.; Jonczyk, A.; Meyer, J.; Dard, M.; Amedee, J. Function of linear and cyclic RGD-containing peptides in osteoprogenitor cells adhesion process. *Biomaterials* **2002**, *23*, 585–596. [CrossRef]
89. Frochot, C.; Di Stasio, B.; Vanderesse, R.; Belgy, M.J.; Dodeller, M.; Guillemin, F.; Viriot, M.L.; Barberi-Heyob, M. Interest of RGD-containing linear or cyclic peptide targeted tetraphenylchlorin as novel photosensitizers for selective photodynamic activity. *Bioorg. Chem.* **2007**, *35*, 205–220. [CrossRef]
90. Maltsev, O.V.; Marelli, U.K.; Kapp, T.G.; Di Leva, F.S.; Di Maro, S.; Nieberler, M.; Reuning, U.; Schwaiger, M.; Novellino, E.; Marinelli, L.; et al. Stable peptides instead of stapled peptides: Highly potent alphavbeta6-selective integrin ligands. *Angew. Chem. Int. Ed. Engl.* **2016**, *55*, 1535–1539. [CrossRef]

91. Aumailley, M.; Gurrath, M.; Muller, G.; Calvete, J.; Timpl, R.; Kessler, H. Arg-Gly-Asp constrained within cyclic pentapeptides. Strong and selective inhibitors of cell adhesion to vitronectin and laminin fragment P1. *FEBS Lett.* **1991**, *291*, 50–54. [CrossRef]
92. Wang, Y.; Xiao, W.; Zhang, Y.; Meza, L.; Tseng, H.; Takada, Y.; Ames, J.B.; Lam, K.S. Optimization of RGD-containing cyclic peptides against alphavbeta3 Integrin. *Mol. Cancer Ther.* **2016**, *15*, 232–240. [CrossRef]
93. Chatterjee, J.; Gilon, C.; Hoffman, A.; Kessler, H. N-methylation of peptides: A new perspective in medicinal chemistry. *Acc. Chem. Res.* **2008**, *41*, 1331–1342. [CrossRef]
94. Chatterjee, J.; Rechenmacher, F.; Kessler, H. N-methylation of peptides and proteins: An important element for modulating biological functions. *Angew. Chem. Int. Ed. Engl.* **2013**, *52*, 254–269. [CrossRef]
95. Nieberler, M.; Reuning, U.; Kessler, H.; Reichart, F.; Weirich, G.; Wolff, K.D. Fluorescence imaging of invasive head and neck carcinoma cells with integrin alphavbeta6-targeting RGD-peptides: An approach to a fluorescence-assisted intraoperative cytological assessment of bony resection margins. *Br. J. Oral Maxillofac. Surg.* **2018**, *56*, 972–978. [CrossRef]
96. Mas-Moruno, C.; Rechenmacher, F.; Kessler, H. Cilengitide: The first anti-angiogenic small molecule drug candidate design, synthesis and clinical evaluation. *Anticancer Agents Med. Chem.* **2010**, *10*, 753–768. [CrossRef]
97. Kapp, T.G.; Rechenmacher, F.; Neubauer, S.; Maltsev, O.V.; Cavalcanti-Adam, E.A.; Zarka, R.; Reuning, U.; Notni, J.; Wester, H.J.; Mas-Moruno, C.; et al. A Comprehensive Evaluation of the Activity and Selectivity Profile of Ligands for RGD-binding Integrins. *Sci. Rep.* **2017**, *7*, 39805. [CrossRef]
98. Stupp, R.; Hegi, M.E.; Gorlia, T.; Erridge, S.C.; Perry, J.; Hong, Y.K.; Aldape, K.D.; Lhermitte, B.; Pietsch, T.; Grujicic, D.; et al. Cilengitide combined with standard treatment for patients with newly diagnosed glioblastoma with methylated MGMT promoter (CENTRIC EORTC 26071-22072 study): A multicentre, randomised, open-label, phase 3 trial. *Lancet Oncol.* **2014**, *15*, 1100–1108. [CrossRef]
99. Zhao, Y.Z.; Lin, Q.; Wong, H.L.; Shen, X.T.; Yang, W.; Xu, H.L.; Mao, K.L.; Tian, F.R.; Yang, J.J.; Xu, J.; et al. Glioma-targeted therapy using Cilengitide nanoparticles combined with UTMD enhanced delivery. *J. Control. Release* **2016**, *224*, 112–125. [CrossRef]
100. Haubner, R.; Gratias, R.; Diefenbach, B.; Goodman, S.L.; Jonczyk, A.; Kessler, H. Structural and functional aspects of RGD-containing cyclic pentapeptides as highly potent and selective integrin αVβ3 antagonists. *J. Am. Chem. Soc.* **1996**, *118*, 7461–7472. [CrossRef]
101. Koivunen, E.; Wang, B.; Ruoslahti, E. Phage libraries displaying cyclic peptides with different ring sizes: Ligand specificities of the RGD-directed integrins. *Bio/technology* **1995**, *13*, 265–270. [CrossRef]
102. Sugahara, K.N.; Teesalu, T.; Karmali, P.P.; Kotamraju, V.R.; Agemy, L.; Girard, O.M.; Hanahan, D.; Mattrey, R.F.; Ruoslahti, E. Tissue-penetrating delivery of compounds and nanoparticles into tumors. *Cancer Cell* **2009**, *16*, 510–520. [CrossRef]
103. Zuo, H. iRGD: A promising peptide for cancer imaging and a potential therapeutic agent for various cancers. *J. Oncol.* **2019**, *2019*, 9367845. [CrossRef]
104. Arap, W.; Pasqualini, R.; Ruoslahti, E. Cancer treatment by targeted drug delivery to tumor vasculature in a mouse model. *Science* **1998**, *279*, 377–380. [CrossRef]
105. Curnis, F.; Longhi, R.; Crippa, L.; Cattaneo, A.; Dondossola, E.; Bachi, A.; Corti, A. Spontaneous formation of L-isoaspartate and gain of function in fibronectin. *J. Biol. Chem.* **2006**, *281*, 36466–36476. [CrossRef]
106. Curnis, F.; Fiocchi, M.; Sacchi, A.; Gori, A.; Gasparri, A.; Corti, A. NGR-tagged nano-gold: A new CD13-selective carrier for cytokine delivery to tumors. *Nano Res.* **2016**, *9*, 1393–1408. [CrossRef]
107. Chen, Y.; Wu, J.J.; Huang, L. Nanoparticles targeted with NGR motif deliver c-myc siRNA and doxorubicin for anticancer therapy. *Mol. Ther.* **2010**, *18*, 828–834. [CrossRef]
108. Stoeltzing, O.; Liu, W.; Reinmuth, N.; Fan, F.; Parry, G.C.; Parikh, A.A.; McCarty, M.F.; Bucana, C.D.; Mazar, A.P.; Ellis, L.M. Inhibition of integrin alpha5beta1 function with a small peptide (ATN-161) plus continuous 5-FU infusion reduces colorectal liver metastases and improves survival in mice. *Int. J. Cancer* **2003**, *104*, 496–503. [CrossRef]
109. Goodman, S.L.; Picard, M. Integrins as therapeutic targets. *Trends Pharmacol. Sci.* **2012**, *33*, 405–412. [CrossRef]
110. Kapp, T.G.; Rechenmacher, F.; Sobahi, T.R.; Kessler, H. Integrin modulators: A patent review. *Expert Opin. Ther. Pat.* **2013**, *23*, 1273–1295. [CrossRef]
111. Hodgins, N.O.; Al-Jamal, W.T.; Wang, J.T.; Klippstein, R.; Costa, P.M.; Sosabowski, J.K.; Marshall, J.F.; Maher, J.; Al-Jamal, K.T. Investigating in vitro and in vivo alphavbeta6 integrin receptor-targeting liposomal

alendronate for combinatory gammadelta T cell immunotherapy. *J. Control. Release* **2017**, *256*, 141–152. [CrossRef]
112. Bergh, J.J.; Lin, H.Y.; Lansing, L.; Mohamed, S.N.; Davis, F.B.; Mousa, S.; Davis, P.J. Integrin alphaVbeta3 contains a cell surface receptor site for thyroid hormone that is linked to activation of mitogen-activated protein kinase and induction of angiogenesis. *Endocrinology* **2005**, *146*, 2864–2871. [CrossRef]
113. Hsieh, M.T.; Wang, L.M.; Changou, C.A.; Chin, Y.T.; Yang, Y.S.H.; Lai, H.Y.; Lee, S.Y.; Yang, Y.N.; Whang-Peng, J.; Liu, L.F.; et al. Crosstalk between integrin alphavbeta3 and ERalpha contributes to thyroid hormone-induced proliferation of ovarian cancer cells. *Oncotarget* **2017**, *8*, 24237–24249. [CrossRef]
114. Lin, H.Y.; Chin, Y.T.; Nana, A.W.; Shih, Y.J.; Lai, H.Y.; Tang, H.Y.; Leinung, M.; Mousa, S.A.; Davis, P.J. Actions of l-thyroxine and nano-diamino-tetrac (Nanotetrac) on PD-L1 in cancer cells. *Steroids* **2016**, *114*, 59–67. [CrossRef]
115. Yalcin, M.; Bharali, D.J.; Dyskin, E.; Dier, E.; Lansing, L.; Mousa, S.S.; Davis, F.B.; Davis, P.J.; Mousa, S.A. Tetraiodothyroacetic acid and tetraiodothyroacetic acid nanoparticle effectively inhibit the growth of human follicular thyroid cell carcinoma. *Thyroid* **2010**, *20*, 281–286. [CrossRef]
116. Hussain, T.; Nguyen, Q.T. Molecular imaging for cancer diagnosis and surgery. *Adv. Drug Deliv. Rev.* **2014**, *66*, 90–100. [CrossRef]
117. Kircher, M.F.; Willmann, J.K. Molecular body imaging: MR imaging, CT, and US. part I. principles. *Radiology* **2012**, *263*, 633–643. [CrossRef]
118. Yu, X.; Song, S.K.; Chen, J.; Scott, M.J.; Fuhrhop, R.J.; Hall, C.S.; Gaffney, P.J.; Wickline, S.A.; Lanza, G.M. High-resolution MRI characterization of human thrombus using a novel fibrin-targeted paramagnetic nanoparticle contrast agent. *Magn. Reson. Med.* **2000**, *44*, 867–872. [CrossRef]
119. Winter, P.M.; Morawski, A.M.; Caruthers, S.D.; Fuhrhop, R.W.; Zhang, H.; Williams, T.A.; Allen, J.S.; Lacy, E.K.; Robertson, J.D.; Lanza, G.M.; et al. Molecular imaging of angiogenesis in early-stage atherosclerosis with alpha(v)beta3-integrin-targeted nanoparticles. *Circulation* **2003**, *108*, 2270–2274. [CrossRef]
120. Anderson, S.A.; Rader, R.K.; Westlin, W.F.; Null, C.; Jackson, D.; Lanza, G.M.; Wickline, S.A.; Kotyk, J.J. Magnetic resonance contrast enhancement of neovasculature with alpha(v)beta(3)-targeted nanoparticles. *Magn. Reson. Med.* **2000**, *44*, 433–439. [CrossRef]
121. Schmieder, A.H.; Winter, P.M.; Caruthers, S.D.; Harris, T.D.; Williams, T.A.; Allen, J.S.; Lacy, E.K.; Zhang, H.; Scott, M.J.; Hu, G.; et al. Molecular MR imaging of melanoma angiogenesis with alphanubeta3-targeted paramagnetic nanoparticles. *Magn. Reson. Med.* **2005**, *53*, 621–627. [CrossRef]
122. Goswami, L.N.; Ma, L.; Cai, Q.; Sarma, S.J.; Jalisatgi, S.S.; Hawthorne, M.F. cRGD peptide-conjugated icosahedral closo-B12(2-) core carrying multiple Gd3+-DOTA chelates for alpha(v)beta3 integrin-targeted tumor imaging (MRI). *Inorg. Chem.* **2013**, *52*, 1701–1709. [CrossRef]
123. Montet, X.; Montet-Abou, K.; Reynolds, F.; Weissleder, R.; Josephson, L. Nanoparticle imaging of integrins on tumor cells. *Neoplasia* **2006**, *8*, 214–222. [CrossRef]
124. Siegel, R.L.; Miller, K.D.; Jemal, A. Cancer statistics, 2019. *CA Cancer J. Clin.* **2019**, *69*, 7–34. [CrossRef]
125. Goldman, E.; Zinger, A.; da Silva, D.; Yaari, Z.; Kajal, A.; Vardi-Oknin, D.; Goldfeder, M.; Schroeder, J.E.; Shainsky-Roitman, J.; Hershkovitz, D.; et al. Nanoparticles target early-stage breast cancer metastasis in vivo. *Nanotechnology* **2017**, *28*, 43lt01. [CrossRef]
126. Mu, Q.; Wang, H.; Zhang, M. Nanoparticles for imaging and treatment of metastatic breast cancer. *Expert Opin. Drug Deliv.* **2017**, *14*, 123–136. [CrossRef]
127. Peiris, P.M.; Schmidt, E.; Calabrese, M.; Karathanasis, E. Assembly of linear nano-chains from iron oxide nanospheres with asymmetric surface chemistry. *PLoS ONE* **2011**, *6*, e15927. [CrossRef]
128. Peiris, P.M.; Bauer, L.; Toy, R.; Tran, E.; Pansky, J.; Doolittle, E.; Schmidt, E.; Hayden, E.; Mayer, A.; Keri, R.A.; et al. Enhanced delivery of chemotherapy to tumors using a multicomponent nanochain with radio-frequency-tunable drug release. *ACS Nano* **2012**, *6*, 4157–4168. [CrossRef]
129. Tao, K.; Fang, M.; Alroy, J.; Sahagian, G.G. Imagable 4T1 model for the study of late stage breast cancer. *BMC Cancer* **2008**, *8*, 228. [CrossRef]
130. Hong, H.; Shi, J.; Yang, Y.; Zhang, Y.; Engle, J.W.; Nickles, R.J.; Wang, X.; Cai, W. Cancer-targeted optical imaging with fluorescent zinc oxide nanowires. *Nano Lett.* **2011**, *11*, 3744–3750. [CrossRef]
131. Wang, Z.L. Splendid one-dimensional nanostructures of zinc oxide: A new nanomaterial family for nanotechnology. *ACS Nano* **2008**, *2*, 1987–1992. [CrossRef]

132. Hahm, J.I. Zinc oxide nanomaterials for biomedical fluorescence detection. *J. Nanosci. Nanotechnol.* **2014**, *14*, 475–486. [CrossRef]
133. Martinez-Carmona, M.; Gun'ko, Y.; Vallet-Regi, M. ZnO nanostructures for drug delivery and theranostic applications. *Nanomaterials* **2018**, *8*, 268. [CrossRef]
134. Cai, W.; Shin, D.W.; Chen, K.; Gheysens, O.; Cao, Q.; Wang, S.X.; Gambhir, S.S.; Chen, X. Peptide-labeled near-infrared quantum dots for imaging tumor vasculature in living subjects. *Nano Lett.* **2006**, *6*, 669–676. [CrossRef]
135. Matea, C.T.; Mocan, T.; Tabaran, F.; Pop, T.; Mosteanu, O.; Puia, C.; Iancu, C.; Mocan, L. Quantum dots in imaging, drug delivery and sensor applications. *Int. J. Nanomed.* **2017**, *12*, 5421–5431. [CrossRef]
136. Smith, B.R.; Cheng, Z.; De, A.; Koh, A.L.; Sinclair, R.; Gambhir, S.S. Real-time intravital imaging of RGD-quantum dot binding to luminal endothelium in mouse tumor neovasculature. *Nano Lett.* **2008**, *8*, 2599–2606. [CrossRef]
137. Schipper, M.L.; Iyer, G.; Koh, A.L.; Cheng, Z.; Ebenstein, Y.; Aharoni, A.; Keren, S.; Bentolila, L.A.; Li, J.; Rao, J.; et al. Particle size, surface coating, and PEGylation influence the biodistribution of quantum dots in living mice. *Small* **2009**, *5*, 126–134. [CrossRef]
138. Jiang, P.; Zhu, C.N.; Zhang, Z.L.; Tian, Z.Q.; Pang, D.W. Water-soluble Ag(2)S quantum dots for near-infrared fluorescence imaging in vivo. *Biomaterials* **2012**, *33*, 5130–5135. [CrossRef]
139. Lin, R.Y.; Dayananda, K.; Chen, T.J.; Chen, C.Y.; Liu, G.C.; Lin, K.L.; Wang, Y.M. Targeted RGD nanoparticles for highly sensitive in vivo integrin receptor imaging. *Contrast Media Mol. Imaging* **2012**, *7*, 7–18. [CrossRef]
140. Vargas, H.A.; Akin, O.; Franiel, T.; Mazaheri, Y.; Zheng, J.; Moskowitz, C.; Udo, K.; Eastham, J.; Hricak, H. Diffusion-weighted endorectal MR imaging at 3 T for prostate cancer: Tumor detection and assessment of aggressiveness. *Radiology* **2011**, *259*, 775–784. [CrossRef]
141. Blasiak, B.; Van Veggel, F.C.J.M.; Tomanek, B. Applications of nanoparticles for MRI cancer diagnosis and therapy. *J. Nanomater.* **2013**, *2013*, 148578. [CrossRef]
142. Akers, W.J.; Zhang, Z.; Berezin, M.; Ye, Y.; Agee, A.; Guo, K.; Fuhrhop, R.W.; Wickline, S.A.; Lanza, G.M.; Achilefu, S. Targeting of alpha(nu)beta(3)-integrins expressed on tumor tissue and neovasculature using fluorescent small molecules and nanoparticles. *Nanomedicine* **2010**, *5*, 715–726. [CrossRef]
143. Gao, Z.; Zhang, L.; Sun, Y. Nanotechnology applied to overcome tumor drug resistance. *J. Control. Release* **2012**, *162*, 45–55. [CrossRef]
144. Schirrmacher, V. From chemotherapy to biological therapy: A review of novel concepts to reduce the side effects of systemic cancer treatment (Review). *Int. J. Oncol.* **2019**, *54*, 407–419.
145. Tian, Y.; Li, S.; Song, J.; Ji, T.; Zhu, M.; Anderson, G.J.; Wei, J.; Nie, G. A doxorubicin delivery platform using engineered natural membrane vesicle exosomes for targeted tumor therapy. *Biomaterials* **2014**, *35*, 2383–2390. [CrossRef]
146. Akhter, S.; Ahmad, I.; Ahmad, M.Z.; Ramazani, F.; Singh, A.; Rahman, Z.; Ahmad, F.J.; Storm, G.; Kok, R.J. Nanomedicines as cancer therapeutics: Current status. *Curr. Cancer Drug Targets* **2013**, *13*, 362–378. [CrossRef]
147. Meyers, J.D.; Doane, T.; Burda, C.; Basilion, J.P. Nanoparticles for imaging and treating brain cancer. *Nanomedicine* **2013**, *8*, 123–143. [CrossRef]
148. Miura, Y.; Takenaka, T.; Toh, K.; Wu, S.; Nishihara, H.; Kano, M.R.; Ino, Y.; Nomoto, T.; Matsumoto, Y.; Koyama, H.; et al. Cyclic RGD-linked polymeric micelles for targeted delivery of platinum anticancer drugs to glioblastoma through the blood-brain tumor barrier. *ACS Nano* **2013**, *7*, 8583–8592. [CrossRef]
149. Graf, N.; Bielenberg, D.R.; Kolishetti, N.; Muus, C.; Banyard, J.; Farokhzad, O.C.; Lippard, S.J. Alpha(V)beta(3) integrin-targeted PLGA-PEG nanoparticles for enhanced anti-tumor efficacy of a Pt(IV) prodrug. *ACS Nano* **2012**, *6*, 4530–4539. [CrossRef]
150. Duncan, R. The dawning era of polymer therapeutics. *Nat. Rev. Drug Discov.* **2003**, *2*, 347–360. [CrossRef]
151. Danhier, F.; Le Breton, A.; Preat, V. RGD-based strategies to target alpha(v) beta(3) integrin in cancer therapy and diagnosis. *Mol. Pharm.* **2012**, *9*, 2961–2973. [CrossRef]
152. Nazli, C.; Demirer, G.S.; Yar, Y.; Acar, H.Y.; Kizilel, S. Targeted delivery of doxorubicin into tumor cells via MMP-sensitive PEG hydrogel-coated magnetic iron oxide nanoparticles (MIONPs). *Colloids Surf. B Biointerfaces* **2014**, *122*, 674–683. [CrossRef]
153. Fu, X.; Yang, Y.; Li, X.; Lai, H.; Huang, Y.; He, L.; Zheng, W.; Chen, T. RGD peptide-conjugated selenium nanoparticles: Antiangiogenesis by suppressing VEGF-VEGFR2-ERK/AKT pathway. *Nanomedicine* **2016**, *12*, 1627–1639. [CrossRef]

154. Paris, J.L.; Villaverde, G.; Cabañas, M.V.; Manzano, M.; Vallet-Regí, M. From proof-of-concept material to PEGylated and modularly targeted ultrasound-responsive mesoporous silica nanoparticles. *J. Mater. Chem. B* **2018**, *6*. [CrossRef]
155. Eldar-Boock, A.; Miller, K.; Sanchis, J.; Lupu, R.; Vicent, M.J.; Satchi-Fainaro, R. Integrin-assisted drug delivery of nano-scaled polymer therapeutics bearing paclitaxel. *Biomaterials* **2011**, *32*, 3862–3874. [CrossRef]
156. Saraf, P.; Li, X.; Wrischnik, L.; Jasti, B. In vitro and in vivo efficacy of self-assembling RGD peptide amphiphiles for targeted delivery of paclitaxel. *Pharm. Res.* **2015**, *32*, 3087–3101. [CrossRef]
157. Babu, A.; Amreddy, N.; Muralidharan, R.; Pathuri, G.; Gali, H.; Chen, A.; Zhao, Y.D.; Munshi, A.; Ramesh, R. Chemodrug delivery using integrin-targeted PLGA-Chitosan nanoparticle for lung cancer therapy. *Sci. Rep.* **2017**, *7*, 14674. [CrossRef]
158. Minotti, G.; Menna, P.; Salvatorelli, E.; Cairo, G.; Gianni, L. Anthracyclines: Molecular advances and pharmacologic developments in antitumor activity and cardiotoxicity. *Pharm. Rev.* **2004**, *56*, 185–229. [CrossRef]
159. Xiong, X.B.; Mahmud, A.; Uludag, H.; Lavasanifar, A. Multifunctional polymeric micelles for enhanced intracellular delivery of doxorubicin to metastatic cancer cells. *Pharm. Res.* **2008**, *25*, 2555–2566. [CrossRef]
160. Muggia, F.M. Doxorubicin-polymer conjugates: Further demonstration of the concept of enhanced permeability and retention. *Clin. Cancer Res.* **1999**, *5*, 7–8.
161. Kim, D.; Lee, E.S.; Oh, K.T.; Gao, Z.G.; Bae, Y.H. Doxorubicin-loaded polymeric micelle overcomes multidrug resistance of cancer by double-targeting folate receptor and early endosomal pH. *Small* **2008**, *4*, 2043–2050. [CrossRef]
162. Guan, H.; McGuire, M.J.; Li, S.; Brown, K.C. Peptide-targeted polyglutamic acid doxorubicin conjugates for the treatment of alpha(v)beta(6)-positive cancers. *Bioconjug. Chem.* **2008**, *19*, 1813–1821. [CrossRef]
163. Xiong, X.B.; Ma, Z.; Lai, R.; Lavasanifar, A. The therapeutic response to multifunctional polymeric nano-conjugates in the targeted cellular and subcellular delivery of doxorubicin. *Biomaterials* **2010**, *31*, 757–768. [CrossRef]
164. Dasari, S.; Tchounwou, P.B. Cisplatin in cancer therapy: Molecular mechanisms of action. *Eur. J. Pharmacol.* **2014**, *740*, 364–378. [CrossRef]
165. Ivanov, A.I.; Christodoulou, J.; Parkinson, J.A.; Barnham, K.J.; Tucker, A.; Woodrow, J.; Sadler, P.J. Cisplatin binding sites on human albumin. *J. Biol. Chem.* **1998**, *273*, 14721–14730. [CrossRef]
166. Graf, N.; Lippard, S.J. Redox activation of metal-based prodrugs as a strategy for drug delivery. *Adv. Drug Deliv. Rev.* **2012**, *64*, 993–1004. [CrossRef]
167. Lee, Y.S.; Chin, Y.T.; Yang, Y.S.H.; Wei, P.L.; Wu, H.C.; Shih, A.; Lu, Y.T.; Pedersen, J.Z.; Incerpi, S.; Liu, L.F.; et al. The combination of tetraiodothyroacetic acid and cetuximab inhibits cell proliferation in colorectal cancers with different K-ras status. *Steroids* **2016**, *111*, 63–70. [CrossRef]
168. Zhang, D.; Tian, A.; Xue, X.; Wang, M.; Qiu, B.; Wu, A. The effect of temozolomide/poly(lactide-co-glycolide) (PLGA)/nano-hydroxyapatite microspheres on glioma U87 cells behavior. *Int. J. Mol. Sci.* **2012**, *13*, 1109–1125. [CrossRef]
169. Mansoori, B.; Mohammadi, A.; Davudian, S.; Shirjang, S.; Baradaran, B. The different mechanisms of cancer drug resistance: A brief review. *Adv. Pharm. Bull.* **2017**, *7*, 339–348. [CrossRef]
170. Zhang, R.X.; Wong, H.L.; Xue, H.Y.; Eoh, J.Y.; Wu, X.Y. Nanomedicine of synergistic drug combinations for cancer therapy-strategies and perspectives. *J. Control. Release* **2016**, *240*, 489–503. [CrossRef]
171. Murugan, C.; Rayappan, K.; Thangam, R.; Bhanumathi, R.; Shanthi, K.; Vivek, R.; Thirumurugan, R.; Bhattacharyya, A.; Sivasubramanian, S.; Gunasekaran, P.; et al. Combinatorial nanocarrier based drug delivery approach for amalgamation of anti-tumor agents in breast cancer cells: An improved nanomedicine strategy. *Sci. Rep.* **2016**, *6*, 34053. [CrossRef]
172. Wang, G.; Wang, Z.; Li, C.; Duan, G.; Wang, K.; Li, Q.; Tao, T. RGD peptide-modified, paclitaxel prodrug-based, dual-drugs loaded, and redox-sensitive lipid-polymer nanoparticles for the enhanced lung cancer therapy. *Biomed. Pharmacother.* **2018**, *106*, 275–284. [CrossRef]
173. Huang, W.; Liang, Y.; Sang, C.; Mei, C.; Li, X.; Chen, T. Therapeutic nanosystems co-deliver anticancer drugs and oncogene SiRNA to achieve synergetic precise cancer chemo-gene therapy. *J. Mater. Chem. B* **2018**, *6*, 3013–3022. [CrossRef]
174. Adams, F.H.; Norman, A.; Mello, R.S.; Bass, D. Effect of radiation and contrast media on chromosomes. *Radiology* **1977**, *124*, 823–826. [CrossRef]

175. Matsudaira, H.; Ueno, A.M.; Furuno, I. Iodine contrast medium sensitizes cultured mammalian cells to X rays but not to gamma rays. *Radiat. Res.* **1980**, *84*, 144–148. [CrossRef]
176. Haume, K.; Rosa, S.; Grellet, S.; Śmiałek, M.A.; Butterworth, K.T.; Solov'yov, A.V.; Prise, K.M.; Golding, J.; Mason, N.J. Gold nanoparticles for cancer radiotherapy: A review. *Cancer. Nanotechnol.* **2016**, *7*, 8. [CrossRef]
177. Shukla, R.; Bansal, V.; Chaudhary, M.; Basu, A.; Bhonde, R.R.; Sastry, M. Biocompatibility of gold nanoparticles and their endocytotic fate inside the cellular compartment: A microscopic overview. *Langmuir* **2005**, *21*, 10644–10654. [CrossRef]
178. Akamatsu, K.; Shimada, M.; Tsuruoka, T.; Nawafune, H.; Fujii, S.; Nakamura, Y. Synthesis of pH-responsive nanocomposite microgels with size-controlled gold nanoparticles from ion-doped, lightly cross-linked poly(vinylpyridine). *Langmuir* **2010**, *26*, 1254–1259. [CrossRef]
179. Zong, J.; Cobb, S.L.; Cameron, N.R. Peptide-functionalized gold nanoparticles: Versatile biomaterials for diagnostic and therapeutic applications. *Biomater. Sci.* **2017**, *5*, 872–886. [CrossRef]
180. Moncharmont, C.; Levy, A.; Guy, J.B.; Falk, A.T.; Guilbert, M.; Trone, J.C.; Alphonse, G.; Gilormini, M.; Ardail, D.; Toillon, R.A.; et al. Radiation-enhanced cell migration/invasion process: A review. *Crit. Rev. Oncol. Hematol.* **2014**, *92*, 133–142. [CrossRef]
181. Bouchard, G.; Therriault, H.; Geha, S.; Bujold, R.; Saucier, C.; Paquette, B. Radiation-induced lung metastasis development is MT1-MMP-dependent in a triple-negative breast cancer mouse model. *Br. J. Cancer* **2017**, *116*, 479–488. [CrossRef] [PubMed]
182. Yao, H.; Zeng, Z.Z.; Fay, K.S.; Veine, D.M.; Staszewski, E.D.; Morgan, M.; Wilder-Romans, K.; Williams, T.M.; Spalding, A.C.; Ben-Josef, E.; et al. Role of α5β1 integrin up-regulation in radiation-induced invasion by human pancreatic cancer cells1. *Transl. Oncol.* **2011**, *4*, 282–292. [CrossRef] [PubMed]
183. Nam, J.M.; Ahmed, K.M.; Costes, S.; Zhang, H.; Onodera, Y.; Olshen, A.B.; Hatanaka, K.C.; Kinoshita, R.; Ishikawa, M.; Sabe, H.; et al. beta1-Integrin via NF-kappaB signaling is essential for acquisition of invasiveness in a model of radiation treated in situ breast cancer. *Breast Cancer Res.* **2013**, *15*, R60. [CrossRef] [PubMed]
184. Hood, J.D.; Cheresh, D.A. Role of integrins in cell invasion and migration. *Nat. Rev. Cancer* **2002**, *2*, 91–100. [CrossRef]
185. Hanahan, D.; Weinberg, R.A. Hallmarks of cancer: The next generation. *Cell* **2011**, *144*, 646–674. [CrossRef]
186. Liang, G.; Jin, X.; Zhang, S.; Xing, D. RGD peptide-modified fluorescent gold nanoclusters as highly efficient tumor-targeted radiotherapy sensitizers. *Biomaterials* **2017**, *144*, 95–104. [CrossRef]
187. Enferadi, M.; Fu, S.Y.; Hong, J.H.; Tung, C.J.; Chao, T.C.; Wey, S.P.; Chiu, C.H.; Wang, C.C.; Sadeghi, M. Radiosensitization of ultrasmall GNP-PEG-cRGDfK in ALTS1C1 exposed to therapeutic protons and kilovoltage and megavoltage photons. *Int. J. Radiat. Biol.* **2018**, *94*, 124–136. [CrossRef]
188. Vilchis-Juarez, A.; Ferro-Flores, G.; Santos-Cuevas, C.; Morales-Avila, E.; Ocampo-Garcia, B.; Diaz-Nieto, L.; Luna-Gutierrez, M.; Jimenez-Mancilla, N.; Pedraza-Lopez, M.; Gomez-Olivan, L. Molecular targeting radiotherapy with cyclo-RGDFK(C) peptides conjugated to 177Lu-labeled gold nanoparticles in tumor-bearing mice. *J. Biomed. Nanotechnol.* **2014**, *10*, 393–404. [CrossRef]
189. Van der Zee, J. Heating the patient: A promising approach? *Ann. Oncol.* **2002**, *13*, 1173–1184. [CrossRef]
190. Bohl, M.A.; Martirosyan, N.L.; Killeen, Z.W.; Belykh, E.; Zabramski, J.M.; Spetzler, R.F.; Preul, M.C. The history of therapeutic hypothermia and its use in neurosurgery. *J. Neurosurg.* **2018**. [CrossRef]
191. Song, C.W.; Park, H.; Griffin, R.J. Improvement of tumor oxygenation by mild hyperthermia. *Radiat. Res.* **2001**, *155*, 515–528. [CrossRef]
192. Bettaieb, A.; Wrzal, P.K.; Averill-Bates, D.A. *Hyperthermia: Cancer treatment and beyond. Cancer Treatment -Conventional and Innovative Approaches*; Rangel, L., Ed.; IntechOpen: Rijeka, Croatia, 2013.
193. Behrouzkia, Z.; Joveini, Z.; Keshavarzi, B.; Eyvazzadeh, N.; Aghdam, R.Z. Hyperthermia: How can it be used? *Oman Med. J.* **2016**, *31*, 89–97. [CrossRef] [PubMed]
194. Kaur, P.; Aliru, M.L.; Chadha, A.S.; Asea, A.; Krishnan, S. Hyperthermia using nanoparticles–Promises and pitfalls. *Int. J. Hyperth.* **2016**, *32*, 76–88. [CrossRef] [PubMed]
195. Riley, R.S.; Day, E.S. Gold nanoparticle-mediated photothermal therapy: Applications and opportunities for multimodal cancer treatment. *Wiley Interdiscip. Rev. Nanomed. Nanobiotechnol.* **2017**, *9*, e1449. [CrossRef]
196. Bucharskaya, A.; Maslyakova, G.; Terentyuk, G.; Yakunin, A.; Avetisyan, Y.; Bibikova, O.; Tuchina, E.; Khlebtsov, B.; Khlebtsov, N.; Tuchin, V. Towards effective photothermal/photodynamic treatment using plasmonic gold nanoparticles. *Int. J. Mol. Sci.* **2016**, *17*, 1295. [CrossRef]

197. Li, Z.; Huang, P.; Zhang, X.; Lin, J.; Yang, S.; Liu, B.; Gao, F.; Xi, P.; Ren, Q.; Cui, D. RGD-conjugated dendrimer-modified gold nanorods for in vivo tumor targeting and photothermal therapy. *Mol. Pharm.* **2010**, *7*, 94–104. [CrossRef]
198. Li, P.; Shi, Y.W.; Li, B.X.; Xu, W.C.; Shi, Z.L.; Zhou, C.; Fu, S. Photo-thermal effect enhances the efficiency of radiotherapy using Arg-Gly-Asp peptides-conjugated gold nanorods that target alphavbeta3 in melanoma cancer cells. *J. Nanobiotechnol.* **2015**, *13*, 52. [CrossRef]
199. Lu, W.; Melancon, M.P.; Xiong, C.; Huang, Q.; Elliott, A.; Song, S.; Zhang, R.; Flores, L.G., 2nd; Gelovani, J.G.; Wang, L.V.; et al. Effects of photoacoustic imaging and photothermal ablation therapy mediated by targeted hollow gold nanospheres in an orthotopic mouse xenograft model of glioma. *Cancer Res.* **2011**, *71*, 6116–6121. [CrossRef]
200. Shi, H.; Yan, R.; Wu, L.; Sun, Y.; Liu, S.; Zhou, Z.; He, J.; Ye, D. Tumor-targeting CuS nanoparticles for multimodal imaging and guided photothermal therapy of lymph node metastasis. *Acta Biomater.* **2018**, *72*, 256–265. [CrossRef]
201. Zheng, S.W.; Huang, M.; Hong, R.Y.; Deng, S.M.; Cheng, L.F.; Gao, B.; Badami, D. RGD-conjugated iron oxide magnetic nanoparticles for magnetic resonance imaging contrast enhancement and hyperthermia. *J. Biomater. Appl.* **2014**, *28*, 1051–1059. [CrossRef]
202. Sangnier, P.A.; Preveral, S.; Curcio, A.; Silva, A.K.A.; Lefevre, C.T.; Pignol, D.; Lalatonne, Y.; Wilhelm, C. Targeted thermal therapy with genetically engineered magnetite magnetosomes@RGD: Photothermia is far more efficient than magnetic hyperthermia. *J. Control. Release* **2018**, *279*, 271–281. [CrossRef] [PubMed]
203. Issels, R.D.; Lindner, L.H.; Verweij, J.; Wust, P.; Reichardt, P.; Schem, B.C.; Abdel-Rahman, S.; Daugaard, S.; Salat, C.; Wendtner, C.M.; et al. Neo-adjuvant chemotherapy alone or with regional hyperthermia for localised high-risk soft-tissue sarcoma: A randomised phase 3 multicentre study. *Lancet Oncol.* **2010**, *11*, 561–570. [CrossRef]
204. Kaur, P.; Hurwitz, M.D.; Krishnan, S.; Asea, A. Combined hyperthermia and radiotherapy for the treatment of cancer. *Cancers* **2011**, *3*, 3799–3823. [CrossRef] [PubMed]
205. Hatzfeld-Charbonnier, A.S.; Lasek, A.; Castera, L.; Gosset, P.; Velu, T.; Formstecher, P.; Mortier, L.; Marchetti, P. Influence of heat stress on human monocyte-derived dendritic cell functions with immunotherapeutic potential for antitumor vaccines. *J. Leukoc. Biol.* **2007**, *81*, 1179–1187. [CrossRef] [PubMed]
206. Vrouenraets, M.B.; Visser, G.W.; Snow, G.B.; van Dongen, G.A. Basic principles, applications in oncology and improved selectivity of photodynamic therapy. *Anticancer Res.* **2003**, *23*, 505–522.
207. Dolmans, D.E.; Fukumura, D.; Jain, R.K. Photodynamic therapy for cancer. *Nat. Rev. Cancer* **2003**, *3*, 380–387. [CrossRef]
208. Wang, D.; Fei, B.; Halig, L.V.; Qin, X.; Hu, Z.; Xu, H.; Wang, Y.A.; Chen, Z.; Kim, S.; Shin, D.M.; et al. Targeted iron-oxide nanoparticle for photodynamic therapy and imaging of head and neck cancer. *ACS Nano* **2014**, *8*, 6620–6632. [CrossRef]
209. Mardilovich, A.; Craig, J.A.; McCammon, M.Q.; Garg, A.; Kokkoli, E. Design of a novel fibronectin-mimetic peptide-amphiphile for functionalized biomaterials. *Langmuir* **2006**, *22*, 3259–3264. [CrossRef]
210. Li, F.; Zhao, Y.; Mao, C.; Kong, Y.; Ming, X. RGD-modified albumin nanoconjugates for targeted delivery of a porphyrin photosensitizer. *Mol. Pharm.* **2017**, *14*, 2793–2804. [CrossRef]
211. Liu, Q.; Pang, M.; Tan, S.; Wang, J.; Chen, Q.; Wang, K.; Wu, W.; Hong, Z. Potent peptide-conjugated silicon phthalocyanines for tumor photodynamic therapy. *J. Cancer* **2018**, *9*, 310–320. [CrossRef]
212. Zhao, J.; Li, S.; Jin, Y.; Wang, J.Y.; Li, W.; Wu, W.; Hong, Z. Multimerization increases tumor enrichment of peptide(-)photosensitizer conjugates. *Molecules* **2019**, *24*, 817. [CrossRef] [PubMed]
213. Wang, J.L.; Xi, Y.; Liu, Y.L.; Wang, Z.H.; Zhang, Q. Combination of targeted PDT and anti-VEGF therapy for rat CNV by RGD-modified liposomal photocyanine and sorafenib. *Invest. Ophthalmol. Vis. Sci.* **2013**, *54*, 7983–7989. [CrossRef] [PubMed]
214. Jang, C.; Lee, J.H.; Sahu, A.; Tae, G. The synergistic effect of folate and RGD dual ligand of nanographene oxide on tumor targeting and photothermal therapy in vivo. *Nanoscale* **2015**, *7*, 18584–18594. [CrossRef] [PubMed]
215. Zhao, N.; Battig, M.R.; Xu, M.; Wang, X.; Xiong, N.; Wang, Y. Development of a dual-functional hydrogel using RGD and anti-VEGF aptamer. *Macromol. Biosci.* **2017**, *17*, 1700201. [CrossRef]

216. Yang, X.; Fan, B.; Gao, W.; Li, L.; Li, T.; Sun, J.; Peng, X.; Li, X.; Wang, Z.; Wang, B.; et al. Enhanced endosomal escape by photothermal activation for improved small interfering RNA delivery and antitumor effect. *Int. J. Nanomed.* **2018**, *13*, 4333–4344. [CrossRef]
217. Guo, S.; Huang, L. Nanoparticles escaping RES and endosome: Challenges for siRNA delivery for cancer therapy. *J. Nanomater.* **2011**, *2011*, 12. [CrossRef]

cancers

MDPI

Review

Active Targeting Strategies Using Biological Ligands for Nanoparticle Drug Delivery Systems

Jihye Yoo [1,2,†], Changhee Park [1,2,†], Gawon Yi [1,2], Donghyun Lee [1,2] and Heebeom Koo [1,2,3,*]

[1] Department of Medical Life Sciences, College of Medicine, The Catholic University of Korea, 222 Banpo-daero, Seocho-gu, Seoul 06591, Korea; yooji0498@catholic.ac.kr (J.Y.); parkch@catholic.ac.kr (C.P.); gawon4292@catholic.ac.kr (G.Y.); a2168989@catholic.ac.kr (D.L.)

[2] Department of Biomedicine & Health Sciences, College of Medicine, The Catholic University of Korea, 222 Banpo-daero, Seocho-gu, Seoul 06591, Korea

[3] Catholic Photomedicine Research Institute, College of Medicine, The Catholic University of Korea, 222 Banpo-daero, Seocho-gu, Seoul 06591, Korea

* Correspondence: hbkoo@catholic.ac.kr

† These authors contributed equally to this work.

Received: 8 April 2019; Accepted: 2 May 2019; Published: 8 May 2019

Abstract: Targeting nanoparticle (NP) carriers to sites of disease is critical for their successful use as drug delivery systems. Along with optimization of physicochemical properties, researchers have focused on surface modification of NPs with biological ligands. Such ligands can bind specific receptors on the surface of target cells. Furthermore, biological ligands can facilitate uptake of modified NPs, which is referred to as 'active targeting' of NPs. In this review, we discuss recent applications of biological ligands including proteins, polysaccharides, aptamers, peptides, and small molecules for NP-mediated drug delivery. We prioritized studies that have demonstrated targeting in animals over in vitro studies. We expect that this review will assist biomedical researchers working with NPs for drug delivery and imaging.

Keywords: nanoparticle; drug delivery; ligand; active targeting; tumor targeting; biodistribution

1. Introduction

The site where a drug is administered is most often very distant from the site of expected therapeutic effect. Thus, there has been significant research in the field of targeted drug delivery. Nanoparticle (NP) drug delivery systems represent the cumulative research efforts of numerous fields, including chemistry, biology, material science, pharmaceutics, and clinical medicine [1]. Commercialized formulations such as Doxil and Abraxane are excellent examples of NP drug delivery systems that have improved therapy in patients [2,3]. NPs can disperse hydrophobic drugs stably in aqueous conditions without aggregation. [4]. Importantly, their physicochemical properties, including size and surface charge, can easily be modified by adjusting the component molecules or fabrication method [5]. NPs can delay early release of drugs in order to allow sufficient time for therapeutic action. NPs also allow for controlled release of drugs, which in some cases can be tailored to respond to specific stimuli such as pH, light, heat, or enzymes [6].

With respect to targeted drug delivery, NPs utilize two basic strategies comprising either passive or active targeting [7]. Passive targeting is based on physicochemical properties [8]. Specifically, when NPs employing a passive targeting release method are injected intravenously, they generally circulate longer in the blood stream compared to free drugs. In angiogenic tissues such as tumors, NPs employing passive targeting penetrate the fenestrated structure of blood vessels more at the disease site, which in turn leads to significant accumulation of the drug, which is aided in part by slow lymphatic drainage. This scenario is referred to as the enhanced permeability and retention (EPR) effect. The EPR effect is

supported by promising data from many reports on NPs [9]. Compared to passive targeting, active targeting relies on a biological interaction between ligands on the surface of NPs and the cell target.

A large number of biological ligands have been identified and studied for facilitating active targeting of NPs [10]. Such biological ligands often bind to specific receptors on the surface of the target cells, and in this way increase cellular uptake of drug-containing NPs and also increase therapeutic efficacy [11]. Compared to singular ligand, an increased density of ligands is advantageous for promoting binding and cellular uptake through the multivalent effect [12]. Various types of ligands have been employed for this purpose, including proteins, polysaccharides, nucleic acids, peptides, and small molecules (Scheme 1). Generally, NPs are functionalized with these ligands by two ways. They can be chemically conjugated or physically adsorbed on the NPs after formation of NPs, or can be linked with NP components, such as polymers, before formation [13,14]. In this review, we discuss different types of biological ligands and review their current applications in NP-based drug delivery systems, focusing primarily on studies reporting promising outcomes in vivo (Table 1).

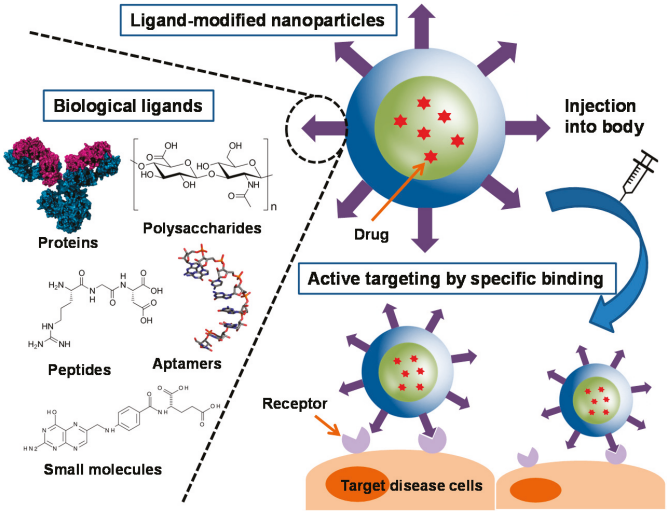

Scheme 1. Illustration of biological ligands for active targeting of nanoparticle drug carriers.

2. Biological Ligands and Their Applications for Nanoparticles

2.1. Proteins and Polysaccharides

Among biological ligands, antibodies have the longest history with respect to targeting specific receptors [15]. Antibodies are tens of kilodaltons in size and have high specificity, consistent with the generalized trend that larger ligands exhibit more specific binding [16]. In particular, many antibodies can be used not only for targeting, but for therapeutic purposes as well [17]. Nevertheless, the large size of antibodies limits their density on the surface of NPs during modification. In 2018, Roncato et al. reported the use of antiepidermal growth factor receptor (EGFR) antibody (cetuximab) in antibody-guided avidin-nucleic-acid nanoassemblies (ANANAS) for efficient cancer therapy (Figure 1) [18]. Specifically, they synthesized poly-avidin cores combined with biotin-conjugated molecules. They evaluated the targeting efficacy of the antibody–drug conjugates (ADCs), which are widely used in personalized cancer therapy. The authors found that cetuximab-guided ANANAS could increase the drug–antibody ratio more than ADCs, which they attributed to the ability of the avidin–biotin interaction to increase the drug capacity of ANANAS carriers. In that same study, ANANAS were modified with biotin-poly (ethylene glycol) (PEG)-cetuximab for targeting, biotin-PEG-Atto488 for imaging, and biotin-hydrazine-doxorubicin for therapy. They also investigated hydrazine bonds, which

are acid-reversible and can release drugs under mild acidic environments such as lysosomes after cellular uptake. Cetuximab-guided ANANAS exhibited faster cellular internalization than both untargeted ANANAS and antibody alone in MDA-MB-231 (EGFR-expressing cells). In MDA-MB-231 tumor-bearing mice, cetuximab-guided ANANAS-treated groups showed improved therapeutic efficacy compared to other groups because of their high drug–antibody ratio and targeting ability with cetuximab.

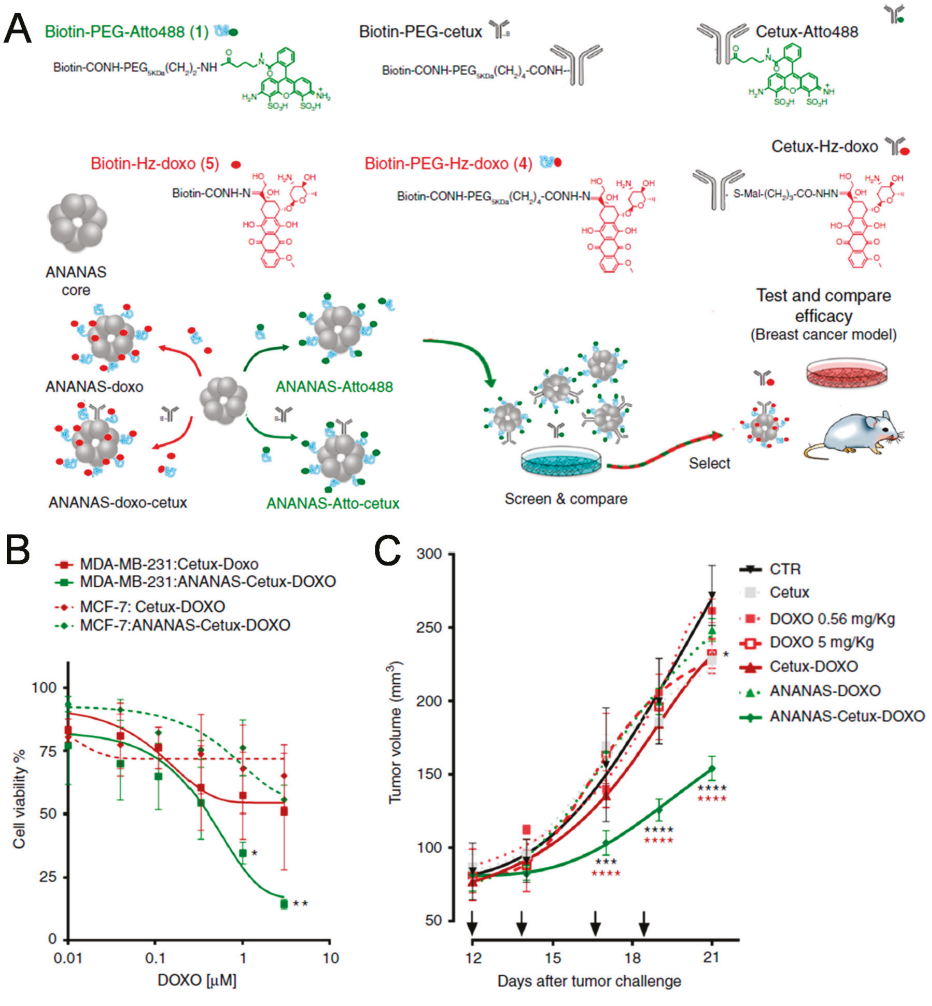

Figure 1. Antibody-conjugated nanoparticles (NPs). (**A**) Schematic illustration of antibody-guided avidin-nucleic-acid nanoassemblies (ANANAS) modified with antiepidermal growth factor receptor (EGFR) antibody (cetuximab) for enhancing cancer targeting. (**B**) Cell viability assay of cetuximab-guided ANANAS in MCF-7 and MDA-MB-231 cell lines. (**C**) Tumor growth in mice bearing MDA-MB-231 tumors after intravenous injection of cetuximab-guided ANANAS. Reproduced with permission from Reference [18].

Affibodies (Afbs) are engineered, high-affinity proteins that are smaller than normal antibodies [19]. Recently, Oh et al. successfully used Afbs for active targeting of NPs [20]. To avoid clearance of NPs by the mononuclear phagocyte system (MPS), Oh et al. suggested a protein corona shield concept.

They decorated the surface of mesoporous silica NPs (MSNs) containing camptothecin (CPT) with human epidermal growth factor receptor 2 (HER2) binding Afbs by supramolecular interaction. The resulting Afb-CPT-MSNs were approximately 270 ± 20 nm in size and had superior colloidal stability that afforded extended blood circulation time without the need for a traditional polyethyleneglycol (PEG) coating. They showed fast cellular uptake in the HER2-receptor-overexpressing SK-BR-3 breast cancer cell line, but not in control MCF-10A cells. Interestingly, in RAW264.7 murine macrophage-like cells, Afb-CPT-MSNs exhibited reduced internalization compared to free CPT, which was otherwise highly cytotoxic. In SK-BR-3 tumor-bearing mice, the Afb-modified NPs accumulated to higher levels in tumor tissue after intravenous injection compared to PEG-coated control NPs. Furthermore, they inhibited tumor growth by approximately 90%, and were found to escape from reticuloendothelial organs during ex vivo experiments. Taken together, these results demonstrated that Afb modification of NPs by protein engineering could be used to enhance the stealth effect of NPs in order to facilitate better escape from MPS compared to PEG coating while minimizing serum protein adsorption due to the presence of a protein corona.

Transferrin (Tf) is an iron-binding glycoprotein that is responsible for iron transport in the body [21]. Tf receptors are highly expressed in specific tissues and cells, which can be targeted by Tf-modified NPs. The Davis group used conjugated NPs to target Tf receptors on the blood side of the blood–brain barrier (BBB) to deliver therapeutic drugs through the BBB [22]. They anticipated that Tf-modified NPs that specifically bind Tf receptors would be unable to pass through the BBB, and thus be limited to the blood side of the BBB. To overcome this potential limitation, they used the acid-cleavable linkage DAK [2,2-bis-(aminoethoxy)-propane] to conjugate Tf to NP cores. DAK exhibits good stability at a neutral pH, with a hydrolysis half-life of 60 min at pH 5.5. Owing to the nature of the DAK linkage, transcytosis of Tf-modified NPs results in separation from the NP core under acidic environments and subsequent release into the parenchyma for therapy. Importantly, the Davis group showed that the cleavable DAK moiety was helpful in facilitating specific delivery to the brain, with an ideal ratio of 200 Tf molecules per NP for this purpose. This strategy of using Tf-modified NPs and cleavable linkages supports the possibility of NP-mediated drug delivery in brain disease, and further drug applications are expected.

Hyaluronic acid (HA) is a polymer capable of binding cell surface receptors for active targeting. HA is a polysaccharide and one the main components of the extracellular matrix along with collagen. HA binds CD44, which is often overexpressed on the surface of cancer cells and is believed to be a representative marker of cancer stem cells [23]. Interestingly, HA can be used simultaneously as a hydrophilic backbone polymer of NPs and a targeting moiety as demonstrated by Choi et al. [24]. Furthermore, HA is degraded by the enzyme hyaluronidase 1 (Hyal-1), which is highly expressed in various malignant cells and thus can accelerate drug release in target tissue. In the study by Choi et al., the HA-NPs consisted primarily of HA modified with PEG and hydrophobic cholanic acids to create a self-assembled amphiphilic structure. The as-prepared HA-NPs were not sequestered by the reticuloendothelial system (RES) and exhibited long blood circulation times, which in turn promoted specific accumulation in tumors. In one study, hydrophobic camptothecin (CPT) was loaded into the HA-NPs as an anticancer therapeutic. In the presence of Hyal-1, the CPT-loaded HA-NPs were rapidly degraded, which in turn led to quick release of CPT. In cancer cells, the CPT-HA-NPs showed dose-dependent cytotoxicity, but their cytotoxicity was highly reduced in normal cells with low CD44 expression. After that, the tumor-targeting capability of CPT-HA-NPs as well as their antitumor effect were also demonstrated in SCC7 and MBA-MB-231 tumor-bearing mice models.

2.2. Peptides

Among targeting ligands, peptides have several advantages such as low cost of production, good stability, and ease of conjugation to the surface of NPs at a high density due to their small size [25]. To target interleukin-4 receptor (IL-4R) expressed in both lung tumor cells and tumor endothelial cells, Chi et al. reported using an IL-4R-binding peptide-1 (IL4RPep-1) with the sequence CRKRLDRNC

identified using a phage-display technique [26]. The IL4RPep-1 showed excellent binding to H226 human lung cancer cells overexpressing IL-4R and was stable in whole serum for up to 4 h. Based on these findings, the authors further developed IL4RPep-1-labeled liposomes incorporating doxorubicin (IL4RPep-1-L-Dox). Cell binding and uptake of IL4RPep-1-L-Dox were more efficient than that of unlabeled liposomes (L-Dox) due to the peptide moiety. Intravenously injected IL4RPep-1-L-Dox into H226 tumor-bearing mice was also found to accumulate more significantly and had greater antitumor activity compared to L-Dox without peptide. Using immunofluorescence, the authors demonstrated that IL4RPep-1-L-Dox was present in vascular endothelial cells of tumor tissues. Taken together, these data confirmed successful targeting of IL4RPep-1-L-Dox to tumor blood vessels with concomitant improvement in chemotherapeutic efficacy.

The arginylglycylaspartic acid (RGD) peptide binds integrins, which are particularly overexpressed in vascular endothelial cells present in tumor tissue, and for this reason is a well-known tumor-targeting peptide [27]. The sequence of the RGD peptide originates from cell attachment proteins including fibronectin, vitronectin, and laminin [28]. In 2018, Lu et al. developed size-shrinkable NPs for enhanced cancer therapy using the RGD peptide as the targeting ligand (Figure 2) [29]. For deeper penetration into tumor tissue, small NPs containing metformin (MET) or doxorubicin (DOX) were linked to the surface of large gelatin nanoparticles (GNP). In addition, Lu et al. generated small NPs containing RGD peptides as well as therapeutic agents to target tumors with overexpression of integrin. They used MET as an anti-inflammatory drug for combination with DOX, and both drugs were conjugated to small NPs via degradable imine bonds. Large GNPs can be degraded by matrix metalloproteinases-2 (MMP-2) overexpressed in cancer, while small NPs decorated with RGD peptide can easily penetrate deeply into tumor tissues. MET and DOX are then released from small NPs after degradation of imine bonds in the acidic environment of tumor tissues. In this way, nuclear factor-kB (NF-kB) inducing cancer-related inflammation can be inhibited by MET, while DOX exerts cytotoxic effects in cancer cells. Both GNP and RGD NPs exhibit improved accumulation in 4T1 and CT26 tumors via targeting ligand RGD and size shrinkage. Coadministration of MET and DOX-containing NPs revealed superior antitumor and antimetastatic effects in 4T1 and CT26 tumor-bearing mice. Furthermore, the anti-inflammatory effect of MET-containing NPs was successfully evaluated during analysis of TNF-α, NF-kB, IL-6, and Ki67.

In addition to the RGD peptide, the iRGD peptide represents an RGD-containing peptide sequence initially characterized by its ability to bind αv integrins expressed on tumor endothelial cells. Interestingly, when the iRGD peptide is cleaved by proteases in tumor cells, it produces a CRGDK/R derivative peptide that has diminished affinity for αv integrin but increased affinity for neuropilin-1 (NRP-1) [30]. This switch in affinities promotes tumor-specific penetration of molecules due to the presence of the CendR peptide motif. These unique characteristics of the iRGD peptide make it useful for enhanced drug delivery in tumor tissues. For example, the Ruoslahti group showed that the iRGD peptide produced increased tumor-specific vascular permeability in five tumor models compared to a control peptide lacking the CendR motif [31]. In particular, even when not conjugated to drugs or NPs, the iRGD peptide effectively increased particle tumor accumulation owing to the natural structure of the iRGD and CendR motifs. Therefore, iRGD combination groups with free drugs or NPs enhance cancer therapy compared to free drug or NP alone. This special ability of iRGD is different from other biological ligands and may be worth pursuing in the future as a way to reduce the amount of chemotherapy needed to treat certain types of cancer [32].

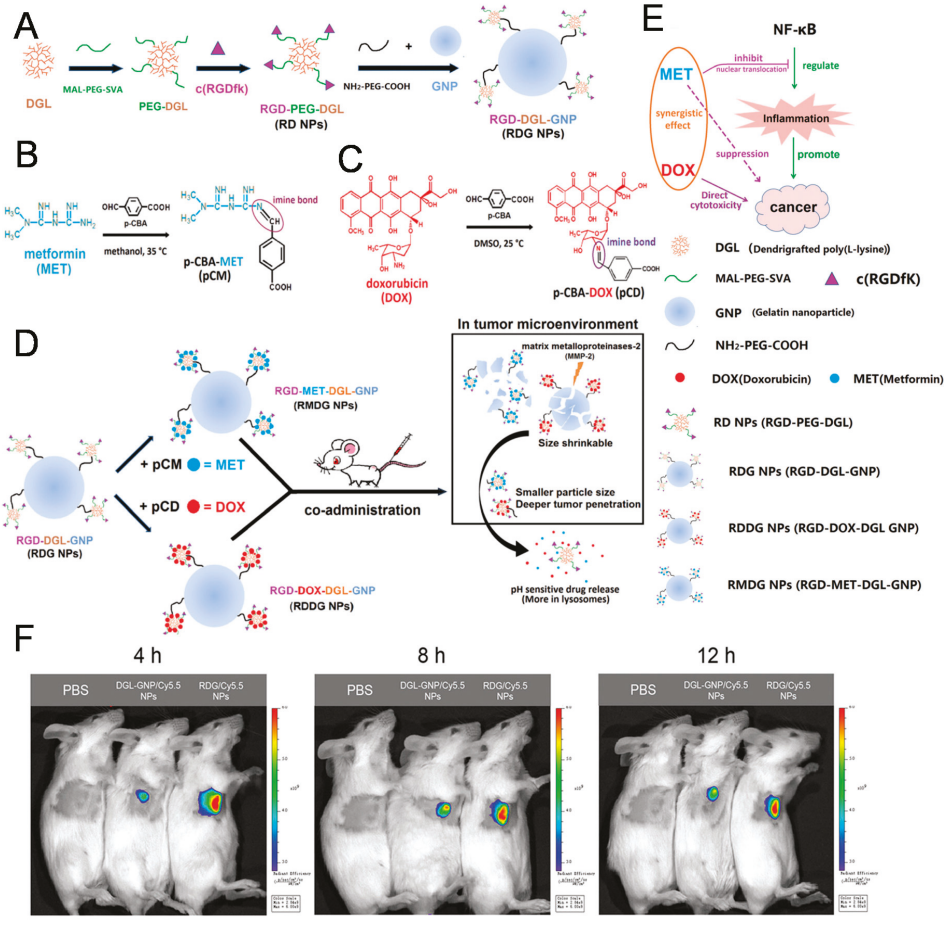

Figure 2. Peptide-conjugated NPs. Schematic illustration of RGD-doxorubicin (DOX)-dendri-grafted poly-L-lysine (DGL)-gelatin nanoparticles (GNP) (RDDG NPs) and RGD-metformin (MET)-DGL-GNP (RMDG NPs). (**A**) Synthetic procedure for RGD-DGL-GNP (RGD NPs). Chemical structure and synthetic procedure for (**B**) 4-Carboxybenzaldehyde (p-CBA)-MET (pCM) and (**C**) p-CBA-DOX (pCD). Illustration of the RDDG NPs and RMDG NPs in the tumor microenvironment (**D**) and their antitumor/anti-inflammatory effects (**E**). (**F**) In vivo fluorescence images showing tumor accumulation of NPs with or without RGD ligand. Reproduced with permission from Reference [29].

2.3. Aptamers

Aptamers are a class of short nucleic acid (DNA or RNA) comprising several nucleotides. Aptamers are small, highly sensitive, biodegradable, and have immunogenicity, making them good candidates for active targeting ligands [33]. In 2018, Duo et al. used the AS-1411 aptamer to target mesoporous silica NPs containing CX-5461 to the nucleus of tumor cells (Figure 3) [34]. The AS-1411 G-rich DNA aptamer specifically recognizes nucleolin, a protein upregulated in many cancer cell lines. Nucleolin, which is present in nucleoli, nucleoplasm, cytoplasm, and on cell surfaces, can facilitate transport of bound NPs to the nucleus after cellular uptake. CX-5461 is a well-known small-molecule inhibitor of rRNA synthesis that triggers prodeath autophagy in tumor cells. In the study by Duo et al., CX-5461-loaded MSNs were coated by polydopamine to increase loading stability, after which AS-1411 aptamers were

conjugated on the surface of NPs. After treatment, the resulting NPs successfully accumulated in the nucleolus of HeLa cells and inhibited cell growth through induced prodeath autophagy. In a HeLa cell xenograft mice model, aptamer-modified NPs exhibited higher accumulation in tumors compared to NPs without aptamers. Correspondingly, tumor growth in vivo was effectively suppressed by the AS-1411 aptamer-modified NPs without significant toxicity.

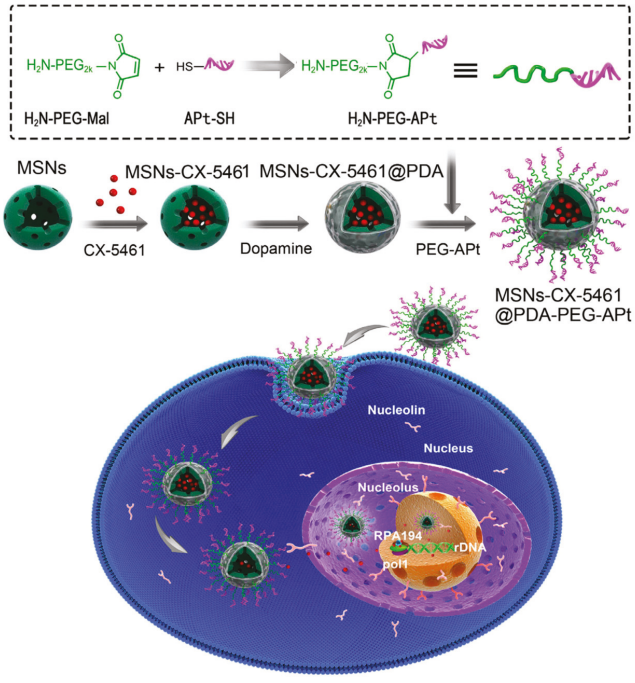

Figure 3. Aptamer-conjugated nanoparticles (NPs). Scheme of CX-5461-loaded mesoporous silica NPs modified with AS-1411 aptamers to increase nucleoli targeting. Reproduced with permission from Reference [34].

Recently, Xi et al. used the GBI-10 aptamer for tumor-targeting of NPs [35]. GBI-10 is a single strand DNA aptamer that strongly interacts with tenascin-C, a protein overexpressed in the extracellular matrix (ECM) of pancreatic ductal adenocarcinoma. For enhanced tissue penetration and cellular uptake, the authors also simultaneously used a cell-penetrating peptide (CPP). The cell-penetrating function of the CPP is not specific to tumor cells, and it was shown that GBI-10 uses electrostatic attraction to avoid nonspecific accumulation at the site of injection. Dimeric camptothecin prodrug (CPTD) was loaded in these NPs modified with aptamer and CPP, which showed greater triggered release under high redox potential after cellular uptake. Cytotoxicity testing showed that the resulting GBI-10 aptamer and CPP-modified NPs containing CPTD (Apt/CPP-CPTD NPs) have a higher IC_{50} than CPP modified NPs (CPP-CPTD NPs) due to the camouflaged CPP. However, Xi et al. asserted that GBI-10 aptamers detach from Apt/CPP-CPTD NPs in tumors secondary to the high-affinity relationship between GBI-10 and tenascin-C. Recovered cell-penetrating ability of Apt/CPP-CPTD NPs was demonstrated by Miapaca 3D tumor spheroid microscopic images. Finally, the Apt/CPP-CPTD NPs were injected intravenously into orthotopic pancreatic cancer xenograft mouse models. Fluorescent images of mice also showed high accumulation in tumor sites at all time points. Accordingly, Apt/CPP-CPTD NPs showed enhanced antitumor efficacy and survival rates in vivo over other control groups, thereby demonstrating successful active targeting of NPs with the GBI-10 aptamer and CPP.

2.4. Small Molecules

Folate (FA) receptors are well known to be overexpressed in solid tumor cells and macrophages, making them attractive targets for many NPs via receptor-mediated endocytosis [36–38]. For example, Lv et al. prepared mesoporous silica NPs (MSNs) modified with FA for active targeting, and decorated NPs using the large gas-filled microbubble (MB) technique [39]. In this method, the gas-filled MB is destroyed under local ultrasound irradiation, resulting in the release of FA-modified MSNs across the endothelial layer and into the target tissue. Using this technique, one study loaded tanshinone IIA (TAN), a hydrophobic drug, into MSNs and demonstrated both a high loading capacity and potent ability to induce tumor cell apoptosis. The FA-modified MSNs and MB also showed negligible cytotoxicity in both HeLa and A549 cells without TAM and which expressed relatively high and low levels of the FA receptor, respectively. However, the MSN-FA-TAN-MB showed enhanced cellular uptake via receptor-mediated endocytosis and increased apoptosis of HeLa cells compared to A549 cells. During in vivo testing with an H22-tumor-bearing mouse model, intravenously injected MSN-FA-TAN-MB showed greater antitumor efficacy when the tumor site was irradiated with ultrasound. These results demonstrated that a combination strategy based on the ultrasound-guided releasing and FA-mediated active targeting of NPs could be used effectively for drug delivery.

Anisamide is a benzamide known to bind sigma-1 receptors overexpressed in cancer cells [40]. In 2017, Huo et al. showed improved vaccine therapy for melanoma using the tyrosinase-related protein 2 (Trp2) vaccine and sunitinib, a known tyrosine kinase inhibitor [41]. Sunitinib inhibits tyrosine kinase activity, thereby blocking tumor growth and inducing tumor apoptosis. As sigma receptors are overexpressed in melanoma, anisamide was employed as a targeting ligand to facilitate efficient delivery of sunitinib to melanoma tumors. Specifically, the authors prepared sunitinib base-loaded polymeric micelles ($SUN_{b\text{-}PM}$) modified with anisamide. In B16F10-tumor bearing mice treated with these modified NPs, the tumor inhibition ratio was the greatest for Trp2 + $SUN_{b\text{-}PM}$. Furthermore, as a result of the immune response elicited by Trp2, the number of CD8+ T cells in Trp2+$SUN_{b\text{-}PM}$ groups was significantly increased. On the other hand, there was a decrease in the abundance of myeloid-derived suppressor cells and T regulator cells, both of which play important roles in immune suppression. They found that T helper 1 and 2 cytokine levels were appropriately altered in order to enhance antitumor immune responses. Based on these findings, the authors concluded that anisamide-modified NPs containing tyrosine kinase inhibitors combined with a vaccine may afford synergistic antitumor effects. The mechanism of anisamide remains controversial. The Leroux group insisted that cellular uptake of anisamide-modified NPs is not related to Sigma-1 receptors [42]. They also suggested the possibility that anisamide binds to Sigma-2 receptors instead of Sigma-1 receptors, and suggested that further studies are needed to identify the exact mechanism of action of anisamide [43].

Table 1. Ligands for active targeting of nanoparticle drug delivery systems.

Type	Ligands (Example)	Advantage/Disadvantage	References
Proteins	Antibodies, transferrin	High specificity/large size, low stability	[18,19,22]
Polysaccharides	Hyaluronic acid	Can be used as polymer backbone of nanoparticles/overexpressed receptors in liver tissue	[24]
Peptides	RGD, IL4RPep-1	Easy fabrication, small size/cleavable by peptidase	[26,29,31]
Aptamers	AS-1411, GBI-10	High specificity, small size/cleavable by nuclease, high cost	[34,35]
Small molecules	Folate, anisamide phenylboronic acid	Small size, very low cost/targets are also expressed in normal tissues	[39,41,44]

In another example showing the feasibility of small molecule targeting ligands, the Kataoka group demonstrated that phenylboronic acid (PBA) strongly binds N-acetylneuraminic acids, which are the main components of sialic acid (SA) compared to other sugars including galactose, mannose, and glucose (Figure 4) [44]. In particular, the difference in binding affinity is further increased at pH 6.5, which is consistent with the acidic intratumoral environment. Taking into consideration the abundance of SA present on the surface of tumor cells, they designed phenylboronic acid (PBA)-installed micelles for drug delivery, specifically, the prepared PBA-modified poly-(ethylene glycol)-b-poly-(L-glutamic acid) (PEG-PLGA) micelles containing dichloro-(1,2-diamino-cyclohexane)-platinum (II) (DACHPt), an anticancer drug. After a nine-hour incubation in vitro, they found large amounts of internalization of PBA-modified micelles in B16F10 tumor cells, while control NPs without PBA exhibited decreased uptake. Further in vivo studies with B16F10 tumor-bearing mice showed that PBA-modified micelles containing DACHPt inhibited both tumor growth and metastasis, which was attributed to their excellent accumulation of tumor cells. However, PBA needs to be applied as a ligand for drug delivery carefully, because the amount of SA varies significantly among different cancer cell lines.

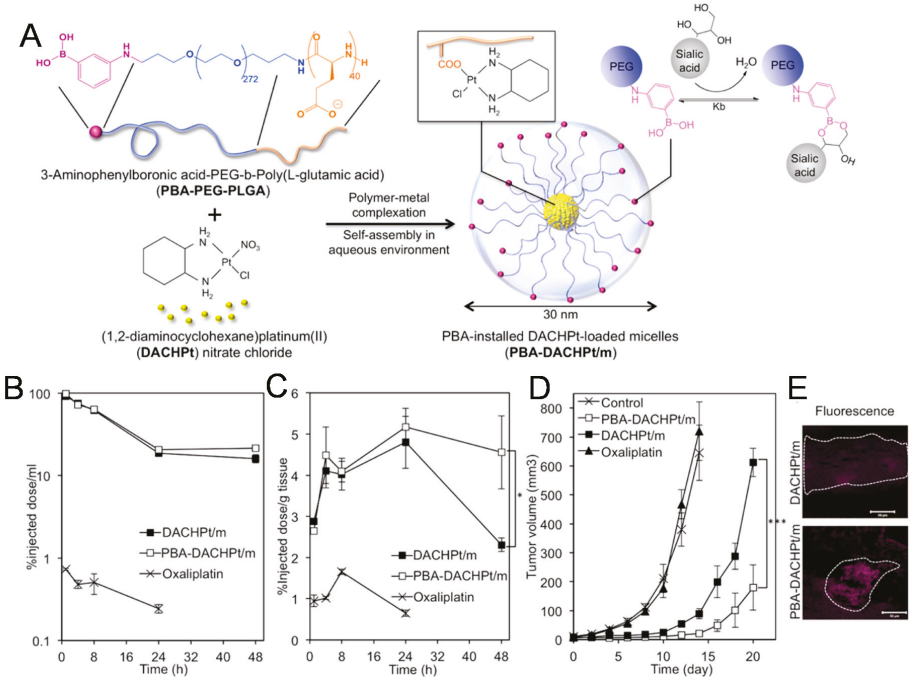

Figure 4. Small molecule-conjugated nanoparticles (NPs). (**A**) Scheme of phenylboronic acid (PBA)-conjugated dichloro-(1,2-diamino-cyclohexane)-platinum (II) (DACHPt)-loaded micelles (PBA-DACHPt/m) by self-assembly via polymer−metal complex formation. (**B**) Blood circulation time of intravenously injected DACHPt/m, PBA-DACHPt/m, and oxaliplatin. (**C**) Tumor accumulation of DACHPt/m and PBA-DACHPt/m in an orthotopic B16F10 mouse model. (**D**) Tumor volume of orthotopic B16F10 tumors after treatment with oxaliplatin (8 mg/kg), DACHPt/m, or PBA-DACHPt/m (3 mg/kg). (**E**) Ex vivo fluorescence images showing tumor tissue accumulation of DACHPt/m and PBA-DACHPt/m. Reproduced with permission from Reference [44].

3. Conclusions

To date, we have summarized the representative examples of biological ligands for targeting of NPs. Various ligands including proteins, carbohydrates, nucleic acids, peptides, and small molecules

are capable of increasing the specific binding of NPs containing drugs to disease cells to increase the efficacy of chemotherapy. Active targeting is a term that is often misunderstood as the ability of a ligand to control and direct the movement of conjugated NPs to target cells in vivo like guided missiles. However, dramatic changes in organ distribution of NPs do not occur in many cases, and the ligands present on NPs only help the binding of NPs on target cells. As observed in the studies of the Davis group, biodistribution and organ distribution of NPs in vivo changed only slightly following conjugation of biological ligands, especially on whole-body imaging [45]. Nevertheless, the ligands significantly enhanced the binding and uptake of NPs after reaching tumor tissue, which may improve therapeutic efficacies, not large-scale distribution [46].

Physicochemical properties such as size, shape, rigidity, or surface properties are very important to determine the large-scale distribution of NPs. It is known that nanoparticles from 10 to 500 nm can move through vessels and accumulate in tumor tissue [9]. Strong cationic charges increase liver accumulation and antifouling PEG modification helps tumor targeting [47]. Recent studies showed that soft NPs are advantageous for accumulation and penetration in tumor tissue [48,49]. In addition, the study of Reuter et al. showed unexpected lower tumor accumulation of RGD peptide-modified NPs compared to control PEG-modified NPs [50]. It demonstrated the importance of physicochemical properties of NPs and the unintended result of ligand modification. Thus, it is important for researchers to consider these properties while at the same time not overestimating the effect of biological ligands [46].

Another important consideration of NP ligands is their cost [51]. For example, antibodies are attractive ligands due to high specificity and diverse targets, but their production and conjugation cost a lot [52]. Development of more efficient methods for coupling of antibodies onto NPs may reduce the cost. From this point of view, small chemical molecules are generally cheaper than proteins or aptamers. Furthermore, first-generation nanomedicines including Doxil and Abraxane have insufficient specificity on their own, while many NPs using biological ligands remain in various stages of clinical development. We expect that drug-eluting, targeted NPs will become increasingly commercialized and available for use in the clinic in the near future to provide greater benefit to reduce side effects and improve therapeutic efficacy.

Author Contributions: J.Y., C.P., and H.K. researched the data for the article. All authors wrote the manuscript together. J.Y., C.P., and H.K. reviewed the manuscript.

Funding: This work was supported by Basic Research Program (2016R1C1B3013951) through the National Research Foundation of Korea (NRF) funded by the Korean Government (Ministry of Science, ICT, & Future Planning).

Conflicts of Interest: The authors declare no conflict of interest.

References

1. Hare, J.I.; Lammers, T.; Ashford, M.B.; Puri, S.; Storm, G.; Barry, S.T. Challenges and strategies in anti-cancer nanomedicine development: An industry perspective. *Adv. Drug Deliv. Rev.* **2017**, *108*, 25–38. [CrossRef]
2. Aaron, C.A.; Balabhaskar, P.; Kapil, P.; Samir, M. Clinical and commercial translation of advanced polymeric nanoparticle systems: Opportunities and material challenges. *Transl. Mater. Res.* **2017**, *4*. [CrossRef]
3. Barenholz, Y. Doxil®—The first FDA-approved nano-drug: Lessons learned. *J. Control. Release* **2012**, *160*, 117–134. [CrossRef] [PubMed]
4. Göke, K.; Lorenz, T.; Repanas, A.; Schneider, F.; Steiner, D.; Baumann, K.; Bunjes, H.; Dietzel, A.; Finke, J.H.; Glasmacher, B.; Kwade, A. Novel strategies for the formulation and processing of poorly water-soluble drugs. *Eur. J. Pharm. Biopharm.* **2018**, *126*, 40–56. [CrossRef]
5. Xie, J.; Lee, S.; Chen, X. Nanoparticle-based theranostic agents. *Adv. Drug Deliv. Rev.* **2010**, *62*, 1064–1079. [CrossRef] [PubMed]
6. Yue, X.; Zhang, Q.; Dai, Z. Near-infrared light-activatable polymeric nanoformulations for combined therapy and imaging of cancer. *Adv. Drug Deliv. Rev.* **2017**, *115*, 155–170. [CrossRef]
7. Petros, R.A.; DeSimone, J.M. Strategies in the design of nanoparticles for therapeutic applications. *Nat. Rev. Drug Discov.* **2010**, *9*, 615–627. [CrossRef]

8. Koo, H.; Huh, M.S.; Sun, I.-C.; Yuk, S.H.; Choi, K.; Kim, K.; Kwon, I.C. In Vivo Targeted Delivery of Nanoparticles for Theranosis. *Acc. Chem. Res.* **2011**, *44*, 1018–1028. [CrossRef] [PubMed]
9. Torchilin, V. Tumor delivery of macromolecular drugs based on the EPR effect. *Adv. Drug Deliv. Rev.* **2011**, *63*, 131–135. [CrossRef]
10. Byrne, J.D.; Betancourt, T.; Brannon-Peppas, L. Active targeting schemes for nanoparticle systems in cancer therapeutics. *Adv. Drug Deliv. Rev.* **2008**, *60*, 1615–1626. [CrossRef]
11. Muhamad, N.; Plengsuriyakarn, T.; Na-Bangchang, K. Application of active targeting nanoparticle delivery system for chemotherapeutic drugs and traditional/herbal medicines in cancer therapy: A systematic review. *Int. J. Nanomed.* **2018**, *13*, 3921–3935. [CrossRef]
12. Montet, X.; Funovics, M.; Montet-Abou, K.; Weissleder, R.; Josephson, L. Multivalent Effects of RGD Peptides Obtained by Nanoparticle Display. *J. Med. Chem.* **2006**, *49*, 6087–6093. [CrossRef] [PubMed]
13. Liu, Y.; Hui, Y.; Ran, R.; Yang, G.-Z.; Wibowo, D.; Wang, H.-F.; Middelberg, A.P.J.; Zhao, C.-X. Synergetic Combinations of Dual-Targeting Ligands for Enhanced In Vitro and In Vivo Tumor Targeting. *Adv. Healthc. Mater.* **2018**, *7*. [CrossRef]
14. Ran, R.; Wang, H.; Liu, Y.; Hui, Y.; Sun, Q.; Seth, A.; Wibowo, D.; Chen, D.; Zhao, C.-X. Microfluidic self-assembly of a combinatorial library of single- and dual-ligand liposomes for in vitro and in vivo tumor targeting. *Eur. J. Pharm. Biopharm.* **2018**, *130*, 1–10. [CrossRef] [PubMed]
15. Alibakhshi, A.; Abarghooi Kahaki, F.; Ahangarzadeh, S.; Yaghoobi, H.; Yarian, F.; Arezumand, R.; Ranjbari, J.; Mokhtarzadeh, A.; de la Guardia, M. Targeted cancer therapy through antibody fragments-decorated nanomedicines. *J. Control. Release* **2017**, *268*, 323–334. [CrossRef]
16. Kim, K.S.; Kim, J.; Kim, D.H.; Hwang, H.S.; Na, K. Multifunctional trastuzumab-chlorin e6 conjugate for the treatment of HER2-positive human breast cancer. *Biomater. Sci.* **2018**, *6*, 1217–1226. [CrossRef] [PubMed]
17. Lewis, P.G.D.; Li, G.; Dugger, D.L.; Crocker, L.M.; Parsons, K.L.; Mai, E.; Blattler, W.A.; Lambert, J.M.; Chari, R.V.J.; Lutz, R.J.; Wong, W.L.T.; et al. Targeting HER2-Positive Breast Cancer with Trastuzumab-DM1, an Antibody-Cytotoxic Drug Conjugate. *Cancer Res.* **2008**, *68*, 9280–9290. [CrossRef]
18. Roncato, F.; Rruga, F.; Porcù, E.; Casarin, E.; Ronca, R.; Maccarinelli, F.; Realdon, N.; Basso, G.; Alon, R.; Viola, G.; Morpurgo, M. Improvement and extension of anti-EGFR targeting in breast cancer therapy by integration with the Avidin-Nucleic-Acid-Nano-Assemblies. *Nat. Commun.* **2018**, *9*. [CrossRef]
19. Smith, B.; Lyakhov, I.; Loomis, K.; Needle, D.; Baxa, U.; Yavlovich, A.; Capala, J.; Blumenthal, R.; Puri, A. Hyperthermia-triggered intracellular delivery of anticancer agent to HER2+ cells by HER2-specific affibody (ZHER2-GS-Cys)-conjugated thermosensitive liposomes (HER2+ affisomes). *J. Control. Release* **2011**, *153*, 187–194. [CrossRef] [PubMed]
20. Oh, J.Y.; Kim, H.S.; Palanikumar, L.; Go, E.M.; Jana, B.; Park, S.A.; Kim, H.Y.; Kim, K.; Seo, J.K.; Kwak, S.K.; et al. Cloaking nanoparticles with protein corona shield for targeted drug delivery. *Nat. Commun.* **2018**, *9*. [CrossRef]
21. Schieber, C.; Bestetti, A.; Lim, J.P.; Ryan, A.D.; Nguyen, T.-L.; Eldridge, R.; White, A.R.; Gleeson, P.A.; Donnelly, P.S.; Williams, S.J.; Mulvaney, P. Conjugation of Transferrin to Azide-Modified CdSe/ZnS Core–Shell Quantum Dots using Cyclooctyne Click Chemistry. *Angew. Chem. Int. Ed.* **2012**, *51*, 10523–10527. [CrossRef] [PubMed]
22. Clark, A.J.; Davis, M.E. Increased brain uptake of targeted nanoparticles by adding an acid-cleavable linkage between transferrin and the nanoparticle core. *Proc. Natl. Acad. Sci. USA* **2015**, *112*, 12486–12491. [CrossRef] [PubMed]
23. Aruffo, A.; Stamenkovic, I.; Melnick, M.; Underhill, C.B.; Seed, B. CD44 is the principal cell surface receptor for hyaluronate. *Cell* **1990**, *61*, 1303–1313. [CrossRef]
24. Choi, K.Y.; Yoon, H.Y.; Kim, J.-H.; Bae, S.M.; Park, R.-W.; Kang, Y.M.; Kim, I.-S.; Kwon, I.C.; Choi, K.; Jeong, S.Y.; et al. Smart Nanocarrier Based on PEGylated Hyaluronic Acid for Cancer Therapy. *ACS Nano* **2011**, *5*, 8591–8599. [CrossRef] [PubMed]
25. Chen, K.; Conti, P.S. Target-specific delivery of peptide-based probes for PET imaging. *Adv. Drug Deliv. Rev.* **2010**, *62*, 1005–1022. [CrossRef] [PubMed]
26. Chi, L.; Na, M.-H.; Jung, H.-K.; Vadevoo, S.M.P.; Kim, C.-W.; Padmanaban, G.; Park, T.-I.; Park, J.-Y.; Hwang, I.; Park, K.U.; et al. Enhanced delivery of liposomes to lung tumor through targeting interleukin-4 receptor on both tumor cells and tumor endothelial cells. *J. Control. Release* **2015**, *209*, 327–336. [CrossRef]

27. Nieberler, M.; Reuning, U.; Reichart, F.; Notni, J.; Wester, H.-J.; Schwaiger, M.; Weinmuller, M.; Rader, A.; Steiger, K.; Kessler, H. Exploring the Role of RGD-Recognizing Integrins in Cancer. *Cancers* **2017**, *9*, 116. [CrossRef]
28. Auernheimer, J.; Dahmen, C.; Hersel, U.; Bausch, A.; Kessler, H. Photoswitched Cell Adhesion on Surfaces with RGD Peptides. *J. Am. Chem. Soc.* **2005**, *127*, 16107–16110. [CrossRef] [PubMed]
29. Lu, Z.; Long, Y.; Cun, X.; Wang, X.; Li, J.; Mei, L.; Yang, Y.; Li, M.; Zhang, Z.; He, Q. A size-shrinkable nanoparticle-based combined anti-tumor and anti-inflammatory strategy for enhanced cancer therapy. *Nanoscale* **2018**, *10*, 9957–9970. [CrossRef]
30. Teesalu, T.; Sugahara, K.N.; Kotamraju, V.R.; Ruoslahti, E. C-end rule peptides mediate neuropilin-1-dependent cell, vascular, and tissue penetration. *Proc. Natl. Acad. Sci. USA* **2009**, *106*, 16157–16162. [CrossRef]
31. Sugahara, K.N.; Teesalu, T.; Karmali, P.P.; Kotamraju, V.R.; Agemy, L.; Greenwald, D.R.; Ruoslahti, E. Coadministration of a Tumor-Penetrating Peptide Enhances the Efficacy of Cancer Drugs. *Science* **2010**, *328*, 1031–1035. [CrossRef]
32. Fadeev, R.; Chekanov, A.; Solovieva, M.; Bezborodova, O.; Nemtsova, E.; Dolgikh, N.; Fadeeva, I.; Senotov, A.; Kobyakova, M.; Evstratova, Y.; et al. Improved Anticancer Effect of Recombinant Protein izTRAIL Combined with Sorafenib and Peptide iRGD. *Int. J. Mol. Sci.* **2019**, *20*, 525. [CrossRef] [PubMed]
33. Jo, H.; Ban, C. Aptamer–nanoparticle complexes as powerful diagnostic and therapeutic tools. *Exp. Mol. Med.* **2016**, *48*. [CrossRef]
34. Duo, Y.; Yang, M.; Du, Z.; Feng, C.; Xing, C.; Wu, Y.; Xie, Z.; Zhang, F.; Huang, L.; Zeng, X.; Chen, H. CX-5461-loaded nucleolus-targeting nanoplatform for cancer therapy through induction of pro-death autophagy. *Acta Biomater.* **2018**, *79*, 317–330. [CrossRef]
35. He, X.; Chen, X.; Liu, L.; Zhang, Y.; Lu, Y.; Zhang, Y.; Chen, Q.; Ruan, C.; Guo, Q.; Li, C.; Sun, T.; Jiang, C. Sequentially Triggered Nanoparticles with Tumor Penetration and Intelligent Drug Release for Pancreatic Cancer Therapy. *Adv. Sci. (Weinh)* **2018**, *5*. [CrossRef]
36. Van Dam, G.M.; Themelis, G.; Crane, L.M.A.; Harlaar, N.J.; Pleijhuis, R.G.; Kelder, W.; Sarantopoulos, A.; de Jong, J.S.; Arts, H.J.G.; van der Zee, A.G.J.; et al. Intraoperative tumor-specific fluorescence imaging in ovarian cancer by folate receptor-[alpha] targeting: First in-human results. *Nat. Med.* **2011**, *17*, 1315–1319. [CrossRef]
37. Nogueira, E.; Gomes, A.C.; Preto, A.; Cavaco-Paulo, A. Folate-targeted nanoparticles for rheumatoid arthritis therapy. *Nanomed. Nanotechnol. Biol. Med.* **2016**, *12*, 1113–1126. [CrossRef] [PubMed]
38. Son, J.; Yang, S.M.; Yi, G.; Roh, Y.J.; Park, H.; Park, J.M.; Choi, M.-G.; Koo, H. Folate-modified PLGA nanoparticles for tumor-targeted delivery of pheophorbide a in vivo. *Biochem. Biophys. Res. Commun.* **2018**, *498*, 523–528. [CrossRef]
39. Lv, Y.; Cao, Y.; Li, P.; Liu, J.; Chen, H.; Hu, W.; Zhang, L. Ultrasound-Triggered Destruction of Folate-Functionalized Mesoporous Silica Nanoparticle-Loaded Microbubble for Targeted Tumor Therapy. *Adv. Healthc. Mater.* **2017**, *6*. [CrossRef] [PubMed]
40. Fitzgerald, K.A.; Malhotra, M.; Gooding, M.; Sallas, F.; Evans, J.C.; Darcy, R.; O'Driscoll, C.M. A novel, anisamide-targeted cyclodextrin nanoformulation for siRNA delivery to prostate cancer cells expressing the sigma-1 receptor. *Int. J. Pharm.* **2016**, *499*, 131–145. [CrossRef] [PubMed]
41. Huo, M.; Zhao, Y.; Satterlee, A.B.; Wang, Y.; Xu, Y.; Huang, L. Tumor-targeted delivery of sunitinib base enhances vaccine therapy for advanced melanoma by remodeling the tumor microenvironment. *J. Control. Release* **2017**, *245*, 81–94. [CrossRef] [PubMed]
42. Dasargyri, A.; Kumin, C.D.; Leroux, J.-C. Targeting Nanocarriers with Anisamide: Fact or Artifact? *Adv. Mater.* **2017**, *29*. [CrossRef]
43. Dasargyri, A.; Hervella, P.; Christiansen, A.; Proulx, S.T.; Detmar, M.; Leroux, J.-C. Findings questioning the involvement of Sigma-1 receptor in the uptake of anisamide-decorated particles. *J. Control. Release* **2016**, *224*, 229–238. [CrossRef] [PubMed]
44. Deshayes, S.; Cabral, H.; Ishii, T.; Miura, Y.; Kobayashi, S.; Yamashita, T.; Matsumoto, A.; Miyahara, Y.; Nishiyama, N.; Kataoka, K. Phenylboronic Acid-Installed Polymeric Micelles for Targeting Sialylated Epitopes in Solid Tumors. *J. Am. Chem. Soc.* **2013**, *135*, 15501–15507. [CrossRef] [PubMed]

45. Bartlett, D.W.; Su, H.; Hildebrandt, I.J.; Weber, W.A.; Davis, M.E. Impact of tumor-specific targeting on the biodistribution and efficacy of siRNA nanoparticles measured by multimodality in vivo imaging. *Proc. Natl. Acad. Sci. USA* **2007**, *104*, 15549–15554. [CrossRef]
46. Choi, C.H.J.; Alabi, C.A.; Webster, P.; Davis, M.E. Mechanism of active targeting in solid tumors with transferrin-containing gold nanoparticles. *Proc. Natl. Acad. Sci. USA* **2010**, *107*, 1235–1240. [CrossRef]
47. Lee, S.; Lee, S.-Y.; Park, S.; Ryu, J.H.; Na, J.H.; Koo, H.; Lee, K.E.; Jeon, H.; Kwon, I.C.; Kim, K.; Jeong, S.Y. In vivo NIRF Imaging of Tumor Targetability of Nanosized Liposomes in Tumor-Bearing Mice. *Macromol. Biosci.* **2012**, *12*, 849–856. [CrossRef]
48. Hui, Y.; Wibowo, D.; Liu, Y.; Ran, R.; Wang, H.-F.; Seth, A.; Middelberg, A.P.J.; Zhao, C.-X. Understanding the Effects of Nanocapsular Mechanical Property on Passive and Active Tumor Targeting. *ACS Nano* **2018**, *12*, 2846–2857. [CrossRef]
49. Na, J.H.; Lee, S.-Y.; Lee, S.; Koo, H.; Min, K.H.; Jeong, S.Y.; Yuk, S.H.; Kim, K.; Kwon, I.C. Effect of the stability and deformability of self-assembled glycol chitosan nanoparticles on tumor-targeting efficiency. *J. Control. Release* **2012**, *163*, 2–9. [CrossRef]
50. Reuter, K.G.; Perry, J.L.; Kim, D.; Luft, J.C.; Liu, R.; DeSimone, J.M. Targeted PRINT Hydrogels: The Role of Nanoparticle Size and Ligand Density on Cell Association, Biodistribution, and Tumor Accumulation. *Nano Lett.* **2015**, *15*, 6371–6378. [CrossRef]
51. Cheng, Z.; Al Zaki, A.; Hui, J.Z.; Muzykantov, V.R.; Tsourkas, A. Multifunctional Nanoparticles: Cost Versus Benefit of Adding Targeting and Imaging Capabilities. *Science* **2012**, *338*, 903–910. [CrossRef] [PubMed]
52. Fleck, L.M. The Costs of Caring: Who Pays? Who Profits? Who Panders? *Hastings Cent. Rep.* **2006**, *36*, 13–17. [CrossRef] [PubMed]

cancers

MDPI

Review

Oncogenic Signaling in Tumorigenesis and Applications of siRNA Nanotherapeutics in Breast Cancer

Nur Izyani Kamaruzman [1], Noraini Abd Aziz [2], Chit Laa Poh [2] and Ezharul Hoque Chowdhury [3,*]

[1] Department of Biomedical Science, Faculty of Medicine, University of Malaya, 50603 Kuala Lumpur, Malaysia; nurizyanikamaruzman@gmail.com

[2] Centre for Virus and Vaccine Research (CVVR), Sunway University, 47500 Subang Jaya, Selangor, Malaysia; norainiaa@sunway.edu.my (N.A.A.); pohcl@sunway.edu.my (C.L.P.)

[3] Jeffrey Cheah School of Medicine and Health Sciences, Monash University Malaysia, 47500 Subang Jaya, Selangor, Malaysia

* Correspondence: md.ezharul.hoque@monash.edu; Tel: +603-5514-4978; Fax: +603-5514-6323

Received: 21 February 2019; Accepted: 8 April 2019; Published: 6 May 2019

Abstract: Overexpression of oncogenes and cross-talks of the oncoproteins-regulated signaling cascades with other intracellular pathways in breast cancer could lead to massive abnormal signaling with the consequence of tumorigenesis. The ability to identify the genes having vital roles in cancer development would give a promising therapeutics strategy in combating the disease. Genetic manipulations through siRNAs targeting the complementary sequence of the oncogenic mRNA in breast cancer is one of the promising approaches that can be harnessed to develop more efficient treatments for breast cancer. In this review, we highlighted the effects of major signaling pathways stimulated by oncogene products on breast tumorigenesis and discussed the potential therapeutic strategies for targeted delivery of siRNAs with nanoparticles in suppressing the stimulated signaling pathways.

Keywords: breast cancer; siRNA; cell signaling; active targeting; passive targeting; EPR effect; oncogenes; nanoparticles; nanomedicine

1. Introduction

Breast cancer is one of most common life-threatening cancers and the second leading cause of female deaths worldwide. About 1.67 million new cases of breast cancer were diagnosed in 2012 worldwide [1]. According to the data revealed by the American Cancer Society, around 266,120 new cases of invasive breast cancer will be diagnosed in American women in 2018 [2]. The statistics emphasized that one in every eight women in the United State of America is at risk of having breast cancer. Based on the Malaysian National Cancer Registry Report (2007–2011), 1 in 30 females is at risk of having breast cancer in a lifetime [3]. The mortality rate of breast cancer in Malaysia is estimated to be ~16.7 to 20 in 100,000 [4].

Breast cancer is the malignant cell growth that originates from the breast cells at the inner lining of the breast ducts or lobules that supply milk [5]. There are stages of breast cancer diagnosis, where at stage 0, the cancer cells are found to be localized at the lobules or ducts of the breast. At stage I, II, and III, the cancer may be defined by the size of the tumors and the area that the cancer cells have spread, such as the chest wall, skin, or the lymph nodes surrounding the breast. At the advanced or metastatic stage (stage IV), the cancer cells have metastasized to other organs or lymph nodes that are further away from the breast [5,6]. Breast cancer is a heterogeneous disease, as there are many distinct genes being overexpressed and acting as key players in the progression of the breast cancer cells [7]. The

expression of breast cancer markers, such as estrogen receptor (ER), human epidermal growth factor receptor 2 (HER2/neu), progesterone receptor (PR), and urokinase plasminogen activator (uPA) has been used to evaluate the progression and aggressiveness of the disease [7–9]. The untreated lesion of the ducts or lobules may lead to proliferation and formation of metastatic cells that can develop the ability to invade blood and lymphatic vessels and metastasize to other parts of the body, such as brain, lung, liver, and bones [10]. The common symptom of the disease is the formation of lumps in the breast. Other than that, patients may also experience changes in the breast's features such as thickening, swelling, distortion, tenderness, skin irritation, redness, nipple abnormalities, and discharge.

Factors that have been associated with increased risk of breast tumorigenesis are sex, age, family history, breast condition, and endogenous estrogens. Females are more frequently diagnosed with breast cancer than males. The risk also increases with age, and postmenopausal women have been considered to have more risk. Women and men with first-degree relatives with breast cancer are shown to be at higher risk of getting the disease compared to those without family history of breast cancer. The mutations of the well-known tumor suppressor genes, *BRCA1* and *BRCA2*, are frequently associated with breast cancer. The faulty genes impairing the DNA repair process increase the chances of breast cancer. Conversion of proto-oncogenes into oncogenes via mutations is one of the prominent causes of the disease, promoting overexpression of growth factor receptors and subsequent cross-talks among their downstream signaling cascades, and can lead to proliferation and survival of cancer cells [11]. Besides that, an increase in mammographic breast density indicates a higher chance of the individual to develop breast cancer [12]. The presence of fat tissues, which can be the source of cholesterol, may increase the production of estrogens in high-density breast. Aromatase is the enzyme that promotes the production of estrogen from the androgens [13]. Other than that, there are studies showing that higher levels of estrogens are associated with the development and progression of breast cancer [14].

Biopsy taken from the mass formed in the breast confirms the presence of malignancy through laboratory screening. To date, there are few treatments of breast cancer such as surgery, radiotherapy, chemotherapy, hormonal therapy, and monoclonal antibody therapy [6]. The surgical procedure involves the removal of the tumors localized in the tissue, and mastectomy, which is the removal of the affected breast. Radiotherapy uses high-energy rays that kill the actively dividing cancerous cells [15]. Chemotherapy for breast cancer is a treatment by delivering cytotoxic drugs either through intravenous injection or oral delivery, allowing the drugs to travel through the blood circulation before reaching the cancer cells [6]. Monoclonal antibody therapy for breast cancer attempts to trigger the immune system to destroy the cancer cells by allowing binding of the antibody with the antigens that are present on the cancer cells. For example, introduction of traztuzumab that targets HER2 on breast cancer cells causes arrest of cancer cells at the G1 phase of the cell cycle, thus reducing the process of cell proliferation. Further, it may down-regulate the expression of HER2 and reduce the dimerization of the receptor [16,17]. Hormonal therapy is performed, for instance, by using estrogen antagonist that blocks the action of estrogen, such as tamoxifen and raloxifene or aromatase inhibitors (anatrozole and exemastene) [6]. As research showed that 70% of the breast cancer cases are estrogen-receptor positive, the usage of estrogen antagonist and aromatase inhibitor is commonly employed to treat breast cancer. As breast cancer is a heterogenous disease, there is rapid growth of ongoing research on developing breast cancer therapeutic strategies to encounter the likely cause of the disease. Triple-negative breast cancer (TNBC) defines the disease without or having less expression of the well-known breast cancer markers like ER, PR, and HER/neu [18], therefore, requiring different treatment approaches. Glycotherapy is one of the potential strategies to target aberrant glycosylation that promotes abnormal cellular activities and carcinogenesis [19]. The aspragine-linked (N-linked) glycoprotein was found to have roles in the progression of breast cancer, such as angiogenesis [20]. Banerjee et al. (2011) has shown that Tunicamycin is able to inhibit angiogenesis in vitro and in vivo. They have observed reduced expression of vascular endothelial growth factor receptors (VGFRs) and N-glycan in the tumor micro-vessels [21]. Another field of research is immunotherapy, which comprises, for instance, targeting the pathway of programmed death 1/ programmed death ligand

1 (PD-1/PD-L1), which involves responses from T-cells [22]. PD-L1 that is expressed by the tumor cells binds to PD-1 proteins expressed by T-cells. The interaction of PD/PD-L1 inhibits T-cells from killing the tumor cells. Atezolizumab (Tecentriq ™) is known as a checkpoint inhibitor and functions as an anti-PD-L1 monoclonal antibody. The inhibition of PD-1/PD-L1 binding enables the killing of tumor cells by T-cells. There are also studies on complementary and alternative medicines (CAM) as a treatment option of breast cancer, such as Ayuverda (traditional Indian medicine) and traditional Chinese medicine [23]. Several patients opted for CAM as they have experienced failures in other treatments. CAM typically employs herbal and botanical therapy (e.g., homeopathy), mental therapy (e.g., meditation and hypnosis), and physical therapy (e.g., acupuncture, massage, yoga, and Chi Gong). Thus far, there lacks scientific evidence of CAM, with no successful clinical trials reported in effectively curing the disease [24].

Numerous short- and long-term effects from the chemotherapy such as risks of cardiac toxicity, development of secondary cancer, neurotoxicity, premature menopause, and effects on sexuality with high costs of drugs and treatments have led to emotional, physical, and financial burden for the patients and the community [25]. Thus, it is crucial to identify key players of the disease's development and to develop effective therapeutic strategies in targeting breast cancer with or without minimal side effects.

2. Signaling Pathways and Oncogene Involvement in Breast Cancer

Cell membrane receptors and ion channels receive stimuli such as hormones, neurotransmitters, antibodies, cytokines, growth factors, and ions from the extracellular region that influence cell signaling [26]. The interactions between the stimuli and the receptors or ion channels may trigger various downstream signaling pathways, such as Mitogen-activated protein kinase (MAPK) and phosphoinositide-3-kinase–protein kinase B (PI3K/AKT) and Ca^{2+} signaling pathways at the intracellular level (Figure 1). The interplay or cross-talks between the signal transduction pathways build up the complexity of breast cancer signaling cascades, thus, complicating the process of curing the disease. The interconnected signaling pathways may induce the breast cancer cells to proliferate and survive under a heterogeneous condition with various up-regulated and down-regulated proteins. Proto-oncogenes and tumor suppressor genes are involved in the maintenance of the normal cell functions such as growth, division, and survival. However, mutations of these genes in the form of deletions, insertions, or substitutions, resulting in gain or loss of functions, may constitutively activate the signaling pathways, initiating the tumorigenesis [27,28]. Thus, identifying the oncogenes and tumor suppressor genes governing the breast cancer signaling pathways is an important goal in therapeutic intervention of breast cancer.

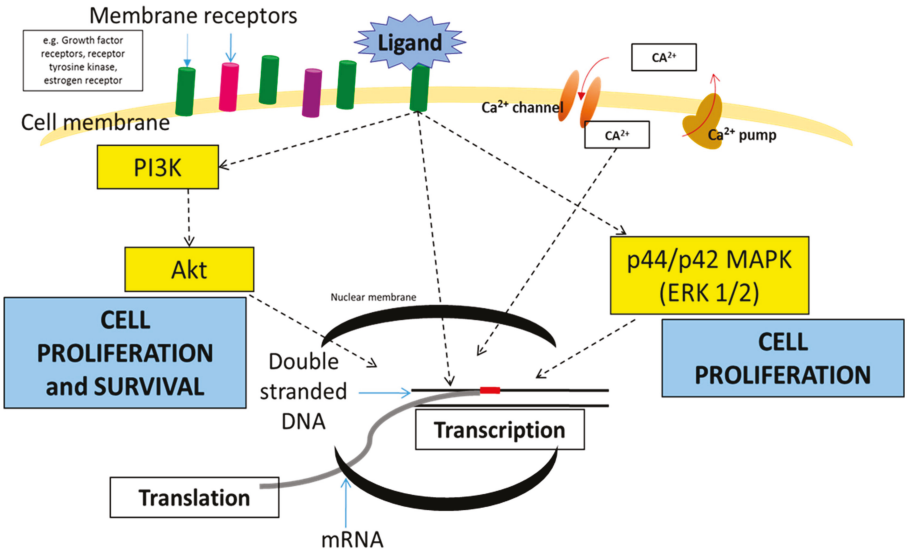

Figure 1. Diagram of several signaling pathways in breast cancer that lead to proliferation and survival of breast cancer cells.

2.1. Mitogen-Activated Protein Kinase (MAPK) Pathway

Gene therapy has been advocated to treat cancers. There are many genes and proteins that are being up- or down-regulated in the signaling pathways, thus promoting the proliferation and survival of breast cancer cells. For example, mitogen-activated protein kinases (MAPKs) are the proteins that function in delivering and amplifying the extracellular signals. Researchers have identified six different groups of MAPKs, which are extracellular signal-regulated kinases (ERK)1/2, ERK3/4, ERK5, ERK7/8, Jun N-terminal kinase (JNK)1/2/3, and the p38 isoforms α/β/γ (ERK6)/δ [29–31]. MAPK signaling through the ERK pathway activation is regularly being activated via the binding of ligand with the cell membrane receptor, such as the receptor tyrosine kinase (RTK). These will later promote the downstream responses of the pathway, for example, the activation of Ras protein. The activation of Ras may lead to subsequent stimulation of ERK1/2 signaling proteins to transmit signals into the nucleus for gene transcription and expression; thus, cell proliferation, survival, apoptosis, and differentiation are turned on [32]. Hyper-expression of MAPK was found in the primary human breast cancer tissue compared to the benign portion, which is related to metastatic potential of the disease [33]. Studies on down-regulating the expression of MAPK have shown the decrease in breast cancer cell proliferation and migration [34].

2.2. PI3K/AKT Pathway

AKT or protein kinase B is also an important factor in regulating the cell proliferation, survival, glycogen metabolism, and motility [35]. It exists in three isoforms in mammals; AKT1, AKT2, and AKT3. Phosphatidylinositol 3-kinase (PI3K) is the vital protein in connecting the signals from the cognate receptor tyrosine kinase towards AKT [36]. Numerous studies have revealed the deregulation and mutations of genes of this pathway in 70% of the breast cancers [37,38]. Upon stimulation by ligand binding to the receptor tyrosine kinase, PI3K signaling pathway may be activated, thus transferring the message down to the AKT pathway, such as the mTOR signaling pathway. The phosphorylation of AKT (pAKT) promotes cellular functions, such as proliferation and survival. However, overexpression of pAKT proteins was found in 33% of ductal carcinoma in situ and in 38% of the invasive breast cancer cases through the immunohistochemistry of tissue microarray [39]. In another study involving siRNA

knockdown targeting the AKT in MCF-7 human breast cancer cell line, the introduction of the siRNA has reduced the expression of AKT and BCL-2 (anti-apoptotic protein) proteins, which may enhance the probability of cancer cell death [40].

2.3. Calcium Signaling Pathway

Calcium ion (Ca^{2+}) is known to be a ubiquitous cellular signal and is one of the important second messengers in cell signaling. It is crucial to maintain its homeostasis in normal cell signaling series. Ca^{2+} is released in cytosol either from internal stores, such as endoplasmic reticulum or from external medium through different cell membrane-associated channels, through the action of Ca^{2+} itself, intracellular messengers, such as inositol-1,4,5-trisphosphate, or the status of intracellular Ca^{2+} storage. It may initiate different types of protein activation or phosphorylation and changes in protein shapes and charges, which may subsequently vary the interactions with other respective components [41]. Moreover, Ca^{2+} plays a role in cell proliferation, as it is involved with the activation of the cyclin-dependent kinases (CDK4 and CDK2) for the progression of the cell cycle from the G1 to S phase [42]. In the pathological environment, malignant cells may acquire the six hallmarks of cancers, as described by Hanahan and Weinberg (2000): (a) Self-sufficiency in growth signals, (b) insensitivity to growth-inhibitory signals, (c) evasion of programmed cell-death (apoptosis), (d) limitless replication potential, (e) sustained angiogenesis, and (f) tissue invasion and metastasis [43]. Any disturbance of Ca^{2+} homeostasis may alter the cell cycle progression and trigger the emergence of one or more of the cancer hallmarks. Di et al. (2015) [44] showed that the overexpression of Rap2B, a GTP-binding protein, increased the intracellular calcium level, thus later promoting the phosphorylation of ERK1/2 in Bcap-37 and MDA-MB-231 breast cancer cells. They also observed increase in proliferation, migration, and invasion of the cancer cells [44].

Endoplasmic reticulum release of Ca^{2+} and subsequent uptake by mitochondria involves programmed cell death. Nevertheless, increases in Ca^{2+} influx activates the survival signaling pathways of the cancer cells. Cancer cells develop an antioxidant system against the reactive oxygen species (ROS) such as hydrogen peroxide (H_2O_2) to maintain cells' activities. H_2O_2 produced by mitochondria mediates cysteine oxidation on transient receptor potential ankyrin 1 (TRPA1). TRPA1, a cation channel on the cell membrane, enables the up-regulation of Ca^{2+} into the cellular region and activates the anti-apoptotic pathway such as the PI3K/AKT signaling pathway [45]. Data analysis from the cancer genome atlas found the overexpression of TRPA1 in breast cancer.

2.4. Notch Signaling Pathway

Notch signaling pathway begins with the interaction of the DSL (Delta/Serrate/LAG-2) ligands on one cell and Notch receptor on the adjacent cell [46]. The signaling pathway is associated with the cellular progression, such as proliferation, apoptosis, angiogenesis, hypoxia, cancer stem cell activity, epithelial to mesenchymal transition (EMT), and metastasis. In breast cancer, Notch receptors and their ligands were found to be overexpressed. Notch receptors have been categorized into four groups, Notch1 to Notch4; while the DSL ligands, which are transmembrane ligands, have five groups (Jagged1, Jagged2, Delta-like1, Delta-like3, and Delta-like4). The expressions of *cyclinA*, *cyclinB*, and *cyclinD1* genes were found to be upregulated in Notch signaling cascade, while the survival of breast cancer cells might be induced via AKT pathway activation by Notch signaling pathway [46–48].

2.5. Hedgehog Signaling Pathway

Hedgehog signaling pathway controls the process of cell proliferation, survival, differentiation, tissue homeostasis, regeneration, and stem cell maintenance [49]. Most of the basal-like breast cancers (BLBC) have the triple negative phenotype of the important receptors (ER−, PR−, and HER2) and are resistant to chemotherapy treatments. The BLBC has an aggressive growth and has the possibility to metastasize to other organs. Mott et al. (2018) has shown that the forkhead-box transcription factor C1 (FOXC1) plays a role in 4T1 murine metastatic breast cancer cell proliferation, migration, and

invasion, although no significant effects were reported in the in vivo study [50]. FOXC1 was found to be overexpressed in BLBC and was able to activate the hedgehog signaling pathway [51]. In another case, this pathway might be initiated by the interaction of modified Hedgehog ligand towards the patched (Ptch1) receptor, a 12-pass transmembrane receptor. This event led to the activation of smoothened (Smo), a seven transmembrane protein that further stimulated multi-complex proteins that contained Gli protein. A zinc finger transcription factor then traveled into the nucleus to initiate the transcription of targeted genes [52,53]. Overexpression of Gli 1 protein (belonging to the family of Gli transcription factors) was observed to be associated with the unfavorable prognosis and survival of the breast cancer cells [54,55].

2.6. JAK/STAT Signaling Pathway

Extracellular stimuli such as cytokines (e.g., interleukins, interferons, and growth factors) can activate the JAK/STAT signaling pathway. JAK or Janus kinase and STAT (signal transducers and activator of transcription) are the intracellular proteins that cooperate with the transmembrane receptor in conveying signals down to the nucleus for DNA transcription and gene expression. STAT acts as the substrate of JAK, becomes phosphorylated, and travels into the nucleus to promote gene transcription. JAK/STAT signaling pathway is involved in stem cell maintenance, hematopoiesis, and participate in the process of inflammatory response. This signaling pathway may promote cell proliferation, differentiation, and has a role in controlling cellular apoptosis. The suppressor of cytokine signaling proteins (SOCS) is the regulator of the JAK/STAT negative feedback loop that functions as competitive inhibitors to STAT while STAT is the stimulator of the transcription of *SOCS* genes [56]. Dolled-Filhart et al. (2003) showed that STAT3 (a protein under the STAT family) and phosphorylated-STAT3 were overexpressed in 69.2% of breast cancer tumors [57]. Other investigations of STAT3 have confirmed the involvement of this protein in breast cancer malignancies [58,59].

2.7. Anti-Apoptotic Signaling Pathway

The anti-apoptotic signaling pathway is another pivotal component in breast cancer maintenance. BCL-2, BCL-XL, BCL-W, MCL-1, and BFL-1/A1 are the anti-apoptotic proteins in the BCL2 family. These gene are overexpressed in many cancers such as prostate, lung, stomach, ovarian, and breast carcinoma [60]. The BCL-2 (B-cell lymphoma 2) protein plays an anti-apoptotic role, leading to prolonged cancer cell survival [61–64]. Activation of the growth factor receptors, such as HER2, could modulate expression of BCL-2 via activation of PI-3 kinase signaling [63]. The cross-talks between the estrogen receptor (ER) with other membrane receptors might induce the transcription of target genes such as *BCL-2* gene expression. BCL-2 functions by inhibiting the pro-apoptotic proteins (e.g., BAD and BAX) in inducing cell death, thus, prolonging the survival of the cancer cells [64].

3. Growth Factor Receptors and Breast Cancer

The expression of the growth factor receptors (GFRs) is an important regulatory element that contributes to cell proliferation and survival. Regularly, the GFRs require ligand binding in order to transmit the downstream commands. The ligands may exist in the forms of growth factors, cytokines, or hormones.

3.1. Epidermal Growth Factor Receptor (EGFR)

The EGFR is a transmembrane receptor that falls under the receptor tyrosine kinase family [10]. The EGFR family consists of four sub-proteins which are EGFR1 to 4 (also known as ErbB 1 to 4). EGFR is regularly activated by the EGF, which acts as the ligand and the downstream signaling cascades such as the Ras/Raf, MAPK, and the PI3K/AKT which may be stimulated to govern cell proliferation and survival [65]. EGFR is one of the receptors that has been associated with the progression of breast cancer and the overexpression of the EGFR is often associated with poor prognosis [66]. Price et al. (1999) has worked on the MDA-MB-231 breast cancer cell line and found that the EGF might stimulate

the migration of the breast cancer cells via the activation of ERK1/2 signaling pathway [67,68]. In the case of molecular apocrine breast cancer (MABC), this molecular subtype of breast cancer is associated with poor prognosis as this subtype has negative expression of the estrogen receptor. Liu et al. (2018) [69] has found 53% of the MABC and non-MABC cases to be positive with EGFR expression via immunohistochemical analysis. The expression of EGFR was alongside the expression of other prominent breast cancer biomarkers such as the androgen receptor and Ki67 protein (the cellular marker for cell proliferation), thus suggesting EGFR is another therapeutic target for breast cancer treatment [69].

3.2. Insulin-Like Growth Factor 1 Receptor (IGF1R)

The IGF1R is a receptor that belongs to the IGFR family. It is a heterodimeric cell membrane receptor that comprises α- (subunit binding site) and β-(linked to the tyrosine kinase domain) chains that are projected towards the extracellular compound; whereas the tyrosine kinase domains are embedded within the layers of cell membrane [11,70]. The binding of IGF1 to the IGF1R results in the auto-phosphorylation of the tyrosine kinases and further activates the downstream signaling cascades, such as the PI3K/AKT and MAPK pathways [65]. The IGF family members, together with the IGF1R, were found to be overexpressed in breast cancer tumors and associated with cancer progression [71].

3.3. Transforming Growth Factor-Beta Receptor (TGF-βR)

TGF-βR has the TGFβ as the protein ligand which is available in the extracellular matrix (ECM) in order to encourage the intracellular signaling pathways [11]. There are three types of TGF-βR which are TGF-βR1, TGF-βR2, and TGF-βR3. The TGFβ1 and TGFβ3 ligands, once activated, will bind to the TGF-βR2, while the TGFβ2 has more affinity towards the TGF-βR3. The interaction between TGF-βR2 and its ligand may encourage the activation of TGF-βR1 [72,73]. Busch et al. (2015) showed that loss of expression of TGF- βR2 in the mammary fibroblast might stimulate tumorigenesis with increased tumor volume in the mouse xenograft model [74].

3.4. Vascular Endothelial Growth Factor Receptor (VEGFR)

The VEGFR is also a tyrosine kinase receptor that has seven immunoglobulin (Ig)-like domains projected at the extracellular region of the cell. The tyrosine kinase domains are rooted within the cell membrane layers (11). The VEGF–VEGFR interaction has often been associated with the angiogenesis or vasculogenesis of blood vessel in tumors, where the enlargement or growing tumors are in need of more nutrients supply as rapid growth rate is usually observed [75]. It has been shown that the growth of breast tumor in the murine model benefited from the expression of VEGFR1 expression [76]. VEGFR2 was confirmed to have roles in breast cancer angiogenesis and the inhibitor [YLL545, a novel synthesized compound from commercially available 1H-pyrazolo[3,4-d]-pyrimidin-4(5H)-one [1] for VEGFR2 has been shown to inhibit the downstream signaling regulators such as phosphor STAT and phosphor ERK1/2 [77]. Another compound named isomangeferin (a xanthone C-glucoside), was shown to bind to the VEGFR2 and suppressed tumor growth, metastasis, and angiogenesis [78].

3.5. Human Epidermal Growth Factor Receptor 2 (HER2/ERBB2)

HER2 is one of the members of receptor tyrosine kinase family that is encoded by *ERBB2* gene. The transmembrane receptor plays important roles in various cellular functions such as cell growth and differentiation [79,80]. However, 20%–30% of amplification of this gene is often seen in tumors of breast cancer [81]. Cross-talks between HER2 and other cell membrane receptors such as estrogen receptor (ER), IGFR, and EGFR may initiate downstream signaling through MAPK and PI-3 kinase pathways in breast cancer cells [82], suggesting the importance to determine the genes crucial in the cross-talks for therapeutic purpose. Moreover, there are other molecules that assist HER2 in governing breast cancer progression. The epithelial cell adhesion molecule (EpCAM) is a membrane glycoprotein that functions as a cell adhesion molecule in normal cells. However, it has been observed to be highly

expressed in cancers including breast cancer [83–85]. N-glycosylation of the EpCAM was observed in parallel with overexpression of HER2 in breast cancer tissues. Furthermore, this event was shown to increase cancer cell proliferation and prevent apoptosis [86]. A study by Peiris et al. (2017) has shown that the co-translational modification of the glycans, such as the N-linked glycans, reduced the binding efficiency of Herceptin towards HER2, thus decreasing the competency of the treatment [87]. Therefore, HER2 and associated glycoproteins could be targeted with an aim to reduce breast cancer progression.

4. siRNA Silencing Technique

Malignancies are often being associated with up-regulation of genes that causes overexpression of oncogenes [88–91]. Genetic manipulation, such as the introduction of the small interfering RNAs (siRNAs) has become one of the promising therapeutic approaches that is rapidly expanding. siRNA is a duplex RNA of 21–28 nucleotides that selectively degrades a mRNA transcript and thereby blocks its translation into a particular protein [92]. In eukaryotes, protein-coding genes are transcribed by RNA polymerase II to produce pre-mRNA which, upon further processing, becomes the mature mRNA [93]. The mature mRNAs travel from the nucleus into the cytoplasm for protein translation by ribosomes. The introduction of exogenous siRNA into the cells results in the formation of the RNA-induced silencing complex (RISC) by assembling with other proteins such as Argonaute and Dicer (Figure 2). Argonaute proteins are then activated to cleave the siRNA to become single stranded. In the cytoplasm, RISC carrying the single stranded siRNA binds to the complementary sequence on the targeted mRNA in a sequence specific manner. Slicer or Argonaute proteins will then cleave the mRNA complementary to the antisense strand in the newly formed double-stranded RISC-mRNA complex. The cleaved mRNA strands are recognized by the cell as aberrant and destroyed; thus, the expression of the targeted gene has successfully been 'silenced' [94,95].

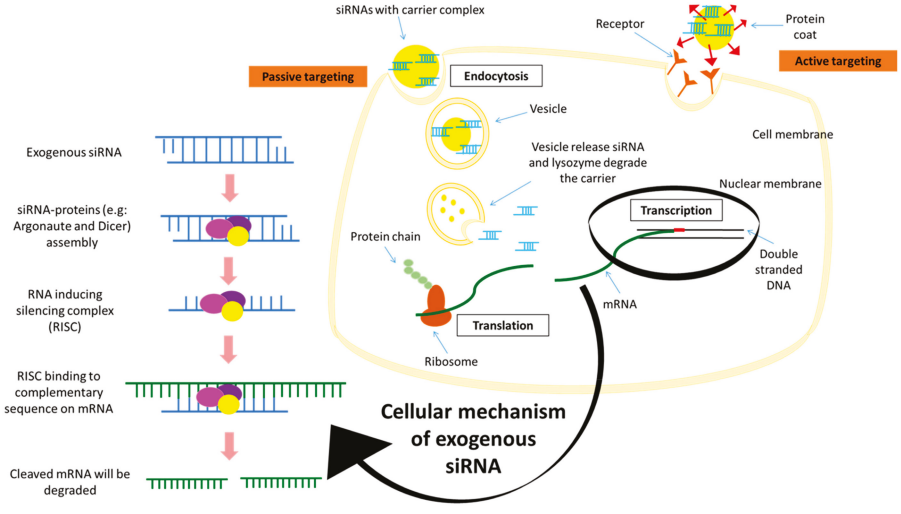

Figure 2. Schematic diagram of the mechanism of small interfering RNA (siRNA) in targeting mRNA for gene silencing (left) and exogenous siRNA duplex delivery into the cytoplasmic region via passive and active targeted delivery (right).

4.1. Advantages of siRNA Delivery

As a promising cancer therapeutic strategy, siRNA has several potential advantages over chemotherapeutic drugs. Firstly, siRNA has a high degree of safety, since it inhibits the post-transcriptional stage of gene expression through complementary base pairing with a target mRNA without interacting with chromosomal DNA; thereby, the risks of mutation and teratogenicity

are less [96]. The second advantage is its high degree of specificity in targeting a particular mRNA through RNA interference system, with the unlimited choice of targets. Another crucial advantage of siRNA is its high efficacy, suppressing the expression of a target gene strikingly in a single cancer cell with just several copies. Synthesis of siRNA is also much cheaper than that of antibodies or proteins.

4.2. Limitations of siRNA Delivery

There are several limitations to the clinical applications of siRNAs as therapeutics. The main challenge is the difficulty in passively delivering the siRNA which carries a negative charge due to the strong anionic phosphate backbone. The cell membrane which carries net negative charges repels the anionic siRNA, thus causing the process of passive diffusion of the exogenous siRNA to be challenging [97]. The water-soluble characteristic of the siRNA has further added hurdles to the process [98]. Despite the remarkable potency of siRNA in silencing specific gene expression, its half-life is too short because of the risk of degradation by serum nucleases which could affect the stability of siRNA, and quick elimination of the degraded products through the kidneys. In addition, 'naked' siRNA is hardly able to penetrate the tissue owing to its negatively charged phosphate backbone that could be repelled by anionic extracellular matrix molecules [99]. Even though siRNA molecules enter the cell through endocytosis, the fusion of endosomes with lysosomes results in degradation of the entrapped siRNAs. Nonetheless, various nanotechnology approaches have been harnessed to design suitable carriers for the siRNA to avoid degradation and assist in cellular delivery. Therefore, a suitable nano-carrier to transport siRNA molecules into tumor cells via endocytosis and subsequently release them in the cytoplasm is the prerequisite for achieving the maximum therapeutic outcomes from siRNA-mediated cleavage of the targeted mRNA. However, nanoparticles are prone to interact with reticuloendothelial system (RES) and hence, require surface modification prior to being used for systemic delivery of siRNA.

5. Delivery Systems of Potential Therapeutic siRNAs

Nanoparticles have emerged in the last few years as an alternative material for advanced diagnostic and therapeutic applications in medicine. A nanoparticle-based drug delivery system has two main targeting systems: Passive and active. Passive targeting relies on enhanced permeability and retention (EPR) effects of leaky vasculature (Figure 3) [99]. Tumor formation leads to underdevelopment of blood vessels that impairs the lymphatic drainage especially surrounding the tumor site. The leakiness of neoplastic blood vessels has great benefit in delivering and accumulating drugs up to 400 nm of size onto target sites [100]. Hobbs et al. (1998) showed that the vasculature of the tumors that was induced subcutaneously in mice had cut-off pore sizes in the range of 200 nm to 1.2 μm [101]. Active targeting includes ligand-mediated targeting, where ligands such as peptides or antibodies with affinity towards the nanoparticles or/and drugs are incorporated. The complex may recognize the targeted cells through binding to the receptors present on the cell surface. Active targeting may further augment the drug-delivery process to be more specific [100,102]. Therefore, it is crucial to identify highly expressed receptors, particularly on the breast cancer cells, to increase their specific binding with the ligands on the siRNA complexes and successful delivery of siRNA to the targeted sites.

Nanoparticles with size ranging 1–100 nm in diameter and large surface area [103] have been designed to bind and deliver siRNA, since naked siRNA is prone to degradation by serum nucleases and clearance by kidneys. Hence, the siRNA needs to be encapsulated with nanoparticles. Moreover, as mentioned above, nanoparticles can also be employed for targeted delivery of siRNA to tumor cells [104]. In addition, nanoparticles have the potential ability to penetrate and accumulate within tumor cells efficiently, as they have enhanced circulation time particularly when they possess hydrophilic coating on their surface, thus allowing for better therapeutics efficacy and, at the same time, minimizing the side effects of drugs. Nanoparticles can easily be imaged to track their progress in vivo.

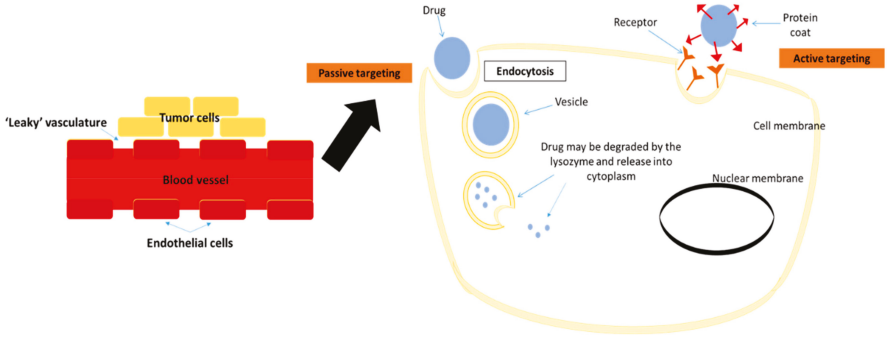

Figure 3. A schematic diagram showing 'leaky' vasculature of blood vessels at the tumor site, thus encouraging passive targeting of drug delivery. Active targeting employs the protein coating on the drug's surface to attract receptor binding upon drug delivery into the target site.

6. Current Targets for Nanoparticles-Facilitated siRNA Silencing

A combination of activated oncogenes and dysfunctional tumor suppressor genes lead to uncontrolled cell growth and blockage of natural apoptotic processes. Since crucial gene mutations responsible for cancer initiation and progression have been identified, the siRNA technology emerges as one of the highly promising approaches in treating breast cancer [105]. siRNA could be effective in cancer treatment as it is able to specifically inhibit any of the cancer-associated genes without being specific to their protein products. siRNA allows us to conceivably target the resistant cells in cancer treatment. Intriguingly, various sets of therapeutic siRNA molecules can be developed to target genes that are correlated with the multiple signaling pathways aberrantly activated in tumors. Nanotechnology is currently being explored in the development of nano-size drugs to efficiently deliver chemotherapy drugs to breast cancer cells and address the toxicity concern in relation to administration of higher doses of the drugs [106]. Introduction of exogenous siRNA into the breast cancer cells might be harnessed in order to overcome dose limitation of the chemotherapeutic drugs in clinical settings. However, since siRNA-loaded nanoparticles are accumulated in several other organs, in addition to the tumor, and the target genes that are overexpressed in breast cancer can also be expressed in those organs although at much lower level, silencing of those genes in non-target genes could produce adverse effects. Therefore, selection of target genes could be of crucial importance for clinical implications of siRNA-based nanotherapeutics. Table 1 showed the targeted genes for siRNA knockdown in breast cancer cells.

siRNA silencing of the MAPK pathway genes by targeting either the raf-1, mekk1, or mlk3 in acute myeloid leukemia (AML) cells was found to knockdown expression levels of between 40% and 60%. The data showed that when MAPK signaling pathway was partially blocked, the apoptosis pathway was upregulated and led to programmed cell death. Multiple siRNAs could be used together to target multiple genes of the MAPK pathway [107]. Bakhtiar et al. (2017) has developed nanoparticles from barium salts targeting the MAPK transcript in MCF-7 cell line and breast tumor in their in vivo study [108]. They have found success in delivery of the siRNAs, thus reducing the cell viability and inhibiting tumor growth. Silencing the MAPK genes specifically in MCF-7 cells caused the suppression of expression MAPK and activation of AKT, two important signaling molecules in both MAPK and PI3K pathways. On the other hand, our data have shown that delivery of selective siRNAs via carbonate apatite nanoparticle against the mRNA transcripts of the growth receptors including Estrogen Receptor 1 (ESR1) along with anti-apoptotic genes (BCL2), or with ERBB2 and EGFR, critically contributes to the induction of cell deaths in human and murine breast cancer cell lines by inhibiting the activation of MAPK and PI3K pathways [82]. Moreover, intravenous delivery of the selected siRNAs was able to retard tumor growth in mice.

Expressions of the BCL-2 and BCL-xL genes could promote cell survival by inhibiting apoptosis. Silencing of BCL-2 with the use of an antisense oligonucleotide appeared to be a promising cancer therapeutic approach. Silencing of Bcl-2 by siRNA followed by treatment with etoposide or doxorubicin had reduced the number of viable cancer cells and sensitized them to drug-induced apoptosis [109]. In addition, a calcium phosphate with polyelthyleneglycol (PEG)-polyanion polymer has recently been used to promote the delivery of siRNAs targeting the anti-apoptotic genes BCL-2 and BCL-xL in human breast cancer cells (MCF-7). The expression of BCL-2 and BCL-xL genes were decreased to 49% and 23%, respectively, after 48 hours of incubation with the respective siRNA. Silencing antiapoptotic genes such as BCL-2 and BCL-xL via the application of siRNAs delivered by hybrid nanoparticles was shown to be an effective and promising strategy against breast cancer [109].

Many cancer cells upregulate the expression of VEGF, thereby promoting angiogenesis that plays a crucial role in tumor development and metastasis. Previous study has shown that silencing VEGF expression by siRNA via polycation liposome-encapsulated calcium phosphate nanoparticles (PLCP) caused significant inhibition of tumor growth and angiogenesis in MCF-7 xenografts mice. Thus, the delivery of VEGF siRNA via PLCP to inhibit angiogenesis could be a promising strategy for breast cancer treatment, particularly when combined with DOX [110].

Since EpCAM, a cell surface molecule, is found to be overexpressed in cancers, Subramaniam et al. (2015) employed a novel aptamer-polyethyleneimine (PEI)-siRNA nanocomplex to target EpCAM in MCF-7 and retinoblastoma cell line (WERI-Rb1). They observed downregulation of EpCAM and inhibition of cell proliferation in the two cell lines [111].

Polo-like kinase 1 (PLK1) is a gene that is vital in cell division and DNA damage response and was found to be expressed in actively dividing cancer cells. PLK1 was targeted in metastatic breast cancer and triple negative breast cancer (TNBC). siRNA against the targeted gene was delivered via polymer-coated mesoporous silica with polyethyleneimine (PEI) and it was shown to inhibit cancer cell migration and invasion in TNBC cells. In the in vivo study, 80% of the target gene knockdown was observed in the mouse lung besides reduction in tumor incidence [112].

Moirangthem et al. (2016) [113] successfully transfected MDA-MB-231 human breast cancer cells with siRNA against uPA and matrix metalloproteinase 9 (MMP9) transcripts via lipid transfection. They showed that the cells were arrested in the S and G2-M after flow cytometry analysis [113]. Li et al. (2014) found that transfection of the siRNA with Lipofectamine 2000 against the cyclin-dependent kinase (CDK) 8 transcript was able to cause a significant decline in cell proliferation in MDA-MB-231 and MCF-7 cell lines [114]. Receptor tyrosine kinase expression, originated from the ROS1 oncogene, was found to be expressed in breast ductal carcinoma. Chua et al. (2013) employed carbonate apatite as the siRNA carrier targeting the c-ROS1 gene in MCF-7 cells. They observed enhancement in chemo-sensitivity of the cells towards cisplatin and paclitaxel treatments [115]. When the siRNA against IKKε was transfected into SK-BR-3 and MCF-7 human breast cancer cell lines, the siRNA was able to significantly reduce cell migration, invasion, and proliferation of both cell lines [116].

Silencing of the cyclin E expression by oligofectamine-facilitated siRNA delivery successfully reduced the expression of the targeted protein and led to apoptosis in SK-BR3, MDA-MB-436, and MDA-MB-157 cell lines. The xenografts of MDA-MB-436 implanted into the nude mice were successfully suppressed by cyclin E knockdown by employing the siRNA silencing technique [117].

HER2 siRNA-based therapeutics delivered using functionalized mesoporous silica nanoparticles coated with a cationic polymer and PEG conjugated to trastuzumab for HER2 targeting was shown to have an excellent safety profile. It could overcome intrinsic and acquired resistance to trastuzumab and lapatinib in HER2-positive breast cancer in vitro and in vivo [118,119]. For the long-term treatment effect of the therapeutic HER2 siRNA, the treated cells grew much slower and showed 67% increase in doubling time than cells that did receive any treatment [120]. The data indicated that the HER2 siRNA-based therapeutic provided a more durable inhibition of HER2 signaling to the cells.

Table 1. List of targeted genes for siRNA knockdown in breast cancer.

Targeted Genes	Delivery Carrier	Cell Line	Animal Model	References
ER, BCL-2, ERBB2,* and *EGFR	Carbonate apatite	MCF-7, MDA-MB-231	Balb/c	[82]
egfr1* and *erbb2	Carbonate apatite	MCF-7	Balb/c	[114]
BCL-2* and *BCL-XL	Calcium phosphate pEG-polyanion	MCF-7	NA	[109]
MAPK	Barium salts nanoparticles	MCF-7	Balb/c	[108]
VEGF	Polycation liposome-encapsulated calcium phosphate nanoparticles (PLCP)	MCF-7	Balb/c	[110]
EpCAM	Polyethyleneimine	MCF-7 and WERI-Rb1	NA	[111]
PLK1	Mesoporous silica coated with PEI and PEG	Bt549 and MDA-MB-231	SCID hairless SHO (Crl:SHO-Prkdc ^{scid} Hr ^{hr})	[112]
uPA* and *MMP9	Interferin transfection reagent	MDA-MB-231	NA	[113]
CDK8	Lipofectamine 2000	MDA-MB-231 and MCF-7	NA	[114]
c-ROS1	Carbonate apatite	MCF-7	NA	[115]
IKKε	Lipofectamine 2000	SK-BR-3 and MCF-7	NA	[116]
Cyclin E	Oligofectamine	SK-BR3, MDA-MB-157, MDA-MB-436, T47D, and MDA-MB-453	Nude mice	[117]
HER2	Mesoporous silica coated with cationic polymer and PEG	BT474	NA	[118]

NA: No information available.

7. Clinical Trials of nano-siRNA for Cancer Therapy

The first clinical trial of siRNA therapeutics was developed in 2004, not long after the discovery of RNAi. The rapid growth of siRNA accelerating into clinical trials is possibly due to the experience acquired during development of antisense and other nucleic acid-based therapies. To date, about 30 siRNA candidates have reached numerous stages of clinical trials for the treatment of different diseases including cancer [121–123]. Approximately one third of the siRNA-based therapeutics in clinical trials are targeted at cancer.

A cyclodextrin polymer-based system designated as CALAA-01 was the first systemic siRNA delivered using targeted nanoparticles in human. The siRNA-nanoparticle formulation contained four components, which includes a duplex synthetic non-chemically modified siRNA, a cyclodextrin-containing polymer, stabilizing agent, and targeting agent that contained the human transferrin protein. The human transferrin functions as targeting ligand. CALAA-01 contained the anti-R2 siRNA targeting ribonucleotide reductase subunit M2 (RRM2) for the treatment of solid tumor. Since RRM2 regulates BCL-2 in various types of cancers and plays an active role in tumor progression, it can serve as a potential target for cancer therapy [122]. A phase-I study involving systemic administration of CALAA-01 showed that the cancer-associated gene was silenced by RNAi mechanism in target tumor cells. In addition, the patients also showed inhibition of tumor growth, as siRNA treatment was able to reduce the expression of the M2 subunit of RRM2 [122,124]. CALAA-01 treatment was carried on until the disease progressed or the treatment may no longer tolerated by the patient. About 21% of the patients discontinued the test for the reason of adverse effects. No objective tumor responses were noticed with the exception of one patient who had stable disease following four months of treatment at the dose 30 mg/m^2 [125].

Besides CALAA-01, Silence Therapeutics conducted a phase-I study of the siRNA therapeutic Atu027 for the treatment of advanced solid tumor [125–127]. Atu027 was formulated as a liposomal particle containing siRNA that targeted protein kinase N3 (PKN3) gene. PKN3 is a downstream effector of PI3K signaling that is believed to be involved in cancer progression through the metastasis process. Inhibition of PKN3 caused significant reduction of tumor growth, as well as reduction of lymph node

metastasis in vivo [128]. Early results showed that after eight weeks of treatment, Atu027 was safe in patients with advanced solid tumor with no further progression of tumors in 41% of patients [127]. Further, a phase-Ib/IIa study for Atu027 in combination with gemcitabine was achieved after the lead-in safety period [129].

ALN-VSP02 was the first dual target of a siRNA drug carried by lipid nanoparticles developed by Alnylam Pharmaceuticals (Cambridge, MA, USA). This Stable Nucleic Acid Lipid Particle (SNALP)-formulated siRNA suppressed not only VEGF, but also the cell-cycle protein kinesin spindle protein (KSP) that promoted cell-cycle arrest and, subsequently, cell death [129–131]. A phase-I dose-escalation study was proposed in 2009. Provisional data from pharmacodynamics measurements showed preliminary evidence of clinical efficacy in the treatment of advanced solid tumor. Nevertheless, the study did not achieve the highest tolerated dose and the trial is still ongoing, to enroll more patients in a dose-escalating manner [121]. Analysis of phase-1 clinical trials showed comparable maximum concentration and area under the curve for VEGF and KSP upon single systemic injection of ALN-VSP. The treatment normalized the tumor vasculature as determined by VEGF mRNA levels and was associated with a decrease in tumor blood flow as observed via DCE-MRI. Further, the mRNA levels of KSP that influence the mitotic cell cycle was also observed by extrahepatic tumor biopsy [125,131]. The pharmacodynamic effect observed in biopsy sample from patients validated the successful delivery of the two siRNAs, indicating stability of the nanoparticles during systemic circulation.

A phase-I clinical trial of siRNA-EphA2-DOPC was recently authorized by the FDA and initiated by the MD Anderson Cancer Center. DOPC (1,2-dioleoylsn-glycero-3-phosphatidylcholine) is based on a type of neutral lipid to enhance siRNA entrapment efficiency. siRNA-EphA2-DOPC was constructed to shut down the activity of a genetic biomarker called EphA2. EphA2 overexpression is common in many human cancers, including breast cancer. EphA2 siRNA incorporated in DOPC nanoliposomes was greatly effective in lowering EphA2 protein levels after a single dose, and significantly reduced tumor growth three weeks after treatment [130].

Another ongoing phase-1 clinical study utilizing siRNA-transfected peripheral blood mononuclear cells (PBMCs) was APN401 for treatment of solid tumors that spread to other areas in the body or have relapsed [130]. APN401 might stop the growth of tumor cells by blocking some of the enzymes needed for cell growth. APN401 is a suspension of autologous PBMCs transfected with a siRNA that knock down Casitas-B-lineage lymphoma protein-b (Cbl-b). A single intravenous infusion of APN401 into patients with resistant solid tumors is possible and safe. This result supported phase-II clinical trials of multiple infusions of APN401 [132].

Other nanomedicines against breast cancer that have been approved or undergoing clinical trials were Myocet, LEP-ETU, EndoTAG-1, Lipoplatin, Genexol-PM, and Narekt-102 [133]. So far, clinical trials have shown great outcomes with no indication of adverse side effects. Moreover, avenues utilizing collateral treatment had produced promising results, hence indicating the possibility of personalized cancer treatment in the future.

8. Conclusions

Chemotherapy as cancer treatment stimulates various side effects that are unbearable for the patients. RNAi technique via siRNA gene silencing should be explored in depth to further develop and enhance tumor targeting treatments, thus making it as an efficient method to combat breast cancer and other cancers. The various oncogenic genes involved in the signaling pathways in breast cancers are suitable candidates for therapeutic targets. The flexibility of employing nanoparticles to deliver siRNAs against single or multiple oncogenic genes has made the treatment strategy highly promising. Moreover, by enabling tumor-selective delivery either through passive and/or active targeting, and subsequently, promoting efficient cellular uptake, nanoparticles could be harnessed to minimize the cost of siRNAs. In addition to that, siRNA might be the solution to increase the treatment efficiency by combating classical drugs resistance.

Funding: This research received funding from Sunway University Research Centre Grant (2018).

Conflicts of Interest: The authors declare no conflict of interest.

References

1. Ferlay, J.; Soerjomataram, I.; Dikshit, R.; Eser, S.; Mathers, C.; Rebelo, M.; Parkin, D.M.; Forman, D.; Bray, F. Cancer incidence and mortality worldwide: Sources, methods and major patterns in GLOBOCAN 2012. *Int. J. Cancer* **2015**, *136*, E359–E386. [CrossRef] [PubMed]
2. Siegel, R.L.; Miller, K.D.; Jemal, A. Cancer statistics, 2018. *CA Cancer J. Clin.* **2018**, *68*, 7–30. [CrossRef]
3. Ministry of Health; National Cancer Registry Department; National Cancer Institute. *Malaysian National Cancer Registry Report (2007–2011)*; Ministry of Health Malaysia: Putrajaya, Malaysia, 2016.
4. Globocan. Breast Cancer: Estimated Incidence, Mortality and Prevalence Worldwide in 2018. 2018. Available online: http://globocan.iarc.fr/Pages/fact_sheets_cancer.aspx (accessed on 5 April 2019).
5. Van Pham, P. Introduction to Breast Cancer. In *Breast Cancer Stem Cells & Therapy Resistance*; Springer International Publishing: Cham, Switzerland, 2015; pp. 1–4.
6. Carlson, N.; King, J. Overview of breast cancer treatment and reconstruction for primary care providers. *J. Midwifery Women's Health* **2012**, *57*, 558–568. [CrossRef]
7. Polyak, K. Heterogeneity in breast cancer. *J. Clin. Investig.* **2011**, *121*, 3786–3788. [CrossRef]
8. Chan, M.; Chang, M.C.; González, R.; Lategan, B.; del Barco, E.; Vera-Badillo, F.; Quesada, P.; Goldstein, R.; Cruz, I.; Ocana, A.; et al. Outcomes of estrogen receptor negative and progesterone receptor positive breast cancer. *PLoS ONE* **2015**, *10*, e0132449. [CrossRef]
9. Tang, L.; Han, X. The urokinase plasminogen activator system in breast cancer invasion and metastasis. *Biomed. Pharmacother.* **2013**, *67*, 179–182. [CrossRef] [PubMed]
10. Mansel, R.E.; Fodstad, O.; Jiang, W.G. Metastasis of breast cancer: An introduction. In *Metastasis of Breast Cancer*; Mansel, R.E., Fodstad, O., Jiang, W.G., Eds.; Springer: Dordrecht, The Netherlands, 2007; pp. 1–5.
11. Tiash, S.; Chowdhury, E.H. Growth factor receptors: Promising drug targets in cancer. *J. Cancer Metastasis Treat.* **2015**, *1*, 190–200.
12. Lokate, M.; Peeters, P.H.; Peelen, L.M.; Haars, G.; Veldhuis, W.B.; van Gils, C.H. Mammographic density and breast cancer risk: The role of the fat surrounding the fibroglandular tissue. *Breast Cancer Res.* **2011**, *13*, R103. [CrossRef] [PubMed]
13. Urlep, Z.; Rozman, D. The interplay between circadian system, cholesterol synthesis, and steroidogenesis affects various aspects of female reproduction. *Front Endocrinol.* **2013**, *4*, 111. [CrossRef]
14. Yaghjyan, L.; Colditz, G.A. Estrogens in the breast tissue: A systematic review. *Cancer Causes Control CCC* **2011**, *22*, 529–540. [CrossRef] [PubMed]
15. Wang, W. Radiotherapy in the management of early breast cancer. *J. Med. Radiat. Sci.* **2013**, *60*, 40–46. [CrossRef]
16. Harbeck, N. HER2-positive breast cancer: Neoadjuvant and adjuvant therapy. In *Handbook of HER2-Targeted Agents in Breast Cancer*; Springer International Publishing: Cham, Switzerland, 2016; pp. 29–49.
17. Figueroa-Magalhães, M.C.; Jelovac, D.; Connolly, R.; Wolff, A.C. Treatment of HER2-positive breast cancer. *Breast (Edinb. Scotl.)* **2014**, *23*, 128–136. [CrossRef] [PubMed]
18. Liedtke, C.; Gonzalez-Angulo, A.M.; Pusztai, L. Definition of triple-negative breast cancer and relationship to basal-like molecular subtype. In *DeVita, Hellman, and Rosenberg's Cancer: Principles and Practice of Oncology*; DeVita, V.T., Lawrence, T.S., Rosenberg, S.A., Eds.; Lippincott Williams & Wilkins: Philadelphia, PA, USA, 2010; pp. 1–6.
19. Wang, M.; Zhu, J.; Lubman, D.; Gao, C. Aberrant glycosylation and cancer biomarker discovery: A promising and thorny journey. *Clin. Chem. Lab. Med.* **2018**, *57*, 407–416. [CrossRef] [PubMed]
20. Cheng, W.; Oon, C. How glycosylation aids tumor angiogenesis: An updated review. *Biomed. Pharmacother.* **2018**, *103*, 1246–1252. [CrossRef] [PubMed]
21. Banerjee, A.; Lang, J.; Hung, M.; Sengupta, K.; Banerjee, S.; Baksi, K.; Banerjee, D. Unfolded Protein Response Is Required innu/nuMice Microvasculature for Treating Breast Tumor with Tunicamycin. *J. Biol. Chem.* **2011**, *286*, 29127–29138. [CrossRef] [PubMed]
22. Kwa, M.; Adams, S. Checkpoint inhibitors in triple-negative breast cancer (TNBC): Where to go from here. *Cancer* **2018**, *124*, 2086–2103. [CrossRef]

23. Thamarajah, L. Complementary and Alternative Therapies for Breast Cancer Worldwide. *Lett. Health Biol. Sci.* **2018**, *4*, 27–32.
24. Barrie, R.C.; Gary, D. Complementary and Alternative Therapies for Cancer. *Oncologist* **2003**, *9*, 80–89.
25. Azim, H.A., Jr.; de Azambuja, E.; Colozza, M.; Bines, J.; Piccart, M.J. Long-term toxic effects of adjuvant chemotherapy in breast cancer. *Ann. Oncol.* **2011**, *22*, 1939–1947. [CrossRef]
26. Nooren, I.M.A.; Thornton, J.M. CHAPTER 4—Molecular Sociology A2—Bradshaw, Ralph A. In *Handbook of Cell Signaling*; Dennis, E.A., Ed.; Academic Press: Burlington, NJ, USA, 2003; pp. 21–26.
27. Chial, H. Proto-oncogenes to Oncogenes to Cancer. *Nat. Educ.* **2008**, *1*, 33.
28. Basu, A.K. DNA damage, mutagenesis and cancer. *Int. J. Mol. Sci.* **2018**, *19*, 970. [CrossRef]
29. Schaeffer, H.J.; Weber, M.J. Mitogen-activated protein kinases: Specific messages from ubiquitous messengers. *Mol. Cell. Biol.* **1999**, *19*, 2435–2444. [CrossRef]
30. Chen, Z.; Gibson, T.B.; Robinson, F.; Silvestro, L.; Pearson, G.; Xu, B.; Wright, A.; Vanderbilt, C.; Cobb, M.H. MAP kinases. *Chem. Rev.* **2001**, *101*, 2449–2476. [CrossRef]
31. Kyriakis, J.M.; Avruch, J. Mammalian mitogen-activated protein kinase signal transduction pathways activated by stress and inflammation. *Physiol. Rev.* **2001**, *81*, 807–869. [CrossRef]
32. Cargnello, M.; Roux, P.P. Activation and function of the MAPKs and their substrates, the MAPK-activated protein kinases. *Microbiol. Mol. Biol. Rev. MMBR* **2011**, *75*, 50–83. [CrossRef]
33. Sivaraman, V.S.; Wang, H.; Nuovo, G.J.; Malbon, C.C. Hyperexpression of mitogen-activated protein kinase in human breast cancer. *J. Clin. Investig.* **1997**, *99*, 1478–1483. [CrossRef]
34. Meng, F.; Zhang, H.; Liu, G.; Kreike, B.; Chen, W.; Sethi, S.; Miller, F.R.; Wu, G. p38gamma mitogen-activated protein kinase contributes to oncogenic properties maintenance and resistance to poly (ADP-ribose)-polymerase-1 inhibition in breast cancer. *Neoplasia* **2011**, *13*, 472–482. [CrossRef]
35. Vivanco, I.; Sawyers, C.L. The phosphatidylinositol 3-Kinase AKT pathway in human cancer. *Nat. Rev. Cancer* **2002**, *2*, 489–501. [CrossRef]
36. Baselga, J. Targeting the phosphoinositide-3 (PI3) kinase pathway in breast cancer. *Oncologist* **2011**, *16* (Suppl. 1), 12–19. [CrossRef]
37. Luo, J.; Manning, B.D.; Cantley, L.C. Targeting the PI3K-Akt pathway in human cancer: Rationale and promise. *Cancer Cell* **2003**, *4*, 257–262. [CrossRef]
38. Wickenden, J.A.; Watson, C.J. Key signaling nodes in mammary gland development and cancer. Signalling downstream of PI3 kinase in mammary epithelium: A play in 3 Akts. *Breast Cancer Res.* **2010**, *12*, 202. [CrossRef]
39. Bose, S.; Chandran, S.; Mirocha, J.M.; Bose, N. The Akt pathway in human breast cancer: A tissue-array-based analysis. *Mod. Pathol.* **2006**, *19*, 238–245. [CrossRef] [PubMed]
40. Shankar, E.; Krishnamurthy, S.; Paranandi, R.; Basu, A. PKCepsilon induces Bcl-2 by activating CREB. *Int. J. Oncol.* **2010**, *36*, 883–888.
41. Clapham, D.E. Calcium signaling. *Cell* **1995**, *80*, 259–268. [CrossRef]
42. Roderick, H.L.; Cook, S.J. Ca^{2+} signaling checkpoints in cancer: Remodelling Ca2+ for cancer cell proliferation and survival. *Nat. Rev. Cancer* **2008**, *8*, 361–375. [CrossRef] [PubMed]
43. Hanahan, D.; Weinberg, R.A. The hallmarks of cancer. *Cell* **2000**, *100*, 57–70. [CrossRef]
44. Di, J.; Huang, H.; Qu, D.; Tang, J.; Cao, W.; Lu, Z.; Cheng, Q.; Yang, J.; Bai, J.; Zhang, Y.; et al. Rap2B promotes proliferation, migration, and invasion of human breast cancer through calcium-related ERK1/2 signaling pathway. *Sci. Rep.* **2015**, *5*, 12363. [CrossRef]
45. Reczek, C.; Chandel, N. ROS Promotes Cancer Cell Survival through Calcium Signaling. *Cancer Cell* **2018**, *33*, 949–951. [CrossRef] [PubMed]
46. Acar, A.; Simoes, B.M.; Clarke, R.B.; Brennan, K. A role for Notch signaling in breast cancer and endocrine resistance. *Stem Cells Int.* **2016**, *2016*, 2498764. [CrossRef]
47. Ling, H.; Sylvestre, J.R.; Jolicoeur, P. Notch1-induced mammary tumor development is cyclin D1-dependent and correlates with expansion of pre-malignant multipotent duct-limited progenitors. *Oncogene* **2010**, *29*, 4543–4554. [CrossRef]
48. Cohen, B.; Shimizu, M.; Izrailit, J.; Ng, N.F.; Buchman, Y.; Pan, J.G.; Dering, J.; Reedijk, M. Cyclin D1 is a direct target of JAG1-mediated Notch signaling in breast cancer. *Breast Cancer Res. Treat.* **2010**, *123*, 113–124. [CrossRef] [PubMed]

49. Kasper, M.; Jaks, V.; Fiaschi, M.; Toftgård, R. Hedgehog signaling in breast cancer. *Carcinogenesis* **2009**, *30*, 903–911. [CrossRef] [PubMed]
50. Mott, L.; Su, K.; Pack, D. Evaluation of FOXC1 as a therapeutic target for basal-like breast cancer. *Cancer Gene Ther.* **2018**, *25*, 84–91. [CrossRef]
51. Han, B.; Qu, Y.; Jin, Y.; Yu, Y.; Deng, N.; Wawrowsky, K.; Zhang, X.; Li, N.; Bose, S.; Wang, Q.; et al. FOXC1 activates Smoothened-independent Hedgehog signaling in basal-like breast cancer. *Cell Rep.* **2015**, *13*, 1046–1058. [CrossRef]
52. Bai, C.B.; Stephen, D.; Joyner, A.L. All mouse ventral spinal cord patterning by hedgehog is Gli dependent and involves an activator function of Gli3. *Dev. Cell* **2004**, *6*, 103–115. [CrossRef]
53. Kasper, M.; Regl, G.; Frischauf, A.M.; Aberger, F. GLI transcription factors: Mediators of oncogenic Hedgehog signaling. *Eur. J. Cancer* **2006**, *42*, 437–445. [CrossRef]
54. Ten Haaf, A.; Bektas, N.; von Serenyi, S.; Losen, I.; Arweiler, E.C.; Hartmann, A.; Knüchel, R.; Dahl, E. Expression of the glioma-associated oncogene homolog (GLI) 1 in human breast cancer is associated with unfavourable overall survival. *BMC Cancer* **2009**, *9*, 298. [CrossRef] [PubMed]
55. Gonnissen, A.; Isebaert, S.; Haustermans, K. Targeting the Hedgehog signaling pathway in cancer: Beyond Smoothened. *Oncotarget* **2015**, *6*, 13899–13913. [CrossRef]
56. Croker, B.A.; Kiu, H.; Nicholson, S.E. SOCS regulation of the JAK/STAT signaling pathway. *Semin. Cell Dev. Biol.* **2008**, *19*, 414–422. [CrossRef] [PubMed]
57. Thomas, S.J.; Snowden, J.A.; Zeidler, M.P.; Danson, S.J. The role of JAK/STAT signaling in the pathogenesis, prognosis and treatment of solid tumours. *Br. J. Cancer* **2015**, *113*, 365–371. [CrossRef]
58. Dolled-Filhart, M.; Camp, R.L.; Kowalski, D.P.; Smith, B.L.; Rimm, D.L. Tissue microarray analysis of signal transducers and activators of transcription 3 (Stat3) and phospho-Stat3 (Tyr705) in node-negative breast cancer shows nuclear localization is associated with a better prognosis. *Clin. Cancer Res.* **2003**, *9*, 594–600. [PubMed]
59. Alvarez, J.V.; Febbo, P.G.; Ramaswamy, S.; Loda, M.; Richardson, A.; Frank, D.A. Identification of a genetic signature of activated signal transducer and activator of transcription 3 in human tumors. *Cancer Res.* **2005**, *65*, 5054–5062. [CrossRef] [PubMed]
60. Kirkin, V.; Joos, S.; Zornig, M. The role of Bcl-2 family members in tumorigenesis. *Biochim. Biophys. Acta* **2004**, *1644*, 229–249. [CrossRef] [PubMed]
61. Oltersdorf, T.; Elmore, S.W.; Shoemaker, A.R.; Amstrong, R.C.; Augeri, D.J.; Belli, B.A. An inhibitor of Bcl-2 family proteins induces regression of solid tumours. *Nature* **2005**, *435*, 677–681. [CrossRef] [PubMed]
62. Klasa, R.J.; Gillum, A.M.; Klem, R.E.; Frankel, S.R. Oblimersen Bcl-2 antisense: Facilitating apoptosis in anticancer treatment. *Antisense Nucleic Acid Drug Dev.* **2002**, *12*, 193–213. [CrossRef]
63. Carpenter, R.L.; Lo, H.W. Regulation of apoptosis by HER2 in breast cancer. *J. Carcinog. Mutagen.* **2013**, *2013* (Suppl. 7), 003.
64. Hata, A.N.; Engelman, J.A.; Faber, A.C. The BCL-2 family: Key mediators of the apoptotic response to targeted anti-cancer therapeutics. *Cancer Discov.* **2015**, *5*, 475–487. [CrossRef]
65. Voudouri, K.; Berdiaki, A.; Tzardi, M.; Tzanakakis, G.N.; Nikitovic, D. Insulin-like growth factor and epidermal growth factor signaling in breast cancer cell growth: Focus on endocrine resistant disease. *Anal. Cell. Pathol. (Amst.)* **2015**, *2015*, 975495. [CrossRef] [PubMed]
66. Harris, A.L.; Nicholson, S.; Sainsbury, R.; Wright, C.; Farndon, J. Epidermal growth factor receptor and other oncogenes as prognostic markers. *J. Natl. Cancer Inst. Monogr.* **1992**, *11*, 181–187.
67. Price, J.T.; Tiganis, T.; Agarwal, A.; Djakiew, D.; Thompson, E.W. Epidermal growth factor promotes MDA-MB-231 breast cancer cell migration through a phosphatidylinositol 3′-kinase and phospholipase C-dependent mechanism. *Cancer Res.* **1999**, *59*, 5475–5478.
68. Witsch, E.; Sela, M.; Yarden, Y. Roles for growth factors in cancer progression. *Physiology* **2010**, *25*, 85–101. [CrossRef] [PubMed]
69. Liu, X.; Feng, C.; Liu, J.; Liu, J.; Li, C.; Xu, C.; Niu, Y. The importance of EGFR as a biomarker in molecular apocrine breast cancer. *Hum. Pathol.* **2018**, *77*, 1–10. [CrossRef]
70. Ullrich, A.; Gray, A.; Tam, A.W.; Yang-Feng, T.; Tsubokawa, M.; Collins, C.; Henzel, W.; Le Bon, T.; Kathuria, S.; Chen, E.; et al. Insulin-like growth factor I receptor primary structure: Comparison with insulin receptor suggests structural determinants that define functional specificity. *EMBO J.* **1986**, *5*, 2503–2512. [CrossRef] [PubMed]

71. LeRoith, D.; Roberts, C.T., Jr. The insulin-like growth factor system and cancer. *Cancer Lett.* **2003**, *195*, 127–137. [CrossRef]
72. Shi, Y.; Massague, J. Mechanisms of TGF-beta signaling from cell membrane to the nucleus. *Cell* **2003**, *113*, 685–700. [CrossRef]
73. Cheifetz, S.; Andres, J.L.; Massague, J. The transforming growth factor-beta receptor type III is a membrane proteoglycan. Domain structure of the receptor. *J. Biol. Chem.* **1988**, *263*, 16984–16991. [PubMed]
74. Busch, S.; Acar, A.; Magnusson, Y.; Gregersson, P.; Ryden, L.; Landberg, G. TGF-beta receptor type-2 expression in cancer-associated fibroblasts regulates breast cancer cell growth and survival and is a prognostic marker in pre-menopausal breast cancer. *Oncogene* **2015**, *34*, 27–38. [CrossRef] [PubMed]
75. Shibuya, M. Vascular endothelial growth factor (VEGF) and its receptor (VEGFR) signaling in angiogenesis: A crucial target for anti- and pro-angiogenic therapies. *Genes Cancer* **2011**, *2*, 1097–1105. [CrossRef] [PubMed]
76. Wu, Y.; Hooper, A.T.; Zhong, Z.; Witte, L.; Bohlen, P.; Rafii, S.; Hicklin, D.J. The vascular endothelial growth factor receptor (VEGFR-1) supports growth and survival of human breast carcinoma. *Int. J. Cancer* **2006**, *119*, 1519–1529. [CrossRef] [PubMed]
77. Zhang, J.; Liu, C.; Shi, W.; Yang, L.; Zhang, Q.; Cui, J.; Fanf, Y.; Li, Y.; Ren, G.; Yang, S.; et al. The novel VEGF receptor 2 inhibitor YLL545 inhibits angiogenesis and growth in breast cancer. *Oncotarget* **2016**, *7*, 41067–41080. [CrossRef] [PubMed]
78. Wang, B.; Shen, J.; Wang, Z.; Liu, J.; Ning, Z.; Hu, M. Isomangiferin, a novel potent vascular endothelial growth factor receptor 2 kinase inhibitor, suppresses breast cancer growth, metastasis and angiogenesis. *J. Breast Cancer* **2018**, *21*, 11–20. [CrossRef]
79. Gutierrez, C.; Schiff, R. HER2: Biology, detection, and clinical implications. *Arch. Pathol. Lab. Med.* **2011**, *135*, 55–62. [PubMed]
80. Rubin, I.; Yarden, Y. The Basic Biology of HER2. *Ann. Oncol.* **2001**, *12* (Suppl. 1), S3–S8. [CrossRef]
81. Mitri, Z.; Constantine, T.; O'Regan, R. The HER2 Receptor in Breast Cancer: Pathophysiology, Clinical Use, and New Advances in Therapy. *Chemother. Res. Pract.* **2012**, *2012*, 743193. [CrossRef]
82. Kamaruzman, N.I.; Tiash, S.; Ashaie, M.; Chowdhury, E.H. siRNAs Targeting Growth Factor Receptor and Anti-Apoptotic Genes Synergistically Kill Breast Cancer Cells through Inhibition of MAPK and PI-3 Kinase Pathways. *Biomedicines* **2018**, *6*, 73. [CrossRef] [PubMed]
83. Carpenter, G.; Red Brewer, M. EpCAM: Another surface-to-nucleus missile. *Cancer Cell* **2009**, *15*, 165–166. [CrossRef]
84. Imrich, S.; Hachmeister, M.; Gires, O. EpCAM and its potential role in tumor-initiating cells. *Cell Adhes. Migr.* **2012**, *6*, 30–38. [CrossRef]
85. Munz, M.; Baeuerle, P.A.; Gires, O. The emerging role of EpCAM in cancer and stem cell signaling. *Cancer Res.* **2009**, *69*, 5627–5629. [CrossRef]
86. Zhang, D.; Liu, X.; Gao, J.; Sun, Y.; Liu, T.; Yan, Q.; Yang, X. The role of epithelial cell adhesion molecule N-glycosylation on apoptosis in breast cancer cells. *Tumor Biol.* **2017**. [CrossRef] [PubMed]
87. Peiris, D.; Spector, A.; Lomax-Browne, H.; Azimi, T.; Ramesh, B.; Loizidou, M.; Welch, H.; Dwek, M. Cellular glycosylation affects Herceptin binding and sensitivity of breast cancer cells to doxorubicin and growth factors. *Sci. Rep.* **2017**, *7*, 43006. [CrossRef] [PubMed]
88. Menard, S.; Tagliabue, E.; Campiglio, M.; Pupa, S.M. Role of HER2 gene overexpression in breast carcinoma. *J. Cell. Physiol.* **2000**, *182*, 150–162. [CrossRef]
89. Daly, R.J.; Binder, M.D.; Sutherland, R.L. Overexpression of the Grb2 gene in human breast cancer cell lines. *Oncogene* **1994**, *9*, 2723–2727.
90. Zollo, M.; Andre, A.; Cossu, A.; Sini, M.C.; D'Angelo, A.; Marino, N.; Budroni, M.; Tanda, F.; Arrigoni, G.; Palmieri, G. Overexpression of h-prune in breast cancer is correlated with advanced disease status. *Clin. Cancer Res.* **2005**, *11*, 199–205.
91. Hayashi, S.I.; Eguchi, H.; Tanimoto, K.; Yoshida, T.; Omoto, Y.; Inoue, A.; Yoshida, N.; Yamaguchi, Y. The expression and function of estrogen receptor alpha and beta in human breast cancer and its clinical application. *Endocr. Relat. Cancer* **2003**, *10*, 193–202. [CrossRef]
92. Ryther, R.C.C.; Flynt, A.S.; Phillips, J.A.; Patton, J.G. siRNA therapeutics: Big potential from small RNAs. *Gene Ther.* **2004**, *12*, 5–11. [CrossRef] [PubMed]
93. Nikolova, D.; Toncheva, D. RNA Interference—Regulations and Application in Oncology. *J. Cancer Mol.* **2008**, *4*, 67–77.

94. Shen, H.; Mittal, V.; Ferrari, M.; Chang, J. Delivery of gene silencing agents for breast cancer therapy. *Breast Cancer Res. BCR* **2013**, *15*, 205. [CrossRef]
95. Bernstein, E.; Denli, A.M.; Hannon, G.J. The rest is silence. *RNA* **2001**, *7*, 1509–1521. [PubMed]
96. Xu, C.-F.; Wang, J. Delivery systems for siRNA drug development in cancer therapy. *Asian J. Pharm. Sci.* **2015**, *10*, 1–12. [CrossRef]
97. Chowdhury, E.H. Strategies for tumor-directed delivery of siRNA. *Expert Opin. Drug Deliv.* **2011**, *8*, 389–401. [CrossRef] [PubMed]
98. Ahmadzada, T.; Reid, G.; McKenzie, D. Fundamentals of siRNA and miRNA therapeutics and a review of targeted nanoparticle delivery systems in breast cancer. *Biophys. Rev.* **2018**, *10*, 69–86. [CrossRef]
99. Torchilin, V.P. Passive and active drug targeting: Drug delivery to tumors as an example. *Handb. Exp. Pharmacol.* **2010**, 3–53. [CrossRef]
100. Danhier, F.; Feron, O.; Preat, V. To exploit the tumor microenvironment: Passive and active tumor targeting of nanocarriers for anti-cancer drug delivery. *J. Control. Release* **2010**, *148*, 135–146. [CrossRef]
101. Hobbs, S.K.; Monsky, W.L.; Yuan, F.; Roberts, W.G.; Griffith, L.; Torchilin, V.P.; Jain, R.K. Regulation of transport pathways in tumor vessels: Role of tumor type and microenvironment. *Proc. Natl. Acad. Sci. USA* **1998**, *95*, 4607–4612. [CrossRef] [PubMed]
102. Upponi, J.R.; Torchilin, V.P. Passive vs. active targeting: An update of the EPR role in drug delivery to tumors. In *Nano-Oncologicals: New Targeting and Delivery Approaches*; Alonso, M.J., Garcia-Fuentes, M., Eds.; Springer International Publishing: Cham, Switzerland, 2014; pp. 3–45.
103. Huang, C.; Zhang, Y.; Yuan, H.; Gao, H.; Zhang, S. Role of nanoparticle geometry in endocytosis: Laying down to stand up. *Nano Lett.* **2013**, *13*, 4546–4550. [CrossRef] [PubMed]
104. Tatiparti, K.; Sau, S.; Kashaw, S.K.; Iyer, A.K. siRNA delivery strategies: A comprehensive review of recent developments. *Nanomaterials* **2017**, *7*, 77. [CrossRef]
105. Bora, R.S.; Gupta, D.; Mukkur, T.K.; Saini, K.S. RNA interference therapeutics for cancer: Challenges and opportunities (review). *Mol. Med. Rep.* **2012**, *6*, 9–15. [CrossRef]
106. Markman, J.L.; Rekechenetskiy, A.; Holler, E.; Ljubimova, J.Y. Nanomedicine therapeutic approaches to overcome cancer drug resistance. *Adv. Drug Deliv. Rev.* **2013**, *65*, 1866–1879. [CrossRef]
107. Mohd Hafiz, M.R.; Zain, M.; Mohd Faiz, F.A.; Mohamed Saifulaman, M.S. Targeted RNAi of the Mitogen-activated Protein Kinase Pathway Genes in Acute Myeloid Leukemia Cells. *Sains Malays.* **2013**, *42*, 1131–1137.
108. Bakhtiar, A.; Kamaruzman, N.I.; Othman, I.; Zain, A.; Chowdhury, E. Intracellular delivery of p53 gene and MAPK siRNA into breast cancer cells utilizing barium salt nanoparticles. *J. Breast Cancer Res. Adv.* **2017**. [CrossRef]
109. De Mello, L.J.; Souza, G.R.; Winter, E.; Silva, A.H.; Pittella, F.; Creczynski-Pasa, T.B. Knockdown of antiapoptotic genes in breast cancer cells by siRNA loaded into hybrid nanoparticles. *Nanotechnology* **2017**, *28*, 175101. [CrossRef] [PubMed]
110. Chen, J.; Sun, X.; Shao, R.; Xu, Y.; Gao, J.; Liang, W. VEGF siRNA delivered by polycation liposome-encapsulated calcium phosphate nanoparticles for tumor angiogenesis inhibition in breast cancer. *Int. J. Nanomed.* **2017**, *12*, 6075–6088. [CrossRef]
111. Subramanian, N.; Kanwar, J.; Athalya, P.; Janakiraman, N.; Khetan, V.; Kanwar, R.; Eluchuri, S.; Krishnakumar, S. EpCAM aptamer mediated cancer cell specific delivery of EpCAM siRNA using polymeric nanocomplex. *J. Biomed. Sci.* **2015**, *22*, 4. [CrossRef] [PubMed]
112. Morry, J.; Ngamcherdtrakul, W.; Gu, S.; Reda, M.; Castro, D.J.; Sangvanich, T.; Gray, J.W.; Yantasee, W. Targeted treatment of metastatic breast cancer by PLK1 siRNA delivered by an antioxidant nanoparticle platform. *Mol. Cancer Ther.* **2017**, *16*, 763–772. [CrossRef] [PubMed]
113. Moirangthem, A.; Bondhopadhyay, B.; Mukherjee, M.; Bandyopadhyay, A.; Mukherjee, N.; Konar, K.; Bhattacharya, S.; Basu, A. Simultaneous knockdown of uPA and MMP9 can reduce breast cancer progression by increasing cell-cell adhesion and modulating EMT genes. *Sci. Rep.* **2016**, *6*, 21903. [CrossRef] [PubMed]
114. Li, X.Y.; Luo, Q.F.; Wei, C.K.; Li, D.F.; Fang, L. siRNA-mediated silencing of CDK8 inhibits proliferation and growth in breast cancer cells. *Int. J. Clin. Exp. Pathol.* **2014**, *7*, 92–100.
115. Chua, M.; Tiash, S.; Fatemian, T.; Noordin, M.I.; Cheong, S.; Chowdhury, E.H. Carbonate apatite-facilitated intracellular delivery of c-ROS1 siRNA sensitizes MCF-7 breast cancer cells to cisplatin and paclitaxel. *Cancer* **2013**, *1*. [CrossRef]

116. Qin, B.; Cheng, K. Silencing of the IKKε gene by siRNA inhibits invasiveness and growth of breast cancer cells. *Breast Cancer Res.* **2010**, *12*, R74. [CrossRef]
117. Liang, Y.; Gao, H.; Lin, S.Y.; Goss, J.A.; Brunicardi, F.C.; Li, K. siRNA-based targeting of cyclin E overexpression inhibits breast cancer cell growth and suppresses tumor development in breast cancer mouse model. *PLoS ONE* **2010**, *5*, e12860. [CrossRef]
118. Gu, S.; Ngamcherdtrakul, W.; Reda, M.; Hu, Z.; Gray, J.W.; Yantasee, W. Lack of acquired resistance in HER2-positive breast cancer cells after long-term HER2 siRNA nanoparticle treatment. *PLoS ONE* **2018**, *13*, e0198141-e. [CrossRef]
119. Ozcan, G.; Ozpolat, B.; Coleman, R.L.; Sood, A.K.; Lopez-Berestein, G. Preclinical and clinical development of siRNA-based therapeutics. *Adv. Drug Deliv. Rev.* **2015**, *87*, 108–119. [CrossRef]
120. Ku, S.H.; Jo, S.D.; Lee, Y.K.; Kim, K.; Kim, S.H. Chemical and structural modifications of RNAi therapeutics. *Adv. Drug Deliv. Rev.* **2016**, *104*, 16–28. [CrossRef]
121. Yin, H.; Kanasty, R.L.; Eltoukhy, A.A.; Vegas, A.J.; Dorkin, J.R.; Anderson, D.G. Non-viral vectors for gene-based therapy. *Nat. Rev. Genet.* **2014**, *15*, 541–555. [CrossRef]
122. Rahman, M.A.; Amin, A.R.; Wang, D.; Koenig, L.; Nannapaneni, S.; Chen, Z.; Wang, Z.; Sica, G.; Chen, Z.G.; Shin, D.M. RRM2 regulates Bcl-2 in head and neck and lung cancers: A potential target for cancer therapy. *Clin. Cancer Res.* **2013**, *19*, 3416–3428. [CrossRef]
123. Davis, M.E.; Zuckerman, J.E.; Choi, C.H.; Seligson, D.; Tolcher, A.; Alabi, C.A.; Yen, Y.; Heidel, J.D.; Ribas, A. Evidence of RNAi in humans from systemically administered siRNA via targeted nanoparticles. *Nature* **2010**, *464*, 1067–1070. [CrossRef]
124. Zuckerman, J.E.; Davis, M.E. Clinical experiences with systemically administered siRNA-based therapeutics in cancer. *Nat. Rev. Drug Discov.* **2015**, *14*, 843–856. [CrossRef] [PubMed]
125. Aleku, M.; Schulz, P.; Keil, O.; Santel, A.; Schaeper, U.; Dieckhoff, B.; Janke, O.; Endruschat, J.; Durieux, B.; Röder, N.; et al. Atu027, a liposomal small interfering RNA formulation targeting protein kinase N3, inhibits cancer progression. *Cancer Res.* **2008**, *68*, 9788–9798. [CrossRef]
126. Schultheis, B.; Strumberg, D.; Santel, A.; Vank, C.; Gebhardt, F.; Keil, O.; Lange, C.; Giese, K.; Kaufmann, J.; Khan, M.; et al. First-in-human phase I study of the liposomal RNA interference therapeutic Atu027 in patients with advanced solid tumors. *J. Clin. Oncol.* **2014**, *32*, 4141–4148. [CrossRef] [PubMed]
127. Santel, A.; Aleku, M.; Roder, N.; Mopert, K.; Durieux, B.; Janke, O.; Endruschat, J.; Dames, S.; Lange, C.; Eisermann, M.; et al. Atu027 prevents pulmonary metastasis in experimental and spontaneous mouse metastasis models. *Clin. Cancer Res.* **2010**, *16*, 5469–5480. [CrossRef] [PubMed]
128. Tao, W.; South, V.J.; Zhang, Y.; Davide, J.P.; Farrell, L.; Kohl, N.E.; Sepp-Lorenzino, L.; Lobell, R.B. Induction of apoptosis by an inhibitor of the mitotic kinesin KSP requires both activation of the spindle assembly checkpoint and mitotic slippage. *Cancer Cell* **2005**, *8*, 49–59. [CrossRef]
129. Tabernero, J.; Shapiro, G.I.; LoRusso, P.M.; Cervantes, A.; Schwartz, G.K.; Weiss, G.J.; Paz-Ares, L.; Cho, D.C.; Infante, J.R.; Alsina, M.; et al. First-in-humans trial of an RNA interference therapeutic targeting VEGF and KSP in cancer patients with liver involvement. *Cancer Discov.* **2013**, *3*, 406–417. [CrossRef] [PubMed]
130. Naing, A.; Lopez-Berestein, G.; Fu, S.; Tsimberidou, A.; Pant, S.; Piha-Paul, S.; Janku, F.; Hong, D.; Sulovic, S.; Meng, X.; et al. EphA2 gene targeting using neutral liposomal small interfering RNA (EPHARNA) delivery: A phase I clinical trial. *J. Clin. Oncol.* **2017**, *35*, TPS2604. [CrossRef]
131. Triozzi, P.L. *APN401 in Treating Patients with Recurrent or Metastatic Pancreatic Cancer, Colorectal Cancer, or Other Solid Tumors That Cannot Be Removed by Surgery*; NCT03087591; NIH: Bethesda, MD, USA, 2017.
132. Triozzi, P.; Kooshki, M.; Alistar, A.; Bitting, R.; Neal, A.; Lametschwandtner, G.; Loibner, H. Phase I clinical trial of adoptive cellular immunotherapy with APN401 in patients with solid tumors. *J. Immunother. Cancer* **2015**, *3* (Suppl. 2), P175. [CrossRef]
133. Li, Y.; Humphries, B.; Yang, C.; Wang, Z. Nanoparticle-Mediated Therapeutic Agent Delivery for Treating Metastatic Breast Cancer-Challenges and Opportunities. *Nanomaterials* **2018**, *8*, 361. [CrossRef]

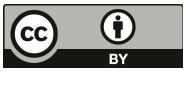

cancers

MDPI

Review

Recent Progress in the Theranostics Application of Nanomedicine in Lung Cancer

Anubhab Mukherjee [1,*], Manash Paul [2,*] and Sudip Mukherjee [3,*]

[1] Department of Translational Neurosciences and Neurotherapeutics, John Wayne Cancer Institute, Providence Saint John's Health Center, 2200 Santa Monica Boulevard, Santa Monica, CA 90404, USA
[2] Division of Pulmonary and Critical Care Medicine, David Geffen School of Medicine, The University of California, Los Angeles (UCLA) Factor Bldg. 10-240, 621 Charles E. Young Dr., Los Angeles, CA 90095, USA
[3] Department of Bioengineering, Rice University, 6500 Main Street, Houston, TX 77005, USA
* Correspondence: anubhabrsv@gmail.com (A.M.); paul_cancerbiotech@yahoo.co.in (M.P.); sudip.mukherjee@rice.edu or sudip.mukherjee1988@gmail.com (S.M.)

Received: 30 March 2019; Accepted: 27 April 2019; Published: 29 April 2019

Abstract: Lung cancer is one of the leading causes of cancer-related death worldwide. Non-small cell lung cancer (NSCLC) causes around 80% to 90% of deaths. The lack of an early diagnosis and inefficiency in conventional therapies causes poor prognosis and overall survival of lung cancer patients. Recent progress in nanomedicine has encouraged the development of an alternative theranostics strategy using nanotechnology. The interesting physico-chemical properties in the nanoscale have generated immense advantages for nanoparticulate systems for the early detection and active delivery of drugs for a better theranostics strategy for lung cancer. This present review provides a detailed overview of the recent progress in the theranostics application of nanoparticles including liposomes, polymeric, metal and bio-nanoparticles. Further, we summarize the advantages and disadvantages of each approach considering the improvement for the lung cancer theranostics.

Keywords: lung cancer; nanomedicine; theranostics; clinical status; cancer therapy

1. Introduction

Lung cancer is one of the prevalent malignancies and leading causes of cancer-related mortality and the most common cancer in men, accounting for an estimated 154,050 deaths in 2018 and worldwide [1–3]. As per the GLOBOCAN, a project of the International Agency for Research on Cancer (IARC), estimation, approximately 18.1 million new cancer cases would have been detected in 2018 [2]. This dreadful disease owes its origin mostly (85%) to long term tobacco smoking [4]. It turns out that at the time of diagnosis lung cancer in many patients has metastasized to other tissues in the body. According to the 2012 global lung cancer statistics, an estimated 1.8 million new cases were reported 58% of which occurred in less developed countries [5]. The American Cancer Society reported over 221,200 estimated new cases of lung cancer and 158,040 death cases in 2015 in the United States [2,3]. Around 85% of lung cancer patients had non-small cell lung cancer while the remaining 15% had small cell lung cancer. The survival rate in lung cancer patients depends primarily on early diagnosis and surgical resection of the tumor tissue is often the preferred therapy [6,7]. Clinically used therapeutic modalities are still associated with a poor outcome: Only <20% five-year overall survival is reported as cancer cells routinely become impervious to drugs. Among all the presently available cancer therapies, chemotherapy is the most widely used treatment strategy for lung cancer. The insufficient drug concentration in the tumor tissue is one of the major impediments retarding the clinical success of lung cancer chemotherapy. To meet this up-hill therapeutic challenge, repeated applications of anti-cancer agents at high concentrations are being used in systemic chemotherapy which is causing adverse side

effects. The commonly observed adverse side effects in chemotherapy based cancer treatments mostly originate from the ability of many potent cytotoxic drugs to penetrate non-cancerous healthy body tissues in addition to tumor tissues [8]. Novel therapeutic modalities for more effective treatment of lung cancer are, therefore, urgently needed.

In recent years, enormous endeavors have been directed toward the development of new warheads and their effective carriers to reduce the probability of occurrences of multi-drug resistance, combinations of hydrophilic with hydrophobic drugs, small interfering RNA (siRNAs) with hydrophobic drugs being majorly explored among them [9]. Global efforts are also being witnessed on delivering potent anti-cancer drugs selectively to tumor tissues by encapsulating the drugs within various types of drug carriers [10–12]. The exo-surfaces of such drug carriers are covalently grafted with tumor-specific targeting motifs including small peptides, aptamers, proteins, and antibodies [13–17].

Much to our intrigue, theranostics (therapy plus diagnostic) nanomedicine has emerged as a propitious paradigm in cancer therapy. It involves advantages of the both world: highly efficacious nanocarriers to ferry cargo while loading onto them both imaging and therapeutic agents. The idea spawned a plethora of nanoparticles, well suitable for drug delivery as well as diagnosis, facilitating the advent of personalized medicine. There exists four crucial aspects to take into account while designing an efficacious nanoplatform based therapeutics: (i) Selecting a potent therapeutic, ranging from small molecule drugs to larger peptide or nucleic acid; (ii) to choose a stable carrier; (iii) to adopt a targeting and drug release strategy; and (iv) to carefully single out an imaging agent [18–24].

The present review is an attempt to update major advancements in lung cancer theranostics: A description of development of various nanosystems (liposomes, polymeric nanoparticles, metal nanoparticles, bio-nanoparticles, etc.) for efficient delivery of an array of theranostics in lung cancer.

2. Lung Cancer: Category, Cause, Molecular Target, and Limitations of Conventional Therapy

Non-small cell lung cancer is the most prevalent cancer and can be further categorized into two major subtypes which include small cell lung cancer (SCLC) and non-small cell lung cancer (NSCLC) based on the histological appearance. Though SCLC is more aggressive but less frequent as compared to NSCLC. NSCLC can be sub-classified into three major histological subtypes: Adenocarcinoma, squamous cell-carcinoma, and large cell-lung cancer. Again, each of the subtypes is distinct and responds differently to available therapies.

Lung carcinogenesis is influenced by the interaction of ecological factors, for example, tobacco smoke, and genetic susceptibility. The cancer susceptibility increases significantly with rare germ line mutations like p53, retinoblastoma, epidermal growth factor receptor (EGFR), etc. Moreover, reduced DNA repair efficiency may also play a critical role in lung carcinogenesis [25]. Chemicals in tobacco smoke are reported to play a major role in lung carcinogenesis. Research advances have provided clear evidence for the role of tyrosine kinases in the pathophysiology of lung cancer. Constitutive kinase activation and downstream signaling may arise due to mutation(s), overexpression, and autocrine paracrine incitement, leading to cancer. Oncogenic activation of tyrosine kinase like EGFR, PIK3CA, MET etc. are frequently observed in NSCLC and thereby offer opportunity for therapeutic targeting [25,26].

Despite the fact that progresses are made in the treatment of non-small cell lung cancer (NSCLC), the five-year survival rate for lung malignant growth has expanded by just 5% in recent years. Surgery serves an important treatment modality of early stage disease but surgery for lung cancer is complex and can have serious consequences. Early detection of lung malignant growth is another hurdle in effective treatment of lung cancer patients. Roughly seventy five percent of patients with lung disease will present symptoms, and the majority of these have an advanced stage of tumor at the time of diagnosis.

The emergence of cancer chemotherapy and radiation therapy is partially effective in the initial stage of NSCLC treatment. Due to the advent of robust sequencing techniques and initiation of large genome wide association studies it is quite clear that molecular heterogeneity exists even in the same

cancer subtypes. Heterogeneity can exist among the primary tumor and the metastatic counterpart, even within the cells of a particular tumor or based on the cell of origin. The molecular diversity and the cancer cells ability to acquire adaptive resistance create a definite challenge in planning an effective therapy [27]. A new approach addressing patient specific molecular specificities and patient centered approach is needed.

3. Alternative Theranostics by Nanomedicine

Nanotechnology is one of the fast growing fields in the area of biomedical science that has been utilized to solve different biological problems including therapeutics and diagnostics. Recently, nanotechnology has been widely utilized for the treatment of various diseases including cancer, diabetes, bacterial infections, cardiovascular diseases, etc. [28–30]. Due to several limitations in the conventional therapeutic strategies for lung cancers, scientists and researchers have focused on the development of the nanoscale therapeutic agents, whereas the delivery system includes liposomal nanoparticles, polymeric nanoparticles, metal nanoparticles, and bio-nano particles. The lung cancer theranostics applications of these nanoparticles has been largely effective due to their small size, that enables them to specifically accumulate in tumor cells due to an enhanced permeability and retention effect (EPR) [31]. Moreover, nanoparticles are easy to functionalize and demonstrates high drug loading due to large surface area to volume [29]. Apart from that, due to good biocompatibility and the capability of overcoming clearance by the kidney effacing long circulation nanoparticles holds edge over conventional therapeutic treatments. Moreover, several nanoparticles displayed multifunctional abilities like imaging, diagnostics, therapeutics, sensing that helps researchers to utilize these nanomaterials for multifunctional biomedical applications in lung cancer theranostics. Here in this review, we have focused on the theranostics applications of various types of nanomaterials that have shown enormous promise for the applications in lung cancer diagnosis and therapy including (a) liposomal nanoparticles, (b) polymeric nanoparticles, (c) bio-nanoparticles, and (d) metal nanoparticles (Figure 1).

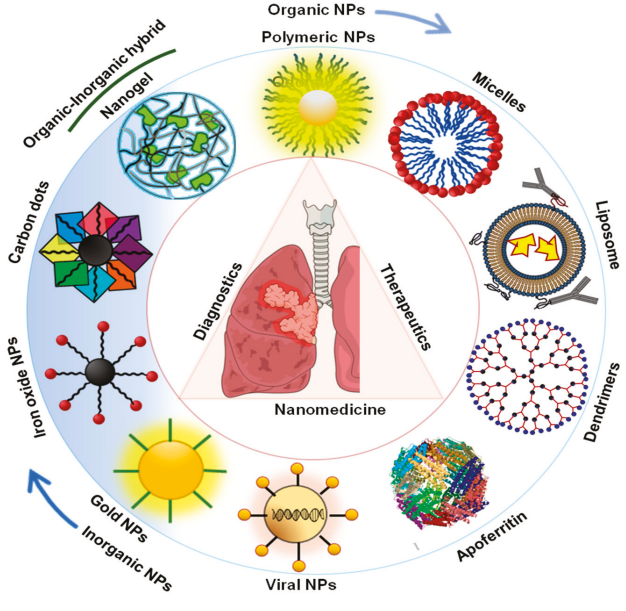

Figure 1. Schematic representation of different theranostics nanomedicine approaches in lung cancer theranostics.

4. Liposomal Nanoparticles for Lung Cancer Theranostics

Liposomes are artificially generated vesicles with a bilayer structure spontaneously formed when natural or synthetic amphiphatic lipids get dispersed in water. Ever since their inception, they have largely been explored as drug delivery vehicles because of their biocompatibility and beneficial safety profile. The bilayer structure of liposomes comprises of phosphatidylcholine, cholesterol, etc. and they are known to carry an array of small molecule and large molecule therapeutics of hydrophobic and hydrophilic origin. Their surface can be modified by grafting polyethylene glycol (PEG), which prolongs their half-life in circulation [32,33]. Doxil and Myocet, two leading Doxorubicin liposomes, received FDA approval in 1995 and 1999, respectively, followed by many of the category [34,35]. Despite availability of around sixteen liposomal drugs in the market as of now, very few formulations are designated as the treatment modality for NSCLC. Here we summarize a few recent examples of liposomes for pulmonary delivery of therapeutics.

In 2014, Cheng et al. [36] exploited EGFR binding affinity of a novel peptide GE11 in doxorubicin-loaded liposomes and characterized them in terms of size distribution, zeta potential, drug entrapment efficiency, and morphology. It turned out that optimal GE11 density was 10% in A549 cytotoxicity. Major involvement of clathrin-mediated endocytosis pathway was also determined by cellular uptake experiments. Using a near infrared (NIR) fluorescence imaging system, they found that the accumulation and retention of the GE-11 modified liposomes was 2.2-fold higher compared to unmodified liposomes [36]. For effective delivery of triptolide (TPL) to NSCLC by pulmonary administration, a dual ligand (anti-carbonic anhydrase IX (anti-CA IX) antibody and CPP33) modified triptolide-loaded liposomes (dl-TPL-lip) was designed, synthesized, and characterized by Lin et al. [37] in 2018. The cell killing ability was evaluated by an apoptosis assay. Importantly, superior tumor penetration and tumor growth inhibition efficacy of the liposomes were further demonstrated using 3D tumor spheroids. Pharmacokinetics studies in rats after endotracheal administration of the liposomal formulations exhibited a lower concentration of TPL in circulation [37]. In 2017, Song et al. [38] came up with a multifunctional targeting liposome for the treatment of NSCLC and achieved better in vivo effects. They decorated the liposome surface by Octreotide (OCT), a synthetic 8-peptide analog of somatostatin that binds to somatostatin receptors overexpressed in a variety of tumors. Two drugs were co-encapsulated in the liposome: Honokiol into the lipid bilayer to reduce tumor metastasis and inhibit vasculogenic mimicry channel formations, and epirubicin into the aqueous core as an antitumor drug. Mechanistic investigation studies revealed that these liposomes could downregulate PI3K, MMP-2, MMP-9, VE-Cadherin, and FAK and activate caspase 3 [38]. In 2013, Mukherjee et al. designed and synthesized a series of guanidinylated cationic amphiphiles and demonstrated that systemic administration of a 19 bp synthetic CDC20 siRNA encapsulated within liposomes of guanidinylated cationic amphiphile with stearyl tails inhibits B16F10 solid tumor growth and intravenous administration of the same liposomal formulation inhibits B16F10 melanoma growth on lung (metastases) in a syngeneic C57BL/6J mouse tumor model [39].

As a suitable alternative, pulmonary drug delivery strategy, i.e., local delivery via inhalation has gained substantial attention of researchers across the globe. This enables us to reach higher local drug concentration to the specific site of action. This also demands a low dose of therapeutics with reduced toxicity. We intend to provide few examples of liposomes to be inhaled as reported in the last two decades: In 2000, Anderson PM and coworkers designed a phase I study to examine the efficacy and toxicity of administering interleukin (IL)-2 liposomes by aerosol to patients with lung metastases. The liposome-aerosol was inhaled for ~20 min thrice a day. The dose chosen was based on previous studies. Nine patients were treated in three cohorts of three patients at varying IU of IL-2 thrice a day. Authors reported that inhalation of IL-2 liposomes is well tolerated with any reduced systemic toxicity [40]. In another phase I dose-escalating study performed by Wittgen et al. [41] safety, efficacy and PK of aerosolized liposomal (sustained release lipid inhalation targeting, SLIT) cis-platin were investigated in patients having lung cancer. In seventeen patients SLIT cis-platin was well tolerated. No nephrotoxicity, ototoxicity, hematologic toxicity, or neurotoxicity was revealed by safety data.

Together, they concluded that the use of aerosolized liposomal cis-platin was feasible and safe [41]. Importantly, in 2010, Makale and co-workers developed a PEGylated DOX liposome with a dextran core, containing iron oxide for MRI contrast and Bodipy for fluorescence and demonstrated robust imaging ability of these nanoparticles (NPs) in an in vivo murine Lewis lung carcinoma model [42]. In 2011, Lowery et al. [43] decorated the surface of a DOX entrapped liposome with a phage displayed peptide HVGGSSV to achieve radiation guided selective drug delivery to tumors. Liposomes were labeled with Alexa Fluor 750 and the biodistribution of the labeled liposomes was studied in a murine Lewis lung carcinoma model by near infrared (NIR) imaging [43]. The liposomes are widely applied for lung cancer theranostics as they show immense promise due to their excellent biocompatibility and biodegradability [44,45]. Moreover, liposomes hold the edges over other nanoparticles as they are useful to load a high amount of therapeutic agents and can be easily controlled for sustained drug delivery [44,45]. However, liposomal nanoparticles have some disadvantages like batch to batch variability, high manufacturing cost, possible drug leakage, etc. [44]. Hence, careful fabrication strategies are required to overcome these challenges and reduction of the cost.

5. Polymeric Nanoparticles for Lung Cancer Theranostics

Polymeric NPs, on the other hand, can be prepared either by nanoprecipitation or a double emulsion method via self-assembly of biodegradable amphiphilic block-copolymers with varying hydrophobicity's between blocks and are suitable for systemic administration. The core-shell structure of polymeric NPs facilitates encapsulation of hydrophobic drugs, extension of circulation time, and sustained drug release. Their surfaces can also be decorated for targeted drug delivery [46,47]. For instance, Genexol-PM is a formulation of paclitaxel and poly (D,L-lactide)-b-polyethylene glycol-methoxy (PLGA-mPEG), which is already marketed for metastatic breast cancer therapy in Korea and other European countries [48,49]. Here we summarize a few recent interesting examples of usage of polymeric NPs for treatment of lung cancer.

In 2015, Jiang [50] developed a nano-carrier encapsulating Crizotinib (approved for EML4-ALK fusion positive lung cancer) within polylactide tocopheryl polyethylene glycol 1000 succinate (PLA-TPGS), which showed a sustained release, induced remarkable cytotoxicity in NCIH3122 lung cancer cells, and noticeable early and late apoptosis. The polymeric nanoparticle followed an endocytosis-mediated cellular uptake [50]. Interestingly, in 2017 Hu et al. [51] reported on the efficiency of paclitaxel (PTX) loaded Polycaprolactone/ Poly (ethylene glycol)/Polycaprolactone (PCEC) nanoparticles combined with chronomodulated chemotherapy for use in lung cancer. The authors set out to map the suitable time of the day for administering drug loaded nano-carriers by making out the crucial role of circadian rhythms in cancer propagation. The combination therapy demonstrated remarkable tumor growth inhibition in vivo, while it turned out that 15HALO is optimal for chemotherapy [51]. Very recently, to circumvent the low targeting capacity of nanoparticles, Wang et al. used mesenchymal stem cells (MSC) as a carrier for drug delivery loaded with nanoparticles with docetaxel (DTX). MSC proved its superiority over fibroblasts in drug loading. Both cellular and animal experiments justified the intercellular translocation of nanoparticles from MSC to cancer cell. It also inhibited primary tumor growth in vivo [52]. Much to our intrigue, Ganesh et al. explored HA-PEI/PEG nano-carriers for CD44-targeted siRNA delivery to lung cancer cells. They undertook a detailed structure-activity study for optimal siRNA encapsulation efficiency. Importantly, the targeted HA-PEI/PEG nanosystems encapsulating SSB/PLK1 siRNA showed higher cellular uptake and sequence specific gene knockdown in vivo both in sensitive and resistant A549 primary and metastatic [53].

Polymer based delivery of chemotherapeutics via inhalation has also made substantial progress in recent years. Kim et al., in 2013, made an attempt to make highly porous PLGA microparticles entrapping doxorubicin where the surface of the particles was decorated with Apo2L/TRAIL (tumor necrosis factor (TNF)-related apoptosis-inducing ligand) that binds selectively to death receptors such as DR4/TRAIL-R1 expressed specifically on cancer cells. The particles got deposited in a mouse lung followed by pulmonary administration and exhibited tumor growth inhibition in nude mice with

H226 metastatic lung cancer cells [54]. Furthermore, for pulmonary inhalation treatment, Feng et al. developed a two-in-one nanosystem comprising of doxorubicin and paclitaxel encapsulated into a porous PLGA microparticles and established a synergy between the two drugs at DOX:PTX 5:1 in vitro. Co-delivery remained superior over their individual counterparts in vivo as well [55]. Khatun et al. [56] demonstrated multifunctional cancer theranostics application of graphene-doxorubicin in a HA nanogel in human lung cancer cell line (A549). This nanocomposite was used as thermo and chemotherapeutic, real-time noninvasive optical imaging, and a controlled drug release [56] (Figure 2). Importantly, in a study performed in 2006, Mitra et al. [57] observed an enhanced tumor targeting the capability of N-(2-hydroxypropyl) methacrylamide (HPMA) copolymers when coupled with RGDfK and RGD4C in C57BL/6NHsd mice bearing Lewis lung carcinoma. They conjugated radionuclides with longer half-life such as 111In compounds to HPMA for scintigraphic imaging and detected contrast enhancement at the tumor site after 24h of injection [57]. In 2010, Gao and co-worker developed an MRI-visible PLA polymeric micelle whose surface was decorated by a peptide RGDLATLRQL directed towards $\alpha v\beta 6$ integrin over-expressing human NSCLC cell H2009. DOX and super-paramagnetic iron oxide nanoparticles (SPIONs) were loaded inside the micelle core for drug delivery and MR imaging, respectively [58]. The polymeric nanoparticles are extensively applied for lung cancer theranostics due to their biocompatibility, biodegradability, high drug pay load, sustained drug release, high scalability, low batch variability, low cost production, and easy tunability [44,45].

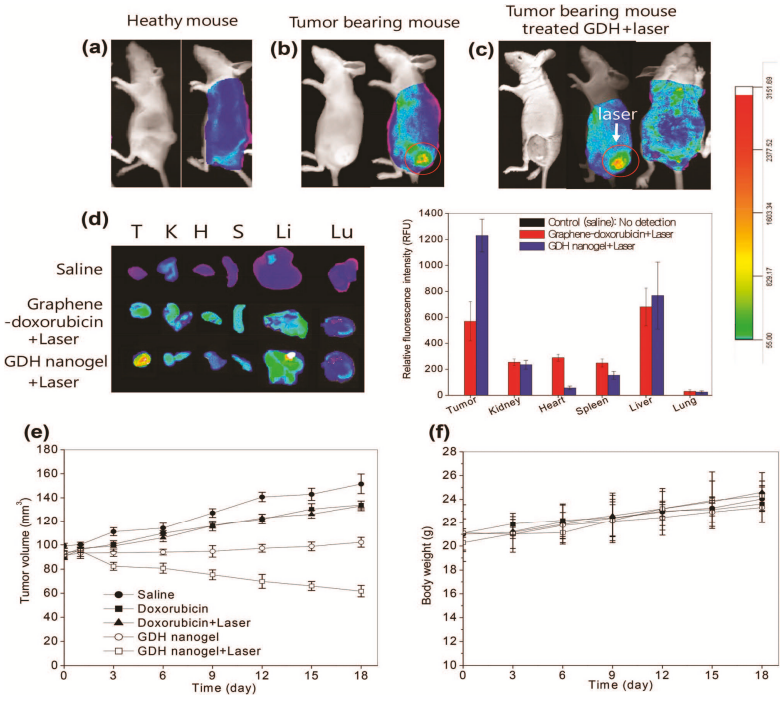

Figure 2. In vivo optical imaging and thermo-chemotherapy using the nanogel. (**a**,**b**) are optical images of healthy mice and tumor bearing mice, respectively. (**c**) Light responsive imaging. The nanogels were intravenously injected and 670 nm laser was applied to the tumors for 30 min. (**d**) Ex vivo imaging and fluorescence intensities of tumors and normal tissues. Organs were arranged in the following order: Tumor (T), kidney (K), heart (H), spleen (S), liver (Li), and lung (Lu). (**e**) Thermo-chemotherapy after treating doxorubicin and the nanogels with and without laser irradiation. (**f**) Body weight changes of mice after treatment with the nanogels. The data were plotted as mean ± SEM (n = 5). Reproduced from [56]. Copyright © 2015 Royal Society of Chemistry.

6. Bio-Nanoparticles for Lung Cancer Theranostics

Due to high biocompatibility, better stability and biodegradability current researchers have shifted their focal point of research towards using the bio-nanoparticles including protein nanoparticles, solid lipid nanoparticles, viral nanoparticles, aptamers, and apoferritin, wherein a bio-mimicking component is incorporated to the therapeutic nanoparticles [59,60]. In the recent past, these types of nanoparticles were successfully designed, synthesized, and utilized for cancer theranostics applications in lung cancer [59,61,62].

6.1. Viral Nanoparticles

Viral nanoparticles (VNPs) obtained from viruses and bacteriophages have gained immense interest for various biomedical applications including drug delivery, biosensing, bioimaging, and vaccine development due to their biocompatibility, flexibility in sizes and shapes, and easy surface modification [63]. Many researchers have developed a combinational approach with chemotherapy and immunotherapy for the treatment of lung cancer due to challenges of drug resistance. Veljanski et al. has published an exciting review about the use genetically modified oncolytic viruses (OVs) with conventional chemotherapies in the treatment of lung cancer. The inability of chemo-drugs to destroy the cancer stem cells is well compensated by OVs-based gene therapy [64]. The cowpea mosaic virus (CPMV) with an average size of ~28 nm has a high potential for vaccination therapy in lung cancer [65].

6.2. Protein-Based Nanoparticles

Protein nanoparticles prepared from a naturally occurring protein, such as gelatin, gliadin, albumin, and legumin have been recently used for the drug and gene delivery purposes either alone or in a mixture with biodegradable polymers in lung cancer therapy due to their excellent biocompatibility, and lack of inflammation in human bronchial cells and high cellular uptake [66–68]. Cationic bovine serum albumin (CBSA) has been utilized for the delivery of siRNA for the metastatic lung cancer therapy [69].

6.3. Apoferritin

Apoferritin is the hollow protein nanocage without the iron core that is composed of self-assembling 24 polypeptide subunits and has internal and external diameters of 8 nm and 12 nm, respectively. Upon removal of the iron core the apoferritin undergoes a process of assembly and disassembly with the change in pH that is extensively utilized for the synthesis of various nanoparticles for lung cancer theranostics [70,71]. Li et al. demonstrated the lung cancer diagnosis of A549 cells by using fluorescence and MR imaging of apoferritin, a ferritin-based multifunctional nanostructure [71]. The authors synthesized multifunctional hybrid nanostructures made of ferritin that showed green fluorescence and had ferrimagnetic iron oxide nanoparticles into the hollow ferritin cavity. This multifunctional apoferritin was used for the imaging $\alpha v\beta 3$ integrin upregulated cancer cells. In another recent paper by Luo et al., demonstrated the use of hyaluronic acid (HA)-conjugated apoferritin nanocages for pH-responsive controlled intracellular prodrug release of the anticancer drug daunomycin (DN), which was encapsulated into the interior of apoferritin [72]. Moreover, the authors modified the apoferritin by HA to target and kill the cancer cells (embryonic lung MRC-5 cells and lung cancer A549 cells) upon binding to the HA-receptor CD44.

Bio-nanoparticles are widely applied for lung cancer theranostics as they demonstrate huge promise due to their good biocompatibility and biodegradability. However, the synthesis strategies can be complex at times and that can increase the cost and time of manufacturing. Hence, more research needed to manufacture these bio-nanoparticles from lab-scale to commercial industrial scale.

7. Inorganic Nanoparticles for Lung Cancer Theranostics

Inorganic nanoparticles have long been used for various biomedical applications including drug delivery, nucleic acid delivery, bio-sensing, diagnostics, imaging, and cancer therapy due to their exciting physico-chemical properties in the nanoscale range [73–76]. Among various inorganic nanoparticles, gold, silver, iron oxides, silica, rare earth oxides, carbon dots, and nanodiamonds were extensively studied in lung cancer theranostics [77–79]. Moreover, these nanoparticles demonstrated prominent cytotoxic effects on various lung cells in vitro and in vivo that depend largely on their size, shape, surface charge, concentration, and time of exposure. An accurate control over these physico-chemical parameters can facilitate their meaningful application in lung cancer theranostics.

7.1. Gold Nanoparticles (AuNPs)

Gold nanoparticles were extensively used for cancer theranostics applications due to easy synthesize and functionalize high biocompatibility, and multifunctional theranostics properties [80–82]. Several research groups utilized AuNPs for lung cancer theranostics [77]. For example, Nanospectra has developed a silica-gold nanoshells stabilized by (poly)ethylene glycol (PEG) for the photothermal therapy to the solid tumors using an NIR light source [83]. More importantly, in a recent clinical trial, AuroLase® was used for the photothermal therapy of primary or metastatic lung tumors (NCT01679470) [84]. In a recent published report by Knights et al. the authors demonstrated the size dependent effects of gold nanorods (AuNRs) on the photoacoustic (PA) imaging response and pulsed-wave photothermal therapeutic (PW-PPTT) efficacy, which is crucial for the clinical translation of AuNRs [77]. Interestingly, the PA intensity increased with the AuNR size due to the overall mass of the nanoparticles. All the different sized AuNRs showed toxicity in lung cancer cells upon laser fluence with a highest cell death in the smallest AuNR treatment, indicating the theranostics potential of AuNRs combined with PW lasers in lung cancer. In another recent report, Ramalingam et al. [85] showed the enhanced anti-cancer efficacy of doxorubicin (DOX) using polyvinylpyrrolidone functionalized AuNPs (Dox@PVP-AuNPs) in lung cancer cells. Mechanistic studies demonstrated that Dox@PVP-AuNPs treatment to lung cancer cells increases reactive oxygen species (ROS) generation, up-regulates the tumor suppressor genes, sensitize mitochondrial membrane potential and further induces apoptosis [85]. Peng et al. exhibited that novel sensors based technology using gold nanoparticles could be used for a non-invasive and inexpensive diagnostic tool for lung cancer [86].

7.2. Iron Oxides Nanoparticles (IONPs)

Supermagnetic iron oxide nanoparticles is extensively used as a MRI contrast agent, and also can be utilized as a delivery carrier in cancer theranostics applications. Iron oxides nanoparticles were long used for various biomedical applications including MRI imaging, drug delivery, magnetic hyperthermia, and cancer theranostics in lung cancer [87–90]. Wang et al., recently demonstrated MRI and magnetic resonance-guided focused ultrasound ablation therapy using iron oxide nanoparticles in lung cancer (Figure 3) [87]. The authors synthesized an epidermal growth factor receptor targeted PEGylated iron oxide nanoparticles (IONPs) for targeted delivery and imaging to lung cancer in an in vitro and in vivo rat xenograft model of human lung cancer (H460). In another study, Sadhuka et al. showed the usage of EGFR-targeted inhalable iron oxide nanoparticles for magnetic hyperthermia in lung cancer [89]. The authors showed that EGFR targeting enhanced the tumor retention of IONPs. Moreover, magnetic hyperthermia treatment by EGFR-targeted IONPs caused in major inhibition of lung tumor growth in in vivo orthotropic lung cancer model.

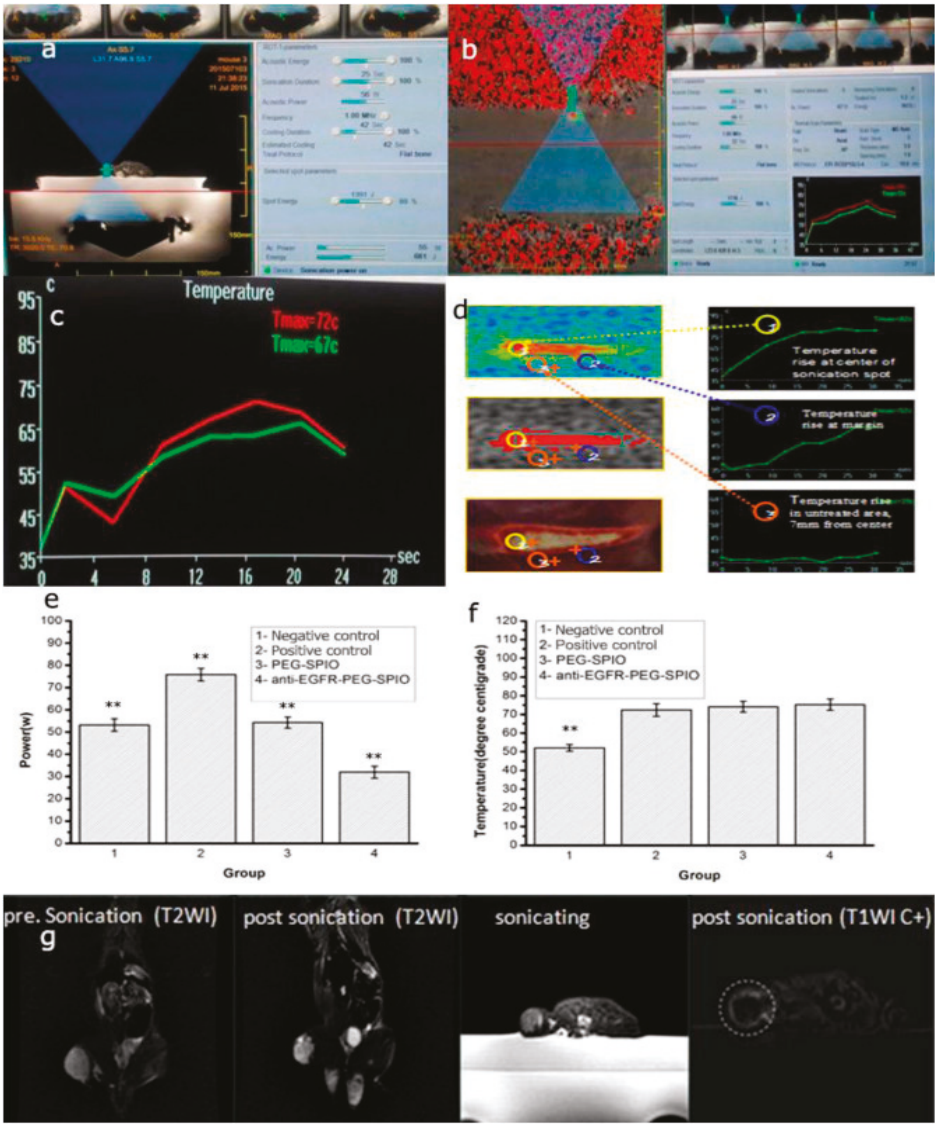

Figure 3. (**a**) Sonication process images. Treatment planning software on the MRgFUS workstation. In total, five sonications are needed to measure the circumference of this tumor. (**b**) Tissue temperature mapping during MRgFUS ablation. (**c**) Real-time temperature change in MRgFUS ablation monitored by MRI. (**d**) Schematic illustration of therapeutic temperature map in tumor center and margin. Sonication energy (**e**) and therapeutic peak temperature (**f**) of negative control (low power, 54 W), control (76 W), PEG-SPIO (54 W), and anti-EGFR-PEG-SPIO (32 W) at 4 h post-injection of SPIO nanoparticles. (**g**) Anti-EGFR-PEG-SPIO group: Coronal T2WI image signal intensity of tumor before treatment and after treatment. The coronal T2WI signal intensities of tumor increased significantly after therapy compared to before therapy (Figure 6g). Enhanced axial T1WI-weighted images after injection of Gd-DTPA. Axial contrast-enhance T1WI subtraction images after injection of Gd-DTPA showed a small focal area of nonperfusion. Reproduced from [87]. Copyright © 2017. Elsevier.

7.3. Silver Nanoparticles (AgNPs)

Silver nanoparticles were long used for various biomedical applications including anti-bacterial applications, anti-cancer applications, fluorescence imaging, and biosensors [91]. Recently, He et al. demonstrated the antitumor activity of biosynthesized AgNPs against lung cancer in in vitro H1299 lung cancer cells and an in vivo xenograft immunodeficient (SCID) mouse model [92]. The potent cytotoxicity effect of AgNPs was showed by trypan blue and MTT assay. Mechanistic studies showed that AgNPs caused apoptosis (increase in caspase-3 and decrease in bcl-2) in lung cancer cells that connected well with an inhibition of NF-κB activity [92]. The cytotoxicity of AgNPs largely depends on their size, shape, morphology, and surface chemistry [93]. In another recent published report, Jeong et al. [94] explored the basic mechanism of hypoxia on AgNPs induced apoptosis that showed the upregulation of HIF-1α expression under both normoxic and hypoxic conditions. Moreover, the AgNPs treatment caused programmed cell death in lung cancer cells but not in normal cells. Notably, HIF-1α protected AgNPs-induced apoptosis by regulating autophagic flux through controlling the ATG5, p62, and LC3-II. Hence, these results suggest that hypoxia-mediated autophagy could be used to inhibit the AgNPs mediated apoptosis involving the HIF-1α as a potential target in lung cancer therapy [94].

7.4. Other Metal Nanoparticles

Among other nanoparticles rare earth, silica, and nanodiamond were used for the cancer theranostics application in lung cancer [95–97]. Wu et al., showed the application of a silica-polymer nanocomposite for p53 gene therapy and near infrared tumor targeted imaging of lung cancer in vitro and in vivo [95]. A nanodiamond (ND) was also utilized for the delivery of paclitaxel in lung cancer therapy. This nanodrug delivery exhibited significant tumor regression ability in immunodeficiency mice, in a lung cancer cell model. Mechanistic studies revealed that ND caused mitotic arrest and apoptosis that led to lung cancer cell death [97]. In another report, Zhang et al. developed a silica based imaging agent to detect a single miRNA in lung cancer cells that can be used for biosensing applications [96]. In another published report, Chen et al. showed the application of micromolar concentration of the neodymium oxide nanoparticles (Nd_2O_3) for the induction of extensive autophagy and immense vacuolization in NSCLC cells [98]. Wu et al. [99] developed a multi-functionalized, carbon dots based theranostics nanoagent that can be used for bioimaging as it emitted visible blue photoluminescence when excited at 360 nm and also can be utilized as a gene delivery vehicle for multiple siRNAs (EGFR and cyclin B1) in lung cancer. Moreover, this nanoagent was found to be accumulated in lung cancer cells by receptor mediated endocytosis in a targeted manner, resulting in improved gene silencing and anti-cancer efficacy.

Scientists and researchers are excited with metal nanoparticles in the recent past due to their small size, high surface to area, easy synthesis and scale up, low cost, multifunctional theranostics applications, exciting physico-chemical properties. However, due to the lack of enough knowledge about their long-term toxicity, pharmacokinetics, pharmacodynamics, and degradability, the clinical translation of these nanomaterials is still not widely possible compared to its other counterparts [29].

8. Clinical Status of the Nanotheranostics in Lung Cancer

Advances in nanoparticle designing and formulations are related to numerous applications in the detection and treatment of malignant growth. Ongoing advances in nanotheranostics in imaging and therapeutics of lung cancer are as follows. Porphyrins due to their favorable photophysical properties have been particularly successful for cancer imaging and photodynamic therapy (PDT). Hematoporphyrin derivative (HpD), porfimer sodium has been approved in over 120 countries since 1993 for the detection and photodynamic therapy of esophageal, lung, superficial bladder, gastric, cervical, and endobronchial cancers [100–102]. Though relatively non-toxic, HpD is not very effective as a primary therapy in lung cancer [103]. Laserphyrin 664 is approved for PDT in Japan for treating early centrally located lung cancer. PET (positron emission tomography) is a nuclear medicine imaging

method, frequently used in combination with FDG (fluorine-18 combined with deoxy-glucose) [104]. FDG is a glucose analogue that is extensively used in cancer staging, restaging and for the analysis of tumor response to treatment. The most frequent application of theranostics is for the palliative treatment of bone metastases from lung cancer. EDTMP marked with 153Sm [105] and 99mTc-MDP an analogue of pyrophosphate similar to bone scanning agents and provides high doses of localized radiation because of its β-particle emissions.

Peptidomimetics like [68Ga]Ga-NODAGA-THERANOST™ is a 3 integrin antagonist first used in humans for lung and breast cancer diagnosis and anti-angiogenic therapy [106]. Ongoing advances in nanotheranostics for drug delivery have been mostly attempted using liposomal formulations. Irinotecan liposome injection (ONIVYDE®) is being investigated versus topotecan in patients with small cell lung cancer after platinum-based first-line therapy (Phase3; 2018–2022 study). To find the highest dose of DOTAP:Chol-fus1 liposomal formulation that can safely be given in combination with tarceva (erlotinib hydrochloride) to patients with NSCLC (Phase2; 2014–2019 study) is currently undergoing. Another trial is investigating the pain management efficiency of liposomal bupivacaine after elective thoracoscopic lobectomy (Phase3; 2018–2021 study) for non-small cell lung cancer.

An exosome is a nano-sized vesicle secreted from different cell types and has a natural ability to carry functional biomolecules, such as small RNAs, DNAs, and proteins in their lumen. This unique signature of particular cells also makes them attractive for use in drug delivery and molecular diagnosis. Moreover, exosomes can be coupled to nanoparticles and used for high precision imaging. Exosomes are considered as an important component in liquid biopsy assessments, which are useful for detecting cancers, including lung cancer. Several studies are currently underway to develop methods of exploiting exosomes for its use as efficient drug delivery vehicles and to develop novel diagnostic modalities. Srivastava et al., 2018 combined the diagnosis of CT and exosome in early lung cancer 2018–2019. Another theranostics-based use of exosome is for the dynamic monitoring circulating tumor DNA in surgical patients with lung cancer, 2017–2023 [107]. Albumin based nanoparticles are in use in different phases of clinical trials for the delivery of paclitaxel, cisplatin in NSCLC [62,108–110].

The development of lung cancer nanotheranostics, with an accentuation on clinical use is limited by several lacunae. The reproducible synthesis of several nanoplatforms with composite structures and its scale-up produces significant complications. Sterility can also hamper such processes. Another important aspect worth considering is nanoparticles-induced cytotoxicity, genotoxicity, and immunotoxicity related to their nanometer size. Industrial vendors and pharmaceutical companies have fewer incentives to move on with theranostics-based blockbusters because of the projected final product price as compared to conventional therapy. Though, coupling therapy with diagnosis together into a single theranostics platform should provide significant advantages but the imaging and tumor targeting components might have different pharmacokinetics and dynamics and can mount a significant manufacturing challenge.

Delay in the transition for theranostics from bench to bedside is mainly due a lack of basic-clinical scientific collaborations. Basic scientists and many clinical scientists lack the information or time to comprehend, envision, oversee cons, and manage the nuances of the multistep compliance guidelines of the clinical trial phases. Being oblivious about the obligation regarding guaranteeing consistency with the guidelines and related regulatory aspects delays the process of bringing cancer theranostics from the laboratory to clinical use. Though FDA is bringing a change in the regulatory changes to the regulatory procedures and developing tools to reduce the development time of theranostics. Weighing the potential benefits to possible adverse health risk assessment of lung cancer nanotheranostics needs to be considered based on scientifically sound, evidence-based and well-controlled clinical studies.

9. Conclusions and Future Perspectives

Theranostics or personalized cancer treatment is proof based, an individualized prescription that warrants the right treatment at the correct time, leading to significant efficacy and improvements of patient's condition and a decrease in medicinal and services costs. Theranostics medicine is

employed for delivering both therapeutic and imaging agents to the targeted area of the body, using a nanotechnology-based delivery platform. Nanomaterials have proved to be tools with tremendous benefit and are now finding application in the clinic. Nanostructures, due to their novel physical properties can often overcome solubility and stability issues through surface modification/wrappings or additional formulation. The integrated approach of combining ligands, drugs, biomolecules, and imaging agents into a functionalized nanoparticle enables targeted drug delivery and diagnostics. Another aspect that aids in the higher therapeutic payload is the high surface area because of their nanosize. Nanoparticle-based targeting specific cancer cells and specific delivery of therapeutic payloads at cancer sites via passive or active targeting can significantly reduce nonspecific toxicity. In spite of the advantages, a lot of unsolved challenges remain including scale-up problems, economical production, the pharmacokinetics of the drug, and the imaging construct. Additional issues with nanotoxicity and regulatory guidelines and hurdles need to be resolved in order to see lung cancer theranostics in the clinic. Though nanotechnology has achieved great strides but still is not used to maximal impact in lung and other malignancies.

With the advent of stronger sequencing, immunohistochemistry, and proteomic techniques, a better understanding of the mechanisms of cancer and identification of new definitive biomarkers are on the way. Greater funding for multi-center cohort studies and the advent of landmark genomic program like the Cancer Genome Atlas (TCGA) and cancer proteome studies the human protein atlas have also created new inroads in the understanding of cancer. In 2018, theranosticsimaging using PSMA (prostate specific membrane antigen) PET (positron emission tomography) and image-guided therapy using PSMA targeted radionucleotide lutetium-177 PSMA617 has shown to be a paradigm-changing practice for improving prostate cancer patient outcomes. The advances of theranostics-based radiomics will span from the current effort to the expected future of using deep learning. Development of theranosticstools for ultrasensitive and quantitative measurement of theranostics biomarkers, ability to diagnose and quantify cancer at its earliest stage with high resolution, and early prediction response to cancer therapy will also depend on how new assisting tools (e.g., artificial intelligence) are going to be harnessed. The integration of all the advances in these allied fields together as cancer theranosticsis poised to revolutionize the future of therapeutics for the ultimate eradication of cancer.

Author Contributions: Conceptualization, A.M. and S.M.; writing—original draft preparation, A.M., M.P. and S.M.; writing—review and editing, A.M., M.P. and S.M.; funding acquisition, M.P. and S.M.

Funding: This research received no external funding. The APC was partially funded by Fondren Library, Rice University, Houston, TX, USA.

Acknowledgments: Sudip Mukherjee acknowledges Fondren Library, Rice University, Houston, TX, United States for partial financial support for the APC of this work. He also acknowledges Omid Veiseh (supervisor/mentor) for providing continuous support for his postdoctoral research. Manash Paul acknowledges Steven Dubinett and Brigitte Gomperts for providing continuous support and mentoring.

Conflicts of Interest: The authors declare no conflict of interest. The authors have no other pertinent affiliations or financial connection with any organization or entity with a financial interest in or financial conflict with the subject matter or materials discussed in the manuscript apart from those disclosed.

References

1. Siegel, R.L.; Miller, K.D.; Jemal, A. Cancer statistics, 2019. *CA Cancer J. Clin.* **2019**, *69*, 7–34. [CrossRef]
2. Bray, F.; Ferlay, J.; Soerjomataram, I.; Siegel, R.L.; Torre, L.A.; Jemal, A. Global cancer statistics 2018: GLOBOCAN estimates of incidence and mortality worldwide for 36 cancers in 185 countries. *CA Cancer J. Clin.* **2018**, *68*, 394–424. [CrossRef] [PubMed]
3. Ferlay, J.; Soerjomataram, I.; Dikshit, R.; Eser, S.; Mathers, C.; Rebelo, M.; Parkin, D.M.; Forman, D.; Bray, F. Cancer incidence and mortality worldwide: Sources, methods and major patterns in GLOBOCAN 2012. *Int. J. Cancer* **2015**, *136*, E359–E386. [CrossRef] [PubMed]
4. Van der Aalst, C.M.; de Koning, H.J. Biochemical verification of the self-reported smoking status of screened male smokers of the Dutch-Belgian randomized controlled lung cancer screening trial. *Lung Cancer* **2016**, *94*, 96–101. [CrossRef]

5. Torre, L.A.; Bray, F.; Siegel, R.L.; Ferlay, J.; Lortet-Tieulent, J.; Jemal, A. Global cancer statistics, 2012. *CA Cancer J. Clin.* **2015**, *65*, 87–108. [CrossRef]
6. Rudokas, M.; Najlah, M.; Alhnan, M.A.; Elhissi, A. Liposome Delivery Systems for Inhalation: A Critical Review Highlighting Formulation Issues and Anticancer Applications. *Med. Princ. Pract.* **2016**, *25*, 60–72. [CrossRef] [PubMed]
7. Miller, K.D.; Siegel, R.L.; Lin, C.C.; Mariotto, A.B.; Kramer, J.L.; Rowland, J.H.; Stein, K.D.; Alteri, R.; Jemal, A. Cancer treatment and survivorship statistics, 2016. *CA Cancer J. Clin.* **2016**, *66*, 271–289. [CrossRef] [PubMed]
8. Cohen, Z.R.; Ramishetti, S.; Peshes-Yaloz, N.; Goldsmith, M.; Wohl, A.; Zibly, Z.; Peer, D. Localized RNAi therapeutics of chemoresistant grade IV glioma using hyaluronan-grafted lipid-based nanoparticles. *ACS Nano.* **2015**, *9*, 1581–1591. [CrossRef]
9. Xiong, X.B.; Lavasanifar, A. Traceable multifunctional micellar nanocarriers for cancer-targeted co-delivery of MDR-1 siRNA and doxorubicin. *ACS Nano.* **2011**, *5*, 5202–5213. [CrossRef]
10. Shen, S.; Xia, J.X.; Wang, J. Nanomedicine-mediated cancer stem cell therapy. *Biomaterials* **2016**, *74*, 1–18. [CrossRef]
11. Tran, T.H.; Nguyen, H.T.; Pham, T.T.; Choi, J.Y.; Choi, H.G.; Yong, C.S.; Kim, J.O. Development of a Graphene Oxide Nanocarrier for Dual-Drug Chemo-phototherapy to Overcome Drug Resistance in Cancer. *ACS Appl. Mater. Interfaces* **2015**, *7*, 28647–28655. [CrossRef] [PubMed]
12. Shahin, M.; Soudy, R.; El-Sikhry, H.; Seubert, J.M.; Kaur, K.; Lavasanifar, A. Engineered peptides for the development of actively tumor targeted liposomal carriers of doxorubicin. *Cancer Lett.* **2013**, *334*, 284–292. [CrossRef] [PubMed]
13. Zhang, X.X.; Eden, H.S.; Chen, X. Peptides in cancer nanomedicine: Drug carriers, targeting ligands and protease substrates. *J. Control. Release* **2012**, *159*, 2–13. [CrossRef] [PubMed]
14. Liu, J.; Wei, T.; Zhao, J.; Huang, Y.; Deng, H.; Kumar, A.; Wang, C.; Liang, Z.; Ma, X.; Liang, X.J. Multifunctional aptamer-based nanoparticles for targeted drug delivery to circumvent cancer resistance. *Biomaterials* **2016**, *91*, 44–56. [CrossRef]
15. Codony-Servat, J.; Garcia-Roman, S.; Molina-Vila, M.A.; Bertran-Alamillo, J.; Gimenez-Capitan, A.; Viteri, S.; Cardona, A.F.; D'Hondt, E.; Karachaliou, N.; Rosell, R. Anti-Epidermal Growth Factor Vaccine Antibodies Enhance the Efficacy of Tyrosine Kinase Inhibitors and Delay the Emergence of Resistance in EGFR Mutant Lung Cancer Cells. *J. Thorac. Oncol.* **2018**, *13*, 1324–1337. [CrossRef] [PubMed]
16. Mukherjee, A.; Waters, A.K.; Babic, I.; Nurmemmedov, E.; Glassy, M.C.; Kesari, S.; Yenugonda, V.M. Antibody drug conjugates: Progress, pitfalls, and promises. *Hum. Antibodies* **2019**, *27*, 53–62. [CrossRef] [PubMed]
17. Lv, S.; Tang, Z.; Li, M.; Lin, J.; Song, W.; Liu, H.; Huang, Y.; Zhang, Y.; Chen, X. Co-delivery of doxorubicin and paclitaxel by PEG-polypeptide nanovehicle for the treatment of non-small cell lung cancer. *Biomaterials* **2014**, *35*, 6118–6129. [CrossRef]
18. Fernandez-Fernandez, A.; Manchanda, R.; McGoron, A.J. Theranostic applications of nanomaterials in cancer: Drug delivery, image-guided therapy, and multifunctional platforms. *Appl. Biochem. Biotechnol.* **2011**, *165*, 1628–1651. [CrossRef]
19. Cong, Y.; Xiao, H.; Xiong, H.; Wang, Z.; Ding, J.; Li, C.; Chen, X.; Liang, X.J.; Zhou, D.; Huang, Y. Dual Drug Backboned Shattering Polymeric Theranostic Nanomedicine for Synergistic Eradication of Patient-Derived Lung Cancer. *Adv. Mater.* **2018**, *30*. [CrossRef]
20. Chi, Y.H.; Hsiao, J.K.; Lin, M.H.; Chang, C.; Lan, C.H.; Wu, H.C. Lung Cancer-Targeting Peptides with Multi-subtype Indication for Combinational Drug Delivery and Molecular Imaging. *Theranostics* **2017**, *7*, 1612–1632. [CrossRef]
21. Arranja, A.G.; Pathak, V.; Lammers, T.; Shi, Y. Tumor-targeted nanomedicines for cancer theranostics. *Pharmacol. Res.* **2017**, *115*, 87–95. [CrossRef]
22. Chowdhury, S.R.; Mukherjee, S.; Das, S.; Patra, C.R.; Iyer, P.K. Multifunctional (3-in-1) cancer theranostics applications of hydroxyquinoline-appended polyfluorene nanoparticles. *Chem. Sci.* **2017**, *8*, 7566–7575. [CrossRef]
23. Muthuraj, B.; Mukherjee, S.; Patra, C.R.; Iyer, P.K. Amplified Fluorescence from Polyfluorene Nanoparticles with Dual State Emission and Aggregation Caused Red Shifted Emission for Live Cell Imaging and Cancer Theranostics. *ACS Appl. Mater. Interfaces* **2016**, *8*, 32220–32229. [CrossRef]
24. Mukherjee, S.; Patra, C.R. Biologically synthesized metal nanoparticles: Recent advancement and future perspectives in cancer theranostics. *Future Sci.* **2017**, *3*, FSO203. [CrossRef]

25. Burstein, H.J.; Schwartz, R.S. Molecular origins of cancer. *N. Engl. J. Med.* **2008**, *358*, 527. [CrossRef]
26. Paul, M.K.; Mukhopadhyay, A.K. Tyrosine kinase—Role and significance in Cancer. *Int. J. Med. Sci.* **2004**, *1*, 101–115. [CrossRef]
27. Jamal-Hanjani, M.; Wilson, G.A.; McGranahan, N.; Birkbak, N.J.; Watkins, T.B.K.; Veeriah, S.; Shafi, S.; Johnson, D.H.; Mitter, R.; Rosenthal, R.; et al. Tracking the Evolution of Non-Small-Cell Lung Cancer. *N. Engl. J. Med.* **2017**, *376*, 2109–2121. [CrossRef]
28. DiSanto, R.M.; Subramanian, V.; Gu, Z. Recent advances in nanotechnology for diabetes treatment. *Wiley Interdiscip. Rev. Nanomed. Nanobiotechnol.* **2015**, *7*, 548–564. [CrossRef]
29. Mukherjee, S.; Patra, C.R. Therapeutic application of anti-angiogenic nanomaterials in cancers. *Nanoscale* **2016**, *8*, 12444–12470. [CrossRef]
30. Yue, X.; Dai, Z. Liposomal Nanotechnology for Cancer Theranostics. *Curr. Med. Chem.* **2018**, *25*, 1397–1408. [CrossRef]
31. Matsumura, Y.; Maeda, H. A New Concept for Macromolecular Therapeutics in Cancer-Chemotherapy—Mechanism of Tumoritropic Accumulation of Proteins and the Antitumor Agent Smancs. *Cancer Res.* **1986**, *46*, 6387–6392.
32. Moghimi, S.M.; Szebeni, J. Stealth liposomes and long circulating nanoparticles: Critical issues in pharmacokinetics, opsonization and protein-binding properties. *Prog. Lipid Res.* **2003**, *42*, 463–478. [CrossRef]
33. Torchilin, V.P. Recent advances with liposomes as pharmaceutical carriers. *Nat. Rev. Drug Discov.* **2005**, *4*, 145–160. [CrossRef] [PubMed]
34. Barenholz, Y. Doxil(R)—The first FDA-approved nano-drug: Lessons learned. *J. Control. Release* **2012**, *160*, 117–134. [CrossRef] [PubMed]
35. Petersen, G.H.; Alzghari, S.K.; Chee, W.; Sankari, S.S.; La-Beck, N.M. Meta-analysis of clinical and preclinical studies comparing the anticancer efficacy of liposomal versus conventional non-liposomal doxorubicin. *J. Control. Release* **2016**, *232*, 255–264. [CrossRef]
36. Cheng, L.; Huang, F.Z.; Cheng, L.F.; Zhu, Y.Q.; Hu, Q.; Li, L.; Wei, L.; Chen, D.W. GE11-modified liposomes for non-small cell lung cancer targeting: Preparation, ex vitro and in vivo evaluation. *Int. J. Nanomed.* **2014**, *9*, 921–935. [CrossRef] [PubMed]
37. Lin, C.; Zhang, X.; Chen, H.; Bian, Z.; Zhang, G.; Riaz, M.K.; Tyagi, D.; Lin, G.; Zhang, Y.; Wang, J.; et al. Dual-ligand modified liposomes provide effective local targeted delivery of lung-cancer drug by antibody and tumor lineage-homing cell-penetrating peptide. *Drug Deliv.* **2018**, *25*, 256–266. [CrossRef]
38. Song, X.L.; Ju, R.J.; Xiao, Y.; Wang, X.; Liu, S.; Fu, M.; Liu, J.J.; Gu, L.Y.; Li, X.T.; Cheng, L. Application of multifunctional targeting epirubicin liposomes in the treatment of non-small-cell lung cancer. *Int. J. Nanomed.* **2017**, *12*, 7433–7451. [CrossRef]
39. Mukherjee, A.; Bhattacharyya, J.; Sagar, M.V.; Chaudhuri, A. Liposomally encapsulated CDC20 siRNA inhibits both solid melanoma tumor growth and spontaneous growth of intravenously injected melanoma cells on mouse lung. *Drug Deliv. Transl. Res.* **2013**, *3*, 224–234. [CrossRef]
40. Skubitz, K.M.; Anderson, P.M. Inhalational interleukin-2 liposomes for pulmonary metastases: A phase I clinical trial. *Anticancer Drugs* **2000**, *11*, 555–563. [CrossRef]
41. Wittgen, B.P.; Kunst, P.W.; van der Born, K.; van Wijk, A.W.; Perkins, W.; Pilkiewicz, F.G.; Perez-Soler, R.; Nicholson, S.; Peters, G.J.; Postmus, P.E. Phase I study of aerosolized SLIT cisplatin in the treatment of patients with carcinoma of the lung. *Clin. Cancer Res.* **2007**, *13*, 2414–2421. [CrossRef]
42. Erten, A.; Wrasidlo, W.; Scadeng, M.; Esener, S.; Hoffman, R.M.; Bouvet, M.; Makale, M. Magnetic resonance and fluorescence imaging of doxorubicin-loaded nanoparticles using a novel in vivo model. *Nanomedicine* **2010**, *6*, 797–807. [CrossRef]
43. Lowery, A.; Onishko, H.; Hallahan, D.E.; Han, Z. Tumor-targeted delivery of liposome-encapsulated doxorubicin by use of a peptide that selectively binds to irradiated tumors. *J. Control. Release* **2011**, *150*, 117–124. [CrossRef]
44. Sercombe, L.; Veerati, T.; Moheimani, F.; Wu, S.Y.; Sood, A.K.; Hua, S. Advances and Challenges of Liposome Assisted Drug Delivery. *Front. Pharmacol.* **2015**, *6*, 286. [CrossRef]
45. Bolhassani, A.; Javanzad, S.; Saleh, T.; Hashemi, M.; Aghasadeghi, M.R.; Sadat, S.M. Polymeric nanoparticles: Potent vectors for vaccine delivery targeting cancer and infectious diseases. *Hum. Vaccin. Immunother* **2014**, *10*, 321–332. [CrossRef]

46. Farokhzad, O.C.; Cheng, J.; Teply, B.A.; Sherifi, I.; Jon, S.; Kantoff, P.W.; Richie, J.P.; Langer, R. Targeted nanoparticle—Aptamer bioconjugates for cancer chemotherapy in vivo. *Proc. Natl. Acad. Sci. USA* **2006**, *103*, 6315–6320. [CrossRef]
47. Torchilin, V.P. Micellar nanocarriers: Pharmaceutical perspectives. *Pharm. Res.* **2007**, *24*, 1–16. [CrossRef]
48. Kim, T.Y.; Kim, D.W.; Chung, J.Y.; Shin, S.G.; Kim, S.C.; Heo, D.S.; Kim, N.K.; Bang, Y.J. Phase I and pharmacokinetic study of Genexol-PM, a cremophor-free, polymeric micelle-formulated paclitaxel, in patients with advanced malignancies. *Clin. Cancer Res.* **2004**, *10*, 3708–3716. [CrossRef]
49. Ahn, H.K.; Jung, M.; Sym, S.J.; Shin, D.B.; Kang, S.M.; Kyung, S.Y.; Park, J.W.; Jeong, S.H.; Cho, E.K. A phase II trial of Cremorphor EL-free paclitaxel (Genexol-PM) and gemcitabine in patients with advanced non-small cell lung cancer. *Cancer Chemother. Pharmacol.* **2014**, *74*, 277–282. [CrossRef]
50. Jiang, Z.M.; Dai, S.P.; Xu, Y.Q.; Li, T.; Xie, J.; Li, C.; Zhang, Z.H. Crizotinib-loaded polymeric nanoparticles in lung cancer chemotherapy. *Med. Oncol.* **2015**, *32*, 193. [CrossRef]
51. Hu, J.; Fu, S.; Peng, Q.; Han, Y.; Xie, J.; Zan, N.; Chen, Y.; Fan, J. Paclitaxel-loaded polymeric nanoparticles combined with chronomodulated chemotherapy on lung cancer: In vitro and in vivo evaluation. *Int. J. Pharm.* **2017**, *516*, 313–322. [CrossRef]
52. Wang, X.S.; Chen, H.Y.; Zeng, X.W.; Guo, W.P.; Jin, Y.; Wang, S.; Tian, R.Y.; Han, Y.J.; Guo, L.; Han, J.M.; et al. Efficient lung cancer-targeted drug delivery via a nanoparticle/MSC system. *Acta. Pharm. Sin. B* **2019**, *9*, 167–176. [CrossRef] [PubMed]
53. Ganesh, S.; Iyer, A.K.; Morrissey, D.V.; Amiji, M.M. Hyaluronic acid based self-assembling nanosystems for CD44 target mediated siRNA delivery to solid tumors. *Biomaterials* **2013**, *34*, 3489–3502. [CrossRef]
54. Kim, I.; Byeon, H.J.; Kim, T.H.; Lee, E.S.; Oh, K.T.; Shin, B.S.; Lee, K.C.; Youn, Y.S. Doxorubicin-loaded porous PLGA microparticles with surface attached TRAIL for the inhalation treatment of metastatic lung cancer. *Biomaterials* **2013**, *34*, 6444–6453. [CrossRef]
55. Feng, T.; Tian, H.; Xu, C.; Lin, L.; Xie, Z.; Lam, M.H.; Liang, H.; Chen, X. Synergistic co-delivery of doxorubicin and paclitaxel by porous PLGA microspheres for pulmonary inhalation treatment. *Eur. J. Pharm. Biopharm.* **2014**, *88*, 1086–1093. [CrossRef]
56. Khatun, Z.; Nurunnabi, M.; Nafiujjaman, M.; Reeck, G.R.; Khan, H.A.; Cho, K.J.; Lee, Y.K. A hyaluronic acid nanogel for photo-chemo theranostics of lung cancer with simultaneous light-responsive controlled release of doxorubicin. *Nanoscale* **2015**, *7*, 10680–10689. [CrossRef] [PubMed]
57. Mitra, A.; Coleman, T.; Borgman, M.; Nan, A.; Ghandehari, H.; Line, B.R. Polymeric conjugates of mono- and bi-cyclic alphaVbeta3 binding peptides for tumor targeting. *J. Control. Release* **2006**, *114*, 175–183. [CrossRef] [PubMed]
58. Guthi, J.S.; Yang, S.G.; Huang, G.; Li, S.; Khemtong, C.; Kessinger, C.W.; Peyton, M.; Minna, J.D.; Brown, K.C.; Gao, J. MRI-visible micellar nanomedicine for targeted drug delivery to lung cancer cells. *Mol. Pharm.* **2010**, *7*, 32–40. [CrossRef] [PubMed]
59. Sivarajakumar, R.; Mallukaraj, D.; Kadavakollu, M.; Neelakandan, N.; Chandran, S.; Bhojaraj, S.; Karri, V.V.S.R. Nanoparticles for the Treatment of Lung Cancers. *J. Young Pharm.* **2018**, *10*, 276–281. [CrossRef]
60. Perepelyuk, M.; Sacko, K.; Thangavel, K.; Shoyele, S.A. Evaluation of MUC1-Aptamer Functionalized Hybrid Nanoparticles for Targeted Delivery of miRNA-29b to Nonsmall Cell Lung Cancer. *Mol. Pharm.* **2018**, *15*, 985–993. [CrossRef]
61. Rizvi, N.A.; Riely, G.J.; Azzoli, C.G.; Miller, V.A.; Ng, K.K.; Fiore, J.; Chia, G.; Brower, M.; Heelan, R.; Hawkins, M.J.; et al. Phase I/II trial of weekly intravenous 130-nm albumin-bound paclitaxel as initial chemotherapy in patients with stage IV non-small-cell lung cancer. *J. Clin. Oncol.* **2008**, *26*, 639–643. [CrossRef]
62. Socinski, M.A.; Okamoto, I.; Hon, J.K.; Hirsh, V.; Dakhil, S.R.; Page, R.D.; Orsini, J.; Yamamoto, N.; Zhang, H.; Renschler, M.F. Safety and efficacy analysis by histology of weekly nab-paclitaxel in combination with carboplatin as first-line therapy in patients with advanced non-small-cell lung cancer. *Ann. Oncol.* **2013**, *24*, 2390–2396. [CrossRef]
63. Li, K.; Nguyen, H.G.; Lu, X.B.; Wang, Q. Viruses and their potential in bioimaging and biosensing applications. *Analyst* **2010**, *135*, 21–27. [CrossRef]
64. Beljanski, V.; Hiscott, J. The use of oncolytic viruses to overcome lung cancer drug resistance. *Curr. Opin. Virol.* **2012**, *2*, 629–635. [CrossRef]

65. Robertson, K.L.; Soto, C.M.; Archer, M.J.; Odoemene, O.; Liu, J.L. Engineered T4 viral nanoparticles for cellular imaging and flow cytometry. *Bioconjug. Chem.* **2011**, *22*, 595–604. [CrossRef]
66. Maham, A.; Tang, Z.; Wu, H.; Wang, J.; Lin, Y. Protein-based nanomedicine platforms for drug delivery. *Small* **2009**, *5*, 1706–1721. [CrossRef]
67. Wiley, J.A.; Richert, L.E.; Swain, S.D.; Harmsen, A.; Barnard, D.L.; Randall, T.D.; Jutila, M.; Douglas, T.; Broomell, C.; Young, M.; et al. Inducible bronchus-associated lymphoid tissue elicited by a protein cage nanoparticle enhances protection in mice against diverse respiratory viruses. *PLoS ONE* **2009**, *4*, e7142. [CrossRef]
68. Lohcharoenkal, W.; Wang, L.Y.; Chen, Y.C.; Rojanasakul, Y. Protein Nanoparticles as Drug Delivery Carriers for Cancer Therapy. *Biomed. Res. Int.* **2014**. [CrossRef]
69. Han, J.F.; Wang, Q.; Zhang, Z.R.; Gong, T.; Sun, X. Cationic Bovine Serum Albumin Based Self-Assembled Nanoparticles as siRNA Delivery Vector for Treating Lung Metastatic Cancer. *Small* **2014**, *10*, 524–535. [CrossRef]
70. Dostalova, S.; Vasickova, K.; Hynek, D.; Krizkova, S.; Richtera, L.; Vaculovicova, M.; Eckschlager, T.; Stiborova, M.; Heger, Z.; Adam, V. Apoferritin as an ubiquitous nanocarrier with excellent shelf life. *Int. J. Nanomed.* **2017**, *12*, 2265–2278. [CrossRef]
71. Li, K.; Zhang, Z.P.; Luo, M.; Yu, X.; Han, Y.; Wei, H.P.; Cui, Z.Q.; Zhang, X.E. Multifunctional ferritin cage nanostructures for fluorescence and MR imaging of tumor cells. *Nanoscale* **2012**, *4*, 188–193. [CrossRef]
72. Luo, Y.; Wang, X.; Du, D.; Lin, Y. Hyaluronic acid-conjugated apoferritin nanocages for lung cancer targeted drug delivery. *Biomater. Sci.* **2015**, *3*, 1386–1394. [CrossRef]
73. Patra, C.R.; Mukherjee, S.; Kotcherlakota, R. Biosynthesized silver nanoparticles: A step forward for cancer theranostics? *Nanomedicine* **2014**, *9*, 1445–1448. [CrossRef]
74. Gao, L.; Fan, K.; Yan, X. Iron Oxide Nanozyme: A Multifunctional Enzyme Mimetic for Biomedical Applications. *Theranostics* **2017**, *7*, 3207–3227. [CrossRef] [PubMed]
75. Lim, E.K.; Kim, T.; Paik, S.; Haam, S.; Huh, Y.M.; Lee, K. Nanomaterials for theranostics: Recent advances and future challenges. *Chem. Rev.* **2015**, *115*, 327–394. [CrossRef]
76. Gaddam, R.R.; Mukherjee, S.; Punugupati, N.; Vasudevan, D.; Patra, C.R.; Narayan, R.; Vsn Kothapalli, R. Facile synthesis of carbon dot and residual carbon nanobeads: Implications for ion sensing, medicinal and biological applications. *Mater. Sci. Eng. C Mater. Biol. Appl.* **2017**, *73*, 643–652. [CrossRef] [PubMed]
77. Knights, O.B.; McLaughlan, J.R. Gold Nanorods for Light-Based Lung Cancer Theranostics. *Int. J. Mol. Sci.* **2018**, *19*, 3318. [CrossRef] [PubMed]
78. Silva, C.O.; Pinho, J.O.; Lopes, J.M.; Almeida, A.J.; Gaspar, M.M.; Reis, C. Current Trends in Cancer Nanotheranostics: Metallic, Polymeric, and Lipid-Based Systems. *Pharmaceutics* **2019**, *11*, 22. [CrossRef]
79. Lee, H.Y.; Mohammed, K.A.; Nasreen, N. Nanoparticle-based targeted gene therapy for lung cancer. *Am. J. Cancer Res.* **2016**, *6*, 1118–1134.
80. Liu, Y.; Ma, W.; Wang, J. Theranostics of Gold Nanoparticles with an Emphasis on Photoacoustic Imaging and Photothermal Therapy. *Curr. Pharm. Des.* **2018**, *24*, 2719–2728. [CrossRef] [PubMed]
81. Balakrishnan, S.; Mukherjee, S.; Das, S.; Bhat, F.A.; Raja Singh, P.; Patra, C.R.; Arunakaran, J. Gold nanoparticles-conjugated quercetin induces apoptosis via inhibition of EGFR/PI3K/Akt-mediated pathway in breast cancer cell lines (MCF-7 and MDA-MB-231). *Cell Biochem. Funct.* **2017**, *35*, 217–231. [CrossRef]
82. Meka, R.R.; Mukherjee, S.; Patra, S.; Chaudhuri, A. Shikimoyl-ligand decorated gold nanoparticles for use in ex vivo engineered dendritic cell based DNA vaccination. *Nanoscale* **2019**, *11*. [CrossRef]
83. Anselmo, A.C.; Mitragotri, S. Nanoparticles in the clinic. *Bioeng. Transl. Med.* **2016**, *1*, 10–29. [CrossRef]
84. Singh, P.; Pandit, S.; Mokkapati, V.; Garg, A.; Ravikumar, V.; Mijakovic, I. Gold Nanoparticles in Diagnostics and Therapeutics for Human Cancer. *Int. J. Mol. Sci.* **2018**, *19*, 1979. [CrossRef] [PubMed]
85. Ramalingam, V.; Varunkumar, K.; Ravikumar, V.; Rajaram, R. Target delivery of doxorubicin tethered with PVP stabilized gold nanoparticles for effective treatment of lung cancer. *Sci. Rep.* **2018**, *8*, 3815. [CrossRef]
86. Peng, G.; Tisch, U.; Adams, O.; Hakim, M.; Shehada, N.; Broza, Y.Y.; Billan, S.; Abdah-Bortnyak, R.; Kuten, A.; Haick, H. Diagnosing lung cancer in exhaled breath using gold nanoparticles. *Nat. Nanotechnol.* **2009**, *4*, 669–673. [CrossRef] [PubMed]
87. Wang, Z.L.; Qiao, R.R.; Tang, N.; Lu, Z.W.; Wang, H.; Zhang, Z.X.; Xue, X.D.; Huang, Z.Y.; Zhang, S.R.; Zhang, G.X.; et al. Active targeting theranostic iron oxide nanoparticles for MRI and magnetic resonance-guided focused ultrasound ablation of lung cancer. *Biomaterials* **2017**, *127*, 25–35. [CrossRef]

88. Ghazani, A.A.; Pectasides, M.; Sharma, A.; Castro, C.M.; Mino-Kenudson, M.; Lee, H.; Shepard, J.A.; Weissleder, R. Molecular characterization of scant lung tumor cells using iron-oxide nanoparticles and micro-nuclear magnetic resonance. *Nanomedicine* **2014**, *10*, 661–668. [CrossRef]
89. Sadhukha, T.; Wiedmann, T.S.; Panyam, J. Inhalable magnetic nanoparticles for targeted hyperthermia in lung cancer therapy. *Biomaterials* **2013**, *34*, 5163–5171. [CrossRef]
90. Noh, M.S.; Jun, B.H.; Kim, S.; Kang, H.; Woo, M.A.; Minai-Tehrani, A.; Kim, J.E.; Kim, J.; Park, J.; Lim, H.T.; et al. Magnetic surface-enhanced Raman spectroscopic (M-SERS) dots for the identification of bronchioalveolar stem cells in normal and lung cancer mice. *Biomaterials* **2009**, *30*, 3915–3925. [CrossRef] [PubMed]
91. Mukherjee, S.; Chowdhury, D.; Kotcherlakota, R.; Patra, S.; Vinothkumar, B.; Bhadra, M.P.; Sreedhar, B.; Patra, C.R. Potential theranostics application of bio-synthesized silver nanoparticles (4-in-1 system). *Theranostics* **2014**, *4*, 316–335. [CrossRef]
92. He, Y.; Du, Z.Y.; Ma, S.J.; Liu, Y.; Li, D.L.; Huang, H.R.; Jiang, S.; Cheng, S.P.; Wu, W.J.; Zhang, K.; et al. Effects of green-synthesized silver nanoparticles on lung cancer cells in vitro and grown as xenograft tumors in vivo. *Int. J. Nanomed.* **2016**, *11*. [CrossRef]
93. Stoehr, L.C.; Gonzalez, E.; Stampfl, A.; Casals, E.; Duschl, A.; Puntes, V.; Oostingh, G.J. Shape matters: Effects of silver nanospheres and wires on human alveolar epithelial cells. *Part Fibre. Toxicol.* **2011**, *8*, 36. [CrossRef]
94. Jeong, J.K.; Gurunathan, S.; Kang, M.H.; Han, J.W.; Das, J.; Choi, Y.J.; Kwon, D.N.; Cho, S.G.; Park, C.; Seo, H.G.; et al. Hypoxia-mediated autophagic flux inhibits silver nanoparticle-triggered apoptosis in human lung cancer cells. *Sci. Rep* **2016**, *6*, 21688. [CrossRef]
95. Wu, H.; Zhao, Y.; Mu, X.; Wu, H.; Chen, L.; Liu, W.; Mu, Y.; Liu, J.; Wei, X. A silica-polymer composite nano system for tumor-targeted imaging and p53 gene therapy of lung cancer. *J. Biomater. Sci. Polym. Ed.* **2015**, *26*, 384–400. [CrossRef]
96. Zhang, J.; Fu, Y.; Mei, Y.; Jiang, F.; Lakowicz, J.R. Fluorescent metal nanoshell probe to detect single miRNA in lung cancer cell. *Anal. Chem.* **2010**, *82*, 4464–4471. [CrossRef]
97. Liu, K.K.; Zheng, W.W.; Wang, C.C.; Chiu, Y.C.; Cheng, C.L.; Lo, Y.S.; Chen, C.; Chao, J.I. Covalent linkage of nanodiamond-paclitaxel for drug delivery and cancer therapy. *Nanotechnology* **2010**, *21*, 315106. [CrossRef]
98. Chen, Y.; Yang, L.; Feng, C.; Wen, L.P. Nano neodymium oxide induces massive vacuolization and autophagic cell death in non-small cell lung cancer NCI-H460 cells. *Biochem. Biophys. Res. Commun.* **2005**, *337*, 52–60. [CrossRef]
99. Wu, Y.-F.; Wu, H.-C.; Kuan, C.-H.; Lin, C.-J.; Wang, L.-W.; Chang, C.-W.; Wang, T.-W. Multi-functionalized carbon dots as theranostic nanoagent for gene delivery in lung cancer therapy. *Sci. Rep.* **2016**, *6*, 21170. [CrossRef]
100. Baskaran, R.; Lee, J.; Yang, S.G. Clinical development of photodynamic agents and therapeutic applications. *Biomater. Res.* **2018**, *22*, 25. [CrossRef]
101. Kato, H.; Horai, T.; Furuse, K.; Fukuoka, M.; Suzuki, S.; Hiki, Y.; Ito, Y.; Mimura, S.; Tenjin, Y.; Hisazumi, H.; et al. Photodynamic therapy for cancers: A clinical trial of porfimer sodium in Japan. *Jpn. J. Cancer Res.* **1993**, *84*, 1209–1214. [CrossRef] [PubMed]
102. Hayata, Y.; Kato, H.; Konaka, C.; Ono, J.; Takizawa, N. Hematoporphyrin derivative and laser photoradiation in the treatment of lung cancer. *Chest* **1982**, *81*, 269–277. [CrossRef]
103. Hayata, Y.; Kato, H.; Konaka, C.; Amemiya, R.; Ono, J.; Ogawa, I.; Kinoshita, K.; Sakai, H.; Takahashi, H. Photoradiation therapy with hematoporphyrin derivative in early and stage 1 lung cancer. *Chest* **1984**, *86*, 169–177. [CrossRef] [PubMed]
104. Ding, X.P.; Zhang, J.; Li, B.S.; Li, H.S.; Wang, Z.T.; Yi, Y.; Sun, H.F.; Wang, D.Q. Feasibility of shrinking field radiation therapy through 18F-FDG PET/CT after 40 Gy for stage III non-small cell lung cancers. *Asian Pac. J. Cancer Prev.* **2012**, *13*, 319–323. [CrossRef] [PubMed]
105. Pacilio, M.; Ventroni, G.; Basile, C.; Ialongo, P.; Becci, D.; Mango, L. Improving the dose-myelotoxicity correlation in radiometabolic therapy of bone metastases with 153Sm-EDTMP. *Eur. J. Nucl. Med. Mol. Imaging* **2014**, *41*, 238–252. [CrossRef] [PubMed]
106. Baum, R.P.; Kulkarni, H.R.; Muller, D.; Satz, S.; Danthi, N.; Kim, Y.S.; Brechbiel, M.W. First-In-Human Study Demonstrating Tumor-Angiogenesis by PET/CT Imaging with (68) Ga-NODAGA-THERANOST, a High-Affinity Peptidomimetic for alphavbeta3 Integrin Receptor Targeting. *Cancer Biother. Radiopharm.* **2015**, *30*, 152–159. [CrossRef] [PubMed]

107. Srivastava, A.; Amreddy, N.; Razaq, M.; Towner, R.; Zhao, Y.; Ahmed, R.; Munshi, A.; Ramesh, R. Exosomes as Theranostics for Lung Cancer. *Adv. Cancer Res.* **2018**, *139*, 1–33.
108. Socinski, M.A.; Langer, C.J.; Okamoto, I.; Hon, J.K.; Hirsh, V.; Dakhil, S.R.; Page, R.D.; Orsini, J.; Zhang, H.; Renschler, M.F. Safety and efficacy of weekly nab(R)-paclitaxel in combination with carboplatin as first-line therapy in elderly patients with advanced non-small-cell lung cancer. *Ann. Oncol.* **2013**, *24*, 314–321. [CrossRef]
109. Green, M.R.; Manikhas, G.M.; Orlov, S.; Afanasyev, B.; Makhson, A.M.; Bhar, P.; Hawkins, M.J. Abraxane, a novel Cremophor-free, albumin-bound particle form of paclitaxel for the treatment of advanced non-small-cell lung cancer. *Ann. Oncol.* **2006**, *17*, 1263–1268. [CrossRef]
110. Zheng, D.; Wang, J.; Guo, S.; Zhao, Z.; Wang, F. Formulations, Pharmacodynamic and Clinical Studies of Nanoparticles for Lung Cancer Therapy—An Overview. *Curr. Drug Metab.* **2018**, *19*, 759–767. [CrossRef]

MDPI
St. Alban-Anlage 66
4052 Basel
Switzerland
Tel. +41 61 683 77 34
Fax +41 61 302 89 18
www.mdpi.com

Cancers Editorial Office
E-mail: cancers@mdpi.com
www.mdpi.com/journal/cancers

MDPI
St. Alban-Anlage 66
4052 Basel
Switzerland

Tel: +41 61 683 77 34
Fax: +41 61 302 89 18

www.mdpi.com

978-3-03943-105-2 (PDF)